

---

# SOIL MECHANICS IN ENGINEERING PRACTICE

---

THIRD EDITION

Karl Terzaghi  
Ralph B. Peck  
Gholamreza Mesri

---

# Soil Mechanics in Engineering Practice

Third Edition

*Karl Terzaghi*

Late Professor of the Practice of Civil Engineering  
Harvard University  
Lecturer and Research Consultant in Civil Engineering  
University of Illinois

*Ralph B. Peck*

Professor of Foundation Engineering, Emeritus  
University of Illinois

*Gholamreza Mesri*

Professor of Civil Engineering  
University of Illinois



A Wiley-Interscience Publication

JOHN WILEY & SONS, INC.

New York • Chichester • Brisbane • Toronto • Singapore



This text is printed on acid-free paper.

Copyright © 1996 by John Wiley & Sons, Inc.

All rights reserved. Published simultaneously in Canada.

Reproduction or translation of any part of this work beyond that permitted by Section 107 or 108 of the 1976 United States Copyright Act without the permission of the copyright owner is unlawful. Requests for permission or further information should be addressed to the Permissions Department, John Wiley & Sons, Inc., 605 Third Avenue, New York, NY 10158-0012.

This publication is designed to provide accurate and authoritative information in regard to the subject matter covered. It is sold with the understanding that the publisher is not engaged in rendering legal, accounting, or other professional services. If legal advice or other expert assistance is required, the services of a competent professional person should be sought.

*Library of Congress Cataloging in Publication Data:*

Terzaghi, Karl, 1883–1963.

Soil mechanics in engineering practice/Karl Terzaghi,  
Ralph B. Peck, Gholamreza Mesri.—3rd ed.

p. cm.

Includes index.

ISBN 0-471-08658-4

1. Soil mechanics. I. Peck, Ralph B. (Ralph  
Brazelton) II. Mesri, Gholamreza, 1940-  
III. Title.

TA710.T39 1995

624.1'5136—dc20

95-6616

Printed in the United States of America

*To Ruth, Marjorie, and Lorna*

# CONTENTS

Preface	xix
Preface to First Edition	xxi
Introduction	xxiii
Symbols	xxv
<b>Part I. Physical Properties of Soils</b>	<b>1</b>
<b>CHAPTER 1. Index Properties of Soils</b>	<b>3</b>
1. Practical importance of index properties	3
2. Principal types of soils	3
3. Size and shape of soil particles	6
4. Properties of very fine soil fractions	6
4.1 Mineralogical composition	6
4.2 Characteristics of principal clay minerals	7
4.3 Role of isomorphous substitution	9
4.4 Cation exchange and adsorbed water	10
4.5 Fabric	12
4.6 Organic soils	15
4.7 Practical significance of colloidal properties	17
5. Mechanical analysis of soils	17
5.1 Methods of mechanical analysis	17
5.2 Abbreviated representation of grain-size characteristics	19
6. Soil aggregate	19
6.1 Introduction	19
6.2 Texture, structure, and consistency	19
6.3 Porosity, water content, unit weight, and density	19
7. Consistency of fine-grained soils	22
7.1 Consistency and sensitivity of undisturbed soils	22
7.2 Consistency of remolded soils	23
7.3 Plasticity chart	24
8. Soil classification	27
8.1 Practical significance of soil classification	27
8.2 Classification based on grain size	27
8.3 Unified soil classification system	28
9. Minimum requirements for adequate soil description	29
<b>CHAPTER 2. Soil Exploration</b>	<b>32</b>
10. Purpose and scope of soil exploration	32
10.1 Definition of soil exploration	32
10.2 Influence of soil conditions on exploratory program	32

10.3	Influence of size of project on exploratory program	34
10.4	Causes of misjudgment of subsoil conditions	34
10.5	Observations during construction	34
11.	Methods of soil exploration	35
11.1	Principal procedures	35
11.2	Boring	35
11.2.1	<i>Methods of drilling</i>	35
11.2.2	<i>Wash borings</i>	35
11.2.3	<i>Rotary drilling</i>	36
11.2.4	<i>Auger borings</i>	37
11.2.5	<i>Hammer drilling</i>	37
11.2.6	<i>Inspection shafts</i>	38
11.3	Sampling	38
11.3.1	<i>Purpose</i>	38
11.3.2	<i>Split-spoon sampling in exploratory drill holes</i>	38
11.3.3	<i>Thin-walled tube samplers</i>	40
11.3.4	<i>Piston samplers</i>	42
11.3.5	<i>Sampling combined with coring</i>	42
11.3.6	<i>Hand-carved samples in clay</i>	44
11.3.7	<i>Block sampling in bore holes</i>	44
11.3.8	<i>Quality of samples</i>	44
11.3.9	<i>Sampling in sand</i>	44
11.4	Subsurface soundings	46
11.4.1	<i>Purpose of subsurface soundings</i>	46
11.4.2	<i>Static sounding methods</i>	47
11.4.3	<i>Dynamic methods</i>	48
11.5	<i>In situ tests</i>	50
11.5.1	<i>Purpose and types</i>	50
11.5.2	<i>Vane tests</i>	50
11.5.3	<i>Pressuremeter</i>	51
11.6	Groundwater investigations	53
11.6.1	<i>Observation wells</i>	53
11.6.2	<i>Piezometers</i>	54
11.7	Geophysical methods	54
12.	Program for subsoil exploration	55
12.1	Type and sequence of operations	55
12.2	Geological considerations	56
12.3	Spacing and depth of exploratory borings	58
12.4	Relative density of sand strata	59
12.5	Permeability of sand strata	61
12.6	Shearing resistance of saturated clays	62
12.7	Compressibility of clay strata	65
12.8	Summary of procedures in subsoil reconnaissance	68
12.9	Discrepancies between reality and assumptions based on subsoil reconnaissance	69
CHAPTER 3.	Hydraulic and Mechanical Properties of Soils	71
13.	Significance of hydraulic and mechanical properties of soils	71
14.	Permeability of soils	71
14.1	Introduction	71
14.2	Definitions and Darcy's flow equation	71
14.3	Permeability of granular soils	73
14.4	Permeability of soft clays	74
14.5	Permeability of sand-clay mixtures	76
14.6	Laboratory permeability tests	78
14.7	<i>In situ</i> permeability tests	79
14.8	Permeability of stratified masses of soil	80
14.9	Particle migration and erosion	81

15.	Effective stress, porewater pressure, and critical hydraulic gradient	83
15.1	Effective stress	83
15.2	Mechanism of effective stress transfer	83
15.3	Effective vertical stress	84
15.4	Critical hydraulic gradient	85
15.5	Porewater pressures resulting from undrained changes in state of stress	87
15.5.1	<i>Porewater pressures resulting from changes in equal all-around total stress</i>	87
15.5.2	<i>Porewater pressures resulting from application of shear stresses</i>	89
15.6	Negative pore pressures in soils	90
15.6.1	<i>Capillarity and suction</i>	90
15.6.2	<i>Drainage by gravity</i>	93
15.6.3	<i>Drainage by desiccation</i>	94
15.6.4	<i>Shrinkage, swelling, and slaking</i>	96
15.7	Electro-osmosis	97
15.8	Frost heave	98
16.	Compressibility of confined layers of soil	100
16.1	Introduction	100
16.2	One-dimensional compression	100
16.3	Void ratio-effective stress relationship	101
16.4	Preconsolidation pressure	103
16.5	Coefficient of earth pressure at rest	104
16.6	Magnitude of settlement	106
16.7	Settlement during secondary consolidation stage	108
16.8	Rate of one-dimensional consolidation	110
16.9	Oedometer test	113
16.10	Heave of expansive soils	116
17.	Stress, strain, and failure in soils	122
17.1	Introduction	122
17.2	Triaxial apparatus and procedure	125
17.3	Other laboratory shear tests	127
17.3.1	<i>Unconfined compression test</i>	127
17.3.2	<i>Direct shear test</i>	127
17.3.3	<i>Direct simple shear test</i>	128
17.3.4	<i>Torsional ring-shear test</i>	129
17.3.5	<i>Plane strain triaxial test</i>	129
17.4	Mohr's rupture diagram and Coulomb's failure equation	130
17.5	Relations among shear stress, shear strain, and time	133
17.5.1	<i>Hyperbolic stress-strain equation</i>	133
17.5.2	<i>Creep equations</i>	134
18.	Behavior of soils in shear	134
18.1	Relation of mineralogy to shear strength	135
18.2	Volumetric response of soils during shear	137
18.2.1	<i>Examples of drained behavior</i>	137
18.2.2	<i>Examples of undrained behavior</i>	139
18.3	Stress path to failure	141
19.	Drained shear strength	146
19.1	Drained shear strength of granular soils	146
19.2	Drained shear strength of cohesive soils	151
19.2.1	<i>Intact shear strength</i>	152
19.2.2	<i>Fully softened shear strength</i>	155
19.2.3	<i>Residual shear strength</i>	158
20.	Undrained shear strength of soils	161
20.1	Undrained failure	161
20.2	Yielding of soil structure	162
20.3	Undrained shear strength in terms of effective stress at failure	167

20.4	Measurement of undrained shear strength	171
20.5	Mobilized field strength based on <i>in situ</i> vane experience	173
20.6	Undrained shear strength from laboratory shear tests	178
20.7	Unconfined compression test	181
20.8	Undrained shear strength of stiff fissured clays	187
20.9	Liquefaction of saturated loose sands	193
20.9.1	Introduction	193
20.9.2	Soils most susceptible to liquefaction	193
20.9.3	Liquefaction behavior	194
20.9.4	Events triggering liquefaction	196
20.9.5	Cyclic yield strength from laboratory tests	198
20.9.6	Cyclic yield strength from <i>in situ</i> penetration tests	204
20.9.7	Undrained critical shear strength	206
21.	Effect of vibrations on soils	208
<b>Part II.</b>	<b>Theoretical Soil Mechanics</b>	<b>211</b>
<b>CHAPTER 4.</b>	<b>Hydraulics of Soils</b>	<b>213</b>
22.	Scope of hydraulic problems	213
23.	Seepage computations	214
23.1	Hydrodynamic equations	214
23.2	One-dimensional steady-state seepage	215
23.3	Two-dimensional steady-state seepage	215
23.4	Computation of seepage and seepage pressure	217
23.5	Construction of flow net	217
23.6	Seepage through soils with transverse isotropy	218
23.7	Seepage toward single well	219
24.	Mechanics of piping	222
24.1	Definition of piping	222
24.2	Mechanics of piping due to heave	222
24.3	Uplift compensation by loaded filters	223
25.	Theory of consolidation	223
25.1	Process of consolidation	223
25.2	Progress of consolidation	224
25.3	Computation of rate of consolidation	226
25.4	Other initial and boundary conditions	229
25.5	Consolidation with vertical drains	231
25.6	Limitations of the theory of consolidation	233
25.7	Application of a consolidation theory to field situations	235
25.8	Theory of expansion	236
<b>CHAPTER 5.</b>	<b>Plastic Equilibrium in Soils</b>	<b>241</b>
26.	Fundamental assumptions	241
27.	States of plastic equilibrium	243
27.1	Fundamental concepts	243
27.2	Local states of plastic equilibrium	244
28.	Rankine's earth-pressure theory	246
28.1	Earth pressure against retaining walls	246
28.2	Active earth pressure of cohesionless soil against smooth vertical walls	246
28.3	Active earth pressure of partly submerged sand supporting a uniform surcharge	247
28.4	Active earth pressure of cohesive soils against smooth vertical surfaces	247



28.5	Passive earth pressure of cohesive soils in contact with smooth vertical surfaces	248
29.	Influence of wall friction on the shape of the surface of sliding	250
30.	Coulomb's theory of active earth pressure against retaining walls	251
30.1	Introduction	251
30.2	Coulomb's theory	251
30.3	Culmann's graphical construction	251
30.4	Earth pressure due to line load	251
31.	Point of application of earth pressure	254
32.	Passive earth pressure against rough contact faces	255
32.1	Definition	255
32.2	Coulomb's theory of the passive earth pressure of sand	255
32.3	Passive earth-pressure of cohesive soils	255
33.	Bearing capacity of shallow footings	258
33.1	Fundamental assumptions	258
33.2	States of plastic equilibrium beneath shallow continuous footings	259
33.3	Approximate methods for computing the bearing capacity of continuous footings	259
33.4	Bearing capacity of footings of finite length	261
34.	Bearing capacity of piers and piles	262
34.1	Definitions	262
34.2	Bearing capacity of cylindrical piers	262
34.3	Bearing capacity of piles	263
34.3.1	<i>Pile formulas</i>	264
34.3.2	<i>Transmission of stresses during driving</i>	265
35.	Stability of slopes	267
35.1	Introduction	267
35.2	Slopes on dry cohesionless sand	267
35.3	General character of slides in homogeneous cohesive soil	267
35.4	Purpose of stability computations	268
35.5	Computation of shearing resistance from slide data	268
35.6	Procedure for investigating stability of slopes	269
35.7	Slope failures under undrained conditions	269
35.8	Slopes on soils with cohesion and internal friction	271
35.9	Irregular slopes on nonuniform soils, circular surface of sliding	272
35.10	Composite surface of sliding	275
36.	Stability of earth dams	277
36.1	Critical states for design	277
36.2	Evaluation of porewater pressures in critical design states	278
36.3	Stability computations	278
36.4	Sources of error in effective stress stability analyses	279
36.5	Seismic stability of earth dams	279
36.5.1	<i>Introduction</i>	279
36.5.2	<i>Seismic shaking with nondegrading shear strength</i>	280
36.5.3	<i>Seismic shaking with degrading shear strength</i>	283
37.	Earth pressure against supports in cuts	283
37.1	Deformation conditions imposed by supports	283
37.2	Cuts in dry or drained sand	284
37.3	Cuts in saturated clay under undrained conditions	285
37.3.1	<i>Heave of the bottom</i>	285
37.3.2	<i>Earth pressure against supports</i>	286
38.	Arching in soils	289

<b>CHAPTER 6.</b>	<b>Settlement and Contact Pressure</b>	<b>291</b>
39.	Introduction	291
39.1	Purpose of settlement investigations	291
39.2	Theoretical approach to settlement problems	291
39.3	Computation of contact pressure	291
40.	Vertical pressure in soil beneath loaded areas	292
40.1	Boussinesq's equations	292
40.2	Pressure distribution in horizontal sections beneath loaded areas	292
40.3	Change of pressure with depth	293
41.	Settlement of foundations	295
41.1	Foundations above confined strata of soft clay	295
41.2	Foundations on unstratified soil	296
42.	Contact pressure and theories of subgrade reaction	298
42.1	Contact pressure on base of rigid footings	298
42.2	Definition of subgrade reaction	298
42.3	Subgrade reaction on rigid foundations	299
42.4	Subgrade reaction on flexible foundations	299
42.5	Horizontal subgrade reaction	300
<b>Part III.</b>	<b>Problems of Design and Construction</b>	<b>301</b>
<b>CHAPTER 7.</b>	<b>Ground Improvement</b>	<b>303</b>
43.	Drainage prior to excavation	303
43.1	Introduction	303
43.2	Methods of drainage	303
43.3	Historical review of drainage techniques	305
43.4	Well-point method	305
43.5	Deep-well drainage method	306
43.6	Eductor well-point system	306
43.7	Bleeder wells	307
43.8	Vacuum method	307
43.9	Drainage by electro-osmosis	308
43.10	Summary of methods of drainage	309
44.	Compaction, preloading, and other methods	310
44.1	Introduction	310
44.2	Compaction of fills	310
44.2.1	<i>Procedure and equipment</i>	310
44.2.2	<i>Compaction of cohesionless soils</i>	311
44.2.3	<i>Compaction of soils with moderate cohesion</i>	312
44.2.4	<i>Effect of compaction on stresses</i>	315
44.3	Compaction of soils in place	319
44.3.1	<i>Procedures and equipment</i>	319
44.3.2	<i>Vibration combined with water jetting</i>	319
44.3.3	<i>Compaction induced by explosives</i>	320
44.3.4	<i>Compaction by dropping weights</i>	320
44.3.5	<i>Pile driving, sand piles, and stone columns</i>	322
44.3.6	<i>Preloading or surcharging without or with vertical drains</i>	322
44.4	Other methods of ground improvement	324
44.4.1	<i>General</i>	324
44.4.2	<i>Injection</i>	324
44.4.3	<i>Electro-osmosis</i>	324
44.4.4	<i>Freezing</i>	324
44.4.5	<i>Heating</i>	324
44.4.6	<i>Chemical additives</i>	325

CHAPTER 8.	Earth Pressure and Stability of Slopes	327
45	Retaining walls	327
45.1	Function and types of retaining walls	327
45.2	Foundations for retaining walls	327
45.2.1	<i>Introduction</i>	327
45.2.2	<i>Safety against sliding</i>	328
45.2.3	<i>Safety against overturning</i>	329
45.2.4	<i>Allowable soil pressure and settlement</i>	329
45.3	Backfill of retaining walls	330
45.3.1	<i>Materials</i>	330
45.3.2	<i>Drainage provisions for retaining walls</i>	330
45.3.3	<i>Provisions to reduce frost action behind retaining walls</i>	331
45.4	External stability of retaining walls	332
45.4.1	<i>Forces acting on retaining walls</i>	332
45.4.2	<i>Use of earth pressure theories for determining external pressure on walls</i>	332
45.4.3	<i>Use of semiempirical rules for estimating external pressure on retaining walls</i>	335
45.5	Internal stability of retaining walls	338
45.5.1	<i>Masonry and concrete walls</i>	338
45.5.2	<i>Reinforced soil</i>	338
45.5.3	<i>Soil nailing</i>	340
45.6	Influence of compaction on rigid vertical walls	344
45.7	Earth pressure against nonyielding retaining walls	345
45.8	Large-scale model tests and field observations	347
45.9	Summary	348
46.	Lateral supports in open cuts	349
46.1	Introduction	349
46.2	Bracing of shallow cuts	350
46.3	Support of deep cuts	350
46.3.1	<i>General considerations in design of support systems</i>	350
46.3.2	<i>Deep cuts in sand</i>	352
46.3.3	<i>Cuts in saturated clay</i>	353
46.3.4	<i>Deep cuts in soft to medium clay</i>	354
46.3.5	<i>Deep cuts in stiff clay</i>	357
46.3.6	<i>Deep cuts in stratified soils</i>	358
46.4	Tiebacks	359
47.	Stability of hillsides and slopes in open cuts	361
47.1	Causes and general characteristics of slope failures	361
47.2	Engineering problems involving the stability of slopes	361
47.3	Standard slopes	362
47.4	Stability of slopes and cuts in sand	363
47.5	Stability of cuts in loess	363
47.6	Slides in fairly homogeneous soft clay	364
47.7	Quick clay flows	364
47.8	Stability of slopes on clay containing layers or pockets of water-bearing sand	365
47.9	Slides in stiff clay	366
47.10	Slopes on shale	367
47.11	Sudden spreading of clay slopes	369
47.12	Slopes on residual soil and weathered rock	370
47.12.1	<i>General</i>	370
47.12.2	<i>Weathered metamorphic rocks</i>	371
47.12.3	<i>Weathered granite</i>	371
47.12.4	<i>Weathered basalts</i>	372
47.12.5	<i>Weathered carbonate rocks</i>	373
47.12.6	<i>Design of slopes</i>	373
47.13	Debris flows	375
47.14	Summary of approach to stability of slopes	375

48.	Design and stability of embankments	377
48.1	Introduction	377
48.2	Early practice in construction of railway and highway fills	377
48.3	Modern practice for railway and highway fills	377
48.4	Levees or dikes	378
48.5	Types of base failure	379
48.6	Methods for investigating stability	379
48.7	Fills on very soft organic silt or clay	379
48.8	Fills on soft homogeneous clay	380
48.9	Varieties of failure by spreading	382
48.9.1	<i>Spreading of fills above fairly homogeneous layers of soft clay</i>	382
48.9.2	<i>Spreading of fills above clay strata with sand or silt partings</i>	382
48.10	Means for increasing stability of fills above thin strata or soft clay	384
48.11	Summary	384
CHAPTER 9.	Foundations	386
49.	Foundations for structures	386
49.1	Types of foundations for structures	386
49.2	Minimum depth of building foundations	386
49.3	Minimum depth of bridge foundations	387
49.4	Allowable pressure on the subsoil	388
50.	Footing foundations	389
50.1	Origin and shortcomings of conventional design methods	389
50.1.1	<i>Loads, resistances, and factors of safety</i>	391
50.2	Footings on sand and nonplastic silt	393
50.2.1	<i>Scope</i>	393
50.2.2	<i>Relevance and limitations of settlement predictions</i>	393
50.2.3	<i>Early application of soil mechanics to settlement prediction</i>	394
50.2.4	<i>Settlement estimates by semiempirical statistical approaches</i>	394
50.2.5	<i>Method using standard penetration test</i>	395
50.2.6	<i>Method using cone penetration test</i>	398
50.2.7	<i>Comparison of standard penetration and cone penetration methods</i>	402
50.2.8	<i>Design of footings on sand and gravel</i>	402
50.3	Footings on clay	405
50.3.1	<i>Footings on expansive clays</i>	407
50.4	Footing foundations located on firm soil above soft layers	408
50.5	Footing on metastable soils	409
50.5.1	<i>Principal types of metastable soils</i>	409
50.5.2	<i>Footings on unsaturated soils with metastable structure</i>	410
50.5.3	<i>Footings on saprolite</i>	411
50.5.4	<i>Compressibility of metastable soils</i>	411
51.	Raft foundations	412
51.1	Comparison between raft and footing foundations	412
51.2	Settlement of raft foundations	413
51.2.1	<i>Rafts on sand</i>	413
51.2.2	<i>Rafts on clay</i>	414
51.3	Design of raft foundations	414
51.4	Heave during basement excavation	416
51.5	Footing foundations on natural rafts	416
51.6	Footings on sand in basements below the water table	417

52.	Pile foundations	417
52.1	Function of piles	417
52.2	Design of pile foundations	418
52.2.1	<i>Historical development</i>	418
52.2.2	<i>Steps in design of a pile foundation</i>	418
52.3	Ultimate loads and safe design loads for single piles	419
52.3.1	<i>Side resistance and point resistance</i>	419
52.3.2	<i>Relations between driving resistance and depth</i>	421
52.3.3	<i>Use of pile-driving formulas for estimating ultimate bearing capacity</i>	421
52.3.4	<i>Use of wave equation in design</i>	422
52.3.5	<i>Determination of bearing capacity by load test</i>	424
52.3.6	<i>Use of wave equation for estimating ultimate bearing capacity</i>	425
52.3.7	<i>Single pile entirely in sand</i>	426
52.3.8	<i>Single pile in sand below weak deposits</i>	431
52.3.9	<i>Side resistance on single pile in saturated clay</i>	432
52.3.10	<i>Action of point-bearing piles</i>	434
52.3.11	<i>Evaluation of safe design load</i>	435
52.4	Ultimate bearing capacity of pile groups	435
52.5	Behavior of pile foundations	436
52.5.1	<i>Friction pile foundations in sand</i>	436
52.5.2	<i>Piles driven through compressible strata into sand or gravel</i>	437
52.5.3	<i>Piles driven to sound bedrock</i>	439
52.5.4	<i>Piles driven into decomposed bedrock</i>	439
52.5.5	<i>Piles driven through compressible strata into stiff clay</i>	440
52.5.6	<i>Piles embedded in firm stratum underlain by soft clay</i>	440
52.5.7	<i>Floating pile foundations in deep soft deposit</i>	440
52.5.8	<i>Heave and lateral movement due to pile driving</i>	442
52.5.9	<i>Efficiency equations</i>	442
52.5.10	<i>Selection of type of pile</i>	443
52.6	Piles subjected to lateral loads	444
52.6.1	<i>Lateral resistance of single piles</i>	444
52.6.2	<i>Lateral resistance of pile groups</i>	445
52.6.3	<i>Effect of repeated lateral loads on vertical piles</i>	445
53.	Pier foundations	446
53.1	Function of piers	446
53.2	Distinction between piers and piles	446
53.3	Caissons	446
53.3.1	<i>Methods of construction</i>	446
53.3.2	<i>Estimate of skin friction during sinking of caissons</i>	447
53.4	Piers constructed in open excavations	448
53.4.1	<i>Piers on sand</i>	448
53.4.2	<i>Piers on clay</i>	449
53.4.3	<i>Hand-excavated shafts</i>	449
53.5	Drilled shafts	450
53.5.1	<i>Methods of construction</i>	450
53.5.2	<i>Construction implications of subsurface conditions</i>	450
53.5.3	<i>Behavior of drilled shafts under compressive load</i>	451
53.5.4	<i>Bearing capacity of drilled shafts</i>	452
53.5.5	<i>Settlement of drilled shafts</i>	454
53.5.6	<i>Load tests on drilled shafts</i>	454

	53.5.7 Uplift capacity of drilled shafts	454
	53.5.8 Drilled shafts in expansive soils	456
	53.5.9 Lateral resistance of drilled shafts	456
CHAPTER 10.	Settlement Due to Extraneous Causes	457
54.	Settlement due to excavation in open cuts	457
54.1	Characteristic movements	457
54.2	Cuts in sand	459
54.2.1	Sand above water table	459
54.2.2	Effect of lowering the water table in sand strata	459
54.3	Cuts in soft to medium clays	460
54.4	Cuts in stiff clays or cohesive sands	464
54.5	Wide cuts with berms	464
54.6	Measures for reduction of settlement	466
55.	Settlement due to increasing stress in subsoil	467
55.1	Effect of adjacent loads	467
55.2	Effect of pumping on clay strata	468
56.	Settlement caused by vibrations	469
56.1	Factors determining magnitude of settlement	469
56.2	Examples of settlement due to induced vibrations	470
56.3	Settlement due to earthquakes	471
56.3.1	Settlement due to drained shaking	471
56.3.2	Settlement due to undrained shaking	472
CHAPTER 11.	Dams and Dam Foundations	474
57.	Types of dams and potential modes of failure	474
57.1	Types of dams and foundations	474
57.2	Causes of failure	474
58.	Mechanisms of subsurface erosion	475
58.1	Influence of geologic factors on mechanics of piping	475
58.2	Mechanics of subsurface erosion	475
58.3	Empirical rules for estimating factors of safety	475
58.4	Subsurface erosion initiated by scour	478
58.5	Means for avoiding subsurface erosion	478
58.6	Susceptibility of soils to erosion	479
59.	Earth and rockfill dams	480
59.1	Basis for design	480
59.2	Seepage control	480
59.3	Cutoffs	480
59.3.1	Efficiency of cutoffs	480
59.3.2	Construction by use of slurry	482
59.3.3	Injected cutoffs in soils	482
59.3.4	Injected curtains in rock	483
59.4	Upstream blankets	484
59.5	Drainage provisions	484
59.6	Zoned dams	484
59.6.1	Purpose of zones	484
59.6.2	Arrangement of zones	485
59.7	Deformation of earth and rockfill dams	486
59.8	Slopes	489
59.9	Materials	490
59.10	Contact between embankment and foundation	492
59.11	Embankment dams with membranes	493
59.11.1	Upstream facings	493
59.11.2	Internal membranes	495
59.11.3	Synthetic membranes and filter fabrics	496



60. Concrete dams on sediments	497
60.1 Modes of failure	497
60.2 Safety with respect to sliding	497
60.3 Settlement considerations	498
References	501
Author Index	523
Subject Index	529

## *Preface*

In 1948 Karl Terzaghi, in the preface to the First Edition, wrote:

Unfortunately the research activities in soil mechanics . . . diverted the attention of many investigators and teachers from the manifold limitations imposed by nature on the application of mathematics to problems in earthwork engineering. As a consequence, more and more emphasis has been placed on refinements in sampling and testing and on those very few problems that can be solved with accuracy. Yet, accurate solutions can be obtained only if the soil strata are practically homogeneous and continuous in horizontal directions. Furthermore, since the investigations leading to accurate solutions involve highly specialized methods of sampling and testing, they are justified only in exceptional cases. On the overwhelming majority of jobs no more than an approximate forecast is needed, and if such a forecast cannot be made by simple means it cannot be made at all. If it is not possible to make an approximate forecast, the behavior of the soil must be observed during construction, and the design may subsequently have to be modified in accordance with the findings. These facts cannot be ignored without defying the purpose of soil mechanics. They govern the treatment of the subject in this book.

In the half-century since these words were written, research in sampling and testing has continued unabated, and a vast literature has accumulated about the properties of soils, much of it directed toward advancing one or another school of thought concerning idealized conceptions of soil behavior. During the same time, remarkable advances in electronic calculation have made theoretical forecasts possible for problems involving complex boundary and stratigraphic conditions. Thus it may no longer be true that if a forecast cannot be made by simple means it cannot be made at all. In exchange for this progress, however, it has become increasingly important that the choice of soil properties used in the analyses be based on a fundamentally correct knowledge of soil behavior.

Part I of this edition is essentially a digest of the findings of research workers concerning the properties of soil

that are of interest to engineers. The digest presents the findings from a fundamental point of view rather than as representing any one school of thought. Because of the many contributions of the research workers, this part of the book has been expanded markedly over that of the previous editions.

Part II, on the other hand, has been increased only slightly, because the essential theoretical tools were already available 50 years ago. The development of finite-element and similar procedures, although changing the mode of many calculations, has not altered this fact. Moreover, the closed-form solutions of the classical theories of elasticity and plasticity permit the simple, rapid approximate calculations that should always be made to provide a "back of the envelope" estimate to permit judging the need for or the reasonableness of the results of any more elaborate calculational procedure.

As in previous editions, Part III deals with the art of getting satisfactory results in earthwork and foundation engineering at a reasonable cost, in spite of the complexity of the structure of natural soil formations and in spite of the inevitable gaps in our knowledge of the soil conditions. The semi-empirical approach described and advocated in this Part has stood the test of time. It has become the hallmark of the practice of geotechnical engineering.

The authors are indebted to Dr. M. T. Davisson, Mr. R. M. Armstrong, and Prof. J. H. Long for their constructive reviews of the chapters on pile and pier foundations. The patient and expert typing of the many successive versions of the text by Mrs. Paul C. Jesse and Mrs. Joyce M. Snider are gratefully acknowledged. The new illustrations for this edition were drawn by Mr. Ron Winburn. Mr. Marawan Shahien provided invaluable assistance in checking the manuscript and in preparing, revising, and solving the problems. Figures and tables from journals, proceedings, and books are reproduced with permission from the respective publishers.

RALPH B. PECK  
GHOLAMREZA MESRI

## *Preface to First Edition*

Soil mechanics originated several decades ago under the pressure of necessity. As the practical problems involving soils broadened in scope, the inadequacy of the scientific tools available for coping with them became increasingly apparent. Efforts to remedy the situation started almost simultaneously in the United States and in Europe, and within a short period they produced an impressive array of useful information.

The initial successes in this field of applied science were so encouraging that a new branch of structural analysis appeared to be in the making. As a consequence, the extent and profundity of the theoretical investigations increased rapidly, and experimental methods were developed to a high degree of refinement. Without the results of these painstaking investigations a rational approach to the problems of earthwork engineering could not have been attempted.

Unfortunately, the research activities in soil mechanics had one undesirable psychological effect. They diverted the attention of many investigators and teachers from the manifold limitations imposed by nature on the application of mathematics to problems in earthwork engineering. As a consequence, more and more emphasis has been placed on refinements in sampling and testing and on those very few problems that can be solved with accuracy. Yet, accurate solutions can be obtained only if the soil strata are practically homogeneous and continuous in horizontal directions. Furthermore, since the investigations leading to accurate solutions involve highly specialized methods of sampling and testing, they are justified only in exceptional cases. On the overwhelming majority of jobs no more than an approximate forecast is needed, and if such a forecast cannot be made by simple means it cannot be made at all. If it is not possible to make an approximate forecast, the behavior of the soil must be observed during construction, and the design may subsequently have to be modified in accordance with the findings. These facts cannot be ignored without defying the purpose of soil mechanics. They govern the treatment of the subject in this book.

Part A deals with the physical properties of soils and Part B with the theories of soil mechanics. These two parts are very short, but they contain all that engineering students and the average engineer need to know about soil mechanics proper at the present time. The heart of the book is Part C.

Part C deals with the art of getting satisfactory results in earthwork and foundation engineering at a reasonable cost, in spite of the complexity of the structure of natural soil strata and in spite of the inevitable gaps in our knowledge of the soil conditions. To achieve this goal the engineer must take advantage of all the methods and resources at his disposal—experience, theory, and soil testing included. Yet all these resources are of no avail unless they are used with careful discrimination, because almost every practical problem in this field contains at least some features without precedent.

Every discussion of practical problems in Part C starts with a critical survey of conventional methods and proceeds step by step to whatever improvements have been realized with the assistance of the results of research in soil mechanics. Therefore, the experienced engineer is advised to start reading the book at the beginning of this part. He should use Parts A and B only for reference, to get information about concepts with which he is not yet familiar. Otherwise he would be obliged to digest a considerable amount of material before he would be in a position to realize its function in his field of interest.

The details of the methods for coping with the practical problems covered by Part C may change as experience increases, and some of them may become obsolete in a few years because they are no more than temporary expedients. Yet the merits of the semiempirical approach advocated in Part C are believed to be independent of time. At the end of each article of Part C the reader will find a list of references. In their choice priority was given to those publications that are likely to foster the urge and capacity for careful and intelligent field observations. In connection with these references it should be emphasized

that some of the discussions and closures may contain more important information than the articles themselves.

Since the field of soil engineering is too broad to be covered adequately in a single volume, various important topics such as highway, airport, and tunnel engineering had to be excluded. Brief references concerning these fields have been assembled in an appendix.

In its early stages, the manuscript was critically studied by Professor C. P. Siess, whose comments were especially helpful. The authors also appreciate the suggestions of the several practicing engineers who read various portions of the text. In particular, they are indebted to Mr. A. E.

Cummings, Mr. O. K. Peck, and Mr. F. E. Schmidt for criticisms of Part C, to Dr. R. E. Grim for review of Article 4, and to Dr. Ruth D. Terzaghi for assistance in the preparation of Article 63.

Tables and figures taken in whole or in part from other sources are acknowledged where they occur in the text. The drawings are the work of Professor Elmer F. Heater. For his co-operative interest and skilful work the authors are indeed grateful.

KARL TERZAGHI  
RALPH B. PECK

# Introduction

*Soil Mechanics in Engineering Practice, Third Edition*, is divided into the following three parts:

- I. Physical Properties of Soils.
- II. Theoretical Soil Mechanics.
- III. Problems of Design and Construction.

Part I deals with the physical and mechanical properties of homogeneous specimens of undisturbed and remolded soils. It discusses those properties which serve as convenient criteria for distinguishing between different soils and provides instructions for describing soils adequately. It also deals with those soil properties that have a direct bearing on the behavior of soil masses during and after construction operations. Part I also deals with the techniques for securing information about the soil conditions at the chosen site by boring, sounding, sampling, and testing. In spite of the great amount of time and labor involved in such exploratory work, the results commonly leave much room for interpretation.

Part II provides the reader with an elementary knowledge of the theories required for solving problems involving the stability or bearing capacity of soils or the interaction between soil and water. All these theories are based on radically simplifying assumptions regarding the mechanical and hydraulic properties of the soils. Nevertheless, when properly applied, the results obtained by means of these approximate procedures are accurate enough for most practical purposes.

Part III deals with the application of our present knowledge of soil behavior and of the theories of soil mechanics to design and construction in the field of foundation and earthwork engineering.

The physical properties of soils could be discussed quite properly in a general study of the engineering properties of materials, and the theories of soil mechanics constitute a part of the general subject of theoretical mechanics. However, design and construction in the field

of foundation and earthwork engineering, which constitutes the third part of this book, is essentially an independent subject in its own right, because it involves methods of reasoning and procedure that have no counterpart in other fields of structural engineering. In all other fields, the engineer is concerned with the effect of forces on structures made of manufactured products such as steel and concrete or carefully selected natural materials such as timber or stone. Since the properties of these materials can be determined reliably, the problems associated with design can almost always be solved by the direct application of theory or the results of model tests.

On the other hand, every statement and conclusion, pertaining to soils in the field involves many uncertainties. In extreme cases the concepts on which a design is based are no more than crude working hypotheses that may be far from the truth. In such cases the risk of partial or total failure can be eliminated only by using what may be called the observational procedure. This procedure consists of making appropriate observations soon enough during construction to detect any signs of departure of the real conditions from those assumed by the designer and of modifying either the design or the method of construction in accordance with the findings.

These considerations determine the subject matter and method of presentation of Part III, which contains a discussion of the general principles of the design of structures such as retaining walls, earth dams, and foundations. The behavior of all such structures depends chiefly on the physical soil properties and the subsoil conditions. Because our knowledge of subsoil conditions is always incomplete, uncertainties inevitably enter into the fundamental design assumptions. These uncertainties require and receive continuous attention in the text. Similar discussions are not required in textbooks pertaining to other fields of structural design, because the reliability of the fundamental assumptions concerning the properties of the other common construction materials can almost always be taken for granted.

## Symbols

$A$ = porewater-pressure coefficient	$C'_\alpha$ = postsurcharge secondary compression index
$A$ ( $\text{m}^2$ ) = area	$C''_\alpha$ = postsurcharge secant secondary compression index defined from $t_l$
$A_c$ = activity = $I_p/\text{CF}$	CF = clay fraction
$A_p$ ( $\text{m}^2$ ) = base area of pile or pier	CRP = constant rate of penetration
$A_r$ = area ratio of sampling spoon	CRS = constant rate of strain oedometer test
$a$ = exponent in empirical expression for component of shear strength resulting from suction	$c$ (kPa) = cohesion intercept
$a_{\max}(\text{gal})$ = maximum ground surface acceleration produced by an earthquake	$c$ (m/s) = compression wave velocity
$a_v$ (1/kPa) = coefficient of compressibility	$c'$ (kPa) = cohesion intercept of Mohr-Coulomb failure envelope in terms of effective stress at failure
$a_{vt}$ (1/s) = compressibility with respect to time	$c(m)$ = constant in <i>Engineering News</i> formula
$a_{vs}$ (1/kPa) = compressibility with respect to effective vertical stress; coefficient of swellability = $\Delta e/\Delta \sigma'_v$	$c_h$ ( $\text{m}^2/\text{year}$ ) = coefficient of consolidation when flow in the horizontal direction
$B$ = porewater-pressure coefficient = $\Delta u/\Delta p$	$c'_m$ (kPa) = cohesion intercept mobilized at undrained yield condition
$B$ (m) = width	$c_{vs}$ ( $\text{m}^2/\text{year}$ ) = coefficient of expansion
$b$ (kPa) = constant in empirical expression for component of shear strength resulting from suction	$c_a$ (kPa) = adhesion between soil and pile, pier, wall, or sheeting
$C$ (any dimension) = constant	$c_v$ ( $\text{m}^2/\text{year}$ ) = coefficient of consolidation
$C$ (1/kPa) = compressibility of soil skeleton	$D$ = discharge factor (in relation to vertical drains)
$C$ (kN) = resultant cohesion	$D$ (m) = depth; diameter; spacing between centers of piles
$C_C$ = coefficient of curvature = $D_{30}^2/D_{10}D_{60}$	$D$ (mm) = grain size
$C_U$ = uniformity coefficient = $D_{60}/D_{10}$	$D_{10}$ (mm) = effective grain size
$C_a$ (kN) = total adhesion	$D_{50}$ (mm) = mean grain size
$C_c$ = compression index = $\Delta e/\Delta \log \sigma'_v$ ; creep ratio	$D_B$ (m) = diameter of bottom of a tapered pile
$C'_c$ = secant compression index from a point defined by the recompression curve and preconsolidation pressure	$D_e$ (mm) = effective grain size
$C_k = \Delta e/\Delta \log k$	$D_f$ (m) = depth of foundation
$C_r$ = recompression index	$D_{fs}$ (m) = depth of spread footings below basement (measured from the basement floor)
$C_s$ = swelling index	$D_r$ = relative density of cohesionless soil
$C_s$ (1/kPa) = compressibility of soil solids	$D_T$ (m) = diameter of top of a tapered pile
$C_{ss}$ = swelling strain index = $\Delta \epsilon_v/\Delta \log \sigma'_v$	DS (m) = vertical drain spacing
$C_{sss}$ = swelling strain suction index = $\Delta \epsilon_v/\Delta \log u_s$	DS = direct shear test
$C_{s\alpha}$ = secondary swelling index = $\Delta e/\Delta \log t$	DSS = direct simple shear test
$C_{ss\alpha}$ = secondary swelling strain index = $\Delta \epsilon_v/\Delta \log t$	$d$ (m) = diameter of pile; distance
$C_w$ = weighted creep ratio (failure by piping)	$d$ (mm) = grain size
$C_w$ (1/kPa) = compressibility of water	$d_b$ (m) = base diameter of drilled shaft
$C_\alpha$ = secondary compression index = $\Delta e/\Delta \log t$	$d_s$ (m) = shaft diameter of drilled shaft



$E$  = efficiency of cutoff  
 $E$  (kPa) = modulus of elasticity  
 $E$  (volt) = difference in electric potential  
 $E$  (kN/m) = normal force on side of slice (stability analysis)  
 $E_i$  (kPa) = initial tangent Young's modulus  
 $E_s$  (kPa) = modulus of deformation computed from pressuremeter measurement  
 $E_s$  (kPa) = drained Young's modulus  
 $E_{pm}$  (kPa) = pressuremeter modulus  
 $E_u$  (kPa) = undrained Young's modulus  
 $EI$  (kPa·m<sup>4</sup>) or (kN·m<sup>2</sup>) = flexural stiffness of pile or wall  
EOP = end-of-primary consolidation  
EOP  $\sigma'_p$  (kPa) = preconsolidation pressure determined from end-of-primary  $e$  vs  $\log \sigma'_v$  curve  
ESSA = effective stress stability analysis  
 $e$  = void ratio  
 $e_0$  = *in situ* void ratio under effective overburden pressure  $\sigma'_{vo}$   
 $e_c$  = critical void ratio  
 $e_{max}$  = void ratio in loosest state  
 $e_{min}$  = void ratio in densest state  
 $e_p$  = void ratio at the end-of-primary consolidation  
 $e_w$  = volume of water per unit volume of solid matter (for saturated soil  $e_w = e$ )  
 $F$  (kN) = reaction; resultant force  
 $F$  = factor of safety  
FS = factor of safety  
 $f$  = coefficient of friction between soil and base of structure  
 $f_s$  (kPa) = push cone penetrometer sleeve resistance  
 $f_s$  (kPa) = sum of friction and adhesion between soil and pile or pier; yield strength of a tie  
 $f_0$  (1/s) = natural frequency (vibrations)  
 $f_i$  (1/s) = frequency of impulse (vibrations)  
 $G_a$  = air-space ratio (drainage)  
 $G_s$  = specific gravity of solid constituents  
 $g$  (gal) = acceleration due to gravity  
 $H$  (m) = thickness of stratum except when used in connection with consolidating layer. In this event,  $H$  = maximum drainage distance  
 $H$  (m) = height of fall of hammer (pile driving)  
 $H_c$  (m) = critical height of slope  
 $h$  (m) = hydraulic head or total head  
 $h_{av}$  (m) = average vertical spacing between struts  
 $h_c$  (m) = height of capillary rise; critical head for failure by piping  
 $h'_c$  (m) = actual hydraulic head at which piping occurs  
 $h_{cc}$  (m) = height of complete saturation of drained soil  
 $h_{cr}$  (m) = greatest height to which the water level in the reservoir could rise with reference to tailwater level without producing failure by piping  
 $h_{cr}$  (m) = critical head for failure by piping according to computation based on line of creep method

$h_L$  (m) = total head loss through a system = headwater elevation minus tailwater elevation  
 $h_r$  = relative vapor pressure  
 $h_{ra}$  = relative humidity  
 $h_w$  (m) = piezometric head  
 $\Delta h$  (m) = potential drop (hydraulics)  
IL = incremental loading oedometer test  
 $I_l$  = liquidity index  
 $I_p$  = plasticity index  
 $I_z$  = vertical strain influence factor  
 $i$  = hydraulic gradient  
 $i_c$  = critical hydraulic gradient  
 $i_e$  (volts/m) = potential gradient, electro-osmosis  
 $i_p$  (kN/m<sup>3</sup>) = pressure gradient  
 $i_x, i_y, i_z$  = hydraulic gradient in  $x$ -,  $y$ -,  $z$ -directions  
 $K$  = ratio between intensities of effective horizontal and effective vertical pressures at a given point in a mass of soil  
 $K_o$  = coefficient of earth pressure at rest (value of  $K$  for initial state of equilibrium)  
 $K_{op}$  = coefficient of earth pressure at rest in normally consolidated young deposits  
 $K_A$  = coefficient of active earth pressure  
 $K_P$  = coefficient of passive earth pressure  
 $K_{PS}$  = coefficient of passive earth pressure during passive shearing  
 $K$  (kPa) = bulk modulus of soil skeleton  
 $K$  (kPa/m) = spring stiffness  
 $K_h$  (kPa/m) = modulus of horizontal subgrade reaction  
 $K_s$  (kPa) = bulk modulus of soil solids  
 $K_s$  (kPa/m) = coefficient of subgrade reaction  
 $K_w$  (kPa) = bulk modulus of water  
 $\dot{K}_r$  = slope of  $\sigma'_h$  vs  $\sigma'_v$  relation in the recompression range  
 $k$  (m/s) = coefficient of permeability  
 $k_l$  (m/s) = coefficient of permeability in direction parallel to bedding planes  
 $k_{ll}$  (m/s) = coefficient of permeability in direction perpendicular to bedding planes  
 $k_e$  (m/s) = coefficient of electro-osmotic permeability  
 $k_h$  (m/s) = coefficient of permeability in the horizontal direction  
 $k_h, k_v$  (kPa/m) = coefficients for computing pressure of backfill against retaining wall  
 $k_{ho}$  (m/s) = *in situ* coefficient of permeability in horizontal direction  
 $k_s$  (m/s) = coefficient of permeability of soil in the smear zone around vertical drain  
 $k_v$  (m/s) = coefficient of permeability in the vertical direction  
 $k_{vo}$  (m/s) = *in situ* coefficient of permeability in vertical direction  
 $k_x, k_y, k_z$  (m/s) = coefficient of permeability in  $x$ -,  $y$ -,  $z$ -directions  
 $L$  (m) = length of line of creep; length; thickness of a soil layer; length of footing

$L_A$  (m) = active zone depth = long-term postconstruction depth within which there is significant swelling and heave

$L_R$  (m) = length of a tie

$L_S$  (m) = depth of seasonal moisture fluctuation

$L_o$  (m) = preconstruction thickness of a compressible layer with void ratio  $e_o$

$l$  (m) = length

$l_w$  (m) = maximum drainage length of vertical drain

$M_c$  (kN/m) = moment of cohesive forces

$m$  = exponent in expression for drained shear strength of overconsolidated clays; exponent in expression for undrained shear strength of clays

$m$  = reduction factor (earth pressures against bracing in open cuts)

$m_v$  (1/kPa) = coefficient of vertical compression =  $\Delta \epsilon_v / \Delta \sigma'_v$  ( $m_v$  differs from coefficient of volume compressibility in that the former includes settlement resulting from the lateral deformation of soil.)

$\bar{m}_v$  (1/kPa) = average coefficient of vertical compression of soil within the depth of influence

$m_\alpha$  = coefficient (stability analysis)

$m_o$  = exponent in the empirical expression for the interrelationship between  $s_{uo}$ ,  $\sigma'_{vo}$ , and  $\sigma'_p$

$m_v$  (1/kPa) = coefficient of volume compressibility

$m_{vs}$  (1/kPa) = coefficient of volume swellability

$N$  = dimensionless factor ( $N_c$ ,  $N_\gamma$ , and  $N_q$  = bearing capacity factors;  $N_s$  = stability factor in theory of stability of slopes); number of blows on sampling spoon during performance of standard penetration test

$N_b$  = base stability number

$N_c$  = equivalent significant number of uniform shear-stress pulses produced by earthquake or imposed in the laboratory

$N_d$  = number of equipotential drops (flow net)

$N_f$  = number of flow channels (flow net)

$N_k$  = cone factor

$N_{60}$  = dynamic standard penetration test blow count corresponding to a combined efficiency of 60%

$\bar{N}_{60}$  = arithmetic mean of the  $N_{60}$ -values within the depth of influence of the footing  $Z_f$

$(N_1)_{60}$  = dynamic standard penetration test blow count corresponding to a combined efficiency of 60% normalized to effective overburden pressure of 100 kPa

$N'_\phi$  = flow value =  $\tan^2 (45^\circ + \phi'/2)$

$n$  = porosity; number of piles in group

$n_a$  = ratio between distance from bottom of lateral support to point of application of earth pressure and total height of lateral support

$n_d$  = depth factor (stability of slopes)

$n_g$  = ratio between maximum acceleration produced by earthquake and acceleration of gravity

$n_h$  (kPa/m) = coefficient of horizontal subgrade reaction

$n_o$  = initial porosity

OCR = overconsolidation ratio =  $\sigma'_p / \sigma'_{vo} = \sigma'_{v \max} / \sigma'_{vo}$

$P$  = percent of grains smaller than given size

$P$  = compression wave

$P$  (kN or kN/m) = resultant pressure, normal force

$P_A$  (kN/m) = active earth pressure if arching is absent (retaining walls; active Rankine state)

PCPT = push cone penetration test

PDA = pile driving analyzer

$P_a$  (kN/m) = active earth pressure if arching is present (bracing in open cuts)

$P_g$  (kN) = resultant force of gravity on particle

$P_p$  (kN/m) = passive earth pressure (May be subdivided into  $[P_p]_I$ , which depends on unit weight of the soil, and  $[P_p]_{II}$ , which depends on cohesion and surcharge.)

$P_s$  (kN) = resultant of forces having seat on surface of particle

$P_w$  (kN/m) = resultant water pressure

$\Delta P_A$  (kN/m) = part of active earth pressure due to line load  $q_1$

$p$  (kPa) = pressure of normal stress; subgrade reaction

$p'$  (kPa) = effective stress =  $(\sigma'_1 + \sigma'_3)/2$

$p_A$  (kPa) = intensity of active earth pressure

$p_L$  (kPa) = limiting pressure reached in pressuremeter

$p_a$  (kPa) = pressure due to atmosphere

$p_k$  (kPa) = capillary pressure

$p_q$  (kPa) = increase in pressure on retaining wall due to surcharge  $q$  per unit of area

$p_{q1}$  (kN/m) = increase in pressure on retaining wall due to surcharge  $q_1$  per unit of length parallel to crest

$p_s$  (kPa) = swelling pressure

$p_s$  (mob) (kPa) = swelling pressure mobilized under field conditions

$p_{si}$  (kPa) = swelling pressure at initial void ratio of specimen

$p_s$  (kPa) = seepage pressure

$Q$  (kN) = concentrated load; strut load

$Q$  (kN) = permanent or dead load on the base of the footing

$Q$  (m<sup>3</sup>) = total discharge per unit of time

QML = quick maintained load

$Q_a$  (kN) = allowable load on pile

$Q_d$  (kN) = ultimate bearing capacity; ultimate static resistance of pile

$Q_d$  (kN or kN/m) = critical load on footing or pier resting on dense or stiff soil (May be subdivided into  $[Q]_I$  due to weight of soil and  $[Q]_{II}$  due to cohesion and surcharge. Bearing capacity of circular footing is denoted by  $Q_{dr}$  and of square footing by  $Q_{ds}$ .)

$Q'_d$  (kN or kN/m) = critical load on footing or pier resting on loose or soft soil

$Q_{dy}$  (kN) = dynamic resistance to penetration of pile

- $Q_f$  (kN) = skin friction (total)  
 $Q_g$  (kN) = ultimate bearing capacity of pile group  
 $Q_p$  (kN) = ultimate bearing capacity resulting from point resistance  
 $Q_s$  (kN) = side resistance of pile or pier  
 $Q_t$  (kN) = live load on footing including that due to wind and snow  
 $Q_t$  (kN) = excess load on footing or raft, consisting of net dead load  $Q_{dn}$  and live load  $Q$ ; load on pile, consisting of  $Q$  exerted by building, and  $[Q]_I + [Q]_{II}$  due to negative skin friction  
 $Q_u$  (kN) = ultimate uplift resistance of drilled shaft  
 $q$  (kPa) = average gross bearing pressure over the foundation  
 $q$  (kPa) = shear stress =  $(\sigma_1 - \sigma_3)/2$   
 $q$  (kPa) = uniformly distributed load; surcharge per unit of area; uniformly distributed line load  
 $q$  (m<sup>3</sup>/day) = seepage rate or flow rate  
 $q_a$  (kPa) = allowable soil pressure  
 $q_c$  (kPa) = the pressure at which the material passes from the elastic into the semiplastic or plastic state  
 $q_c$  (kPa) = push cone penetrometer tip resistance  
 $\bar{q}_c$  (kPa) = weighted mean of the measured  $q_c$  values of the sublayers within the thickness  $Z_I$   
 $q_d$  (kPa) = ultimate bearing capacity  
 $[q_d]_1$  = ultimate bearing capacity for dense or stiff soil. Value for loose or soft soil denoted by  $[q_d]_2$ . Bearing capacity of circular footing denoted by  $q_{dr}$ , and of square footing by  $q_{ds}$ .  
 $q_p$  (kPa) = bearing capacity of soil beneath base of pile or pier  
 $q_t$  (kPa) = cone tip resistance  
 $q_u$  (kPa) = unconfined compressive strength  
 $q_v$  (m<sup>3</sup>/day) = flow rate in vertical direction  
 $q_w$  (m<sup>3</sup>/day) = discharge capacity of vertical drain  
 $R$  = ratio of size of filter material to size of material to be protected  
 $R$  (m) = radius of influence of well; radius of curvature of deformed slope  
 $R_f$  = parameter used in hyperbolic stress strain equation  
 $R_s$  = total surcharge ratio  
 $R'_s$  = effective surcharge ratio  
 $r$  (m) = radius  
 $r_d$  = reduction factor to seismic shear stress computed assuming rigid-body ground response  
 $r_e$  (m) = radius of soil discharging water into a vertical drain  
 $r_f$  (m) = radius of friction circle (stability of slopes)  
 $r_m$  (m) = radius of mandrel used to install vertical drain  
 $r_s$  (m) = radius of smear zone around vertical drain  
 $r_u$  = porewater pressure coefficient =  $u/\sigma_v$   
 $r_w$  (m) = radius of vertical drain  
 $r_0$  = radius of logarithmic spiral  
 $S$  (kN/m) = total sliding resistance between base of dam and subsoil  
 $S$  (mm) = settlement; heave; penetration of pile under hammer blow  
 $S$  = shear wave  
 $SML$  = slow maintained load  
 $SPTC$  = soldier-pile tremie-concrete  
 $S_c$  (mm) = settlement at end of construction and application of permanent live load  
 $S_e$  (mm) = temporary elastic compression of pile under hammer blow  
 $S_p$  (mm) = settlement at end-of-primary consolidation  
 $S_r$  = degree of saturation  
 $S_t$  = degree of sensitivity  
 $SQD$  = specimen quality designation  
 $s$  (kPa) = shearing resistance; shear strength; drained shear strength  
 $s_f$  (kPa) = average shearing resistance along the surface of sliding located within a fill  
 $s_u$  (kPa) = undrained shear strength  
 $s_u$  (critical) (kPa) = undrained shear strength of liquefied sand  
 $s_u$  (mob) (kPa) = undrained shear strength mobilized in full-scale field failures; undrained shear strength mobilized during stage construction  
 $s_u$  (yield) (kPa) = undrained shear strength mobilized at the triggering of liquefaction  
 $s_{uo}$  (DSS) (kPa) = preconstruction undrained shear strength measured by direct simple shear test  
 $s_{uo}$  (FV) (kPa) = preconstruction undrained shear strength measured by field vane test  
 $s_{uo}$  (TC) (kPa) = preconstruction undrained shear strength measured by triaxial compression test  
 $s_{uo}$  (TE) (kPa) = preconstruction undrained shear strength measured by triaxial extension test  
 $s_{uo}$  (UC) (kPa) = preconstruction undrained shear strength measured in unconfined compression test  
 $s_{uo}$  (UU) (kPa) = preconstruction undrained shear strength from unconsolidated undrained compression test  
 $s_{uo}$  (kPa) = preconstruction undrained shear strength  
 $s_{uo}$  (mob) (kPa) = undrained shear strength mobilized in full-scale field instabilities  
 $T$  (kN/m) = shear force on side of slice (stability analysis)  
 $T$  (degrees centigrade) = temperature  
 $T_c$  = construction time factor  
 $T_r$  = time factor for radial consolidation (vertical compression with radial flow)  
 $T_s$  (kN/m) = surface tension of liquid  
 $T_v$  = time factor for one-dimensional consolidation in vertical direction  
 $TC$  = triaxial compression test  
 $TE$  = triaxial extension test

$t$  (s) = time  
 $t_c$  (days) = construction time  
 $t_l$  (days) = postsurcharge time at which secondary compression reappears  
 $t_{pr}$  (days) = time required to complete primary rebound after removal of surcharge  
 $t'_{ps}$  (days) = time required to complete primary consolidation under surcharge  
 $t_p$  (days) = duration of primary consolidation  
 $t'_s$  (days) = duration of surcharging  
 $U$  = average degree of consolidation  
 $U$  (kN/m) = total neutral pressure on base of dam; total excess hydrostatic pressure  
 $U_r$  = average degree of consolidation assuming radial flow only  
 $U_z$  = average degree of consolidation assuming vertical flow only  
 $UC$  = unconfined compression test  
 $UU$  = unconsolidated undrained triaxial compression test  
 $USSA$  = undrained strength stability analysis  
 $u$  (kPa) = porewater pressure  
 $u'$  (kPa) = excess porewater pressure  
 $u_a$  = pressure in air or vapor phase of soil  
 $u'_b$  (kPa) = excess porewater pressure at the bottom of oedometer specimen in a constant rate-of-strain oedometer test  
 $u'_i$  (kPa) = initial excess porewater pressure  
 $u_o$  (kPa) = preconstruction porewater pressure  
 $u_s$  (kPa) = suction; reference static or steady-state porewater pressure  
 $u_{sf}$  (kPa) = postconstruction suction  
 $u_{so}$  (kPa) = preconstruction suction  
 $\Delta u$  (kPa) = porewater pressure change caused by all-around pressure or by shear stress  
 $V$  (m<sup>3</sup>) = total volume  
 $V_v$  (m<sup>3</sup>) = total volume of voids  
 $v$  (m/s) = discharge velocity  
 $v_s$  (m/s) = seepage velocity  
 $v_x, v_y, v_z$  (m/s) = discharge velocity component in  $x$ -,  $y$ -,  $z$ -directions  
 $W$  (kN or kN/m) = weight  
 $W_H$  (kN) = weight of ram of pile driver  
 $W_p$  (kN) = weight of pile  
 $W'_p$  (kN) = weight of pile less the weight of displaced soil  
 $W_s$  (kN) = effective weight of the soil (total weight of soil reduced by hydrostatic uplift) that was located above the base of the footing prior to excavation  
 $w$  = water content in percent of dry weight  
 $w_l$  = liquid limit  
 $w_o$  = natural water content in percent of dry weight  
 $w_p$  = plastic limit  
 $w_s$  = shrinkage limit

$Z_l$  (m) = depth of influence below which the vertical strains under the foundation are negligible  
 $z$  (m) = depth, position, or elevation head  
 $z_c$  (m) = depth of tension cracks  
 $\alpha$  = angle  
 $\alpha$  = pressuremeter rheological coefficient  
 $\alpha$  = reduction factor on strength of clay adjacent to shaft of pier  
 $\beta$  (degrees) = slope angle  
 $\gamma$  (kN/m<sup>3</sup>) = total unit weight  
 $\gamma'$  (kN/m<sup>3</sup>) = submerged unit weight  
 $\gamma_d$  (kN/m<sup>3</sup>) = dry unit weight, unit weight of soil if water is entirely replaced by air  
 $\gamma_w$  (kN/m<sup>3</sup>) = unit weight of water  
 $\gamma_s$  (kN/m<sup>3</sup>) = average unit weight of solid constituents  
 $\gamma_{sat}$  (kN/m<sup>3</sup>) = unit weight in saturated state  
 $\Delta$  = change  
 $\Delta$  (kN/m) = energy lost in pile driving  
 $\delta$  (degrees) = angle of wall friction; angle between resultant stress on plane and normal to plane  
 $\delta_h$  (mm) = lateral movement  
 $\delta_{h\max}$  (mm) = maximum lateral movement  
 $\epsilon$  = base of Napierian logarithms; unit strain  
 $\epsilon_c$  = compression strain index =  $\Delta\epsilon_v/\Delta \log \sigma'_v$   
 $\epsilon_f$  = axial strain at failure  
 $\epsilon_R$  = reference strain  
 $\epsilon_v$  = vertical strain  
 $\epsilon_\alpha$  = secondary compression strain index =  $\Delta\epsilon_v/\Delta \log t$   
 $\dot{\epsilon}$  = axial strain rate  
 $\dot{\epsilon}_1$  = reference axial strain rate  
 $\dot{\epsilon}_f$  = axial strain rate imposed in a constant rate of strain oedometer test  
 $\dot{\epsilon}_p$  = imposed axial strain rate producing zero excess porewater pressure in a constant rate of strain oedometer test  
 $\eta$  (kN/m<sup>2</sup>) = viscosity  
 $\theta$  (degrees) = angle; central angle  
 $\lambda$  = creep parameter  
 $\mu$  = field vane correction factor for embankment and foundation stability analysis; micron  
 $\mu_{UC}$  = correction factor for unconfined compression test on specimens from  $D$  to  $B$  quality  
 $\mu_s$  = field vane correction factor for slope stability analysis  
 $\mu_t$  = time-to-failure correction factor for undrained shear strength from laboratory tests  
 $\nu$  = Poisson's ratio  
 $\rho_d$  (Mg/m<sup>3</sup>) = density in dry state  
 $\rho_s$  (Mg/m<sup>3</sup>) = average density of solid constituents  
 $\rho_{sat}$  (Mg/m<sup>3</sup>) = density in saturated state  
 $\rho_w$  (Mg/m<sup>3</sup>) = density of water  
 $\sigma$  (kPa) = total normal stress  
 $\sigma'$  (kPa) = effective normal stress  
 $\sigma_1$  (kPa) = major principal stress  
 $\sigma_2$  (kPa) = intermediate principal stress

$\sigma_3$  (kPa) = minor principal stress  
 $\sigma'_1$  (kPa) = effective major principal stress  
 $\sigma'_2$  (kPa) = effective intermediate principal stress  
 $\sigma'_3$  (kPa) = effective minor principal stress  
 $\sigma'_c$  = preconsolidation pressure or critical pressure resulting from secondary compression  
 $\sigma'_{1c}$  (kPa) = effective major principal stress after consolidation and before undrained shear  
 $\sigma'_{3c}$  (kPa) = effective minor principal stress after consolidation and before undrained shear  
 $\sigma'_{\alpha o}$  (kPa) = *in situ* effective normal stress on a plane with orientation  $\alpha$  to the horizontal  
 $\sigma'_h$  (kPa) = effective horizontal pressure  
 $\sigma'_n$  (kPa) = effective normal stress on a plane  
 $\sigma'_p$  (kPa) = preconsolidation pressure  
 $\sigma'_{pl}$  (kPa) = preconsolidation pressure measured in isotropic consolidation test  
 $\sigma'_s$  (kPa) = isotropic effective stress in an undisturbed specimen  
 $\sigma_v$  (kPa) = total vertical stress  
 $\sigma'_v$  (kPa) = effective vertical stress  
 $\sigma'_{vc}$  (kPa) = vertical consolidation pressure  
 $\sigma_{ver}$  (kPa) = critical pressure at which the bearing plate on unsaturated soils with metastable structure plunged into the ground  
 $\sigma_{vf}$  (kPa) = postconstruction total vertical stress  
 $\sigma'_{vf}$  (kPa) = final effective vertical stress =  $\sigma'_{vo} + \Delta \sigma'_v$   
 $\sigma'_{\max}$  (kPa) = maximum past pressure  
 $\sigma_{vo}$  (kPa) = preconstruction total vertical stress  
 $\sigma'_{vo}$  (kPa) = *in situ* effective vertical stress, effective overburden pressure  
 $\sigma'_{vs}$  (kPa) = maximum effective vertical stress reached before the removal of surcharge  
 $\Delta \sigma_a$  (kPa) = axial stress imposed during the second step of a triaxial test

$\tau$  (kPa) = shear stress  
 $\tau$  (seismic) (kPa) = equivalent uniform shear stress pulse produced by an earthquake  
 $\tau_c$  (kPa) = shear stress carried by soil after consolidation and before undrained shear  
 $\tau_h$  (kPa) = shear stress on horizontal planes  
 $\tau_{\max}$  (kPa) = maximum shear stress pulse produced by an earthquake  
 $\tau_s$  (kPa) = shear stress applied under undrained conditions followed by consolidation  
 $\tau_v$  (kPa) = shear stress on vertical planes  
 $\tau_{\alpha o}$  (kPa) = *in situ* shear stress on a plane with orientation  $\alpha$  to the horizontal  
 $\Phi$  = velocity potential (flow net)  
 $\phi'$  (degree) = effective-stress friction angle; angle of internal friction; angle of shearing resistance  
 $\phi'_{cv}$  (degree) = constant-volume friction angle  
 $\phi'_d$  (degree) = component of friction angle produced by dilation  
 $\phi'_g$  (degree) = component of friction angle of granular soils resulting from geometrical interference  
 $\phi'_m$  (degree) = effective-stress friction angle mobilized at undrained yield condition  
 $\phi'_p$  (degree) = component of friction angle of granular soils resulting from particle rearrangement  
 $\phi'_s$  (degree) = secant friction angle for granular soils  
 $\phi'_\mu$  (degree) = angle of interparticle sliding friction  
 $\Psi$  = function defining flow lines  
 $\ln a$  = Naperian (natural) logarithm of  $a$   
 $\log a$  = logarithm of  $a$  to the base 10  
 $ab$  = distance  $ab$  measured along a straight line  
 $\widehat{ab}$  = distance  $ab$  measured along an arc  
 $\approx$  means approximately equal  
 15.3 indicates Eq. 3 in Article 15. The article number appears at the top of each right-hand page.

## **PART I**

### ***Physical Properties of Soils***

The subject matter of Part I is divided into four chapters. The first deals with the procedures commonly used to discriminate among different soils or among different states of the same soil. The second deals with the methods and program of soil exploration. The third is concerned

with the hydraulic and mechanical properties of soils and with the experimental methods used to determine numerical values representative of these properties. The fourth chapter deals with the physical processes involved in the drainage of soils.



## CHAPTER 1

### *Index Properties of Soils*

#### ARTICLE 1 PRACTICAL IMPORTANCE OF INDEX PROPERTIES

In geotechnical engineering, more than in any other field of civil engineering, success depends on practical experience. The design of ordinary soil-supporting or soil-supported structures is necessarily based on simple empirical rules, but these rules can be used safely only by the engineer who has a background of experience. Large projects involving unusual features may call for extensive application of scientific methods to design, but the program for the required investigations cannot be laid out wisely, nor can the results be interpreted intelligently, unless the engineer in charge of design possesses a large amount of experience.

Since personal experience is necessarily somewhat limited, the engineer is compelled to rely at least to some extent on the records of the experiences of others. If these records contain adequate descriptions of the soil conditions, they constitute a storehouse of valuable information. Otherwise, they may be misleading. Consequently, one of the foremost aims in attempts to reduce the hazards in dealing with soils has been to find simple methods for discriminating among the different kinds of soil in a given category. The properties on which the distinctions are based are known as *index properties*, and the tests required to determine the index properties are *classification tests*.

The nature of any soil can be altered by appropriate manipulation. Vibrations, for example, can transform a loose sand into a dense one. Hence, the behavior of a soil in the field depends not only on the significant properties of the individual constituents of the soil mass, but also on those properties that are due to the arrangement of the particles within the mass. Accordingly, it is convenient to divide index properties into two classes: *soil grain properties* and *soil aggregate properties*. The principal soil grain properties are the size and shape of the grains and, in clay soils, the mineralogical character of the smallest grains. The most significant aggregate prop-

erty of cohesionless soils is the relative density, whereas that of cohesive soils is the consistency.

The discussion of soil grain and aggregate properties is preceded by a description of the principal types of soil, and it is followed by a condensed review of the minimum requirements for adequate soil descriptions to be incorporated in the records of field observations.

#### ARTICLE 2 PRINCIPAL TYPES OF SOILS

The materials that constitute the earth's crust are rather arbitrarily divided by the civil engineer into the two categories, *soil* and *rock*. Soil is a natural aggregate of mineral grains that can be separated by such gentle mechanical means as agitation in water. Rock, on the other hand, is a natural aggregate of minerals connected by strong and permanent cohesive forces. Since the terms "strong" and "permanent" are subject to different interpretations, the boundary between soil and rock is necessarily an arbitrary one. As a matter of fact, there are many natural aggregates of mineral particles that are difficult to classify either as soil or as rock. In this text, however, the term soil will be applied only to materials that unquestionably satisfy the preceding definition.

Although the terminology described in the preceding paragraph is generally understood by civil engineers, it is not in universal use. To the geologist, for example, the term rock implies all the material that constitutes the earth's crust, regardless of the degree to which the mineral particles are bound together, whereas the term soil is applied only to that portion of the earth's crust that is capable of supporting vegetation. Therefore, the civil engineer who makes use of information prepared by workers in other fields must understand the sense in which the terms soil and rock are used.

On the basis of the origin of their constituents, soils can be divided into two large groups, those that consist chiefly of the results of chemical and physical rock weathering, and those that are chiefly of organic origin. If the products of rock weathering are still located at the place

where they originated, they constitute a *residual soil*. Otherwise they constitute a *transported soil*, regardless of the agent that performed the transportation.

Residual soils that have developed in semiarid or temperate climates are usually stiff and stable and do not extend to great depth. However, particularly in warm humid climates where the time of exposure has been long, residual soils may extend to depths of hundreds of meters. They may be strong and stable, but they may also consist of highly compressible materials surrounding blocks of less weathered rock (Article 47.12). Under these circumstances they may give rise to difficulties with foundations and other types of construction. Many deposits of transported soils are soft and loose to a depth of more than a hundred meters and may also lead to serious problems.

Soils of organic origin are formed chiefly *in situ*, either by the growth and subsequent decay of plants such as peat mosses or by the accumulation of fragments of the inorganic skeletons or shells of organisms. Hence a soil of organic origin can be either organic or inorganic. The term *organic soil* ordinarily refers to a transported soil consisting of the products of rock weathering with a more or less conspicuous admixture of decayed vegetable matter.

The soil conditions at the site of a proposed structure are commonly explored by means of test borings or test shafts. The inspector on the job examines samples of the soil as they are obtained, classifies them in accordance with local usage, and prepares a boring log or shaft record containing the name of each soil and the elevation of its boundaries. The name of the soil is modified by adjectives indicating the stiffness, color, and other attributes. At a later date the record may be supplemented by an abstract of the results of tests made on the samples in the laboratory.

The following list of soil types includes the names commonly used for field classification.

*Sand* and *gravel* are cohesionless aggregates of rounded subangular or angular fragments of more or less unaltered rocks or minerals. Particles with a size up to 2 mm are referred to as sand, and those with a size from 2 mm to 200 mm as gravel. Fragments with a diameter of more than 200 mm are known as *boulders*.

*Hardpan* is a soil that has an exceptionally great resistance to the penetration of drilling tools. Most hardpans are extremely dense, well-graded, and somewhat cohesive aggregates of mineral particles.

*Inorganic silt* is a fine-grained soil with little or no plasticity. The least plastic varieties generally consist of more or less equidimensional grains of quartz and are sometimes called *rock flour*; whereas the most plastic types contain an appreciable percentage of flake-shaped particles and are referred to as *plastic silt*. Because of its smooth texture, inorganic silt is often mistaken for clay, but it may be readily distinguished from clay without

laboratory testing. If shaken in the palm of the hand, a pat of saturated inorganic silt expels enough water to make its surface appear glossy. If the pat is bent between the fingers, its surface again becomes dull. This procedure is known as the *shaking test*. After the pat has dried, it is brittle and dust can be detached by rubbing it with the finger. Silt is relatively impervious, but if it is in a loose state it may rise into a drill hole or shaft like a thick viscous fluid. The most unstable soils of this category are known locally under different names, such as bull's liver.

*Organic silt* is a fine-grained more or less plastic soil with an admixture of finely divided particles of organic matter. Shells and visible fragments of partly decayed vegetable matter may also be present. The soil ranges in color from light to very dark gray, and it is likely to contain a considerable quantity of  $H_2S$ ,  $CO_2$ , and various other gaseous products of the decay of organic matter which give it a characteristic odor. The permeability of organic silt is very low and its compressibility very high.

*Clay* is an aggregate of microscopic and submicroscopic particles derived from the chemical decomposition of rock constituents. It is plastic within a moderate to wide range of water content. Dry specimens are very hard, and no powder can be detached by rubbing the surface of dried pats with the fingers. The permeability of clay is extremely low. The term *gumbo* is applied, particularly in the western United States, to clays that are distinguished in the plastic state by a soapy or waxy appearance and by great toughness. At higher water contents they are conspicuously sticky.

*Organic clay* is a clay that owes some of its significant physical properties to the presence of finely divided organic matter. When saturated, organic clay is likely to be very compressible, but when dry its strength is very high. It is usually dark gray or black and it may have a conspicuous odor.

*Peat* is a somewhat fibrous aggregate of macroscopic and microscopic fragments of decayed vegetable matter. Its color ranges between light brown and black. Peat is so compressible that it is almost always unsuitable for supporting foundations. Various techniques have been developed for carrying earth embankments across peat deposits without the risk of breaking into the ground, but the settlement of these embankments is likely to be large and to continue at a decreasing rate for many years.

If a soil is made up of a combination of two different soil types, the predominant ingredient is expressed as a noun, and the less prominent ingredient as a modifying adjective. For example, silty sand indicates a soil that is predominantly sand but contains a small amount of silt. A sandy clay is a soil that exhibits the properties of a clay but contains an appreciable amount of sand.

The aggregate properties of sand and gravel are described qualitatively by the terms *loose*, *medium*, and *dense*, whereas those of clays are described by *hard*, *stiff*,

*medium*, and *soft*. These terms are usually evaluated by the boring foreman or inspector on the basis of several factors, including the relative ease or difficulty of advancing the drilling and sampling tools and the consistency of the samples. However, since this method of evaluation may lead to a very erroneous conception of the general character of the soil deposit, the qualitative descriptions should be supplemented by quantitative information whenever the mechanical properties are likely to have an important influence on design. The quantitative information is commonly obtained by means of laboratory tests on relatively undisturbed samples (Article 11.3), or by suitable *in situ* tests (Articles 11.4 and 11.5).

A record of the color of the different strata encountered in adjacent borings reduces the risk of errors in correlating the boring logs. Color may also be an indication of a real difference in the character of the soil. For example, if the top layer of a submerged clay stratum is yellowish or brown and stiffer than the underlying clay, it was probably exposed temporarily to desiccation combined with weathering. Terms such as mottled, marbled, spotted, or speckled are used when different colors occur in the same stratum of soil. Dark or drab colors are commonly associated with organic soils.

Under certain geological conditions soils form that are characterized by one or more striking or unusual features such as a root-hole structure or a conspicuous and regular stratification. Because of these features, such soils can easily be recognized in the field and, consequently, they have been given special names by which they are commonly known. The following paragraphs contain definitions and descriptions of some of these materials.

*Till* is an unstratified glacial deposit of clay, silt, sand, gravel, and boulders.

*Tuff* is a fine-grained water- or wind-laid aggregate of very small mineral or rock fragments ejected from volcanoes during explosions.

*Loess* is a uniform, cohesive, wind-blown sediment, and is commonly light brown. The size of most of the particles ranges between the narrow limits of 0.01 and 0.05 mm. The cohesion is due to the presence of a binder that may be predominantly calcareous or clayey. Because of the universal presence of continuous vertical root holes, the permeability in vertical direction is usually much greater than in horizontal directions; moreover, the material has the ability to stand on nearly vertical slopes. True loess deposits have never been saturated. On saturation the bond between particles is weakened and the surface of the deposit may settle.

*Modified loess* is a loess that has lost its typical characteristics by secondary processes, including temporary immersion, erosion and subsequent deposition, chemical changes involving the destruction of the bond between the particles, or chemical decomposition of the more perishable constituents such as feldspar. Thorough chemical

decomposition produces *loess loam*, characterized by greater plasticity than other forms of modified loess.

*Diatomaceous earth* (kieselguhr) is a deposit of fine, generally white, siliceous powder composed chiefly or wholly of the remains of diatoms. The term diatom applies to a group of microscopic unicellular marine or freshwater algae characterized by silicified cell walls.

*Lake marl* or *boglime* is a white fine-grained powdery calcareous deposit precipitated by plants in ponds. It is commonly associated with beds of peat.

*Marl* is a rather loosely used term for various fairly stiff or very stiff marine calcareous clays of greenish color.

*Shale* is a clastic sedimentary rock mainly composed of silt-size and clay-size particles. Most shales are laminated and display fissility; the rock has a tendency to split along relatively smooth and flat surfaces parallel to the bedding. When fissility is completely absent, the clastic sedimentary deposit is called mudstone or clay rock. Depending on clay mineralogy, void ratio, and degree of diagenetic bonding or weathering, compressive strength of shales may range from less than 2.5 MPa to more than 100 MPa.

*Adobe* is a term applied in the southwestern United States and other semiarid regions to a great variety of light-colored soils ranging from sandy silts to very plastic clays.

*Caliche* refers to layers of soil in which the grains are cemented together by carbonates deposited as a result of evaporation. These layers commonly occur at a depth of several meters below the surface, and their thickness may range up to a few meters. A semiarid climate is necessary for their formation.

*Varved clay* consists of alternating layers of medium gray inorganic silt and darker silty clay. The thickness of the layers rarely exceeds 10 mm, but occasionally very much thicker varves are encountered. The constituents were transported into freshwater lakes by melt water at the close of the Ice Age. Varved clays are likely to combine the undesirable properties of both silts and soft clays.

*Bentonite* is a clay with a high content of montmorillonite (Article 4). Most bentonites were formed by chemical alteration of volcanic ash. In contact with water, dried bentonite swells more than other dried clays, and saturated bentonite shrinks more on drying.

Each term used in the field classification of soils includes a great variety of different materials. Furthermore, the choice of terms relating to stiffness and density depends to a considerable extent on the person who examines the soil. Consequently, the field classification of soils is always more or less uncertain and inaccurate. More specific information can be obtained only by physical tests that furnish numerical values representative of the properties of the soil.

The methods of soil exploration, including boring and sampling, and the procedures for determining average

numerical values for the soil properties are discussed in Chapter 2.

### ARTICLE 3 SIZE AND SHAPE OF SOIL PARTICLES

The size of the particles that constitute soils may vary from that of boulders to that of large molecules.

Grains larger than approximately 0.06 mm can be inspected with the naked eye or by means of a hand lens. They constitute the *very coarse* and *coarse* fractions of the soils.

Grains ranging in size from about 0.06 mm to 2  $\mu$  (1  $\mu$  = 1 micron = 0.001 mm) can be examined only under the microscope. They represent the *fine fraction*.

Grains smaller than 2  $\mu$  constitute the *very fine fraction* (*clay size fraction, CF*). Grains having a size between 2  $\mu$  and about 0.1  $\mu$  can be differentiated under the microscope, but their shape cannot be discerned. The shape of grains smaller than about 1  $\mu$  can be determined by means of an electron microscope. Their molecular structure can be investigated by means of X-ray analysis.

The process of separating a soil aggregate into fractions, each consisting of grains within a different size range, is known as *mechanical analysis*. By means of mechanical analysis, it has been found that most natural soils contain grains representative of two or more soil fractions. The general character of mixed-grained soils is determined almost entirely by the character of the smallest soil constituents. In this respect soils are somewhat similar to concrete. The properties of concrete are determined primarily by the cement, whereas the aggregate, which constitutes most of the concrete, is inert. The "aggregate," or the inert portion of a mixed-grained soil, comprises about 80 or 90% of the total dry weight. The decisive or active portion constitutes the remainder.

Very coarse fractions, for example gravel, consist of rock fragments each composed of one or more minerals. The fragments may be angular, subangular, rounded, or flat. They may be fresh, or they may show signs of considerable weathering. They may be resistant or crumbly.

Coarse fractions, exemplified by sand, are made up of grains usually composed chiefly of quartz. The individual grains may be angular, subangular, or rounded. Some sands contain a fairly high percentage of mica flakes that make them very elastic or springy.

In the fine and very fine fractions, any one grain usually consists of only one mineral. The particles may be angular, flake-shaped, or tubular. Rounded particles, however, are conspicuously absent. Exceptionally, the fine fraction contains a high percentage of porous fossils, such as diatoms or radiolaria, that produce abnormal mechanical properties. In general, the percentage of flaky constituents

in a given soil increases with decreasing grain size of the soil fraction.

If the size of most of the grains in an aggregate of soil particles is within the limits given for any one of the soil fractions, the aggregate is called a *uniform soil*. Uniform very coarse or coarse soils are common, but uniform very fine or colloidal soils are very seldom encountered. All clays contain fine, very fine, and colloidal constituents, and some clays contain even coarse particles. The finest grain-size fractions of clays consist principally of flake-shaped particles.

The widespread prevalence of flake-shaped particles in the very fine fractions of natural soils is a consequence of the geological processes of soil formation. Most soils originate in the chemical weathering of rocks. The rocks themselves consist partly of chemically very stable and partly of less stable minerals. Chemical weathering transforms the less stable minerals into a friable mass of very small particles of secondary minerals that commonly have a scale-like or flaky crystal form, whereas the stable minerals remain practically unaltered. Thus the process of chemical weathering reduces the rock to an aggregate consisting of fragments of unaltered or almost unaltered minerals embedded in a matrix composed chiefly of discrete scaly particles. During subsequent transportation by running water the aggregate is broken up, and the constituents are subjected to impact and grinding. The purely mechanical process of grinding does not break up the hard equidimensional grains of unaltered minerals into fragments smaller than about 10  $\mu$  (0.01 mm). On the other hand, the friable flake-shaped particles of secondary minerals, although initially very small, are readily ground and broken into still smaller particles. Hence, the very fine fractions of natural soils consist principally of flake-shaped particles of secondary minerals.

### ARTICLE 4 PROPERTIES OF VERY FINE SOIL FRACTIONS

#### 4.1 Mineralogical Composition

The most important grain property of fine-grained soil materials is the mineralogical composition. If the soil particles are smaller than about 0.002 mm, the influence of the force of gravity on each particle is insignificant compared with that of the electrical forces acting at the surface of the particle. A material in which the influence of the surface charges is predominant is said to be in the *colloidal state*. The colloidal particles of soil consist primarily of *clay minerals* that were derived from rock minerals by weathering, but that have crystal structures differing from those of the parent minerals.

All the clay minerals are crystalline hydrous aluminosilicates having a lattice structure in which the atoms are arranged in several layers, similar to the pages of a book.

The arrangement and the chemical composition of these layers determine the type of clay mineral.

The basic building blocks of the clay minerals are the silica tetrahedron and the alumina octahedron. These blocks form tetrahedral and octahedral layers (Fig. 4.1), different combinations of which produce a unit sheet of the various types of clays.

A single particle of clay may consist of many sheets or films piled one on another. Because each sheet or film has a definite thickness but is not limited in dimensions at right angles to its thickness, clay particles are likely to exhibit flat or curved terraced surfaces. The surfaces carry residual negative electrical charges, but the broken edges may carry either positive or negative charges in accordance with the environment.

In problems of interest to the civil engineer, clay particles are always in contact with water. The interactions among the clay particles, the water, and the various materials dissolved in the water are primarily responsible for the properties of the soil consisting of the particles.

The characteristics of the principal clay minerals are described in the following paragraphs.

#### 4.2 Characteristics of Principal Clay Minerals

*Kaolinite* is one of the most common clay minerals in sedimentary and residual soils (Grim 1968, Swindale 1975). A unit sheet of kaolinite, which is approximately 0.7 nm ( $\text{nm} = 10^{-9} \text{ m}$ ) thick, is composed of one aluminum octahedral layer and one silicon tetrahedral layer, joined together by shared oxygens. A typical particle of kaolinite consists of a stack of sheets forming a stiff hexagonal plate with flat-faced edges. It is about 100 nm in thickness with a breadth/thickness of about 5 to 10, and a specific surface of 5 to 15  $\text{m}^2/\text{g}$ . The scanning electron microscope (SEM) photomicrograph in Fig. 4.2 shows a range of particle sizes and shapes including terraced surfaces where packets of 0.7-nm sheets terminate.

*Halloysite* is one of the most common minerals in residual soils, particularly those derived from volcanic parent material. It is a member of the kaolin subgroup of clay minerals. A unit sheet of hydrated halloysite, including one molecular layer of water, is approximately

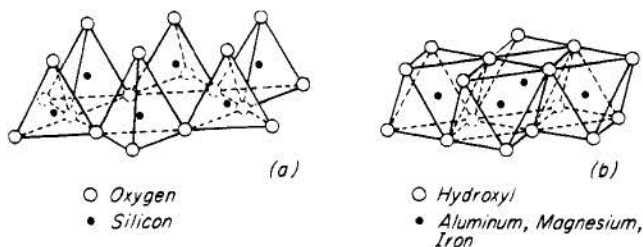


**Figure 4.1** (a) Tetrahedral layer. (b) Octahedral layer. (After Grim 1968)

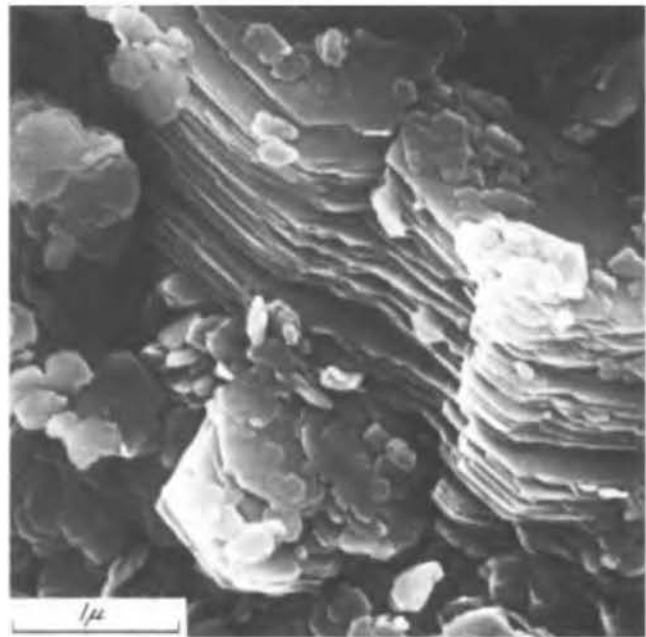


**Figure 4.2** Photomicrograph of kaolinite.

1 nm thick. A typical particle has the shape of a hollow tube or prism with outside and inside diameters of 70 and 40 nm, respectively, and is 300 to 500 nm long. The intersheet water in the hydrated halloysite is removed irreversibly starting at 60° to 75°C.

*Allophane*, a major constituent of young residual soils formed from volcanic ash, is an amorphous hydrous aluminosilicate commonly associated with halloysite (Grim 1968, Fieldes and Claridge 1975, Wesley 1973). In some residual soils, the transition to halloysite from allophane, which forms at early stages of weathering, is not well defined. Allophane consists of very loosely packed chains of silica tetrahedra and alumina octahedra, *cross-linked* at a relatively small number of points. In the natural state, it exists as microaggregates of extremely fine particles of the order of several nanometers and specific surface areas of 250 to 800  $\text{m}^2/\text{g}$ . The allophane aggregates or clusters are relatively incompressible. They are sometimes cemented by iron or aluminum oxides, and they enclose a large amount of water. Since the aggregates are susceptible to structural breakdown upon mechanical manipulation, as by heavy equipment, a deposit of allophane may change from a granular material to a plastic sticky mass that cannot be handled easily. The natural aggregates do not readily lose water; however, when water is removed and the fabric shrinks, the process cannot be reversed. The resulting soil, with silt- and sand-sized particles that are quite hard, is practically nonplastic.

*Illite* is the most common clay mineral in stiff clays and shales as well as in postglacial marine and lacustrine soft clay and silt deposits (Grim 1968, Radoslovich 1975, Reichenbach and Rich 1975). It is often present, some-



times interstratified with other sheet silicates, in sedimentary and residual soils, except in residual soils derived from amorphous volcanic material. Illite is also referred to as fine-grained mica and weathered mica.

The crystal structure of illite is similar to that of muscovite mica in the macroscopic form. However, in microscopic illite particles the stacking of the sheets is not so regular as in well-crystallized micas, and weathering may remove intersheet  $K^+$  from the edges of the plates. The resulting illite particles, with terraced surfaces where one or more unit sheets terminate, have frayed and tattered edges, are flexible and elastic, are 10 to 30 nm in thickness, have a breadth/thickness of 15 to 30, and have a specific surface of 80 to 100  $m^2/g$ . A SEM photomicrograph of illite particles is shown in Fig. 4.3.

*Chlorite* is a clay mineral commonly associated with micas and illite, but is usually a minor component (Grim 1968, Bailey 1975). A unit sheet of chlorite, which is about 1.4 nm thick, consists of one biotite mica sheet in which all octahedral sites are occupied by magnesium and one brucite sheet, an octahedral layer in which magnesium atoms are in octahedral coordination with hydroxyls. The biotite mica and brucite sheets are strongly bonded together. The unit sheets are stacked and are connected to each other by hydrogen bonding of surface oxygens of the tetrahedral layer of mica and surface hydroxyls of brucite. The size and platyness of chlorite particles are similar to those of illite. However, in contrast to illite, in which the unit sheets are bonded by potassium, the hydrogen bonding between chlorite sheets results in pseudohexagonal or *euheral*-shaped platelets that are flexible but inelastic.

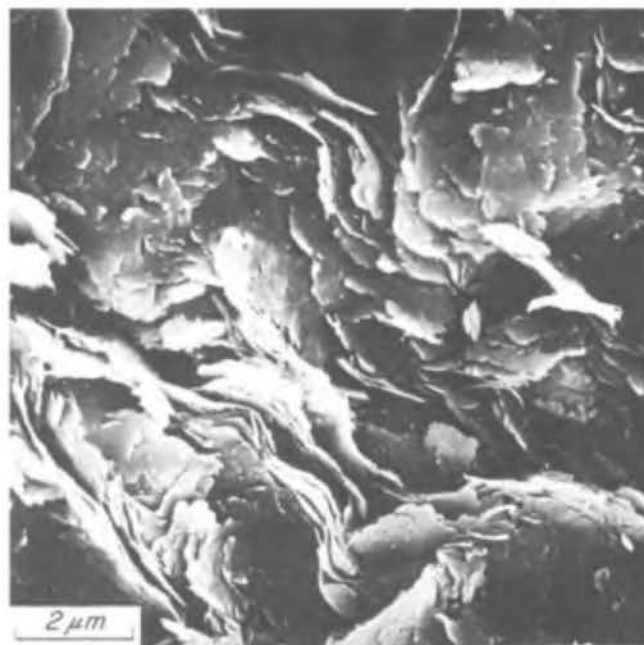


Figure 4.3 Photomicrograph of illite.

*Montmorillonite*, the most common member of a group of clay minerals known as *smectites*, is the dominant clay mineral in some clays and shales and in some residual soils derived from volcanic ash (Grim 1968, Mering 1975). Relatively pure seams of montmorillonite are found in some deposits, Wyoming bentonite being the best-known example. A unit sheet of montmorillonite is similar to that of the micas. In montmorillonite, octahedral Al is partially replaced by Mg atoms. Each isomorphous replacement (Article 4.3) produces a unit negative charge at the location of the substituted atom, which is balanced by exchangeable cations, such as  $Ca^{+2}$  and  $Na^+$  situated at the exterior of the sheets. In a packet of montmorillonite in the anhydrous state, where as many as 10 unit sheets are in contact, the stacking of the sheets is disordered in the sense that the hexagonal cavities of the adjacent surfaces of two neighboring sheets are not matched face-to-face. In a hydrous environment, water molecules penetrate between the sheets and separate them by 1 nm (i.e., four molecular layers of water).

In sodium montmorillonite, the *exchange capacity* is satisfied by Na cations. If the electrolyte concentration in water is less than 0.3 N, further separation of unit sheets takes place to more than 3 nm by *diffuse double-layer repulsion* (Article 4.4). The resulting particles of sodium montmorillonite in water are thin films 1 nm thick, with breadth-to-thickness ratios in excess of 100 and specific surfaces as much as 800  $m^2/g$ . In calcium montmorillonite, the electrostatic attraction of the Ca cations links the successive sheets together and prevents separation beyond 1 nm. The resulting domains of 8 to 10 unit sheets, which are separated from each other by up to four molecular layers of water, experience minimal swelling. Among clay minerals, sodium montmorillonite has the smallest and most filmy particles, as is shown by the SEM photomicrograph in Fig. 4.4.

*Attapulgite* is a fibrous clay mineral composed of silica chains linked together by oxygens along their longitudinal edges to form single laths or bundles of laths (Grim 1968, Hénin and Caillère 1975). Water molecules fill the interstices between the chains. The particles of attapulgite are relatively rigid, 5 to 10 nm thick, 10 to 20 nm wide, and 0.1 to 1  $\mu m$  in length, as shown in the SEM, Fig. 4.5. The specific surface of the bundles is about 150  $m^2/g$ , but it can be much higher for dispersed single laths. Attapulgite, frequently associated with carbonate rocks, is not a very common clay mineral in soil deposits. However, when present, it results in unusual physical properties such as a very high plastic limit, a very high plasticity index, and high frictional resistance (Articles 7.2 and 19.2).

#### Mixed-layer Clay Minerals

Particles in some soils are composed of regularly or randomly interstratified unit sheets of two or more types

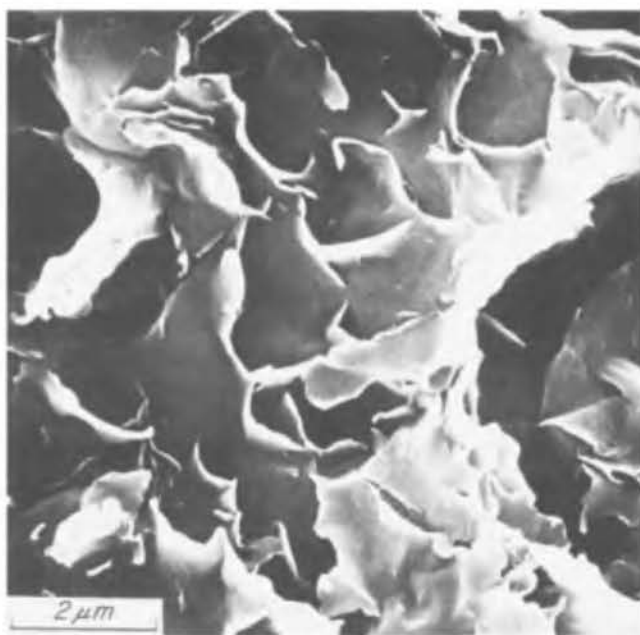


Figure 4.4 Photomicrograph of montmorillonite.

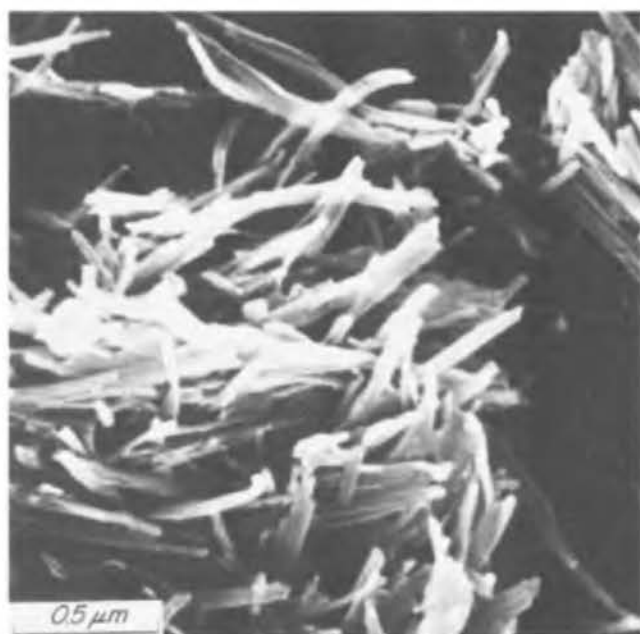


Figure 4.5 Photomicrograph of attapulgite.

of clay minerals (MacEwan and Ruiz-Amil 1975). For example, a marine or lacustrine clay deposit may include regularly alternating montmorillonite-illite particles, and a volcanic ash residual soil may contain randomly interstratified halloysite and hydrated halloysite. These mixed-layer clay minerals often represent an intermediate phase in the transformation, by weathering or through a diagenetic process, of one mineral to another mineral, such as that of mica to montmorillonite or vice versa. However,

the physical properties of interstratified clay minerals are not well defined, inasmuch as a wide range of combinations is possible. Mixed-layer clay mineral particles possess properties generally representative of the constituent minerals.

### 4.3 Role of Isomorphic Substitution

Isomorphic substitution is the replacement of a cation in the mineral structure by another cation of lower electrovalence. The difference in the valences leads to a negative charge, and the difference in size of the cations produces a distortion of the mineral structure. Both effects tend to decrease the resistance of a mineral structure to chemical and mechanical weathering. Quartz is a space-lattice silicate composed of silica tetrahedrons,  $(\text{SiO}_4)^{-4}$  linked together by primary valence bonds to form a three-dimensional network with the formula  $\text{SiO}_2$ . There is no isomorphous substitution in quartz, and each silica tetrahedron is firmly and equally braced in all directions. As a result, quartz has no planes of weakness and is very hard and highly resistant to mechanical and chemical weathering. Quartz is not only the most common mineral in sand- and silt-sized particles of soils, but quartz or amorphous silica is frequently present in colloidal (1 to 100 nm) and molecular ( $<1$  nm) dimensions (Mitchell 1975). In some young soils of volcanic origin, clay-sized particles may consist essentially of silica, an appreciable proportion of which is amorphous. The boundary between quartz and amorphous silica, however, is not distinct, inasmuch as physical processes such as grinding may render crystalline quartz amorphous.

In feldspar, some of the silicon atoms are replaced by aluminum. This results in a negative charge and in distortion of the crystal structure, because Al atoms are larger than Si atoms. The negative charge is balanced by taking in cations such as  $\text{K}^+$ ,  $\text{Na}^+$ , and  $\text{Ca}^{+2}$  in orthoclase, albite, and anorthite feldspars, respectively. The distortion of the lattice and the inclusion of the cations cause cleavage planes that reduce the resistance of feldspars to mechanical and chemical weathering. For these reasons, feldspars are not so common as quartz in the sand-, silt-, and clay-sized fractions of soils, even though feldspars are the most common constituent of the earth's crust.

Common micas such as muscovite and biotite are often present in the silt- and sand-sized fractions of soils. In a unit sheet of mica, which is 1 nm thick, two tetrahedral layers are linked together with one octahedral layer. In muscovite, only two of every three octahedral sites are occupied by aluminum cations, whereas in biotite all sites are occupied by magnesium. In well-crystallized micas one fourth of the tetrahedral  $\text{Si}^{+4}$  are replaced by  $\text{Al}^{+3}$ . The resulting negative charge in common micas is balanced by intersheet potassiums. In a face-to-face stacking of sheets to form mica plates, the hexagonal holes on opposing tetrahedral surfaces are matched to enclose the

intersheet potassium. Perfect cleavage occurs along the K-plane, however, as the intersheet bond strength of  $(\text{KO}_{12})^{-23}$  is only 1/12 of the bond strength of  $(\text{SiO}_4)^{-4}$  inside the sheets.

There is very little isomorphous substitution in kaolinite, the particles of which are formed by hydrogen bonding of unit sheets. The edge charge is important, because the particles are thick and the edge surface area is significant. The edge charge, which results from broken bonds and exposed oxygens at the edges of the particles, may be positive or negative in accordance with the pH of the water. When the pH is low (acidic condition), excess  $\text{H}^+$  ions associate with the oxygens at the edge of the particles, and give the edge a net positive charge. When the pH is high,  $\text{H}^+$  ions disassociate from the edge, which then becomes negatively charged. In mica and illite a major part of the negative charge resulting from isomorphous substitution is neutralized by K atoms which also connect the successive unit sheets to each other to form particles.

#### 4.4 Cation Exchange and Adsorbed Water

Cations that neutralize the net negative charge on the surface of soil particles in water are readily exchangeable with other cations. The exchange reaction depends mainly on the relative concentrations of cations in the water and also on the electrovalence of the cations. Cation exchange capacity, measured in milliequivalents of cations per gram of soil particles, is a measure of the net negative charge on the soil particles, resulting from isomorphous substitution and broken bonds at the boundaries. The values of the cation exchange capacity for the principal clay minerals are indicated in Table 4.1. Montmorillonite has a relatively large exchange capacity because its particles may consist of single unit sheets. Very fine particles of other minerals such as mica and quartz also carry a net negative charge in water as a result of broken bonds at the boundaries. However, even in the range of small particle sizes in which nonclay minerals occur in soils, the exchange capacity is relatively small.

**Table 4.1 Cation Exchange Capacity of Principal Clay Minerals**

Mineral	Cation Exchange Capacity (meq/g)
Kaolinite	0.03–0.1
Illite	0.2–0.3
Chlorite	0.2–0.3
Attapulgite	0.2–0.35
Hydrated halloysite	0.4–0.5
Montmorillonite	0.8–1.2

The highly polar water molecule has the ability to form strong bonds with the surface of soil particles, as well as with the exchangeable cations that surround it. The strong short-range adsorption forces hold one to four molecular layers of water at the surface of the soil particles. This water is said to be *adsorbed*. It is of most importance if the particles are very small, such as films of sodium montmorillonite 1 nm thick, and is insignificant if they are large, such as 200- $\mu\text{m}$  grains of quartz sand.

If a soil particle is surrounded by water, the exchangeable cations are not attached to it. Its negative electrical charge tends to attract the cations, but the cations diffuse toward the lower cation concentration away from the particle. Therefore, the soil particle is surrounded by a domain known as an *electric double layer* (van Olphen 1977, Mitchell 1976). The inner layer of the double layer is the negative charge on the surface of the soil particle. The outer layer is the excess of cations and deficiency of anions with respect to the concentration in the free water not influenced by the force field of the particle. The cation concentration has a finite value near the surface of the particle and decreases exponentially with distance to the concentration of the cations in the free pore water. The thickness of double-layer water, which is determined by the valence of the exchangeable cations and by the electrolyte concentration in free pore water, can exceed 50 nm. Thick double-layer water develops with exchangeable cations of low electrovalence such as  $\text{Na}^+$ , and in free pore water of low electrolyte concentration, as in freshwater rivers and lakes. On the other hand, exchangeable cations of high valence such as  $\text{Ca}^{+2}$  and high electrolyte concentration as in the marine environment tend to depress the thickness of the double-layer water. Thus, in general, a soil particle is covered by a 1-nm layer of adsorbed water, surrounded by 1 to > 50 nm of double-layer water, enveloped in turn by free water. Double-layer water is most significant in sodium montmorillonite because of its very small and filmy particles.

When soil particles approach each other, as during deposition or consolidation, a number of long-range and short-range interparticle forces influence their geometrical arrangement and interaction. Repulsion develops when two soil particles approach each other and their double layers come in contact. The particles will remain dispersed unless they are pushed together by an external force, such as the weight of overburden, equal to the repulsive force. For example, a pressure of 500 kPa is required to bring two face-to-face-oriented sodium montmorillonite particles, in 0.01 N electrolyte concentration, to within 4 nm of each other. An increase in electrolyte concentration depresses double-layer thickness and allows closer approach of the particles, which aggregate into *flocs*. The flocs of clay-mineral particles may settle simultaneously, without segregation, with other fine particles and with silt-sized particles of quartz, mica, and



feldspars. On the other hand, in a freshwater lacustrine environment flocculation is absent, and segregated varved clay and silt deposits develop.

Adsorbed water layers must be removed for soil particles to approach within less than 1 nm of each other. Enormous external pressures are required to squeeze them out. For example, a pressure of 125 MPa is required to bring two parallel plates of montmorillonite or mica to within 0.5 nm of each other, and a pressure of 400 MPa is required to remove the last molecular layer of water. Such magnitudes of contact pressure are likely to develop only at mineral-to-mineral contact points of sand-sized and larger particles, where in general the force per particle can be large and the contact area very small. This is illustrated in Figs. 4.6 through 4.9, which show an assemblage of sand grains, close-ups of grain-to-grain contacts, and a magnified smooth fracture surface, respectively. It is apparent that the area of contact between grains is extremely small and that even small forces between grains would produce very high pressures. At the other extreme, it is unlikely that geologic pressures due to overburden on clays and shales or typical construction loads could squeeze adsorbed water from between plates of montmorillonite in which the force per particle is small and the contact area, as compared with the size of the particles, is very large. Edge-to-face contact in sodium montmorillonite is also unlikely, because the highly flexible films cannot be pushed together. In kaolinite, short-range edge-to-face contact between particles is possible, because the particles are relatively large. As a result of their small breadth-to-thickness ratio, they are rather stiff and thus

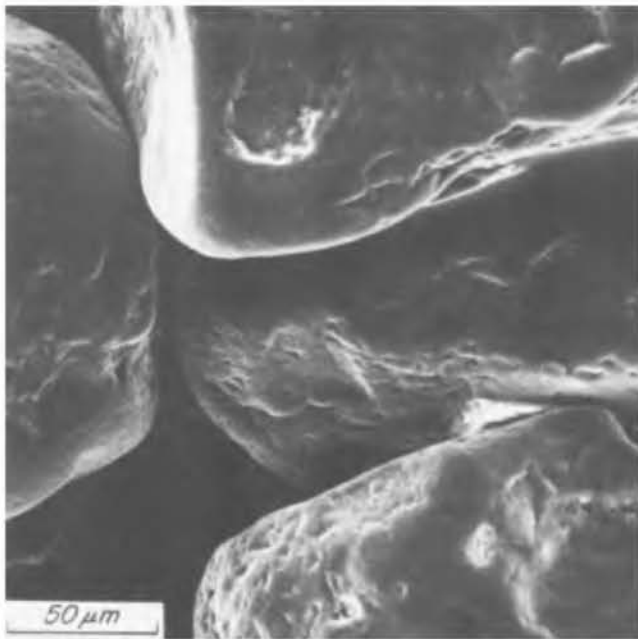


**Figure 4.6** Photomicrograph of Lake Michigan beach sand particles.

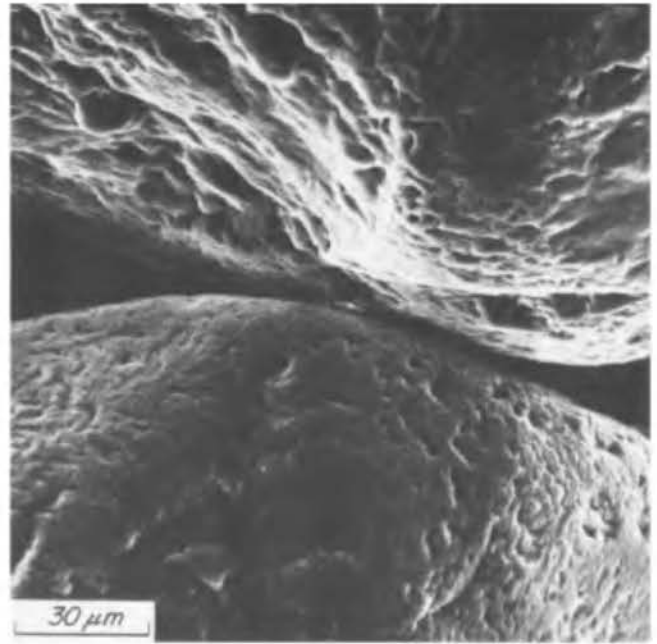


**Figure 4.7** Photomicrograph of contact between grains of quartz sand.

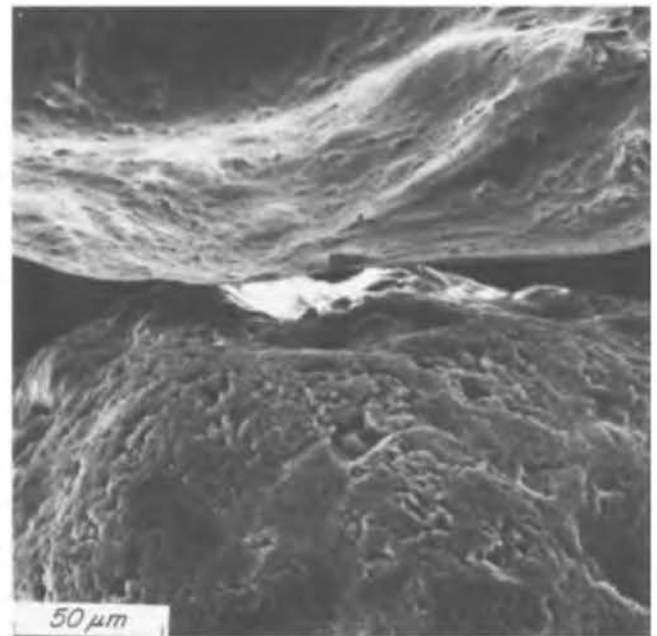


**Figure 4.8** Photomicrograph of contact between grains of dune sand.

are capable of transmitting forces parallel to the plates. The particle size and shape of illite suggest a behavior intermediate between those of kaolinite and montmorillonite, but closer to the former.

Mineral-to-mineral contact is established after the last molecular layer of water is desorbed and the very short range repulsion of approaching mineral surfaces is over-

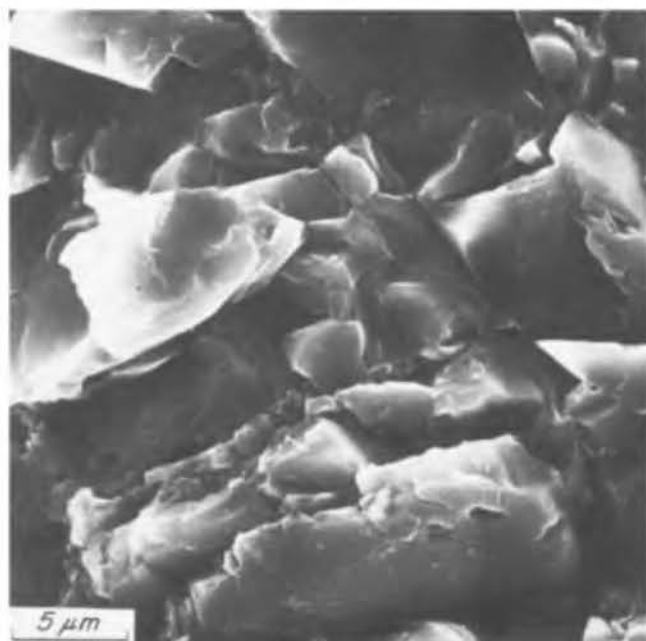


**Figure 4.9** Magnification of “smooth” fracture surface of quartz.

come. This type of contact is required for developing primary valence bonding between the particle surfaces or, alternatively, for engaging microscopic roughness of the contact surfaces, such as protruding lattice points or regions. It is also required for generating sliding frictional resistance.

Although cementing between mineral grains is a significant factor in rocks such as sandstone and even in residual soils at the early stages of weathering, the nature and extent of microscopic cementing in soils is not well established. The existence of rather stable aggregates of clay minerals in most clay and shale deposits, and the brittle behavior of soils such as certain soft clays from eastern

Canada, suggest a possible cementing action by molecular coatings of carbonates or silicates on the surface of soil particles that are connected to each other. For example, such an interparticle bonding may be responsible for the rather high water content of the soft clays from eastern Canada as compared with their relatively inactive mineral composition. However, most soft and stiff clay deposits as well as granular soils are uncemented.

#### 4.5 Fabric

The term *fabric* describes the geometrical arrangement of soil particles with respect to each other. During sedimentation of very fine-grained soil particles in quiet fresh water, the elementary mineral units tend to settle individually. The resulting sediment has a random geometrical arrangement in which the mineral particles have no pronounced preferred orientation. As overburden accumulates, the platy or elongated particles tend to rotate into more horizontal positions, whereupon the sediment becomes more anisotropic but retains its random microfabric. If the supply of sediment is seasonal, the coarser sediments, which settle more quickly than the finer ones, soon cease to accumulate during the periods of low inflow, and only the finer particles continue to settle out. The result is a segregated fabric, of which a varved clay is an example. On the other hand, if the sediment accumulates in salt water, flocculation occurs, and all mineral types with elementary particles from fine clay-size to coarse silt-size settle simultaneously to form a random unsegregated deposit.

Most fine-grained natural soil deposits consist of a mixture of mineral types that often include sheet silicates as well as space lattice silicates and some carbonates. This is illustrated by the mineralogical composition of several soft-clay deposits listed in Table 4.2. A typical soft-clay deposit includes, in addition to illite and chlorite and some montmorillonite, substantial amounts of quartz

**Table 4.2** Mineralogical Composition of Soft Clays

Clay	Total mineral content (%)							Clay mineral content (%)			
	Clay Mineral	Quartz	Plagioclase	K-feldspar	Amphibole	Calcite	Dolomite	Illite	Chlorite	Montmorillonite	Other
Boston Blue	30	35	24	8	3	0	0	74	21	5	0
St. Hilaire	32	23	21	0	8	9	8	55	39	6	0
Berthierville	21	37	25	0	17	0	0	53	34	13	0
La Grande	11	29	25	7	0	10	17	70	30	0	0
Väsby	38	33	16	13	0	0	0	67	14	9	10
Pisa*	73	14	5	0	0	6	0	60	16	24†	0

\* Also contains 2% pyrite.

† Mixed-layer: 17% illite/montmorillonite and 7% chlorite/montmorillonite.

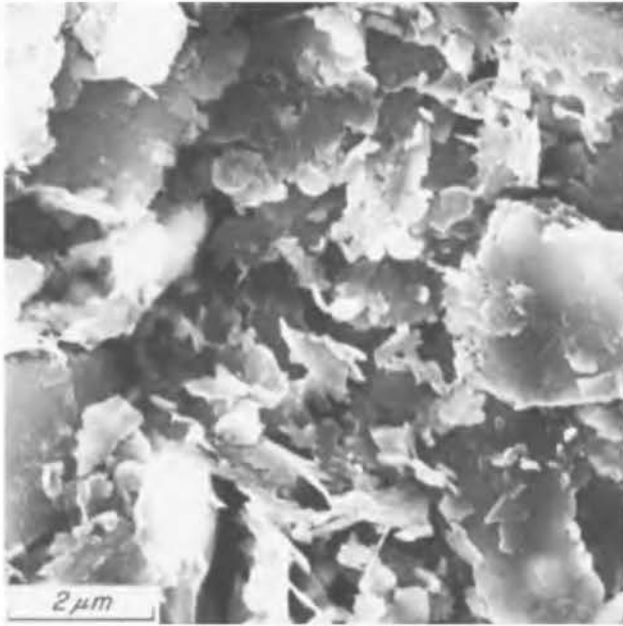


**Figure 4.10** Fabric of undisturbed Boston blue clay.

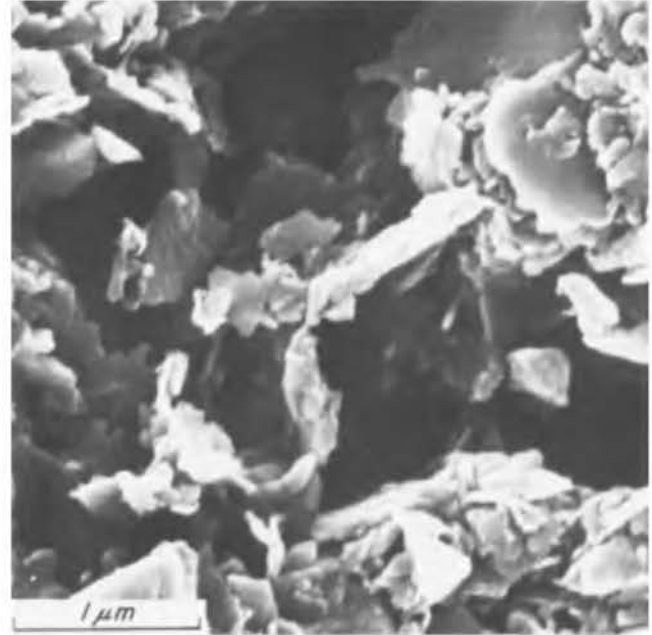


**Figure 4.11** Fabric of undisturbed St. Hilaire clay.

and feldspar and some carbonates. Some of the very fine minerals may have been eroded from shales and were probably already in an aggregated form when they reached the sedimentation basin.

The SEM photomicrographs of natural soft-clay deposits in Figs. 4.10 through 4.15 generally suggest more or less flocculated- or aggregated-random fabrics. The mineralogical composition of these clays is shown in Table 4.2 and their index properties are presented in Table 4.3. Boston Blue Clay is a glacial outwash deposited

about 14,000 years ago in coastal brackish water. The sample described in Fig. 4.10 and Tables 4.2 and 4.3 was a firm to stiff clay preconsolidated by desiccation. St. Hilaire clay and Berthierville clay are postglacial clays deposited about 10,000 years ago in the inland Champlain Sea. La Grande clay is a postglacial clay deposited 6,000 to 8,000 years ago in the marine environment of the Tyrrell Sea. Väsby clay is a recent postglacial marine clay from the eastern central coast of Sweden. Pancone clay

**Table 4.3** Index Properties of Soft Clays

No.	Clay	$w_o$ (%)	$w_l$ (%)	$w_p$ (%)	CF (-2 $\mu$ m%)	$\sigma'_{vo}$ (kPa)	$\sigma'_p/\sigma'_{vo}$	$\phi'$ Degrees
1	Boston Blue	27–30	34	17	40	155	3.20–3.50	30
2	St. Hilaire	61–68	55	23	77	83	1.40–1.57	26
3	Berthierville	57–63	46	24	36	39	1.30–1.40	27
4	La Grande	55–58	64	26	52	83	1.75–2.00	28
5	Väsby	94–103	121	40	67	28	1.20–1.34	23
6	Pisa-Pancone	54–65	86	35	72	124	1.57–2.02	23
7	Mexico City	421–574	500	150	27	58	1.40–1.60	45

$w_o$  = natural water content (Article 6).

$w_l$  = liquid limit (Article 7.2).

$w_p$  = plastic limit (Article 7.2).

CF = clay fraction (Article 8.2).

$\sigma'_{vo}$  = effective vertical overburden pressure (Article 15.3).

$\sigma'_p$  = preconsolidation pressure (Article 16.4).

$\phi'$  = effective-stress friction angle (Article 19.2).



**Figure 4.12** Fabric of undisturbed Berthierville clay.

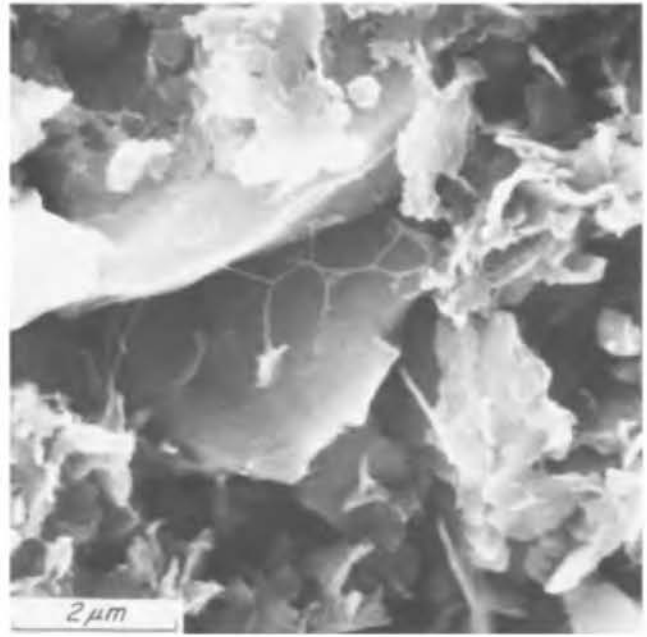


**Figure 4.14** Fabric of undisturbed Väsby clay.

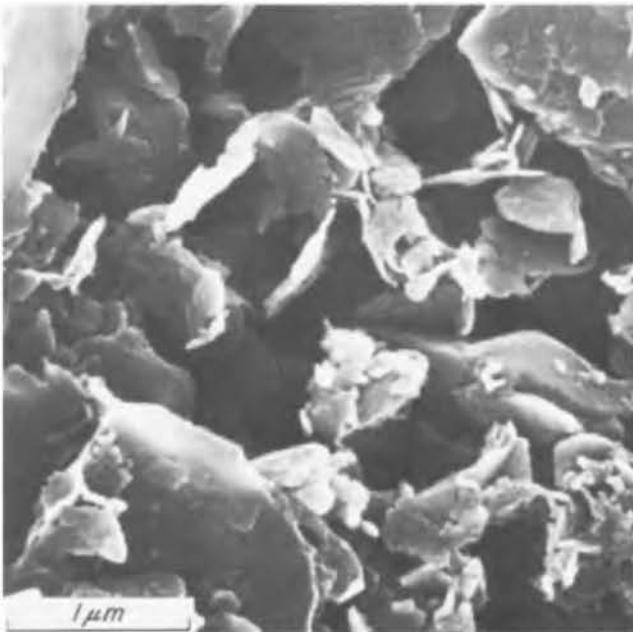


**Figure 4.13** Fabric of undisturbed LaGrande clay.

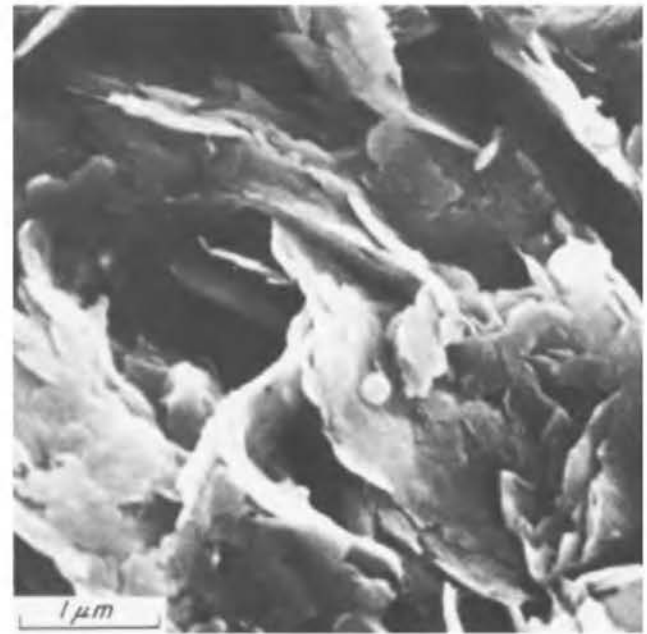


**Figure 4.15** Fabric of undisturbed Pancone clay.

from Pisa was deposited 7,000 years ago in a marine environment. The salt concentration in the pore water of these brackish or marine deposits has been substantially reduced, through either leaching or diffusion, following crustal rebound that elevated the clay deposits above the sea level after withdrawal of glacial ice (Bjerrum 1954, Kenney 1964).

The fabric of the postglacial soft clays from eastern Canada is very open, and their natural water content is high in comparison with their mineralogical composition and liquid limit. A slow rate of deposition accompanied by simultaneous development of interparticle bonds by carbonates and possibly silicates apparently is responsible for the special fabrics (Quigley 1980). When the salt content of these clays was subsequently reduced by leach-





**Figure 4.16** Fabric of undisturbed Mexico City clay.

ing or diffusion leading to a tendency for particle dispersion, the clays acquired the characteristics to lose most of their strength and to liquefy when subjected to remolding at constant water content (Bjerrum 1954).

Not all soft-clay deposits have a mineralogical composition similar to those in Table 4.2. Mexico City clay is a dramatic example of soft clay derived from volcanic material. It consists of about 5 to 10% sand-sized concretionary particles composed of calcium carbonate; 55 to 65% silt-sized siliceous diatoms; 20 to 30% clay-sized particles (10% interlayered montmorillonite, with exchangeable cations that are mostly sodium, and the remainder biogenic or volcanogenic silica); and 5 to 10% organic material. Thus, Mexico City clay is largely composed of microfossils that mainly are siliceous skeletons and skeletal fragments of diatoms. Apparently the large quantities of silica released by the volcanic ash as it underwent weathering initiated a great bloom of diatoms in the Pleistocene lake waters of the valley of Mexico. The undisturbed fabric of Mexico City clay is shown in Fig. 4.16, and photomicrographs of the silt-sized fraction are shown in Figs. 4.17 and 4.18. Figure 4.16 shows that Mexico City clay has an open flocculated-random fabric. The highly poriferous skeletal fragments are mainly responsible for such unusual properties as very high plastic and liquid limits, a very high friction angle, and great loss of strength upon manipulation. Similar high values of plastic limit and friction angle are displayed by volcanic ash residual soils of Japan, which contain allophane and halloysite.



**Figure 4.17** Silt-size fraction of Mexico City clay showing poriferous whole geometric forms and fragments of diatoms.

In contrast to the random fabric or structure of most natural clays, clays that have been sheared by tectonic activity, by sliding, or even by manipulation in the laboratory or by construction activities, are likely to lose their flocculated, random structure. They are then said to have a *dispersed*, highly *oriented* fabric. In this state they are likely to have properties quite different from those of clays with a flocculated or aggregated random fabric.

#### 4.6 Organic Soils

Organic substances in soil range from macroscopic incompletely decomposed plant and animal residues to microscopic dark-colored humus. Humus includes products of advanced decomposition of organic residues, products of microbial resynthesis, precipitates of dissolved organic compounds, and organic molecules in solution (Gieseking 1975a). Organic substances are composed mainly of carbon, oxygen, and hydrogen. However, different organic parent materials, various aerobic and anaerobic conditions of degradation, and different degrees of humification produce organic substances with a wide range of molecular structure and particle morphology. A highly poriferous and flexible cellular structure is the most important characteristic of organic coarse particles, which are either fibrous or granular. Organic fine substances, usually smaller than 100 μm, consist of irregularly shaped organic skeletons such as cell fragments and tissue parts, as well as of globular organic precipitates smaller than 1 μm, and of 3- to 9-nm organic polymolecules. Organic fine substances are negatively charged and



**Figure 4.18** Silt-size fraction of Mexico City clay showing poriferous whole geometric forms and fragments of diatoms.

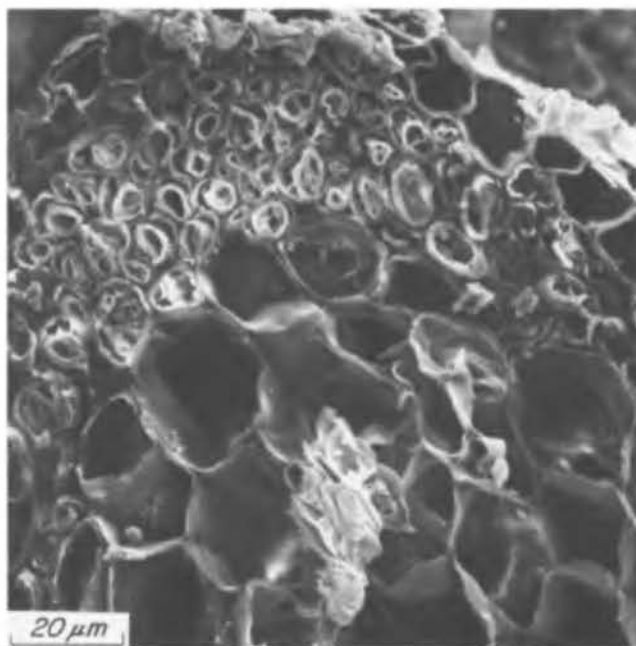


**Figure 4.20** Photomicrograph of a poriferous cellular peat particle.



**Figure 4.19** Photomicrograph of fibrous Middleton peat.

display a substantial cation exchange capacity which increases with degree of humification and is strongly influenced by the hydrogen ion concentration in the pore water. Cations such as calcium, magnesium, potassium, sodium, and also iron and aluminum, replace hydrogen at the exchange sites of organic polymolecules. The cation

exchange capacity of very fine humic substances may be as high as 1.5 to 5.0 meq/g.

Soil fabrics characterized by organic coarse particles, as in fibrous peat, hold a considerable amount of water because they are generally very loose, and also because organic particles are hollow and largely full of water. This is illustrated in Figs. 4.19 and 4.20 by SEM photomicrographs of a light brown fibrous peat from Middleton, Wisconsin, with natural water content and void ratio in the range of 610 to 830% and 11.1 to 14.2, respectively. In organic fine substances, water of hydration and double-layer water are important. In general, the water-holding capacity of peats decreases with increased degree of decomposition. In a high-pH, alkaline environment, organic fine substances disperse into globular polyanions as small as 3 to 9 nm. In a low-pH, acidic environment or in high-electrolyte concentration, the polyanions coagulate to form large flocs of a more or less globular shape. Organic polyanions that pigment the surface of fine mineral particles such as clay minerals result in stable clay-humus complexes that promote loose and open fabric in organic soft clays and silts. Globular organic polyanions attach themselves, directly through hydrogen bonding or through adsorbed cations, to specific sites at the surface of minerals and thus promote flocculation and aggregation of mineral particles.

Drying of organic coarse particles causes shrinkage of thin-walled tissues and collapse of cell structure and thereby decreases particle porosity and water-holding capacity. It also promotes aggregation of organic substances, whereupon organic precipitates bind mineral par-

ticles into stable aggregates. Even without drying and at moderate laboratory temperatures, the organic solid content of soil is susceptible to degradation, decomposition, dissolution, and therefore to loss. Scorching, irreversible dehydration, and oxidation of organic substances begin at about 60°C.

#### 4.7 Practical Significance of Colloidal Properties

The foregoing sections of this article have made it clear that the properties of the very fine soil fractions are of outstanding engineering importance. They have also indicated that an understanding of these properties has its roots in physical chemistry, colloidal chemistry, clay mineralogy, and organic chemistry. Notwithstanding the fundamental importance of these scientific disciplines, a detailed quantitative knowledge of none of them is needed in geotechnical engineering practice, because the influence of the various scientific findings is reflected in the numerical values of the index properties and of the strength, deformation, and hydraulic properties determined by means of engineering tests and used in engineering calculations. To know the percentages of, say, illite and sodium montmorillonite in a deposit where a landslide has developed gives the engineer insight into the causes of the slide and may suggest the relative applicability of certain remedial measures, but it is the quantitative influence of the very fine soil fraction, as determined by engineering tests and analyses, that is of primary value in assessing and solving most problems in applied soil mechanics.

#### Selected Reading

The first three references include a review of the history and development of geotechnical engineering from the earliest times up to 1985. The remaining references deal with mineralogy, physico-chemistry, fabric, and structure of soils.

- Kerisel, J. (1985). "The history of geotechnical engineering up until 1700," *Proc. 11th Int. Conf. Soil Mech. and Found. Eng.*, San Francisco, Golden Jubilee Volume, pp. 3–93.
- Peck, R. B. (1985). "The last sixty years," *Proc. 11th Int. Conf. Soil Mech. Found. Eng.*, San Francisco, Golden Jubilee Volume, pp. 123–133.
- Skempton, A. W. (1985). "A history of soil properties, 1717–1927," *Proc. 11th Int. Conf. Soil Mech. Found. Eng.*, San Francisco, Golden Jubilee Volume, pp. 95–121.
- Terzaghi, K. (1925). "Structure and volume of voids of soils," in *Erdbaumechnik auf Bodenphysikalischer Grundlage*, pp. 10–13, translated by A. Casagrande in *From Theory to Practice in Soil Mechanics*, New York, John Wiley & Sons, Inc., (1960), pp. 146–148.
- Casagrande, A. (1932b). "The structure of clay and its importance in foundation engineering," *J. Boston Soc. Civil Engrs.*, **19**, No. 4, p. 168.

- Skempton, A. W. and R. D. Northey (1952). "The sensitivity of clays," *Géot.*, **3**, p. 30–53.
- Rosenqvist, I. T. (1953). "Considerations on the sensitivity of Norwegian quick clays," *Géot.*, **3**, pp. 195–200.
- Bjerrum, L. (1954). "Geotechnical properties of Norwegian marine clays," *Géot.*, **4**, pp. 49–69.
- Kenney, T. C. (1964). "Sea-level movements and the geological histories of the post-glacial marine soils at Boston, Nicolet, Ottawa, and Oslo," *Géot.*, **15**, No. 3, pp. 203–230.
- Grim, R. E. (1968). *Clay Mineralogy*, 2nd, ed. New York, McGraw-Hill, 596 p.
- Rowe, P. W. (1972). "The relevance of soil fabric to site investigation practice," *Géot.*, **22**, No. 2, pp. 195–300.
- Gieseking, J. E. (1975a). *Soil Components. Volume 1: Organic Components*, New York, Springer-Verlag, 534 p.
- Gieseking, J. E. (1975b). *Soil Components. Volume 2: Inorganic Components*, New York, Springer-Verlag, 684 p.
- Mitchell, J. K. (1993). *Fundamentals of Soil Behavior*, 2nd ed, New York, John Wiley & Sons, Inc., 450 p.
- Van Olphen, H. (1977). *An Introduction to Clay Colloid Chemistry*, 2nd ed., New York, John Wiley & Sons, Inc., 318 p.
- Quigley, R. M. (1980). "Geology, mineralogy and geochemistry of Canadian soft soils: a geotechnical perspective," *Canadian Geotech. J.*, **17**, No. 2, pp. 261–285.

## ARTICLE 5 MECHANICAL ANALYSIS OF SOILS

### 5.1 Methods of Mechanical Analysis

The purpose of mechanical analysis is to determine the size of the grains that constitute a soil and the percentage of the total weight represented by the grains in various size ranges. The most direct method for separating a soil into grain-size fractions is the use of sieves. However, since the openings of the finest mesh readily available have a width of 0.07 mm, the use of sieves is restricted to analysis of clean sands. If a soil contains grains smaller than 0.07 mm, it may be separated into two parts by washing with water. As the water becomes turbid, it is drawn off. The coarser portion of the soil remains in the container and can be subjected to a sieve analysis. The soil particles in the turbid liquid, which are too fine to be collected on sieves, can be subjected to wet mechanical analysis.

The methods for performing wet mechanical analysis are based on Stokes's law, which determines the velocity at which a spherical particle of given diameter settles in a quiet liquid. In the method commonly used for engineering purposes, 20 to 40 g of clay soil or 50 to 100 g of sandy soil are mixed with one liter of water, agitated, and poured into a container. The density of the suspension is measured at various times by means of a hydrometer of special design. At any given time, the size of the largest particles remaining in suspension at the level of the hydrometer can be computed by means of Stokes's law, whereas the weight of the particles finer than that size can be computed from the density of the suspension

at the same level. The performance of a test requires several days.

By means of wet mechanical analysis, soil fractions can be separated down to a size of about  $0.5\mu$ . Still finer fractions can be obtained by means of a centrifuge, but the results of such refined methods are of interest only in connection with scientific research.

Agitation in water transforms many clays into suspensions, not of individual particles, but of flocs. To break up the flocs into individual grains, or to disperse the soil, a deflocculating agent must be added to the water. The most common errors in the results of wet mechanical analysis are caused by inadequate dispersion.

The results of wet mechanical analysis are not strictly comparable to those of sieve analysis, because soil grains are never exactly spherical, and the smallest ones are commonly of a flaky shape. In a sieve analysis the width of the flake is measured, whereas the dimension determined by means of wet mechanical analysis is the diameter of a sphere that sinks at the same rate as the flake. This diameter may be much smaller than the width of the actual flake.

The most convenient representation of the results of a mechanical analysis is the semilogarithmic grain-size curve shown in Fig. 5.1. The abscissas of this curve represent the logarithm of the grain size. The ordinates represent the percentage  $P$ , by weight, of grains smaller than the size denoted by the abscissa. The more uniform the grain size, the steeper is the slope of the curve; a vertical line represents a perfectly uniform powder. The most important advantage of a semilogarithmic plot is that the grain-size curves of soils having equal uniformity are identical in shape, regardless of the average grain size. In addition, the horizontal distance between two curves of the same shape is equal to the logarithm of the ratio of the average grain sizes of the corresponding soils.

Figure 5.2 shows several typical grain-size curves. Curve *a* is a common type. It closely resembles the normal frequency curve that represents one of the fundamental laws of statistics. Since grain size is a statistical phenomenon, attempts have been made to use the terms and con-

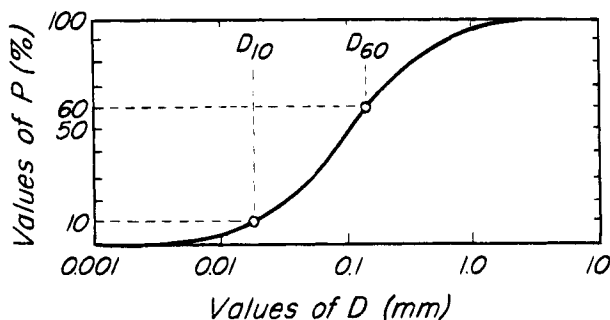


**Figure 5.1** Semilogarithmic plot of results of mechanical analysis.

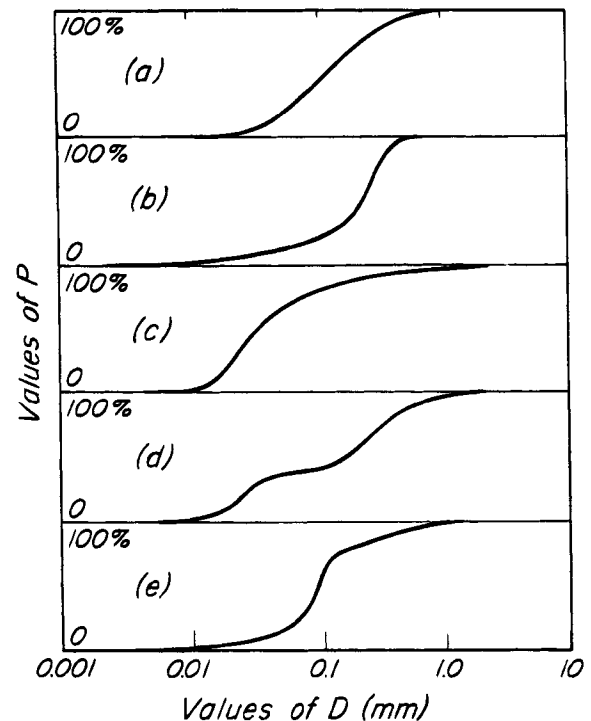


**Figure 5.2** Typical grain-size curves. (a) Normal frequency curve. (b and c) Curves for soils having coarser and finer fractions of different uniformity. (d and e) Composite curves.

cepts of statistics to describe the results of mechanical analyses. Such refinements, however, are usually not warranted in connection with soil mechanics for engineering purposes.

If a sample has the grain-size distribution shown in Fig. 5.2*a*, the uniformity of the fraction having grains larger than  $D_{50}$  (corresponding to  $P = 50\%$ ) is approximately equal to that of the fraction having grains smaller than  $D_{50}$ . If the distribution resembles that shown in *b*, the coarser half of the sample is relatively uniform, whereas the size of the grains in the finer half varies over a wide range. Conversely, the distribution represented in *c* corresponds to a sample in which the coarser grains are of widely different sizes and the finer ones are more uniform. The curves represented in *d* and *e* are said to be *composite*.

The grain-size curves of immature residual soils are usually similar to that shown in Fig. 5.2*b*. With increasing age of the soil, the average grain size decreases because of weathering, and the curves become more nearly straight (Fig. 5.2*a*). The grain-size curves of mature soils resemble that shown in Fig. 5.2*c*. Distributions represented by *b* and *c* are also common among soils of glacial or fluvioglacial origin. Absence of a medium grain size in a sedimentary soil, as exemplified by the curve in Fig. 5.2*d*, is common among sand-gravel mixtures that were deposited by swiftly flowing rivers carrying a large load of sediment.



Gravels of this type are said to be poorly, or gap, graded. A curve such as that in Fig. 5.2d may also be obtained if the materials from two different layers are mixed before the mechanical analysis is performed.

A conspicuous break in the continuity of the grain-size curve may also indicate the simultaneous deposition of the soil by two different agents. For instance, one fraction might be washed into a glacial lake by a river and another fraction dropped from melting ice floats. Thus, a knowledge of the shape of grain-size curves may assist in determining the geological origin of a soil and thereby reduce the risk of error in the interpretation of the data obtained from test borings.

## 5.2 Abbreviated Representation of Grain-Size Characteristics

In order to represent the essential results of the mechanical analysis of a great number of soils, it may be convenient to express the grain-size characteristics of each soil either by numerical values indicative of some characteristic grain size and of the degree of uniformity or else by names or symbols that indicate the dominant soil fraction. The most common procedure based on numerical values is known as Allen Hazen's method. On the basis of a great number of tests with filter sands, Hazen (1892) found that the permeability of these sands in a loose state depends on two quantities that he called the effective size and the uniformity coefficient. The *effective size* is the diameter  $D_{10}$  that corresponds to  $P = 10\%$  on the grain-size diagram. In other words, 10% of the particles are finer and 90% coarser than the effective size. The *uniformity coefficient*  $C_U$  is equal to  $D_{60}/D_{10}$ , wherein  $D_{60}$  is the grain size corresponding to  $P = 60\%$ . A third characteristic of the grain-size distribution, useful in the classification of soils (Article 8.3), is the *coefficient of curvature*  $C_C$ , defined as  $D_{30}^2/D_{10} D_{60}$ .

Hazen's findings led other investigators to the more or less arbitrary assumption that the quantities  $D_{10}$  and  $C_U$  are also suitable for expressing the grain-size characteristics of mixed-grained natural soils. With increasing knowledge concerning fine-grained soils, it has become evident that the character of such soils depends chiefly on the finest 20% and that it might be preferable to select  $D_{20}$  and  $D_{70}$  as the significant quantities. However, the advantage is not sufficiently important to justify a departure from well-established procedure. The use of symbols to indicate the grain-size characteristics of a soil is described in Article 8.3.

## Selected Reading

Techniques for performing mechanical analyses and other classification tests are described in Section 4 of the *Annual Book of ASTM Standards*.

# ARTICLE 6 SOIL AGGREGATE

## 6.1 Introduction

The term *aggregate* refers to the soil itself, in contrast to its constituent parts. Qualitatively, soil aggregates may differ in texture and consistency. Quantitatively, they may differ in porosity, relative density, water and gas content, and consistency. The qualitative information is obtained in the field by visual inspection. It constitutes the basis for preparing the boring logs or other records that describe the succession of strata in the underground. The quantitative information is obtained by means of laboratory and field tests. Without such information the description of any soil is inadequate.

## 6.2 Texture, Structure, and Consistency

The term *texture* refers to the degree of fineness and uniformity of a soil. It is described by such expressions as *floury*, *smooth*, *gritty*, or *sharp*, in accordance with the sensation produced by rubbing the soil between the fingers.

The term *structure* may refer to the *fabric* of the aggregate, as described in Article 4.5. It may also refer to features acquired after deposition, such as the root holes contained in loess (Article 2). Stiff clays may also contain tubular root holes extending to a depth of several meters below the surface, or they may be divided by hair cracks into prismatic or irregular fragments that fall apart as soon as the confining pressure is removed. Such hair cracks are known as *joints*. Striations produced by movements along the walls of the joints are known as *slickensides*. The origin, nature, and practical implications of such defects of soil strata are discussed in Chapter 2.

The term *consistency* refers to the degree of adhesion between the soil particles and to the resistance offered against forces that tend to deform or rupture the soil aggregate. The consistency is described by such terms as *hard*, *stiff*, *brittle*, *friable*, *sticky*, *plastic*, and *soft*. The more nearly a soil approaches the characteristics of a clay, the greater is the variety of states of consistency in which it may be found. The degree of plasticity is sometimes expressed by the terms *fat* and *lean*. A lean clay is one that is only slightly plastic because it contains a large proportion of silt or sand. Further information concerning the consistency of clays is given in Article 7.

## 6.3 Porosity, Water Content, Unit Weight, and Density

The *porosity*  $n$  is the ratio of the volume of voids to the total volume of the soil aggregate. The term *volume of voids* refers to that portion of the volume of the soil not occupied by mineral grains.

The *void ratio*  $e$  is the ratio of the volume of voids to the volume of the solid substance. If

$V$  = total volume

$V_v$  = total volume of voids

then

$$n = \frac{V_v}{V} \quad (6.1a)$$

and

$$e = \frac{V_v}{V - V_v} \quad (6.1b)$$

The relation between void ratio and porosity is expressed by the equations,

$$e = \frac{n}{1 - n} \quad (6.2a)$$

and

$$n = \frac{e}{1 + e} \quad (6.2b)$$

The porosity of a stable mass of identical cohesionless spheres depends on the manner in which the spheres are arranged. In the densest possible arrangement,  $n$  is equal to 26%, and in the loosest state to 47%. Natural sands are found with porosities varying from about 25 to 50%. The porosity of a natural sand deposit depends on the shape of the grains, the uniformity of grain size, and the conditions of sedimentation.

The effect of the shape of the grains on the porosity of the aggregate can be demonstrated by mixing various percentages of mica with a uniform angular sand. If the percentage of mica, by weight, is equal successively to 0, 5, 10, 20, and 40, the porosities of the resultant mixtures when loosely dumped into a vessel are about 47, 60, 70, 77, and 84%, respectively (Gilboy 1928). The porosity of soft natural clays, which contain an appreciable percentage of flat particles, usually ranges between 30 and 60%. It can even exceed 90%.

Because of the great influence of the shape of the grains and of the degree of uniformity on the porosity, the porosity itself does not indicate whether a soil is loose or dense. This information can be obtained only by comparing the porosity of the given soil with that of the same soil in its loosest and densest possible states. The looseness or denseness of sandy soil can be expressed numerically by the *relative density*  $D_r$ , defined by the equation

$$D_r = \frac{e_{\max} - e}{e_{\max} - e_{\min}} \quad (6.3)$$

in which  $e_{\max}$  = void ratio of the soil in its loosest stable state

$e_{\min}$  = void ratio in the densest state that can be obtained in the laboratory

$e$  = void ratio of the soil in the field

To bring a medium or coarse sand into its loosest state, corresponding to the void ratio  $e_{\max}$ , the sand is first dried and then poured from a small height into a vessel. Fine and very fine sands may in some instances be brought into the loosest state by mixing a sample with enough water to transform it into a thick suspension that is then allowed to settle; the value of  $e_{\max}$  is equal to the final void ratio of the sediment. In other instances the loosest state can be established by carefully depositing the sand in a slightly moist state, such that the capillary forces produce an artificially loose structure, and by then permitting a very slow upward flow of water that causes the unstable structure to collapse. The densest state of clean sands can be established by prolonged vibrations, under a small vertical load, at a frequency of 20 to 30 Hz.

The relative density of sand has a well-defined meaning because its value is practically independent of the static pressure to which the sand is subjected. It depends primarily on the procedure used in placing and compacting the sand. On the other hand, the degree of density of clays and other cohesive soils depends chiefly on the loads that these soils have carried and, in some instances, on the rate at which the loads were applied. The degree of density of these soils is most clearly reflected by the liquidity index  $I_L$  (Article 7.2).

The *water content*  $w$  of a soil is defined as the ratio of the weight of water to the dry weight of the aggregate. It is usually expressed as a percentage. In sands located above the water table, part of the voids may be occupied by air. If  $e_w$  represents the volume occupied by water per unit volume of solid matter, the ratio,

$$S_r(\%) = \frac{100 V_w}{V_v} = \frac{100e_w}{e} \quad (6.4)$$

represents the *degree of saturation*. The degree of saturation of sands is commonly expressed by such words as dry or moist. Table 6.1 gives a list of such descriptive terms and of the corresponding degrees of saturation. The nomenclature represented in Table 6.1 applies only to sands or very sandy soils. A clay in the state of desiccation represented by  $S_r = 90\%$  might be so hard that it would be called dry instead of wet.

Coarse sands located above the water table are usually humid. Fine or silty sands are moist, wet, or saturated. Clays are almost always completely or nearly saturated, except in the layer of surface soil that is subject to seasonal variations of temperature and moisture. If a clay contains gas, the gas is present in bubbles scattered throughout

**Table 6.1 Degree of Saturation of Sand in Various States**

Condition of Sand	Degree of Saturation (%)
Dry	0
Humid	1–25
Damp	26–50
Moist	51–75
Wet	76–99
Saturated	100

the material. The bubbles may be composed of air that entered the deposit during sedimentation, or of gas produced at a later date by chemical processes such as the decomposition of organic material. The gas may be under pressure great enough to cause the clay to expand energetically at constant water content if the confining pressure is decreased. The determination of the gas content of a clay is extremely difficult. It requires special equipment and is not a routine test.

The water content itself is a significant index property, especially with respect to the consistency of clays (Article 7). Of even greater importance, however, is the state of stress of the water in the voids of the soil. The *porewater stress*, which may be either positive or negative with respect to atmospheric pressure, is fundamentally related to the behavior of the soil under field conditions. This relationship is at the heart of much of the subject matter of the remainder of this book. Porewater stress is variously referred to as *porewater pressure*, *pore pressure*, or *neutral stress* (Article 15).

The *density* of the soil aggregate is defined as the mass of the aggregate (soil plus water) per unit of volume. It depends on the density of the solid constituents, the porosity of the aggregate, and the degree of saturation. It may be computed as follows:

Let

$\rho_s$  = average density of solid constituents

$\rho_w$  = density of water

$n$  = porosity (expressed as a ratio)

The density of dry soil ( $S_r = 0\%$ ) is

$$\rho_d = (1 - n)\rho_s \quad (6.5)$$

and of saturated soil ( $S_r = 100\%$ ) is

$$\rho_{\text{sat}} = (1 - n)\rho_s + n\rho_w = \rho_s - n(\rho_s - \rho_w) \quad (6.6)$$

Similarly, the *unit weight* of the soil aggregate is defined as the weight of the aggregate (soil plus water) per unit of volume. It depends on the unit weight of the solid constituents, the porosity of the aggregate, and the degree of saturation. It may be computed as follows:

Let

$\gamma_s$  = average unit weight of solid constituents

$\gamma_w$  = unit weight of water

$n$  = porosity (expressed as a ratio)

The unit weight of dry soil ( $S_r = 0\%$ ) is

$$\gamma_d = (1 - n)\gamma_s \quad (6.7)$$

and of saturated soil ( $S_r = 100\%$ ) is

$$\gamma_{\text{sat}} = (1 - n)\gamma_s + n\gamma_w = \gamma_s - n(\gamma_s - \gamma_w) \quad (6.8)$$

The density and unit weight of the principal solid constituents of soils are given in Table 6.2. For sand grains the average density is usually about 2.65 Mg/m<sup>3</sup>. For clay particles the density varies from 2.5 to 2.9 with a statistical average of approximately 2.7 Mg/m<sup>3</sup>.

Given in Table 6.3 are the porosity, the saturated density, and the saturated unit weight of typical soils. For sandy soils the values for dry soil have also been included. The values have been computed on the assumption that  $\rho_s$  is 2.65 Mg/m<sup>3</sup> for sandy soils and 2.70 Mg/m<sup>3</sup> for clays. The tabulated values should be considered only as approximations. Before final computations are made on a given job, the actual density or unit weight of the soil should always be determined.

The *specific gravity* of the solid constituents is defined as  $G_s = \rho_s/\rho_w = \gamma_s/\gamma_w$ .

### Problems

1. A sample of saturated clay weighed 1526 g in its natural state, and 1053 g after drying. Determine the natural water content. If the specific gravity of the solid constituents was 2.70, what was the void ratio? The porosity? The total unit weight?

Ans.  $w = 44.9\%$ ;  $e = 1.21$ ;  $n = 0.55$ ;  $\gamma = 17.3 \text{ kN/m}^3$ .

**Table 6.2 Density of Most Important Soil Constituents**

	Mg/m <sup>3</sup>		Mg/m <sup>3</sup>
Gypsum	2.32	Dolomite	2.87
Montmorillonite	2.50–2.80	Aragonite	2.94
Orthoclase	2.56	Biotite	3.0–3.1
Kaolinite	2.60	Augite	3.2–3.4
Illite	2.66–2.72	Hornblende	3.2–3.5
Chlorite	2.6–3.0	Limonite	3.8
Quartz	2.66	Hematite,	4.3±
Talc	2.7	hydrous	
Calcite	2.72	Magnetite	5.17
Muscovite	2.8–2.9	Hematite	5.2

Larson and Berman (1934).

**Table 6.3 Porosity, Void Ratio, Density, and Unit Weight of Typical Soils in Natural State**

Description	Porosity, $n$ (%)	Void ratio ( $e$ )	Water content, $w$ (%)	Density (Mg/m <sup>3</sup> )		Unit Weight (kN/m <sup>3</sup> )	
				$\rho_d$	$\rho_{sat}$	$\gamma_d$	$\gamma_{sat}$
1. Uniform sand, loose	46	0.85	32	1.43	1.89	14.0	18.5
2. Uniform sand, dense	34	0.51	19	1.75	2.09	17.2	20.5
3. Mixed-grained sand, loose	40	0.67	25	1.59	1.99	15.6	19.5
4. Mixed-grained sand, dense	30	0.43	16	1.86	2.16	18.2	21.2
5. Glacial till, very mixed-grained	20	0.25	9	2.12	2.32	20.8	22.7
6. Soft glacial clay	55	1.2	45		1.77	12.0	17.4
7. Stiff glacial clay	37	0.6	22		2.07	16.7	20.3
8. Soft slightly organic clay	66	1.9	70		1.58	9.1	15.5
9. Soft very organic clay	75	3.0	110		1.43	6.7	14.4
10. Soft bentonite	84	5.2	194		1.27	4.2	12.5

$w$  = water content when saturated, in percent of dry weight.

$\rho_d$  = density in dry state.

$\rho_{sat}$  = density in saturated state.

$\gamma_d$  = unit weight in dry state.

$\gamma_{sat}$  = unit weight in saturated state.

2. A sample of hardpan had a weight of 129.1 g and a volume of 56.4 cm<sup>3</sup> in its natural state. Its dry weight was 121.5 g. The specific gravity of the solid constituents was found to be 2.70. Compute the water content, the void ratio, and degree of saturation.

Ans.  $w = 6.3\%$ ;  $e = 0.25$ ;  $S_r = 67\%$ .

3. The density of a sand backfill was determined by field measurements to be 1.75 Mg/m<sup>3</sup>. The water content at the time of the test was 8.6%, and the specific gravity of solid constituents was 2.60. In the laboratory the void ratios in the loosest and densest states were found to be 0.642 and 0.462, respectively. What were the void ratio and the relative density of the fill?

Ans.  $e = 0.616$ ;  $D_r = 14\%$ .

4. A dry quartz sand sample weighs 1.54 Mg/m<sup>3</sup>. What is its density when saturated?

Ans.  $\rho = 1.96$  Mg/m<sup>3</sup>.

5. A sample of silty clay had a volume of 14.88 cm<sup>3</sup>. Its weight at the natural water content was 28.81 g and after oven-drying was 24.83 g. The specific gravity of solid constituents was 2.70. Calculate the void ratio and the degree of saturation of the sample.

Ans.  $e = 0.617$ ;  $S_r = 70\%$ .

6. Given the values of porosity  $n$  for the soils in Table 6.3, check the values of void ratio  $e$ , water content  $w$ , density  $\rho$ , and unit weight  $\gamma$ . For soils 1 to 5,  $G_s = 2.65$ ; for soils 6 to 10,  $G_s = 2.70$ .

## ARTICLE 7 CONSISTENCY OF FINE-GRAINED SOILS

### 7.1 Consistency and Sensitivity of Undisturbed Soils

The consistency of clays and other cohesive soils is usually described as *soft*, *medium*, *stiff*, or *hard*. The most direct quantitative measure of consistency is the load per unit of area at which unconfined prismatic or cylindrical samples of the soil fail in a compression test. This quantity is known as the *unconfined compressive strength* of the soil. Values of the compressive strength corresponding to the various degrees of consistency are given in Table 7.1.

**Table 7.1 Consistency of Clay in Terms of Unconfined Compressive Strength**

Consistency	Unconfined Compressive Strength, $q_u$ (kPa)
Very soft	Less than 25
Soft	25–50
Medium	50–100
Stiff	100–200
Very stiff	200–400
Hard	Over 400

Clays share with many other colloidal substances the property that kneading or working at unaltered water content makes the material softer. The process of kneading or working is commonly referred to as *remolding*, and clays that have been subjected to the process are called *remolded clays*. The softening effect is probably due to three different causes: destruction of the orderly arrangement of the water molecules and ions in the adsorbed layers, reorientation of clay plates from edge-face arrangement to a predominantly face-face interaction, and injury to the structure that the clay acquired during sedimentation and consolidation. That part of the loss of strength caused by the disturbance of the adsorbed layers and reorientation of clay plates may be gradually regained, at unaltered water content, after the working has ceased. The remainder, probably caused by permanent alteration of the structure, is irrecoverable unless the water content of the clay is reduced. The ratio between these two parts of the loss of strength is very different for different clays.

The term *sensitivity* indicates the effect of remolding on the consistency of a clay, regardless of the physical nature of the causes of the change. The degree of sensitivity is different for different clays, and it may also be different for the same clay at different water contents. If a clay is very sensitive, a slide may turn it into a mass of lubricated chunks capable of flowing on a gently sloping base, whereas a similar slide in a clay with low sensitivity merely produces a conspicuous local deformation. The change in consistency produced by the disturbance of a sensitive clay is always associated with a change of the permeability.

The degree of sensitivity  $S_i$  of a clay is expressed by the ratio between the unconfined compressive strength of an undisturbed specimen and the strength of the same specimen at the same water content but in a remolded state. That is,

$$S_i = \frac{\text{Unconfined compressive strength undisturbed}}{\text{Unconfined compressive strength remolded}} \quad (7.1)$$

The values of  $S_i$  for most clays range between 2 and about 4. For sensitive clays they range from 4 to 8. However, extrasensitive clays are encountered with values of  $S_i$  between 8 and 16, and in some localities clays with even higher sensitivities are found; these are known as *quick clays*. High degrees of sensitivity may be due to a very loose structure, or to leaching of soft glacial clays deposited in salt water and subsequently uplifted. The quick clays of Scandinavia and of eastern Canada are of this category. On the other hand, the extra-sensitive clays of Mexico City were derived from the decomposition of volcanic ash.

The remolded strengths of some saturated clays may be so low that an unconfined specimen cannot stand without excessive deformation under its own weight. Under these conditions the degree of sensitivity  $S_i$  may be evaluated by comparing the undisturbed and remolded shearing strength determined by such other procedures as the vane shear test (Article 11.5.2).

## 7.2 Consistency of Remolded Soils

After a cohesive soil has been remolded, its consistency can be changed at will by increasing or decreasing the water content. Thus, for instance, if the water content of a clay slurry is gradually reduced by slow desiccation, the clay passes from a liquid state through a plastic state and finally into a solid state. The water contents at which different clays pass from one of these states into another are very different. Therefore, the water contents at these transitions can be used for identification and comparison of different clays. However, the transition from one state to another does not occur abruptly as soon as some critical water content is reached. It occurs gradually over a fairly large range in the value of the water content. For this reason every attempt to establish criteria for the boundaries between the limits of consistency involves some arbitrary elements. The method that has proved most suitable for engineering purposes was taken over from agronomy. It is known as Atterberg's method, and the water contents that correspond to the boundaries between the states of consistency are called the *Atterberg limits* (Atterberg 1911).

The *liquid limit*  $w_l$  is the water content in percent of the dry weight at which two sections of a pat of soil having the dimensions shown in Fig. 7.1 barely touch each other but do not flow together when subjected in a cup to the impact of sharp blows from below. The personal equation has an important influence on the test results. In order to eliminate this factor, a standardized mechanical device is used (Casagrande 1932a).

The *plastic limit*  $w_p$  or lower limit of the plastic state is the water content at which the soil begins to crumble when rolled out into thin threads.

The record of the results of the plastic-limit test should also contain a statement as to whether the threads, immediately before crumbling, were very tough like those of a gumbo, moderately tough like those of an average gla-

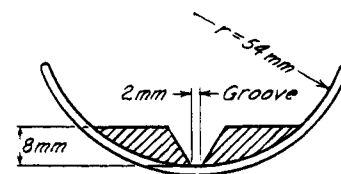


**Figure 7.1** Cross-section through soil pat for liquid-limit test (after Casagrande 1932a).

cial clay, or weak and spongy like those of an organic or of a micaceous inorganic soil.

The *shrinkage limit*  $w_s$  or lower limit of volume change is the water content below which further loss of water by evaporation does not result in a reduction of volume. As soon as the soil passes below the shrinkage limit its color becomes slightly lighter.

Performance of the liquid and plastic limit tests is specified in ASTM D4318. The shrinkage limit test is specified in ASTM D427.

The range of water content within which a soil possesses plasticity is known as the *plastic range*, and the numerical difference between the liquid limit and the plastic limit is the *plasticity index*  $I_p$ . As the water content  $w$  of a cohesive soil approaches the lower limit of the plastic range, the stiffness and degree of compaction of the soil increase. The ratio,

$$I_L = \frac{w - w_p}{w_l - w_p} = \frac{w - w_p}{I_p} \quad (7.2)$$

is called the *liquidity index* of the soil. If the water content of a natural soil stratum is greater than the liquid limit (liquidity index greater than 1.0), remolding transforms the soil into a thick viscous slurry. If the natural water content is less than the plastic limit (liquidity index negative), the soil cannot be remolded. The unconfined compressive strength of undisturbed clays with a liquidity index near unity commonly ranges between 30 and 100

kPa. If the liquidity index is near zero, the compressive strength generally lies between 100 and 500 kPa.

In addition to the Atterberg limits, a knowledge of the *dry strength* is useful in the identification and comparison of cohesive soils. The strength of air-dry specimens of clay ranges from about 200 kPa to more than 20 MPa, and a trained experimenter can distinguish among the degrees of *very low*, *low*, *medium*, *high*, and *very high*, merely by pressing an angular fragment of the soil between the fingers. The strength is called medium if the fragment can be reduced to powder only with great effort. Fragments with very high strength cannot be injured at all, whereas those of very low strength disintegrate completely on gentle pressure. The fragments should be obtained by molding a cylindrical specimen about 25 mm high and 25 mm in diameter from a paste at a water content close to the plastic limit. After the cylinder has dried at room temperature, it is broken into smaller pieces, and fragments for the examination are selected from the interior of the specimen.

### 7.3 Plasticity Chart

It has been observed (Casagrande 1932a) that many properties of clays and silts, such as their dry strength, their compressibility, their reaction to the shaking test, and their consistency near the plastic limit, can be correlated with the Atterberg limits by means of the *plasticity chart* (Fig. 7.2). In this chart, the ordinates represent the plastic-

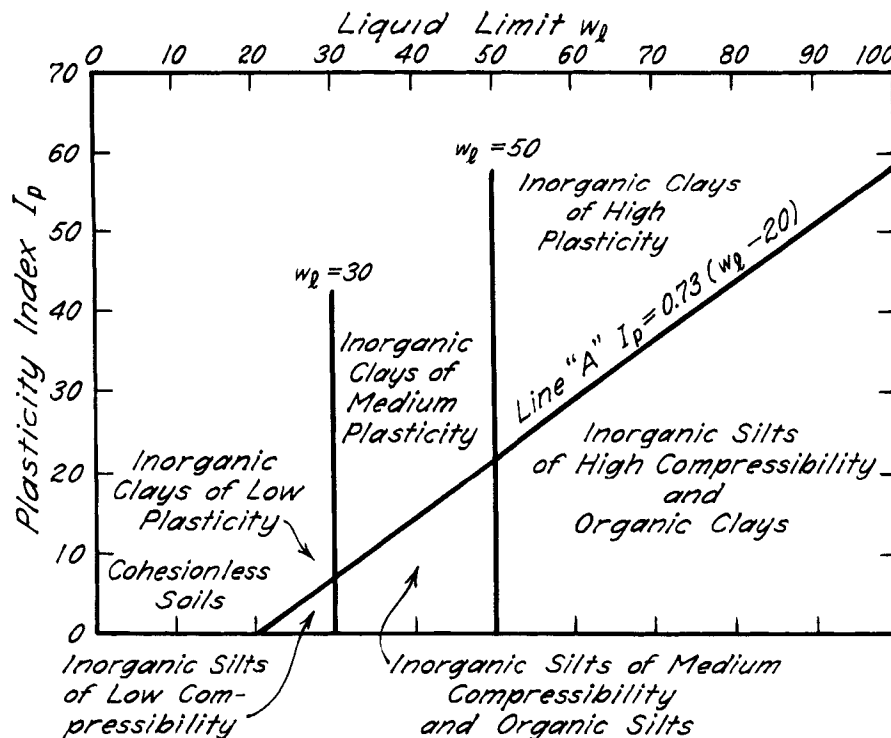


Figure 7.2 Plasticity chart (after Casagrande 1932a).

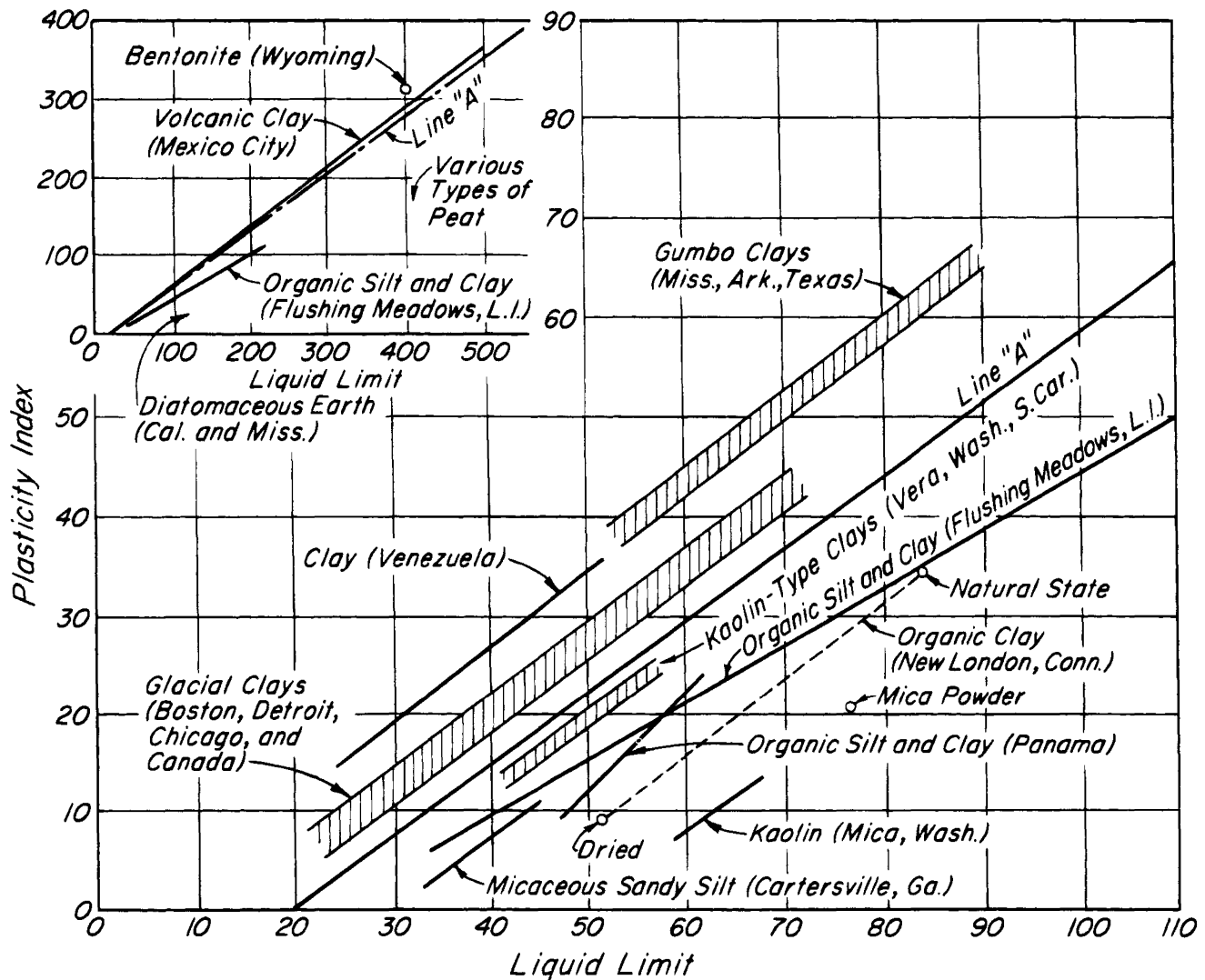


Figure 7.3 Relation between liquid limit and plasticity index for typical soils (after Casagrande 1932a).

ity index  $I_p$  and the abscissas the corresponding liquid limit  $w_L$ .

The chart is divided into six regions, three above line A and three below. The group to which a given soil belongs is determined by the name of the region that contains the point representing the values of  $I_p$  and  $w_L$  for the soil. All points representing inorganic clays lie above line A, and all points for inorganic silts lie below it. Therefore, if a soil is known to be inorganic, its group affiliation can be ascertained on the basis of the values of  $I_p$  and  $w_L$  alone. However, points representing organic clays are usually located within the same region as those representing inorganic silts of high compressibility, and points representing organic silts in the region assigned to inorganic silts of medium compressibility. Usually, the organic soils can be distinguished from the inorganic by their characteristic odor and their dark-gray or black color.

In doubtful cases the liquid limit should be determined for an oven-dry specimen as well as a fresh one. If drying decreases the value of the liquid limit by 30% or more, the soil may usually be classified as organic, although in some instances other constituents, such as the clay mineral halloysite, similarly lower the liquid limit. Finally, if an inorganic and an organic soil are represented in Fig. 7.2 by approximately the same point, the dry strength of the organic soil is considerably greater than that of the inorganic soil. Experience has shown that the points which represent different samples from the same soil stratum define a straight line that is roughly parallel to line A. As the liquid limit of soils represented by such a line increases, the plasticity and the compressibility of the soils also increase. The dry strength of inorganic soils represented by points on lines located above A increases from medium for samples with a liquid limit below 30

to very high for samples with a liquid limit of 100. On the other hand, if the line representative of inorganic samples from a given stratum is located at a considerable distance below A, the dry strength of samples with a liquid limit less than 50 is very low, and that of samples with a liquid limit close to 100 is only medium. In accordance with these relationships, the dry strength of inorganic soils from different localities but with equal liquid limits increases in a general way with increasing plasticity index. Figure 7.3 shows the plasticity characteristics of several well-defined types of clay.

The samples required for Atterberg-limit tests need not be undisturbed, and the technique of making the tests is simple. A great amount of useful information can be derived from the test results. Therefore, the investigation

of statistical relations between the Atterberg limits and the other physical properties of cohesive soils is a promising field for research. Every well-established statistical relation of this type broadens the scope of conclusions that can be drawn from the results of limit tests. Two useful relations of this kind are shown in Figs. 19.7 and 20.20

However, empirical relations between the physical properties of soils and their Atterberg limits, based on data from sedimentary deposits consisting of clay minerals commonly found in temperate climates, are not likely to apply to certain residual soils formed under humid tropical conditions, particularly from volcanic materials. These soils are likely to display a characteristic yellow, red, or brown color. In some (latosols), the predominant clay

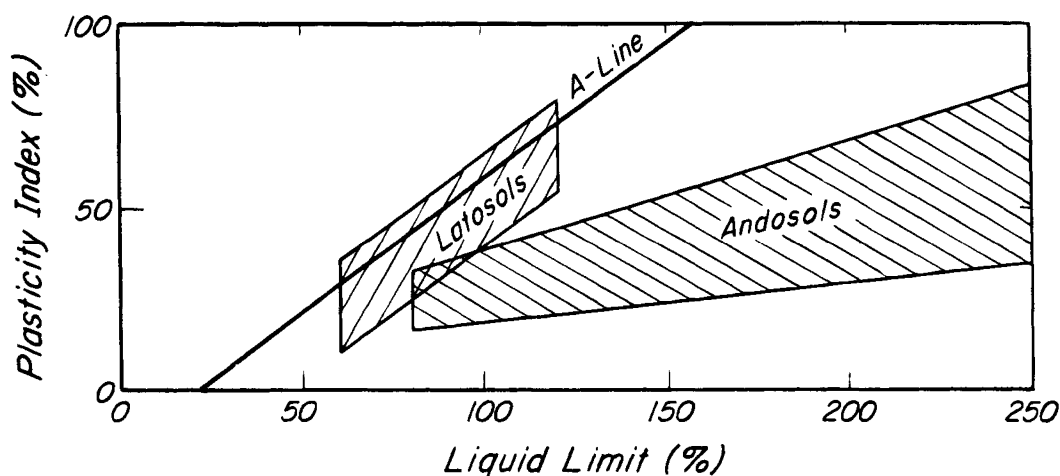


Figure 7.4 Latosols and Andosols from Java, Indonesia (after Wesley 1973).

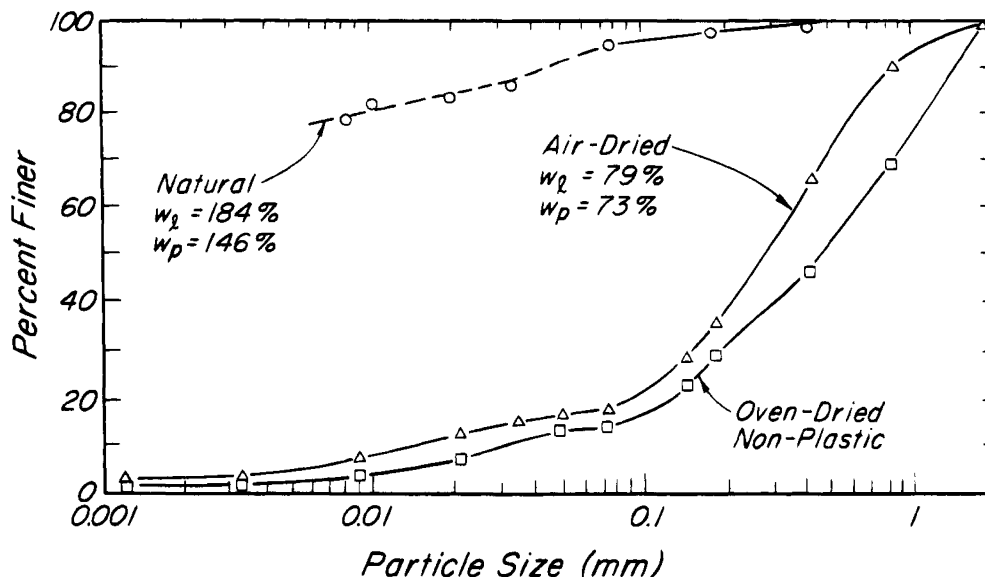


Figure 7.5 Particle size distribution and Atterberg limits for sample of residual soil from Indonesia (data from Wesley 1973).



mineral is halloysite; the water is held in the pores of clusters or aggregates that are cemented together. Therefore, at the same water content or liquid limit the soils have lower compressibility and significantly higher shear strength than soils consisting of the clay minerals more commonly found in temperate climates. In others (andosols), the predominant clay mineral is allophane; a major part of the pore water is trapped within the soil particles and, consequently, the plastic limit is unusually high and the plasticity index correspondingly low (Fig. 7.4). When dried, removal of the water causes the porous clusters to shrink irreversibly to form hard grains. The resulting effects on the Atterberg limits and grain-size distribution for one such material are shown in Fig. 7.5.

### Selected Reading

The classic study of the Atterberg limits and their uses for engineering purposes is Casagrande, A. (1932a). "Research on the Atterberg limits of soils," *Public Roads*, 13, pp. 121–136.

Atterberg, A. (1911). "On the investigation of the physical properties of soils and the plasticity of clays," *Int. Mitt. Bodenkunde (German)*, 1, p. 10.

## ARTICLE 8 SOIL CLASSIFICATION

### 8.1 Practical Significance of Soil Classification

Ever since the physical properties of soils became a matter of interest, frequent attempts have been made to correlate the results of simple classification tests with the soil parameters needed for solving practical problems. Most of the early correlations were related to the grain-size characteristics. The results of the endeavors to base systems of classification exclusively on grain size, however, were consistently disappointing. Attempts to compute the coefficient of permeability of soils on the basis of the results of mechanical analysis failed because the permeability depends to a large extent on the shape of the grains, which can be very different for soils with identical grain-size characteristics. Attempts to correlate the grain-size characteristics of fine-grained soils such as silt or clay with the angle of internal friction have been even less successful. The reason is illustrated by Fig. 8.1.

In Fig. 8.1 the heavy uppermost curve is the *grain-size frequency curve* for a glacial clay from southeastern Canada. On the horizontal axis are plotted the logarithms of the grain size. The area of the strip located above an arbitrary grain-size range, for instance  $2\ \mu$  to  $1\ \mu$ , represents the quantity of soil particles within this range, in percent of the total weight of the dried clay. According to the diagram the macroscopic fraction ( $>0.06\ \text{mm}$ ), like that of most other clays, consists chiefly of quartz. The microscopic fraction ( $0.06$  to  $0.002\ \text{mm}$ ) consists

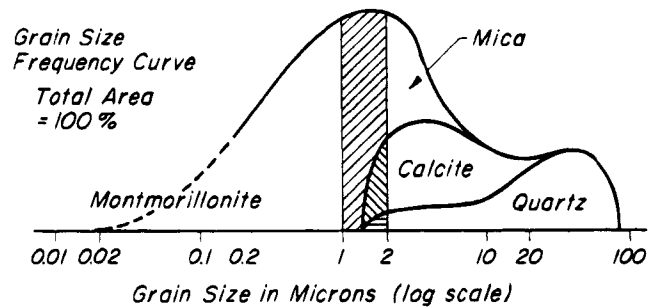


**Figure 8.1** Grain size and mineralogical composition of a glacial marine clay (courtesy R. E. Grim).

partly of quartz and calcite and partly of mica flakes. The mica content of this fraction is very different for different clays, and it has a decisive influence on the compressibility and other properties of the clay. The colloidal fraction ( $<0.002\ \text{mm}$ ) consists almost exclusively of montmorillonite, whereas that of other clays may consist chiefly of clay minerals of the kaolin or illite groups. The physical properties of the clay depend to a large extent on the type of clay mineral that dominates the colloidal fraction. They also depend to a large extent on the substances that are present in the adsorbed layers (Article 4). Hence, two clays with identical grain-size curves can be extremely different in every other respect.

Because of these conditions, well-defined statistical relations between grain-size characteristics and significant soil properties such as the angle of internal friction have been encountered only within relatively small regions where all the soils of the same category, such as all the clays or all the sands, have a similar geological origin. In such regions the grain-size characteristics can be used as a basis for judging the significant properties of the soils. This is commonly and successfully done. However, none of the procedures that grow out of experience in such regions can safely be used outside the boundaries of the region where they originated.

Since the properties of fine-grained soils can be correlated in a general way with the plasticity of the materials, classification systems for such soils are preferably based on the Atterberg limits rather than on grain size. Classification of mixed-grained soils containing both coarse and fine fractions should be based not only on the grain-size characteristics of the coarse fractions but also on the plasticity of the fine and very fine fractions.

### 8.2 Classification Based on Grain Size

In spite of their shortcomings, soil classifications based on grain-size characteristics, such as the one shown in Table 8.1, are widely used, especially for preliminary or general descriptions. It is customary, in connection with such classifications, to assign the names of soils, such as "silt" or "clay," to different grain-size fractions. However,

**Table 8.1 Soil Classification Based on Grain Size**

Soil	Diameter (mm)	Sieve Size*
Boulders	Over 300	12 in.
Cobbles (rounded)	300–75	12 in.–3 in.
Gravel	75–4.76	3 in.–No. 4
Coarse	75–19	3 in.–3/4 in.
Fine	19–4.76	3/4 in.–No. 4
Sand	4.76–0.074	No. 4–No. 200
Coarse	4.76–2.0	No. 4–No. 10
Medium	2.0–0.42	No. 10–No. 40
Fine	0.42–0.074	No. 40–No. 200
Fines	Less than 0.074	No. 200
(Silt size)	0.074–0.002	
(Clay size)	Less than 0.002	

\* ASTM D422.

(After USBR 1974).

any system of classification based on grain size alone is likely to be misleading, because the physical properties of the finest soil fractions depend on many factors other than grain size (see Article 4). For example, according to any one of the commonly used classifications, a soil consisting of quartz grains of colloidal size should be called a clay, whereas in reality it does not possess even a remote resemblance to clay. Hence, if the words “silt” or “clay” are used to express grain size, they should be combined with the word “size,” as in the expression “clay-size particle.” The term *fine* is often used to describe the fraction of a soil that passes the No. 200 sieve (0.074 mm), and the term *clay-size fraction* (CF) the fraction with sizes smaller than 0.002 mm.

### 8.3 Unified Soil Classification System

The unsatisfactory nature of systems of soil classification based on grain size alone led to a critical review of the problem (Casagrande 1948) and the proposal of the Unified Soil Classification System, adopted in 1952 by the U.S. Corps of Engineers and Bureau of Reclamation, and subsequently by many other organizations (USBR 1963).

According to this system, all soils are divided into three major groups: coarse-grained, fine-grained, and highly organic (peaty). The peaty soils are readily identified by the characteristics listed in Article 2. The boundary between coarse-grained and fine-grained soils is taken to be the 200-mesh sieve (0.074 mm). In the field the distinction is based on whether the individual particles can be seen with the unaided eye. If more than 50% of the soil by weight is judged to consist of grains that can be distinguished separately, the soil is considered to be coarse-grained.

The coarse-grained soils are divided into gravelly (G) or sandy (S) soils in accordance with whether more or less than 50% of the visible grains are larger than the No. 4 sieve (4.75 mm.). They are each divided further into four groups:

- W*: *clean* (less than 5% finer than 0.074 mm); *well graded* (uniformity coefficient  $C_U$  greater than 4 for gravels or 6 for sands, and coefficient of curvature  $C_C$  between 1 and 3).
- P*: *clean* (less than 5% finer than 0.074 mm); *poorly graded* ( $C_U$  less than 4 for gravels or 6 for sands, or gap-graded because  $C_C$  not between 1 and 3).
- C*: *dirty* (more than 12% finer than 0.074 mm); *plastic clayey fines* ( $I_P$  greater than 7%, also plots above A-line in plasticity chart).
- M*: *dirty* (more than 12% finer than 0.074 mm); *non-plastic silty fines* ( $I_P$  less than 4%, or plots below A-line in plasticity chart).

The soils are represented by symbols such as *GW* or *SP*. Borderline materials are represented by a double symbol, as *GW-GP*.

The fine-grained soils are divided into three groups: inorganic silts (*M*), inorganic clays (*C*), and organic silts and clays (*O*). The soils are further divided into those having liquid limits lower than 50% (*L*), or higher (*H*).

The distinction between the inorganic clays *C* and the inorganic silts *M* and organic soils *O* is made on the basis of a modified plasticity chart (Fig. 8.2). Soils *CH* and *CL* are represented by points above the A-line, whereas soils *OH*, *OL*, and *MH* correspond to positions below. Soils *ML*, except for a few clayey fine sands, are also represented by points below the A-line. The organic soils *O* are distinguished from the inorganic soils *M* and *C* by their characteristic odor and dark color or, in doubtful instances, by the influence of oven-drying on the liquid limit (Article 7). In the field, the fine-grained soils can

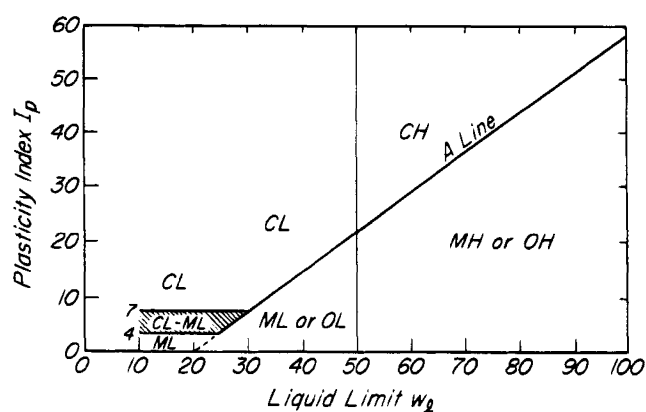


**Figure 8.2** Modified Plasticity Chart for use with Unified Soil Classification System. Soils represented by points within shaded area are considered borderline and are given dual symbols (after USBR 1974).

be differentiated by their dry strength, their reaction to the shaking test, or their toughness near the plastic limit (Article 7). The pertinent characteristics are indicated in Table 8.2. Borderline materials are represented by a double symbol, as *CL-ML*.

The Unified Soil Classification System permits reliable classification on the basis of relatively few and inexpensive laboratory tests. With experience it also provides a practicable basis for visual or field classification. Like all procedures based on grain size or the properties of remolded materials, it cannot take into consideration the characteristics of the intact materials as found in nature. Hence, it can serve only as a starting point for the description of the engineering properties of soil masses or soil deposits.

### Selected Reading

The definitive discussion of soil classification, as well as the basis for the Unified Soil Classification System, are contained in Casagrande, A. (1948). "Classification and identification of soils," *Trans. ASCE*, **113**, pp. 901–992.

For a more detailed discussion, see ASTM D2487.

## ARTICLE 9 MINIMUM REQUIREMENTS FOR ADEQUATE SOIL DESCRIPTION

In Article 8 suitable procedures were described for dividing soils into several large groups on the basis of their grain-size characteristics and their plasticity. If the group to which a given soil belongs is known, the more outstanding physical characteristics of the soil are also generally known. However, each group includes soils with a great

variety of properties and, furthermore, every soil can occur in the field in very different states. In order to distinguish among the individual members of each group and the different states of each member, two different procedures can be used. Either the principal groups can be subdivided further, or else the group name can be supplemented by numerical values representing the pertinent index properties.

The first of these two procedures is suitable for classifying the soils within geographically limited districts, because within such districts the number of different types and states of soil is likely to be fairly limited. Consequently, the method is used extensively and to advantage by local construction organizations such as state highway departments. However, attempts to use a similar procedure for establishing a universal system of soil classification have little prospects for success, because the required terminology would inevitably be so complex that it would lead to ultimate confusion.

The second procedure, on the other hand, can be used profitably under any circumstances, provided those index properties that are indicative of the essential physical characteristics of the soil are chosen. The properties required for adequate description of the various types of soil are summarized in Table 9.1. The soils listed in this table have been described in Article 2, which contains all the information required for at least a tentative classification of the soil. After the type has been recognized, the engineer turns to Table 9.1 and performs all the soil tests prescribed for this type. The test results represent the criteria for distinguishing among different soils of the same type.

With the exception of till, hardpan, and peat, all the soils listed in Table 9.1 consist either exclusively of coarse grains such as sand and gravel, or exclusively of fine grains having the size of silt or clay particles. Soils that consist of a mixture of these ingredients are regarded as composite. To describe a composite soil, it is first necessary to determine the natural void ratio  $e$ , the natural water content  $w$ , and the grain-size distribution. The soil is then divided into two parts, one consisting of all the grains larger than about 0.07 mm (width of the openings in the 200-mesh sieve), and the other of the remainder. The coarse fraction is submitted to the classification tests prescribed for sand and gravel, and the remainder to those for silts and clays.

If the soils encountered on a given job are submitted to tests other than those listed in Table 9.1, the significant results of these tests should be included in the record. Since soil strata are seldom homogeneous, even an apparently homogeneous soil stratum cannot be considered adequately described unless the index properties of several samples from the stratum have been determined. The record should also contain a brief

**Table 8.2 Classification of Fine-Grained Soils Unified Soil Classification System**

Group	Dry Strength	Reaction to Shaking Test	Toughness at Plastic Limit
ML	None to very low	Rapid to slow	None
CL	Medium to high	None to very slow	Medium
OL	Very low to medium	Slow	Slight
MH	Very low to medium	Slow to none	Slight to medium
CH	High to very high	None	High
OH	Medium to high	None to very slow	Slight to medium

Table 9.1 Data Required for Soil Identification

Type of Soil	General Information						Results of Classification Tests											
							Intact Samples <sup>1</sup>						Disturbed Samples					
	Color	Odor <sup>2</sup>	Texture <sup>3</sup>	Dilatancy <sup>4</sup>	Grain properties <sup>5</sup>	Dry strength <sup>6</sup>	Natural void ratio $e^7$	Natural water content $w$	Unit weight, natural state	Unit weight, oven-dried $\gamma_d$	Unconf. compressive strength $q_u$	Sensitivity $S_t^8$	Max. void ratio $e_{\max}^9$	Min. void ratio $e_{\min}^{10}$	Liquid limit $w_L^{11}$	Plastic limit $w_p^{12}$	Mechanical analysis <sup>13</sup>	Carbonate content <sup>14</sup>
Hardpan <sup>15</sup>	x	-	x	-	x	-	-	-	x	-	-	-	-	-	-	-	-	-
Sand, gravel	x	-	-	-	x	-	x	-	-	-	-	-	x	-	-	-	-	-
Inorganic silt	x	-	x	x	-	x	-	x	x	x	x	x	-	-	x	x	x	x
Organic silt	x	x	x	x	-	x	-	x	x	x	x	x	-	-	x	x	x	x
Clay	x	-	x	-	-	x	-	x	x	x	x	x	-	-	x	x	-	x
Organic clay	x	x	x	-	-	x	-	x	x	x	x	x	-	-	x	x	-	x
Peat	x	x	x	-	x	-	-	-	x	x	-	-	-	-	-	-	-	-
Till	x	-	-	-	x	-	x	x	x	-	-	-	x	x	-	-	x	-
Tuff, fine-grained	x	-	x	-	-	x	-	-	x	x	x	x	-	-	x	x	x	-
Loess <sup>16</sup>	x	-	x	x	-	x	x	x	x	x	x	-	x	x	x	x	x	x
Modified loess	x	-	x	x	-	x	x	x	x	x	x	-	x	x	x	x	x	x
Adobe	x	-	x	x	-	x	x	x	x	x	x	-	x	x	x	x	x	x
Marl	x	-	x	x	-	x	-	x	x	x	x	x	-	-	x	x	x	x
Lake marl	x	-	x	x	-	x	-	x	x	x	x	x	-	-	x	x	x	x
Gumbo	x	-	x	-	-	x	-	x	x	x	x	x	-	-	x	x	x	x

<sup>1</sup> If no undisturbed or tube samples were obtained, use the spoon samples (Article 11.3.2).

<sup>2</sup> If the odor is faint, heat the sample slightly. This intensifies the odor.

<sup>3</sup> Describe appearance of fresh fracture of intact sample (granular, dull, smooth, glossy). Then rub small quantity of soil between the fingers, and describe sensation (floury, smooth, gritty, sharp). If large specimens break up readily into smaller fragments describe appearance of walls of cracks (dull, slickensided) and average spacing of cracks.

<sup>4</sup> Perform shaking test, page 4. Describe results (conspicuous, weak, none) depending on intensity of phenomena observed.

<sup>5</sup> Describe shape (angular, subangular, subrounded, rounded, well rounded) and mineralogical characteristics of macroscopic soil particles only. Mineralogical characteristics include types of rocks and minerals represented among the grains as far as they can be discerned by inspection under the hand lens. Describe rock fragments (fresh, slightly weathered, or thoroughly decomposed; hard or friable). If a sand contains mica flakes, indicate mica content (slightly, moderately, or very micaceous). In connection with peat, the term grain properties refers to the type and state of preservation of the predominant visible remnants of plants such as fibers, twigs, or leaves.

<sup>6</sup> Crush dry fragment between fingers and indicate hardness (very low, low, medium, high, very high).

<sup>7</sup> If no undisturbed samples were obtained, substitute results of standard penetration test (Article 11.3.2) or equivalent.

<sup>8</sup> Applies only to clay and fine silt at a water content above the plastic limit.

<sup>9</sup> Prepare sample as described on page 20.

<sup>10</sup> Determine as described on page 20 for sands or gravels, or for other materials by means of Proctor method, page 312.

<sup>11</sup> If soil may be organic, determine  $w_L$  first in fresh state and then after drying in oven at 105°C.

<sup>12</sup> In addition to numerical value of  $w_p$ , state whether threads were tough, firm, medium, or weak.

<sup>13</sup> Present results either in form of semilogarithmic graph, or else by numerical values of  $D_{10}$  and  $C_u = D_{60}/D_{10}$  (Article 5) accompanied by adjectives indicating the type of grain-size grading (see Fig. 5.2.)

<sup>14</sup> Calcium carbonate content can be detected by moistening the dry material with HCl. Describe result of test (strong, weak, or no effervescence).

<sup>15</sup> Add to data on texture a description of general appearance, structure, and degree of cohesiveness of chunks in fresh state and after soaking in water.

<sup>16</sup> Add to data on texture a description of the macroscopic features of the loess, such as diameter and spacing of root holes.

statement of whatever can be learned about the geological history of the stratum.

Most large engineering construction organizations, such as the Corps of Engineers of the United States Army, the United States Bureau of Reclamation, and many state highway departments, maintain soil laboratories in which classification tests are made routinely. However, the results of these tests are of such practical importance that they should also be made by every engineer who deals with soils. The performance of the tests increases familiarity with the various properties of the soils and the test results greatly increase the value of the engineer's field records.

After personally testing several dozen samples of soil from one locality, the engineer can estimate the index properties of most of the soils from that locality without any tests and can discriminate among different soils or

different states of the same soil which previously seemed identical.

Every engineer should develop the habit of expressing the plasticity and grain-size characteristics of soils by numerical values rather than by adjectives. The grading of a sand should be expressed by the estimated value of the uniformity coefficient,  $C_U = D_{60}/D_{10}$  (Article 5) and not by the words "well graded" or "poorly graded." The degree of plasticity should be indicated by the estimated value of the plasticity index  $I_p$  (Article 7) and not by the words "trace of plasticity" or "highly plastic." This habit is so important that it should be encouraged from the beginning by the instructor in the classroom. The use of the numerical system prevents misunderstandings and is an incentive to check from time to time the degree of accuracy of the estimates. Without occasional check tests the progressive deterioration of the ability to estimate may pass unnoticed.

## CHAPTER 2

### *Soil Exploration*

#### ARTICLE 10 PURPOSE AND SCOPE OF SOIL EXPLORATION

##### 10.1 Definition of Soil Exploration

The design of a foundation, an earth dam, or a retaining wall cannot be made intelligently unless the designer has at least a reasonably accurate conception of the physical properties of the soils involved. The field and laboratory investigations required to obtain this essential information constitute the *soil exploration*.

Until about the 1930s soil exploration was consistently inadequate because rational methods for soil investigation had not yet been developed. On the other hand, at the present time the amount of soil exploration and testing and the refinements in the techniques for performing the investigations are often quite out of proportion to the practical value of the results. To avoid either of these extremes, the exploratory program must be adapted to the soil conditions and to the size of the job.

##### 10.2 Influence of Soil Conditions on Exploratory Program

If the foundation of an important structure is to be established above a fairly homogeneous layer of clay, a considerable amount of soil testing of samples of excellent quality may be justified because the test results permit a relatively accurate forecast of both the amount and the rate of settlement. On the basis of such a forecast, it may be possible to eliminate the danger of harmful differential settlement at reasonable expense by appropriate distribution of the loads or by suitable adjustment of the depths of subbasements beneath different parts of the structure, or it may become clear that a deep foundation is necessary. On the other hand, if a similar structure is to be located above a deposit consisting of pockets and lenses of sand, clay, and silt, the same amount of testing would add very little to the information that could be obtained merely by determining the index properties of several dozen representative samples extracted from exploratory drill holes. Additional data of far greater significance than

those obtainable from extensive laboratory soil tests could be secured in a shorter time and at less expense by subsurface soundings along closely spaced vertical lines, because such soundings would disclose whatever weak or compressible spots might be located between drill holes. The discovery of such spots is more important than an accurate knowledge of the properties of random samples.

The preceding remarks demonstrate that, if the soil profile is complex, an elaborate program of soil testing is likely to be out of place. Hence, the methods of soil exploration must be chosen in accordance with the type of soil profile at the site of the construction operations. The following paragraphs describe the significant characteristics of the principal types of soil profiles commonly encountered in the field.

The term *soil profile* indicates a vertical section through the subsoil that shows the thickness and sequence of the individual strata. The term *stratum* is applied to a relatively well-defined layer of soil in contact with other layers of conspicuously different character. If the boundaries between strata are more or less parallel, the soil profile is said to be *simple* or *regular*. If the boundaries constitute a more or less irregular pattern, the soil profile is called *erratic*.

From the ground surface to a depth of about 2 m, and in some localities to a greater depth, the physical properties of the soil are influenced by seasonal changes of moisture and temperature and by such biological agents as roots, worms, and bacteria. The upper part of this region is known as the A-horizon. It is subject primarily to the mechanical effects of weathering and to the loss of some constituents due to leaching. The lower part is referred to as the B-horizon, where part of the substances washed out of the A-horizon are precipitated and accumulate.

The properties of the soils in the A- and B-horizons are chiefly the concern of agronomists and road builders. Foundation and earthwork engineers are interested pri-

marily in the underlying parent material. Beneath the B-horizon the character of the soil is determined by the raw materials from which it is derived, by the method of deposition, and by subsequent geological events. The individual strata that constitute the soil profile beneath the B-horizon may be fairly homogeneous, or they may be composed of smaller elements having properties that depart more or less from the average. The shape, size, and arrangement of these smaller elements constitute the *primary structure* of the deposit. Because most soils have been deposited under water, the most common primary structure is *stratification*. If the individual layers are not thicker than about 20 mm and are of roughly equal thickness, the soil is called *laminated*. For example, the varved clays described in Article 2 are laminated soils. The action of ice, landslides, torrential streams, and several other agents leads to the formation of deposits with an *erratic structure*. Such deposits have no well-defined pattern. The more the structure of a mass of soil approaches the erratic type, the more difficult it is to determine the average values of the soil properties and the more uncertain is the result.

In stiff clays and other soils with great cohesion the primary structure may be associated with a *secondary structure* that develops after the soil is deposited. Most important among the secondary structural characteristics are systems of hair cracks, joints, or slickensides. Hair cracks and joints occur commonly in flood-plain clays consisting of layers, each of which was temporarily exposed to the atmosphere after deposition. Shrinkage caused cracks to form during the period of exposure. Slickensides are smoothly polished surfaces that may be the result of volume changes produced by chemical processes or of deformations produced by gravity or tectonic forces involving slippage along the walls of existing or newly formed joints. Secondary structure is also present in many residual soils in the form of relict joints, shears, or other features present in the rock before weathering reduced the material to a soil.

If a cohesive stratum has a well-developed secondary structure, the results of laboratory or field penetration tests may give an erroneous conception of its mechanical properties. Therefore, in connection with such soils, the engineer must rely on judgment based on experience with similar materials and, in some instances, on large-scale field tests.

Experience has shown that the physical properties of almost every natural soil stratum vary to a considerable extent in the vertical direction and to a smaller degree in horizontal directions. This fact is strikingly demonstrated by the variation in natural water content of clays that appear on visual inspection to be homogeneous. The results of an investigation of the variation in water content within a layer of clay in Boston are shown in Fig. 10.1. The variations within a 300-mm layer are shown in Fig.

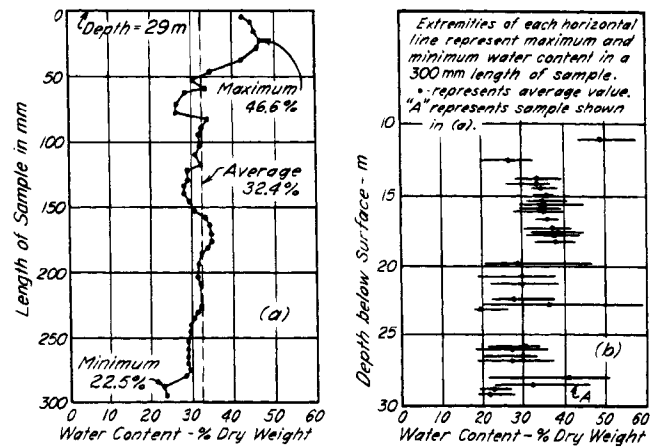


**Figure 10.1** Variation in natural water content of clay from one drill hole in Boston. (a) Variation within vertical distance of 300 mm. (b) Variation throughout entire boring (after Fadum 1948).

10.1a and those within a 20-m layer in Fig. 10.1b. If a mass of clay appears to be stratified or lenticular, its water content is likely to vary with depth in a manner like that shown in Fig. 10.2.

If a soil stratum is nonuniform, adequate information concerning the variations in the soil properties can be obtained only by securing continuous cores from top to bottom of the stratum and performing soil tests on every part of the core material, or else by performing suitable tests in the field. Field tests of one type, exemplified by subsurface soundings, furnish continuous records of the variations in penetration resistance of the stratum. Those

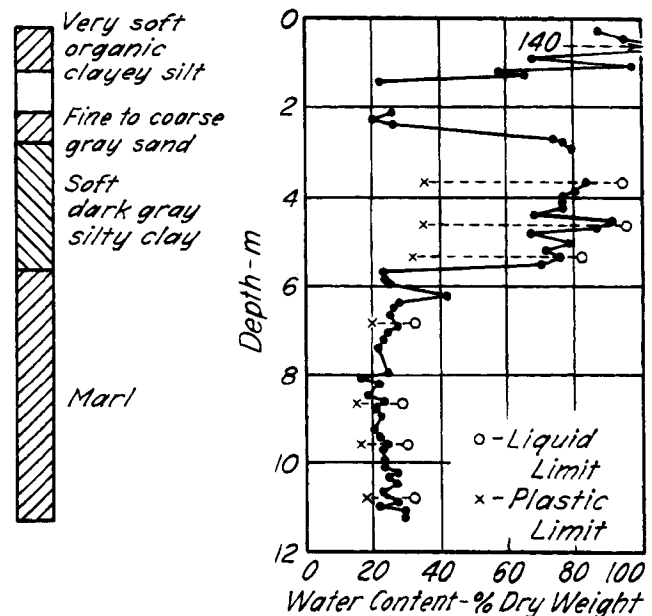


**Figure 10.2** Variation in natural water content of samples from boring in composite shore deposit.

of a second type, represented by pumping tests for determining permeability, furnish average values of the soil property under investigation.

### 10.3 Influence of Size of Project on Exploratory Program

In the preparation of a program for soil exploration the magnitude of the job must also be considered. If the proposed construction operation involves only a small expenditure, the designer cannot afford to include more in the investigation than a small number of exploratory borings and a few classification tests on representative soil samples. The lack of accurate information concerning the subsoil conditions must be compensated by using a liberal factor of safety in design. On the other hand, if a large-scale construction operation is to be carried out under similar soil conditions, the cost of even a thorough and elaborate subsoil investigation is usually small compared to the savings that can be realized by utilizing the results in design and construction, or compared to the expenditures that would arise from a failure due to erroneous design assumptions. Hence, on large projects extensive subsoil investigations are likely to be justified.

To adapt the exploratory program to the requirements of a given job and to obtain the essential data at minimum expenditure of time and money, the engineer in charge must be familiar with the tools and processes available for exploring the soil, with the methods for analyzing and digesting the results of laboratory and field tests, and with the uncertainties involved in the results obtained by the different methods of soil exploration. These subjects are discussed in the following two sections.

### 10.4 Causes of Misjudgment of Subsoil Conditions

Irrespective of the subsoil conditions and the program for borings and soundings, the exploration furnishes information only concerning the sequence of materials along vertical lines, commonly spaced no closer than 15 m, and concerning the significant physical properties of what are believed to be representative materials. On the basis of this rather fragmentary information, the designer is compelled to construct a soil profile by interpolation between drill holes or soundings, to divide the subsoil into zones consisting of materials with approximately the same engineering properties, and to estimate for each zone the average values of the pertinent soil parameters. Hence, the degree of reliability of the results of the computations depends entirely on the differences between the real and the ideal subsoil. If an unfavorable difference of an essential nature has escaped attention, the design may turn out to be unsatisfactory in spite of conscientious subsoil exploration.

Experience has shown that the causes of serious misjudgment of the subsoil conditions may be divided into three categories:

1. Influence on the test results of excessive soil disturbance or of significant differences between test and field conditions.
2. Failure to recognize or judge correctly the most unfavorable subsoil conditions compatible with the field data.
3. Inadequate contact between the design and construction organizations, resulting in failure to detect significant departures of conditions or of construction procedures from those the designer anticipated or specified (Terzaghi 1958a, 1963).

### 10.5 Observations during Construction

Design based on the most unfavorable assumptions is inevitably uneconomical, but no other procedure provides the designer in advance of construction with the assurance that the soil-supported structure will not develop unanticipated defects. However, if the project permits modifications of the design during construction, large savings can often be made by designing on the basis of the most probable rather than the most unfavorable possibilities. The gaps in the available information are filled by observations during construction, and the design is modified in accordance with the findings. This basis of design is called the *observational procedure*.

The observational procedure was practiced successfully throughout the ages in tunnel engineering, because the construction of permanent tunnel linings was usually preceded by the installation of temporary supports, and the observation of the performance of the temporary supports furnished the information required for adapting the design of the permanent lining to unanticipated unfavorable subsoil conditions. On the other hand, in earth-dam and foundation engineering the permanent structures are designed before the construction operations start, and the consequences of unanticipated sources of trouble do not appear until the structure is in an advanced state of construction or is in service.

To use the observational procedure in earthwork engineering, two requirements must be satisfied. First, the presence and general characteristics of weak or compressible zones must be disclosed by the results of the subsoil exploration before construction. Second, special provisions must be made to secure quantitative information concerning the undesirable characteristics of these zones during construction before it is too late to modify the design in accordance with the findings. These requirements could not have been satisfied until the mechanics of interaction between soil and water were clearly understood and adequate means for observation were developed. For projects of various kinds, the data required for



practicing the observational procedure are obtained by measuring pore pressures and piezometric levels; loads and stresses; horizontal, vertical, and angular displacements; and quantity of seepage. The means for making the measurements are well described in the literature (Dunnicliff 1988). Some examples of the observational procedure are given in Chapters 9 to 11. More detailed accounts of modifications of design during construction are given in the list of suggested reading.

### Selected Reading

Examples of the observational procedure, in which the design was modified as a consequence of observations during construction, are contained in the following references.

- Graftio, H. (1936). "Some features in connection with the foundation of Svir 3 hydro-electric power development," *Proc. 1st Int. Conf. Soil Mech., Cambridge MA*, **1**, pp. 284–290. Note especially the means to adapt the design and construction to the elastic properties of the ground.
- FitzHugh, M. M., J. S. Miller and K. Terzaghi (1947). "Shipways with cellular walls on a marl foundation," *Trans. ASCE*, **112**, pp. 298–324.
- Zeevaert, L. (1957). "Foundation design and behavior of Tower Latino Americana in Mexico City," *Géot.*, **7**, No. 3, pp. 115–133.
- Casagrande, A. (1960). "An unsolved problem of embankment stability on soft ground," *Proc. 1st Panamerican Conf. Soil Mech. and Found. Eng., Mexico*, **2**, pp. 721–746.
- Terzaghi, K. (1960d). "Stabilization of landslides," Series of memoranda contained in *From theory to practice in soil mechanics*, New York, John Wiley and Sons, pp. 409–415.
- Terzaghi, K. and T. M. Leps (1960). "Design and performance of Vermilion dam," *Trans. ASCE*, **125**, pp. 63–100.
- Terzaghi, K. and Y. Lacroix (1964). "Mission dam, an earth and rockfill dam on a highly compressible foundation," *Géot.*, **14**, pp. 14–50.
- Casagrande, A. (1965). "Role of the 'calculated risk' in earthwork and foundation engineering," *ASCE J. Soil Mech.*, **91**, No. SM4, July, pp. 1–40.
- Peck, R. B. (1969). "Advantages and limitations of the observational method in applied soil mechanics," *Géot.*, **19**, No. 1, pp. 171–187.

## ARTICLE 11 METHODS OF SOIL EXPLORATION

### 11.1 Principal Procedures

Every subsurface exploration should be preceded by a review of all available information concerning the geological and subsurface conditions at or near the site (Article 12.1). In most instances this information must be supplemented by the results of more direct investigations. The first direct step is usually to drill several holes into the ground by an expedient method and to obtain fairly intact

samples of soil from every stratum encountered by the drilling tools. In addition, more refined sampling operations, field tests, or both may be required. The samples provide material for an investigation of the soil properties by means of laboratory tests. Field tests such as subsurface soundings, in-place shear tests, or pumping tests supply direct information concerning the details of the soil profile and values for the physical properties of the soils *in situ*.

Under some circumstances geophysical methods of exploration may be useful. By means of observations at the ground surface they provide information regarding the position of the boundary between soil and rock. If the rock is sound and its upper surface is not too uneven, the position and topography of the rock surface can be determined more cheaply and rapidly than by borings. Under favorable conditions geophysical methods have also been used successfully to determine the location of the boundaries between different soil strata and to obtain information about the physical properties of these strata. However, geophysical methods should not be relied on unless the findings are adequately checked by borings or other direct means of investigation.

The methods by which samples are obtained are selected to suit the requirements of the project. On the other hand, the procedures for drilling the holes through which the samplers are inserted into and removed from the ground are determined largely by economy and site conditions. As a rule any one of several methods of drilling may be used in connection with a given sampling procedure. Therefore, in the following sections the methods of boring and sampling are described separately.

### 11.2 Boring

#### 11.2.1 Methods of Drilling

The cheapest and most expedient procedures for making borings are wash boring, rotary drilling, and auger drilling. Shallow holes up to about 3m deep are usually made with augers. To make deeper borings any of the methods can be used.

#### 11.2.2 Wash Borings

The most primitive equipment for making a wash boring (Mohr 1943) usually includes a set of 1.5-m lengths of pipe 60 mm in diameter, known as *casing*, which serves to support the walls of the hole; a weight for driving the casing into the ground; a derrick for handling the weight and casing; and wash pipe, 25 mm in diameter, in 1.5-m or 3-m lengths. A hose connection is made through a swivel head to the top of the wash pipe, and the lower end of the pipe is fitted with a chopping bit (Fig. 11.2c) provided with water ports so that the wash water can be pumped down the wash pipe and forced out of the ports. The equipment also includes a tub to store the water and a hand- or power-operated pump.

To start a wash boring (Fig. 11.1), the derrick is erected and a 1.5-m length of casing is driven about 1 m into the ground. A tee is attached to the top of the casing with its stem in a horizontal position, and a short pipe is inserted horizontally in the stem. The tub is placed under the end of the short pipe and filled with water. The wash pipe is lifted to a vertical position by means of a hand rope that passes over a pulley at the top of the derrick and is lowered into the top of the casing. The pump is started and water is circulated from the tub through the swivel head into the wash pipe, from which it emerges at the chopping bit and rises in the annular space between the wash pipe and the casing. It returns to the tub, carrying cuttings of soil, through the tee and horizontal pipe at the top of the casing. As the water circulates, the wash pipe is churned up and down and is rotated at the bottom of each stroke to cut the soil loose. The hole is advanced by the churning and washing, and additional casing is driven as needed.

While drilling proceeds, the driller observes the color and general appearance of the mixture of soil and water that comes out of the hole. Whenever a conspicuous change is noticed, the wash water is turned off and a spoon sample (Article 11.3.2) is taken. Spoon samples

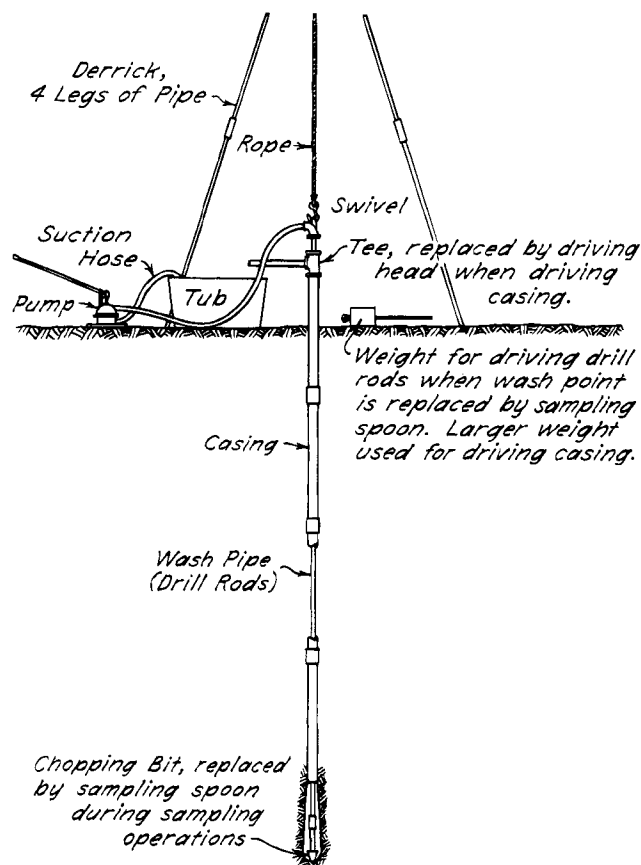


**Figure 11.1** Primitive apparatus for making wash boring (after Mohr 1943).

are also secured, one for each 1.5 m of depth, if the character of the subsoil appears to remain unaltered. Departures from this procedure may lead to serious misjudgment of the subsoil conditions. Even if the sampling is done conscientiously, the presence of clay strata within a stratum of sand may remain unnoticed.

When the boring operations are discontinued, for example to take a spoon sample, the water should be allowed to come to equilibrium in the casing. At this stage the elevation of the water table should be determined and recorded. It is not uncommon for water to rise from deeper strata to very much higher elevations than from the upper strata. Failure to recognize such a condition may have serious consequences. Less commonly the reverse condition may be encountered.

The advantage of the simple equipment described in the preceding paragraphs is that an experienced and conscientious driller, by the feel of the wash pipe as it is churned and rotated and by the color of the wash water, can usually detect changes in the character of the materials. Therefore, it is often possible to establish the elevations of the boundaries between lenses or strata with reasonable accuracy and to stop drilling to take samples representative of all the materials penetrated. The other methods of drilling, or more elaborate wash-boring equipment, do not share this advantage. Nevertheless, they are widely used because of their economy and speed. Their shortcomings with respect to the detection of changes in the subsurface conditions must be compensated by more frequent or even continuous sampling.

### 11.2.3. Rotary Drilling

The essential features of rotary drilling are similar to those of wash boring except that the drill rods and cutting bit are rotated mechanically while the hole is being advanced. The cutting bit contains ports from which the circulating water emerges and lifts the cuttings as it rises in the annular space outside the drill rods. The rods while rotating are pressed downward mechanically or hydraulically. They can be withdrawn and the cutting bit replaced by a sampling spoon whenever a sample is required.

In rotary drilling the circulating fluid often consists not of water but of *drilling mud*, usually a suspension of bentonite of a creamy consistency and a density of 1.09 to 1.15 Mg/m<sup>3</sup>. The higher density of the fluid with respect to that of water facilitates removal of the cuttings, and the slightly thixotropic character of the mud helps to prevent the accumulation of cuttings at the bottom of the hole in the interval of time between drilling and sampling. Moreover, the mud forms a thin layer of cohesive material on the walls of the hole which usually prevents the caving of those parts of the hole that are located in soil with little or no cohesion. Therefore, except for a short section at the top of the hole, casing may often be unnecessary. The use of drilling mud, however, prevents determining

the piezometric levels corresponding to the various pervious strata through which the hole may pass.

#### 11.2.4. Auger Borings

Shallow borings are almost universally made by means of augers. The auger, usually of the type shown in Fig. 11.2*a*, is turned into the soil for a short distance and then withdrawn with the soil clinging to it. The soil is removed for examination, the auger again inserted into the hole and turned further. If the hole fails to stand open to permit the insertion of the auger because of squeezing from the sides or because of caving, it must be lined with a casing having an inside diameter somewhat larger than the diameter of the auger. The casing should be driven to a depth not greater than that of the top of the next sample and should be cleaned out by means of the auger. The auger is then inserted into the clean hole and turned below the bottom of the casing to obtain the sample. Auger borings cannot be made in sand below the water table because the material will not adhere to the auger.

Cohesive soil brought to the surface by the auger contains all its solid constituents, but the structure of the soil is completely destroyed, and the water content is likely to be greater than that of the soil in place. Hence, the use of augers as drilling tools does not eliminate the necessity for obtaining spoon samples whenever the drill hole reaches a new stratum. Only the spoon samples

should be considered representative of the character of the undisturbed soil.

If a relatively firm stratum such as a layer of gravel is located above a very soft one, it is not unusual for an auger boring to fail to disclose the real position of the boundary between the two strata. In one instance the existence of a 2.5-m stratum of soft clay between two thick gravel layers was overlooked. In another the boundary between a bed of gravel and an underlying stratum of soft clay was reported 3 m below its real position. Errors of this type are caused by driving the casing below the level at which the auger is operating. The casing pushes or drags stony material into the clay layer. The errors can be avoided by keeping the cutting tool as far in advance of the casing as the character of the soil permits.

By means of mechanized equipment, auger borings can also be made to depths greater than 50 m and with diameters up to a meter or more. *Continuous flight augers* consist of segments that can be turned into the ground whereupon another segment is attached to the upper end, the assembly is again turned into the ground, another segment is attached, and the procedure repeated. The cuttings rise to the surface on the spirals, but the depth from which any given material comes cannot be ascertained. Therefore, the auger must be withdrawn frequently to permit examination of the material clinging to the bottom, or preferably to permit sampling. The *hollow-stem auger* (Fig. 11.3), a variation of the continuous flight auger, permits sampling below the bottom of the auger without removing the auger from the hole. It also eliminates the need for casing.

#### 11.2.5 Hammer Drilling

Drilling through deposits containing or consisting of cobbles and boulders is usually impractical by any of the foregoing procedures. Such materials, as well as other types, can be penetrated by the Becker hammer drill. The unique feature of the equipment is a double-walled casing, consisting of two concentric heavy pipes, driven into the ground by a diesel pile-driving hammer. Only the outer pipe is struck by the hammer; the inner pipe is separated from it by neoprene cushions except at the bottom where both pipes are attached to a hollow drill bit. As the casing is driven, compressed air is forced down the annulus between the pipes and then rises, carrying the choppings, through the inner pipe. The choppings may consist of intact soil particles with sizes up to the inside diameter of the drill bits, of fragments of larger particles broken by the bit, or of cylindrical masses of cohesive materials if clays are present. The choppings are passed through a cyclone separator. They represent all the materials through which the bit has advanced, but in a completely disturbed state. Cohesive soils are sometimes forced from the inner casing through a flexible tube to the ground where they may be laid out and inspected. By careful

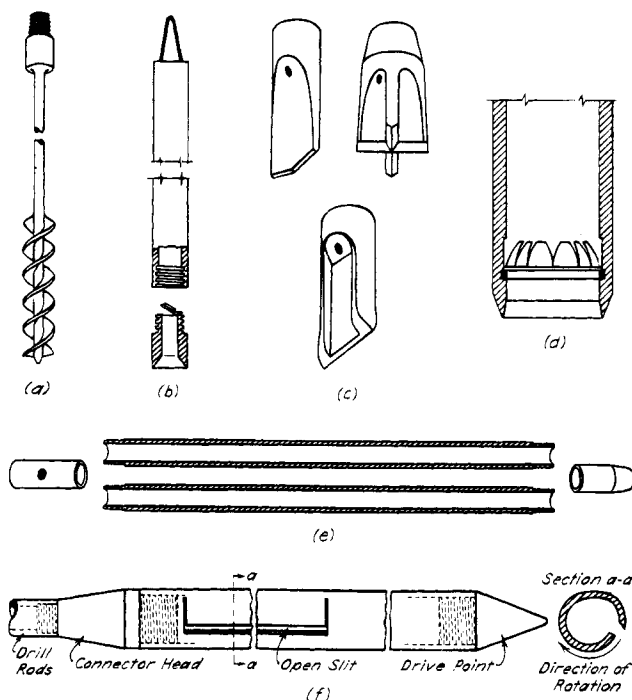


**Figure 11.2** Sampling tools for exploratory borings. (a) Earth auger. (b) Bailer. (c) Chopping bits. (d) Spring core catcher. (e) Split spoon sampler. (f) Scraper bucket.

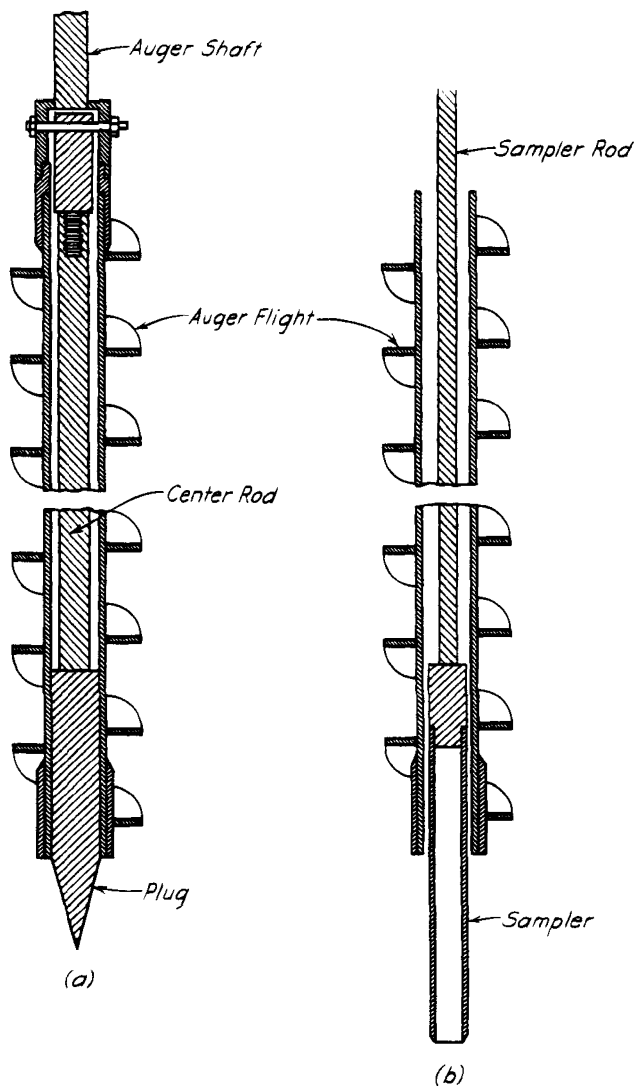


**Figure 11.3** Hollow stem auger. (a) Plugged while advancing auger. (b) Plug removed and sampler inserted to sample soil below auger.

attention to the character of the choppings as they appear, an approximate idea of the gross stratigraphy can be obtained. Penetration rates of as much as 30 m per hour can often be achieved.

### 11.2.6 Inspection Shafts

In stiff cohesive soils or stable sands above the water table it may be possible to auger a hole large enough for an inspector to be lowered to observe or sample the material. The inspection is made within the protection of a cage with windows through which the soil can be reached. In some localities such procedures are used extensively.

Many soils contain explosive or lethal gases. Therefore, no inspector should descend into such a hole until the air at the bottom has been sampled and adequate ventilation provided.

## 11.3 Sampling

### 11.3.1 Purpose

The cuttings or washings from exploratory drill holes are inadequate to furnish a satisfactory conception of the engineering characteristics of the soils encountered, or even of the thicknesses and depths of the various strata. On the contrary, such evidence more often than not is grossly misleading and has been responsible for many foundation failures.

Proper identification of the subsurface materials requires that samples be recovered containing all the constituents of the materials in their proper proportions. Moreover, evaluation of the appropriate engineering properties, such as the strength, compressibility, or permeability, may require the performance of laboratory tests on fairly intact or even virtually undisturbed samples. The expenditure of time and money increases rapidly as the requirements become more stringent with respect to the degree of disturbance that can be tolerated and with increasing diameter of sample. Therefore, on small projects or in the initial exploratory stages of large or complex projects, it is usually preferable to obtain relatively inexpensive, fairly intact samples from the exploratory drill holes. On the basis of the information obtained from these samples, the necessity for more elaborate sampling procedures can be judged.

### 11.3.2 Split-spoon Sampling in Exploratory Drill Holes

To obtain soil samples from exploratory drill holes, a *sampling spoon* is attached to the bottom of the wash pipe or the drill rod in place of the bit and is lowered to the bottom of the hole. It is forced or driven into the soil to obtain a sample and is then removed from the hole.

Sampling spoons for small-diameter exploratory borings commonly consist of a pipe with an inside diameter of about 40 mm and a length of 300 to 600 mm. The pipe is split lengthwise, as shown in Fig. 11.2e. Consequently the sampler is called a *split spoon*. While the sample is being taken, the two halves of the spoon are held together at the ends by short pieces of threaded pipe. One piece serves to couple the spoon to the wash pipe. The other, which has been sharpened, serves as the cutting edge while the spoon is driven into the soil.

According to the usual practice, the soil is extracted from the spoon by the foreman or the inspector, who inspects and classifies the material and places a small portion of it in a glass jar that is covered tightly and shipped to the engineer for visual inspection. Preferably, fairly large samples should be removed from the spoon, sealed in airtight jars, carefully identified, and shipped to a laboratory for determination of the index properties. Only part of each sample should be used for the tests. The

remainder should be retained in the jars, to be available for inspection by the bidders.

Clay samples obtained by means of a sampling spoon retain at least part of the characteristics of the undisturbed soil. On the other hand, samples of soils with a high permeability are almost always thoroughly compacted whether the soil *in situ* is loose or even fairly dense. Hence, the samples fail to inform the investigator on the relative density of the soil, although, as a rule, this property is far more significant than the character of the soil grains themselves.

A simple and widely used method of obtaining at least some information concerning the degree of compactness or the stiffness of the soil *in situ* consists of counting the number of blows of the drop weight required to drive the sampling spoon a specified distance into the ground. In the 1930's the Raymond Concrete Pile Co. standardized the equipment and procedures to be used by its various offices and began to correlate the results with construction experience (Fletcher 1965). The usefulness of the correlations led to the designation of the procedure as the *standard penetration test* (SPT) (Terzaghi and Peck 1948) or the *dynamic standard penetration test* (DSPT). The essential features included a drop hammer weighing 140 lb (63.5 kg) falling through a height of 30 in. (0.76 m) onto an anvil at the top of the drill rods, and a split spoon having an external diameter of 2 in. (50.8 mm) and a length of 30 in. (0.76 m). The spoon was attached to the drill rods and lowered to the bottom of the drill hole after the hole had been cleaned. After the spoon reached the bottom, the number of blows of the hammer was counted to achieve three successive penetrations of 6 in. (0.15 m). The number of blows for the first 6 in. was disregarded because of the disturbance likely to exist at the bottom of the drill hole; the numbers for the second and third 6-in. increments were added and designated the *standard penetration resistance*,  $N$ .

The procedure was widely adopted throughout the world, but it was soon recognized that the results were influenced by several factors that determined the amount of energy actually transmitted to the drill rods by the drop hammer. These factors fall into two categories: those that decrease the velocity of the drop hammer below the free-fall velocity for a 30-in. drop just before impact and those associated with the energy loss at impact (Skempton 1986). The first depend on the mechanism for releasing the drop hammer from its raised position, and the second on the details of the striking parts including the anvil between the hammer and drill rods.

By far the most frequently used procedure for operating the drop hammer is to lift the hammer by means of a rope held by the driller and looped around a rotating drum or *cathead*. By pulling the rope the operator can mobilize friction between the rope and cathead to exert a pull on the hammer; by releasing the pull when the hammer has

been lifted 30 in. the operator then permits the hammer to fall. The fall is inhibited to some extent by the residual friction between the rope and cathead and also by friction in the sheave or pulley at the top of the derrick. Somewhat different practices have developed in different countries regarding the dimensions of the cathead and the number of turns of the rope around it, as well as in the thickness or stiffness of the rope. To eliminate the friction losses associated with this procedure, trigger mechanisms have been developed to release the hammer freely from the specified 30-in. height. Measurements of hammer velocity at impact (Kovacs 1979, Yoshimi and Tokimatsu 1983) have indicated that the trigger mechanisms permit almost 100% of the free-fall energy to be developed before the impact, whereas the use of a cathead with the usual two turns of rope reduces the energy delivered to about 70% of the free-fall potential. The advantage of the more efficient trigger mechanisms is offset in many instances, however, by the greater expense of the equipment and the appreciably greater time required for the tests.

The ratio of the energy actually transmitted to the rods to that delivered by the hammer depends primarily on the efficiency of the anvil which, in turn, is a function of its weight. It varies from about 60% for heavy anvils to about 80% for light ones.

The combined efficiency, representing the ratio of the energy that reaches the rod to the available potential energy of the hammer, ranges from about 45 to 78% (Skempton 1986). In general, most correlations are based on  $N$ -values corresponding to a combined efficiency of about 60%.  $N$ -values corresponding to this efficiency are designated as  $N_{60}$ .

Values of  $N$  are also influenced by the length of the drill rods, by the presence or absence of liners in the standard split spoon, and by the diameter of the borehole. Approximate corrections to the measured  $N$ -values are indicated in Table 11.1.

**Table 11.1 Approximate corrections to Measured  $N$  Values**

Rod length:	>10 m	1.0
	6–10 m	0.95
	4–6 m	0.85
	3–4 m	0.75
Standard sampler		1.0
US sampler without liners		1.2
Borehole diameter:	65–115 mm	1.0
	150 mm	1.05
	200 mm	1.15

After Skempton (1986).

Details of the equipment and procedures are specified in ASTM D 1586. The standard split spoon is shown in Fig. 11.4.

In cohesionless or nearly cohesionless sand located below the water table, the sand is likely to drop out of the spoon while it is being lifted from the bottom of the drill hole. Bailers (Fig. 11.2*b*) are unsatisfactory, because the churning operation required to fill them washes the fine particles out of the sand. In order to recover sand samples that contain all their constituents, it is necessary to experiment with other devices such as a sampling spoon equipped with a core catcher made of spring steel (Fig. 11.2*d*). The core catcher is attached to the walls of the lower end of the sampling spoon. As the spoon is lifted, the springs bend toward the center of the sample and, if no coarse particle becomes caught between them, they join to form a dome-shaped bottom that supports the sample.

If the sampling spoon equipped with core catcher fails to retain the sand, reasonably complete samples can be obtained from 100-mm holes by means of the scraper bucket shown in Fig. 11.2*f*. It has an internal diameter of 60mm and a length of 0.75m. The lower end is plugged with a conical shoe. The upper half of the bucket is provided with a vertical slit. One side of the wall adjoining the slit is bent out and sharpened to form a cutting edge. The sampler is driven for its full length into the bottom of the hole and rotated in the direction shown in the figure, whereupon the cutting edge scrapes off the adjoining soil. The scraped-off material accumulates first in the lower half of the sampler and later in the upper part. The sample is thoroughly disturbed and partly segregated, but the loss of fines is very small.

If a stratum of gravel is encountered, no samples can be recovered from exploratory drill holes with a diameter as small as 60mm. It may even be impossible to drive the casing through the stratum, whereupon the hole must

be abandoned. The next hole should be lined with a casing having a diameter of at least 100mm.

### 11.3.3 Thin-walled Tube Samplers

If the project calls for reliable information concerning the shearing resistance or stress-deformation characteristics of a deposit, the degree of disturbance of the samples must be reduced to the minimum compatible with the benefits to be obtained from the information. Whatever type of sampler is used, a certain amount of disturbance of the soil is inevitable.

The degree of disturbance depends on the manner in which the sampler is forced into the soil and on the dimensions of the sampler. The greatest disturbance is caused by driving the sampler into the soil by successive blows of a hammer, and the best results can be obtained if the sampler is pushed into the ground at a high and constant speed. For samples of a given diameter forced into the soil by the same process, the degree of disturbance depends on the area ratio.

$$A_r(\%) = 100 \frac{D_e^2 - D_i^2}{D_i^2} \quad (11.1)$$

in which  $D_e$  is the external diameter and  $D_i$  is the internal diameter of the sampler (Hvorslev 1948). The area ratio of the split spoon for the standard penetration test is 112%, whereas the value should not exceed about 20% if disturbance is to be nominal.

If the exploratory borings are lined with casing having an internal diameter of 60 mm, the largest sampling device that can be used has an external diameter of 50 mm. Reasonably satisfactory samples can be obtained in 50-mm samplers made of steel tubing about 1.5 mm thick. Such samplers have an area ratio of about 13%. The tubes commonly have a length of 0.75 to 0.9 m. The lower ends are beveled to a cutting edge and are given a slight

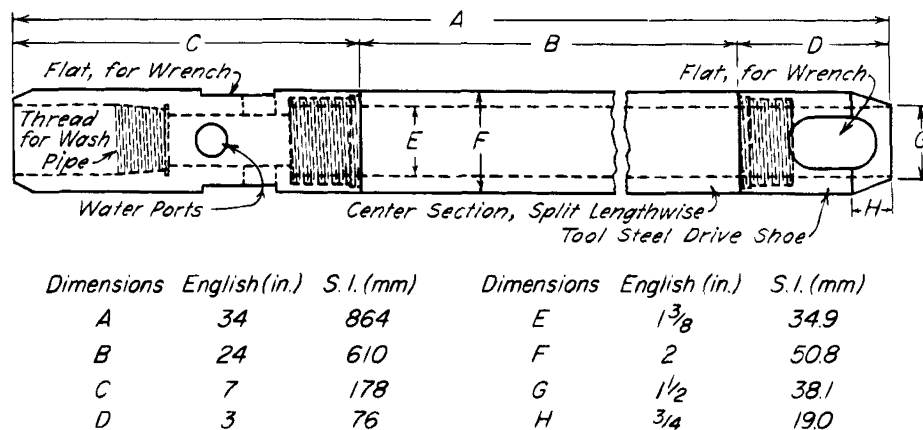


Figure 11.4 Split barrel sampler for Standard Penetration Test.

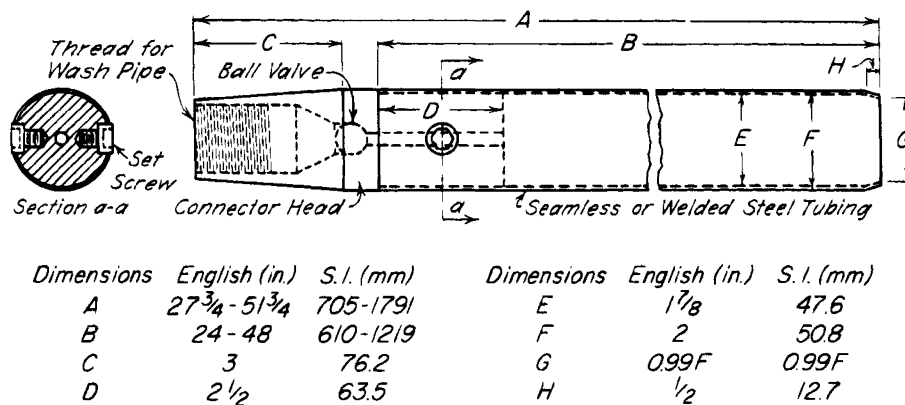


Figure 11.5 Fifty-millimeter thin-walled tube sampler.

inside clearance. The upper ends are fitted for attachment to the drill rods (Fig. 11.5).

To take a sample, the foreman attaches a tube to the bottom of the drill rods and lowers it into the hole that has previously been cleaned by a cleaning spoon or by washing. The sampler is then pushed downward from the bottom of the hole for a distance about 0.15 m less than the length of the tube. Preferably, the sampler is forced down in one rapid continuous movement. Driving with a hammer should be avoided. When the sampler has been forced down, the drill rods are rotated to shear the end of the sample, and the sampler is removed. The material at each end of the tube is carefully cleaned out for a short distance and smoothed so that metal disks can be inserted to protect the faces of the soil sample. Microfine wax is then poured against the metal disks to form a seal.

Details of samplers and procedures are specified in ASTM D-1587.

Usually, after two samples have been recovered, the casing is advanced to within about 0.1 m of the bottom of the hole and is cleaned out by a spoon or a water jet. The next two samples are then taken. By repeating this procedure, an almost continuous core record of the clay strata can be obtained. During all these steps the hole should remain filled with water. The casing should not be driven into the clay below a given level until the sampling operations have been carried out for at least the length of one sampling tube below this level. Otherwise, the sample consists not of relatively undisturbed soil but of material that has been forced into the casing. If the clay is very soft, it may squeeze into the hole left by the sampler so rapidly that casing must be driven before the next sample can be obtained. If the soil is fairly stiff, several samples can be taken in succession before additional casing is needed.

If tube samples have been taken on a given job, it is desirable to investigate the extent to which the consistency of the clay has been affected by the sampling operations. However, such information can be obtained only

at sites where the clay is exposed either in open excavations or on the bottom of shafts. Several sampling tubes are pushed into the clay on the bottom of the excavation and are allowed to remain in the soil while a bench containing the tubes is cut in the clay. A large sample is then carefully carved from the bench, and finally the filled sampling tubes are recovered.

Investigations of this kind were carried out in clays of various consistencies in tunnels of the Chicago subway. The results of tests at one location are shown in Fig. 11.6,

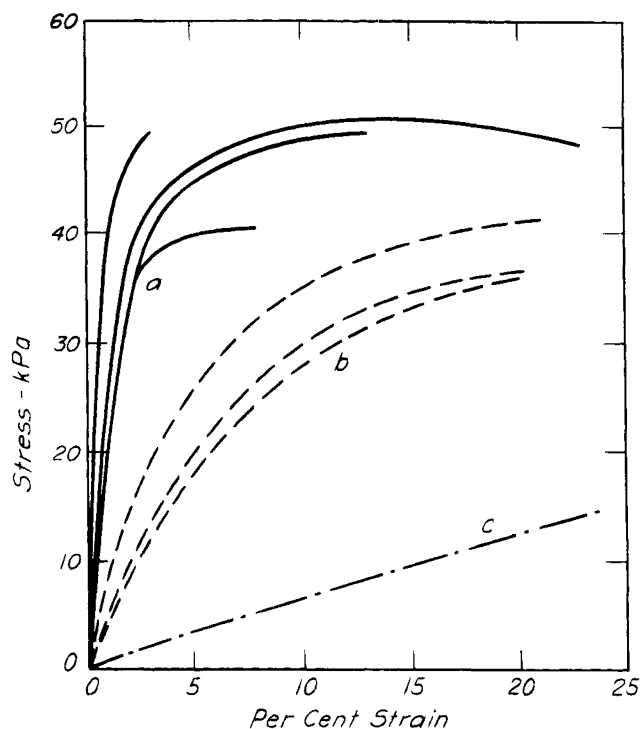


Figure 11.6 Stress-strain curves obtained by means of unconfined compression tests on Chicago clay. (a) Undisturbed samples cut from bench in tunnel. (b) 50-mm tube samples of same clay. (c) Completely remolded samples.

in which the plain curves *a* represent the stress-strain relations obtained by means of unconfined compression tests on the hand-carved samples, and the dash curves *b* those on the tube samples. The dash-dotted curve *c* represents the relation for one of the samples completely remolded at unaltered water content. On the basis of the results of several tests of this kind, it was concluded that the unconfined compressive strength of 50-mm tube samples of the clay was roughly equal to 75% of that of the hand-cut samples, whereas complete remolding reduced the strength of the hand-cut samples to 30% of its original value.

Similar samplers with a diameter of 90 mm are also in common use. With tube samplers of larger diameter the difficulty of retaining the samples increases, and samplers of other types are likely to be more satisfactory.

### 11.3.4 Piston Samplers

Part of the disturbance associated with tube sampling, especially in soft nonuniform cohesive soils, arises because the various portions of the soil *in situ* are not represented in the sample at their true thicknesses. When the empty sampler begins its downward thrust, the adhesion and friction on the outside of the tube combined with the tendency for the bottom of the drill hole toward instability may cause the soil to rise into the tube faster than the rate of descent of the tube. On the other hand, after the tube is partly filled, the adhesion and friction between the tube and the sample oppose the rise of the sample. Under extreme conditions the initial portion of the sample may act as a plug capable of displacing soft seams or layers so that they do not enter the sampler at all (Hvorslev 1948).

These conditions can be greatly improved by providing the sampling tube with a piston (Fig. 11.7) that closes the lower end of the tube until the sampler has arrived at the level of the top of the sample to be taken. The piston is then held at this elevation, in contact with the soil, while the tube is advanced around the piston and into the soil. In the early part of the stroke the presence of the piston prevents the entrance of a greater length of sample than the amount of penetration of the tube. In the later part of the stroke, the top of the sample cannot pull away from the piston without creating a vacuum; hence, at this stage the presence of the piston assists the rise of the sample into the tube. After the sampling tube has been advanced, the piston is fixed in its new position with respect to the tube, both elements are rotated to separate the sample from the underlying soil, and piston and tube are removed from the hole.

Piston samplers with small area ratios are capable of furnishing excellent samples of cohesive soils even if very soft and sensitive. The necessity for a separate piston rod rising through the drill rods to the ground surface

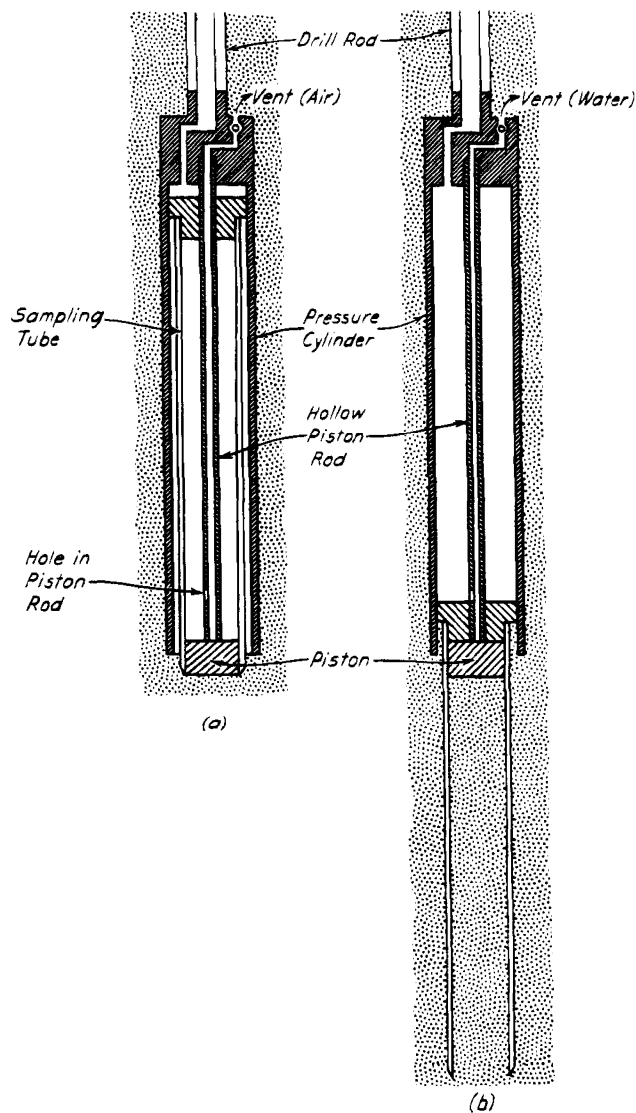


**Figure 11.7** Piston sampler of hydraulically operated type. (a) Lowered to bottom of drill hole, drill rod clamped in fixed position at ground surface. (b) Sampling tube after being forced into soil by water supplied through drill rod.

can be eliminated by using a hydraulically operated mechanism (Osterberg 1952).

### 11.3.5 Sampling Combined with Coring

Sampling by forcing thin-walled tubes into the soil cannot be done if the soil is too stiff or compact to permit penetration without damaging the cutting edge or buckling the tube. Moreover, even if a tube could be advanced by driving, the resulting disturbance, especially in brittle materials, would be excessive. In deposits containing successive soft and hard layers, the likelihood of successful sampling by tube or piston samplers is very remote.

Under these circumstances the *Pitcher sampler*, in which rock-coring techniques are adapted to tube sam-



pling, may prove satisfactory. The essential elements of the sampler are shown in Fig. 11.8. While the sampler is being lowered into the hole the thin-walled tube is suspended from the cutter barrel, and drilling fluid circulates downward through the tube and flushes the cuttings from the bottom of the hole. When the tube encounters the bottom it is pushed upward with respect to the cutter barrel, whereupon circulation is diverted downward in the annular space between tube and barrel, beneath the rotating cutter barrel, and upward alongside the barrel. If the soil to be sampled is soft, the spring at the head of the tube keeps the cutting edge of the tube well below the cutter barrel and the tube is pushed into the soil in a manner similar to that in ordinary tube sampling. If the soil is hard, the spring is compressed until the cutting edge of the tube is forced above the level of the bottom of the cutter barrel. As the barrel rotates it cuts an annular

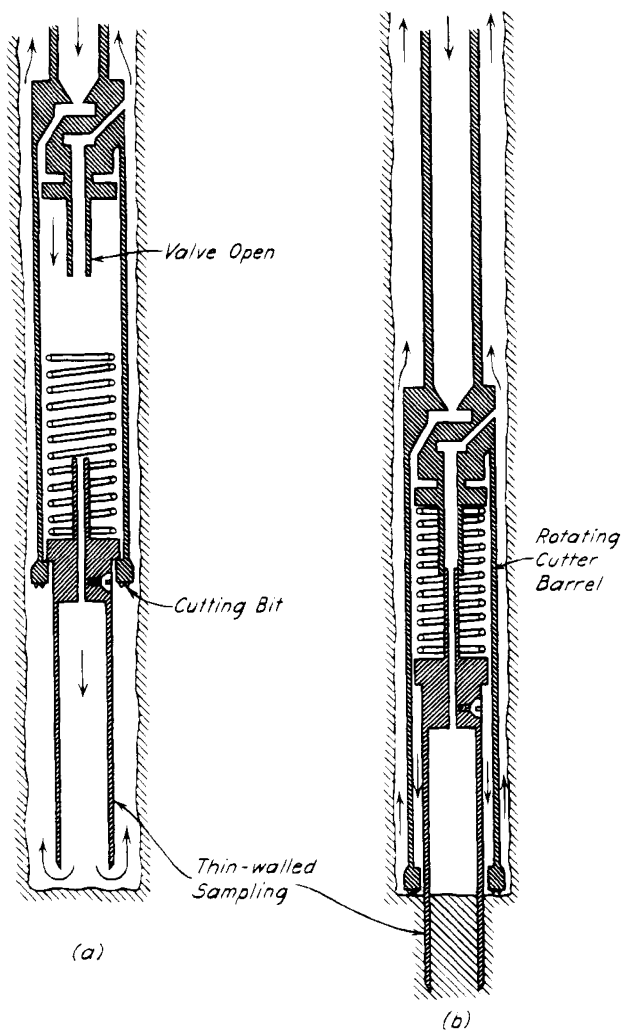


**Figure 11.8** Diagrammatic sketch of Pitcher sampler. (a) Sampling tube suspended from cutter barrel while being lowered into hole. (b) Tube forced into soft soil ahead of cutter barrel by spring.

ring leaving a cylinder of soil over which the tube sampler slides and protects the sample against further erosion by the circulating fluid. In this manner the sampler adapts itself to the consistency of the soil.

Another modification of rock-coring techniques, in which the sample enters a core barrel, has been used extensively by the United States Army Engineers and the United States Bureau of Reclamation in combination with a sampling tool known as the *Denison sampler* (Johnson 1940). Drilling mud is introduced into the hole in suspension through a set of hollow drill rods. The core barrel is located within a larger barrel (Fig. 11.9) provided with cutting teeth on the lower end. While drilling proceeds, the outer barrel rotates. The drilling mud flows downward through the annular space between the two barrels. It escapes through the openings between the cutting teeth and rises between the outer barrel and the walls of the hole into the upper part of the drill hole. The sampler has a length of 0.6 m and an inner diameter of 150 mm. It contains a thin cylindrical lining within which the sample may be removed from the tool, and it is equipped with a spring core catcher similar to that shown in Fig. 11.2d. While drilling proceeds, the sampler is pushed into the ground by means of jacks exerting a pressure between 10 and 20 kN. The jacks react against the drilling rig.

Stiff to hard cohesive soils including soft shales have been obtained successfully by the Denison sampler. In many instances even slightly cohesive or silty sands have

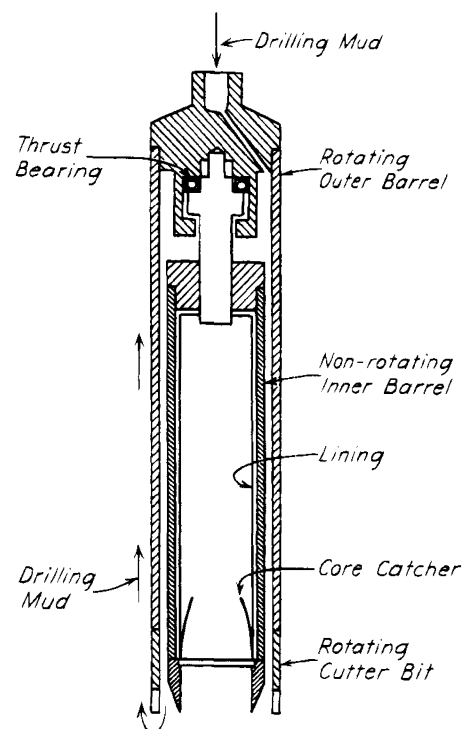


**Figure 11.9** Diagrammatic sketch showing principal features of Denison sampler.

been recovered with little disturbance. However, when used in clean sand below the water table, the sampler may come out of the hole empty. Strata of gravel may interfere with the drilling operations to such an extent that the drill hole must be abandoned.

### 11.3.6 *Hand-carved Samples in Clay*

On construction projects involving shafts, cuts, or tunnels in clays, the opportunity may exist to recover undisturbed samples without the necessity for drill holes. To obtain a large-diameter undisturbed sample in an open excavation or tunnel, the clay around the location of the proposed sample is carefully carved away, leaving a block somewhat larger than the sample standing in the form of a pedestal. Soft clay is usually carved with the aid of a tightly drawn piano wire or a loop of thin strap steel. In stiffer materials a knife or spatula may be more suitable.

The container for the sample consists of a thin-walled metal can with no projecting lugs or rim. When the pedestal has been carved into a size several centimeters larger than the final dimensions of the sample, the container, with top removed, is inverted and placed on top of the pedestal. The pedestal is carefully trimmed to the diameter of the container, a few centimeters at a time. As carving proceeds, the container is forced down. When it is full, the pedestal is cut off below the can by means of the piano wire. The soil is trimmed flush with the end of the container, and any voids left between the sample and the container are filled by pouring microfine wax around the periphery of the sample. Finally a metal top is placed on the container and sealed.

Samples obtained in this manner may be less disturbed, under many circumstances, than those recovered by any other procedure. On the other hand, if the relief of stress caused by the excavation is great enough to cause significant strains in the material to be sampled, the stress-deformation characteristics of the material may be unduly altered even before trimming the sample begins.

### 11.3.7 *Block Sampling in Bore Holes*

To reduce the stress relief associated with carving block samples, the sample may be trimmed while submerged in a drill hole filled with water or bentonite slurry. The Sherbrook sampler, for example, was developed to recover samples of quick clay with a diameter of 250 mm and a height of about 350 mm (Lefebvre and Poulin 1979). The sampler is lowered to the bottom of a 400-mm-diameter, fluid-filled borehole. Three cutting tools, each mounted on the bottom of a pipe connected to a drill rod, as shown schematically in Fig. 11.10, carve out a cylindrical annulus about 50 mm thick as the drill rod is rotated and gradually lowered. Drilling fluid emerges at the cutting tools, removes the cuttings, and stabilizes the wall of the bore hole. When the cutting tools reach

the bottom of the intended sample, components of a horizontal diaphragm, fastened at each cutting tool and located in the annular slot while drilling is in progress, are activated to close and thereby cut off the sample at its bottom. The closed diaphragm supports the sample as it is slowly withdrawn from the slurry-filled drill hole. Unless pieces of gravel are encountered that are displaced by the cutting tools, the recovered samples are of excellent quality.

The Laval sampler (LaRoche et al. 1981) can also obtain samples of excellent quality in sensitive clays to depths of 15 to 20 m. The samples, with diameters of 200 mm, are obtained in thin-walled tubes without a piston by overcoring in a slurry-filled hole.

### 11.3.8 *Quality of Samples*

It is apparent from the foregoing descriptions of various sampling methods that all samples experience disturbance; moreover, generally, the better the quality of the sample, the more expensive and time-consuming its recovery is likely to be. For some purposes, such as determining the index properties or evaluating the bearing capacity of the foundation of an inexpensive structure on a medium to stiff clay, the expense of obtaining samples of the highest quality may not be justified. On the other hand, when the compressibility or shearing strength of a soft clay must be known to evaluate the settlement or stability of a critical embankment or structure, even the best of samples may barely be adequate. Consequently, there is a need to establish a quantitative measure of the quality of samples, especially for soft clays and silts. One such measure, suggested by Andresen and Kolstad (1979) is the magnitude of the volumetric strain of a specimen when subjected in an oedometer test (Article 16.9) to the *in situ* vertical stress  $\sigma'_{vo}$  or in triaxial compression test (Article 17.2) to the effective vertical and lateral stresses under which it existed in the field. This is discussed further in Articles 16.9 and 20.4. Table 11.2 shows the specimen quality designation (SQD) based on the volumetric strain measured in the laboratory test. This characterization of specimen quality is mainly applicable to cohesive soils with values of overconsolidation ratio (Article 16.4) less than about 3 to 5.

### 11.3.9 *Sampling in Sand*

A distinction must be made between sampling in sand above and below the water table. Above the water table the soil moisture imparts to the sand a trace of cohesion. Samples of the slightly cohesive sand can be secured from drill holes for identification by means of sampling spoons equipped with core catchers (Fig. 11.2d). Less disturbed samples can be recovered by means of thin-walled piston samplers. Such samples are adequate for study of the grain-size distribution and stratification.

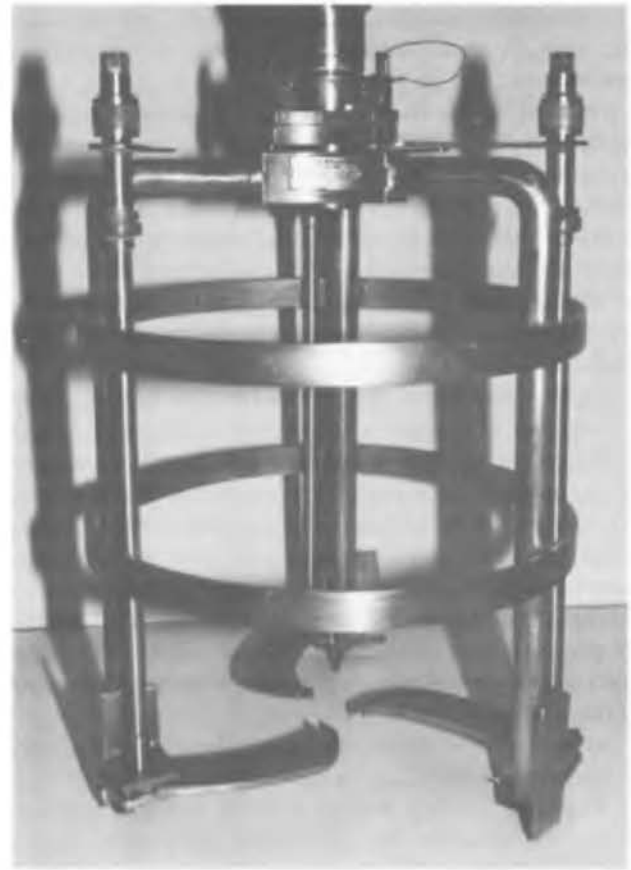
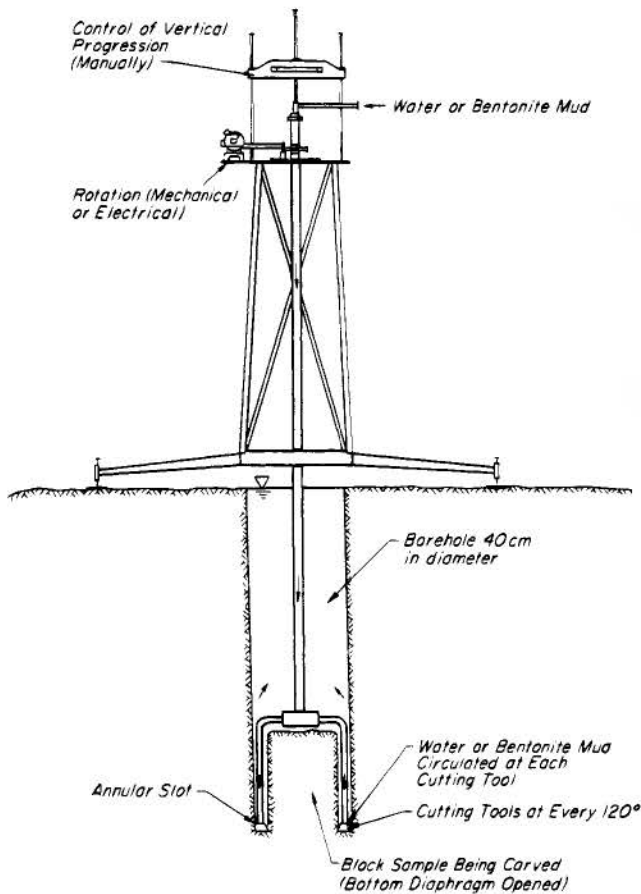


**Figure 11.10** (a) Diagrammatic sketch of Sherbrooke apparatus for carving block sample beneath drill hole (From Lefebvre and Poulin 1979). (b) Photograph of Sherbrooke sampler (Courtesy of G. Lefebvre).

**Table 11.2 Specimen Quality in Terms of Volumetric Strain**

Volumetric Strain (%)	Specimen Quality Designation
< 1	A
1–2	B
2–4	C
4–8	D
> 8	E

However, in most unsaturated sands the sampling operation is likely to cause a change in volume of the material that enters the sampler. Hence, if the nature of the job requires information concerning the natural void ratio of the sand, special procedures must be used. In many instances the most satisfactory procedure is to carve the samples from a shaft excavated for the purpose.

Before a sample is taken from a shaft, a bench is cut in the sand at the bottom. The surface of the sand is carefully leveled, and on it is placed a cylindrical metal shell with its axis in a vertical direction. The shell, of thin sheet steel, commonly has a diameter of 125 or 150 mm and a length of about 150 mm. It is pushed gently into the sand for its full length so that it encases a cylinder of sand. The surrounding sand is trimmed away, and the top of the sample is sealed with a metal cap that fits over the shell. If the surface of the sample is not level with the top of the shell, the space is filled with paraffin before the cap is attached. A shovel is used to cut off the sample several centimeters below the shell, and the sample is inverted. The surplus sand is removed so that the surface now on top can also be sealed with a metal cap.

Sands from below the water table ordinarily cannot be retained in the types of samplers in common use. Moreover, their void ratio is likely to be markedly altered unless the area ratio of the sampler is small. Satisfactory samples can sometimes be recovered by means of piston samplers, especially if the soil contains occasional cohe-

sive zones that may plug the bottom of the tube and retain the sand. In most instances, however, more elaborate procedures must be used.

Because of side friction a sample of saturated sand can be held in a tube, provided that at least a small capillary tension can be maintained in the pore water at the bottom of the tube. The tension cannot, exist, of course, if the bottom of the tube is submerged. Bishop (1948) devised sampling equipment in which compressed air is used to create capillary stresses that permit a sample to be recovered, but the equipment is complex and is rarely used.

As one alternative, the water table may be lowered to a level below the base of the sand stratum and a shaft excavated in the drained sand. If the shaft is unwatered by pumping from a sump, the water that flows toward the sump is likely to loosen the structure of the sand or, if the sand is already loose, the shaft may be invaded by a mixture of sand and water. For these reasons satisfactory results can be obtained only if the water table is lowered by pumping from well points (Article 43.4). The water level should be maintained at least 1 m below the bottom of the shaft.

As another alternative, undisturbed samples of water-bearing cohesionless sands and gravels can be obtained by an *in situ* freezing method (Adachi 1989). Yoshimi et al. (1985) describe the successful application of the method to obtain high-quality undisturbed samples of saturated loose and dense sands. At one site a 75-mm hole was drilled to a depth of 10 m with a rotary drilling machine using bentonite mud, and a 73-mm-diameter and 6-mm-thick steel pipe was placed in the hole. After plugging the bottom and removing the drilling fluid from inside the pipe, a copper pipe 15.9 mm in diameter and 3.5 mm thick was placed in the steel pipe as shown in Fig. 11.11a. Liquid nitrogen was supplied through the copper pipe for about 40 h to freeze the soil around the steel pipe to a diameter of about 600 mm. A 607-mm core barrel with hardened metal teeth was advanced around the frozen column of soil to a depth of 10.5 m using a boring machine and chilled bentonite mud (Fig. 11.11b.) The upper part of the frozen sand melted, because the temperature of the bentonite mud was not kept low enough; however, a large sample of sand below a depth of about 8 m was obtained as shown in Fig. 11.11c. The frozen sample was cut into blocks, wrapped in heavy vinyl sheet, and transported to the laboratory in a refrigerated truck. For undrained cyclic triaxial tests (Article 20.9) cylindrical specimens of frozen sand were trimmed. The frozen specimens were allowed to thaw after they were assembled in the triaxial apparatus (Article 17.2) and subjected to a confining pressure of 30 kPa. Such a procedure is very expensive and requires elaborate equipment.

Finally, water-bearing cohesionless sand below the bottom of a drill hole may be transformed into a cohesive

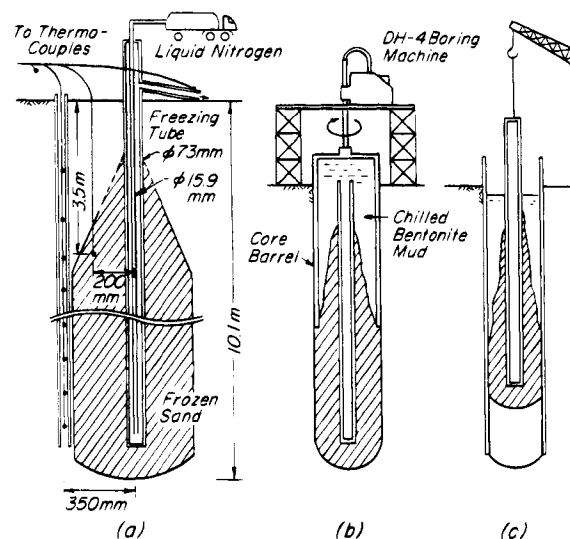


Figure 11.11 Undisturbed sampling of saturated sand by *in situ* freezing method (after Yoshimi et al. 1985).

material, whereupon it can be sampled by methods appropriate for clays. The transformation has been accomplished by injection of asphalt emulsion removed, after the sample has been recovered, by a solvent (Bruggen 1936), and by freezing a plug in the lower end of the sampling tube (Fahlquist 1941). These procedures are rather expensive and require elaborate equipment.

Fortunately, in most problems in practice, sufficiently reliable information concerning the properties of sands below the water table can be obtained by indirect means such as penetration or pumping tests.

## 11.4 Subsurface Soundings

### 11.4.1 Purpose of Subsurface Soundings

Subsurface soundings are used for exploring layers of soil with an erratic structure. They are also used to make sure that the subsoil does not contain exceptionally soft spots located between drill holes and to get information on the relative density of soils with little or no cohesion.

Experience shows that erratic soil profiles are far more common than regular ones. The results of test borings in subsoils with an erratic structure leave a dangerously wide margin for interpretation unless the spacing between drill holes is very small, and the cost of a set of closely spaced drill holes is likely to be prohibitive unless the area under investigation is also very small. Fortunately, significant changes in the character of the subsoil are commonly associated with a change in the resistance of the soil against penetration.

The effect of the relative density of sand on the penetration resistance is well known to every engineer experienced in pile driving. If the sand is very dense, a pile cannot be driven deeper than 3 to 5 m. Driving is very hard, and the resistance to penetration increases rapidly

with depth. If the sand is very loose, piles can be driven to any depth, and the increase of resistance with depth is small.

The variation of the penetration resistance of a soil along vertical lines can be determined rapidly at moderate expense by tests known as *subsurface soundings*. The tool used to make the tests is a *penetrometer*. One of the most widely used procedures for measuring resistance to penetration is the *standard penetration test*, described in Article 11.3.2, in which the penetrometer is the standard split spoon itself.

Whereas the standard penetration test furnishes only one value of resistance for each 1.5 m of depth, or under special conditions one value for each 0.75 m, many other types of subsurface soundings yield continuous or almost continuous penetration records.

If subsurface soundings are to be used to full advantage, the technique must be adapted to the soil conditions. For this reason a great many different procedures have been developed. They can be divided into two large groups, static and dynamic. In the static methods the sounding rod is pushed into the ground by static pressure. The dynamic methods consist of driving the rod by the impact of a drop hammer.

#### 11.4.2 Static Sounding Methods

Static sounding tools still in use were developed about 1917 by the Swedish State Railways (Fellenius et al. 1922), about 1927 by the Danish Railways (Godskesen 1936), and about 1935 by the Department of Public Works in the Netherlands (Barentsen 1936). Of these the latter, known as the *Dutch Cone* apparatus, has found wide application. In its primitive form it consists of a  $60^\circ$  cone with a base area of  $1000 \text{ mm}^2$  (Fig. 11.12a.) attached to the lower end of a 15-mm rod surrounded by a 20-mm pipe (Fig. 11.12c). The cone is pushed 0.5 m into the ground at a rate of 10 mm/s by one or two men who apply part of their weight to a crossbar attached to the upper end of the rod. The pressure exerted on the rod is registered by a Bourdon gage connected to a hydraulic cylinder located below the crossbar. After each downward stroke, the pipe is pushed down 0.5 m, and the stroke is repeated. The pressure exerted on the rod during each stroke is plotted against depth. The individual penetration records (Fig. 11.12d) furnish the data for constructing consistency profiles (Fig. 11.12e).

The original Dutch Cone apparatus is still useful for rapid detailed surveys of erratic deposits of soft clays, silts, and peats. One sounding to a depth of 12 m can be made in about 15 min. The equipment has been refined and mechanized, and in some models has been equipped with electric sensors, for rapid and detailed investigation of many types of deposits.

The most widely used mechanical device is the friction-cone penetrometer, Fig. 11.13a (Begemann 1953), or

*Push-Cone Penetrometer* (PCPT). The dimensions of the tip are the same as those of the original Dutch cone, but a jacket or sleeve is located above the tip to permit measuring the frictional resistance or adhesion separately from the point resistance. The assembly is pushed into the ground by drill rods (step 1, Fig. 11.13a) to the depth at which the measurements are to be made. The point is then pushed further, by a small rod inside the drill rods, at a rate of 20 mm/s while the force applied to the rods is measured. After the point has penetrated 40 mm the friction jacket is engaged, whereupon the point and sleeve advance together. The force applied to the inner rod then measures the sum of the point and frictional resistance. The frictional resistance is calculated as the difference between the two forces. The procedure is repeated at vertical intervals of 0.2 m. The point resistance  $q_c$  is calculated by dividing the force required to advance the point by the area of the point ( $1000 \text{ mm}^2$ ); the frictional resistance  $f_s$  is obtained by dividing the frictional force by the area of the sleeve in contact with the soil. It is inherent in the device that the point and frictional resistance are not determined at exactly the same depths. The rods are usually forced into the ground by a hydraulic jack reacting against a frame held down by ground anchors, or reacting against the weight of a truck-mounted mobile unit.

Penetrometers with electric sensing units, both with and without friction sleeves, are used increasingly. They usually have the same external dimensions as the original Begemann device so that advantage can be taken of the widespread experience with the mechanical cone. The Fugro penetrometer, Fig. 11.13b, is representative of several types; it has been found useful not only for investigating sites on land but also for underwater soundings for such structures as off-shore oil platforms. Because it is not necessary to advance the point independently of the friction sleeve, both resistances can be measured simultaneously and a continuous record obtained except for the necessary breaks when the drill rods must be extended.

Some cone penetrometers are equipped with porous filters to permit the direct measurement of the porewater pressure. Such a device is termed a *piezocone*. The one illustrated in Fig. 11.13c (Campanella et al. 1983) incorporates the porous filter directly behind the conical point. In other devices the filters have been placed closer to the point; experience indicates that in some soils the pressures measured at different locations differ significantly. The arrangement in Fig. 11.13c seems preferable, but in any event the location should be recorded.

Penetrometers of the dimensions shown cannot penetrate more than a few meters in dense sands, but they have been used to depths up to 40 m or more in soft soils. Below depths of about 20 m considerable deviations from verticality may occur, and the actual depth of the penetrometer may be inaccurately inferred from the length

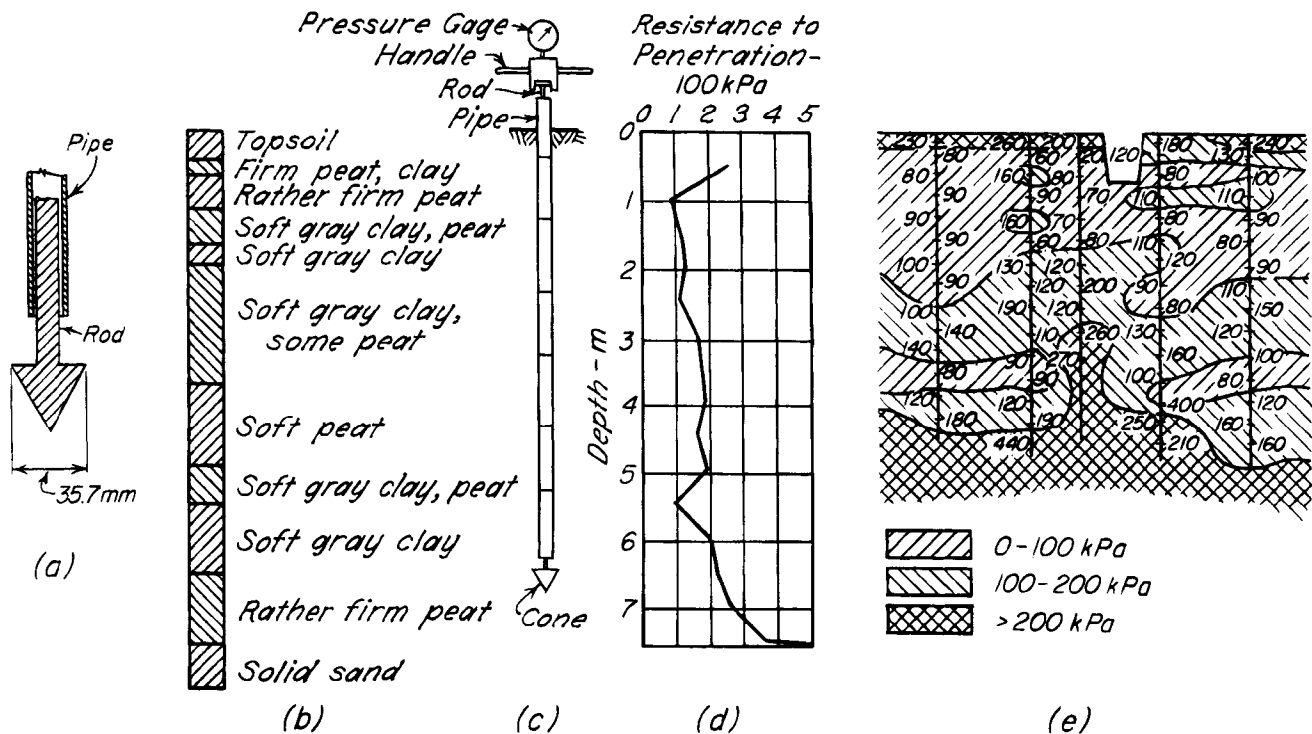


**Figure 11.12** (a) Original Dutch cone penetrometer. (b) Soil profile. (c) Penetrometer assembly. (d) Record from single penetration profile. (e) Soil profile along route of highway, showing variation in penetration resistance (after Barentsen 1936).

of the string of drill rods. To permit taking account of the deviation, some electric penetrometers are equipped with a sensor to measure the deviation. The device illustrated in Fig. 11.13c is an example.

Although the dimensions of the penetrometers shown in Fig. 11.13 are considered standard (ASTM D3441), larger devices for reaching greater depths or investigating more resistant soils have been used successfully for special applications.

Inasmuch as no samples are obtained by use of penetrometers, boring and sampling are needed for definitive information about the type of soil being investigated. Nevertheless, it has been found that the *friction ratio*  $f_s/q_c$  can be correlated in a general way with the type of soil (Begemann 1965). One such classification is shown in Fig. 11.14. It should be used with caution, however, because the presence of thin layers of different materials or of extrasensitive soils, among other possibilities, may lead to an erroneous classification.

The use of the cone resistance  $q_c$  in design, as well as other information derived from penetrometer data, is discussed in subsequent articles.

The cone penetration test and the standard penetration test (Article 11.3.2) are the most widely used tools giving quantitative data in soil exploration. With the aid of various empirical correlations the results have been applied

to a variety of practical problems, as discussed in Part III. Several comparisons have indicated that for sands the ratio between cone resistance  $q_c$  and standard penetration resistance  $N$  or  $N_{60}$  is a function primarily of the median particle size  $D_{50}$  of the sand, as illustrated in Fig. 11.15. On the basis of this relation, design procedures developed on the basis of one type of test can be used even if the available data are obtained from tests of the other type.

#### 11.4.3 Dynamic Methods

Dynamic sounding methods consist of driving a rod or casing with a drive point into the ground by means of a drop hammer and measuring the number of blows to achieve a given penetration. The most widely used procedure is the *standard penetration test* described in Article 11.3.2. The various uses and interpretations of this test are discussed in subsequent sections.

Inasmuch as the diameter of the spoon for the standard penetration test is only 50 mm, it is unsuitable for investigating deposits consisting largely of cobbles or boulders. Yet, the relative density of such deposits is often the overriding factor in determining their behavior under foundations, during pile driving, or in earthquakes. In many instances, general information is needed regarding the structure of deposits of erratic composition, such as river or shore deposits consisting of lenses of silt or

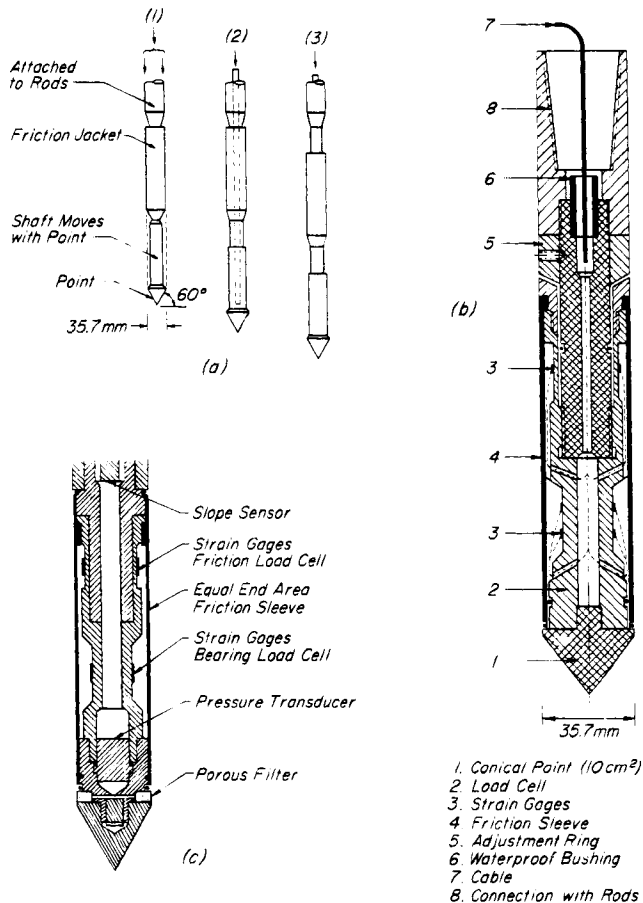


**Figure 11.13** Sleeve penetrometers. (a) Begemann Dutch cone (after Alperstein and Leifer 1976). (b) Fugro electric friction cone (after Hunt 1984). (c) Piezocone (after Campanella et al. 1983).

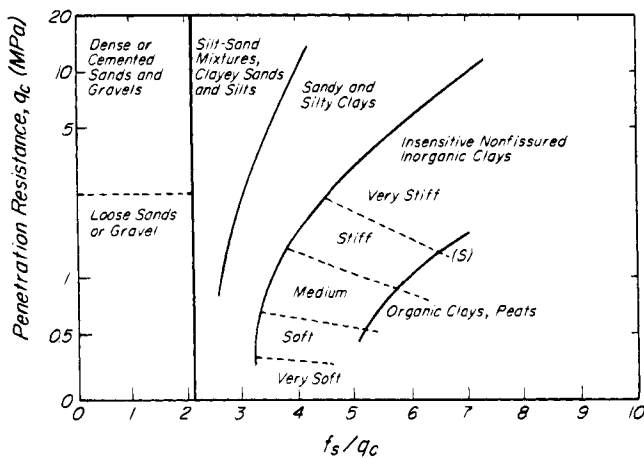


**Figure 11.14** Soil classification based on Begemann cone penetrometer tests (after Hunt 1984, based on Alperstein and Leifer 1976, Sanglerat 1972, and Schmertmann 1970).

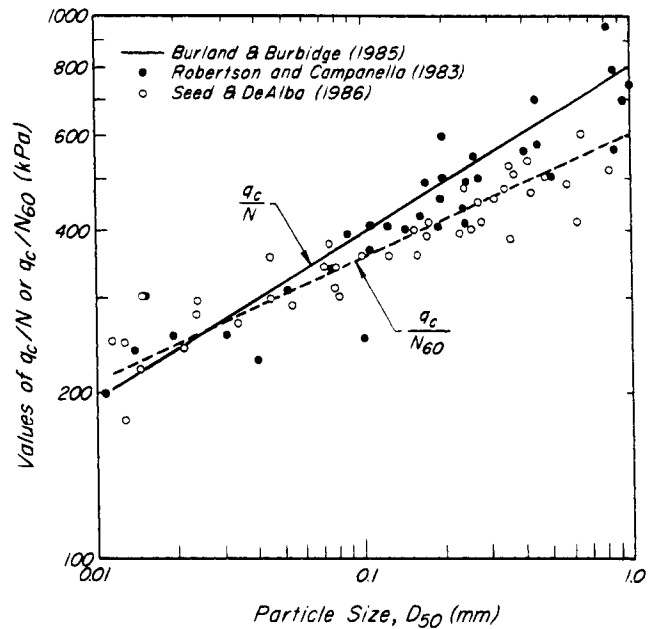


**Figure 11.15** Relation between cone penetration resistance  $q_c$  and standard penetration  $N$  or  $N_{60}$  values of sands as related to the median particle size  $D_{50}$  of the sands.

clay embedded in sands, gravels, and cobbles of variable relative density. If cobbles and boulders are not too prevalent, useful information can often be obtained by penetrometers consisting of sacrificial drive points of conical shape driven into the ground on the bottom of a pipe of somewhat smaller diameter than the base of the point. One such arrangement is shown in Fig. 11.16. A 50-mm conical point is inserted in an extra-strong, flush-joint steel pipe that is assembled in 1.5-m sections. Attached to the cone is a short stem fitting a 12-mm hole in a plug that is screwed into the lower end of the string of pipes. The pipe is driven into the ground by means of a 0.72-kg drive weight that falls 0.75 m, and a record is kept of

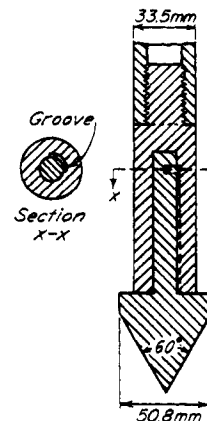


**Figure 11.16** Expendable drive-point penetrometer.

the number of blows per 0.3 m. After the pipe is driven to refusal it is recovered, whereas the point remains in the ground. Several such soundings per day can be made to a depth of 20 or 30 m. Since the diameter of the cone is larger than that of the pipe, the side friction is likely to be small compared with the point resistance. As the depth of the point increases, the weight of the pipe also increases; hence, the relation between relative density and penetration resistance is to some extent dependent on the depth.

Where numerous cobbles and boulders are present more rugged equipment is needed. Under some circumstances steel rails or H-piles have been driven by a pile driver and the blows per unit of penetration recorded. Such procedures can give only qualitative information, but may nevertheless be useful.

Quantitative data regarding very coarse-grained deposits can be obtained by use of the Becker hammer drill (Article 11.2.5) by counting the blows of the pile hammer per unit of penetration of the casing. Because the rising column of air and choppings leads to erratic results, the open bit normally used in hammer drilling is replaced by a plugged bit; consequently, if samples are required, a separate hole must be made with the use of an open bit. For granular materials various correlations have been developed between the number of blows to advance the Becker drill 0.3 m and the standard penetration  $N_{60}$ -value. The most reliable correlations take into account the dimensions of the casing and drill bit and the hammer energy actually delivered to the casing. Since the diesel hammers used are of the closed-ended type, the delivered energy is a function of the pressure in the bounce chamber, which can be measured during the driving. A rational and reasonably reliable method for calculating the corrected Becker values  $N_{BC}$  to be correlated with the  $N_{60}$  values for the standard penetration test has been developed on this basis (Harder and Seed 1986). However, a preferable procedure may be to determine the maximum energy transferred to the top of the Becker pile by field measurements of force and velocity during impact (Sy and Campa-nella 1993) by methods developed in connection with pile driving (Article 52.3.6).

## 11.5 In Situ Tests

### 11.5.1 Purpose and Types

Boring and sampling provide the means for identifying the types of soil at a site. The samples furnish material for determining the index properties and, if undisturbed samples are obtained, for physical tests in the laboratory. Soundings may provide indirect information regarding the types of soil and their consistency. In cohesive soils static soundings can be interpreted to indicate the shearing resistance of the material, whereas in granular materials both static and dynamic soundings provide data from

which the relative density or angle of internal friction can be estimated. Often such information is adequate for routine design.

When the critical materials have been identified and evaluated with respect to the requirements of the job, it is often found necessary to determine their engineering properties as accurately as possible. Although in some instances the required information can best be obtained by testing undisturbed samples, the disturbance due to sampling and handling may be appreciable, and more reliable data can often be obtained by investigations of specific properties by *in situ* tests. Several of the more widely used tests are described in this article; the interpretation is discussed subsequently in connection with specific applications.

### 11.5.2 Vane Tests

One of the most versatile and widely used devices for investigating the undrained shearing strength (Article 20) and sensitivity of soft deposits of clay is the *vane shear apparatus* (Carlson 1948, Cadling and Odenstad 1950). In its simplest form it consists of a four-bladed rectangular vane (Fig. 11.17a) fastened to the bottom of a vertical rod. The standard vane has a height-to-diameter ratio of 2 and is 55 or 65 mm in diameter and 110 or 130 mm in height. The blades consist of 1.95-mm, high-strength steel plate welded to a steel rod. The SGI-Geonor vane (Andresen and Bjerrum 1958) is pushed into the ground with a 36-mm steel pipe casing connected to a sheath that houses the vane. The casing isolates a 16-mm diameter torsion rod from the soil. The device is pushed down with the vane withdrawn into the sheath. When the desired depth is reached, the torsion shaft is unlocked and the vane is pushed 0.5 m out of the sheath. It is then rotated at the rate of 0.1°/s by a crank handle, and the torque is measured. The vane is withdrawn into the sheath, which is then advanced to the next depth, and the process is repeated. The tests can be conducted at intervals of 0.5 m. The Roctest vane is designed without a protective casing or sheath. A 20-mm torsion rod is used to push the vane into the ground and is in contact with the soil, but a slip coupling allows the rod torque to be measured separately from the total torque of rod and vane. The difference is the torque required to turn the vane.

The shearing resistance of the soil can be computed from the torque and dimensions of the vane (Article 20.5). If the vane is rotated rapidly through several revolutions, the soil becomes remolded and the shearing strength can be determined again. In this manner the sensitivity can be calculated. However, the degree of disturbance caused by rotating the vane differs from that obtained by kneading a sample in the laboratory; therefore, the numerical values of sensitivity determined by the two procedures are not strictly comparable.



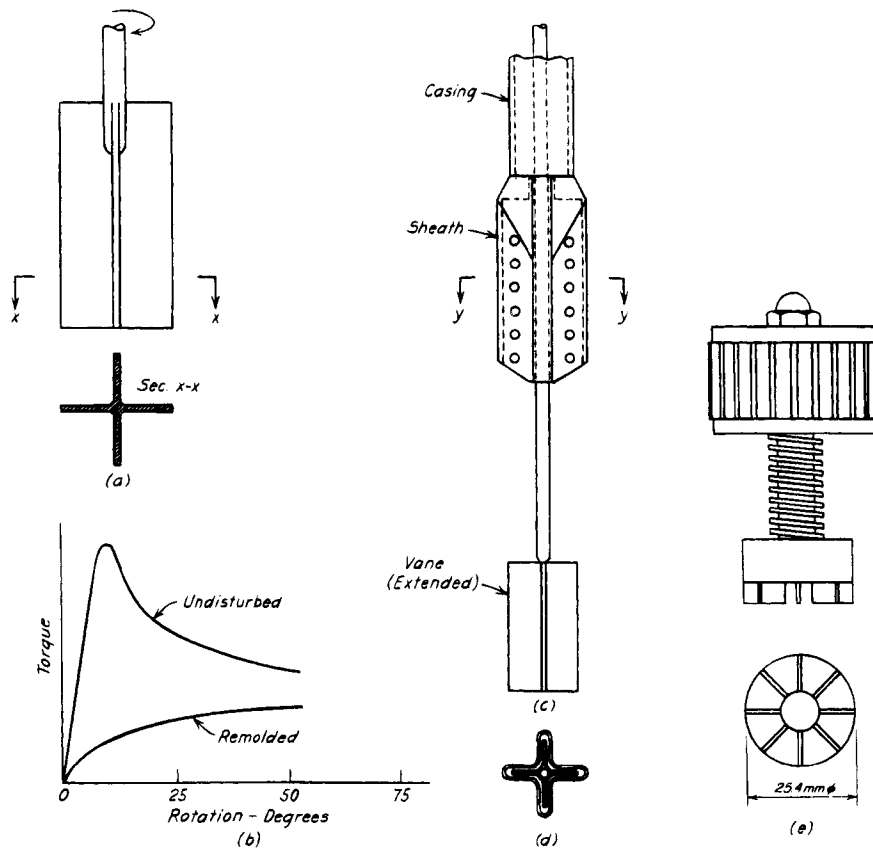


**Figure 11.17** Vane shear apparatus. (a) Simple four-bladed vane. (b) Typical torque-rotation curves for soft sensitive clay. (c) Sheath for advancing vane without drill hole. (d) Section y-y through sheath before advancing vane (after Cadling and Odenstad 1950). (e) Torvane.

If the soil contains layers or even thin laminations of sand or dense silt, the torque may be much greater than that required if the layers were not present. When these conditions prevail, the results of vane tests may be misleading. Other limitations are discussed in Article 20.5.

A modification of the vane, convenient for investigating the strength of clays in the walls of test pits in the field or for rapid scanning of the strength of tube or split-spoon samples, is the *torvane*, Fig. 11.17e. The vanes are pressed to their full depth into the clay below a flat surface, whereupon a torque is applied through a calibrated spring until the clay fails along the cylindrical surface circumscribing the vanes and, simultaneously, along the circular surface constituting the base of the cylinder. The value of the shear strength is read directly from the indicator on the calibrated spring. An example of a rapid survey of a clay deposit by means of this device is discussed in Article 12.6.

### 11.5.3 Pressuremeter

The pressuremeter, developed by Menard in the late 1950's, provides information about the stress-strain properties and strength of a soil by expanding the walls of a

drill hole while the radial pressure and corresponding radial deformation are measured. The device usually consists of an assembly of three cylindrical cells with flexible walls: an upper guard cell, a middle measuring cell, and a lower guard cell (Fig. 11.18a). The assembly is lowered into a drill hole of the same nominal diameter as the cell, and the cells are inflated. The measuring cell is inflated by increments of water pressure; the water pressure is measured to indicate the radial pressure applied to the surrounding soil, and the volume of water is observed as a measure of the average radial displacement during the increment. The guard cells are also inflated, to the same or somewhat smaller pressure as the measuring cell, to ensure a nearly cylindrical two-dimensional state of stress around the measuring cell by reducing end effects. The guard cells are pressurized by gas or, in some models, by water.

The measuring-cell pressure must be corrected for the difference in elevation between the cell and the pressure gage and for the pressure required to inflate the cell without external resistance. A small correction is also required to account for the expansion of the measuring cell tubing under pressure.

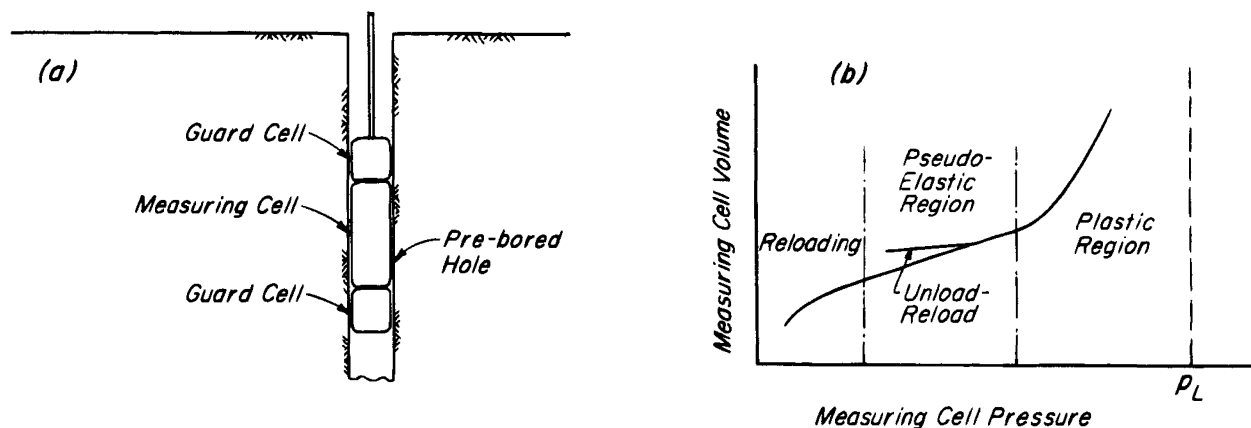


**Figure 11.18** (a) Schematic diagram of pressuremeter in borehole. (b) Typical pressure-volume curve (after Hartman and Schmertmann 1975).

For a test at a given elevation the volume of the cell is plotted as a function of the corrected cell pressure. The results typically are similar to the curve in Fig. 11.18b. At low cell pressures the relation is nonlinear, largely because the fit between the probe and the drill hole is imperfect and the soil just outside the hole may be disturbed. At increased pressures the relation becomes approximately linear; this range of pressure is designated the pseudoelastic region. At still greater pressures the volume increases at an increasing rate and approaches a limiting value  $p_L$ . The slope of the pseudoelastic portion is designated the *pressuremeter modulus*  $E_{pm}$ ; it constitutes a measure of the stiffness of the soil. Numerically it is calculated as

$$E_{pm} = (1 + \nu)2V \frac{\Delta p}{\Delta V} \quad (11.2)$$

in which  $V$  is the initial volume of the cell plus the additional volume corresponding to the pressure  $p$ . The value of Poisson's ratio  $\nu$  is usually taken as 0.33. The limit pressure  $p_L$  is determined by plotting the pressure against the reciprocal of the volume. At pressures above the pseudoelastic region this plot is usually linear. It is extrapolated somewhat arbitrarily to a volume twice the original volume of the measuring cell. The value  $p_L$  so determined is said to correspond to failure of the surrounding soil.

The pressuremeter modulus  $E_{pm}$  has been related empirically (Menard 1965) to the modulus of deformation  $E_s$  of the soil for use in calculations based on the theory of elasticity as

$$E_s = \frac{E_{pm}}{\alpha} \quad (11.3)$$

in which  $\alpha$  was termed by Menard the *rheological coefficient*. According to Menard the value of  $\alpha$  depends on the type of soil and the ratio  $E_{pm}/p_L$  as indicated in Table 11.3, modified from Menard (1965) by Briaud (1992).

The results of a pressuremeter test are sensitive to the degree of disturbance to which the immediately surrounding soil has been subjected. In loose sands below water table it may be preferable to drive the probe with a small drop hammer or to push it against a reaction. In such circumstances the probe is protected by a casing with longitudinal slots that allow the cells to expand. In materials that permit a dry or slurry-filled hole to stand open, the hole may be drilled with a flight auger. Typical washing methods for advancing borings are likely to cause excessive irregularities in the walls of the hole.

Normally one test is made for each meter of depth. The pressure increments are selected to reach the estimated point of failure in about 10 equal increments; the deformations for each increment are observed at 15, 30, and 60 s.

The Menard pressuremeter provides a fairly rapid method for obtaining quantitative data regarding *in situ* lateral stresses, deformation characteristics that can be applied to calculation of lateral movements, and shearing strength of the soils as a function of depth. Its principal shortcoming is the necessity to insert it into a drilled hole around which the soil inevitably relaxes and experiences change in stress before the probe is inserted. The effects of the relaxation together with the imperfect initial contact between the probe and the wall of the hole are to reduce or, in some instances, even to eliminate the range of pressure within the linear pseudoelastic region, and thus to introduce errors in evaluating the original *in situ* lateral stresses and the pressuremeter modulus.

To reduce such errors several modified types of pressuremeters have been developed. The modifications include the ability of the probe to excavate its own hole as it descends and thus greatly to reduce the effects of disturbance and stress changes. Such self-boring devices (Baguelin et al. 1974, Wroth and Hughes 1974, Denby and Clough 1980) have been used with considerable success in soft to stiff clays, but the time required to advance

**Table 11.3 Menard's  $\alpha$  Factor**

Soil Type	Peat		Clay		Silt		Sand		Sand and Gravel	
	$E_{pm}/p_L$	$\alpha$	$E_{pm}/p_L$	$\alpha$	$E_{pm}/p_L$	$\alpha$	$E_{pm}/p_L$	$\alpha$	$E_{pm}/p_L$	$\alpha$
Over consolidated		1	>16	1	>14	2/3	> 12	1/2	>10	1/3
Normally consolidated	For all values	1	9–16	2/3	8–14	1/2	7–12	1/3	6–10	1/4

the probe and take one set of observations is several hours in contrast to several minutes for the Menard type. Consequently, self-boring pressuremeters have thus far been used primarily for research.

If the properties of a soil are strongly anisotropic, as for example a soft clay with numerous sand strata, the results from lateral expansion of the cells of any type of pressuremeter may be misleading with respect to such properties as the vertical compressibility of the soil mass. An extensive description of the equipment, its calibration and use, and applications to practical problems is found in Briaud (1992).

### 11.6 Groundwater Investigations

The behavior of soil is profoundly influenced by the presence of water in the voids, by the soil's permeability, and by the stress in the water. At a minimum, an adequate subsurface investigation requires determination of the elevation of the groundwater table or tables, together with enough information to assess the permeability of the various components of the soil mass. In many problems a knowledge of the state of stress in the pore water is essential. This article describes the procedures used in routine subsurface exploration to investigate the groundwater conditions. They are compatible with the normal process of drilling, sampling, and penetration testing. More refined methods are required in many instances. They are discussed in connection with specific problems in subsequent sections of the book.

The *groundwater table*, *groundwater level*, or *phreatic surface* is defined as the elevation at which the pressure in the water is equal to that of the atmosphere. Above groundwater level the soil may be fully or partially saturated, but the water is held in the voids by capillarity and the stress in the water is negative with respect to atmospheric pressure (Article 15.6). In principle, if a drill hole will stand open or if its sides are supported by a perforated or screened tube, water will ultimately fill the hole to an elevation corresponding to the groundwater level. This principle is generally used to investigate groundwater conditions during exploratory drilling. It provides definitive results, however, only in soils such as gravels and sands permeable enough to furnish water

to the drill hole without significantly altering the groundwater conditions. In less permeable soils the time required to supply the water is so great that the water level in the drill hole does not come to equilibrium within a reasonable time of observation, and in feebly permeable soils such as clay, a state of equilibrium at which the correct groundwater level can be observed may never be reached.

Furthermore, if a highly permeable deposit contains one or more layers or zones of less permeable soil, the less permeable zones may divide the deposit into layers having different groundwater levels. Under these conditions an open hole provides a means for flow to occur from one layer to another, and the water level in the hole may not correctly reflect the groundwater level in any of the permeable layers or, at best, will approximately indicate the piezometric level of only the most permeable layer.

In spite of these limitations, information regarding the groundwater level in pervious deposits is so important to design and construction that careful observations should always be made and recorded, if circumstances permit, during exploratory drilling. If the drill hole is cased, each advance of the hole beyond the casing should be followed by observations of inflow or outflow of water and, if practicable, of the equilibrium level attained by the water in the casing. It is customary, in any event, to note the water level on completion of the hole and after allowing the hole to stand overnight or for 24 h before backfilling. Use of drilling mud to stabilize the walls of drillholes precludes obtaining this useful information.

In addition to the information obtained at the time of drilling, further data are often obtained by converting the drill holes to observation wells (Article 11.6.1) or by installing piezometers (Article 11.6.2).

If penetration tests are made in pervious granular soils by means of a piezocone (Article 11.4.2), a continuous record is obtained of porewater pressure as a function of depth.

#### 11.6.1 Observation Wells

The groundwater level observed at the time the subsurface investigations are made is not likely to be either the maximum or the minimum that may be experienced dur-

ing the year or from year to year, whereas the design of the proposed facility or the construction procedure should take such fluctuations into account. To obtain the necessary data in pervious soils, permanent observation wells may be installed in which the water level is measured periodically. The wells in their simplest form consist of a pipe connected to a screened or slotted section that is lowered into a drillhole, whereupon the casing is withdrawn. The depth to the water in the pipe is determined by sounding, or a float can be installed that actuates a recording device at the ground surface. Such installations are simple and relatively inexpensive, but they produce valid results only in pervious deposits sufficiently homogeneous to exhibit only one groundwater table. In stratified deposits with several water tables, or in feebly permeable materials in which the time lag in the wells would be appreciable, more refined installations known as piezometers are required.

### 11.6.2 Piezometers

In contrast to observation wells, which may be open to the entire column of soil through which they pass, piezometers measure the water pressure at a selected level in the formation. In its simplest form a piezometer is similar to an observation well, except that the screened or slotted section at the bottom of the pipe has a length of a meter or less and is embedded in a pocket of sand. The rest of the drill hole around the pipe is backfilled with an impervious material as the casing is withdrawn or, if the casing is left in place above the screened section, the space between the casing and riser pipe is similarly backfilled. Separate installations are made, each with its screen at an appropriate depth, if the phreatic surfaces are to be determined for different layers in the deposit.

Simple installations of this type are satisfactory only in such pervious soils as gravels and sands. In finer materials the time for equilibrium becomes excessive and, if the groundwater level is itself subject to fluctuations, the results inevitably are erroneous. Under these conditions the time to equilibrium may be reduced by decreasing the diameter of the riser pipe, thereby reducing the flow into the piezometer needed to make the measurement, or by the use of electrically or pneumatically operated sensors that permit measurement of the water pressure with negligible flow. The choice among the various possibilities depends on the specific characteristics of the site and the requirements of design or construction, and the corresponding investigations go beyond the scope of soil exploration. These matters will be discussed in appropriate sections of the text.

## 11.7 Geophysical Methods

At the beginning of this article it was mentioned that various kinds of information regarding subsoil conditions

can be obtained by means of geophysical methods, without the aid of borings or soundings.

Some of the geophysical methods are based on the dependence of the geometry of every field of force on the location of the boundaries between the substances that occupy the field. The field of force may already exist, as for example the gravitational or the magnetic field of the earth, or it may be created artificially, for instance by sending an electric current through the ground located between two electrodes embedded in the ground.

The geometry of any field of force in a perfectly homogeneous medium is independent of the physical properties of the medium. It is simple and can be determined accurately by theory. The distortion of the field produced by the existence of an internal boundary depends on those physical properties of the substances located on either side of the boundary that create the field or that have a decisive influence on its intensity. Hence, the most suitable method for locating the boundary between two types of rock or soil is determined by the type of field of force that will be distorted most conspicuously by the difference between the properties of these materials. If their unit weights are very different, a gravitational method may be indicated. If their unit weights are almost equal but their electric conductivities are very different, the electric potential or resistivity method may be used to advantage.

To locate the position of an internal boundary the pattern of the real field of force at the surface of the ground is determined by suitable surface observations. This pattern is compared with the one determined by computation based on the assumption that the seat of the field is perfectly homogeneous. The position of the internal boundary is ascertained on the basis of the difference between the real and the ideal patterns.

A second group of geophysical methods, known as seismic methods, is based on the dependence of the rate of propagation of elastic waves on the elastic properties of the media through which the waves travel. If a wave arrives at the boundary between two media with different elastic properties, part of it is reflected and part is refracted. To determine the position of an internal boundary, for instance between hard and soft rock or between soil and rock, a small shock is produced at the ground surface by a hammer blow or by firing an explosive in a shallow hole, and the time is measured at which the reflected or the refracted waves arrive at different points on the surface. On the basis of the results of the observations the position of the internal boundary can be computed, provided the boundary is well defined and not too uneven.

Seismic methods can also be used to determine directly the velocity of propagation of seismic waves. These waves are of two kinds, compression ( $P$ ) and shear ( $S$ ) waves. In  $P$ -waves the soil particles move forward and backward in the direction of propagation, whereas in  $S$ -

waves the motion is transverse to the direction of propagation. The velocities are characteristic for different soils and, for a given soil, of its stiffness or relative density. Knowledge of the velocities is particularly useful in judging the effectiveness of compaction of sands and gravelly sands in connection with their susceptibility to liquefaction (Article 20.9). Because the velocity of *P*-waves is different above and below the groundwater table whereas that of *S*-waves is not, the latter velocity is evaluated more often. In *crosshole tests* at least two vertical drill-holes cased with plastic pipe are spaced at 3 m or more. In one, at successive depths, a vertical impulse is delivered to the wall of the hole by a vibrator or a blow to the top of a rod with a short enlargement in contact with the wall at the bottom of the rod. The time of the impulse and that of the arrival of the *S*-wave at the same depth in the adjacent hole are recorded, and the velocity is calculated as the distance between the holes divided by the elapsed time. In contrast to  $N_{60}$ -values determined by the standard penetration test, the shear-wave velocities represent average properties for the intervening mass of sand rather than discrete, sometimes quite scattered, numerical values.

In civil engineering, only the seismic and electrical resistivity methods are used to any significant extent, sometimes in conjunction with each other. The principal application of the seismic method is to locate the surface of the bedrock. If the thickness of the weathered top layer of the rock is small and the rock surface is not too uneven, the results are usually reliable. In fact, if a sedimentary overburden contains many boulders, a survey by boring may be almost impracticable, whereas a seismic survey may be as simple and reliable as if the boulders did not exist. In some instances the depth to the surface of a stiff or hard deposit of soil beneath soft overlying sediments can be determined. Since the velocity of seismic waves is much greater in saturated than in unsaturated soils, the method can also be used to locate the water table in pervious soils. On the other hand, the presence of a soft layer below a stiffer one cannot ordinarily be detected.

The resistivity method has been found useful in defining the boundaries between soils of low resistivity such as soft clays and soft organic deposits, and materials of higher resistivity such as sands, gravels, or bedrock. Materials having low resistivities can be detected even if they underlie those of high resistivities. The method can be used from the surface of a body of water. On the other hand, the boundaries cannot usually be detected between an organic soil and soft clay, or between stiff clay and soft clay shale, or between loose sand and coarse-grained sandstone. In all applications, the interpretation requires calibration of the equipment over known materials in the immediate area (Moore 1961).

Readily portable seismic and resistivity equipment has been developed for civil engineering purposes. With such

equipment, exploration can often be carried out economically and rapidly over large areas. Under some circumstances the use of both types of equipment may facilitate interpretation. For instance, it may not be possible on the basis of a seismic survey to determine whether an inferred boundary is the water table or bedrock; a resistivity survey might permit the distinction because rock ordinarily has a high resistivity compared to that of waterbearing strata. The results of a geophysical survey, however, should always be checked by at least a few borings.

### Selected Reading

- Hvorslev, M. J. (1948). *Subsurface exploration and sampling of soils for civil engineering purposes*, Waterways Experiment Station Vicksburg, MS, 465 pp.
- Cambefort, H. (1955). *Forages et sondages* (Borings and soundings), Paris, Eyrolles, 396 pp.
- Lowe, J. (1960). "Current practice in soil sampling in the United States," *Hwy. Res. Board Special Rept. 60*, pp. 142–154.
- Sanglerat, G. (1965). *Le pénétromètre et la reconnaissance des sols* (The penetrometer and soil exploration), Paris, Dunod, 230 pp.

## ARTICLE 12 PROGRAM FOR SUBSOIL EXPLORATION

### 12.1 Type and Sequence of Operations

Whatever the project, the engineer should keep in mind that most subsoils were formed by geological processes that changed at random in space and time. Because of the decisive influence of geological factors on the sequence, shape, and continuity of the soil strata, the first step in any subsoil exploration should always be an investigation of the general geological character of the site. The more clearly the geology is understood, the more efficiently can the program for soil exploration be laid out. The second step is to make exploratory drill holes that furnish more specific information regarding the general character and the thickness of the individual strata. These two steps are obligatory. All others depend on the size of the job and the character of the soil profile.

On routine jobs, such as the design and construction of foundations for apartment houses of moderate size in districts with known foundation conditions, no further investigations are needed. The soil testing can be limited to the determination of the index properties (see Table 9.1) of spoon samples obtained from the exploratory borings. The test results serve to correlate the soils with others previously encountered on similar jobs. Hence, they make it possible to utilize past experience. The gaps in the information obtained from the exploratory drill holes are compensated by a liberal factor of safety. Whenever information can be obtained by inspection of existing structures in the vicinity, this opportunity should not be overlooked.

The soil exploration on large projects may call for the determination of one or several of the following: relative density of sand strata, permeability of sand strata, shearing resistance of clay strata, or compressibility of clay strata. In every instance the program of the exploration should be prepared in accordance with the amount of useful information that can be derived from the results of laboratory or field tests. With increasing complexity of the soil profile the usefulness of elaborate laboratory investigations rapidly decreases. If the soil profile is erratic, the efforts should be concentrated not on obtaining accurate data regarding the physical properties of individual soil samples, but on obtaining reliable information regarding the structural pattern of the subsoil. Attempts to obtain this information by means of boring and testing are likely to be wasteful. Since erratic soil profiles are far more common than simple and regular ones, the instances are relatively rare in which elaborate and large-scale soil testing is justified from a practical point of view. In the following discussion of the means for obtaining reliable information concerning the subsoil conditions, the influence of the degree of complexity of the soil profile on the practical value of soil testing is consistently emphasized.

## 12.2 Geological Considerations

Most natural soil deposits represent one of the following principal types: river-channel deposits, flood-plain deposits, delta deposits, shore deposits, glacial deposits, wind-laid deposits, deposits formed by sedimentation in standing water, and residual soils formed in place by weathering. The only ones likely to have a fairly regular structure are the flood-plain and wind-laid deposits and those formed in large bodies of standing water at a considerable distance from the shore. All the others are likely to be distinguished by large and erratic variations, at least in consistency or relative density, and usually in grain size as well.

In the upper reaches of river systems, *river-channel deposits* generally occupy the bottoms of valleys carved out of rock. In the lower reaches they may be laid down in winding and interlaced channels eroded out of the broad sheet of fine-grained sediments that have previously been deposited by the river under different conditions of sedimentation. The average grain size decreases with increasing distance from the source, and at any one point it is likely to increase in a general way with increasing depth below the surface. However, the details of stratification are always erratic, and both grain size and relative density vary in an unpredictable manner. Still more abrupt and conspicuous are the variations in *glacial outwash* deposited by the melt waters along the rim of continental ice sheets.

*Flood-plain deposits* are laid down during the high-water season on both sides of the lower courses of rivers. They commonly consist of continuous layers of silt or

clay of fairly uniform thickness, separated from each other by equally persistent layers of coarser sediments. However, at any point or line the continuity of these strata can be broken by bodies of other sediments occupying troughs or abandoned river channels (Kolb and Shockley 1959). If such a body is located between two drill holes, its presence may escape attention. Several well-known foundation accidents have been ascribed to this cause.

*Delta deposits* are formed where water courses enter bodies of standing water. The main features of deltas are simple, but the details of their structure can be very complex, as shown in Fig. 12.1, because the currents that transport the sediments shift continually.

*Shore deposits* are composed of sediments that were eroded by waves or carried into a body of standing water by rivers and transported and deposited by shore currents. They generally consist of sand and gravel. However, as a result of important fluctuations in the lake or sea level combined with the shifting of the water courses that cross the coastal belt, the sand and gravel deposits may alternate in an intricate manner with layers or pockets of silt, clay, or peat. Deposits of this kind are referred to as *composite shore deposits*. Figure 12.7 and the upper half of Fig. 10.2 illustrate the structure of deposits of this type.

The constituents of *glacial deposits* were picked up and transported by ice and laid down when the ice melted. The wasting away of ice sheets always alternates with periods of temporary growth and advancement. The advancing ice plows up or deforms previously deposited layers of glacial material. Furthermore, at the ice rim random sorting and shifting are carried on by the streams of water that emerge from beneath the ice. Hence, glacial deposits are among the most erratic with which the engineer has to deal. Irregular pockets and lenses of fine- and coarse-grained materials intermingled with boulders may follow each other in a chaotic manner (Fig. 12.1).

In contrast to glacial deposits, *wind-laid sediments* are remarkably uniform. However, their boundaries may be very irregular, because the wind may drop its burden in irregular heaps on very uneven surfaces. Furthermore, the fine-grained varieties known as loess (Article 2) may completely lose their original homogeneity on account of local leaching or weathering. Many faulty foundations on loess have resulted from the failure of the designers to recognize the existence of these partial alterations.

The various transporting agencies, running water, ice, and wind, deposit only part of their solid burden on their way or at the end of their path. The remainder is carried into large bodies of standing water such as lakes, bays, or the open ocean. Once they get beyond the narrow zone in which the shore currents travel, they are acted on by no force other than gravity. Therefore, in contrast to all other sedimentary deposits, those formed in large bodies of standing water usually have a relatively simple structure that reflects the periodic or progressive changes in

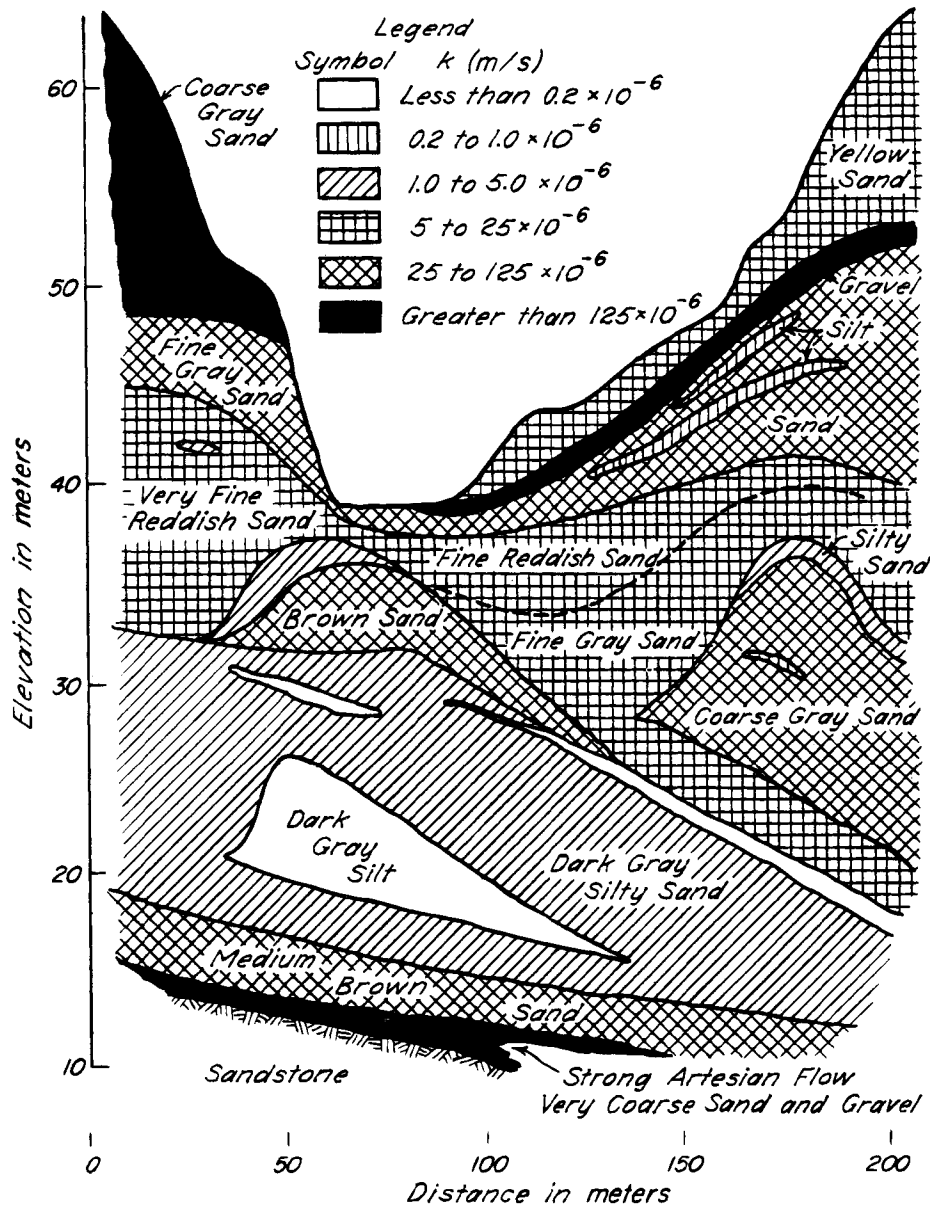


**Figure 12.1** Permeability profile of relatively homogeneous glacial delta deposit near Chippopee, MA.

the character of the material that enters the region of sedimentation. It is also influenced to some extent by the chemical composition of the water.

The effect of the seasonal changes in the character of the suspended material is disclosed by the water-content diagram (Fig. 10.1b). On account of this effect, the scattering of the water content from the average is as great for vertical distances as small as a few centimeters as it is for the entire depth. Still more conspicuous is the effect of seasonal changes on the structure of sediments that were laid down in freshwater lakes under arctic conditions such as those prevailing in the northern United States and in Canada during the Ice Age. In the summertime,

the suspended material in the offshore parts of the lakes consisted of silt and clay, because the coarser materials such as sand and gravel had already been laid down as delta deposits at the mouths of the rivers. The silt particles settled out during the summer. During the winter, however, no new material was carried into the lakes because the rivers were completely frozen. Hence, beneath the ice crust, only clay particles that did not settle during the summer were deposited. Therefore, the sediment is composed of light-colored summer layers consisting of silt with some clay, and dark-colored winter layers consisting chiefly of clay. Each varve consisting of one silt and one clay layer represents the deposit of one year.



These deposits are the varved clays (Fig. 12.2) mentioned in Article 2. The thickness of the varve is commonly less than 1 or 2 cm, but exceptionally as much as a meter. It depends on the amount of material washed into the lake during the summer season. Deposits of such clay are very common in both North America and Europe north of the 40th parallel. They are a prolific source of serious construction difficulties.

If similar arctic rivers enter a bay of the ocean instead of a freshwater lake, the segregation according to particle size is much less perfect because the salts contained in the sea water cause flocculation of the clay particles. Consequently, most of the clay is deposited simultaneously with the silt.

The preceding review has shown that nature created an infinite variety of structural patterns ranging from the simple stratification of offshore deposits formed in large lakes to the utterly complex structure of masses of gravel, sand, and silt that were laid down, plowed up, distorted, locally eroded, and redeposited along the rim of a continental ice sheet. The character of residual soils, on account of variations in the parent material and in the degree of weathering, is no less complex. If borings are made in a mass of soil at two points 25 or 50 m apart, the engineer knows the character and the sequence of the strata along two vertical lines. Between these two lines the strata may be continuous. However, they may also wedge out at a short distance from each line, and the sequence of strata halfway between the two borings may not have the remotest resemblance to that at either one. An intelligent program for supplementary soil investigations can be prepared only by an engineer who is familiar with the elements of physical geology and with the geology of the region in which the site is located.

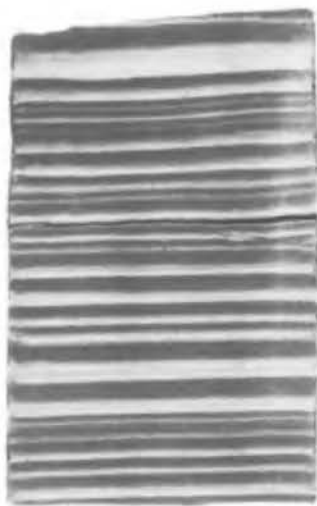


**Figure 12.2** Section through undisturbed sample of varved clay taken in well-designed sampler of 100 mm diameter (courtesy M. J. Hvorslev).

Geological literature is indexed extensively in publications of the various state and national geological surveys and by such organizations as the Geological Society of America. Several useful sources are listed at the end of this article.

Insight concerning the geology of a site can often be gained by a study of aerial photographs. Experts in air-photo interpretation from a geomorphic point of view can usually define the surficial geology and make valuable inferences about subsurface conditions. Such interpretations are virtually mandatory for large projects including dams and reservoirs, transportation routes, or landslide control.

In short, the engineer should cultivate the capacity for geological observation and interpretation as an essential element in subsurface exploration, should use existing geological information, and should develop skill in air-photo interpretation. On large and complex projects the services of a professional geologist may be needed to assist in the planning and interpretation of the subsurface exploration.

### 12.3 Spacing and Depth of Exploratory Borings

The spacing between exploratory drill holes is presently often governed by convention and not by rational considerations. On building sites the borings are commonly spaced at about 15 to 20 m in both principal directions. On subway or earth-dam projects a spacing of 30 m is generally considered the minimum. However, if the line is very long or the site very large, the spacing is often as great as 60 m. Even at that spacing the required amount of drilling and testing may be very large.

Standardization of the spacing of exploratory drill holes has obvious disadvantages. If the soil profile is very simple, the customary spacing is too small, whereas if the profile is erratic, the spacing is excessive. To avoid the loss of time and money due to drilling superfluous bore holes, subsurface soundings can often be used to advantage. A sounding, which is cheaper and more expedient than a drill hole, may be made at each point where convention would call for a drill hole. If all the penetration diagrams are similar, the soil profile is likely to be simple. Exploratory drill holes are required at only one or two locations where average conditions prevail, and near those few points where the penetration diagrams indicate maximum deviations from the statistical average. If the geology of the site involves the possibility that the continuity of the strata may be disrupted locally by channel fillings or other bodies of foreign material, supplementary soundings should be made wherever there is any surface indication of the presence of a compressible inclusion, such as a shallow depression on the surface of the ground. If a sounding encounters such an inclusion, an exploratory drill hole should be made near by to determine the type of soil of which the inclusion consists.



If the penetration diagrams obtained from the exploratory soundings are very different, the soil profile is likely to be erratic, and intermediate soundings should be made until the penetration data are complete enough to leave no doubt concerning the general shape and trend of the boundaries between the fine-grained and coarse-grained, and the loose and dense parts of the deposit. Yet, no more drill holes are required than those few needed to determine the types of soil located between the different surfaces of discontinuity or to find out whether a body of exceptionally resistant or nonresistant soil consists of sand or clay.

The depth to which exploratory drill holes should be made is likewise more or less standardized. This practice is not only wasteful but also dangerous. Many buildings have been seriously damaged by settlement due to the consolidation of soft clay strata located below the depth to which the subsoil was explored. Yet, no general rules can be established for selecting this depth, because for a given weight and given dimensions of a structure the depth at which the seat of settlement is located depends to a large extent on the soil profile. The following paragraphs illustrate the factors that should be considered before the depth of the drill holes is specified.

If it is certain for geological reasons or from the results of previous borings in the vicinity that the subsoil of a group of buildings does not contain any strata of clay or soft silt, it is sufficient to explore the subsoil at the site of each building to a depth between 5 to 10 m below subgrade, in accordance with the size and weight of the building. The size of the area occupied by the group is irrelevant, because the compressibility of sand strata decreases rapidly with increasing depth and, consequently, each building settles almost as if the others did not exist.

On the other hand, if the subsoil of a group of buildings contains soft strata, the seat of settlement may be located at a depth greater than the width of the entire area occupied by the buildings because, even at a depth of 50 or 75 m, a moderate increase of the pressure on a thick stratum of soft clay may produce a settlement of more than 300 mm (Article 51). Hence, the depth to which the subsoil should be explored depends primarily on the absence or presence of compressible strata.

If the geology of the site indicates that clay or silt strata may be located at great depth below the surface, or if nothing whatsoever is known concerning the subsoil conditions, a rough estimate should be made of the intensity and distribution of the pressures that will be produced in the subsoil by the proposed group of buildings, as well as by any fill that may be placed on the site. The procedure is described in Article 40. On the basis of this estimate, the greatest depth  $D_{\max}$  can be evaluated at which the presence of a thick layer of soft clay with a high liquid limit may still have a significant influence on settlement.

The first drill hole should be made to this depth. All the other borings and subsoil soundings can be discontinued at a depth of about 3 m below the base of the lowest clay or silt stratum that was encountered within the depth  $D_{\max}$ . This procedure should be followed regardless of whether the character of the upper soil strata may call for a footing, raft, or pile foundation.

The following example illustrates the possible consequences of disregarding this procedure. A group of factory buildings was constructed on a tidal flat. None of the buildings was more than 12 m wide. The subsoil was explored by borings to a depth of 30 m. Within this depth there was a gradual transition from soft silt near the surface to sand with variable density at a depth of more than 20 m. Because of the high compressibility of the top strata, it was decided to support the buildings on piles 20 to 30 m long. To the surprise of the engineers in charge of the job, the buildings started to settle during construction, and in the course of three years the settlement increased to more than 600 mm. Subsequent soil investigations showed that the settlement was due to the consolidation of a stratum of soft clay 10 m thick, located at a depth of about 35 m below yard level.

If bedrock is encountered within the depth  $D_{\max}$ , the topography of the rock surface must be determined at least approximately by sounding or boring, because the depressions in the rock surface may be filled with very compressible sediments that are encountered in only the deepest drill holes. The omission of this precaution also has repeatedly been the cause of unexpected settlement.

The results of the exploratory borings and subsurface soundings should be assembled in a report containing all the information that was secured concerning the geology of the site, a list of the index properties of all the spoon samples that were taken, and a record of the results of the penetration tests. On the basis of this report it can be decided whether or not supplementary investigations are required concerning the relative density and permeability of the sand strata and the shearing resistance and compressibility of the clay strata.

## 12.4 Relative Density of Sand Strata

The relative density of sand strata, Eq. 6.3, has a decisive influence on the angle of internal friction of the sand (Article 19.1), on the ultimate bearing capacity (Article 33), and on the settlement of footings resting on the sand. If a submerged sand is very loose, a sudden shock may transform it temporarily into a sand suspension with the properties of a thick viscous liquid (Article 20.9). In a dense state the same sand is insensitive to shock and is perfectly suitable as a base for even very heavy structures. For this reason the relative density of a sand is far more important than any of its other properties, except possibly its permeability.

While the exploratory borings are being made, some information regarding the relative density of the sand strata encountered in the drill holes can be obtained by performing the standard penetration test (Article 11.3.2) whenever a spoon sample is taken. In view of the outstanding importance of the relative density, the standard penetration test should be considered an essential part of the boring operation. Table 12.1 gives an approximate relation between the number of blows  $N_{60}$  and the relative density.

The relation, Table 12.1, should be used with caution and only if the penetration tests are conducted conscientiously. If the sand is located below the water table, an inexperienced driller may allow the water level in the casing to fall below the piezometric level in the sand at the location of the test, whereupon the sand may become quick and be transformed into a loose state; the  $N_{60}$ -value will then be too low. The mere removal of the drill rods at a rate too rapid to permit water to replace the volume of the rods may cause such a lowering of the water level. On the other hand, boulders or cobbles several centimeters larger than the diameter of the spoon may give excessively high  $N_{60}$ -values.

In saturated fine or silty sands of moderate to high relative density, and having an effective grain size between 0.1 and 0.05 mm, the number of blows may be abnormally great because of the tendency of such materials to dilate during shear under undrained conditions (Art. 18.2). Hence, in such soils the standard penetration test should be supplemented by more reliable procedures, or the results should be interpreted conservatively.

The value  $N_{60}$  of the standard penetration resistance is also influenced by the overburden pressure at the depth at which the test is made. In many practical problems, such as the design of spread footings on sand, the influence of the overburden pressure on  $N_{60}$  is comparable to its influence on the stiffness of the sand, and a correction to the value of  $N_{60}$  is not explicitly required. In other problems, particularly those concerned with the liquefaction of sand (Article 20.9.6), however, a correction is necessary. The corrected values of  $N_{60}$  are designated as  $(N_1)_{60}$ ; they may be calculated by means of Eq. 20.37.

**Table 12.1 Relative Density of Sands According to Results of Standard Penetration Test**

No. of Blows, $N_{60}$	Relative Density
0-4	Very loose
4-10	Loose
10-30	Medium
30-50	Dense
Over 50	Very dense

On important jobs the information obtained from the standard penetration tests concerning the relative density of the sand should be supplemented by subsurface soundings. These soundings furnish continuous records of the variation of the penetration resistance with depth. However, the resistance against the penetration of a penetrometer into sand, or the energy required to produce a given penetration, depends not only on the relative density of the sand but also on the dimensions of the drive point and the stem and, to some extent, on the shape of the grains and the grain-size distribution. Hence, every new method of subsurface sounding and every use of the method in an unexplored locality call for a set of calibration tests that furnish the data for interpreting the penetration records.

A rough calibration can be achieved by making a subsurface sounding next to a drill hole in which standard penetration tests were performed. More cumbersome but also more reliable are *standard load tests* at different depths below a point close to the location of a subsurface sounding. The tests are made on a bearing plate 300 mm square, resting on a horizontal surface of the sand. No backfill or surcharge is placed within 1 m of the plate. The relation between load and settlement for such tests on several different sands is shown in Fig. 12.3a. Curves 1 and 2 were obtained from tests on very dense sand, curve 4 on sand of medium density, and curve 5 on loose sand. With increasing relative density the bearing capacity increases rapidly, and the settlement under a given load decreases. Figure 12.3a shows, in accordance with field experience and in contrast to a widespread opinion, that the grain size has no influence on the relative density and bearing capacity of a sand.

On the basis of the results of standard load tests such as those shown in Fig. 12.3a, the relative density of the sand can be determined by means of the diagram (Fig. 12.3b). For this purpose the curves obtained from the load tests are introduced into the diagram. The position of the curve with reference to the boundaries shown in the figure indicates the relative density of the sand.

The standard load test may, however, furnish misleading results if the grain size of the sand is fine or very fine and if the sand contains appreciable soil moisture. On account of the apparent cohesion due to the capillary forces (Article 15.6), the sand may seem stronger and less compressible than it would if no soil moisture were present. The influence of the apparent cohesion decreases rapidly with increasing width of the loaded area; it may be too great to ignore if the test area is as small as 300 mm square.

Still more accurate information regarding the relative density of sand strata can be obtained by laboratory tests on undisturbed samples hand carved from test shafts or taken from drill holes by one of the procedures described in Article 11.3.9. The shafts or borings are made near

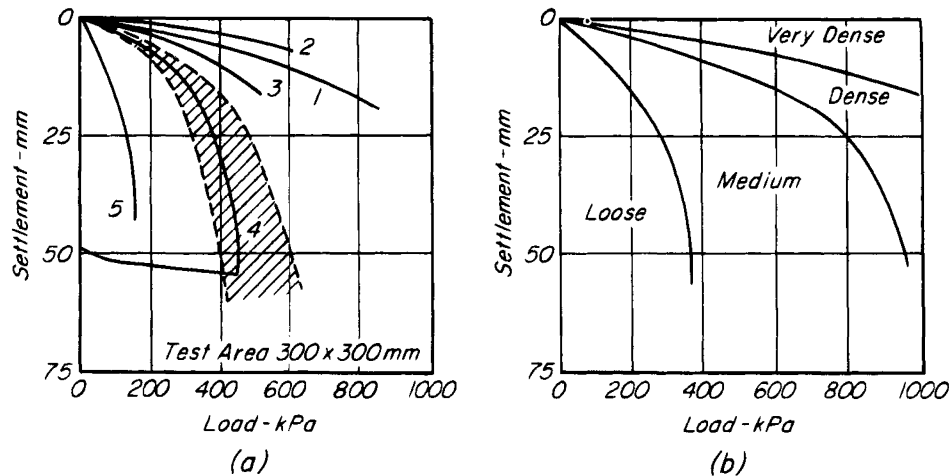


**Figure 12.3** (a) Relation between load and settlement of bearing plate 300 mm square resting on the surface of sand. Curve 1 represents dense clean fine sand in caisson 8 m below river bottom; curve 2 represents very dense fine sand in open excavation 8 m below ground surface in Lynn, Massachusetts; curve 3 represents damp sand of medium density hand-compacted by tamping in layers; curve 4 represents medium-dense sand at bottom of shaft 9 m deep in Houston Street, New York. Shaded area indicates range for curves obtained between depths of 6 and 18 m; curve 5 represents loose, coarse, clean, and very sharp sand at bottom of open excavation near Muskegon, Michigan. (b) Chart for estimating relative density of sand on basis of results of standard load test on bearing plate 300 mm square.

points at which subsurface soundings were previously performed. By correlating the test results with the corresponding resistances to penetration, the data are obtained for accurate interpretation of the results of all the other subsurface soundings. However, the instances are rare in which such refinements are warranted.

### 12.5 Permeability of Sand Strata

Reliable information on the permeability of sand strata may be required for either of two purposes. It may be necessary to estimate the quantity of water that will flow toward an excavation with specified dimensions, at a given position of the water table. Or it may be required to determine the depth to which the cutoff beneath a dam on a permeable foundation must be made to reduce the seepage losses from the reservoir to less than a specified amount.

The data for estimating the flow of water toward an excavation are obtained most conveniently by means of pumping tests (Article 14.7). The results of the tests make it possible to compute the average coefficient of permeability (Article 14.2) of the subsoil in horizontal directions. Once this coefficient is known, problems concerning the flow of water toward the proposed excavation can be solved on the basis of the laws of hydraulics. If the project calls for lowering the water table by means of filter wells (Article 43), the well system can be laid out and an estimate can be made of the capacity of the pumps required for maintaining the water table below the bottom of the excavation during construction.

To solve cutoff and seepage problems, it is necessary to determine not only the average permeability of the subsoil but also the major variations of the permeability within the sand strata located beneath and beside the water-retaining structure. This can be accomplished by means of permeability tests on fairly continuous series of samples obtained from a large number of drill holes. However, natural deposits are never homogeneous. The water percolates through them along more or less tortuous lines following lenses and layers composed of the coarsest constituents, and their permeability in a vertical direction is usually much smaller than that in a horizontal one. Therefore, laboratory investigations of any kind cannot be expected to disclose more than the order of magnitude of the permeability of the deposit even if the tests are performed by causing the water to flow through undisturbed samples separately in horizontal and vertical directions. Furthermore, the cores are never continuous. A single seam of silt located between two adjoining samples of sand may have a radical influence on the ratio of horizontal to vertical permeability. The occurrence of such seams is not uncommon (Fig. 12.4).

For these reasons the use of undisturbed samples for permeability tests is hardly justified. Results no less reliable can be obtained by testing samples recovered from drill holes by means of a sampling spoon equipped with a core catcher (Fig. 11.2d) or by a scraper bucket (Fig. 11.2j). If the samples are recovered in a spoon, their constituents should be thoroughly mixed before testing. After making 15 or 20 permeability tests on samples from

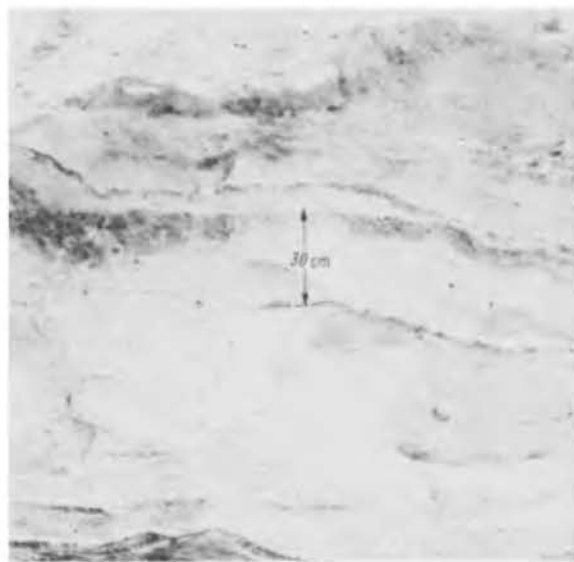


**Figure 12.4** Silt seams in medium uniform sand. The presence of the seams could not be detected by ordinary test borings. Yet they reduce the permeability of the sand stratum in the vertical direction to a small fraction of that in horizontal directions.

a given stratum, a technician can estimate the coefficient of permeability of the others on the basis of their texture and general appearance. The estimates and test results can be adjusted to take into account the difference between the relative density of the remolded and the in-place material. The ratio of horizontal to vertical permeability can be judged on the basis of Eqs. 14.12 and 14.13.

Elaborate investigations of this nature are rarely justified economically. The determination of the permeability of natural deposits below the water table by *in situ* permeability tests (Article 14.7) is always more reliable than that by laboratory tests.

Procedures have been developed to evaluate the permeability of sand strata located above the water table on the basis of the quantity of water that percolates into the soil from that part of a drill hole extending below the casing. The results are at best no more than crude estimates and may be unreliable, because the flow pattern into the soil is unknown and the formation of a filter skin at the entrance surface can hardly be avoided. The procedure (Zangar 1953) is similar to that described in connection with *in situ* permeability tests in drill holes below the water table.

## 12.6 Shearing Resistance of Saturated Clays

If a project involving clay soils calls for an investigation of the stability of slopes, the computation of the lateral pressure against the bracing of open cuts, or an estimate of the ultimate bearing capacity of embankments, footings, or rafts, the shearing resistance of the clay must be

determined. If the water content of the clay will not change significantly during the period when the slopes are unsupported or during the lifetime of the temporary bracing of the open cuts, or if the factor of safety of footings is a minimum before the water content can decrease on account of the loading, the undrained shearing strength (Article 20.6) governs the behavior of the clay. Under many conditions of practical importance, this strength is approximately equal to one-half the unconfined compressive strength  $q_u$  of undisturbed samples. The undrained shearing strength can also be determined directly by means of the vane or torvane (Fig. 11.17), and indirectly by means of the cone penetrometer (Article 11.4.2) or pressuremeter (Article 11.5.3).

During the drilling of exploratory holes the shearing resistance of the clay can be crudely estimated on the basis of the record of the standard penetration test. Table 12.2 shows the approximate relation between the unconfined compressive strength and the penetration resistance  $N_{60}$ . However, at a given value of  $N_{60}$  the scatter of the corresponding values of  $q_u$  from the average is very large. The estimate can be improved by making compression tests on the spoon samples, but the values of  $q_u$  are likely to be too low because of the disturbance associated with the *SPT* sampler and procedure. A much better estimate can be obtained by making laboratory tests on samples from thin-walled tube samplers (Article 11.3.3.).

One procedure for investigating the undrained strength and other pertinent characteristics of a clay deposit is described in the following paragraphs. It is intended to suggest a fruitful approach, rather than to constitute a rigid prescription. The samples are obtained by means of tube-sample borings that furnish practically continuous cores. To obtain fairly reliable average values, the spacing between the sample borings should not exceed 30 m. If it is known in advance that the soil profile is fairly regular and that tube sample borings will be required, continuous samples are taken in all those sections of the exploratory holes that are located within clay strata. In the sections located between clay strata, spoon samples are extracted and standard penetration tests are made.

The samples are delivered to the laboratory in sealed tubes commonly 750 or 900 mm long. Preferably, all the clay samples from one hole should be tested in the sequence in which they followed each other in the drill hole in a downward direction. Each sample is ejected from its tube by means of a close-fitting plunger in such a manner that the sample continues to move with respect to the tube in the same direction as it entered; if excessive side friction causes too much disturbance during ejection, the tube is cut into 150-mm sections, the soil itself is cut by means of a wire saw, and each section is ejected.

For routine testing each sample is cut into sections with lengths equal to about three times the diameter; that is, 50-mm tube samples should be cut into about 150-

**Table 12.2** Relation of Consistency of Clay, Number of Blows  $N_{60}$  on Sampling Spoon, and Unconfined Compressive Strength

Consistency	$q_u$ (kPa)					
	Very Soft	Soft	Medium	Stiff	Very Stiff	Hard
$N_{60}$	<2	2–4	4–8	8–15	15–30	>30
$q_u$	<25	25–50	50–100	100–200	200–400	>400

mm sections. If the uppermost clay-core section from a given tube appears to be relatively undisturbed, it is submitted to an unconfined compression test first in its natural state and then in a completely remolded state at the same water content. The ratio between the two values of the compressive strength is a measure of the sensitivity of the clay (Article 7.1). After the test, the sample is divided lengthwise into two parts. One-half is used for a water-content determination, and the other is stored in a jar with an airtight cover. The same set of tests is made during subsequent operations whenever a sample is encountered that differs noticeably from its predecessor in consistency, color, or general appearance. A change in consistency is revealed by a noticeable change of the resistance of the clay to deformation between the fingers. The uppermost samples in each tube may be appreciably more disturbed than the others. If this is the case, the compression tests should be performed on one of the less disturbed samples.

The samples following the first one are split lengthwise. One entire half is used for a water-content determination. The other half should be set aside in a fairly humid atmosphere with its plane surface facing upward, whereupon it starts to dry slowly. At an intermediate state of desiccation the details of stratification become clearly visible. At that state a record should be made of the details of stratification, indicating the color and approximate thickness of the individual layers, the degree of perfection of the stratification, and other visible features. The records are later used for preparing a general description of the characteristics of the stratification of the clay. A few representative specimens are photographed.

Each 150-mm section is used for water-content determination and visual inspection. If the experimenter examines five or six samples in this manner without noticing a conspicuous change, the next section is submitted to an unconfined compression test in its natural state, as well as to the water-content determination. This procedure is continued until a sample is encountered that differs materially from its predecessor. This sample is submitted to the same tests as the very first one, whereupon the routine procedure is resumed.

If a more detailed record of the consistency is desired, each of the 150-mm sections mentioned in the preceding paragraph is sliced lengthwise into halves and one or two small-diameter torvane tests (Fig. 11.17e) are made on the cut face of one of the halves. The other half is used for determinations of water content, studies of stratification, and other appropriate tests. Figure 12.5 shows the results of such a detailed survey on samples of stratified highly sensitive silty clays involved in landslides caused by the Good Friday earthquake in Anchorage (Shannon and Wilson 1964). The values of sensitivity were calculated on the basis of miniature vane tests on completely remolded portions of the samples at the locations where the torvane tests were made.

After all the foregoing tests on samples from one drill hole have been made, the Atterberg limits are determined on representative specimens of those samples that were submitted to compression tests in both the natural and remolded states. The results of the tests are represented in diagrams such as that shown in Fig. 12.5. The diagrams should be accompanied by a brief description of the characteristics of the stratification of the clay (not shown in the figure).

If the investigation is made for the purpose of estimating the factor of safety of slopes with respect to sliding or of fills with respect to spreading, the knowledge of the details of stratification is at least as important as that of the strength of the clay, because the major part of the potential surface of sliding may be located in one or more seams of water-bearing fine sand or coarse silt and not in the clay. In such instances a detailed and well-illustrated description of the characteristics of the stratification should be prepared. A few typical samples of the stratified layers should be set aside for further investigation. This investigation consists of determining the natural water content and the Atterberg limits of each of the layers of which the sample is composed. Figure 12.6 shows the results of such an investigation.

In any event the opportunity should be sought to investigate the degree of disturbance of the tube samples as described in Article 11.3.3.

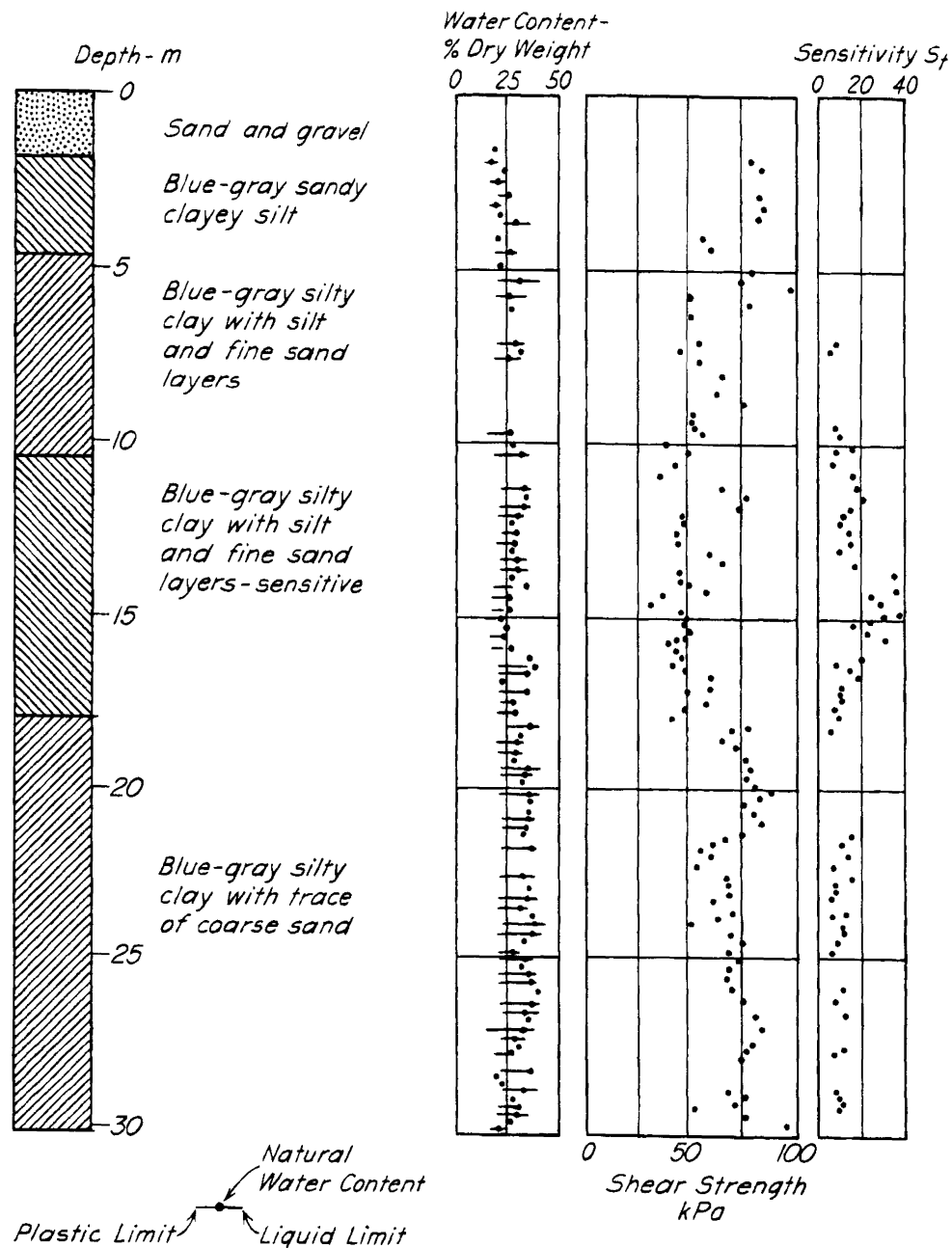


**Figure 12.5** Results of detailed study of strength, Atterberg limits, and natural water content of borings in clays associated with landslides caused by earthquake in Anchorage, Alaska on Good Friday, 1964 (after Shannon and Wilson 1964).

All the preceding discussions refer to the investigation of fairly homogeneous clay strata. If the clay strata contained in the subsoil have a variable thickness and consistency, the method of investigation must be modified. Instead of concentrating on soil tests, the engineer should attempt to investigate the topography of the upper and lower boundaries of the clay layers and to locate the softest and hardest parts of the layers. The most expedient

method to obtain this information is to make numerous sub-surface soundings supplemented by exploratory drill holes. After the results of these investigations are assembled, two or three tube-sample borings are made. These borings should be located at the best and the worst spots of the site. Within the bodies of soil located between the clay strata, spoon samples are taken and standard penetration tests are made, whereas within the clay strata

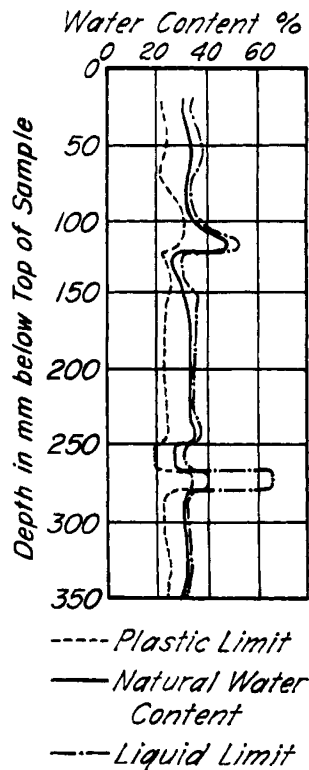


**Figure 12.6** Diagram showing variations of index properties within a 300-mm layer of soft glacial clay.

continuous tube samples are secured. Figure 12.7 represents a boring of this type. The boring was made in a composite shore deposit located on one of the slopes of a drowned valley. On the left side is shown an abstract of the foreman's record. The first diagram is the penetration record of a subsurface sounding made a short distance from the drill hole. The last two diagrams contain the results of the soil tests.

Figure 12.8 represents the results of a survey of the unconfined compressive strength of a glacial clay deposit intermediate between regular and erratic. The individual clay strata were not homogeneous enough to justify assigning definite average values to their physical properties. Yet the project called for general information concerning the compressive strength of the clay and its variations in both horizontal and vertical directions. To satisfy these demands, tube sample borings were made at points 60 m apart, and the cores obtained from these borings were submitted to the same tests that are made on continuous cores from homogeneous strata. Subsequent tunneling operations showed that the profiles realistically disclosed the general character of the clay strata encountered in the different tunnel sections. As would be expected, between drill holes the scattering of the properties of the clay from the average was important and called for continual vigilance during construction, but a more

detailed subsoil investigation would have been impracticable and uneconomical (Terzaghi 1943a).

## 12.7 Compressibility of Clay Strata

The compressibility of clay strata is of interest as a source either of progressive settlement or else of delay in the increase of shearing resistance produced by superimposed load. Whatever the practical implications of the compressibility may be, a reliable forecast of its effects can be made only if the clay strata are continuous and fairly homogeneous.

If the subsoil contains a continuous and fairly homogeneous clay stratum, the settlement of the surface due to superimposed loads is at every point roughly proportional to the average pressure that the loads produce in the clay beneath this point. The intensity and distribution of the pressure in the clay can be computed by means of the methods described in Article 40. On the basis of the results of the computations and those of soil tests, the settlements due to the loads can be computed, and curves of equal settlement can be constructed.

On minor jobs involving foundations above fairly homogeneous clay strata, no soil investigations are required other than routine tests on spoon samples. These include determination of the natural water content and of the liquid and plastic limits. The compressibility can then be estimated on the basis of general or regional statistical correlations. For example, the compressibility as measured by the compression index  $C_c$  (Article 16.6) is related to the natural water content for sedimented clays, silts, and peats as shown in Fig. 16.3. In specific localities, such as Boston or Chicago, approximately linear relations are found between the *compression ratio*  $C_c/(1 + e_0)$ , determined from consolidation tests, and the natural water content (Fig. 12.9). Where such relations exist, they permit estimating  $C_c$  and making settlement calculations (Eq. 16.18) reliable enough for many purposes. Moreover, whenever consolidation tests are made for a particular project, such correlations should be developed, not only as an aid in interpreting the pattern of compressibility for the soils at the project, but also to add to the storehouse of data for the locality.

Correlations between compressibility and water content or liquid limit may underestimate the compressibility of a sensitive clay that suffers structural breakdown under the added stress caused by the construction. To avoid this eventuality in a locality where experience is lacking, the sensitivity should be investigated in at least one boring by means of compression or vane tests on tube samples of C quality or better, or by means of field vane tests (Article 11.5.2). If the sensitivity exceeds about 15, the routine investigation outlined above should be supplemented by more refined investigations.



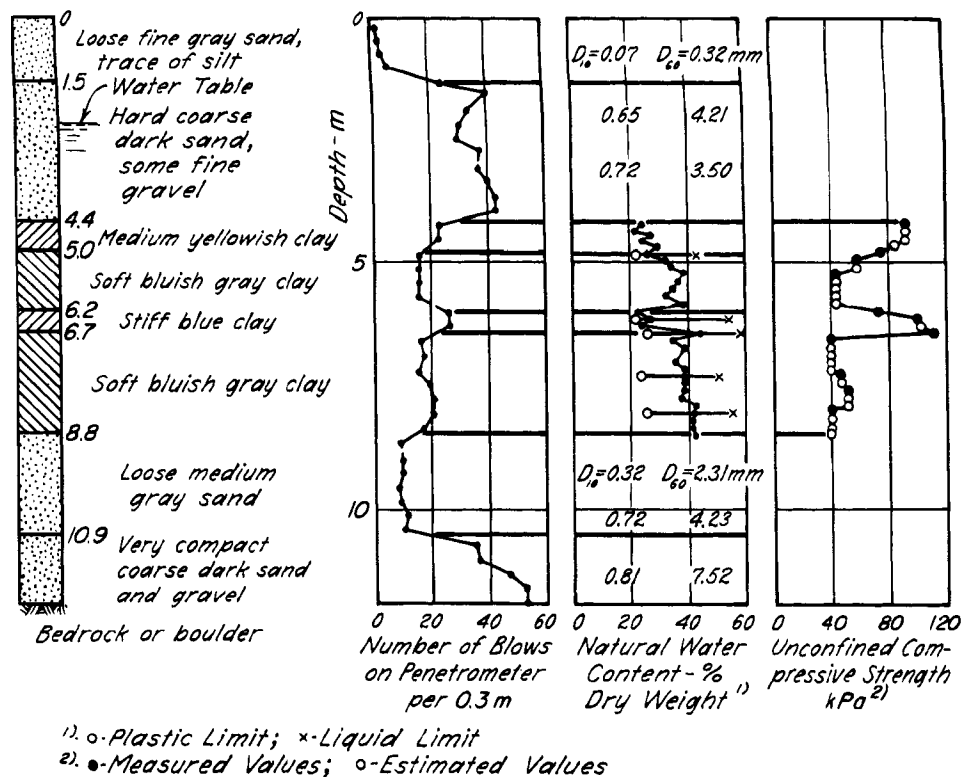


**Figure 12.7.** Diagram representing boring record, penetration record, and results of soil tests on samples from drill hole through composite shore deposit.

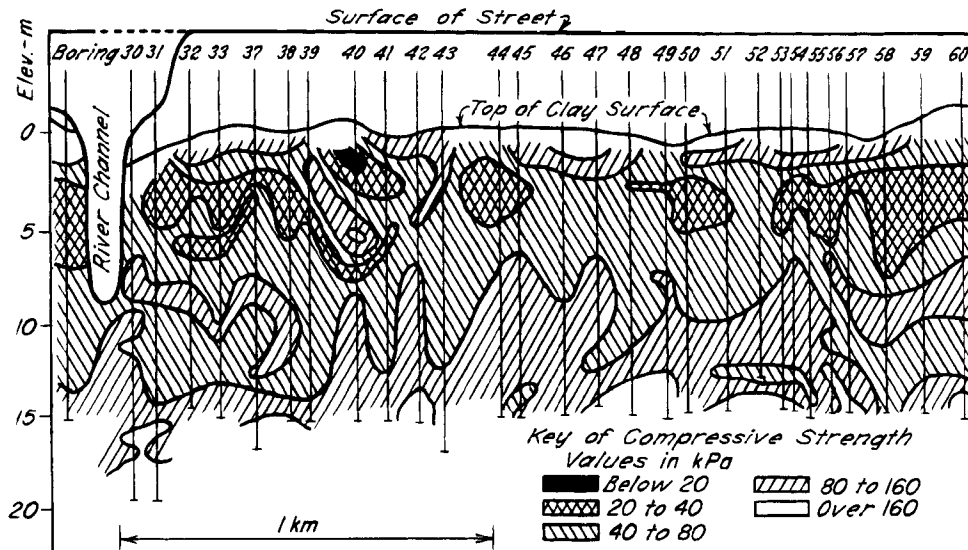


**Figure 12.8** Diagram showing variations in unconfined compressive strength of somewhat erratic glacial clay deposit in Chicago (after Terzaghi 1943a).

On important jobs that call for accurate settlement forecasts, supplementary investigations are required. These include tube-sample borings, from which continuous tube samples are obtained, spaced not more than 30 m. The samples are submitted to the same tests as those described

for the investigation of the shearing resistance of homogeneous clay strata, except that the sensitivity does not need to be evaluated on samples from more than one boring.

After the water-content profiles for all the tube-sample borings have been plotted in diagrams similar to Fig. 12.5,



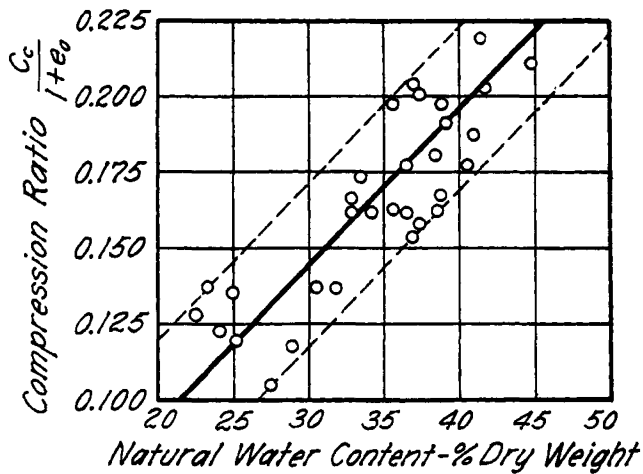


**Figure 12.9** Statistical relation between natural water content and compression ratio for samples of clay from boring in Boston, MA (after Fadum 1941).

one representative boring is selected. Near this boring an undisturbed sample boring is made that furnishes samples of at least *B* quality to be submitted to consolidation tests.

Because of the great amount of time and labor involved in the performance of consolidation tests (Article 16.9), these tests cannot be made on most jobs on more than 10 or 15 samples without undue delay. Yet, even in relatively homogeneous clay strata the physical properties of the clay are likely to change to a considerable extent from point to point. Consequently, the compressibility characteristics of a clay can be determined at a reasonable expense only on the basis of statistical relationships between the compressibility and the index properties of the clay.

Finally, on very large and expensive jobs, such as the construction of airport runways on deep fills over thick compressible sediments in bays or estuaries, or the construction on sensitive clays of dams to retain reservoirs at a given elevation, reliable forecasts of long-term settlements are required. The supplementary information to be obtained for such forecasts is described in Article 16.

Figure 52.15 illustrates the degree of accuracy that can be achieved in computing the distribution of the settlement over the base area of a building located above fairly homogeneous clay strata. The real distribution is shown on the left-hand side, and the computed on the right. The structure itself is complex but symmetrical. No such results can be obtained if the profile of the subsoil of a building is erratic, because the settlement of buildings on such subsoils depends not only on the intensity and the distribution of the loads but also on the variations in the compressibility of the subsoil in horizontal directions. In addition, the rate of settlement can change from place to place, because it depends on the degree of continuity of layers and pockets of cohesionless material present in

the subsoil. Figure 12.10 illustrates such a profile. It represents the results of test borings in a composite shore deposit located at the south shore of Lake Erie. More than 100 borings were made, and the spacing between drill holes did not exceed 30 m. Yet the borings records did not indicate whether or not the layers of clay encountered in the drill holes were continuous.

If the profile of the subsoil of a proposed structure is erratic an extensive program of undisturbed sample borings and elaborate soil investigations is entirely out of place. Information of far more practical value can be obtained by means of numerous subsurface soundings supplemented by exploratory drill holes. The results of such investigations inform the designer of the location of the softest and the most resistant spots beneath the base of the building. At the location of the softest clay, an undisturbed sample boring may be made to obtain information on the details of stratification and on the compressibility of the clay that was encountered in the exploratory holes. The maximum settlement is estimated on the basis of the procedures described in Article 41. In judging whether the proposed structure can stand the estimated settlement, the spacing between the hardest and the softest spots of the subsoil is taken into consideration. The results of even very elaborate soil investigations would hardly add anything to the information obtained by the recommended procedure.

## 12.8 Summary of Procedures in Subsoil Reconnaissance

According to the preceding discussions, a subsoil reconnaissance involves several successive stages. The first step is to decide on the depth and spacing of the exploratory borings.

If the proposed structure is a building, current practice calls for about one drill hole for every 250 m<sup>2</sup> of the area covered by the building. If a retaining wall is to be constructed or an open cut to be made, it is customary to make at least one drill hole for every 30 m of length of the wall or the cut. However, these rules are based on convention rather than rational considerations. If the subsoil is erratic, more useful information can usually be obtained in less time and at a smaller expense by combining the exploratory borings with subsurface soundings.

The depth to which the exploratory drill holes should be made depends on whether the subsoil may contain layers of soft clay. If the local geological conditions or the conditions revealed by earlier test borings in the vicinity exclude this possibility, the drill holes do not need to be made to a depth of more than 5 or 10 m below subgrade. On the other hand, if the subsoil may contain layers of soft clay at an unknown depth, a sound decision regarding the minimum depth of the test borings can be made only on the basis of the results of a rough estimate of the maximum depth at which the presence of clay strata may

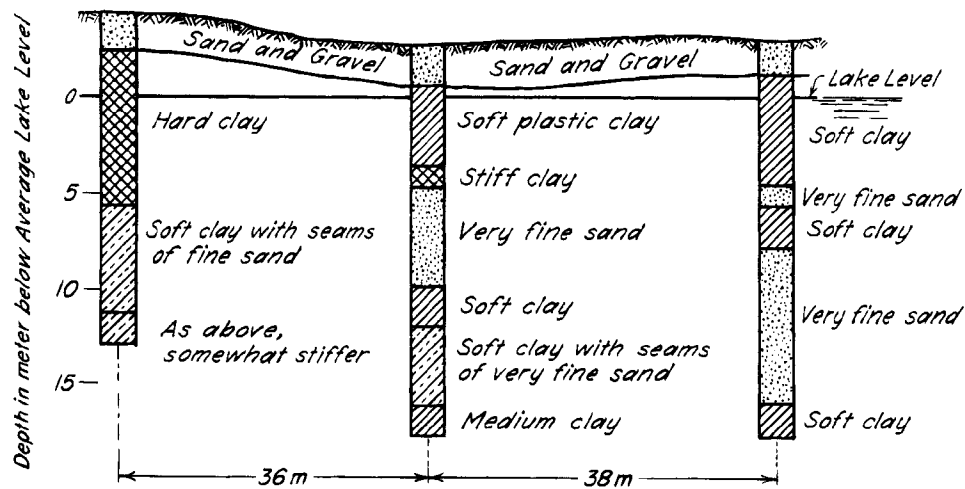


Figure 12.10 Erratic shore deposit, Lake Erie near Cleveland.

still have a significant influence on the performance of the proposed structure.

The subsequent investigations depend on the size of the job, the nature of the design problems, and the subsoil conditions.

On routine jobs such as the foundations of ordinary buildings or bridges, no investigations are needed beyond the routine tests on the spoon samples (see Table 9.1). Large or unusual jobs may call for one or more of the supplementary investigations described under the preceding subheadings. After the results of these investigations are digested, the engineer must then judge whether the conclusions based on the data can be considered final or whether the remaining uncertainties require an observational procedure during construction. Because of the important practical implications of these uncertainties, they are discussed in detail in Article 12.9.

The preceding summary demonstrates that subsoil reconnaissance is seldom a simple procedure requiring only conscientious adherence to a set of hard and fast rules. Unless the investigator is guided by mature judgment and has had a varied practical experience in this field, much time and money may be wasted.

In connection with each step, a thorough knowledge of the geology of sedimentary and other unconsolidated masses is an asset of inestimable value, because factual knowledge is always limited to soil conditions along vertical lines spaced far apart. The results of interpolation and the estimate of possible scattering can be very misleading unless the investigator has a fairly clear conception of the anatomy of the body of soil under investigation. A knowledge of the geology of the region is also needed to confirm whether clay beds beneath the building site have ever been subjected to greater loads than at present and, if so, to provide a basis for estimating the magnitude of the additional pressure.

The larger the job, the more necessary it is to supplement the results of the soil investigations by information obtained from airphoto interpretation and purely geological sources, because on large jobs a detailed soil survey is likely to be a physical impossibility.

## 12.9 Discrepancies between Reality and Assumptions Based on Subsoil Reconnaissance

The results of the subsoil reconnaissance for every job, large or small, are ultimately condensed into a set of assumptions that constitute the basis for design. The steps that lead to this final result involve various processes of interpolation and correlation based on statistical relationships. Therefore, the assumptions are always to some extent at variance with reality. However, the importance of these inevitable discrepancies is very different for different types of assumptions. This fact is explained in detail in the following paragraphs.

Assumptions regarding the angle of internal friction of sandy soils, the relative density of sand strata, or the average compressibility of clay strata belong in one category. The errors associated with these assumptions depend chiefly on the number and quality of the field tests that furnish the basic data. Hence, faulty assumptions in this category can safely be blamed on inadequate soil reconnaissance, provided the soil profile is relatively simple. It should always be assumed that loose submerged sands may liquefy on slight provocation unless they are compacted by artificial means.

The accurate determination of the permeability of soil strata of any kind on the basis of the results of soil tests is impracticable, because the permeability depends on structural details of the strata that cannot be detected by any method of soil exploration. However, if the method for investigating the permeability is selected judiciously

and used intelligently, fairly reliable limiting values can be obtained under almost any circumstances. The difference between the limiting values and the real average value cannot be determined, but for many practical purposes only a knowledge of the limiting values is needed.

By far the most unreliable information is obtained when attempts are made to predict the porewater pressures in stratified sand layers or in beds of clay containing thin seams or layers of more permeable material. The intensity and distribution of porewater pressures, under given hydraulic boundary conditions, depend on unexplorable structural details, even more than does the average coefficient of permeability of such strata. Hence, if the factor of safety of a foundation with respect to failure, or that of a mass of soil with respect to sliding, depends on porewater pressures, the fundamental assumptions regarding the porewater pressures should not be trusted under any circumstances, regardless of the care with which the subsoil has been explored.

In such instances the assumptions on which the design is based should be considered as nothing more than the expression of a working hypothesis, subject to revision on the basis of the results of observations made in the field during construction. Practically all the failures of the foundations of dams and other hydraulic structures can be attributed to unjustified confidence in assumptions of some kind, and many of the failures could have been avoided by appropriate field observations during the construction period. Considering the loss of life and capital involved in the failure of an important hydraulic structure, reliance on the assumptions on which the original design was based and omission of the field observations required for investigating the real conditions must, at the present state of our knowledge, be classified as unpardonable neglect.

Even though the computed values of the porewater pressure cannot be relied on, the computations should always be made, because the results serve a vital purpose. They constitute the basis for evaluating the possible dangers, for preparing the program of field observations needed to detect impending dangers during construction, and for interpreting the results of these observations.

### Selected Reading

The relationships among geological conditions, engineering properties, and exploratory procedures are discussed or exemplified in the following publications.

- Belcher, D. J. (1945). "The engineering significance of soil patterns," *Photogrammetric Engineering*, **11**, No. 2, pp. 115–148.
- Lee, C. H. (1953). "Building foundations in San Francisco," *Proc. ASCE*, **79** (Separate 325), 32 pp.
- Sowers, G. F. (1953). "Soil and foundation problems in the southern Piedmont region," *Proc. ASCE*, **80** (Separate 416), 18 pp.

- Bjerrum, L. (1954). "Geotechnical properties of Norwegian marine clays," *Géot.*, **4**, No. 2, pp. 49–69.
- Peck, R. B. and W. C. Reed (1954). "Engineering properties of Chicago subsoils," *U. of Ill. Eng. Exp. Sta. Bull.* **423**, 62 pp.
- Terzaghi, K. (1955a). "Influence of geological factors on the engineering properties of sediments," *Economic Geology*, Fiftieth Anniversary Volume, pp. 557–618.
- Marsal, R. J. and M. Mazari (1962). *El subsuelo de la Ciudad de Mexico* (The subsoil of Mexico City). U. of Mexico, Faculty of Engineering, 2nd ed., 614 pp.
- Woods, K. B., R. D. Miles, and C. W. Lovell, Jr. (1962). "Origin, formation, and distribution of soils in North America," Chapter 1 in *Foundation engineering*, G. A. Leonards, ed., New York, McGraw-Hill, pp. 1–65.
- Lumb, P. (1965). "The residual soils of Hong Kong," *Géot.*, **15**, No. 2, pp. 180–194.

The following references contain examples of exploratory programs adapted to the conditions at the site and the requirements of the report.

- Terzaghi, K. (1929c). "Soil studies for the Granville dam at Westfield, Mass.," *J. New Engl. Water Works Assn.*, **43**, pp. 191–223. Permeability survey of glacial outwash adjoining a reservoir site. The capillary rise method used in this study has been superseded by other procedures.
- Peck, R. B. (1940). "Sampling methods and laboratory tests for Chicago subway soils," *Proc. Purdue Conf. on Soil Mech.*, pp. 140–150. Investigation of physical properties of somewhat erratic glacial clays in connection with tunneling operations.
- Brown, F. S. (1941). "Foundation investigation for the Franklin Falls dam," *J. Boston Soc. Civil Engrs.*, **28**, pp. 126–143. Reprinted in *Contributions to soil mechanics 1941–1953*. Boston Society of Civil Engineers, pp. 2–19.
- Peck, R. B. (1953). "Foundation exploration—Denver Coliseum," *Proc. ASCE*, **79** (Separate 326), 14 pp. Investigation of erratic sand and gravel deposits and location of boundary of filled area.
- Peck, R. B., (1954). "Foundation conditions in the Cuyahoga River valley," *Proc. ASCE* **80** (Separate 513), 20 pp.
- Teixeira, A. H. (1960). "Typical subsoil conditions and settlement problems in Santos, Brasil," *Proc. 1st Panamerican Conf. on Soil. Mec.*, Mexico, **1**, pp. 149–177.
- Monahan, C. J. (1962). "John Day lock and dam: foundation investigations," *Proc. ASCE*, **88**, No. PO4, pp. 29–45. Exploration of five-mile stretch of river for selection of damsite, requiring geological, geophysical, and engineering studies.

The following references deal with methods of subsoil exploration.

- Sanglerat, G. (1972). *The Penetrometer and Soil Exploration*, Elsevier, Amsterdam.

- Proc. 1st European Symp. on Penetration Testing*, Stockholm, 1, 2:1, 2:2 (1974).
- Proc. 2nd European Symp. on Penetration Testing*, Amsterdam, 1 & 2 (1982).
- Hunt, R. E. (1984). *Geotechnical Engineering Investigation Manual*, McGraw-Hill, New York, 983 p.
- Proc. In Situ '86*, ASCE Speciality Conf. on Use of In Situ Tests in Geotech. Eng., ASCE Geotech. Spec. Publ. No. 6, Blacksburg (1986).
- Proc. ASCE Specialty Conf. on In Situ Measurement of Soil Properties*, Raleigh, 1 & 2 (1975).
- Proc. Int. Symp. on Soil Sampling: State-of-the-Art on Current Practice of Soil Sampling*, Singapore (1979).
- Proc. Symp. on Cone Penetration Testing and Experience*, Geotech. Eng. Div., ASCE (1981).
- Meigh, A. C. (1987). "Cone penetration testing," *CIRIA Ground Eng. Rpt: In Situ Testing*, Butterworth Publishers, Stoneham, MA.
- Proc. 1st Int. Symp. on Penetration Testing*, Orlando, 1 & 2 (1988).
- Proc. Penetration Testing Conf.*, organized by Inst. of Civil Engineers, London (1988).
- Lunne, T., S. Lacasse, N. S. Rad, and L. Décourt (1990). "SPT, CPT, pressuremeter testing and recent developments on in situ testing," *Norwegian Geotech. Inst. Publ.* 179, 89 p.

## CHAPTER 3

# *Hydraulic and Mechanical Properties of Soils*

### ARTICLE 13 SIGNIFICANCE OF HYDRAULIC AND MECHANICAL PROPERTIES OF SOILS

In Chapter 1, we dealt with the index properties of soils. Because these properties reflect the general character of a given soil, they serve to indicate the extent to which soils from different localities may or may not be similar. In addition, they constitute the basis for recording construction experience and for using this experience on subsequent jobs.

Foundation and earthwork engineering is based chiefly on experience. However, civil engineering in general did not emerge from a state of relative stagnation until the accumulated stock of experience became fertilized by applied science. The function of science was to disclose the relations between events and their causes.

To establish these relations in the realm of foundation and earthwork engineering, it was necessary to investigate the physical properties of the different types of soils, just as it was necessary in structural engineering to investigate the properties of steel and concrete. A given steel or concrete is adequately described for most practical purposes if its strength and modulus of elasticity are known. On the other hand, practical problems involving soils may require the consideration of a variety of soil properties. Foremost among these are the permeability, the compressibility, the resistance against shear, and the stress-deformation relationships. In the following articles, these properties are discussed in detail.

### ARTICLE 14 PERMEABILITY OF SOILS

#### 14.1 Introduction

A material is said to be permeable if it contains continuous voids. Because such voids are contained in all soils including the stiffest clays, and in practically all nonmetallic construction materials including sound granite and neat cement, all these materials are permeable. Furthermore, the flow of water through all of them obeys approximately

the same laws. Hence, the difference between the flow of water through clean sand and through sound granite is merely one of degree.

The permeability of soils has a decisive effect on the cost and the difficulty of many construction operations, such as the excavation of open cuts in water-bearing sand, or on the rate at which a soft clay stratum consolidates under the influence of the weight of a superimposed fill. Even the permeability of dense concrete or rock may have important practical implications, because water exerts a pressure on the porous material through which it percolates. This pressure, which is known as *seepage pressure*, can be very high. The erroneous but widespread conception that stiff clay and dense concrete are impermeable arose because the entire quantity of water that percolates through such materials toward an exposed surface is likely to evaporate, even in a very humid atmosphere. Consequently, the surface appears to be dry. However, since the mechanical effects of seepage are entirely independent of the rate of percolation, the absence of visible discharge does not imply the absence of seepage pressures. Striking manifestations of this fact may be observed while an excavation is being made in very fine rock flour. The permeability of this material is very low. Yet, a slight change in the pressure conditions in the pore water may suffice to transform a large quantity of the material into a semiliquid.

#### 14.2 Definitions and Darcy's Flow Equation

Water flows through soils in response to a gradient in *total* or *hydraulic head* ( $h$ ) defined as

$$h = z + \frac{u}{\gamma_w} \quad (14.1)$$

Total head is illustrated in Fig. 14.1, in which  $a$  and  $b$  represent two points on a flow line in soil. The vertical elevation of each point is defined by the position head  $z$  in reference to a datum. At each point a standpipe, known as a *piezometer* or *piezometric tube*, has been installed

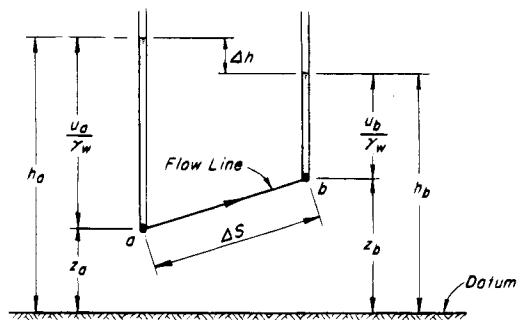


**Figure 14.1** Definition of total head  $h$  in terms of position head  $z$  and piezometric head  $u/\gamma_w$ .

to indicate the level to which the water rises at these points. The water level in the piezometer at  $a$  is designated the *piezometric level* at  $a$ , and the vertical distance from this level to point  $a$  is the *piezometric head*,  $u_a/\gamma_w$ , at  $a$ , where  $u_a$  is the *porewater pressure* at point  $a$ . Regardless of the relative magnitudes of  $z_a$  and  $z_b$  or of  $u_a/\gamma_w$  and  $u_b/\gamma_w$ , water can flow only if  $h_a$  differs from  $h_b$ . Since in Fig. 14.1  $h_a$  is larger than  $h_b$ , water flows from  $a$  to  $b$ , and the head loss between  $a$  and  $b$  is

$$\Delta h = h_a - h_b \quad (14.2)$$

The rate of loss of total head through the soil is defined as the *hydraulic gradient*,

$$i = -\lim_{\Delta s \rightarrow 0} \frac{\Delta h}{\Delta s} = -\frac{dh}{ds} \quad (14.3)$$

where  $\Delta s$  is the macroscopic or apparent flow distance between points  $a$  and  $b$ . The line connecting points  $a$  and  $b$  is a *flow line*.

The *discharge velocity*,  $v$ , is defined as the quantity of water that percolates per unit of time across a unit area of a section oriented normal to the flow lines. Since, in a statistically isotropic porous material, the porosity of a plane section is equal to the volume porosity  $n$ , the average *seepage velocity*,  $v_s$ , at which water percolates through the voids of the material is equal to the discharge velocity divided by the porosity. If the term velocity is used without qualification in connection with permeability, it always indicates the discharge and not the seepage velocity.

Darcy (1856) made observations of the rate of flow of water through saturated granular soils and obtained the empirical relationship

$$v = ki \quad (14.4)$$

where, in the macroscopic or apparent flow direction  $s$ ,  $v$  is the discharge velocity,  $i$  is the hydraulic gradient, and  $k$  is defined as the *coefficient of permeability*. Subsequent measurements have shown that the Darcy equation of fluid motion accurately defines the relationship between

discharge velocity and hydraulic gradient in all saturated fine- and coarse-grained soils unless, in very coarse-grained soils, the flow is so rapid as to be turbulent. Because the hydraulic gradient is dimensionless, the coefficient of permeability has the units of velocity (e.g., m/s). Table 14.1 indicates the approximate range of values of  $k$  for soils of various gradations.

The coefficient of permeability is a measure of the ease with which water flows through permeable materials. It is inversely proportional to the viscosity of water, which decreases with increasing temperature as shown in Fig. 14.2. Therefore, permeability measurements at laboratory temperatures should be corrected with the aid of Fig. 14.2, before application to field temperature conditions, by means of the equation

$$k_f = \frac{\eta_t}{\eta_f} k_t \quad (14.5)$$

where  $k_f$  and  $k_t$  are the coefficients of permeability corresponding to the field and test temperatures, respectively, and  $\eta_f$  and  $\eta_t$  are the corresponding viscosities. It is customary to report values of  $k_t$  at a standard temperature of 20°C.

Several factors may alter the permeability of a given soil. Occluded air bubbles in otherwise saturated soils block flow channels and decrease permeability. Since the bubbles decrease in size with increasing water pressure, the coefficient of permeability of such a soil also increases with increasing water pressure. In clays with root holes or open cracks, percolation is almost inevitably associated with internal erosion. The detached particles gradually clog the narrowest parts of the water passages, whereupon the coefficient of permeability may decrease to a small fraction of its initial value. In compacted soils composed of desiccated clay or shale fragments, percolation of water may lead to slaking and dispersion of clay particles. In well-compacted homogeneous fills, this leads to a decrease in the coefficient of permeability with time. In poorly compacted clays with open continuous voids and cracks, dispersed clay particles are carried away by percolating water, and the permeability increases with time. Hence, Darcy's flow equation may be invalid unless the volume and shape of the water passages remain independent of porewater pressure and time.

Mathematical analyses and measurements of flow through permeable media have demonstrated that the permeability is determined mainly by the areas of the individual pores normal to the direction of flow, the shape of the pores along the direction of flow, and the total area of pores per unit of area normal to the direction of flow. The size of the soil particles, often dictated by mineralogy and aggregation or dispersion, determines the size of individual pores. The shape and arrangement of the particles determine the shape of the pores; and the size, shape,

**Table 14.1 Permeability and Drainage Characteristics of Soils\***

Coefficient of Permeability $k$ (m/s)												
	$10^0$	$10^{-1}$	$10^{-2}$	$10^{-3}$	$10^{-4}$	$10^{-5}$	$10^{-6}$	$10^{-7}$	$10^{-8}$	$10^{-9}$	$10^{-10}$	$10^{-11}$
Drainage	Good						Poor		Practically Impervious			
Soil types	Clean gravel	Clean sands, clean sand and gravel mixtures				Very fine sands, organic and inorganic silts, mixtures of sand silt and clay, glacial till, stratified clay deposits, etc.			"Impervious" soils, e.g., homogeneous clays below zone of weathering			
						"Impervious" soils modified by effects of vegetation and weathering						

\* After Casagrande and Fadum (1940).

and arrangement of the pores together determine the porosity. In stiff clays and shales, as well as in rocks, macropores produced by fissures, joints, and cracks exert a major influence on the permeability.

### 14.3 Permeability of Granular Soils

The permeability of granular soils depends mainly on the cross-sectional areas of the pore channels. Since the average diameter of the pores in a soil at a given porosity increases in proportion to the average grain size, the permeability of granular soils might be expected to increase as the square of some characteristic grain size, designated as the *effective grain size*,  $D_e$ . Extensive investigations of filter sands by Hazen (1892) led to the equation

$$k(\text{m/s}) = C_e D_e^2 \quad (14.6)$$

in which the parameter  $C_e$  includes the effects of the shape of the pore channels in the direction of flow and of the total volume of pores as determined by such proper-

ties as grain shape and gradation. The effective grain size best fitting Eq. 14.6 was found by Hazen to be the 10% size  $D_{10}$  (Article 5). The permeability data in Fig. 14.3 approximate a straight line with a slope equal to 2, consistent with Eq. 14.6. These data indicate an average value of  $C_{10} = 10^{-2}$  when  $k$  is expressed in m/s and  $D_{10}$  in mm. According to the data in Fig. 14.3, Eq. 14.6 may underestimate or overestimate the permeability of granular soils by a factor of about 2.

Laboratory studies by Kenney et al. (1984) on the permeability of granular filters, using natural sands and

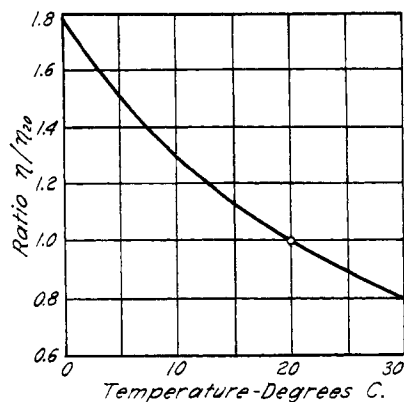


**Figure 14.2** Relation between temperature and viscosity of water.

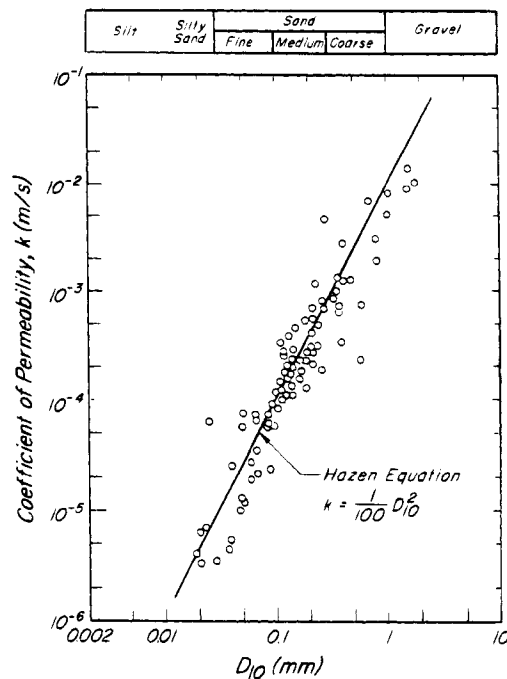


**Figure 14.3** Hazen equation and data relating coefficient of permeability and effective grain size of granular soils (after Loudon 1952).

gravels with subangular grains, indicate that gradation, as expressed by uniformity coefficients  $C_U = D_{60}/D_{10}$  ranging from 1.04 to 12, has little influence on permeability in comparison to the influence of the size of the small particles. The permeability is controlled by  $D_5$  or  $D_{10}$ , because the spaces between the large particles are filled with smaller particles and the smaller particles control the size of the pore channels. Kenney et al. concluded that  $D_5$  would have been a better choice for the effective grain size, because  $C_5$  has a narrower range of values than  $C_{10}$  or  $C_{15}$  for materials of differing gradation. This is shown by Fig. 14.4. All specimens represented in Fig. 14.4 were compacted by vibration to values of relative density in excess of 80%. Thus the permeability data in Fig. 14.4 correspond to a smaller range of relative density than those in Fig. 14.3.

The permeability of granular soils may decrease substantially on account of the presence of even small amounts of fine silt- and clay-sized particles. The mineralogy and degree of aggregation or dispersion of the fines determine the magnitude of the decrease in permeability. Figures 14.5 and 14.6 show data on values of  $k$  for clay minerals in water and in nonpolar fluids, respectively. Both water, which is highly polar, and monovalent adsorbed sodium cations promote dispersion and small particle sizes. Of the three principal clay minerals, montmorillonite has the smallest particle size and kaolinite the largest, with illite occupying an intermediate position. At the same void ratio, illite is about 200 times and kaolinite about 200,000 times more permeable than montmorillonite. Figure 14.5 also shows that the permeability of clay minerals depends strongly on void ratio.

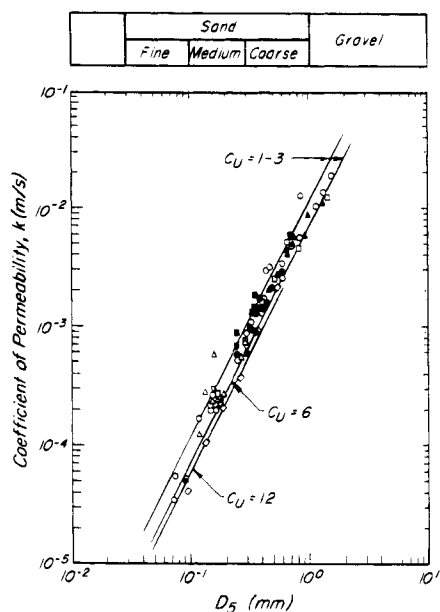


**Figure 14.4** Influence of gradation on permeability of granular soils (after Kenney et al. 1984).

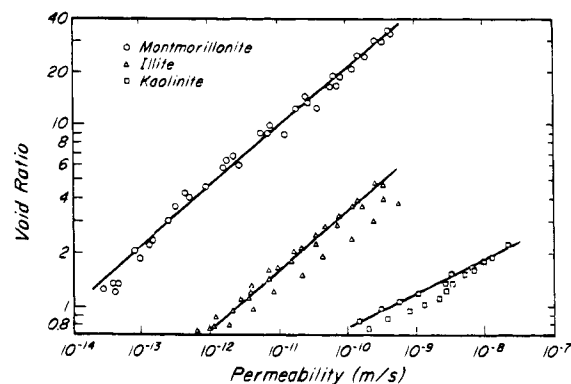


**Figure 14.5** Permeability of sodium clay minerals in water (Mesri and Olson 1971).

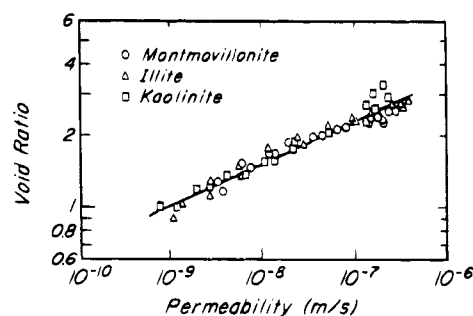


**Figure 14.6** Permeability of sodium clay minerals in carbon tetrachloride or benzene (after Mesri and Olson 1971).

The permeability data in Fig. 14.6 pertain to clay minerals in benzene or carbon tetrachloride, which are nonpolar fluids that promote complete aggregation of clay mineral particles. Aggregation is most significant for the small and thin plates of montmorillonite and illite and is less so for the large and thick plates of kaolinite. After aggregation, the size of montmorillonite and illite particles approaches that of large kaolinite particles, and the three clay minerals display similar relations between permeability and void ratio. The significant aggregation effect on clay minerals of nonpolar fluids must be considered in the design of clay liners that are used to contain chemical wastes.

The foregoing paragraph demonstrates that the coefficient of permeability, as customarily defined in soil mechanics, is a property not only of the soil but also of the fluid. Unless otherwise indicated, values of  $k$  refer to the permeability in water; this value is often designated as the *hydraulic conductivity*.

#### 14.4 Permeability of Soft Clays

Most soft clay deposits of marine and lacustrine origin are composed of a mixture of minerals that are likely to include illite and chlorite, substantial amounts of quartz and feldspar, and some montmorillonite, micas, and car-



bonates. The fabric of soft clays, especially those of marine origin, is often flocculated or aggregated. Figure 14.7 shows that the coefficient of permeability in the vertical direction, at *in situ* void ratio  $e_0$ , is correlated with the clay fraction (CF) (Article 8.2) and with the activity  $A_c = I_p/CF$ . The correlation exists because the activity reflects mineralogy which, in turn, determines particle size and thus pore size. Moreover, the permeability is related directly to  $e_0$  but inversely to the clay-size fraction (CF), because high values of CF correspond to small and tortuous pores. Values of  $k_{vo}$  for soft clays are commonly near  $1 \times 10^{-9}$  m/s. In fact, values of  $k_{vo}$  for a majority of soft clays fall within the narrow range of  $5 \times 10^{-10}$  m/s to  $5 \times 10^{-9}$  m/s for a number of reasons. With decreasing clay mineral and organic content, or with increasing silt content, soft clays come to equilibrium under natural sedimentation-consolidation conditions at increasingly small void ratios. Thus, the combination of large void ratios but small void sizes in clays of high plasticity leads to permeabilities similar to those in silty clays with smaller void ratios but larger void sizes. Furthermore, the flocculated or aggregated fabric, which occurs most commonly in soft clays, somewhat affects the influence of mineral composition on the size, shape, and total volume of the pores.

Several independent factors can lead to anisotropy in the permeability of soft clay deposits, in which the coefficient of permeability  $k_{ho}$  in horizontal directions is higher than  $k_{vo}$ . One factor may be an inherent anisotropy of the clay fabric resulting from a predominant horizontal orientation of plate-shaped or elongated clay mineral particles. However, most soft clay deposits of marine origin have an overall random fabric, since they consist of a more or less homogeneous mixture of clay minerals, which are flocculated or aggregated, and of space-lattice minerals. Thus, in soft clays of marine origin,  $k_{ho}/k_{vo}$  rarely exceeds 1.5 and often is near 1.0. A second possible source of anisotropy in the permeability of lacustrine soft clay

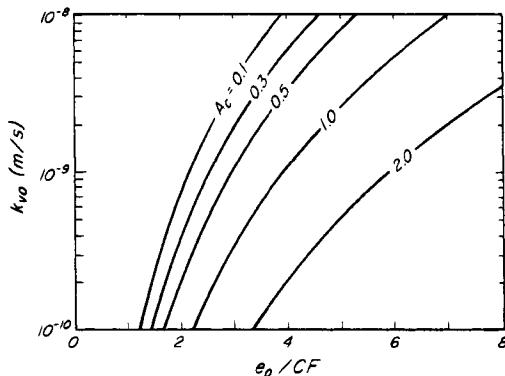


**Figure 14.7** *In situ* permeability of soft clays in relation to initial void ratio,  $e_0$ ; clay fraction, CF; and activity  $A_c$  (After Mesri et al. 1994).

deposits is their varved nature. However, even in varved clay deposits,  $k_{ho}/k_{vo}$  rarely exceeds 5 and is often less than 3. This is regarded by Kenney (1963, 1976) to be a consequence of gradual as opposed to abrupt variation of gradation and permeability in the vertical direction within the silt and clay varves. In highly segregated clay deposits the value of  $k_{ho}/k_{vo}$  may reach 10 (Ladd and Wissa 1970). A third factor that may lead to values of  $k_{ho}/k_{vo}$  greater than one in soft clay deposits is the presence of thin horizontal silt or sand layers. Continuous pervious layers, if identified during subsurface investigations, can be treated as drainage boundaries or as sublayers with high permeability. However, inclusions of silt and sand may be horizontally discontinuous. Such inclusions contribute to  $k_{ho}$ , especially when vertical drains are used (Article 44.3.6), and must be taken into account if  $k_{ho}/k_{vo}$  is calculated from full-scale field observations.

Consolidation of soft clays (Article 16) may involve a significant decrease in void ratio and therefore of permeability. The relationships between  $e$  and  $\log k_v$  for a number of soft clays are shown in Fig. 14.8. The decrease in permeability with decreasing void ratio may be expressed in terms of  $C_k = \Delta e / \Delta \log k$ . For a given decrease in void ratio, large values of  $C_k$  imply small decreases in permeability, whereas small values of  $C_k$  correspond to large decreases. The shape of the  $e$  vs  $\log k$  curves in the compression range is such that  $C_k$  gradually decreases with compression. However, for most soft clays, the initial portion, starting from the field conditions up to about 20% vertical strain, can be represented by a constant value of  $C_k$ . Typical values of  $C_k$  correspond to a range in  $C_k/C_c$  of 1/2 to 2, where the compression index  $C_c = \Delta e / \Delta \log \sigma'_v$  (Article 16.6) is evaluated just beyond the preconsolidation pressure (Mesri and Rokhsar 1974). For

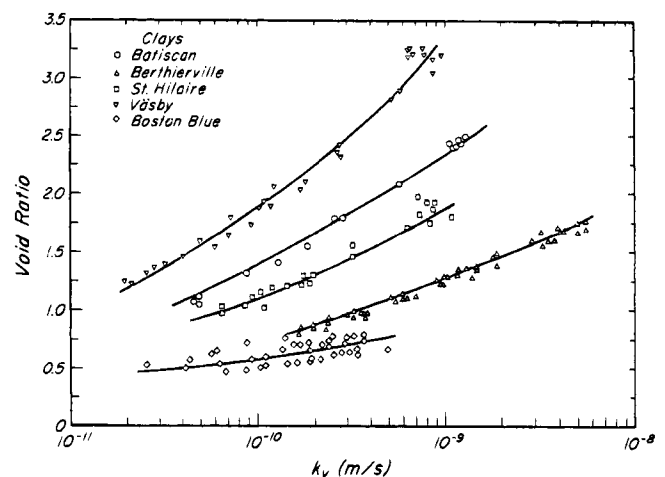


**Figure 14.8** Results of falling-head and constant-head permeability tests on undisturbed samples of soft clays.

most soft clay deposits an empirical correlation,  $C_k = 0.5 e_0$ , between  $C_k$  and *in situ* void ratio  $e_0$  is excellent.

#### 14.5 Permeability of Sand-Clay Mixtures

Compacted mixtures of sand and bentonite are often used as blankets or liners to form seepage barriers against fluids, including leachates from disposal facilities.

In ideal homogeneous mixtures with bentonite to sand ratios of about 10%, hydrated bentonite occupies all the voids between the sand particles. The permeability  $k_m$  of ideal sand-bentonite mixtures is controlled by the permeability  $k_b$  of the bentonite:

$$\begin{aligned} k_m &= k_b \left[ \frac{\text{Cross-sectional area through bentonite}}{\text{Total cross-sectional area of mixture}} \right] \\ &= k_b \left[ \frac{\text{Total volume} - \text{sand volume}}{\text{Total volume}} \right] \\ &= k_b \left[ 1 - \frac{\gamma_{dm}}{(1-r)G_s\gamma_w} \right] \end{aligned} \quad (14.7)$$

where  $\gamma_{dm}$  is the dry unit weight of the mixture,  $\gamma_w$  the unit weight of water,  $G_s$  the specific gravity of the sand, and  $r$  the ratio of the dry masses of bentonite and sand. For many mixtures,  $k_m \approx k_b/2$ . The void ratio  $e_b$  of the bentonite in an ideal saturated sand-bentonite mixture depends on the amount of dry bentonite in the mixture and on the volume between sand particles that is occupied by hydrated bentonite:

$$e_b = \left( 1 + \frac{1}{r} \right) \frac{G_b\gamma_w}{\gamma_{dm}} - \frac{G_b}{rG_s} - 1 \quad (14.8a)$$

where  $G_b$  is the specific gravity of bentonite. For  $G_b \approx G_s$

$$e_b = e_m \left( 1 + \frac{1}{r} \right) \quad (14.8b)$$

where  $e_m$  is the void ratio of the mixture. The upper limit of  $e_b$  is the free-swell void ratio of the bentonite (i.e., void ratio at zero effective stress, Article 15.1, on wetting). Void ratios calculated from Eq. 14.8 that are larger than the free-swell void ratio indicate the presence of voids not occupied by hydrated bentonite.

Kenney et al. (1992) measured the permeability of sand-bentonite mixed with either distilled water, referred to as fresh water, or a solution of 40 g NaCl/l, referred to as salt water. The bentonite consisted mainly of montmorillonite with sodium the dominant exchangeable cation. The liquid limits of the bentonite in fresh water and in salt water were 500% and 105%, respectively. To determine the permeability  $k_b$  of the bentonite, samples were mixed with water at water contents near to or larger than the corresponding liquid limit and were consolidated one-dimensionally (Article 16.2) to an  $e_b$  in the range of

1.5 to 10 at which falling-head permeability tests (Article 14.6) were conducted. The results are presented in Fig. 14.9. Bentonite in fresh water is highly dispersed, with small flow channels and low permeability. At the same values of void ratio, saltwater bentonite is an order of magnitude more permeable than freshwater bentonite, because in salt water the sheets of montmorillonite are flocculated into large units that lead to large flow channels and high permeability.

Frequently the permeant passing through a seepage barrier is chemically different from the original pore fluid used for mixing. Kenney et al. (1992) used salt water to permeate bentonite mixed and consolidated in fresh water, and conversely they used fresh water to permeate bentonite mixed and consolidated in salt water; no change in void ratio was allowed. Figure 14.9 shows that the reduction in salt concentration led to significant dispersion and to decreases in pore size and permeability of more than an order of magnitude. The permeability increased by only small amounts when fresh water was replaced by salt water. Such a large increase in salt concentration would lead to significant flocculation in suspensions of bentonite, such as bentonite grouts and slurries, in which montmorillonite particles have freedom to move. However, at void ratios of 3 to 10, which are significantly less than the free-swell void ratio of 25 for the bentonite in fresh water, the montmorillonite sheets apparently were not free to rearrange themselves into packets and flocs.

The sand used in the tests of Kenney et al. (1992) ranged in grain size from 0.07 to 1.2 mm; in a dense state its coefficient of permeability was  $10^{-4}$  m/s. Two different procedures were used to prepare mixtures of the sand with bentonite: remolding, to approximate ideal homogeneous mixtures, and compacting, to approximate field construction procedures. In the first, homogeneous

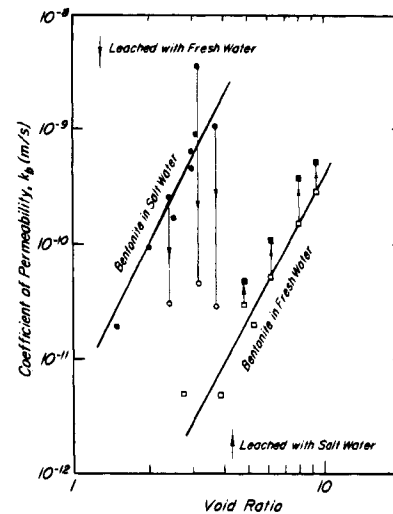


**Figure 14.9** Permeability of bentonite in fresh water and in salt water (after Kenney et al. 1992).

mixtures of sand and bentonite were prepared by thorough mixing at water contents nearly twice as great as the optimum water content (Article 44). The mixtures were then subjected to one-dimensional consolidation until the dry unit weights were in the range of 15 to 18 kN/m<sup>3</sup>. In the second, either dry or moist sand was mixed with dry bentonite, followed by mixing and addition of more water. The samples were then compacted dynamically in the permeameter by using a miniature compaction hammer and a compaction energy per unit volume equal to standard Proctor compaction (Article 44.2.3). For bentonite to sand ratios of 4 to 20%, the standard Proctor compaction energy resulted in values of maximum dry unit weight in the range of 17.4 to 18.5 kN/m<sup>3</sup>. The compacted specimens were subjected to an effective vertical stress equal to 60 kPa and were saturated by back-pressuring before the permeability was measured. The results of compaction and permeability tests on one such mixture are presented in Fig. 14.10. Some mixtures were made using distilled water and some using salt water.

In the first series of permeability tests, made on remolded samples, the same fluids used for mixing were used as permeants. The results are plotted in Fig. 14.11 together with the relationships for ideal mixtures computed using Eqs. 14.7 and 14.8 and  $k_b$  data from Fig. 14.9. The measured  $k_m$  values agree quite well with the calculated relationships for ideal homogeneous mixtures.

Clay barriers in the field are constructed by compacting the sand-bentonite mixtures. Kenney et al. carried out permeability tests on compacted sand-bentonite mixtures in fresh water. The permeability of such a mixture is influenced by the compaction water content, especially when considerably less than  $w_{opt}$ . On the dry side of the optimum water content, the montmorillonite particles are aggregated into stiff clusters that create large flow channels. When compaction is carried out at water contents in the range of  $w_{opt}$  to  $1.5 w_{opt}$ , the particles are dispersed

and produce small flow channels. The dark band in Fig. 14.11 indicates measured permeabilities of compacted sand-bentonite mixtures that were both mixed and permeated with fresh water. For  $B/S$  values of 12% or more, the behavior of compacted samples was similar to that predicted for ideal mixtures. However, the measured permeabilities of compacted mixtures having  $B/S$  values less than 12% are larger than those of ideal mixtures. This indicates that, at mixing water contents of  $w_{opt}$  to  $1.5 w_{opt}$ , the bentonite content and degree of dispersion were not sufficient to fill all the pores between the sand particles. Kenney et al. concluded that the most important factor affecting the permeability of a sand-bentonite mixture is the number of spaces that are devoid of bentonite. This number is greatest at small  $B/S$  values and diminishes for large values of  $B/S$  and with improved mixing. Another important factor is the water content at the time of mixing and compaction. Higher water contents lead to dispersion, to more uniform distribution of bentonite, and therefore to smaller values of permeability. Mixing is likely to be more thorough in the laboratory than in the field, where inadequate distribution of bentonite is probable. Therefore, laboratory values of permeability should be considered as lower limiting values.

Sand-bentonite mixtures prepared in fresh water were permeated with salt water, and mixtures remolded in salt water were permeated with fresh water. The corresponding permeability measurements are shown in Fig. 14.11; they indicate that the mixtures behaved similarly to the bentonite (Fig. 14.9). Replacement of salt water with fresh water resulted in significant dispersion of the montmorillonite flocs and a decrease in permeability by as much as two orders of magnitude, even though no expansion of the mixture was observed. On the other hand, in the range of void ratio encountered in either the remolded and consolidated or compacted and consolidated mixtures, the clay particles did not have sufficient space and freedom to permit them to reorganize into larger units. Therefore, for mixtures compacted or remolded in fresh water, permeation by salt water increased  $k_m$  by a factor of less than 5. In the field, moreover, there may be inadequate distribution of bentonite. In zones of inadequate bentonite content the bentonite may exist at large void ratios. In the presence of salt water, the bentonite may flocculate and result in large channels that allow concentrated seepage.

In Fig. 14.11, the permeability values of the mixtures are extrapolated by dashed lines to  $B/S = 0$  to reference  $k_m$  to the permeability of the sand ( $10^{-4}$  m/s) and to show the marked reductions of permeability that result from even small contents of bentonite. Moreover, mixtures with very small values of  $B/S$  may be unstable because the void ratio of bentonite in the voids may exceed the free-swell void ratio. In such a situation, dispersed bentonite

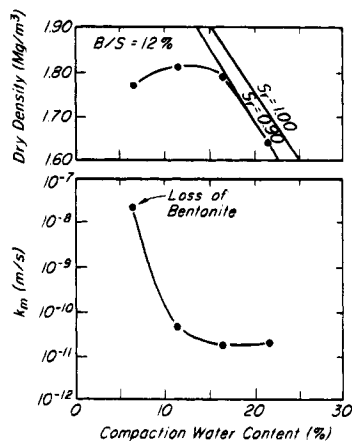


**Figure 14.10** Results of compaction and permeability tests on a sand-bentonite mixture (after Kenney et al. 1992).

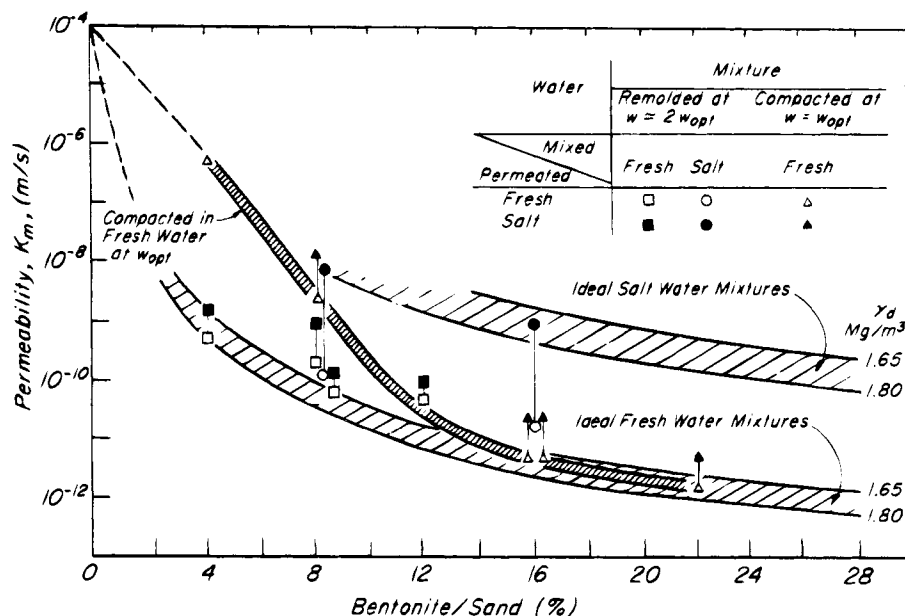


Figure 14.11 Permeability of sand-bentonite mixtures (after Kenney et al. 1992).

particles may be removed by water percolating through the mixture.

#### 14.6 Laboratory Permeability Tests

The principal types of apparatus for determining the coefficient of permeability of soil samples are illustrated in Fig. 14.12. Either constant-head or falling-head permeability tests can be performed on all types of soils. However, the constant-head permeameter (a and b) is more suitable for very permeable soils, and the falling-head permeameter (c) for less permeable ones. To perform a test with either of these types of apparatus, a hydraulic

gradient is established within the sample, whereupon water flows through the soil.

In the constant-head permeameter (Fig. 14.12a), the total head loss is kept constant through a specimen of length,  $L$ , and cross-sectional area,  $A$ , and the discharge,  $Q$ , is measured as a function of time. The quantity,  $\Delta Q$ , corresponding to an increment of time,  $\Delta t$ , is constant, and the permeability is calculated from Darcy's flow equation expressed as

$$k = \frac{L}{Ah_L} \frac{\Delta Q}{\Delta t} \quad (14.9)$$

where  $h_L$  is the constant head loss through the specimen, and  $\Delta Q$  is the quantity of flow measured during the elapsed time,  $\Delta t$ .

In the falling-head permeameter (Fig. 14.12c) the water flows out of a tube  $P$  with cross-sectional area  $a$  through the sample, which has a larger cross-sectional area  $A$ . The coefficient of permeability is computed on the basis of the observed rate at which the water level descends in tube  $P$  while the water level in the vessel  $V$  remains unchanged. Darcy's equation leads to a linear relation between  $\log h_L$  and time. The constant slope of a plot of  $\log h_L$  versus  $t$  is used to compute the permeability

$$k = \frac{2.3aL}{A} \frac{\Delta \log h_L}{\Delta t} \quad (14.10)$$

where  $h_L$  is the total head loss through the sample at elapsed time  $t$ .

Permeability measurements on soft clays are generally carried out as a part of incrementally loaded oedometer tests (Article 16.9). Falling-head or constant-head perme-

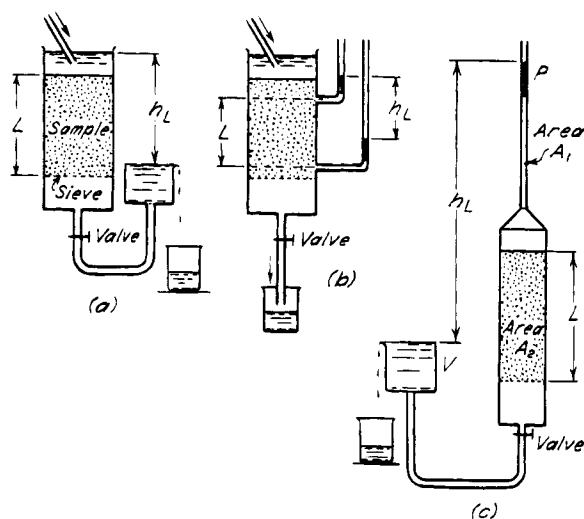


Figure 14.12 (a and b) Constant-head permeameters; (c) falling-head permeameter.

ability tests are carried out during the secondary compression stage (Article 16.7). Permeability measurements at several void ratios are used to define the  $e$  vs  $\log k$  relationship. Another reliable method for determining the permeability of soft clays uses the results of excess pore-water pressure measurements during constant rate of strain oedometer tests (Article 16.9). The permeability of clays can also be computed by analyzing the deformation vs time data from an incrementally loaded oedometer test, together with a theory of consolidation. The necessary equations and procedures are presented in Article 25.

#### 14.7 In Situ Permeability Tests

Preliminary information about the order of magnitude and variability of the coefficient of permeability of a natural pervious stratum can be obtained by permeability tests in exploratory borings while drilling proceeds. The observations during drilling should also furnish information concerning the presence or absence of free communication between pervious strata encountered in the holes.

Most of the common procedures used in connection with drill holes are based on the principle of the falling-head permeability test. The hole is cased from the ground surface to the top of the zone to be tested and extends without support for a suitable depth below the casing. Usually the uncased part of the hole has a roughly cylindrical shape. If the pervious stratum is not too thick, the hole is preferably extended through the full thickness; otherwise the hole penetrates only part of the pervious material.

If the pervious zone is below the water table, the test may be carried out by adding water to raise the water level in the casing and then allowing the water level to descend toward its equilibrium position. The elevation is measured as a function of time, and the coefficient of permeability is calculated by means of the expression

$$k = \frac{1}{C} \frac{A(\Delta h / \Delta t)}{r'_0 h'_m} \quad (14.11)$$

where  $\Delta h$  is the drop in water level in the casing during an interval of time  $\Delta t$ ,  $A$  is the inside cross-sectional area of the casing,  $h'_m$  is the mean distance during the interval  $\Delta t$  from the water level in the casing to the equilibrium water level in the pervious zone, and  $r'_0$  is the mean radius of the roughly cylindrical hole below the casing. The coefficient  $C$  is a dimensionless quantity that depends on the shape of the cylindrical hole and the depth of penetration into the pervious layer. Values of  $C$  for various conditions are given in Fig. 14.13 (Zangar 1953).

In a falling-head test in a drill hole it is likely that fines suspended in the water may form a filter skin over the walls and bottom of the hole in the pervious material; consequently, the observed permeability may be too small. The error may be avoided by bailing the water from the casing until the water level is below that of the

pervious stratum and by measuring the elevation of the water level at various times as it rises toward its equilibrium position. The value of  $k$  can be calculated by Eq. 14.11 as before. However, if the permeable stratum is cohesionless the water level cannot be lowered too far or the hole will collapse and the cohesionless material may rise into the casing.

The results of such tests are little more than an indication of the order of magnitude of the coefficient of permeability. More reliable information is obtained from pumping tests on test wells.

The usual diameter of a pumping-test well is about 300 mm. Observation wells should be established in two lines, one in the direction of normal groundwater flow and the other perpendicular to it. At least two, and preferably four, observation wells should be established in each line. The observation wells should permit entrance of water over most of the thickness of the aquifer. The initial groundwater level should be observed in all the wells for a period long enough to establish the amount and nature of any fluctuations that normally occur at the site. Pumping should then be started at a constant rate of discharge and the water levels measured in the observation wells.

The theory of radial flow toward a pumping well, including the equations for calculating the coefficient of permeability from the results of measurements in the observation wells when equilibrium is reached, is outlined in Article 23. In most practical problems, however, the permeability is evaluated on the basis of measurements made before equilibrium in the observation wells is achieved (Theis 1935, Jacob 1950). The nonequilibrium methods also provide insight regarding the existence and influence of sources of groundwater infiltration, barriers to flow, and other characteristics of the aquifer. Their application has developed into a specialty practiced by groundwater hydrologists whose expertise is useful in the planning and interpretation of pumping tests.

The permeability of soft clays has been measured *in situ* by falling-head tests in piezometers that are driven in place or installed in boreholes. Field investigations by Tavenas et al. (1986) show that piezometers fitted with porous bronze elements and installed by driving into position are subject to clogging and cause remolding of the soil and a reduction in void ratio and permeability. Such *in situ* measurements may grossly underestimate horizontal permeability of soft clays. However, the permeability measured by falling head tests in soft clay deposits, using a nonclogging, self-boring permeameter (Tavenas et al. 1986) was found to be in good agreement with laboratory measurements on undisturbed specimens. Because *in situ* tests measure only horizontal permeability at the *in situ* void ratio, do not provide any information on the change in permeability with change in void ratio, and even when reliable are rather expensive and time consuming, laboratory permeability tests on undis-

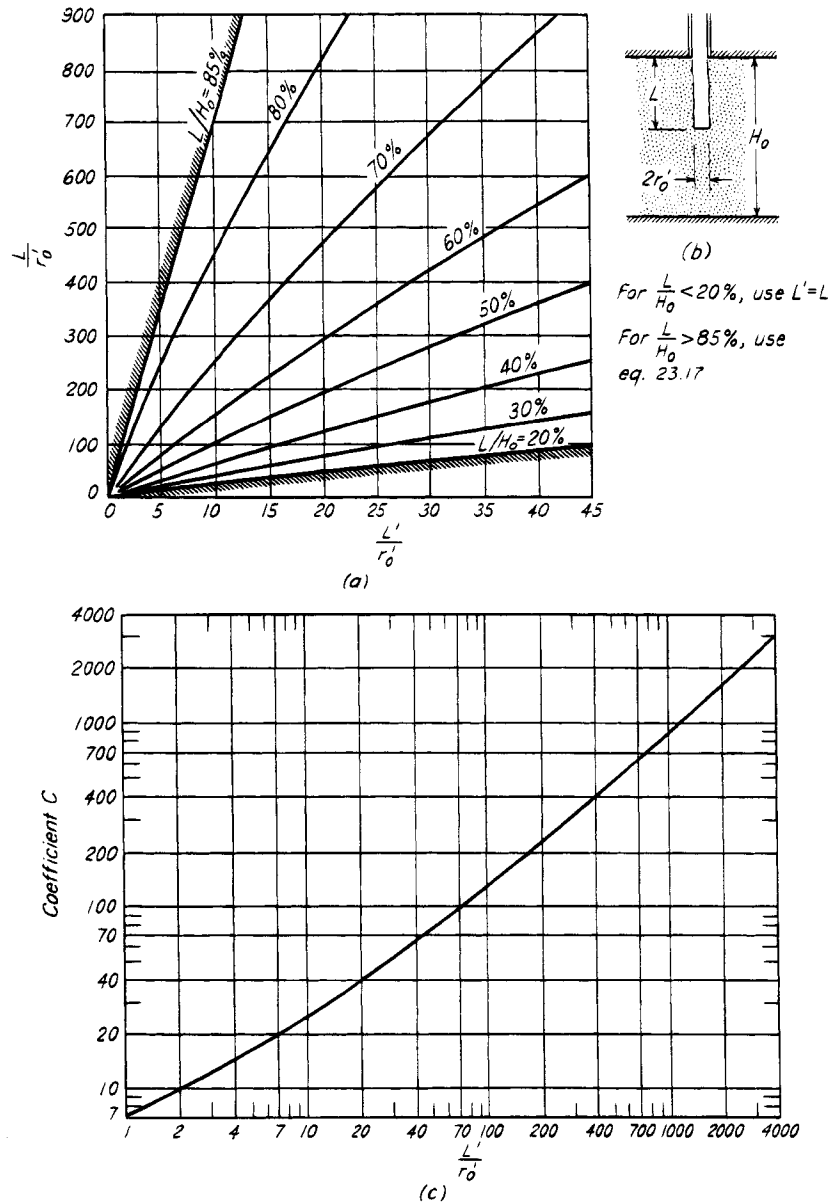


**Figure 14.13** Permeability test in open drill hole into pervious stratum. (a) Chart for determining ratio  $L'/r_o$  for various penetrations  $L/H_o$  shown in (b). (c) Chart for determining coefficient  $C$  for use in Eq. 14.11 (after Zangar 1953).

turbed specimens are preferable for determining the permeability of uniform soft clay and silt deposits.

#### 14.8 Permeability of Stratified Masses of Soil

Natural transported soils commonly consist of layers that have different permeability. To determine the average coefficient of permeability of such deposits, representative samples are secured from each of the layers and are tested. Once the values of  $k$  are known for the individual strata, the averages can be computed by using the following method. Let

$k_1, k_2 \dots k_n$  = coefficients of permeability of the individual strata

$H_1, H_2 \dots H_n$  = thicknesses of corresponding strata

$H = H_1 + H_2 + \dots H_n$  = total thickness

$k_I$  = average coefficient of permeability parallel to bedding planes (usually horizontal)

$k_{II}$  = average coefficient of permeability perpendicular to bedding planes (usually vertical)

If the flow is parallel to the bedding planes, the average discharge velocity  $v$  is

$$v = k_i i = \frac{1}{H} [v_1 H_1 + v_2 H_2 + \cdots v_n H_n]$$

Furthermore, because the hydraulic gradient must be the same in every layer,

$$k_i i = \frac{1}{H} [k_1 i H_1 + k_2 i H_2 + \cdots k_n i H_n]$$

whence

$$k_i = \frac{1}{H} [k_1 H_1 + k_2 H_2 + \cdots k_n H_n]$$

or

$$k_i = \sum_{j=1}^n \frac{H_j}{H} k_j \quad (14.12)$$

For flow at right angles to the bedding planes, the hydraulic gradient across the individual layers is denoted by  $i_1, i_2 \dots i_n$ . The hydraulic gradient across the series of layers is  $h_L/H$ , where  $h_L$  equals the total loss in head. The principle of continuity of flow requires that the velocity be the same in each layer. Therefore

$$v = \frac{h_L}{H} k_{II} = k_1 i_1 = k_2 i_2 = \cdots k_n i_n$$

Also,

$$h_L = H_1 i_1 + H_2 i_2 + \cdots + H_n i_n$$

Combining these equations, we obtain

$$k_{II} = \frac{H}{\frac{H_1}{k_1} + \frac{H_2}{k_2} + \cdots \frac{H_n}{k_n}}$$

or

$$k_{II} = \frac{1}{\sum_{j=1}^n \frac{H_j}{H} \frac{1}{k_j}} \quad (14.13)$$

It can be demonstrated theoretically that for every stratified mass  $k_{II}$  must be less than  $k_f$ .

### 14.9 Particle Migration and Erosion

Wherever seepage crosses a boundary from a finer to coarser material or emerges from a soil into an open space, such as a riverbank or a drillhole, the potential exists for some particles to migrate out of the finer material. The migration may have serious consequences. It may cause the clogging of packing or backfill around wells or of drains (Article 43.5) or it may result in the formation of erosion tunnels and sinkholes (Article 58.4). Indeed, subsurface or internal erosion has been one of

the most prevalent causes of catastrophic failure of earth and rockfill dams (Article 57.2).

The migration can be prevented by covering the surface of the finer material across which the seepage emerges with a *filter* consisting of a suitably graded coarser material having voids small enough to block the passage of the fine materials through the filter but large enough not to impede the escape of the water. Under some circumstances, filter fabrics are used to serve the same purpose. Filters are used extensively to prevent internal erosion and to control seepage in embankment dams.

The requirements for satisfactory filters have been determined by experiment (Terzaghi 1922, Bertram 1940, Kenney et al. 1985, Sherard et al. 1984). Terzaghi concluded that particles of the material to be protected (the *base material*) do not pass through a filter if the  $D_{15}$  size of the filter is not greater than 4 times the  $d_{85}$  size of the finest base material, whereas the permeability of the filter is adequate if the  $D_{15}$  size of the filter is at least 4 times the  $d_{15}$  size of the coarsest base material. These requirements, illustrated in Fig. 14.14, have been found to be conservative and have been widely used in practice. Indeed, subsequent tests (Fig. 14.15) indicate that a ratio  $D_{15}/d_{85} = 5$  is adequate. Two precautions should be taken, however: (1) the filter, to minimize the effects of inevitable segregation during placement, should not be broadly or gap graded (Article 5), because otherwise the segregation would lead to nests of coarse material into or through which fines may migrate (Ripley 1986); (2) if the base material consists of strata or lenses of widely differing grain sizes, different filters must be used to protect the different base materials. Because the filter must also be capable of carrying away the water without developing excessive pressures, a series of filters may be required, each more pervious than the previous one, and each designed as if the previous one were the base material. Such an assemblage is known as a *graded filter*. Alternatively, under some circumstances, a suitably designed

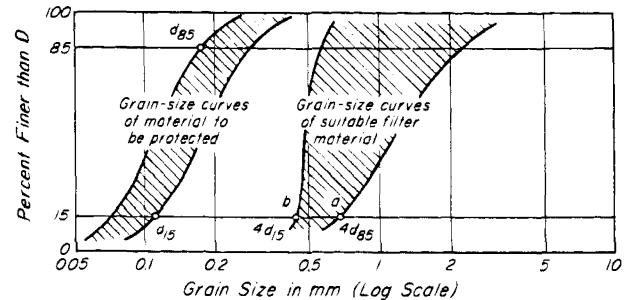


**Figure 14.14** Diagram illustrating original Terzaghi specifications for grain size of material suitable for filter. Left-hand shaded area encloses all grain-size curves for material to be protected; right-hand area indicates range within which curves for filter material must lie.

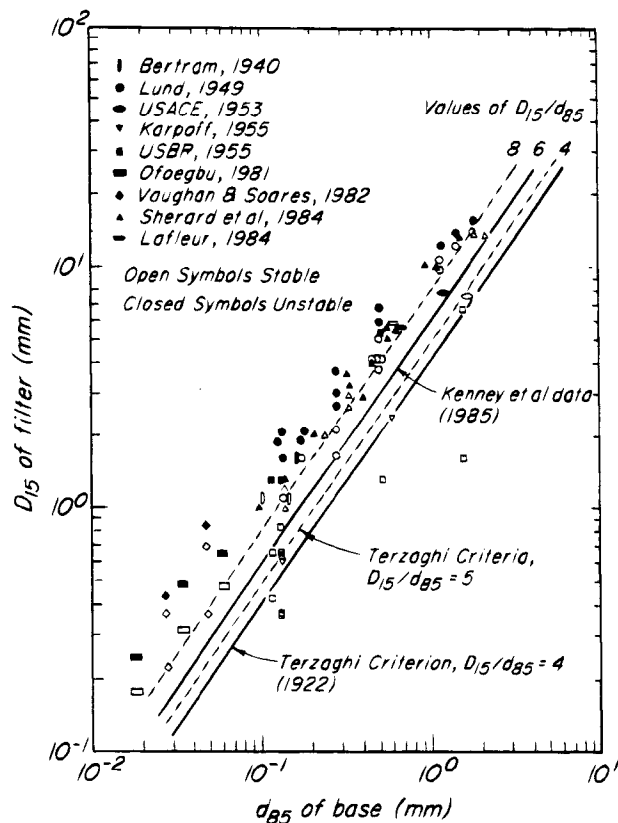


Figure 14.15 Results of various filter experiments.

perforated drain pipe may be incorporated in the filter (Cedergren 1989).

Some naturally occurring base materials with very broad or gap gradings may themselves be unstable internally when subjected to seepage flow; the fine particles may move into or through large voids in the coarse fraction and thus permit concentration of flow and even formation of sinkholes. The susceptibility to internal instability can be checked (Lowe 1988) by separating the grain-size curve into two parts at an arbitrarily chosen point and comparing the  $d_{15}$  size of the coarser fraction to the  $d_{85}$  size of the finer fraction. If the ratio is less than 4 or 5, the material can be considered internally stable or self-filtering.

Most filter experiments have been carried out using granular bases, and the filter criteria were originally developed for granular materials. Since it is generally difficult to define and measure the particle sizes of silts and clays, it is prudent to base filter selection for fine-grained soils on field experience. According to Ripley (1986), a clean cohesionless sand is not only capable of effectively filtering even the finest silt and clay soils generally found in nature, but it also resists segregation during construction. This conclusion is supported by others (e.g., Lowe 1988). Sands typically used for concrete, having a  $D_{15}$  of about 0.25 to 0.5 mm and a uniformity

coefficient of about 1.5 to 2, can serve as a conservative filter to block even the finest clays.

### Problems

1. A sample of coarse sand, 15 cm high and 5.5 cm in diameter, was tested in a constant-head permeameter. Water percolated through the soil under a hydrostatic head of 40 cm for a period of 6.0 s. The discharge water was collected and found to weigh 400 g. What was the coefficient of permeability at the void ratio and temperature of the test?

Ans.  $k = 1.05 \times 10^{-2}$  m/s.

2. A bed of sand consists of three horizontal layers of equal thickness. The value of  $k$  for the upper and lower layers is  $1 \times 10^{-6}$  m/s, and of the middle layer is  $1 \times 10^{-4}$  m/s. What is the ratio of the average permeability of the bed in the horizontal direction to that in the vertical direction?

Ans. 23.

3. An undisturbed sample of soft clay has a void ratio  $e_0$  of 1.62 and a coefficient of permeability  $k_{v0}$  of  $2 \times 10^{-9}$  m/s. Estimate the value of  $k_v$  for the soft clay sample at a void ratio of 1.20.

Ans.  $k_v = 6 \times 10^{-10}$  m/s.

### Selected Reading

The following references deal with permeability of soils.

- Louden, A. G. (1952). "The computation of permeability from simple soil tests," *Géot.*, **3**, No. 4, pp. 165–183.
- Kenney, T. C. (1963). "Permeability ratio of repeatedly layered soils," *Géot.*, **13**, No. 4, pp. 325–333.
- Mesri, G. and R. E. Olson (1971). "Mechanisms controlling the permeability of clays," *Clays and Clay Minerals*, **19**, No. 3, pp. 151–158.
- Chan, H. and T. C. Kenney (1973). "Laboratory investigation of permeability ratio in New Liskeard varved soil," *Canadian Geotech. J.*, **10**, No. 3, pp. 453–472.
- Kenney, T. C. and H. T. Chan (1973). "Field investigation of permeability ratio of New Liskeard varved soil," *Canadian Geotech. J.*, **10**, No. 3, pp. 473–488.
- Kenney, T. C. (1976). "Formation and geotechnical characteristics of glacial-lake varved soils," *Bjerrum Memorial Volume*, Norwegian Geotechnical Institute, Oslo, pp. 15–39.
- Tavenas, F., P. Leblond, P. Jean and S. Leroueil (1983a). "The permeability of natural soft clays. Part I: Methods of laboratory measurement," *Canadian Geotech. J.*, **20**, No. 4, pp. 629–644.
- Tavenas, F., P. Leblond, P. Jean and S. Leroueil (1983b). "The permeability of natural soft clays. Part II: Permeability characteristics," *Canadian Geotech. J.*, **20**, No. 4, pp. 645–660.
- Tavenas, F., M. Tremblay, G. Larouche and S. Leroueil (1986). "In situ measurement of permeability in soft clays," *Proc. In Situ '86*, ASCE Specialty Conf. on Use of *In Situ* Testing in Geotech. Eng., Blacksburg, pp. 1034–1048.
- Mesri, G. and A. F. Cepeda-Diaz (1987). "Permeability of shales," *Proc. 8th Panamerican Conf. on Soil Mech. and Found. Eng.*, Cartagena, Colombia, pp. 89–100.



Mesri, G., T. W. Feng, S. Ali and T. M. Hayat (1994). "Permeability characteristics of soft clays," *Proc. 13th Int. Conf. on Soil Mech. and Found. Eng.*, New Delhi, 2, pp. 187–192.

## ARTICLE 15 EFFECTIVE STRESS, POREWATER PRESSURE, AND CRITICAL HYDRAULIC GRADIENT

### 15.1 Effective Stress

Figure 15.1a shows a cross-section through a thin layer of soil that covers the bottom of a container. If a load  $\sigma$  per unit of area is applied to the surface of the sample, for example by covering it with lead shot, the void ratio of the soil decreases from  $e_0$  to  $e_1$ . The pressure  $\sigma$  also produces a change in all the other mechanical properties of the soil, such as its shearing resistance. For this reason, it is known as an *effective pressure*. It is given the symbol  $\sigma'$ .

If, instead, the vessel is filled with water to such a height  $h_w$  that  $h_w = \sigma/\gamma_w$ , the normal stress on a horizontal section through the sample is also increased by  $\sigma$ . Nevertheless, the increase in pressure due to the weight of the water does not have a measurable influence on the void ratio or on any other mechanical property of the soil such as the shearing resistance. Therefore, the pressure produced by the water load is called a *neutral pressure*. It is said to be zero if it is equal to atmospheric pressure. Hence, the neutral pressure is equal to the piezometric head  $h_w$  times the unit weight of water  $\gamma_w$ , or

$$u = \gamma_w h_w \quad (15.1)$$

The total normal stress  $\sigma$  at any point on a section through a saturated soil consists, therefore, of two parts. One part,  $u$ , acts in the water and in the solid in every direction with equal intensity; this part is known as the *neutral stress* or the *porewater pressure*. The remaining

part  $\sigma' = \sigma - u$  represents an excess over the neutral stress  $u$  and has its seat exclusively in the solid phase of the soil. This fraction of the total stress is called the *effective stress*.

A change in the neutral stress produces practically no volume change and has practically no influence on the stress conditions for failure, whereas all the measurable effects of a change in stress, such as compression, distortion, and a change in shearing resistance, are due exclusively to changes in the effective stress  $\sigma'$ . Hence, every investigation of the stability or settlement of a saturated body of soil requires the knowledge of both the total and neutral stresses, and the equation

$$\sigma = \sigma' + u \quad (15.2)$$

is one of the most important in soil mechanics (Terzaghi 1936b).

### 15.2 Mechanism of Effective Stress Transfer

Equation 15.2 defines the effective stress  $\sigma'$  for a saturated soil in terms of the total stress  $\sigma$  and the porewater pressure  $u$ , both of which are externally controlled. The equation makes no assumptions about the interparticle forces that transmit the effective stress from one particle to another, and it provides no information about them. The balance between total stress that pushes the particles together and porewater pressure that pushes them apart is in equilibrium with the difference between interparticle repulsions and attractions. These forces operate at spacings between particles that may range from zero to several nanometers. Effective stress can be transmitted from one particle to another through mineral-to-mineral contact at zero particle spacing, through adsorbed water at up to about 1-nm spacing, and through double-layer water at 1- to more than 20-nm spacing. In a soil with a wide range of particle sizes and arrangements, effective stress may be transmitted from particle to particle through mineral-to-mineral contact, through adsorbed water, and through double-layer water.

In coarse granular soils such as sand and gravel, effective stress is transmitted from one particle to another mainly through mineral-to-mineral contacts. Because the surfaces of large particles are rough at a microscopic scale (Figs. 4.6–4.8), the force per particle resulting from  $\sigma - u$  may be large. Yet, because the contact area is very small, the contact stresses are very high, and the adsorbed water is readily squeezed out. An increase in effective stress should then result in an increase in mineral-to-mineral contact area and, therefore, in a substantial increase in interparticle shearing resistance through primary valence bonding or microscopic surface to surface interlocking.

On the other hand in fine-grained soils, including clay minerals, adsorbed water is not readily squeezed out from between the particles, especially when the particles inter-

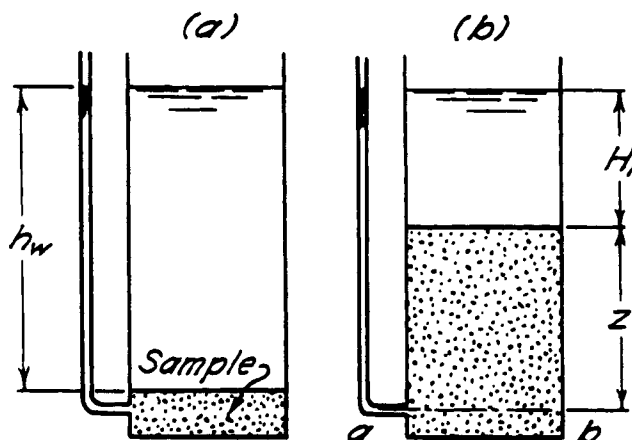


Figure 15.1 Apparatus for demonstrating difference between effective stress and porewater pressure or neutral stress.

act face to face. In this event the force per particle resulting from  $\sigma - u$  is small, and the interacting area of the adjacent particles is relatively large. An increase in effective stress may squeeze out one or more molecular layers of water and decrease the particle spacing through which the attractive forces operate and hold the particles together. In very fine-grained soils, oriented face to face, the effective stress may be transmitted from one particle to another through double-layer water. An increase in effective stress that squeezes out part of the double-layer water may not result in any significant increase in shearing resistance, however. For example, in sodium montmorillonite, where the predominant particle interaction is face to face and effective stress is transmitted mainly through adsorbed water or double-layer water, the angle of shearing resistance may approach zero (Article 18). That is, an increase in external effective stress  $\sigma - u$  may result in no increase in shearing resistance.

A change in effective stress results in a change in void volume; an increase produces compression and a decrease, expansion or swelling. For a given change in  $\sigma - u$ , the largest volume change occurs if the effective stress is transmitted through double-layer water, and the least if it is transmitted through mineral-to-mineral contact. Internal equilibrium among interparticle forces is not reached by the time an external effective stress change comes to a stop, whether it is caused by a change in total stress at constant porewater pressure, by a change in porewater pressure at constant total stress, or both. A readjustment of particles and redistribution of interparticle forces follows for a long time at constant effective stress and results in an additional change in void volume. The additional change is known as *secondary compression* after an effective stress increase and *secondary swelling* after an effective stress decrease.

It is evident that the mechanism of the transfer of effective stress from one particle to another is complex. Fortunately, although no theoretical basis for Eq. 15.2 has been found, its empirical basis is so well established that a quantitative knowledge of the interparticle reactions is not needed.

### 15.3 Effective Vertical Stress

The effective vertical stress in a saturated soil is equal to the total vertical stress,  $\sigma_v$ , minus the porewater pressure,  $u$ .

$$\sigma'_v = \sigma_v - u \quad (15.3)$$

The total vertical stress at any point in a soil profile is determined by the total unit weight and the thickness of all material (including free water above the ground surface) above that point. For a uniform soil layer of total unit weight,  $\gamma$

$$\sigma_v = z\gamma \quad (15.4)$$

where  $z$  is the depth of the point of stress calculation below the ground surface. For several uniform layers of different unit weights,

$$\sigma_v = \sum_{j=1}^n H_j \gamma_j \quad (15.5)$$

where  $H_j$  is the thickness of material of unit weight,  $\gamma_j$ .

In a hydrostatic condition, the rate of increase in porewater pressure with depth is equal to the unit weight of water,  $\gamma_w$ . The porewater pressure at any point in the soil is determined by the vertical distance to the water table above that point. For a soil deposit of total unit weight,  $\gamma$ , with the water table at the ground surface, the effective vertical stress is

$$\sigma'_v = z\gamma - z\gamma_w = z(\gamma - \gamma_w) = z\gamma' \quad (15.6)$$

The quantity  $\gamma'$  is the *submerged unit weight* of the soil. It is equal to the difference between the total unit weight,  $\gamma$ , of the soil and the unit weight of water,  $\gamma_w$ . For several layers of uniform soil of different unit weights, with the water table at the ground surface,

$$\sigma'_v = \sum_{j=1}^n H_j \gamma'_j \quad (5.7)$$

If the water table is at depth  $z_1$  below the ground surface, the soil located above the water table is not submerged. It then contributes  $z_1\gamma$  to the effective vertical stress at depths below the water table.

For steady-state seepage in the vertical direction, the porewater pressure from the definition of total or hydraulic head (Eq. 14.1) is

$$u = \gamma_w h - \gamma_w z \quad (15.8)$$

and

$$\frac{du}{dz} = \gamma_w \frac{dh}{dz} - \gamma_w \quad (15.9)$$

Within each homogeneous layer of constant hydraulic gradient,  $i = dh/dz$ , the change in porewater pressure with depth is

$$\frac{du}{dz} = \gamma_w \pm i\gamma_w \quad (15.10)$$

The plus sign corresponds to a hydraulic head increasing with depth and water flowing upward, whereas the minus sign represents a hydraulic head decreasing with depth and water flowing downward. Since  $du/dz = \gamma_w$  corresponds to the hydrostatic condition, it is apparent that steady-state seepage in the vertical direction changes  $du/dz$  by the amount  $i\gamma_w$ . The quantity  $i\gamma_w$ , which has the dimensions of unit weight, is called the *volumetric seepage force*. It produces a *seepage pressure*  $i\gamma_w dz$ .

Because the effective vertical stress is related linearly to the porewater pressure

$$\sigma'_v = \sigma_v - u \quad (15.3)$$

and because in the hydrostatic condition, from Eq. 15.6,

$$\frac{d\sigma'_v}{dz} = \gamma' \quad (15.11)$$

then, in the steady-state seepage condition,

$$\frac{d\sigma'_v}{dz} = \gamma' \pm i\gamma_w \quad (15.12)$$

The plus sign corresponds to downward flow in which the volumetric seepage force acts in the direction of gravity, and the minus sign to upward flow in which the seepage force acts opposite to the direction of gravity.

For a stratified soil profile subjected to steady-state seepage in the vertical direction

$$\sigma'_v = \sum_{j=1}^n (\gamma'_j \pm i_j \gamma_w) H_j \quad (15.13)$$

where  $\gamma'_j$ ,  $i_j$  and  $H_j$  are the submerged unit weight, hydraulic gradient, and thickness of layer  $j$  above the point at which  $\sigma'_v$  is computed.

The physical significance of the foregoing discussion can be demonstrated by means of the apparatus shown in Fig. 15.2a. The cylindrical vessel A contains a layer of dense sand resting on a screen. The thickness of the layer is  $H$ , and the rim of the vessel is located at a distance  $H_1$  above the top of the sand. The space below the screen communicates through a tube with vessel B. The water level is maintained at the elevation of the upper rim of each vessel. Hence, whatever the position of the water level in B, the total vertical stress on a horizontal section at depth  $z$  below the surface of the sand is always equal to  $\sigma_v$  (Eq. 15.4). The corresponding effective vertical stress  $\sigma'_v$  is equal to  $\sigma'_v = \sigma_v - u$ . Hence, if the porewater

pressure decreases or increases by  $\Delta u$ , the effective vertical stress increases or decreases by the same amount, or

$$\Delta\sigma'_v = \pm\Delta u \quad (15.14)$$

As long as the water level in both vessels is at the same elevation, the effective pressure at depth  $z$  is equal to  $\sigma'_v = z\gamma'$  (Eq. 15.6). If the vessel B is lowered through a distance  $h_L$ , water percolates through the sand in a downward direction under a hydraulic gradient  $i = h_L/H$ . The porewater pressure at depth  $H$  is reduced by  $h_L \gamma_w = iH\gamma_w$ , and that at any other depth  $z$  is proportionately reduced by the amount  $\Delta u = iz\gamma_w$ . The effective stress is increased by the same amount.

On the other hand, if the vessel B is lifted through a distance  $h_L$ , the porewater pressure at depth  $z$  increases by  $\Delta u = iz\gamma_w$ , and the effective stress decreases to

$$\sigma'_v = z\gamma' - iz\gamma_w \quad (15.15)$$

The increase  $\Delta u$  of the porewater pressure is caused exclusively by the transition of the porewater from a stationary state into a state of flow. The corresponding *seepage pressure* is produced by the friction between the percolating water and the surface of the particles and can be described as a "drag." If the water percolates in a downward direction, the friction between the water and the soil particles drags the particles down and thereby increases the effective pressure in the sand. On the other hand, if the water flows in an upward direction, the friction tends to lift the soil grains.

#### 15.4 Critical Hydraulic Gradient

As soon as the hydraulic gradient  $i$  in Eq. 15.15 becomes equal to

$$i_c = \frac{\gamma'}{\gamma_w} \quad (15.16)$$

the effective stress becomes equal to zero at any depth in the layer of sand. In other words, the average seepage pressure becomes equal to the submerged weight of the sand. The value  $i_c$  represents the *critical hydraulic gradient*.

Figure 15.2b illustrates the mechanical effect of the upward flow of water on the properties of the sand. In this diagram, the abscissas represent the hydraulic gradient, and the ordinates the corresponding discharge velocity. The curve  $Oab$  represents the relation between discharge velocity and hydraulic gradient as the hydraulic gradient is steadily increased. As long as  $i$  is less than  $i_c$ , the discharge increases in accordance with Darcy's flow equation (Eq. 14.4) in direct proportion to  $i$ , and the value of  $k$  remains constant. This fact indicates that the mutual position of the sand grains remains practically unaltered. However, when  $i$  becomes equal to  $i_c$ , as indicated by point  $a$  on  $Oab$ , the discharge

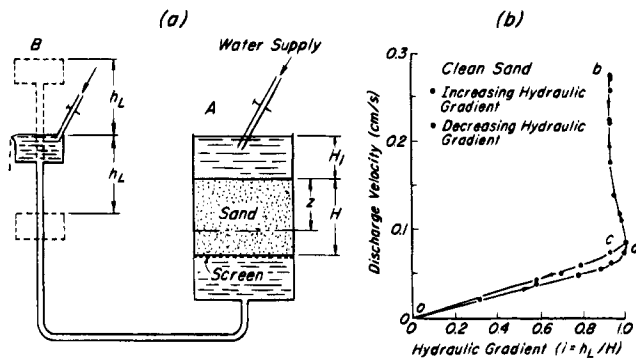


**Figure 15.2** (a) Apparatus for illustrating hydraulic conditions associated with boiling of sand. (b) Relation between upward hydraulic gradient and discharge velocity through sand in apparatus shown in (a).

increases suddenly, and the coefficient of permeability increases correspondingly. If a weight previously rested on the surface of the sand, it now sinks down as if the sand were a liquid.

Beyond point  $a$ , as  $h_L$  is increased, the void ratio and thickness of the sand layer increase and  $i$  gradually decreases, but the discharge velocity continues to increase. If, after point  $b$  is reached,  $h_L$  is decreased, the decrease in discharge velocity and the associated change in  $i$  are indicated by the line  $bcO$ . As soon as  $i$  becomes roughly equal to  $i_c$ , the permeability remains constant throughout any further decrease of  $i$ . Since the line  $Oc$  is located above the line  $Oa$ , the corresponding coefficient of permeability is greater than the original value. This suggests that the event represented by the portion  $ab$  of the line  $Oab$  causes a permanent increase in the void ratio of the sand.

The process represented by the step  $ab$  is accompanied by a violent and visible agitation of the sand particles. Hence, it is commonly referred to as *boiling* or as a *quick condition* of the sand. Sand starts to boil in any open excavation if the ground water rises toward the bottom of the excavation at a hydraulic gradient greater than the critical value  $i_c$ . It has often been claimed that boiling occurs only in certain types of sand known as quicksands. In reality, it takes place in every sand and even in gravel, as soon as the hydraulic gradient becomes equal to  $i_c$ .

The boiling of granular soils can be prevented by constructing a weighted filter above the area in which the seepage emerges from the ground. A properly designed filter has almost no effect on the porewater pressure in the soil. Hence, its entire weight serves to increase the effective vertical pressure and to keep the sand particles in their original positions.

### Problems

1. A sand is composed of solid constituents having a density of  $2.60 \text{ Mg/m}^3$ . The void ratio is 0.572. Compute the density of the sand when dry and when saturated, and compare with the effective density when submerged.

Ans.  $\rho_d = 1.652$ ;  $\rho = 2.014$ ;  $\rho' = 1.016 \text{ Mg/m}^3$ .

2. The water table in a deep deposit of very fine sand is 1 m below the ground surface. Above the water table, the sand is saturated by capillary water. The density of the saturated sand is  $2.03 \text{ Mg/m}^3$ . What is the effective vertical pressure on a horizontal plane at a depth of 4 m below the ground surface?

Ans. 50.2 kPa.

3. A submerged stratum of clay has a thickness of 15 m. The average water content of samples taken from the stratum is 54%, and the specific gravity of the solid constituents is 2.78. What is the effective vertical pressure, due to the weight of the clay, at the base of the stratum?

Ans. 104 kPa.

4. The density of the particles of a sand is  $2.66 \text{ Mg/m}^3$ , the porosity in the loose state is 45%, and in the dense state is 37%. What is the critical hydraulic gradient for these two states?

Ans. 0.91; 1.05.

5. A large open excavation was made in a stratum of stiff clay with a saturated density of  $1.76 \text{ Mg/m}^3$ . When the depth of the excavation reached 7.5 m, the bottom rose, gradually cracked, and was flooded from below by a mixture of sand and water. Subsequent borings showed that the clay was underlain by a bed of sand with its surface at a depth of 11 m. Compute the elevation to which the water would have risen from the sand into a drill hole before the excavation was started.

Ans. 6.2 m above top of sand.

6. A soil profile consists of 3 m of clean sand ( $\gamma = 19 \text{ kN/m}^3$ ) over 6 m of marine clay ( $\gamma = 16 \text{ kN/m}^3$ ,  $k_v = 10^{-9} \text{ m/s}$ ) over 3 m of silty clay ( $\gamma = 17 \text{ kN/m}^3$ ,  $k_v = 2 \times 10^{-9} \text{ m/s}$ ). The water table is 2.5 m below the ground surface. A piezometer placed at 7 m below the ground surface indicates a piezometric head of 6 m. Assuming a one-dimensional flow condition in the vertical direction, compute the flow rate in  $\text{m}^3/\text{day}/\text{m}^2$ . Also, compute at middepth of the silty clay the total vertical stress, effective vertical stress, and porewater pressure.

Ans.  $q_v = 3.24 \times 10^{-5} \text{ m}^3/\text{day}/\text{m}^2$ ;  $\sigma_v = 179 \text{ kPa}$ ;  $\sigma'_v = 74 \text{ kPa}$ ;  $u = 105 \text{ kPa}$ .

7. A soil profile consists of 2 m of sand ( $\gamma = 18 \text{ kN/m}^3$ ,  $k_v = 4 \times 10^{-2} \text{ m/day}$ ) over 3 m of silt ( $\gamma = 17 \text{ kN/m}^3$ ,  $k_v = 1 \times 10^{-3} \text{ m/day}$ ) over 2 m of clay ( $\gamma = 16 \text{ kN/m}^3$ ,  $k_v = 5 \times 10^{-4} \text{ m/day}$ ) over gravel. The water table is 0.5 m below the ground surface. A piezometer placed at the top of the gravel layer measures a porewater pressure of 42 kPa. Assuming a one-dimensional flow condition in the vertical direction, compute the flow rate in  $\text{m}^3/\text{day}/\text{m}^2$ . Also compute, at middepth of the clay layer, the porewater pressure, total vertical stress, and effective vertical stress.

Ans.  $q_v = 3.33 \times 10^{-4} \text{ m}^3/\text{day}/\text{m}^2$ ;  $u = 38.5 \text{ kPa}$ ;  $\sigma_v = 103 \text{ kPa}$ ;  $\sigma'_v = 64.5 \text{ kPa}$ .

8. A soil profile consists of 3 m of clean sand ( $\gamma = 18 \text{ kN/m}^3$ ) over 10 m of silt ( $\gamma = 17 \text{ kN/m}^3$ ,  $k_v = 1 \times 10^{-8} \text{ m/s}$ ) over 12 m of clay ( $\gamma = 17 \text{ kN/m}^3$ ,  $k_v = 4 \times 10^{-9} \text{ m/s}$ ) over gravel. Piezometers installed at middepth of the silt layer and at the top of the gravel layer measure, respectively, piezometric heads of 4 m and 3 m. Assuming one-dimensional flow in the vertical direction, compute the flow rate in  $\text{m}^3/\text{year}/10,000 \text{ m}^2$ . Also, compute at 16 m below the ground surface the total vertical stress, effective vertical stress, and porewater pressure.

Ans.  $q_v = 1622 \text{ m}^3/\text{year}/10,000 \text{ m}^2$ ;  $\sigma_v = 275 \text{ kPa}$ ;  $\sigma'_v = 219 \text{ kPa}$ ;  $u = 56 \text{ kPa}$ .

### Selected Reading

The history and significance of the concept of effective stress are discussed by A. W. Skempton in "Terzaghi's discovery of effective stress," included in *From theory to practice in soil mechanics*, New York, John Wiley and Sons, 1960, pp. 42–53.

### 15.5 Porewater Pressures Resulting from Undrained Changes in State of Stress

The preceding sections in this article have demonstrated that the behavior of soils depends exclusively on the conditions of effective stress. If the soil is saturated, the influence of pore pressures, such as those due to the flow of water, is determined in accordance with the equation

$$\sigma = \sigma' + u \quad (15.2)$$

The pore pressure  $u$  in an element of soil may result from the flow of water through, into, or out of the element, as described in Articles 15.3 and 15.4. It may also occur under *undrained conditions*, in which no flow takes place into or out of the element. Two undrained conditions are of interest for their fundamental significance. The first (Article 15.5.1) is associated with a change in equal all-around total stress on the element. The second (Article 15.5.2) is the result of shear stresses that may occur at least temporarily during an earthquake, on rapid application of a load such as a building or fill above a relatively impermeable soil, or in some soil tests in which a specimen is enclosed within a sealed impermeable membrane while external stresses are applied. The *triaxial test*, Article 17.2, is the most widely used means for investigating undrained behavior. In it, a specimen can be subjected to various states of stress, and the deformations and resulting changes in pore pressure measured.

From Eq. 15.2 it is evident that, in saturated soils, the change in effective stress on any plane is  $\Delta\sigma' = \Delta\sigma - \Delta u$ , where the change in total stress  $\Delta\sigma$  is readily determined from a consideration of statics or by means of elastic stress distribution. The main difficulty is evaluating the change in porewater pressure  $\Delta u$ . For this purpose, it is generally convenient to identify the principal planes and to define the change in the state of total stress in terms of the *principal changes in total stress*,  $\Delta\sigma_1$ ,  $\Delta\sigma_2$ , and  $\Delta\sigma_3$ . At any point in a soil there exist three mutually perpendicular planes, called *principal planes* on which no shear stresses act. The *principal stresses*  $\sigma_1$ ,  $\sigma_2$ , and  $\sigma_3$  are the maximum, intermediate, and minimum value, respectively, of normal stresses on principal planes.

#### 15.5.1 Porewater Pressures Resulting from Changes in Equal All-Around Total Stress

Skempton (1954a) defined the change in porewater pressure  $\Delta u$  resulting from undrained changes in equal all-around total stress  $\Delta\sigma$  in terms of the porewater pressure coefficient  $B = \Delta u/\Delta\sigma$ . Bishop (1973, 1976) derived an expression for the  $B$ -coefficient of saturated soils in terms of the compressibility  $C$  of the soil skeleton, the compressibility  $C_w$  of the pore water, and the compressibility  $C_s$  of the solids forming the skeleton. For a soil element of total volume  $V$  and of porosity  $n$ , the volume of the pore water within the element is  $nV$  and the volume of the solids forming the skeleton is  $(1 - n)V$ . The volume

changes resulting from the application of  $\Delta\sigma$  without drainage are evaluated by imposing, in a first stage, a change in total stress and in porewater pressure equal in magnitude to  $\Delta u$  and, in a second stage, a change in total stress of magnitude  $\Delta\sigma - \Delta u$  at constant porewater pressure. Although Bishop's analysis and the resulting conclusions concerning the  $B$ -coefficient are applicable to both total stress increments and total stress decrements, in the following description of the volume changes, only a pressure increment is considered.

The first stage produces: (i) A decrease in volume of the pore water equal to  $nVC_w\Delta u$ ; (ii) A decrease in volume of the solids equal to  $(1 - n)VC_s\Delta u$ ; (iii) A decrease in overall volume of soil skeleton equal to  $VC_s\Delta u$ . The second stage produces: (iv) A decrease in volume of the soil solids equal to  $VC_s(\Delta\sigma - \Delta u)$ ; (v) A decrease in overall volume of the soil skeleton equal to  $VC(\Delta\sigma - \Delta u)$ . For an undrained application of  $\Delta\sigma$ , in which there is no drainage of pore water out of the element, the decrease in the volume of the soil skeleton, given by summing (iii) and (v), must be equal to the decrease in volume of the pore water (i) and of the soil solids (ii) and (iv):

$$VC_s\Delta u + VC(\Delta\sigma - \Delta u) = nVC_w\Delta u + (1 - n)VC_s\Delta u + VC_s(\Delta\sigma - \Delta u)$$

This results in the following expression for  $B = \Delta u/\Delta\sigma$

$$B = \frac{1}{1 + n \frac{C_w - C_s}{C - C_s}} \quad (15.14)$$

Equation 15.14 shows that  $B = 1$  for saturated geotechnical materials for which  $C$  is significantly larger than  $C_s$  and is also large as compared to  $C_w$ . This is the case for all soils, as well as for fissured or jointed rock masses. The bulk modulus of pure water,  $K_w = 1/C_w$ , is 2100 MPa. The bulk modulus of minerals that are common in soils and rocks,  $K_s = 1/C_s$ , has values in the range of 36,000 to 69,000 MPa. In comparison, the bulk modulus of the soil skeleton,  $K = 1/C$ , for a dense sand may be less than 30 MPa and that for a soft clay may be less than 3 MPa. Therefore, when saturated soils and fissured and jointed rock masses are subjected, under an undrained condition, to an equal all-around total stress increment or decrement  $\Delta\sigma$ , the porewater pressure increases or decreases respectively by an amount equal to  $\Delta\sigma$ , and there is no change in the state of effective stress.

For intact rocks, however, for which  $C$  may approach  $C_s$ , the  $B$ -coefficient is less than unity. Values of  $\Delta u/\Delta\sigma$  computed from the porewater-pressure response of intact specimens of Vermont Marble (porosity 2.1%, coefficient of permeability  $5 \times 10^{-12}$  m/s, and unconfined compressive strength 48 to 97 MPa) are shown in Fig. 15.3. A back pressure of 1.32 MPa was required to obtain a fully

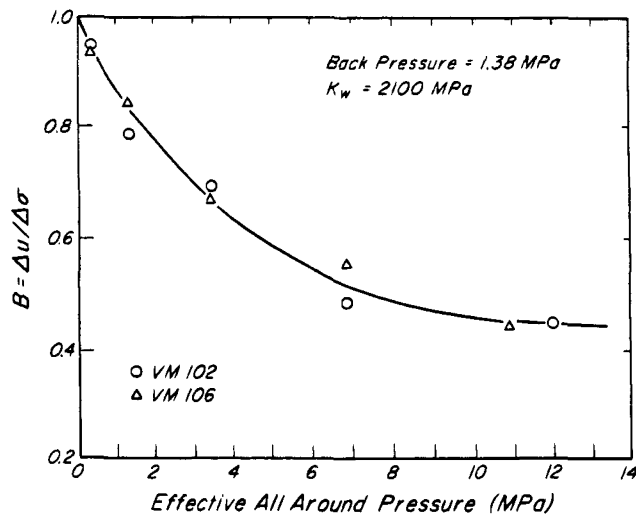


**Figure 15.3** Measured values of porewater pressure parameter  $B$  for intact specimens of Vermont marble as a function of the effective all-around confining pressure (after Mesri et al. 1976).

saturated condition with  $K_w = 2100$  MPa. Even though the rock specimens, 54 mm in diameter and 127 mm long, had no visible fissures or cracks, the apparently intact rock was sufficiently microfissured to display a  $B$ -value of unity at an effective confining pressure of zero. However, as the effective confining pressure increased and microfissures were closed, the compressibility of the rock skeleton decreased rapidly, and values of  $B$  became less than 1. At an effective confining pressure of 12 MPa, the measured value of  $B = 0.45$  and Eq. 15.14 lead to a  $K$  value of 45,000 MPa, which is rather close to the measured value  $K_s = 69,000$  MPa for the marble.

The bulk modulus of water decreases dramatically if the water contains even a very small volume of gas. For example,  $K_w$  may decrease by a factor of 100 as the degree of saturation decreases from 100% to 99% (Kirkebo 1994). Values of  $B$  in the range of 0.4 to 0.7 have been measured for compacted soils at a degree of saturation of 99% (Campbell 1973). Figures 15.4 and 15.5 show the behavior of four compacted specimens of Champaign till, a well-graded glacial till from Champaign, Illinois, with liquid limit, plastic limit, and clay size fraction of 24%, 16%, and 18%, respectively. The specimens were compacted by applying, under a laterally constrained condition, a static axial pressure of 276 kPa and maintaining it for 2 min. Figure 15.4 shows that the initial degree of saturation of the compacted specimens ranged from 31 to 74%. The specimens were set up in a triaxial cell (Article 17.2) and were subjected to increments of equal all-around pressure under an undrained condition while the porewater pressure was measured. The increases in porewater pressure in response to the increments of equal all-around pressure are shown in Fig. 15.5. In all cases, the increases in porewater pressure in response to the

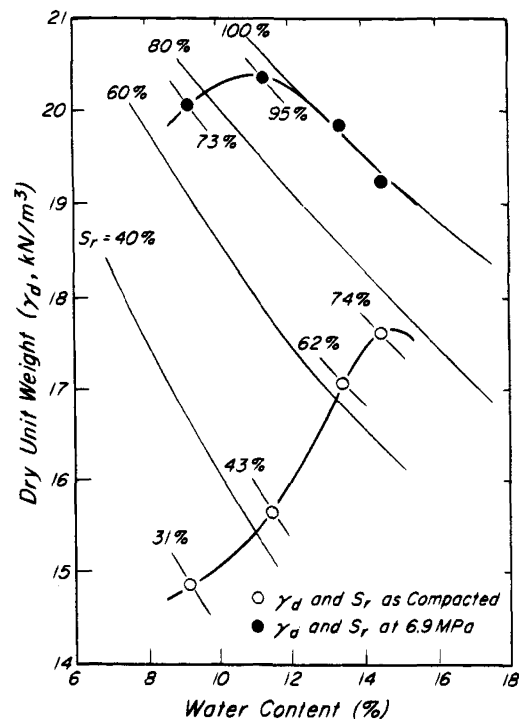


**Figure 15.4** Relation between dry unit weight and water content of Champaign till after compaction and after undrained compression under an equal all-around pressure of 6.9 MPa (after Campbell 1973).

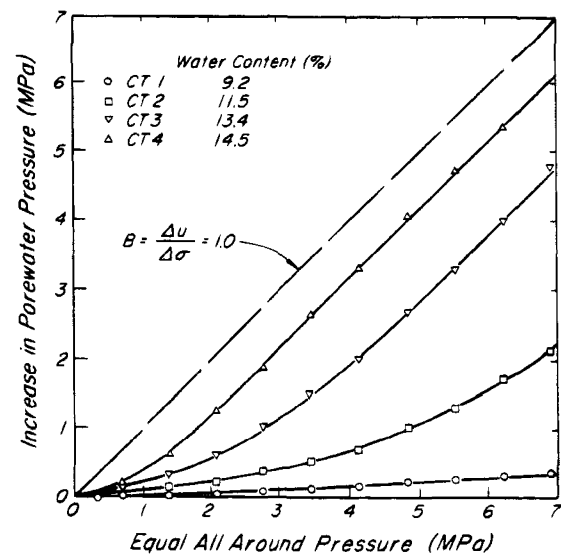


**Figure 15.5** Porewater pressure response of specimens of Champaign till (Fig. 15.4) subjected to increments of equal all-around pressure under undrained conditions (after Campbell 1973).

initial increments of all-around pressure were small and corresponded to values of  $B$  significantly less than unity. Even though the specimens were sealed, volume change occurred on account of compression of the air. The corresponding increases in porewater pressure were less than  $\Delta\sigma$ , but in all four specimens  $\Delta u/\Delta\sigma$  increased with the increase in equal all-around pressure.

The value of  $\Delta u/\Delta\sigma$  for the specimen that was compacted near the optimum water content and had an initial degree of saturation of 74% increased rapidly, and the incremental  $B$ -coefficient became equal to unity at an equal all-around pressure of about 2 MPa. At this stage the slope of the line (Fig. 15.5) representing the relation between porewater pressure increase and cell pressure became equal to that for a saturated material. As the total confining pressure was increased, air was compressed and dissolved in the pore water, and the degree of saturation increased. Beyond the total confining pressure of 2 MPa, the porewater-pressure response of this specimen reflected the behavior of a saturated soil. At this pressure, the free air was completely dissolved whereupon the specimen became saturated. Indeed, direct measurements of volume change, used in computing the increase in dry unit weight shown in Fig. 15.4, indicated a degree of saturation near 100%. According to the porewater-pressure response in Fig. 15.5, the specimen, which had an initial degree of saturation of 62%, became fully saturated at an equal all-around pressure of about 5 MPa. This is confirmed by the degree of saturation determined from the volume change measurements, Fig. 15.4. On the other hand, Fig. 15.5 shows, for the specimens with initial degrees of saturation of 43% and especially 31%, that even though  $\Delta u/\Delta\sigma$  increased with the total confining pressure, the incremental  $B$ -coefficient did not reach unity in the equal all-around pressure range up to 6.9 MPa. Figure 15.4 shows that the degrees of saturation of these specimens at the total confining pressure of 6.9 MPa were 95% and 73%, respectively.

The data in Figs. 15.4 and 15.5 show that the porewater-pressure response of unsaturated soils subjected to increments of equal all-around pressure depends strongly on the degree of saturation. A simple relationship between the  $B$ -coefficient and the degree of saturation does not exist, however, because the porewater-pressure response also depends on the magnitude of  $C$ , which is determined by the composition of the soil, its structure (for example, the method and degree of compaction), and the amount of compression produced by the total confining pressure.

In inorganic soils and rocks,  $C_s$  is always less than  $C_w$  and thus  $B$  is not expected to have values greater than unity. However, in fully saturated organic soils such as fibrous peat, if the porous fibers contain occluded gas,  $C_s$  may be greater than  $C_w$  and  $B$  may slightly exceed unity. In a series of laboratory tests on a fibrous peat, values of  $B = 1.01$  to  $1.02$  were measured repeatedly.

### 15.5.2 Porewater Pressures Resulting from Application of Shear Stresses

When the changes in state of total stress lead to algebraically unequal *principal changes in stress*,  $\Delta\sigma_1$ ,  $\Delta\sigma_2$ , and  $\Delta\sigma_3$ , the soil is subjected to changes in shear stresses. All soils and rocks tend to experience volume change when subjected to a change in shear stress. Under undrained conditions, the tendency for volume change is manifested in the form of shear-induced pore pressures. Because the change in state of stress may involve a rotation of the principal planes, the pore-pressure response is expressed in terms of *principal changes in total stress* rather than in terms of the changes in the preshear principal stresses (Law and Holtz 1978). For example, irrespective of the preshear directions of  $\sigma_1$ ,  $\sigma_2$ , and  $\sigma_3$ , if the principal changes in total stress are  $-20$  kPa,  $0$ , and  $10$  kPa, then  $\Delta\sigma_3 = -20$  kPa,  $\Delta\sigma_2 = 0$ , and  $\Delta\sigma_1 = 10$  kPa.

A change in the state of total stress, defined by  $\Delta\sigma_1$ ,  $\Delta\sigma_2$ , and  $\Delta\sigma_3$ , is equivalent to an equal all-around change in total stress  $\Delta\sigma_3$  plus the shear stresses  $\Delta\sigma_1 - \Delta\sigma_3$ , and  $\Delta\sigma_2 - \Delta\sigma_3$ . Therefore, for a saturated soil with  $B = 1$ , the change in porewater pressure in an undrained condition may be expressed as

$$\Delta u = \Delta\sigma_3 + A_1(\Delta\sigma_1 - \Delta\sigma_3) + A_2(\Delta\sigma_2 - \Delta\sigma_3) \quad (15.15)$$

When  $\Delta\sigma_2 = \Delta\sigma_3$  the following expression proposed by Skempton (1954) is obtained

$$\Delta u = \Delta\sigma_3 + A(\Delta\sigma_1 - \Delta\sigma_3) \quad (15.16)$$

Even though Eq. 15.16 is a convenient means of normalizing shear-induced porewater pressure in terms of the change in shear stress, it has not found wide application in practice. The reason is that shear-induced porewater pressure, and thus the  $A$ -coefficient, are highly dependent not only on the composition and structure of the soil, but also on the mode of shear or the stress path to failure (Article 18.2.2). Therefore, it has not been possible to generalize information regarding the magnitude and behavior of the  $A$ -coefficient and to develop an empirical database for estimating shear-induced porewater pressures for effective stress stability analyses of undrained soil failures (Article 20.3). However, the general outline of the behavior of shear-induced porewater pressure in saturated soils and the associated  $A$ -coefficient is well established. For example, soils and rocks that tend to contract on application of shear stresses develop positive shear-induced porewater pressures that lead to positive values of the  $A$ -coefficient. For contractive soil and rock conditions (Article 18.2), values of  $A$  from slightly above zero to higher than 2 have been measured in the laboratory. Very loose and open fabrics of clay, silt, and fine sand that may exist at relatively high consolidation pressures tend to collapse on application of shear stresses, and thus lead to high values of the  $A$ -coefficient. On the

other hand, a clay soil with an overconsolidation ratio near 6 to 8, on application of shear stresses, may display little tendency for either contraction or expansion and may develop zero shear-induced porewater pressures and values of  $A$  near zero. Highly overconsolidated dense soils and rocks that are very dilatant (Article 18.2), especially when they exist under relatively low effective confining pressures, develop very high negative shear-induced porewater pressures. Values of  $A$  for even highly overconsolidated clays and dense rocks, however, are rarely less than about  $-0.3$ , because the overconsolidation or densification that promotes the highly dilatant tendency also increases the resistance to shear and thus increases the magnitude of the shear stress required to deform the soil or rock structure and elicit dilatant response.

In summary, soils exist at a void ratio determined by their existing effective stress condition. When they are subjected to changes in shear stresses, they have a tendency to change their void ratio. If an undrained condition prevails and the change in void ratio is not possible, soils alter the existing effective stress condition by generating pore pressures. If the tendency of a saturated soil is to contract upon shear, the soil develops positive porewater pressures in an undrained condition, and thus decreases the imposed effective stresses. On the other hand, the tendency for expansion develops negative porewater pressures and increases the imposed effective stresses. Because the effective stress condition determines the behavior of soils, shear-induced porewater pressures that alter the effective stress condition in soils are of practical importance.

### Selected Reading

- Skempton, A. W. (1954). "The pore-pressure coefficients  $A$  and  $B$ ," *Géot.*, **4**, No. 4, pp. 143–147.
- Bishop, A. W. (1973). "The influence of an undrained change in stress on the pore pressure in porous media of low compressibility," *Géot.*, **23**, No. 3, pp. 435–442.
- Bishop, A. W. (1976). "The influence of system compressibility on the observed pore-pressure response to an undrained change in stress in saturated rock," *Géot.*, **26**, No. 2, pp. 371–375.
- Mesri, G., K. Adachi and C. R. Ullrich (1976). "Pore pressure response in rock to undrained change in all-round stress," *Géot.*, **26**, No. 2, pp. 317–330.
- Law, K. T. and R. D. Holtz (1978). "A note on Skempton's 'A parameter with rotation of principal stresses'," *Géot.*, **28**, No. 1, pp. 57–64.

## 15.6 Negative Pore Pressure in Soils

### 15.6.1 Capillarity and Suction

The terms *water level*, *water table*, and *phreatic surface* designate the locus of the levels to which water rises in observation wells in free communication with the voids

of the soil *in situ*. The water table can also be defined as the surface at which the neutral stress or porewater pressure  $u_w$  (Article 15.1) in the soil is equal to zero.

If the water contained in a soil were subject to no force other than gravity, the soil above the water table would be perfectly dry. In reality, every soil in the field is completely saturated for a certain distance above the water table and is partly saturated above this level. The water that occupies the voids of the soil located above the water table constitutes *soil moisture*.

If the lower part of a mass of dry soil comes into contact with water, the water rises in the voids to a certain height above the free-water surface. The upward flow is attributed to the *surface tension* of the water. The seat of the surface tension is located at the boundary between air and water. Within the boundary zone the water is in a state of tension comparable to that in a stretched rubber membrane attached to the walls of the voids of the soil. However, in contrast to the tension in a stretched membrane, the surface tension in the boundary film of water is unaffected by either the contraction or stretching of the film.

The phenomenon of capillary rise can be demonstrated by immersing into water the lower end of a very small-diameter glass tube known as a capillary tube. As soon as the lower end of the tube comes into contact with the water, the attraction between the glass and the water molecules combined with the surface tension of the water pull the water up into the tube to a height  $h_c$  above the water level (Fig. 15.6a). The height  $h_c$  is known as the *height of capillary rise*. The upper surface of the water assumes the shape of a cup, called the *meniscus*, that joins the walls of the tube at an angle  $\alpha$  known as the *contact angle*. The value of  $\alpha$  depends on the material that constitutes the wall and on the type of impurities that cover it. For glass tubes with chemically clean or

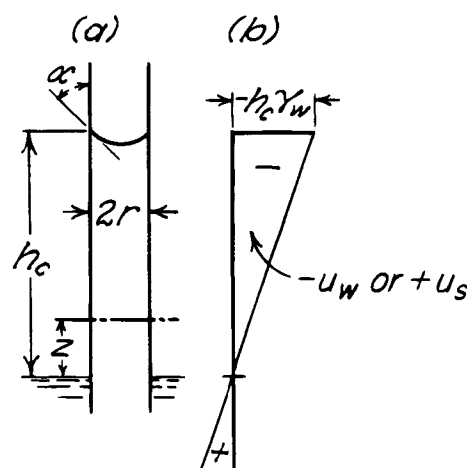


**Figure 15.6** (a) Rise of water in capillary tube. (b) State of stress of water in capillary tube.



wetted walls  $\alpha$  is equal to  $0^\circ$ , and the water rises in such tubes to the greatest height compatible with the diameter of the tube and the surface tension of the water. If the walls are not chemically clean,  $\alpha$  is likely to have some value intermediate between  $0^\circ$  and  $90^\circ$ , and the corresponding height of capillary rise is smaller than  $h_c$  for  $\alpha = 0^\circ$ . If the walls are covered with a thin film of grease,  $\alpha$  is greater than  $90^\circ$ , and the meniscus is located below the free-water level. This phenomenon is ascribed to a repulsion between the molecules of the water and the grease.

If  $T_s$  denotes the surface tension per unit of length of contact, and  $\rho_w g$  the unit weight of water, equilibrium requires that

$$h_c \pi r^2 \rho_w g = 2 \pi r T_s \cos \alpha$$

from which

$$h_c = \frac{2T_s}{r\rho_w g} \cos \alpha \quad (15.19)$$

The value of  $T_s$  decreases slightly with increasing temperature. At room temperature it is about 75 mN/m, and  $\rho_w$  is equal to 1 Mg/m<sup>3</sup>. Therefore, approximately

$$h_c(m) = \frac{150}{r(m)} \cos \alpha \quad (15.20)$$

Above the free-water level the hydrostatic pressure in the water  $u_w$  is negative. At an elevation  $z$  it is

$$u_w = -z\gamma_w = -u_s \quad (15.21)$$

where  $u_s = z\gamma_w$  is designated the *suction*.

It may be noted in Fig. 15.6a that atmospheric pressure  $u_a$  acts on the meniscus at the top of the column of water as well as on the surface of the body of free water into which the bottom of the capillary tube is inserted. Under these circumstances the air pressure  $u_a$  has no effect on the height of capillary rise  $h_c$ . Strictly speaking, the suction is defined as

$$u_s = (u_a - u_w) \quad (15.22)$$

where  $u_a$  is the air pressure above the meniscus. Hence, Eq. 15.21 is applicable only if the air-water interface is open to the atmosphere, and  $u_a$  is atmospheric gage pressure.

In contrast to capillary tubes, the continuous voids in soils and most other porous materials have a variable width. They communicate with each other in every direction and constitute an intricate network of voids. If such a network is invaded by water from below, the lower part of the network becomes completely saturated. In the upper part, however, the water occupies only the narrowest voids, and the wider ones remain filled with air. In the laboratory, the rise of water into the voids of a dry sand due to surface tension can be demonstrated by the test

arrangement shown in Fig. 15.7a. The sand is poured into an upright glass tube with a screen across the bottom. The bottom of the tube is then placed just below a free-water surface, whereupon the water rises into the sand. That part of the sand in which the voids become partly or completely occupied by liquid assumes a dark color, whereas the remainder is light. To a height  $h_{cc}$  above the water level the sand is completely saturated. Between  $h_{cc}$  and  $h_c$  it is partially saturated, as shown in Fig. 15.7b. The height  $h_c$  is called the *height of capillary rise*. Figure 15.7c shows the time rate at which the upper surface of the moistened zone approaches its equilibrium position at elevation  $h_c$ .

As the effective grain size decreases, the size of the voids also decreases, and the height of capillary rise increases. The height  $h_c$  (m) is approximately equal to

$$h_c = \frac{C}{eD_{10}} \quad (15.23)$$

in which  $e$  is the void ratio,  $D_{10}$  (mm) is Allen Hazen's effective size (Article 5), and  $C$  is an empirical coefficient that depends on the shape of the grains and on the surface impurities. It ranges between 0.01 and 0.05. However, because the decrease in permeability associated with a decrease in effective size reduces the rate of capillary rise, the height to which water will rise within a specified time, such as 24 hr, is a maximum at some intermediate grain size. In Fig. 15.8 the abscissas represent the logarithm of the grain size of a uniform quartz powder in a fairly dense state, and the ordinates represent the height to which the water rises in 24 hr. The height of rise is a maximum for a grain size of about 0.02 mm. For a 48-hr rise the optimum grain size would be slightly smaller.

Capillary forces are able to raise water against the force of gravity not only into capillary tubes or the voids in columns of dry soil, but also into narrow open channels or V-shaped grooves. This fact can be demonstrated by the apparatus shown in Fig. 15.9. If the highest point of the groove is located below the level to which the surface tension can lift the water, the capillary forces will pull

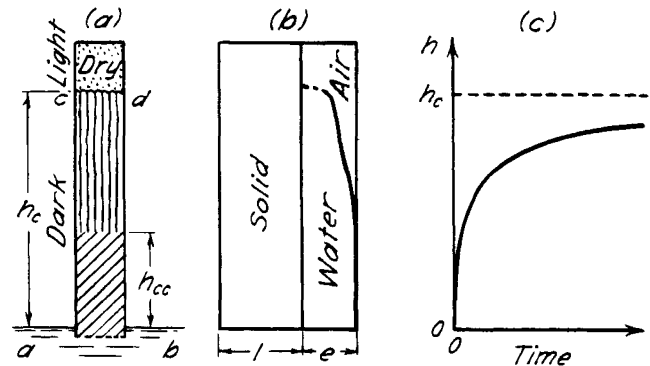


Figure 15.7 Capillary rise of water into dry sand.

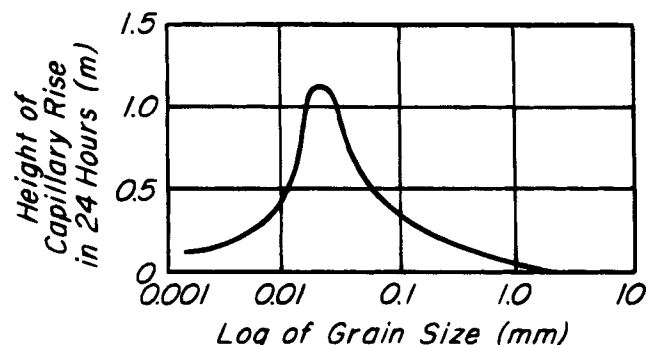


Figure 15.8 Relation between grain size of uniform quartz powder and height of capillary rise for 24 hr period (after Atterberg 1908).

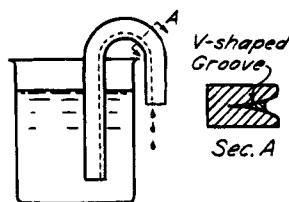


Figure 15.9 Capillary flow through V-shaped groove.

the water into the descending part of the groove and will slowly empty the vessel. This process is known as *capillary siphoning*. The same process may also occur in the voids of a soil in the field. For example, water may flow over the crest of an impermeable core in a dam or dike, as shown in Fig. 15.10, even though the elevation of the free-water surface is below that of the crest of the core. Capillary siphoning over the crest of cores was found to cause a loss of 26 m<sup>3</sup>/day for a length of 19 km of the canal between Berlin and Stettin in Germany. The impermeable core of the dikes extended 0.3m above the water table. When the height of the core was increased 0.4m, the loss was reduced to 6 m<sup>3</sup>/day.

Between the heights  $h_{cc}$  and  $h_c$  (Fig. 15.7a) some of the void space is occupied by continuous channels of air. The remainder is occupied by threads of water. Because these threads are also continuous, the stress in the water up to an elevation  $h_c$  is governed by Eq. 15.21. However, if a sand is only moist, the water particles do not communicate with each other, and Eq. 15.21 is not applicable.

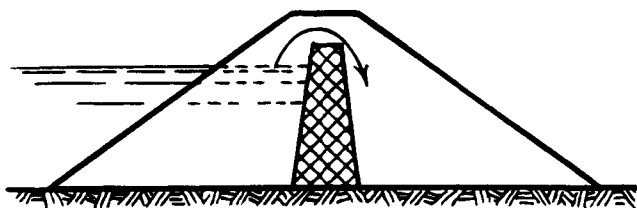


Figure 15.10 Capillary flow over impermeable core in earth fill.

The water contained in a moist sand is known as *contact moisture* because each drop of water surrounds a point of contact between two soil grains, as shown in Fig. 15.11. The surface tension at the boundary between the water and the air in the adjoining voids pulls the soil grains together with a force  $P$  known as the *contact pressure*. The frictional resistance produced by the contact pressure has the same effect as if the sand had a certain amount of cohesion, known as *apparent cohesion* (see Figs. 15.14,a and b). As soon as the sand is immersed, the surface tension is eliminated, the contact pressure becomes equal to zero, and the sand disintegrates.

The mechanical effect of the apparent cohesion due to contact moisture depends on the relative density of the sand. If the sand is dense, the cohesion increases its shearing resistance to such an extent that vertical slopes with a height of a few meters can stand without lateral support. On the other hand, if a damp sand is loosely deposited, for instance by dumping, the apparent cohesion prevents the soil particles from settling into stable positions and reduces the bearing capacity of the sand almost to zero. The volume of such a sand may exceed that of the same sand in a loose dry state by 20 to 30%. This phenomenon is known as *bulking*. Because the forces that maintain the grains in their unstable positions are extremely small, bulking occurs only within a meter or so below the surface of the sand. Watering reduces the porosity of the sand to that of the same sand in a dry or saturated loose state because it eliminates the surface tension of the water.

In very fine-grained soils the height of capillary rise may be many meters and the suction  $u_s$  correspondingly great. Moreover, in such soils the difference in concentration of the cations in the electric double layer surrounding the particles (Article 4.4) and in the free water farther from the particles generates an *osmotic suction* that may be very large. The total suction is made up of the capillary or *matric suction* and the osmotic suction, although the two are not necessarily strictly additive (Nelson and Miller 1992). In most geotechnical problems, changes in osmotic suction are small in comparison with changes in matric suction, and changes in total suction are due almost entirely to changes in matric suction. Consequently, the

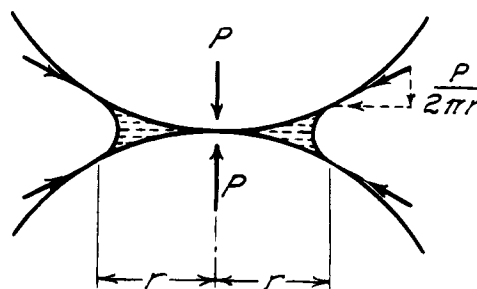


Figure 15.11 Forces produced by contact moisture.

effects of practical importance result primarily from changes in matric suction. Total suction is of interest because it is the quantity measured directly in some of the methods by which suction is investigated in the laboratory and in the field (Fredlund and Rahardjo 1993). In this book  $u_s$  refers to total suction; in coarse- to fine-grained soils it is likely to be primarily matric suction, whereas in very fine-grained soils such as clays it is likely to include a substantial component of osmotic suction.

### 15.6.2 Drainage by Gravity

In engineering practice soil is drained where it is desirable to eliminate seepage pressure, to reduce the danger of frost damage, or to increase the shearing resistance of the soil by reducing the neutral stresses. Drainage consists of lowering the water table below the base of the mass of soil that requires protection or reinforcement. The techniques and practical applications of drainage are discussed in Article 43. After a brief description of the various categories of drainage, the remainder of this section deals with drainage due to gravity alone.

In sand part of the water that flows out of the voids by gravity is replaced by air (*drainage by air invasion*). However, very fine-grained soils remain in a saturated state, and the volume of the voids of the soil decreases by an amount equal to that of the expelled water (*drainage by consolidation*).

The drainage of any type of soil can also be accomplished by evaporation from a surface exposed to the atmosphere. This process is called *drainage by desiccation*. In different types of soil it can take place by air invasion, by consolidation, or by air invasion preceded by consolidation.

Very fine-grained soils can also be drained by passing an electric current through them. This procedure is known as *drainage by electro-osmosis*. If the uppermost part of a saturated mass of very fine-grained soil is exposed to a temperature below the freezing point, water is drawn out of the lower part and accumulates in the upper part where it forms ice layers. The seepage pressure of the percolating water consolidates the layer of soil located beneath the zone of freezing. Therefore, it may be said that this layer is subject to *drainage by frost action*.

The smallest value to which the water content of a soil can be reduced by drainage is known as the *water-holding capacity* of the soil. To obtain numerical values for comparing the water-holding capacity of different soils, various laboratory procedures are used. In *gravity methods*, the water drains out of the sample under the influence of gravity alone. In *suction methods*, the force of gravity is augmented by applying a vacuum at the bottom of the sample or air pressure at the top. In *centrifuge methods*, the gravity forces are replaced by inertia forces of much greater intensity.

If the void ratio of a soil after drainage, the unit weight of the solid soil particles, and the water-holding capacity are known, the degree of saturation  $S_r$  (Eq. 6.4) and the air-space ratio  $G_a$  of the drained soil can be computed. The *air-space ratio* is defined by the equation,

$$G_a = \frac{\text{Air space}}{\text{Total void space}} = 1 - \frac{S_r(\%)}{100} \quad (15.24)$$

Curves *A* and *B* in Fig. 15.12 represent the relation between the air-space ratio and the effective grain size  $D_{10}$  for different soil fractions that were drained by two different methods. The data for plotting curve *A* were obtained by submitting saturated samples to drainage by suction. A vacuum was applied for 2 hr at the bottom of samples 100 mm high. Curve *B* represents the results of tests made by the centrifuge method, in which the samples were subjected for 2 min to a force 18,000 times that of gravity (Lebedeff 1928).

In the laboratory the drainage of sand under the influence of gravity continues for years at a decreasing rate, even if the sand is fairly coarse. Figure 15.13*a* represents two samples of sand 2 1/2 years after the start of drainage. In both samples the air-space ratio increased quite rapidly with increasing elevation above the water table, as shown in Fig. 15.13*b*. Furthermore, even at the end of 2 1/2 years, the average air-space ratio of both samples was still increasing (King 1899).

In the field every process of drainage by gravity is accompanied by an occasional inflow of water from rain or melting snow and ice. The effect of the recharge on the average moisture content of a drained soil in the field depends not only on the amount of recharge and evaporation, but also to a considerable extent on details of stratification. Furthermore, experience indicates that the air-space ratio for a drained soil in the field is practically independent of the elevation above the water table, whereas in drained laboratory specimens it increases consistently in an upward direction, as shown in Fig. 15.13*b*. Hence, there is no definite relation between the water-holding capacity of a soil after drainage in the laboratory and that of the same soil after drainage in the field. This can be seen by comparing the laboratory curves *A* and *B* in Fig. 15.12 with curve *C*. The shaded area surrounding curve *C* represents the relation between air-space ratio and effective grain size of various soils after gravity drainage in the field under climatic conditions similar to those in the east-central part of the United States. Observations in regions with different climatic conditions may lead to very different curves. Yet no field curves can be expected to have more than the general trend in common with the laboratory curves.

Fortunately, in connection with engineering operations, the quantity of water drained out of the ground is seldom of importance. Of much greater significance are the

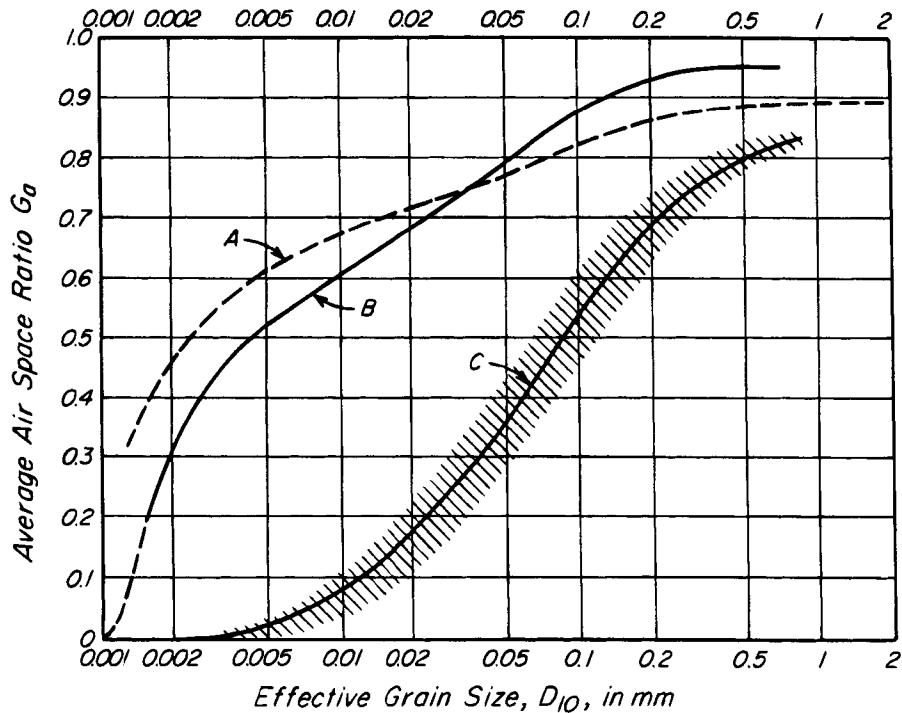


**Figure 15.12** Relation between grain size and degree of saturation after drainage. Curve A (after Zunker 1930) obtained by suction method; curve B (after Lebedeff 1928) by centrifuge method; curve C by field measurements.

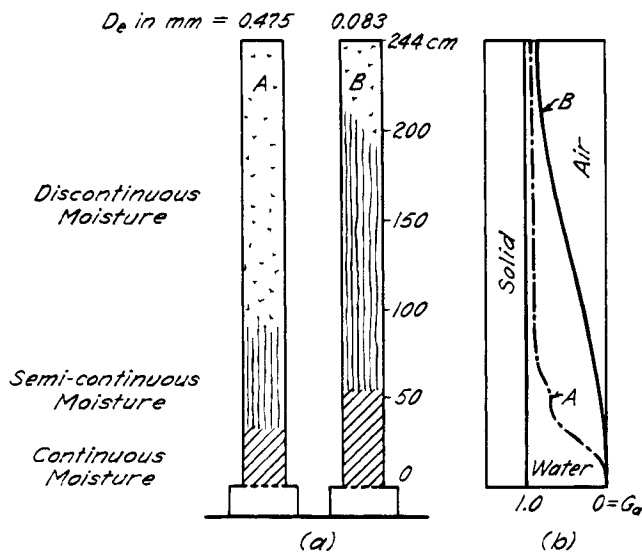


**Figure 15.13** Soil moisture in two different samples of sand after drainage for 2.5 years in laboratory (after King 1899).

mechanical effects of the drainage and the time required to produce them.

Theoretical methods for estimating the rate of drainage by air invasion are still rather unsatisfactory. Hence, to estimate the time required for draining a sand stratum, the engineer must rely primarily on experience. The drainage of a stratum of clean coarse sand by pumping from

filter wells spaced not in excess of 10 m can usually be accomplished within a few days (very rapid drainage). On the other hand, the same operation in a very fine sand may require several months (slow drainage). The methods available for draining soils and the conditions for their successful application are discussed in Article 43. The settlements associated with lowering the water table are the subject of Article 55.2.

### 15.6.3 Drainage by Desiccation

If a specimen of soft clay is exposed to the air, water is drawn from the interior of the specimen toward the surface where it evaporates. During this process, the clay becomes stiffer and finally very hard. The state at which evaporation ceases depends on the relative humidity of the surrounding air. Water evaporates at every air-water boundary unless the relative humidity of the air is at least equal to a certain value that is a function of the tension in the water. The *relative humidity*  $h_{ra}$  is defined as the ratio between the weight of water vapor actually contained in the air at a given temperature and the greatest quantity of vapor that can be contained in the air at the same temperature. In humid climates the relative humidity commonly ranges between 0.15 and 0.95 and exceptionally reaches 0.99. If the relative humidity of the air above a free-water surface is smaller than 1.0, water evaporates until the relative humidity of the superincumbent air is equal to 1.0, or until the water has completely evaporated.

If the water is in a state of tension, it ceases to evaporate at a lower value of relative humidity. This lower value  $h_r$  is designated as the *relative vapor pressure* of the water. Within a temperature range of 10° to 30°C, and a relative vapor-pressure range of 0.7 to 1.0, the relation between the suction  $u_s$  in the water and the relative vapor pressure  $h_r$  of the water can be expressed approximately by the equation

$$u_s \text{ (MPa)} = -135 \ln h_r \quad (15.25)$$

For example, if  $h_r = 0.90$ ,  $u_s = 15$  MPa. Hence, if the suction in an exposed specimen of clay is equal to 15 MPa, the water content of the clay does not remain constant unless the relative humidity of the surrounding air is equal to 0.90. If the relative vapor pressure is smaller, the clay continues to lose water by evaporation, whereas, if it is greater, water condenses on the surface of the clay and causes the clay to swell until the suction drops to the value determined by Eq. 15.25. This fact can be used as a basis for computing the suction in fine-grained porous materials such as clays.

If the water evaporates at the ends of a capillary tube having a radius  $r$ , the curvature of the menisci and the suction  $u_s$  increase until  $u_s$  equals  $h_c \rho_w g$ . Substitution of  $h_c = u_s / \rho_w g$  into Eq. 15.20 leads to

$$u_{s \text{ max}} \text{ (MPa)} = \frac{150}{r(m)} \quad (15.26)$$

Further evaporation causes the water to withdraw into the interior of the tube at a constant neutral stress. A similar process takes place in the pore water of desiccating soils. When a soil dries,  $u_s$  first increases until it assumes the greatest value compatible with the size of the voids at the surface of the soil. Further evaporation causes air to penetrate the specimen, whereupon the color of the soil changes from dark to light. At the beginning of this second stage, the water content of the specimen is equal to the shrinkage limit (Article 7.2). However, during this stage, the suction  $u_s$  can increase further because the water withdraws into the narrowest corners and grooves. Evaporation does not cease until the relative vapor pressure  $h_r$  (Eq. 15.25) becomes equal to the relative humidity  $h_{ra}$ .

The water that remains in the dried soil constitutes the contact moisture mentioned in Article 15.6.1. After desiccation at room temperature, the water content of soils ranges from almost zero for clean sand to 6 or 7% for typical clays. The corresponding air-space ratio ranges from 1.0 to about 0.8. At this state a perfectly clean sand is cohesionless, whereas a clay is very hard.

If an oven-dried soil specimen is cooled in contact with the atmosphere, its water content increases. The water taken up by the soil particles from the surrounding atmosphere is called the *hygroscopic moisture*. The amount of hygroscopic moisture varies for a given specimen with

the temperature and relative humidity of the air. In a general way it increases with decreasing grain size. For sands it is negligible. For silty soils it is very small, yet sufficient to induce bulking. In clay it may amount to more than 5% of the dry weight.

When an air-dry clay specimen is heated to a temperature somewhat above the boiling point of water, its water content decreases slightly. At this stage some of the physical properties of the clay undergo changes that appear to be permanent. The changes are disclosed by permanent changes in the Atterberg limits. Further increase of the temperature to several hundred degrees Celsius above the boiling point leads to actual fusion between the grains at their points of contact. This process produces a strong and permanent bond between the grains and gives the clay the characteristics of a solid body. The transformation of sand-clay mixtures into brick occurs in a similar manner.

The rate at which water evaporates from the surface of clay specimens under given conditions of exposure decreases with decreasing water content. At the liquid limit the rate of evaporation is approximately equal to that from a free surface. At such a surface the rate of evaporation depends on the temperature, the relative humidity, and the wind velocity. In the United States the area of lowest evaporation from large free-water surfaces is the Great Lakes region, where the rate of evaporation ranges from 0.4 to 0.5 m per year. To the west and south of the Great Lakes region it gradually increases. It amounts to about 1.8 m in southwest Texas and southeast New Mexico. In the central parts of the Imperial Valley, California, values up to 2.2 m per year have been recorded. Even if a clay sample coated with paraffin is stored in a humid room, it gradually shrinks away from its shell. This shrinkage indicates the escape of water vapor through invisible but continuous voids in the paraffin.

As the water content of a desiccating clay decreases, the rate of evaporation also decreases because the suction in the pore water increases. According to Eq. 15.25 the increase in suction involves a decrease in the relative vapor pressure. Such a decrease has the same retarding effect on the rate of evaporation at constant relative humidity as an increase of the relative humidity has on the rate of evaporation from a free-water surface.

Below the shrinkage limit the rate of evaporation is further retarded, because the relative humidity of the air in the voids is always higher than in the adjoining open air. As soon as the relative vapor pressure in the pore space becomes equal to the relative humidity of the surrounding air, further evaporation ceases. If the relative humidity then increases, the water content of the clay increases slightly.

While a soil is drying, suction develops in the pore water. This suction increases with decreasing water con-

tent, whereas the total normal stress on a given section through the soil remains practically unaltered. Because the total normal stress is equal to the sum of the neutral and effective stresses, the increasing suction or tension in the porewater involves an equivalent increase of the effective pressure. As desiccation increases the suction in the pore water from zero to  $u_s$ , the surface tension simultaneously produces an effective all-around pressure

$$p_k = u_s \quad (15.27)$$

This pressure is known as *capillary pressure*. It increases the shearing resistance of the soil along any section by

$$\Delta s = p_k \tan \phi' \quad (15.28)$$

wherein  $\phi'$  represents the angle of internal friction for sand or the consolidated-undrained value of the angle of shearing resistance for clays (Article 18).

At the shrinkage limit, air invades the voids of the specimen and the soil moisture ceases to be continuous. The tension in the water that remains in the clay produces contact pressures, as illustrated in Fig. 15.11, and the contact pressures in turn produce shearing resistance. However, because of the discontinuity of the pore water, the relation between  $\Delta s$  and  $u_s$  is no longer governed by Eqs. 15.27 and 15.28.

Because of capillary pressure even perfectly cohesionless materials such as fine clean sands may temporarily acquire the characteristics of cohesive materials. Consequently, samples of the material possess a definite compressive strength when unconfined. Because the cohesion of such soils disappears completely after immersion, it is referred to as *apparent cohesion*.

The water content at which the unconfined compressive strength  $q_u$  of a desiccating soil sample is a maximum depends chiefly on the grain size. This statement is illustrated by Fig. 15.14, which shows the effect of a decrease of the water content due to desiccation on the compressive strength of three different soils. The water content of each soil at the shrinkage limit is denoted by  $w_s$ . For values of  $w$  smaller than  $w_s$  the degree of saturation (Eq. 6.4) is approximately equal to  $100w/w_s$ .

For a perfectly clean fine sand moistened with distilled water (Fig. 15.14a),  $q_u$  is a maximum for a degree of saturation of about 80%. Further desiccation ultimately reduces  $q_u$  to zero. However, if the interstices are filled with tap water, the impurities are precipitated during evaporation and form a very thin but continuous layer that adheres to the grains and interconnects them at their points of contact. Thus, during the last stage of desiccation, the sand acquires a slight cohesion, as indicated in Fig. 15.14a by the dash line.

The relation between  $w$  and  $q_u$  for a fine silty sand is shown in Fig. 15.14b. As the water content approaches the shrinkage limit, the strength increases. At the shrinkage limit, air invades the voids of the specimen, and the

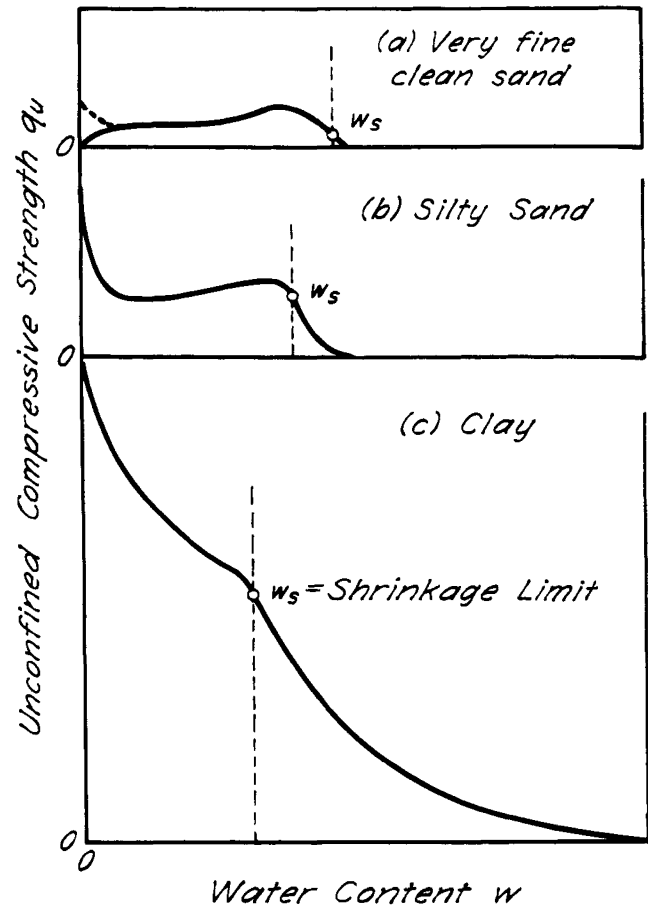


**Figure 15.14** Unconfined compressive strength of various soils at water contents above and at various stages of desiccation below the shrinkage limit (b and c, after Atterberg 1916).

strength decreases gradually until the degree of saturation becomes approximately equal to 10%. Thereafter it increases and becomes greater than at the shrinkage limit (Atterberg 1916).

The strength of clays (Fig. 15.14c) below the shrinkage limit increases at an increasing rate as the dry state is approached.

#### 15.6.4 Shrinking, Swelling, and Slaking

In nature desiccation takes place whenever the surface of the soil is not permanently flooded. The apparent cohesion of very fine-grained silty sands due to periodic desiccation may be quite large. Because rain water does not expel more than a small part of the air contained in the voids, the cohesion survives even wet spells of long duration. Consequently, such soils have often been mistaken, particularly in semiarid and arid regions, for soft rocks. However, if the surface of the soil is flooded, the cohesion gradually disappears, and the soil may start to slide.

The desiccation of a soft clay layer proceeds very slowly from the exposed surface in a downward direction

and leads to the formation of a crust that becomes thicker with age. If such a crust is buried beneath clay sediments and is permanently flooded, it constitutes a stiff precompressed layer located between soft normally loaded strata. Thick layers of soft clay can be consolidated by circulating hot dry air through systems of ventilation tunnels, but such a procedure is rarely economical.

In semiarid regions such as western Texas the desiccation of clays in the dry season often proceeds to a depth of 6 m or more (Simpson 1934). Within this depth the clay is broken up by shrinkage cracks. During the rainy season water enters the cracks, and the clay swells. The swelling causes an important rise of the ground surface. Beneath areas covered by buildings the loss of water due to evaporation is very much smaller than the corresponding loss beneath the adjacent areas. Hence, the water content of the clay located beneath the covered areas increases for many years at a decreasing rate and causes a heave of the central part of the areas with reference to their outer boundaries. The amount of heave is practically independent of the weight of the buildings, but its effect on the buildings is very similar to that of unequal settlement. Under unfavorable climatic and soil conditions, the heave can, in the course of time, become a large fraction of a meter.

If the basement floor of a centrally heated building rests on clay, the pore water of the clay may evaporate through the voids of the concrete, whereupon the clay shrinks away from the concrete and deprives the floor of its support. This undesirable development can be prevented by covering the surface of the clay with a bituminous layer before placing the concrete. The quantitative aspects of shrinking and swelling are discussed in Article 16.10.

When a dried specimen of clay (Fig. 15.15) is rapidly immersed in water, the outer portions of the specimen become saturated, and air is trapped in the inner portions. The pressure in the air produces a tension in the solid skeleton that is likely to cause failure in tension along some surface such as *ab*. This process is known as *slaking*. It is responsible for the breaking up and ultimate sloughing of unprotected clay slopes.

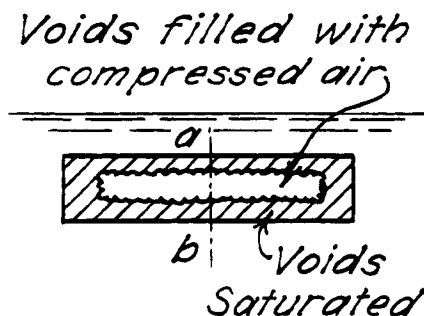


Figure 15.15 Diagram illustrating slaking of dried clay.

## 15.7 Electro-osmosis

If two electrodes are driven into a saturated soil and an electric current is made to flow from one to the other, the water contained in the soil migrates from the positive electrode (anode) toward the negative one (cathode). If the cathode consists of a well point, the water seeps into it, whence it can be removed by pumping.

The movement of the water is due to the negative charge carried by the surface of the soil particles (see Article 4). Consequently, positively charged ions in the water are attracted toward the soil particles, and the film of water adjacent to the soil (double-layer water, Article 4) is positively charged because of the preponderance of positive ions. Although there is no sharp boundary between the positively charged and the free water, for present purposes the seat of the electric charges may be regarded as the electric double layer (Article 4).

The positive ions, which are concentrated in the double-layer water, are attracted by the negative electrode and repelled by the positive one. Hence, the double-layer water together with the enclosed column of free water migrates toward the cathode (Fig. 15.16a). The flow of water produced by the electric current is known as an *electro-osmotic phenomenon*.

In electro-osmotic flow the velocity is constant over the cross-section of the entire column of water surrounded by the double layer, whereas the velocity of gravity flow through a capillary increases from the walls toward the center of the tube as shown in Fig. 15.16b.

The velocity  $v$  at which water flows by electro-osmosis through a cylindrical tube is given approximately by the equation

$$v = \frac{CedE}{\eta l} \quad (15.29)$$

where  $e$  = electric charge per unit of area of the walls of the tube

$E$  = difference in electric potential of the two ends of the tube

$d$  = thickness of the electric double layer

$\eta$  = viscosity of the water

$l$  = length of the tube

$C$  = numerical coefficient.

For a given material constituting the tubes and for a relatively small range in temperature,  $e$ ,  $d$ , and  $\eta$  are approximately constant and Eq. 15.29 may be rewritten as

$$v = k_e i_e \quad (15.30)$$

where  $k_e$  is designated the *coefficient of electro-osmotic permeability*, and  $i_e$  is the potential gradient  $E/l$ . The coefficient of electro-osmotic permeability is expressed as the velocity of flow under a unit potential gradient. Although the width of capillaries in a bundle of capillary tubes is constant, whereas that of the voids in soils varies

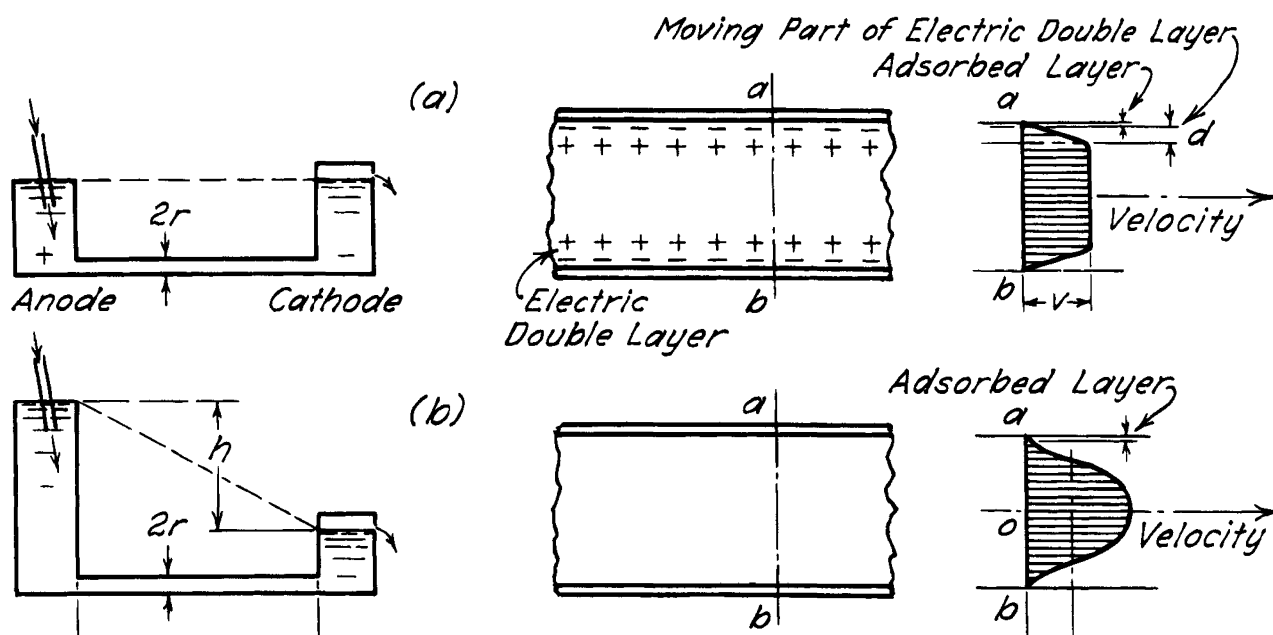


**Figure 15.16** Diagrams illustrating difference between flow through capillaries and soils produced by an electric current (a) and a hydraulic head (b).

from point to point, Eq. 15.30 represents at least crudely the velocity of electro-osmotic flow through soils. It is analogous to Eq. 14.4, which represents the flow of water under the influence of a hydraulic gradient.

In contrast to the hydraulic coefficient of permeability  $k$ , which varies over an extremely wide range that depends on the size of the voids in the soil and, consequently, on the grain size, the coefficient of electro-osmotic permeability is almost independent of grain size. For most soils it lies within the range  $0.4$  to  $0.6 \times 10^{-6}$  m/s. Hence, for such fine-grained soils as silts, which cannot be drained effectively by gravity, electro-osmosis may prove particularly advantageous (Casagrande 1949, 1962).

As soon as the electrical potential is applied to the soil, water starts to flow toward the cathode. Seepage pressures (Article 23.4) are immediately set up which, if directed away from the exposed face of an excavation, may greatly increase the stability of the excavation. Consequently, stabilization of cut slopes in saturated silty soils is one of the more common applications of electro-osmosis (Article 47).

The application of an electrical potential to a compressible fine-grained soil such as clay leads to expulsion of water at the cathodes and, therefore, to consolidation of the clay. The consolidation is not only associated with an increase of strength, but also with the formation of cracks and fissures, especially near the anodes. The anodes are generally corroded away as metallic ions are transported into the soil; the deposition of these ions, as well as the replacement of low-valent ions by those carrying higher charges, lead to permanent changes in the

Atterberg limits and other physical characteristics of the soils.

### 15.8 Frost Heave

If the water contained in the voids of a saturated clean sand or gravel freezes, the structure of the soil remains unchanged. Freezing merely increases the volume of each void by 9% because of the expansion of the water contained in the void. On the other hand, if a saturated fine-grained soil freezes, the process involves the formation of lenses of clear ice oriented roughly parallel to the surface exposed to low temperature. The thickness of the individual ice lenses may increase to several centimeters and the soil subject to freezing assumes the character of a stratified material consisting of alternate lenses of soil and clear ice (Taber 1930).

Although the molecular mechanics involved in the formation of the ice lenses and the intensity of the forces involved have been the subject of intensive investigation, a quantitative understanding of the phenomena has not yet been achieved. Nevertheless, the conditions for the formation of the lenses and the means for preventing it are well established (Casagrande 1931, Beskow 1935).

Ice lenses develop only in fine-grained soils. However, the critical grain size marking the boundary between soils that are subject to ice-lens formation and those that are not depends on the uniformity of the soil. In perfectly uniform soils ice lenses do not develop unless the grains are smaller than 0.01 mm. Fairly uniform soils must contain at least 10% of grains smaller than 0.02 mm. The formation of ice lenses in mixed-grained soils requires,



as a rule, that grains with a size less than 0.02 mm constitute at least 3% of the total aggregate. In soils with less than 1% of grains smaller than 0.02 mm ice lenses are not formed under any conditions which may be encountered in the field.

Figure 15.17 represents three cylindrical specimens of a fine saturated silt. Specimen *a* is surrounded by air, whereas the lower ends of specimens *b* and *c* are immersed in water. The temperature of the upper end of each specimen is kept below the freezing point. In *a* the water that enters the ice lenses is drawn out of the lower part of the specimen. As a consequence, the lower part consolidates in the same manner as if the water were pulled toward a surface of evaporation at the upper end. The growth of the ice lenses probably continues until the water content of the lower part is reduced to the shrinkage limit. Because all the water entering the ice lenses comes from within the specimen, the sample is referred to as a *closed system*. The volume increase associated with the freezing of a closed system does not exceed the volume increase of the water contained in the system. It ranges between about 3 and 5% of the total volume.

In *b* the water required for the initial growth of the ice lenses is also drawn out of the specimen, whereupon the lower part of the sample consolidates. However, as the consolidation progresses, more and more water is drawn from the pool of free water located below the specimen. Finally, both the rate of flow toward the zone of freezing and the water content of the unfrozen zone through which the water percolates become constant. Such a sample constitutes an *open system*. The total thickness of the ice lenses contained in such a system can, at least theoretically, increase indefinitely.

The open system represented by sample *b* can be transformed into a closed system by inserting a layer of coarse-grained material between the zone of freezing temperature and the water table, as shown by *c*. Because the water

cannot rise by capillarity through the coarse layer, the upper part of the sample represented in *c* constitutes a closed system.

In engineering practice open systems are encountered wherever the vertical distance between the water table and the frost line is smaller than the height of capillary rise of the soil. Because the water that migrates out of the groundwater reservoir is continually replenished, the ice lenses grow continually during the frost periods, and the ground surface located above the zone of freezing rises. This phenomenon is commonly known as *frost heave*. Even in regions with moderate winter climate, such as New England, frost heaves up to 150 mm are not uncommon. Because the thickness of the ice lenses reflects very conspicuously the variations of the permeability of the underlying soil, the frost heave is usually nonuniform. Consequently, highway pavements located above the heaving zone are likely to be broken up. Subsequent thaws transform the soil containing the ice lenses into a zone of soft supersaturated material. This condition is likely to be even more detrimental to pavements than the preceding heave.

The tendency of the ice lenses to develop and grow increases rapidly with decreasing grain size. On the other hand, the rate at which the water flows in an open system toward the zone of freezing decreases with decreasing grain size. Hence it is reasonable to expect that the worst frost-heave conditions would be encountered in soils having an intermediate grain size. As a matter of fact, experience has shown that the greatest difficulties with frost heave occur in fine silts and sand-silt mixtures, somewhat finer than the soils for which the capillary rise in a 24-hr period is a maximum (see Fig. 15.8). In a body of soil with given grain-size characteristics, constituting a closed system, the intensity of the growth of ice lenses increases with increasing compressibility of the soil.

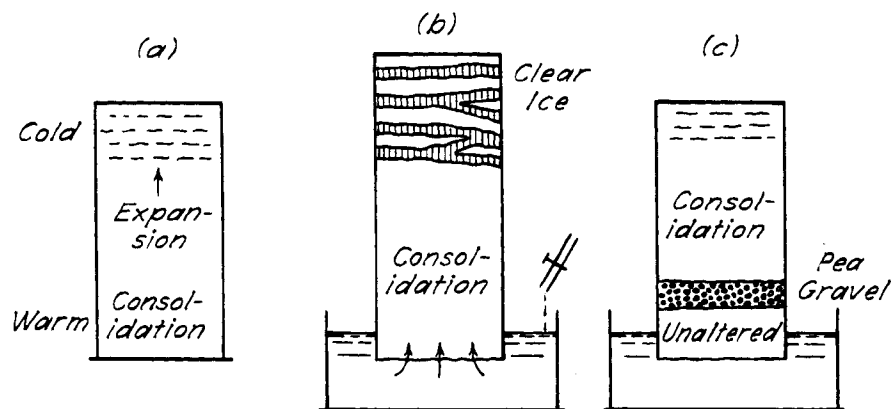


**Figure 15.17** Diagram illustrating frost action in soils. (a) Closed system; (b) open system; (c) method of transforming open into closed system by a layer of coarse sand that intercepts capillary flow toward zone of freezing.

Frost action in humid regions with severe winters constitutes a counterpart to the annual volume changes due to desiccation in semiarid regions with hot summers, such as central Texas. It not only damages roads but also displaces retaining walls (see Article 45.5) and lifts shallow foundations. However, by inserting a layer of gravel between the highest water table and the frost line, the body of soil subject to freezing can be transformed from an open into a closed system, and frost heave can usually be kept within tolerable limits.

### Selected Reading

- Casagrande, A. (1931). "Discussion: A new theory of frost heaving," *Proc. Hwy. Res. Board*, **11**, pp. 168–172.
- Beskow, G. (1935). "Tjälbildningen och Tjällyftningen med Särskild Hänsyn till Vägar och Järnvägar" (Soil freezing and frost heaving with special application to roads and railroads). *Sveriges Geologiska Undersökning, Stockholm*, Series Cv, No. 375, 242 pp.
- Osterberg, J. O. (1940). "A survey of the frost-heaving problem," *Civil Eng.*, **10**, pp. 100–102. Contains a condensed bibliography on the subject.
- Physics of the Earth—Part IX. "Hydrology"* (1942). Edited by O. E. Meinzer, New York, McGraw-Hill, 1st ed., pp. 331–384. Review of present knowledge concerning soil moisture.
- Yong, R. N. and B. P. Warkentin (1966). "Soil freezing and permafrost," Chapter 12 in *Introduction to Soil Behavior*. New York, MacMillan, pp. 391–428.
- Frivik, P. E., N. Janbu, R. Saetersdal, and L. I. Finborud (1980). "Ground freezing 1980," *Developments in Geotech. Eng.*, vol. 28, Elsevier, Amsterdam, 411 p.

## ARTICLE 16 COMPRESSIBILITY OF CONFINED LAYERS OF SOIL

### 16.1 Introduction

Fills and embankments that are wide compared with the thickness of the underlying compressible ground produce a one-dimensional state of compression of the ground. When a large area is loaded uniformly, every element of soil at every depth is confined by adjacent elements that are subjected to the same state of stress. There is no horizontal deformation of the soil except near the boundaries of the loaded area. A state of one-dimensional compression is also approximated in a clay layer loaded by a foundation, if the layer is overlain and confined by a desiccated crust or granular layer thick enough to minimize heave of the clay around the foundation. A similar deformation boundary condition exists when a foundation is placed deep enough that the surrounding overburden prevents lateral deformation of the clay located directly below the foundation. The thicker the overlying layers and the thinner the compressible clay, the more closely the deformation condition in the clay approximates one-

dimensional compression. The one-dimensional compression condition is also favored when the compressible ground is underlain by a stiff layer such as a dense granular soil or bedrock. Horizontal shearing resistances at the top and bottom boundaries of confined clay strata appreciably restrain the strata from stretching in horizontal directions.

Beneath embankments, storage facilities, and footings of limited size in comparison with the thickness of the compressible ground, the ideal one-dimensional state of compression does not exist. Some settlement is then caused by lateral displacement of soil from under the loaded area. However, inclinometer measurements of the lateral deformation of soil at the boundaries of embankments and storage facilities show that settlements resulting from lateral deformation are generally small compared with those resulting from compression if the factor of safety against undrained instability during construction or loading remains greater than about 1.4. The settlement caused by flow of soil from under the structure is then likely to be less than 10% of the end-of-primary settlement (Article 16.3) resulting from compression of the voids (Mesri et al. 1994).

Hence, the information required for computing settlement due to compression of clay strata under confined or other conditions that approximate one-dimensional compression can be derived from compression tests on laterally confined specimens. The tests are known as *consolidation tests*, and the apparatus in which they are conducted is termed an *oedometer*, Article 16.9. If the computed settlements are found to exceed a tolerable amount, the foundation is redesigned.

### 16.2 One-Dimensional Compression

In this section, the compressibility of soil is described for the condition of one-dimensional compression. The discussion is most applicable to transported saturated clays and silts. Settlement due to one-dimensional compression results only from decrease in the volume of the voids and can be analyzed in terms of effective vertical stress.

Every natural soil is characterized by its composition and structure (Articles 3 and 4). These two attributes are not completely independent of each other, because certain compositions favor particular types of structure. For example, a soil composed of quartz tends to have equidimensional rounded or angular particles and under natural conditions stabilizes at relatively low void volumes, whereas a soil composed of illite has plate-shaped particles and the potential to exist at high void volumes. However, even a soil with a particular composition may have different structures. An obvious example is a natural soil in its undisturbed and remolded states.

In addition to the mechanical and physicochemical conditions of deposition and to postdepositional changes

in composition, soil structure is determined by the effective-stress history. The effective vertical stress  $\sigma'_v$  is defined by the total vertical stress  $\sigma_v$  and the porewater pressure  $u$ , both of which are external to the soil structure (Article 15.3). Because of the particulate nature of soil and the existence of various interparticle bonds, some of which are viscous, the internal structural response to a change in the external effective stress is time-dependent. Thus, a soil's structure is determined not only by the effective stress but also by its time-history or aging. The existing state of consolidation of a natural soil is defined by the *in situ* void ratio  $e_o$  and the effective overburden pressure  $\sigma'_{vo}$ .

Any combination of composition and structure that allows a soil to exist at a high volume of voids, as indicated by a high natural water content or void ratio, results in the potential for large volume changes. In most settlement problems the composition of a soil is not altered by the construction or loading, and compression takes place exclusively in response to an increase in effective vertical stress. The natural soil structure adjusts to a new external condition of effective stress by experiencing a decrease in the volume of voids. The compression response to the initial increments of effective stress is strongly influenced by the natural structure of the soil. However, after the initial compression begins to alter the natural structure, the compressibility increasingly reflects the composition. The effective vertical stress at which major changes in the natural soil structure begin to take place is called the *preconsolidation pressure* and is denoted by  $\sigma'_p$ . In the range from  $\sigma'_{vo}$  to  $\sigma'_p$ , designated the *recompression range*, the soil structure accommodates the increased effective stress without significant interparticle displacement. In this stress range, the compression results from the deformation of the soil structure, which involves only minor slip at interparticle contacts. The greater the interparticle bonding and cementation, the greater is the resistance to compression in the recompression range, and the more abrupt is the transition from recompression to compression, because major interparticle slip begins the process of destructuration at the preconsolidation pressure.

In the range beyond  $\sigma'_p$ , known as the *compression range*, significant particle rearrangement is required to develop interparticle resistance to the increased effective stress. In highly bonded soils this rearrangement involves considerable compression, not only to accommodate the additional effective stress but also to compensate for the interparticle bond resistance destroyed by the compression beyond  $\sigma'_p$ . This is especially true for deposits of marine clay and silt that were leached by seepage or diffusion subsequent to the development of a preconsolidation pressure by aging (Mesri 1993). Because the chemical alteration took place at a  $\sigma'_{vo}$  less than  $\sigma'_p$ , the fabric and void ratio of these clays remain substantially

unchanged and correspond to their composition before leaching. When these clays are destructured by consolidation beyond  $\sigma'_p$ , a major change in fabric and thus large compression take place in the transition from the fabric and structure of the original unleached clay to those of the present leached clay. In general, however, for all soils in the compression range, the compressibility decreases continuously as the effective stress and the corresponding compression increase.

### 16.3 Void Ratio-Effective Stress Relationship

Even in the absence of time-dependent changes in total stress and groundwater level or reference porewater pressure, the compression of saturated soils is time-dependent because it is the result of two separate mechanisms, each of which is time-dependent. This can be illustrated by the following basic equation relating void ratio, effective stress, and time

$$\frac{de}{dt} = \left( \frac{\partial e}{\partial \sigma'_v} \right)_t \frac{d\sigma'_v}{dt} + \left( \frac{\partial e}{\partial t} \right)_{\sigma'_v} = a_{vs} \frac{d\sigma'_v}{dt} + a_{vt} \quad (16.1)$$

where the subscripts  $v$ ,  $s$ , and  $t$  denote vertical, stress, and time, respectively. The first term is time-dependent because the increase in effective stress always requires time due to the finite permeability of soils. This component of the time-lag is minimal for relatively permeable granular soils compared with silts or clays. The second term expresses the effect of the various internal components of effective stress; after an increase in effective stress, time is required to reach internal equilibration among the interparticle forces. This component of time-dependent behavior is also less important for coarse-grained than for fine-grained soils because of the limited types of interparticle forces in coarse-grained soils compared with the forces acting between particles of the very fine fraction.

The first term in Eq. 16.1 represents the *hydrodynamic*, and the second term the *structural* time-dependent mechanism. Inasmuch as both mechanisms are related to the development of the internal components of effective stress in the soil, both are controlled by effective stress. However, it is not possible to evaluate the time-dependent responses of the various internal components of  $\sigma'_v$  separately. Consequently, the compression rate  $de/dt$  is for convenience expressed separately with respect to effective stress by  $a_{vs}$  and with respect to time by  $a_{vt}$ . The distinction is entirely arbitrary, however, because there are no differences between the mechanisms of volume change due to the changes in external effective stresses and those due to the redistribution of internal interactions. All the mechanisms of volume change, including the deformation, displacement, and aggregation or dispersion of particles; the distortion of adsorbed water films; and

the contraction or expansion of double layers, can operate during changes in external effective stress and with time.

When an increment  $\Delta\sigma_v$  of total vertical stress is applied to a saturated soft clay or silt, a porewater pressure  $\Delta u$  develops. In one-dimensional compression at the instant of loading,  $\Delta u$  is equal to  $\Delta\sigma_v$ , because the compressibility of the soil structure far exceeds the compressibility of both the water and the soil solids (Article 4). This increment of porewater pressure is termed *excess porewater pressure*, because it is in excess of an equilibrium porewater pressure. Given time, the excess porewater pressure dissipates, with a corresponding increase in effective stress. The period of time during which the excess porewater pressure dissipates is called the *primary consolidation stage*. The *secondary consolidation stage* corresponds to the period after the dissipation of the excess porewater pressure. Although it is true that, during secondary compression, water is discharged from the soil by a porewater pressure gradient generated by the tendency of soil structure to compress as indicated by  $a_{vt}$ , the excess porewater pressure producing this gradient is so small that it need not be considered in analysis of secondary compression. On this premise, primary and secondary compression can be unambiguously defined by integrating Eq. 16.1 to obtain the total compression from the instant at which  $\Delta\sigma_v$  is applied to any elapsed time  $t$ . Thus

$$\int_0^t de = \int_0^{t_p} \left[ a_{vs} \frac{d\sigma'_v}{dt} + a_{vt} \right] dt + \int_{t_p}^t a_{vt} dt$$

The first integral from  $t = 0$  to  $t_p$ , at which the excess pore pressure is practically zero, is the primary compression, and the second integral from  $t_p$  to any elapsed time  $t$  is the secondary compression. During secondary consolidation, when the effective vertical stress  $\sigma'_v$  is essentially constant, the only contribution to the volume decrease comes from  $a_{vt}$ , whereas during primary consolidation both  $a_{vs}$  and  $a_{vt}$  contribute to the compression.

During primary consolidation,  $a_{vs}$  and  $a_{vt}$  are not constants; both vary with elapsed time and with the location of the soil element with respect to the drainage boundary. Furthermore, there is no obvious relationship between values of  $a_{vt}$  during secondary compression and those of  $a_{vt}$  during primary compression. Although it is possible to observe the settlement as a function of time during secondary consolidation and to evaluate  $a_{vt}$ , it is not yet possible to separate the contributions of  $a_{vs}$  and  $a_{vt}$  to the observed settlements during primary consolidation. For most practical applications this does not create a serious difficulty, because the void ratio-effective vertical stress relationship corresponding to the end-of-primary (EOP) consolidation has been found to be independent of the duration of the primary consolidation stage. This finding is known as the *uniqueness of EOP  $e$  vs  $\sigma'_v$*  (Mesri and

Choi 1985b). Consequently, the EOP  $e$  vs  $\sigma'_v$  data from small-scale laboratory samples can be used directly to compute the magnitude of the settlement of layers in the field without the need to evaluate  $a_{vs}$  and  $a_{vt}$  separately. In contrast, modeling the time rates of settlement and porewater pressure dissipation during the primary consolidation stage requires assumptions regarding the behavior of  $a_{vs}$  and  $a_{vt}$  (Mesri and Choi 1985a) (Article 25).

Examples of EOP void ratio-effective vertical stress relationships for typical samples of three natural clays are shown in Fig. 16.1. The procedures for developing the relationships in the laboratory are discussed in Article 16.9. The composition of Mexico City clay,  $w_l = 500\%$ ,  $w_p = 150\%$ , allows it to exist at unusually high natural void ratios; natural water contents in the range of 200 to 600% are not uncommon. Even at such high void ratios, the structure of the clay initially resists compression until the preconsolidation pressure  $\sigma'_p$  is exceeded. Beyond

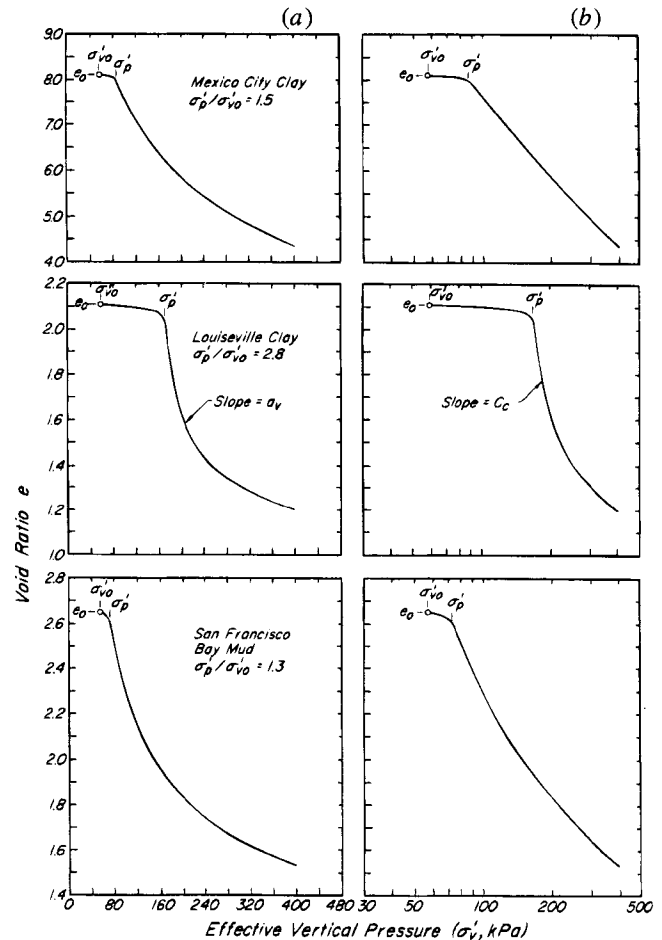


**Figure 16.1** Relation between end-of-primary void ratio and effective vertical pressure for natural clays from Mexico City, Louisville, and San Francisco (top to bottom). Effective vertical pressure plotted (a) to natural scale and (b) to logarithmic scale.

$\sigma'_p$ , the large compressibility in the compression range reflects the high natural void ratio. Louiseville clay,  $w_l = 65\%$ ,  $w_p = 28\%$ , is one of the highly sensitive clays of eastern Canada that have a highly bonded structure. Unless significant mineralogical changes occurred after deposition, the bonds most likely developed early during deposition and consolidation and thus allowed the clay to stabilize at a relatively high natural water content. In the broad recompression range from  $\sigma'_{vo}$  to  $\sigma'_p$  the structural bonds resist compression until the recompression strains break them, whereupon the compressibility increases dramatically. For such clays at a given initial void ratio, the higher the preconsolidation pressure, the larger is the compressibility beyond  $\sigma'_p$ . Because of its composition, the sample of San Francisco Bay mud,  $w_l = 89\%$ ,  $w_p = 37\%$ , stabilized at a relatively high water content. Its preconsolidation pressure is slightly higher than the present effective overburden pressure, possibly because of aging. In the compression range beyond  $\sigma'_p$ , the compressibility of all soils decreases continuously with the increase in effective vertical stress.

Curves expressing the relation between void ratio and effective stress, such as those in Fig. 16.1, do not necessarily correspond to EOP consolidation. They may be plotted, for example, for a time  $t$  greater than  $t_p$ . Under these conditions they will include not only the primary but also a portion of the secondary compression.

#### 16.4 Preconsolidation Pressure

The preconsolidation pressure  $\sigma'_p$ , at which major structural changes including the breakdown of interparticle bonds and interparticle displacement begin to occur, is one of the most important properties of soft clays. It defines the boundary between stiff and soft deformation response of a soil to loading. The magnitude of the preconsolidation pressure is best expressed in terms of the value of  $\sigma'_p/\sigma'_{vo}$ , known as the *overconsolidation ratio*, OCR. Measured magnitudes of  $\sigma'_p/\sigma'_{vo}$  for a variety of natural soft clays are in the range of 1.2 to 3 except within the desiccated crust, where they may be much higher. One or more mechanical and physicochemical mechanisms contribute to the development of the increased interparticle resistance to compression in soft clays and thus to the magnitude of  $\sigma'_p$ . Geologically, the best-known process is preloading, in which the increased resistance to compression is the result of previous consolidation of the clay under past effective vertical pressures higher than that of the existing effective overburden. Geological loading and unloading by thick sediments or glacial ice have produced the most highly overconsolidated clays. In soft clays and silts, fluctuations of the water table, underdrainage, minor erosion of sediments, and light ice and snow loads may have contributed to preconsolidation. Preconsolidation is also produced by desiccation of soils located above the water table (Article 15.6.3). Other processes

such as freezing and thawing, and chemical changes caused by precipitation and oxidation, also operate within the zone above the water table, known as the crust or weathered zone, and influence interparticle bonding and the preconsolidation pressure. If a layer of stiff clay is located above a layer of soft clay of the same type, it is likely that the upper layer has been precompressed by desiccation. Furthermore, if the upper layer was exposed to the atmosphere for a long time, it is also likely to be discolored by oxidation. In some instances, stiff crusts may have formed below the water table by subaqueous weathering or cation exchange (Moum and Rosenqvist 1957).

Increased interparticle resistance and therefore preconsolidation pressure also develop when a soft clay or silt experiences secondary compression. For example, post-glacial marine and lacustrine clays have experienced 5 to 10 thousand years of secondary compression. In these clays, values of  $\sigma'_p/\sigma'_{vo}$  as high as 1.4 to 1.6 may have developed by secondary compression alone. Thixotropic changes in structure and improved interparticle bonding through chemical changes with or without cementing agents also contribute to the magnitude of the preconsolidation pressure. The highest values of  $\sigma'_p/\sigma'_{vo}$ , such as those in the very sensitive and brittle clays of eastern Canada, have probably developed with the help of cementing by silicate or carbonate complexes. No other type of interparticle resistance is strong and brittle enough to produce the very flat recompression curves and abrupt transition to the compression range characteristic of these clays. A decrease in the volume of voids is not needed to produce the thixotropic increase in structural resistance that results from the reorientation of plate-shaped clay particles to edge-face short-range interaction, from the reorganization of ions, or from chemical changes such as cation exchange and cement bonding.

It is likely that more than one mechanism contributes to the development of increased resistance to compression of a natural soft clay. Soils that are known not to have been subjected to effective vertical stresses higher than the present effective overburden pressure and that display values of  $\sigma'_p/\sigma'_{vo} = 1$  are called *normally consolidated*. Only very young soil deposits, or those that either in the field or laboratory have just completed primary consolidation in response to a recent loading, can be expected to lack a recompression behavior and to have values of  $\sigma'_p/\sigma'_{vo}$  equal to unity. Soft clays that have experienced one or more mechanisms of secondary compression, thixotropic strengthening, or chemical increase in interparticle resistance, have values of  $\sigma'_p/\sigma'_{vo}$  greater than unity.

Soils that have been subjected to effective vertical pressures in excess of the present effective overburden are called *precompressed* or *overconsolidated*. The degree of overconsolidation is expressed as the *overconsolidation ratio*,  $OCR = \sigma'_{vmax}/\sigma'_{vo}$ , where  $\sigma'_{vmax}$  is the maximum

past pressure. Overconsolidated soils include those that are lightly or heavily preloaded by snow, ice, or sediments, as well as soils that have been preconsolidated as a result of earlier water table lowering or underdrainage. They also include desiccated crusts in which the maximum past pressure is the equal all-around suction that developed in dry environments. If the maximum past pressure  $\sigma'_{vmax}$  was smaller than about 400 kPa, the clay may still be soft. If it was much greater, however, the clay is stiff. Since the magnitude of  $\sigma'_{vmax}$  cannot be readily determined for natural soil deposits, the OCR is defined by  $\sigma'_p/\sigma'_{vo}$ , irrespective of the cause of the precompression pressure.

In summary, the precompression behavior of a clay can be due to the weight of soil strata that were removed by erosion, to the weight of ice that melted away, to desiccation, or to aging by processes such as secondary compression. If the precompression is due to a uniform load that has been removed,  $\sigma'_p - \sigma'_{vo}$  is the same at every point along a vertical line below the ground surface, and  $\sigma'_p/\sigma'_{vo}$  gradually decreases with depth. If the precompression is due to desiccation,  $\sigma'_p - \sigma'_{vo}$  and  $\sigma'_p/\sigma'_{vo}$  decrease in a downward direction from the former surface of evaporation. However, if precompression is due to secondary compression aging,  $\sigma'_p/\sigma'_{vo}$  remains constant and  $\sigma'_p - \sigma'_{vo}$  increases with depth.

### 16.5 Coefficient of Earth Pressure at Rest

A condition of laterally constrained one-dimensional deformation prevailed during sedimentation-consolidation and erosion-rebound of most natural soil deposits and currently exists in most soils with a level ground surface. The *coefficient of earth pressure at rest*  $K_o$  is the ratio of the effective horizontal pressure  $\sigma'_h$  to the effective vertical pressure  $\sigma'_v$  in a soil that currently exists under the condition of zero horizontal deformation, with principal planes that are horizontal and vertical. That is,

$$K_o = \frac{\sigma'_h}{\sigma'_v} \quad (16.2)$$

The fraction of the force of gravity that is transmitted to the vertical planes is a function of the angle of internal friction mobilized under the laterally constrained deformation condition. Consequently, the external horizontal support required to maintain the condition of zero horizontal deformation decreases with an increase in the mobilized angle of internal friction. Jaky (1944) developed an equation relating  $K_o$  and the maximum available angle of internal friction  $\phi'$  by analyzing a talus of granular soil standing at the angle of repose. He assumed the angle of repose to be equal to the angle of internal friction  $\phi'$ . This is a reasonable assumption for sedimented, normally consolidated young materials for which the angle of repose is equal to the constant-volume friction angle

$\phi'_{cv}$  (Article 19.1) (Cornforth 1973). For these soils  $\phi'_{cv}$  is practically equal to  $\phi'$ . Thus, Jaky's equation for  $K_o$  applies to sedimented normally consolidated young clays and granular materials that have not been densified by aging, precompression, or preshearing, for example, by vibration. This condition exists in the oedometer test (Article 16.9) at the end-of-primary consolidation in the compression range. The corresponding  $\sigma'_h/\sigma'_v$  is denoted by  $K_{op}$ . The Jaky (1944) analysis, after a simplification (Jaky 1948, Mesri and Hayat 1993b), leads to

$$K_{op} = 1 - \sin \phi' \quad (16.3)$$

Oedometer tests with horizontal pressure measurements, on loose granular soils as well as clays and silts in the compression range, lead to values of  $K_{op}$  that generally agree with Eq. 16.3. Values measured for clays and silts and for granular soils correspond to a range in  $\phi'$  of 18° to 43°, and measured values of  $K_{op}$  range from 0.31 to 0.67 (Mesri and Hayat 1993b).

The foregoing statements are illustrated by Fig. 16.2, which presents the results of an oedometer test with horizontal pressure measurements on a sample of Saint Alban clay, a material with a well-developed structure, for which  $w_l = 43\%$ ,  $I_p = 22\%$ ,  $\phi' = 30^\circ$ . Its *in situ* OCR,  $\sigma'_p/\sigma'_{vo}$  (Article 16.4), is 2.42. The progress of consolidation is shown by the EOP relation between the void ratio and the effective vertical pressure  $\sigma'_v$ ; the corresponding effective horizontal pressures  $\sigma'_h$  are shown as a function of  $\sigma'_v$ . The value of  $K_o$  (Eq. 16.2) can be obtained from the stress path, which starts from the *in situ* stress condition  $\sigma'_{vo} = 33$  kPa and  $\sigma'_{ho} = K_o\sigma'_{vo} = 27$  kPa, at which  $K_o$  has the value of  $27/33 = 0.82$ . At a vertical stress  $\sigma'_p$  structural breakdown occurred, whereupon the stress path assumed a slope  $K_{op}$  corresponding to that of an unstructured material, and because of the lack of structure the backward projection of the stress path passes through the origin. The slope, 0.48, of the stress path above  $\sigma'_p$  is therefore equal to  $K_{op}$ . However, after a waiting period of 33 days during which secondary compression aging occurred, the value of  $\sigma'_h$  increased and the stress path, although again approaching the slope  $K_{op}$ , remained permanently above the projection of the portion between  $\sigma'_p$  and the pressure at which the waiting period began.

Because most natural soil deposits have experienced some degree of densification by aging, precompression, or preshearing, rarely is the *in situ*  $K_o$  equal to  $K_{op}$ . For example, for the Saint Alban clay (Fig. 16.2), field and laboratory measurements (Tavenas et al. 1975, Mesri and Feng 1988, Mesri and Hayat 1993b) lead to an *in situ*  $K_o$  in the range of 0.77 to 0.85, and most soft clay deposits of marine or lacustrine origin display values in the range of 0.6 to 1.2. In soft clay and silt deposits, values of  $K_o$  greater than  $K_{op}$  result from secondary compression aging

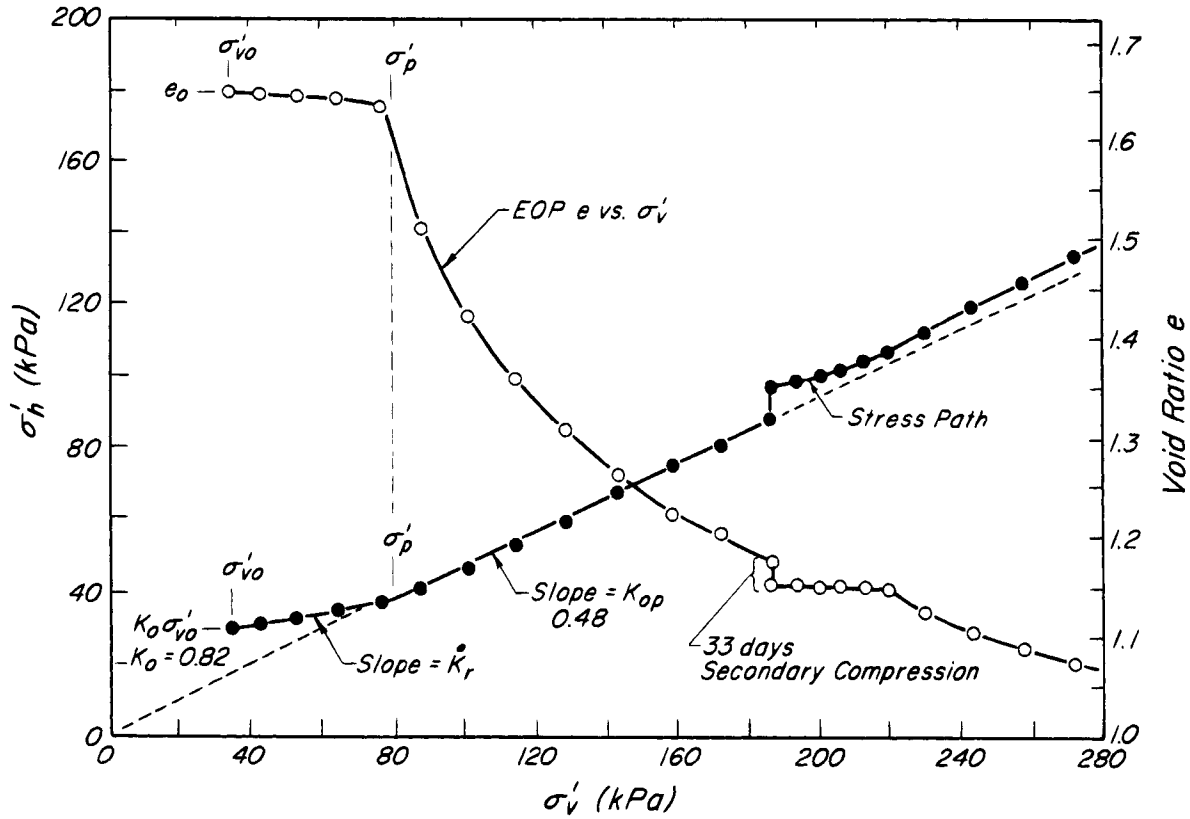


**Figure 16.2** Results of oedometer test with horizontal pressure measurements on undisturbed sample of soft, sensitive St. Alban clay.

and from precompression effects of erosion, porewater pressure fluctuation, and desiccation.

Field and laboratory methods for direct measurement of *in situ*  $\sigma'_{ho}$  and thus of  $K_o$  in natural soil deposits are quite difficult to carry out and require special expertise and considerable care. Hence, various empirical procedures have been proposed. The following equation is suggested for estimating the *in situ*  $K_o$  in marine or lacustrine soft clay and silt deposits that have not been pre-sheared (Mesri and Hayat 1993b).

$$K_o = \dot{K}_r + \frac{\sigma'_p}{\sigma'_{vo}} (K_{op} - \dot{K}_r) \quad (16.4)$$

where  $\dot{K}_r$  is the slope of  $\sigma'_h$  vs  $\sigma'_v$  in the recompression range, as illustrated in Fig. 16.2. A value of  $\dot{K}_r = K_{op}/2$  is typical and leads to

$$K_o = \frac{1}{2} K_{op} \left( \frac{\sigma'_p}{\sigma'_{vo}} + 1 \right) \quad (16.5)$$

The Jaky Eq. 16.3 can be substituted into Eq. 16.5, and thus only  $\sigma'_p/\sigma'_{vo}$  and  $\phi'$  are required for estimating the *in situ*  $K_o$ .

For estimating the coefficient of earth pressure at rest for highly overconsolidated stiff clays, shales, and granular soils that have not experienced preshearing, the following empirical equation is applicable:

$$K_o = (1 - \sin \phi'_{cv}) \left( \frac{\sigma'_p}{\sigma'_{vo}} \right)^{\sin \phi'_{cv}} \quad (16.6a)$$

or, alternatively,

$$K_o = K_{op} \left( \frac{\sigma'_p}{\sigma'_{vo}} \right)^{(1-K_{op})} \quad (16.6b)$$

The upper limit of  $K_o$  from Eq. 16.6 is the coefficient of passive earth pressure  $K_p$  (Article 27). Although Eq. 16.6 and even Eq. 16.5 are applicable to granular soils as well as to clays, undisturbed sampling, especially of clean granular soil deposits, for the measurement of  $\sigma'_p$  is quite difficult.

Preshearing of soils by vibration or compaction leads to a significant increase in  $K_o$ . Simple empirical equations, however, are not available for estimating the  $K_o$  of compacted clays, or granular soils that have been densified by vibration (Peck and Mesri 1987, Peck 1993, Mesri and Hayat 1993a, Mesri et al. 1993). Moreover, preshearing of natural soil deposits by such processes as ice movement

over preglacial clays, severe desiccation, ground shaking of granular soils, or excavation of adjacent ground permanently alters the *in situ*  $K_o$  (Chan and Morgenstern 1986, Jefferies et al. 1987). For example, passive preshearing is likely to increase the *in situ*  $K_o$  above the values predicted by Eqs. 16.5 and 16.6. The *in situ*  $K_o$  of old sand deposits that have experienced a large number of ground shaking events should be higher than  $K_o$  in recent deposits. Empirical procedures have been suggested for estimating the preshearing effect on  $K_o$  of natural soil deposits (Mesri and Hayat 1993b).

### 16.6 Magnitude of Settlement

The most general expression for the settlement resulting from one-dimensional compression is

$$S = \frac{\Delta e}{1 + e_o} L_o \quad (16.7)$$

where  $L_o$  is the initial thickness of the consolidating layer. For computing the settlement that takes place during the primary consolidation stage, the value of  $\Delta e$  can be taken directly from the end-of-primary (EOP)  $e$  vs  $\sigma'_v$  relationship, between  $\sigma'_{vo}$  and  $\sigma'_{vf} = \sigma'_{vo} + \Delta\sigma'_v$ . It is often more convenient, however, to summarize consolidation data and compute settlement by using compressibility parameters rather than the  $e$  vs  $\sigma'_v$  curves. The slope of the  $e$  vs  $\sigma'_v$  curve is the coefficient of compressibility,  $a_v = \Delta e / \Delta\sigma'_v$ , or in terms of vertical strain,  $m_v = \Delta\epsilon_v / \Delta\sigma'_v$ . In the compression range,  $a_v$  generally decreases rapidly with increasing  $\sigma'_v$  (Fig. 16.1a), and is therefore not convenient for use in a simple settlement equation. It is more usual to plot the void ratio against the logarithm of effective vertical pressure (Fig. 16.1b). In an  $e$  vs  $\log \sigma'_v$  plot the slope  $\Delta e / \Delta \log \sigma'_v$  in the recompression range is termed the *recompression index*  $C_r$ , and that in the compression range the *compression index*  $C_c$ . If the recompression slope can be characterized by a single value of  $C_r$  and if  $C_c$  is a constant in the range of  $\sigma'_p$  to  $\sigma'_{vf}$ , then Eq. 16.7 can be rewritten as:

$$S = \frac{C_r}{1 + e_o} L_o \log \frac{\sigma'_p}{\sigma'_{vo}} + \frac{C_c}{1 + e_o} L_o \log \frac{\sigma'_{vf}}{\sigma'_p} \quad (16.8a)$$

or

$$S = \frac{C_c}{1 + e_o} L_o \left( \frac{C_r}{C_c} \log \frac{\sigma'_p}{\sigma'_{vo}} + \log \frac{\sigma'_{vf}}{\sigma'_p} \right) \quad (16.8b)$$

Equation 16.8b is useful because  $C_r$  can be estimated from an empirical database for  $C_r/C_c$  as discussed subsequently in this article. Thus, the important consolidation properties to be evaluated for settlement analyses are  $C_c$  and  $\sigma'_p$ .

For the best estimates of settlement, values of  $C_c$  and  $\sigma'_p$  are determined from the results of oedometer tests

(Article 16.9) on undisturbed specimens of high quality. Under certain circumstances, however, for example, during the siting stage of a project or if only an approximate value of settlement is needed, it is useful to obtain an estimate of  $C_c$  from an empirical correlation with a simple soil property such as the natural water content  $w_o$ . A direct relationship between compression index and natural water content should exist because both are controlled by composition and structure which, in turn, control both the *in situ* void ratio at which a soil comes to equilibrium and the compressibility after the soil structure yields at the preconsolidation pressure. Such a correlation is shown in Fig. 16.3. The points for soft clay and silt deposits correspond to the range of consolidation pressure from  $\sigma'_p$  to  $2\sigma'_p$ .

The composition of the soil, mainly the mineralogy of the particles, is the most important factor that directly determines both  $w_o$  and  $C_c$ . Any soil that comes to equilibrium at high void ratio under typical overburden pressures displays high compressibility when subjected to an increase in effective vertical stress beyond  $\sigma'_p$ . Peat deposits, for example, come to equilibrium at high water contents of 200 to 1500% and display values of  $C_c$  typically in the range of 2 to 12, because a large amount of water is held within and among the particles. Mexico City clay possesses a unique composition (Fig. 4.16) that allows it to exist *in situ* at high water contents of 200 to 600% and to display unusually high values of  $C_c$ . Clay and silt deposits contain clay minerals such as illite and montmorillonite, very fine amorphous particles, and organic mat-

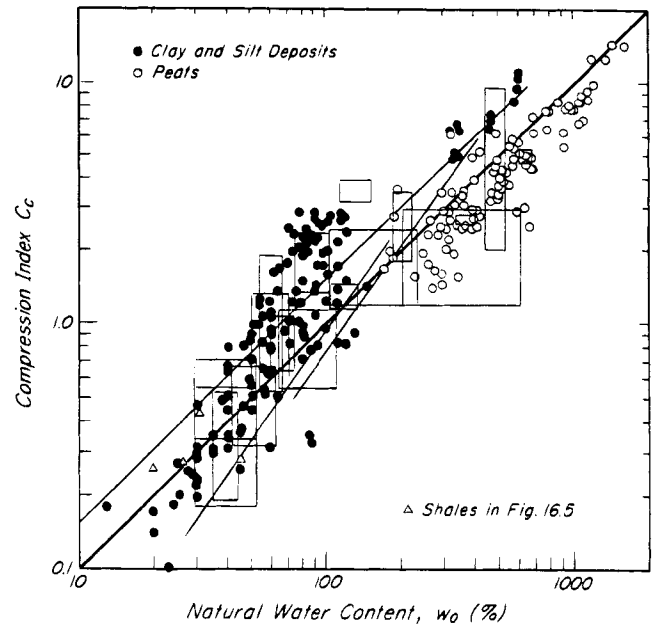


**Figure 16.3** Empirical correlation between compression index and *in situ* water content for clay and silt deposits, for shales from Fig. 16.5, and for peats.



ter, all of which contribute to high values of *in situ* water content and  $C_c$ .

The relation between  $C_c$  and  $w_o$  is also influenced by two other factors. For any soil composition, the  $e$  vs  $\log \sigma'_v$  compression curve is nonlinear over a wide range of values of  $\sigma'_v$ , and  $C_c$  decreases continuously with increasing consolidation pressure. This is illustrated in Fig. 16.4 by the  $e$  vs  $\log \sigma'_v$  relationship for a clay specimen sedimented in the laboratory. The specimen, which consisted mainly of illite and some mixed-layer montmorillonite, had a  $w_l = 110\%$ ,  $w_p = 35\%$ , and  $CF = 100\%$ . After sedimentation in 35 g/l sodium chloride, it had a void ratio of 3.5. Figure 16.4 shows the compression curve  $abdf$ , three rebound curves  $bc$ ,  $de$ , and  $fg$ , and two recompression curves  $cb$  and  $ed$ . The compression index  $C_c$  for the compression curve  $abdf$  continuously decreases with increasing consolidation pressure  $\sigma'_v$ . Thus, both  $w_o$  and  $C_c$  decrease with the increase in effective overburden pressure. Most of the data indicating low values of  $w_o$  and  $C_c$  in Fig. 16.3 correspond to inorganic soils of low plasticity and small clay-mineral content. However, some correspond to stiff clays and shales for which the  $e$  vs  $\log \sigma'_v$  curves are shown in Fig. 16.5. The values of  $C_c$

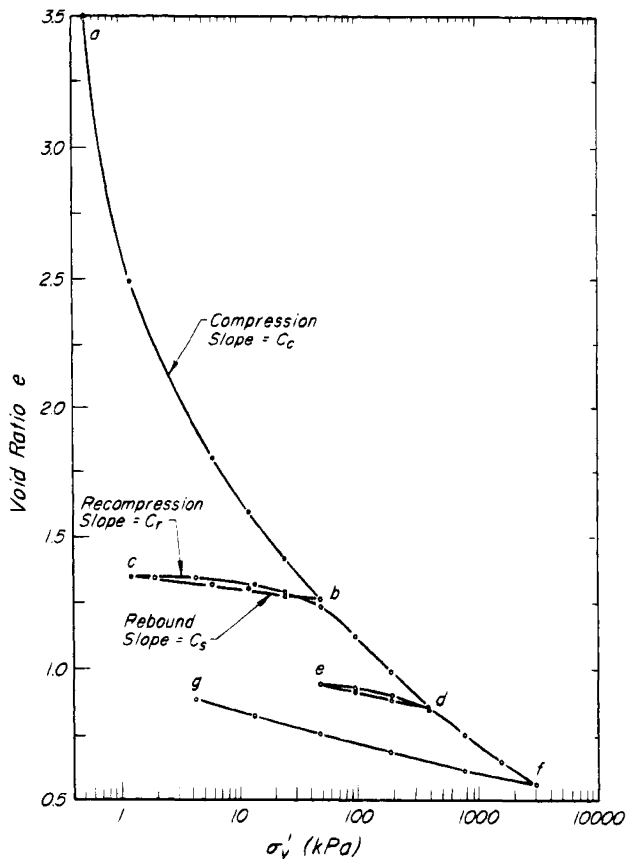


**Figure 16.4** Relation between end-of-primary void ratio and log effective vertical stress for a clay after sedimentation in 35 g/l sodium chloride solution.

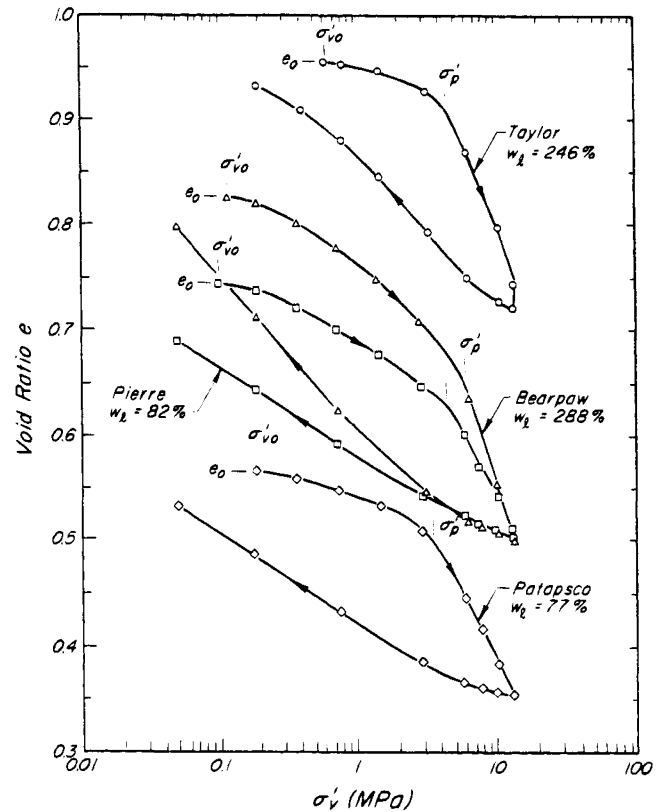


**Figure 16.5** End-of-primary  $e$  vs  $\log \sigma'_v$  relationships for four expansive shales.

for shales are low not because of their composition but because of the high values of  $\sigma'_v$  at which the compression range is encountered. For the shales in Fig. 16.5 the values of  $\sigma'_p$  are in the range of 3000 to 5000 kPa, whereas for most of the soft clays in Fig. 16.3 values of  $\sigma'_p$  are less than 200 kPa.

The second factor that influences the relationship between  $C_c$  and  $w_o$  is the structure of the soil as determined by arrangement of particles and interparticle forces. In general, such factors as flocculation and interparticle bonding, which allow a soil to come to equilibrium at high *in situ* water content, also lead to a high  $C_c$  beyond  $\sigma'_p$ . However, in some highly structured clays and silts such as the soft clays of eastern Canada, the influence of structure is more significant on  $\sigma'_p$  than on *in situ* water content. These soils display relatively high values of  $\sigma'_p/\sigma'_{v0}$  and exceptionally high compressibility immediately beyond  $\sigma'_p$ . The values of  $C_c$  that lie above the general trend in Fig. 16.3 in the range of  $w_o$  from 50 to 100% correspond to these clays. Moreover, for these materials, the values of  $C_c$  in Fig. 16.3 correspond to the secant  $C'_c$  from  $\sigma'_p$  to  $2\sigma'_p$ , as discussed at the end of this section. For smaller increases of effective stress beyond  $\sigma'_p$ ,  $C_c$  for these clays can be higher than 3 and as high as 7 to 8.

As a result of geological unloading or aging, most natural soil deposits display a preconsolidation pressure. Therefore, for typical construction loading, all or part of the increase of  $\sigma'_v$  is in the recompression range. Inasmuch as the recompression index,  $C_r = \Delta e / \Delta \log \sigma'_v$ , is significantly smaller than  $C_c$ , the contribution of  $C_r$  to settlement in many practical problems is insignificant compared with that of  $C_c$ , and precise knowledge of  $C_r$  is not required. However, if even moderate differential settlement would damage a heavy structure on stiff clays or shales, for example, a reliable estimate of  $C_r$  would be needed. An accurate estimate of  $C_r$  is also required for predicting porewater pressure dissipation in soft clay deposits under embankment loading.

Values of  $C_r$  are commonly referenced to those of  $C_c$  between  $\sigma'_p$  and  $2\sigma'_p$ . Most values of the ratio  $C_r/C_c$  are in the range of 0.02 to 0.2. Very low values, even lower than 0.02, correspond to highly structured and bonded soft clay and silt deposits. High values correspond to micaceous silts and fissured stiff clays and shales. For the latter materials,  $C_c$  is relatively small because of the high value of  $\sigma'_p$ , and  $C_r$  is large as a result of the presence of fissures. Measured values of  $C_r$  are highly sensitive to soil disturbance and the oedometer testing procedure (Article 16.9). Any process that leads to destructuration, opening of fissures, or softening before control over  $\sigma'_v$  is established in the oedometer test, is likely to lead to an overestimate of  $C_r$ . It is generally preferable to estimate  $C_r$  from empirical information unless reliable oedometer tests are feasible on A-quality undisturbed specimens, preferably taken from test shafts (Table 11.2).

The  $e$  vs  $\log \sigma'_v$  curves in Fig. 16.1b show that for some soils a single value of  $C_c$  cannot be used to define the entire compression curve beyond  $\sigma'_p$ . Although for most purposes the recompression settlement can be estimated by using a constant  $C_r$ , it is a serious oversimplification to represent the compression curve for highly structured clays by a single value of  $C_c$ . In settlement computations this problem can be avoided by using the EOP  $e$  vs  $\log \sigma'_v$  curve directly together with Eq. 16.7. Otherwise, consolidation data may be summarized in terms of a modified compression index  $C'_c$ , defined in Fig. 16.6. The values of  $C'_c$  are determined from the  $e$  vs  $\log \sigma'_v$  curves and plotted as in Fig. 16.7. The settlement equation then becomes

$$S = \frac{C_r}{1 + e_o} L_o \log \frac{\sigma'_p}{\sigma'_{v0}} + \frac{C'_c}{1 + e_o} L_o \log \frac{\sigma'_{vf}}{\sigma'_p} \quad (16.9)$$

### 16.7 Settlement During Secondary Consolidation Stage

Examples of the behavior of natural clays during the secondary consolidation stage are shown in Fig. 16.8. Compression is expressed in terms of decrease in void

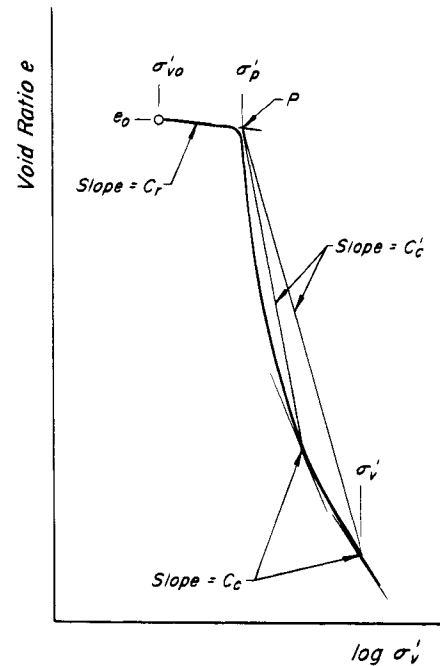


**Figure 16.6** Definition of secant  $C'_c$  as compared with tangent  $C_c$ .

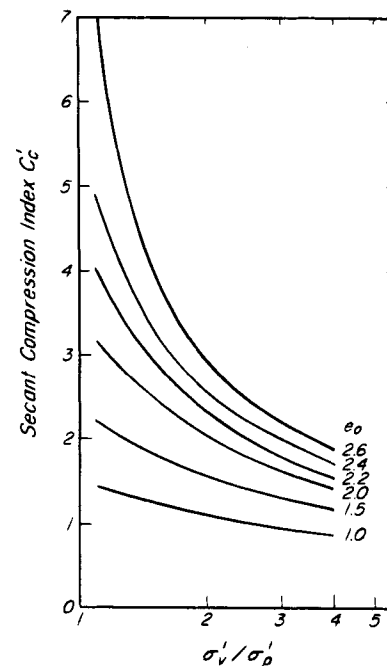


**Figure 16.7** Values of secant  $C'_c$  for a soft clay deposit summarized from a series of oedometer test results.

ratio, and time has been normalized with respect to the duration  $t_p$  of the primary consolidation stage. The rate of compression decreases continuously during the secondary consolidation stage. The general expression for the settlement resulting from secondary compression under a final pressure  $\sigma'_{vf}$  is

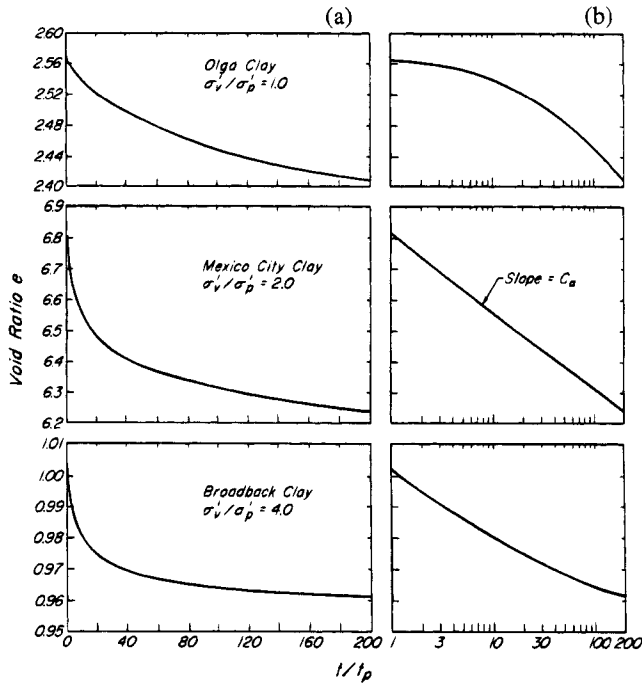


**Figure 16.8** Examples of secondary compression for natural clay.

$$S = \frac{\Delta e}{1 + e_o} L_o \quad (16.10)$$

The value of  $\Delta e$  between  $t/t_p = 1$  and any required time can be read directly from the  $e$  vs  $t/t_p$  curve corresponding to the particular final pressure  $\sigma'_{vf}$ . Often, however, it is preferable to evaluate the secondary settlement in terms of compressibility parameters. It is then convenient to plot secondary compression against the logarithm of time, as in Fig. 16.8b. The *secondary compression index*,  $C_\alpha = \Delta e / \Delta \log t$ , defines the slope of the  $e$  vs  $\log t$  curve in the secondary compression range. For a constant  $C_\alpha$  between  $t_p$  and  $t$ , Eq. 16.10 is rewritten as

$$S = \frac{C_\alpha}{1 + e_o} L_o \log \frac{t}{t_p} \quad (16.11)$$

The magnitude of secondary settlement depends not only on the compressibility parameter  $C_\alpha$ , but also on the value of  $t/t_p$ . In the laboratory the value of  $t/t_p$  can be very large, mainly because the duration of the primary consolidation stage for laboratory samples is generally small. On the other hand, in the field the values of  $t_p$  for layers of soil can range from several months to many years, and for the typical useful life of a structure the value of  $t/t_p$  rarely exceeds 100 and is often less than 10. Exceptions are encountered, however, in clays containing permeable layers, in peats, in certain residual soils with high initial permeability, and in deposits in which vertical drains are installed (Article 25.5) to accelerate primary consolida-

tion. In any event, as  $t/t_p$  decreases, the secondary settlement becomes less and less significant.

Because the interparticle mechanisms responsible for compression over time are the continuation of the response of the soil to an increase in effective stress, it is reasonable to expect the magnitudes of the compressibilities with respect to effective stress and to time to be related. Indeed, for any soil, it is found that at any  $(\sigma'_v, t)$  during secondary compression the ratio  $C_\alpha/C_c$  is a constant in both the recompression and compression ranges (Mesri and Godlewski 1977). This is illustrated in Fig. 16.9 for undisturbed specimens of Brown Mexico City clay with  $w_o = 313$  to  $340\%$ ,  $w_l = 361\%$ ,  $w_p = 91\%$ , and  $\sigma'_p/\sigma'_{vo} = 1.4$ . The value of  $C_c = \Delta e / \Delta \log \sigma'_v$  in the ratio  $C_\alpha/C_c$  expresses the variable slope of the  $e$  vs  $\log \sigma'_v$  curve in both recompression and compression; moreover, in general,  $C_\alpha = \Delta e / \Delta \log t$  does not remain constant with time. Hence, the secondary compression index  $C_\alpha$  may remain constant, decrease, or increase with time in the range of consolidation pressure in which  $C_c$  remains constant, decreases, or increases with  $\sigma'_v$ , respectively (Mesri and Godlewski 1977, Mesri and Castro 1987). For a fundamental understanding of the compressibility of soils, which is essential for developing theories of consolidation and for interpreting field settlement observations and laboratory consolidation data, an appreciation of the behavior of  $C_\alpha$  with time is needed. However, because in the field the value of  $t/t_p$  is often small,  $C_\alpha$  can often be assumed to be independent of time for settlement analysis.

Values of  $C_\alpha/C_c$  are shown in Table 16.1. For all geotechnical materials the total range is 0.01 to 0.07; the midpoint of the range, 0.04, is also the most common value for inorganic clays and silts. The value of  $C_\alpha$  in the early stages of secondary compression, for example

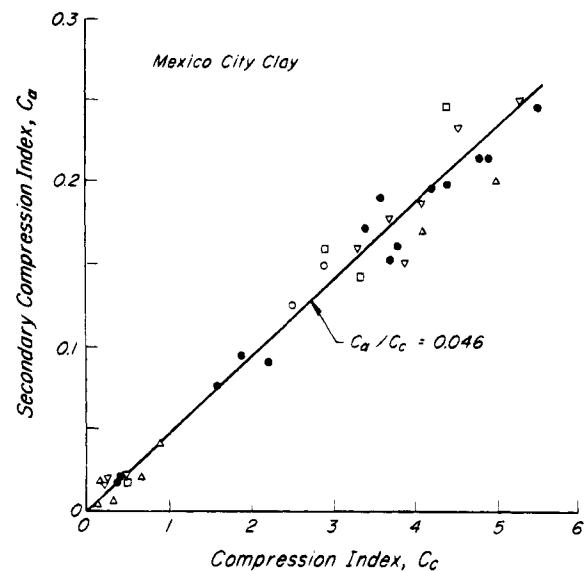


**Figure 16.9** An example of relation between  $C_\alpha$  and  $C_c$ .

**Table 16.1 Values of  $C_\alpha/C_c$  for Geotechnical Materials**

Material	$C_\alpha/C_c$
Granular soils including rockfill	$0.02 \pm 0.01$
Shale and mudstone	$0.03 \pm 0.01$
Inorganic clays and silts	$0.04 \pm 0.01$
Organic clays and silts	$0.05 \pm 0.01$
Peat and muskeg	$0.06 \pm 0.01$

from  $t_p$  to  $10 t_p$ , is computed from  $C_\alpha/C_c$  together with  $C_c$  from the EOP  $e$  vs  $\log \sigma'_v$  curve. Thus, Eq. 16.11 can be written as:

$$S = \frac{C_\alpha/C_c \times C_c}{1 + e_o} L_o \log \frac{t}{t_p} \quad (16.12)$$

Equation 16.12 shows that the magnitude of the secondary settlement is determined by  $C_c$ , which depends in turn on the normalized final pressure  $\sigma'_{vf}/\sigma'_p$  at which secondary compression takes place. When  $\sigma'_{vf}$  is completely in the recompression range, i.e., when  $\sigma'_{vf}/\sigma'_p$  is less than 0.7, then, even though  $t_p$  is small,  $C_c$  (which is under this condition equal to  $C_r$ ) also remains very small, and secondary settlement is not significant. On the other hand, when the final effective pressure  $\sigma'_{vf}$  is near  $\sigma'_p$ ,  $t_p$  may still be small, but  $C_c$  may increase dramatically if it is evaluated on the basis of  $e$  vs  $\log \sigma'_v$  curves corresponding to  $t$  larger than  $t_p$ . Secondary settlement can then be the largest component of the total settlement (Mesri et al. 1994). At consolidation pressures  $\sigma'_{vf}$  in the compression range beyond  $\sigma'_p$ , if there are no vertical drains,  $t_p$  is generally large relative to the design life of most structures, and the secondary settlement is an insignificant component of the total settlement.

When the final consolidation pressure  $\sigma'_{vf}$  is in the compression range beyond  $\sigma'_p$ , and  $t_p$  is small because vertical drains have been installed, then postconstruction secondary settlement can be significant and possibly unacceptable. It can be minimized, however, by surcharging. The surcharging effort is expressed as the *total surcharge ratio*,  $R_s = (\sigma_{vs}/\sigma'_{vf}) - 1$ , and the *surcharging time ratio*  $t'_s/t'_{ps}$ , where  $\sigma_{vs}$  is equal to  $\sigma'_{vf} + \Delta\sigma_{vs}$ ,  $\sigma'_{vf}$  is the final effective vertical stress after removal of surcharge,  $\Delta\sigma_{vs}$  is the total surcharge pressure,  $t'_s$  is the duration of the surcharge, and  $t'_{ps}$  is the time to EOP compression under surcharge (Fig. 16.10). Alternatively, the surcharging effort may be expressed as the *effective surcharge ratio*,  $R'_s = (\sigma'_{vs}/\sigma'_{vf}) - 1$ , where  $\sigma'_{vs}$  is the maximum effective vertical stress reached before the removal of surcharge. When  $t'_s/t'_{ps} = 1$ , then  $R'_s = R_s$ .

The removal of surcharge leads to rebound, including *primary rebound* up to  $t_{pr}$  and *secondary rebound* that

levels off at  $t_l$  and is followed by secondary compression, as illustrated in Fig. 16.10. Both  $t_{pr}$  to EOP rebound after removal of surcharge and  $t_l$  at which secondary compression reappears are measured from the time at which the surcharge load is removed. The interrelationship between  $C_\alpha$  and  $C_c$  explains and permits prediction of postsurcharge secondary compression behavior (Mesri and Feng 1991). In general, the *postsurcharge secondary compression index*,  $C'_\alpha$ , defined in Fig. 16.10 is initially small and gradually increases with time. At large values of  $t$ , the behavior of the secondary compression index  $C'_\alpha$  depends on the shape of the EOP  $e$  vs  $\log \sigma'_v$  curve at  $\sigma'_{vs}$ . It continues to increase, levels off, or levels off and then decreases with time, respectively, for  $\sigma'_{vs}$  values at which  $C_c$  increases, remains constant, or decreases with consolidation pressure.

Because  $C'_\alpha$  is not constant with time, for practical settlement analysis a secant  $C''_\alpha$  is defined from the time  $t_l$  at which postsurcharge secondary compression begins to any  $t$  at which postsurcharge secondary compression is to be evaluated (Fig. 16.10). Values of  $C''_\alpha$  may be obtained from Fig. 16.11, derived from laboratory oedometer surcharging tests on undisturbed specimens of soft clays (Mesri and Feng 1991). The values are normalized with respect to  $C_\alpha$  at  $\sigma'_{vf}$  without surcharging. Postsurcharge secondary settlement can then be computed by means of Eq. 16.13.

$$S = \frac{C''_\alpha}{1 + e_o} L_o \log \frac{t}{t_l} \quad (16.13)$$

where  $C''_\alpha$  corresponds to  $t/t_l$ . For any soft clay, the values of  $C_\alpha/C_c$ ,  $C_c$  at  $\sigma'_{vf}$  on the EOP compression curve, and  $R'_s$  can be used to obtain  $C''_\alpha$  from Fig. 16.11. These values can then be entered into Eq. 16.13, rewritten as:

$$S = \frac{C''_\alpha/C_\alpha \times C_\alpha/C_c \times C_c}{1 + e_o} L_o \log \frac{t}{t_l} \quad (16.14)$$

Postsurcharge secondary compression appears after primary and secondary rebound. The duration of primary rebound depends on the rebound characteristics of the soil as well as on the permeability and drainage boundary conditions. Therefore,  $t_{pr}$  is computed using a theory of time rate of expansion (Article 25.8). The value of  $t_l$  is determined from the empirical correlation between  $t_l/t_{pr}$  and  $R'_s$  shown in Fig. 16.12. This figure shows that the time to the appearance of postsurcharge secondary compression increases with surcharging effort.

## 16.8 Rate of One-Dimensional Consolidation

One-dimensional settlement results from the compression of voids. In terms of void ratio, the rate of compression of a sublayer is expressed by

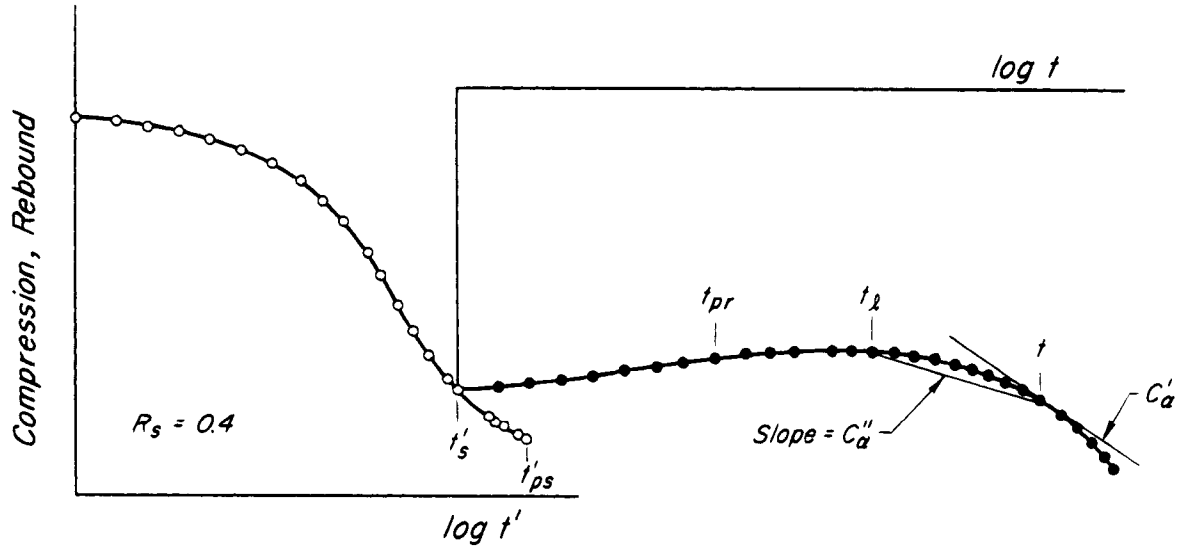


Figure 16.10 Definition of  $t_l$ , tangent  $C'_a$  and secant  $C''_a$ .

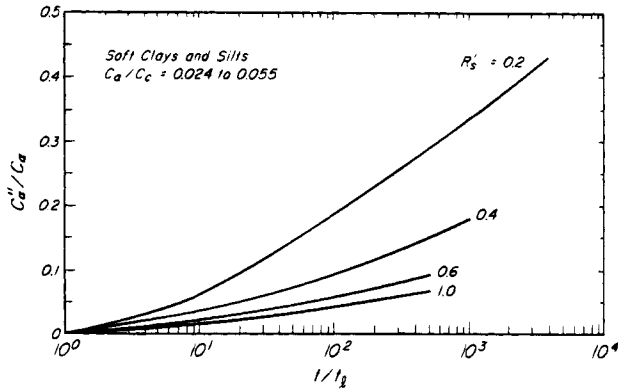


Figure 16.11 Postsurcharge secondary compression index for deposits of soft clay and silt.

$$\frac{de}{dt} = a_{vs} \frac{d\sigma'_v}{dt} + a_{vt} \quad (16.1)$$

The rate of compression  $de/dt$  is determined by the two compressibility parameters  $a_{vs}$  and  $a_{vt}$  and by the rate of increase in effective stress  $d\sigma'_v/dt$ . During the primary consolidation stage, both compressibility parameters contribute to the compression, whereas during the secondary consolidation stage,  $d\sigma'_v/dt$  by definition is zero and the rate of compression is equal to  $a_{vt}$ .

Two factors may be responsible for the time-dependent increase in effective stress. One is a time-dependent loading or a decrease in reference porewater pressure with time. However, a more fundamental factor is the nature of the response of a saturated soil to one-dimensional loading (Article 25). Because the compressibility of the soil structure is much greater than that of water or of soil solids, an increase in total vertical stress produces an equal increase in porewater pressure. This increment of

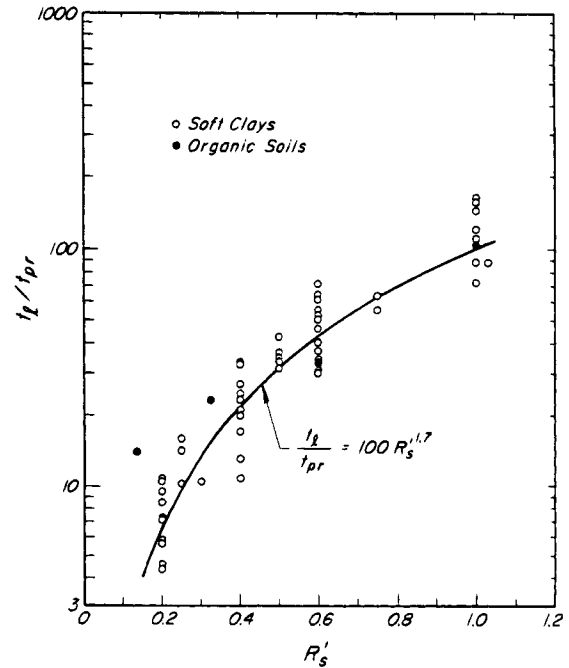


Figure 16.12 Empirical correlation between  $t_l/t_{pr}$  at which postsurcharge secondary compression occurs, and effective surcharge ratio  $R'_s$ .

porewater pressure is called the *excess porewater pressure*  $u'$ , because it is in excess of a reference static or steady-state porewater pressure. A gradient in excess porewater pressure,  $\partial u'/\partial z$ , develops within a sublayer of the soil toward a drainage boundary at which the porewater pressure is at the reference state. As the pore water flows out of the sublayer, the coefficient of permeability controls the rate of flow in accordance with the Darcy flow equation (Article 14.2). In the vertical direction,

$$v_z = \frac{k_v}{\gamma_w} \frac{\partial u'}{\partial z} \quad (16.15)$$

The smaller the coefficient of permeability of the sublayer and the greater the distance of the sublayer from the drainage boundary, the longer is the time required for the pore water to flow out. Moreover, because the water that leaves the sublayer does so because the void space it occupies is being compressed, the more compressible the soil, the longer the time required to discharge the excess water.

The generation and dissipation of excess porewater pressure are illustrated in Figs. 16.13 and 16.14 for two pressure increments applied to a saturated clay layer. The clay is free to drain from the top, but the bottom boundary is impermeable. Four piezometers located at the quarter points in depth measure the porewater pressure during consolidation. The void ratio-effective stress relationship of the soil (Fig. 16.15a) shows that the pressure increment from 28 to 55 kPa is completely within the recompression range, whereas the 110- to 152-kPa increment spans the preconsolidation pressure. In both instances, at the instant of loading all four piezometers measure a porewater pressure equal to the applied pressure increment. Consolidation begins as the excess porewater pressure starts to dissipate. The curve representing the distribution of excess porewater pressure with depth at any time is known as an *isochrone*.

After the application of the pressure increment, because the total vertical stress remains constant, the increase  $d\sigma'_v/dt$  in effective vertical stress with time is equal to

the decrease  $-du'/dt$  in excess porewater pressure. The rate of excess porewater pressure dissipation is substituted for the rate of effective stress increase in Eq. 16.1 to obtain

$$-\frac{du'}{dt} = \frac{\frac{de}{dt} - \left(\frac{\partial e}{\partial t}\right)_{\sigma'_v}}{\left(\frac{\partial e}{\partial \sigma'_v}\right)_t} = \frac{\frac{de}{dt} - a_{vt}}{a_{vs}} \quad (16.16)$$

Eq. 16.16 shows the effect of the compressibility parameters  $a_{vs}$  and  $a_{vt}$  (Article 16.3) on the rate of porewater pressure dissipation. An increase in either  $a_{vs}$  or  $a_{vt}$  slows dissipation. In fact, the rate of excess porewater pressure dissipation is inversely related to the compressibility  $a_{vs}$ . For pressure increments within the recompression range, the porewater pressure dissipates rapidly because  $a_{vs}$  is small. This applies, for instance, to the pressure increment from 28 to 55 kPa in Fig. 16.15a. The same is initially true for the pressure increment from 110 to 152 kPa. However, when the effective vertical pressure reaches  $\sigma'_p$  the value of  $a_{vs}$  abruptly increases and there is a dramatic reduction in the rate of porewater pressure dissipation. During consolidation, the decrease in the coefficient of permeability also slows the rate of porewater pressure dissipation (Fig. 16.15b). However, the decrease in permeability is always gradual, whereas the changes in compressibility can be abrupt with correspondingly abrupt changes in the rate of excess porewater pressure dissipation.

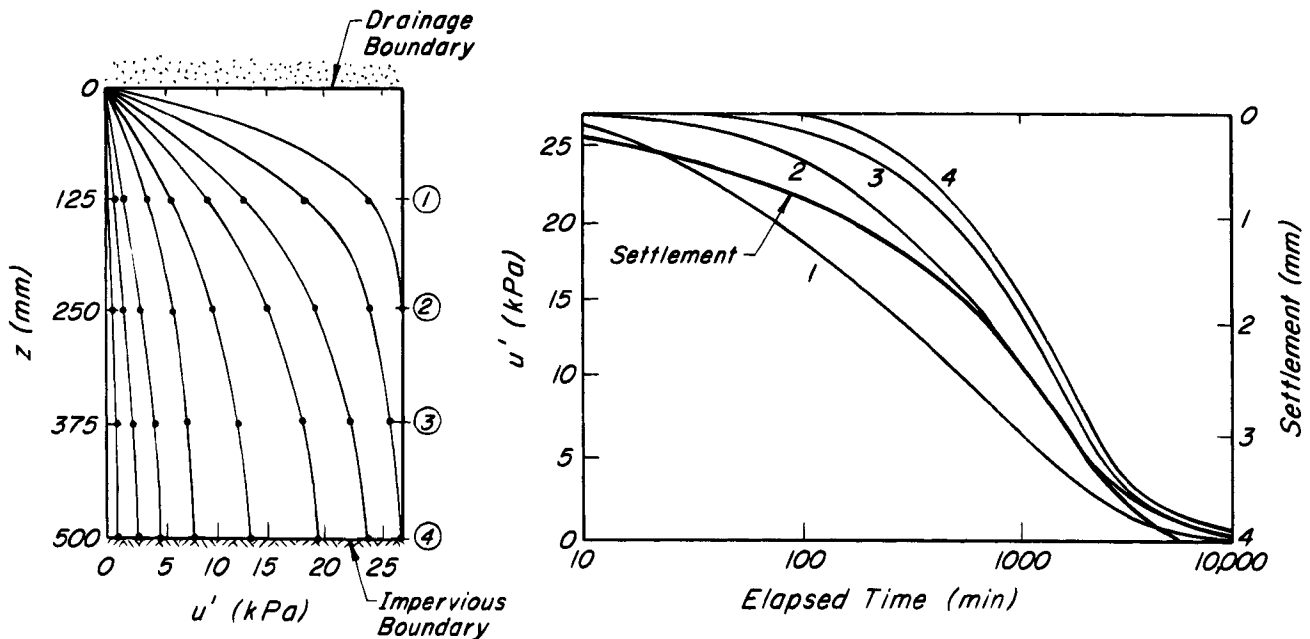
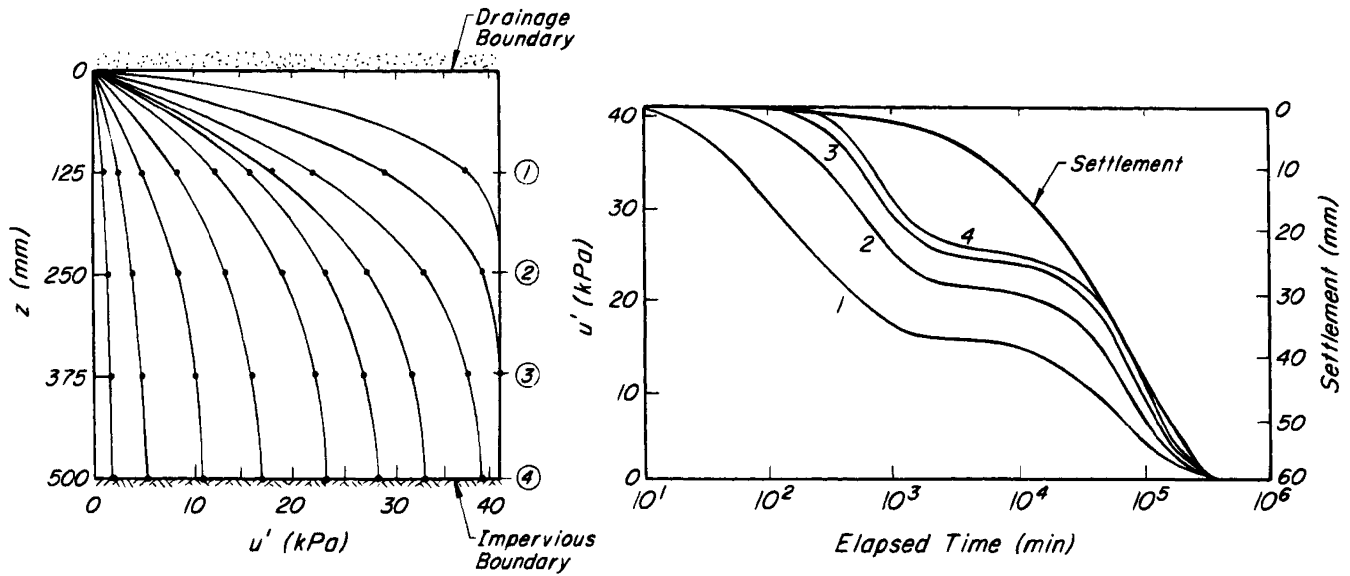
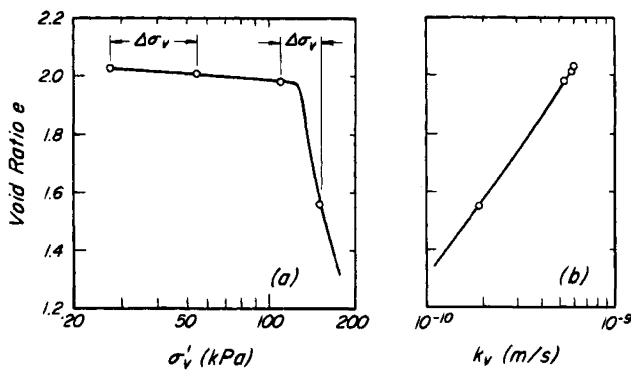


Figure 16.13 Excess porewater pressure behavior for a pressure increment within the recompression range.



**Figure 16.14** Excess porewater pressure behavior for a pressure increment spanning the preconsolidation pressure.



**Figure 16.15** (a) Relation between  $e$  and  $\log \sigma_v$  and (b) Corresponding relation between  $e$  and  $\log k_v$  for the pressure increments in Figs. 16.13 and 16.14.

During the primary consolidation stage, the rates of excess porewater pressure dissipation and compression are different for various sublayers located at different distances from the drainage boundary. To evaluate the rates of compression and of excess porewater pressure dissipation for the sublayers and the rate of settlement of the consolidating layer, Eq. 16.1 must be combined with the hydrodynamic equation of flow and solved simultaneously for the layer as a whole (Article 25.4). During secondary consolidation the rate of compression of a sublayer is

$$\frac{dS}{dt} = \frac{0.434}{1 + e_o} L_o \frac{C_\alpha}{t} \quad (16.17)$$

The rate of secondary settlement of the consolidating layer is the average of the rates of compression for the

sublayers, weighted in accordance with the thickness of the sublayers.

### 16.9 Oedometer Test

The oedometer test closely approximates the one-dimensional deformation and drainage boundary conditions of confined layers of soil in the field. Vertical compression or settlement results only from the compression of voids, because the specimen is confined in a stiff ring. For example, a lubricated highly polished stainless steel ring, having a diameter-to-height ratio of 3 or more, is customarily used to approximate as closely as possible the unyielding, frictionless, inert, and impervious lateral boundary condition assumed in the interpretation of the test. A confining ring with a sharp edge is used to cut an undisturbed specimen directly into the test ring. Any pebbles or shells that are encountered by the cutting ring are carefully removed and the void is backfilled with soil. Vertical load is applied to the top of the soil specimen through a rigid cap, and the compression is measured by a dial indicator. Drainage may be allowed from both the top and bottom faces of the specimen through rigid porous stones. In some tests, however, drainage is allowed only from the top of the specimen, and porewater pressure is measured at the bottom.

In the most common oedometer testing procedure, the incremental loading (IL) test, each increment of load is applied instantaneously and is allowed to act long enough to define the end-of-primary (EOP) void ratio  $e_p$ . If the excess porewater pressure is measured at the bottom of the specimen, the EOP consolidation, by definition, is reached when the excess porewater pressure dissipates to zero or to a very small value such as 1 kPa. If the excess

porewater pressure is not measured, EOP consolidation is determined by a graphical procedure applied to the deformation-time curve for each load increment (Taylor 1948, Casagrande and Fadum 1940). When Taylor's procedure is used, each increment is maintained for the period of time  $t_p$  required to complete primary consolidation. When the Casagrande procedure is used, some secondary compression must be allowed beyond  $t_p$ . Oedometer tests with porewater pressure measurements indicate that the Casagrande procedure leads to values of  $e_p$  practically equal to those defined by excess porewater pressure measurements, whereas the Taylor procedure may underestimate  $e_p$  for soils that experience significant destructuration during the pressure increment.

When information on  $C_\alpha = \Delta e / \Delta \log t$  is required, secondary compression is allowed for about one log cycle of time at two or three values of  $\sigma'_v$ , preferably in the compression range. The values of  $C_\alpha$ , together with the corresponding values of  $C_c$  at the same  $\sigma'_v$  from the EOP  $e$  vs  $\log \sigma'_v$  curves, are used to define the value of  $C_\alpha/C_c$  for the soil. This value together with the EOP  $e$  vs  $\log \sigma'_v$  relationship is used to compute  $C_\alpha$  for all values of  $\sigma'_v$  in the recompression as well as in the compression range. Pressure-increment ratios of 1/2 to 1 in the recompression and compression ranges, and of 1/2 in the  $\sigma'_v/\sigma'_p$  range of 0.5 to 2, provide a sufficient number of ( $e$ ,  $\sigma'_v$ ) data points for an adequate definition of the shape of the EOP  $e$  vs  $\log \sigma'_v$  relationship of most soils. Smaller values of  $\Delta \sigma'_v/\sigma'_v$  prolong the oedometer test and cannot be used readily because, in the absence of porewater pressure measurements, it may not be possible to define the EOP consolidation by means of the empirical procedures of Casagrande or Taylor (Mesri and Godlewski 1977, Mesri 1987).

Practically continuous EOP  $e$  vs  $\log \sigma'_v$  curves are defined, even for highly structured soils that experience an abrupt structural change at  $\sigma'_{p^*}$ , by the constant-rate-of-strain (CRS) oedometer testing procedure in which the specimen is subjected to a constant rate of axial deformation and the vertical load is measured by a stiff load cell. Drainage is allowed from the top of the specimen, and porewater pressure is measured at the bottom. The values of the excess porewater pressures can be used to compute the coefficient of permeability as the test progresses. For any soil, an imposed axial strain rate  $\dot{\epsilon}_p$  can be computed that induces near-zero excess porewater pressure throughout the recompression and compression ranges, and that results in an  $e$  vs  $\log \sigma'_v$  relationship practically identical with the EOP  $e$  vs  $\log \sigma'_v$  from an IL oedometer test (Mesri and Feng 1992). Imposed axial strain rates slower than  $\dot{\epsilon}_p$  permit secondary compression to occur after primary consolidation and cause underestimation of the EOP  $\sigma'_{p^*}$ . Tests at strain rates significantly faster than  $\dot{\epsilon}_p$ , which induce excess porewater pressures corresponding to  $u_h/\sigma_v$  values greater than 15%, are unreliable because

they lead to significant variation in void ratio and effective stress from top to bottom of the specimen throughout the test. There are, however, two disadvantages of using an imposed strain rate equal to  $\dot{\epsilon}_p$  for CRS oedometer testing: a test on typical soft clays may require more than 2 weeks; and because the excess porewater pressure at the bottom of the specimen is near zero, calculation of the coefficient of permeability using  $u'_b$  is not possible. An imposed axial strain rate  $\dot{\epsilon}_t = 10 \dot{\epsilon}_p$ , which produces values of  $u'_b/\sigma_v$  less than 15%, results in oedometer-test durations of about 2 days for typical soft clays and allows reliable calculation of the coefficient of permeability. For typical soft clays,  $10 \dot{\epsilon}_p$  is about  $2 \times 10^{-6} \text{ s}^{-1}$  (Mesri and Feng 1992). For these clays the value of  $(\sigma'_p)_{10 \dot{\epsilon}_p}$  is about 10% greater than  $(\sigma'_p)_{\dot{\epsilon}_p}$ . The field EOP  $e$  vs  $\log \sigma'_v$  relationship for settlement analysis is constructed as shown in Fig. 16.16, by starting from point  $(e_o, \sigma'_{vo})$  and drawing a curve parallel to the recompression curve up to the preconsolidation pressure EOP  $\sigma'_p = (\sigma'_p)_{\dot{\epsilon}_p}$ . Thereafter, a curve is drawn parallel to the compression curve while keeping  $(\sigma'_v)_{\dot{\epsilon}_p}/(\sigma'_v)_{10 \dot{\epsilon}_p}$  constant and equal to 0.90.

Oedometer tests for settlement analysis of soft clays should be made on undisturbed specimens with specimen quality designations SQD (Table 11.2) equal to or better than *B*. *A*-quality specimens are preferred, but *B*-quality specimens are acceptable. In either case, for settlement analysis, a field EOP  $e$  vs  $\log \sigma'_v$  curve must be constructed to exclude the effect of sample disturbance from the results of the oedometer test. The empirical procedure described in the preceding paragraph for constructing the

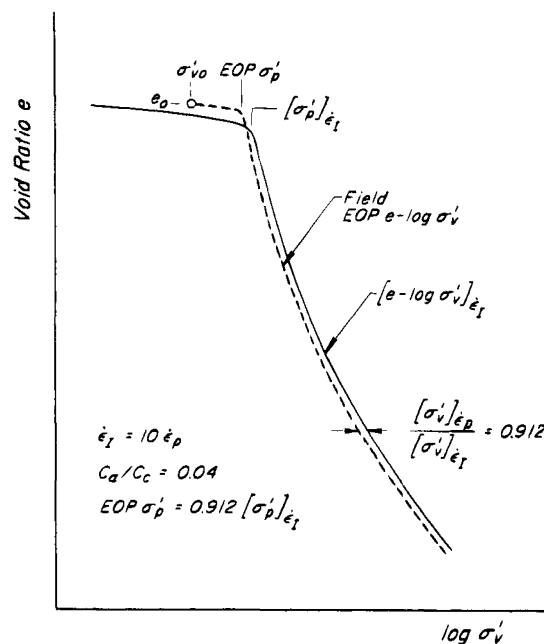


**Figure 16.16** Procedure for constructing field EOP  $e$  vs  $\log \sigma'_v$  curve from  $e$  vs  $\log \sigma'_v$  curve obtained in CRS oedometer test at an imposed strain rate  $\dot{\epsilon}_f = 10\dot{\epsilon}_p$ .



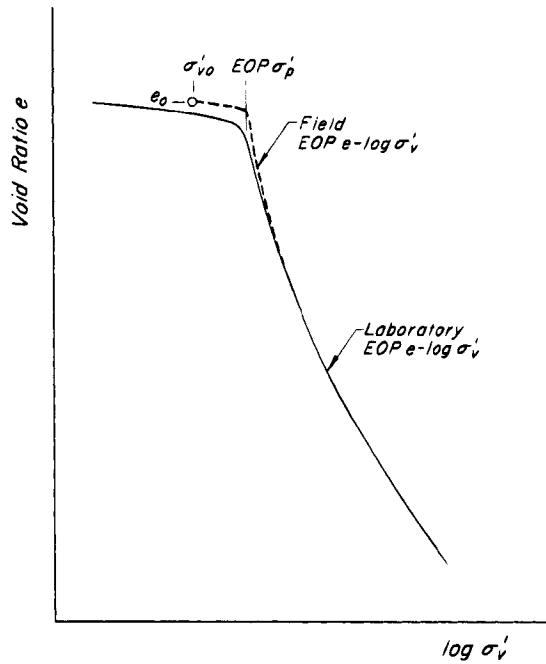


**Figure 16.17** Procedure for constructing field EOP  $e$  vs  $\log \sigma'_v$  curve from laboratory EOP  $e$  vs  $\log \sigma'_v$  curve from incrementally loaded IL odometer test.

field EOP  $e$  vs  $\log \sigma'_v$  curve accomplishes this for the CRS odometer test. A procedure for constructing the field EOP  $e$  vs  $\log \sigma'_v$  curve on the basis of IL odometer test results is illustrated in Fig. 16.17. The field EOP  $e$  vs  $\log \sigma'_v$  relationship starts at point  $(e_o, \sigma'_{vo})$ , proceeds at a recompression index  $C_r$  to the preconsolidation pressure EOP  $\sigma'_p$ , and then gradually joins the laboratory EOP compression curve. Several methods have been proposed for determining the preconsolidation pressure from the results of odometer tests (Sallfors 1975, Graham et al. 1982). The one most commonly used is illustrated in Fig. 16.18 (Casagrande 1936b). Through point  $c$ , at which the radius of curvature is a minimum, a horizontal line is drawn. The bisector of the angle between this line and

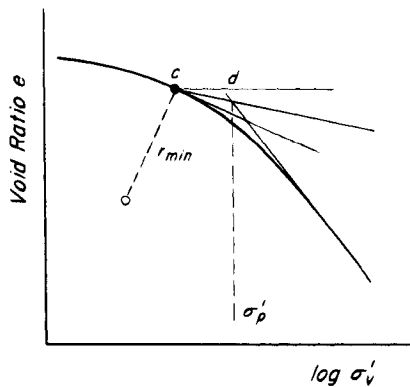


**Figure 16.18** Casagrande graphical construction for estimating preconsolidation pressure  $\sigma'_p$ .

the tangent to the  $e$  vs  $\log \sigma'_v$  curve at  $c$  intersects the upward extension of the compression curve at point  $d$ . The abscissa of  $d$  is considered to be equal to  $\sigma'_p$ .

Sample disturbance increases the slope of the recompression curve,  $C_r = \Delta e / \Delta \log \sigma'_v$ . The recompression index for constructing the field EOP  $e$  vs  $\log \sigma'_v$  curve should be taken equal to or smaller than  $C_r$  from the laboratory EOP recompression curve. The correct value of  $C_r$  can be estimated from odometer tests on A-quality specimens or from empirical information regarding  $C_r/C_c$ , where  $C_c$  is the compression index from  $\sigma'_p$  to  $2\sigma'_p$ . To construct the field  $e$  vs  $\log \sigma'_v$  curve for heavily preconsolidated clays,  $C_r$  can be estimated by means of a graphical procedure (Schmertmann 1953) illustrated in Fig. 16.19. The procedure requires unloading the sample in decrements, after  $\sigma'_p$  has been exceeded, to obtain a laboratory rebound curve. From the point representing the *in situ*  $(e_o, \sigma'_{vo})$  a line is drawn parallel to the rebound curve; its intersection with the vertical at  $\sigma'_p$  is denoted by  $P$ . The field  $e$  vs  $\log \sigma'_v$  curve starts at  $(e_o, \sigma'_{vo})$ , recompresses to a point just below  $P$  and then gradually joins the laboratory compression curve. The logic behind this empirical construction procedure is apparent from the rebound-recompression curves in Fig. 16.4.

All available subsurface information, including vertical profiles of natural water content and total unit weight, and water table and preconstruction porewater pressure profiles, are used for an accurate definition of the *in situ* void ratio  $e_o$  and the preconstruction effective overburden pressure  $\sigma'_{vo}$  of each undisturbed soil specimen. The field EOP  $e$  vs  $\log \sigma'_v$  curve constructed on the basis of odometer test results is used for computing the settlement resulting from primary consolidation. It is also used,

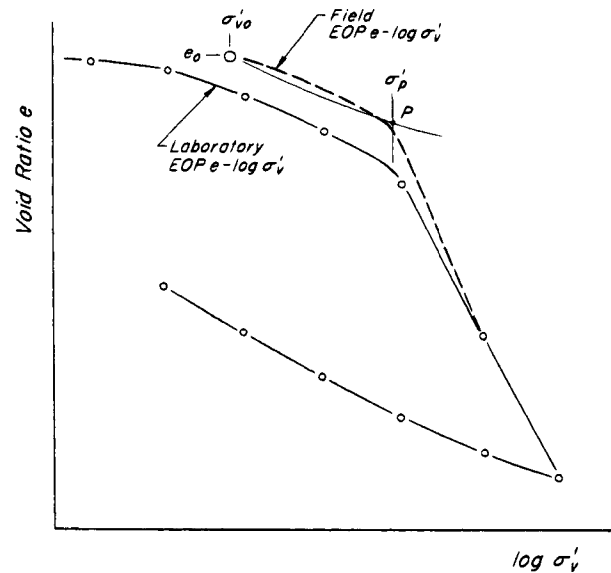


**Figure 16.19** Procedure for constructing field EOP  $e$  vs  $\log \sigma'_v$  curve for heavily preconsolidated clay.

together with the value of  $C_\alpha/C_c$  for the soil, to determine  $C_\alpha$  for calculating the secondary settlement at any postconstruction  $\sigma'_{vf}$ .

As stated previously, at consolidation pressures  $\sigma'_{vf}$  in the compression range beyond  $\sigma'_p$ , if there are no vertical drains,  $t_p$  is generally large relative to the design life of most structures, and the secondary settlement is an insignificant component of the total settlement. Moreover, in some instances, the preconsolidation pressure  $\sigma'_p$  only slightly exceeds the existing overburden pressure  $\sigma'_{vo}$ , and the additional pressure due to a building or fill is almost entirely within the compression range. Under these circumstances a conservative approximate value for the settlement at EOP can be determined by setting  $\sigma'_p = \sigma'_{vo}$  in Eq. 16.8 whereupon

$$S = \frac{C_c}{1 + e_o} L_o \log \frac{\sigma'_{vf}}{\sigma'_{vo}} \quad (16.18)$$

This is the classical equation for primary consolidation, in which  $C_c$  can be determined by oedometer tests or by means of site-specific or general statistical correlations such as those discussed in Article 12.7.

### 16.10 Heave of Expansive Soils

Expansive soils, which usually contain the clay mineral montmorillonite, include sedimentary and residual soils, claystones, and shales. In arid and semiarid climates, they exist in a moisture-deficient, unsaturated condition. A main reason for foundation heave is a construction-related change in the moisture environment.

Expansive soils possess an *intrinsic expansiveness* in that they contain particles that bend and store significant elastic energy and that hold considerable amounts of adsorbed and double-layer water. Intrinsic expansiveness is determined by the mineralogy of the soil solids, the chemistry of the pore water, and the degree of aggregation of the particles. The most important fundamental variables are particle size and shape, which are controlled by mineralogy, aggregation, and chemistry of the pore water; the latter also controls the thickness of the double-layer water. The chemistry of the pore water refers mainly to the type of exchangeable cations and the electrolyte concentration. The highest intrinsic expansiveness is associated with very small and thin particles such as those of montmorillonite with monovalent exchangeable sodium cations, having free pore water with low electrolyte concentration, and being in the most disaggregated state.

Simple indicators of intrinsic expansiveness are the liquid limit,  $w_l$ , which is a measure of the ability of the soil composition to hold water, and the clay fraction,  $CF$ , which indicates the ability of particles to stay in suspension. These index properties, however, may not reliably indicate the role of aggregation, because an arbitrary degree of soil disaggregation is inherent in evaluating  $w_l$  and  $CF$ .

*Potential expansiveness* is determined not only by intrinsic expansiveness but also by the void ratio. In soil at a low void ratio, some particles have been deformed and have stored recoverable energy, some adsorbed water has been expelled from interparticle contacts or short-range interaction zones, and part of the double-layer water between particles has been forced out. If the external agent that has produced the low void ratio is removed, the soil will assert its potential expansiveness. This is illustrated by Table 16.2, in which the swelling index  $C_s = \Delta e / \Delta \log \sigma_v$  indicates intrinsic expansiveness and the swelling pressure  $p_s$  indicates potential expansiveness. *Swelling pressure* is the pressure that a soil or rock exerts against an unyielding support such as a tunnel lining or a basement wall (Mesri et al. 1994). Sodium montmorillonite, which has very high intrinsic expansiveness as indicated by the value of  $C_s$ , displays very high potential expansiveness because its swelling pressure decreases very little as its void ratio increases. On the other hand, kaolinite displays low potential expansiveness, because it has a small value of  $C_s$  and thus its swelling pressure decreases dramatically with any increase in void ratio.

The external variables that control the void ratio in unsaturated soils with air voids that are connected to the atmosphere are usually the total confining pressure and the suction (Eq. 15.19). The confining pressure is usually the total vertical stress  $\sigma_v$ , which pushes soil particles together. It arises from the weight of overburden and structures. The suction  $u_s$ , which pulls soil particles together, is the result of a moisture deficient environment that denies the soil full access to water.

The vertical strain  $\epsilon_v$  is a more practical variable than the void ratio for evaluating the heave of unsaturated expansive soils. Expansiveness is expressed in terms of the *swelling strain index*,  $C_{ss} = \Delta \epsilon_v / \Delta \log \sigma_v$ , *secondary swelling strain index*,  $C_{ssa} = \Delta \epsilon_v / \Delta \log t$ , and *swelling strain suction index*,  $C_{sss} = \Delta \epsilon_v / \Delta \log u_s$ . The two components of the heave, associated with the changes in vertical stress and suction, respectively, can then be computed by means of the equations:

$$(S)_{\Delta \sigma_v} = \sum^{L_{\Delta \sigma_v}} \left[ L C_{ss} \left( \log \frac{\sigma_{vo}}{\sigma_{vf}} + \frac{C_{ssa}}{C_{ss}} \log \frac{t}{t_p} \right) \right] \quad (16.19)$$

$$(S)_{\Delta u_s} = \sum^{L_{\Delta u_s}} \left[ L C_{sss} \log \frac{u_{so}}{u_{sf}} \right] \quad (16.20)$$

where  $\sigma_{vo}$  and  $u_{so}$  are the preconstruction total vertical stress and suction, and  $\sigma_{vf}$  and  $u_{sf}$  are the corresponding values for the postconstruction condition. The secondary swelling during an elapsed time  $t$  starts at  $t_p$ , the time required to complete primary swelling. Data on magnitudes of  $C_{ss}$  and  $C_{sss}$  for clays and shales are summarized in Figs. 16.20 and 16.21, respectively. The difference between  $C_{ss}$  of reconstituted and of undisturbed

**Table 16.2** Intrinsic Expansiveness and Potential Expansiveness of Clay Minerals\*

Clay	$p_s$ at $e = 1$ kPa	$p_s$ at $e = 1.5$ kPa	$C_s$ from $e = 1.0$ to $e = 1.5$
Sodium montmorillonite (low EC)	3500	1050	0.956
Sodium montmorillonite (high EC)	3500	850	0.814
Calcium montmorillonite (low EC)	1500	115	0.448
Sodium illite (low EC)	350	60	0.653
Sodium illite (high EC)	350	33	0.488
Calcium illite (low EC)	275	12	0.368
Kaolinite	29	0.3	0.250

\* Data from Olson and Mesri (1970).

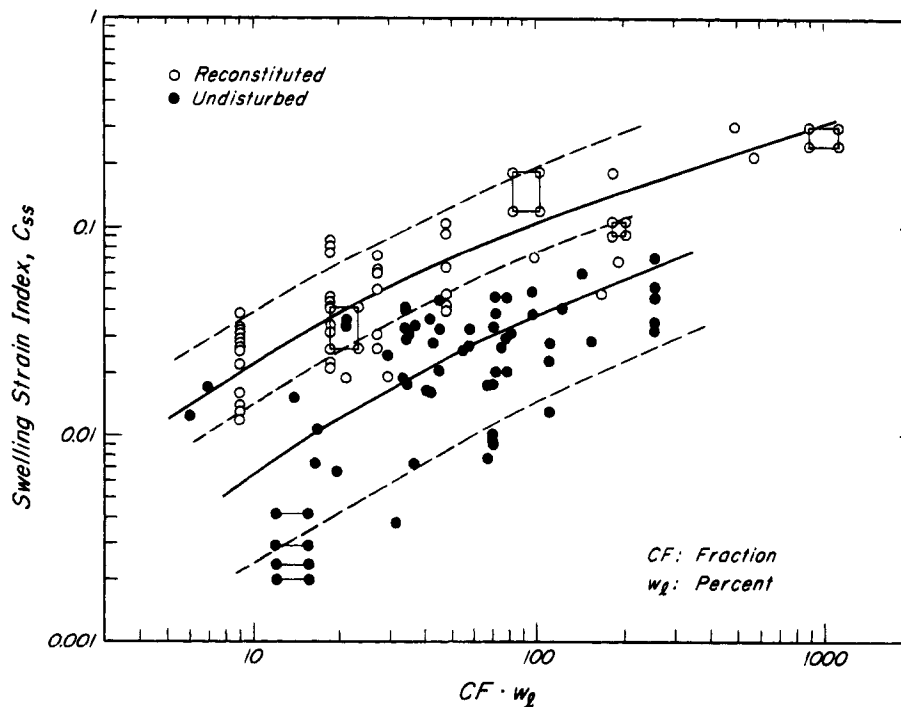


**Figure 16.20** Swelling strain index  $C_{ss}$  of soils as a function of clay fraction, CF, and liquid limit  $w_L$ .

claystones and shales mainly reflects aggregation, which exists in the undisturbed soil but is broken up by drying and slaking in the preparation of reconstituted specimens.

Swelling continues with time after unloading and dissipation of negative excess porewater pressures. The volume increase that takes place at constant effective vertical stress is referred to as *secondary swelling*. The slope of the  $e$  vs  $\log t$  curve during secondary volume increase is called the *secondary swelling index*,  $C_{s\alpha} = \Delta e / \Delta \log t$ . The magnitude of  $C_{s\alpha}$  is directly related to the swelling index  $C_s$  where both  $C_{s\alpha}$  and  $C_s$  correspond to the same void ratio and effective vertical stress during unloading. Whereas for any given soil the value of  $C_\alpha / C_c$  is a con-

stant, and whereas for all geotechnical materials considered together  $C_\alpha / C_c$  does not exceed 0.07 (Article 16.7),  $C_{s\alpha} / C_s$  increases with overconsolidation ratio,  $OCR = \sigma'_{vmax} / \sigma'_v$ , and may have values as high as 1.0. Because  $C_s$  and  $C_{s\alpha}$  both increase with  $OCR$ ,  $C_{s\alpha}$  should increase with time (Mesri et al. 1978). The relatively high values of  $C_{s\alpha} / C_s$  as compared with  $C_\alpha / C_c$  are to be expected. In general, compression is a process of progressive *strengthening* of soil structure, whereas swelling represents progressive *weakening*. In shales and claystones diagenetic bonds that aggregate clay minerals should reduce the magnitude of swell during the primary swelling stage; and, together with structural discontinuities, such as fis-

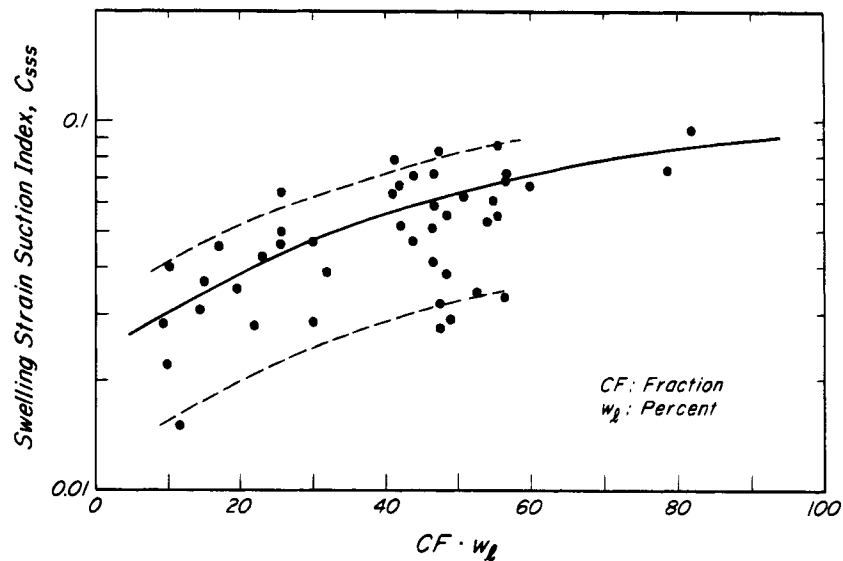


**Figure 16.21** Swelling strain suction index  $C_{ss}$  of soils as a function of clay fraction, CF, and liquid limit  $w_L$ .

tures and slickensides, should accelerate the rate of excess porewater pressure dissipation. Therefore, major structural deterioration including disaggregation takes place after the dissipation of excess porewater pressures, i.e., during secondary swelling.

Even though  $C_{s\alpha}/C_s$  increases with OCR, the magnitude of  $C_{s\alpha}/C_s$  for any given clay or shale is independent of the magnitude of the maximum past pressure  $\sigma'_{vmax}$ , of time during the secondary swelling stage, and of whether unloading is from recompression or the compression range (Cepeda-Diaz 1987). Figure 16.22 shows  $C_{s\alpha}/C_s$  versus OCR data for undisturbed Bearpaw shale samples from three different locations. The liquid limits of the Bearpaw shale samples from Fort Peck, Billings, and Saskatchewan were 288%, 68%, and 128%, respectively. The unloading of the Billings and Saskatchewan samples was from 3.2 MPa in the recompression range, whereas that of Fort Peck was from 1.6 and 3.2 MPa in the recompression, and from 6.6 and 14.1 MPa in the compression range. Secondary swelling measurements on undisturbed oedometer specimens of more than two dozen shales (Mesri et al. 1978, Cepeda-Diaz 1987) suggest the following relation between  $C_{s\alpha}/C_s$  and OCR:

$$\frac{C_{s\alpha}}{C_s} = \alpha (OCR)^{1/2} \quad (16.21)$$

The most typical values of  $\alpha$  are in the range of 0.01 to 0.02. The secondary swelling strain index  $C_{ss\alpha}$  is estimated from  $C_{ss\alpha}/C_{ss}$  which is equal to  $C_{s\alpha}/C_s$ .

The decrease in  $\sigma_v$  may result from the grading of a site; from excavation for a basement, highway, or spillway; or from other construction activities (Article 46.3.4). The

thickness of the expansive soil that contributes to significant heave depends primarily on the areal extent of the excavation. The variation of  $\Delta\sigma_v$  over the depth  $L_{\Delta\sigma_v}$ , as well as the magnitude of  $L_{\Delta\sigma_v}$ , may be estimated from elastic stress distribution (Article 40).

Expansive soils that are not flooded or submerged are subjected to suction. In an unsaturated expansive soil with air voids connected to the atmosphere, the environment competes with the soil for the available moisture. Thus, all the external sources that either supply moisture or extract it from the environment influence the suction. The environmental conditions that control initial preconstruction suction in expansive soil profiles include: (1) climate, including precipitation and evaporation; (2) topography, including surface fissures that determine surface drainage, water penetration, and runoff; (3) vegetation, including plants, shrubs, and trees depleting moisture by transpiration; (4) water tables, both deep and perched, as determined by the hydrogeology of the site; and (5) climatic events, such as back-to-back rainy seasons or prolonged drought. The depth of soil within which there is moisture deficiency is defined by the deep water table, as shown in Fig. 16.23. The desiccated zone  $L_D$  above the deep water table may be from several meters to more than 50 m thick. The near-surface portion of the desiccated zone is subject to seasonal fluctuations in moisture content and suction. The depth of seasonal moisture fluctuation  $L_s$  is a function of the magnitude and frequency of surface wet-dry cycles, the intensity and depth of fissures and cracks, and the coefficients of suction-swelling and suction-shrinking of the soil, which determine the rate of wetting and drying. Typical values of  $L_s$  are in the range of 1 to 5 m.

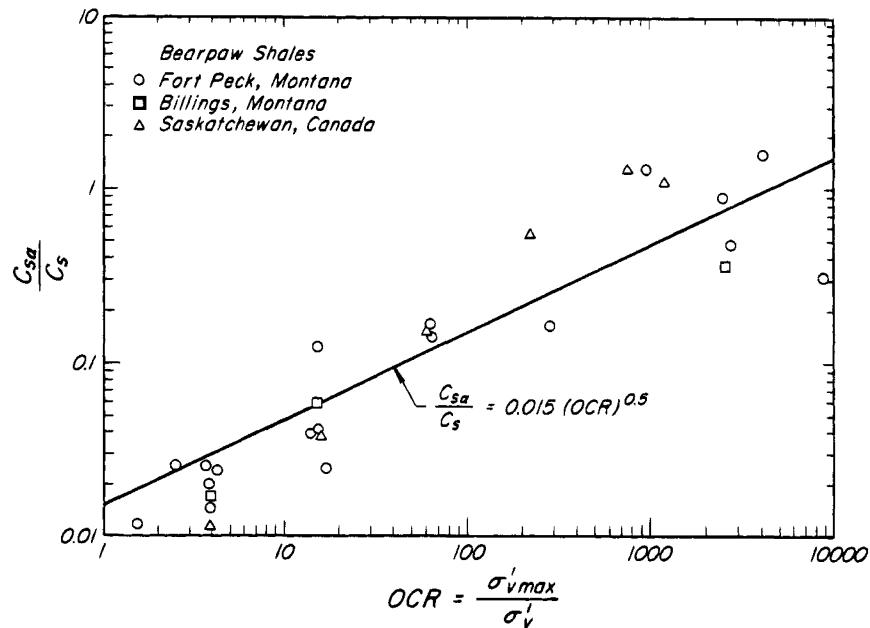


**Figure 16.22** Values of ratio of secondary swelling index to swelling index as a function of overconsolidation ratio for Bearpaw shales from different localities in the United States and Canada.

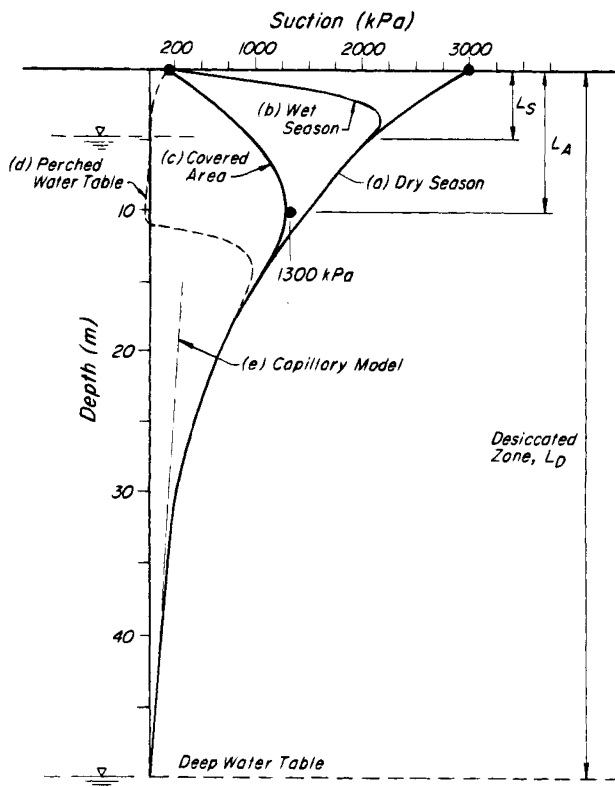


**Figure 16.23** Examples of suction profiles. (a) Preconstruction in dry season; (b) preconstruction in wet season; (c) postconstruction beneath covered area; (d) postconstruction above perched water table.

To compute the heave by using Eq. 16.20, the values of preconstruction and postconstruction suction are required. The most direct approach for obtaining the preconstruction suction profile is *in situ* measurement by psychrometer or filter paper (e.g., Baker et al. 1973, Nelson and Miller 1992, Chen 1988). A psychrometer measures relative humidity, which is then converted to suction by means of Eq. 15.25. However, direct measurement of suction in the field is seldom straightforward or economically feasible. In such a situation, the suction may be estimated from empirical information (Mesri and Shahien 1994). For example, the preconstruction maximum near-surface suction, which ranges from 1500 to 5000 kPa, may be estimated from the wilting point of native vegetation (Lytton 1992, McKen 1992). The postconstruction minimum near-surface suction, resulting from moisture movement in vapor form and unsaturated flow but in the absence of flooding, may be estimated from the field water-holding capacity. The typical range is 10 to 300 kPa, but the most common values are 100 to 200 kPa. The long-term postconstruction depth within which there is significant swelling and heave is called the *active zone depth*,  $L_A$  (Fig. 16.23). This depth, which is determined by the availability of moisture, may range from  $L_s$  to  $L_D$ . Values of  $L_A$ , typically twice the seasonal depth of moisture fluctuation, have been reported in the range of 3 to 15 m. The most common values for semiarid and arid climates are from 4 to 8 m. The suction at the base of the active zone is called the *equilibrium suction*. Its value

depends on the climate and the depth of the deep water table; it ranges typically between 100 and 3000 kPa.

A perched water table may develop after a site on expansive soil has been fully developed, for example, by residential construction with extensive paved surfaces and lawns. Water from precipitation, surface irrigation, and leaky utility lines is trapped on top of the unweathered expansive soil. Such a near-surface evaporation barrier may also lead to a rise in the deep water table. A perched water table may significantly alter the postconstruction suction profile and the depth of the active zone. This is illustrated by the dash profile in Fig. 16.23.

Laboratory oedometer tests with suction control can be used to establish relations among vertical strain, suction, and total vertical stress. The results of a series of tests on undisturbed specimens of Onderstepoort clay are shown in Fig. 16.24. The preconstruction stress condition for the undisturbed specimen is defined by  $\sigma_{vo} = 45$  kPa and  $u_{so} = 4500$  kPa. The data in Fig. 16.24, together with Eq. 16.19 and preconstruction and postconstruction values of suction, can be used to compute the heave. For example, for a 1-m-thick sublayer and  $u_{sf} = 200$  kPa, the average value of  $C_{ss} = 0.052$  between  $u_{so}$  and  $u_{sf}$  leads to a computed heave of 70 mm. When preconstruction and postconstruction suction data are not available, a heave equation in terms of swelling pressure can be used. For a sublayer of thickness  $L$ , overburden pressure  $\sigma_{vo}$ , and swelling pressure  $p_s$ , the heave can be estimated from

$$S = C_{ss} L \log \frac{p_s}{\sigma_{vo}} \quad (16.22)$$

On the assumption that, after construction, the expansive

soil will not be flooded, a value of  $p_s = 3000$  kPa and an average value of  $C_{ss} = 0.036$  between  $\sigma_{vo}$  and  $p_s$ , when substituted in Eq. 16.22, indicate a heave of 66 mm, quite comparable to the 70 mm computed by using suction.

Oedometer test results with suction control are often not readily available. The relation between  $\epsilon_v$  and  $p_s$  is then obtained from oedometer specimens that are submerged during the test. Constant volume, free swell, or deformation controlled unloading tests can be used to obtain the relation between vertical strain and swelling pressure for the flooded condition (Mesri et al. 1994). The data in Fig. 16.24 for Onderstepoort clay suggest that oedometer tests on submerged specimens may overestimate  $p_s$  and  $C_{ss}$  (represented by the slope of the curves), and thus the heave for expansive soils that are not flooded. However, Fig. 16.24 also shows that, at least for this undisturbed expansive soil,  $C_{ss}$  is not highly dependent on suction. Furthermore, additional test results on Onderstepoort clay (Fig. 16.25) show that the  $\epsilon_v$  vs  $u_s$  relation on wetting displays a critical suction below which there is no heave and thus no decrease in swelling pressure. Therefore, oedometer test results on submerged specimens, or even estimates of swelling pressure together with values of  $C_{ss}$  from Fig. 16.20, may be used to obtain a first estimate of heave for expansive soils subjected to wetting.

Expansive soils that gain access to water develop a swelling pressure against an unyielding stiff support that prevents full swelling. In most instances of sampling or field excavation, some expansion of claystone or shale takes place. Therefore, information on swelling pressure should be reported in terms of the relation between strain

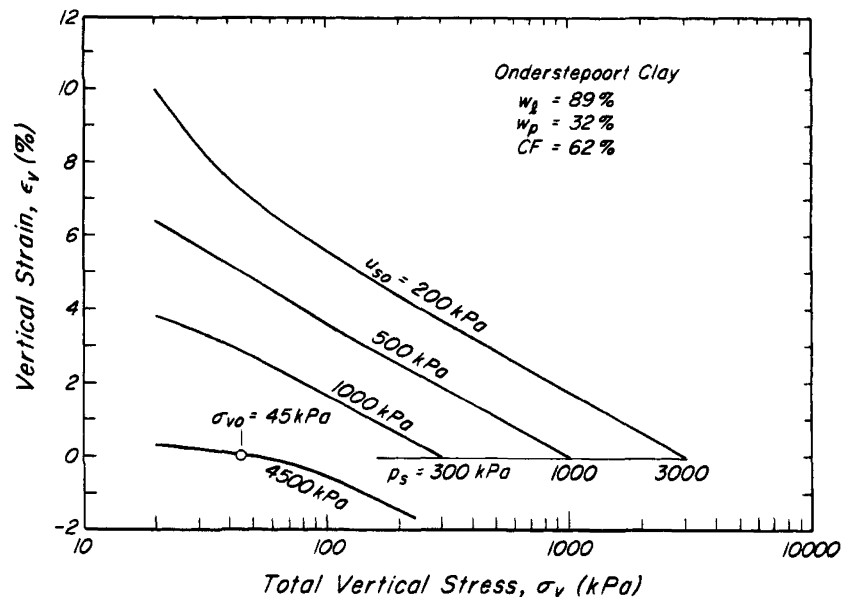


**Figure 16.24** Relation between vertical strain and vertical stress  $\sigma_v$  at different values of suction for Onderstepoort clay (data from Meintjes 1992).

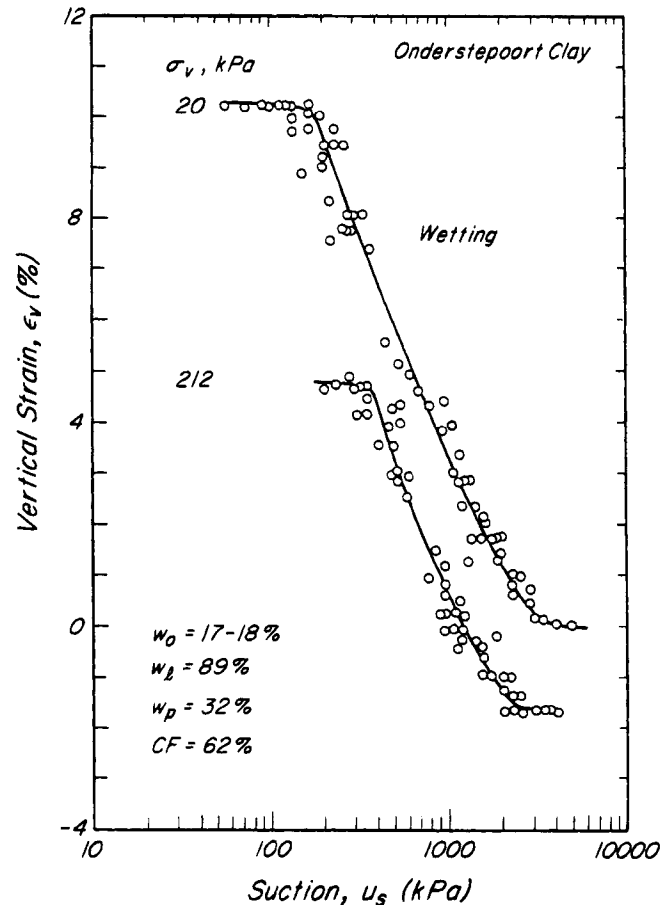


**Figure 16.25** Swelling of Onderstepoort clay showing a condition of limiting heave upon wetting (data from Meintjes 1992).

and pressure rather than as a single value of a swelling pressure. The swelling pressure  $p_s$  (mob) may be significantly smaller than the swelling pressure  $p_{si}$  measured at the initial void ratio of an undisturbed specimen, as shown by the relation (Mesri et al. 1994)

$$p_s (\text{mob}) = p_{si} \exp\left(-2.3 \frac{\epsilon - \epsilon_i}{C_{ss}}\right) \quad (16.23)$$

where  $\epsilon$  is the volumetric strain, for a particular excavation-support situation, of the ground around the stiff support with respect to the preconstruction void ratio, and  $\epsilon_i$  is the volumetric strain of the specimen starting from the same void ratio. The volumetric strain around the excavation may develop as a result of opening of fissures, joints, and cracks during excavation and may increase further if the support is compressible. In most field excavation-support construction,  $\epsilon$  is greater than  $\epsilon_i$  of an undisturbed specimen; therefore  $p_s$  (mob) is significantly less than  $p_{si}$ . Most swelling pressure measurements are carried out on submerged specimens. The data in Fig. 16.25 show that significantly smaller swelling pressures may be mobilized in the field if the expansive soil is not flooded and some suction remains in the soil.

### Problems

1. A wide fill will apply a uniform pressure of 100 kN/m<sup>2</sup> to the surface of a soil profile consisting of 3 m of weathered clay ( $\gamma = 17.6$  kN/m<sup>3</sup>,  $e_o = 1.2$ ,  $C_c = 0.5$ ,  $\sigma'_p/\sigma'_{vo} = 5$ ,  $C_r/C_c = 0.2$ ) over 7 m of marine clay ( $\gamma = 16.0$  kN/m<sup>3</sup>,  $e_o = 1.8$ ,  $C_c = 1.5$ ,  $\sigma'_p/\sigma'_{vo} = 1.8$ ,  $C_r/C_c = 0.1$ ) over 5 m of lacustrine clay ( $\gamma = 16.3$  kN/m<sup>3</sup>,  $e_o = 1.7$ ,  $C_c = 1.2$ ,  $\sigma'_p/\sigma'_{vo} = 1.0$ ,  $C_a/C_c = 0.05$ ) over granular till. The water table is 3 m below ground surface. Compute settlement resulting from primary consolidation of: (a) weathered clay and (b) marine clay. Compute settlement resulting from consolidation of the lacustrine clay after 50 years assuming that primary consolidation is completed in 14 years.

Ans. 7 cm; 53 cm; 68 cm.

2. A soil profile consists of 10 m of sand ( $\gamma = 17.6$  kN/m<sup>3</sup>) over 3 m of soft clay ( $\gamma = 17.3$  kN/m<sup>3</sup>,  $e_o = 1.6$ ,  $C_c = 1.3$ ,  $\sigma'_p/\sigma'_{vo} = 1.3$ ,  $C_r/C_c = 0.2$ ) over gravel. The water table is 3 m below the ground surface and a hydrostatic condition exists throughout the soil profile. Before constructing a structure at the site, the clay layer is preconsolidated by lowering the water table by 3 m and pumping from the gravel layer at such a rate that piezometric head in the gravel drops by 6 m. Compute the settlement resulting from primary consolidation of the clay layer assuming that pumping continues for a long time.

Ans. 8 cm.

3. The soil profile at a site consists of 2.5 m of sand ( $\gamma = 20 \text{ kN/m}^3$ ) over 3 m of soft clay ( $\gamma = 15 \text{ kN/m}^3$ ,  $e_o = 2.1$ ,  $C_c = 1.2$ ,  $\sigma'_p/\sigma'_{vo} = 1.5$ ,  $C_r/C_c = 0.1$ ,  $C_\alpha/C_c = 0.04$ ) over coarse sand. The ground water table is 2 m below the ground surface. Before construction of a structure at the site, a 3-m-thick fill ( $\gamma = 20 \text{ kN/m}^3$ ) is placed over a 10-hectare area. After the placement of the fill, the ground water table is expected to rise by 1.5 m. Compute settlement (a) resulting from the primary consolidation of the soft clay and (b) after 30 years assuming that primary consolidation is completed in 280 days.

Ans. 14 cm; 21 cm.

4. A 3-m-thick wide fill ( $\gamma = 19 \text{ kN/m}^3$ ) is placed over a soil profile consisting of 6 m of plastic clay ( $\gamma = 16 \text{ kN/m}^3$ ,  $e_o = 1.7$ ,  $C_c = 1.2$ ,  $\sigma'_p/\sigma'_{vo} = 1.4$ ,  $C_r/C_c = 0.15$ ) over 10 m of organic silt ( $\gamma = 16 \text{ kN/m}^3$ ,  $e_o = 1.2$ ,  $C_c = 0.8$ ,  $\sigma'_p/\sigma'_{vo} = 1.0$ ,  $C_r/C_c = 0.1$ , and  $C_\alpha/C_c = 0.06$ ) over dense sand. The water table is at the surface of the plastic clay. Compute the settlement resulting from: (a) primary consolidation of the plastic clay, and (b) consolidation of organic silt after 30 years assuming that primary consolidation is completed in 7 years.

Ans. 153 cm; 112 cm.

5. A 3-m-thick wide granular fill ( $\gamma = 20 \text{ kN/m}^3$ ) is to be placed on a site with a soil profile consisting of a 5.5 m clayey silt layer ( $\gamma = 17.8 \text{ kN/m}^3$ ,  $e_o = 1.25$ ,  $C_c = 0.5$ ,  $\sigma'_p/\sigma'_{vo} = 5.2$ ,  $C_r/C_c = 0.15$ ) over 11.5 m of silty clay ( $\gamma = 17.1 \text{ kN/m}^3$ ,  $e_o = 1.48$ ,  $C_c = 1.66$ ,  $\sigma'_p/\sigma'_{vo} = 1.4$ ,  $C_r/C_c = 0.10$ , and  $C_\alpha/C_c = 0.037$ ) over granular till. The water table is at the ground surface. Compute the settlement resulting from: (a) primary consolidation of the clayey silt and (b) compression of the silty clay after 100 years assuming that primary consolidation is completed in 30 years.

Ans. 20 cm; 94 cm.

### Selected Reading

- Lea, N. D. and C. O. Brawner (1963). "Highway design and construction over peat deposits in lower British Columbia," *Highway Research Record*, No. 7, pp. 1–32.
- Bjerrum, L. (1967). "Engineering geology of normally consolidated marine clays as related to settlement of buildings," *Géot.*, **17**, No. 2, pp. 83–118.
- Olson, R. E. and G. Mesri (1970). "Mechanisms controlling the compressibility of clays," *J. Soil Mech. and Found. Eng.*, ASCE, **96**, No. 6, pp. 1863–1878.
- Mesri, G., A. Rokhsar, and B. F. Bohor (1975). "Composition and compressibility of typical samples of Mexico City clay," *Géot.*, **25**, No. 3, pp. 527–556.
- Mesri, G., K. Adachi, and C. R. Ullrich (1976). "Pore pressure response in rock to undrained change in all-round stress," *Géot.*, **25**, No. 2, pp. 317–330.
- Mesri, G. and P. M. Godlewski (1977). "Time- and stress-compressibility interrelationship," *J. Geotech. Eng.*, ASCE, **103**, No. 5, pp. 417–430.
- Mesri, G. and Y. K. Choi (1985b). "The uniqueness of the End-Of-Primary (EOP) void ratio-effective stress relationship," *Proc. 11th Int. Conf. on Soil Mech. and Found. Eng.*, San Francisco, **2**, pp. 587–590.
- Mesri, G. (1987). "Fourth law of soil mechanics: A law of compressibility," *Proc. of Int. Symp. on Geotech. Eng. of Soft Soils*, Mexico City, **2**, pp. 179–187.
- Mesri, G. and A. Castro (1987). "The  $C_\alpha/C_c$  concept and  $K_o$  during secondary compression," *J. Geotech. Eng.*, ASCE, **112**, No. 3, pp. 230–247.
- Mesri, G. and T. W. Feng (1991). "Surcharging to reduce secondary settlement," *Proc. Int. Conf. on Geotech. Eng. for Coastal Development—Theory to Practice*, Yokohama, **1**, pp. 359–364.
- Mesri, G. and T. M. Hayat (1993b). "The coefficient of earth pressure at rest," *Canadian Geotech. J.*, **30**, No. 4, pp. 647–666.
- Mesri, G., M. C. Pakbaz, and A. F. Cepeda-Diaz (1994). "Meaning, measurement and field application of swelling pressure of clay shales," *Géot.*, **44**, No. 1, pp. 129–145.
- Mesri, G., and M. Shahien (1994). "Foundations on expansive soils," *Keynote Lecture, 2nd Geotech. Eng. Conf.*, Cairò, **2**, 138–171.
- Mesri, G., T. D. Stark, M. A. Ajlouni, and C. S. Shen (1997). "Secondary compression of peat with and without surcharging," *J. Geotech. Eng.*, ASCE, **123**, No. 5.

## ARTICLE 17 STRESS, STRAIN, AND FAILURE IN SOILS

### 17.1 Introduction

If the settlement of a foundation is due chiefly to the consolidation of strata of soft soil located between layers of relatively incompressible material, it can be computed or estimated as explained in Article 16. However, this procedure is valid only if the horizontal deformation of the compressible layers is negligible in comparison with the vertical deformation. Otherwise local application of load causes a deformation of the soil mass in every direction. The stress-strain properties that determine the deformation are too complex to be expressed in simple equations of general applicability. They are best investigated by laboratory tests on undisturbed samples subjected to initial stresses and subsequent stress changes comparable with those in the field. Many other problems in applied soil mechanics require similar investigations; these include changes in earth pressure against retaining walls caused by movement of the walls, the magnitude and distribution of loads in the supports in braced open cuts, and the deformation of embankments and their foundations.

Furthermore, if the stresses reach certain critical values, the soil will fail. In a few instances, tensile stresses may cause cracks that may be of practical importance, but in most engineering problems only the resistance to shear requires consideration. It governs, for example, the stability of foundations and dams, as well as the stability of slopes and the behavior of landslides. The complexity of the stress-deformation-failure properties of soil, as compared with those of most structural materials, is exacer-



bated by the influence of pore pressure. This influence must be taken into account in the laboratory tests used to investigate soil behavior.

All laboratory tests for determining stress, strain, and strength of soils are conducted in two steps. In the first step, an initial stress condition, preferably similar to the preconstruction condition existing in the field, is established in the soil specimen. For example, before an embankment is constructed on a soft clay deposit with a level ground surface, each soft clay element exists under an effective vertical stress  $\sigma'_{vo}$ , effective horizontal stresses  $K_o\sigma'_{vo}$ , and a hydrostatic porewater pressure  $u_o$ . To determine the stress-strain and strength characteristics of the soft clay to be used in evaluating its response to the embankment construction, an undisturbed cylindrical specimen may be placed in a triaxial apparatus (Article 17.2) and subjected in the first step to a vertical axial stress equal to  $\sigma'_{vo} + u_o$ , a horizontal radial stress equal to  $K_o\sigma'_{vo} + u_o$  and a porewater pressure  $u_o$ . In this manner the *in situ* stress and porewater pressure conditions are reestablished in the laboratory specimen before the second and main step of the test. The porewater pressure  $u_o$  during the first step may be imposed to maintain the *in situ* degree of saturation and to minimize oxidation-related biochemical aging of the specimen (Lessard 1982). As a second example, an element of saturated sand beneath a level ground surface also exists under a  $\sigma'_{vo}$ ,  $K_o\sigma'_{vo}$ , and  $u_o$  condition before seismic shear stresses are imposed by an earthquake. Therefore, an undisturbed specimen in a direct simple shear apparatus (Article 17.3.3) may also be subjected in the first step to a vertical axial stress equal to  $\sigma'_{vo}$ . In this apparatus, however, the radial stress cannot be controlled, and it is not a simple matter to impose a porewater pressure. Moreover, it is assumed that the radially constrained application of  $\sigma'_{vo}$  in the direct simple shear apparatus develops an effective radial stress approximately equal to  $K_o\sigma'_{vo}$ , and that the absence of  $u_o$  does not significantly influence the behavior of the saturated sand during the second step.

To overcome the limitations of apparatus or to simplify the testing procedure, a stress and porewater pressure condition approximating but not identical to the *in situ* condition is often imposed in the first step. In the triaxial apparatus, the *in situ* stress condition is often approximated by a mean stress, and the soil specimen is subjected to an equal all-around pressure equal to  $\sigma'_{vo} (1 + 2 K_o)/3$ . In a direct simple shear test, sand specimens from an embankment dam are often subjected to a normal stress, and the *in situ* shear stresses existing in the embankment before seismic shaking are ignored. In a similar simplification, in the first step of a direct shear test (Article 17.3.2), a specimen of stiff clay from a shear zone in a natural slope is subjected only to a normal stress, and the shear stresses are ignored that exist in the slope even

before an excavation or toe failure imposes additional shear stresses that cause a landslide.

During the first step of most tests, drainage is permitted, and the specimen is free to expel or take in water. Such a test is called *consolidated*. This terminology, however, is somewhat misleading. For example, when the *in situ* stress condition is reimposed on an *ideally undisturbed specimen*, even when drainage is permitted, the specimen should not experience volume change (Article 11.3.8). Nevertheless, some consolidation may occur during the first step of such a test; it reflects either the undesirable effects of sample disturbance or imposed values of  $\sigma'_{vo}$  and  $K_o\sigma'_{vo}$  that do not correspond to the actual *in situ* condition, or both. Thus, in this particular usage, the term *consolidated* refers to restoration of the state of consolidation of the soil that existed *in situ* before sampling and not to the undesirable volume changes that may take place during the first step of the test.

In some tests, drainage is not permitted during the first step and the test is called *unconsolidated*. This terminology is also misleading, because all soil specimens, whether undisturbed or reconstituted, have experienced consolidation in one form or another to attain the consistency of a soil before they were set up in a shear apparatus. Thus, the terminology *unconsolidated* refers only to the drainage condition during the first step of the test and not to the true consolidation condition of the soil specimen.

For analyses of some practical problems, the stress-strain properties and strength of the soil are required at consolidation stresses different from those existing in the preconstruction *in situ* condition. For example, when an embankment is constructed in stages on a soft clay deposit, deformation and stability analyses of the second stage require knowledge of the stress-strain properties and strength of the clay after consolidation under the first stage. To evaluate the behavior of an earth dam, the stress-strain characteristics and strength of each compacted layer are required after the layer is subjected to the overburden of subsequent lifts. Information on shear strength may be required either in terms of effective stresses before shear (consolidation stresses) or in terms of effective stresses at a failure condition. To obtain this type of information, several soil specimens are subjected to different consolidation pressures in the first step. The range of consolidation pressure or of effective stress at failure should correspond as closely as practicable to that expected in the full-scale field situation. After each increment of pressure, primary consolidation and less than a half-cycle of secondary compression should be allowed. Large secondary compression of soft clays, silts, and loose sands should be avoided, especially when relationships are being developed between consolidation pressure and small-strain undrained modulus or undrained shear strength, because secondary consolidation has the effect of increasing the consolidation pressure. This increase

can be estimated by means of the empirical relation  $\sigma'_c = \sigma' (t/t_p)^{C_\alpha/C_c}$  (Mesri and Choi 1979), where  $\sigma'_c$  is the consolidation pressure that determines the undrained modulus and the undrained strength that will be measured in the second step,  $\sigma'$  is the imposed consolidation pressure under which secondary consolidation takes place,  $t_p$  is the duration of primary consolidation,  $t$  is the total duration of the pressure increment, and  $C_\alpha/C_c$  is defined in Article 16.7. For example, if a specimen of soft clay is subjected in the first step of a direct simple shear test to  $\sigma'_v = 100$  kPa in the compression range, and if primary consolidation is completed in 120 min but the consolidation pressure is maintained for 24 h, then a value of  $C_\alpha/C_c = 0.04$  leads to  $\sigma'_c = 110$  kPa. Thus, the undrained modulus and undrained strength measured in the second step would correspond to a consolidation pressure of 110 kPa rather than 100 kPa.

It is not possible to perform the first step in most *in situ* tests for determining the stress-strain properties and strength of soils. The initial effective stress condition is already established, and it is generally difficult to alter the consolidation stress condition in the field. The volume changes or porewater pressure changes that may precede the main step of *in situ* tests are undesirable consequences of soil disturbance during the insertion of the vane, pressuremeter, or other device.

The second step in the testing procedure is intended to simulate or represent a natural or construction-related process that subjects the soil to changes in shear stresses. Various modes of shear that may be encountered under full-scale field conditions are approximated by using different types of apparatus and methods of application of shear stress. Either increments or decrements of stress are imposed on the specimen and deformations are measured, or a deformation is imposed (often at a constant rate) on the specimen and the resulting changes in stress are measured. A test of the former type, which is carried out under *stress control*, is more realistic, but the latter, which is under *strain control*, is more convenient.

All soils tend to experience volume change when they are subjected to changes in shear stress (Articles 15.5, 18.2). If, during the second step, the soil specimen is able to experience volume change throughout the shearing process, the test is called *drained*. A drained second step must be preceded by a *consolidated* first step. If, on the other hand, volume changes are prevented during the second step, the test is called *undrained*. An undrained second step may follow either a *consolidated* or *unconsolidated* first step. When drainage is prevented, the tendency for volume change leads to shear-induced porewater pressures (Articles 15.5, 18.2).

Drained and undrained tests, respectively, attempt to duplicate fully drained and fully undrained shearing conditions in the field. Drained tests are usually carried out on soils that in the field respond in *drained* fashion to

typical natural and construction-related shearing processes. For example, permeable granular soils, with the exception of saturated sands subjected to dynamic loading, display a drained response to most natural and man-made events (Article 19.1). Critical instability conditions in stiff clays and shales also develop most often in a drained condition (Article 19.2). Therefore, drained tests are most appropriate for granular soils and stiff clays and shales. On the other hand, soft clays and silts in most shearing situations (Article 20.1) and loose saturated sands subjected to dynamic shearing (Article 20.9) display an undrained response. Therefore, undrained tests are most often used for soft clays and silts and for dynamic cyclic shearing of saturated loose sands.

A fully drained test is one during which no shear-induced porewater pressures develop in the specimen. This condition is achieved by applying shear stresses at such a rate that shear-induced volume changes have an opportunity to take place. That is, the shear stresses are applied at a rate slow enough to allow water to flow into or out of the specimen in response to dilative or contractive tendencies, respectively. Porewater pressures are rarely measured in drained tests; the drained condition is ensured by selecting an appropriate shearing rate such that no appreciable porewater pressures are developed within the specimen. The estimate of the imposed rate of shear is based on an application of the Terzaghi theory of consolidation (Article 25) to the dissipation of shear-induced excess porewater pressures (Bishop and Henkel 1962, Bishop and Gibson 1963). It is important that a test categorized as drained should actually be drained, because in the interpretation of the test results, shear-induced porewater pressure is assumed to be zero.

Two factors must be considered in selecting the rate of shear for undrained tests: (a) undrained stress-strain properties and strength are dependent on the rate of shearing and (b) shear strains and associated shear-induced porewater pressure distributions in most laboratory specimens are not uniform. Both the undrained modulus and undrained shear strength decrease with a decrease in the rate of shearing, because the soil structure creeps under sustained shear stresses. Therefore, the imposed shearing rate should correspond to a widely used standard rate. For example, correction factors for strain rate or time to failure, applied to the undrained strength measured in laboratory tests to obtain the field strength, correspond to standard rates of shear (Article 20.6). Only the first factor (a) is considered in selecting the imposed rate of shear, unless shear-induced porewater pressures must be measured for defining the effective stress path to failure and the undrained shear strength in terms of the effective stress condition at failure. The second factor (b) requires consideration in most laboratory tests, because boundary effects cause the soil specimen to experience nonuniform deformation, and the resulting shear-induced porewater

pressures are not uniform throughout the specimen. The porewater pressure measurements should be made near the center of the soil specimen where deformations are largest. However, the porewater pressures are often measured at the boundaries of the specimen where, as a result of boundary constraints, the deformations are smaller. To avoid the error, the imposed shearing rate must be slow enough to permit porewater pressure equalization between the shear zone and the boundaries of the specimen. The appropriate imposed rates of deformation for complete porewater pressure equalization are also estimated by an application of the Terzaghi consolidation theory (Bishop and Henkel 1962, Blight 1963).

In summary, the imposed shearing rates for undrained tests without porewater pressure measurements are standard rates that allow measurement of undrained stress-strain properties and of undrained strength. In undrained tests with shear-induced porewater pressure measurements, the imposed shearing rate must allow complete porewater pressure equalization for accurate measurement of shear-induced porewater pressures in the shear zone.

Undrained tests with porewater pressure measurement often include a pressure saturation step between the first and second steps. In this intermediate step, a porewater pressure is imposed on the specimen without changing the effective stress condition. One reason for this step is to subject the fluid in the sample and in the drainage connections to a pressure (often referred to as *back pressure*) sufficient to compress and dissolve any air that might be present, and thus to decrease the compressibility of the system and obtain rapid porewater pressure response during the second step. A second reason is that an initial back pressure allows measurement of negative porewater pressures generated in dilatant soils, without in fact subjecting the pore water to tension, which may cause formation of vapor bubbles, or *cavitation*, at about  $-100$  kPa. For proper measurement of shear-induced porewater pressures in the second step, dilatant soils are subjected to a back pressure no less than the maximum negative shear-induced porewater pressure expected during the test.

## 17.2 Triaxial Apparatus and Procedure

In a triaxial test a cylindrical specimen of soil, typically 38 mm or more in diameter and with a height to diameter ratio of 2, is subjected to an equal all-around pressure, known as the *cell pressure*, in addition to an axial stress that may be varied independently of the cell pressure. The axial stress may be positive or negative. If it is positive, the test is a *triaxial compression* (TC) test; if negative, a *triaxial extension* (TE) test.

The basic features of typical triaxial apparatus are shown diagrammatically in Fig. 17.1. The cylindrical sur-

face of the sample is covered by a rubber membrane sealed by rubber O-rings to a pedestal at the bottom and to a cap at the top. The assemblage is contained in a chamber into which cell fluid may be admitted under any desired pressure; this pressure acts laterally on the cylindrical surface of the sample through the rubber membrane and vertically through the top cap. The additional axial stress is applied by means of a piston passing through a frictionless bushing at the top of the chamber. A test may be carried out under *stress control*, in which the axial stress is increased or decreased as determined arbitrarily by the operator, or under *strain control*, in which a predetermined rate of axial deformation is imposed and the axial stress required to maintain the rate of deformation is observed. In either test the vertical deformation of the sample is measured.

A porous disk is placed against the bottom of the sample and is connected to the outside of the chamber by tubing. By means of this connection, the pressure in the water contained in the pores of the sample can be measured if drainage is not allowed. Alternatively, flow may be permitted through the connection and the quantity of water passing into or out of the sample measured.

In the first step of a triaxial test, the soil specimen is subjected either to a uniform all-around cell pressure or to an axial stress greater than the radial stress. To achieve the latter condition, an axial stress in addition to the uniform all-around cell pressure is imposed on the specimen. In *consolidated* tests, the final consolidation stress condition is reached in increments with pressure increment ratios equal to or less than one. The specimen is allowed to consolidate or swell freely until the imposed axial and radial stresses are carried entirely by effective stresses within the specimen. Pressure increment ratios of less than one are required particularly for tests in which the axial stress differs from the radial stress, e.g., to reestablish the *in situ*  $\sigma'_{vo}$ ,  $K_0\sigma'_{vo}$  stress condition in a soft clay specimen. The increments of axial stress and radial stress are kept small enough to avoid undrained shear strains or to minimize radial strains.

In drained tests or undrained tests without porewater pressure measurements, the second step directly follows the first step. However, in undrained triaxial tests with porewater pressure measurements, the soil specimen is *back-pressured* before the second step. With drainage prevented, the cell pressure is increased by an increment, and if the soil is fully saturated, a porewater pressure of equal magnitude should be measured (Article 15.5.1). Thus, the second step starts with the effective stress condition established during the first step, plus an initial porewater pressure.

Triaxial tests with stress control are desirable as they more closely simulate the actual field conditions. However, triaxial tests with strain control are more common, because the procedure is easier and the interpretation of

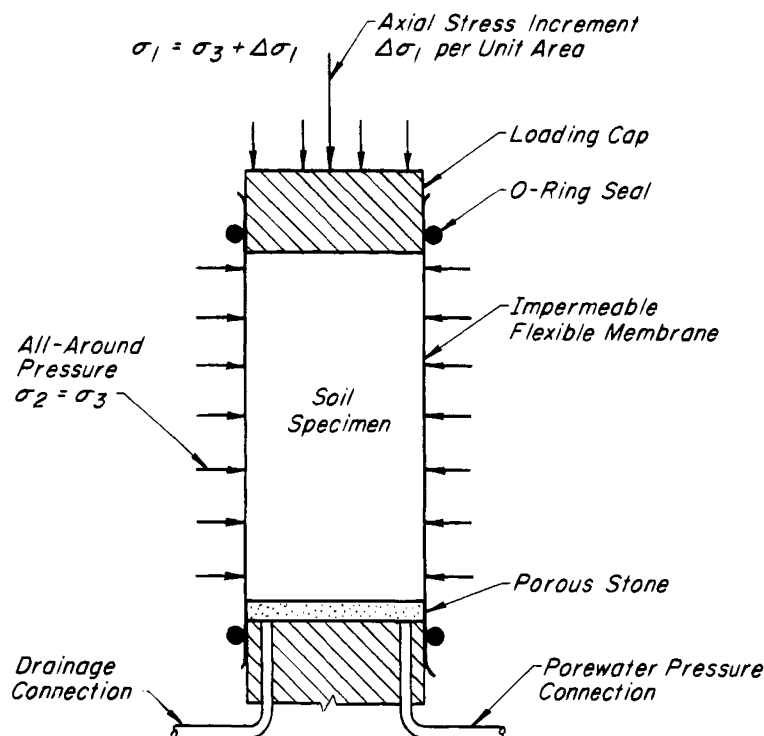


Figure 17.1 Soil specimen in a triaxial test.

results is more straightforward. In a triaxial compression test, the specimen is subjected, at a constant cell pressure, to a constant rate of axial compression, and the resulting imposed axial stress is measured with a proving ring or a load cell. The axial deformation is measured by a dial gage. In a triaxial extension test, the specimen is subjected to axial extension while the cell pressure is kept constant. Axial deformation is continued until a failure condition or failure conditions are reached. For example, in an undrained triaxial compression test, axial compression is imposed until a yield strength at small axial strain and then a postyield, large-strain strength at an axial strain of about 10% are measured (Article 18.2.2). In a drained triaxial compression test on a dense sand, axial compression is imposed until maximum strength and then ultimate strength are reached.

In triaxial tests in which the cell pressure is kept constant, the total radial stress during the second step is equal to the radial stress at the end of the first step. In drained tests, the effective radial stress during the second step is equal to the effective radial stress at the end of the first step. In consolidated undrained triaxial tests, the effective radial stress during the second step is equal to the effective radial stress at the end of first step minus the shear-induced porewater pressure, which may be positive or negative.

In drained triaxial tests, the effective axial stress during the second step is equal to the effective axial stress at the end of first step plus the axial stress imposed during

the second step,  $\Delta\sigma_a$ , which is positive for compression tests and negative for extension tests. In undrained triaxial tests, the effective axial stress during the second step is equal to the effective axial stress during the first step plus or minus  $\Delta\sigma_a$ , for compression or extension, respectively, minus the shear-induced porewater pressure, which may be positive or negative. In undrained triaxial compression or extension tests in which shear-induced porewater pressure is not measured, the effective stress condition at the beginning of the second step together with the axial stress change  $\Delta\sigma_a$  during the second step, at both yield and large strain, define the undrained stress-strain characteristics and the strength as a function of the consolidation pressure.

Because the cylindrical specimen in the triaxial cell is surrounded by a thin flexible membrane that is subjected to a uniform cell fluid pressure, the radial boundary of the specimen is free of shear stresses; shear stresses that may develop at the top and bottom boundaries of the specimen are ignored. Thus, the vertical and horizontal planes in a triaxial specimen are considered to be principal planes. For example, in a drained triaxial compression test on a specimen consolidated under an equal all-around pressure, the minor and intermediate principal planes are vertical and the major principal plane is horizontal. At the end of the first step,  $\sigma'_1 = \sigma'_2 = \sigma'_3 = \text{cell pressure}$ . During the second step,  $\sigma'_2 = \sigma'_3 = \text{cell pressure}$ , and  $\sigma'_1 = \text{cell pressure plus the axial stress } \Delta\sigma'_1 \text{ imposed during the second step}$ . Therefore,  $\Delta\sigma_1 = \sigma'_1 - \sigma'_3 =$

$\sigma_1 - \sigma_3$ . During the second step in an undrained triaxial compression test on a specimen consolidated under an equal all-around pressure,  $\sigma'_2 = \sigma'_3 =$  cell pressure at the end of the first step minus the shear-induced porewater pressure, and  $\sigma'_1 = \sigma'_3$  during the second step plus  $\Delta\sigma_1$ . Thus,  $\Delta\sigma_1 = \sigma'_1 - \sigma'_3 = \sigma_1 - \sigma_3$ . Therefore, for drained and undrained triaxial tests on specimens that are subjected during the first step to an equal all-around pressure, the axial stress imposed during the second step is called the *principal stress difference* or *stress difference*.

### 17.3 Other Laboratory Shear Tests

Although the triaxial test is widely used for investigating the shear strength of soils, it has several limitations that restrict its applicability to certain types of problems. It is, moreover, a relatively expensive test to perform. Consequently, several other kinds of equipment are used for routine subsurface investigations or for determining the shear strength under conditions to which the triaxial test is unsuited. In the first category are the unconfined compression test and the direct shear test; in the second are simple shear tests, ring- and torsion-shear tests, reversal direct shear tests, and several forms of cyclic shear tests. A brief description of the equipment and procedure for these tests is presented before the discussion in Article 18 of the shear strength characteristics of soils.

#### 17.3.1 Unconfined Compression Test

The unconfined compression (UC) test is used widely to determine the consistency of saturated clays and other cohesive soils (Article 7.1). A cylindrical vertical specimen with a height-to-diameter ratio of about 2 and typically 38 mm or more in diameter is set up between end plates. A vertical load is applied incrementally at such a rate as to produce a vertical strain of about 1 to 2% per minute. This rate is so rapid relative to the drainage of the sample that there is no time for significant volume change in spite of the absence of a membrane to seal the sample. The unconfined compressive strength is considered to be equal to the load at which failure occurs, or at which the axial strain reaches 20% if there is no sudden failure, divided by the cross-sectional area of the sample at the time of failure. The significance of the test is discussed in Article 20.7.

The unconfined compression test is a special case of the *unconsolidated-undrained* (UU) triaxial test, in which the sample is enclosed in a membrane, placed in the triaxial apparatus, and subjected to a confining pressure. The axial load is then increased. No drainage is permitted from the sample under the influence of either the confining pressure or the axial stress. As compared to the unconfined compression test, the UU test reduces the likelihood of a premature failure along a defect such as a fracture in the sample.

#### 17.3.2 Direct Shear Test

The oldest method for investigating the shearing resistance of soils is the *direct-shear test* (DS). It is performed by means of the apparatus illustrated in Fig. 17.2. The apparatus consists of an upper box that is stationary and a lower one that can be moved in a horizontal direction. The specimen is located between two porous stones that serve as drains during the first and second steps of the test. The surfaces of contact between the sample and the porous stones are grooved, as shown in the figure, to prevent slippage between sample and stones during shear. Because drainage is not readily controlled, the direct shear apparatus is most suitable for consolidated-drained tests, especially on granular soils and stiff clays and shales. Because the specimen is confined by the rigid upper and lower shear boxes, volume changes of the specimen during both the first and second steps are measured by a vertical deformation dial gauge in contact with the upper porous stone.

In the first step, a vertical load  $\sigma$  per unit of area is applied to the upper stone and is maintained long enough that the vertical load is carried entirely by effective vertical stresses within the specimen. This is accomplished by reading the vertical deformation dial with time and interpreting the progress of consolidation as for an oedometer test (Articles 16 and 25). In the second step, the lower box is subjected to a constant rate of horizontal displacement, and the imposed horizontal shear force  $\tau$  per unit of area is measured by a proving ring or load cell that keeps the upper box stationary. The lower box is displaced at such a rate that no appreciable shear-induced porewater pressures develop during the second step. This rate is determined by the same approach as that used to estimate the rate of axial deformation for drained triaxial tests (Article 17.2). The shear-induced volume changes as a function of shear displacement are measured with the vertical deformation dial gauge.

A main advantage of the direct shear test is that a clay or shale specimen can be oriented to measure the shear strength along a plane of weakness. This capability is most suitable for testing presheared or precut stiff clay, shale, or rock specimens in which the shearing resistance along a plane of discontinuity is required. Also, the shearing resistance after a large shear displacement can be measured by using the reversing direct shear method in which the direction of shearing is reversed several times to accumulate large shear displacement along a plane of discontinuity as occurs in a fault zone in the field. Another advantage of the direct shear test is that, because clay or shale specimens about 20 mm thick are commonly used, *consolidation* during the first step and a *drained* condition in the second step are achieved fairly rapidly.

The direct shear apparatus, however, has several inherent disadvantages. Foremost among these are the change

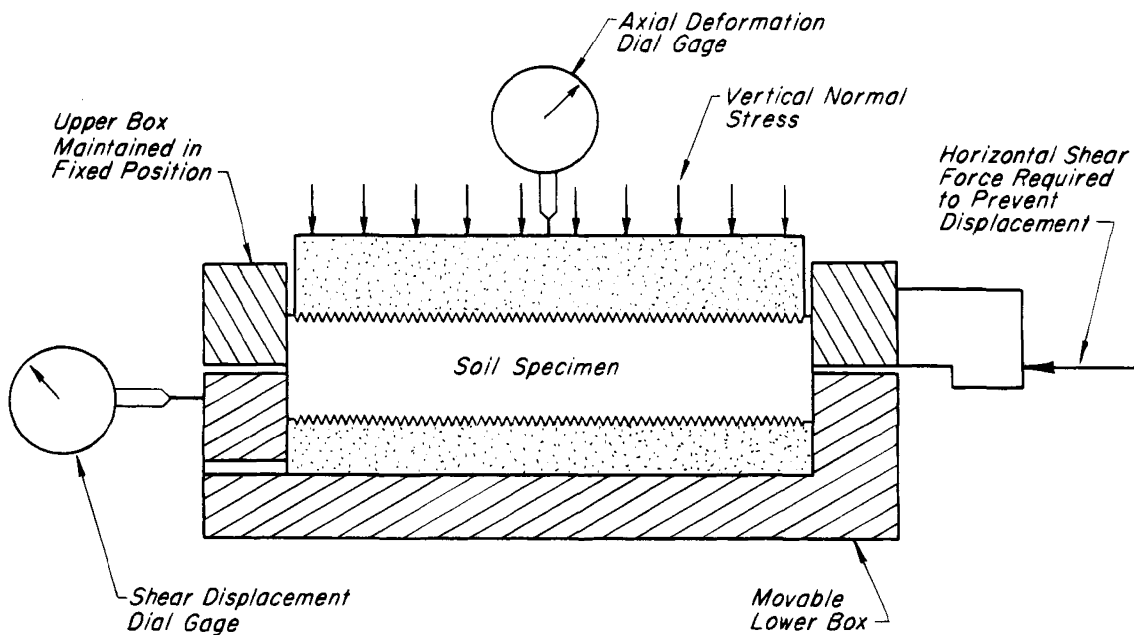


Figure 17.2 Soil specimen in a direct shear test.

in area of the surface of sliding as the test progresses, and the nonuniform distribution of shearing strains and shearing stresses over the potential surface of sliding. As the horizontal displacement of the lower box increases, the area of contact between the upper and the lower half of the sample decreases. This problem is minimized in typical direct shear tests by restricting the shearing displacement in each direction to about 5 mm and attaining large shear displacement by the reversing shear procedure. To avoid an area correction, direct shear test results may be interpreted in terms of the ratio  $\tau/\sigma'$  of shear force per unit area to effective normal force per unit area.

In a direct shear specimen, shear failure does not take place simultaneously at every point of the potential surface of sliding. Progressive failure (Article 17.4) starts at the two edges and proceeds toward the center (Roscoe 1953, Hvorslev 1960). Therefore, the peak value of the shearing resistance indicated by the test results is lower than the real peak value. Because the distribution of shearing strains is nonuniform and the thickness of the shear zone is not well defined, the magnitude of shear strain as a function of shear displacement is not known. Also, the principal directions are not known, and the principal stresses cannot be determined readily for the direct shear specimen (Hansen 1961). Although most of these disadvantages may be minimized by increasing the ratio of the length in the direction of shear to the thickness of the specimen (typical values of the ratio are 3 to 6), the most practical interpretation of common direct shear tests is in terms of the relationship between  $\tau/\sigma'$  and shear displacement.

### 17.3.3 Direct Simple Shear Test

The direct simple shear (DSS) was developed to simulate the conditions in a thin shear zone separating two essentially rigid masses that slide with respect to each other, a condition approached in some landslides that occur along a planar surface or along horizontal or gently inclined portions of a slip surface. The form of the apparatus developed by the Norwegian Geotechnical Institute (Bjerrum and Landva 1966) is shown diagrammatically in Fig. 17.3. The sample is contained in a cylindrical rubber membrane reinforced with a spiral winding of wire that prevents lateral deformation during consolidation under vertical loading but allows horizontal displacements during shear. Drainage is permitted through the top and bottom plates. The soil is sheared by moving the top plate horizontally at a constant rate, while the height of the specimen is kept constant by adjusting the vertical load. In this fashion the volume of the sample is kept constant. The change in vertical pressure required to maintain the constant volume is equal to the increase in shear-induced porewater pressure that would occur in an undrained test with constant vertical total stress (Dyvic et al. 1987). The peak horizontal shear stress is defined as the undrained shear strength.

The NGI direct simple shear apparatus is most suitable for undrained tests on soft clays and silts (Articles 18.3, 20.6). This apparatus also allows a close simulation in the laboratory of the stress-deformation conditions under level ground during an earthquake. Therefore, the cyclic direct simple shear test, including multidirectional shak-

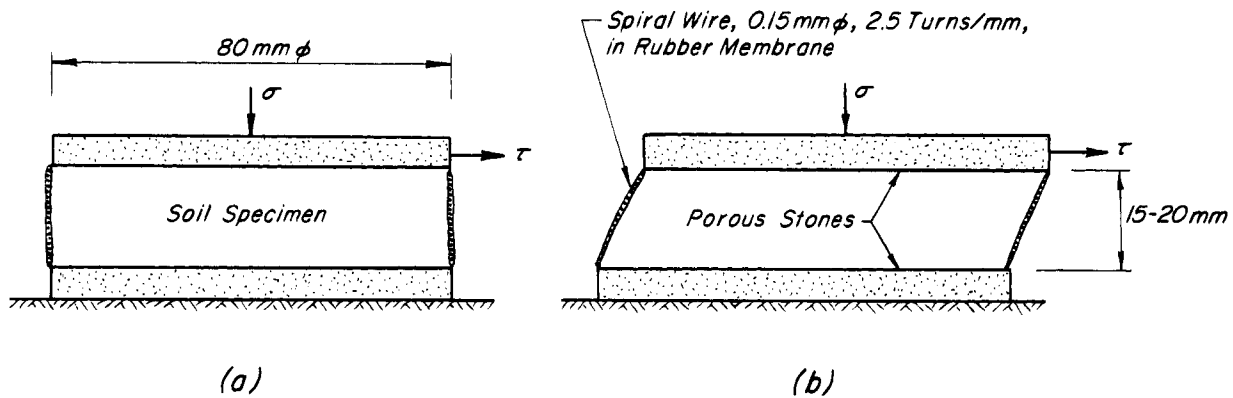


**Figure 17.3** Soil specimen in the NGI version of the direct simple shear apparatus (a) before shearing and (b) during shear.

ing, has been used to investigate the liquefaction characteristics of loose sands (Article 20.9). When the direct simple shear test is used to simulate undrained failure in sloping ground, during the first step the specimen is consolidated under a normal stress and a shear stress on the horizontal plane.

#### 17.3.4 Torsional Ring-Shear Test

All the foregoing tests lack the ability to investigate the shearing resistance of soils at very large strains or displacements; the reversing direct shear test (Article 17.3.2) leaves open the question whether the effect of many back-and-forth displacements is indeed equivalent to a unidirectional displacement of the same total magnitude. To investigate this question, the torsional *ring-shear apparatus* has been devised to permit shear-stress measurements over unlimited displacements (Hvorslev 1936, 1939, LaGatta 1970, Bishop et al. 1971, Bromhead 1979). A simplified section of the apparatus developed jointly by the Norwegian Geotechnical Institute and Imperial College is shown in Fig. 17.4. The soil specimen has the shape of a ring with a rectangular cross-section; the outside diameter, inside diameter, and thickness of the specimen are 152 mm, 102 mm, and 20 mm, respectively. The inside and outside of the specimen are confined by metal rings, and the top and bottom are in contact with annular porous ceramic plates with sharpened fins to minimize slip at soil-ceramic interfaces. In the first step, the specimen is subjected to an effective vertical stress. In the second step, the specimen is sheared by rotating the lower half while the upper half reacts against a torque arm, held in place by a proving ring at each end, that measures the tangential load. Failure occurs on the horizontal plane that passes through the boundary between the upper and lower confining rings. The average shear stress on the failure surface can be calculated with knowledge of the torque applied to the upper annular porous plate.

Torsional ring-shear apparatus is mainly suited for drained shear tests. Because of the extreme nonuniformity of strains and shear stresses, especially for specimens with high ratio of width of ring to mean diameter, the apparatus is suitable only for measurement of the residual shear strength of clays and shales (Article 19.2.3). Its only advantage over the direct shear test is that uninterrupted shear displacement of any magnitude can be readily achieved on the horizontal slip surface. Its many disadvantages include most of those of the direct shear apparatus. In addition, most torsional ring-shear apparatus are complex, and the preparation of ring-shaped undisturbed specimens, especially of fissured clays and shales, is very difficult. A simplified ring-shear apparatus has been developed by Bromhead (1979). This apparatus has been used successfully by Stark and Eid (1994) to measure the residual strength of reconstituted precut specimens of stiff clays and shales.

#### 17.3.5 Plane Strain Triaxial Test

Many civil engineering works have great lengths compared with their other dimensions. Hence, a large number of stability problems involving dikes, embankments and cuts for roads and railways, retaining walls, and strip footings approximate a plane strain condition in which no deformation occurs in the direction at right angles to the displacement. The three principal stresses acting at a point in the soil in plane strain may all have different values; the intermediate principal stress acts along the axis of zero deformation. Several devices have been constructed to investigate the influence of the plane strain condition and of the intermediate principal stress on the strength of soils (Wood 1958, Cornforth 1964). The equipment is complex and is not well suited to routine investigations, but the results of research are useful in modifying the strengths obtained from the conventional symmetrical triaxial test to plane strain situations in the field (Article

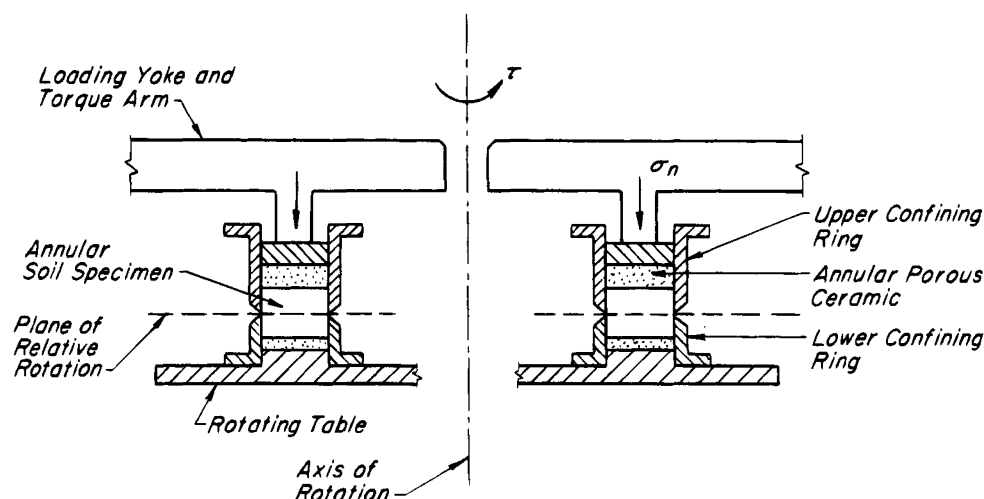


**Figure 17.4** Soil specimen in NGI-Imperial College ring shear apparatus (after Bishop et al. 1971).

19.1). Plane-strain specimens are of rectangular prismatic shape with a height to width ratio comparable to that of a triaxial specimen; the length, height, and width of the soil specimens in Cornforth's plane strain apparatus were 400 mm, 100 mm, and 50 mm, respectively. The sides of the sample were covered by a rubber membrane sealed to a pedestal at the bottom and to a rectangular cap at the top. An *end clamp* with facing plates in contact with the rubber membrane at the ends of the specimen prevented changes in the length of the specimen during shear. A thin coating of silicon grease was used between the membrane and end plates to minimize end friction. In the first step of a consolidated-drained test, for example, a specimen may be subjected to a vertical stress  $\sigma'_{vo}$  and a horizontal stress  $K_o \sigma'_{vo}$ . In the second step, while  $\sigma'_3 = K_o \sigma'_{vo}$  is kept constant by the cell pressure, a vertical stress increment  $\Delta \sigma_1$  is applied, and  $\Delta \sigma_2$  is measured with an instrumented end clamp. However, measuring  $\Delta \sigma_2$ , reducing end friction to a negligible value, and maintaining sufficient clearance between the top plate and side plates represent difficult experimental problems that can be solved only in apparatus intended for research.

#### 17.4 Mohr's Rupture Diagram and Coulomb's Failure Equation

Soils, like most solid materials, fail either in tension or in shear. Tensile stresses may cause the opening of cracks that, under some circumstances of practical importance, are undesirable or detrimental. In most engineering problems, however, only the resistance to failure by shear requires consideration.

Shear failure starts at a point in a mass of soil when, on some surface passing through the point, a critical combination of shearing and normal stresses is reached. Various types of equipment have been developed to deter-

mine and investigate these critical combinations. At present the most widely used is the triaxial apparatus described in Article 17.2. Because it is assumed that only principal stresses are applied to the boundaries of the specimen in this equipment, the state of stress on any other than principal planes must be determined indirectly.

According to the principles of mechanics, the normal stress and the shearing stress on a plane inclined at angle  $\alpha$  to the plane of the major principal stress and perpendicular to the plane of the intermediate principal stress (Fig. 17.5a) are determined by the following equations

$$\sigma' = \frac{1}{2}(\sigma'_1 + \sigma'_3) + \frac{1}{2}(\sigma'_1 - \sigma'_3) \cos 2\alpha \quad (17.1)$$

$$\tau = \frac{1}{2}(\sigma'_1 - \sigma'_3) \sin 2\alpha \quad (17.2)$$

These equations represent points on a circle in a rectangular system of coordinates (Fig. 17.5b) in which the horizontal axis is that of normal stresses and the vertical axis is that of shearing stresses. Similar expressions may be written for the normal and shearing stresses on planes on which the intermediate principal stress acts. The corresponding components of stress are represented by points on the dash circles plotted on the same axes in Fig. 17.5b. Because, in the usual triaxial compression test, the major principal stress acts in a vertical direction and the cell pressure represents both the intermediate and minor principal stresses, which are equal, we are generally concerned with only the outer circle associated with the major and minor principal stresses  $\sigma'_1$  and  $\sigma'_3$ . This is known as the *circle of stress*.

Every point, such as *D*, on the circle of stress represents the normal stress and shearing stress on a particular plane inclined at an angle  $\alpha$  to the direction of the plane of the major principal stress. From the geometry of the figure it can be shown that the central angle  $AO'D$  is equal to  $2\alpha$ .



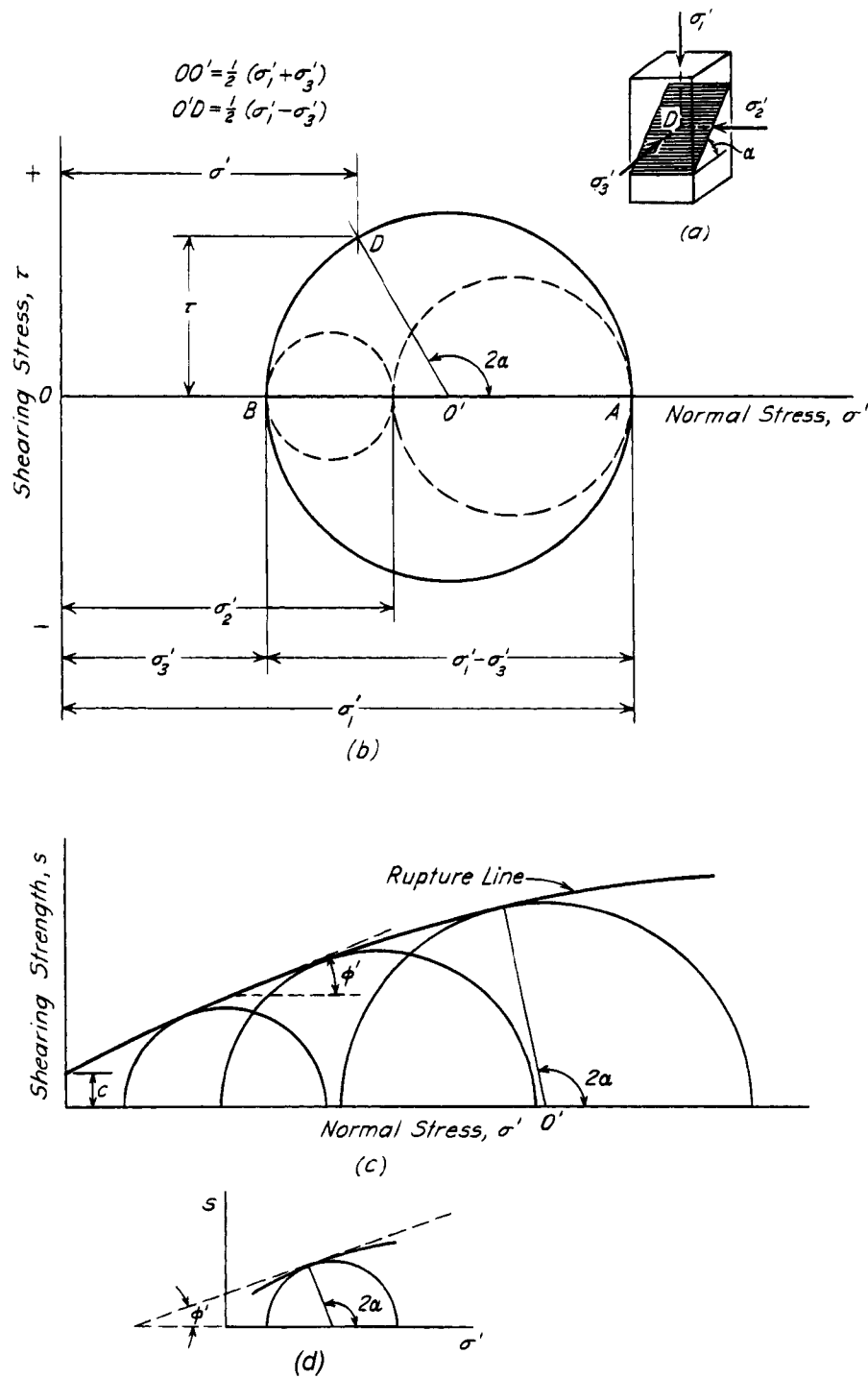


**Figure 17.5** Diagram illustrating Mohr's circle of stress and rupture diagrams. (a) Principal stresses and inclined plane on which normal and shearing stresses  $\sigma'$  and  $\tau$  act; (b) circle of stress; (c) rupture line from series of failure circles; (d) relation between angles  $\alpha$  and  $\phi'$ .

If the principal stresses  $\sigma'_1$  and  $\sigma'_3$  correspond to a state of failure in the specimen, then at least one point on the circle of stress must represent a combination of normal and shearing stresses that led to failure on some plane through the specimen. Moreover, if the coordinates of

that point were known, the inclination of the plane on which failure took place could be determined from a knowledge of the angle  $\alpha$ .

If a series of tests is performed and the circle of stress corresponding to failure is plotted for each of the tests,

at least one point on each circle must represent the normal and shearing stresses associated with failure. As the number of tests increases indefinitely, and if the material is homogeneous and isotropic, it is apparent that the envelope of the failure circles (Fig. 17.5c) represents the locus of points associated with failure of the specimens. The envelope is known as the *rupture line* for the given material under the specific conditions of the series of tests.

From the geometry of Fig. 17.5d it may be seen that for any failure circle

$$2\alpha = 90^\circ + \phi'$$

Therefore the angle between the plane on which failure occurs and the plane of the major principal stress is

$$\alpha = 45^\circ + \frac{\phi'}{2} \quad (17.3)$$

In general the rupture line for a series of tests on a soil under a given set of conditions is curved. However, a segment of the curve may be approximated by a straight line with the equation

$$s = c + \sigma' \tan \phi' \quad (17.4)$$

This expression is known as *Coulomb's equation*. In this equation the symbol  $\tau$ , representing shearing stress, is replaced by  $s$ , known as the *shearing resistance* or *shearing strength*, because points on the rupture line refer specifically to states of stress associated with failure. The parameters  $c$  and  $\phi'$  are defined on Fig. 17.5c and are explained in detail in Articles 18 and 19.

In soil mechanics the mathematical solution of stability problems is preceded by the experimental determination of the values  $c$  and  $\phi'$  and by the subsequent replacement of the real soil by an ideal plastic material to which the shear characteristics  $c$  and  $\phi'$  are assigned. This replacement involves the assumption that both  $c$  and  $\phi'$  are independent of strain. Therefore, the soils should not fail until the shearing stress at every point along a continuous potential surface of sliding reaches the value  $s$  defined by Eq. 17.4. Failures of this type are called *simultaneous*. The stress-strain curve for a triaxial test of an ideal plastic material exhibiting simultaneous failure, therefore, resembles one of those shown in Fig. 17.6a. Failure is said to occur when the stress difference reaches the value  $\Delta\sigma_f$ , and there is no ambiguity about the position of the rupture line plotted on the basis of effective stresses.

In contrast, the stress-strain curve for a real soil is likely to exhibit a peak corresponding to a small strain (Fig. 17.6b) whereupon the value of  $\Delta\sigma$  that the specimen can support decreases from its maximum value  $\Delta\sigma_f$  and approaches, at large strains, a smaller value  $\Delta\sigma_u$  designated the *ultimate value*. The position of the rupture line then depends on which value of  $\Delta\sigma$  is considered to represent failure. Peak values of  $\Delta\sigma$  correspond to the

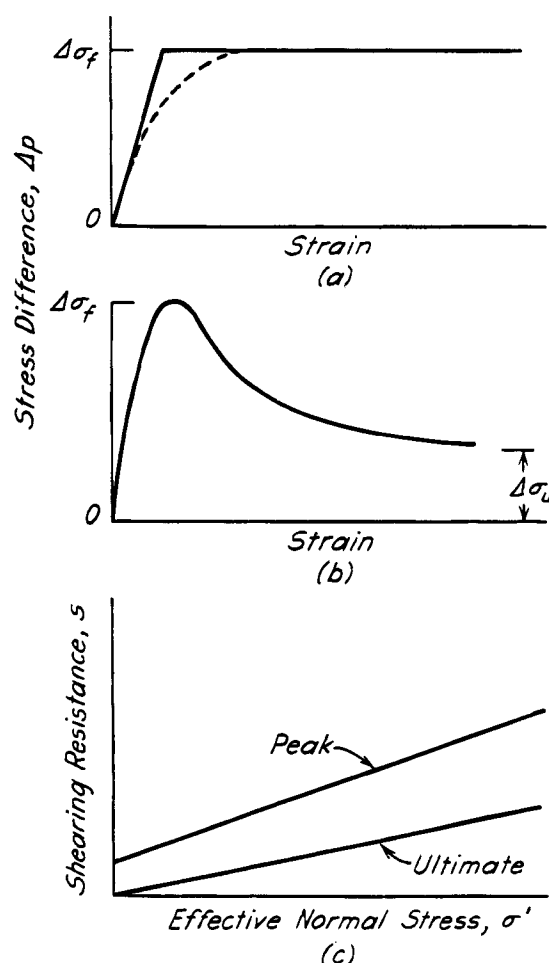


**Figure 17.6** (a) Stress-strain curves for ideal plastic material exhibiting simultaneous failure; (b) stress-strain curve for real soil, illustrating peak and ultimate strengths; (c) typical rupture lines for peak and ultimate strengths of same soil.

upper rupture line (Fig. 17.6c). On the other hand, if the lower limit of the shearing strength is of interest, a rupture line based on ultimate values may be constructed. However, whenever a material is characterized by a stress-strain curve exhibiting a peak, the conditions for simultaneous failure are likely to be violated, because even in a homogeneous material the strains along a potential surface of sliding are not likely to be uniform. Consequently, the soil along part of the surface of sliding may be exerting its peak strength whereas that along the remainder may be exerting a smaller value. Under these conditions failure starts at the point where the shearing stress becomes equal to  $s$  (Eq. 17.4) and from this point is likely to spread over the balance of the potential surface of failure. Failures of this type are said to be *progressive*. They invalidate the results of computations based on the conventional assumption of simultaneous failure.

Because of these differences between real and ideal soils, stability computations based on test results and on Eq. 17.4 are strictly valid only for the ideal plastic material that was substituted for the real soil. The practical consequences of the observed differences between real soils and their ideal substitutes must be compensated by adequate factors of safety. The importance of the differences depends on the type of soil and, for a given soil, on its load history.

### 17.5 Relations Among Shear Stress, Shear Strain, and Time

Relations among shear stress, shear strain, and time are required for determining deformations or forces in soils that are subjected to external shear stresses. This information is used to estimate, for example, the deformation of soil toward excavations such as open cuts or tunnels, or for estimating loads that are imposed by soil on supports or linings that partly or completely constrain soil deformation. The relations between shear stress and shear strain are highly dependent on the previous strain history of the soil structure, the mode of imposed shear, and the drainage conditions. Therefore, simple forms of shear stress-shear strain relations that adequately describe the behavior of different soils over a wide range of values of shear strain are not available. Nevertheless, certain simple stress-strain equations have been successfully used to estimate the interaction between soil that is subjected to shear stresses by loading or excavation and structures that constrain the soil deformation. One such relationship is the hyperbolic equation, which is described in the following discussion in terms of the axial stress and axial strain of the triaxial compression test. It has been found to be particularly useful in finite element analyses (Duncan and Chang 1970).

#### 17.5.1 Hyperbolic Stress-Strain Equation

The equation of a rectangular hyperbola in terms of stress difference  $\sigma_1 - \sigma_3$  and axial strain  $\epsilon$  is (Kondner 1963)

$$\sigma_1 - \sigma_3 = \frac{\epsilon}{a + b\epsilon} \quad (17.5)$$

The initial tangent modulus  $E_i$  of Eq. 17.5 is

$$E_i = \left. \frac{d(\sigma_1 - \sigma_3)}{d\epsilon} \right|_{\epsilon=0} = \frac{1}{a}$$

and the ultimate value of  $\sigma_1 - \sigma_3$  at infinite strain is

$$(\sigma_1 - \sigma_3)_{ult} = \lim_{\epsilon \rightarrow \infty} \frac{\epsilon}{a + b\epsilon} = \frac{1}{b}$$

The maximum value  $(\sigma_1 - \sigma_3)_{ult}$  of the stress difference for the hyperbolic stress-strain curve is reached at infinite strain, whereas the observed maximum  $(\sigma_1 - \sigma_3)_f$  for

soils occurs at a finite strain  $\epsilon_f$ . To force the hyperbolic curve to pass through the observed point of failure  $[\epsilon_f, (\sigma_1 - \sigma_3)_f]$ , a fitting ratio  $R_f$  is introduced such that

$$R_f = \frac{(\sigma_1 - \sigma_3)_f}{(\sigma_1 - \sigma_3)_{ult}} = \frac{(\sigma_1 - \sigma_3)_f}{1/b}$$

Equation 17.5 can be rewritten as

$$\frac{\epsilon}{\sigma_1 - \sigma_3} = a + b\epsilon$$

which indicates that a plot of  $\epsilon/(\sigma_1 - \sigma_3)$  against  $\epsilon$ , referred to as the transformed stress-strain plot, is a straight line with slope  $b$  and intercept  $a$ .

In evaluating the initial tangent modulus  $E_i = 1/a$  from the transformed plot of the observed data, it is often noted that at small strains the data points do not plot on the straight line; i.e., at small strains the observed data do not fit the hyperbolic stress-strain model. The departure of the initial portion of the stress-strain curve from the hyperbolic shape could represent actual soil behavior (e.g., an initial linear stress-strain curve should plot as a horizontal line in the transformed diagram), or it could result from experimental problems related to the soil sample or testing procedures. Thus, in general,  $1/a$  does not represent the initial tangent modulus  $E_i$  of the observed stress-strain curve. It is the initial slope of the best hyperbolic fit extrapolated to zero strain. The modulus evaluated by this procedure for undrained triaxial compression tests is denoted by  $E_u$ .

Substituting  $R_f$  and  $E_u$  into Eq. 17.5 we obtain

$$\epsilon = \frac{2}{E_u/s_u} \left( \frac{D}{1 - R_f D} \right) \quad (17.6)$$

where  $s_u = (\sigma_1 - \sigma_3)_f/2$  is the undrained shear strength

$D = (\sigma_1 - \sigma_3)/(\sigma_1 - \sigma_3)_f$  is the shear stress level

Substituting  $\epsilon = \epsilon_f$  and  $(\sigma_1 - \sigma_3) = (\sigma_1 - \sigma_3)_f$ , we obtain an expression for  $R_f$  in terms of  $E_u/s_u$  and strain at failure  $\epsilon_f$ :

$$R_f = 1 - \frac{2}{(E_u/s_u)\epsilon_f}$$

In terms of a reference strain  $\epsilon_R = 2/(E_u/s_u)$  (Hardin and Drnevich 1972) illustrated in Fig. 17.7

$$R_f = 1 - \epsilon_R/\epsilon_f$$

The values of  $E_u/s_u$  for most soils are in the range of 200 to 2000. The most typical values of  $R_f$  corresponding to  $\epsilon_f > 4\%$  and  $E_u/s_u > 400$  are in the range of 0.75 to 1.0. However, smaller values of  $\epsilon_f$  and  $E_u/s_u$  lead to values of  $R_f < 0.75$ .

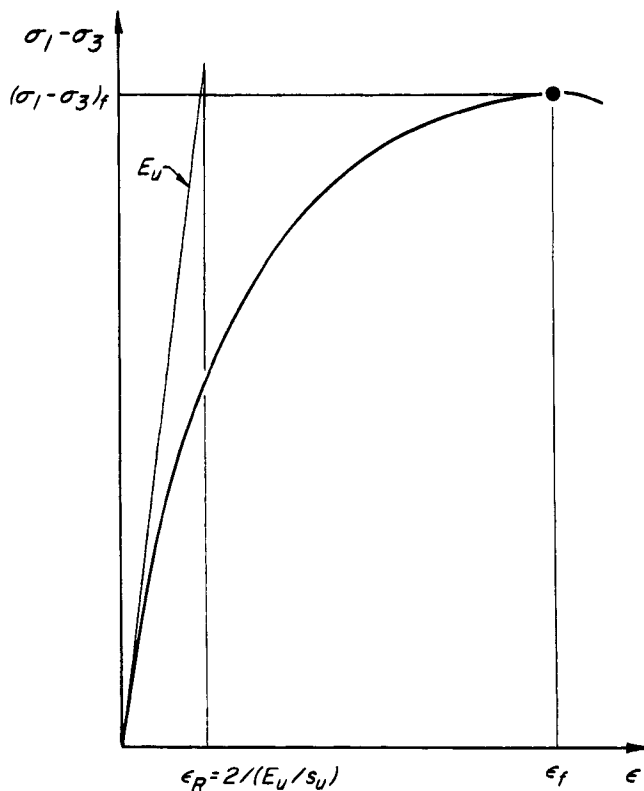


**Figure 17.7** Definition of  $\epsilon_f$ ,  $(\sigma_1 - \sigma_3)_f$ ,  $E_u$  and  $\epsilon_R$  for hyperbolic curve.

### 17.5.2 Creep Equations

The term *creep* is used to describe shear strains that develop at constant external shear stresses. Information on creep characteristics of soil structure is required for evaluating the influence of time or rate of deformation on laboratory or *in situ* measurement of the stress-strain and strength properties of soils. The relation between shear strain and time is also required for determining the deformation of soil with time after loading or excavation, or for estimating changes with time of loads imposed by soil on structures that constrain deformation. Although such relations, of general applicability to different soils, modes of shear, and drainage conditions, are not currently available, certain simple equations have been successfully used for estimating time-dependent loads produced by squeezing ground on tunnel supports (Semple 1973, Phienweja 1987).

The creep equation is presented in this article in terms of axial strain in the undrained triaxial compression test. The equation in terms of elapsed time  $t$  is

$$\epsilon = \frac{2}{(E_u/s_u)_1} \frac{D_1}{1 - (R_f)_1 D_1} \left( \frac{t}{t_1} \right)^\lambda \quad (17.7a)$$

and in terms of axial strain rate  $\dot{\epsilon}$  is

$$\epsilon = \frac{2}{(E_u/s_u)_1} \frac{D_1}{1 - (R_f)_1 D_1} \left( \frac{\dot{\epsilon}}{\dot{\epsilon}_1} \right)^{-c} \quad (17.7b)$$

where  $\lambda$  = the slope of  $\ln \epsilon$  vs  $\ln t$  at fixed values of  $D_1$

$c = \lambda/(1 - \lambda)$  is the slope of  $\ln \epsilon$  vs  $\ln \dot{\epsilon}$  at fixed values of  $D_1$

$D_1 = (\sigma_1 - \sigma_3)/(\sigma_1 - \sigma_3)_f$  for  $t_1$  or  $\dot{\epsilon}_1$  is the shear stress level.

In Eq. 17.7,  $t_1$  is a reference time,  $\dot{\epsilon}_1$  is a reference axial strain rate, and  $D_1$ ,  $(E_u/s_u)_1$  and  $(R_f)_1$  are defined by using the stress-strain curve corresponding to  $t_1$  or  $\dot{\epsilon}_1$ . An empirical expression for  $\lambda$  in the  $E_u/s_u$  range of 100 to 600 is  $\lambda = (E_u/s_u)/6000$  (Mesri et al. 1981). Therefore,  $E_u/s_u$  and  $\epsilon_f$  are the only soil parameters required for estimating stress-strain-time behavior by means of Eq. 17.7.

### Selected Reading

- Bishop, A. W. and D. J. Henkel (1962). *The Measurement of Soil Properties in the Triaxial Test*, 2nd ed., London, Edward Arnold, 228 p.
- Laboratory Shear Testing of Soils, ASTM STP No. 361 (1963).
- Bjerrum, L. and A. Landva (1966). "Direct simple-shear tests on a Norwegian quick clay," *Géot.*, **16**, No. 1, pp. 1-20.
- Bishop, A. W., G. E. Green, V. K. Garga, A. Andresen, and J. D. Brown (1971). "A new ring shear apparatus and its application to the measurement of residual strength," *Géot.*, **21**, No. 4, pp. 273-328.
- Parry, R. H. G. (1971). "Stress-strain behavior of soils," *Proc. of the Roscoe Memorial Symp.*, Edited by R. H. G. Parry, G. T. Foulis & Co., Ltd., Oxfordshire, England, 752 p.
- Mesri, G., E. Febres-Cordero, D. R. Shields, and A. Castro (1981). "Shear stress-strain-time behavior of clays," *Géot.*, **31**, No. 4, pp. 537-552.
- Richards, A. F., Editor (1988). *Vane Shear Strength Testing in Soils: Field and Laboratory Studies*, ASTM STP No. 1014.

## ARTICLE 18 BEHAVIOR OF SOILS IN SHEAR

In all problems involving earth pressures, bearing capacity of foundations, landslides, and the stability of slopes in cuts or fills, the essential ingredient for a successful solution is a proper evaluation of the shear strength of the soil or soils involved. Yet, unfortunately, shearing resistance is a complex phenomenon that cannot generally be described by a few simple rules or evaluated by routine performance of a few simple tests. Although the behavior of some soils under some circumstances can be predicted reliably on the basis of simple routine tests and procedures, that of the same soils under other circumstances or of other soils may require insight based on the best information and most sophisticated techniques available.

During the past several decades a vast amount of research has aimed at a better understanding of the behavior of soils of various geological origins and stress history

as they approach and reach shear failure. This article presents the useful findings in a systematic manner that will give the practitioner the required insight. This is accomplished by presenting digests of the properties and shear behavior of the principal types of soil, from which the practitioner can form conclusions as to the shear strength that can reasonably be assumed in connection with a particular problem or as to the type of additional investigations that may be needed.

Article 18.1 relates shear strength in general to the fundamental mineralogical properties of soil materials; it is intended to enhance the engineer's insight regarding the causes of certain behavior. The remainder of Articles 18 through 20 summarizes aspects of the research findings pertinent to engineering practice. The summaries are generally in the form of plots conveying not only the trends and relations derived from the work of the various investigators but also the variations or scatter from these trends. With this information the engineer can judge the degree of conservatism appropriate for a given design.

### 18.1 Relation of Mineralogy to Shear Strength

Shearing resistance in soils is the result of resistance to movement at interparticle contacts. Each contact can transmit normal force from one particle to another across an area that increases or decreases as the normal force increases or decreases. Bonds (Article 4.4) form across the contact areas and, together with any particle interlocking, resist tangential or sliding movements and thus create shearing resistance. The main bonding mechanism, the primary valence bond (in which surface atoms at interparticle contact are joined by sharing and transferring electrons), develops in response to the effective normal stress in the assemblage of particles. It is, therefore, of a physical nature. Other types of bonds may also contribute to the resistance; these include chemical bonds or cementation, which connect soil particles through a solid substance such as recrystallized calcium carbonate.

All these bonds increase with increasing interparticle contact area. Therefore, any mechanism that increases interparticle area contributes to shearing resistance. Effective normal stress establishes the interparticle contacts at which bonds form; in general, an increase in effective normal stress produces an increase of interparticle contact area and thus an increase in shearing resistance.

In some soils, if an increase in effective normal stress is followed by an equal decrease, the contact area may remain larger than the contact area before the stress changes took place. However, if the effective normal stress is reduced to zero, all physical and chemical interparticle bonds are broken, because the interparticle contact area reduces to zero. Chemical bonds or interparticle links, which develop at contacts after soil particles are brought together by an effective normal stress, break as a result of deformations at interparticle contact points

when the effective normal stress decreases. Thus, chemical bonding is unlikely to survive an effective stress decrease to zero, and soils have no shearing resistance at zero effective normal stress.

The physicochemical nature of the bonds at interparticle contacts is of engineering significance because of the insight it provides into the behavior of soils during shear. In practice, however, the behavior is related to more convenient indicators that integrate the physicochemical effects and that can be measured more readily. The more important of these indicators and the way in which they reflect the influence of the bonding are discussed in the following paragraphs.

Density is one important general indicator of shearing resistance. Porosity, void ratio, and water content reflect density for various types of soil. Composition influences shearing resistance by controlling the densities attainable under normal geologic and construction conditions. The influence of composition is illustrated in Fig. 18.1, in which are shown the shearing resistances of several different soils in the range of effective normal stress from 0 to 700 kPa. For example, at an effective normal pressure of 300 kPa the shearing resistance of compacted rockfill composed of 0.6- to 200-mm angular particles of quarried basalt (Marsal 1973) is 370 kPa, whereas at the other extreme the shearing resistance of a clay composed of sodium montmorillonite particles is only 33 kPa. The main reason for the difference in the shearing resistance of these two soils of extremely different compositions and those of the intermediate compositions is the difference in their void ratios, as shown in Table 18.1; the compacted rockfill has a void ratio of 0.37, compared with 3.71

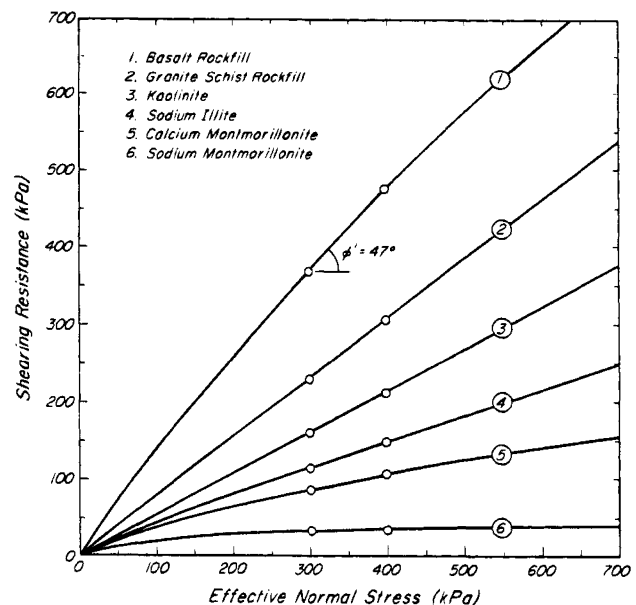


Figure 18.1 Influence of composition on shearing resistance of various soils.

**Table 18.1 Void Ratio and Shearing Resistance of Soil Materials at 300 kPa**

Composition	$e$	$s$ (kPa)	$\phi'$
Basalt rockfill	0.37	367	47°
Granitic schist rockfill	0.63	231	37°
Kaolinite	0.95	160	28°
Sodium illite	1.29	115	19°
Calcium montmorillonite	1.68	86	12°
Sodium montmorillonite	3.71	33	2°

for the consolidated sodium montmorillonite. Moreover, during shear at a 300-kPa effective normal stress, a much larger interparticle contact area is mobilized in the rockfill than in sodium montmorillonite. The void ratio attainable under normal geologic and construction conditions is related mainly to the size, shape, surface characteristics, and strength of the particles. The mineralogy of soil particles and the physicochemical environment influence shearing resistance only indirectly through their control of these important particle characteristics.

For a soil of given composition, increased density, as indicated by decreased void ratio, generally implies an increase in interparticle contact area and, thus, in shearing resistance. Although at any state of effective stress, density is an important indicator of shearing resistance, a unique relationship between shearing resistance and density is not to be expected for soils of different compositions, because for any combination of density and effective stress, even in the absence of chemical bonding, different degrees of physical bonding are possible on account of differences in the nature of the soil particles. Additional differences in shearing resistance at any density and state of effective stress can be caused by the presence of different degrees of chemical bonding.

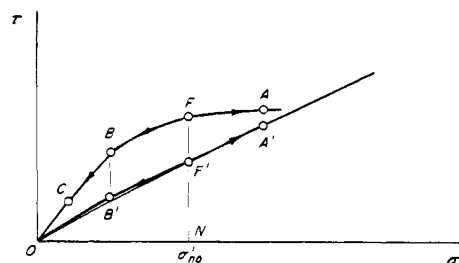
Figure 18.1 shows that, as the effective normal stress increases within the range of 0 to 700 kPa, there is a dramatic increase in the shearing resistance of basalt rockfill and only a relatively small increase in the shearing resistance of sodium montmorillonite. For example, because of the difference in the increase of mobilized interparticle contact area, an increase in effective normal stress from 300 to 400 kPa increases the shearing resistance of the rockfill by 107 kPa as compared with only 4 kPa for sodium montmorillonite. As the effective normal stress becomes greater, the contact area increases significantly in the rockfill, but the adsorption complex permits very little increase in the sodium montmorillonite.

The change in shearing resistance that is directly related to the change in effective normal stress, and therefore to physical bonding, is called *frictional resistance*. The rate of increase of the frictional resistance with effective nor-

mal stress is expressed as the *angle of friction*  $\phi'$ . Table 18.1 shows that, at an effective normal stress of 300 kPa, the angle of friction of the basalt rockfill is 47°, whereas that of sodium montmorillonite is only 2°. Figure 18.1 indicates that the friction angle decreases as the effective normal stress increases. This behavior is a consequence of the decrease in the rate of increase of contact area as the effective normal stress increases. In granular soils such as rockfill, it is caused mainly by the crushing of particle contacts and the polishing of particle surfaces, whereas in soils containing platy clay minerals it is the result of increased face-to-face orientation and interaction of the particles. The face-to-face orientation of clay particles, each surrounded by adsorbed water, decreases the likelihood of particle contact and thus of primary valence bonding.

Changes in effective stress directly control physical bonding between soil particles, and indirectly affect chemical bonding if it exists. An increase in effective stress produces an increase in physical bonding, whereas a decrease produces the opposite result. On the other hand, either an increase or a decrease in effective stress from the condition at which interparticle chemical bonding developed leads to breakage of chemical bonds.

Ideally, the friction angle should represent only the contribution of physical bonding to shearing resistance. However, in cemented soils it is not generally possible to identify the separate contributions of physical and chemical bonding during a change in effective stress. This point is illustrated in Fig. 18.2. A soil has formed and has developed chemical bonding under an effective normal pressure  $\sigma'_{no}$ . The shearing resistance of the soil at the existing effective-stress condition is defined by point  $F$ . At the same effective normal stress, point  $F'$  defines the corresponding shearing resistance of the same soil without chemical bonding. As the effective normal stress increases or decreases, the shearing resistance of the soil without chemical bonding increases along  $F'A'$  or decreases along  $F'B'$ , with an angle of friction  $\phi'$  of 26°. Chemical bonding alters the response of the soil to a change in effective stress by resisting particle rearrangements that may either increase or decrease physical bonding and may break chemical bonds. The net increase in shearing resistance along  $FA$ , in response to

**Figure 18.2** Effect of cementation bonding on friction angle.

an increase in effective stress, represents some loss of chemical bonding and some increase in physical bonding. The decrease in shearing resistance along  $FB$  includes loss of chemical bonds as well as a reduction in physical bonding. A significant part of the reduction in shearing resistance along  $BC$  represents loss of chemical bonding. The rates of change in shearing resistance along  $FA$ ,  $FB$ , and  $BC$  correspond to  $5^\circ$ ,  $25^\circ$ , and  $39^\circ$ , respectively. These values, which represent the combined changes in chemical and physical bonding, if interpreted as representing the angle of friction (Fig. 18.1), would give a misleading impression of the composition of the soil.

## 18.2 Volumetric Response of Soils During Shear

Density, effective stress, and soil structure are the three important variables that determine the shearing resistance of soils. It is a distinctive characteristic of soils that, during the mobilization of shearing resistance, shear deformation is accompanied by a change in either density or effective stress. Furthermore, the nature and magnitude of this change depend on the preshear density and effective-stress condition as well as on the soil structure. In saturated soils, density change during shear is achieved by expelling or by taking in water, and effective-stress change is brought about through an increase or a decrease in porewater pressure.

The mechanism responsible for a volume or porewater pressure change is the tendency of soil particles to rearrange themselves during shear. If water can leave or enter the soil, the tendency for particle rearrangement manifests itself as a change in volume and, consequently, in density. If volume change is not possible, the porewater pressure change produces a change in effective stress. Soils of low preshear density, such as loose sands and silts and soft clays, tend to compress during shear. On the other hand, soils of high density, such as dense sands and gravels and stiff clays and shales, tend to expand; however, as the preshear effective confining pressure increases, the tendency for volume increase is suppressed.

In a drainage-controlled laboratory test, it is possible to bring any soil to failure under a fully drained or fully undrained condition (Article 17.1). In the field, however, because of their high permeability, granular soils generally reach failure under drained conditions and mobilize drained shear strength. Exceptions are saturated very loose sands that can liquefy under an undrained condition (Article 20.9). Soft clays generally tend to fail under undrained conditions, because their low permeability permits little drainage during construction or application of loading, and if drainage should occur it would lead to an increase in strength. Shearing of stiff clays tends to cause a decrease in porewater pressure, an increase in effective stress, and thus an increase in shear strength, but a reduction in effective stress due to excavation induces volume increase, softening, and reduction in strength. The net

effect is that failure, if it occurs, usually takes place under drained conditions.

Soil structure, i.e., the nature and arrangement of soil particles and interparticle forces and bonds, also influences volumetric response during shear. Chemical bonding, for example, which allows a soil deposit to come to equilibrium in a loose condition, can be expected to unleash a large tendency for volume decrease when broken during shear. On the other hand, it is possible to have combinations of preshear density, effective stress, soil structure, and mode of shearing that produce no tendency for volume change during shear. For example, platy clay particles that are highly oriented along a preexisting shear plane show little tendency for rearrangement during further shear displacement.

Typical examples of volume change in drained tests and porewater pressure change in undrained tests are presented in the remainder of Article 18.2 to illustrate general features of volumetric response of soils during shear. The corresponding stress-strain curves are also shown. They are discussed in Article 18.3 in connection with stress path to failure.

### 18.2.1 Examples of Drained Behavior

Stress-strain and volume change relationships for drained plane-strain compression tests (Article 17.3.5) on a saturated sand from Brasted, England, are shown in Fig. 18.3 (Cornforth 1961, 1964). For this sand, having 95% of its grain sizes between 0.1 and 0.6 mm, the minimum and

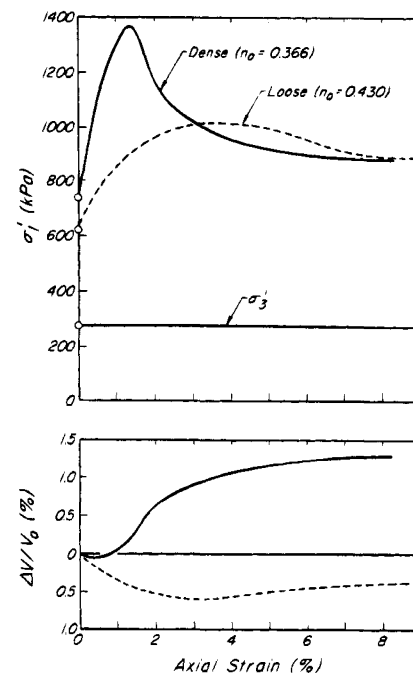


**Figure 18.3** Stress-strain and volume-change relationships for drained plane-strain tests on saturated Brasted sand (data from Cornforth 1961).

maximum porosities were 0.322 and 0.442, respectively. For both loose and dense specimens the major principal stress increased to a maximum and then decreased and leveled off at an ultimate value. As axial strain increased, both the loose and dense samples experienced volume decrease followed by volume increase. The loose sample experienced large compression with net volume decrease at both maximum and ultimate major principal stress, whereas the dense sample, after a small decrease in volume, dilated strongly with a net volume increase at both maximum and ultimate stresses. In both samples, the rate of volume increase with respect to axial strain (dilation rate) was a maximum at the maximum stress and was almost zero at the ultimate condition.

Stress-strain and volume change relationships for drained triaxial compression (TC) tests on saturated rockfill from Pyramid dam are shown in Fig. 18.4 (Marachi et al. 1972). After compaction, both specimens were dense and had an initial porosity of 0.310. Before shear, however, one sample was consolidated under an equal all-around pressure of 210 kPa, whereas the other sample was consolidated under 4500 kPa. The sample sheared under the low confining pressure behaved as a dense specimen showing significant dilative tendency. The sample consolidated under a high confining pressure, however, exhibited large volume decrease. The test results confirm that an increase in effective confining pressure decreases the tendency for volume increase. In these tests, particle rearrangement during shear into a denser condition was strongly aided by particle crushing at interparticle contact points.

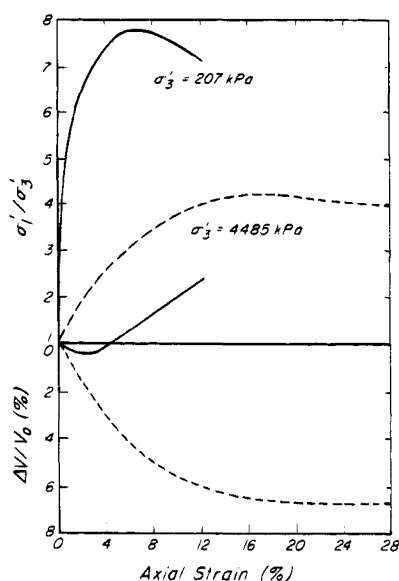


**Figure 18.4** Stress-strain and volume-change relationships for triaxial compression tests on dense rockfill (data from Marachi et al. 1972).

Stress-strain and volume-change relationships for drained triaxial compression tests on undisturbed specimens of stiff London clay are shown in Fig. 18.5 (Bishop et al. 1965). The clay was taken from a depth of 35 m and had a natural water content of 25.5%, liquid limit of 70%, and plastic limit of 27%. *In situ* effective overburden pressure, preconsolidation pressure, and coefficient of earth pressure at rest (Article 16.5) were estimated to be 390 kPa, 4100 kPa, and 2.1, respectively. Figure 18.5a shows that the drained stress-strain and volume-change behavior of a highly overconsolidated clay is qualitatively similar to that of a dense sand. Shear stress reaches a peak value and then drops to a value, known as the *fully softened strength*, at which volume increase levels off (Article 19.2.2). The brittle nature of the failure at maximum stress, as indicated by the sharp peak of the stress-strain curve, is associated with the formation of a distinct slip plane. The influence of effective confining pressure on an overconsolidated clay is similar to that on a dense sand. On the other hand, Fig. 18.5b shows that in the London clay specimen consolidated to an equal all-around pressure of 4400 kPa, a value exceeding the preconsolidation pressure, only a small decrease in shear stress was observed after the peak, and the specimen showed a volume reduction throughout the test except for a small increase that occurred at large strains toward the end. This behavior is similar to that of an insensitive normally consolidated soft clay.

The behavior of dense sands and highly overconsolidated clays differs in that in dense sands the maximum dilation rate is achieved at the strain corresponding to the maximum shear stress, whereas in overconsolidated clays

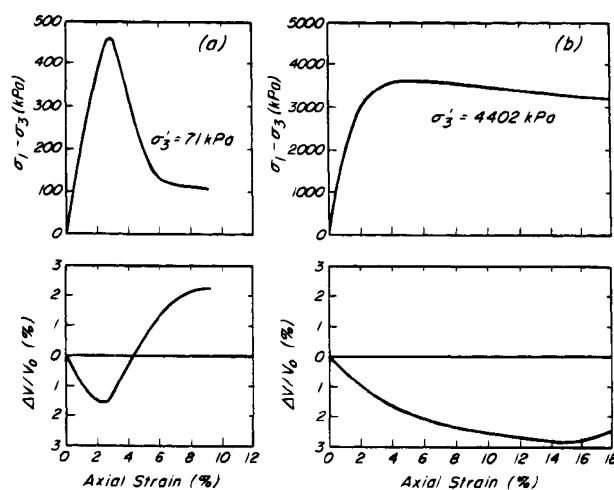


**Figure 18.5** Stress-strain and volume-change relationships for triaxial compression tests on undisturbed stiff London clay. (a) Sample consolidated under all-around pressure  $\sigma'_3$  less than preconsolidation pressure. (b) Sample consolidated under all-around pressure  $\sigma'_3$  greater than preconsolidation pressure (data from Bishop et al. 1965).



dilatancy does not begin until the peak shear stress is reached. The dilatant behavior of overconsolidated clays is due to the breaking of interparticle bonds and the formation of a major slip plane along which the dense clay fabric has an opportunity to swell and soften.

If it were possible to continue shear displacement along the slip plane, the shearing resistance would reduce to the *residual value*. Large relative displacement between two stiff clay blocks helps to give platy clay particles in the thin shear zone an orientation parallel to the slip plane and produces minimum shearing resistance. The reduction of strength to a residual value represents another difference between granular soils, in which resistance decreases to the ultimate strength after a strain of 10 or 20%, and soils that contain clay minerals, in which resistance decreases from the fully softened to the residual strength as strains become very large. The triaxial test is not suitable for determining residual strength because only limited deformation along a slip plane is possible in the apparatus. The reversing direct shear test (Article 17.3.2) or the torsional ring-shear test (Article 17.3.4) can be used to measure the reduction in shearing resistance from the fully softened to the residual condition.

### 18.2.2 Examples of Undrained Behavior

The results of a series of consolidated undrained triaxial compression tests on sand are shown in Figs. 18.6 through 18.8 (Castro 1969). The material, Banding sand,

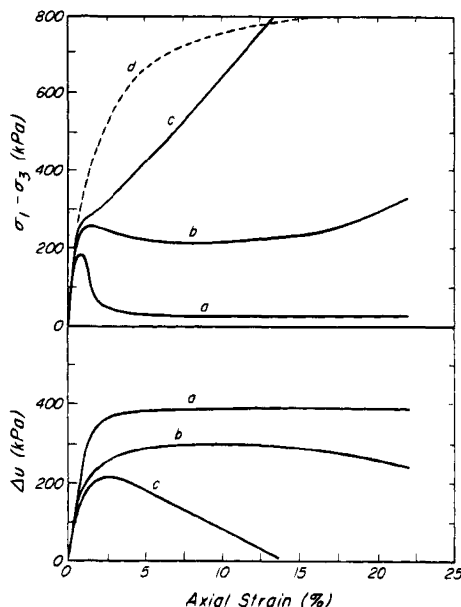


**Figure 18.6** Stress-strain and shear-induced porewater pressure behavior of Banding sand in undrained triaxial compression tests. Curves *a*, *b*, and *c* refer to samples of different relative density. Curve *d* represents results of drained test on sample identical with that represented by *a* (data from Castro 1969).

is a uniform, clean, fine quartz sand with subrounded to subangular grains and minimum and maximum void ratios of 0.50 and 0.84, respectively. Specimens were sheared using axial stress control (Article 17.2) by applying axial loads in increments. At three different relative densities three types of stress-strain and porewater pressure responses were observed during undrained shear, as shown in Fig. 18.6. All three specimens were consolidated to an equal all-around pressure of 400 kPa; the void ratios of specimens *a*, *b*, and *c* after consolidation were 0.748, 0.689, and 0.681, respectively. As soon as the loosest specimen, *a*, failed, at a maximum  $(\sigma_1 - \sigma_3) = 190$  kPa, it deformed in 0.18 s from an axial strain of 0.8% to more than 20%. A substantial increase in porewater pressure took place that resulted in a decrease in effective confining pressure from 400 to 10 kPa. For axial strains larger than about 6% the specimen deformed continuously at a  $(\sigma_1 - \sigma_3)$  of only 20 kPa. The rapid rate of increase in porewater pressure, great loss of strength, and large strains that developed in the undrained test are characteristic of *liquefaction failure* (Article 20.9) of saturated uniform fine loose sands. For comparison the stress-strain curve for an identical specimen, *d*, sheared under drained conditions, is shown. It was also consolidated to 400 kPa.

The medium dense specimen *c* showed a dilative response during undrained shear. The porewater pressure reached a maximum at a strain of about 2.5%, after which it started to decrease and became zero at 14% strain. Axial loading was stopped at this strain, but if the test had been continued, the shear-induced porewater pressure would have become negative. The stress-strain curve shows an inflection point at an axial strain of about 2% at which the porewater pressure was a maximum. For axial strains beyond 3%, a practically linear increase in shear resistance developed as the porewater pressure decreased.

Specimen *b*, which was only slightly looser than specimen *c*, experienced behavior intermediate between liquefaction failure and dilation. It behaved similarly to the specimen that liquefied, except that the rapid deformation and associated dilatancy stopped itself at about 19% strain.

The specimen represented by Fig. 18.7 was practically identical with specimen *a* and was similarly consolidated to an effective confining pressure of 400 kPa. However, it was subjected to axial cyclic loads under undrained conditions. The axial load oscillated between zero and a maximum compressive load. Just after the accumulated strain reached about 1%, liquefaction occurred. The characteristics of the stress-strain and porewater pressure behavior were very similar to those for specimen *a* (Fig. 18.6), which developed liquefaction with monotonically increasing shear stress and strain. Since strain and pore-

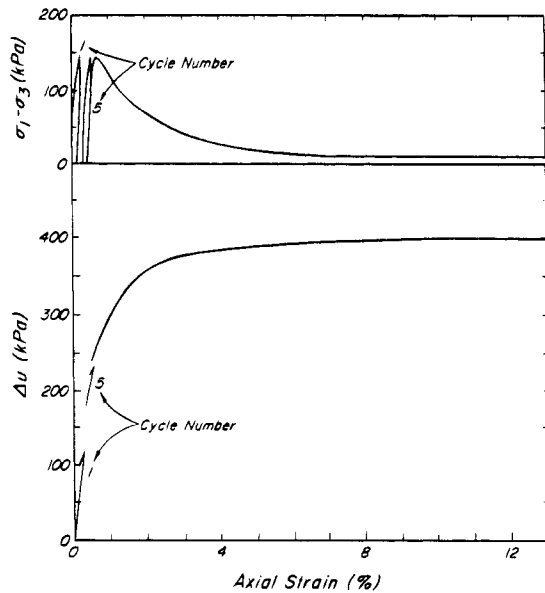


**Figure 18.7** Stress-strain and shear-induced porewater pressure behavior of Banding sand in undrained cyclic triaxial compression test (data from Castro 1969).

water pressure accumulate in the cyclic test, liquefaction occurred at a maximum  $(\sigma_1 - \sigma_3)$  of only 150 kPa, compared with the 190 kPa required for monotonic loading.

In contrast to the isotropically consolidated specimens discussed above, the three specimens represented in Fig. 18.8 were anisotropically consolidated to a major principal stress  $\sigma'_{10}$  and to minor principal stresses  $\sigma'_{30}$ . After consolidation, axial loads were increased under undrained

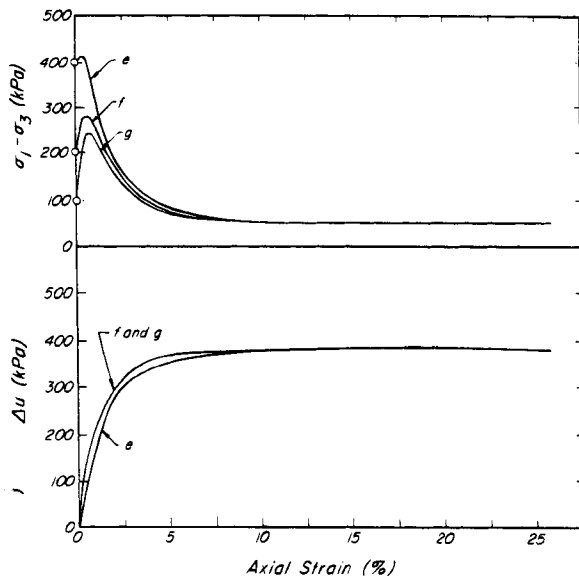


**Figure 18.8** Stress-strain and shear-induced porewater pressure behavior of Banding sand in  $K_o$ -consolidated undrained triaxial compression tests (data from Castro 1969).

conditions. Unlike in isotropically consolidated specimens, the initial value of  $(\sigma_1 - \sigma_3)$  in tests on anisotropically consolidated specimens was not zero. As the additional  $(\sigma_1 - \sigma_3)$  was applied under undrained conditions, each of the three specimens developed a peak strength at an axial strain smaller than 1%, after which the resistance of the specimens decreased and remained constant beyond an axial strain of about 8%. The general characteristics of the postpeak stress-strain and porewater pressure behavior are similar to those of specimen *a* in Fig. 18.6. The major difference between the isotropically and anisotropically consolidated specimens is dramatically illustrated by specimen *e*, in which failure was induced by the undrained application of an axial load after consolidation of only 10 kPa. The  $(\sigma_1 - \sigma_3)$  applied to this specimen during anisotropic consolidation was about half of the drained strength of the specimen. If the specimen had been loaded further under drained conditions, an increase in axial stress of about 400 kPa would have been required to induce failure. However, during undrained loading, the small additional  $(\sigma_1 - \sigma_3) = 10$  kPa resulted in liquefaction failure.

The volume changes in the drained tests on London clay (Fig. 18.5) have their counterparts in the porewater pressure changes in the consolidated undrained triaxial compression tests shown in Fig. 18.9. The specimen that was subjected to an effective confining pressure of 103 kPa before shear behaved like a highly overconsolidated clay. It first exhibited positive porewater pressure, and then dilation occurred and the porewater pressure became negative. On the other hand, the specimen that was consolidated under an equal all-around pressure of 5930 kPa behaved like an insensitive normally consolidated clay.

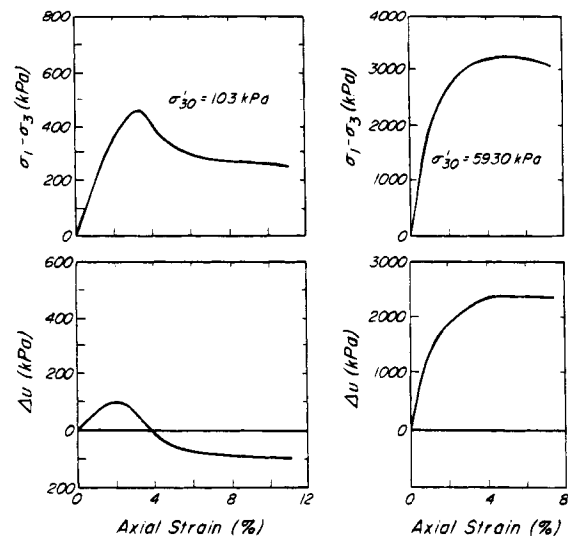


**Figure 18.9** Stress-strain and shear-induced porewater pressure behavior of undisturbed London clay in undrained triaxial compression tests (data from Bishop et al. 1965).

The porewater pressure increased and then leveled off after the peak stress was reached.

Undrained shear test results on three specimens of a very sensitive highly structured silty clay sample from the Broadback River valley in Quebec are shown in Fig. 18.10. The material had a liquid limit of 27%, plastic limit of 19%, and natural water content of 42%; values of effective overburden pressure, preconsolidation pressure, and field-vane undrained shear strength were 63 kPa, 133 kPa, and 20 kPa, respectively. Before undrained shear, all three specimens were subjected under drained conditions to an axial stress equal to the effective overburden pressure. In two triaxial tests, a lateral pressure corresponding to a ratio of  $\sigma'_3/\sigma'_1$  equal to 0.55 was applied during the drained phase. During the undrained phase, the lateral pressure was held constant. In the TC test the axial stress was increased; in the TE test it was decreased. The compression or extension was achieved by either pushing or pulling in the axial direction at a constant rate of axial deformation. The third specimen was tested in direct simple shear (DSS, Article 17.3.3) at a constant rate of horizontal deformation. The shear stresses in Fig. 18.10 have been normalized with respect to the preconsolidation pressure

of the sample. The plotted shear stress for the triaxial tests is taken equal to  $(\sigma_1 - \sigma_3)/2$ ; that for the simple shear test is the measured horizontal shear stress. In Fig. 18.10 the final direction of the shear stress is considered to be positive, so that the TE test starts from a negative shear stress that increases to zero and then becomes positive. The shear strain for the triaxial tests has been taken as 1.5 times the axial strain, on the premise that  $\gamma/2 = (\epsilon_1 - \epsilon_3)/2$  and  $\epsilon_3 = -\epsilon_1/2$ , where  $\gamma$  = shear strain and  $\epsilon_1$  and  $\epsilon_3$  = principal strains.

In all three tests the shear stress reached a peak and then dropped and leveled off at a large strain. The peak undrained shear stress in the TE test was considerably less than that in the TC test, partly because in the former test the direction of shear stress was opposed to the direction of shear stress during consolidation of the sample in the field. During reversal of shear stress, significant numbers of interparticle bonds were broken before peak stress was reached. In addition, as discussed in Article 18.3, during undrained compression of this clay to peak strength the effective stress increased, whereas during the extension test, it decreased. The stress condition in the simple shear test was intermediate between those in the TC and TE tests. Also, the DSS test involved distortion of the whole sample; consequently, progressive failure caused the peak stress to be reached at larger strain.

In the triaxial tests, compression or extension to peak strength was almost elastic and produced positive or negative porewater pressure, respectively. The formation of a major slip plane in the compression test led to a temporary dilatant pore pressure response. However, continued shear distortion of the soft clay in the shear zone produced a porewater pressure increase in both the compression and the extension tests. In the simple shear test, in which the whole soft clay specimen was subjected to distortion, porewater pressure continuously increased and tended to level off at large strains.

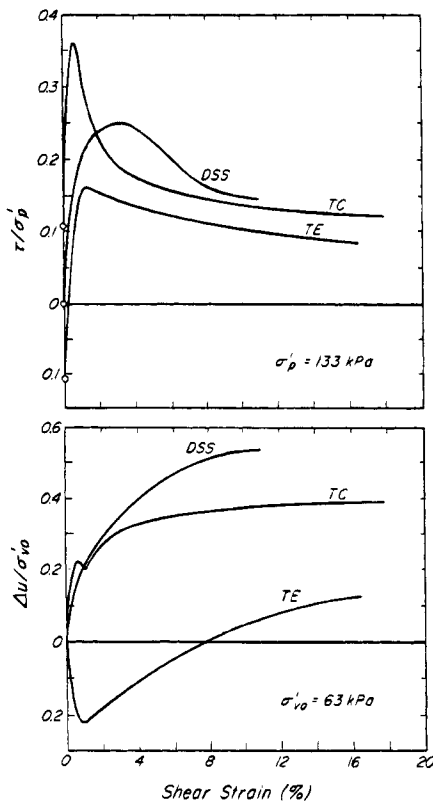


**Figure 18.10** Stress-strain and shear-induced porewater pressure behavior of highly sensitive Broadback clay in undrained triaxial compression, simple shear, and triaxial extension tests (data from Lefebvre et al. 1983).

### 18.3 Stress Path to Failure

The shearing resistance of soil on a surface of sliding is a function of the effective normal stress acting on that surface. During mobilization of shearing resistance, whether in the field or in most laboratory or *in situ* strength tests, a combination of changes in both shear stress and effective normal stress brings the soil to failure. Changes in effective normal stress are caused by changes in total normal stress, porewater pressure, or both. Under all undrained shear conditions in the field and laboratory, shear-induced porewater pressure either increases or decreases the effective normal stress on the surface of shear. In both drained and undrained triaxial tests, shearing involves changes in effective normal stress as well as in shear stress. In the drained direct shear test, on the other hand, the effective normal stress on the imposed

shear plane remains practically constant during shear. It increases slightly as the test progresses, because the area of the imposed shear plane decreases while the applied normal force remains constant.

Thus, to interpret laboratory or field strength tests and to select strength parameters for stability analysis, it is useful to examine the manner in which the effective normal stress and the shear stress change during mobilization of the shearing resistance; that is, to determine the *stress path* to failure.

Before the stress path to failure can be examined, the plane must be selected on which the stresses are to be represented. In some situations a preexisting slip plane in the field or an imposed failure surface, as in direct shear and simple shear tests, predetermines the plane of interest. However, under other circumstances, as in the triaxial test wherein the known stresses are the principal stresses, a choice must be made. One possibility is the plane on which slip will eventually take place. For example, on the assumption that the failure plane will make an angle of  $45^\circ + \phi'/2$  with the major principal plane, the state of stress on a plane making  $60^\circ$  with the major principal plane (for an angle of friction  $\phi' = 30^\circ$ ) might be appropriate. Usually, however,  $\phi'$  is not known in advance, and an assumption as to the orientation of the failure plane may be misleading. Stress paths for other planes may be instructive. One common choice is the plane of maximum shear stress, on which the shear stress is equal to  $(\sigma'_1 - \sigma'_3)/2$  and the effective normal stress is  $(\sigma'_1 + \sigma'_3)/2$ . In general, the stress path starts from the preshear

effective stress conditions. For some laboratory tests, however, it is useful to consider the stress path during the preshear consolidation phase as well.

Figure 18.11 shows stress paths, for the plane of maximum shear stress, for eight triaxial compression tests on saturated, loose Ham River sand (Bishop 1971). The initial porosities of the specimens averaged 0.454; the minimum and maximum porosities were 0.38 and 0.48. All samples except sample 11 were consolidated under equal all-around pressure. Samples 5, 6, and 7 were subjected to consolidated-drained tests, and samples 10, 9, and 8 to consolidated-undrained tests. In all the undrained tests the shear-induced porewater pressure was measured, so it is possible to plot the effective stress paths to failure. The dramatic influence of drainage during shear on the effective stress path and, therefore, on the mobilized strength can be seen by comparing either tests 10 and 6 or tests 8 and 7. For example, samples 8 and 7 were consolidated under an equal all-around pressure of 6820 kPa and then the axial stress was increased. In the drained test (7), a maximum value of  $(\sigma_1 - \sigma_3)/2$  of 6890 kPa was reached as compared with 1720 kPa for the undrained test (8). An examination of the effective stress path for the drained test (7) shows that there was a continuous increase in effective normal stress  $(\sigma'_1 + \sigma'_3)/2$  to the maximum  $(\sigma_1 - \sigma_3)/2$ . In the undrained test (8), however, there had been a significant decrease in effective stress by the time the maximum  $(\sigma_1 - \sigma_3)/2$  was reached. This behavior is compatible with the observation that in a drained test on loose sand a

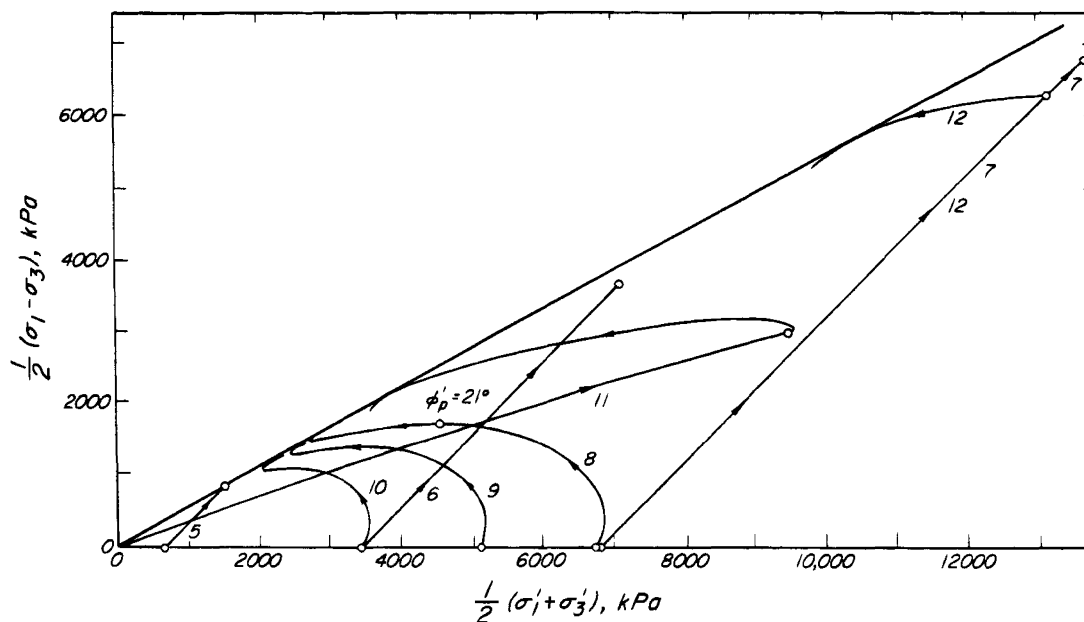


**Figure 18.11** Stress paths for drained and consolidated-undrained tests on saturated loose Ham River sand. The number next to each stress path refers to the corresponding sample (after Bishop 1971).

significant decrease in porosity occurs during shear, whereas in an undrained test the porosity remains constant. The effective stress paths for the drained tests do not readily show the decrease in shear stress after the maximum is reached, because the descending path coincides with the one for increasing  $(\sigma'_1 + \sigma'_3)/2$ . On the other hand, the stress paths for the undrained tests show that the shear stress reaches a maximum that is followed by a decrease. The decrease may be followed by an increase just before failure occurs.

Sample 11 was consolidated anisotropically under a confining stress  $\sigma'_3$  equal to about one half of the axial stress  $\sigma'_1$ . The linear portion of the stress path represents the consolidation phase, but during this phase the sample was subjected to considerable shear. The sample was then sheared to failure under undrained conditions. Sample 12 was subjected to drained shear after isotropic consolidation. Before failure was reached, however, the drains were turned off and the test was completed under undrained conditions.

An important point is illustrated by the stress paths of samples 11 and 12. Both samples were able to withstand large shear stresses under the drained condition, but when the shearing became undrained, specimen 11 could sustain an additional  $(\sigma_1 - \sigma_3)/2$  of only 100 kPa, and specimen 12 could carry no additional shear stress at all.

Other examples of undrained stress paths are shown in Fig. 18.12 for the tests on Banning sand represented by the stress-strain curves in Fig. 18.6 (Castro 1969). These stress paths have been plotted for a plane making  $60^\circ$  with the major principal plane. In Fig. 18.12a, for sample *a*, which liquefied, there was an enormous decrease in effective normal stress throughout the test, so that finally the sample could sustain a shear stress of only 20 kPa. On the other hand, in specimen *b* liquefaction was averted after maximum shear stress by a decrease in porewater pressure and thus an increase in effective stress and shear strength. Specimen *c* had a tendency to dilate shortly after the initial maximum shear stress was reached, and a significant decrease in porewater pressure produced major increases in effective stress and mobilized strength. Figure 18.12b shows that the cumulative effective stress path in undrained cyclic compression was identical with that observed in monotonic loading of specimen *a* in Fig. 18.12a. Both initially very loose samples liquefied because of the continued increase in porewater pressure and the corresponding decreases in effective stress and shearing resistance.

The stress paths in Fig. 18.12c confirm the behavior illustrated by samples 11 and 12 in Fig. 18.11. The magnitude of the increment of undrained shear stress that can be carried by a sample depends on the shear-stress condition in the sample during the drained phase. Specimen 1 could carry some additional shear stress, whereas speci-

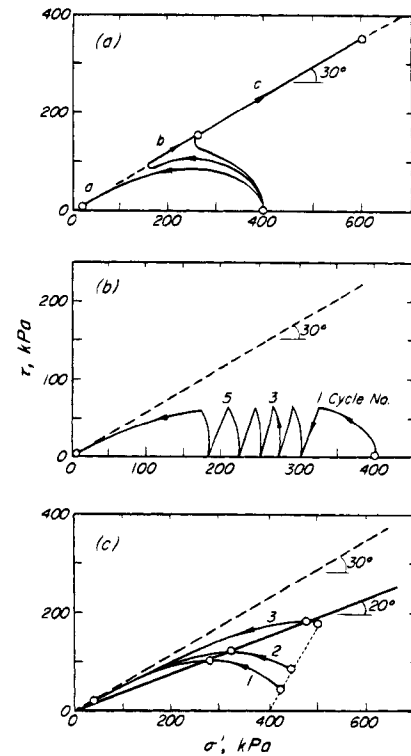


**Figure 18.12** Undrained stress paths for  $60^\circ$  plane for tests on Banning sand represented by stress-strain curves in Fig. 18.6 (data from Castro 1969).

men 3 could not sustain any additional shear stress under undrained conditions.

Examples of stress paths for undrained triaxial extension tests on saturated Ham River sand (Bishop 1971) are shown in Fig. 18.13. Two samples were consolidated to the same void ratio of 0.789, one under an equal all-around pressure and the other under  $\sigma'_3/\sigma'_1 = 0.55$ . The failure of the anisotropically consolidated sample in triaxial extension involved a change in the direction of the major principal

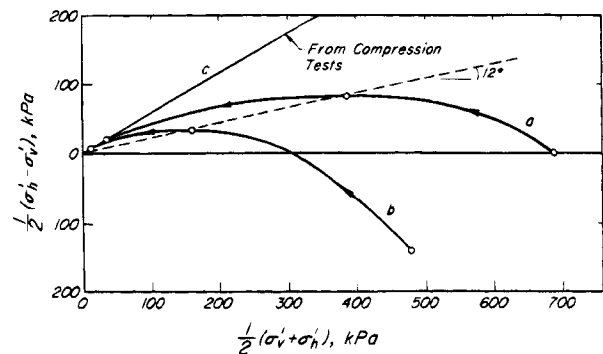


**Figure 18.13** Stress paths for consolidated-undrained triaxial extension tests on saturated Ham River sand. Curves *a* and *b* refer to isotropically and anisotropically consolidated specimens, respectively. Curve *c* shows results of compression test for comparison (data from Bishop 1971).

stress under undrained conditions. Although the void ratios of the two samples were the same, the maximum shear stress that could be reached in the anisotropically consolidated sample was only 40% of the value attained in the isotropically consolidated sample.

Figure 18.14 shows effective stress paths for six undrained TC tests on undisturbed samples of highly overconsolidated intact London clay (Bishop et al. 1965). The water contents of the samples after equilibration under isotropic effective confining pressure are also given. During the undrained TC tests, the effective normal stress either increased (as in sample E75), or remained practically constant (as in E48). In addition, the results are shown of an undrained test on a sample of the same material reconstituted and consolidated in the laboratory. The stress path for this test is typical of a normally consolidated insensitive clay. A stress path is also shown for a drained test of an intact sample taken to its peak strength and then to the fully softened condition (Article 19.2.2). Unfortunately, it is not generally possible to obtain a continuous stress path for a highly overconsolidated clay including the peak, fully softened, and residual strength conditions. The triaxial compression test, commonly used for the measurement of peak strength, is only occasionally continued to the fully softened condition, and it is unsuitable for the measurement of residual strength. The main reasons are that after the formation of a slip plane it is not possible to control the state of stress in the sample, to determine readily the area of the shear plane, or to

produce large relative displacement along the slip plane. Thus, different types of specimens (such as intact, remolded or reconstituted, and precut) and different kinds of apparatus (such as triaxial and direct shear) are often used for the measurement of peak, fully softened, and residual strengths. In effect, when a precut sample is used for the measurement of residual strength, the sample is taken through the peak and fully softened condition during sample preparation.

The stress paths shown in Fig. 18.15 correspond to the highly sensitive soft Broadback clay described in Article 18.2. The results of seven undrained shear tests are shown, including three TC, three TE, and one DSS. In Fig. 18.15 the stress paths correspond to  $(\sigma'_1 - \sigma'_3)/2$  and  $(\sigma'_1 + \sigma'_3)/2$  for the triaxial tests, and to  $\tau$  and  $\sigma'$  for the DSS test. The stress paths for tests 1 and 2, in which the samples were subjected to an identical *in situ* effective stress condition before undrained shear, show that in triaxial compression the effective stress increases continuously to the maximum strength (test 1), whereas during the extension test (test 2), it decreases. The peak undrained strengths reached in these two tests are dramatically different (e.g., compare points *a* and *b*). The DSS test gives a peak strength between the compression and extension values. The remaining four specimens, 4, 5, 6, and 7, were consolidated using  $\sigma'_3/\sigma'_1 = 0.55$  to a stress condition beyond the preconsolidation pressure. Therefore, these samples of originally highly sensitive clay were significantly destructured during consolidation. For

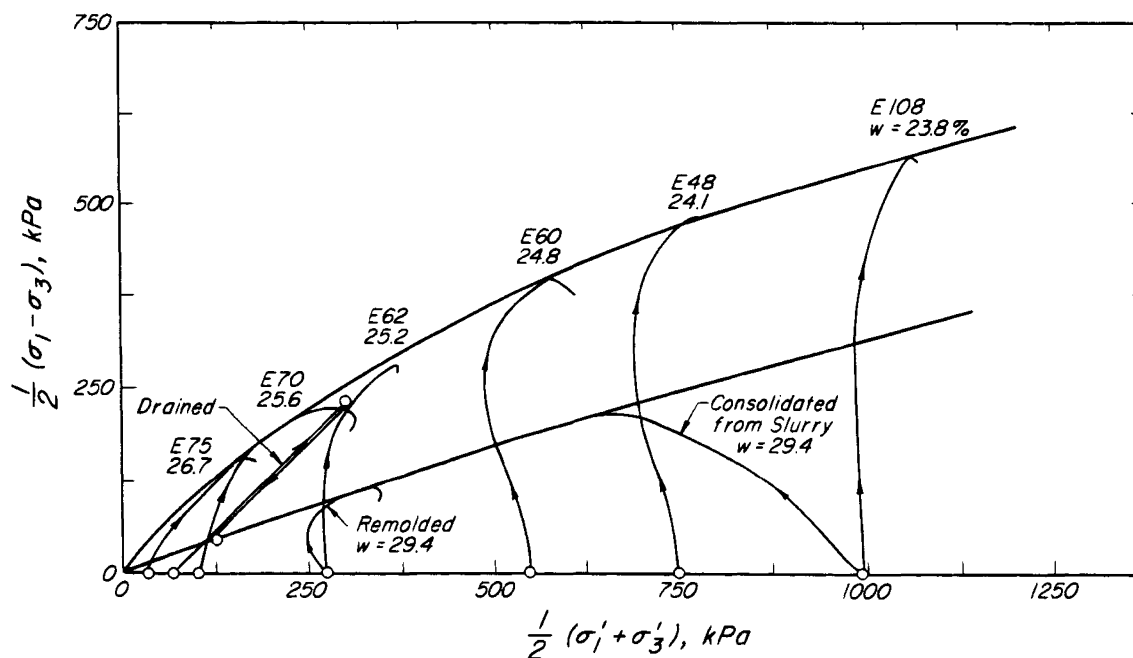


**Figure 18.14** Effective stress paths for undrained triaxial compression tests on undisturbed, overconsolidated intact London clay. For comparison, results are also shown for a remolded sample, a sample consolidated from a slurry, and a sample tested under drained conditions (data from Bishop 1971).

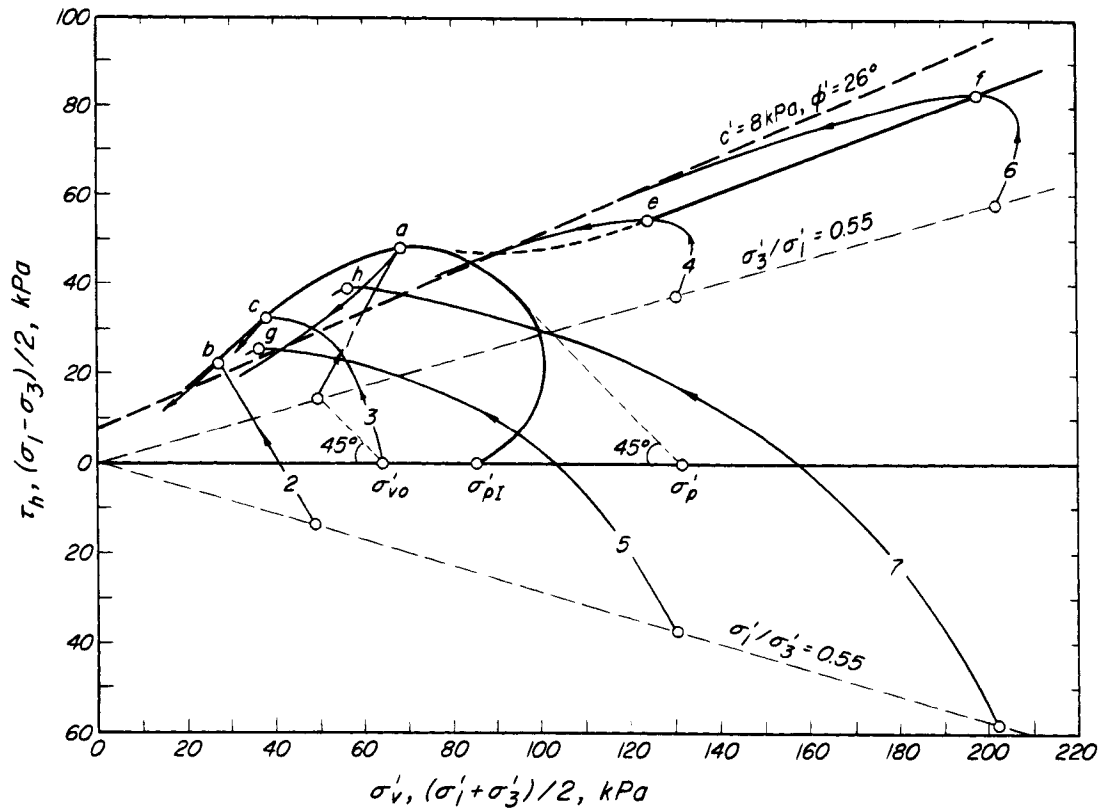


Figure 18.15 Stress paths for samples of highly sensitive Broadback clay under undrained shear.

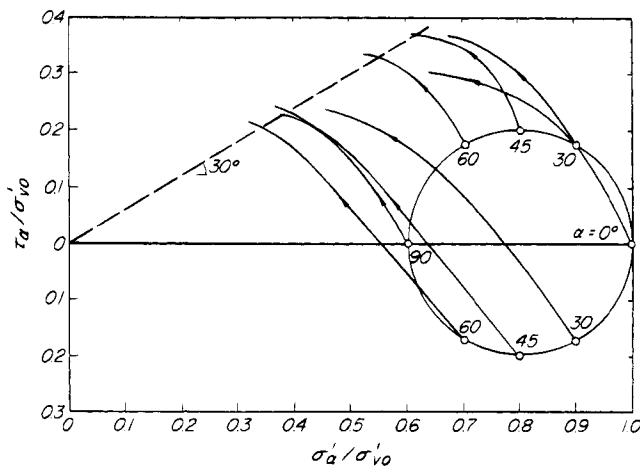
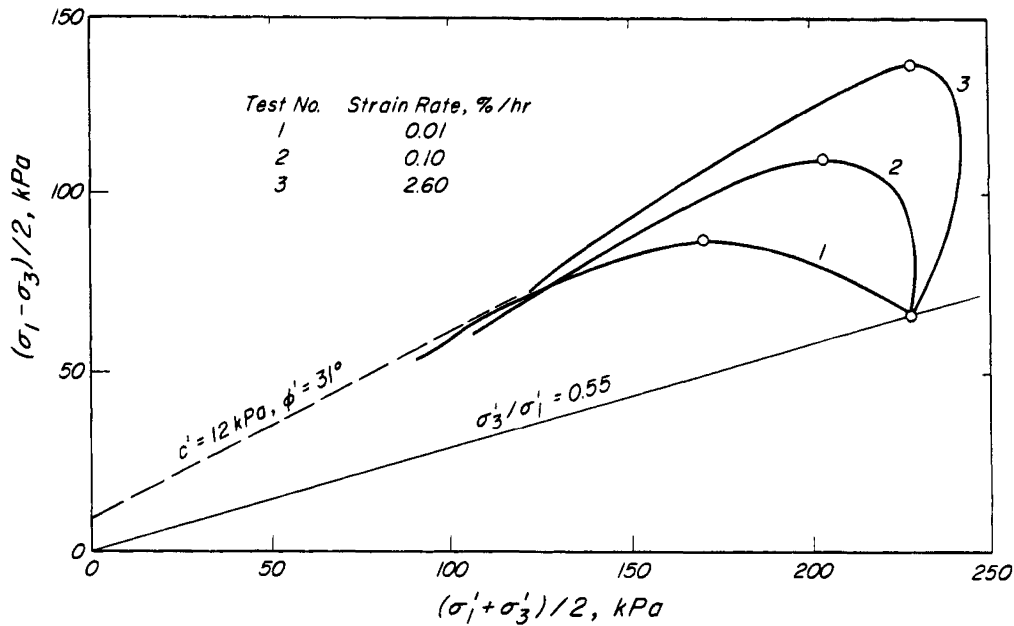


Figure 18.16 Stress paths for simple shear tests on plastic Drammen clay. Values of  $\alpha$  refer to the orientation of the samples with respect to the horizontal (data from Bjerrum and Soydemir 1972).

example, by comparing the effective stress paths for tests 1 and 4, one can see the difference in undrained behavior of a clay that starts from the *in situ* stress condition, and of the same clay after consolidation beyond the *in situ* preconsolidation pressure. A comparison of either tests

4 and 5 or tests 6 and 7 shows the dramatic difference in the stress paths for compression and extension tests, and the equally dramatic difference in mobilized maximum undrained strength (e.g., compare points *e* and *g* or *f* and *h*). For these tests the difference in effective stress at maximum shear stress, for extension as compared to compression failure, is notable.

The constant volume DSS tests represented in Fig. 18.16 were performed to study undrained shear strength anisotropy in soft clays (Bjerrum and Soydemir 1972). The undisturbed samples of plastic Drammen soft clay used for these tests are characterized by natural water content, liquid limit, and plastic limit values of 55%, 62%, and 33%, respectively, and  $\sigma'_p/\sigma'_{v0} = 1.5$ . The DSS samples were cut at orientations  $\alpha$  to the horizontal of  $0^\circ$ ,  $30^\circ$ ,  $45^\circ$ ,  $60^\circ$ , and  $90^\circ$ . The *in situ* state of stress on any plane before shear,  $(\sigma'_{\alpha 0}, \tau_{\alpha 0})$ , was defined in terms of effective overburden pressure,  $\sigma'_{v0}$ , and the corresponding effective horizontal stress,  $K_0 \sigma'_{v0}$ . A value of  $K_0 = 0.6$  was assumed. For example, in the  $\alpha = 0^\circ$  test the specimen was cut horizontally (with the axis of the cylindrical disc vertical), and under drained conditions in the simple shear apparatus it was subjected to  $\sigma'_{\alpha 0} = \sigma'_{v0}$  and  $\tau_{\alpha 0} = 0$ . Then, under constant volume conditions,  $\tau_\alpha$  was increased using a shearing strain rate of 0.9%/h. The specimen for the  $\alpha = 90^\circ$  test was cut vertically and subjected to  $\sigma'_{\alpha 0} = 0.6 \sigma'_{v0}$  and  $\tau_{\alpha 0} = 0$  before undrained



**Figure 18.17** Influence of rate of shear on stress paths for consolidated-undrained tests on a soft clay consolidated beyond the preconsolidation pressure (data from Lefebvre et al. 1983).

shear. Two  $\alpha = 90^\circ$  tests were performed. In one test, the undrained shear stress was applied in the vertical direction to approximate sliding in the vertical direction along a vertical plane. In the other, the shear stress was applied in the horizontal direction to approximate the mode of shear in the field vane test (Article 11.5.2). For these two tests, the observed undrained behavior was almost identical.

For the  $\alpha = 30^\circ, 45^\circ$ , and  $60^\circ$  tests the samples were cut at the corresponding angles to the horizontal and subjected to  $(\sigma'_{\alpha o}, \tau_o)$  equal to  $(0.9 \sigma'_{vo}, 0.18 \sigma'_{vo})$ ,  $(0.8 \sigma'_{vo}, 0.2 \sigma'_{vo})$  and  $(0.7 \sigma'_{vo}, 0.18 \sigma'_{vo})$ , respectively. In the compression tests,  $\tau_\alpha$  was increased in the direction of  $\tau_{\alpha o}$ , whereas in the extension specimens it was applied in the direction opposite to  $\tau_{\alpha o}$ . Because the radial stress is not measured in the DSS apparatus, the state of stress in the specimen is not completely defined. Therefore, the stress paths in Fig. 18.16 correspond to the state of stress on the  $\alpha$ -planes. Figure 18.16 dramatically illustrates that the undrained shear strength of a soft clay is not a constant soil property and that the mobilized undrained shear strength depends on the orientation of the shear plane with respect to the direction of deposition and consolidation, as well as on the mode of undrained shear. Figure 18.16 also illustrates that, although in the DSS apparatus only a shear stress is applied to the specimen, the effective normal stress decreases because of the tendency of the soft clay to consolidate during shear.

Figure 18.17 shows the influence of the rate of shear on the undrained stress path of a soft clay consolidated to the compression range,  $\sigma'_{vc}/\sigma'_p = 1.33$ . The clay had

a liquid limit of 44%, a plastic limit of 23%, and water content of 41%. The standard axial strain rate used in most laboratories for the measurement of undrained shear strength is 0.6%/h. It is apparent that strain rate had a significant effect on the undrained shear strength of this clay. The stress path for sample 3 might not truly represent the behavior of the sample, because the porewater pressure is commonly measured at the base of the sample and the strain rate of this test might not have been slow enough for proper equalization of shear-induced porewater pressure throughout the specimen (Article 17.1).

## ARTICLE 19 DRAINED SHEAR STRENGTH

### 19.1 Drained Shear Strength of Granular Soils

The drained shear strength of granular soils is related to the ease with which particles can move in the general direction of shear. If relative particle movement takes place only in that direction, as in sliding of one particle on a flat surface, then the drained shear strength is determined by the angle of interparticle sliding friction,  $\phi'_\mu$ . Values of  $\phi'_\mu$  for minerals and rocks that commonly form the particles of granular soils, including rockfill, are given in Tables 19.1 and 19.2. They range from  $20^\circ$  to  $40^\circ$ , or more commonly from  $25^\circ$  to  $35^\circ$ . Frictional resistance between two flat surfaces is derived from primary valence bonding at contact points. On a more macroscopic level, it could be reasoned that the magnitude of  $\phi'_\mu$  is determined by surface microroughness that comes into play during shear. This roughness is related to the strength, texture, and hardness of the surface, which in turn are



**Table 19.1 Sliding Friction Angle of Minerals in Water**

Mineral	$\phi'_\mu$ , Range, deg (Typical Value)
Quartz	22–35 (26)
Feldspar	36–38 (37)
Hornblende	31
Calcite	31–34 (33)
Anthracite	31
Chalk	30

**Table 19.2 Sliding Friction Angle of Flat Rock Surfaces in Water in  $\sigma'_n$  Range of 0.07 to 7 MPa**

Rock	$q_u$ (MPa)	$\phi'_\mu$ Range, deg (Typical Value)	
		Lapped No. 600 grit	Sand- blasted
Lower granite	227	23–28	30–34
basalt		(26)	(31)
Oneta dolomite	90	23–26	30–35
		(25)	(32)
Bedford limestone	48	29–35	35–38
		(33)	(36)
Solenhofen	248	31–35	34–35
limestone		(33)	(35)
Fine-grained Grand	193	23–28	27–33
Coulee granite		(25)	(30)
Berea sandstone	76	24–26	30–34
		(25)	(32)
Schistose gneiss	97	20–26	22–27
		(23)	(24)
Hackensack	124	24–30	25–31
siltstone		(27)	(28)

Data from Coulson (1970).

determined by the crystal structure of the minerals and intercrystalline bonding. For example, high values of  $\phi'_\mu$  for limestone (37°), as opposed to quartzite (30°), result from a combination in the lower-strength limestone of more effective microinterlocking, lower hardness, and larger grain texture.

During shearing of a granular mass such as a sand, gravel, or rockfill, particle movement does not occur exclusively in the general direction of shear. In dense granular soils under low confining pressure, particles push adjacent grains out of the way or move up and over them,

as indicated by the expansion or dilation of the granular mass during shear. Intense dilation suggests not only closely packed and interlocked grains, but also the climbing of grains over adjacent grains to move in the direction of shear. Particle pushing and climbing, termed geometrical interference or interlocking, generate resistance in addition to  $\phi'_\mu$ .

As effective confining pressure increases, pushing adjacent particles out of the way or climbing over them becomes more difficult. Relative particle displacements are accomplished more and more through particle crushing or shattering. With increased particle crushing, relative particle movements occur mainly in the direction of shear, and thus geometrical interference is minimized. Grain breakage is determined largely by particle strength; however, it is also affected by particle shape, gradation, size, and porosity. Particle breakdown is favored by angularity of particles, especially those of quarried rock (which contain fresh defects such as fissures and cracks), by uniform gradation, by large particles (which are more likely to include defects), and by high initial porosity. At any effective confining pressure, uniform gradation and high porosity lead to high contact stresses and thus particle crushing. On the other hand, with high-strength grains and in well-graded dense granular masses with subrounded grains, particle crushing begins only at high confining pressures. The geometrical interference component of strength may disappear at an effective confining pressure corresponding to values of  $\sigma'_n$  that may range from 1.5 to 15 MPa; the range depends on the strength of the grains and other factors. The lower limit may apply to a poorly graded angular quarried mica gneiss, crushed chalk, or anthracite, and the upper limit to a well-graded subrounded alluvial sand and gravel composed of basalt or quartzite.

The decrease in the geometrical interference component of shear strength with increasing effective confining pressure leads to a curved strength envelope in the Mohr diagram, as shown in Fig. 19.1. The friction angle,  $\phi'$ , defined by the slope of the strength envelope, consists of two components, interparticle sliding friction,  $\phi'_\mu$ , and geometrical interference,  $\phi'_g$ . Thus

$$\phi' = \phi'_\mu + \phi'_g \quad (19.1)$$

The value of the geometrical interference component  $\phi'_g$  ranges from 0° at high effective confining pressures, where particle movement is achieved through sliding and particle crushing, to 30° or more at low effective confining pressures, where relative movement involves pushing adjacent particles out of the way and climbing over them. The geometrical interference itself may be expressed as the sum of  $\phi'_d$ , produced by dilation or particle climbing, and  $\phi'_p$ , caused by particle pushing and rearrangement:

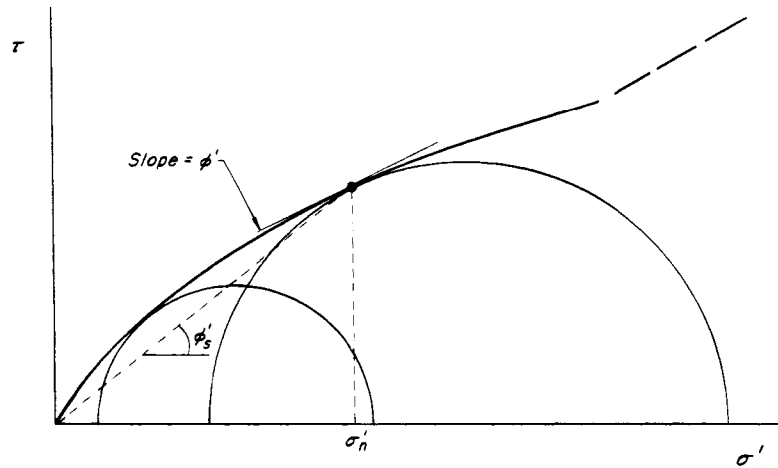


Figure 19.1 Strength envelope in Mohr diagram for a dense granular soil.

$$\phi'_g = \phi'_d + \phi'_p \quad (19.2)$$

As the initial porosity of a granular soil increases, the contribution of the dilation component  $\phi'_d$  decreases. In the loose condition, particles move in the general direction of shear mainly by pushing adjacent particles out of the way. This type of particle interaction is indicated by contraction of the granular mass during shear. At a particular initially high porosity  $n_o^*$ , volumetric strain levels off at maximum strength and thereafter remains constant. For this initial loose condition,  $\phi'_d = 0$  and

$$\phi' = \phi'_\mu + \phi'_p \quad (19.3)$$

The  $\phi'_p$  component of the friction angle, which develops by particles pushing adjacent particles out of the way at constant volume, has values typically in the range of  $5^\circ$  to  $6^\circ$ . The magnitude of  $\phi'$  corresponding to the initial condition  $n_o^*$ , for which there is no tendency for volume change as the contraction rate levels off at maximum strength, is designated the constant volume friction angle,  $\phi'_{cv}$ .

At the initial porosity corresponding to  $\phi' = \phi'_{cv}$  interparticle sliding friction,  $\phi'_\mu$  is fully mobilized, and particles pushing adjacent particles generate an additional  $\phi'_p$  resistance of  $5^\circ$  to  $6^\circ$ . In some granular soils such as fine sands, it may be possible under field or laboratory conditions to attain initial porosities looser than  $n_o^*$  (Bjerrum et al. 1961). After shear deformation of these very loose sands starts, some particles cannot keep up with the movement of adjacent particles, and the contraction rate  $d(V/V_o)/d\epsilon$  remains greater than zero throughout shearing. In this range of porosity the contribution of  $\phi'_p$  disappears, and even interparticle sliding friction may not be fully mobilized. Thus,  $\phi'$  can actually be less than  $\phi'_\mu$ , as illustrated in Fig. 19.2. For such very loose sands, undrained shear strength (Article 20) is more relevant.

The triaxial compression test is one of the most common methods of determining  $\phi'$  and is the source of most

of the existing data on the friction angle of granular soils. In the TC test, particles have the freedom to move in any direction, and this maximum degree of freedom minimizes geometrical interference. In the field, deformation boundary conditions are often closer to plane-strain shear in which deformation is constrained in one direction. This constraint reduces the degree of freedom of particle movement and maximizes geometrical interference. Thus, in general:

$$\phi'(\text{plane-strain shear}) \geq \phi'(\text{triaxial shear}) \quad (19.4)$$

The difference between plane-strain and triaxial  $\phi'$  becomes small when there is no significant tendency for geometrical interference. Existing data on the relationship between plane strain  $\phi'$  and triaxial  $\phi'$ , summarized in Fig. 19.3, indicate a maximum difference of  $8^\circ$ .

Water has no significant effect on the interparticle sliding resistance,  $\phi'_\mu$ , in the range of particle surface roughness commonly encountered under natural conditions. However, water can influence the drained shear strength of granular soils by its possible effect on the grain strength and thus on  $\phi'_g$ . If, for example, the grains are weathered and contain fissures or pores with fillings that can be softened by water, particle breakage increases and geometrical interference can be expected to decrease. In quarried rockfills, water weakens particle contacts, most probably through a slaking process, and particle breakage increases.

The secant friction angle  $\phi'_s$ , defined in Fig. 19.1, is a convenient parameter for expressing a curved strength envelope for granular soils. The drained shear strength of a granular soil on any plane with an effective normal stress  $\sigma'_n$  is given by:

$$s = \sigma'_n \tan \phi'_s \quad (19.5)$$

where the value of  $\phi'_s$  depends on the magnitude of  $\sigma'_n$ . Existing data on the drained shear strength of granular

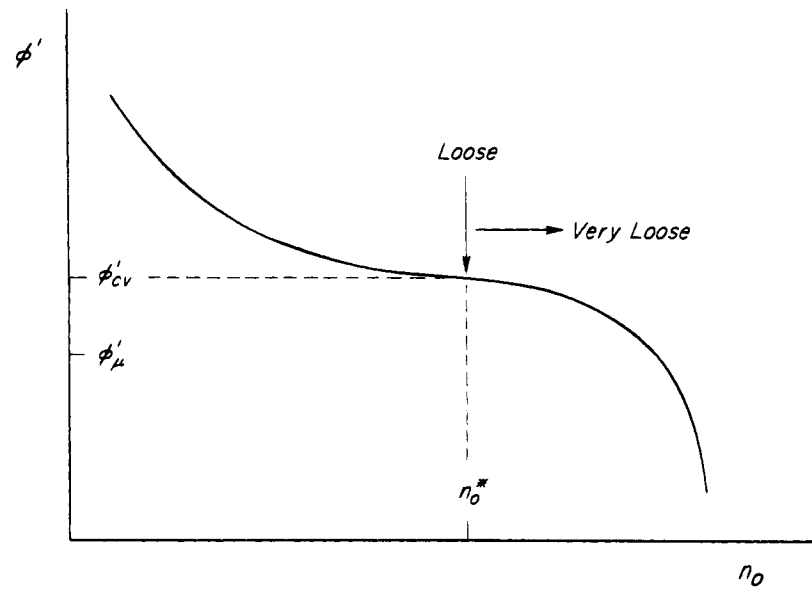


Figure 19.2 Behavior of  $\phi'$  as porosity increases from dense to loose and very loose.

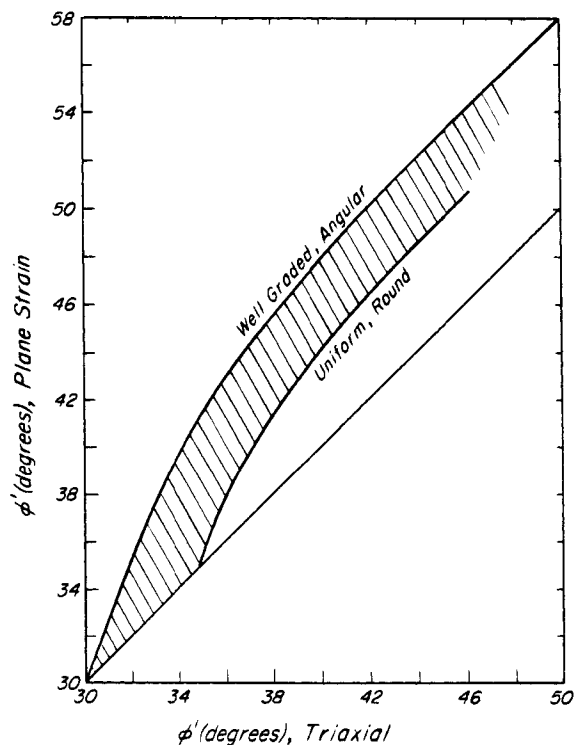


Figure 19.3 Relation between plane-strain  $\phi'$  and triaxial  $\phi'$  for granular soils.

soils have been used to prepare Fig. 19.4. Most of the data are from triaxial compression tests. At low confining pressures the value of  $\phi'_s$  ranges from  $35^\circ$  to  $60^\circ$ , whereas at high confining pressures it is approximately equal to  $\phi'_\mu$ . The values of  $\phi'_s$  for sand and sandy gravel correspond to alluvial subrounded particles of very sound, strong,

massive minerals or rocks. The values also depend on the initial porosity and, to some extent, on gradation, which influences geometrical interference by minimizing particle breakage. Initial porosities in the range of 0.15 to 0.35 are achieved only in well-graded gravel and granular soils that consist of particles larger than coarse sand. Uniform sands have porosities generally in the range of 0.35 to 0.55.

If sand particles are uniform and rounded, the value of  $\phi'_s$  for low values of  $\sigma'_n$  is about  $4^\circ$  lower than for subrounded particles; however, the difference gradually decreases as  $\sigma'_n$  increases, as illustrated in Fig. 19.4. Thus, the data in Fig. 19.4 include practically every type of sand or gravel, as well as larger alluvial particles of strong massive minerals and rocks.

The quarried rockfill data included in Fig. 19.4 (e.g., Charles and Watts 1980) represent five grades of rockfill, from grade A down to grade E, of which the particle strengths are specified in Table 19.3. However, more than the particle strength is involved in the difference between the grades. For example, grade A rockfill corresponds not only to a strong rock, such as a basalt, with particle  $q_u = 240$  MPa, but also to material that possesses moderate to high  $\phi'_\mu$ , in the range of  $30^\circ$  to  $35^\circ$ , and is well graded. These qualities make a very low initial porosity of 0.17 attainable with a good compaction procedure. At the other extreme, a combination of a very weak rock, such as weathered mica gneiss with particle  $q_u = 70$  MPa, low  $\phi'_\mu$  of  $22^\circ$  to  $25^\circ$ , and poor gradation, results in a lower limit for initial porosity of about 0.4 with good compaction effort.

The values of  $\phi'_s$  for a sand composed of weak- or intermediate-strength particles can be estimated from Fig.

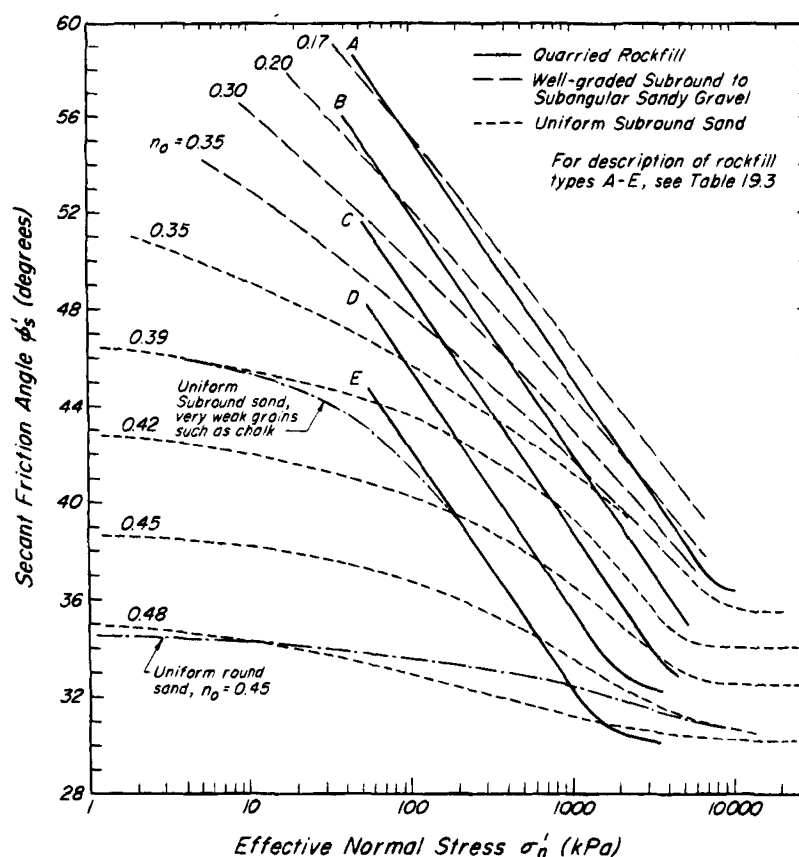


Figure 19.4 Values of secant friction angle for granular soils.

Table 19.3 Unconfined Compressive Strength of Particles for Rockfill Grades in Fig. 19.4

Rockfill Grade	Particle $q_u$ (MPa)
A	$\geq 220$
B	165–220
C	125–165
D	85–125
E	$\leq 85$

19.4 by starting with the values of  $\phi'_s$  for the strong particles at low  $\sigma'_n$  and merging to the corresponding rockfill as  $\sigma'_n$  increases. The procedure is illustrated in Fig. 19.4 for a uniform, subrounded sand with very weak grains of material such as chalk.

Because undisturbed sampling of granular soils is difficult, the friction angle  $\phi'$  of sand deposits is often estimated from the results of *in situ* penetration tests (e.g., Schmertmann 1975, Broms and Flodin 1988). In quartz sands, in which compressibility associated with grain crushing is not a significant factor, the friction angle  $\phi'$  and the effective confining pressure  $\sigma'_{ho} = K_o \sigma'_{vo}$  are the

main factors that determine the penetration resistance. It is, therefore, reasonable to expect that, for normally consolidated young sands, a correlation should exist between  $\phi'$  and the penetration resistance measured by the dynamic standard penetration test DSPT (Article 11.3.2) or the push-cone penetration test PCPT (Article 11.4.2), when the penetration resistances are normalized to take into account the effective confining pressure. The normalized values for the PCPT tip resistance  $q_c$  may be taken as

$$q_{c1} = q_c(100/\sigma'_{vo})^{1/2}$$

and for the DSPT as

$$(N_1)_{60} = N_{60}(100/\sigma'_{vo})^{1/2}$$

where  $\sigma'_{vo}$  is in kPa (Liao and Whitman 1985).

The best data on the correlation between  $\phi'$  and  $q_c$  were obtained from  $q_c$  measurements in large calibration chambers (Holden 1971, Veismanis 1974, Parkin et al. 1980, Chapman and Donald 1981, Baldi et al. 1981, Villet and Mitchell 1981). The friction angle  $\phi'$  was determined from drained triaxial compression tests at confining pressures approximately equal to the values of  $\sigma'_{ho}$  in the calibration chamber. The correlation has been generally confirmed by predictions based on bearing capacity the-

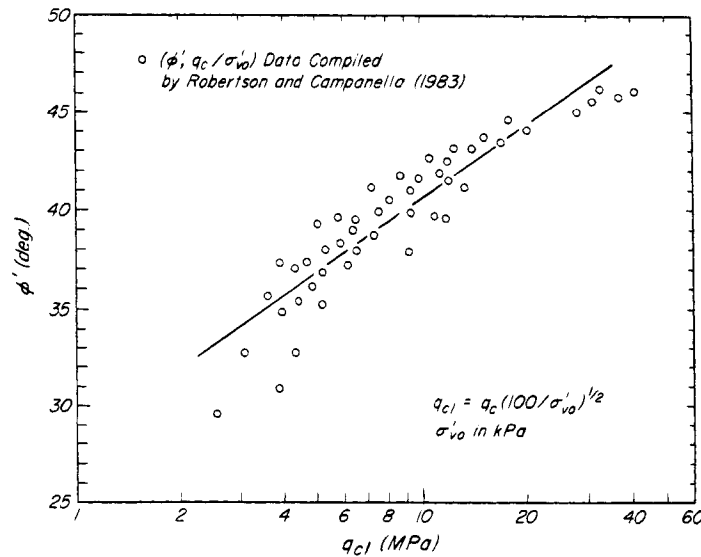


**Figure 19.5** Empirical correlation between friction angle  $\phi'$  of sands and normalized push cone tip penetration resistance.

ory (de Beer 1948, Meyerhof 1961, Janbu and Senneset 1974, Durgunoglu and Mitchell 1975, Mitchell and Keaveny 1986). Data compiled by Robertson and Campanella (1983) are plotted in terms of  $q_{c1}$  in Fig. 19.5. The correlation is mainly applicable to normally consolidated young sand deposits composed of quartz and feldspars. It underestimates by several degrees the friction angle of compressible carbonate sands with crushable particles, and it overestimates by several degrees the friction angle of overconsolidated or aged sands with values of  $\sigma'_{ho}$  higher than those in normally consolidated young deposits (Schmertmann 1975).

The correlation between  $\phi'$  and  $(N_1)_{60}$  in Fig. 19.6 is based on various proposals for the relationship between  $\phi'$  and standard penetration blow count  $N$  (Peck et al. 1953, De Mello 1971, Schmertmann 1975, Stroud 1988). It underestimates  $\phi'$  for calcareous sands with crushable particles and overestimates  $\phi'$  for overconsolidated sands (Stroud 1988). Figure 19.6 also includes relations between  $\phi'$  and  $(N_1)_{60}$  determined from the empirical correlation in Fig. 19.6 together with  $q_c/N_{60}$  values of 400 and 500 kPa for sand deposits. The two different empirical correlations between  $\phi'$  and  $q_c$  and between  $\phi'$  and  $N_{60}$ , which have originated from separate databases, lead to comparable values of  $\phi'$  for sands.

## 19.2 Drained Shear Strength of Cohesive Soils

The drained shear strength of normally consolidated cohesive soils is defined by the friction angle  $\phi'$ , as follows:

$$s = \sigma' \tan \phi' \quad (19.6)$$

The effective normal stress  $\sigma'$  on the plane of shear is determined by the total normal stress and the equilibrium

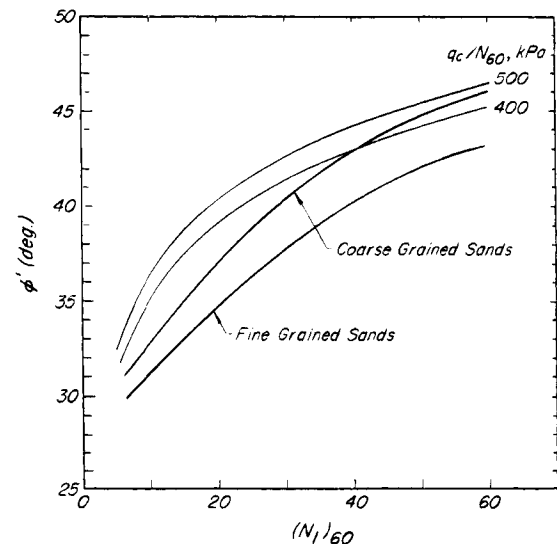


**Figure 19.6** Empirical correlation between friction angle  $\phi'$  of sands and normalized standard penetration blowcount.

hydrostatic or steady porewater pressure condition. The friction angle  $\phi'$ , which corresponds to a more or less random arrangement of particles, is mainly a function of the clay mineral content and clay mineralogy of the composition. Values of  $\phi'$  for the full range of clay compositions are shown in Fig. 19.7. Among the pure clay minerals, sodium montmorillonite (consisting of filmy particles) has the lowest value of  $\phi'$ , whereas attapulgite (with interlocking fibers) exhibits the highest value. Typical values of  $\phi'$  for soft clay, stiff clay, and shale constituents are in the range of 25° to 35°, 20° to 35°, and 15° to 35°, respectively. The water-filled and rough surface-

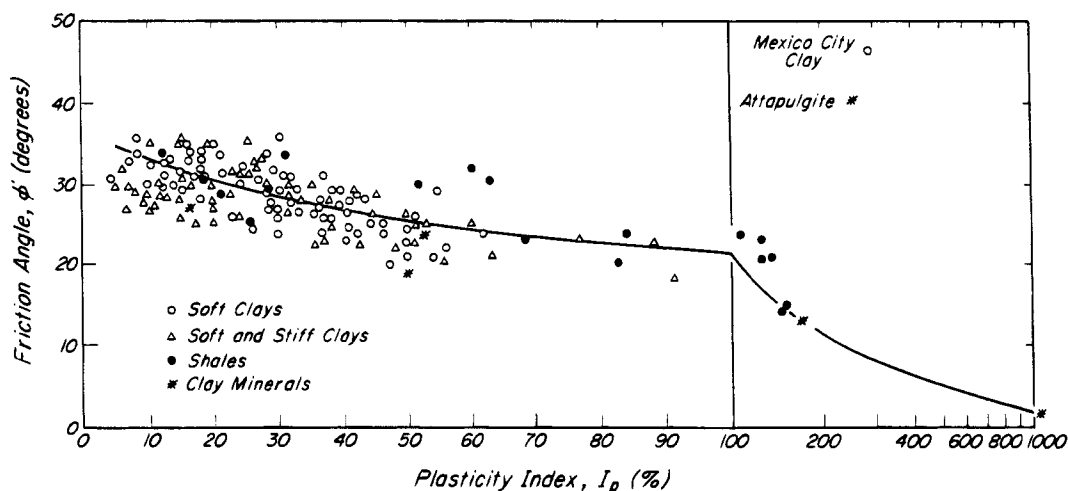


**Figure 19.7** Values of friction angle  $\phi'$  for clays of various compositions as reflected in plasticity index.

textured diatom shell fragments that make up the matrix of Mexico City clay are capable of generating unusually large friction angles while retaining an exceptionally large amount of water. At each plasticity index, different values of  $\phi'$  result from the difference in clay size fraction of soils and from the difference in effective normal stress at which  $\phi'$  was measured. The high values of  $\phi'$  correspond to soils with clay size fraction of less than 20% and effective normal stresses less than 50 kPa. The low values are representative of soils with clay size fraction of greater than 50%, subjected to effective normal stresses of higher than 400 kPa. Torsional ring-shear tests by Stark and Eid (1994) show that  $\phi'$  may decrease by  $4^\circ$  as the clay size fraction increases from less than 20% to more than 50% or as effective normal stress increases from less than 50 kPa to more than 400 kPa. Although there is a strong correlation between friction angle and plasticity index, the significant scatter of the data around the empirical relationship shown in Fig. 19.7 indicates that  $\phi'$  should be measured directly on major projects. The drained triaxial compression test on specimens normally consolidated under an equal all-around pressure is most suitable for determining  $\phi'$ .

The drained shear strength of an overconsolidated clay should ordinarily be greater than the drained strength of the same constituents in a normally consolidated state, mainly because the overconsolidated clay has a smaller preshear void ratio. However, the mobilized or available drained shear strength of heavily overconsolidated clays strongly depends on their condition before shear and when they reach failure. An overconsolidated clay mobilizes its intact strength at failure only if it has remained in an intact condition during geological unloading and associated swelling, remains intact in response to a construction operation that eventually leads to a failure, and reaches its peak resistance at the instant of a global instability.

On the other hand, an overconsolidated clay has available at the instant of slip only its fully softened shear strength if it has been badly fissured and jointed during the removal of overburden or of lateral support by erosion, has softened further in response to an excavation process that leads to a long-term drained failure, or has been involved in severe progressive failure. An overconsolidated clay mass that has already experienced large displacements along a major plane of shear can mobilize only the residual shear strength if movements are reactivated along the preexisting shear surface. The presence in the fabric of an overconsolidated cohesive soil of discontinuities, such as brecciations, slickensides, fissures, joints, and shears, becomes an increasingly important factor in relation to the available drained shear strength at failure as preconsolidation pressure, overconsolidation ratio, plasticity, and, therefore, stiffness and brittleness increase.

### 19.2.1 Intact Shear Strength

The drained intact shear strength of a saturated overconsolidated clay is commonly expressed in terms of the intercept  $c'$  and the angle  $\phi'$  of a failure envelope in the Mohr diagram, as

$$s = c' + \sigma' \tan \phi' \quad (19.7)$$

In general the angle  $\phi'$  in Eq. 19.7 is not comparable to the friction angle in Eq. 19.6. An example of a failure envelope for an intact sample of an overconsolidated London clay is shown in Fig. 19.8. The sample was taken from a depth of 35 m below ground level, and the best estimates of  $\sigma'_{v0}$  and  $\sigma'_p$  are 390 kPa and 4100 kPa, respectively. London clay was deposited under marine conditions in the Eocene period about 30 million years ago. Subsequently, uplift and erosion in Tertiary and Pleistocene times removed 170 m to 340 m of overlying sediments. The failure envelope of the overconsolidated clay

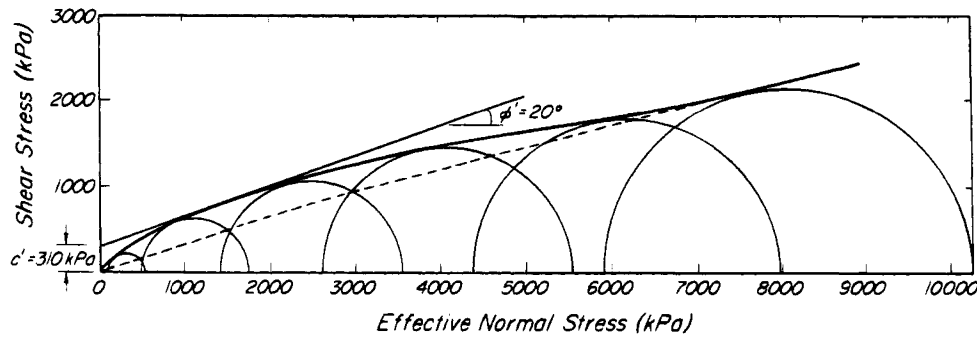


**Figure 19.8** Mohr envelope for a sample of intact London clay from a depth of 35 m (data from Bishop et al. 1965).

shows a very marked curvature before it merges with the envelope corresponding to the normally consolidated condition. There is a significant change in slope and intercept in passing from a low-stress to a high-stress range:  $c'$  and  $\phi'$  change from 100 kPa and  $30^\circ$ , respectively, in the lower range to 790 kPa and  $10^\circ$  in the upper range. This type of nonlinear failure envelope is characteristic of the intact shear strength of overconsolidated soft clays, stiff clays, and shales. Therefore, in reporting the values of  $c'$  and  $\phi'$ , the effective normal stress range to which they correspond must be specified. For example, in Fig. 19.8 the combination  $c' = 310$  kPa,  $\phi' = 20^\circ$  corresponds only to the  $\sigma'$  range of 1000 to 2000 kPa. Outside this range, the same set of strength parameters would greatly overestimate the intact strength of this clay.

Because the intact strength envelope depends strongly on the preconsolidation pressure and overconsolidation ratio, a summary of such strengths for a variety of overconsolidated soft and stiff clays and shales in terms of the values of  $c'$  and  $\phi'$  has little meaning. For this reason, the drained strength of an overconsolidated clay is expressed in terms of the drained strength of the same constituents in the normally consolidated state as

$$s = \sigma' \tan \phi' \cdot \text{OCR}^{1-m} \quad (19.8)$$

According to Eq. 19.8, the drained intact strength of an overconsolidated clay is greater by a factor of  $\text{OCR}^{1-m}$  than the drained shear strength of the same constituents in a normally consolidated state as given in Eq. 19.6. The overconsolidation ratio, OCR, in Eq. 19.8 is defined in terms of the effective normal stress at which the failure envelope of the overconsolidated clay joins the envelope for the normally consolidated condition.

Values of the exponent  $m$  for soft and stiff clays and shales are presented in Table 19.4. The term intact refers to completely undisturbed and unfissured materials, whereas *destructured* describes slightly fissured stiff clays and shales, and soft clays that have been sheared beyond the yield surface to a large-strain condition. Destructured does not refer to fully softened stiff clays and shales or

**Table 19.4** Values of  $m$  in Eq. 19.8

Material	$m$	
	Intact	Destructured
Cemented soft clays	0.4–0.5	0.5–0.7
Stiff clays and shales	0.5–0.6	0.6–0.8
Soft clays	0.6–0.7	0.7–0.9

remolded soft clays for which the values of  $m$  are expected to range from 0.9 to 1. The lowest values of  $m$  are obtained for bonded or cemented soft clays such as those of eastern Canada. Beneath level ground such clays exhibit OCR values between 1.5 and 3, whereas in natural or cut slopes the OCR ranges from 2 to 20. The low values of  $m$  define the portion of the failure envelope above the normally consolidated strength envelope (Eq. 19.6).

Frequently the available intact strength is significantly modified by fissuration and softening. The considerable variation in strength of what is believed to be intact material is most likely associated with the degree of fissuring of the clay. This is best illustrated by a comparison of drained strengths of undisturbed samples of an overconsolidated clay taken from various depths below the ground surface. For London clay, peak strength parameters in the effective normal stress range of 100 kPa to 600 kPa, as measured in 60-mm direct shear tests or 38-mm-diameter triaxial compression tests, are compared in Table 19.5. A change in the nature and scale of the fissure pattern accounts for the marked decrease in the value of  $c'$  as the depth decreases. For London clay the mean spacing of the randomly oriented fissures decreases and the number of fissures per unit volume increases as the upper surface of the clay is approached. This suggests that stress release together with chemical and physical weathering play an important role in the genesis of fissures. Fissures within the top 12 m of London clay are typically between 25 and 75 mm long and rarely exceed

**Table 19.5 Intact Strength of London Clay, as Modified by Fissuration**

Depth (m)	Values of Parameters in Eq. 19.7	
	$c'$ (kPa)	$\phi'$
2–3	7	20°
3–7	15	20°
7–10	31	20°
35	100	30°

150 mm; at the lower elevations, the fissures are more widely spaced. Beneath level ground high lateral pressures tend to keep the fissures closed, whereas in areas of sloping ground lateral stress release may lead to their opening.

Large slopes of failure envelopes for intact samples in the low effective stress range, such as 30° for London clay in Table 19.5, reflect the aggregated nature of the fabric of intact overconsolidated clay and interparticle friction resulting from interlocking of the aggregations. These slopes may give a misleading impression of the frictional characteristics of the components of the clay, which are reflected in a more meaningful way by the normally consolidated or fully softened  $\phi'$  in Eq. 19.6, or the residual friction angle  $\phi'_r$ . Data in Table 19.5 also show that before large displacements concentrate along a major plane of shear, the slope of the intact failure envelope does not drop below the fully softened friction angle, the value of which for London clay is near 20°. Thus, for fissured clays, the difference in degree of fissuration is mainly reflected in the magnitude of the cohesion intercept  $c'$ .

The intact strength of nonfissured overconsolidated clays is independent of the size of undisturbed specimens used to measure it. It is also independent of whether drained tests or undrained tests with porewater pressure measurements are carried out. On the other hand, where the spacing of the fissures is small in comparison with the size of the specimens, the drained shear strength of a fissured clay, such as that encountered at shallow depths in London, strongly depends on the size of the specimen in relation to the fissure spacing. The influence of the ratio of specimen size to fissure spacing is reflected mainly in the measured value of  $c'$ ; small specimens with low frequency of fissures generally indicate large values of  $c'$ . This creates a serious problem in measuring and selecting strength parameters for stability analyses in overconsolidated clays. Gradual opening or elongation of fissures resulting from the effects of excavation or sampling disturbance, including delay in testing, can lead to an underestimation of the intact strength available *in situ*. For

example, on the assumption that London clay at a depth of 35 m below ground surface is practically free from fissures, the intact strength measured using high-quality block samples, as shown in Fig. 19.8, should be available at that depth to provide the bearing capacity of deep bored cylindrical foundations that are constructed in place without disturbing the clay or allowing time for the fissures to open. One mechanism, however, that could lead to an available strength at 35-m depth less than the intact strength in Fig. 19.8 is progressive failure along a global slip surface, because the overlying fissured zones may require higher strain to mobilize their peak strength.

More often, fissures lead to an overestimation of the available strength in full-scale field problems, because laboratory tests can rarely be made on samples large enough to be representative of the fissured nature of the clay. This is especially important for excavations and cut slopes less than 10 to 20 m deep. Both drained long-term and short-term strengths of a fissured clay mass can be appreciably lower than the strength of the intact clay between the fissures. There is abundant evidence that in overconsolidated fissured clays the cohesion intercept  $c'$  prevailing at the time of a long-term drained failure is far less than the value measured in conventional laboratory tests on small specimens (Mesri and Abdel-Ghaffar 1993). For London clay the ratio of the short-term strength of fissured and jointed clay masses in the field to the undrained strength measured on 38-mm-diameter triaxial compression specimens is in the range of 55% to 75%. Back analyses of first-time slope failures in London clay suggest that even the drained strength measured on large-diameter samples overestimates the strength available on the slip surface in the field. A value of  $c'$  equal to 7 kPa was measured using triaxial compression specimens up to 260 mm in diameter, as compared with the back-calculated  $c'$  of only 1.0 kPa from the average field strength mobilized when a slope failure occurred. The angle  $\phi'$  was assumed to be 20° in both cases. In excavated slopes it is possible that, during the decades that are required for the increase in porewater pressure from the initially low values following stress reduction during excavation to the steady seepage values, fissures open as a result of small movements associated with the removal of lateral support. The clay may soften along these fissures until global failure occurs. Another factor that can contribute to a lower  $c'$  available on a slip surface is progressive failure induced by the joints and fissures.

The decrease in cohesion intercept  $c'$  by fissuration or other weathering mechanisms in overconsolidated clay is related to the difference between fully softened  $\phi'$  and residual  $\phi'_r$ . For London clay, which has a  $\phi'_r$  value of about one-half  $\phi'$ , fissuration has a significant effect on the drained strength, reflected in a small value of  $c'$ . On the other hand, in low plasticity boulder clays of glacial origin ( $I_p < 20\%$ ) as well as silty soft clays in eastern



Canada, the postpeak large-strain values of  $c'$  in the range of 5 to 10 kPa measured in laboratory tests are also mobilized in long-term slope failures in the field. Most of the clay fraction in these clays is composed of mechanically pulverized rock flour. For clays of low plasticity, Fig. 19.7 shows that the values of  $\phi'$  are near  $30^\circ$ , and according to Fig. 19.16 the difference between  $\phi'_s$  and  $\phi'$  is small. This suggests that clays with low clay content and plasticity are generally unfissured or, as discussed later, that the small difference between  $\phi'$  and  $\phi'_s$  minimizes the influence of fissures on available shear strength. Typical unsheared fissures and joints exhibit a matt surface texture. In London clay this consists of mounds and depressions of the order of 0.1 mm high and 0.2 to 0.4 mm in diameter, without clay-particle reorientation at the fissure surface. However, some fissures are slickensided with a polished and striated surface, or are coated with a thin clay gouge. These features suggest some particle orientation on particular fissures during the mobilization of peak strength.

In summary, whenever the intact strength is used in design or analysis, the significance of existing or potential fissures on the  $c'$  available during a global instability must be examined. The size of the specimen in tests for the measurement of drained strength should reflect, as much as is practically feasible, the frequency of fissures in the field. Further reductions in the measured  $c'$  may be necessary to take into account the possible influence of progressive failure, because  $c'$  and  $\phi'$  of even a representative specimen may not be mobilized simultaneously on all segments of a global slip surface. Whenever reliance is placed on  $c'$  for stability of a mass of clay, local experience should be examined carefully or a conservative approach adopted.

In unsaturated soils that are not submerged or flooded, a suction is imposed on the soil by the moisture-deficient environment which denies the soil full access to water. In unsaturated soils with air voids connected to the atmosphere, the total normal stress acts as an effective confining pressure and pushes the soil particles together. In such a soil, and at a constant suction, the increase in shear strength with increasing total normal stress is determined by the friction angle  $\phi'$ . This is illustrated in Fig. 19.9 by a series of suction-controlled direct shear tests on Guadalix Red clay (Escario et al. 1989). At zero suction, the saturated undisturbed clay displays a cohesion intercept  $c'$ . On the other hand, Fig. 19.10 shows that at a constant normal stress, the increase of shear strength with increasing suction becomes insignificant even in the practical range of suction values up to 4 MPa. The initial slope of the  $s$  vs  $u_s$  relationship is equal to  $\tan \phi'$ , because at  $u_s = 0$  the soil is saturated, and an increment of suction represents a decrease in porewater pressure or an increase in effective stress. However, as the suction increases and the soil becomes unsaturated, the Terzaghi relation (Eq. 15.2) between effective stress and porewater pressure

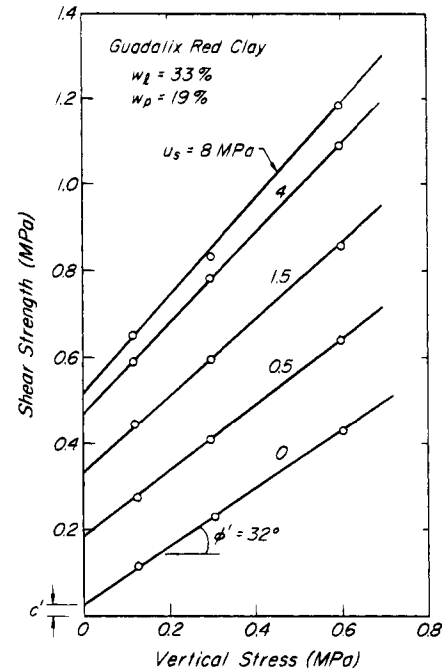


**Figure 19.9** Results of direct shear tests with suction control on Guadalix red clay (data from Escario et al. 1989).

becomes invalid, and a decrease occurs in the component of suction that pulls the soil particles together and generates shearing resistance. For practical purposes, the drained shear strength of unsaturated soils may be expressed as (Abramanto and Carvalho 1989)

$$s = c' + \sigma \tan \phi' + b u_s^a \quad (19.9)$$

Laboratory shear-strength measurements on undisturbed and compacted unsaturated soils in the range of suction up to 4 MPa lead to a mean value of  $a = 0.5$  and values of  $b$  in the range of 2 to 10 (Fig. 19.11). Equation 19.9 and Fig. 19.9 suggest that, at a constant suction, the suction-related shear-strength term is equivalent to a cohesion intercept that is permanently available only in the absence of submergence or a flooding. For example, for a soil with  $\phi' = 30^\circ$ , a value of  $b = 6$  (Fig. 19.11), together with  $a = 0.5$  and a modest suction of 100 kPa, indicate a significant suction-related cohesion intercept of 60 kPa. This explains why slopes in unsaturated residual soils may be steep, and why shallow failures occur in these slopes in the rainy seasons as the soil becomes saturated and suction is lost.

### 19.2.2 Fully Softened Shear Strength

The fully softened drained shear strength of an overconsolidated clay, which may develop under highly fissured and jointed conditions without the presence of a preexisting shear surface, is defined by Eq. 19.6. It is equal to the friction angle  $\phi'$  of clay of the same composition in a normally consolidated state, such as that produced by

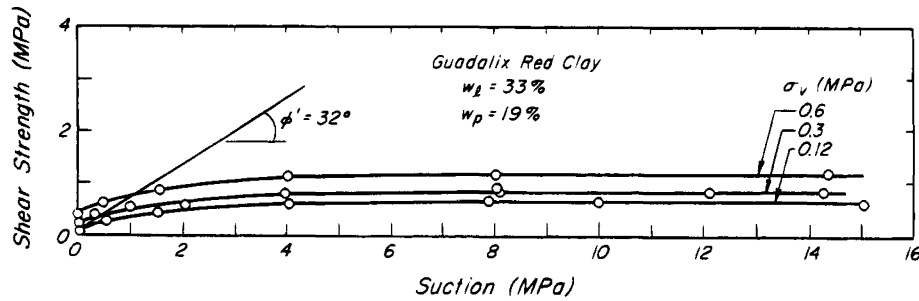


**Figure 19.10** Influence of suction on shear strength at constant vertical-pressure Guadalix red clay (data from Escario et al. 1989).

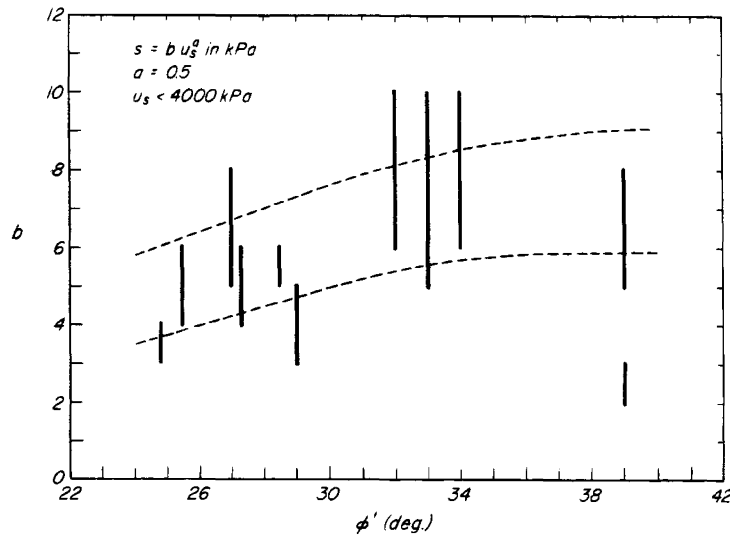


**Figure 19.11** Summary of shear-strength measurements with suction control on undisturbed and on compacted unsaturated soils.

laboratory consolidation from a slurry. The failure envelope of a normally consolidated clay or the fully softened strength envelope, like those in Figs. 19.8 and 19.12, exhibits a slight curvature that indicates a decrease in  $\phi'$  with increasing effective normal stress. Even in the random fabric that corresponds to the fully softened condition, increased effective confining pressure leads to increased face-to-face and reduced edge-to-face interaction among the plate-shaped particles. This results in decreased frictional resistance. For the normally consolidated London clay composition represented in Fig. 19.8,  $\phi'$  starts at  $21^\circ$  in the low-pressure range, whereas it has a value of  $17^\circ$  at high effective normal stresses. Back analyses of first-time slides in stiff fissured clays on the basis of a value of fully softened  $\phi'$  from laboratory tests at moderately high effective normal pressures and the best estimate of steady porewater pressure conditions may indicate a small cohesion intercept  $c'$ . For example, back analyses of first time slides in London clay, using  $\phi' = 20^\circ$  and values of pore pressure taken as  $0.3\sigma_{vs}$ , suggest a value of  $c' = 1$  kPa (Fig. 19.13). Such a result indicates that the fully softened failure envelope was

slightly nonlinear, or that a drained strength slightly greater than the fully softened value was available at the time of the slips. That is, either the assumed  $\phi'$  slightly underestimated the fully softened  $\phi'$  within the effective normal pressure range of less than 50 kPa, or a small cohesion intercept had survived fissuration and progressive failure.

The fully softened failure envelope for an overconsolidated clay can be determined by using intact specimens, intact specimens containing a distinct fissure or joint, or reconstituted normally consolidated specimens (Fig. 19.14). For samples consolidated from a slurry and for shear tests along a fissure or joint, the peak strength defines the fully softened failure envelope. When intact specimens are used, or when specimens are remolded at water contents less than the liquid limit, the fully softened strength corresponds to the postpeak shear stress at which the increase in water content during shear levels off. Both drained tests and undrained tests with porewater pressure measurements can be used to define the fully softened failure envelope. The triaxial compression test is suitable for practically every type

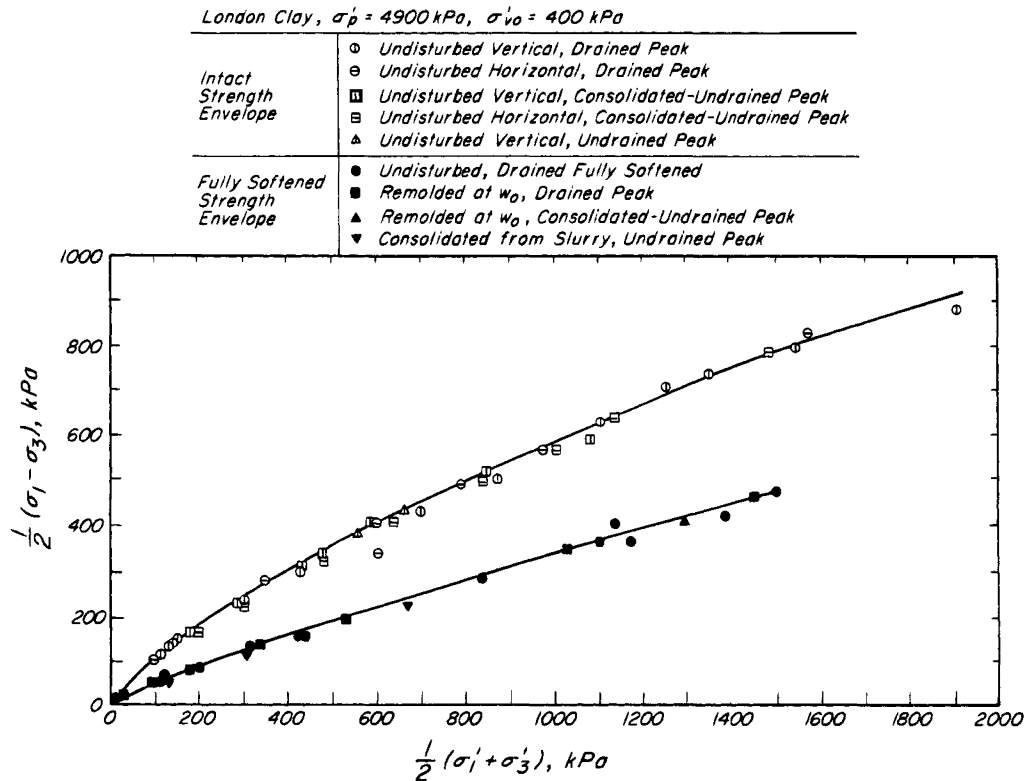


**Figure 19.12** Intact and fully softened strengths of samples of London clay from depth of 35 m (Bishop et al. 1965).

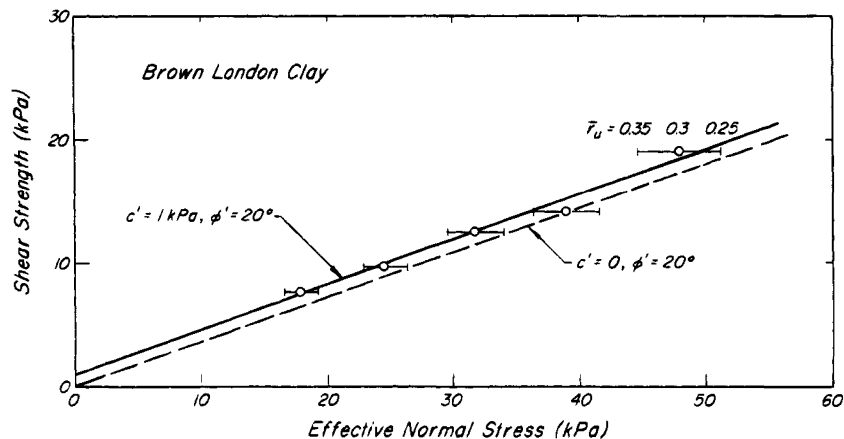


**Figure 19.13** Fully softened shear strengths of brown London clay back-calculated from first-time slides in cuts more than 45 years old (after Skempton 1977).

of specimen and for drained as well as undrained tests. The direct shear test (Article 17.3.2) may be useful for specimens containing a single distinct fissure or joint. However, specimens remolded at a water content higher than the liquid limit or specimens normally consolidated from slurry are preferred for the measurement of fully softened shear strength. Special care must be exercised

on intact specimens to achieve, in the shear zone at the fully softened condition, complete porewater pressure equilibration and softening in drained tests, or complete porewater pressure equalization in undrained tests. Moreover, for intact samples, it may be difficult to define the area of the shear zone and to control axial loads after the formation of distinct shear planes.

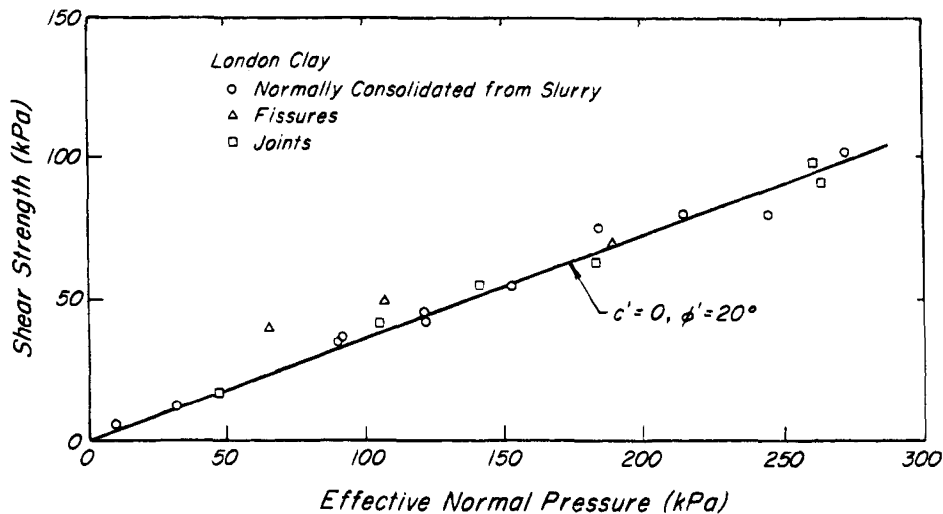


Figure 19.14 Fully softened shear strengths of London clay from laboratory tests (after Skempton 1977).

### 19.2.3 Residual Shear Strength

The residual shear strength in highly overconsolidated stiff cohesive soils that contain plate-shaped clay minerals is reached after large shear displacements have occurred along a continuous major plane of discontinuity. The decrease in shearing resistance from the fully softened to the residual condition results from reorientation of platy particles into a direction parallel to the direction of shearing with correspondingly increased face-to-face interaction of the particles. Residual shear strength is defined in terms of the residual friction angle as

$$s = \sigma' \tan \phi'_r \quad (19.10)$$

A drained failure condition generally prevails during reactivation of a slip on preexisting shear surfaces that have reached the residual condition. This is mainly because there is little tendency for volume change in the oriented clay particles in the shear zone, and partly because the small thickness of the shear zone as compared with the adjoining clay blocks facilitates rapid pore pressure equilibration. Therefore, the effective normal stress in Eq. 19.10 is defined by the steady porewater pressure condition.

The reason for the decrease in shearing resistance is that when particles are oriented face to face, it is difficult to establish short-range contact between them and thus to generate shearing resistance. In relation to residual strengths, particle size and degree of platyness are the most important characteristics of minerals. As particle size decreases and platyness increases, the interparticle contact pressure decreases, edge-to-edge interlocking is minimized, and residual shear strength decreases.

For cohesive soils containing plate-shaped clay minerals, a correlation should exist between  $\phi'_r$  and index prop-

erties such as the liquid limit. The liquid limit is a measure of the ability of the soil constituents to hold water. Water associates with soil particles either through hydration of particle surfaces (adsorbed water) or hydration of the ions surrounding the surfaces (double-layer water). As the particle size decreases and, therefore, as the particle surface area per unit weight increases, the liquid limit should increase. Although for the common clay minerals kaolinite, chlorite, illite, and montmorillonite, platyness and particle size are correlated (as particle size decreases, platyness increases) and platyness may contribute to the ability of particles to hold adsorbed and double-layer water, no simple relationship exists between particle shape and water-holding capacity. For example, needle-shaped attapulgite may have a liquid limit of 345%. Thus, although a correlation between  $\phi'_r$  and liquid limit is expected because each is directly or indirectly related to one or both of the fundamental factors of particle size and platyness, it is also apparent that such a correlation need not be unique. Figure 19.15 shows the trend of decreasing  $\phi'_r$  with increasing liquid limit, clay size fraction, and effective normal stress on the shear surface for stiff clays and shales. For materials with liquid limit in the range of 60 to 200% and clay size fraction more than 50%, the residual friction angle decreases with effective normal stress because high effective normal stresses enhance face-to-face particle orientation during shear displacement.

The magnitude of the fully softened friction angle  $\phi'_s$ , which corresponds to a random arrangement of particles, reflects the ability of particles to establish short-range interaction and interlocking. For example, stiff plates of kaolinite, like the rotund particles of quartz, are able to establish short-range, edge-to-face interaction and inter-

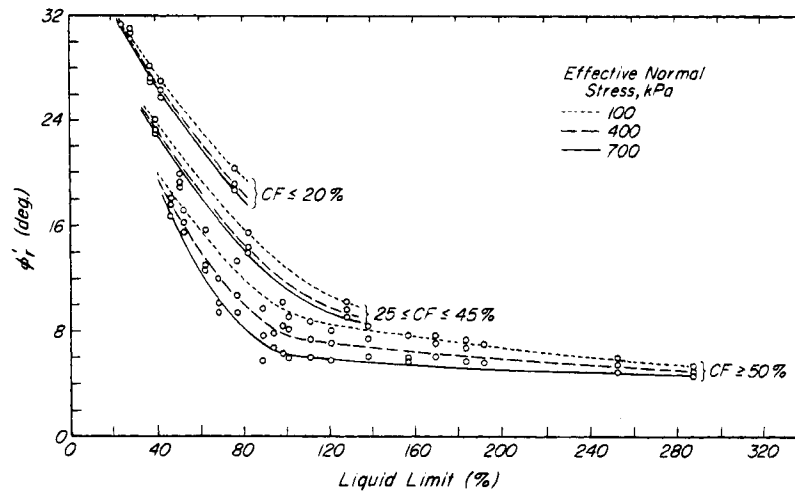


**Figure 19.15** Secant residual friction angle as a function of liquid limit, clay size fraction, and effective normal stress on slip plane (after Stark and Eid 1994).

ference during shear. In contrast, highly flexible films of montmorillonite are capable of doing neither. As the platyness increases, even in a random arrangement of particles, the predominant particle interaction is face to face, because particle edges can bend easily. Thus, a relationship between  $\phi'$  and  $\phi_r'$  should exist because both depend on the fundamental variables of particle size and platyness. Figure 19.16 shows that at two extreme compositions the values of  $\phi'$  and  $\phi_r'$  approach each other. For stiff clays in general, the lower limit is defined by sodium

montmorillonite with 1-nm-thick filmy particles. For such a composition, the predominant particle interaction is face to face for both highly oriented and random fabrics, and values of  $\phi'$  and  $\phi_r'$  are very small and close to each other. At the other extreme are the compositions with nonplaty particles of minerals such as quartz. The decrease in drained shear strength from fully softened to residual, in terms of the difference ( $\phi' - \phi_r'$ ), is a maximum at intermediate compositions. These correspond to clays and shales with values of  $\phi_r'$  in the range of 8 to 12°. For these materials the value of ( $\phi' - \phi_r'$ ) can be in the range of 10 to 20°.

In the field, residual shear strength is mobilized only by reactivation of shearing on preexisting shear planes on which previous large shear displacements have already taken the clay past the peak and fully softened to the residual condition. These conditions may exist, for example, where the ground has been previously sheared by landsliding or other geological processes (Brooker and Peck 1993). Residual shear strength in the laboratory is measured most conveniently by using precut specimens from either undisturbed blocks or reconstituted and consolidated samples. This method concentrates the shear strains at the flat boundary between the two intact stiff blocks, and the residual condition is reached after a total shear displacement in the order of 50 mm. Such a displacement can be achieved cumulatively by using drained reversal direct shear tests (Article 17.3.2). The torsion shear apparatus (Article 17.3.4) allows uninterrupted shear displacement of any magnitude in one direction, but specimen preparation and testing procedure are complex and costly. Use of this type of apparatus is generally unnecessary. Residual shear strength can also be measured by starting from an intact specimen or by using shear surfaces from slip zones in the field. However, for

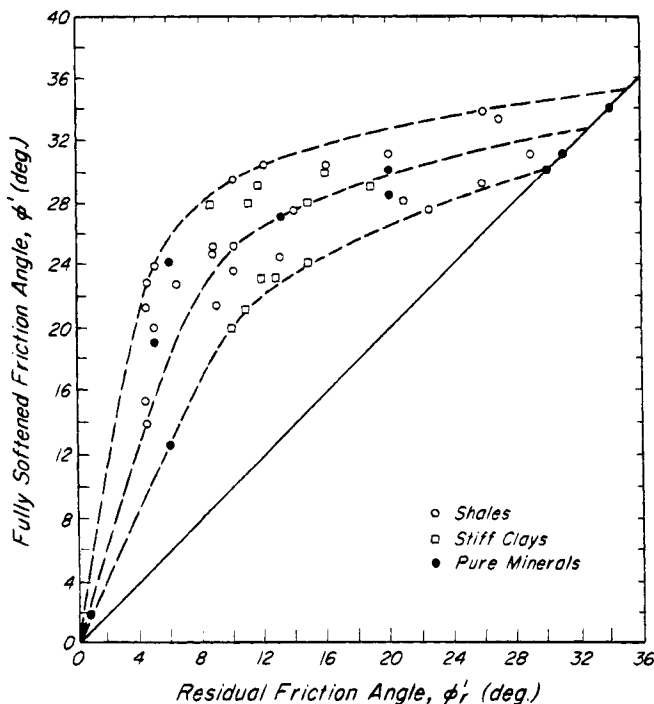


**Figure 19.16** Relationship between fully softened  $\phi'$  and residual  $\phi_r'$ .

intact specimens, shear displacements larger than 50 mm may be required to reach the residual strength.

By far the most complete data on residual shear strength, in terms of both laboratory measurements and field behavior, are available for London clay with a composition consisting primarily of illite with some quartz, kaolinite, montmorillonite, and calcite. Residual shear strengths measured by laboratory tests are compared in Figs. 19.17 and 19.18 with drained shear strength back-calculated from reactivated natural slopes. According to these data, the residual shear-strength envelope defined by laboratory direct shear tests on slip surfaces and by back analysis of unstable natural slopes exhibits a negligible curvature in the effective normal pressure range of 0 to 300 kPa. The data in Fig. 19.17 can be expressed with sufficient accuracy by a straight line of slope  $\phi'_r = 12^\circ$  passing through the origin. Data in Figs. 19.17 and 19.18 show that residual shear strengths, measured by drained direct shear tests on samples of London clay containing natural shear surfaces, compare very well with values derived from back analysis of reactivated landslides. The field residual shear strength was also reliably determined by multiple reversal direct shear tests on cut-plane samples. The ring-shear results in Fig. 19.18, which were obtained after large shear displacements of as much as 500 mm, define a conservative lower limit to the field values, because movement in the ring-shear apparatus is concentrated on a single plane on which maximum particle orientation is achieved. In landslides, however, movement is often accommodated on several different surfaces.

## Problems

1. To evaluate shear strength to be used in stability analysis of a slope, two drained direct shear tests have been performed on samples of a highly overconsolidated clay. One test was carried out on a remolded sample under effective vertical stress of 300 kPa, and a shear strength of 121 kPa was measured. The second test was carried out on a precut sample under effective vertical stress of 300 kPa, and a shear strength of 48 kPa was measured. On the basis of previous field experience with the overconsolidated plastic clay, it is expected that the

peak (intact) strength envelope will show a cohesion intercept  $c'$  (mob) of 10 kPa for effective normal stress range near 200 kPa. Compute the shear strength to be used on a segment of a slip surface on which the effective normal stress is 200 kPa, if the slip plane passes through: (a) material that is badly fissured and jointed; however, there is no preexisting continuous plane of discontinuity; (b) material that contains a preexisting plane of discontinuity oriented in the direction of global movement; (c) material that according to bore hole records appears to be free of joints and fissures and there is no preexisting plane of discontinuity; and (d) if for condition (b) the factor of safety was equal to 1.2, compute the factor of safety if the porewater pressure at the slip plane increases by 50 kPa.

Ans. 81 kPa; 32 kPa; 91 kPa; 0.90.

2. The following laboratory data are available on the drained shear strength of a highly overconsolidated stiff clay at an effective normal stress range near 100 kPa: peak strength,  $c' = 10$  kPa,  $\phi' = 22^\circ$ ; fully softened strength,  $c' = 0$ ,  $\phi' = 21^\circ$ ; residual strength,  $c' = 0$ ,  $\phi'_r = 12^\circ$ . Factor of safety for slope stability analysis is defined as F.S. = (mobilized shear strength)/(shear stress). For one segment of a slip surface in a slope, the effective normal stress is 100 kPa and the factor of safety (for the segment) with respect to peak strength is 1.7. For the same segment compute: (a) F.S. with respect to the fully softened strength; (b) F.S. with respect to residual strength; (c) if the F.S. of the segment in part (b) also represented the F.S. of the whole slope, would you consider the slope to be stable or unstable?; (d) describe a method that could be used to improve the stability of the slope without making any excavations.

Ans. 1.29; 0.72;

3. For a glacial stiff clay ( $I_p = 12\%$ ,  $\sigma'_p = 3000$  kPa), the shape of the nonlinear peak-strength failure envelope is defined by  $m = 0.8$ . The friction angle  $\phi'$  of the clay composition determined from a series of drained triaxial compression tests on reconstituted normally consolidated specimens is  $28^\circ$ . The residual friction angle  $\phi'_r$  determined from drained reversal direct shear tests on remolded precut specimens is  $20^\circ$ . (a) Compute the peak drained shear strength in a direct shear test of a laboratory specimen that is reconstituted from the glacial clay and normally consolidated to 120 kPa. For an effective stress stability analysis (ESSA) of an existing natural slope, at the bottom of a slice on which  $\sigma'_n = 120$  kPa, compute the shear strength available for stability if: (b) there is no preexisting

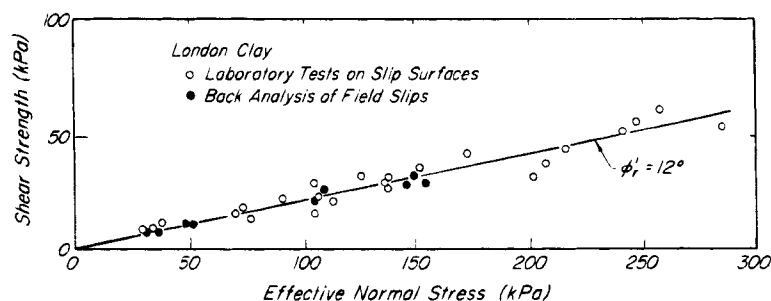
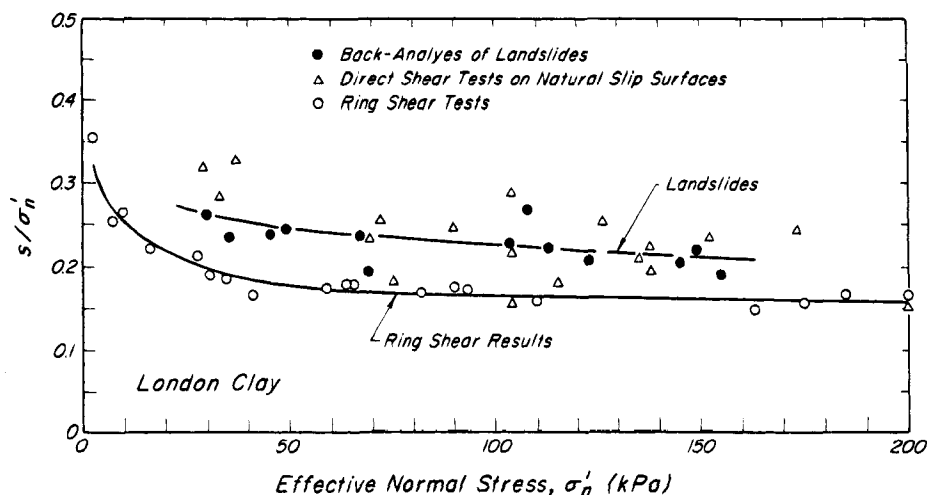


Figure 19.17 Residual shear strength of London clay from laboratory tests and from back-analysis of slides in field (after Skempton 1985).



**Figure 19.18** Comparison of residual shear strengths of London clay from direct shear tests on slip surfaces in landslides, from ring-shear tests, and from back-analysis of landslides (data from Chander 1984).

continuous plane of discontinuity but the clay contains a random system of microfissures, and (c) there is a major shear zone along which there have been 3m of previous shear displacement.

Ans. 64, 64, 44 kPa.

4. The failure envelope for drained peak (intact) strength of a highly overconsolidated clay exhibits pronounced curvature in the low effective normal stress range. For this reason intact strength is defined using different values of intercept and angle of failure envelope for each range of effective normal stress  $\sigma'_n$ . An intact specimen of this clay is consolidated under an equal all-around pressure of 50 kPa and then axial stress is increased under drained conditions until the maximum principal stress difference of 135 kPa is reached. Compute: (a) angle of the Mohr-Coulomb failure envelope for this stress condition, assuming an intercept of 10 kPa; (b) drained shear strength on the failure surface of the specimen, defined by the Mohr-Coulomb failure criterion; (c) drained shear strength of a normally consolidated specimen of the same clay composition, on a failure surface with the same effective normal stress as in part (b) on the assumption that the angle of internal friction  $\phi'$  is 20°; (d) fully softened shear strength of the intact specimen, on a failure surface with an effective normal stress as in part (b); and (e) residual shear strength on a preexisting shear surface of the overconsolidated clay, with an effective normal stress as in part (b) and for a residual friction angle  $\phi'_r$  equal to 10°.

Ans. 30°; 58 kPa; 30 kPa; 30 kPa; 15 kPa.

### Selected Reading

- Bishop, A. W., D. L. Webb, and P. I. Lewin (1965). "Undisturbed samples of London clay from the Ashford Common shaft: Strength-effective stress relationships," *Géot.*, **14**, No. 1, pp. 1–31.
- Bishop, A. W. (1966). "The strength of soils as engineering materials," *Géot.*, **16**, No. 2, pp. 91–128.
- Kenney, T. C. (1967a). "The influence of mineral composition on the residual strength of natural soils," *Proc. Geotech.*

*Conf. on Shear Strength Properties of Natural Soils and Rocks*, Oslo, **1**, pp. 123–129.

- Bishop, A. W. (1971). "Shear strength parameters for undisturbed and remolded soil specimens," *Proc. of the Roscoe Memorial Symp.*, Edited by R. H. G. Parry, Cambridge Univ., pp. 3–58.
- Marsal, R. J. (1973). "Mechanical properties of rockfill," *Embankment Dam Engineering*, Casagrande Vol., Wiley, New York, pp. 109–200.
- Kenney, T. C. (1977). "Residual strengths of mineral mixtures," *Proc. 9th Int. Conf. on Soil Mech. and Found. Eng.*, Tokyo, **1**, pp. 155–160.
- Skempton, A. W. (1977). "Slope stability of cuttings in brown London clay," *Proc. 9th Int. Conf. on Soil Mech. and Found. Eng.*, **3**, pp. 261–270.
- Chandler, R. J. (1984). "Recent European experience of landslides in overconsolidated clays and soft rocks," *Proc. IV Int. Symp. on Landslides*, **1**, pp. 61–81.
- Skempton, A. W. (1985b). "Residual strength of clays in landslides, folded strata and the laboratory," *Géot.*, **35**, No. 1, pp. 3–18.
- Mesri, G. and A. F. Cepeda-Diaz (1986). "Residual shear strength of clays and shales," *Géot.*, **36**, No. 2, pp. 269–274.
- Escario, V., J. F. T. Jucá, and M. S. Coppe (1989). "Strength and deformation of partly saturated soils," *Proc. 12th Int. Conf. on Soil Mech. and Found. Eng.*, Rio de Janeiro, **1**, pp. 43–46.
- Mesri, G. and M. E. M. Abdel-Ghaffar (1993). "Cohesion intercept in effective stress stability analysis," *J. Geotech. Eng.*, ASCE, **119**, No. 8, pp. 1229–1249.

## ARTICLE 20 UNDRAINED SHEAR STRENGTH OF SOILS

### 20.1 Undrained Failure

Undrained shear strength is mobilized when failure occurs before any significant dissipation of shearing-induced

porewater pressures takes place. In saturated soils, undrained failure is equivalent to mobilizing shearing resistance at constant volume and, therefore, is not associated with any change in water content. Combinations of shearing rates and drainage boundary conditions that would lead to undrained failure are at least conceptually possible in any soil, including soft to stiff clays and silts, fissured clays and shales, or fine to coarse granular soils. In the field, for example, an undrained failure may be induced in a stiff clay by rapidly making a deep excavation or by rapidly loading a test pier. In principle, with ideal laboratory apparatus, shearing rate, and drainage conditions, it should be possible to carry out an undrained shear test on any soil or rock.

However, during typical construction and geologic events, undrained instability develops mainly under the condition of contractive shear. This condition is determined by the compressibility and permeability of the soil, as well as by the confining pressure during shear. During contractive shear the mechanism of deformation that attempts to mobilize frictional shearing resistance also unleashes a strong tendency for the soil structure to contract under the prevailing confining pressure. This tendency, which is not realized either because of low permeability or rapid shearing, produces large positive porewater pressures with an associated decrease in effective stress. A contractive shear condition generally exists in soft clays, silts, and loose deposits of clean sand when loaded by an embankment, foundation, excavation, or slope. Construction times up to several months may be associated with undrained failure in soft clays and silts of low permeability, but in loose sands with a high permeability, undrained instability requires dynamic shearing by such events as seismic shaking. Moreover, although soft clays, silts, and loose sands inherently possess high compressibility, they require moderate to high confining pressures during shear to develop the contractive shear condition. Such confining pressures are generally present on the failure surfaces produced by embankment and foundation loading and on the base failure surfaces of deep braced excavations for shafts and basements. They also occur on deep-seated surfaces under slopes failing retrogressively after an initial slope failure produces a steep scarp.

The most extensive experience relative to the undrained shear strength mobilized in the field exists for soft clays, silts, and loose clean sands, because, for typical construction and geologic events, undrained instability develops only under contractive-shear soil conditions. Thus, the undrained shear strength of these materials is of primary importance in geotechnical analysis and design. Accordingly, the following discussion of undrained shear strength is concerned mainly with soft clays and silts under static loading and with loose sands under dynamic loading. Some data on the undrained shear strength of stiff clays

and shales are summarized, not because undrained instability commonly develops in these materials, but rather because undrained test results are frequently used to characterize them.

## 20.2 Yielding of Soil Structure

Undrained instability under contractive shear conditions begins when the soil structure yields. At yield, the soil structure begins to break down, the compressibility of the soil increases significantly and, consequently, the porewater pressure increases. Because of the associated reduction in effective stress, the frictional resistance may remain constant or decrease substantially, even though the mobilized friction coefficient may continue to increase with strain until rupture is reached. Thus, the yield stress represents the maximum shear stress the soil structure can mobilize under undrained conditions without undergoing large irrecoverable deformations. After undrained yielding, deformations increase rapidly and lead to rupture.

The structure of natural soils represents an interparticle equilibrium that develops during deposition and consolidation. As deposition occurs and overburden increases under a horizontally constrained consolidation condition, the frictional resistance of the soils results in an effective horizontal stress less than the effective vertical stress. The value of the coefficient of horizontal pressure after primary consolidation,  $K_{op} = \sigma'_h/\sigma'_v$ , is in the range of 0.43 to 0.66 for typical soils with  $\phi'$  values ranging from  $20^\circ$  to  $35^\circ$  (Article 16.5). During secondary compression, the soil particles continue to rearrange themselves, with a net decrease in void volume. Increased interparticle resistance to deformation results from more efficient particle packing and enhanced interlocking of rough particle surfaces. A typical increase caused by secondary compression during geologic aging of soft clay and silt deposits is 40%; however, it can be as much as 100%. There are indications that the effective horizontal stress increases slightly during secondary compression. For a typical aging period of 10,000 years, the coefficient of horizontal pressure may increase, for example, from  $K_{op} = 0.55$  to  $K_o = 0.75$ . It appears, however, that the anisotropy of soil structure that develops in response to primary consolidation under the  $K_{op}$  condition is not significantly diminished by the subsequent increase in effective horizontal stress.

The yield stress for any mode of loading depends on the rate at which the load is applied, because the yielding of soil structure is a time-dependent phenomenon. The criterion governing a complete yield of soil structure is a *limiting* or *critical* strain condition. For slow rates of loading, creep at interparticle contacts causes strain to accumulate. The yield stress decreases as the time to complete yield increases, because more interparticle bonds are broken and more contractive particle rearrangement is realized before complete yielding. At



slow rates of deformation, adjacent soil particles have time to rearrange themselves in a contractive manner and higher porewater pressures build up than at fast rates. At fast rates there is increased tendency for geometric interference, because adjacent particles do not have a chance to rearrange themselves in a contractive manner. For most soft clays and silts, a tenfold increase in time to yield or a tenfold decrease in imposed strain rate typically produces about a 10% decrease in yield stress. However, the time effect becomes slight at very slow rates of loading.

The average yield stress mobilized by an element of soil may be smaller than the maximum yield stress that the soil structure could sustain for a given mode and rate of loading. Simultaneous mobilization of the maximum yield stress is possible only if the strains in the element are uniform. Inasmuch as the stresses and strains are frequently nonuniform, yielding develops progressively by starting in the more severely stressed zones and spreading. The effect of time on yield stress contributes to progressive yielding. Most susceptible to progressive yielding are the highly structured soft clays and silts that display a large postyield decrease in shearing resistance.

Because the structure of soil is anisotropic and is in equilibrium under a  $K_o$  stress condition, the yield stress is also anisotropic and varies with the direction in which the stresses are applied relative to the vertical. Each mode of loading corresponds to a yield point in, for example, the  $q = (\sigma'_1 - \sigma'_3)/2$  and  $p' = (\sigma'_1 + \sigma'_3)/2$  stress space. The oedometer test represents one mode of loading that may be imposed on a soil specimen to cause yielding under a drained condition. The effective stress path and the corresponding compression curve are shown in Fig. 20.1 for a vertical specimen of a structured soft clay subjected to the oedometer mode of loading starting from the *in situ* ( $\sigma'_{vo}$ ,  $K_o \sigma'_{vo}$ ) point. The preconsolidation pressure  $\sigma'_p$  corresponds to the effective major principal stress at yield. At effective vertical stresses less than the yield stress compression of the specimen is small and mostly recoverable. At stresses exceeding the yield stress, the compression is relatively large and mostly irrecoverable.

The oedometer mode of loading represents only one of an infinite number of stress paths that may be imposed on a soil element to cause yielding. A sufficient number of yield points defines a *yield envelope* for the soil element. The distortions of drained and undrained specimens are closely similar in the region of stress space enclosed by the yield envelope. In drained tests the specimens suffer large volume compression and associated distortion as the stress path crosses the yield envelope. In the undrained condition yield occurs when the structure of the soil breaks down and relatively high porewater pressures develop. The distance from the starting point ( $\sigma'_{vo}$ ,  $K_o \sigma'_{vo}$ ) to the yield envelope is a measure of the maximum

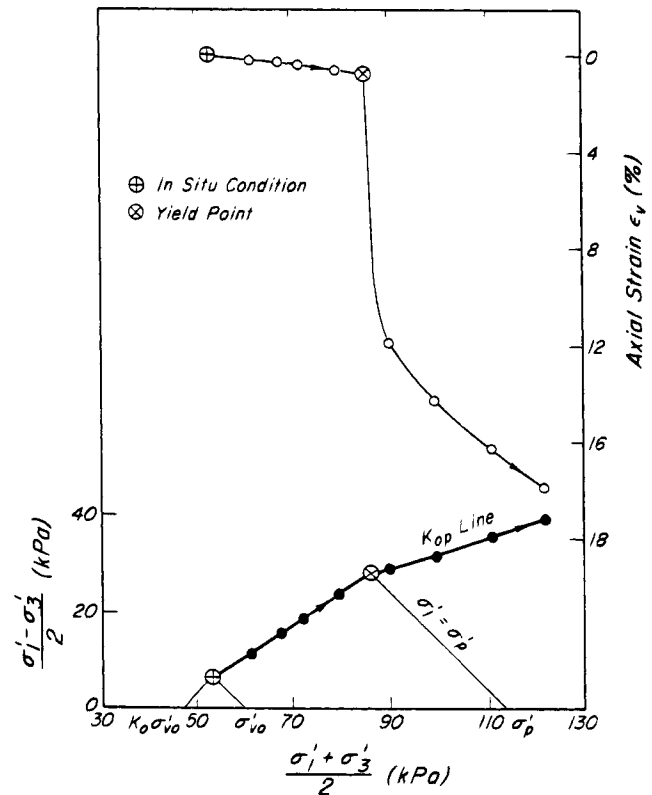


Figure 20.1 Stress path to yield in an oedometer test.

stress change that can be imposed on the soil before yielding.

Yield envelopes corresponding to four different preconsolidation pressures on samples from various depths in a soft blue plastic clay from Winnipeg, Canada are shown in Fig. 20.2. The natural water contents, liquid limits and plasticity indices are in the range of 54 to 63%, 65 to 85%, and 35 to 60%, respectively. The clay is somewhat unusual in that it contains significant montmorillonite in addition to illite, kaolinite, quartz, dolomite, and some gypsum and feldspar. As compared to most postglacial soft clays, it has a low friction angle of  $\phi' = 17.5^\circ$ . There is no evidence of geologic preloading since deposition. However, the  $\sigma'_p$  profile reflects possible effects of deep winter frost penetration and strong summer evaporation from the ground surface. Values of  $\sigma'_p/\sigma'_{vo}$  corresponding to the 8 to 12 m depths of the specimens represented in Fig. 20.2 range from 1.5 to 4.0. Triaxial specimens 76 mm in diameter and 140 mm high, trimmed from block samples, were first  $K_o$ -consolidated to their estimated *in situ* stresses. They were then loaded under drained conditions in increments along approximately linear stress paths in the  $(q, p')$  space. Each load increment was maintained for one day. Yield points were determined from plots of shear stress *versus* axial strain and volumetric strain *versus* effective mean stress.

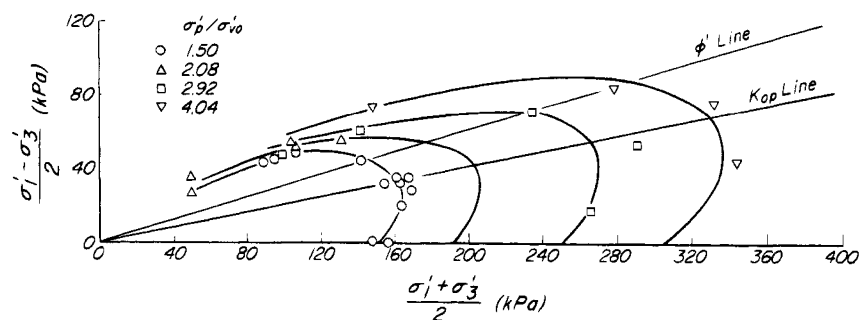


Figure 20.2 Yield envelopes for Winnipeg clay (after Graham et al. 1983).

The position of the yield envelope in the  $(q, p')$  space is fixed by the preconsolidation pressure  $\sigma'_p$ , which varies with depth, and by the coefficient of horizontal pressure  $K_{op}$ , which is fairly constant for a soft clay deposit. The yield envelope has a more or less elliptical shape and is nearly centered about the  $K_{op}$  line such that the yield stress for isotropic consolidation,  $\sigma'_{pi}$ , is significantly less than  $\sigma'_p$  for one-dimensional consolidation. The shape of the yield envelope, which is a reflection of the soil structure and its degree of anisotropy, is also reasonably unique for a given soft clay deposit. Thus, if the yield envelopes are normalized with respect to the corresponding preconsolidation pressures, a unique yield envelope for the entire deposit is obtained, as shown for the Winnipeg clay in Fig. 20.3.

Yield envelopes for three other soft clays are shown in Figs. 20.4 to 20.7. Figure 20.4 presents the yield envelopes obtained by similar tests on specimens prepared from 200-mm-diameter clay samples taken at three different depths from a deposit at St. Alban, Quebec. The clay, a shoreline Champlain Sea deposit, has low to medium plasticity and a low porewater salinity in the range of 0.3 to 0.9 g/l. Typical values of natural water content, liquid limit, and plasticity index range from 60 to 90%, 40 to 50%, and 17 to 23%, respectively. Although St. Alban clay has not been subjected to any significant geologic preconsolidation, it has developed a structure due to aging corresponding to  $\sigma'_p / \sigma'_{v0}$  values of 2.1 to 2.3.

Plastic Drammen clay from Norway is a postglacial marine deposit with a porewater salt concentration of 25 g/l. Its natural water content, liquid limit, and plasticity index range from 50 to 54%, 50 to 60%, and 25 to 35%. The clay has never been subjected to loads greater than the present overburden. However, it has developed values of  $\sigma'_p / \sigma'_{v0}$  in the range of 1.4 to 1.6 as a result of 3000 years of aging. Thin-walled fixed-piston samples, 95 mm in diameter, were used for the drained and undrained tests represented in Fig. 20.6. In undrained triaxial shear tests, the yield point is defined at the peak principal stress difference.

The yield envelope for Ottawa clay, another Champlain Sea deposit, is shown in Fig. 20.7. Block samples were obtained at a depth of 5.4 m and had a preconsolidation pressure of 200 kPa. Typical values of natural water content, liquid limit, and plasticity index were 80%, 90%, and 60%, respectively. Drained triaxial compression and extension tests were carried out according to a variety of effective stress paths and with both stress and strain controlled loading (Mitchell and Wong 1973). At stresses exceeding the preconsolidation pressure  $\sigma'_p$ , the clay exhibited a typical Mohr-Coulomb failure envelope for normally consolidated young clays with  $\phi' = 27^\circ$  in both compression and extension.

Because yielding is a time-dependent phenomenon, yield points on a yield envelope ideally should correspond to the same strain rate or time to yield. Frequently, how-

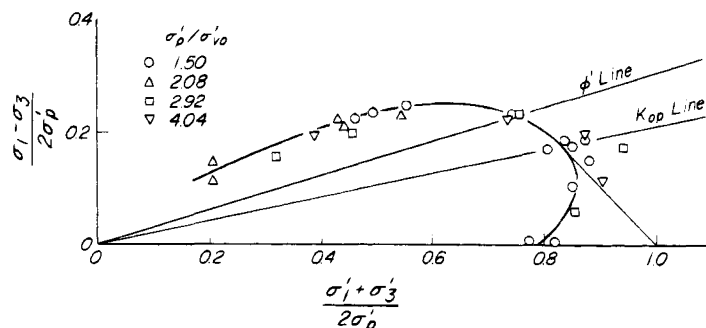


Figure 20.3 Normalized yield envelope for Winnipeg clay.

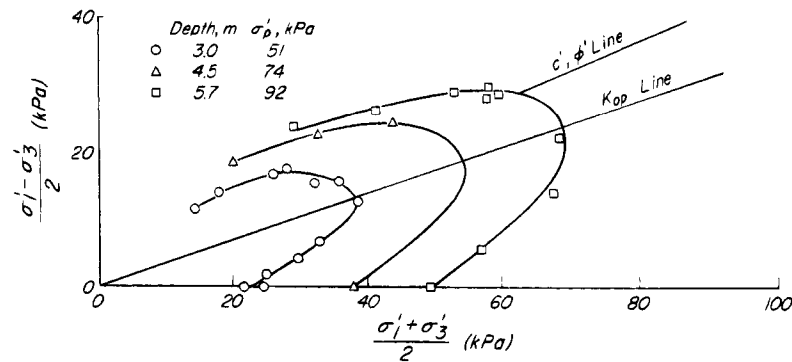


Figure 20.4 Yield envelopes for St. Alban clay (after Tavenas and Leroueil 1977, 1978).

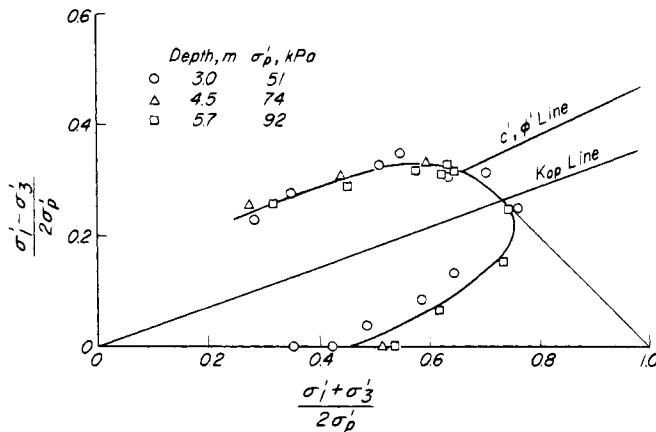


Figure 20.5 Normalized yield envelope for St. Alban clay.

rates are selected to ensure porewater pressure equilibration throughout the soil specimen for the proper measurement of the porewater pressure. In consolidation tests and drained shear tests, loading rates or imposed strain rates must allow complete dissipation of excess or shearing-induced porewater pressures. Such testing requirements may lead to different times to yield in various types of tests and may be partly responsible for the scatter in the yield points that define a yield envelope. Another possible source of scatter, in addition to spatial variability in mineralogy and structure within a soft clay deposit and random error in testing, is different degrees of progressive yielding for different modes of loading.

The time to reach yield at the preconsolidation pressure in a standard oedometer test is approximately equal to the typical time of a few hours to reach yield at peak shear stress in undrained shear tests with porewater pressure

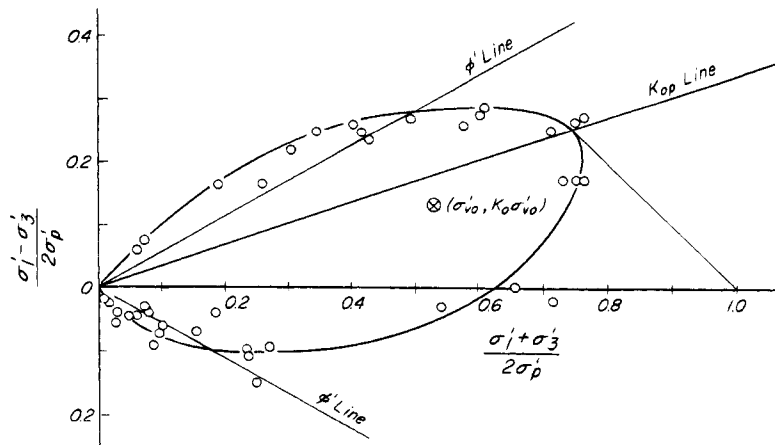


Figure 20.6 Normalized yield envelope for plastic Drammen clay (after Larsson and Sallfors 1981).

ever, it is not possible to fulfill this condition completely because of the different requirements for different types of undrained shear, drained shear, and consolidation tests (Article 17.1). For example, in undrained shear tests with porewater pressure measurement, loading rates or strain

measurement. Thus, it is reasonable to define a yield envelope by using the yield points from a standard consolidation test and from undrained shear tests with porewater pressure measurements, and to normalize yield envelopes in terms of the end-of-primary preconsolidation pressure.

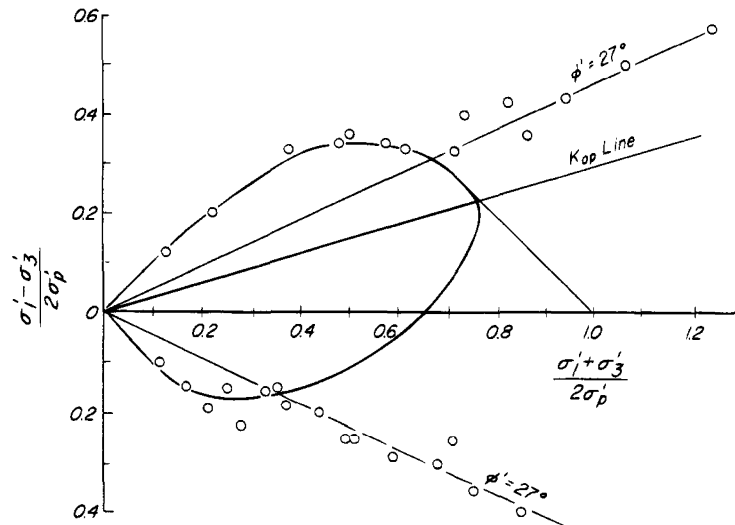


Figure 20.7 Normalized yield envelope for Ottawa clay (after Mitchell and Wong 1973).

However, undrained shear strengths from rapid tests such as the unconfined compression or *in situ* vane, which typically force yield in a few minutes, as well as undrained strengths mobilized in full-scale failures in the field, which may reach yield in weeks, are also frequently normalized in terms of the preconsolidation pressure from the standard oedometer test. This is an acceptable practice as long as the difference in times to yield in the oedometer test and in the undrained shear is kept in mind while relating undrained shear strength to preconsolidation pressure data.

The shape and location of yield envelopes for soft clays and silts in stress space confirm that different modes of undrained shear mobilize different magnitudes of undrained shear strength. For example, in an undrained triaxial compression test starting from the *in situ* ( $\sigma'_{vo}$ ,  $K_o \sigma'_{vo}$ ) condition, the applied shear stress is in the same direction as the *in situ* shear stress. Therefore, most of the interparticle bonds and the particle interference of the soil structure contribute to the yield strength mobilized in the compression mode of shear. On the other hand, in an undrained triaxial extension test, the shear stress is applied in the direction opposite to the shear stress condition under which the soil structure was at equilibrium. As soon as shearing begins, interparticle bonds are broken and interlocks are disengaged. Thus, full structural resistance is not available when complete yielding takes place.

In general, different modes of shear mobilize different magnitudes of undrained shear strength and lead to different ratios  $s_{uo}/\sigma'_p$  of undrained shear strength to preconsolidation pressure for any particular soil deposit. However, a unique normalized yield envelope for a given soft clay deposit has important practical implications with respect to the normalized parameters. For example, it implies that the ratio of the preconsolidation pressure for isotropic

loading  $\sigma'_{pI}$  to the oedometer preconsolidation pressure  $\sigma'_p$  is a constant for a soil deposit and is independent of  $\sigma'_p/\sigma'_{vo}$ . Data in Fig. 20.8 show that  $\sigma'_{pI}/\sigma'_p$  is almost a constant for a large number of soft clay deposits from eastern Canada. Values of  $\sigma'_{pI}/\sigma'_p$  for soft clays and silts from North America, Europe, and South East Asia are shown in Fig. 20.9. For most soft clays and silts,  $\sigma'_{pI}/\sigma'_p$ , although widely scattered, is roughly 0.65. The existence of a unique normalized yield envelope also suggests the possibility of a constant  $s_{uo}/\sigma'_p$  independent of  $\sigma'_p/\sigma'_{vo}$ , for any one mode and rate of shear of a soft clay deposit. *In situ* and laboratory undrained shear strength measurements support this possibility. Figure 20.10 shows undrained shear strength measurements by the *in situ* vane for six soft clay deposits. These data are presented in terms of  $s_{uo}/\sigma'_{vo}$  to show that, for undrained

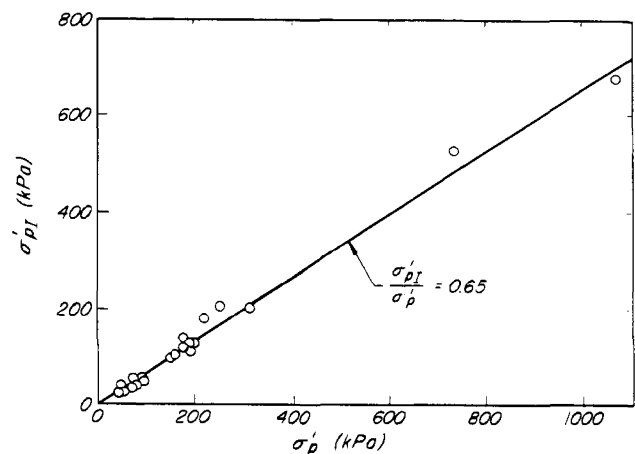
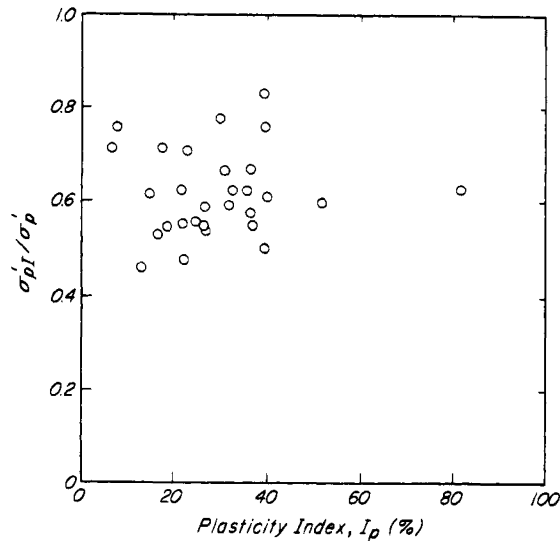


Figure 20.8 Comparison, for soft clays of Eastern Canada, of preconsolidation pressure for isotropic loading with oedometer preconsolidation pressure  $\sigma'_p$  (after Leroueil et al. 1983).



**Figure 20.9** Ratio of preconsolidation pressure for isotropic loading to oedometer preconsolidation pressure for various soft clays.

shear strengths mobilized by starting from the *in situ* ( $\sigma'_{vo}$ ,  $K_o \sigma'_{vo}$ ), the parameter  $m_o$  defined by Eq. 20.1 is equal to unity.

$$\frac{s_{uo}}{\sigma'_{vo}} = \left[ \frac{s_{uo}}{\sigma'_{vo}} \right] \frac{\sigma'_p}{\sigma'_{vo}} = 1 \left( \frac{\sigma'_p}{\sigma'_{vo}} \right)^{m_o} \quad (20.1)$$

For  $m_o = 1$ , Eq. 20.1 leads to

$$\frac{s_{uo}}{\sigma'_p} = \left( \frac{s_{uo}}{\sigma'_{vo}} \right) \frac{\sigma'_p}{\sigma'_{vo}} = 1 \quad (20.2)$$

The conclusion, of considerable practical importance, is reached that  $s_{uo}(FV)/\sigma'_p$  is a constant for a given soil deposit and is independent of  $\sigma'_p/\sigma'_{vo}$ . For the data in Fig. 20.10,  $\sigma'_p/\sigma'_{vo}$  has values in the range of 1.2 to 6.

Similar shear strength data from laboratory undrained shear tests, such as triaxial compression, triaxial extension, and direct simple shear tests, are shown in Fig. 20.11. For the triaxial tests, the undrained shear strength is defined as  $s_u = (\sigma_1 - \sigma_3)/2$ . For all practical purposes it is seen that  $m_o = 1$ . Thus it is reasonable to conclude that for any one mode and rate of shear,  $s_{uo}/\sigma'_p$  of a natural soil deposit may be taken as a constant independent of  $\sigma'_p/\sigma'_{vo}$  for values of the latter in the range of 1.2 to 8.

It should be realized that  $[s_{uo}/\sigma'_{vo}]$  at  $\sigma'_p/\sigma'_{vo} = 1$  is only an intercept and does not necessarily correspond to any *in situ* or laboratory consolidation condition. Moreover, in natural soil deposits for which  $\sigma'_p/\sigma'_{vo}$  has values generally greater than unity, the ratio  $s_{uo}/\sigma'_{vo}$  has no physical meaning and is not a useful parameter. The parameter  $s_{uo}/\sigma'_p$ , on the other hand, can be used for estimating  $s_{uo}$  if the preconsolidation pressure  $\sigma'_p$  can be evaluated. For a particular mode and rate of shear of a soil deposit it

can be obtained directly from a plot of  $s_{uo}$  against the corresponding  $\sigma'_p$ , as is illustrated in Fig. 20.12.

### 20.3 Undrained Shear Strength in Terms of Effective Stress at Failure

Because the effective stress is the most important factor determining the shearing resistance of soils, it is attractive to attempt to express shear strength in terms of effective stress. An expression for undrained shear strength in terms of effective stress at failure could be used to define shear strength for analyses of failures in the field that develop under undrained conditions. Such an expression could also help interpret undrained strength measurements made in shear tests that subject soil to different modes and rates of shear and to explain the magnitudes of normalized strength parameters such as  $s_{uo}(FV)/\sigma'_p$  and  $s_{uo}(TC)/\sigma'_p$ . To be useful, however, the expression for undrained shear strength must define yield shear stress in terms of the effective stress conditions at yield, because the limiting stress for undrained failure under contractive conditions is the yield point. The implications of this requirement may be appreciated by considering the Mohr-Coulomb equation in the following form:

$$s_{uo} = c'_m + (\sigma - u) \tan \phi'_m \quad (20.3)$$

The parameters  $c'_m$  and  $\phi'_m$  are, respectively, the cohesion intercept and friction angle mobilized at yield, and the porewater pressure  $u$  is the sum of the hydrostatic or steady-seepage porewater pressure  $u_o$  and the shearing-induced porewater pressure  $\Delta u$ . The anisotropic and time-dependent nature of yielding suggests that  $\Delta u$ , which reflects the contractive response of the soil structure, must depend on the mode and rate of loading. For example, modes of shear that cause significant damage to the soil structure, and slow rates of shear that allow time for the damage to be realized before yield, should lead to high porewater pressures at yield. It is evident that predicting shearing-induced porewater pressures is almost as difficult as predicting the undrained shear strength itself. This problem has been recognized, and it is generally agreed that the use of Eq. 20.3 is limited to cases in which the porewater pressures corresponding to the most critical condition are measured or can be estimated with reasonable accuracy. In practice, it is often difficult to predict shearing-induced porewater pressures accurately under contractive shear conditions; this is an important limitation to the use of undrained shear strength expressed in terms of effective stress at failure.

It is equally important, however, that the parameters  $c'_m$  and  $\phi'_m$  in Eq. 20.3 are in general not respectively equal to  $c'$  and  $\phi'$  that correspond to rupture. The yield point is reached at relatively small strain, whereas  $\phi'$  is mobilized after large strain. The cohesion intercept  $c'$ , which corresponds to a soil structure that has been significantly altered by deformation, differs from  $c'_m$  at yield.

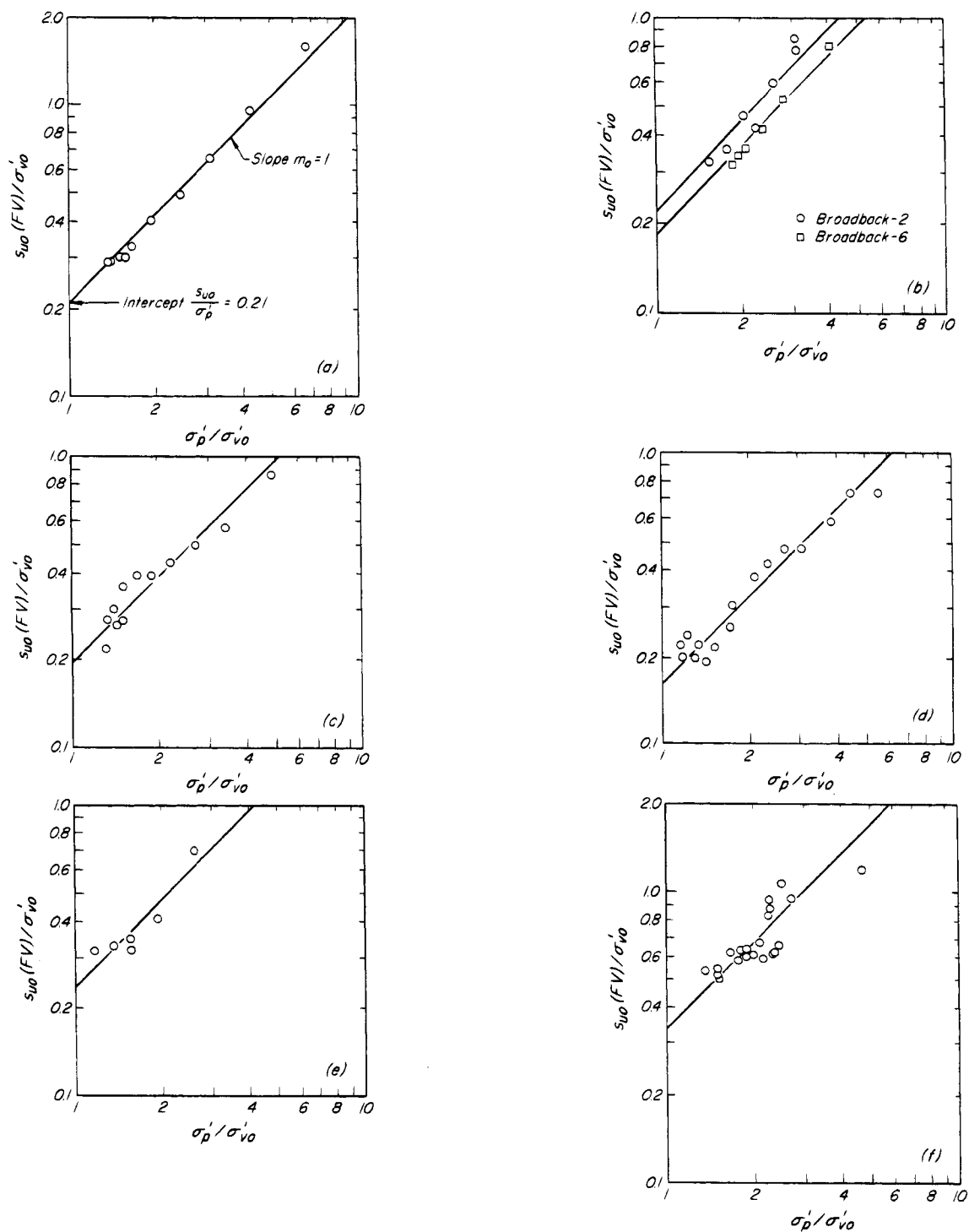


**Figure 20.10** Undrained shear strength from *in situ* vane tests. (a) Soft clay from Persian Gulf; (b) James Bay clays; (c) Connecticut Valley varved clay; (d) Boston blue clay; (e) Persian Gulf clay; (f) Natsushima clay from Tokyo Bay (data from Hanzawa and Kishida 1982, Ladd et al. 1983, Lacasse et al. 1978, Hanzawa et al. 1979).

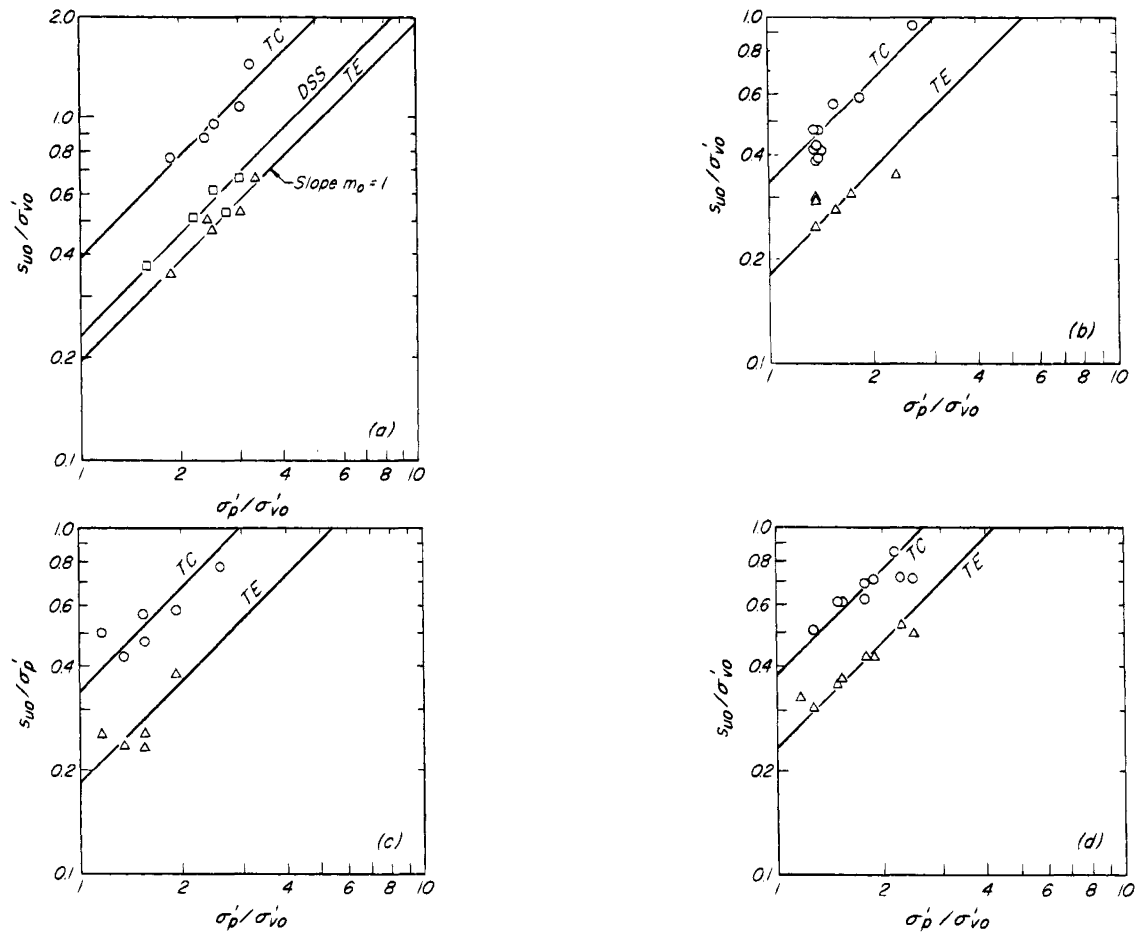


**Figure 20.11** Laboratory undrained shear strengths from triaxial compression, direct simple shear, and triaxial extension tests on various clays. (a) James Bay clay; (b) Belfast clay; (c) Persian Gulf clay; (d) Natsushima clay from Tokyo Bay (data from Lefebvre et al. 1983, Crooks and Graham 1976, Hanzawa et al. 1979).

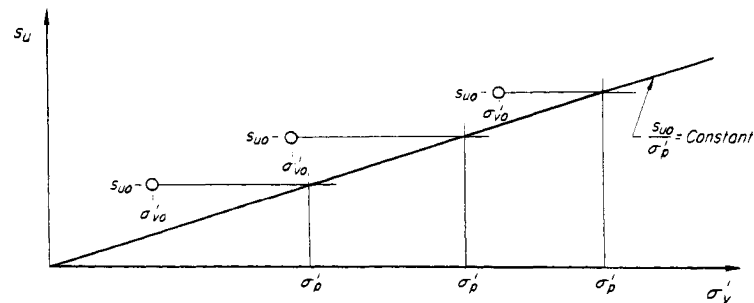


**Figure 20.12** Values of undrained shear strength and preconsolidation pressure for different depths in a clay deposit.

For bonded or loose soil structures, the friction  $\phi'_m$  that is mobilized at yield may be less than 50% of the frictional resistance  $\phi'$  mobilized after large deformation. Because the natural soil structure has been substantially destroyed by the time the large-strain rupture condition is reached,  $c'$  and  $\phi'$  are practically independent of the mode and rate of shear. They are evaluated by shear tests on several specimens consolidated to different pressures larger than  $\sigma'_{vo}$  or  $\sigma'_p$ . Although consolidation at pressures larger than  $\sigma'_{vo}$  and, especially,  $\sigma'_p$  damages the natural soil structure, the damage does not invalidate the determination of  $c'$  and  $\phi'$  because these parameters correspond to the large-strain shear condition, reached after the natural soil structure is substantially destroyed. On the other hand,  $c'_m$  and  $\phi'_m$  depend on the mode and rate of shear, as well as on the extent of progressive yielding. It is practically impossible to evaluate  $c'_m$  and  $\phi'_m$  by means of shear tests that start from the *in situ* stress condition ( $\sigma'_{vo}$ ,  $K_o$   $\sigma'_{vo}$ ). Shear tests in which the soil is consolidated to effective stresses in the range of  $\sigma'_{vo}$  to  $\sigma'_p$  or more are conducted on specimens that have experienced different degrees of destructuration before shear. The "failure envelope" defined by the yield points of such tests does not properly represent the  $c'_m$  and  $\phi'_m$  for the natural soil structure that are mobilized in tests starting from the *in situ* ( $\sigma'_{vo}$ ,  $K_o$   $\sigma'_{vo}$ ) consolidation condition. In summary, tools for determining the mobilized friction and cohesion at yield are not yet available. Moreover, it is generally difficult to estimate shearing-induced porewater pressures. Thus Eq. 20.3 cannot be readily used to define the undrained shear strength for a significant number of undrained instability problems in soft clay, silt, or loose sand.

There are, however, some problems involving instability in soft clay and silt in which the shear strength can be computed by using Eq. 20.3: (1) if shearing-induced porewater pressures remain small and can be ignored, or (2) if the porewater pressures can be measured readily or estimated with reasonable accuracy, and if  $c'_m$  and  $\phi'_m$  can be approximated or replaced by  $c'$  and  $\phi'$ , respectively.

For clay and silt embankments compacted near optimum water content (Article 44.2.3), the porewater pressures can be measured in the field or computed with the aid of such laboratory undrained shear tests as the triaxial compression test on specimens of the compacted soil. To express the results, the porewater pressure parameter  $\Delta u / \Delta \sigma_v$  may be used. Furthermore, because these soils are remolded, yield and rupture conditions almost coincide, and  $c'_m$  and  $\phi'_m$  can be determined on compacted specimens in a series of drained triaxial compression tests or undrained triaxial compression tests with pore pressure measurements. For recently compacted nearly saturated clays, such as those compacted wet of optimum during embankment construction,  $c'_m$  is close to zero, and  $\phi'_m$

may be estimated from the empirical  $\phi'$  against  $I_p$  correlation in Fig. 19.7.

The condition of shearing-induced porewater pressures so near to zero that they may be ignored, and of  $c'_m$  and  $\phi'_m$  values that may be estimated or replaced by  $c'$  and  $\phi'$ , respectively, is encountered in the initial sliding of natural or cut slopes in soft clay. The event that triggers the initial slide may be loading the slope by a fill, excavation, or erosion at the toe, rapid seasonal variations in pore pressures, or ground shaking. The surfaces of sliding of initial slope failures in soft clays and silts are relatively shallow, where the confining pressures on the soft clay elements are relatively small; therefore, a principal requirement for contractive shear is not satisfied. The formation of the slope has in effect produced soft clays with high overconsolidation ratios in the range of 3 to 15. Therefore, the tendency for contraction of the soil structure is reduced, and shearing-induced porewater pressures are near zero. Two other factors, separately or together, may contribute to keeping the shearing-induced porewater pressures small and, in effect, making the failures of these soft clays substantially drained: (1) frequently, the materials that are involved in the initial slides are weathered and fissured; (2) for the stress conditions encountered in soft clay slopes, the coefficient of consolidation is generally very high. As a result of these factors, shearing-induced porewater pressures may dissipate rapidly, and the porewater pressure in Eq. 20.3 can be taken equal to the static or steady-state seepage pressures, which can be measured or computed reliably.

The fissured nature of weathered clay and the brittle strain-softening behavior of soft clay at low confining pressures lead to progressive failure (Article 17.4). When limiting equilibrium for the slope is reached, most of the elements on the slip surface may have already reached the large-strain rupture strength. It is then reasonable to replace  $c'_m$  and  $\phi'_m$  by  $c'$  and  $\phi'$ , respectively. For soft clays and silts the values of  $c'$  are generally less than 10 kPa, and the friction angle  $\phi'$  may be estimated from the empirical relationship between  $\phi'$  and  $I_p$  (Fig. 19.7). The large-strain failure envelope of a soft clay for determining  $c'$  and  $\phi'$  may be defined by drained triaxial compression tests on undisturbed samples. For example, values of  $c'$  and  $\phi'$  in the range of 5 to 10 kPa and 27 to 35°, respectively, determined by such tests, together with porewater pressure measurements in unfailed slopes, have led to reliable prediction of initial slope failures in the soft clays of eastern Canada (Kenney 1967b, Lefebvre 1981, Tavenas 1984).

The preceding assumptions in relation to the shearing-induced porewater pressures and strength parameters, however, are not valid for deep-seated soft clay landslides, including retrogressive failures that may be triggered by the initial slope failures. Deep-seated relatively flat slip surfaces that may develop within unweathered soft clays



below almost level ground are subjected to high confining pressures, and contractive shear soil conditions exist. The undrained yield strength, which determines stability for this condition, cannot be easily computed with the aid of Eq. 20.3, and an alternative approach must be used.

## 20.4 Measurement of Undrained Shear Strength

For many contractive-shear soil conditions, it is not possible to express the undrained shear strength in terms of the strength parameters  $c'_m$  and  $\phi'_m$  and the effective-stress state at failure. The alternative is to measure the undrained shear strength directly. However, the undrained shear strength of an element of soil is not a unique value; it depends on the way in which the soil is brought to failure. Modes of shear that take full advantage of the resistance of the natural soil structure and that minimize progressive yielding mobilize the highest undrained shear strength. The more rapidly the shear stress is applied, the greater the measured undrained shear strength. Thus, different *in situ* or laboratory testing devices and procedures that subject soil to different modes and rates of shear and that involve different degrees of progressive yielding measure different values of undrained shear strength. The most common methods of obtaining or directly measuring the undrained shear strength are field vane (FV) shear tests and laboratory unconfined compression (UC), triaxial compression (TC), triaxial extension (TE), and direct simple shear (DSS) tests. The vane device (Article 11.5.2) is inserted into the ground and then rotated to measure the undrained shear strength. Laboratory shear tests require that samples of *in situ* soil be obtained. Although most *in situ* and laboratory shear devices test a relatively small element of soil, this limitation is rarely a serious problem in the measurement of the undrained shear strength of soft clays, silts, and loose sands.

The measurement of undrained shear strength, perhaps more than any other soil property, is affected by soil disturbance before shearing. Disturbance is involved in both *in situ* testing and in sampling and laboratory testing, although it may be easier to minimize or at least to standardize the effect of disturbance for *in situ* tests than for sampling and testing in laboratory devices. Because of disturbance, the undrained shear strength measured *in situ* or on specimens in the laboratory is usually smaller than the undrained shear strength of a truly undisturbed soil. The magnitude of the reduction varies considerably with the type of soil. The effect of disturbance is generally greater in brittle silty clays of relatively high permeability than in ductile plastic clays of low permeability. Moreover, it depends on the mode of shear used to measure the undrained shear strength. Its significance is greater in modes of shear that cause little disruption of soil structure before yield, and is less in modes that damage soil structure before yield is reached.

The *in situ* vane shear device (Article 11.5.2) tests soil in its natural environment. Insertion of the vane into soft clays and silts, however, causes displacements and changes in stress that disrupt the natural structure of the soil around the vane. Moreover, the undrained shear strength measured 1 day after inserting the vane can be more than 20% higher than that obtained from a standard test carried out about 5 min after insertion. Consolidation increases the strength of the soil around the vane and also increases the adhesion between the blades of the vane and the soil; this minimizes progressive yielding during rotation of the vane. The increase in undrained shear strength  $s_{uo}$  (FV) with time confirms that the natural soil structure is disturbed during the penetration of the vane. Although this disturbance cannot be eliminated completely, its adverse effect on the applicability of the test results can be minimized by standardization of equipment (e.g., vane stem diameter and blade thickness) and operation (e.g., delay time between penetration and rotation).

All specimens of natural soil deposits tested in laboratory shear devices experience disturbance. The disturbance may have occurred during sampling and handling in the field, during transit to the laboratory, and during laboratory storage and trimming of specimens for the tests. The most serious mechanism of disturbance is shear distortion of the natural soil structure produced by displacement of the soil during conventional tube sampling (Article 11.3.3) and careless handling of the sample thereafter. Other mechanisms of disturbance, which operate especially during long storage periods, are redistribution of water from the outside to the relatively less disturbed inside of the sample that is eventually tested, and chemical changes including oxidation. Because considerable handling of the soil takes place after sampling and there is variable opportunity for additional sample disturbance, it is not practicable to quantify the quality of specimens in terms of sampling devices and procedures. However, a good indicator of the quality of a shear specimen is the specimen quality designation (SQD) (Article 11.3.8) (Table 11.2). Soft clay and silt block samples of A quality can be obtained from excavations or test pits. The Sherbrooke and Laval sampling devices (Article 11.3.7) can take samples of A quality down to depths of 15 to 20 m. However, for most projects soft clay and silt samples of B quality are adequate. They can be obtained by using 54- to 95-mm fixed-piston, thin-walled tube samplers with area ratios not exceeding about 10% (Article 11.3.4). The sampler must be pushed, not driven, into the ground.

Although Table 11.2 is a good indicator of the quality of shear specimens, it does not offer a unique assessment of the effect of disturbance on the undrained shear strength of every type of soil. The same magnitude of volumetric strain may imply a smaller disturbance-related reduction in undrained shear strength for plastic soft clays than for

lean clayey silts. Specimen disturbance leads to highly variable laboratory undrained shear strength measurements, especially from unconsolidated undrained (*UU*) tests (Article 17.3.1). The unconfined compression undrained shear strengths,  $s_{uo}$  (*UC*), of tube samples of *D* quality can be less than 50% of those of samples of *A* quality.

Another important factor in laboratory measurement of undrained shear strength is the consolidation pressure. The best laboratory data on the undrained shear strength of natural soft clays and silts are obtained by subjecting, before shear, specimens of *B* to *A* quality to the same effective stresses they carried in the field. The effective overburden pressure  $\sigma'_{vo}$  is determined from measurements of unit weight and porewater pressure. The value of  $K_o$  in  $\sigma'_{ho} = K_o \sigma'_{vo}$  is estimated from previous experience or from empirical relationships (Article 16.5).

The reduced water content that results from the application of the *in situ* ( $\sigma'_{vo}$ ,  $K_o \sigma'_{vo}$ ) stress condition does not necessarily result in a net gain in strength of specimens of *B* and even *C* quality, because sample disturbance produces a reduction in strength. Destruction of interparticle bonds may have a greater effect than the decrease in particle spacing. The laboratory undrained shear strength data in Fig. 20.11 were obtained on specimens of *B* to *A* quality that were subjected to ( $\sigma'_{vo}$ ,  $K_o \sigma'_{vo}$ ) stress conditions before shear.

Specimens of soil are often consolidated in the laboratory to effective stresses higher than the *in situ* ( $\sigma'_{vo}$ ,  $K_o \sigma'_{vo}$ ) before being subjected to undrained shear. This procedure is logical if the purpose is to obtain information on the gain in undrained shear strength after consolidation under loads from a structure or embankment. The information is particularly useful for stage filling of storage facilities or stage construction of embankments on soft clays or silts. On the other hand, the view has sometimes been expressed that consolidating specimens, before undrained shear, to effective stresses greater than the *in situ* condition allows the undrained strength of samples of even poor quality to be evaluated. However, the more disturbance the sample has suffered, the greater is the volume change expected in the laboratory under the *in situ* ( $\sigma'_{vo}$ ,  $K_o \sigma'_{vo}$ ) stress condition. Subjecting specimens of *D* quality to the field effective stress condition does not restore the natural structure of the soil, and the water content at the end of the consolidation stage is usually significantly less than the *in situ* water content. Therefore, in general, *D* to *C* quality specimens consolidated to effective stresses below the preconsolidation pressure cannot provide information on the *in situ* strength. On the other hand, if the samples are consolidated beyond the preconsolidation pressure, the undrained strength ratios  $s_{uo}/\sigma'_p$  can be estimated from the  $s_u/\sigma'_{vc}$  data obtained in the normally consolidated range.

For overconsolidated stiff fissured clays, the undrained shear strength increases significantly while specimens are consolidated in the recompression range from  $\sigma'_{vo}$  to  $\sigma'_p$ . Laboratory measurements for stiff fissured London clay specimens of *A* quality are shown in Fig. 20.13 and are replotted in normalized form in Fig. 20.14. The slope in the compression range in Fig. 20.13 is equal to 0.27. The linear segment in Fig. 20.14 may be expressed as (Ladd et al. 1977):

$$\frac{s_u}{\sigma'_{vc}} = \left[ \frac{s_u}{\sigma'_{vc}} \right]_{\frac{\sigma'_p}{\sigma'_{vc}}=1} \left( \frac{\sigma'_p}{\sigma'_{vc}} \right)^m \quad (20.4)$$

For these data,  $(s_u/\sigma'_{vc})_{\sigma'_p/\sigma'_{vc}=1}$  is merely an intercept and is not equal to the slope  $s_u/\sigma'_{vc} = 0.27$  in the normally consolidated range. The value  $m = 0.41$  for this clay is considerably less than unity; this indicates a significant increase in  $s_u$  in the recompression range. Part of the increase is probably due to disturbance that caused fissures in the specimen to open and reduce  $s_{uo}$  at  $\sigma'_{vo}$ . The fissures closed as the consolidation pressure increased from  $\sigma'_{vo}$  to  $\sigma'_p$ .

On the other hand, if specimens of soft clay and silt are subjected to laterally constrained consolidation in the recompression range from  $\sigma'_{vo}$  to  $\sigma'_p$ , the undrained shear strength may increase or decrease slightly or may remain constant. It may remain constant because frictional gain in strength is achieved at the expense of loss of interparticle chemical bonds. For these materials,  $m = 1$  in the range from  $\sigma'_{vo}$  to  $\sigma'_p$  that corresponds to the value of  $\sigma'_p/\sigma'_{vo}$  for which  $s_{uo}/\sigma'_p$  is a constant for any one mode and rate of shearing. Therefore, it is reasonable to assume that, in the recompression range from  $\sigma'_{vo}$  to  $\sigma'_p$ , the undrained shear strength remains constant and equal to  $s_{uo}$ . Note that whereas Eq. 20.1 compares values of undrained shear strength at different locations in a natural soil deposit, Eq. 20.4 describes the undrained shear strength of a single element of soil subjected to consolidation from  $\sigma'_{vo}$  to  $\sigma'_p$ .

For consolidation pressures  $\sigma'_{vc}$  greater than  $\sigma'_p$ , the undrained shear strength increases linearly with  $\sigma'_{vc}$ . A set of results for ( $\sigma'_{vc}$ ,  $K_{op} \sigma'_{vc}$ ) consolidated triaxial compression and extension tests on Natsushima Tokyo Bay clay is shown in Fig. 20.15. For some soft clays and silts,  $s_u/\sigma'_{vc}$  measured in the normally consolidated range is equal to  $s_{uo}/\sigma'_p$  of the natural soil structure. However, for other soils, especially for chemically bonded lean clay silts,  $s_u/\sigma'_{vc}$  differs from  $s_{uo}/\sigma'_p$ , as is illustrated in Fig. 20.16. The reason for the difference is not apparent, especially within the framework of the yield envelope concept. In the absence of  $s_{uo}/\sigma'_p$  data,  $s_u$  in the recompression range, equal to  $s_{uo}$ , is computed as

$$s_{uo} = \frac{s_u}{\sigma'_{vc}} \sigma'_p \quad (20.5)$$

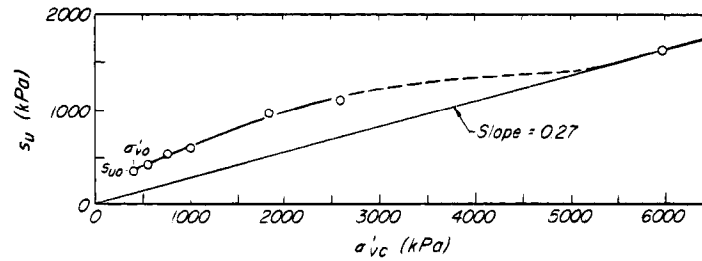


**Figure 20.13** Relation between undrained shear strength and consolidation pressure for London clay (data from Bishop et al. 1965).

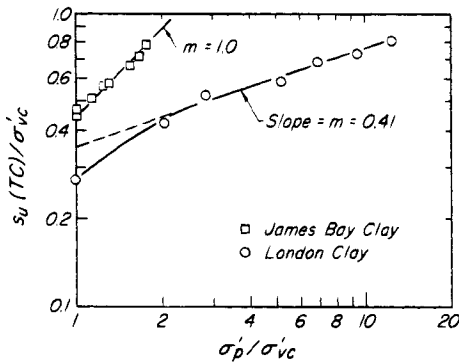


**Figure 20.14** Comparison of relation between undrained shear strength and consolidation pressure for soft James Bay clay and stiff London clay.

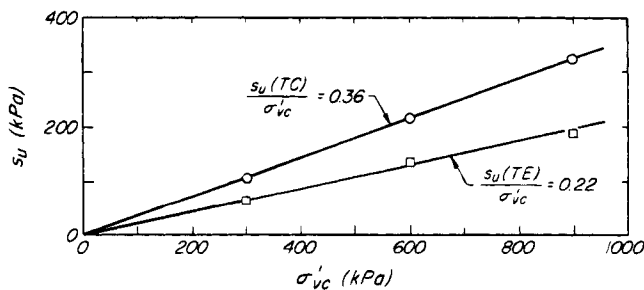


**Figure 20.15** Increase in undrained shear strength with consolidation pressure of Natsushima Tokyo Bay clay for  $\sigma'_{vc}$  greater than  $\sigma'_p$  (data from Hanzawa 1979).

If specimens of *B* to *A* quality are unavailable,  $\sigma'_p$  may be estimated from other measurements such as piezocone soundings (Article 11.4.2) (Mayne and Holtz 1988).

To simplify testing procedure and minimize costs, specimens of *B* to *A* quality of soft clay and silt are often subjected, before undrained shear, not to the  $(\sigma'_{vo}, K_o \sigma'_{vo})$  stress condition, but to an all-around effective confining pressure equal to the *in situ* effective vertical stress,  $\sigma'_{vo}$ . Data in Fig. 20.9 show that for most soft clays and silts,  $\sigma'_{pl}/\sigma'_p$ , although widely scattered, is roughly 0.65. Thus, for soft clays and silts with  $\sigma'_p/\sigma'_{vo}$  values greater than about 1.5, consolidation under an isotropic pressure equal to  $\sigma'_{vo}$  may not significantly damage the natural soil structure. Such undrained compression tests lead to  $s_{uo}(TC)/\sigma'_p$  values comparable with those from specimens that are subjected to the  $(\sigma'_{vo}, K_o \sigma'_{vo})$  stress condition. However, consolidation under isotropic pressure should decrease the difference between  $s_{uo}(TC)/\sigma'_p$  and  $s_{uo}(TE)/\sigma'_p$  as compared with the difference for specimens consolidated under  $(\sigma'_{vo}, K_o \sigma'_{vo})$  conditions. Consequently, extension tests starting from an isotropic consolidation pressure equal to  $\sigma'_{vo}$  may overestimate  $s_{uo}(TE)/\sigma'_p$ . The values of  $s_u(TC)/\sigma'_{vc}$  in the normally consolidated range, obtained from isotropic consolidation tests, are equal to or as much as 10% greater than the values obtained in the  $(\sigma'_{vc}, K_{op} \sigma'_{vc})$  compression range.

## 20.5 Mobilized Field Strength Based on In Situ Vane Experience

Inasmuch as gravity is the main driving force causing instability in the field, two-dimensional plane-strain

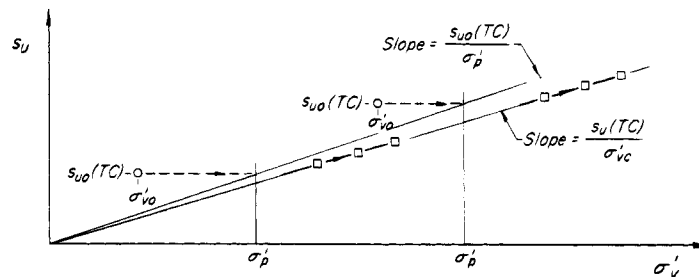


**Figure 20.16** Example of difference between  $s_{uo}/\sigma'_p$  and  $s_u/\sigma'_{vc}$ .

shearing occurs in vertical planes and on vertical, inclined, or horizontal shear surfaces. On inclined segments the mode of shearing may either be active, in the direction of the geostatic shear stresses, or passive, opposite to the original direction of the shear stresses. On a single surface of sliding, some segments may be subjected to different modes of shear; for example, the surface of sliding in a soft clay beneath an embankment may include segments subjected to compressive shear, simple shear, and extension shear (see Fig. 20.23). Differing conditions of restraint may be associated with plane-strain or triaxial shearing. Thus, it is evident that a single laboratory or *in situ* testing device or procedure cannot duplicate all the modes of shear along a full-scale slip surface in the field; each type of test corresponds mainly to one mode of shear. Moreover, the mode of shear for some tests, such as the horizontal shearing on a vertical surface that occurs in the *in situ* vane test, does not correspond to any actual failure condition in the field.

Mobilization of the undrained shear strength of clays under embankment, footing, or excavation loading usually occurs over a period of weeks. In laboratory and *in situ* undrained shear tests, however, the clay is brought to yield within a few minutes (as in *in situ* vane and unconfined compression tests), or hours (as in triaxial compression, triaxial extension, and direct simple shear tests). The mobilized undrained shear strength of clays and silts decreases as the time to failure increases. Thus, the undrained shear strength measured by *in situ* or laboratory tests in minutes to hours can be considerably greater than the strength mobilized in field instabilities over a much longer time. Retrogressive sliding (Article 47.7), however, may develop rapidly and mobilize undrained shear strengths corresponding to short times to failure.

When combinations of soil structure and modes of shear lead to a postpeak reduction in shearing resistance, full peak strengths are not mobilized simultaneously for all elements along a slip surface. On a portion of the surface of sliding that is subjected to a single mode of shear, simultaneous mobilization of the peak shear strength is possible only if the strains are uniform. In general this is not the case, and yielding develops progressively from the more severely stressed into the less stressed zones. When sliding finally occurs over the full segment of the slip surface, some of the elements have been strained beyond the peak. Moreover, a surface of sliding may consist of segments each subjected to a different mode of shear. Brittle modes of shear reach undrained yield at a small strain and display strain softening before more ductile modes mobilize their peak resistance. Under an embankment loading, the compression segment of the slip surface is strained beyond its peak strength and loses resistance before the strengths along the horizontal slip surface and the extension segment are fully mobilized. Thus, nonuniform strains and unequal strains to yield for

different modes of shear, separately or together, lead to progressive yielding on the surfaces of sliding in the field. When global instability develops, the average undrained shear strength mobilized along the surface of sliding may be significantly less than the average of the peak strengths of the modes of shear on that surface. The likelihood of progressive failure is especially great for highly structured loose brittle soft clays and silts.

In summary, the undrained shear strength mobilized on a full-scale surface of sliding in the field may be significantly different from the strength measured by *in situ* or laboratory tests, because (1) a shear test does not, in general, duplicate the modes of shear along a slip surface in the field; (2) undrained shear strength in the field is mobilized over a much longer period than in shear tests; (3) progressive failure is more significant on the surface of sliding, which is subjected to more than one mode of shear in the field, than in a test element subjected mainly to one mode of shear; and (4) soil disturbance is a factor only in the tests. Thus, before the undrained shear strength measured in shear tests is used in a stability analysis, either it must be corrected for the effects of strength anisotropy, time to failure, progressive yielding, and soil disturbance, or it must be calibrated against the strength mobilized in full-scale failures. The most practical approach, and the one that established the usefulness of soil mechanics, is to calibrate *in situ* or laboratory test values against undrained shear strengths back-calculated from actual failures. The usefulness of a shear test for obtaining undrained shear strength is measured by its simplicity, the reproducibility of its results, and whether the values it yields have been calibrated against the observed behavior of a significant number of failures. So far, the most comprehensive calibration in soft clays and silts has been carried out for the *in situ* vane shear test (Article 11.5.2).

The ratio of the cross-sectional area of the standard vane blades to that of the circle circumscribed by the vane is about 10%. Insertion of the vane, analogous to intrusion of a sampling tube, disturbs the natural soil structure (Kimura and Saitoh 1983). This has been confirmed by using vanes of different blade thicknesses. *In situ* vane tests were carried out by La Rochelle et al. (1973) in Saint Louis clay from eastern Canada using vanes with blade thicknesses of 1.6, 1.95, 3.1, and 4.7 mm. Figure 20.17 shows that the undrained shear strength decreases with increasing blade thickness. Soil disturbance caused by the intrusion of the vane has also been confirmed by *in situ* vane tests with different waiting periods between vane insertion and rotation. Data from vane tests by Torstensson (1977) in two Swedish soft clays and by Roy and Leblanc (1988) in two soft clays of eastern Canada are shown in Fig. 20.18. As the porewater pressures developed by the intrusion of the vane dissipate, the soil consolidates and the vane strength increases.

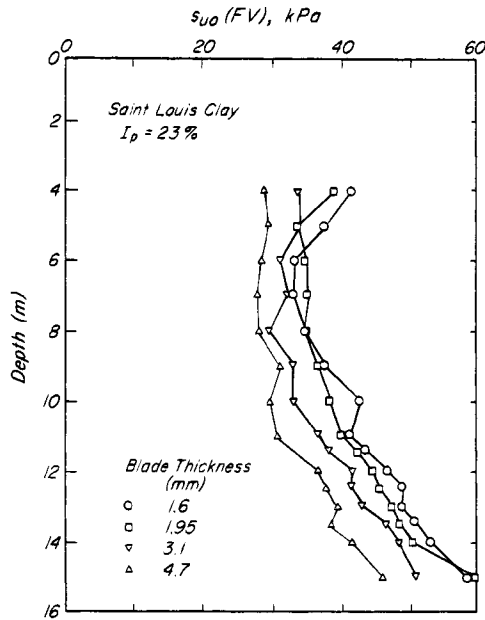


**Figure 20.17** Influence of disturbance due to thickness of vane blade on measured shear strength (after La Rochelle et al. 1973).

However, the measured increase, for example, after 1 week, does not necessarily indicate the total effect of the disturbance on undrained strength, and  $s_u(FV)$  at 1 week could be significantly less than the undrained shear strength of the undisturbed soil subjected to the same mode and rate of shear. The soil disturbance associated with *in situ* vane shear testing of soft clays and silts is of practical importance, however, only if the test deviates from the standard equipment and procedure, because this equipment has been calibrated against full-scale failures in the field. It is thus extremely important that standard vane dimensions, waiting period, and rotation rate, are used throughout the world.

The conventional interpretation of the vane test is based on the assumption that the clay shears along the side and ends of the cylinder circumscribing the rectangular vane. The vane strength is derived from shearing in the top and

bottom horizontal planes and from shearing horizontally in the vertical cylindrical surface. On the assumption that the shear stress distribution is uniform on the vertical as well as the horizontal surfaces, the torque required to turn the vane is

$$T = \frac{\pi D^2 H \tau_v}{2} + \frac{\pi D^3 \tau_h}{6} \quad (20.6)$$

where  $D$  and  $H$  are the diameter and height of the vane, and  $\tau_v$  and  $\tau_h$  are the shear stresses on the vertical and horizontal planes, respectively. For  $H = 2D$ :

$$T = \pi D^3 \left( \tau_v + \frac{\tau_h}{6} \right) \quad (20.7)$$

If  $\tau_v = \tau_h = s_{uo}(FV)$ , the vane strength is computed from the measured peak torque by:

$$s_{uo}(FV) = \frac{6T}{7\pi D^3} \quad (20.8)$$

A plot of a shear stress against rotation angle from a vane test is shown in Fig. 20.19. Equation 20.7 shows that the vane strength is derived mainly from horizontal shearing on the vertical surface. This mode of shear approximates the direct simple shear of a horizontal specimen subjected to an axial consolidation pressure equal to  $K_o \sigma'_{vo}$ . In lean, brittle, and chemically bonded clays, progressive yielding may be initiated at the edges of the blades where the soil is more intensely strained than along the rest of the cylindrical shear zone.

Although the effective stress path to yield in a vane test cannot be defined, the strength for the standard vane shear rate of about 1/2% shear strain per minute or a few minutes to failure corresponds to a point on the yield surface. This implies a constant  $s_{uo}(FV)/\sigma'_p$ , independent of  $\sigma'_p/\sigma'_{vo}$  for a homogeneous soft clay deposit. Indeed, the vane strengths at different depths in a soft clay deposit can often be defined by a single value of  $s_{uo}(FV)/\sigma'_p$ . The values of  $s_{uo}(FV)/\sigma'_p$  for different soft clay and silt deposits have been collected and compared in terms of their liquid limits or plasticity indices. The first set of

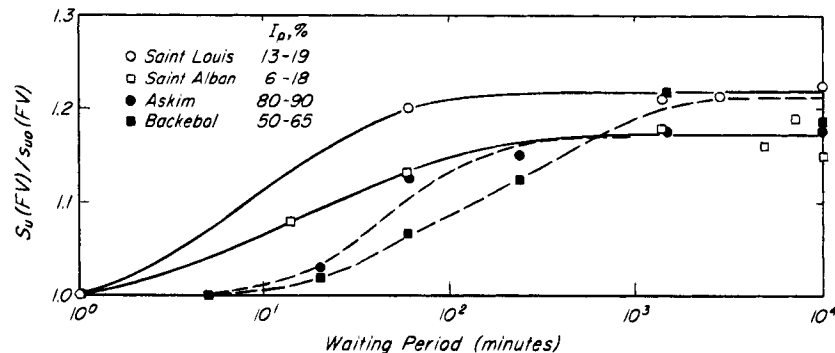


**Figure 20.18** Influence on measured shear strength of waiting period during field vane test.

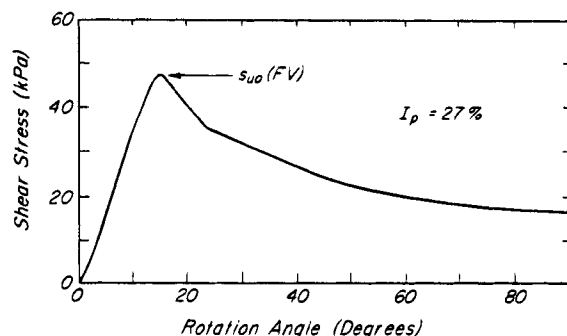


**Figure 20.19** Typical relation from *in situ* vane test between shear stress and rotation angle.

data, published by Skempton (1948), shows an increase in  $s_{uo} (FV)/\sigma'_p$  with the increase in liquid limit. Subsequent data on  $s_{uo} (FV)/\sigma'_p$  for different clays have been compiled in terms of the plasticity index (Skempton 1954b, 1957) and the liquid limit (Hansbo 1957). As a part of a comprehensive study of a number of soft clays that were involved in failures, Bjerrum (1972, 1973) developed typical relations between  $s_{uo} (FV)/\sigma'_{vo}$  and plasticity index for young clays, and between  $s_{uo} (FV)/\sigma'_{vo}$  as well as  $\sigma'_p/\sigma'_{vo}$  and plasticity index for aged clays. Combining the  $s_{uo} (FV)/\sigma'_{vo}$  and  $\sigma'_p/\sigma'_{vo}$  data of Bjerrum for aged clays and comparing the results with  $s_{uo} (FV)/\sigma'_{vo}$  of young clays, Mesri (1975) obtained a practically unique relationship between  $s_{uo} (FV)/\sigma'_p$  and plasticity index for both young and aged clays. This result is consistent with a constant  $s_{uo} (FV)/\sigma'_p$  independent of  $\sigma'_p/\sigma'_{vo}$  for any soft clay deposit. A comprehensive compilation of  $s_{uo} (FV)/\sigma'_p$  data, by Tavenas and Leroueil (1987), is shown in Fig. 20.20 together with the relationship based on Bjerrum's curves. Departures from standard equipment and procedures for the measurements of vane strength, preconsolidation pressure, and plasticity index are partly responsible for the scatter.

In Sweden, shear strength values obtained in laboratory tests were calibrated against mobilized strength back-calculated from stability analyses of loading tests on piles, failed railway embankments; and slopes (Jakobson 1946). When the field vane test was introduced, it was believed that the vane undrained shear strength was equal to the average strength mobilized along the surface of sliding in the field, and that no correction was required. It soon became clear that, in general, the vane strength was not equal to the mobilized strength, and a correction factor had to be introduced before the vane strength could be used in a stability analysis. For example, a computed factor of safety greater than one for a failed embankment on a soft clay deposit indicated that  $s_{uo} (FV)$  was greater than the average strength value mobilized along the surface of sliding at failure. Reduction factors were then recommended by the Swedish Geotechnical Institute for the *in situ* vane undrained shear strength (Osterman 1960).

Bjerrum (1972, 1973) analyzed well-documented embankment, footing, and excavation failures in terms of *in situ* vane undrained shear strength. The computed factors of safety based on circular arc analyses (Article 35.9) were plotted against the plasticity indices of the soils and a straight line was fitted through the data points. Using this line Bjerrum recommended the *in situ* vane correction factor  $\mu = 1/FS$  shown in Fig. 20.21. The mobilized undrained shear strength is computed from

$$s_{uo} (\text{mob}) = \mu s_{uo} (FV) \quad (20.9)$$

Additional data for embankment failures, compiled by Ladd et al. (1977), Menzies and Simons (1978), and Tavenas and Leroueil (1980) show more scatter of the individual cases from the Bjerrum correction curve. The data points in Fig. 20.21 come from different parts of the world, and the scatter in part is related to differences in equipment and procedures used for determining vane strength and plasticity index. The scatter is also related

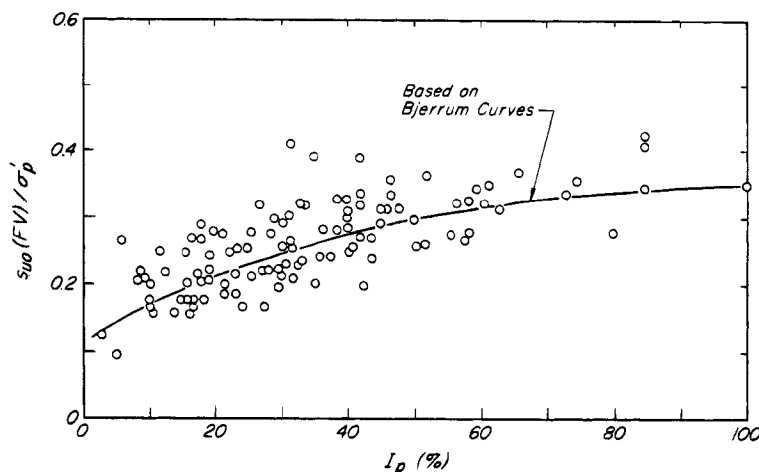


**Figure 20.20** Undrained shear strengths from field vane tests on inorganic soft clays and silts.

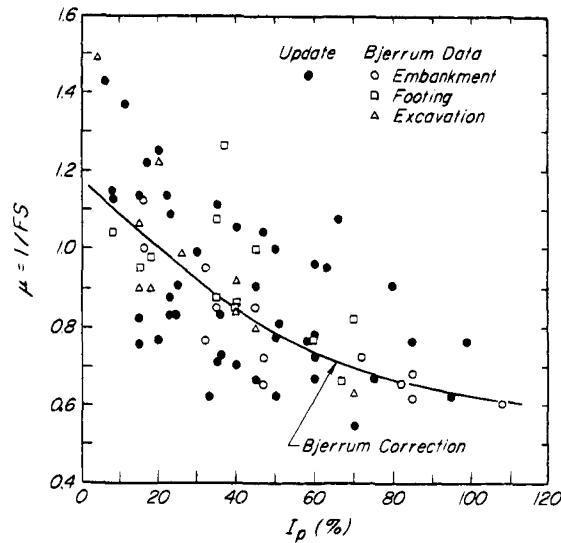


Figure 20.21 Bjerrum's field vane correction factor.

to the influence on the computed factor of safety of ignoring the three-dimensional end effects of the surface of sliding (Azzouz et al. 1981, 1983) and of the difference in strengths mobilized within the embankment and in the crust on the underlying foundation soil (Lefebvre et al. 1988). The discrepancy between the mobilized strength and the vane shear strength is attributed to soil disturbance in the vane test, to progressive yielding, and to the difference in mode of shear and time to failure between the vane test and full-scale instability. The more plastic the clay, the smaller the effect of soil disturbance on  $s_{uo}$  (FV), the smaller the difference due to mode of shear and progressive yielding, and the greater the difference in time to failure. The *in situ* vane strength modified by Bjerrum's correction factor represents the best available calibrated information on undrained shear strength of inorganic soft clays and silts for stability analysis of embankments, footings, and excavations.

Mesri (1975) showed that by associating Bjerrum's correction factor in Fig. 20.21 with the relationship between  $s_{uo}$  (FV)/ $\sigma'_p$  and plasticity index in Fig. 20.20, the mobilized undrained shear strength for stability analysis can be expressed, independently of the plasticity index, as

$$s_{uo}(\text{mob}) = 0.22 \sigma'_p \quad (20.10)$$

Equation 20.10 represents an alternative method for determining the mobilized undrained shear strength of inorganic soft clays and silts for the stability analysis of embankments, footings, and excavations. The preconsolidation pressure  $\sigma'_p$  is evaluated either by oedometer tests using samples of B to A quality or, in the absence of such specimens, by empirical correlations based on *in situ* tests such as the piezocone penetrometer.

The relation between  $s_{uo}$  (FV)/ $\sigma'_p$  and plasticity index in Fig. 20.20 is not applicable to young organic soft clays and silts. The values of  $s_{uo}$  (FV)/ $\sigma'_p$  for these soils frequently plot considerably above the average relationship for inorganic clays and silts. The fiber content of organic soils may act as localized reinforcement or drainage veins across the relatively thin shear zone in the vane test and lead to vane strengths that are too high. Moreover, these soils are highly susceptible to disturbance during sampling and preparation for testing, so that  $\sigma'_p$  is often underestimated by the oedometer test. Alternatively, the molecular organic residues that connect soil particles may provide resistance against relative particle movement, with a maximum effect in rapid undrained shear, but a smaller contribution in drained oedometer loading. For these reasons, Eq. 20.9 may overestimate and Eq. 20.10 may underestimate the mobilized undrained shear strength for organic clays and silts. For organic soils, excluding peats, an additional reduction factor of 0.85 should be used in Eq. 20.9, and  $s_{uo}(\text{mob})/\sigma'_p = 0.26$  should be used in place of Eq. 20.10.

Initial failures of natural slopes, or failures after several months or years of slopes formed by excavation or previous sliding, in soft clays that are nearly normally consolidated have been successfully analyzed using the *in situ* vane shear strength. In these slope failures, the surface of sliding has an average inclination generally larger than 20°. The failures are long-term instabilities in the sense that porewater pressures generated during excavation or previous sliding tend to dissipate within a few months, before the slopes fail. However, in slopes on overconsolidated clays factors of safety computed using the *in situ* vane shear strength are too high (Bjerrum and Kjaernsli 1957). Leroueil et al. (1983) and Tavenas (1984) back-analyzed failures of natural slopes and cuts in soft clays of eastern Canada with  $\sigma'_p/\sigma'_{vo}$  values as high as 4, and discovered that the shear strength mobilized at failure was, in general, much lower than  $s_{uo}$  (FV). The computed factor of safety increased linearly with  $\sigma'_p/\sigma'_{vo}$ . The values of  $s_{uo}$  (FV) and  $\sigma'_p/\sigma'_{vo}$  at each depth both corresponded to the soft clay below the level ground at the top of the slope. The values of the computed factors of safety compiled by Tavenas (1984) have been used to compute a correction factor,  $\mu_s = 1/FS$ , shown in Fig. 20.22. The mobilized strength for initial slope-failure analysis is estimated as:

$$s_{uo}(\text{mob}) = \mu_s s_{uo}(\text{FV}) \quad (20.11)$$

The most conservative interpretation of the data in Fig. 20.22 is

$$FS(\text{computed}) = \frac{\sigma'_p}{\sigma'_{vo}} \quad (20.12)$$

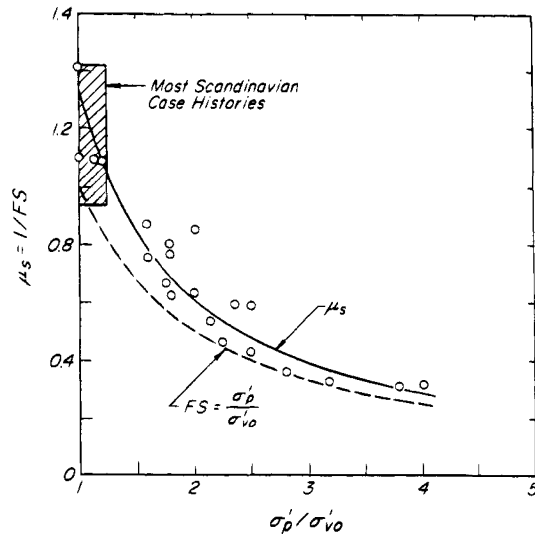


**Figure 20.22** Vane correction factor for analysis of initial slope failure (data from Leroueil et al. 1983).

or

$$\frac{s_{uo} \text{ (FV)}}{s_{uo} \text{ (mob)}} = \frac{\sigma'_p}{\sigma'_{vo}} \quad (20.13)$$

Equation 20.13 leads to

$$s_{uo} \text{ (mob)} = \sigma'_{vo} \frac{s_{uo} \text{ (FV)}}{\sigma'_p} \quad (20.14)$$

Because for a soft clay deposit,  $s_{uo} \text{ (FV)}/\sigma'_p$  is a constant, Eq. 20.14 shows that the mobilized shear strength is directly related to the effective vertical stress below the top of the slope. This agrees with the observation that most initial slope failures tend to occur in wet seasons when the water table is high and  $\sigma'_{vo} = \sigma_{vo} - u_o$  is low. Equation 20.14 can be used for assessing the long-term stability of natural slopes or cuts in soft clays against initial sliding. In highly structured loose quick-clay silts, initial slope failure may lead to retrogressive landsliding, including large flakes on nearly horizontal slip planes.

## 20.6 Undrained Shear Strength from Laboratory Shear Tests

Undrained shear strength depends on the mode of shear and differs in different directions in the ground. The corrected vane undrained shear strength is the average mobilized value for the modes of shear that occur along a circular surface of sliding in field instabilities. The values of undrained shear strength mobilized in different directions can be measured by laboratory shear tests that simulate distinct modes of shear. The tests most widely used are triaxial compression, triaxial extension, and direct simple shear. The relevance of these tests to the modes

of shear along a circular slip surface is illustrated in Fig. 20.23.

A triaxial compression or extension test is performed on a cylindrical vertical specimen typically 38 mm in diameter and 76 mm in height. The specimen is set up in the triaxial cell and is subjected to consolidation stresses under a drained condition. If the specimen is of *B* to *A* quality (Table 11.2), it is subjected to the *in situ* ( $\sigma'_{vo}$ ,  $K_o \sigma'_{vo}$ ) consolidation stress condition. When samples of only *D* to *C* quality are available, or when it is necessary to measure the increase in undrained shear strength due to consolidation, the specimen is subjected to ( $\sigma'_{vc}$ ,  $K_{op} \sigma'_{vc}$ ) consolidation, in which the vertical consolidation pressure  $\sigma'_{vc}$  has values in the range of  $1.5 \sigma'_p$  to  $4 \sigma'_p$ . During the undrained shear, the vertical stress is increased for the compression test (*TC*) and decreased for the extension test (*TE*) while the horizontal stress is kept constant. For triaxial shear tests, the peak value of principal stress difference is used to define the undrained shear strength as

$$s_{uo} = \frac{1}{2} (\sigma_1 - \sigma_3)_f \quad (20.15)$$

The change in vertical stress during the shearing stage is usually imposed by subjecting the specimen to a constant rate of axial compression or extension. If the purpose of the test is to define undrained shear strength according to Eq. 20.15, a standard imposed strain rate, such as 0.01%/min, is recommended. However, if it is necessary to define the effective stress condition during shear, the porewater pressure in the specimen is measured. The imposed strain rate, which must be selected to allow proper measurement of shearing-induced porewater pressure, is then governed by the permeability of the soil; the time to the yield point for different soils may vary from one-half to several hours.

In the triaxial compression test (*TC*), which simulates the active mode of shear in the field, the shear stresses are increased in the same direction as the already existing geostatic shear stresses. The natural soil structure remains fairly intact until it yields at small axial strain. Most soft

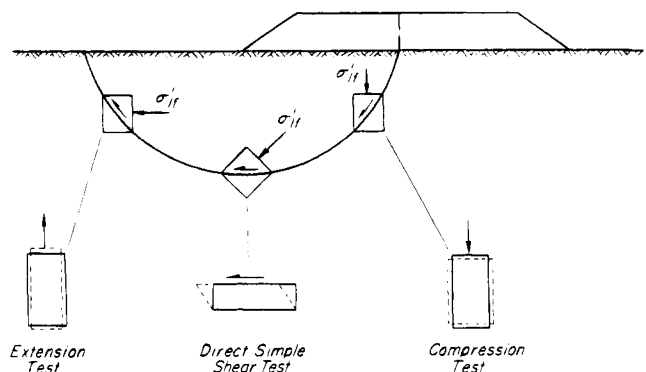


**Figure 20.23** Relevance of laboratory shear tests to modes of shear on a surface of sliding in the field (after Bjerrum 1972).



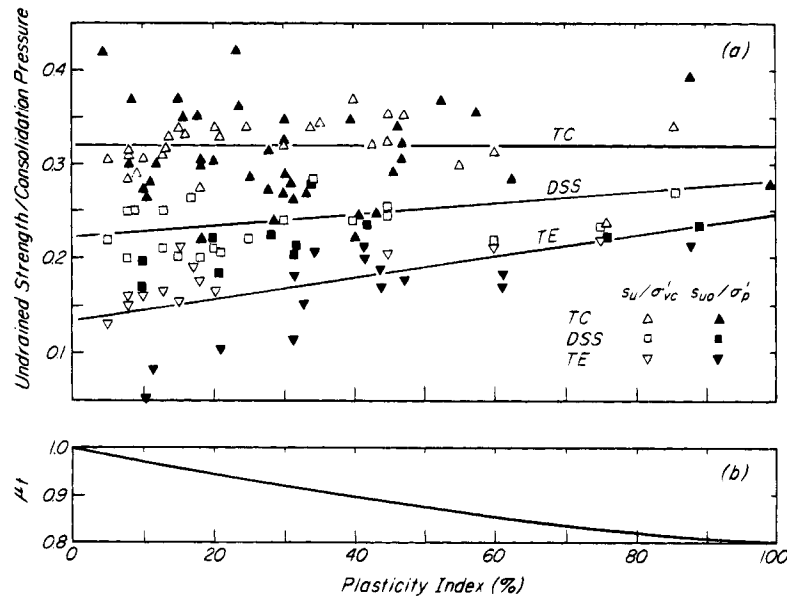


**Figure 20.24** (a) Ratios of undrained shear strength to consolidation pressure from laboratory tests. (b) Correction factor to be applied to laboratory test results to account for difference in time to failure in field.

clays and silts exhibit pronounced strain-softening behavior after yield in the triaxial compression mode of shear. In the triaxial extension test (TE), which simulates the passive mode of shear in the field, shear stresses are increased in the opposite direction to the initial geostatic shear stresses. During the test the shear stresses decrease to zero and then increase in the opposite direction. Considerable disruption of the natural soil structure occurs before final yield is reached at relatively large axial strain, and strain softening is insignificant thereafter.

The direct simple shear test (DSS) is used to simulate the mode of shear along horizontal or gently inclined portions of a slip surface. The state of stress in the specimen cannot be defined from a knowledge of the effective normal stress  $\sigma'_v$  and shear stress  $\tau_h$  on the horizontal plane. The shearing mode causes a rotation of the principal planes by about  $45^\circ$ , and the degree of disruption of the natural soil structure before yield is intermediate between the triaxial compression and extension modes of shear. A horizontal displacement rate, such as 0.006 mm/min, is selected so that porewater pressures in the specimen remain zero throughout the test. Therefore, different shear rates are used for different soils.

A summary of the undrained shear strengths of several natural soft clay and silt deposits is shown in Fig. 20.24. Before undrained shearing the specimens were subjected under drained conditions either to the same ( $\sigma'_{vo}$ ,  $K_o \sigma'_{vo}$ ) stresses as they carried in the field, or to ( $\sigma'_{vc}$ ,  $K_{op} \sigma'_{vc}$ ) stresses up to several times the preconsolidation pressure  $\sigma'_p$ . The data were compiled by Crooks (1981), Graham et al. (1982), Jamiolkowski et al. (1985), Chandler (1988),

and Ladd (1991). The relative positions of the TC, TE, and DSS yield points on a yield envelope are shown in Fig. 20.25. Inasmuch as the states of stress in the direct simple shear device and the *in situ* vane test cannot be defined, the DSS stress path shown is a plot of  $\tau_h/\sigma'_p$  against  $\sigma'_v/\sigma'_p$ , and the stress path for the vane shear has merely been sketched. In general, the values of  $s_{uo}$  (TC)/ $\sigma'_p$  are equal to or larger than  $s_u$  (TC)/ $\sigma'_{vc}$ ,  $s_{uo}$  (DSS)/ $\sigma'_p$  are about equal to  $s_u$  (DSS)/ $\sigma'_{vc}$ , and  $s_{uo}$  (TE)/ $\sigma'_p$  are equal to or smaller than  $s_u$  (TE)/ $\sigma'_{vc}$ . The data in Fig. 20.25 demonstrate that most soft clays and silts exhibit significant undrained shear-strength anisotropy that is generally most important in lean clays, especially if the clays are also highly structured and bonded. The ratio between  $s_u$  (TC)/ $\sigma'_{vc}$  and  $s_u$  (TE)/ $\sigma'_{vc}$  is of the order of 2 for lean clays

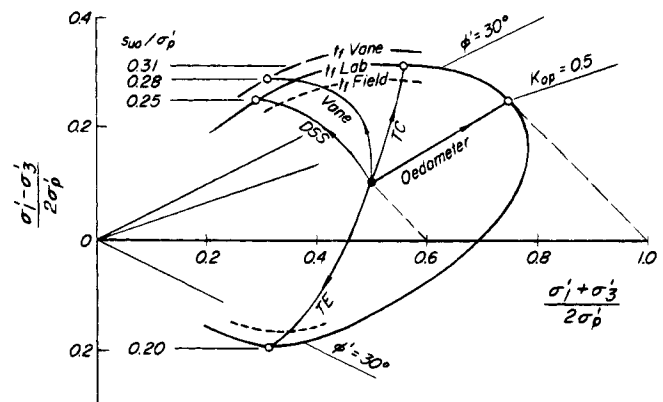


**Figure 20.25** Stress path to yield in different shear tests.

and silts and reduces with increasing plasticity to about 1.5. For some highly structured bonded lean clays, the values of  $s_{uo}(TC)/\sigma'_p$  are 2.5 to 3.5 times as large as  $s_{uo}(TE)/\sigma'_p$ . The values of  $s_{uo}(DSS)/\sigma'_p$ , as well as  $s_u(DSS)/\sigma'_{vc}$ , lie approximately midway between  $s_{uo}(TC)/\sigma'_p$  and  $s_{uo}(TE)/\sigma'_p$  or  $s_u(TC)/\sigma'_{vc}$  and  $s_u(TE)/\sigma'_{vc}$ . The relative magnitudes of  $s_{uo}(TC)/\sigma'_p$ ,  $s_{uo}(DSS)/\sigma'_p$ , and  $s_{uo}(TE)/\sigma'_p$  or of  $s_u(TC)/\sigma'_{vc}$ ,  $s_u(DSS)/\sigma'_{vc}$ , and  $s_u(TE)/\sigma'_{vc}$  reflect different shapes of the yield envelope for various soils.

For any one mode of shear, a unique relationship between  $s_{uo}/\sigma'_p$  or  $s_u/\sigma'_{vc}$  and the plasticity index should not be expected. However, part of the scatter of the data in Fig. 20.24 is related to different degrees of specimen disturbance, especially for  $(\sigma'_{vo}, K_o \sigma'_{vo})$  tests, to generally variable testing procedures in terms of the imposed consolidation stress condition and rate of shear, and to inconsistent interpretation of data to define  $s_{uo}$  or  $s_u$  as well as  $\sigma'_p$  or  $\sigma'_{vc}$ . It is probably reasonable to assume that the average linear relationships in Fig. 20.24a provide an acceptable estimate of the values of  $s_{uo}/\sigma'_p$  or  $s_u/\sigma'_{vc}$  for the three modes of shear.

The time to failure in laboratory shear tests is generally measured in hours, whereas mobilization of the undrained shear strength in field instability situations requires weeks. The laboratory undrained shear-strength values must be corrected to the time to failure encountered in the field. There is no consistent relationship between plasticity index and reduction in undrained shear strength due to creep. Independently of plasticity, the undrained shear strength decreases by about 5 to 10% for every tenfold increase in the time to failure in the range of time from that for laboratory shear tests to that involved in field instabilities. The undrained shear strength under a footing or embankment loading begins to increase after a consolidation time that depends on the permeability and thus on the plasticity of the soil. Therefore, the time to failure for field instabilities is likely to increase with plasticity index, and there is a larger opportunity for a creep reduction in undrained shear strength. The time-to-failure reduction factor,  $\mu_t$ , shown in Fig. 20.24b, should be applied to the undrained shear strength values from laboratory *TC*, *TE*, and *DSS* tests to obtain the mobilized strength for stability analysis. The empirical correction factor has been established from a consideration of typical times to failure for embankment instabilities and laboratory shear tests (Mesri 1989).

The values of  $s_{uo}/\sigma'_p$  or  $s_u/\sigma'_{vc}$  from a particular type of laboratory shear test can be used to compute the undrained shear strength on a slip surface that is subjected to the same mode of shear. For example,  $s_{uo}(DSS)/\sigma'_p$  may be used, after correction for time to failure, to define undrained shear strength along a long gently inclined slip plane of a flake slide, as follows:

$$s_{uo}(\text{mob}) = \mu_t s_{uo}(\text{DSS}) \quad (20.16)$$

For calculation of embankment stability, an average of the shear strengths obtained in *TC*, *DSS*, and *TE* tests should be used. It may be assumed that the slip surface consists of equal segments of compression, direct simple, and extension modes of shear. For strain-softening clays and silts, because of progressive failure, the average undrained strength mobilized along the slip surface is less than the sum of the peak strengths. To account for the effect of progressive failure a strain compatibility approach has been recommended by Koutsoftas and Ladd (1985) and is illustrated in Fig. 20.26. The shear strain for triaxial tests is computed as 1.5 times the axial strain. The technique assumes that the shear strain all along a potential slip surface is uniform at the moment global instability develops. The stress-strain curves of the three tests are combined to obtain an average stress-strain curve, the peak of which defines the mobilized strength. The calculations on Fig. 20.26 show that correction for progressive failure for a highly structured clay reduces the available strength by less than 10%. Unless the soil exhibits very pronounced postpeak reduction in undrained resistance and, in addition, the compression mode occurs over a major portion of the sliding surface, such a refinement is often not practical or justified. It is preferable to compute the average mobilized strength for a given  $\sigma'_p$  by

$$s_u(\text{mob}) = \frac{1}{3} \left( \frac{s_{uo}(TC)}{\sigma'_p} + \frac{s_{uo}(DSS)}{\sigma'_p} + \frac{s_{uo}(TE)}{\sigma'_p} \right) \sigma'_p \mu_t \quad (20.17)$$

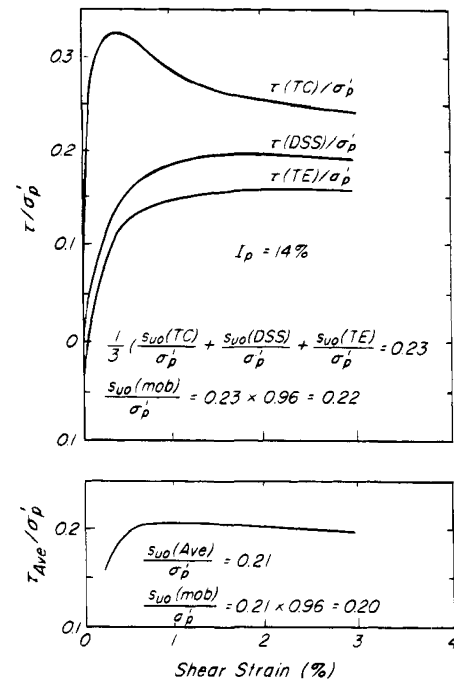


Figure 20.26 Application of strain compatibility method to highly structured clay (after Lefebvre et al. 1988).

When Eq. 20.17 is applied to the average lines in Fig. 20.24 for the three modes of shear, it is found that, independently of the plasticity index,

$$s_u (\text{mob}) = 0.22 \sigma'_p \quad (20.18)$$

This empirical result, based on laboratory undrained shear strength data, is identical with the conclusion reached from the calibration of *in situ* vane strength with full-scale embankment, footing, and excavation failures. The empirical Eq. 20.18 offers a reliable alternative for evaluating the mobilized average undrained strength to be used in circular arc stability analyses of embankment and footing. Because, in general,  $s_{uo} (DSS)/\sigma'_p$  is approximately the average of  $s_{uo} (TC)/\sigma'_p$  and  $s_{uo} (TE)/\sigma'_p$ , Eq. 20.18 can also be used to obtain the undrained shear strength on horizontal or gently inclined sliding surfaces. The mobilized undrained strengths on the active and passive portions of a wedge-type slip surface (Article 35.10) can be estimated from the following equations:

$$s_{uo} (\text{AC}) = s_{uo} (\text{TC}) \mu_t \quad (20.19)$$

$$s_{uo} (\text{PA}) = s_{uo} (\text{TE}) \mu_t \quad (20.20)$$

For strain-softening clays and silts, an additional reduction factor of 10 to 20% may be required in Eq. 20.19 to account for progressive yielding along the slip surface.

The procedures for computing  $s_{uo} (\text{mob})$  are also applicable to  $s_u (\text{mob})$  after consolidation in the field. For example, the following equation is suitable for computing the mobilized strength, after consolidation, on a circular arc or a long gently inclined slip surface:

$$s_u (\text{mob}) = 0.22 \sigma'_{vc} \quad (20.21)$$

where  $\sigma'_{vc}$  is the vertical consolidation pressure greater than  $\sigma'_p$ .

In general, obtaining undrained shear strength data from laboratory *TC*, *TE* and *DSS* shear testing of soil samples from borings is more expensive and time consuming than determining strength values from *in situ* vane tests. The data and analyses presented in this article suggest that the more economical and less time-consuming calibrated vane strength may be at least as reliable as undrained strength information from laboratory tests.

## 20.7 Unconfined Compression Test

The unconfined compression test (Article 17.3.1) is one of the most widely used tests for the measurement of compressive strength of construction materials. It is also one of the oldest tests for determining the undrained shear strength of saturated soft clays and silts. The undrained shear strength,  $s_u (UC)$ , is defined in terms of unconfined compressive strength  $q_u$  as:

$$s_{uo} (UC) = \frac{1}{2} q_u \quad (20.22)$$

For a saturated clay specimen of A quality there are

three fundamental differences between an unconfined compression test and a triaxial compression test from the *in situ* ( $\sigma'_{vo}$ ,  $K_o \sigma'_{vo}$ ): (1) The unconfined compression specimen starts undrained shear from an isotropic effective stress  $\sigma'_s$ , equal to the negative porewater pressure resulting from the release of the *in situ* ( $\sigma'_{vo}$ ,  $K_o \sigma'_{vo}$ ) stress condition. The value of  $\sigma'_s$  is generally less than  $\sigma'_{vo}$  and decreases with specimen disturbance. For specimens of A quality, however, the preshear effective stress condition, corresponding to a point inside the yield envelope (Article 20.2), does not have a significant effect on the undrained shear strength in the compression mode of shear. Therefore, the initial effective stress condition does not lead to a significant difference between  $s_{uo} (UC)$  and  $s_{uo} (TC)$ . However, with an increase in specimen disturbance, the difference between  $s_{uo} (UC)$  and  $s_{uo} (TC)$  increases, because the laboratory application of ( $\sigma'_{vo}$ ,  $K_o \sigma'_{vo}$ ) and the associated consolidation counteract part of the effect of soil disturbance on  $s_{uo}$ . (2) Unconfined compression tests on different types of clays and silts typically reach failure in a few minutes, 10 to 100 times faster than triaxial compression tests from ( $\sigma'_{vo}$ ,  $K_o \sigma'_{vo}$ ). In this range of strain rate, the undrained shear strength could be some 5 to 15% greater than if determined at the tenfold smaller rate to failure in a triaxial test. (3) Because of the absence of any confining pressure, a premature failure through a weak zone may terminate an unconfined compression test. The significance of this factor increases with the stiffness and the presence of fissures in the specimen. For typical soft clays, premature failure is not likely to decrease the undrained shear strength by more than 5%.

The unconfined compression test is a special case of the unconsolidated undrained (*UU*) triaxial compression test (Article 17.3.1). In the *UU* test the specimen is subjected to equal all-around pressure under undrained conditions, and no overall water content change is allowed. The axial stress is then increased to produce an axial strain rate of about 1 to 2% per minute until failure occurs. For completely saturated soft clays and silts, the undrained shear strength is independent of the total confining pressure. The increase in equal all-around pressure results only in an equal increase in porewater pressure, and the effective stress remains unchanged (Article 15.5.1). This is illustrated in Fig. 20.27, which shows the relationship between undrained shear strength and total normal stress for one *UC* and three *UU* tests on saturated Boston Blue clay. It also illustrates that:

$$s_{uo} (UU) = s_{uo} (UC) = \frac{1}{2} q_u = \frac{1}{2} (\sigma_1 - \sigma_3)_f \quad (20.23)$$

The *UU* as compared with the *UC* test tends to decrease the scatter in the  $s_{uo}$  data, even for soft saturated clays, because it minimizes the possibility of premature failure.

The results of a series of undrained compression (*UU*) tests on 38-mm-diameter and 76-mm-high vertical speci-

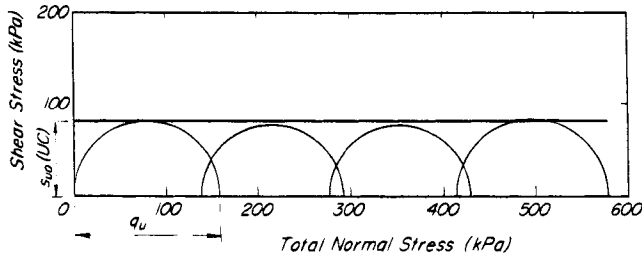


**Figure 20.27** Relation between undrained shear strength and total normal stress for Boston blue clay.

mens of Boston Blue Clay are shown in Fig. 20.28. Block samples of A quality were hand carved at a depth of 13.7 m, and had the following index properties:  $w_o = 26\%$ ,  $w_l = 34\%$ , and  $I_p = 16\%$ . The *in situ* consolidation stress condition was defined by  $\sigma'_{vo} = 155$  kPa,  $K_o = 0.90$ , and  $\sigma'_p/\sigma'_{vo} = 3.0$ . The only difference between the unconfined compression test (UC) and the unconsolidated undrained compression test (UU) is that a total confining pressure, under which no drainage was permitted, was applied in the latter test. The 5% difference between  $s_{uo}$  (UC) and  $s_{uo}$  (UU) is related to premature failure in the unconfined compression test. The UC and UU tests reached failure about 10 times faster than the TC test. In spite of this,  $s_{uo}$  (TC) was about 4% higher than  $s_{uo}$  (UU). Since the strain rate effect was about 5% for the UC and UU tests with respect to that of the TC test, the disturbance resulting from the release of the *in situ* stress evidently reduced the undrained strength by about 9%. In this instance the

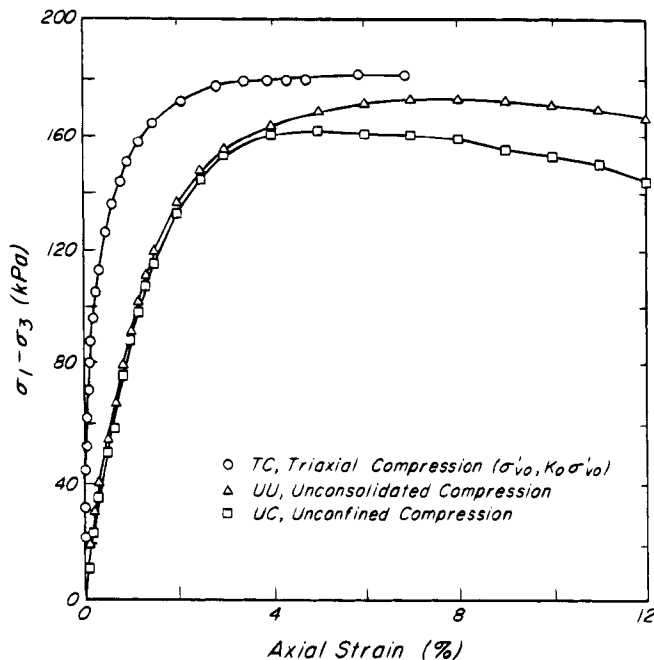


**Figure 20.28** Undrained compression tests on Boston blue clay.

effect of disturbance was almost offset by the rapid strain rate, and  $s_{uo}$  (UU) was almost equal to  $s_{uo}$  (TC). In general, for saturated soft clays, it is reasonable to ignore the difference between  $s_{uo}$  (UC) and  $s_{uo}$  (UU), and to conclude that for specimens of A quality:

$$s_{uo} \text{ (UC)} = s_{uo} \text{ (TC)} \quad (20.24)$$

Unconfined compression or unconsolidated undrained compression tests are usually carried out on tube samples from boreholes, and the soil specimens are of C to D quality. Figures 11.6 and 20.29 show comparisons of  $s_{uo}$  (UC) data from tube and block samples of Chicago blue clay. The values of natural water content, liquid limit, and plasticity index for this clay are in the range of 23 to 30%, 30 to 35%, and 12 to 17%, respectively. Figure 20.29 shows that  $s_{uo}$  (UC) from 51-mm Shelby tube samples is about 70% of  $s_{uo}$  (UC) from block samples. It may be recalled that, irrespective of the plasticity of the clay,  $s_{uo}$  (TC)/ $\sigma'_p$  equals approximately 0.32 (Fig. 20.24). A reduction to 70% of this value leads to 0.22. The latter value, in agreement with Eq. 20.18, is the best estimate for the average mobilized undrained strength ratio on a circular arc surface of sliding. Thus, for Chicago blue clay, the compression mode and rapid shearing rate of the unconfined compression test counterbalance soil disturbance, and  $s_{uo}$  (UC) from the 51-mm Shelby tube samples provides an excellent estimate of the average mobilized strength on a slip surface in the field.

Figure 20.30 shows a comparison of undrained shear-strength values from unconfined compression tests, and from triaxial compression tests consolidated under  $(\sigma'_{vo}, K_o \sigma'_{vo})$ , on soft Natsushima clay from Tokyo Bay. The specimens of 38 mm diameter were trimmed from 75-mm thin-walled fixed piston samples of C to B quality.

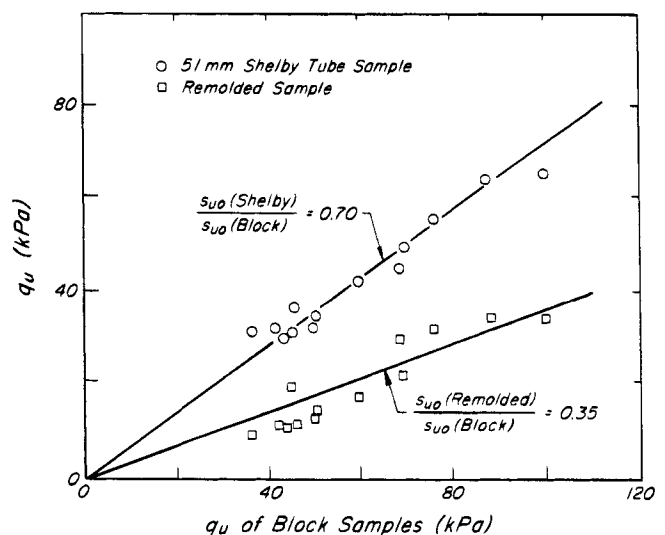


**Figure 20.29** Effect of sample disturbance on undrained shear strength of Chicago clay.

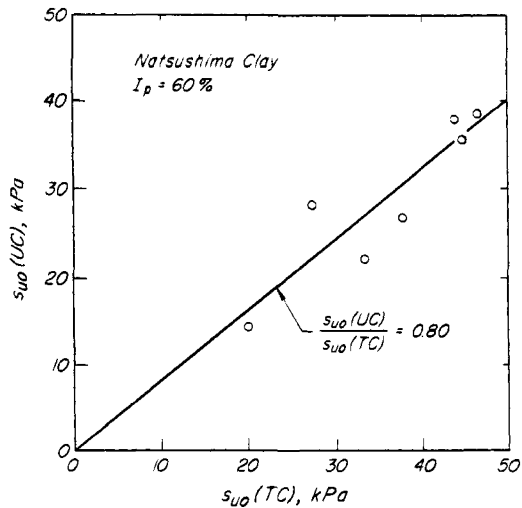


**Figure 20.30** Relation between undrained shear strengths from unconfined compression and triaxial compression tests on Natsushima clay (data from Hanzawa and Kishida 1982).

The values of natural water content, liquid limit, and plasticity index are 80 to 90%, 100 to 110%, and 60%, respectively. For specimens of *B* quality  $s_{uo}(UC)$  for this clay is about 80% of  $s_{uo}(TC)$ . Inasmuch as 80% of 0.32 is 0.26,  $s_{uo}(UC)$  should overestimate the average mobilized strength on a circular arc sliding surface. Figure 20.31 shows that the values of  $s_{uo}(UC)$  for Natsushima clay are approximately equal to the average of  $s_{uo}(TC)$  and  $s_{uo}(TE)$ . From Fig. 20.24b, at  $I_p = 60\%$ , a time-to-failure correction factor of 0.85 must be applied to  $s_{uo}(TC)$  and

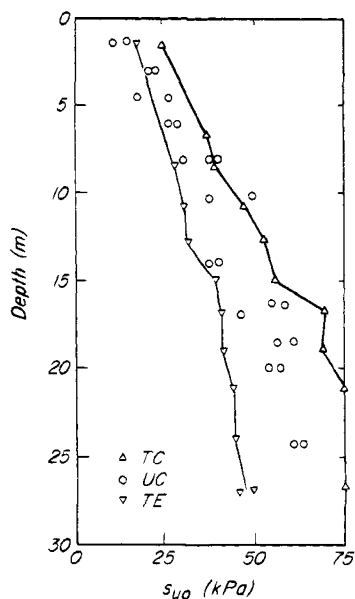


**Figure 20.31** Comparison of values of undrained shear strength from unconfined compression, triaxial compression, and triaxial extension tests on Natsushima clay (data from Hanzawa and Kishida 1982).

$s_{uo}(TE)$  to obtain the mobilized strength in full-scale field failures. The product of 80% of  $0.32 \times 0.85$  again indicates 0.22 to be the best estimate for the average mobilized undrained strength ratio on a circular arc surface of sliding.

Unfortunately, in spite of the consistent  $s_{uo}(UC)$  information from extensive and reliable unconfined compression tests on Chicago blue clay and Natsushima clay, in general the effect of specimen disturbance on  $s_{uo}(UC)$  can be very large and quite variable. The limiting disturbed soil is defined by complete remolding and is best quantified by the sensitivity, defined as

$$S_t = \frac{s_{uo}(\text{undisturbed})}{s_{uo}(\text{remolded})} \quad (20.25)$$

Any consistent method can be used to determine undisturbed and remolded strength values. The remolded undrained strength of some soft clays and silts, however, is so small that special equipment must be used to measure it. Figure 20.32 dramatically illustrates that the completely disturbed  $s_{uo}$  in extreme cases can be 1000 times smaller than the undisturbed strength. Figure 20.33 suggests that the correlation between  $S_t$  and liquidity index (Fig. 20.32) is strongly determined by the unique relationship between remolded undrained shear strength and liquidity index. The data in Fig. 20.33 were obtained by Norman (1958), Leroueil et al. (1983), and Locat and Demers (1988), and include soft clay and silt deposits from around the world. It is interesting to note that the liquid limit corresponds to a remolded undrained shear strength of 1.5 to 2.5 kPa (Casagrande 1958). The quick clays, which in the remolded state display the consistency of a thick liquid, have remolded undrained shear strengths generally less than 0.2 kPa.

Because of the enormous range between remolded and undisturbed undrained shear strengths, experience with

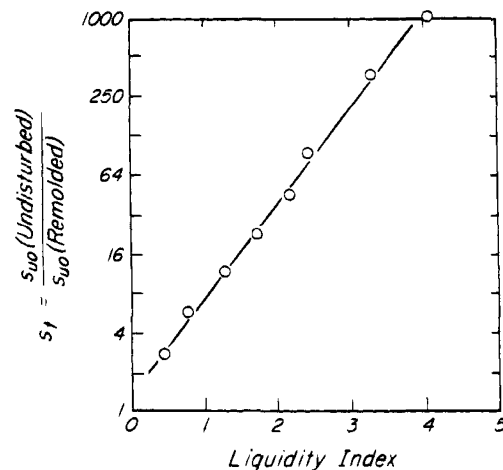


**Figure 20.32** Relation between sensitivity and liquidity index (after Bjerrum 1954).

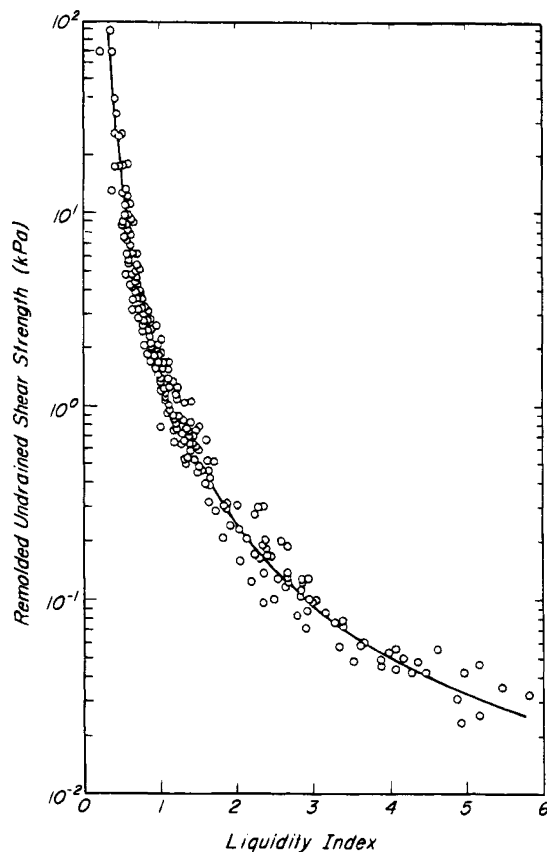


**Figure 20.33** Relation between undrained shear strength and liquidity index of clays from around the world.

$s_{uo}$  (UC) based on borehole samples can vary within fairly wide limits for different soil types and degrees of soil disturbance. It is difficult to determine a general calibration of  $s_{uo}$  (UC) against field experience for specimens that may range in quality from *E* to *B*. Ohta et al. (1989) have computed a correction factor for  $s_{uo}$  (UC) by comparing the undrained shear strength from the unconfined compression test to the average mobilized strength on the surface of sliding of failed embankments. Their data, together with additional cases of embankment failures on soft clays and silts, are shown in Fig. 20.34. The  $s_{uo}$  (UC) data for the cases summarized in this figure correspond to tube samples of *D* to *B* quality. The correction factor for  $s_{uo}$  (UC),

$$\mu_{uc} = \frac{s_{uo}(\text{mob})}{s_{uo}(\text{UC})} \quad (20.26)$$

is compared with the Bjerrum correction factor for *in situ* vane undrained strength. In spite of the limited number of data points and the significant scatter, the data in Fig. 20.34 suggest that specimen disturbance causes  $s_{uo}$  (UC) values to be generally smaller than  $s_{uo}$  (FV). However, in the plasticity index range of 20 to 60%,  $s_{uo}$  (UC) values from tube samples are comparable to the  $s_{uo}$  (FV) values.

For plasticity indices outside this range, and especially for lean loose clay silts,  $s_{uo}$  (UC) from tube samples may significantly underestimate the average mobilized strength on a circular arc surface of sliding. Finally, the data in Fig. 20.34 show that, over a fairly significant range of plasticity, the value of  $\mu_{uc}$  is close to unity. This explains successful local applications of the unconfined compression test, in the United States, England, and Japan, on the assumption that  $s_{uo}(\text{mob}) = s_{uo}(\text{UC})$ . On the other hand, if samples of *B* to *A* quality are used in the unconfined compression test, the  $s_{uo}$  (UC) values for stability analysis may lead to unconservative factors of safety.

The unconfined compression test should not be used for fissured clays, because a premature failure is likely to terminate the test. A premature failure may also occur in highly dilatant dense silts, by cavitation resulting from large negative shearing-induced porewater pressures. For both materials *UU* tests with a large enough all-around pressure must be used (Bishop and Eldin 1950). The fissures that open up upon sampling stiff clays, shales, mudstones, and siltstones generally are unsaturated. Therefore, even an undrained application of a confining pressure closes them and causes a significant increase in undrained strength with total confining pressure. Figure 20.35 shows a series of *UU* tests on Newport fissured siltstone, with natural water content, liquid limit, and plasticity index of 9, 30, and 13%, respectively. A similar increase in undrained strength with total confining pressure is observed in unsaturated compacted soils, as is illustrated in Fig. 20.36 for Goose Lake clay, which has a liquid limit of 31% and a plasticity index of 14%. The specimens compacted at a water content of 6.3% had an initial degree of saturation of 28%. As the total confining pressure increases on such unsaturated soils, the air voids compress and an increase in density and undrained shear strength occurs (Article 15.5.1). The undrained strength increases with total confining pressure until all air has been compressed and dissolved in the pore water of the specimen. The steep slope of the relation between undrained strength and confining pressure for the specimen compacted at a water content of 6.3% suggests that, even under an equal all-around pressure of 7 MPa, the specimen was still substantially unsaturated. On the other hand, specimens compacted on the wet side of optimum (Article 44.2.3), with an initial degree of saturation of 90%, became saturated under a confining pressure of about 0.5 MPa and behaved as saturated soils thereafter (Article 15.5.1).

## Problems

1. An undisturbed specimen of silty clay is set up in the triaxial cell and is consolidated by subjecting it to an equal all-around pressure of 750 kPa and a back pressure of 250 kPa.

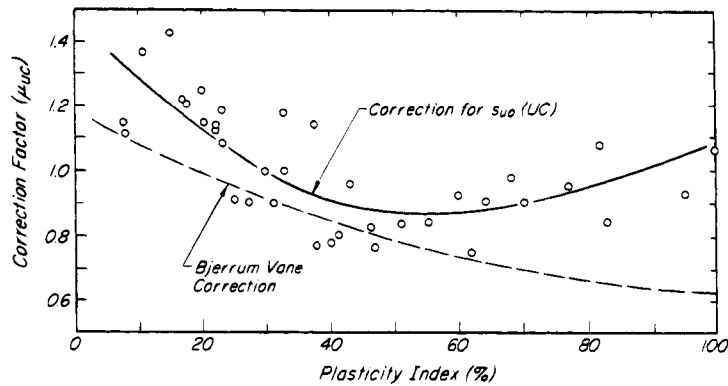


**Figure 20.34** Correction factor for undrained shear strength from unconfined compression tests on tube samples.

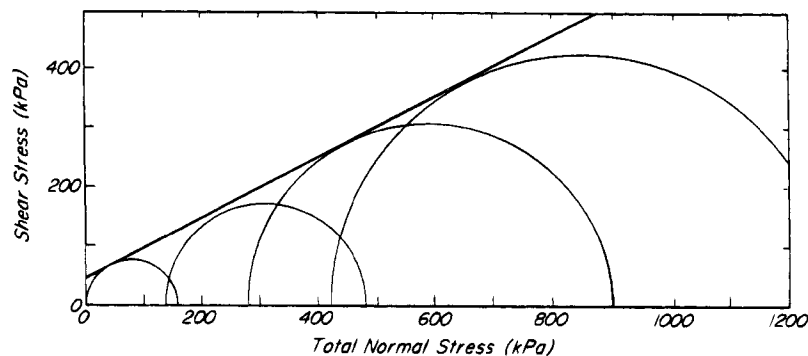


**Figure 20.35** Relation between undrained shear strength and total normal stress for Newport fissured siltstone (after Golder and Skempton 1948).

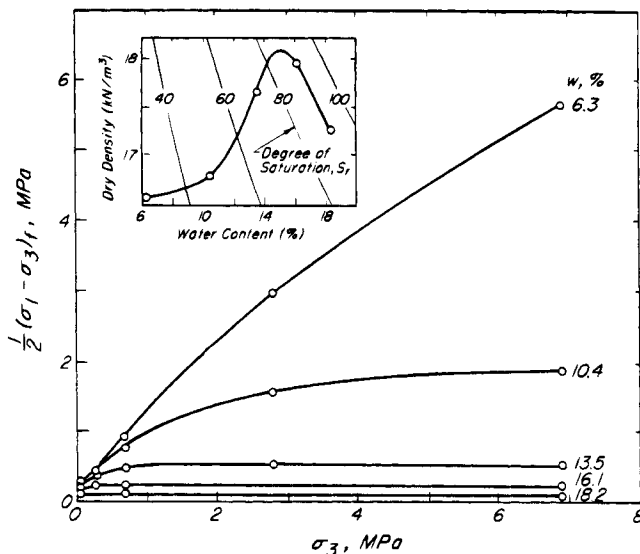


**Figure 20.36** Relation between undrained shear strength and total confining pressure for Goose Lake clay (Olson and Parola 1968).

After the sample reaches equilibrium in terms of porewater pressure under this equal all-around pressure and back-pressure condition, the drainage lines are turned off and the axial stress is increased. At failure, the total porewater pressure measured is 550 kPa and the increase in axial stress is 333 kPa. Compute: (a) undrained shear strength of the specimen, (b) undrained shear strength to consolidation pressure ratio for the particular mode of shear, (c) friction angle (assuming cohesion intercept to be zero).

Ans. 166 kPa; 0.33; 27°.

2. A soft clay specimen is normally consolidated in the triaxial cell under an equal, all-around pressure of 200 kPa. Then the drainage lines are turned off and the cell pressure is increased by 300 kPa. A porewater pressure of 300 kPa is measured. Under constant cell pressure, the axial stress is increased, measuring at failure  $\Delta\sigma_1 = 110$  kPa and  $\Delta u = 120$  kPa. A second specimen of the same clay is normally consolidated under an equal all-around pressure of 70 kPa. Under undrained conditions the axial stress is increased to failure. For the second specimen compute: (a)  $\Delta\sigma_1$  at failure, (b)  $\Delta u$  at failure, and (c) undrained shear strength  $s_u$  (TC). A third specimen is normally consolidated under an equal all-around pressure of 70 kPa and the axial stress is increased to failure under drained conditions. For the third specimen com-

pute: (d)  $\Delta\sigma_1$  at failure, and (e) drained shear strength. What assumptions did you have to make in order to use the test data on the first specimen to predict the behavior of the second and third specimens?

Ans. 38, 42, 19, 96, 44 kPa.

3. An undisturbed sample of soft clay is taken from a depth at which  $\sigma'_{vo} = 50$  kPa and  $\sigma'_p = 100$  kPa. A specimen is set up in the triaxial cell and under a fully drained condition is subjected to a final equal all-around pressure of 250 kPa. After primary consolidation, the drainage valves are turned off, the cell pressure increased by 200 kPa, and a porewater pressure of 200 kPa is measured. The specimen is then sheared by increasing the axial stress. At failure, the increase in axial stress is  $\Delta\sigma_1 = 160$  kPa and the total measured porewater pressure is 344 kPa. For this laboratory consolidated specimen compute: (a) undrained shear strength, (b) friction angle  $\phi'$ , (c) compressive strength if the same specimen had been sheared to failure under the fully drained condition.

Ans. 80 kPa; 25°; 377 kPa.

4. An undisturbed specimen of soft clay is set up in the triaxial apparatus, and under a drained condition is subjected to *in situ* stresses  $\sigma'_{vo} = 40$  kPa and  $\sigma'_{ho} = 24$  kPa. The value of  $\sigma'_p/\sigma'_{vo} = 1.6$  has been obtained from one-dimensional consolidation tests. (a) What factors determine the magnitude of volume change of the specimen on reapplication of the *in situ* stresses? After the specimen comes to equilibrium, the drainage lines are turned off and the cell pressure is increased by 100 kPa; and a porewater pressure of 100 kPa is measured after 1 min and then remains constant as a function of time. (b) What can you say about the degree of saturation of the specimen and system as well as about such factors as membrane and system leakage? Then, the axial stress is increased while keeping the cell pressure constant. An additional axial stress of 24 kPa is required to reach undrained failure at an axial strain of 1% at which the shear-induced porewater pressure is 20 kPa. Compute: (c) coefficient of earth pressure at rest,  $K_o$ , (d) undrained shear strength of this specimen for the triaxial compression mode of shear,  $s_u$  (TC), (e) undrained shear-strength ratio  $s_u$  (TC)/ $\sigma'_p$  for the triaxial compression mode of shear.

Ans. 0.60; 20 kPa; 0.31.

5. An undisturbed soft clay specimen is set up in a triaxial cell and is subjected to an axial stress of 100 kPa and a radial stress of 60 kPa. After the specimen comes to equilibrium under drained conditions, drainage valves are turned off and cell pressure is increased by 200 kPa. A porewater pressure of 200 kPa is observed. Then, under undrained conditions, the axial stress is increased up to an axial strain of 8%. A maximum axial stress of 130 kPa is reached at an axial strain of 1% after which the axial stress decreases and levels off at 110 kPa at axial strain of 8%. The porewater pressures measured by a transducer are 230 kPa and 250 kPa at axial strains of 1% and 8%, respectively. Compute: (a) undrained shear strength  $s_u$  (TC) at maximum axial stress (i.e., at axial strain of 1%), (b) preconsolidation pressure  $\sigma'_p$  of this specimen, (c)  $\phi'$  at axial strain of 8% assuming  $c' = 7$  kPa, and (d) Skempton's A-parameter at axial strains of 1% and 8%.

Ans. 35 kPa; 109 kPa; 33°; 1, 5.

6. A soft clay specimen with  $\sigma'_p/\sigma'_{vo} = 1.4$  and  $\sigma'_{vo} = 50$  kPa is set up in a triaxial apparatus and consolidated under an

equal all-around pressure of 100 kPa. Then the drainage lines are turned off, the cell pressure is increased by 150 kPa, and a porewater pressure of 150 kPa is measured. Axial stress is then increased and the specimen reaches failure at  $\Delta\sigma_1 = 64$  kPa, at which a total porewater pressure of 214 kPa is measured by a transducer. Compute the following: (a) undrained shear strength ( $s_u = (\sigma_1 - \sigma_3)_f/2$ ) to preconsolidation pressure ratio of the soft clay corresponding to the compression mode of shear, (b) unconfined compressive strength of an "A"-quality undisturbed clay specimen from the same depth, (c) speculate on part (b) for a "C"-quality specimen, (d)  $\phi'$  of the soft clay, (e) compressive strength of the soft clay if it is consolidated under equal all-around pressure of 100 kPa and subjected to the drained triaxial compression mode of shear.

Ans. 0.32; 45 kPa; 34 kPa; 28°; 177 kPa.

7. At a particular depth A in a soft clay deposit with  $I_p$  in the range of 40 to 55%, the following have been computed or measured:  $\sigma'_{vo} = 60$  kPa,  $\sigma'_p = 108$  kPa, and  $s_u$  (FV) = 28 kPa. Making necessary assumptions, at a depth B where  $\sigma'_{vo} = 90$  kPa, compute the following: (a)  $s_u$  (UC) for a specimen with SQD of C, (b) a first estimate of  $s_u$  (DSS). If a first-stage embankment construction produces increase in total vertical stress of 85 kPa at depth B, compute: (c)  $s_u$  (FV) immediately after construction of the first stage of embankment, (d)  $s_u$  (FV) after completion of primary consolidation under embankment load. If you had to carry out USSA for the embankment construction, compute (e)  $s_u$  (mob) for the first-stage embankment construction, (f)  $s_u$  (mob) for a second-stage embankment construction after completion of primary consolidation under the first stage.

Ans. 36, 36, 42, 46, 36, 39 kPa.

8. For an inorganic soft clay deposit, *in situ* vane shear testing and one-dimensional consolidation tests have established the following properties:  $s_u$  (FV)/ $\sigma'_p = 0.28$  and  $\sigma'_p/\sigma'_{vo} = 1.7$ . At a particular depth where  $\sigma'_{vo} = 80$  kPa, compute: (a) undrained shear strength by *in situ* vane test. A 2-m-high granular embankment with  $\gamma = 20$  kN/m<sup>3</sup> is constructed at the site (first stage); compute: (b) undrained shear strength to be used (at that particular depth) for stability analysis during first-stage construction, (c)  $s_u$  (FV) after primary consolidation is completed under the weight of first-stage embankment. In a second-stage construction, the embankment height is increased by 2 m (total height of 4 m); compute (d) undrained shear strength to be used for stability analysis during the construction of a third stage, after primary consolidation under the second stage is completed.

Ans. 38, 30, 38, 35 kPa.

9. At a particular depth A in a soft clay deposit, the following properties have been computed or measured:  $\sigma'_{vo} = 65$  kPa,  $\sigma'_p = 100$  kPa, and  $s_u$  (FV) = 30 kPa. Assuming that  $\sigma'_p/\sigma'_{vo}$  is constant for this soft clay deposit, at a depth B where  $\sigma'_{vo} = 90$  kPa, compute: (a)  $s_u$  (FV). A first-stage embankment load produces an increase in total vertical stress of 40 kPa at point B; compute (b)  $s_u$  (FV) immediately after embankment construction, (c)  $s_u$  (FV) 6 months after embankment construction. During a second stage of embankment loading, the height is increased so that the increase in total vertical stress (first stage and second stage together) is 70 kPa; compute (d)  $s_u$  (FV) immediately after construction of second stage of embankment and (e)  $s_u$  (FV) after primary consolidation under the embank-



ment load. If you had to carry out USSA for the embankment construction, compute: (f)  $s_u$  (mob) for first-stage embankment construction, and (g)  $s_u$  (mob) for second-stage embankment construction.

Ans. 42, 42, 42, 42, 48, 30, 30 kPa.

### Selected Reading

- Bjerrum, L. (1972). "Embankments on soft ground," *ASCE Conf. on Performance of Earth and Earth-Supported Structures*, Purdue University, **2**, pp. 1–54.
- Bjerrum, L. (1973). "Problems of soil mechanics and construction on soft clays," *Proc. 8th Int. Conf. on Soil Mech. and Found. Eng.*, **3**, pp. 111–159.
- Larsson, R. (1980). "Undrained shear strength in stability calculation of embankments and foundations on soft clays," *Can. Geotech. J.*, **17**, No. 4, pp. 591–602.
- Trak, B., P. LaRoche, F. Tavenas, S. Leroueil, and M. Roy (1980). "A new approach to the stability analysis of embankments on sensitive clays," *Can. Geotech. J.*, **17**, No. 4, pp. 526–544.
- Tavenas, F. and S. Leroueil (1981). "Creep and failure of slopes in clays," *Can. Geotech. J.*, **18**, No. 1, pp. 106–120.
- Jamiolkowski, M., C. C. Ladd, J. T. Germaine, and R. Lancelotta (1985). "New developments in field and laboratory testing of soils," *Proc. 11th Int. Conf. on Soil Mech. and Found. Eng.*, San Francisco, **1**, pp. 57–153.
- Chandler, R. J. (1988). "The in situ measurement of the undrained shear strength of clays using the field vane," *Proc. Int. Symp. on Vane Shear Strength Testing in Soils: Field and Laboratory Studies*, ASTM STP No. 1014, pp. 13–44.
- Locat, J., and D. Demers (1988). Viscosity, yield stress, remolded strength, and liquidity index relationships for sensitive clays. *Can. Geotech. J.*, **25**, No. 4, pp. 799–806.
- Mesri, G. (1989). "A re-evaluation of  $s_u$  (mob) =  $0.22 \sigma'_p$  using laboratory shear tests," *Can. Geotech. J.*, **26**, No. 1, pp. 162–164.

### 20.8 Undrained Shear Strength of Stiff Fissured Clays

Stiff overconsolidated clays generally are fissured. The spacing of fissures may vary from less than 5 mm near the ground surface to more than 500 mm at 30 m depth. The orientation of the fissures is generally random. Some fissures are curvilinear and have polished and slickensided surfaces. More often they are planar with a matt surface texture.

The presence of fissures has a profound effect on the full-scale field behavior of stiff clays, on their response to *in situ* testing, and on their response to sampling and laboratory testing. To an extent that depends on their frequency, orientation, and nature, fissures reduce the strength of the clay mass below that of the intact material. No shearing resistance is available in open fissures, and the resistance mobilized along closed fissures may be considerably less than that of the intact clay. The stiffer

the intact clay, the greater the relative weakening effect of the fissures.

Stiff clays have a tendency to dilate when they are sheared. In an undrained condition this tendency would be expected to result in a decrease in porewater pressure. However, in stiff clays shear strains and associated pore pressures are very localized. Even for undrained boundary conditions, pore water drains locally into the thin shear zones from adjacent intact materials. For this reason, fully undrained shear strength probably cannot be mobilized in stiff fissured clays except possibly during transient loading. The influence of strain rate on the mobilized undrained shear strength of stiff fissured clays is mainly the result of internal redistribution of pore water and associated softening of shear zones. In laboratory undrained shear tests, for example, the water content in the shear zone increases with increasing time to failure.

For soft clays the difference between  $s_u$  (mob) and  $s_u$  (test) is explained by the effects on the soil microstructure of soil disturbance, mode of shear, progressive failure, and time to failure. The difference between  $s_u$  (mob) and  $s_u$  (test) for stiff clays is related to the effects of these same factors on the soil macrofabric produced by the fissures. Because of the fissures the undrained shear strength of a fissured clay mass may be only one quarter to one half the undrained strength of intact material. Soil disturbance in stiff clays opens and extends fissures in the network and develops new fissures in response to stress relief and distortion. The mode of shear determines the proportion of the fissures involved in the slip surface as well as the magnitude of confining pressure on the fissured mass. For example, in the triaxial compression test, the influence of fissures is significant, because there is appreciable freedom as to the direction in which slip can occur. On the other hand, an *in situ* vane in a fissured clay crust cuts a cylindrical slip surface that passes mainly through intact material. Both progressive failure and an increase in size of the sheared volume relative to the spacing of fissures increase the proportion of fissures to intact material along the slip surface. The rate of shear and time to failure determine the extent of moisture movement to fissures in the shear zone and of local softening. For all these reasons, it is generally reasonable to expect a significant difference between the undrained shear strength mobilized in a stiff fissured clay mass by full-scale excavation or foundation loading, and the undrained shear strength measured by laboratory or *in situ* testing of a small volume of clay.

The most extensive data on mass undrained shear strength or  $s_u$  (mob) of stiff fissured clays have been obtained from plate loading tests made at the bottom of boreholes or from pile loading tests. The value of  $s_u$  (mob) is computed by means of bearing-capacity theory (Article 34) from the measured failure load. An example of  $s_u$  (mob) determined from pile load tests on stiff fissured

Boom clay is shown in Fig. 20.37 (DeBeer et al. 1977). These data show that the mass undrained shear strength mobilized under the base of a pile at 10 m depth decreases with the increase in diameter of the pile.

The laboratory undrained shear strength of stiff fissured clays at the *in situ* water content is usually determined by unconsolidated undrained (UU) triaxial compression tests. Conventional tests are carried out on specimens with diameters in the range of 38 to 100 mm and heights equal to twice the diameter. Confining pressures equal to the *in situ* total overburden pressure are applied. Typical axial compression rates correspond to time to failure of 15 to 30 min.

It is hardly possible to obtain truly undisturbed specimens of stiff fissured clays even when large-diameter tube or block samples are taken. Sampling and specimen preparation involve stress relief which allows fissures to open. The extent of fissure opening and possible moisture redistribution is related to the length of time during which the reduction in confining stresses prevails. Hence, the laboratory undrained shear strength decreases as the elapsed time between sampling and testing increases. However, the most important factor affecting the results of laboratory measurement of the undrained shear strength of stiff fissured clays is the size of the specimen. The undrained shear strength of undisturbed samples decreases with increasing dimensions of the specimens. In the triaxial compression test a slip plane may develop fully along favorably oriented fissures or partly along fissures and partly through intact material. An increase in size of the specimen relative to fissure spacing increases the probability of inclusion of fissures in the slip plane and thus decreases the undrained strength of the specimen.

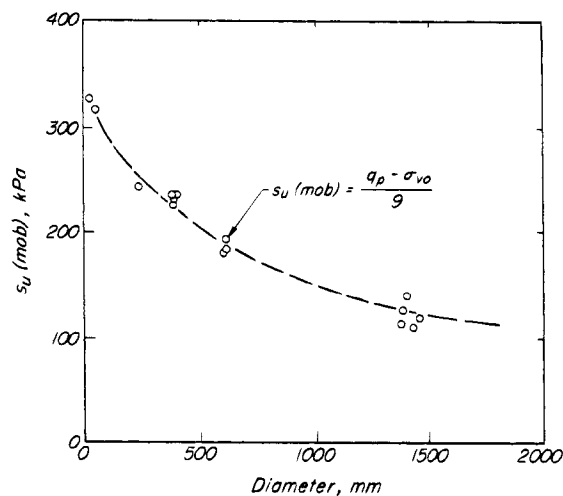


**Figure 20.37** Mobilized undrained shear strength of Boom clay at 10-m depth as a function of diameter of pile (data from De Beer et al. 1977).

Figure 20.38 illustrates the influence of specimen size relative to fissure spacing on the measured undrained shear strength of London clay at Hendon (Marsland 1974). At Hendon, London clay extends to the ground surface. The range in the spacing of fissures increases from 5 to 25 mm at a depth of 5 m to 75 to 325 mm at a depth of 25 m. Undisturbed samples were taken with 98-mm-diameter thin-walled tube samplers. Constant rate of strain UU triaxial compression tests on 38-mm- and 98-mm-diameter specimens reached failure in about 30 min. *In situ* loading tests on 865-mm-diameter plates were made in 900-mm-diameter boreholes at depths of 6.1, 12.2, 18.3, and 24.4 m below ground level (Marsland 1971). The time between drilling the borehole and loading the test plate was kept as short as possible; it varied from 60 to 120 min in accordance with the amount of preparation required. The test surface was carefully prepared before placing a layer of quick-setting plaster onto which the test plate was bedded. The load was applied by a hydraulic jack to give a constant rate of penetration of 2.5 mm/min. The time to failure was about 30 min, roughly corresponding to that for the triaxial tests.

Down to a depth of 9 m the average undrained shear strengths measured on both 38-mm- and 98-mm-diameter samples were in reasonable agreement with those

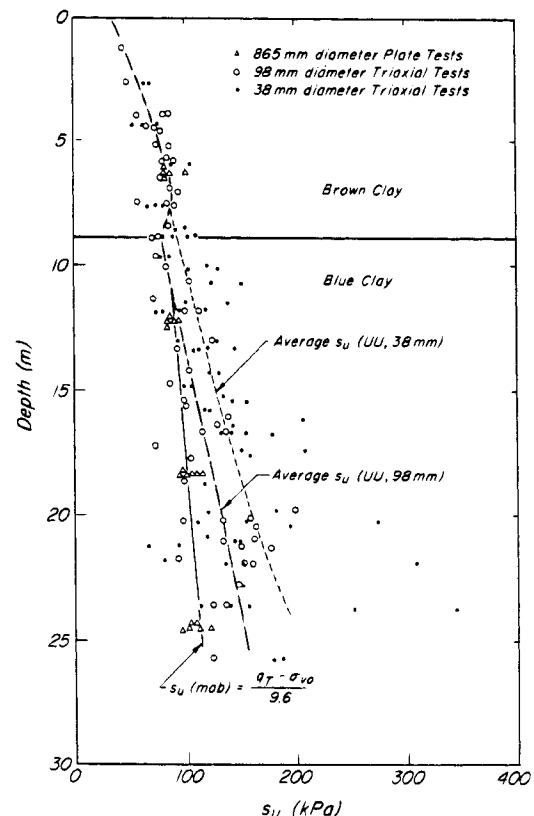


**Figure 20.38** Undrained shear strength of London clay at Hendon (data from Marsland 1974).

obtained from the 865-mm plate load tests. Above this depth the spacing of the fissures was small, and both the 38- and 98-mm-diameter specimens were representative of the fissured clay mass. At a depth of about 12 m the strengths measured on 98-mm-diameter specimens were still in close agreement with the plate load tests, but those measured on 38-mm-diameter specimens were 30% higher. As the spacing of the fissures became greater with depth, the differences between the laboratory and large plate load tests also increased. At a depth of 18 m the undrained shear strengths from 38-mm-diameter specimens were 50% greater, whereas those from 98-mm-diameter specimens were 20% greater than those mobilized by the plate load tests. When the size of the triaxial specimen was equal to or smaller than the fissure spacing, some specimens containing few or no fissures were much stronger than the mass average, whereas others with a single favorably inclined fissure were weaker; hence, the scatter of  $s_u$  (UU) data increased with decreasing specimen size and increasing depth. The increase in scatter with depth is also partly related to the greater opening of fissures due to relief of higher *in situ* stresses.

In general, with decreasing specimen size there is a gradual increase in  $s_u$  (UU) between  $s_u$  (mob) of the clay mass and  $s_u$  (intact). However, the difference between  $s_u$  (UU) and  $s_u$  (mob) begins to become significant only when the height of the specimen is less than the fissure spacing. Therefore, if the laboratory  $s_u$  (UU) is to be used directly to represent  $s_u$  (mob) of a fissured mass, the tested specimens should be large enough to include some fissures.

The difficulties of obtaining representative specimens in stiff fissured clays are great and the scatter of individual  $s_u$  (UU) results using 38-mm-diameter specimens is large and increases with depth. Moreover, sampling of fissured clays and specimen preparation for laboratory testing involve operations that cannot be readily standardized, and there is variable opportunity for soil disturbances. Hence, it may be preferable to use *in situ* penetration tests for estimating undrained shear strength and to specify standard equipment and procedures for the *in situ* tests.

One such *in situ* test is the push cone penetration test (PCPT) (Article 11.4.2). Bearing capacity theory (Article 33.3) indicates that the net bearing capacity ( $q_t - \sigma_{vo}$ ) of an area for constant volume undrained loading is equal to  $N_c \cdot s_u$ , where  $N_c$  is a bearing-capacity factor that depends on the shape and depth of the loaded area, and  $s_u$  is the undrained shear strength. For a deep pile of circular cross-section, for example,  $N_c = 9$ . Under the conditions of the cone penetration test,  $s_u$  is represented by  $s_u$  (cone). In general,  $s_u$  (cone), which is mobilized in a few seconds, is of limited practical value. Thus, the bearing capacity equation is written as

$$q_t - \sigma_{vo} = N_k (\text{test}) \cdot s_u (\text{test})$$

where  $N_k$  (test) is a cone factor that corresponds to  $s_u$  (test) which may be selected to be  $s_u$  (FV),  $s_u$  (UU), or even  $s_u$  (mob). In other words, cone penetration resistance may be calibrated against any useful measurement of undrained shear strength. The most useful data on  $N_k$  values of stiff fissured clays have been obtained from UU tests on 100-mm-diameter specimens. Thus

$$N_k (\text{UU}, 100 \text{ mm}) = \frac{q_t - \sigma_{vo}}{s_u (\text{UU}, 100 \text{ mm})} \quad (20.27)$$

Figure 20.38 has been prepared using data collected by Marsland and co-workers (Marsland and Powell 1979, Marsland and Quarterman 1982, Powell and Quarterman 1988). To appreciate the source of the difference between  $N_c = 9$  (Skempton 1951, Meyerhof 1951) and  $N_k$  (UU, 100 mm) values in the range of 11 to 30 as indicated in Fig. 20.39, the role of fissures and strain rate must be considered. In typical laboratory tests,  $s_u$  (UU) is mobilized in about 1200 s, as compared with 2 s for  $s_u$  (cone). The strain rate or structural creep effect on  $s_u$  of stiff clays, excluding the part associated with local softening, is about a 7% decrease in  $s_u$  for every tenfold increase in the time to failure. Thus the effect introduces a factor of 1.2 into Eq. 20.27 when  $s_u$  (cone) is replaced by  $s_u$  (UU). The major portion of the remaining difference between  $N_k$  (UU, 100 mm) and  $1.2 N_c = 11$  is related to the fissured nature of stiff clays and to local softening during undrained shear. The fissures contribute to the difference between  $s_u$  (cone) and  $s_u$  (UU, 100 mm) as a result of the difference between strength along fissures and through intact materials, and as a result of a strain rate effect associated with local softening. Both effects should increase with the plasticity of the clay. Therefore, the value of  $N_k$  (UU, 100 mm) depends on fissure spacing and plasticity index.

In laboratory triaxial compression tests there is appreciable freedom of direction in which slip can occur. Fissure strength dominates  $s_u$  (UU, 100 mm) until the fissure spacing exceeds 200 to 300 mm. In contrast, the direction of motion of a cone is fixed, and slip planes are forced either to pass through the intact clay or to take longer paths along the fissures. Whichever occurs, the penetration resistance increases rapidly with increasing fissure spacing. For fissure spacings larger than about the diameter of the cone, the cone bearing capacity substantially reflects the intact strength of the clay. The difference between  $s_u$  (cone) and  $s_u$  (UU, 100 mm) and, therefore, the magnitude of  $N_k$  (UU, 100 mm) reaches a maximum at a fissure spacing of about two to four times the diameter of the cone. The fissure and local softening effects are most significant for marine clays of high plasticity for which the difference between fissure strength and intact strength is large. Fissures have less influence on the  $N_k$

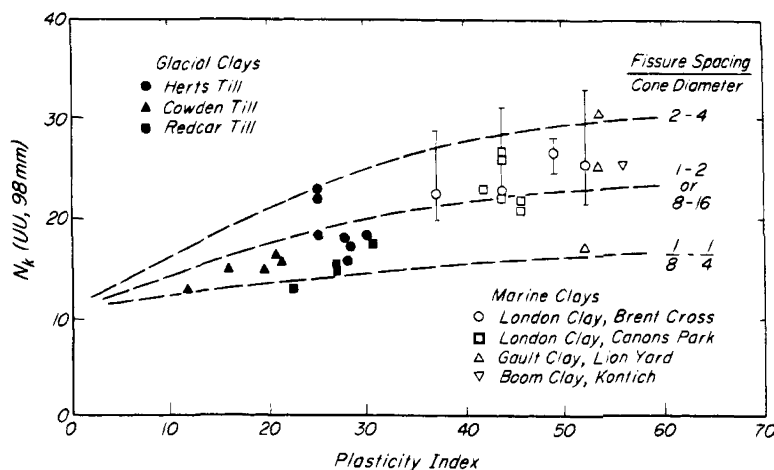


**Figure 20.39** Cone factors for stiff fissured clays as a function of fissure spacing and plasticity index (data from Powell and Quarterman 1988).

( $UU$ , 100 mm) of glacial clays of low plasticity. Moreover, glacial clays are also more likely to be free from fissures and other discontinuities. For fissure spacings less than about one sixth the diameter of the cone, slip occurs mainly along the discontinuities, and the cone-bearing capacity reflects the effect of the fissures. The difference between  $1.2 N_c$  and  $N_k$  ( $UU$ , 100 mm) is then related to local softening and to the sample disturbance effect on  $s_u$  ( $UU$ ).

In summary, for fissure spacings larger than about one sixth the diameter of the standard cone, the *PCPT* tests a relatively small volume of the clay mass in a few seconds. The values of  $N_k$  ( $UU$ , 100 mm) should be larger than  $N_c = 9$ , and generally in the range of 11 to 30. Figure 20.39 can be used together with information on the plasticity index and fissure spacing to estimate  $N_k$  ( $UU$ , 100 mm) for stiff fissured clays. However, for large construction projects, the cone should be calibrated locally by making a limited series of  $s_u$  ( $UU$ , 100 mm) measurements.

Information on  $N_k$  ( $UU$ , 100 mm) is useful because, down to the considerable depth in which fissure spacing does not exceed 200 to 300 mm,  $s_u$  (mob) from large plate load tests is approximately equal to  $s_u$  ( $UU$ , 100 mm). This is illustrated in Fig. 20.40, in which the values of  $N_k$  ( $UU$ , 98 mm) and  $N_k$  (plate, 865 mm) are plotted for the sites in Fig. 20.39. In the London clay below a depth of about 15 m,  $s_u$  ( $UU$ , 100 mm) may have overestimated the mass shear strength  $s_u$  (mob) to some degree, possibly because the increased fissure spacing at depth led to the testing of a disproportionately large number of intact triaxial samples. Although  $s_u$  ( $UU$ , 100 mm) provides a good estimate of  $s_u$  (mob) for plate diameters of about 500 to 600 mm, Fig. 20.40 suggests that, with increasing fissure spacing at depth and for larger plates,  $s_u$  (mob) may be only 70% of  $s_u$  ( $UU$ , 100 mm).

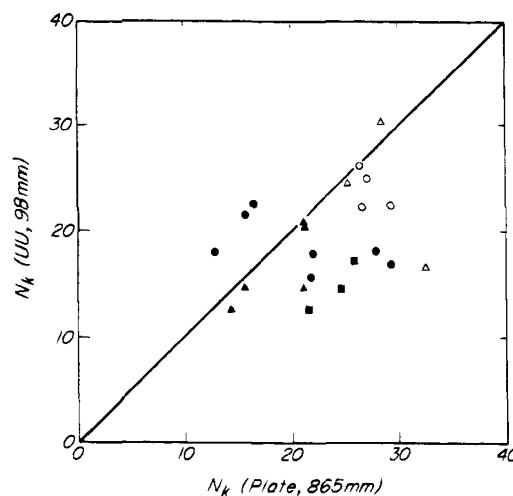


**Figure 20.40** Comparison for stiff fissured London clay of undrained shear strength as determined from 98-mm specimens, and strength mobilized beneath 865-mm bearing plates. Strengths are expressed in terms of cone factor  $N_k$ .

The most comprehensive correlations between undrained shear strength and *DSPT* blow count  $N_{60}$  (Article 11.3.2) have been reported by Stroud (1974) for stiff to hard fissured clays and weak rocks. *DSPT* blow counts were correlated with undrained shear strengths from  $UU$  triaxial compression tests on 102-mm-diameter specimens. At each site, a good correlation between  $s_u$  ( $UU$ , 102 mm) and  $N_{60}$  values was found, with a constant  $s_u$  ( $UU$ , 102 mm)/ $N_{60}$  which was practically independent of depth and independent of fissure spacing up to at least 200 mm. The scatter of  $N_{60}$  values at any one site was generally much less than the scatter of  $s_u$  ( $UU$ , 102 mm), particularly at depth. Apparently, driving a thick-walled sampler 300 mm into the ground tests a large enough volume of material to average the effect of fissures.

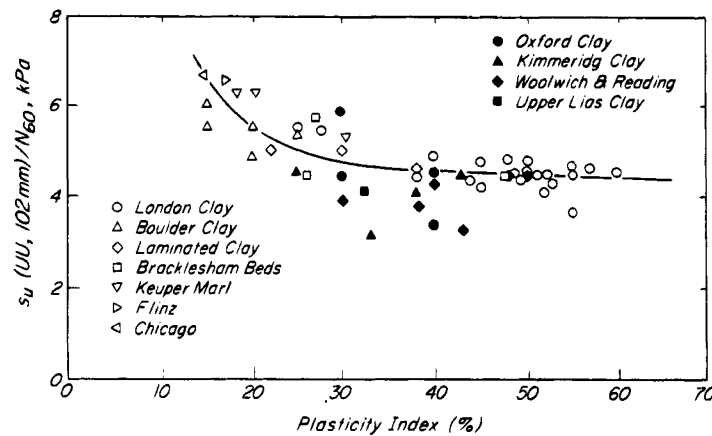


**Figure 20.41** Correlation between plasticity index and ratio of undrained shear strength derived from 102-mm cone penetration tests to standard-penetration test  $N_{60}$  values (data from Stroud 1974).

The values of  $s_u$  (UU, 102 mm)/ $N_{60}$  for a variety of clays and weak rocks, including 31 sites in London clay, are plotted against plasticity index in Fig. 20.41. The quantity  $s_u$  (UU, 102 mm)/ $N_{60}$  decreases with plasticity index, and has typical values in the range of 4 to 6 kPa. It appears that at any one plasticity index the lower values of  $s_u$  (UU, 102 mm)/ $N_{60}$  correspond to harder clays. It is likely that as the intact clay becomes harder the weakening effect of fissures becomes relatively more significant on  $s_u$  (UU, 102 mm) than on  $N_{60}$ . The values of  $s_u$  (UU, 102 mm) computed using the  $N_{60}$  profile together with the corresponding values of  $s_u$  (UU, 102 mm)/ $N_{60}$  are shown in Fig. 20.42 for all the sites in London clay. The mass undrained shear strengths of London clay estimated from over 120 large deep plate loading tests from 13 sites are also plotted in Fig. 20.42. The plate diameters ranged from 195 to 1830 mm, with an average of 575 mm. The average trend of  $s_u$  (UU, 102 mm) with depth as determined from  $N_{60}$  values agrees quite well with the undrained shear strength of the clay mass. Thus, for London clay:

$$s_u(\text{mob}) = 4.4 N_{60} \text{ (kPa)} \quad (20.28)$$

The  $s_u(\text{mob})/N_{60}$  of 4.4 for London clay with a typical plasticity index of 50% may be compared with the ratio 6.7 for Chicago glacial clays, with an average plasticity index of 15%, which is also plotted in Fig. 20.41. Thus, it would appear that the information concerning  $s_u$  (UU, 102 mm)/ $N_{60}$  in Fig. 20.41 can be used, together with  $DSPT$   $N_{60}$  values, to estimate  $s_u(\text{mob})$  for foundation stability analyses involving a wide range of clays.

A useful empirical correlation exists between  $q_c$  values of  $PCPT$  and  $N_{60}$  values of  $DSPT$  for granular soils (Fig. 11.15). A comparatively limited set of data suggests that values of  $q_c/N_{60}$  for stiff fissured clays increase from 75 to 125 kPa as the plasticity index increases from 15 to 65%. However, the most typical value of  $q_c/N_{60}$  for clays

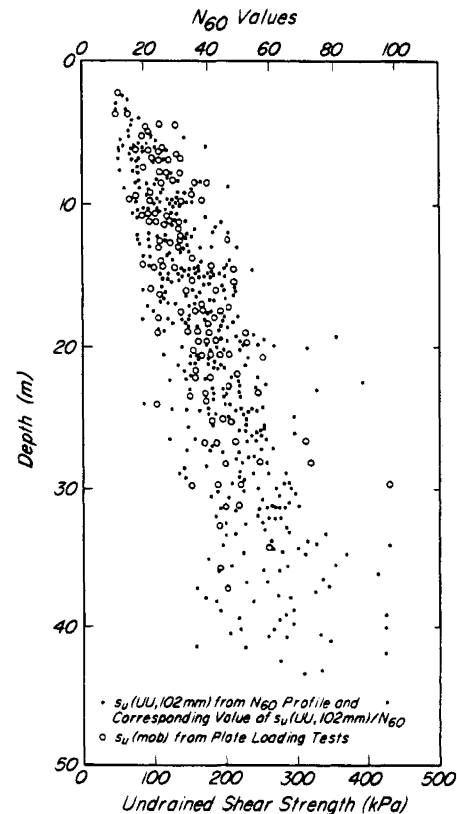


**Figure 20.42** Comparison of undrained shear strengths of London clay from standard penetration tests, calibrated against unconsolidated undrained tests on 100-mm-tube samples, with shear strengths derived from plate loading tests (data from Stroud 1974).

is 100 kPa, which may be compared with the range of 200 to 900 kPa for granular soils. The value of  $q_c/N_{60} = 100$  kPa is quite consistent with the  $N_k$  (UU, 100 mm) and  $s_u$  (UU, 100 mm)/ $N_{60}$  data in Figs. 20.39 and 2.41, respectively. For example, for a clay with  $I_p = 15\%$ ,

$N_k(UU, 100 \text{ mm}) = 15$  and  $s_u(UU, 100 \text{ mm})/N_{60} = 6.5$ . These values result in  $q_c/N_{60} = 98$ . For a clay with  $I_p = 60\%$ ,  $N_k(UU, 100 \text{ mm}) = 25$  and  $s_u(UU, 100 \text{ mm})/N_{60} = 4.4$ . For these values,  $q_c/N_{60} = 110$ . In these comparisons the values of  $N_k(UU, 100 \text{ mm})$  were increased by 10% because  $\sigma_{v0}$  was ignored.

End of construction or maximum loading is the most critical condition for the stability of foundations. The stability of excavations in stiff fissured clays, however, decreases with time as the undrained shear strength decreases toward the fully softened condition. Stress release caused by excavation and associated deformations lead to the opening of fissures and to a decrease in porewater pressure. Stiff clays are strong enough that the fissures remain open at considerable depth (Terzaghi 1936c). A time-dependent process of straining and softening of the clay is initiated by the excavation unloading. Although the factor of safety reaches its minimum value under long-term equilibrium porewater pressure conditions, temporary excavations for basements, trenches, and shafts can fail under undrained conditions if they are made too steep and deep. In the absence of a preexisting continuous plane of shear, the long-term permanent stability of slopes and walls in stiff fissured clays is governed by the fully softened shear strength defined by  $\phi'$  and the steady porewater pressure condition. In temporary works, where stability during construction or shortly thereafter is of interest, it may be evaluated using undrained shear strength.

Straining and softening of stiff fissured clays, involving opening of fissures and increase in water content in the slip zone, is a progressive and time-dependent process. Steep and deep cuts which subject the clay to high shear stress levels strain rapidly to failure soon after excavation, before significant softening, and mobilize high undrained shear strength. Flat slopes strain slowly to failure after significant softening and mobilize lower undrained shear strength. The concept of time-dependent mobilized undrained strength is supported by slope angle, slope height, and time-to-failure data in London clay, compiled by Skempton (1977) and plotted by Leonards (1979) and Tavenas and Leroueil (1981), as in Fig. 20.43. The time-dependent softening process is also confirmed by the increase in  $\bar{r}_u$  with time in cuttings in London clay (Skempton 1977, Chandler 1984). The porewater pressure coefficient  $\bar{r}_u$  is the average value of  $r_u = u/\sigma_v$  around the slipsurface, where  $u$  is total porewater pressure and  $\sigma_v$  is total overburden pressure. Measurements of porewater pressure associated with long-term drained slips in London clay show values of  $\bar{r}_u$  typically within the range of 0.25 to 0.35. The time-dependent softening process in slopes on fissured clays is discussed in Article 51.9. In the laboratory, Saito and Uezawa (1961) and Finn and Shead (1973), using load-controlled triaxial compression tests, determined a relationship between time to failure

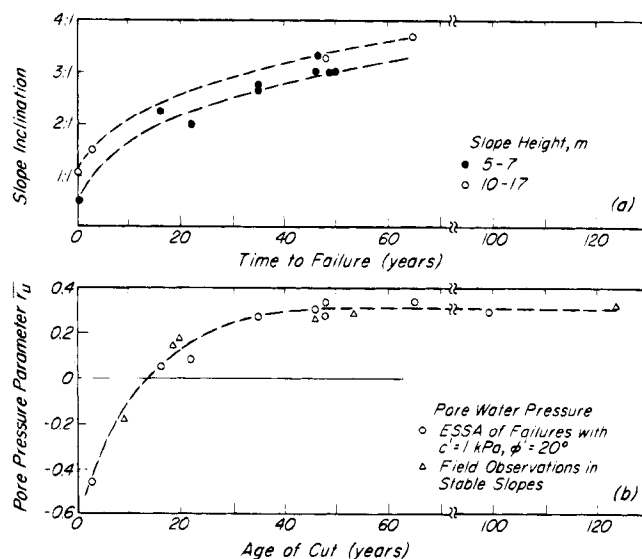


**Figure 20.43** Long-term behavior of cuts in London clay. (a) Relation among inclination of slope, height of slope, and time to failure (Leonards 1979, Tavenas and Leroueil 1981); (b) Relation between porewater pressure parameter  $r_u$  and age of cut (Skempton 1977, Chandler 1988).

and strain rate immediately before acceleration to failure; the relation is independent of consolidation history and drainage conditions and is applicable to a wide variety of clays. Saito (1965) and Tavenas and Leroueil (1981) have shown that the same relationship is applicable to full-scale failures in stiff and soft clays in Japan, England, Belgium, South Africa, Canada, and France. The relationship from the laboratory tests and field data is shown in Fig. 20.44. Stable deformation conditions in slopes correspond to small constant strain rates or strain rates

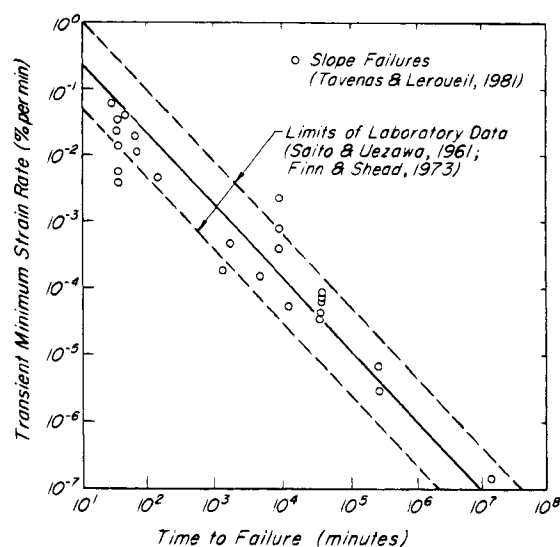


**Figure 20.44** Relation between strain rate and time to failure in clay slopes.

that decrease with time. Laboratory and field observations suggest that once a minimum is reached and strain rate starts to increase, it continues to accelerate and eventually leads to failure. The application of this relation to stability of slopes in stiff clays is discussed in Article 47.9.

### Selected Reading

- Skempton, A. W. and P. LaRochelle (1965). "The Bradwell slip: A short-term failure in London clay," *Géot.*, **15**, No. 3, pp. 221–242.
- Marsland, A. (1971). "Large in situ tests to measure the properties of stiff fissured clay," *Proc. 1st Australian Conf. on Geomech.*, Melbourne, **1**, pp. 180–189.
- Marsland, A. (1974). "Comparisons of the results from static penetration tests and large in situ plate tests in London clay," *Proc. European Symp. on Penetration Testing*, Stockholm.
- Stroud, M. A. (1974). "The standard penetration test in insensitive clays and soft rocks," *Proc. European Symp. on Penetration Testing*, Stockholm, **2.2**, pp. 367–375.
- Leonards, G. A. (1979). "Stability of slopes in soft clay," *6th Pan American Conf. Soil Mech. and Found. Eng.*, Lima.
- Marsland, A. and J. J. M. Powell (1979). "Evaluating the large-scale properties of glacial clays for foundation design," *Proc. 2nd Conf. on Behavior of Offshore Structures*, **1**, pp. 435–464.
- Tavenas, F. and S. Leroueil (1981). "Creep and failure of slopes in clays," *Can. Geotech. J.*, **18**, No. 1, pp. 106–120.
- Marsland, A. and R. S. T. Quarterman (1982). "Factors affecting the measurement and interpretation of quasi static penetration tests on clays," *Proc. European Symp. on Penetration Testing II*, Amsterdam, **2**, pp. 697–702.
- Powell, J. J. M. and R. S. T. Quarterman (1988). "The interpretation of cone penetration tests in clays, with particular reference to rate effects," *Proc. 1st Int. Symp. on Penetration Testing*, Orlando, **2**, pp. 903–909.

## 20.9 Liquefaction of Saturated Loose Sands

### 20.9.1 Introduction

The sudden drop of shear strength under undrained conditions from the yield strength to the substantially smaller critical state strength is known as liquefaction. It may be triggered by the dynamic application of a single large increment of shear stress, as by a sudden toe failure of a slope, or by the repeated application of smaller shear-stress increments and decrements by the ground shaking associated with an earthquake or explosion. The loss in shear strength affects a sizeable part of the mass rather than only the sand along a surface of sliding. The loss of strength is so significant that the sand temporarily assumes the consistency of a heavy liquid. The consequences of liquefaction include flow slides of sloping ground, lateral displacement of retaining structures and bridge abutments, tilting, sinking, and complete failure of foundations, breaking up of the ground, boiling of sand through breaks to the ground surface and basements, and

floating of buried light structures such as storage tanks. The damage is most severe when the liquefied zone is thick and the overlying confining mantle is relatively thin. The possibility of liquefaction is judged by comparing the anticipated dynamic shear stresses with the undrained shear strength of the sand at yield. The stability of a confined liquefied sand is analyzed by comparing the shear stresses to the undrained shear strength of the sand at the critical-state condition (Articles 20.9.3, 20.9.7).

### 20.9.2 Soils Most Susceptible to Liquefaction

Cohesionless soil deposits are susceptible to liquefaction if they are loose enough to be contractive and are of sufficiently low permeability to experience no significant drainage during the period of ground shaking. These characteristics in turn are determined by the size, gradation, shape, surface characteristics, and arrangement of the grains as controlled by the method of deposition, geologic age, and stress history of the deposit.

Clean fine sands and nonplastic silty sands containing less than 5% fines passing the No. 200 sieve are the most susceptible to liquefaction, because they are likely to be deposited in a loose condition and to have a permeability low enough to permit little drainage during the period of ground shaking in zones that are more than about 5 m from a drainage boundary. Coarse sands and gravels are less likely than fine sands to come to equilibrium at very high void ratios, and their much higher permeability enables them to drain rapidly unless they are unusually thick or are bounded by less pervious layers. Nevertheless, liquefaction has developed in gravels in the field (Harder and Seed 1986). The liquefaction potential of sands with a fines content higher than 5% depends on the amount and plasticity of the fines. Plastic fines impede separation of sand grains during shaking and thus provide increased resistance to liquefaction. Deposits of narrowly graded sands are more susceptible to liquefaction than broadly graded ones, because they are more likely to have come to equilibrium in a loose condition such that during shear considerable contraction is required to encounter interference from adjacent grains. Widely graded sands are less susceptible because they are likely to form a more stable structure under natural depositional environments. On the basis of the results of sieve analyses on soils that did or did not liquefy during past earthquakes, Tsuchida (1970) proposed the grain-size distribution boundary curves in Fig. 20.45a. The lower boundary reflects the influence of plastic fines in decreasing the ability of sand to contract during shaking. The zone between the upper boundaries corresponds to coarse soils with coefficients of permeability greater than  $10^{-3}$  to  $10^{-2}$  m/s. Sands most susceptible to liquefaction have coefficients of permeability in the range of  $10^{-5}$  to  $10^{-3}$  m/s.

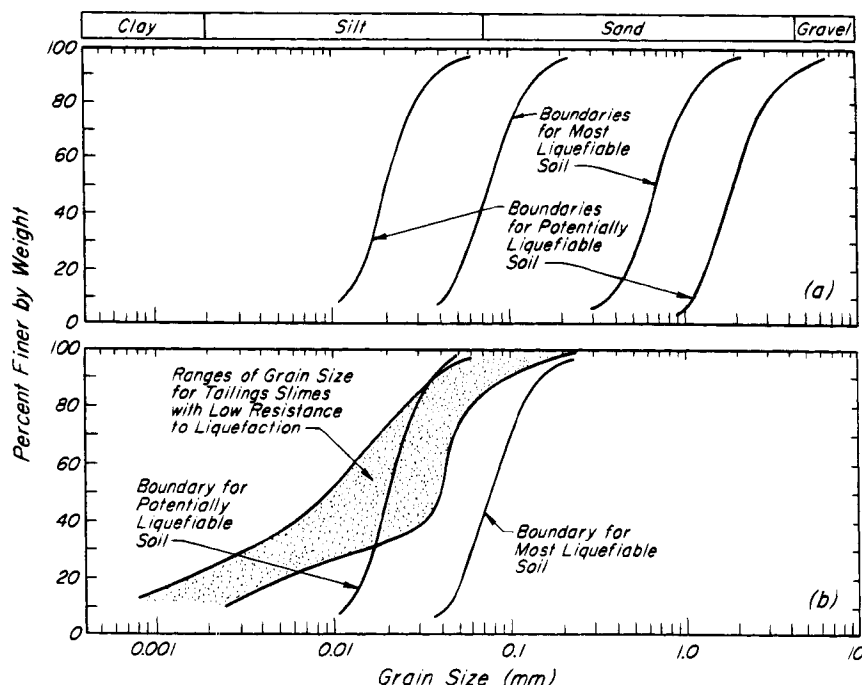


**Figure 20.45** (a) Gradation curves defining limits of liquefiable and nonliquefiable soils (after Tsuchida 1970). (b) Range of grain sizes for tailings dams with low resistance to liquefaction (after Ishihara 1985).

According to Fig. 20.45a, natural soil deposits with  $D_{50}$  less than 0.02 mm or larger than 2.0 mm do not liquefy. On the other hand, mine tailings of crushed rock and other wastes are highly susceptible to liquefaction, even though they contain significant amounts of silt and clay size particles, because these fines are composed of nonplastic solids. Grain size distribution curves for the fine-grained tailings obtained from several disposal ponds and their susceptibility to liquefaction are shown in Fig. 20.45b.

Sand deposits with rounded or subrounded grains are more susceptible than those with angular grains. Contraction in sands with rounded grains results from grain rearrangement, whereas in angular sands it is achieved partly through grain crushing.

Liquefaction is possible for clean sands having a relative density looser than about 40 to 60%; the susceptibility within this range depends on the confining pressure. Among natural deposits, only geologically young post-Pleistocene alluvial deposits, especially those formed within the last several hundred years, contain layers of sand loose enough to be susceptible to liquefaction. Recent hydraulically deposited fills of fine sand and nonplastic silt, fine-grained tailings from mining operations, or chemical wastes are also likely to be very loose. Beach sand deposits are dense enough to resist liquefaction because the grains have been subjected to horizontal movement by the compactive effect of waves. Old sediments are likely to be denser than recent ones, partly

because they may have already been subjected to many severe ground shakings. After the consolidation that follows liquefaction they are more resistant to liquefaction. Aging under drained conditions and preconsolidation substantially contribute to a more stable sand structure and are other reasons why the liquefaction potential of deposits in the field is influenced by their age. According to Finn (1981), fine particles appear to separate the larger sand grains in recent hydraulic fills and young natural deposits. This leads to unstable deposits that may contract under shaking. In older deposits these finer particles tend to have been squeezed out, and there seem to be more substantial contacts between the sand grains.

### 20.9.3 Liquefaction Behavior

Liquefaction refers to the postyield undrained behavior of contractive sands (Casagrande 1936a, 1975). The phenomenon is exemplified by two specimens of Banning sand, a narrowly graded fine quartz sand with subrounded to subangular grains, tested in triaxial compression. Both specimens displayed a tendency to contract up to the undrained yield point (Fig. 20.46), and both developed shear-induced porewater pressure equal to about 52% of the equal all-around consolidation pressure. After yield, however, one behaved like a loose material and the other like a dense one. The "loose" specimen responded to the sustained shear stress in a contractive manner in which the porewater pressure increased and the undrained shear strength substantially decreased. It liquefied, and its resis-



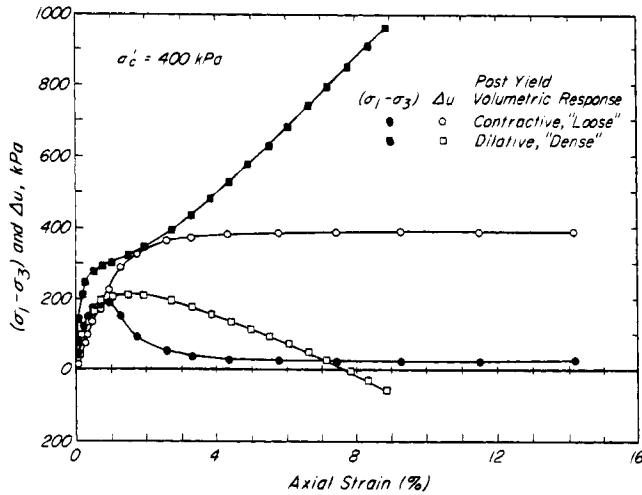


**Figure 20.46** Postyield contractive and dilative responses of samples of Banding sand (data from Castro 1969).

tance to deformation leveled off at a very small undrained shear strength. The sudden and substantial increase in porewater pressure after yield indicates major changes in the arrangement of the sand grains. The “dense” specimen, on the other hand, had a tendency to dilate following yield, and the effective stress and undrained shear strength increased and arrested further deformation.

The shear stress that triggers liquefaction is determined by the *yield strength*, whereas the shear stress that can be sustained by the completely liquefied sand is the *critical strength*. The factors governing the liquefaction of Banding sand were investigated in a series of monotonically and cyclically loaded undrained triaxial tests by Castro (1969). The results of those tests in which liquefaction developed are plotted in Fig. 20.47. The tests were carried out at initial effective confining pressures  $\sigma'_{3c}$  of 30, 100, 400, and 1000 kPa on specimens consolidated to void ratios in the range of 0.672 to 0.778. At the critical condition the friction angle of the sand is fully mobilized. Therefore, it is possible to compute the undrained critical strength from the equation:

$$s_u(\text{critical}) = \sigma'_3(\text{critical}) \frac{\sin \phi'}{1 - \sin \phi'} \quad (20.29)$$

where  $\sigma'_3(\text{critical}) = \sigma'_{3c} - u(\text{critical})$ ,  $\sigma'_{3c}$  is the equal all-around consolidation pressure, and  $u(\text{critical})$  is the shear-induced porewater pressure at the critical condition. For all specimens of Banding sand that displayed post-yield contractive response,  $\phi' = 30^\circ$ . The values of  $s_u(\text{critical})$  computed using Eq. 20.29 and the measured shear-induced porewater pressure at the critical condition are plotted in Fig. 20.47.

Because  $\phi' = 30^\circ$  for Banding sand, according to Eq. 20.29,  $s_u(\text{critical}) = \sigma'_3(\text{critical})$ . Thus, the critical undrained shear strength line *C* in Fig. 20.47 is also the Casagrande critical state line, which defines the boundary

between the “loose” and “dense” conditions of a sand. All combinations of void ratio and consolidation pressure located above the critical state line represent conditions that result in a postyield contractive response. Because the tendency to dilate decreases as the effective confining pressure increases, the greater the consolidation pressure, the denser the sand must be to be safe against liquefaction. All points below the critical state line represent states of the sand which would develop dilative response after yield and would be safe against liquefaction.

The sand with the combination of high void ratio and high consolidation pressure that results in the point at the greatest distance from the critical state line suffers the largest drop in strength and is most susceptible to liquefaction. The ratio  $s_u(\text{yield})/\sigma'_{1c}$  is a constant on the critical state line and on lines parallel to it, as shown in the figure. These lines also represent contours of constant  $e_o - e_c$ , where  $e_o$  is the initial void ratio of the specimen, and  $e_c$  is the critical void ratio at the consolidation pressure  $\sigma'_{1c}$ . The ratio  $s_u(\text{yield})/\sigma'_{1c}$  decreases with the increase in  $e_o - e_c$ . For all monotonically strained specimens of Banding sand that displayed postyield contractive response,  $u(\text{yield})/\sigma'_{1c} = 0.52$ , where  $u(\text{yield})$  is the shear-induced porewater pressure at yield. Therefore, it is possible to compute the friction angle mobilized at yield for contours of constant  $s_u(\text{yield})/\sigma'_{1c}$ . Mobilized friction angles of  $17^\circ$ ,  $20^\circ$ , and  $23^\circ$  correspond to the  $s_u(\text{yield})/\sigma'_{1c}$  contours of 0.20, 0.25, and 0.30, respectively.

Yielding that triggers liquefaction of a sand may be produced by a single monotonic or a repeated cyclic application of shear stress under undrained conditions. Repeated application of shear stresses smaller than the monotonically strained yield strength, but larger than the undrained critical strength, can cause the sand structure to yield and trigger liquefaction. This is illustrated in Fig. 20.48. Figure 20.49 shows that, for a particular mode of shearing, the shear stress required to cause yield in undisturbed specimens of a narrowly graded fine sand with rounded particles decreases as the number of cycles of shear stress increases. The yield strength from cyclic tests on Banding sand, in which the cyclic load oscillated between zero and a compression load, are also plotted in Fig. 20.47. Four to twelve repeated applications of these shear stresses were required to trigger yield and liquefaction. The relation between critical strength and void ratio is independent of the mode of undrained shear, whereas the yield strength is influenced by such factors as full-cycle or half-cycle shearing and reversal of the shear stress.

If an element of sand carried a shear stress during consolidation, the shear stress causing undrained yield is generally larger than the undrained shear strength of a similar element consolidated under an equal all-around pressure. In the former element, the sand structure could adjust to part of the applied shear stress under a drained

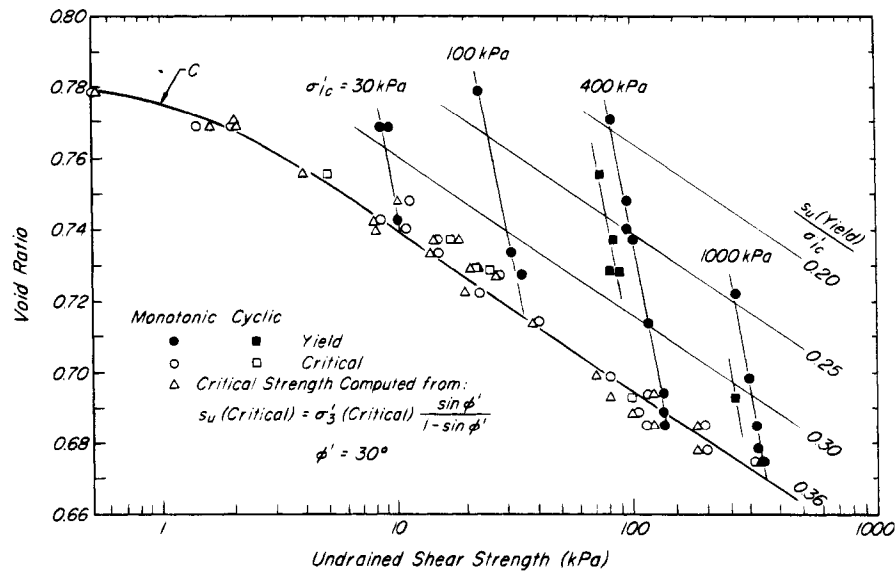


**Figure 20.47** Undrained shear strength of specimens of Banding sand consolidated under equal all-around pressure (data from Castro 1969).

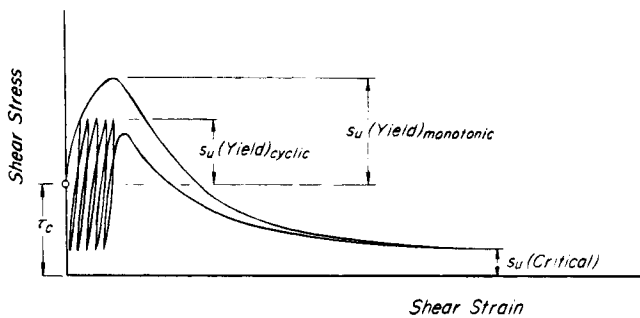


**Figure 20.48** Definition of undrained shear strength at yield and at critical condition.

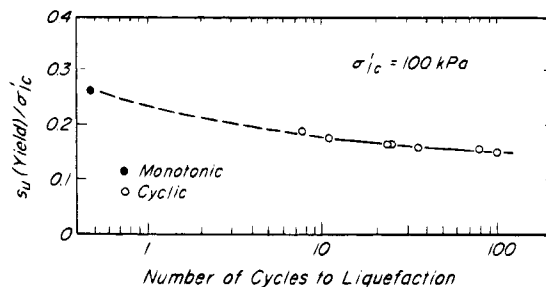


**Figure 20.49** Decrease in shear stress required to cause yield with increase in number of stress cycles (data from Hanzawa et al. 1980).

condition. However, the increment of undrained shear stress required to produce yield in the element already subjected to a substantial consolidation shear stress could be significantly less than the undrained yield strength of a similar element consolidated under a zero shear-stress condition. For one very loose specimen of Banding sand

at a void ratio of 0.725, subjected to a lateral stress of 400 kPa and a maximum shear stress of 51 kPa during consolidation, the shear stress at yield was 120 kPa, but the undrained shear-stress increment to reach yield was 69 kPa. On the other hand, at the same void ratio and equal all-around consolidation pressure of 400 kPa, the undrained shear-stress increment to reach yield was 110 kPa. Thus, an undrained shear-stress increment of 69 kPa triggered liquefaction in an element that already carried a shear stress, as compared with 110 kPa required for yield of an element that started from the zero shear-stress condition. The undrained shear strength at the critical condition, however, is practically independent of the consolidation shear stress, because the critical undrained strength is independent of the original sand structure and the manner in which yield is initiated.

#### 20.9.4 Events Triggering Liquefaction

A dynamic event is characterized by the magnitude of the energy that is released at its source. For example, an earthquake is characterized by its magnitude on the Richter scale. The intensity of ground shaking of a rock formation underlying a liquefaction site is a function of the spatial geometry and orientation of the zone of energy release with respect to the site, the hypocentral distance of the source from the site, and the geologic characteristics of the rocks along the wave transmission path from source to site. Figure 20.50 shows rock accelerations as a function of epicentral distance from the source of energy release for earthquakes of 6.5 to 6.8 Richter magnitude. The local soil stiffness and damping characteristics at the site determine the dynamic soil response to wave motions resulting from shaking in the underlying rock formation.

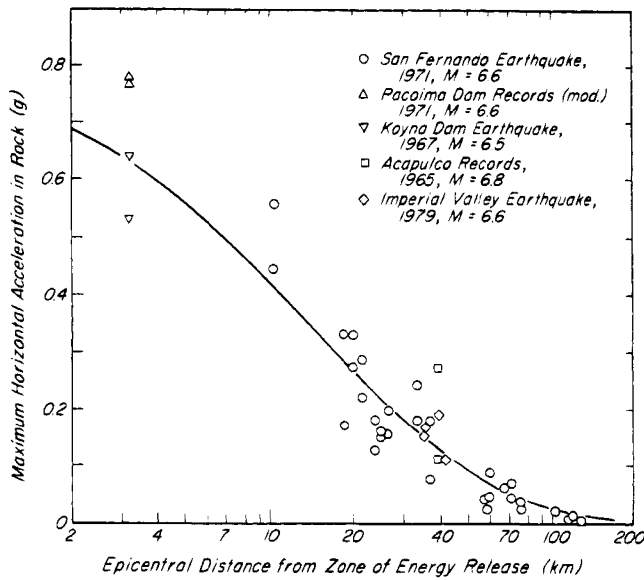


**Figure 20.50** Maximum accelerations in rock produced by earthquakes of Richter magnitude of about 6.6 (data from Seed and Idriss 1982).

During an earthquake, elements of soil are subjected to all forms of wave motions. Generally, the vertical component of rock motion is ignored as it has little effect on the shear stresses that develop in the overlying soil. The most significant deformations and shear stresses induced in elements of soil by an earthquake result from the upward propagation of horizontal shear waves from bedrock. Actual earthquakes generate multidirectional patterns of horizontal motions involving changes in direction. For both level and sloping ground, however, horizontal shear stresses produced by earthquake shaking are usually calculated by one-directional response analysis using the stronger of the recorded motions, usually measured in east-west and north-south directions. One-directional dynamic response evaluation using one-dimensional wave propagation theory provides time histories of seismic horizontal shear stresses at each depth in the soil deposit.

The actual time history of horizontal shear stress at any point in a soil deposit during an earthquake has an irregular form as illustrated by Fig. 20.51, a time-history of horizontal shear stress determined by response analysis for a site in Niigata during the 1964 earthquake of Richter magnitude 7.3 and epicentral distance of 56 km. In laboratory tests, however, it is convenient to use cyclic shear stresses of constant amplitude and frequency. The irregular shear-stress pulses of an actual earthquake are therefore converted to a presumably equivalent significant number  $N_c$  of uniform pulses of shear stress,  $\tau$  (seismic), having an amplitude of 65% of the maximum shear stress in the irregular time history. Seed and Idriss (1971) found, by examining time histories of shear stresses for a number

of earthquakes, that the average equivalent uniform shear stress is about 65% of the maximum shear stress. Both  $\tau$  (seismic) and  $N_c$  can be approximated by visual inspection and appropriate weighing of shear-stress levels in the irregular time history from a response analysis. Undrained simple shear tests using actual time histories of accelerations recorded in recent earthquakes have shown that one-directional regular shaking can be chosen to be equivalent in its effect to multidirectional irregular shaking (Nagase 1985).

Seed and Idriss (1971) developed a simplified procedure for estimating  $\tau$  (seismic) and  $N_c$  for depths less than 15 m in relatively level ground. The soil layer near the ground surface is assumed to move as a rigid body in the horizontal direction. The shear stress induced at a depth  $z$  is equal to the acceleration at the ground surface times the mass of soil lying above that depth:

$$\tau_{\max} = \frac{a_{\max}}{g} \sigma_{vo} \quad (20.30)$$

where  $a_{\max}$  is the maximum ground surface acceleration in gals,  $g$  is the acceleration due to gravity (980 gals), and  $\sigma_{vo}$  is the total overburden pressure at the depth under consideration. Because the soil column in reality moves as a deformable body, the actual shear stress is less than that given by Eq. 20.30:

$$\tau_{\max} = \frac{a_{\max}}{g} \sigma_{vo} r_d \quad (20.31)$$

where  $r_d$  is a reduction factor varying from a value of 1 at the ground surface to a value of 0.9 at a depth of 10 m according to the empirical equation (Iwasaki et al. 1978b)

$$r_d = 1 - 0.01 z \quad (20.32)$$

where  $z$  is the depth in meters. The equivalent uniform seismic shear-stress ratio is

$$\frac{\tau \text{ (seismic)}}{\sigma'_{vo}} = 0.65 \frac{a_{\max}}{g} \frac{\sigma_{vo}}{\sigma'_{vo}} r_d \quad (20.33)$$

in which  $\sigma'_{vo}$  is the effective overburden pressure at the depth under consideration before seismic stresses are applied.

Figure 20.52 shows that the duration of the strong phase of ground shaking is directly related to the magnitude of the earthquake. Therefore, a correlation should exist between the number of significant shear-stress pulses and the earthquake magnitude. Seed and co-workers (e.g., Seed 1979a) collected data on the equivalent number of uniform shear-stress pulses for several earthquakes. These results are shown in Fig. 20.53 and provide a means of selecting  $N_c$  for earthquakes of different magnitude. Typical durations of strong motion earthquakes are 5 to

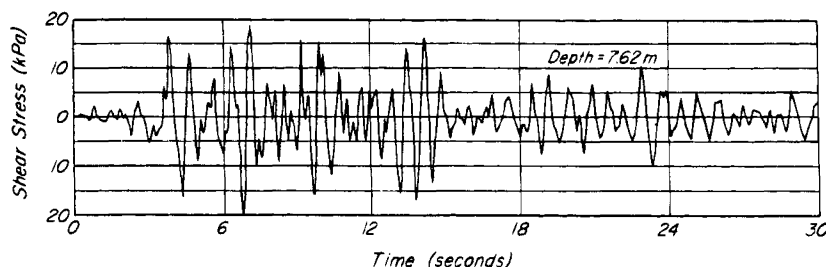


**Figure 20.51** Variation of seismic shear stress with time, as determined by response analysis (after Seed and Idriss 1967).

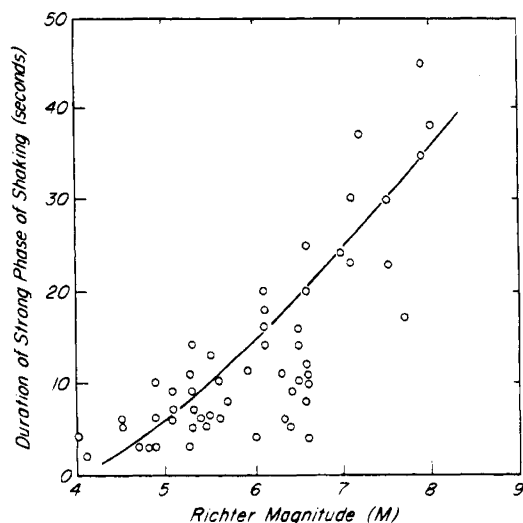


**Figure 20.52** Duration of strong phase of shaking as a function of earthquake magnitude (data after Donovan 1972).

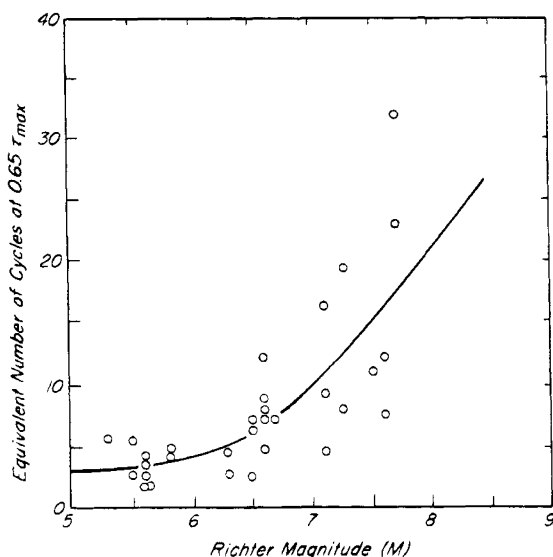


**Figure 20.53** Equivalent number of shear-stress cycles at  $0.65 \tau_{\max}$ , based on strongest component of ground motion (data after Seed 1979a).

40 s during which there are 5 to 30 significant shear-stress cycles.

### 20.9.5 Cyclic Yield Strength from Laboratory Tests

Soil elements in a sand deposit with a level ground surface are subjected to the sequence of stress conditions shown in Fig. 20.54. Before the earthquake, horizontal and vertical planes are subjected to  $\sigma'_{vo}$  and  $K_o \sigma'_{vo}$ , respectively, where  $K_o$  is the coefficient of earth pressure at rest. No shear stresses exist on these planes. During the earthquake, while total vertical stress remains constant, the horizontal and vertical planes are subjected to the seismic shear stress,  $\tau$  (seismic), which reverses direction several times during the ground shaking. Figure 20.54 closely represents the stress and deformation conditions on soil elements subjected to one component of earthquake motion under the free field or directly below structures and embankments. Direct simple shear apparatus (Article 17.3.3) allows a close simulation in the laboratory of these stress and deformation conditions. A laterally constrained saturated sand specimen is consolidated under an effective vertical stress  $\sigma'_{vc}$  and then a fully-reversing horizontal shear stress,  $s_u$  (yield, DSS), is applied under undrained conditions and cycled  $N_c$  times until the specimen liquefies. The results of such a test are expressed in terms of the ratio of cyclic yield strength to vertical consolidation pressure,  $s_u$  (yield, DSS)/ $\sigma'_{vc}$ , and the results of a series of tests are indicated by a plot of  $s_u$  (yield, DSS)/ $\sigma'_{vc}$  against  $N_c$ . In an ideal DSS test an undisturbed saturated specimen is consolidated under the *in situ* effective overburden pressure,  $\sigma'_{vo}$ , to preserve the natural sand structure, before it is subjected to undrained cyclic shear. A sinusoidal or pulsating pattern of shear stress is applied with a constant frequency, typically in the range of 0.5

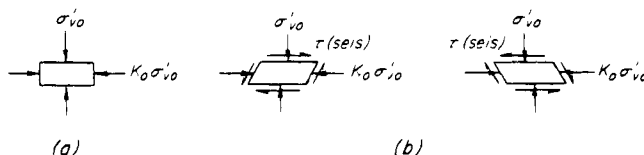


**Figure 20.54** Stress conditions under level ground (a) before and (b) during earthquake.

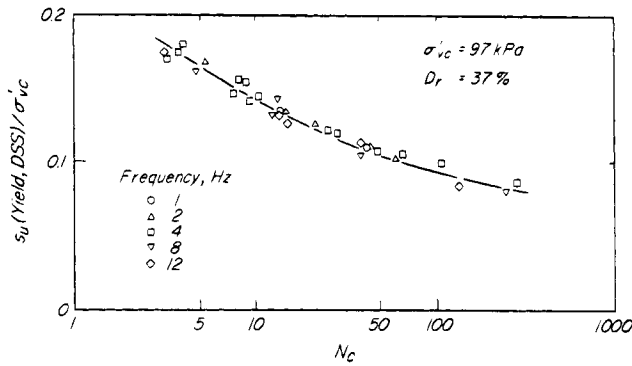


**Figure 20.55** Cyclic direct simple shear tests on Bandaijima sand (data after Yoshimi and Oh-Oka 1975).

to 5 Hz for strong motion earthquakes. Laboratory cyclic shear test results such as those in Fig. 20.55 show that  $s_u(\text{yield})/\sigma'_{vc}$  is nearly independent of the frequency of the cyclic shear stress in the range of 0.05 to 10 Hz. Torsion shear apparatus was used to obtain the data in Fig. 20.55 on reconstituted specimens of Bandaijima sand from Niigata (Yoshimi and Oh-Oka 1975).

A standard direct simple shear test simulates the effect of cyclic straining in one direction only, whereas multidirectional horizontal shaking occurs during actual earthquakes. The effect of multidirectional shaking on the relation between  $s_u(\text{yield})/\sigma'_{vc}$  and  $N_c$  of a sand has been investigated by two-directional and rotational direct simple shear tests with the results shown in Fig. 20.56 for Fuji River sand with subangular grains, a mean grain size of 0.40 mm, a uniformity coefficient of 3.2, and minimum and maximum void ratios of 0.481 and 1.032, respectively. The results indicate lower cyclic  $s_u(\text{yield})$  strength

under multidirectional shaking than under one-directional shaking. That is, multidirectional shaking requires a smaller seismic shear stress than one-directional shaking to produce yielding of the sand structure and to trigger liquefaction.

In reality, the direct simple shear test is by no means simple, and reliable equipment is not readily available. Serious problems are frequently encountered with DSS testing of loose sands. The stress distribution within the specimen is not uniform, and it is difficult to prevent slippage along the top and bottom loading plates. Therefore, undrained cyclic shear tests on saturated sand are most often performed using triaxial shear apparatus, which is widely available. A cylindrical saturated sand specimen is consolidated under an equal all-around pressure,  $\sigma'_{1c}$ . Then, while the lateral stress is kept constant, axial stresses of equal magnitude in compression and extension are applied under undrained conditions  $N_c$  times until the specimen liquefies. The test results are presented in terms of  $s_u(\text{yield}, T)/\sigma'_{1c}$ , where  $s_u(\text{yield}, T) = (\sigma_1 - \sigma_3)_{\text{cyclic}}/2$ . The most serious shortcoming of the undrained cyclic shear test in the triaxial apparatus as compared with direct simple shear is that the condition of equal all-around pressure is different from the *in situ* stress condition and leads to a disturbance of the natural sand structure. To minimize such effects of disturbance,  $\sigma'_{1c}$  values near  $\sigma'_{v0}$  should be used. Undrained cyclic shear tests on Monterey No. 0 sand carried out in triaxial and direct simple shear apparatus are compared in Fig. 20.57. This is a clean uniform sand from Monterey, California, with rounded to subrounded particles mainly of quartz and feldspar. It has a mean grain diameter of 0.36 mm, a coefficient of uniformity of 1.5, and minimum

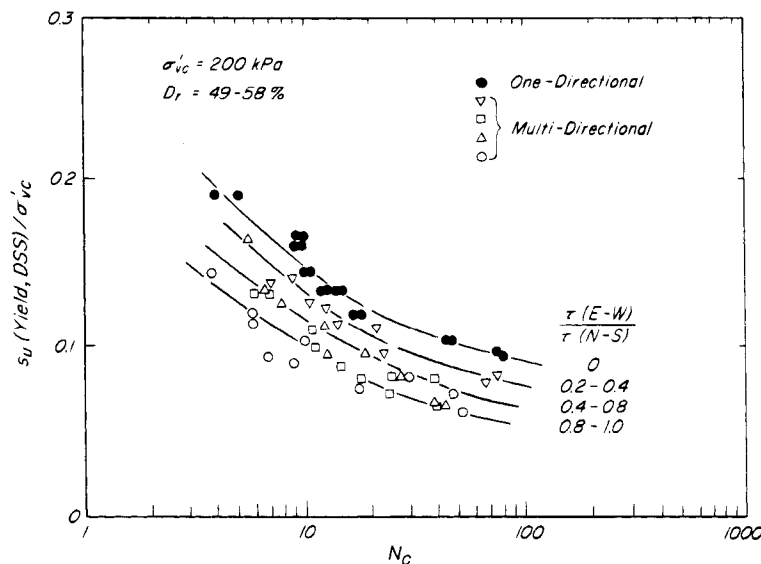


**Figure 20.56** Multidirectional direct simple shear tests on Fuji River sand (data after Ishihara and Yamazaki 1980).

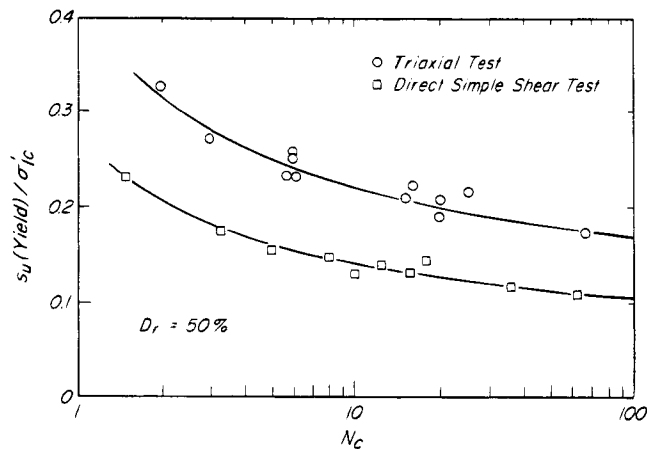


**Figure 20.57** Results of cyclic shear tests on Monterey No. 0 sand (data after De Alba et al. 1975).

and maximum void ratio of 0.53 and 0.85, respectively. Reconstituted normally consolidated saturated specimens were used. According to the behavior of this sand, supported by similar comparisons on other sands:

$$\frac{s_u(\text{yield, DSS})}{\sigma'_{vc}} = 0.64 \frac{s_u(\text{yield, T})}{\sigma'_{lc}} \quad (20.34)$$

As would be expected, the undrained shear strength of a loose sand is a function of the mode of shear. For one very loose sand from the Persian Gulf, a series of consolidated, monotonically sheared undrained tests on undisturbed specimens resulted in  $s_u(TC)/\sigma'_{vo} = 0.33$ ,  $s_u(IC)/\sigma'_{vo} = 0.26$ ,  $s_u(DSS)/\sigma'_{vo} = 0.21$ , and  $s_u(TE)/\sigma'_{vo} = 0.08$  (Hanzawa 1980). On the basis of data such as those in Fig. 20.57, a reduction factor of 0.64 is applied to values of  $s_u(\text{yield, T})/\sigma'_{lc}$  before they are used in liquefaction analysis of seismic shaking conditions similar to those represented in Fig. 20.54.

In the laboratory, the yield strength of a natural sand can be reliably determined only by using undisturbed specimens in which the structure of the natural deposit remains intact. Techniques such as tube sampling, block

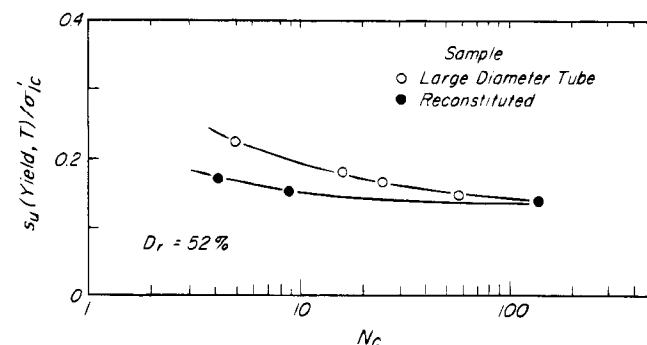


**Figure 20.58** Cyclic yield strength of Niigata sand (data from Ishihara 1985).

sampling, and *in situ* freezing and coring are available. However, it is practically impossible to recover completely undisturbed samples of loose clean sand deposits. A representative specimen for an undrained cyclic shear test should be not only undisturbed but also subjected to the same effective stress as it carried in the field before sampling. Application of the *in situ* effective stresses to a natural specimen of loose sand results in a decrease in void ratio, of a magnitude that depends on the degree of sample disturbance. However, with the possible exception of very young normally consolidated sands, this increase in density may not compensate for the loss of interparticle resistance, because rough particle surface interlocks are disengaged by particle movements during sampling.

Cyclic yield strengths of Niigata sand specimens cut from large-diameter tube samples are compared in Fig. 20.58 with those of specimens reconstituted to the *in situ* density by pluviation under water. The sand has a mean grain size of 0.30 mm and a uniformity coefficient of 2.6. The deposit consists of clean sand dumped into the river between 1945 to 1955. The difference in cyclic yield strengths of undisturbed and reconstituted specimens at the same void ratio is more pronounced when the number of cycles required for liquefaction is small. The difference decreases with the increase in  $N_c$ , because cyclic loading also disturbs the natural soil structure. Data such as those in Figs. 20.58 and 20.59 illustrate the effect of sample disturbance on cyclic yield strength. Because some disturbance of the natural sand structure is likely even with the best sampling techniques, it is not possible to know the cyclic yield strength of a truly undisturbed element in the field. Moreover, the increase in the cyclic resistance associated with the increase in density on reapplication of the field effective stress condition is unlikely to compensate fully for the reduction in yield strength resulting from the disturbance of the natural sand structure.

The structure of a natural sand deposit is conditioned not only by the process of deposition, but also by aging, preconsolidation, and preshearing. Drained aging, preconsolidation, and preshearing that does not lead to liquefaction followed by reconsolidation, all prestrain the structure of sand, increase its yield strength, and thus increase its resistance to liquefaction. It is well known that young alluvial sands are much more susceptible to liquefaction than older sediments. During the earthquake of 1964, alluvial sands and hydraulic fills placed in Niigata after the late 19th century all liquefied, whereas much older deposits did not.

For natural soft clay and silt deposits,  $s_{uo}/\sigma'_p$  is a more meaningful indicator of undrained shear strength than  $s_{uo}/\sigma'_{vo}$  or  $s_u/\sigma'_{vc}$ , because the undrained shear strength of soft clays and silts is determined mainly by the preconsolidation pressure. The undrained yield strength of sands is also strongly influenced by their preconsolidation pressure. Unfortunately, however, in contrast to clays and

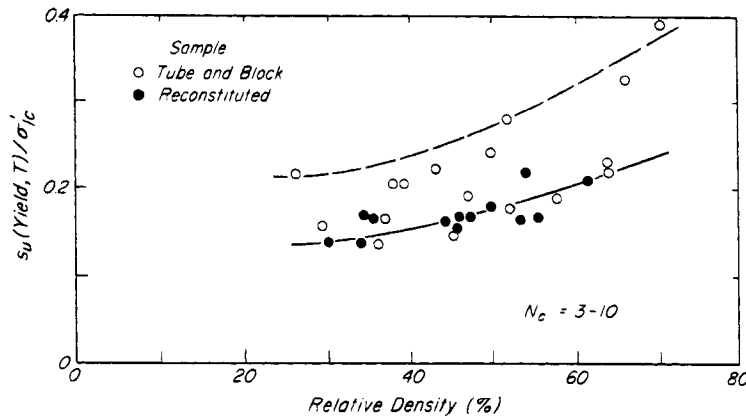


**Figure 20.59** Effect of sample disturbance on cyclic yield strength of Niigata sand (data from Ishihara 1985).

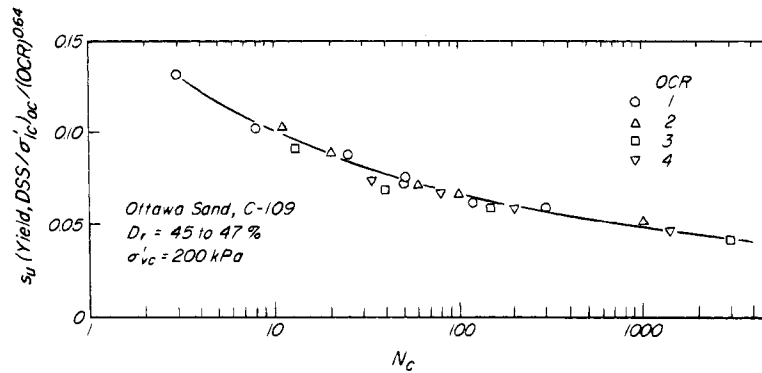


**Figure 20.60** Effect of overconsolidation on cyclic yield strength of Ottawa sand (data from Finn 1981).

silts, for which  $\sigma'_p$  can be determined by oedometer tests on undisturbed specimens, it is not possible to determine the preconsolidation pressure of clean sands readily. Therefore, yield strengths of sands usually have been measured and reported in terms of  $s_u$  (yield) /  $\sigma'_{vc}$ . For a fundamental interpretation of the undrained shear strength of a natural sand deposit,  $s_u$  (yield) /  $\sigma'_{vc}$  is even less meaningful than  $s_{uo}$  (yield) /  $\sigma'_{vo}$ . The results of a series of cyclic undrained direct simple shear tests on reconstituted specimens of Ottawa sand C-109 are shown in Fig. 20.60. This quartz sand consisting of rounded particles has a mean grain size of 0.40 mm, a uniformity coefficient of 1.5, and minimum and maximum void ratios of 0.50 and 0.85, respectively. The data can be expressed as follows:

$$\left[ \frac{s_u \text{ (yield, DSS)}}{\sigma'_{vc}} \right]_{OC} = \left[ \frac{s_u \text{ (yield, DSS)}}{\sigma'_{vc}} \right]_{NC} (\text{OCR})^{0.64} \quad (20.35)$$

where  $s_u$  (yield, DSS)<sub>OC</sub> and  $s_u$  (yield, DSS)<sub>NC</sub> are the cyclic yield strengths of overconsolidated and normally consolidated sand, respectively, both defined at the same  $N_c$ . These data show that overconsolidation can signifi-

cantly increase the undrained yield strength of a clean sand deposit. Furthermore, for preconsolidated natural sand deposits, the magnitude of  $s_u$  (yield, DSS) /  $\sigma'_{vc}$  or  $s_u$  (yield, T) /  $\sigma'_{lc}$  would also be expected to depend on the magnitude of  $\sigma'_{vc}$  or  $\sigma'_{lc}$  that is used to measure  $s_u$  (yield). Overconsolidation of a sand, which generally involves a minor increase in relative density, produces more efficient particle interlocking and particle surface interference, leading to a significant reduction in the tendency of sand to contract during shear. Cyclic yield strength data on four other overconsolidated sands, in addition to those in Fig. 20.60, indicate values of the exponent in Eq. 20.35 in the range of 0.35 to 0.64.

Aging of clean sands under constant external conditions results mainly from secondary compression. The increase in resistance to contraction is caused by slight movement of grains into more stable positions and improved engaging of surface roughnesses at grain contacts. The aging effect on undrained yield strength is illustrated in Figs. 20.61 and 20.62 by cyclic test results on undisturbed specimens of the hydraulic fine to coarse silt and sand fills in Upper and Lower San Fernando

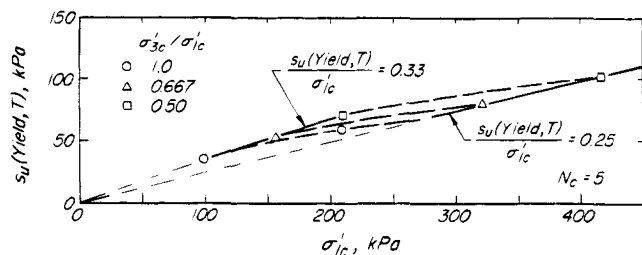


**Figure 20.61** Cyclic undrained yield strength at Upper San Fernando hydraulic fill (data from Seed et al. 1973).

dams. During the Richter magnitude 6.6 earthquake of 1971, which produced 15 s of strong shaking at the dam sites with a peak acceleration of 0.6 g in the bedrock, the Upper San Fernando dam strained but did not fail. The upstream part of the Lower San Fernando dam, however, failed and spread 75 m into the reservoir. The failure was triggered by liquefaction of the hydraulic sand fill near the base of the embankment. At the time of the San Fernando earthquake, the hydraulic sand fills were about 55 years old. Undrained cyclic triaxial shear tests were carried out on undisturbed saturated specimens 7.1 cm in diameter and 17.8 cm in height. San Fernando hydraulic sand fills are fine to coarse silty sands with mean grain size of 0.05 to 1.0 mm, uniformity coefficient of 7 to 10, and relative density of 50 to 54%. Before the undisturbed specimens were subjected to undrained cyclic axial loading they were consolidated under magnitudes of  $\sigma'_{3c}/\sigma'_{1c}$  believed to exist in the dam before the earthquake shaking. Figure 20.61 shows that the specimens that were consolidated in the low range of  $\sigma'_{1c}$  displayed a higher value of  $s_u(\text{yield}, T)/\sigma'_{1c}$  than those that were consolidated under higher axial stresses. The aging effect that produced the  $s_u(\text{yield}, T)/\sigma'_{1c} = 0.33$  at the low-consolidation

pressure range was destroyed by high consolidation pressures that led to a  $s_u(\text{yield}, T)/\sigma'_{1c} = 0.25$ . A similar consolidation pressure effect is shown in Fig. 20.62 wherein  $s_u(\text{yield}, T)/\sigma'_{1c}$  is plotted against  $N_c$  data for the hydraulic fill of the Lower San Fernando dam. The magnitudes of  $s_u(\text{yield}, T)/\sigma'_{1c}$  in the  $\sigma'_{1c}$  range of 100 to 210 kPa are significantly higher than those in the range of 315 to 420 kPa. However, the difference tends to decrease with increasing number of cycles to liquefaction, because cyclic loading also disturbs the aged sand structure.

Whereas for normally consolidated young clays,  $s_u(\text{yield})/\sigma'_c$  is practically independent of the consolidation pressure  $\sigma'_c$ ,  $s_u(\text{yield})/\sigma'_c$  of normally consolidated young sands may depend on the consolidation pressure. An increase in consolidation pressure may enhance contractive behavior and thus decrease  $s_u(\text{yield})/\sigma'_c$ . This effect is illustrated in Fig. 20.63 for the Banning sand data in Fig. 20.47 and a compression  $e$  vs  $\log \sigma'_c$  curve starting from zero relative density at  $\sigma'_c = 1$  kPa. The decrease in  $s_u(\text{yield})/\sigma'_{1c}$  with  $\sigma'_{1c}$  is shown in reference to  $s_u(\text{yield})/\sigma'_{1c}$  at  $\sigma'_{1c} = 100$  kPa. The data show that the effect of the consolidation pressure on  $s_u(\text{yield})/\sigma'_c$  of normally consolidated young Banning sand is relatively small. Moreover, there are indications that for other sands of certain grain shape and gradation, in the relative density range at which liquefaction is possible and in the practical range of values of consolidation pressure, the consolidation pressure effect on  $s_u(\text{yield})/\sigma'_{1c}$  of normally consolidated young sand is negligible. In contrast, values of  $s_u(\text{yield}, T)/\sigma'_{1c}$  for the San Fernando hydraulic fills are also shown in Fig. 20.63. For this case, a major part of the  $\sigma'_{1c}$  effect on  $s_u(\text{yield}, T)/\sigma'_{1c}$  is related to aging of the hydraulic fill. The data in Figs. 20.61 to 20.63

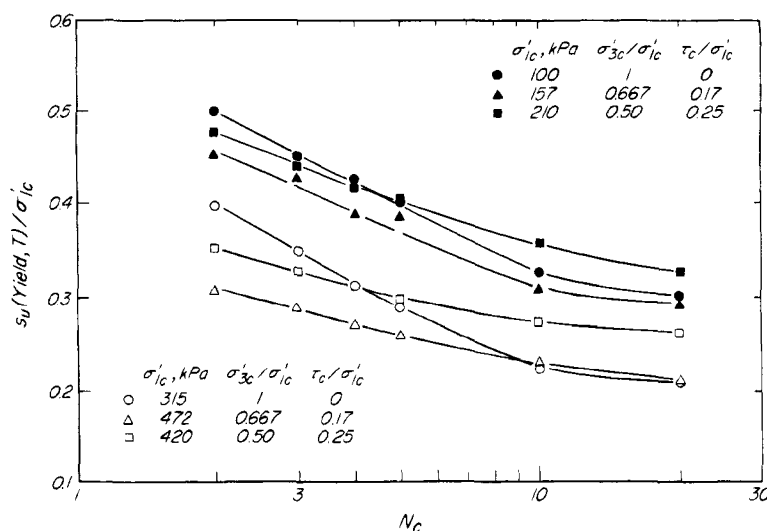


**Figure 20.62** Cyclic undrained yield strength of Lower San Fernando hydraulic fill (data from Seed et al. 1973).



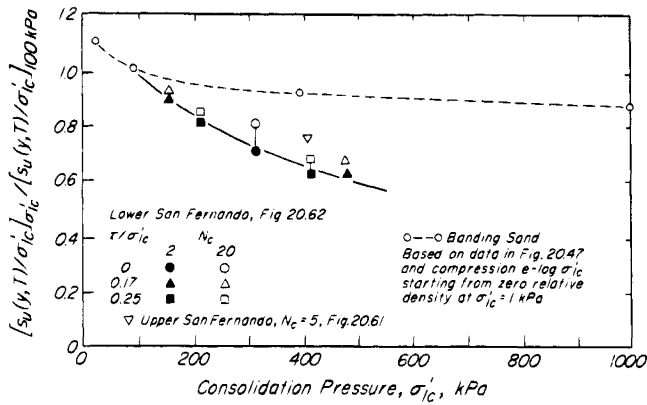


**Figure 20.63** Effect of consolidation pressure on  $s_u$  (yield)/ $\sigma'_{vc}$  of normally consolidated young Banding sand; effect of consolidation pressure and aging on  $s_u$  (yield)/ $\sigma'_{vc}$  of San Fernando hydraulic fill (data from Castro 1969, Seed et al. 1973).

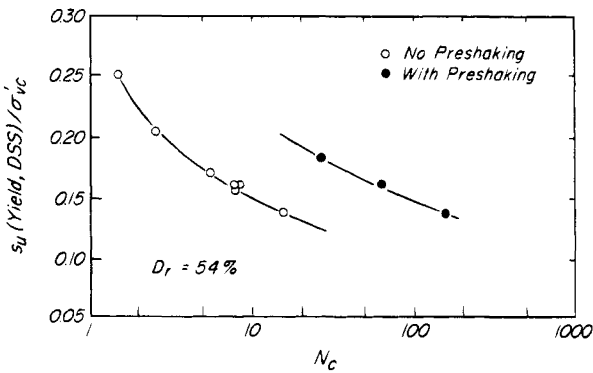


**Figure 20.64** Effect of preshaking and reconsolidation on cyclic yield strength of Monterey No. 0 sand (data from Seed et al. 1977).

confirm that for natural sand deposits that are overconsolidated or aged,  $s_u$  (yield,  $T$ )/ $\sigma'_{vc}$  should depend on the magnitude of  $\sigma'_{vc}$  that is used to consolidate the undisturbed specimens. Consolidation of an undisturbed specimen of a natural sand deposit beyond the *in situ* condition may result in substantially reduced resistance to liquefaction. Undrained cyclic yield strength data for a limited number of sands reconstituted and subjected to drained aging in the laboratory, as well as a comparison of  $s_u$  (yield) values of undisturbed and freshly reconstituted specimens of aged sand deposit (Harder 1988), suggest that  $s_u$  (yield)/ $\sigma'_{vc}$  may increase 5 to 10% for each tenfold increase in age of the deposit.

Undrained preshearing followed by reconsolidation has been shown to have a significant effect on the subsequent cyclic undrained behavior of sand specimens (Vaid et al. 1989). Preshaking of loose sands by earthquakes of small to moderate magnitude should lead to a small increase in density and a substantial increase in yield strength. Small cyclic preshearing ( $\tau_s/\sigma'_{vc}$ ,  $N_c$ ) that does not trigger yielding of the sand structure and contractive deformation

causes slight movement at particle contacts and produces better interlocking among the grains and increased resistance to subsequent cyclic loading. Large cyclic preshearing, which stretches and yields the sand structure, leads to particle rearrangement and disengages grain surface interlocks, even after reconsolidation may significantly decrease subsequent resistance to liquefaction.

Seed et al. (1977) used large-scale shaking table tests, simulating the DSS mode of shear, to study the preshearing effect on the cyclic yield strength of reconstituted Monterey 0 sand. The sand specimen, deposited at a relative density of 54.0%, was subjected to  $\tau_s/\sigma'_{vc} = 0.185$  five times, which corresponds to  $N_c = 2 \frac{1}{2}$  cycles. After each small shock, the sand was allowed to reconsolidate under the initial effective vertical stress,  $\sigma'_{vc}$ . At the conclusion of preshearing the relative density of the sand had increased to 54.7%. The specimen was then subjected to a large shock to determine  $s_u$  (yield) required to cause it to liquefy. The  $s_u$  (yield)/ $\sigma'_{vc}$  of specimens having no previous seismic shaking and those specimens subjected to low levels of seismic shocks are compared in Fig. 20.64. The cyclic undrained behavior after preshearing is directly related to the magnitude of prestrain accumulated at the end of preshearing that did not produce liquefaction. For Ottawa C-109 sand at a relative density of 36% and subjected to  $\sigma'_{vc} = 250$  kPa and  $\sigma'_{3c}/\sigma'_{vc} = 0.80$ , the number of cycles of  $s_u$  (yield,  $T$ )/ $\sigma'_{vc} = 0.125$  to trigger liquefaction increased from 14 for a sand with no preshearing, to 38 for a preaxial strain of 0.1%, and to 125 for a preaxial strain of 0.2% (Vaid et al. 1989).

Cyclic direct simple shear tests starting from the ( $\sigma'_{vc}$ ,  $K_o \sigma'_{vc}$ ) stress condition, and cyclic axial loading tests in the triaxial apparatus starting from equal all-around pressure  $\sigma'_{vc}$ , simulate preshaking ground conditions where there are no permanent shear stresses on the horizontal planes. For sand elements located beneath the edge of an embankment or structure, or within sloping ground, significant permanent shear stresses exist on horizontal planes. Thus, before application under undrained conditions of seismic shear stress,  $\tau$  (seismic), the sand element is already carrying a shear stress,  $\tau_c$ , under drained conditions. For a given void ratio, the decrease in strength from yield to critical state increases with increasing initial shear stress acting on the sand. The initial shear stress may also influence the magnitude of cyclic  $s_u$  (yield) that is required to trigger liquefaction. In fact, for very loose sands the initial shear stress moves the element close to the yield condition and, as  $\tau_c$  increases, a smaller cyclic  $s_u$  (yield) is required to trigger liquefaction. Cyclic torsion shear test results, Fig. 20.65, illustrate the effect of  $\tau_c/\sigma'_{vc}$  on the liquefaction resistance of a very loose Bandajima sand.

For dense sands, initial shear stress has a beneficial effect, because  $\tau_c$  increases dilatant tendency and therefore yield strength. The ratio of cyclic shear strength to consoli-

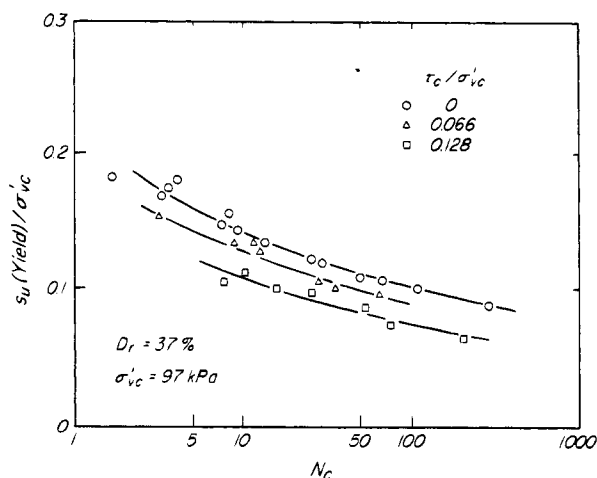


**Figure 20.65** Effect of permanent shear stress on cyclic yield strength of loose Bandaijima sand (after Yoshimi and Oh-Oka 1975).

dation pressure,  $s_u(\text{yield})/\sigma'_{vc}$  or  $s_u(\text{yield})/\sigma'_{lc}$ , to cause liquefaction in loose to medium sands having relative density values in the range of 45 to 55%, is practically independent of the permanent shear-stress magnitudes encountered under the edges of structures or in sloping ground. This important conclusion is illustrated by the cyclic yield strength data of San Fernando dam hydraulic fills in Figs. 20.61 and 20.62. These data show that the magnitude of  $\sigma'_{lc}$  has a much more significant effect on the relation between  $s_u(\text{yield})/\sigma'_{lc}$  and  $N_c$  of these loose sands than does  $\tau_c$ . The magnitude of  $\tau_c/\sigma'_{lc}$  may have a rather complex effect on the relation between  $s_u(\text{yield})/\sigma'_{lc}$  and  $N_c$ , because the relative magnitudes of  $\tau_c/\sigma'_{lc}$  and  $s_u(\text{yield})/\sigma'_{lc}$  may or may not reverse the direction of the total shear stress during the cyclic shear test. Cyclic loading that involves a change in total shear-stress direction should lead to liquefaction in a smaller number of cycles.

Undrained yield strength data from standard cyclic shear tests with  $\tau_c = 0$  can be used for liquefaction analysis of loose to medium sands beneath the edge of embankments and structures and in sloping ground. However,  $s_u(\text{yield})/\sigma'_{vc}$  or  $s_u(\text{yield})/\sigma'_{lc}$  data from the standard tests with  $\tau_c = 0$  on very loose sands must be reduced before they are used in liquefaction analyses where significant permanent shear stresses exist on the horizontal planes. Laboratory cyclic test data on very loose sands (Rollins and Seed 1990, Seed and Harder 1990) suggest the reduction factor

$$\left[ \frac{s_u(\text{yield})}{\sigma'_{vc}} \right]_{\tau_c} = \left[ \frac{s_u(\text{yield})}{\sigma'_{vc}} \right]_{\tau_c=0} \left( 1 - 2 \frac{\tau_c}{\sigma'_{vc}} \right) \quad (20.36)$$

which is applicable to values of  $\tau_c/\sigma'_{vc}$  less than 0.40, for sands with  $D_r$  values of 25 to 40%.

### 20.9.6 Cyclic Yield Strength from *In Situ* Penetration Tests

The cyclic yield strengths of *in situ* deposits may differ significantly from those of laboratory specimens reconstituted to *in situ* density. Geologic deposition, aging, preconsolidation, and preshearing, which may have conditioned the structure of sand deposits in the field, cannot be reproduced in the laboratory. On the other hand, extraction and testing of truly undisturbed specimens of clean sands are extremely difficult, time consuming, and expensive, if at all possible. In addition, a laboratory testing approach to determining cyclic yield strength suffers from the uncertain effects of sample disturbance and the accuracy with which laboratory tests simulate field consolidation and seismic loading conditions. Thus, even the most reliable laboratory cyclic  $s_u$  (yield) data may not represent  $s_u$  (yield, mob) in the field during actual earthquakes. An alternative approach to determining liquefaction resistance is to correlate the field performance of soil deposits during actual earthquake shaking directly with some readily measurable *in situ* characteristic. In the great majority of cases where it is known whether or not liquefaction occurred during an earthquake, the Standard Penetration Resistance (DSPT) and grain-size distribution are the properties of the sand deposit most commonly available for characterizing its condition. After the Niigata earthquake of 1964, Japanese engineers developed direct empirical correlations between liquefaction-related earthquake damage and DSPT  $N_{60}$  values. The evidence of liquefaction includes sand boils, breaking of the ground, settlement or bearing capacity failure of structures, lateral displacement of foundations, and uplifting of buried pipelines and tanks. The most extensive field performance data for soil deposits which did or did not liquefy during past earthquakes have been summarized in Fig. 20.66 in terms of DSPT  $N_{60}$  values and the earthquake seismic shear-stress ratio  $\tau$  (seismic)/ $\sigma'_{vo}$ . For the data shown in Fig. 20.66 this ratio has been computed using Eq. 20.33. At each site the layer with the lowest penetration resistance was considered to be the critical layer and the average  $N_{60}$  value was selected as representative of that layer. In addition to the advantage of DSPT due to its widespread use in areas where earthquakes have occurred, it is quite reasonable to expect a correlation between the cyclic yield strength and the dynamic penetration resistance of sands. Both should be affected by such factors as the density, aging, preconsolidation, and preshearing of the sand.

Liquefaction may occur at some depth below the ground surface and its effects may not be evidenced unless the liquefied layer is sufficiently extensive and the mantle of unliquefied soil is relatively thin. Ishihara and Ogawa (1978) examined the sites of past earthquakes and concluded that, for earthquakes of Richter magnitude 7.5,

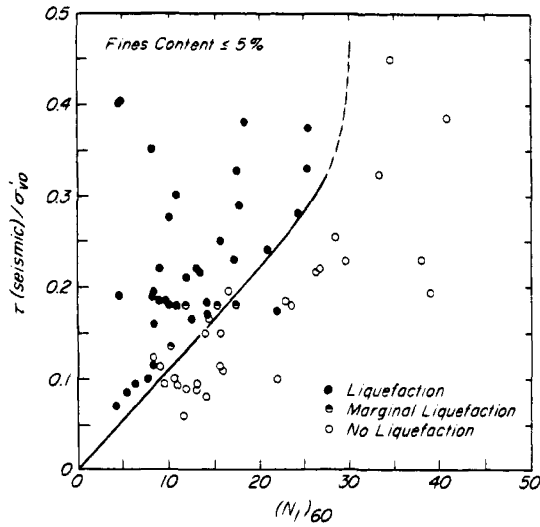


**Figure 20.66** Field evidence of liquefaction and nonliquefaction summarized in terms of seismic shear-stress ratio and DSPT penetration resistance corresponding to effective overburden pressure of 100 kPa and rod energy ratio of 60% (data after Seed et al. 1984).

surface damage may not be evident when the thickness of the liquefied layer exceeds 3 m if the thickness of cover is more than 3 m. If the thickness of the liquefied layer is less than 3 m, the thickness of cover must be more than the thickness of the liquefied layer to prevent liquefaction-induced damage to surface structures. The thickness of cover required to avoid surface evidence of liquefaction should increase with the intensity of shaking. The limiting thickness of 3 m corresponds to an  $a_{\max}/g$  value of about 0.2. If  $a_{\max}/g$  increases to 0.3 or to 0.4 to 0.5, then the limiting thickness increases to about 6 m and 9 m, respectively.

Because the DSPT blow count,  $N_{60}$ , for a given sand is a function of the effective overburden pressure, the measured values are converted to a blow count  $(N_1)_{60}$  corresponding to a standard effective overburden pressure. On the basis of an examination of laboratory and field data Liao and Whitman (1985) proposed the relationship between DSPT penetration resistance and effective overburden pressure

$$N_1 = N \left( \frac{100}{\sigma'_{vo}} \right)^{1/2} \quad (20.37)$$

where  $\sigma'_{vo}$  is in kPa. The most common values of  $\sigma'_{vo}$  for the depths from which field performance data have been obtained are in the range of 50 to 150 kPa. For this reason,  $\sigma'_{vo} = 100$  kPa is a rational choice for the reference effective overburden pressure. The values of  $(N_1)_{60}$  in Fig. 20.66 were computed by using Eq. 20.37.

The relation between  $s_u(\text{yield, mob})/\sigma'_{vo}$  and  $(N_1)_{60}$  may be defined, up to  $(N_1)_{60} = 20$ , by a line that separates sands that did or did not liquefy, as follows:

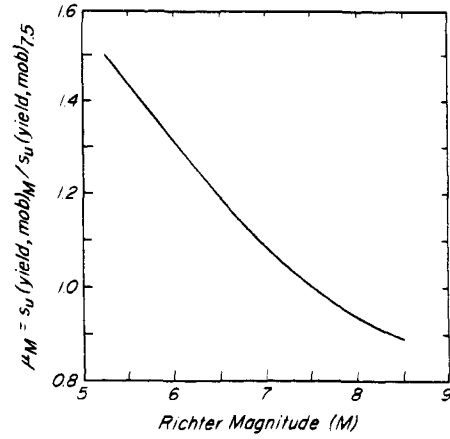


**Figure 20.67** Correction factor for influence of earthquake magnitude on mobilized yield strength from field evidence of liquefaction and nonliquefaction (data from Seed et al. 1985).

$$\left[ \frac{s_u(\text{yield, mob})}{\sigma'_{vo}} \right]_{7.5} = 0.011(N_1)_{60} \quad (20.38)$$

Most of the field performance data have been collected for earthquakes of Richter magnitudes close to 7.5. On the basis of a limited amount of field performance data for earthquake magnitudes different from 7.5, as well as laboratory cyclic strength data where equivalence of earthquake magnitude and number of cycles is evaluated in terms of the empirical relation in Fig. 20.53, lines separating liquefaction and nonliquefaction have been defined for events of other magnitudes. These results lead to the correction factors in Fig. 20.67, which can be used to obtain  $s_u(\text{yield, mob})/\sigma'_{vo}$  for any magnitude  $M$  from the  $s_u(\text{yield, mob})/\sigma'_{vo}$  line separating liquefaction and nonliquefaction in Fig. 20.66 for  $M = 7.5$ .

The line separating liquefiable and nonliquefiable sands in Fig. 20.66 is based on the field performance of clean sands with a fines content, passing No. 200 mesh, of less than 5%. It significantly underestimates the  $s_u(\text{yield, mob})$  of silty sand deposits. Apparently, the degree of drainage during DSPT decreases with the increase in the fines content, and thus the measured blow count underestimates the liquefaction resistance of contractive silty sands. On the basis of field performance data on silty sands, as well as laboratory cyclic shear tests on sands with different fines content, Eq. 20.39 can be used to determine  $s_u(\text{yield, mob})$  of silty materials with  $(N_1)_{60}$  values up to 20:

$$\left[ \frac{s_u(\text{yield, mob})}{\sigma'_{vo}} \right]_{\text{FC}} = 0.011[(N_1)_{60} + \Delta(N_1)_{60}] \quad (20.39)$$

where  $\Delta(N_1)_{60}$  is plotted in Fig. 20.68. The empirical correction in Fig. 20.68 is based on the behavior of silty sands with fines content of plasticity index in the range

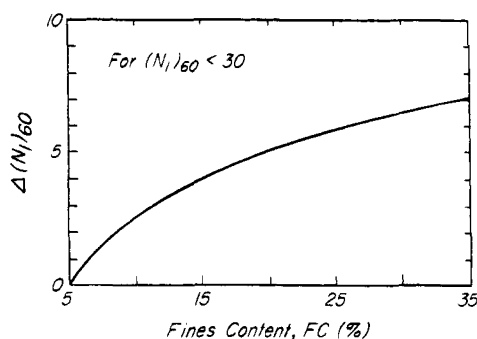


**Figure 20.68** Correction for  $(N_1)_{60}$  of silty sands in determining mobilized yield strength by using Eq. 20.39 (data from Seed et al. 1985).

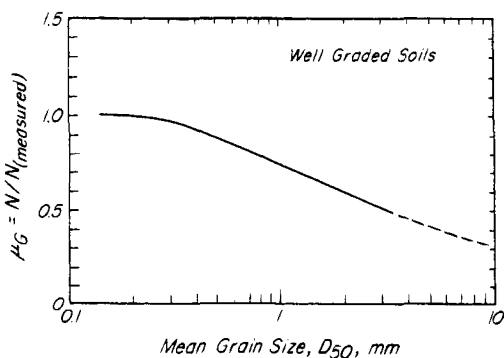


**Figure 20.69** Correction factor for measured DSPT penetration resistance of gravelly soils (from Tokimatsu 1988).

of 20 to 40%. No correction to Eq. 20.38 is needed if the plasticity index of the fines passing No. 200 mesh is less than 20%.

In a number of cases liquefaction of gravelly soils has been observed during earthquakes (Harder and Seed 1986). The DSPT provides an inaccurate impression of the liquefaction resistance of gravelly soils because of the large size of particles compared with the dimensions of the sampler. The gravel content increases the penetration resistance without significantly increasing the cyclic yield strength. Tokimatsu (1988) recommends applying the reduction factors to measured  $N_{60}$ , shown in Fig. 20.69, before they are used in Fig. 20.66 or in Eq. 20.38 to obtain  $s_u$  (yield, mob) for liquefaction analysis. Alternatively, the Becker Hammer Drill (Article 11.2.5) and a correlation between  $N_{BC}$  and  $N_{60}$  may be used to obtain  $(N_1)_{60}$  values.

Although DSPT is the most widely used site exploration tool, *PCPT* is sometimes preferred because it provides a continuous record of penetration resistance more rapidly than does the DSPT, and it is less susceptible than DSPT to testing procedure errors, especially in loose sands. However, a significant database, in terms of cone penetration resistance, on field performance during actual earthquakes is not yet available. It is presently preferable

to convert  $q_c$  to  $N_{60}$  using an empirical correlation such as the one shown in Fig. 11.15, and then to proceed with the liquefaction evaluation by using the DSPT experience.

### 20.9.7 Undrained Critical Shear Strength

A soil that has completely liquefied is still capable of sustaining a shear stress at constant volume. This shear stress is known as the *undrained critical strength*  $s_u$  (critical) or, in the literature, as the *steady-state strength* (Poulos 1981) or *residual strength* (Seed 1987). If a potential slip surface crosses a zone that may liquefy, the possibility of liquefaction is determined by comparing the shear stresses on the slip surface with  $s_u$  (yield), but a stability analysis must be based on the value of  $s_u$  (critical) along the portion of the slip surface within the liquefied zone.

Laboratory tests on reconstituted samples have demonstrated that the value of  $s_u$  (critical) for a given sand is primarily a function of the void ratio (Castro 1969). The relation is exemplified by Fig. 20.70, which shows the results of undrained critical strength data obtained in 1985 for a reevaluation of the liquefaction-related failure of the Lower San Fernando dam during the 1971 earthquake. Monotonically loaded consolidated-undrained triaxial compression tests were carried out on specimens of the hydraulic fill from the downstream shell. Because the values of  $s_u$  (critical) in Fig. 20.70 change rapidly with small changes in void ratio, applicability of such tests is of doubtful reliability, because it is extremely difficult to determine the *in situ* void ratio of cohesionless soils such as clean sands. The slope of the  $e$  vs  $\log s_u$  (critical) line in Fig. 20.70 is a function mainly of grain shape and is, therefore, fairly constant for a given sand deposit; how-

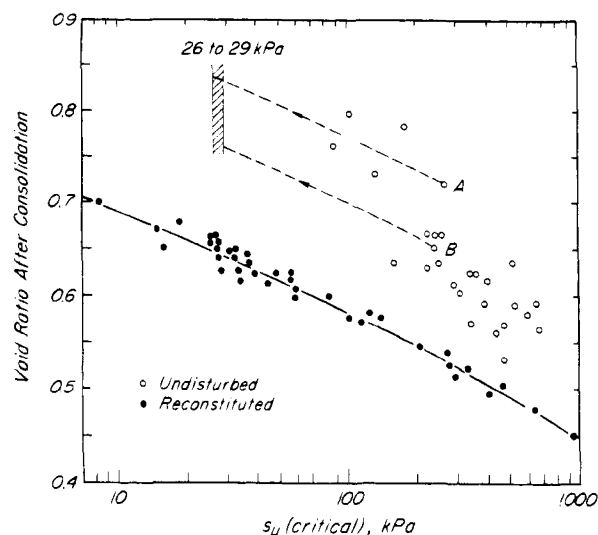


**Figure 20.70** Critical strength of Lower San Fernando hydraulic fill sampled and tested in 1985 (Bulk Sample 7; data from Marcuson et al. 1990).

ever, the position of the line is moderately dependent on the mode of shear and the magnitude of consolidation pressure and is very sensitive to gradation and fines content (Poulos et al. 1985, Vaid et al. 1990, Konrad 1990).

The reconstituted specimens of sandy silt represented by Fig. 20.70 had a median grain size of 0.07 mm. Undisturbed specimens, having median grain sizes from 0.02 to 0.2 mm, were tested similarly. Although there was no significant difference between the average gradation curves for the undisturbed and the reconstituted specimens, a striking difference in the values of  $s_u$  (critical) for the undisturbed and reconstituted samples at a given void ratio was evident. Marcuson et al. (1990) attributed the difference to the stratified nature of the undisturbed specimens, as a result of which the grain-size analysis of a whole specimen would not properly represent the gradation and fines content of the strata controlling  $s_u$  (critical). However, because all the points representing the undisturbed samples lie above the relation for the reconstituted samples, it seems evident that other factors have an influence.

In an alternative approach (Seed 1987), postearthquake values of  $s_u$  (mob) were calculated by back analysis of embankment failures involving liquefied materials and were correlated to the results of standard penetration tests  $(N_1)_{60}$ . Such correlations have been used widely but the results leave a considerable margin of uncertainty, because a large range of values of  $s_u$  (mob) corresponds to a given value of  $(N_1)_{60}$ .

A similar approach was used to back-calculate the values of  $s_u$  (critical, mob)/ $\sigma'_{vo}$  shown in Fig. 20.71 for a number of embankment failures. The values of  $\sigma'_{vo}$  used to normalize  $s_u$  (critical, mob) were determined for mid-depth of the layer that was reported to have liquefied. In making the calculations the final postfailure deformed geometry was used, because the original configuration

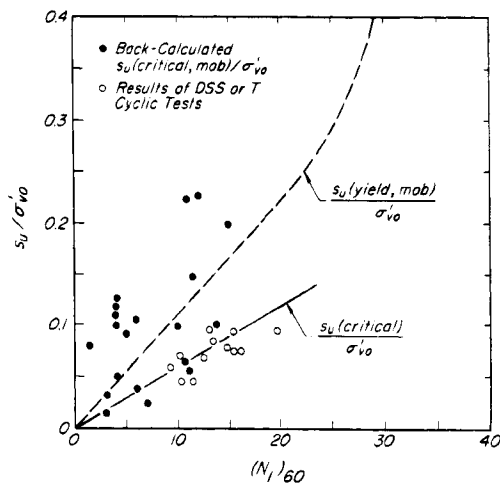


**Figure 20.71** Relation between  $s_u$  (critical)/ $\sigma'_{vo}$  and  $(N_1)_{60}$  for clean sand (fines content not greater than 5%).

before sliding cannot reflect the geometry corresponding to the suddenly reduced shear strength in the liquefied zone.

Also shown in Fig. 20.71 is the curve from Fig. 20.66 that defines  $s_u$  (yield, mob) and separates soils that liquefy from those that do not. The location of many points, representing back-calculated values of  $s_u$  (critical, mob), above this curve suggests that in many instances significant drainage took place during postliquefaction flow, and that by the time the liquefied mass came to rest,  $s_u$  (critical, mob) was actually equal to or greater than  $s_u$  (yield, mob). That is, during the flow of liquefied sand some drainage may occur and constant volume conditions may not prevail.

The stability of an existing slope at the instant of liquefaction is governed, however, by the constant-volume  $s_u$  (critical), not by the partially drained back-calculated  $s_u$  (critical, mob). Therefore, the stability analysis of an existing slope should be based on the original geometry and the constant-volume shearing resistance  $s_u$  (critical). These considerations suggest a third approach for determining the *in situ* value of  $s_u$  (critical) for analyzing the stability of a liquefied sand. In developing this approach, for each sand, laboratory measurements of both  $s_u$  (yield) and  $s_u$  (critical) at the same  $\sigma'_{vc}$  are used. It is assumed that for clean sands,  $s_u$  (yield, DSS)/ $\sigma'_{vc}$  or  $0.64 s_u$  (yield, T)/ $\sigma'_{1c}$  at  $N_c = 15$  is equal to  $s_u$  (yield, mob)/ $\sigma'_{vo}$  from Eq. 20.38. The results of the tests, when substituted in Eq. 20.38, can then be used to evaluate the corresponding values of  $(N_1)_{60}$ . The available data on

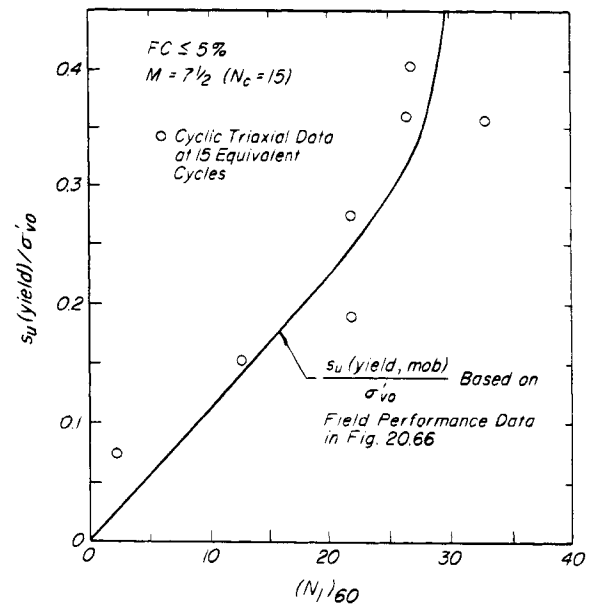


**Figure 20.72** Comparison of  $s_u$  (yield, DSS)/ $\sigma'_{vo}$  from laboratory tests on undisturbed samples of high quality to field performance data (data from Tokimatsu 1988, Ishihara and Koga 1981).

$[s_u \text{ (critical)}/\sigma'_{vc}, (N_1)_{60}]$  are represented by open circles in Fig. 20.71. The relation between  $s_u \text{ (critical)}/\sigma'_{vc}$  and  $(N_1)_{60}$  can be represented by the empirical equation

$$\frac{s_u \text{ (critical)}}{\sigma'_{vo}} = 0.006(N_1)_{60} \quad (20.40)$$

Eq. 20.40 is based on a limited number of data points for nine sands, because laboratory testing of sands has rarely included measurement of both cyclic yield strength to obtain  $s_u$  (yield) at  $N_c = 15$  and  $s_u$  (critical). However, Eq. 20.40 seems to be a reasonable expression for *in situ*  $s_u$  (critical), as it includes the low values of  $s_u$  (critical, mob) that were apparently mobilized under completely undrained conditions. For the upstream hydraulic fill of Lower San Fernando dam, which liquefied, Eq. 20.40 leads to  $s_u$  (critical) = 17 kPa for values of  $(N_1)_{60} = 14$  and  $\sigma'_{vo} = 200$  kPa.

For sands with a fines content more than 5%, Eq. 20.40 should be replaced by

$$\frac{s_u \text{ (critical)}}{\sigma'_{vo}} = 0.006[(N_1)_{60} + \Delta(N_1)_{60}] \quad (20.41)$$

where  $\Delta(N_1)_{60}$  is defined in Fig. 20.68.

At a given site, standard penetration tests can be performed, and  $(N_1)_{60}$  can be used together with Eqs. 20.40 or 20.41 to compute  $s_u \text{ (critical)}/\sigma'_{vo}$ . Alternatively, in addition to DSPT measurements, a program of sampling and laboratory testing can be carried out. By using the measured values of  $0.64 s_u \text{ (yield, } T)/\sigma'_{1c}$  at  $N_c = 15$  and  $s_u \text{ (critical)}/\sigma'_{1c}$  together with Eq. 20.38, a site-specific relation between  $s_u \text{ (critical)}/\sigma'_{1c}$  and  $(N_1)_{60}$  can be established. The measured values of  $(N_1)_{60}$  can be used to determine  $s_u \text{ (critical)}/\sigma'_{vo}$ . This approach does not require an accurate knowledge of the *in situ* void ratio of the sand.

It is of considerable interest to compare  $s_u$  (yield,  $DSS$ )/ $\sigma'_{vc}$  or  $s_u$  (yield,  $T$ )/ $\sigma'_{1c}$  at  $N_c = 15$  from laboratory tests on undisturbed samples with the values indicated by Eq. 20.38 where  $(N_1)_{60}$  values have been determined in the field. Such a comparison has been made by Tokimatsu (1988) using the data from cyclic undrained triaxial shear tests on clean sands. High-quality undisturbed specimens were obtained by *in situ* freezing and coring and were consolidated under an equal all-around pressure equal to the *in situ*  $\sigma'_{vo}$  before they were subjected to a sinusoidal axial load of constant amplitude. The results, together with a few additional data (Ishihara and Koga 1981) are shown in Fig. 20.72. The laboratory yield strength data from undisturbed specimens are consistent with Eq. 20.38, which is based on field records of liquefaction during earthquakes.

### Selected Reading

Castro, G. (1969). "Liquefaction of sands," *Harvard Soil Mechanics Series*, No. 81, Cambridge, 111 p.

- Seed, H. B. and I. M. Idriss (1971). "Simplified procedure for evaluating soil liquefaction potential," *J. Soil Mech. Found. Eng., ASCE*, **97**, No. 9, pp. 1249–1273.
- Casagrande, A. (1975). "Liquefaction and cyclic deformation of sands: A critical review," *Proc. 5th Pan American Conf. on Soil Mech. and Found. Eng.*, Buenos Aires; also published as *Harvard Soil Mechanics Series*, No. 88, Cambridge.
- Seed, H. B. (1979a). "Soil liquefaction and cyclic mobility evaluation for level ground during earthquakes," *J. Geotech. Eng., ASCE*, **105**, No. 2, pp. 201–255.
- Finn, W. D. L. (1981). "Liquefaction potential: Development since 1976," *Proc. Int. Conf. on Recent Advances in Geotech. Earthquake Eng. and Soil Dynamics*, Rolla, MO pp. 655–681.
- Seed, H. B., I. M. Idriss, and I. Arango (1983). "Evaluation of liquefaction potential using field performance data," *J. Geotech. Eng., ASCE*, **109**, No. 3, pp. 458–482.
- Ishihara, K. (1985). "Stability of natural deposits during earthquakes," *Proc. 11th Int. Conf. Soil Mech. and Found. Eng.*, **1**, pp. 321–376.
- Seed, H. B., K. Tokimatsu, L. F. Harder, and R. M. Chung (1985). "Influence of SPT procedures in soil liquefaction resistance evaluations," *J. Geotech. Eng., ASCE*, **111**, No. 12, pp. 1425–1445.
- Seed, H. B. and P. De Alba (1986). "Use of SPT and CPT tests for evaluating the liquefaction resistance of sands," *Proc. In Situ '86, ASCE Specialty Conf. on Use of In Situ Testing in Geotech. Eng.*, STP No. 6, Blacksburg, pp. 281–302.
- Stark, T. D. and G. Mesri (1992). "Undrained shear strength of liquified sands for stability analysis," *J. Geotech. Eng., ASCE*, **118**, No. 11, pp. 1727–1746.
- Ishihara, K. (1993). "Liquefaction and flow failure during earthquakes," *Géot.*, **43**, No. 3, pp. 351–415.

## ARTICLE 21 EFFECT OF VIBRATIONS ON SOILS

It is a matter of common experience that vibrations due to pile driving, traffic, or the operation of machinery usually increase the density of a sand and cause its surface to subside. Damage to buildings may be caused by the subsidence and is often the subject of lawsuits against the parties responsible for the vibrations. On the other hand, vibrations are also one of the most economical means for compacting embankments of sand or natural layers of loose sand before the construction of foundations (Article 44). Hence, the effect of vibrations on soils may be harmful or beneficial, but it always deserves attention.

To investigate the factors that influence the compacting effect of vibration, apparatus shown diagrammatically in Fig. 21.1a (Hertwig et al. 1933) has been used. It consists of a bearing plate and two equal eccentric weights that rotate in opposite directions. The total force exerted on the ground by the base plate of the apparatus consists of a static force equal to the weight of the equipment, plus a pulsating force with a maximum value equal to the centrifugal force of the two eccentric weights. The num-

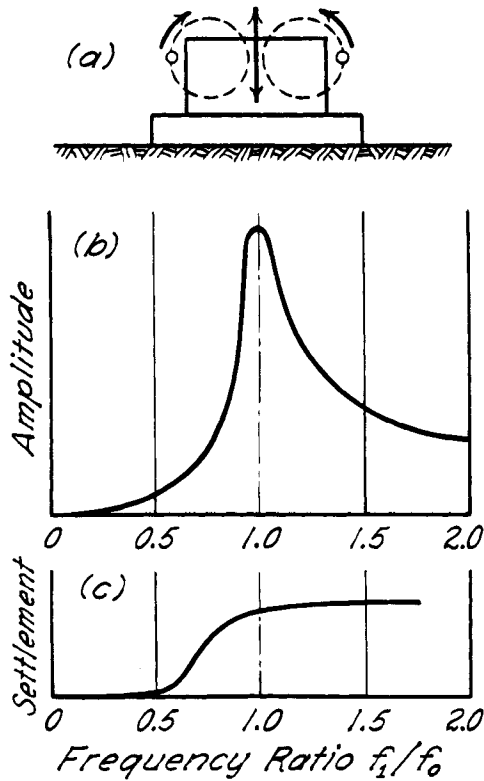


**Figure 21.1** (a) Principle of soil vibrator. (b) Relation between frequency and amplitude of vibrations. (c) Relation between frequency and settlement of vibrator base (after Hertwig et al. 1933).

ber of revolutions of the eccentric weights per unit of time is the *frequency*, usually expressed in Hz (cycles/s). The greatest vertical distance through which the base moves from its equilibrium position is called the *amplitude* of vibration of the base. At a certain frequency the amplitude is a maximum (see Fig. 21.1b). This frequency is approximately equal to the natural frequency  $f_0$  of the vibrator and the vibrating portion of the supporting soil.

The term *natural frequency* indicates the frequency of the vibrations that ensue if a body with well-defined boundaries is acted on by a single impulse. If the impulse is periodic, the amplitude of the resulting *forced vibrations* increases as the frequency  $f_1$  of the impulse approaches the natural frequency of the body. At a frequency close to the natural frequency, the amplitude is a maximum. This state is called *resonance*. In Fig. 21.1b it is represented by a peak.

Table 21.1 contains values of the resonant frequency of a vibrator such as that shown in Fig. 21.1 operating on different soils and soft rocks (Lorenz 1934). The vibrator had a mass of 2700 kg and a contact area of 1 m<sup>2</sup>. The values were obtained by steadily increasing the frequency of the impulse up to and beyond the occurrence of resonance.

**Table 21.1** Resonant Frequency of Vibrator on Various Types of Soil

Supporting Soil or Rock	Frequency (Hz)
Loose fill	19.1
Dense artificial cinder fill	21.3
Fairly dense medium sand	24.1
Very dense mixed-grained sand	26.7
Dense pea gravel	28.1
Soft limestone	30.0
Sandstone	34.0

The resonant frequency depends not only on the properties of the supporting soil but also to a certain extent on the weight and dimensions of the vibrator. These variables have been investigated by the U.S. Corps of Engineers in two series of tests, one on a cohesive silty clay and the other on cohesionless sand. The mass of the vibrator and its base varied from 6,000 to 30,000 kg, the diameters of the loaded areas from 1.5 to 5 m, and the contact areas from 2 to 20 m<sup>2</sup>. Several modes of vibration were induced separately (WES 1963). The results have substantially extended the range of the pertinent variables, but do not differ fundamentally from those illustrated in Fig. 21.1.

If a particular vibrator is used on different soils, the resonant frequency increases with increasing density and decreasing compressibility of the soil. By taking advantage of this fact, extensive use has been made of such equipment for determining the degree of compaction of artificial fills and for comparing the effectiveness of different methods of compaction.

If a vibrator operates on sand, the sand beneath the bearing plate becomes compacted. At constant frequency of the impulses, the size of the zone of compaction increases at a rate that decreases with time. The ultimate size of the zone depends on the intensity of the periodic impulses exerted by the vibrator and on the initial density of the sand. Beyond the boundaries of this zone the density of the sand remains practically unchanged.

Because the vibrator rests on the surface of the zone of compaction, the process of compaction is associated with a settlement of the vibrator. If the frequency of the impulse is gradually increased, the corresponding settlement of the vibrator increases as shown in Fig. 21.1c. As the resonant frequency is approached, the settlement increases rapidly and becomes many times greater than the settlement produced by a static load of the same magnitude as the pulsating force. The range of frequencies within which the increase of settlement is greatest is called the *critical range*. It seems to extend from  $1/2$  to  $1 1/2$  times the resonant frequency.

If the frequency of a vibrating engine supported on sand is within the critical range for the sand, the resulting settlement is very much greater than that which would be caused by the equivalent static forces. The frequency of vibrations caused by the slight but inevitable eccentricity of the rotating parts of steam turbines happens to be within the critical range for sand. Therefore, foundations for steam turbines on strata of loose sand settle excessively unless the sand is artificially compacted before the turbine foundations are constructed. Whatever the subsoil conditions may be, it is advisable to make special provisions to reduce the amplitude of the forced vibrations.

The effect of vibration on clays is far less conspicuous than on sand because the cohesive bond between clay particles interferes with intergranular slippage. Nevertheless, even a soft clay consolidates to a moderate extent

when it is continually subjected to intense vibrations having a frequency close to the natural frequency of the clay.

In reality, vibrating engines oscillate not only vertically but in several other modes each of which may be characterized by a different resonant frequency. The resulting motions are very complex and cannot usually be predicted reliably, although for simple cases the resonant frequencies can be approximated (Barkan 1962, Lysmer and Richart 1966).

Similar phenomena of resonance may be induced if a vibrator is mounted at the top of a pile. The principle has found application in pile driving. In this instance the vibrator is operated at the natural frequency of longitudinal vibrations in the pile itself, whereupon the pile may penetrate readily into the ground (ASCE 1961).



## PART II

### *Theoretical Soil Mechanics*

This part of the book contains theories dealing with the interaction between soil and water (Chapter 4), with the limiting conditions for the equilibrium of soil masses (Chapter 5), and with the deformations produced by external forces (Chapter 6).

For the most part the theories presented lead to relatively simple closed-form solutions in which soils are modeled as perfectly elastic or perfectly plastic bodies having a few simple properties that can be represented by numerical values such as the modulus of elasticity  $E$  or the angle of internal friction  $\phi'$ . In spite of the gross oversimplification that these limitations impose on modeling the behavior of real soils, the closed-form solutions serve a useful purpose. They provide insight to the behavior that may be anticipated; with judicious selection of values for the soil properties involved, they permit rough estimates of the quantities to be predicted; and they serve as standards against which the results of more elaborate methods of calculation can be compared. Often they provide all the theoretical input needed for design. Taken as a whole, these theories are referred to as *classical soil mechanics*.

In recent years powerful new procedures, made practical by electronic calculation, have been developed that permit numerical solutions of problems involving complex boundary conditions and that allow the physical

properties of the soils to be modeled with greater realism. Complex stress-strain relations can be taken into account, as can a variety of yield conditions and creep relationships. The procedures are categorized as finite-difference, finite-element, and boundary-discretization methods. Each has its advantages and disadvantages with respect to its applicability to a specific problem. Choice of the procedure, and selection and verification of the appropriate software, require expertise in numerical methods of analysis. As specialized as this expertise may be, however, it is more prevalent than the judgment required to select the most realistic formulation of the physical properties of the soils involved and to sense the magnitude of the errors associated with the difference between the postulated and the actual behavior. The need to check the validity of the results of calculations by means of field observations is not diminished by virtue of use of the more sophisticated procedures; indeed, the contrary is more likely.

This book does not deal with the techniques for numerical methods of analysis, a specialty in its own right, although the physical properties that govern the validity of constitutive relations were presented in Part I. Where pertinent the results of numerical analyses that have contributed to engineering practice are incorporated in Part III.

## CHAPTER 4

### *Hydraulics of Soils*

#### ARTICLE 22 SCOPE OF HYDRAULIC PROBLEMS

The interaction between soil and percolating water enters into several groups of problems in earthwork engineering. One group involves the estimate of the quantity of water that will enter a pit during construction, or the quantity of stored water that will be lost by percolation through a dam or its subsoil (Article 23). A second group deals with the influence of the permeability on the rate at which the excess water drains from loaded clay strata (Article 25). A third group deals with the effect of the seepage pressure on the stability of slopes and foundations. Because the problems of this group also involve consideration of the equilibrium of masses of soil, discussion of hydraulic problems in this category will be deferred to Chapter 5, "Plastic Equilibrium in Soils."

The theoretical solution of each of these problems is based on the assumption that the mass of soil through which the water percolates is homogeneous or that it is composed of a few homogeneous strata with well-defined boundaries. Similar assumptions will be made in the derivation of the theories dealing with earth pressure, stability, and settlement. However, the practical implications of the assumptions are fundamentally different in the hydraulic problems.

Earth pressure, settlement, and often stability depend merely on the average values of the soil properties involved. Therefore, even a considerable scattering of the values from the average is of little practical consequence. On the other hand, in connection with hydraulic problems, apparently insignificant geologic details may have a decisive influence on both the amount of seepage and the distribution of the seepage pressures throughout the soil. The following example illustrates this point.

If a thick deposit of sand contains a few thin layers of dense fine silt or stiff clay, the presence of these layers has practically no effect on the lateral pressure exerted by the sand against the bracing of an open cut above the water table, on the ultimate bearing capacity of the sand,

or on the settlement of a structure resting on the sand. Hence, in connection with these problems the presence of such layers can safely be ignored, and it makes no difference whether or not they were noticed in the soil exploration.

On the other hand, in connection with any practical problem involving the flow of water through the sand, for instance from a pond on the upstream side of a row of sheet piles to the downstream side, the presence or absence of thin layers of relatively impermeable soil is of decisive importance. If one of the layers is continuous and located above the lower edge of the sheet piles, it intercepts the flow almost completely. If the layers are discontinuous, it is impossible to estimate their influence on the amount and direction of the seepage without knowing the degree of their continuity. Yet, this degree cannot be determined by any practicable means. As a matter of fact, test borings may not even disclose the presence of the layers at all.

Every natural soil stratum and every man-made earth fill contain undetected or undetectable inclusions of material with exceptionally high or low permeability, and the location of the horizontal boundaries of these inclusions can only be a matter of conjecture. Therefore, the difference between reality and the results of any investigation involving the flow of water through soil can be very important, irrespective of the thoroughness and care with which the subsoil is explored. Yet, if no investigation is made at all, the engineer is entirely at the mercy of chance. Consequently, sound engineering calls for the following procedure in dealing with hydraulic problems. The design should be based on the results of a conscientious hydraulic investigation. However, during the entire period of construction and, if necessary, for several years afterward, all the field observations should be made that are required for finding out whether or to what extent the real hydraulic conditions in the subsoil differ from the assumed ones. If the observations show that the real conditions are less favorable than the designer anticipated, the design must

be modified in accordance with the findings. By means of this procedure, which is illustrated by several examples in Part III, many dam failures could have been avoided.

## ARTICLE 23 SEEPAGE COMPUTATIONS

### 23.1 Hydrodynamic Equations

Fluid flow through porous media is governed by hydrodynamic equations that take into account the physicochemical state of the fluid, consider the interaction with the porous media of the fluid in *motion*, and ensure the *continuity* of the fluid. In the analysis of the flow of water through saturated soils, the state of the fluid is characterized by a constant density independent of porewater pressure. Darcy's flow equation (Article 14.2) is assumed to describe the interaction of the moving water with the soil structure. Continuity is ensured by requiring that the net volume of water flowing per unit of time into or out of an element of soil be equal to the change per unit of time of the volume of water in that element. Figure 23.1 shows an element of saturated soil. The lengths of the sides are  $dx$ ,  $dy$ , and  $dz$ . Because the quantity of flow per unit of time, the *rate of flow*, is a scalar quantity, we can evaluate the individual rates of flow in the  $x$ -,  $y$ -, and  $z$ -directions and then add them to obtain the net flow of water into or out of the element.

The discharge velocity vector at the center of the soil element in Fig. 23.1 has components  $v_x$ ,  $v_y$ , and  $v_z$  in the  $x$ -,  $y$ -, and  $z$ -directions, respectively. At the center of the element, the rate of flow in the  $x$ -direction is  $v_x dy dz$ , where  $dy dz$  is the area of the element perpendicular to the  $x$ -direction. The rate of flow in the  $x$ -direction into the soil element is

$$\left( v_x - \frac{\partial v_x}{\partial x} \frac{dx}{2} \right) dy dz$$

and the rate of flow in the  $x$ -direction out of the element is

$$\left( v_x + \frac{\partial v_x}{\partial x} \frac{dx}{2} \right) dy dz$$

Note that  $\partial v_x / \partial x$  is the rate of change in  $v_x$  in the  $x$ -

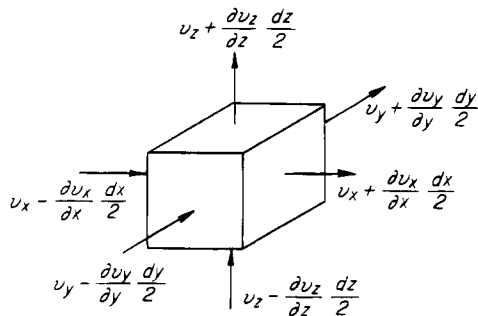


**Figure 23.1** Components of discharge velocity at six faces of an element of soil.

direction, and  $(\partial v_x / \partial x) dx/2$  is the total change in  $v_x$  between the center and a face of the element. The net rate of flow into or out of the soil element in the  $x$ -direction is the algebraic sum of the flow rates in and out

$$\frac{\partial v_x}{\partial x} dx dy dz$$

A similar analysis leads to

$$\frac{\partial v_y}{\partial y} dx dy dz \quad \text{and} \quad \frac{\partial v_z}{\partial z} dx dy dz$$

in the  $y$ - and  $z$ -directions. The net volume of water flowing per unit of time into or out of the element of soil is then

$$\left( \frac{\partial v_x}{\partial x} + \frac{\partial v_y}{\partial y} + \frac{\partial v_z}{\partial z} \right) dx dy dz$$

which by definition is equal to the change per unit of time of the volume of water in the element. Since the volume of water in the element is  $n dx dy dz$ , where  $n$  is the porosity, the equation of continuity is

$$\left( \frac{\partial v_x}{\partial x} + \frac{\partial v_y}{\partial y} + \frac{\partial v_z}{\partial z} \right) dx dy dz = -\frac{\partial}{\partial t} (n dx dy dz) \quad (23.1)$$

The minus sign indicates that the net change is positive if there is a net volume decrease.

For the steady-state seepage condition, in which the change per unit of time of the volume of water in the element is zero, we obtain

$$\frac{\partial v_x}{\partial x} + \frac{\partial v_y}{\partial y} + \frac{\partial v_z}{\partial z} = 0 \quad (23.2)$$

By combining Eq. 23.2 with Eq. 14.4 we obtain

$$v_x = k_x i_x = k_x \frac{\partial h}{\partial x}, \quad v_y = k_y i_y = k_y \frac{\partial h}{\partial y}, \quad \text{and} \quad v_z = k_z i_z = k_z \frac{\partial h}{\partial z}$$

On the assumption that  $k_x$ ,  $k_y$ , and  $k_z$  are constants in the  $x$ -,  $y$ -, and  $z$ -directions, respectively, Eq. 23.2 becomes

$$k_x \frac{\partial^2 h}{\partial x^2} + k_y \frac{\partial^2 h}{\partial y^2} + k_z \frac{\partial^2 h}{\partial z^2} = 0 \quad (23.3)$$

For isotropic soils,  $k_x = k_y = k_z = k$ . By introducing a velocity potential  $\Phi = kh$  such that

$$v_x = \frac{\partial \Phi}{\partial x}, \quad v_y = \frac{\partial \Phi}{\partial y}, \quad \text{and} \quad v_z = \frac{\partial \Phi}{\partial z},$$

we obtain

$$\frac{\partial^2 \Phi}{\partial x^2} + \frac{\partial^2 \Phi}{\partial y^2} + \frac{\partial^2 \Phi}{\partial z^2} = 0 \quad (23.4)$$

If a soil is anisotropic, it may be treated as if it were isotropic by introducing the following transformation of the  $x$ -,  $y$ -, and  $z$ -dimensions

$$x' = x \sqrt{\frac{k_o}{k_x}}, \quad y' = y \sqrt{\frac{k_o}{k_y}}, \quad z' = z \sqrt{\frac{k_o}{k_z}} \quad (23.5)$$

whereupon

$$\frac{\partial^2 \Phi}{\partial x'^2} + \frac{\partial^2 \Phi}{\partial y'^2} + \frac{\partial^2 \Phi}{\partial z'^2} = 0 \quad (23.6)$$

and its permeability

$$k = \sqrt{\frac{k_x k_y k_z}{k_o}} \quad (23.7)$$

where  $k_o$  is any reference permeability, such as  $k_o = 1$  m/s or  $k_o = k_z$ .

### 23.2 One-Dimensional Steady-State Seepage

When the flow is in only one direction, for example in the vertical or  $z$ -direction, then Eq. 23.3 reduces to

$$\frac{d^2 h}{dz^2} = 0$$

Integration of this differential equation leads to

$$\frac{dh}{dz} = C_1$$

where  $C_1$  is a constant independent of  $z$ . This means that, for one-dimensional steady-state seepage in a homogeneous soil layer, the hydraulic gradient is a constant along the direction of flow. A second integration leads to  $h = C_1 z + C_2$ , where  $C_2$  is a constant independent of  $z$ . This means that, for one-dimensional steady-state seepage, the hydraulic head  $h$  in each homogeneous soil layer varies linearly in the direction of flow. By combining this conclusion with the definition of  $h$  in terms of piezometric head and elevation head, we obtain

$$u = D_1 z + D_2 \quad (23.8)$$

This result indicates that, for one-dimensional steady-state seepage, the porewater pressure in each homogeneous soil layer varies linearly in the direction of flow. On the basis of these conclusions, any one-dimensional flow problem can be solved to obtain the rate of seepage and the porewater pressure profile.

One-dimensional steady-state seepage problems often involve flow through more than one homogeneous layer. The soil profile may consist of fairly homogeneous distinct layers 1, 2, . . . ,  $n$  with thicknesses  $H_1, H_2, \dots, H_n$ , vertical coefficients of permeability,  $k_{v1}, k_{v2}, \dots, k_{vn}$ , and horizontal coefficients of permeability,  $k_{h1}, k_{h2}, \dots, k_{hn}$ . When one-dimensional flow is perpendicular to the strati-

fication, then

$$q_{v1} = q_{v2} = \dots = q_{vn} \quad (23.9)$$

and

$$h_L = \sum_{j=1}^n \Delta h_j \quad (23.10)$$

Here  $q_{v1}, q_{v2}, q_{vn}$  are the vertical flow rates through layers, 1, 2, and  $n$ , respectively;  $\Delta h_1, \Delta h_2$ , and  $\Delta h_n$  are the hydraulic head losses in those layers; and  $h_L$  is the hydraulic head loss through the entire stratified soil profile. Thus,

$$q_{v1} = k_{v1} \frac{\Delta h_1}{H_1}, \quad q_{v2} = k_{v2} \frac{\Delta h_2}{H_2}, \quad \text{and} \quad q_{vn} = k_{vn} \frac{\Delta h_n}{H_n}$$

The value of  $h_L$  is equal to headwater elevation minus tailwater elevation. Water flows from the headwater side toward the tailwater side. In using Eq. 23.8 to compute  $u$  from  $h$  and  $z$ , it is usually advantageous to select the tailwater elevation as the datum. Note that Eqs. 23.9 and 23.10 together result in  $n$  equations with  $n$   $\Delta h_j$  unknowns. After determining  $\Delta h_1, \Delta h_2, \dots, \Delta h_n$  and, therefore, the variation of  $h$  with depth, the porewater pressure at any depth is computed from  $u = \gamma_w (h - z)$ .

When the flow is perpendicular to the bedding planes, Eq. 14.11 shows that the overall permeability of the stratified profile is the weighted harmonic mean of the individual permeabilities. Therefore, the overall flow rate in the vertical direction is influenced most strongly by the least pervious layers. In fact, the hydraulic head loss can be assumed to be negligible in a soil layer a hundred times more pervious than another layer of comparable thickness. By making this assumption the number of unknowns in Eqs. 23.9 and 23.10 is reduced and the seepage calculations are simplified.

When the flow is parallel to the bedding planes, then according to Eq. 14.12 the overall permeability in the direction of flow is the weighted mean of the individual permeabilities  $k_{h1}, k_{h2}, \dots, k_{hn}$ . Thus, in this case, the overall rate of flow is influenced most strongly by the most pervious layers, and flow through the less pervious layers is negligible.

### 23.3 Two-Dimensional Steady-State Seepage

Two-dimensional seepage is illustrated in Fig. 23.2. Water escapes from a pond by percolation through the subsoil of a single sheet-pile cofferdam. The row of sheet piles is assumed to be impermeable. The piles are driven to a depth  $D$  into a homogeneous isotropic sand stratum having a thickness  $D_1$ . The sand rests on a horizontal impermeable base. The hydraulic head loss  $h_L$  (Article 14) is kept constant. Water entering the sand at the upstream surface travels along curves known as *flow lines*. Curve  $AB$ , marked by arrows, is one such flow line.

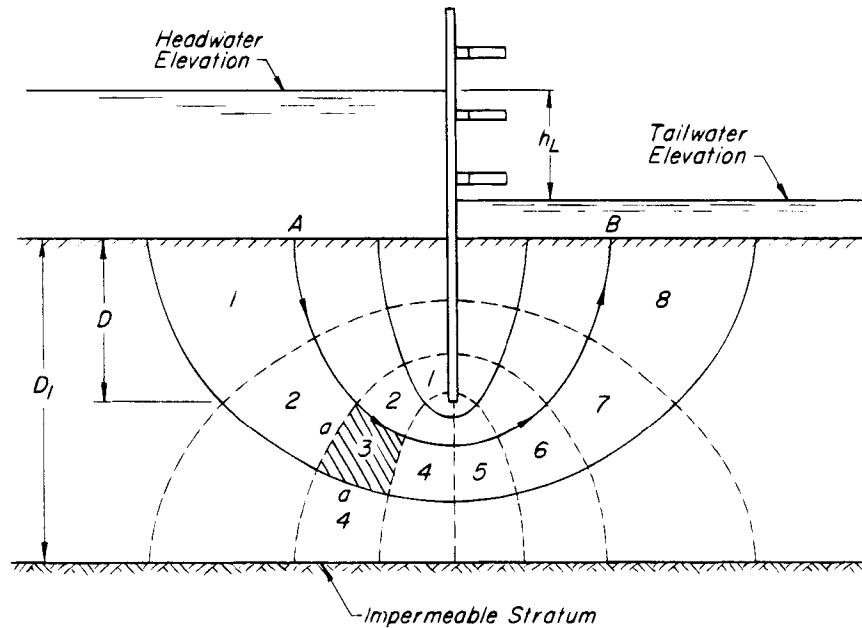


**Figure 23.2** Flow of water around lower edge of single row of sheet piles in a homogeneous isotropic soil.

For seepage in only the  $xz$  plane, the equation of continuity reduces to

$$k_x \frac{\partial^2 h}{\partial x^2} + k_z \frac{\partial^2 h}{\partial z^2} = 0$$

The anisotropic soil can be transformed into an isotropic soil by keeping the natural  $z$ -dimension while transforming the  $x$ -dimension according to Eq. 23.5

$$x' = x \sqrt{\frac{k_z}{k_x}}$$

The permeability of the transformed soil, according to Eq. 23.7, is  $k = \sqrt{k_x k_z}$ .

For isotropic soils, the continuity equation in terms of the velocity potential  $\Phi = kh$  is

$$\frac{\partial^2 \Phi}{\partial x^2} + \frac{\partial^2 \Phi}{\partial z^2} = 0 \quad (23.11)$$

This expression, known as Laplace's equation, describes the variation of hydraulic head in a two-dimensional flow of water through soil. Each curve corresponding to a constant  $\Phi$ , and therefore constant  $h$ , is called an *equipotential line*. A set of equipotential lines completely defines the distribution of hydraulic head and, therefore, together with Eq. 14.1, the porewater pressure in the soil.

A function such as  $\Phi$  that satisfies Laplace's equation is a harmonic function that has a conjugate harmonic function  $\Psi$  related to  $\Phi$  as follows:

$$\frac{\partial \Psi}{\partial x} = -\frac{\partial \Phi}{\partial z} = v_z \quad \text{and} \quad \frac{\partial \Psi}{\partial z} = \frac{\partial \Phi}{\partial x} = v_x \quad (23.12)$$

The equation of a tangent to a flow line in the  $xz$  plane is

$$\frac{dz}{dx} = \frac{v_z}{v_x}$$

By substituting for  $v_z$  and  $v_x$  in terms of  $\Psi$  from Eq. 23.12 one can show that each curve corresponding to a constant  $\Psi$  describes a flow line. Therefore, Laplace's equation in terms of  $\Psi$  describes the flow lines. Furthermore, the relations in Eq. 23.12 show that in homogeneous and isotropic soil, the functions  $\Phi$  and  $\Psi$  are orthogonal. That is, flow lines and equipotential lines intersect at right angles. A complete set of flow lines and equipotential lines is called a *flow net*.

Every strip located between two adjacent flow lines, such as  $\Psi_1$  and  $\Psi_2$  in Fig. 23.3, is called a *flow channel*.

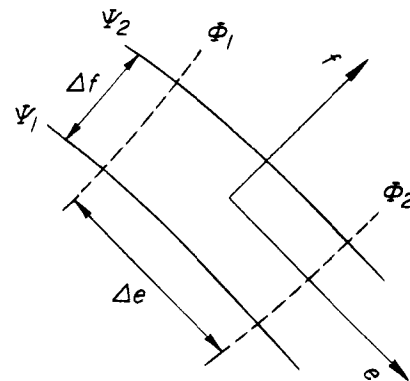


**Figure 23.3** Field formed by two flow lines and two equipotential lines.

The flow rate,  $\Delta q$ , is constant along each channel, and is equal to  $\Delta\Psi = \Psi_2 - \Psi_1$ . Every section located between two adjacent equipotential lines, such as  $\Phi_1$  and  $\Phi_2$  in Fig. 23.3, is known as a *field*. The *potential drop* or hydraulic head loss,  $\Delta h$ , is a constant and is equal to  $h_2 - h_1$ .

### 23.4 Computation of Seepage and Seepage Pressure

To derive the equation necessary for computing the quantity of seepage, we shall consider the net formed by the flow lines and equipotential lines in Fig. 23.3. To simplify the derivation we use the *ef* coordinate system formed by the tangents to the flow line and equipotential line at the center of the net. Thus, the discharge velocity vector at the center of the net has components  $v_e$  and  $v_f$ . From relations 23.12 we have

$$v_e = \frac{\Delta\Phi}{\Delta e} = \frac{\Delta\Psi}{\Delta f}$$

or

$$\Delta\Psi = \frac{\Delta f}{\Delta e} \Delta\Phi$$

By substituting  $\Delta q = \Delta\Psi$  and  $\Delta\Phi = k \Delta h$  we obtain for the flow rate in one flow channel

$$\Delta q = k \frac{\Delta f}{\Delta e} \Delta h$$

To simplify the computation of seepage, we construct the flow net such that  $\Delta f = \Delta e$ ; that is, such that every field is square. On this assumption, we obtain  $\Delta q = k \Delta h$ , where  $\Delta h$  is the potential drop between  $\Phi_2$  and  $\Phi_1$ . If  $h_L$  is the hydraulic head loss from upstream to downstream, and  $N_d$  is the number of potential drops ( $N_d = 8$  in Fig. 23.2), the potential drop is equal to

$$\Delta h = \frac{h_L}{N_d}$$

and

$$\Delta q = k \frac{h_L}{N_d}$$

If  $N_f$  is the total number of flow channels ( $N_f = 4$  in Fig. 23.2), the seepage  $q$  per unit of time per unit distance in the  $y$ -direction (unit of width of sheet piles in Fig. 23.2) is

$$q = k h_L \frac{N_f}{N_d} \quad (23.13)$$

By means of this equation the seepage can be computed readily, after the flow net has been constructed.

The porewater pressure at any point in the soil is computed from the definition of the hydraulic head,  $u = \gamma_w (h - z)$ .

The force of the hydraulic head on the upstream side of the cubical element 3 with side  $a$  in Fig. 23.2 is  $a^2 \times 6 \Delta h \gamma_w$ , whereas the force on the downstream side is  $a^2 \times 5 \Delta h \gamma_w$ . The difference between these two forces

$$P_s = a^2 \Delta h \gamma_w = a^3 \frac{\Delta h}{a} \gamma_w$$

is transferred by the water onto the soil skeleton. Because  $\Delta h/a$  is equal to the hydraulic gradient  $i$  and  $a^3$  is the volume of the element, the water exerts a pressure against the soil equal to

$$p_s = i \gamma_w \quad (23.14)$$

per unit of volume. This is known as the *volumetric seepage pressure*. It has the dimension of a unit weight, and at any point its line of action is tangent to the flow line.

### 23.5 Construction of Flow Net

The data required for plotting a flow net can be obtained by solving Laplace's equations for  $\Phi$  and  $\Psi$ , but an analytical solution is not practicable unless the boundary conditions are very simple. The boundary conditions corresponding to most hydraulic structures do not satisfy this condition. Computer software is available for solving many problems of practical interest, but the output provides the engineer with little insight into the reasonableness of the solutions. On the other hand, flow nets can be constructed graphically by trial and error to any desired accuracy and to satisfy even complex geometries and boundary conditions; in carrying out the construction, the engineer gains invaluable insight into the problem at hand. Even if a computer solution is used, it should be validated by a graphical flow net, the construction of which will greatly aid the engineer's judgment in assessing the critical features of a practical problem.

The steps in performing the graphical construction are illustrated in Fig. 23.4. In this figure *a* represents a vertical section through an overflow dam with a sheet-pile cutoff wall.

Before starting the construction of the flow net, we must examine the hydraulic boundary conditions of the problem and ascertain their effect on the shape of the flow lines. The upstream and downstream ground surfaces in Fig. 23.4*a* represent equipotential lines. The base of the dam and the sides of the cutoff wall represent the uppermost flow line, and the base of the pervious stratum represents the lowest flow line. The other flow lines lie between these two, and their shapes must represent a gradual transition from one to the other. Furthermore, all the flow lines must be vertical where they meet the upstream and downstream ground surfaces. The first step in constructing the flow net is to draw several smooth curves representing flow lines (plain curves in Fig. 23.4*b*) that satisfy these requirements. Then several equipotential lines, which should intersect the flow lines at right angles,

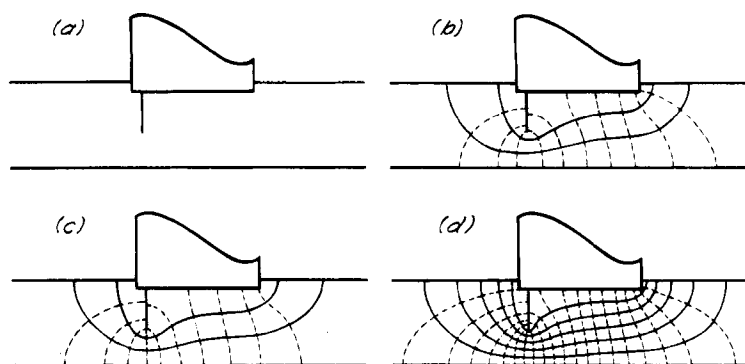


**Figure 23.4** Steps in constructing a flow net. (a) Cross-section through pervious stratum; (b) result of first attempt to construct flow net; (c) result of adjusting flow net constructed in (b); (d) final flow net.

are drawn so that the fields are at least roughly square. In this manner a first rough approximation to the flow net is obtained.

The next step is to examine the trial flow net carefully to detect the most conspicuous defects. In the trial flow net shown in Fig. 23.4b, the flow lines and the equipotential lines do intersect at approximately right angles, but several of the fields are not yet square. Therefore, a new flow net is drawn in which the fields are more nearly square. The process of adjustment is continued until all of the fields are roughly square. The flow net at this stage is represented by Fig. 23.4c.

Finally, the fields in Fig. 23.4c are subdivided, and the flow net is adjusted until each small field is square. The result is shown in Fig. 23.4d. Each field in Fig. 23.4c has been subdivided into four small fields, and minor inaccuracies have been eliminated.

For all practical purposes the flow net is satisfactory as soon as all the fields are roughly square. Even an apparently inaccurate flow net gives remarkably reliable results. Figures 23.5 and 23.6 may serve as a guide for constructing flow nets that satisfy various hydraulic boundary conditions. The flow net in Fig. 23.6a contains one line that represents a free-water surface located entirely within the pervious medium. Along this surface, the vertical distance between each adjacent pair of equipotential lines is a constant and is equal to  $\Delta h$ .

Every flow net is constructed on the assumption that the soil within a given stratum through which the water percolates is uniformly permeable. In a natural soil stratum, the permeability varies from point to point, especially along lines at right angles to the boundaries of the stratum. Therefore, the difference between even a very roughly sketched flow net and an accurate one is commonly small compared with the difference between the flow pattern in the real soil and that indicated by the accurate flow net. Because of this universal condition,

refinements in the construction of flow nets or elaborate model studies are entirely unwarranted.

The use of models based on the analogy between the flow of water in a pervious medium and the flow of electricity in a conductor affords a convenient means for constructing a flow net such as Fig. 23.6a that contains a free-water surface. However, assembling the necessary equipment is not warranted unless many flow nets of this type have to be drawn. Computer software is also available.

### 23.6 Seepage through Soils with Transverse Isotropy

The flow nets shown in Figs. 23.2 to 23.6 have been constructed on the assumption that the soil is hydraulically isotropic. In nature every mass of soil is more or less stratified. Therefore, as stated in Article 14.8, the average permeability  $k_x$  in a direction parallel to the planes of stratification is always greater than the average permeability  $k_z$  at right angles to these planes. To construct a flow net for such a stratified mass of soil, we substitute for the real soil a homogeneous material having horizontal and vertical permeabilities equal to  $k_x$  and  $k_z$ , respectively. A medium with such properties is said to possess *transverse isotropy*.

To prepare a flow net for a homogeneous medium with transverse isotropy, we proceed as follows: A drawing is made showing a vertical section through the permeable layer parallel to the direction of flow. The horizontal scale of the drawing is reduced by multiplying all horizontal dimensions by  $\sqrt{k_z/k_x}$ . For this transformed section we construct the flow net as if the medium were isotropic. The horizontal dimensions of this flow net are then increased by multiplying them by  $\sqrt{k_x/k_z}$ . The quantity of seepage is obtained by substituting the quantity,

$$k = \sqrt{k_x k_z}$$

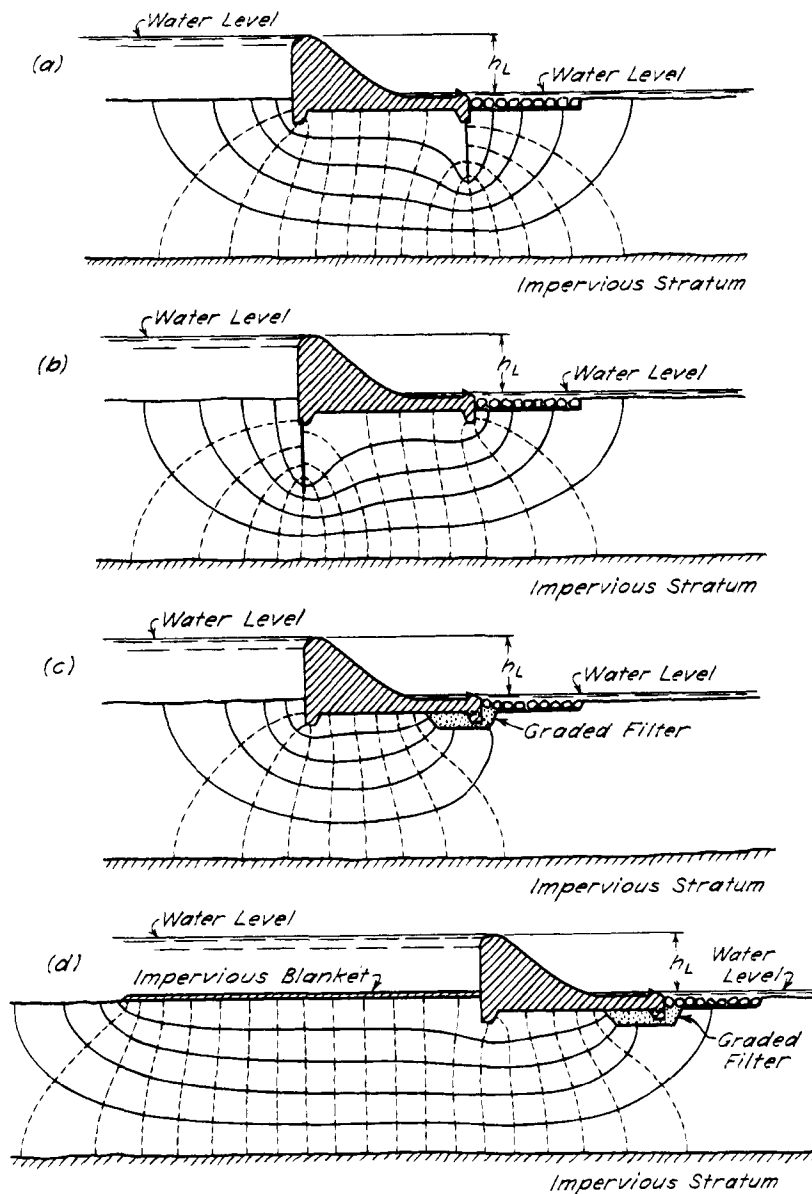


**Figure 23.5** Seepage through homogeneous sand beneath base of concrete dam (after Casagrande 1935a).

into Eq. 23.13. The expression for the quantity of seepage per unit width of the medium is then

$$q = h_L \frac{N_f}{N_d} \sqrt{k_x k_z} \quad (23.15)$$

The procedure is illustrated by Fig. 23.7.

The average value of  $k_x$  for almost all natural soil strata is considerably greater than  $k_z$ . However, the ratio  $k_x/k_z$  ranges from about two or three to several hundred, and there is no way to determine the value accurately for a given deposit. Therefore, it is advisable to sketch two flow nets, one on the basis of the greatest probable value for  $k_x/k_z$ , and the other on the basis of the least probable

one. In selecting these values, consideration should be given to the fact that  $k_x/k_z$  cannot be less than unity, nor greater than the ratio between the coefficients of permeability of the most and least permeable layers. For design purposes, that flow net should be retained that represents the most unfavorable conditions, or else provisions should be made to ascertain during construction whether the difference between the real and the anticipated seepage conditions is on the side of safety.

### 23.7 Seepage toward Single Well

Figure 23.8a is a vertical section through a well, with radius  $r_0$ , extending to the bottom of a pervious horizontal



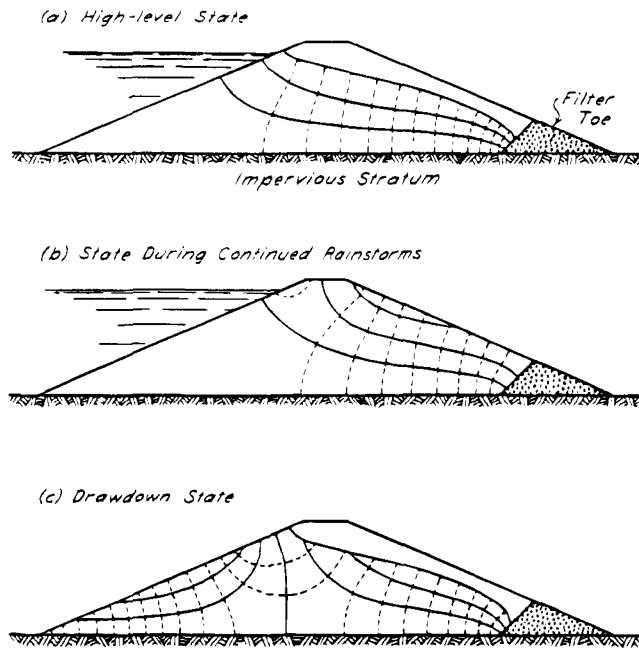


Figure 23.6 Seepage through imaginary homogeneous dam consisting of very fine clean sand.

layer located between impervious deposits. The layer has a thickness  $H_0$  and a uniform coefficient of permeability  $k$ . By pumping at a constant rate  $q$  from the well until a steady state of flow is achieved, the height of the water in the well with respect to the bottom of the pervious layer is lowered from  $H_1$  to  $H$ , and that in observation wells at distance  $r$  is lowered from  $H_1$  to  $h$ . It is assumed that the water flows toward the well in horizontal, radial directions. The total flow rate across the boundary of any cylindrical section of radius  $r$  is then, according to Eq. 14.4,

$$q = kiA = k \frac{dh}{dr} 2\pi r H_0$$

Whence, by integration

$$q = \int_{r_1}^{r_2} \frac{dr}{r} = 2\pi H_0 k \int_{h_1}^{h_2} dh$$

$$q = \frac{2\pi H_0 k (h_2 - h_1)}{\ln \frac{r_2}{r_1}} \quad (23.16)$$

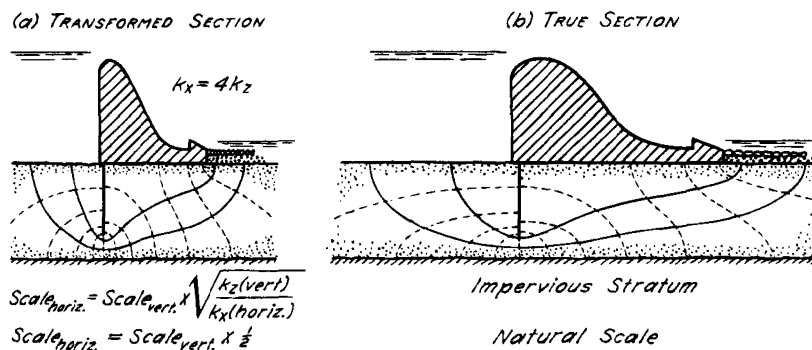


Figure 23.7 Construction of flow net if coefficients of permeability of sand stratum are different in horizontal and vertical directions.

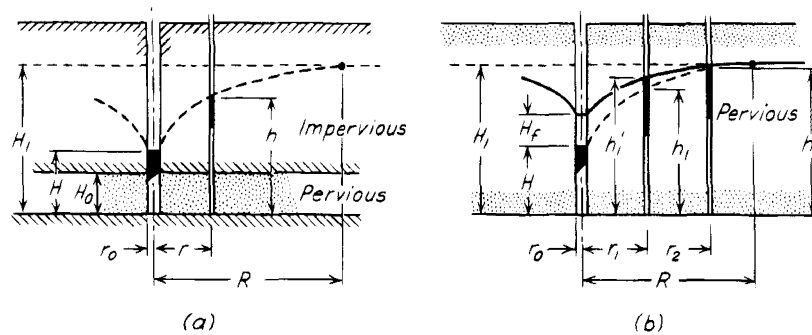


Figure 23.8 Diagram illustrating flow of water toward well during pumping test: (a) if piezometric level lies above pervious layer; (b) if free-water surface lies within pervious layer.

Or, if the well is being pumped to evaluate  $k$ ,

$$k = \frac{q}{2\pi H_0(h_2 - h_1)} \ln \frac{r_2}{r_1} \quad (23.17)$$

The permeability can be determined most accurately by measuring  $h_1$  and  $h_2$  at corresponding radii  $r_1$  and  $r_2$ . However, a rough estimate can be made by making use of the conditions that  $h_1 = H$  at  $r_1 = r_0$ , and that at a large value of  $r_2 = R$ ,  $h_2$  approaches  $H_1$ . The dimension  $R$ , known as the *radius of influence* of the well, represents the distance beyond which the water table remains essentially horizontal. It does not need to be known with accuracy because as  $R/r_0$  increases by a factor of 10,  $\ln(R/r_0)$  merely doubles. Hence, if at least the order of magnitude of  $R$  is known,  $k$  can be approximated without the assistance of observation wells.

If, on the other hand, the well penetrates to the bottom of an open pervious layer (Fig. 23.8b) the water table at the boundary of the well cannot be drawn down to the water level within the well itself because a considerable quantity of flow enters the well through the exposed free surface  $H_f$ . The discharge from such a well was first evaluated (Dupuit 1863) on the simplifying assumptions that  $H_f = 0$  (dash curve in Fig. 23.8b), and that at any radius  $r$  the hydraulic gradient causing horizontal flow toward the well is equal to the slope of the assumed drawdown curve at the radius  $r$ . On these assumptions

$$q = kiA = k \frac{dh}{dr} 2\pi rh$$

whence

$$q = \frac{\pi k(h_2^2 - h_1^2)}{\ln \frac{r_2}{r_1}} \quad (23.18)$$

or

$$k = \frac{q}{\pi(h_2^2 - h_1^2)} \ln \frac{r_2}{r_1} \quad (23.19)$$

For the boundary conditions  $h_1 = H$  at  $r_1 = r_0$  and  $h_2 = H_1$  at  $r_2 = R$ ,

$$q = \frac{\pi k(H_1^2 - H^2)}{\ln \frac{R}{r_0}} \quad (23.20)$$

Both theory (Boreli 1955) and experiments (Babbitt and Caldwell 1948) have demonstrated that Eq. 23.20 leads to reliable values of  $q$  even if  $H$  is reduced to zero. On the other hand, the difference between the ordinates  $h_1$  and  $h_1'$  of the Dupuit drawdown curve and that determined by taking proper account of the presence of the discharge surface  $H_f$  becomes significant at distances from the well less than about 1.0 to 1.5  $H_1$  and increases rapidly as the well is approached or as  $H$  decreases.

## Problems

1. The sand beneath the dams shown in Fig. 23.5 has a permeability in every direction of  $4 \times 10^{-5}$  m/s. The head  $h_L$  is 8 m. Compute the seepage loss in cubic meters per day per lineal meter along the axis of each dam.

Ans. 9.2, 9.2, 15.4, 6.9 m<sup>3</sup>/day

2. Estimate the hydrostatic uplift pressure in excess of that at tailwater level, at a point midway between the upstream and downstream faces of the concrete base of the dams of problem 1.

Ans. 4.8, 2.7, 1.8, 0.8 m of head.

3. The subsoil of the dam shown in Fig. 23.3b contains a horizontal layer of silt, 3 cm thick, that intersects the row of sheet piles a short distance above the bottom of the piles. There are no means for detecting the presence of such a layer by any practicable method of soil exploration. The coefficient of permeability of the sand is  $4 \times 10^{-5}$  m/s, whereas that of the silt is  $2 \times 10^{-8}$  m/s. The total thickness of the sand stratum upstream from the dam is 17.6m, and the lower edge of the sheet piles is located 8 m above the base of the sand. (a) Describe how the influence of the silt layer on the seepage loss could be evaluated on the assumption that the silt layer is continuous over a large area. (b) Describe the effect on the seepage loss of gaps in the silt layer. (c) How can the degree of continuity of the silt layer be determined in advance?

Ans. (a) The silt layer has the same effect as increasing the thickness of the sand layer from 17.6 to 77.6m, and the penetration of the sheet piles from 9.6 to 69.6m. Therefore, the seepage loss could be evaluated by sketching a flow net for these fictitious soil conditions. Because the gap beneath the sheet piles in the fictitious profile is small compared with the depth of sheet-pile penetration, the loss of water computed on the basis of this flow net would be only a small fraction of that through the sand without a silt layer. (b) Depending on the size and location of the gaps in the layer, a discontinuous silt layer may have any effect varying from almost nothing to that of a continuous layer. (c) It cannot.

4. Compute the seepage loss per meter of length of the dam shown in Fig. 58.6b, assuming  $k = 1 \times 10^{-5}$  m/s. Estimate the uplift pressure on the base of the dam at the back of the high masonry section.

Ans. 9.07 m<sup>3</sup>/day/m; 19.6 m of head.

5. The average coefficient of permeability of the stratified sand beneath the dam shown in Fig. 23.7 is  $16 \times 10^{-6}$  m/s in the horizontal direction and  $4 \times 10^{-6}$  m/s in the vertical direction. What is the seepage loss per lineal meter of dam, when the head is 10 m?

Ans. 1.73 m<sup>3</sup>/day/m.

6. Construct the flow net for the dam shown in Fig. 23.7 if the value of  $k$  is equal to  $36 \times 10^{-6}$  m/s in the horizontal direction and  $4 \times 10^{-6}$  m/s in the vertical direction. The base width of the dam is 25 m, the thickness of the pervious layer is 11.5 m, and the length of the sheet piles is 9 m. The head is 10m. What is the seepage loss per lineal foot of dam? Compare this value with the seepage loss beneath the same dam if  $k$  is equal to  $12 \times 10^{-6}$  m/s in every direction.

Ans.  $3.46; 2.25 \text{ m}^3/\text{day}/\text{m}$ .

7. What is the approximate intensity of the horizontal hydrostatic excess pressure against the left-hand side of the sheet-pile wall in Fig. 58.6a at the lowest point of the wall?

Ans.  $128 \text{ kPa}/\text{m}$ .

### Selected Reading

Casagrande, A. (1935b). "Seepage through dams," *J. New England Water-Works Assn.*, **51**, No. 2, pp. 131–172. Reprinted in *Contributions to soil mechanics 1925–1940* Boston Soc. of Civil Engrs., 1940, and as *Harvard Univ. Soil Mech. Series No. 5*. A classic presentation of the flow-net method and its applications.

The following treatises deal with advanced aspects of seepage computations:

Muskat, M. (1937). *The Flow of Homogeneous Fluids through Porous Media*, New York, McGraw-Hill, 763 pp. Reprinted by J. W. Edwards, Ann Arbor, 1946.

Polubarinova-Kochina, P. Ya. (1962). *Theory of ground water movement*. Translated from the Russian by J. M. R. de Wiest, Princeton Univ. Press, 613 pp.

Harr, M. E. (1962). *Groundwater and Seepage*. New York, McGraw-Hill, 315 pp.

Rushton, K.R. and S.C. Redshaw (1979). *Seepage and Groundwater Flow*, John Wiley & Sons, Inc., New York, 339 pp.

An excellent presentation of the fundamentals of seepage, with applications, is contained in Cedergren, H. R. (1989): *Seepage, drainage, and flow nets*, New York, 3rd ed., John Wiley and Sons, 465 pp.

## ARTICLE 24 MECHANICS OF PIPING

### 24.1 Definition of Piping

Many dams on soil foundations have failed by the apparently sudden formation of a pipe-shaped discharge channel or tunnel located between the soil and the foundation. As the stored water rushed out of the reservoir into the outlet passage, the width and depth of the passage increased rapidly until the structure, deprived of its foundation, collapsed and broke into fragments that were carried away by the torrent. An event of this type is known as a *failure by piping*.

Failures by piping can be caused by two different processes. They may be due to scour or subsurface erosion that starts at springs near the downstream toe and proceeds upstream along the base of the structure or some bedding plane (Article 58). Failure occurs as soon as the upstream or intake end of the eroded hole approaches the bottom of the reservoir. The mechanics of this type of piping defy theoretical approach. However, piping failures have also been initiated by the sudden rise of a large body of soil adjoining the downstream toe of the structure. A failure of this kind occurs only if the seepage pressure of the water that percolates upward through the soil beneath the toe becomes greater than the effective weight

of the soil. Failures of the first category will be referred to as *failures by subsurface erosion*, and those of the second as *failures by heave*. The following paragraphs deal exclusively with failures by heave.

The magnitude and distribution of the excess hydrostatic pressure are determined by the flow net. In Article 23 it was emphasized that the theoretical flow net is never identical with the one that represents the flow of water through the real soil strata. Indeed, the two flow nets may have no resemblance whatsoever. Therefore, the results of theoretical investigations into the mechanical effects of the flow of seepage serve merely as a guide for judgment and as a basis for planning appropriate installations for surveillance during and after construction.

### 24.2 Mechanics of Piping due to Heave

The mechanics of failure by piping due to heave are illustrated by Fig. 24.1a which represents a vertical section through one side of a single-wall sheet-pile cofferdam. To a depth  $h_1$  below the water level, the soil outside the cofferdam consists of coarse gravel, whereas the gravel within the cofferdam has been removed by dredging. The gravel rests on a bed of uniform sand. The loss of head in the gravel is so small that it can be disregarded. We wish to compute the factor of safety  $F$  with respect to piping, after the water level on the inside has been pumped down to the surface of the sand.

Before making this computation, we shall consider the hydrostatic conditions at the instant of failure. As soon as the water level within the cofferdam is lowered by pumping, water begins to flow downward through the sand on the left side of the sheet piles and upward on the right. The excess hydrostatic pressure on a horizontal section such as  $Ox$  (Fig. 24.1b) reduces the effective pressure on that section. As soon as the average effective pressure on and above a portion of  $Ox$  near the sheet piles becomes equal to zero, the water that flows through the sand can straighten and widen the flow channels without meeting any resistance. This process greatly increases the permeability of the sand adjoining the sheet

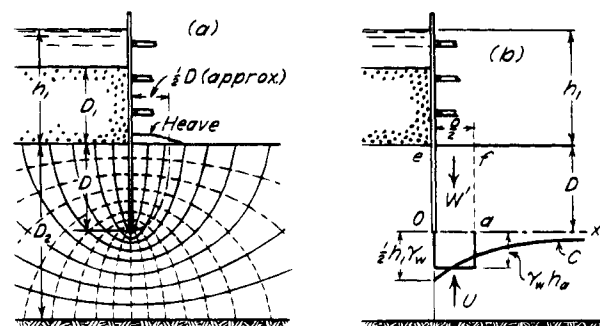


**Figure 24.1** Use of flow net to determine factor of safety of row of sheet piles in sand with respect to piping. (a) Flow net; (b) forces acting on sand within zone of potential heave.

piles, as explained in Article 15.4, and it diverts an additional part of the seepage toward this zone. The surface of the sand then rises (see Fig. 24.1a). Finally, the sand starts to boil, and a mixture of water and sand rushes from the upstream side of the sheet piles, through the space below the lower edge of the sheet piles, and toward the zone where the boiling started.

By model tests (Terzaghi 1922) it has been found that the rise of the sand occurs within a distance of about  $D/2$  from the sheet piles. The failure, therefore, starts within a prism of sand having a depth  $D$  and a width  $D/2$ . At the instant of failure the effective vertical pressure on any horizontal section through the prism is approximately equal to zero. At the same time the effective lateral pressure on the sides of the prism is also approximately zero. Therefore, piping occurs as soon as the excess hydrostatic pressure on the base of the prism becomes equal to the effective weight of the overlying sand.

To compute the excess hydrostatic pressure a flow net must be constructed. After this has been done (Fig. 24.1a) the intensity of this pressure can be determined readily at every point on the base of the prism at depth  $D$  by means of the procedure described in Article 23. In Fig. 24.1b these values are represented by the ordinates of curve  $C$  with reference to a horizontal axis through  $O$ . Within the distance  $D/2$  from the sheet piles the average excess hydrostatic pressure on the base of the prism has the value  $\gamma_w h_a$ , and the total excess hydrostatic pressure on the base is  $U = \frac{1}{2} D \gamma_w h_a$ . Failure by piping occurs as soon as  $U$  becomes equal to the effective weight of the sand which, in turn, is equal to the submerged weight  $W' = \frac{1}{2} D^2 \gamma'$ . Therefore, the factor of safety with respect to piping is

$$F = \frac{W'}{U} = \frac{D\gamma'}{h_a\gamma_w} \quad (24.1)$$

In a similar manner, we may compute the factor of safety for a dam with a sheet-pile cutoff.

### 24.3 Uplift Compensation by Loaded Filters

If the factor of safety against failure by piping is too small, it may be increased by establishing on top of the prism *Oafe* (Fig. 24.1b) an inverted filter which has a weight  $W$ . The presence of the filter does not alter the excess hydrostatic pressure  $U$ , but it increases the effective weight of the prism from  $W'$  to  $W' + W$ . Hence, it increases the factor of safety with respect to piping from  $F$  (Eq. 24.1) to

$$F' = \frac{W + W'}{U} \quad (24.2)$$

The stabilizing effect of loaded inverted filters has been demonstrated repeatedly by experiment and by experience with filter-protected structures. To be effective, the filters

must be coarse enough to permit the free outflow of the seepage water, but fine enough to prevent the escape of soil particles through their voids. The design of filters to satisfy both requirements is discussed in Article 14.9.

### Problems

1. In Fig. 24.1 the head  $h_L$  is 7.6 m. The penetration of the sheet piles into the sand layer is 5.8 m. If the saturated unit weight of the sand is  $18.1 \text{ kN/m}^3$ , what is the weight of an inverted filter required to increase the factor of safety with respect to piping to 2.5?

Ans. 16 kPa.

2. The sand layer mentioned in problem 1 contains a seam of clay too thin to be detected by the boring crew, but thick enough to constitute a relatively impermeable membrane. The numerical data regarding the head and the depth of sheet piles are identical with those given in problem 1. The clay seam is located within a meter above the lower edge of the sheet piles. Its left-hand boundary is located within a meter upstream from the sheet piles, and on the downstream side it is continuous. On the downstream side the sand stratum carries an inverted filter weighing 16 kPa which provides a factor of safety of 2.5 on the assumption that the sand contains no obstacle against flow. (a) To what value does the clay seam reduce the factor of safety? (b) What procedure could be used to detect the danger?

Ans. (a) 0.83. The sand at the downstream side of the sheet piles would blow up as soon as the head reached 6.4 m. (b) Install a single observation well on the downstream side of the sheet piles, with its lower end within a meter below the level of the bottom of the sheet-pile wall.

## ARTICLE 25 THEORY OF CONSOLIDATION

### 25.1 Process of Consolidation

If the load on a layer of saturated soil such as clay is increased, the layer is compressed, and excess water drains out of it. This constitutes a process of *consolidation* (Article 16). During the process the quantity of water that leaves a thin horizontal slice of the soil is larger than the quantity that enters it. The difference is equal to the decrease in volume of the layer; thus the continuity condition expressed by Eq. 23.1 is applicable.

The added pressure or load per unit of area that produces the consolidation is known as the *consolidation pressure increment*. At the instant of its application, it is carried almost entirely by the water in the voids of the soil (see Article 16). Therefore, at the beginning of a process of consolidation, there is an initial excess pressure in the water almost exactly equal to the consolidation pressure increment. As time goes on, the excess porewater pressure decreases, and the effective vertical pressure in the layer correspondingly increases. At any point within the consolidating layer, the value  $u'$  of the excess porewater pressure at a given time may be determined from

$$u' = u - u_s \quad (25.1)$$

in which  $u$  is the total porewater pressure and  $u_s$  is the reference static or steady-state porewater pressure in the consolidating layer. At the end of primary consolidation the excess porewater pressure  $u'$  becomes equal to zero, and the entire consolidation pressure increment becomes an effective stress transmitted through the structure of the soil. If the consolidation pressure increment at any point is denoted by  $\Delta\sigma_v$ , equilibrium requires that

$$\Delta\sigma_v = \Delta\sigma'_v + u' \quad (25.2)$$

Here  $\Delta\sigma'_v$  represents that portion of the consolidation stress increment which, at a given time, is transmitted through the structure of soil and  $u'$  is the corresponding excess porewater pressure.

In Article 16 it was pointed out that the consolidation of a layer may be considered to consist of two stages: the *primary consolidation* stage during which the applied consolidation stress increment is transferred from the pore water to the soil skeleton, and the *secondary consolidation* stage that follows the end of the primary phase (*EOP*). Empirical methods were developed for predicting the rate and amount of secondary consolidation on the basis of laboratory data (Article 16.7). Procedures were also described for predicting the total magnitude of *EOP* consolidation but not of the rate of its development; that is, the magnitude of the rate of transfer of the excess porewater pressure  $u'$  to effective vertical pressure  $\Delta\sigma'_v$ , (Eq. 25.2). The *theory of consolidation* is concerned with this phenomenon, often referred to as the *hydrodynamic lag*; its publication (Terzaghi 1923a), with its clear implication of the concept of effective and porewater stresses, is often considered to mark the beginning of modern soil mechanics.

## 25.2 Progress of Consolidation

Because  $\Delta\sigma_v$  in Eq. 25.2 is a constant, the progress of consolidation at a given point can be visualized by observing the variation of  $u'$  at that point.

Figure 25.1 illustrates the consolidation of a compressible layer located between two layers of sand. Because of the construction of a large building or the placement of a fill on the ground surface, the compressible layer is subjected to a consolidation stress increment  $\Delta\sigma_v$ . It is assumed that  $\Delta\sigma_v$  does not vary from top to bottom of the layer. Furthermore, it is assumed that the layer can drain freely at both its upper and lower surfaces and that within the layer the water flows only in a vertical direction.

The progress of consolidation within the layer can be studied by observing the porewater pressure at a number of points on a vertical line through the layer. Porewater pressure observations at five elevations, points 1 through 5, and at two stages of consolidation are shown in Fig.

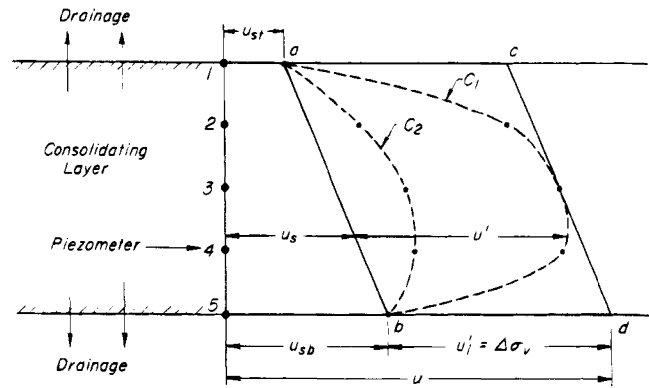


**Figure 25.1** Diagram illustrating consolidation of a layer of clay between two pervious layers.

25.1. The reference porewater pressure  $u_s$  in Fig. 25.1 corresponds to a hydrostatic condition with values of  $u_{st}$  and  $u_{sb}$  at the top and bottom of the layer, respectively. Its distribution corresponds to the porewater pressure condition in the layer before the application of load. It also represents the porewater pressure condition at the end of the primary consolidation stage when the excess porewater pressure throughout the layer has dissipated to zero. In some field situations, however, the hydrostatic or steady-state porewater pressure condition to which the excess porewater pressure is referenced may change during the long primary consolidation stage. This might occur, for example, because of a gradual rise of the water table under an embankment.

The distribution of the porewater pressure  $u$  through the consolidating layer immediately after the application of load is represented by line  $cd$ . The distribution of the initial excess porewater pressure  $u'_i$  through the layer is the difference between the porewater pressures defined by lines  $cd$  and  $ab$ . Therefore, for the type of loading illustrated in Fig. 25.1, the initial excess porewater pressure is constant with depth. Immediately after the application of load, water from the consolidating layer begins to flow toward the drainage boundaries and the excess porewater pressure begins to dissipate. According to Article 16, the consolidation of a layer of clay proceeds from the drainage surface or surfaces toward the interior. Hence, at an early stage of consolidation the porewater pressures for the central part of the layer are still unchanged, whereas those for the outer points have already dropped as shown by the isochrone  $C_1$ . In a more advanced stage, represented by  $C_2$ , the porewater pressures at all depths have dropped, and  $u'$  decreases from the central part toward zero at the drainage surfaces. Finally, at  $t = t_p$  all excess porewater pressure disappears and the final isochrone is represented by the line  $ab$ .

Consolidation of a uniform soft clay from Berthierville, Canada ( $w_o = 56$ – $61\%$ ;  $w_l = 46\%$ ;  $w_p = 24\%$ , and  $\sigma'_p/\sigma'_{vo} = 1.31$ ) is illustrated in Fig. 25.2 by the results

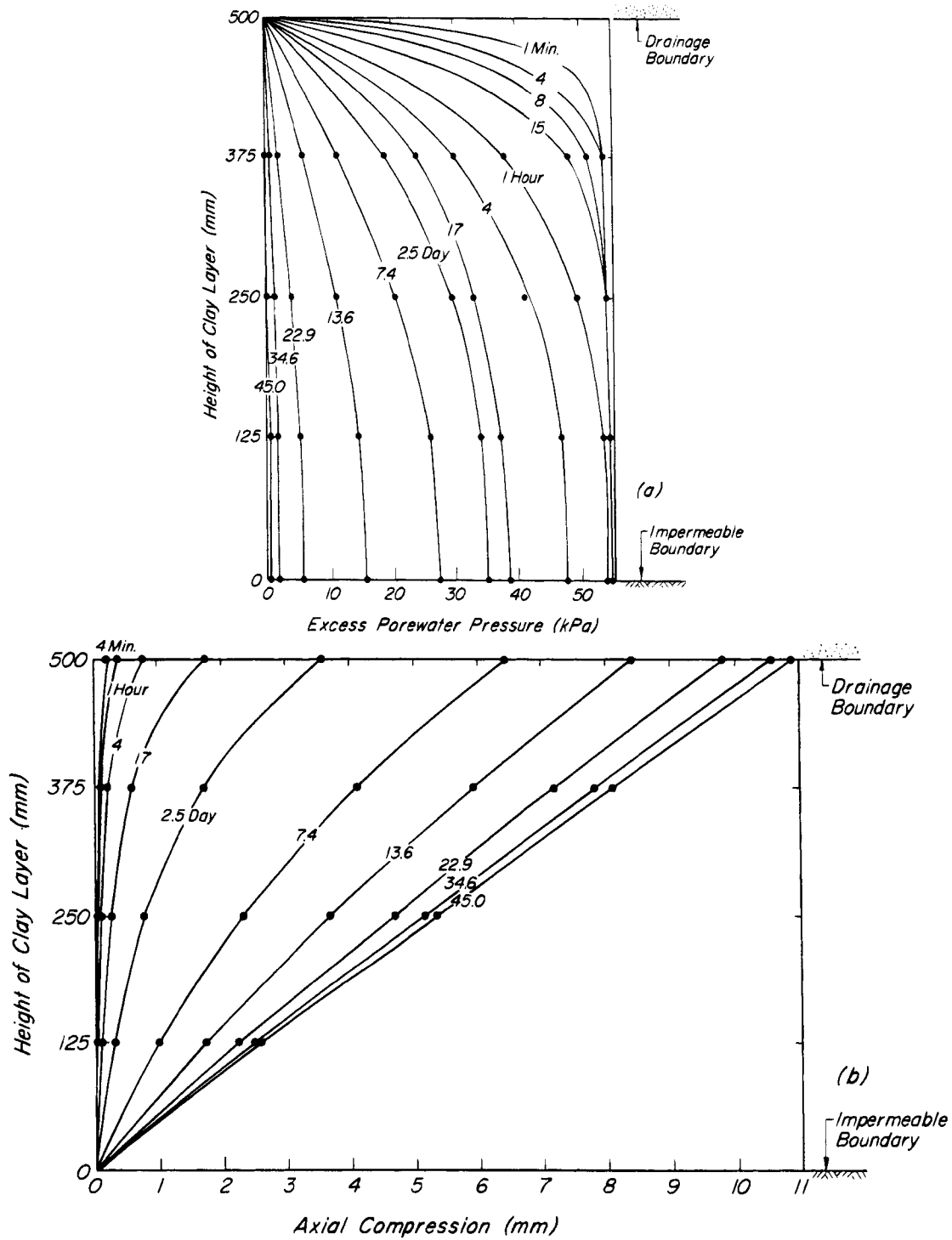


**Figure 25.2** (a) Observed distribution of excess porewater pressure during consolidation of a soft clay layer; (b) observed distribution of vertical compression during consolidation of a soft clay layer.

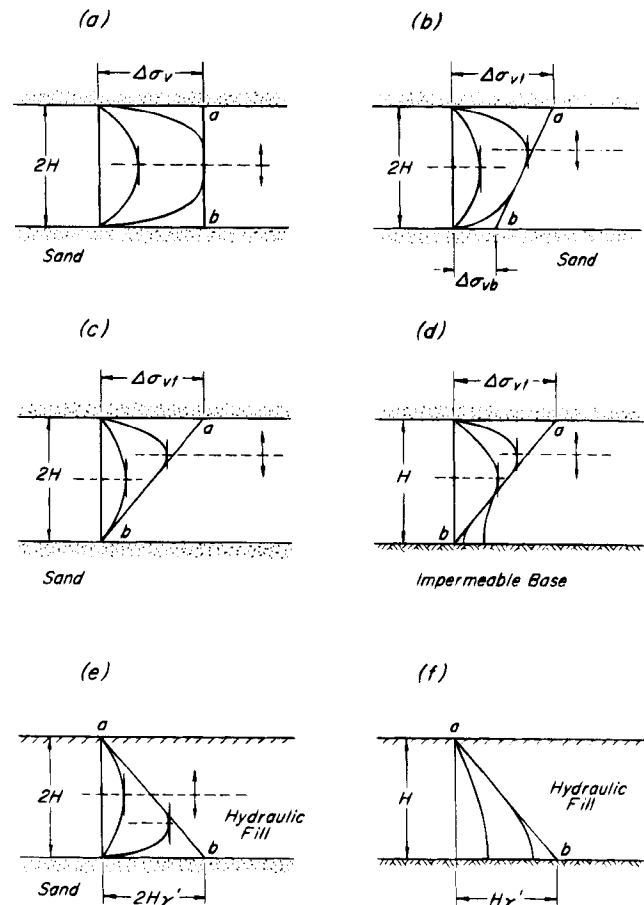
of measurements of excess porewater pressure and vertical compression. The measurements were carried out on a specimen 500 mm thick with a freely draining top and an impermeable bottom boundary (Mesri and Choi 1985b, Mesri and Feng 1986). The consolidation pressure increment of 55 kPa, from 83 to 138 kPa, was completely in the compression range. At the instant of application of the increment, an excess porewater pressure of 55 kPa was measured throughout the height of the clay layer. The measurements of excess porewater pressure and axial compression both showed that consolidation of the clay layer progressed from the top drainage surface toward the impermeable bottom boundary. Therefore, at the early stages of consolidation, the effective stresses and void ratios near the impermeable boundary of the layer were still unchanged, whereas near the drainage boundary the effective stresses increased and the void ratios decreased. As the end of primary consolidation was reached throughout the height of the layer in about 45 days, the excess porewater pressures approached zero and the axial compressive strain became practically uniform from top to bottom of the layer.

Figure 25.3 shows isochrones for different initial and boundary conditions. If the consolidating layer is free to drain through both its upper and lower surfaces, the layer is called an *open layer*, and its thickness is denoted by  $2H$ . If the water can escape through only one surface, the layer is called *half-closed*. The thickness of half-closed layers is denoted by  $H$ . In Fig. 25.3, the layers labeled *a*, *b*, *c*, and *e* are open, whereas the layers *d* and *f* are half-closed.

Figure 25.3a is a simplified replica of Fig. 25.1 in which the reference pressure  $u_s$  is not shown. The diagram represents the consolidation of an open layer of clay under the influence of a consolidation stress increment that is uniform from top to bottom of the layer.

If the consolidating layer is fairly thick with respect to the width of the loaded area, the consolidation pressure increment due to the weight of a structure or a fill decreases with depth in a manner similar to that indicated by the curve  $C_a$  (Fig. 40.6). Under the simplifying assumption that the decrease of the pressure with depth is linear, the initial isochrone may be represented by the line  $ab$  in Fig. 25.3b, and the consolidation pressure increments at the top and bottom of the layer are  $\Delta\sigma_{vt}$  and  $\Delta\sigma_{vb}$ , respectively.

If the consolidating layer is very thick compared with the width of the loaded area, the pressure  $\Delta\sigma_{vb}$  is likely to be very small compared with  $\Delta\sigma_{vt}$ . Under this condition it can be assumed with sufficient accuracy that  $\Delta\sigma_{vb} = 0$ . The corresponding isochrones are shown in Fig. 25.3c for an open layer, and in Fig. 25.3d for a half-closed layer. It should be noticed that the consolidation of the half-closed layer in Fig. 25.3d is associated with



**Figure 25.3** Isochrones representing progress of consolidation of a clay layer for different distributions of excess porewater pressures and different drainage boundary conditions (modified from Terzaghi and Fröhlich 1936).

a temporary swelling of the clay in the lower part of the layer.

Figure 25.3 *e* and *f* illustrates the consolidation of hydraulically placed layers acted on by no force other than their own weight. The consolidation that occurs during construction is disregarded. The fill shown in Fig. 25.3e rests on a stratum of sand (open layer), whereas that in Fig. 25.3f rests on an impermeable stratum (half-closed layer). At a time  $t = 0$ , the entire submerged weight of the soil in either layer ( $\gamma'$  per unit of volume) is carried by the water, and the consolidation pressure increment increases from zero at the surface to  $H\gamma'$  at the base. Therefore, the final result of the consolidation is the same for both layers. However, the difference in the shape of the isochrones for intermediate stages of consolidation indicates that the rate at which the final stage is approached is very different for the two layers.

### 25.3 Computation of Rate of Consolidation

On the assumption that the excess water drains out only along vertical lines, an analytical procedure can be devel-

oped for computing the rate of consolidation for processes such as those illustrated in Fig. 25.3. The continuity equation for one-dimensional flow in the vertical direction (Eq. 23.1) is

$$\frac{\partial v_z}{\partial z} dx dy dz = -\frac{\partial}{\partial t} (n dx dy dz)$$

The Darcy equation in terms of excess porewater pressure is

$$v_z = -\frac{k_v}{\gamma_w} \frac{\partial u'}{\partial z}$$

Assuming that the coefficient of permeability  $k_v$  is the same at every point in the consolidating layer and for every stage of consolidation, and expressing the porosity  $n$  in terms of void ratio  $e$ , we obtain

$$\frac{k_v}{\gamma_w} \frac{\partial^2 u'}{\partial z^2} dx dy dz = \frac{\partial}{\partial t} \left( \frac{e}{1+e} dx dy dz \right)$$

If we assume that the changes in void ratio during consolidation are small,  $(1+e)$  can be approximated by  $(1+e_0)$ , where  $e_0$  is the initial void ratio of the consolidating element and  $e$  is the current void ratio during consolidation. Then,  $(dx dy dz)/(1+e_0)$ , which is equal to the volume of the solids in the element, is independent of time, and we have

$$\frac{k_v}{\gamma_w} \frac{\partial^2 u'}{\partial z^2} dx dy dz = \frac{\partial e}{\partial t} \frac{dx dy dz}{1+e}$$

or

$$\frac{k_v}{\gamma_w} \frac{\partial^2 u'}{\partial z^2} = \frac{1}{1+e} \frac{\partial e}{\partial t} \quad (25.3)$$

Equation 25.3 is the hydrodynamic equation of one-dimensional consolidation based on the assumptions that the coefficient of permeability is constant and the strains are small during consolidation.

If we assume that the time lag of the compression is caused exclusively by the finite permeability of the soil, so that in Eq. 16.1  $a_{vt} = 0$ , and if we assume further that in Eq. 16.1  $a_{vs}$  is equal to  $-a_v$ , which is the same at every point in the layer and for every stage of consolidation, then Eq. 16.1 becomes

$$\frac{de}{dt} = a_v \frac{d\sigma'_v}{dt}$$

If the total vertical stress  $\sigma_v$  and the reference porewater pressure  $u_s$  remain unchanged during consolidation, then  $d\sigma'_v/dt = -du'/dt$ , and Eq. 25.3 becomes

$$\frac{k_v}{\gamma_w} \frac{\partial^2 u'}{\partial z^2} = \frac{a_v}{1+e} \frac{\partial u'}{\partial t}$$

In terms of  $m_v = a_v/(1+e)$ , where  $m_v = \Delta \epsilon_v / \Delta \sigma'_v$  and  $\epsilon_v$  is vertical strain, we have

$$\frac{1}{\gamma_w} \frac{k_v}{m_v} \frac{\partial^2 u'}{\partial z^2} = \frac{\partial u'}{\partial t}$$

By introducing the coefficient of consolidation  $c_v$  defined as

$$c_v = \frac{1}{\gamma_w} \frac{k_v}{m_v} \quad (25.4)$$

we obtain

$$c_v \frac{\partial^2 u'}{\partial z^2} = \frac{\partial u'}{\partial t} \quad (25.5)$$

The dependent variable  $u'$  is a function of the independent variables  $z$  and  $t$ . In the partial differential Eq. 25.5,  $u'$  is differentiated twice with respect to  $z$  and once with respect to  $t$ . Consequently, the solution of Eq. 25.5 requires two boundary conditions in terms of  $z$  and an initial condition in terms of  $t$ . These conditions depend on the drainage boundaries and the loading as shown in the diagrams in Fig. 25.3. The boundary conditions that determine the consolidation of a half-closed layer and a uniform consolidation pressure increment in Fig. 25.4 may serve as an example. The initial condition is

At  $t = 0$  and at any distance  $z$  from the impermeable surface, the excess porewater pressure is equal to  $\Delta \sigma_v$ ; that is  $u'(z, 0) = \Delta \sigma_v$ .

The boundary conditions are

At any time  $t$  other than zero at the drainage surface  $z = H$ , the excess porewater pressure is zero; that is  $u'(H, t) = 0$ .

At any time  $t$  other than zero at the impermeable surface  $z = 0$ , the hydraulic gradient is zero; that is  $\partial u' / \partial z (0, t) = 0$ .

The differential Eq. 25.5 can be solved subject to any set of initial and boundary conditions to obtain an expres-

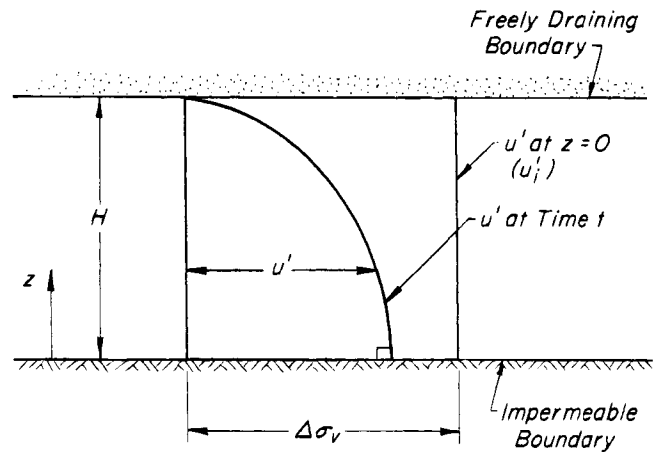


Figure 25.4 Isochrone for half-closed layer subjected to a uniform initial excess porewater pressure distribution.



sion for the excess porewater pressure. A solution using the Fourier expansion method leads to

$$u'(z, t) = \Delta\sigma_v \sum_{m=0}^{\infty} \frac{2}{M} \sin\left(M \frac{z}{H}\right) \exp(-M^2 T_v) \quad (25.6)$$

where  $M = \pi (2m + 1)/2$ ,

$$T_v = \frac{c_v t}{H^2} \quad (25.7)$$

is a pure number called the *time factor*, and  $H$  is the maximum drainage distance.

The *degree of compression* of a sublayer during consolidation is

$$U(z, t) = \frac{e_0 - e}{e_0 - e_p} \quad (25.8)$$

where  $e_p$  is the void ratio when the excess porewater pressure becomes zero. Because a linear time-independent relationship between void ratio and effective vertical stress is assumed in formulating the theory of consolidation represented by Eq. 25.5, the degree of compression defined by Eq. 25.8 is identical with the degree of effective vertical stress increase. This in turn is equal to the degree of excess porewater pressure dissipation

$$U(z, t) = \frac{u'_i - u'}{u'_i}$$

The degree of consolidation of the layer of thickness  $H$  is

$$U = \frac{s}{s_p} \quad (25.9)$$

where  $s_p$  is the settlement of the layer when the excess porewater pressure becomes zero throughout the thickness  $H$ . The expression for  $U$  as a function of the time factor  $T_v$  is obtained by integrating with respect to  $z$  the degree of excess porewater pressure dissipation of the sublayers. For example, from Eq. 25.6 we obtain

$$U = 1 - \sum_{m=0}^{\infty} \frac{2}{M^2} \exp(-M^2 T_v) \quad (25.10)$$

Equation 25.5 can be solved to obtain excess porewater pressure isochrones and  $U = f(T_v)$  for any set of initial and boundary conditions such as those in Fig. 25.3. Several  $U - T_v$  curves are shown in Fig. 25.5. For an open layer (thickness  $2H$ ) the relationship between  $U$  and  $T_v$  is determined by Eq. 25.10 and the curve  $C_1$  for all cases in which the initial excess porewater pressure varies linearly with  $z$ . Therefore, the curve  $C_1$  represents the solution for all the initial and boundary conditions represented by Fig. 25.3 *a*, *b*, *c*, and *e*. If the initial excess porewater pressure is uniform throughout the consolidating layer,

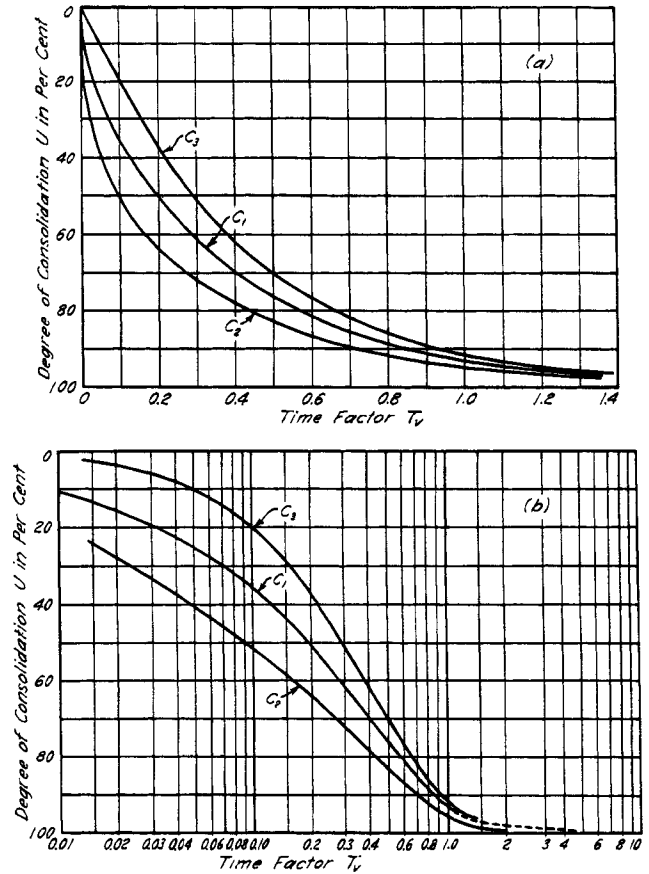


**Figure 25.5** Relation between degree of consolidation and time factor. In (a) the time factor is plotted to an arithmetic and in (b) to a logarithmic scale. The curves  $C_1$ ,  $C_2$ , and  $C_3$  correspond to different conditions of loading and drainage, represented by *a*, *d*, and *f*, respectively, in Fig. 25.3 (after Terzaghi and Fröhlich 1936).

curve  $C_1$  also represents the rate of consolidation for a half-closed layer with thickness  $H$ .

If the consolidation pressure increment for a half-closed layer decreases from some value  $\Delta\sigma_{v_i}$  at the top to zero at the bottom, as shown in Fig. 25.3*d*, the relation between  $U$  and  $T_v$  is given by the curve  $C_2$ . If it increases from zero at the top to  $\Delta\sigma_{v_b}$  at the bottom, as in Fig. 25.3*f*, the relation is given by curve  $C_3$ . Figure 25.5*b* shows the curves  $C_1$  to  $C_3$  plotted to a semilogarithmic scale from which small values of  $U$  can be obtained more accurately. In the arithmetic plot, Fig. 25.5*a*, the initial part of the curve  $C_1$  has a parabolic shape. In fact, up to a degree of consolidation of 60% the relation between  $U$  and  $T_v$  is accurately defined by  $U = 2 \sqrt{T_v/\pi}$ .

The coefficient of consolidation  $c_v$  at any  $\sigma'_v$  is either computed by using Eq. 25.4 after directly measuring  $k_v$  and taking  $m_v$  (Eq. 25.3*a*) from the EOP  $e$  vs  $\sigma'_v$  curve, or it is determined from the definition of the time factor by Eq. 25.7. In the latter procedure it is usual to compute

$c_v = 0.2 H^2 / t_{50}$ , where the time factor 0.2 from curve  $C_1$  in Fig. 25.5 (which is applicable to the commonly used double-drained incremental loading oedometer test) corresponds to the elapsed time  $t_{50}$  required to complete 50% primary consolidation (Casagrande and Fadum 1940; Taylor 1948). Alternative graphical interpretations of the theory of consolidation for estimating  $c_v$  from settlement vs time data have also been used (e.g., Asaoka 1978). Values of  $c_v$  computed using Eq. 25.4 together with direct measurements of  $k_v$  are shown in Fig. 25.6. The magnitude of  $c_v$  in the recompression range is generally larger than that in the compression range. The abrupt decrease in  $c_v$  near the preconsolidation pressure in some clays reflects the change in  $m_v$  as the soil passes from the recompression to the compression range. The ratio of  $c_v$  in recompression to that in compression ranges from about 100 for a highly structured soft clay from eastern Canada to about 2 for a Boston Blue clay overconsolidated by desiccation. For typical soft clays, however, the ratio is in the range of 5 to 10. The value of  $c_v$  is practically constant in the recompression range. In the compression range, it either remains constant or increases moderately with increasing  $\sigma'_v$ . Data on  $c_v$  in the compression range for a large number

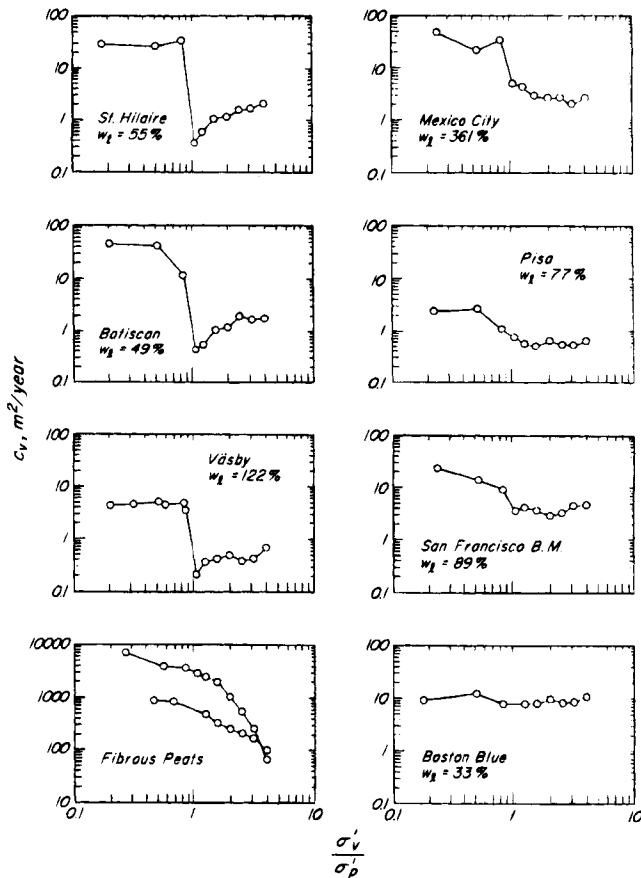


**Figure 25.6** Coefficient of consolidation of various soils as a function of the consolidation pressure  $\sigma'_v$ .

of clays are plotted in Fig. 25.7. Although in a general way  $c_v$  decreases with increasing liquid limit, for clays with a given liquid limit  $c_v$  varies widely.

#### 25.4 Other Initial and Boundary Conditions

It is obvious that the predictions of the time rate of settlement are not even approximately correct unless the assumed hydraulic boundary conditions are in accordance with the drainage conditions in the field. Every continuous sand or silt seam located within a bed of clay acts like a drainage layer and accelerates consolidation of the clay, whereas discontinuous lenses of sand and silt have no such effect. If test boring records indicate that a bed of clay contains partings of sand or silt, the engineer is rarely able to find out whether the partings are continuous. In such instances the theory of consolidation can be used to determine only upper and lower limiting values for the rate of settlement. The real rate remains unknown until it is observed.

In Figs. 25.1, 25.3, and 25.4 the upper and lower boundaries of the consolidating layer are assumed to be either freely draining ( $u' = 0$ ) or impermeable ( $\partial u' / \partial z = 0$ ). In the field the behavior of a boundary layer may lie somewhere between these extremes. This is illustrated in Fig. 25.8 which represents a consolidating layer of thickness  $H$  and permeability  $k_v$ , separated from freely draining upper and lower surfaces by incompressible layers of thickness  $H_t$  and  $H_b$  and finite permeability  $k_{vt}$  and  $k_{vb}$ , respectively. Equation 25.5 has been solved subject to these boundary conditions and a uniform initial excess porewater pressure distribution with depth (Mesri 1973). The drainage capacity of the adjacent incompressible layers is characterized by the drainage factors

$$R_t = \frac{k_{vt} H}{k_v H_t}$$

and

$$R_b = \frac{k_{vb} H}{k_v H_b}$$

The solutions indicate that values of  $R$  equal to 0.1 and 100 closely approximate impermeable and freely draining boundaries, respectively. For example, the  $U$  vs  $T_v$  curve in Fig. 25.8 that corresponds to  $R_b = 0.1$  and  $R_t = 100$  is very close to curve  $C_1$  in Fig. 25.5.

The  $U$  vs  $T_v$  curves in Figs. 25.5 and 25.8 correspond to solutions of Eq. 25.5 in which it is assumed that the consolidation pressure increment is applied instantaneously at  $t = 0$ . In the field, construction operations that may lead to consolidation take time. Under these loading conditions the consolidation pressure increment, and therefore the initial excess porewater pressure, reach their final values after weeks, months, or sometimes years. Equation 25.5 can be solved readily by assuming a linear

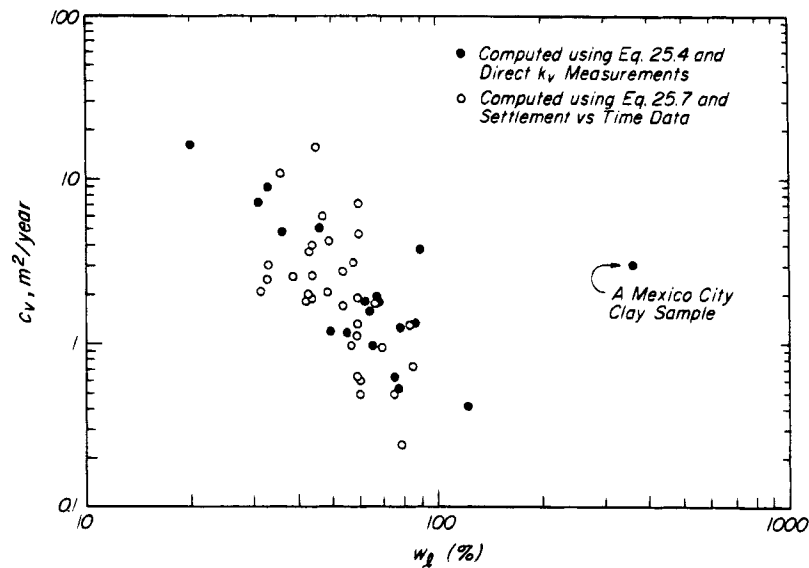


**Figure 25.7** Comparison of coefficients of consolidation of various clays computed by use of direct measurements of  $k_v$  and computed from settlement-time data.

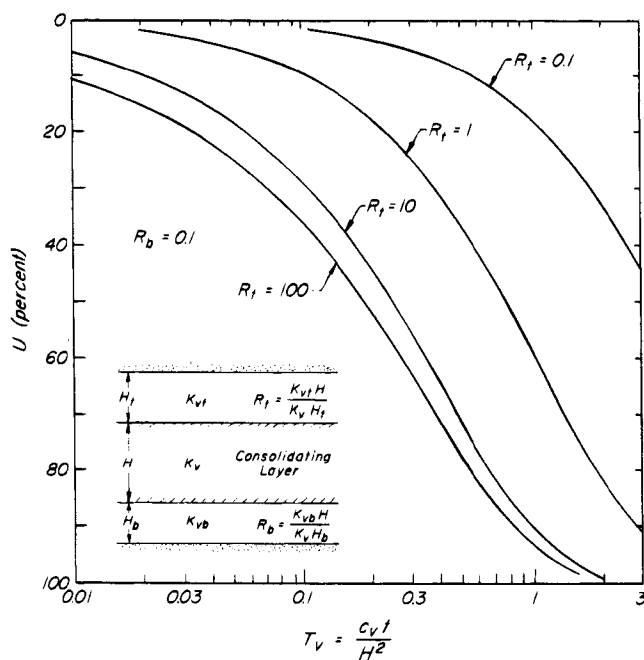


**Figure 25.8** Relation between degree of consolidation and time factor for impeded drainage boundaries.

increase with time of  $\Delta\sigma_v$ , and therefore of  $u'_i$ , up to the end-of-construction time  $t_c$ . Thereafter,  $\Delta\sigma_v$  is assumed to remain constant. The  $U$  vs  $T_v$  relationship in Fig. 25.9 is a function of the *construction time factor*  $T_{vc} = c_v t_c / H^2$ . The combinations of  $c_v$ ,  $H$ , and  $t_c$  that produce values of  $T_{vc}$  less than 0.01 closely approximate instantaneous loading; the  $U$  vs  $T_v$  curve corresponding to 0.01 is very close to curve  $C_1$  in Fig. 25.5.

The initial excess porewater pressure distributions in Fig. 25.3, *b*, *c*, and *d*, could result from dewatering operations that decrease the porewater pressure at the top or bottom boundaries of the consolidating layer, or at both. Consolidation resulting from such operations closely approximates one-dimensional compression and one-dimensional flow in the vertical direction. The initial conditions in Fig. 25.3 *b*, *c*, and *d*, may also result from the distribution of  $\Delta\sigma_v$  with depth that occurs when the consolidating layer is thick with respect to the width of the loaded area. Under these conditions, consolidation is not likely to be one-dimensional. Usually, loading and deformation boundary conditions are such that the compression is more or less one-dimensional, and one-dimensional settlement analysis provides reliable estimates of the EOP settlement. Nevertheless, in these situations, the flow of water is likely to be three-dimensional (two-dimensional for plane-strain loading conditions), and the horizontal flow is likely to accelerate the process of consolidation.

A three-dimensional theory of consolidation was developed by Biot in 1941. With respect to the fundamental assumptions, it is practically identical with the one-dimensional Terzaghi theory except that it includes the flow of water in all directions. The Biot theory, or simpler versions of it (Rendulic 1937, Gibson and Lumb 1953), may be used to evaluate the contribution of horizontal flow to the rate of consolidation (Gibson and McNamee 1957, Gibson 1961, Christian et al. 1972, Davis and Poulos 1972). Two sets of  $U$  vs  $T_v$  curves from Davis and Poulos (1972) are shown in Figs. 25.10 and 25.11 to illustrate this contribution. Figure 25.10 corresponds

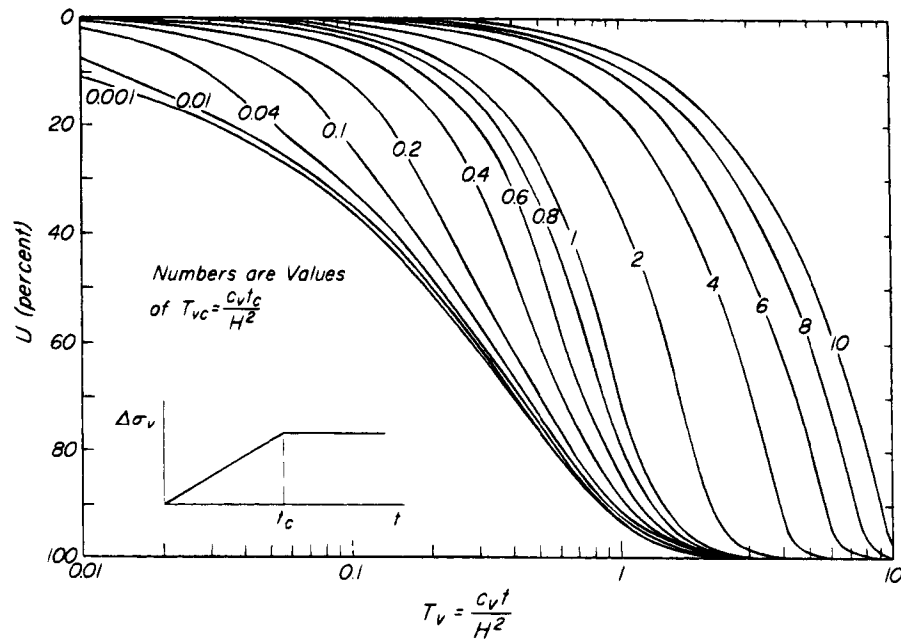


**Figure 25.9** Relations between degree of consolidation and time factor for time-dependent increase in consolidation pressure.

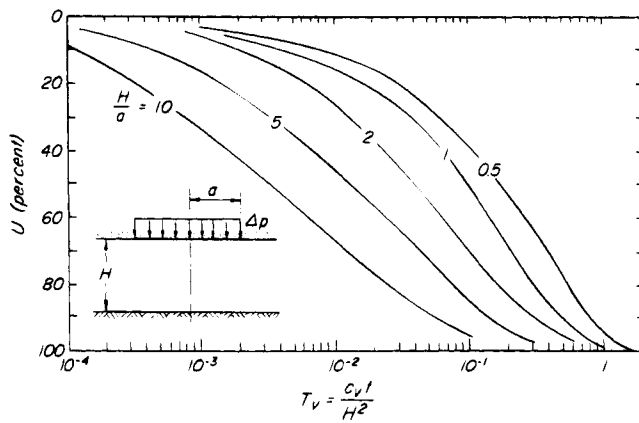


**Figure 25.10** Consolidation under a uniform pressure over a circular area on the assumption of three-dimensional flow of the water (after Davis and Poulos 1972).

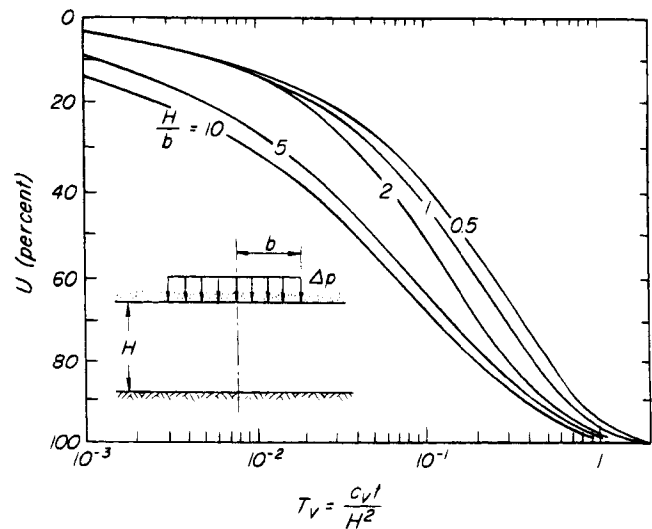


**Figure 25.11** Consolidation under a uniform pressure over a long strip on the assumption of two-dimensional flow of the water (after Davis and Poulos 1972).

to a uniform pressure  $\Delta p$  applied over a circular area of radius  $a$  to the upper surface of a half-closed consolidating layer of thickness  $H$ . A similar condition is shown in Fig. 25.11, except that the uniform pressure  $\Delta p$  is applied over a long strip of width  $2b$ . The  $U$  vs  $T_v$  curves corresponding to  $H/a$  and  $H/b$  values of 0.5 differ only slightly from curve  $C_1$  (Fig. 25.5). However, for values of  $H/a$  or  $H/b$  greater than 1, horizontal flow makes a substantial contribution to the rate of consolidation. The  $U$  vs  $T_v$  curves in Figs. 25.10 and 25.11 correspond to the center of the loaded area and were obtained by assuming  $k_h = k_v$ . In the field, if  $k_h$  is greater than  $k_v$ , the contribution of horizontal flow may be

even more significant, especially beneath the boundaries of the loaded area.

### 25.5 Consolidation with Vertical Drains

The primary consolidation of fairly thick soft clay layers subjected to permanent reclamation fills, embankments, or temporary preloads may require a considerable time if the excess water flows out of the clay in only the vertical direction. For example, the primary consolidation

of a soft clay layer with a maximum drainage distance of 5 m may require more than 10 years. To accelerate primary consolidation, vertical drains may be installed (Article 44.3.6). They are especially effective in stratified soils such as varved clays, in which the permeability is larger in the horizontal than in the vertical direction.

In the absence of a permeable granular layer above the consolidating layer, the drains are connected to a drainage blanket placed on the ground surface. Vertical drains often penetrate fully through the consolidating layer and into a permeable lower boundary. Such a drain is open at both top and bottom, and its length is denoted by  $2l_w$ , where  $l_w$  is the maximum drainage length. If the drain partially penetrates the consolidating layer, it is open only at the top, and its length is denoted by  $l_w$ .

The radius  $r_w$  of a circular sand drain is typically in the range of 80 to 300 mm. The equivalent radius  $r_w$  of wick drains with a rectangular cross-section is computed as  $r_w = (a + b)/\pi$ , where  $a$  and  $b$  are the thickness and width of the drain, respectively (Hansbo 1979). Typical values of  $a$  and  $b$  of 3.2 to 4.0 mm and 93 to 100 mm, respectively, lead to values of  $r_w$  in the range of 31 to 33 mm.

Vertical drains are usually installed in a triangular pattern at a spacing  $DS$  in the range of 1 to 5 m (Figs. 25.12 and 25.13). The radius  $r_e$  of the soil cylinder discharging water into a vertical drain is 0.525  $DS$ .

The function of a vertical drain is to accept radial flow of water from the consolidating ground, transport it in the vertical direction, and discharge it into a top or bottom drainage layer, or both, with as little hydraulic resistance as possible. However, most vertical drains have a finite discharge capacity,  $q_w = \pi r_w^2 k_w$ , where  $k_w$  is the permeability of the drain. Therefore, the horizontal permeability of the consolidating soil and the maximum drainage length  $l_w$  of the drain determine whether a vertical drain

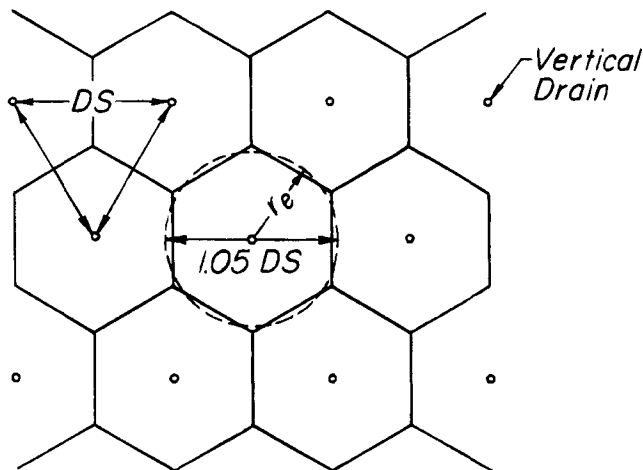


**Figure 25.12** Triangular pattern of installation of vertical drains.

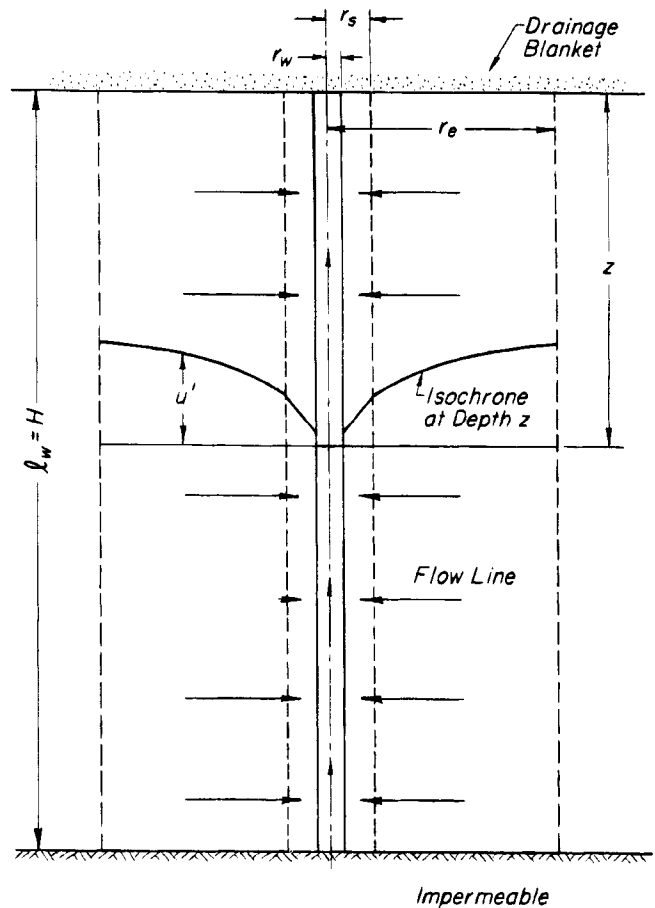


**Figure 25.13** Vertical drain of radius  $r_w$ , smear zone of radius  $r_s$ , and consolidating soil cylinder of radius  $r_e$ . Flow lines based on assumption of no vertical flow of water. Isochrone at depth  $z$  drawn on assumption of well resistance.

may drain freely or may display a well resistance. The discharge factor  $D$  is defined as

$$D = \frac{q_w}{k_h l_w^2} \quad (25.10)$$

where  $k_h$  is the horizontal permeability of the consolidating layer and  $q_w$  and  $l_w$  pertain to the vertical drain. Analyses of field performance of wick drains (Article 44.3.6) in soft clay deposits indicate that well resistance is negligible when  $D$  is greater than 5 (Mesri and Lo 1991). That is, the minimum discharge capacity  $q_w$  (min) of vertical drains, required for negligible well resistance, is  $q_w$  (min) =  $5 k_{ho} l_w^2$ . The most typical values of  $k_{ho}$  and  $l_w$  for soft clay and vertical drain installations lead to values of  $q_w$  (min) in the range of 2 to 80 m<sup>3</sup>/year. However, these magnitudes of discharge capacity are required only at the beginning of consolidation. As  $k_h$  decreases during consolidation, less water enters the drain during a given time and, therefore, a smaller  $q_w$  (min) is required to discharge the water with negligible hydraulic

resistance. The value of  $D = 5$  together with  $k_{ho}$  specify the upper limit for  $q_w$  (min) which decreases approximately according to Eq. 25.10 as  $k_h$  decreases. Therefore, if the initial  $q_w$  (min) required for negligible well resistance is  $10 \text{ m}^3/\text{year}$ , and  $k_h$  decreases by a factor of 2 by the time 50% primary consolidation is completed, then the minimum discharge capacity required beyond 50% consolidation is less than  $5 \text{ m}^3/\text{year}$ .

Installation of vertical drains creates a cylinder of disturbed soil or *smear zone* of external radius  $r_s$  around the drain. In this zone the permeability and preconsolidation pressure are reduced and the compressibility is increased. The decrease in horizontal permeability is most significant for laminated soils such as varved clays, and the increase in compressibility is most significant for highly structured clays.

For one-dimensional vertical compression together with vertical and radial flow, Eq. 25.5 becomes

$$c_v \frac{\partial^2 u'}{\partial z^2} + c_h \left( \frac{\partial^2 u'}{\partial r^2} + \frac{1}{r} \frac{\partial u'}{\partial r} \right) = \frac{\partial u'}{\partial t} \quad (25.11)$$

where  $c_h = k_h / \gamma_w m_v$ . The excess porewater pressure  $u'$  is a function of time as well as of  $z$  and  $r$ . Carillo (1942) showed that the solution of Eq. 25.11 can be obtained by combining separate solutions for vertical compression by vertical flow and vertical compression by radial flow. The excess porewater pressure and degree of consolidation, at any time, were found to be

$$u'_{zr} = \frac{u'_z u'_r}{u'_i} \quad (25.12)$$

and

$$U = 1 - (1 - U_z)(1 - U_r) \quad (25.13)$$

where  $u'_z$  and  $u'_r$  are the excess porewater pressures for vertical flow only and for radial flow only, respectively, and  $U_z$  and  $U_r$  are the corresponding degrees of consolidation. Relying on Carillo's contribution, most formulations of the rate of consolidation with vertical drains have considered only the radial flow of water through the consolidating layer and have ignored the vertical flow. The contribution of vertical flow is taken into account using the solution of Eq. 25.5 together with the Carillo equations. Vertical flow through the consolidating layer is likely to be significant when  $H$  is small and  $DS$  is large.

Barron (1944) formulated the rate of consolidation of a layer with fully penetrating vertical drains on the basis of the same assumptions regarding the permeability and compressibility of the soil as those that were made in developing Eq. 25.5. Assuming no smear zone, no well resistance, and equal vertical strain at any depth throughout the consolidation process, he found

$$U = 1 - \exp \left[ \frac{-2T_r}{F_n} \right] \quad (25.14)$$

where  $U$  is the degree of consolidation for radial flow only,  $n = r_e / r_w$ ,  $F_n = \ln(n) - 3/4$  for values of  $n$  greater than 10, and

$$T_r = \frac{c_h t}{r_e^2} \quad (25.15)$$

Later expressions for vertical compression with radial flow into a vertical drain include the effect of a smear zone of radius  $r_s = s r_w$  with permeability and compressibility different from those of the undisturbed soil, and the effect of a vertical drain having a finite permeability  $k_s$  or discharge capacity  $q_w$  (Barron 1948, Hansbo 1979, 1981, Zeng and Xie 1989). For example, the formulations by Hansbo (1981) and Zeng and Xie (1989) include a smear zone with permeability  $k_s$  different from  $k_h$  of the undisturbed layer but with the same compressibility as that of the undisturbed soil. They can be used to illustrate, for a value of  $k_s = k_h/2$ , the effect of the magnitudes of  $n$ ,  $q_w$ , and  $s$  on the  $U$  vs  $T_r$  relationship (Fig. 25.14). Figure 25.14a shows that  $n$  has a relatively small effect on the  $U$  vs  $T_r$  relation; however, it has a significant effect on the rate of consolidation because of its influence on  $r_e = n r_w$  in the time factor  $T_r$  (Eq. 25.15).

A value of  $s = 1$  means that there is no smear zone. For sand drains  $r_w = r_m$ , and the value of  $s$  is unlikely to exceed 4. However, for wick drains  $r_w$  is significantly smaller than the radius  $r_m$  of the mandrel used to install them. Therefore, even a value of  $r_s/r_w = 2$ , for typical values of  $r_m = 80 \text{ mm}$  and  $r_w = 32 \text{ mm}$ , leads to  $s = 5$ .

Analyses of field performance of wick drains suggest that in most soft clays the mobilized discharge capacity of prefabricated drains of high quality is comparable to the minimum discharge capacity required for negligible well resistance (Mesri and Lo 1991). Drains of poor quality or drains that are damaged during installation are represented by a value of  $q_w$  equal to  $q_w$  (min)/10 in Fig. 25.14c.

## 25.6 Limitations of the Theory of Consolidation

The theory of consolidation that has been formulated in this article and solved for various initial and boundary conditions, including three-dimensional flow of water and consolidation with vertical drains, is based on a number of important assumptions that limit its validity. It has been assumed that:

1. The coefficient of permeability  $k_v$  or  $k_h$  remains constant during consolidation.
2. The relation between void ratio or vertical strain and effective vertical stress is linear; that is, the coefficient of compressibility  $a_v$  or  $m_v$  remains constant during consolidation.

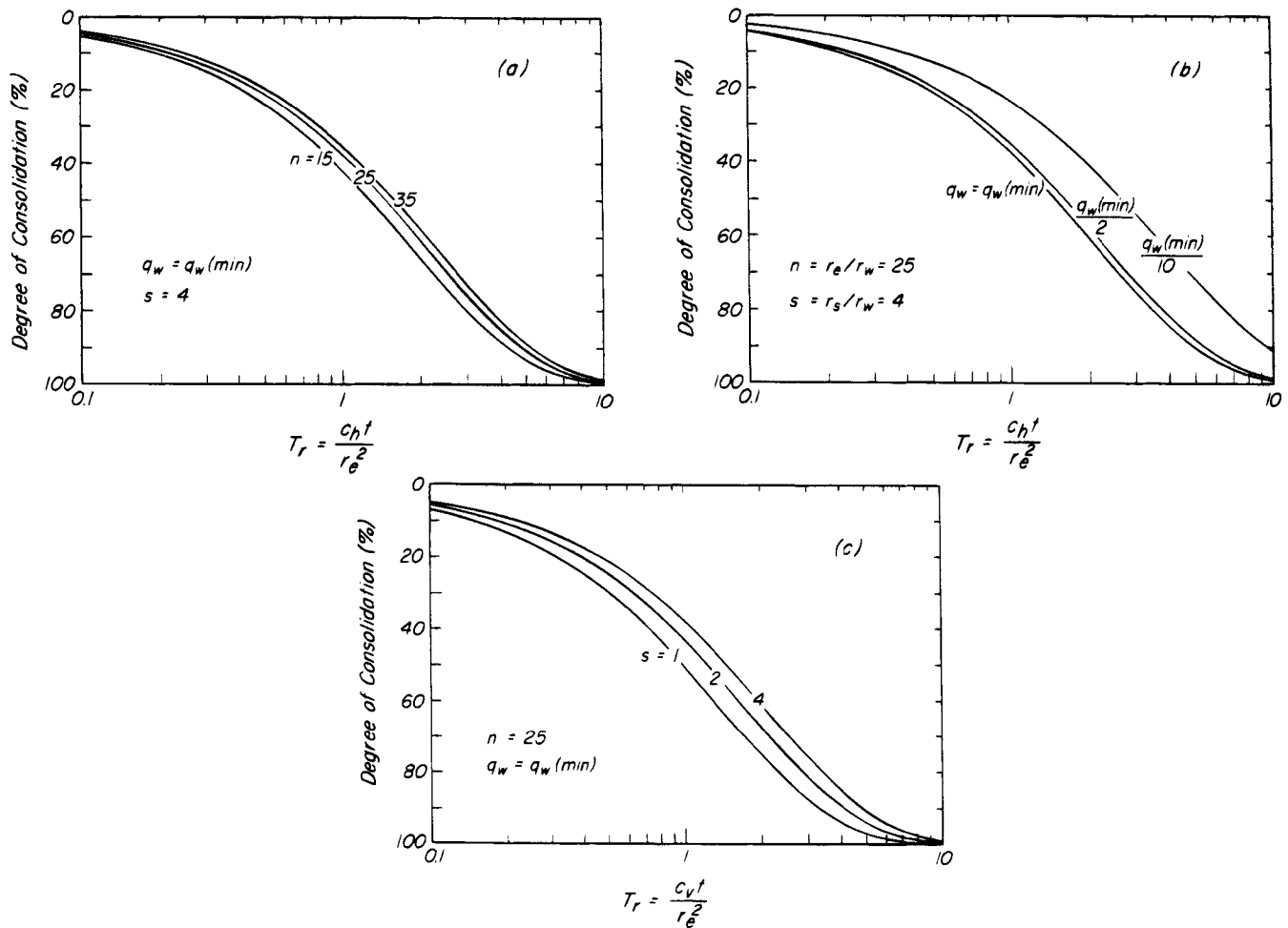


**Figure 25.14** Relations between degree of consolidation and time factor for radial flow into a vertical drain. Loading is assumed to be instantaneous and excess porewater pressure constant with depth. (a) different drain spacing; (b) different mobilized discharge capacity; (c) different size of smear zone.

3. The relation between void ratio and effective vertical stress is independent of time; that is,  $a_{vt}$  is zero throughout the consolidation process.

A theory of consolidation is used primarily to predict the progress of settlements that are expected to be large. Such settlements are associated with values of the final effective vertical stress,  $\sigma'_{vf} = \sigma'_{vo} + \Delta\sigma_v$ , in the compression range; that is, beyond the preconsolidation pressure  $\sigma'_p$  (Fig. 25.15). The consolidation associated with an increase in effective vertical stress from  $\sigma'_{vo}$  to  $\sigma'_{vf}$  involves a decrease in void ratio from  $e_0$  to  $e_p$  and thus a substantial decrease in permeability. The permeability of each sublayer is initially  $k_{vo}$ ,  $k_{ho}$  and decreases during consolidation. Because the consolidation of a layer proceeds from the drainage boundary toward the interior, the decrease in permeability starts at sublayers adjacent to the drainage surface and influences the rate of consolidation in the interior. Thus, during the consolidation of an initially

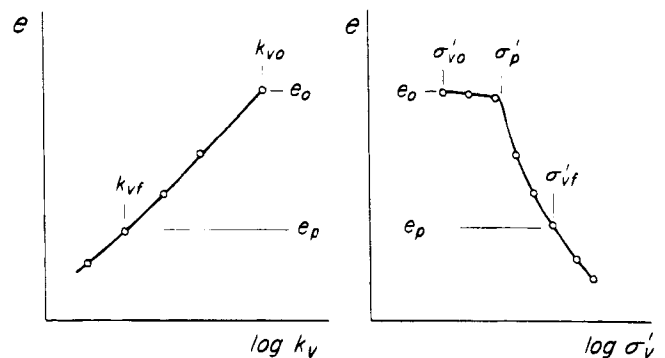


**Figure 25.15** Changes in permeability and compressibility during an increment of consolidation pressure.

homogeneous layer characterized by  $k_{vo}$  and  $k_{ho}$ ,  $k_v$  and  $k_h$  vary with both time and location until the end of primary consolidation is reached.

Figure 16.1 shows that when a consolidation pressure increment spans the preconsolidation pressure,  $a_v$  is initially small in the recompression range, increases abruptly as  $\sigma'_p$  is exceeded, and then decreases continuously as  $\sigma'_v$  increases in the compression range. Thus, in most practical situations involving the consolidation of soft clays,  $a_v$  or  $m_v$  does not remain constant during consolidation.

It is possible to reformulate the theory of consolidation by making more realistic assumptions with respect to the permeability and compressibility of the soil as consolidation proceeds. For example, the decrease in  $k_v$  or  $k_h$  may be expressed in terms of the  $C_k$  between the initial void ratio  $e_0$  and the EOP void ratio  $e_p$  (Article 14.4). The relation between void ratio and effective vertical stress may be approximated by a constant recompression index  $C_r$  in the recompression range from  $\sigma'_{vo}$  to  $\sigma'_p$ , and by a constant compression index  $C_c$  in the compression range from  $\sigma'_p$  to  $\sigma'_{vf}$  (Mesri and Rokhsar 1974). Alternatively the  $e$  vs  $\log k_v$ ,  $e$  vs  $\log k_h$ , and  $e$  vs  $\log \sigma'_v$  curves may be digitized and directly input into a numerical solution of the consolidation equation by use of a computer (Mesri and Choi 1985a, Mesri and Lo 1989). For some soils and for consolidation pressure increments that are completely in the compression range,  $C_k/C_c = 1$ . Under these conditions the decrease in  $m_v$  compensates for the decrease in  $k_v$  or  $k_h$ , and  $c_v$  or  $c_h$  remains practically constant during consolidation. Therefore, in some situations, the assumption of a constant  $c_v$  or  $c_h$  during consolidation may be reasonable and may lead to realistic predictions of the rate of settlement. However, the dissipation of porewater pressure at any point in the consolidating layer is highly dependent on the relation between void ratio and effective vertical stress. Reliable settlement analysis, especially excess porewater pressure prediction, requires realistic assumptions regarding the permeability and compressibility of the consolidating layer (Mesri and Choi 1979).

It has been observed repeatedly in both laboratory tests and in the field that when the excess porewater pressure approaches zero, the settlement does not come to a stop. Secondary compression continues beyond the end of primary consolidation. However, the assumption that  $a_{vt} = 0$  excludes secondary compression. Consequently, the  $U$  vs  $T$  curves in Figs. 25.5, 25.8, 25.9, 25.10, 25.11, and 25.14 and therefore the  $s$  vs  $t$  curves of the theory of consolidation level off at the end of primary consolidation.

The  $C_\alpha/C_c$  law of compressibility (Article 16.7) predicts and explains secondary settlement as a function of time for any value of  $\sigma'_{vf}$ . When the EOP  $e$  vs  $\log \sigma'_v$  relation is nearly linear and thus  $C_c$  is constant near  $\sigma'_{vf}$ , the progress of secondary settlement can be computed

by Eq. 16.12. If the EOP  $e$  vs  $\log \sigma'_v$  curve is highly nonlinear near  $\sigma'_{vf}$  and thus  $C_c$  changes with  $\sigma'_v$ , a graphical construction can be used to compute the secondary settlement as a function of time (Mesri and Godlewski 1977, 1979, Mesri and Shahien 1993). The progress of post-surge secondary settlement is determined by Eq. 13.13. Information on the duration  $t_p$  of the primary consolidation stage after loading or on the duration  $t_{pr}$  of the primary rebound stage after the removal of surcharge, in addition to the compressibility parameters, is required for computing the rate of secondary settlement. The value of  $t_p$  is obtained by using a theory of consolidation, and  $t_{pr}$  is determined with a theory of expansion. Most often,  $t_p$  or  $t_{ps}$  is approximated by the time required to complete 95% primary consolidation or primary expansion. For example, by using the Terzaghi theory of consolidation and the curve  $C_1$  in Fig. 25.5,  $t_p$  is computed by means of Eq. 25.7, and  $T_v = 1.13$ . When vertical drains are used, then  $t_p$  is computed by using Eq. 25.15. From the Barron Eq. 25.14 and, for example,  $n = 25$ ,  $T_r$  is found to be 3.7 for  $U = 95\%$ .

The assumption of  $a_{vt} = 0$  ignores the contribution of compressibility with time during the primary consolidation stage. The compression of a sublayer that occurs during the time that an increment of effective vertical stress acts, however, consists of the contributions of both  $a_{vs}$  and  $a_{vt}$ . Whereas  $a_{vt}$  during the secondary compression stage is well defined by direct measurements, the evaluation of  $a_{vs}$  and  $a_{vt}$  during primary consolidation is not practicable. In the absence of observed data, the assumption that  $a_{vt} = 0$  has been replaced by alternative assumptions (e.g., Berry and Poskitt 1972, Mesri and Rokhsar 1974). Mesri and Choi (1985a), for example, assume that the EOP  $e$  vs  $\log \sigma'_v$  curve is independent of the duration of primary consolidation. The EOP  $e$  vs  $\log \sigma'_v$  curve from the oedometer test is used with a constant  $C_\alpha/C_c$  to estimate  $a_{vs}$  and  $a_{vt}$  for increments of time during the primary consolidation stage. This approach has no effect on the magnitude of the EOP settlement and leads to predictions of rate of settlement that are in good agreement with direct observations (Mesri et al. 1994).

The hydrodynamic equation of consolidation can also be reformulated without assuming small strains during consolidation (Gibson et al. 1967). However, for most consolidation problems involving soft clay deposits, the small strain approximation is not a serious limitation (Mesri and Rokhsar 1974). On the other hand, a finite strain or large strain formulation may be more appropriate for consolidation of clay dredgings and slurries.

## 25.7 Application of a Consolidation Theory to Field Situations

In the field the consolidating layer rarely consists of a single homogeneous soil with respect to permeability and



compressibility. More often it consists of one or more distinct geologic deposits, and within each deposit such soil properties as  $e_0$ ,  $k_{vo}$ ,  $k_{ho}$ , and  $\sigma'_p$  may vary significantly with depth. With the help of the computer, it is no longer necessary to idealize the compressible soil profile into a single homogeneous layer. The compressible soil is divided into a number of consolidating sublayers, each with its own values of  $e_0$ ,  $k_{vo}$ ,  $k_{ho}$ ,  $C_k$ ,  $C_r$ ,  $C_c$ ,  $\sigma'_{vo}$ ,  $\sigma'_p$  (or its own  $e$  vs  $\log k_v$ ,  $e$  vs  $\log k_h$ , and EOP  $e$  vs  $\log \sigma'_v$  curves), as well as  $\sigma'_{vf}$  and  $C_\alpha/C_c$ . A numerical scheme is used with a computer to solve the differential equation of consolidation (Mesri and Choi 1985a, Mesri and Lo 1989). At the interface between adjacent sublayers  $j$  and  $j + 1$  the following conditions are satisfied with respect to the excess porewater pressure and flow rate:

$$u'_j = u'_{j+1}$$

and

$$\left[ \frac{1 + e_0}{1 + e} \right]_j k_{vj} \frac{\partial u'_j}{\partial z} = \left[ \frac{1 + e_0}{1 + e} \right]_{j+1} k_{vj+1} \frac{\partial u'_{j+1}}{\partial z}$$

Vertical drains may be installed before or during construction of a fill or embankment. The drains may fully or partially penetrate the compressible soil profile. The compressibility and permeability of the smear zone surrounding the vertical drain differ from those of the undisturbed soil and differ among the consolidating sublayers. Field construction schedules often include several stages of loading intervening with rest periods before the end of construction; therefore, in general  $\Delta\sigma$ , does not increase linearly from  $t_o$  to  $t_c$ . Such drainage and loading conditions are best treated with a numerical solution with the aid of a computer program. The computer program ILLICON (Mesri and Choi 1985a, Mesri and Lo 1989), for example, incorporates all the foregoing factors.

To illustrate the capabilities of such a procedure, field observations of ground surface settlement over a period of 25 years are shown in Fig. 25.16 for test fills of granular materials at Skå-Edeby, Sweden (Hansbo 1960, Hansbo et al. 1981). Within the compressible clay profile 12 m thick including the crust, the values of  $w_o$ ,  $w_l$ , and  $\sigma'_p/\sigma'_{vo}$  are in the ranges, respectively, of 45 to 120%, 60 to 150%, and 1.1 to 2.0 (most typical values 1.2 to 1.3). The diameters of the fills range from 30 to 70 m. At four locations, displacement-type sand drains of 180 mm diameter were installed in a triangular pattern at spacings of 0.9, 1.5, and 2.2 m. At one location no vertical drains were used. The drains, 12 m long, penetrated into a granular till underlying the clay.

For a settlement analysis using the ILLICON computer program, the compressible soil profile was divided into seven consolidating sublayers, each with its own values of  $e_0$ ,  $\sigma'_{vo}$ ,  $\sigma'_{vf}$ , EOP  $e$  vs  $\log \sigma'_v$  and  $k_{vo}$  (Mesri and Lo 1989, Lo 1991). For the entire compressible profile, con-

stant values of  $C_k/e_0$ ,  $C_\alpha/C_c$ ,  $k_{ho}/k_{vo}$ ,  $k_{so}/k_{vo}$ , and  $r_s/r_w$  were used. The discharge capacity of the sand drains was computed to be 450 m<sup>3</sup>/year which is more than adequate for negligible well resistance. For the smear zone within each sublayer an EOP  $e$  vs  $\log \sigma'_v$  relation was used consisting of a straight line joining  $(\sigma'_{vo}, e_0)$  and  $(\sigma'_{vf}, e_p)$  of the undisturbed soil.

The predictions of ground surface settlements are shown by the continuous curves in Fig. 25.16. The measurements and predictions both show that the sand drains significantly accelerated the rate of primary consolidation and that the magnitude of the increase was a function of the spacing of the drains. For example, with the 0.9-m drain spacing, primary consolidation was completed in about 500 days, whereas without vertical drains it would require more than 30 years. Where the vertical drains were used, primary consolidation was completed within the period of observation and secondary compression was observed thereafter. Because at all sublayers except the crust,  $\sigma'_{vf}$  was significantly larger than  $\sigma'_p$ , the EOP settlement was large and, in comparison, the secondary settlement during the period of observation was small, especially for the drain spacing of 2.2 m.

## 25.8 Theory of Expansion

Time-dependent expansion or swelling of saturated soils in fundamental respects is completely analogous to consolidation. Excavation of overburden or removal of a temporary surcharge results in a decrease in total vertical stress and in an identical decrease in porewater pressure, whereas the effective vertical stress remains unchanged. The porewater pressure at the permeable boundary layers quickly returns to the equilibrium reference condition. The gradient in excess porewater pressure (excess in a negative sense because the porewater pressure in the expanding layer is less than the reference equilibrium porewater pressure) causes water to flow through the boundary surfaces into the expanding layer as the excess negative porewater pressure dissipates. The increase in porewater pressure, the associated decrease in effective vertical stress, and the expansion of the void volume represent the primary expansion stage. Secondary expansion follows the end of primary expansion.

Examples of swelling of saturated shales subjected to a decrement in expansion pressure are shown in Figs. 25.17 and 25.18 (Cepeda-Diaz 1987). The index properties of the Patapsco shale sample from Washington, D.C. were  $w_o = 21.6\%$ ,  $w_l = 77\%$ ,  $w_p = 25\%$ , and  $w_s = 11\%$ . The undisturbed specimen, 15 mm thick, was subjected to a pressure decrement of 144 kPa, from  $\sigma'_{vi} = 192$  kPa to  $\sigma'_{vf} = 48$  kPa. Drainage took place from the permeable top, and porewater pressure was measured at the impermeable bottom of the specimen. At an elapsed time of 4 min an excess porewater pressure of about 142 kPa was observed, which dissipated to zero in about 6000 min.

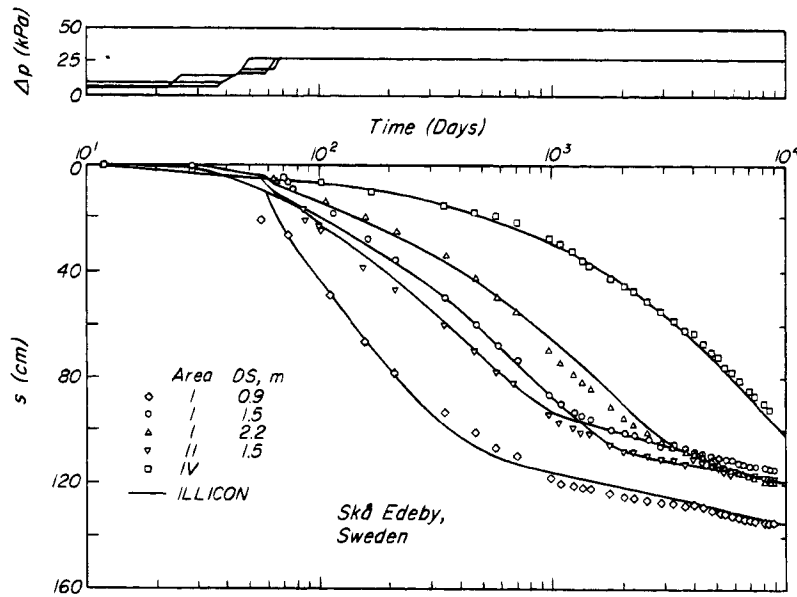


**Figure 25.16** Observed and computed settlements of ground surface under embankments on a soft clay deposit at Skå Edeby, Sweden.

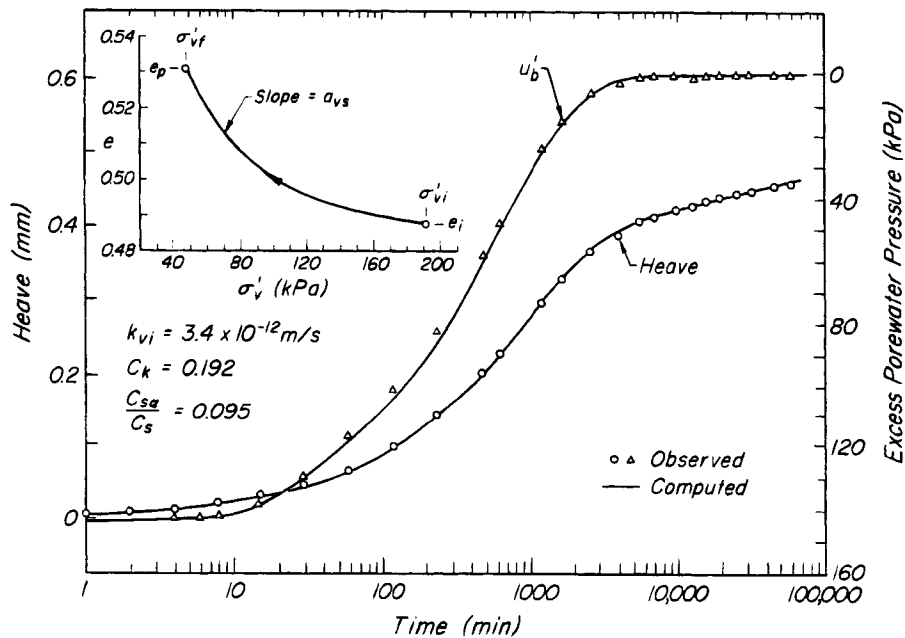


**Figure 25.17** Observed and computed behavior of Patapsco shale subjected to a decrement in expansion pressure.

Secondary swelling followed at a constant effective vertical stress of 48 kPa. The index properties of the Pierre shale sample from Limon, Colorado were  $w_o = 24.3\%$ ,  $w_l = 82\%$ ,  $w_p = 30\%$ , and  $w_s = 13\%$ . The undisturbed specimen, 12 mm thick, was subjected to a pressure decrement of 45 kPa, from  $\sigma'_{vi} = 58$  kPa to  $\sigma'_{vf} = 13$  kPa. At an elapsed time of 2 min, an excess porewater pressure of 45 kPa was measured that dissipated to zero in about

5000 min. Thereafter, at constant effective vertical stress, secondary swelling was observed.

Secondary swelling at  $\sigma'_{vf}$  begins at  $t_p$ , which is the time required to complete primary swelling. The value of  $C_{sa}/C_s$  is used (Article 16.10), together with  $C_s$  from the unloading EOP  $e$  vs  $\log \sigma'_v$  curve. Because  $C_{sa}/C_s$  and in some cases  $C_s$  increase with  $OCR$ ,  $C_{sa}$  is expected to increase with time. This increase is most significant

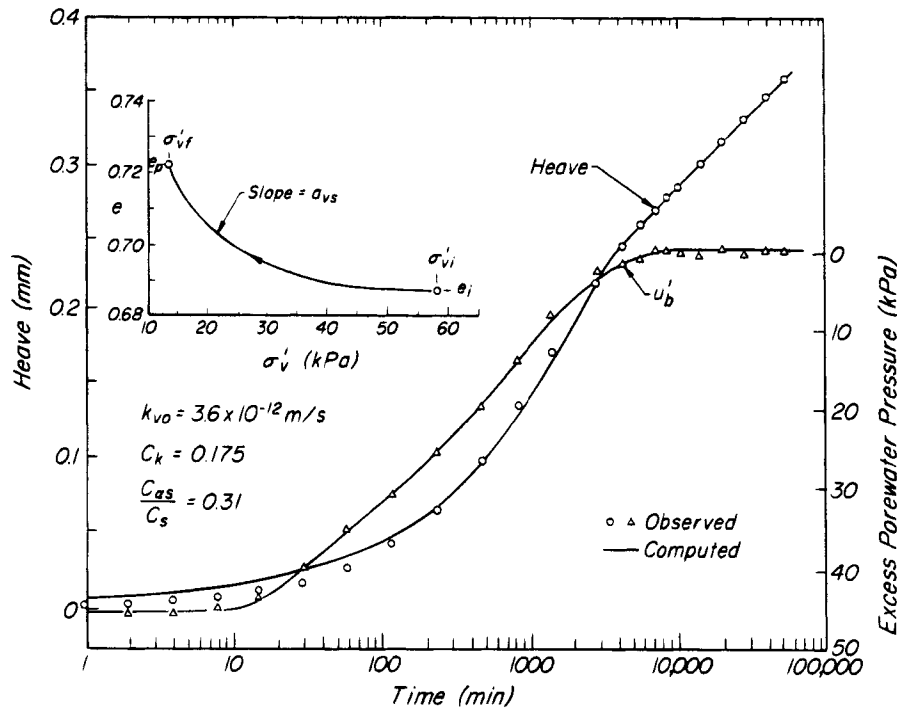


Figure 25.18 Observed and computed behavior of Pierre shale subjected to a decrement in expansion pressure.

at very high values of  $OCR$ , and for those expansive clays and shales for which  $C_s$  dramatically increases with a decrease in  $\sigma'_{vi}$ . However, in many practical situations, where the unloading  $EOP$   $e$  vs  $\log \sigma'_v$  relation is approximately linear, and for values of  $t/t_p$  less than 10, a constant  $C_{sa}$  can be used to estimate heave resulting from secondary swelling.

The theory of consolidation is applicable to the time rate of expansion of saturated soils (Terzaghi 1931), except that time is related to the time factor in terms of the coefficient of expansion,  $c_{vs} = k_v/\gamma_w m_{vs}$ , where  $m_{vs} = \Delta \varepsilon_v/\Delta \sigma'_v$  is determined from the  $EOP$  rebound curve. Values of  $c_{vs}$  for shales as well as for soft clay deposits are shown as a function of overconsolidation ratio in Fig. 25.19. For unloading from the compression range,  $a_{vs}$  or  $m_{vs}$  increases significantly during rebound, whereas in comparison the increase in  $k_v$  is relatively small. Therefore,  $c_{vs}$  decreases dramatically during a decrement in expansion pressure. Because  $m_{vs}$  starts with a very small value at  $\sigma'_{vi}$  and increases with decrease in  $\sigma'_v$ , the assumption of a constant  $m_{vs}$  between  $\sigma'_{vi}$  and  $\sigma'_{vf}$  significantly underestimates the rate of excess porewater pressure dissipation. That is, observed excess porewater pressures in cut slopes and adjacent to underground excavations dissipate faster than predicted by the theory of expansion. However, the  $U$  vs  $T_v$  curves in Figs. 25.5, 25.8, 25.9, 25.10, and 25.11, together with an appropriate value of  $c_{vs}$ , provide acceptable estimates of the rate of expansion

and heave. Furthermore, the decrease in  $c_{vs}$  with overconsolidation ratio is not so dramatic when the unloading is from the recompression range.

The theory of expansion has been reformulated to take into account the increases in  $m_{vs}$  and  $k_v$  during primary expansion (Mesri et al. 1978). The reformulation also includes, in terms of  $C_{sa}/C_s$ , the contribution of  $a_{vi}$  for expansion. Comparisons of predicted time rate of heave and dissipation of excess porewater pressure by the reformulated theory are shown in Figs. 25.17 and 25.18. The insets in these figures show the significant increase in  $a_{vs}$  during the decrements in expansion pressure. These results, together with measurements and predictions for other shales (Cepeda-Diaz 1987), show that for a reliable prediction of the rate of decrease in effective stress after unloading, the variation of  $a_{vs}$  must be included.

Time-dependent expansion and associated heave follow excavation of overburden or any other process of unloading. Time-dependent heave also follows a reduction in preconstruction suction that exists above the water table. A portion of this suction becomes an excess negative porewater pressure with respect to the postconstruction equilibrium condition where the ground surface is covered by an impermeable slab for a building, road, runway, canal, or spillway, and the moisture equilibrium between precipitation-evaporation and the water table is altered. To predict the time rate of heave, a formulation of unsaturated flow in expansive soils must then be used

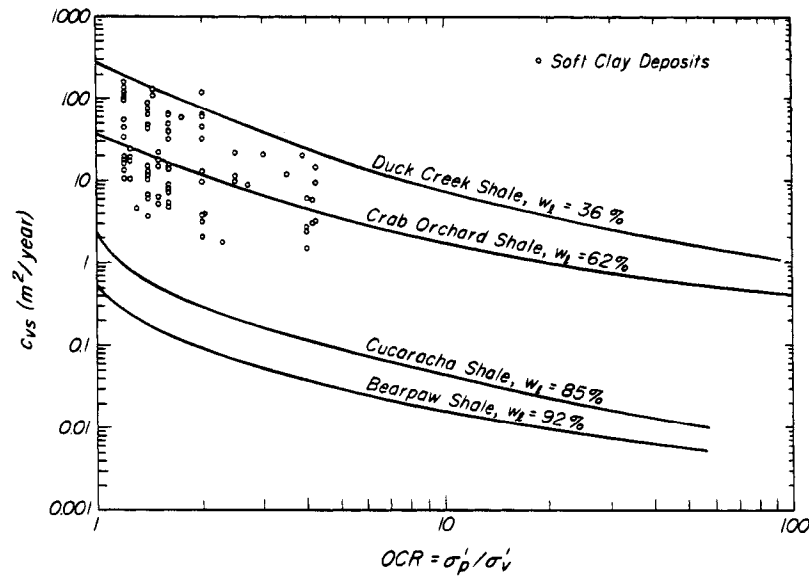


**Figure 25.19** Coefficient of expansion for various shales and soft clays unloaded from the compression range.

(Sokolov and Amir 1973, Yong 1977). Such a formulation must take into account the significant decrease in permeability that occurs with the increase in degree of saturation and with the associated internal slaking and dispersion (Jayawickrama and Lytton 1992).

### Problems

1. A wide fill (3 m thick and  $\gamma = 19.2 \text{ kN/m}^3$ ) is placed on a site with a soil profile consisting of 1.5 m of sand ( $\gamma = 19 \text{ kN/m}^3$ ) over 6 m of plastic clay ( $\gamma = 16 \text{ kN/m}^3$ ,  $e_0 = 1.7$ ,  $C_c = 1.2$ ,  $\sigma'_p/\sigma'_{vo} = 1.4$ ,  $C_r/C_c = 0.15$ ) over 10 m of organic silt ( $\gamma = 16 \text{ kN/m}^3$ ,  $e_0 = 1.2$ ,  $C_c = 0.8$ ,  $\sigma'_p/\sigma'_{vo} = 1$ ,  $C_r/C_c = 0.1$ ,  $C_\alpha/C_c = 0.06$ ,  $c_v = 0.04 \text{ m}^2/\text{day}$ ) over coarse sand. The water table is 1.5 m below the ground surface. Compute the settlement resulting from primary consolidation of the plastic clay. Assuming the plastic clay is impermeable compared with the organic silt, compute settlement resulting from compression of the organic silt after 30 years. Using the same assumption, sketch excess porewater pressure isochrones in the organic silt corresponding to 10%, 50%, and 95% primary consolidation.

Ans. 0.60 m; 0.88 m.

2. A soil profile consists of 6 m of sand ( $\gamma = 17.6 \text{ kN/m}^3$ ) over 3 m of silty clay ( $\gamma = 16.6 \text{ kN/m}^3$ ,  $e_0 = 1.1$ ,  $C_c = 1.5$ ,  $\sigma'_p/\sigma'_{vo} = 1.2$ ,  $C_r/C_c = 0.1$ , and  $c_v = 6 \times 10^{-3} \text{ m}^2/\text{day}$ ) over gravel. The water table is 2 m below the ground surface. The plan is to pump water from cased wells that penetrate into the gravel layer at such a rate that the water level in the wells will be 8 m below the ground surface. Compute settlement resulting from the primary consolidation of the silty clay layer when the steady-state seepage condition is established. Compute the time required for 95% primary consolidation of the silty clay layer. Sketch excess porewater pressure isochrones corresponding to average degree of consolidation of 0%, 5%, 50%, and 95%.

Ans. 0.16 m; 423 days.

3. A soil profile consists of 10 m of sand ( $\gamma = 17.6 \text{ kN/m}^3$ ) over 3 m of organic clay ( $\gamma = 16 \text{ kN/m}^3$ ,  $e_0 = 1.6$ ,  $C_c = 1.3$ ,  $\sigma'_p/\sigma'_{vo} = 1.3$ ,  $C_r/C_c = 0.2$ ,  $C_\alpha/C_c = 0.05$ , and  $c_v$  in compression range =  $0.02 \text{ m}^2/\text{day}$ ) over gravel. The water table is 3 m below the ground surface. Before constructing a structure on the site, the organic clay is precompressed by lowering the water table by 3 m and pumping from the gravel layer at such a rate that the piezometric head in the gravel drops by 6 m. Compute the settlement resulting from 80% primary consolidation of the clay layer. Sketch excess porewater pressure isochrones corresponding to 0%, 80%, and 95% average degree of consolidation. After 95% primary consolidation is reached, pumping is stopped so that the water table in sand and the porewater pressure in the gravel return to the original condition. The structure is constructed; it produces an effective vertical stress increase in the clay barely exceeding that produced by precompression. Compute the settlement of the structure after 30 years resulting from the secondary compression of the organic clay.

Ans. 0.06 m; 0.20 m.

4. A 7-m-thick granular fill ( $\gamma = 20 \text{ kN/m}^3$ ) is to be placed over a 20-m-thick deposit of silty clay ( $\gamma = 16 \text{ kN/m}^3$ ,  $e_0 = 1.76$ ,  $C_c = 0.9$ ,  $\sigma'_p/\sigma'_{vo} = 1.6$ ,  $C_r/C_c = 0.2$ ,  $c_v = 4 \times 10^{-3} \text{ m}^2/\text{day}$ ,  $c_h/c_v = 3$ , and  $C_\alpha/C_c = 0.04$ ) over decomposed fractured granite. The water table is near the ground surface. Computations show that considerable time would be required for primary consolidation of the silty clay if drainage is in the vertical direction only. Therefore, it is decided to speed up consolidation by using prefabricated vertical drains ( $r_w = 33 \text{ mm}$ ) with a spacing of 1 m, in a triangular pattern, and fully penetrating the silty clay layer. Compute: (a) settlement resulting from primary consolidation of silty clay, (b) time required for 95% primary consolidation, and (c) secondary settlement 50 years after construction of the fill.

Ans. 3.1 m; assuming no well resistance and no smear effect, 70 days; however, assuming vertical drain discharge

capacity of  $5 \text{ m}^3/\text{year}$ , a smear zone with  $r_s/r_m = 2$ , radius of mandrel  $r_m = 100 \text{ mm}$ , and  $k_s/k_v = 1$ , we obtain 178 days; using  $t_p = 178 \text{ days}$ ,  $0.52 \text{ m}$ .

5. A 7-m-thick gravel fill ( $\gamma = 19 \text{ kN/m}^3$ ) is to be placed over a soil profile consisting of 3 m of stiff fissured crust ( $\gamma = 18 \text{ kN/m}^3$ ) over 17 m of gray plastic clay ( $\gamma = 16 \text{ kN/m}^3$ ,  $e_0 = 1.76$ ,  $C_c = 0.90$ ,  $\sigma'_p/\sigma'_{vo} = 1.4$ ,  $C_r/C_c = 0.1$ ,  $C_\alpha/C_c = 0.04$ ,  $c_v = 10^{-3} \text{ m}^2/\text{day}$ , and  $c_h = 3 \times 10^{-3} \text{ m}^2/\text{day}$ ) over 10 m of silty clay ( $\gamma = 17 \text{ kN/m}^3$ ,  $e_0 = 1.5$ ,  $C_c = 0.75$ ,  $\sigma'_p/\sigma'_{vo} = 2.5$ ,  $C_r/C_c = 0.1$ ,  $C_\alpha/C_c = 0.05$ ,  $c_v$  (recompression)  $= 5 \times 10^{-2} \text{ m}^2/\text{day}$ ,  $c_v$  (compression)  $= 5 \times 10^{-3} \text{ m}^2/\text{day}$ ) over coarse sand. The water table is 3 m below the ground surface. In order to speed up the primary consolidation of the plastic clay, vertical band drains ( $r_w = 32 \text{ mm}$ , triangular pattern) with a spacing of 1.5 m are installed penetrating to the top of the silty clay. Compute settlement of the ground surface after 1, 3, and 50 years.

Ans. Ignoring well resistance, smear effect, compression of the crust, and vertical water flow through gray plastic clay, 1.06 m, 1.43 m, 1.72 m.

### Selected Reading

Solutions for the consolidation of masses of soil having various boundary conditions may be found in the following references.

- Terzaghi, K. and O. K. Fröhlich (1936). *Theorie der Setzung von Tonschichten* (Theory of settlement of clay layers). Leipzig, Deuticke, 166 pp.
- Barron, R. A. (1948). "Consolidation of fine-grained soils by drain wells," *Trans. ASCE*, **113**, pp. 718–742.
- Hansbo, S. (1960). "Consolidation of clay, with special reference to influence of vertical sand drains," *Proc. Swedish Geotechnical Institute*, **18**, Linköping.
- Gibson, R.E., G. L. England, and M.J.L. Hussey (1967). "The theory of one-dimensional consolidation of saturated clays," *Géot.*, **17**, No. 3, pp. 261–273.
- Davis, E.H. and H.G. Poulos (1972). "Rate of settlement under two- and three-dimensional conditions," *Géot.*, **22**, No. 1, pp. 95–114.
- Mesri, G. and A. Rokhsar (1974). "Theory of consolidation for clays," *J. Geotech. Eng., ASCE*, **100**, No. 8, pp. 889–904.
- Hansbo, S. (1979). "Consolidation of clay by band-shaped prefabricated drains," *Ground Eng.*, **12**, No. 5, pp. 16–25.
- Hansbo, S. (1981). "Consolidation of fine-grained soils by prefabricated drains," *Proc. 10th Int. Conf. Soil Mech. and Found. Eng.*, Stockholm, **3**, pp. 677–682.
- Mesri, G. and Y.K. Choi (1985a). "Settlement analysis of embankments on soft clays," *J. Geotech. Eng., ASCE*, **111**, No. 4, pp. 441–464.
- Mesri, G. and D.O.K. Lo (1989). "Subsoil investigation: the weakest link in the analysis of test fills," *The Art and Science of Geotechnical Engineering At the Dawn of the Twenty-first Century*, Prentice-Hall Inc., Englewood Cliffs, N.J., pp. 309–335.
- Lo, D.O.K. (1991). *Soil Improvement by Vertical Drains*, Ph.D. thesis, Univ. of Illinois at Urbana-Champaign.
- Mesri, G. and D.O.K. Lo (1991). "Field performance of prefabricated vertical drains," *Proc. Int. Conf. on Geotech. Eng. for Coastal Development—Theory to Practice*, Yokohama, **1**, pp. 231–236.
- Mesri, G., D.O.K. Lo, and T.W. Feng (1994). "Settlement of embankments on soft clays," *Proc. Settlement '94*, ASCE Specialty Conf. Geotech. Spec. Publ. No. 40, **1**, pp. 8–56.

## CHAPTER 5

### *Plastic Equilibrium in Soils*

#### ARTICLE 26 FUNDAMENTAL ASSUMPTIONS

This chapter deals with the earth pressure against lateral supports such as retaining walls or the bracing in open cuts, with the resistance of the earth against lateral displacement, with the bearing capacity of footings, and with the stability of slopes. Problems of this type require comparing the magnitudes of two sets of forces: those that tend to resist a failure and those that tend to produce it. Such an investigation is called a *stability calculation*. To make a stability calculation, the position of the potential surface of sliding must be determined and the resistance against sliding along this surface must be computed or estimated.

In reality both the forces tending to resist failure and those tending to produce it involve inherent uncertainties and, consequently, so does the *factor of safety*, defined as the quotient of these two quantities. The probabilistic nature of both the resistances and the driving forces has been the subject of considerable study and is recognized in building codes applicable to structures and their foundations; it will be discussed in Part III. In this chapter the principles of stability calculations are presented as if the pertinent quantities can be evaluated deterministically.

The sliding resistance  $s$  per unit of area depends not only on the type of soil but also on the effective normal stress  $\sigma - u$  on the surface of sliding and a number of other factors. These were discussed in Articles 18 through 20.

For mathematical treatment of stability problems, simplified expressions for shear strength are used. For dry or saturated granular soils, for saturated normally consolidated clays, and for fully softened stiff clays:

$$s = (\sigma - u) \tan \phi' \quad (26.1)$$

where  $\phi'$  is a friction angle independent of the effective normal stress  $\sigma - u$  at failure and is constant throughout the soil. For saturated overconsolidated or aged clays,

$$s = c' + (\sigma - u) \tan \phi' \quad (26.2)$$

where  $c'$  and  $\phi'$  are a cohesion intercept and a friction angle, respectively; both are independent of the effective normal stress at failure and are constant throughout the soil mass. For unsaturated cohesive soils,

$$s = c + \sigma \tan \phi' \quad (26.3)$$

where  $c = c' + b u_s^a$  (Eq. 19.9), and  $c'$  and  $\phi'$  are a cohesion intercept and a friction angle, respectively. The parameters  $a$  and  $b$  as well as suction  $u_s$  are assumed not to vary throughout the soil mass; constant values of  $c$  and  $\phi'$ , independent of total normal stress at failure  $\sigma$ , are used in the analysis. In reality the failure envelopes of dense granular soils and overconsolidated clays are curved, and  $c'$  and  $u_s$  may vary with depth. Thus the selection of appropriate values of  $\phi'$ ,  $c'$  and  $c$  for a particular problem requires experience and judgment (Article 19).

The investigation of failure based on Eqs. 26.1 or 26.2 is called *effective stress stability analysis* (ESSA). The ESSA terminology is also applicable to Eq. 26.3, because in unsaturated soils with air voids that are connected to the atmosphere and with constant suction, the frictional shearing resistance determined by  $\phi'$  is directly proportional to  $\sigma$ . When ESSA is applied to drained failures, the porewater pressure in Eqs. 26.1 and 26.2 is determined from the ground water level, or from a flow net if steady seepage exists. When ESSA is used for mathematical analysis of undrained failures, the porewater pressure term must also include porewater pressures resulting from loading or unloading and associated shearing deformations (Article 15.5). Considerable care must be taken in selecting  $c'$  and  $\phi'$  for undrained failure of contractive soils (Article 20.1).

More often, the shear strength for constant volume undrained failures is defined as

$$s = s_u \quad (26.4)$$

where  $s_u$  is an average mobilized undrained shear strength

assumed to have the same value at all depths and all directions. Equation 26.4 is most suitable for undrained stability analyses of saturated soft clays and silts and for loose sands, in which the undrained shear strength  $s_u$  is independent of the total normal stress. An investigation of failure based on Eq. 26.4 is called an *undrained strength stability analysis* (USSA). Because the undrained shear strength may vary with depth and is highly dependent on mode of shear and time to failure, the selection of the appropriate value of the average mobilized undrained shear strength for a particular problem requires experience and judgment (Article 20). When the undrained shear strength varies with depth in an irregular but distinct manner, the soil should be considered to consist of layers having different values of average mobilized undrained shear strength. In rare instances, such as in an earth dam constructed from a homogeneous cohesive soil, the undrained shear strength may increase linearly with depth or with the consolidation pressure  $\sigma'_{vo}$ . The relationship between undrained shear strength and consolidation pressure may be included in a mathematical analysis as a linear relationship between undrained shear strength and effective normal stress before loading or unloading; i.e., before the associated shear deformation.

Each of the stability problems will be solved first for a dry ( $u = 0$ ) cohesionless sand to which Eq. 26.1 is applicable and then for a cohesive material to which Eqs. 26.2 or 26.3 applies. After the ability to solve problems on the basis of these two equations is achieved, similar problems dealing with partly or completely submerged sand or with saturated clay under undrained conditions can readily be solved.

In a partly submerged mass of sand in which the water is at rest, the neutral stress  $u$  at any depth  $z$  below the water table is

$$u = \gamma_w z$$

This stress reduces the effective unit weight of that part of the sand below water level from  $\gamma$  to the submerged unit weight  $\gamma'$  (Eq. 15.6). Hence a stability calculation dealing with a partly submerged sand can be made on the assumption that the sand is dry, provided that the unit weight  $\gamma$  of the soil below water level is replaced by  $\gamma'$ . The pressure exerted by a partly submerged mass of sand against a lateral support is equal to the sum of the pressure of the sand, computed on the basis just mentioned, and the full water pressure. However, if the water percolates through the voids of the soil instead of being stagnant, this procedure is not applicable because the seepage pressure of the percolating water must be taken into account. Problems dealing with seepage pressure are discussed in Articles 35 and 36.

Theoretical expressions derived on the basis of Eq. 26.2 or Eq. 26.3 can be applied to stability analyses in which the shear strength is expressed by Eq. 26.4. The

equation for the undrained shear strength of saturated soils in terms of *total stress* is

$$s = c + \sigma \tan \phi \quad (26.5)$$

where  $c = s_u$  and  $\phi = 0$ . Because the mathematical forms of Eqs. 26.2, 26.3, and 26.5 are identical, they lead to the same mathematical expressions for solving stability problems. Thus, by appropriate substitutions for the intercept and angle, mathematical expressions for the undrained stability of saturated soils are obtained in terms of  $s_u$ .

The condition for failure represented by Eq. 26.2 corresponds to Mohr's rupture diagram in which the failure envelope is a straight line (Fig. 26.1). Consequently, a definite relation exists at failure between the major and minor principal stresses  $\sigma'_1$  and  $\sigma'_3$ , respectively. By geometry

$$\sigma'_1 + d = OA + AB = OA(1 + \sin \phi')$$

$$\sigma'_3 + d = OA - AB = OA(1 - \sin \phi')$$

whence

$$\sigma'_1 = \sigma'_3 \frac{1 + \sin \phi'}{1 - \sin \phi'} + d \left( \frac{1 + \sin \phi'}{1 - \sin \phi'} - 1 \right)$$

But

$$d = c' \frac{\cos \phi'}{\sin \phi'} = c' \frac{\sqrt{1 - \sin^2 \phi'}}{\sin \phi'}$$

Therefore

$$\sigma'_1 = \sigma'_3 \frac{1 + \sin \phi'}{1 - \sin \phi'} + 2c' \sqrt{\frac{1 + \sin \phi'}{1 - \sin \phi'}}$$

$$\sigma'_1 = \sigma'_3 \tan^2 \left( 45^\circ + \frac{\phi'}{2} \right) + 2c' \tan \left( 45^\circ + \frac{\phi'}{2} \right)$$

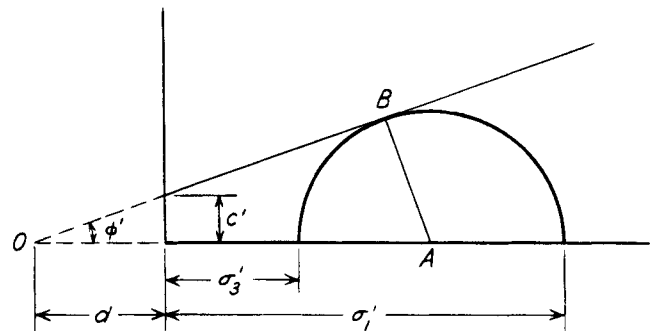


Figure 26.1 Mohr rupture diagram for condition in which failure envelope is straight line.

Or, if

$$N_{\phi'} = \tan^2\left(45^\circ + \frac{\phi'}{2}\right) \quad (26.6)$$

$$\sigma'_1 = \sigma'_3 N_{\phi'} + 2c'\sqrt{N_{\phi'}} \quad (26.7)$$

The quantity  $N_{\phi'}$  is known as the *flow value*. If  $c' = 0$ ,

$$\sigma'_1 = \sigma'_3 N_{\phi'} \quad (26.8)$$

and if the condition for failure is represented by Eq. 26.4 ( $\phi = 0$ ,  $N_{\phi} = 1$ )

$$\sigma_1 = \sigma_3 + 2s_u \quad (26.9)$$

## ARTICLE 27 STATES OF PLASTIC EQUILIBRIUM

### 27.1 Fundamental Concepts

A body of soil is in a *state of plastic equilibrium* if every part of it is on the verge of failure. Rankine (1857) investigated the stress conditions corresponding to those states of plastic equilibrium that can be developed simultaneously throughout a semi-infinite mass of soil acted on by no force other than gravity. States of plastic equilibrium identical with those which Rankine considered are referred to as *Rankine states of plastic equilibrium*. A discussion of the Rankine states in a semi-infinite mass is primarily an introduction to the more complicated states of plastic equilibrium encountered in connection with practical problems.

The Rankine states are illustrated by Fig. 27.1. In this figure,  $AB$  represents the horizontal surface of a semi-infinite mass of cohesionless dry sand with a unit weight  $\gamma$ , and  $E$  represents an element of the sand with a depth  $z$  and a cross-sectional area equal to unity. Because the element is symmetrical with reference to a vertical plane, the effective normal stress on the base

$$\sigma'_v = \gamma z \quad (27.1)$$

is a principal stress. As a consequence, the effective normal stresses  $\sigma'_h$  on the vertical sides of the element at depth  $z$  are also principal stresses.

According to Eq. 26.8, the ratio between the major and minor principal stresses in a cohesionless material cannot exceed the value

$$\frac{\sigma'_1}{\sigma'_3} = N_{\phi'} = \tan^2\left(45^\circ + \frac{\phi'}{2}\right)$$

Because the vertical principal stress  $\sigma'_v$ , in the mass of sand shown in Fig. 27.1a, can be either the major or the minor principal stress, the ratio  $K = \sigma'_h/\sigma'_v$  can assume any value between the limits,

$$K_A = \frac{\sigma'_h}{\sigma'_v} = \frac{1}{N_{\phi'}} = \tan^2\left(45^\circ - \frac{\phi'}{2}\right) \quad (27.2)$$

and

$$K_P = \frac{\sigma'_h}{\sigma'_v} = N_{\phi'} = \tan^2\left(45^\circ + \frac{\phi'}{2}\right) \quad (27.3)$$

After a mass of sand has been deposited by either a natural or an artificial process,  $K$  has a value  $K_0$  intermediate between  $K_A$  and  $K_P$  and

$$\sigma'_h = K_0 \sigma'_v \quad (27.4)$$

wherein  $K_0$  is an empirical coefficient known as the *coefficient of earth pressure at rest*. Its value depends on the relative density of the sand, the process by which the deposit was formed, and its subsequent stress history (Article 16.5).

To change the value of  $K$  for a mass of sand from  $K_0$  to some other value, it is necessary to give the entire mass an opportunity either to stretch or to be compressed in a horizontal direction. Because the weight of sand above any horizontal section remains unchanged, the effective vertical pressure  $\sigma'_v$ , is unaltered. The horizontal pressure  $\sigma'_h = K\sigma'_v$ , however, decreases if the mass stretches and increases if it compresses.

As the mass stretches, any two vertical sections such as  $ab$  and  $cd$  move apart, and the value of  $K$  decreases until it becomes equal to  $K_A$  (Eq. 27.2). The sand is then in what is known as the *active Rankine state*. In this state the intensity of the effective horizontal pressure at any depth  $z$  is equal to

$$\sigma'_h = K_A \sigma'_v = K_A \gamma z = \gamma z \frac{1}{N_{\phi'}} \quad (27.5)$$

in which  $K_A$  is called the *coefficient of active earth pressure*. The distribution of pressure over the sides and base of an element such as  $E$  is shown in Fig. 27.1b. Further stretching of the mass has no effect on  $\sigma'_h$  (Eq. 27.5), but sliding occurs along two sets of plane surfaces as indicated on the right-hand side of Fig. 27.1a. According to Eq. 17.5, such surfaces of sliding intersect the direction of the minor principal stress at the angle  $45^\circ + \phi'/2$ . Because the minor principal stresses in the active Rankine state are horizontal, the shear planes rise at an angle of  $45^\circ + \phi'/2$  with the horizontal. The pattern formed by the traces of the shear planes on a vertical section parallel to the direction of stretching is known as the *shear pattern*.

A horizontal compression of the entire mass of sand causes  $ab$  to move toward  $cd$ , as shown in Fig. 27.1c. As a consequence, the ratio  $K = \sigma'_h/\sigma'_v$  increases. As soon as  $K$  becomes equal to  $K_P$  (Eq. 27.3) the sand is



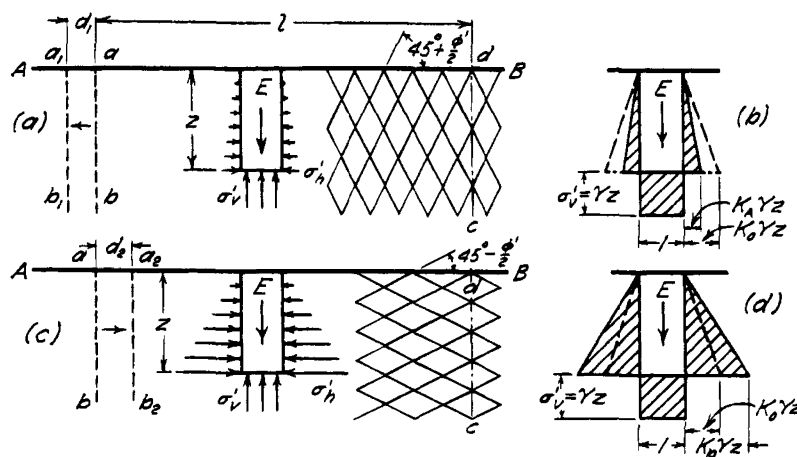


**Figure 27.1** (a, b) Diagrams illustrating active Rankine state in semi-infinite mass of sand; (c, d) corresponding diagrams for passive Rankine state.

said to be in the *passive Rankine state*. At any depth  $z$  the horizontal pressure is

$$\sigma'_h = K_p \sigma'_v = K_p \gamma z = \gamma z N_{\phi'} \quad (27.6)$$

in which  $K_p$  is the *coefficient of passive earth pressure*. Because the minor principal stress in the passive Rankine state is vertical, the surfaces of sliding rise at an angle of  $45^\circ - \phi'/2$  with the horizontal, as shown in Fig. 27.1c.

The active and the passive Rankine states constitute the two limiting states for the equilibrium of the sand. Every intermediate state, including the state of rest, is referred to as a *state of elastic equilibrium*.

## 27.2 Local States of Plastic Equilibrium

The Rankine states illustrated by Fig. 27.1 were produced by uniformly stretching or compressing every part of a semi-infinite mass of sand. They are known as *general states of plastic equilibrium*. However, in a stratum of real sand, no general state of equilibrium can be produced except by a geologic process such as the horizontal compression by tectonic forces of the entire rock foundation of the sand strata. Local events, such as the yielding of a retaining wall, cannot produce a radical change in the state of stress in the sand except in the immediate vicinity of the source of the disturbance. The rest of the sand remains in a state of elastic equilibrium.

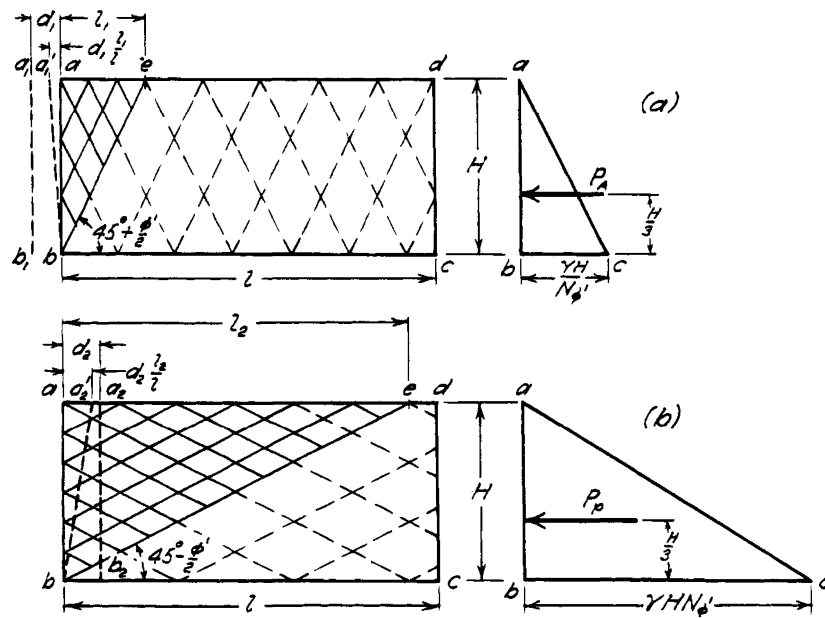
Local states of plastic equilibrium can be produced by very different processes of deformation. The resulting states of stress in the plastic zone and the shape of the zone itself depend to a large extent on the type of deformation and on the degree of roughness of the surface of contact between the soil and its support. These factors constitute the *deformation* and the *boundary conditions*. The practical consequences of these conditions are illustrated by Figs. 27.2 and 27.3.

Figure 27.2a is a vertical section through a prismatic box having a length  $l$  equal to the distance between the

vertical sections  $ab$  and  $cd$  in Fig. 27.1. If dry sand is deposited in the box by the same process that was responsible for the formation of the semi-infinite mass represented in Fig. 27.1, the states of stress in both masses are identical. They represent states of elastic equilibrium.

When the state of the semi-infinite mass of sand (Fig. 27.1a) was changed from that of rest to the active Rankine state, the vertical section  $ab$  moved through the distance  $d_1$ . To change the state of the entire mass of sand contained in the box (Fig. 27.2a) into the active Rankine state, the wall  $ab$  must be moved through the same distance. This constitutes the deformation condition. While the wall  $ab$  (Fig. 27.2a) moves out, the height of the mass of sand decreases, and its length increases. These movements involve displacements between the sand and all the surfaces of the box which it contacts. If the contact surfaces are rough, shearing stresses will develop along vertical and horizontal planes. Because the shearing stresses on these planes are zero in the active Rankine state, this state cannot materialize unless the sides and bottom of the box are perfectly smooth. This requirement constitutes the boundary condition for the transition of the sand in the box to the active Rankine state. If this condition is satisfied, the sand passes into an active Rankine state as soon as the wall  $ab$  reaches the position  $a_1b_1$ . At this stage, the unit stretch of the soil is  $d_1/l$ . Any further movement of the wall causes slippage along the two sets of surfaces of sliding indicated by dash lines in Fig. 27.2a, but the stress conditions remain unchanged.

If the wall  $ab$  is perfectly smooth but the bottom of the box is rough, the sand located between the wall  $ab$  and the potential surface of sliding  $be$  is free to deform in exactly the same manner as it does in a box with a smooth bottom, but the state of stress in the balance of the sand cannot change materially because the friction along the bottom prevents the required deformation. Hence, an outward movement of the wall  $ab$  produces



**Figure 27.2** (a) Diagrams illustrating local active Rankine state in sand contained in rectangular box; (b) corresponding diagrams for local passive Rankine state.

an active Rankine state within only the wedge-shaped zone  $abe$ . Because the width of the wedge increases from zero at the bottom to  $l_1$  at the top, the unit stretch  $d_1/l$  required to establish the active Rankine state in the wedge is attained as soon as the left-hand boundary of the wedge moves from  $ab$  to  $a_1'b$  (Fig. 27.2a). This is the deformation condition for the development of an active Rankine state within the wedge. As soon as the wall  $ab$  passes beyond this position, the wedge slides downward and outward along a plane surface of sliding  $be$  which rises at an angle of  $45^\circ + \phi'/2$  with the horizontal.

If the wall  $ab$  is pushed toward the sand, and if both the walls and the bottom of the box are perfectly smooth, the entire mass of sand is transformed into the passive Rankine state (Fig. 27.2b) as soon as the wall moves beyond a distance  $d_2$  from its original position. The planes of sliding rise at an angle of  $45^\circ - \phi'/2$  with the horizontal. If the wall  $ab$  is perfectly smooth but the bottom of the box is rough, the passive Rankine state develops only within the wedge-shaped zone  $abe$ . The transition from the elastic to the plastic state does not occur until  $ab$  moves into or beyond the position  $a_2'b$ .

If the end of the box is free to move outward at the bottom but is restrained at the top, as indicated in Fig. 27.3, the sand fails by shear along some surface of sliding as soon as the tilt becomes perceptible, because the deformations compatible with an elastic state of equilibrium are very small. However, even at the state of failure, the sand between the wall and the surface of sliding does not pass into the active Rankine state because the upper part of the wall cannot move, and, as a consequence, the

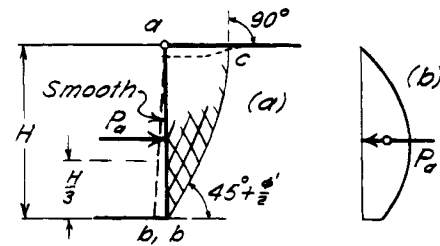


**Figure 27.3** Failure of sand behind smooth vertical wall when deformation condition for active Rankine state is not satisfied. (a) Section through back of wall; (b) stress against back of wall.

deformation condition for the active Rankine state within the sliding wedge is not satisfied.

Theoretical and experimental investigations regarding the type of failure caused by a tilt of the lateral support about its upper edge have led to the conclusion that the surface of sliding starts at  $b$  (Fig. 27.3a) at an angle of  $45^\circ + \phi'/2$  with the horizontal and that it becomes steeper until it intersects the ground surface at a right angle. The upper part of the sliding wedge remains in a state of elastic equilibrium until the lower part of the wedge has passed completely into a state of plastic equilibrium. The distribution of pressure against the lateral support is roughly parabolic (Fig. 27.3b) instead of triangular (Fig. 27.1b).

Similar investigations regarding the effect of pushing the bottom of the support toward the soil (Fig. 27.4a) have shown that the surface of sliding rises from  $b$  at an angle  $45^\circ - \phi'/2$  with the horizontal and that it also

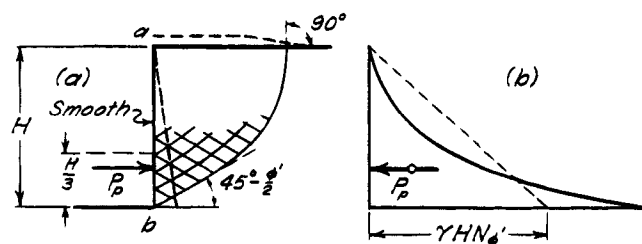


**Figure 27.4** Failure of sand behind smooth vertical wall when deformation condition for passive Rankine state is not satisfied. (a) Section through back of wall; (b) stress on back of wall.

intersects the ground surface at a right angle. The corresponding distribution of pressure is shown in Fig. 27.4b.

### Selected Reading

A general discussion of the application of the theory of plasticity to states of limiting equilibrium, including problems of earth pressure, stability of slopes, and bearing capacity, is contained in Sokolovski, V. V. (1960). *Statics of Soil Media*. Translated from the Russian by D. H. Jones and A. N. Schofield, London, Butterworths, 237 pp. Mathematical methods for solving problems with mixed boundary conditions are developed in Hansen, B. (1965). *A Theory of Plasticity for Ideal Frictionless Materials*, Copenhagen, Teknisk Forlag, 471 pp.

Chen, W.F. (1975). *Limit analysis and soil plasticity, Developments in Geotechnical Engineering*, 7, Elsevier, Amsterdam, 638 pp.

## ARTICLE 28 RANKINE'S EARTH-PRESSURE THEORY

### 28.1 Earth Pressure against Retaining Walls

Retaining walls serve the same function as the vertical sides of the box shown in Fig. 27.2. The soil adjoining the wall is known as the *backfill*. It is always deposited after the wall is built. While the backfill is being placed, the wall yields somewhat under the pressure. The ultimate value of the pressure depends not only on the nature of the soil and the height of the wall but also on the amount of yield. If the position of the wall is fixed, the earth pressure is likely to retain forever a value close to the earth pressure at rest (Article 27). However, as soon as a wall yields far enough, it automatically satisfies the deformation condition for the transition of the adjoining mass of soil from the state of rest into an active state of plastic equilibrium. Hence, the factor of safety of a retaining wall capable of yielding must be adequate with respect to the active earth pressure, but does not need to be investigated for greater values of earth pressure.

Although the back of every real retaining wall is rough, approximate values of the earth pressure can be obtained

on the assumption that it is smooth. In the following paragraphs, this assumption is made. Methods for obtaining more accurate values will be described in subsequent articles.

### 28.2 Active Earth Pressure of Cohesionless Soil against Smooth Vertical Walls

If the surface of a sand backfill is horizontal, and if the back of the retaining wall is vertical and perfectly smooth, the magnitude and the distribution of pressure against the back of the wall are identical with those of the active pressure against the fictitious plane *ab* in Fig. 27.1a. Therefore, the earth pressure can be computed on the basis of the equations already derived. In reality, there are no perfectly smooth surfaces. However, the equations based on this assumption are so simple that they are quite commonly used for evaluating the earth pressure against real retaining walls and other structures acted on by earth pressure. It is shown subsequently that the roughness of the back of a wall commonly reduces the active and increases the passive earth pressure. Hence, as a rule, the error associated with the assumption is on the safe side.

Furthermore, in one case of great practical importance, the assumption of a smooth vertical wall is almost strictly correct. This case is illustrated by Fig. 28.1, which represents a cantilever wall. If such a wall yields under the influence of the earth pressure, the sand fails by shear along two planes rising from the heel of the wall at angles of  $45^\circ + \phi'/2$  with the horizontal. Within the wedge-shaped zone located between these two planes, the sand is in the active Rankine state, and no shearing stresses act along the vertical plane *ab* through the heel. Hence, the earth pressure against this plane is identical with that against a smooth vertical wall.

If the sand backfill is perfectly dry, the active pressure against a smooth vertical wall at any depth *z* is

$$\sigma_h' = \gamma z \frac{1}{N_{\phi'}} \quad (27.5)$$

It increases in simple proportion to the depth, as indicated

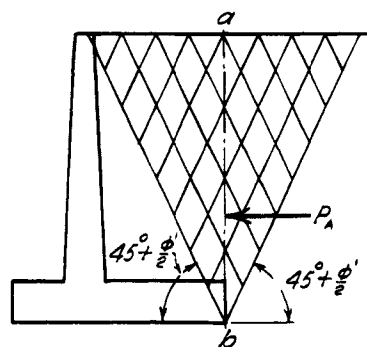


**Figure 28.1** Failure of sand behind cantilever retaining wall; deformation condition for active Rankine state is almost satisfied.

by the pressure triangle  $abc$  (Fig. 27.2a). The resultant pressure or force against the wall is

$$P_A = \int_0^H \sigma'_h dz = \frac{1}{2} \gamma H^2 \frac{1}{N_{\phi'}} \quad (28.1)$$

The point of application of  $P_A$  is located at a height  $H/3$  above  $b$ .

If the wall is pushed into the position  $a_2'b$  in Fig. 27.2b the pressure  $\sigma'_h$  against the wall assumes a value corresponding to the passive Rankine state,

$$\sigma'_h = \gamma z N_{\phi'} \quad (27.6)$$

and the resultant pressure against the wall becomes equal to

$$P_P = \int_0^H \sigma'_h dz = \frac{1}{2} \gamma H^2 N_{\phi'} \quad (28.2)$$

### 28.3 Active Earth Pressure of Partly Submerged Sand Supporting a Uniform Surcharge

In Fig. 28.2a the line  $ab$  represents the smooth vertical back of a wall with height  $H$ . The effective unit weight of the sand when dry is  $\gamma$  and when submerged is  $\gamma'$  (see Article 15); the unit weight of water is  $\gamma_w$ . The surface of the horizontal backfill carries a uniformly distributed surcharge  $q$  per unit of area. Within the backfill the water table is located at depth  $H_1$  below the crest of the wall. The angle of internal friction of both the dry and submerged sand is assumed to be  $\phi'$ .

As the wall yields from position  $ab$  into position  $a'b$ , the pressure against its back decreases from the value of the earth pressure at rest to that of the active Rankine pressure. In Article 26, it was shown that the entire effect of the porewater pressure on the effective stresses in the sand can be taken into account by assigning to the submerged part of the sand the submerged unit weight  $\gamma'$  (Eq. 15.6). Within the depth  $H_1$  the pressure on the

wall due to the weight of the adjoining sand is represented by the triangle  $ace$  in Fig. 28.2b. At any depth  $z'$  below the water table the effective vertical pressure on a horizontal section through the sand is

$$\sigma'_v = H_1 \gamma + z' \gamma'$$

For the corresponding horizontal active Rankine pressure we obtain by means of Eq. 27.5

$$\sigma'_h = \frac{\sigma'_v}{N_{\phi'}} = (H_1 \gamma + z' \gamma') \frac{1}{N_{\phi'}} \quad (28.3)$$

The resultant effective horizontal pressure below the water level is represented by the area  $bced$  in Fig. 28.2b. To this force must be added the resultant water pressure,

$$P_w = \frac{1}{2} \gamma_w H_2^2 \quad (28.4)$$

which acts against the lower part  $cb$  of the wall. In Fig. 28.2b, the water pressure is represented by the triangle  $def$ .

If the fill carries a uniformly distributed surcharge  $q$  per unit of area, the effective vertical stress  $\sigma'_v$  increases at any depth by  $q$ , and the corresponding horizontal active Rankine pressure increases by

$$\Delta \sigma'_h = \frac{q}{N_{\phi'}} \quad (28.5)$$

In Fig. 28.2b the pressure produced by the surcharge  $q$  is represented by the area  $aejihg$ .

### 28.4 Active Earth Pressure of Cohesive Soils against Smooth Vertical Surfaces

In Fig. 28.3a the line  $ab$  represents the smooth vertical back of a wall in contact with an unsaturated cohesive soil having a unit weight  $\gamma$  located above the water table. The shearing resistance of the soil is defined by Eq. 26.3

$$s = c + \sigma \tan \phi'$$

The relation between the extreme values of the principal

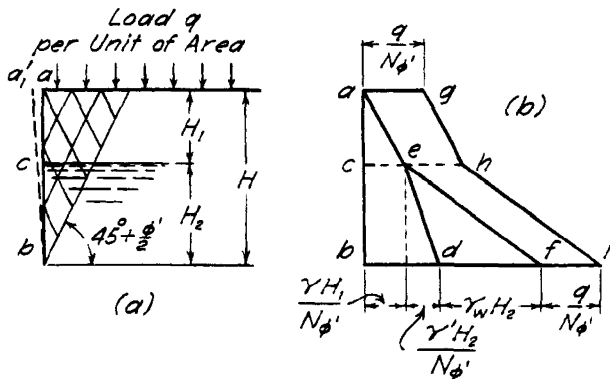


**Figure 28.2** Active earth pressure of partly submerged sand supporting a uniform surcharge. (a) Section through back of supporting structure; (b) pressure against back of structure.

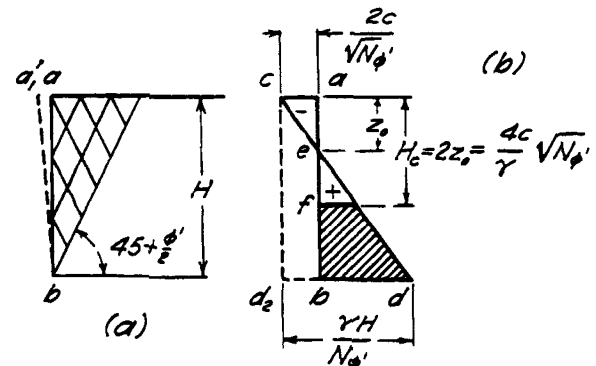


**Figure 28.3** Failure of clay behind smooth vertical wall when deformation condition for active earth pressure is satisfied. (a) Section through back of wall; (b) pressure against back of wall.

stresses in such soils is determined by the expression,

$$\sigma_1 = \sigma_3 N_{\phi'} + 2c\sqrt{N_{\phi'}} \quad (26.7)$$

wherein  $\sigma_1$  and  $\sigma_3$  are the major and minor total principal stresses, respectively, and

$$N_{\phi'} = \tan^2\left(45^\circ + \frac{\phi'}{2}\right) \quad (26.6)$$

is the flow value. In Article 17.4 it is also shown that the surfaces of sliding intersect the direction of the minor principal stress at an angle  $45^\circ + \phi'/2$ , regardless of the value of  $c$  (Eq. 26.2).

Because the back of the wall is smooth, the vertical principal stress at depth  $z$  below the horizontal surface of the backfill is  $\sigma_v = \gamma z$ . Before the support  $ab$  moves, it is acted on by the earth pressure at rest. In this state the horizontal stress  $\sigma_h$  is the minor principal stress. An outward movement of the support into or beyond the position  $a'b$  reduces  $\sigma_h$  to the value corresponding to the active Rankine pressure. Substituting  $\sigma_v = \sigma_1 = \gamma z$  and  $\sigma_h = \sigma_3$  into Eq. 26.2, we obtain

$$\sigma_h = \gamma z \frac{1}{N_{\phi'}} - 2c \frac{1}{\sqrt{N_{\phi'}}} \quad (28.6)$$

This stress at any depth  $z$  is represented by the horizontal distance between the lines  $ab$  and  $cd$  in Fig. 28.3b. At depth,

$$z_0 = \frac{2c}{\gamma} \sqrt{N_{\phi'}} \quad (28.7)$$

the stress  $\sigma_h$  is equal to zero. At a depth less than  $z_0$ , the pressure against the wall is negative, provided that a crack does not open up between the wall and the uppermost part of the soil. The resultant horizontal earth pressure against the wall is

$$P_A = \int_0^H \sigma_h dz = \frac{1}{2} \gamma H^2 \frac{1}{N_{\phi'}} - 2c \frac{H}{\sqrt{N_{\phi'}}} \quad (28.8)$$

If the wall has a height,

$$H = H_c = \frac{4c}{\gamma} \sqrt{N_{\phi'}} = 2z_0 \quad (28.9)$$

the resultant earth pressure  $P_A$  is equal to zero. Hence, if the height of a vertical bank is smaller than  $H_c$ , the bank should be able to stand without lateral support. However, the pressure against the wall increases from  $-2c/\sqrt{N_{\phi'}}$  at the crest to  $+2c/\sqrt{N_{\phi'}}$  at depth  $H_c$ , whereas on the vertical face of an unsupported bank the normal stress is zero at every point. Because of this difference the greatest depth to which a cut can be excavated without lateral support of its vertical sides is slightly smaller than  $H_c$  (see Article 35).

If the cohesive soil above the water table is practically saturated so that it is justifiable to express the extreme values of the principal stresses by Eq. 26.9, then

$$P_A = \frac{1}{2} \gamma H^2 - 2s_u H \quad (28.10)$$

and

$$H_c = \frac{4s_u}{\gamma} \quad (28.11)$$

Because the soil does not necessarily adhere to the wall, it is generally assumed that the active earth pressure of cohesive soils against retaining walls is equal to the pressure represented in Fig. 28.3b by the triangular area  $bde$ , equal to area  $cdd_2$  - area  $cebd_2$ . Therefore,

$$P_A = \frac{1}{2} \gamma H^2 \frac{1}{N_{\phi'}} - 2cH \frac{1}{\sqrt{N_{\phi'}}} + \frac{2c^2}{\gamma} \quad (28.12)$$

In terms of Eq. 26.9,

$$P_A = \frac{1}{2} \gamma H^2 - 2s_u H + \frac{2s_u^2}{\gamma} \quad (28.13)$$

## 28.5 Passive Earth Pressure of Cohesive Soils in Contact with Smooth Vertical Surfaces

If the face  $ab$  of the wall or block that supports the soil and its uniform surcharge  $q$  is pushed toward the backfill as indicated in Fig. 28.4a, the horizontal principal stress  $\sigma_h$  increases and becomes greater than  $\sigma_v$ . As soon as  $ab$  arrives at or beyond the position  $a'_2b$ , which represents the deformation condition for the passive Rankine state, the stress conditions for failure (Eq. 26.2) are satisfied. Because  $\sigma_h$  represents the major principal stress, we may substitute  $\sigma_h = \sigma_1$  and  $\sigma_v = \sigma_3 = \gamma z + q$  into Eq. 26.2 and obtain

$$\sigma_h = \gamma z N_{\phi'} + 2c\sqrt{N_{\phi'}} + qN_{\phi'} \quad (28.14)$$

The stress  $\sigma_h$  can be resolved into two parts. One part

$$[\sigma_h]_I = \gamma z N_{\phi'}$$

increases like a hydrostatic pressure in simple proportion to depth. In Fig. 28.4b the stresses  $[\sigma_h]_I$  are represented by the width of the triangle  $c_1c_2d_2$  with the area

$$[P_P]_I = \frac{1}{2} \gamma H^2 N_{\phi'} \quad (28.15)$$

The point of application of  $[P_P]_I$  is located at an elevation  $H/3$  above  $b$ . The quantity  $[P_P]_I$  represents the resultant passive earth pressure of a cohesionless material with an angle of internal friction  $\phi'$  and a unit weight  $\gamma$ .

The second part of  $\sigma_h$  is

$$[\sigma_h]_{II} = 2c\sqrt{N_{\phi'}} + qN_{\phi'}$$

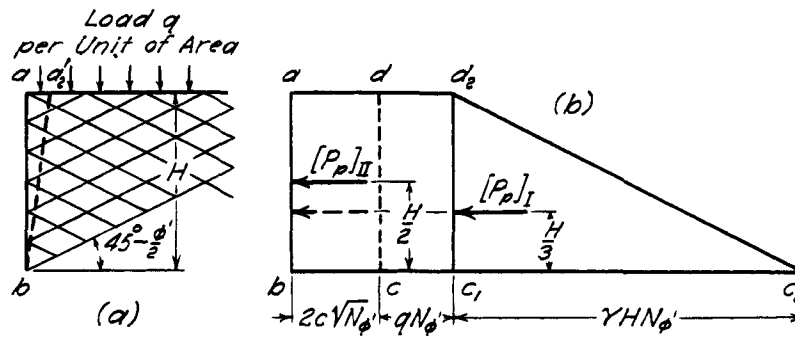


**Figure 28.4** Failure of clay behind smooth vertical wall when deformation condition for passive earth pressure is satisfied. (a) Section through back of wall; (b) stress on back of wall.

This part is independent of the depth. It is represented by the width of the rectangle  $abc_1d_2$  in Fig. 28.4b. The horizontal force is equal to the area of the rectangle. Hence,

$$[P_p]_{II} = H(2c\sqrt{N_{\phi'}} + qN_{\phi'}) \quad (28.16)$$

The point of application of  $[P_p]_{II}$  is at mid-height of the surface  $ab$ . Since Eq. 28.16 does not contain the unit weight  $\gamma$ , the value  $[P_p]_{II}$  can be computed on the assumption that the backfill is weightless. From Eqs. 28.15 and 28.16, we find that the resultant passive earth pressure is

$$P_p = [P_p]_I + [P_p]_{II} = \frac{1}{2}\gamma H^2 N_{\phi'} + H(2c\sqrt{N_{\phi'}} + qN_{\phi'}) \quad (28.17)$$

According to the preceding discussion,  $P_p$  can be computed by two independent operations. First,  $[P_p]_I$  is computed on the assumption that the cohesion and the surcharge are zero ( $c = 0$ ,  $q = 0$ ). The point of application of  $[P_p]_I$  is located at the lower third point of  $H$ . Second,  $[P_p]_{II}$  is computed on the assumption that the unit weight of the backfill is zero ( $\gamma = 0$ ). The point of application of  $[P_p]_{II}$  is at the midpoint of  $H$ . In the following articles this simple procedure is used repeatedly for determining the point of application of the passive earth pressure of cohesive soils. The subdivision of  $P_p$  into the two parts  $[P_p]_I$  and  $[P_p]_{II}$  is strictly correct only when the back of the wall is vertical and perfectly smooth. For all other conditions, the procedure is approximate.

### Problems

1. A wall with a smooth vertical back 3 m high retains a mass of dry cohesionless sand that has a horizontal surface. The sand weighs  $18 \text{ kN/m}^3$  and has an angle of internal friction of  $36^\circ$ . What is the approximate resultant pressure against the wall, if the wall is prevented from yielding? If the wall can yield far enough to satisfy the deformation condition for the active Rankine state?

*Ans.* A unique relationship between  $K_0$  and  $\phi'$  for densified sands does not exist. Using the correlation between  $K_0$  and

$\phi'$  in Fig. 44.6 and assuming  $K_{op} = 0.5$  leads to  $K_0 = 0.65$ ;  $53 \text{ kN/m}$ ;  $21 \text{ kN/m}$ .

2. The water level behind the wall described in problem 1 rises to an elevation 1 m below the crest. The submerged unit weight of the sand is  $10 \text{ kN/m}^3$ . If the deformation condition for the active Rankine state is satisfied, what is the resultant pressure that the earth and water exert against the wall? At what height above the base does the resultant of the earth and water pressures act?

*Ans.*  $37 \text{ kN/m}$ ;  $0.86 \text{ m}$ .

3. What is the resultant lateral pressure against the yielding wall in problem 1, if the sand mass supports a uniformly distributed load of  $20 \text{ kPa}$ ? At what height above the base of the wall is the center of pressure?

*Ans.*  $37 \text{ kN/m}$ ;  $1.2 \text{ m}$ .

4. The space between two retaining walls with smooth backs is filled with sand weighing  $18 \text{ kN/m}^3$ . The foundations of the walls are interconnected by a reinforced concrete floor, and the crests of the walls by heavy steel tie rods. The walls are 5 m high and 17 m apart. The surface of the sand is used for storing pig iron weighing  $15 \text{ kPa}$ . If the coefficient of the earth pressure at rest is  $K_0 = 0.50$ , what is the resultant pressure against the walls before and after the application of the surcharge?

*Ans.*  $113 \text{ kN/m}$ ;  $150 \text{ kN/m}$ .

5. A smooth vertical wall 6 m high is pushed against a mass of soil having a horizontal surface and an undrained shear strength  $s_u = 35 \text{ kPa}$ . The unit weight of the soil is  $17 \text{ kN/m}^3$ . Its surface carries a uniform load of  $10 \text{ kPa}$ . What is the total passive Rankine pressure? What is the distance from the base of the wall to the center of pressure? Determine the intensity of lateral pressure at the base of the wall.

*Ans.*  $786 \text{ kN/m}$ ;  $2.61 \text{ m}$ ;  $182 \text{ kPa}$ .

6. A smooth vertical wall 4 m high is pushed against an overconsolidated clay ( $\gamma = 19 \text{ kN/m}^3$ ,  $c' = 3 \text{ kPa}$ ,  $\phi' = 30^\circ$ , and average  $s_u = 120 \text{ kPa}$ ). The water table in the overconsolidated clay is 1 m below the ground surface. The surface of the overconsolidated clay carries a uniform load of  $25 \text{ kPa}$ . Using the Rankine theory calculate the resultant pressure per lineal meter against the wall when the clay behind the wall fails (a) in an undrained condition, and (b) in a drained condition. (c)

What are the distances from the base of the wall to the center of pressure in cases (a) and (b)?

Ans. 1212 kN/m; 708 kN/m; 1.9 m; 1.7 m.

## ARTICLE 29 INFLUENCE OF WALL FRICTION ON THE SHAPE OF THE SURFACE OF SLIDING

The back of the wall in Fig. 29.1a is assumed to be rough. Otherwise it is identical with that shown in Fig. 27.2a. The backfill consists of clean sand. If the wall moves outward, the sliding wedge subsides, and the sand moves downward along the back of the wall. The downward movement of the sand with reference to the wall develops frictional forces that cause the resultant active earth pressure to be inclined at an angle  $\delta$  to the normal to the wall. This angle is known as the *angle of wall friction*. It is considered positive when the resultant reaction is oriented such that its tangential component acts in an upward direction (Fig. 29.1a). Advanced theoretical analyses (Ohde 1938) as well as experiments have shown that the corresponding surface of sliding  $bc$  consists of a curved lower portion and a straight upper part. Within the section  $adc$  of the sliding wedge the shear pattern is identical with the active Rankine pattern (Fig. 27.2a). Within the area  $adb$  the shear pattern consists of two sets of curved lines.

If the wall is forced down with reference to the backfill, for instance by the action of a heavy load on its crest, the value of  $\delta$  becomes negative, and the curvature of the lower part of the surface of sliding is reversed, as shown in Fig. 29.1b.

If the wall is pushed toward the fill, the movement is resisted by the passive earth pressure. If the weight of

the wall is greater than the friction between the sand and the wall, the sand rises with reference to the wall, and the reaction to the resultant passive earth pressure acts at an angle  $\delta$  with the normal to the back of the wall. The tangential component of this force tends to prevent the rise of the sand. Under this condition the angle  $\delta$  (Fig. 29.1c) is considered positive. The straight portion of the surface of sliding rises at an angle  $45^\circ - \phi'/2$  with the horizontal. Within the isosceles triangle  $adc$  the shear pattern is identical with that shown in Fig. 27.2b, and the material is in the passive Rankine state. Within the area  $adb$  both sets of lines which constitute the shear pattern are curved.

If the weight of the wall is smaller than the friction between the sand and the wall, the angle between the normal to the back of the wall and the reaction to the resultant passive pressure is smaller than  $\delta$ . Finally, if the wall is acted on by an upward force equal to the sum of the weight of the wall and the friction between the sand and the wall, the resultant passive earth pressure is oriented as shown in Fig. 29.1d, and the angle of wall friction is considered negative. The curvature of the curved portion of the surface of sliding is reversed.

The deformation conditions for the plastic states represented by the shear patterns in Fig. 29.1, *a* and *b*, require a certain minimum lengthening of every horizontal element of the wedge. The deformation conditions for the plastic states represented in Fig. 29.1, *c* and *d*, require a certain minimum shortening of every horizontal element. These requirements are the equivalent of those for producing the active or passive Rankine states in the backfill of a perfectly smooth wall, as illustrated by Fig. 27.2, *a* and *b*.

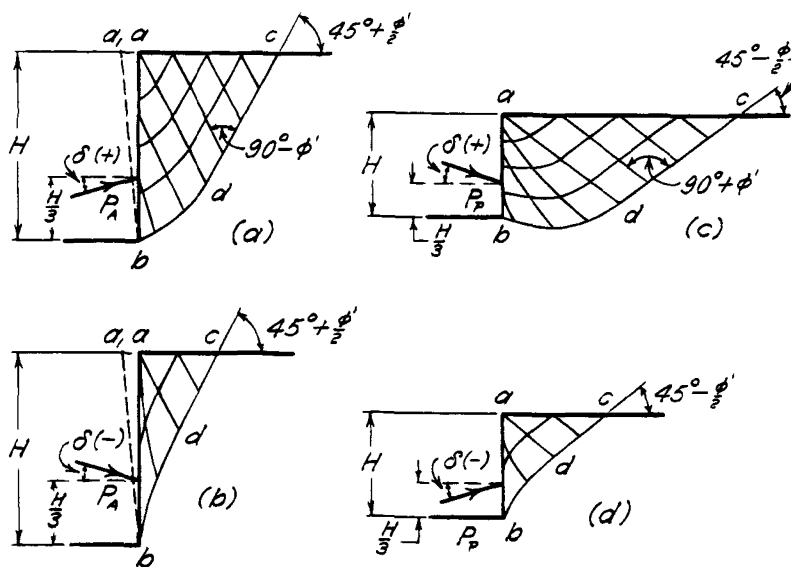


Figure 29.1 Shear patterns associated with failure of sand behind rough vertical wall.

## ARTICLE 30 COULOMB'S THEORY OF ACTIVE EARTH PRESSURE AGAINST RETAINING WALLS

### 30.1 Introduction

Because the back of every real retaining wall is rough to some extent, the boundary conditions for the validity of Rankine's theory are seldom satisfied, and earth-pressure computations based on this theory usually involve an appreciable error. Most of this error can be avoided by using Coulomb's theory (Coulomb 1776). Coulomb's method can be adapted to any boundary condition, but, in exchange, it involves a simplifying assumption regarding the shape of the surface of sliding. However, the error due to this assumption is commonly small compared with that associated with the use of Rankine's theory. When the boundary conditions for the validity of Rankine's theory are satisfied, the two theories lead to identical results.

Both Coulomb's and Rankine's theories are based on the assumptions that the wall is free to move into or beyond position  $a_1b$  (Fig. 29.1a) and that the water contained in the voids of the soil does not exert any appreciable seepage pressure. It is also quite obviously assumed that the soil properties that appear in the equations have definite values that can be determined.

### 30.2 Coulomb's Theory

The surface of sliding in the backfill of a real retaining wall is slightly curved, as shown in Fig. 29.1,  $a$  and  $b$ . To simplify the computations, Coulomb assumed it to be plane. The error due to disregarding the curvature is quite small, however.

The forces that act on the sliding wedge are shown in Fig. 30.1a in which the straight line  $bc_1$  is arbitrarily assumed to represent the surface of sliding. The wedge  $abc_1$  is in equilibrium under the weight  $W_1$ , the reaction to the resultant earth pressure  $P_1$ , and the reaction  $F_1$ . The reaction  $F_1$  is inclined at the angle  $\phi'$  to the normal to  $bc_1$  because the frictional resistance is assumed to be fully developed along the surface of sliding. If the retaining wall rests on a firm foundation, the force  $P_1$  is inclined to the normal to the back of the wall at the angle of wall friction  $+\delta$ , as indicated by the solid arrow in the figure. On the other hand, if it is likely that the wall may settle more than the backfill, the force  $P_1$  will be inclined at the angle  $-\delta$ , as shown by the dash arrow. Because the magnitude of  $W_1$  is known and the directions of all three forces are also known, the resultant earth pressure  $P_1$  can be scaled from the polygon of forces (Fig. 30.1b). Inasmuch as  $bc_1$  is not necessarily the real surface of sliding, similar constructions are made to determine the resultant earth pressures  $P_2$ ,  $P_3$ , etc., for other arbitrarily selected surfaces  $bc_2$ ,  $bc_3$ , etc. (not shown). The greatest value of the resultant earth pressure obtained

in this manner is equal to the resultant active earth pressure  $P_A$ .

### 30.3 Culmann's Graphical Construction

An expedient method was devised by Culmann (1875) for performing the graphical constructions described in the preceding paragraph. It is illustrated in Fig. 30.1c. The first step in Culmann's procedure is to trace the line  $bS$  which passes through the bottom edge  $b$  of the back of the wall and rises at the angle  $\phi'$  above the horizontal base of the backfill. This line is known as the *slope line* because it represents the natural slope of the backfill material. The next step is to trace the *earth-pressure line*  $bL$ , which is located below the slope line and which intersects it at the angle  $\theta$ . The angle  $\theta$  is equal to the angle between the vertical and the direction of the resultant earth pressure  $P_A$ , as shown in Fig. 30.1. It depends on the angle of wall friction  $\delta$  and the inclination  $\alpha$  of the back of the wall.

To determine the resultant earth pressure  $P_1$  exerted by a wedge located above an arbitrary plane surface of sliding  $bc_1$ , it is first necessary to compute the weight  $W_1$  of this wedge. This weight is laid off along  $bS$  at any convenient scale of forces. Thus point  $d_1$  is obtained. The line  $d_1e_1$  is then traced parallel to  $bL$ . Since the triangle  $e_1d_1b$  in Fig. 30.1c is similar to the force polygon (Fig. 30.1b), the distance  $d_1e_1$  is equal to the resultant earth pressure corresponding to the surface of sliding  $bc_1$ . To find the resultant active earth pressure  $P_A$ , the construction is repeated for different planes  $bc_2$ , etc. The points  $e_1$ ,  $e_2$ , etc., are connected by a curve  $C$ , known as the *Culmann line*, and a tangent to  $C$  is traced parallel to  $bS$ . The distance  $ed$  represents  $P_A$ , and the real surface of sliding passes through point  $e$ .

### 30.4 Earth Pressure Due to Line Load

Figure 30.2 is a section through a wall that supports a mass of sand with an inclined surface. Along a line parallel to the crest of the wall, at a distance  $ac'$  from the crest, the surface of the backfill carries a load  $q$  per unit of length of the line. The procedure for determining the resultant active earth pressure against the wall is essentially the same as that illustrated in Fig. 30.1c. However, if the right-hand boundary of a wedge intersects the ground surface to the right of  $c'$ , the distance to be laid off on the slope line  $bS$  is proportional to the weight of the sand that constitutes the wedge, plus the line load  $q$  (Fig. 30.2).

If the ground surface carried no surcharge, the Culmann line  $C$  (dash curve) in Fig. 30.2 would correspond to the line  $C$  in Fig. 30.1c. If the surface carries a line load  $q$  at some point  $c'$ , the Culmann line consists of two sections. The section to the left of plane  $bc'$  is identical with  $C$ , because the wedges bounded by planes to the left of  $bc'$  carry no surcharge. On the right side of  $bc'$  the Culmann line for the loaded backfill is located above  $C$ , as



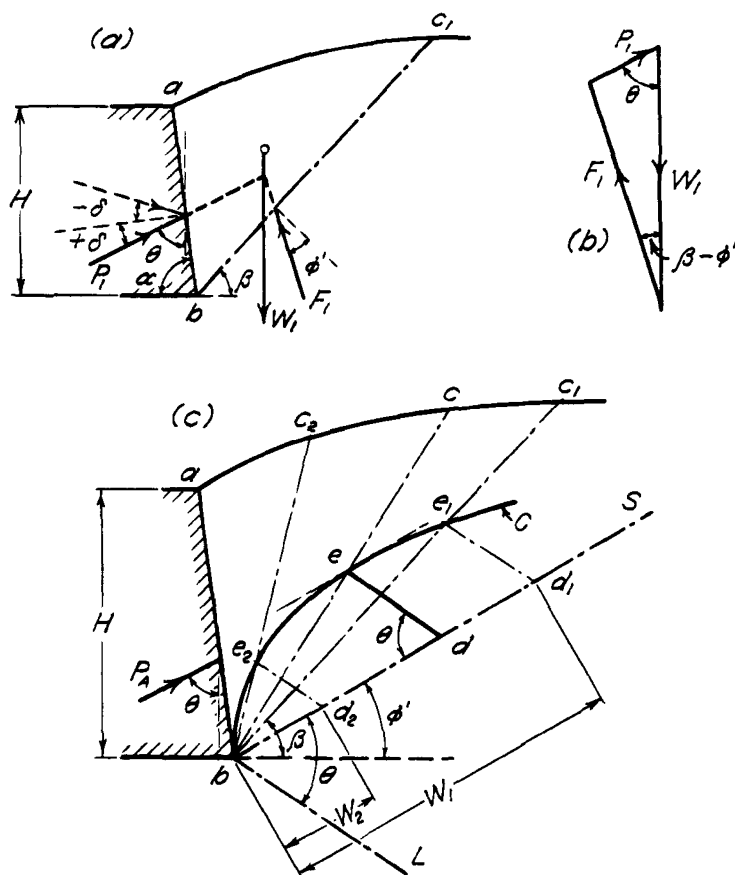


**Figure 30.1** (a, b) Diagrams illustrating assumptions on which Coulomb's theory of active earth pressure is based; (c) Culmann's graphical method for determining earth pressure of sand.

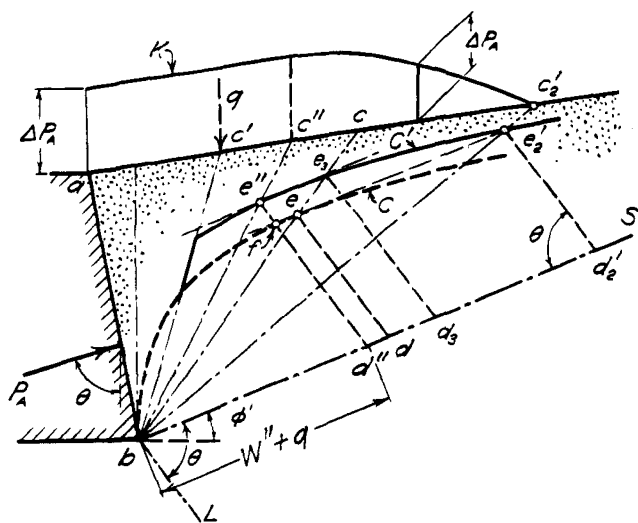


**Figure 30.2** Culmann's graphical method for determining earth pressure exerted by sand backfill that carries a line load.

indicated by the solid curve  $C'$  in Fig. 30.2, because every wedge bounded by a plane to the right of  $bc'$  is acted on by the weight  $q$ . Therefore the complete Culmann line consists of the curve  $C$  to the left of  $bc'$ , and the curve  $C'$  to the right. It has a discontinuity at the plane  $bc'$  which passes through the point of application of the line load.

If the load is located on the left side of  $c'_2$  the value of the resultant active earth pressure exerted by the loaded backfill corresponds to the greatest distance between the Culmann line  $C'$  and the slope line  $bS$  measured in a direction parallel to the earth pressure line  $bL$ . If the line load acts at any position on the surface of the fill between points  $a$  and  $c''$ , the greatest distance is  $d''e''$ . Therefore, the slip occurs along the plane  $bc''$  which passes through  $e''$ . The quantity  $d''e'' - de$  represents that part  $\Delta P_A$  of the resultant active earth pressure due to the line load  $q$ .

The ordinates of the curve  $K$  (Fig. 30.2) with reference to the ground surface represent the values of  $\Delta P_A$  corresponding to the various positions  $c'$  at which  $q$  may be located. Between  $a$  and  $c''$ ,  $K$  is straight and parallel to the surface of the backfill because  $\Delta P_A$  is independent of the position of  $q$  between these two points.

If  $q$  moves to the right beyond  $c''$  to such a position as  $c$ , the Culmann line consists of the dash curve  $C$  to the left of  $bc$  and the solid curve  $C'$  to the right. The maximum value  $P_A$  of the earth pressure is represented by the line  $e_3d_3$ . The failure plane passes through the point  $e_3$  and intersects the ground surface at the line of application of  $q$ . As the line of application of  $q$  moves to the right, the value of  $\Delta P_A$  decreases steadily as indicated by the ordinates of curve  $K$  (Fig. 30.2) until at  $c'_2$  it becomes equal to zero.

Finally, if the line of action of  $q$  is at  $c'_2$ , the value of the resultant earth pressure  $e'_2d'_2$ , determined by means of curve  $C'$ , is equal to the value  $ed$  that represents the resultant active earth pressure when there is no surcharge. If  $q$  moves to the right of  $c'_2$ , the resultant earth pressure determined by means of  $C'$  becomes smaller than  $ed$ . Hence, if the line load acts on the right side of  $c'_2$ , it no longer has any effect on the active earth pressure, and the surface of sliding has the same position  $bc$  as it does for a backfill that carries no surcharge. The greater the line load  $q$ , the farther  $c'_2$  moves to the right. Therefore, the distance within which  $q$  has an influence on the earth pressure depends on the magnitude of  $q$ .

Culmann's method is chiefly used if the wall has an inclined or broken back, and if the backfill has an irregular surface or carries a surcharge. If a vertical wall supports a cohesionless backfill with a horizontal surface, it is more expedient to obtain the value of  $P_A$  from charts prepared for this purpose. Figure 30.3 consists of two different charts of this kind.

### Problems

1. A vertical retaining wall 6.1 m high supports a cohesionless fill that weighs  $18.4 \text{ kN/m}^3$ . The upper surface of the fill rises from the crest of the wall at an angle of  $20^\circ$  with the horizontal. The angle of internal friction is  $28^\circ$ , and the angle of wall friction is  $20^\circ$ . By Culmann's method compute the total active earth pressure against the wall.

Ans.  $155 \text{ kN/m}$ .

2. The stem of a cantilever retaining wall is 11 m high. It retains a storage pile of cohesionless iron ore. The wall has a cross-section symmetrical about its vertical center line. At the top its width is 1.83 m and at the base of the stem is 3.66 m. From a point on the back of the wall 1.22 m below the crest, the surface of the ore pile rises at an angle of  $35^\circ$  with the horizontal to a maximum height of 19.8 m above the base of the stem. The remainder of the pile is level. If  $\phi'$  and  $\delta$  are each equal to  $36^\circ$  and  $\gamma$  is  $25.6 \text{ kN/m}^3$  what is the total lateral pressure of the ore above the base of the stem? If the entire lateral force against the stem is resisted by steel tie rods 7.62 cm square, stressed to 186 MPa, what spacing of the rods is required?

Ans.  $713 \text{ kN/m}$ ; 1.52 m.

3. A vertical wall 5.5 m high supports a cohesionless fill weighing  $16.8 \text{ kN/m}^3$ . The surface of the fill is horizontal. The

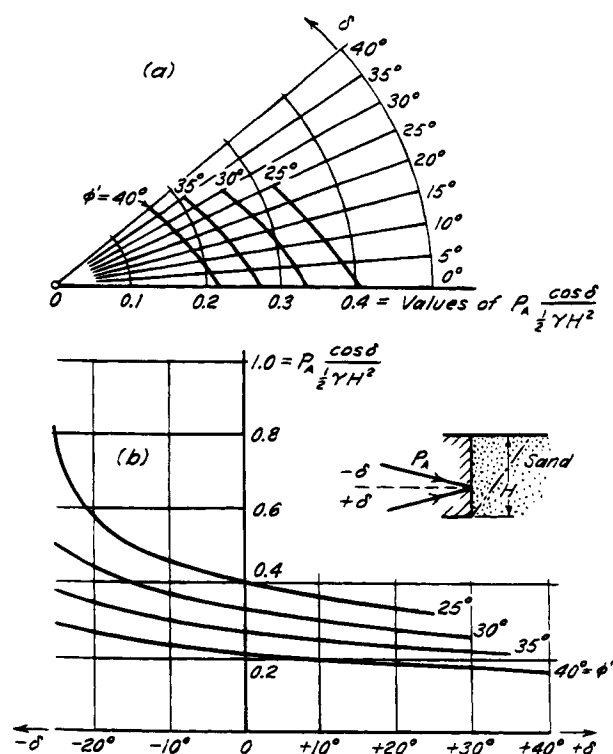


Figure 30.3 Two types of charts that furnish coefficients for computation of active earth pressure ( $a$  after Syffert 1929).

values of  $\phi'$  and  $\delta$  are  $31^\circ$  and  $20^\circ$ , respectively. The fill supports two line loads of  $29.2 \text{ kN/m}$ , parallel to the crest of the wall, at distances of 2.45 and 3.95 m, respectively. Compute the value of the total active earth pressure against the wall. Determine the horizontal distance from the back of the wall to the point at which the surface of sliding intersects the surface of the fill.

Ans.  $92 \text{ kN/m}$ ; 3.96 m.

4. A retaining wall 4.57 m high with a vertical back is just adequate to support a level fill of sand having a unit weight of  $18.4 \text{ kN/m}^3$  and a value of  $\phi'$  equal to  $32^\circ$ . The value of  $\delta$  is  $20^\circ$ . A vertical load of  $73 \text{ kN/m}$  is to be added along a line parallel to the crest of the wall. What is the minimum horizontal distance at which the load can be located from the back of the wall without increasing the earth pressure against the wall?

Ans. 4.94 m.

5. If the fill in problem 3 carries no surcharge, what is the magnitude of the active earth pressure? Check the graphical computation by means of the charts, Fig. 30.3

Ans.  $71 \text{ kN/m}$ .

### Selected Reading

Details of calculation of earth pressure by the graphical trial wedge method, identical in principle with Culmann's method, are given for a variety of conditions and for materials possessing both  $c$  and  $\phi'$  by Huntington, W. C. (1957). *Earth Pressures and Retaining Walls* New York, John Wiley and Sons, 534 pp.

### ARTICLE 31 POINT OF APPLICATION OF EARTH PRESSURE

The procedure described in Article 30 makes it possible to determine the magnitude of the total earth pressure provided its direction is known. However, it does not furnish any information regarding the point of application of the resultant pressure. To get this information, Coulomb assumed that every point on the back of a wall represents the foot of a potential surface of sliding. For example, the point  $d$  on the curved line  $ab$  in Fig. 31.1a represents the lower extremity of a potential surface of sliding  $de$ . The resultant earth pressure  $P_A$  on  $ad$  can be computed by means of Culmann's procedure as described in Article 30. If the depth to the foot of the potential surface of sliding is increased from  $z$  to  $z + dz$ , the resultant earth pressure is increased by

$$dP_A = p_A dz$$

where  $p_A$  is the average pressure over the increment of depth  $dz$ . Therefore,

$$p_A = \frac{dP_A}{dz} \quad (31.1)$$

By means of this equation the distribution of the earth pressure on the back of the wall can be determined. When the distribution is known, the point of application of the resultant pressure can be located by a suitable analytical or graphical method. At any point the line of action of the pressure  $p_A$  makes an angle  $\delta$  with the normal to the back of the wall.

In practice, this method is rather cumbersome. Therefore, simplified methods are used that give approximately the same results. For instance, in Fig. 31.1a, the point of application  $O_1$  is located approximately at the point of intersection of the back of the wall and a line  $OO_1$ , which is parallel to the surface of sliding  $bc$  and which passes through the center of gravity  $O$  of the sliding wedge  $abc$ .

Figures 31.1b and c illustrate a simplified method for estimating the position of the point of application of the additional resultant pressure  $\Delta P_A$  produced by a line load  $q$ . The lines  $bc$ ,  $bc''$ , etc., correspond to the lines  $bc$ ,  $bc''$ , etc., in Fig. 30.2. If  $q$  acts between  $a$  and  $c''$  (Fig. 31.1b),  $b'c'$  is traced parallel to the surface of sliding  $bc''$ , and  $a'c'$  is traced parallel to  $bS$ , the slope line (see Fig. 30.2). The force  $\Delta P_A$  acts at the upper third-point of  $a'b'$ . If  $q$  acts between  $c''$  and  $c'_2$ ,  $a'c'$  is traced parallel to  $bS$ , and  $\Delta P_A$  acts at the upper third-point of  $a'b$ , as shown in Fig. 31.1c.

All these procedures are based on Coulomb's assumption that every point on the back of a wall represents the foot of a potential surface of sliding. This assumption is justified in connection with retaining walls, because most such walls can hardly fail without yielding in a manner that satisfies the deformation condition for the plastic state. Coulomb, however, did not specify this deformation condition. Consequently, the theory was commonly used for computing the active earth pressure against lateral supports that did not satisfy the deformation condition, such as the bracing in open cuts (Article 37). Because it was found that the results of the computations did not

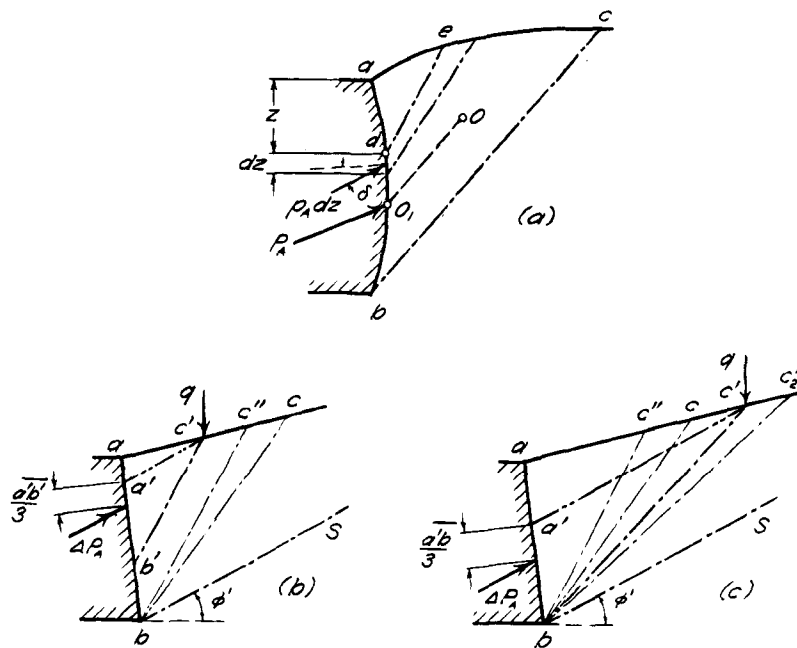


Figure 31.1 Diagrams illustrating simplified procedure for determining point of application of active earth pressure.

agree with reality, many experienced engineers concluded that the theory as such was unreliable. Therefore, it should be emphasized that Coulomb's theory is as satisfactory as any theory in structural engineering, provided the deformation condition for its validity is satisfied.

### Problems

1. At what distance above the base of the stem of the retaining wall of problem 2, Article 30, does the resultant earth pressure act?

Ans. 3.29 m.

2. Locate the center of pressure of the added earth pressure due to each of the two line loads in problem 3, Article 30, on the assumption that the influence of each of the two loads can be considered separately.

Ans. 3.05 m; 2.06 m from the bottom of the wall.

## ARTICLE 32 PASSIVE EARTH PRESSURE AGAINST ROUGH CONTACT FACES

### 32.1 Definition

In the broadest sense, the term passive earth pressure indicates the resistance of a mass of soil against displacement by lateral pressure. The object that exerts the lateral pressure may consist of the foundation of a retaining wall, the outer face of the buried part of a sheet pile bulkhead, or a block of masonry such as the abutment of a loaded arch. It may also consist of a mass of soil that exerts a horizontal pressure because it supports a vertical load. The soil beneath a loaded footing acts in this manner. Because the stability of almost any lateral earth support and the bearing capacity of every shallow foundation depend to some extent on the passive earth pressure, the problem of computing this pressure is of outstanding practical importance.

The surface of contact between the soil and the object that exerts the lateral pressure is called the *contact face*. Coulomb computed the passive earth pressure against rough contact faces on the simplifying assumption that the surface of sliding is plane (Fig. 32.1, *a* and *b*). The error due to this assumption is always on the unsafe side. If the angle of wall friction  $\delta$  is small, the surface of sliding is really almost plane and the error is tolerable. However, if  $\delta$  is large, the error is excessive, and Coulomb's method should not be used.

### 32.2 Coulomb's Theory of the Passive Earth Pressure of Sand

The Coulomb value of the resultant passive earth pressure can be determined graphically by Culmann's method. The procedure is identical with that described in Article 30 except that the slope line  $bS$  (Fig. 30.1c) must be drawn at an angle  $\phi'$  below the horizontal instead of above.

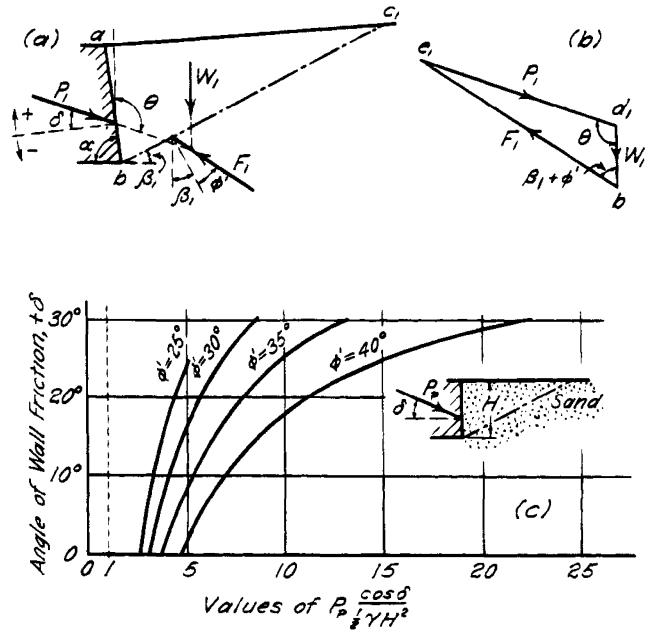


Figure 32.1 (a, b) Diagrams illustrating assumptions on which Coulomb's theory of passive earth pressure is based; (c) chart that furnishes coefficients for computation of passive earth pressure.

Figure 32.1c shows the influence of the angle of wall friction  $\delta$  on the Coulomb value of the resultant passive earth pressure. According to this chart, the earth pressure increases rapidly with increasing values of the angle of wall friction. However, if  $\delta$  is greater than about  $\phi'/3$ , the surface of sliding is strongly curved (Fig. 29.1c). As a consequence, the error due to Coulomb's assumption of a plane surface increases rapidly. For  $\delta = \phi'$  it may be as great as 30%. Hence, for values of  $\delta$  greater than  $\phi'/3$ , the curvature of the surface of sliding must be taken into consideration.

### 32.3 Passive Earth Pressure of Cohesive Soils

To illustrate the methods for determining the passive earth pressure without assuming a plane surface of sliding, the problem illustrated by Fig. 32.2 will be solved. In this figure  $ab$  is a section through a contact face that is pushed toward a mass of unsaturated cohesive soil with the water table below the surface of sliding. The shearing resistance of the soil is determined by Eq. 26.3,

$$s = c + \sigma \tan \phi'$$

The surface of the soil is horizontal. The angle of wall friction is denoted by  $\delta$ , and the total adhesion between the soil and the contact face by  $C_a$ . The real surface of sliding is  $bde$ . It consists of a curved part  $bd$  and a straight part  $de$ . According to Article 29, the soil within the isosceles triangle  $ade$  is in the passive Rankine state. Therefore, the shearing stresses on the vertical section  $df$  are zero,

and the force  $P_d$  on this section is horizontal. It can be computed by Eq. 28.17. The body of soil  $abdf$  is acted on by the following forces: its weight  $W$ ; the force  $P_d$ ; the resultant  $C$  of the cohesion along  $bd$ ; the adhesion  $C_a$  along  $ab$ ; the resultant  $F$  of the normal and frictional stresses along  $bd$ ; and the resultant  $P_p$  of the normal and frictional components of the passive earth pressure.

Because the point of application of  $P_p$  is not known, we use the approximations discussed at the end of Article 28 and replace  $P_p$  by the two forces,  $[P_p]_I$  and  $[P_p]_{II}$ . Each of these forces acts at an angle  $\delta$  with the normal to the contact face. One force  $[P_p]_I$  maintains equilibrium with the weight of the mass  $abdf$  and the friction due to the weight. The other,  $[P_p]_{II}$ , maintains equilibrium with the cohesion on the surface of sliding and the friction due to forces other than the weight. The force  $[P_p]_I$  acts at the lower third-point of  $ab$ , whereas  $[P_p]_{II}$  acts at the midpoint. Because the point of application and the direction of each of these forces are known, we may compute each force individually. The resultant of these two forces represents the resultant passive earth pressure  $P_p$ .

The methods for determining the real shape of the surface of sliding are so involved that they are unsuitable for practical purposes. However, sufficiently accurate results can be obtained on the simplifying assumption that the curved portion  $bd$  of the real surface of sliding is either an arc of a circle or a logarithmic spiral that has the equation,

$$r = r_0 e^{\theta \tan \phi'} \quad (32.1)$$

In the following paragraphs, the curved part of the surface of sliding is assumed to be a logarithmic spiral. Since the spiral is tangent at  $d$  to the straight part  $de$  of the surface of sliding, the center  $O$  of the spiral must be located on the line  $aD$  (Fig. 32.2) which is inclined at  $45^\circ - \phi'/2$  to the horizontal. According to Eq. 32.1, every radius of the spiral makes an angle  $\phi'$  with the normal to the spiral at the point where it intersects the curve. Because  $\phi'$  is the angle of internal friction, the resultant  $dF$  of the normal stress and the frictional resis-

tance on any element of the surface of sliding also makes an angle  $\phi'$  with the normal to the element, and its direction coincides with that of the radius that subtends the element. Because every radius of the spiral passes through point  $O$ , the resultant  $F$  of the normal and frictional forces on  $bd$  also passes through the center  $O$ . This fact is used in the following calculations.

To compute  $[P_p]_I$  (the value of  $P_p$  if  $c = 0$ ), we arbitrarily select a surface of sliding  $bd_1e_1$  (Fig. 32.3a) consisting of the logarithmic spiral  $bd_1$  with its center at  $O_1$ , and the straight line  $d_1e_1$  which makes an angle of  $45^\circ - \phi'/2$  with the horizontal. The lateral pressure required to produce a slip on this surface is designated as  $[P_1]_I$ . We then evaluate the force  $[P_{d_1}]_I$  which acts at the lower third-point of  $f_1d_1$ , by means of the equation,

$$[P_{d_1}]_I = \frac{1}{2} \gamma H_{d_1}^2 N_{\phi'}$$

Finally, we take moments of the forces  $[P_1]_I$ ,  $[P_{d_1}]_I$ ,  $W_1$ , and  $[F_1]_I$  about  $O_1$ . Because the moment of  $[F_1]_I$  about  $O_1$  is zero,

$$[P_1]_I l_1 = W_1 l_2 + [P_{d_1}]_I l_3$$

from which

$$[P_1]_I = \frac{1}{l_1} (W_1 l_2 + [P_{d_1}]_I l_3) \quad (32.2)$$

The value of  $[P_1]_I$  is plotted to scale above  $f_1$ . It is represented by the point  $C'_1$ . Similar computations are performed for other arbitrarily selected surfaces of sliding, and a curve  $[P]_I$  is drawn through the points  $C'_1$ , etc. If the soil has no cohesion ( $c = 0$ ), the second component  $[P_p]_{II}$  of the passive earth pressure  $P_p$  is equal to zero, and the value of  $P_p$  is represented by the minimum ordinate of the curve  $[P]_I$  at point  $C'$ . The surface of sliding passes through the point  $d$  which is located on  $aD$  vertically below  $C'$ .

If the soil possesses cohesion, we must also compute  $[P_p]_{II}$  (the value of  $P_p$  if  $\gamma = 0$ ). To calculate the value  $[P_1]_{II}$  which corresponds to the arbitrary surface of sliding

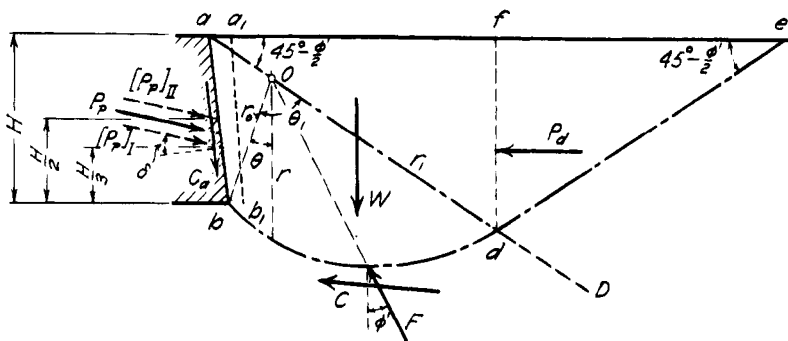


**Figure 32.2** Diagram illustrating assumptions on which theory of passive earth pressure against rough contact faces is based.

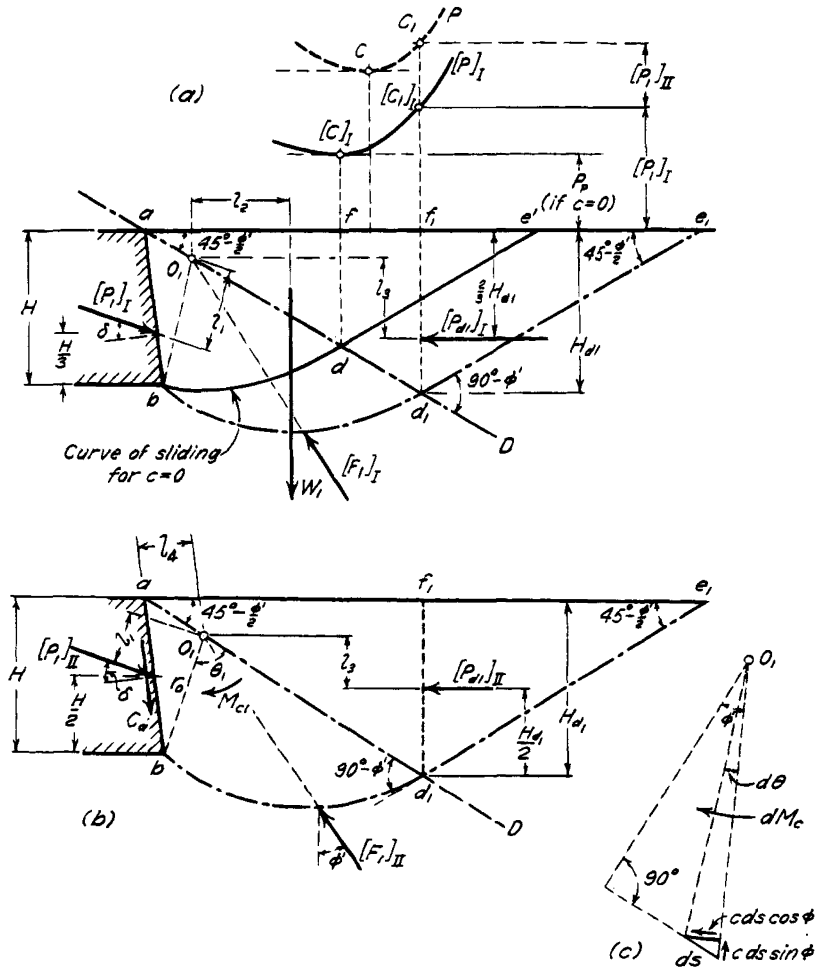


**Figure 32.3** Logarithmic spiral method for determining passive earth pressure. (a) Forces entering into computation of component due to weight of soil, neglecting cohesion; (b) forces entering into computation of component due to friction and cohesion, neglecting weight of soil; (c) diagram illustrating computation of moment due to cohesion.

$bd_1e_1$ , we must consider the forces involved in the computation (see Fig. 32.3b). The value of  $[P_{d_1}]_{II}$  is obtained by making  $q = 0$  and  $H = H_{d_1}$  in Eq. 28.16. Hence,

$$[P_{d_1}]_{II} = 2cH_{d_1}\sqrt{N_{\phi'}}.$$

The point of application of this force is at the midheight of  $d_1f_1$ . The influence of the cohesion along the curve  $bd_1$  may be evaluated by considering an element having a length  $ds$  (Fig. 32.3c). The cohesion along the length  $ds$  is equal to  $c ds$ . The moment of  $c ds$  about  $O_1$  is

$$dM_c = rc ds \cos \phi' = rc \frac{r d\theta}{\cos \phi'} \cos \phi' = cr^2 d\theta$$

and the moment of the total cohesion along  $bd_1$  is

$$M_{c_1} = \int_0^{\theta_1} dM_c = \frac{c}{2 \tan \phi'} (r_1^2 - r_0^2) \quad (32.3)$$

The force  $[F_1]_{II}$  passes through  $O_1$ . By taking moments about this point, we obtain

$$[P_1]_{II}l_1 = M_{c_1} + [P_{d_1}]_{II}l_3 - C_a l_4$$

from which

$$[P_1]_{II} = \frac{1}{l_1} (M_{c_1} + [P_{d_1}]_{II}l_3 - C_a l_4) \quad (32.4)$$

In Fig. 32.3a the value  $[P_1]_{II}$  is plotted to scale at  $C_1$  above point  $C'_1$ . Because  $[P_1]_I$  and  $[P_1]_{II}$  represent the forces required to overcome the two parts of the resistance against sliding along the same surface  $bd_1e_1$ , the ordinate of point  $C_1$  represents the total force required to produce a slip along this surface. Similarly, values of  $[P]_{II}$  are obtained for other arbitrary surfaces of sliding, and a curve  $P$  is drawn through the points  $C_1, \dots$ . The passive earth pressure  $P_p$  is represented by the minimum ordinate of the curve  $P$ , and the surface of sliding passes through a point on  $aD$  directly below the point  $C$  at which curve  $P$  is closest to  $ae_1$ . The total force against the contact face is equal to the resultant of  $P_p$  and the adhesion force  $C_a$ .

The shape of the curved part of the real surface of sliding is intermediate between that of an arc of a circle and that of a spiral. Because the difference between the shapes of these two curves is small, the error due to replacing the real curve by either a circle or a logarithmic spiral is negligible. As a matter of fact, comparisons between the approximate and the exact methods have shown that values of the passive earth pressure computed by means of the approximate methods are at least as accurate as values of the active earth pressure computed by Coulomb's method in which it is assumed that the real slightly curved surface of sliding is a plane.

The preceding investigations are based on the assumption that the mass of soil adjoining the contact face is pushed into a position located entirely beyond  $a_1b_1$  (Fig. 32.2). If the upper part of the contact face does not advance so far as  $a_1b_1$ , the surface of sliding is curved throughout its full length, and only the lowest part of the sliding mass passes into the passive Rankine state. If the lower part of the face stops short of  $a_1b_1$ , the soil adjoining this part does not pass into a state of plastic equilibrium at all. In these instances, the resultant passive earth pressure and its distribution over the contact face depend on the type of restriction imposed on the movement of the contact face.

### Problems

1. Construct a logarithmic spiral for  $\phi' = 36^\circ$ . The value of  $r_0$  should be taken as 1 cm, with values of  $\theta$  ranging from  $-30^\circ$  to  $270^\circ$ .

2. Compute by the logarithmic-spiral method the resultant passive earth pressure against a vertical face in contact with a sand fill having a level surface. The contact face is 6.1 m high, and the angle of wall friction is  $+20^\circ$ . The fill has a unit weight of  $17.9 \text{ kN/m}^3$  and an angle of internal friction of  $36^\circ$ . To facilitate use of the spiral constructed in problem 1, the graphical solution should be laid out on tracing paper. Use the scale 1 cm = 1 m

Ans. 2555 kN/m.

3. Compute the value of passive earth pressure in problem 2, assuming a plane surface of sliding.

Ans. 2920 kN/m.

4. Compute the resultant passive earth pressure against the contact surface of problem 2 if, in addition to frictional resistance, the soil possesses a cohesion intercept of 24 kPa. The adhesion between the soil and the contact face is also 24 kPa. Locate the resultant earth pressure  $P_A$ .

Ans. 3725 kN/m; 2.44 m above base.

### Selected Reading

Tables of active and passive earth pressures, for materials possessing friction, cohesion, or both, and for all angles of wall friction, are contained in Caquot, A. and J. Kerisel

(1948). *Tables for the Calculation of Passive Pressure, Active Pressure and Bearing Capacity of Foundations*. Translated from the French by Maurice A. Bec., Paris, Gauthier-Villars, 120 pp.

## ARTICLE 33 BEARING CAPACITY OF SHALLOW FOOTINGS

### 33.1 Fundamental Assumptions

When a load is applied on a limited portion of the surface of a soil, the surface settles. The relation between the settlement and the average load per unit of area may be represented by a *settlement curve* (Fig. 33.1). If the soil is fairly dense or stiff, the settlement curve is similar to curve  $C_1$ . The abscissa  $[q_d]_1$  of the vertical tangent to the curve represents the *bearing capacity* of the soil. If the soil is loose or fairly soft, the settlement curve may be similar to  $C_2$ , and the bearing capacity is not always well defined. The bearing capacity of such soils is commonly assumed to be equal to the abscissa  $[q_d]_2$  of the point at which the settlement curve becomes steep and straight.

In practice, loads are transmitted to the soil by means of footings, as shown in Fig. 33.2. The footings may be *continuous*, having a long rectangular shape, or they may be *spread footings*, which are usually square or circular. The *critical load* is the load per unit of length of a continu-

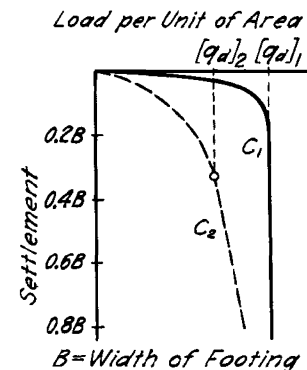


Figure 33.1 Relation between intensity of load and settlement of a footing on  $C_1$  dense or stiff and  $C_2$  loose or soft soil.

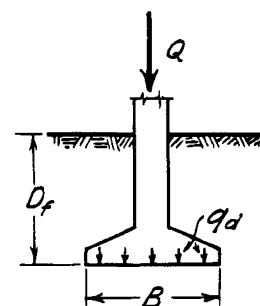


Figure 33.2 Section through continuous shallow footing.

ous footing or the total load on a spread footing at which the soil support fails. The distance from the level of the ground surface to the base of the footing is known as the *depth of foundation*  $D_f$ . A footing that has a width  $B$  equal to or greater than  $D_f$  is considered a *shallow footing*. In computations dealing with shallow footings, the weight of the soil above the base level of the foundation may be replaced by a uniform surcharge,

$$q = \gamma D_f \quad (33.1)$$

This substitution simplifies the computations. The error involved is small and on the safe side.

### 33.2 States of Plastic Equilibrium Beneath Shallow Continuous Footings

The results of mathematical investigations concerning the state of plastic equilibrium beneath continuous footings are not fully satisfactory. No general solution has been found that rigorously satisfies Eqs. 26.2 or 26.3 and also takes into account the weight of the soil, the influence of the depth of surcharge  $D_f$ , and the real distribution of vertical and horizontal forces on the base of the footing. Furthermore, the existing theories commonly assume that the volume of the soil does not change as the critical load is approached. Yet these shortcomings are not of serious practical importance because the accuracy of even approximate solutions is limited by our ability to evaluate the appropriate physical properties of the soil that enter into the equations rather than by the defects in the theories themselves.

The following general conclusions can be drawn from the theoretical studies. If the base of a continuous footing rests on the surface of a weightless soil with shear strength corresponding to Eq. 26.2 or 26.3, the loaded soil fails, as shown in Fig. 33.3a, by plastic flow along the composite surface  $fede f_1$ . This region can be divided into five zones, one marked *I* and two pairs of zones marked *II* and *III*. Because of friction and adhesion between the soil and the base of the footing, zone *I* remains in an elastic state. It acts as if it were part of the footing and penetrates the soil like a wedge. Its boundaries rise at an angle of  $45^\circ + \phi'/2$  with the horizontal. In zones *II* and *III* shear patterns develop. Those in zone *III* are identical with that for the passive Rankine state (Article 27); the boundaries for the passive Rankine zone rise at  $45^\circ - \phi'/2$  with the horizontal. The zones *II* located between *I* and *III* are known as *zones of radial shear*, because the lines that constitute one set in the shear pattern in these zones radiate from the outer edge of the base of the footing. These lines are straight. The lines of the other set are logarithmic spirals with their centers located at the outer edge of the base of the footing. The bearing capacity per unit of area is found to be (Prandtl 1921)

$$q_d = N_c c \quad (33.2)$$

where  $c$  is the cohesion intercept and  $N_c$ , known as a *bearing capacity factor*, depends only on  $\phi'$ . It is equal to

$$N_c = \cot \phi' \left[ \epsilon^{\pi \tan \phi'} \tan^2 \left( 45^\circ + \frac{\phi'}{2} \right) - 1 \right] \quad (33.3)$$

If the surface of the ground is acted on by a uniformly distributed surcharge  $q$  the shear pattern remains the same and the bearing capacity is increased by an amount  $N_q q$  (Reissner 1924) where

$$N_q = \epsilon^{\pi \tan \phi'} \tan^2 \left( 45^\circ + \frac{\phi'}{2} \right) \quad (33.4)$$

from which

$$N_c = \cot \phi' (N_q - 1) \quad (33.5)$$

If the shear strength is defined by Eq. 26.5,  $c = s_u$ , and  $\phi = 0^\circ$ . The spirals then become arcs of circles and the corresponding values of  $N_c$  and  $N_q$  become  $(2 + \pi)$  and 1.0, respectively. Hence, for a footing at the ground surface

$$q_d = (2 + \pi) s_u = 5.14 s_u \quad (33.6)$$

where  $s_u$  is the average mobilized undrained shear strength. Moreover, for  $\phi = 0^\circ$  the shear pattern and Eq. 33.6 remain valid even if the weight of the soil is not zero.

The right side of Fig. 33.3a shows the deformations of the soil located within the zones of plastic flow. The soil in zones *III* is compressed laterally. Its surface rises and terminates at the side of the footing in a sharp edge that conveys the impression that the soil has been punched.

If the soil is cohesionless but possesses friction and weight, the shear pattern is represented by Fig. 33.3b. The boundaries of the elastic zone *I* are curved. The two branches intersect at  $d$  at an angle of  $90^\circ - \phi'$  and the boundaries  $de$  and  $de_1$  of the zones *II* merge smoothly at  $d$  into the boundaries of zone *I*. In zone *II* the radial lines are curved. In zone *III* the shear pattern again corresponds exactly to that of the passive Rankine state. A rigorous general solution for the bearing capacity under these conditions has not been obtained but solutions for particular cases are available (Lundgren and Mortensen 1953).

### 33.3 Approximate Methods for Computing the Bearing Capacity of Continuous Footings

Real soils possess weight and in general exhibit both cohesion and friction. Moreover, the bases of most footings are located at least a short distance below the surface of the surrounding ground. Rigorous methods are not available for computing the bearing capacity under these circumstances, but for practical purposes no other than approximate methods are needed.



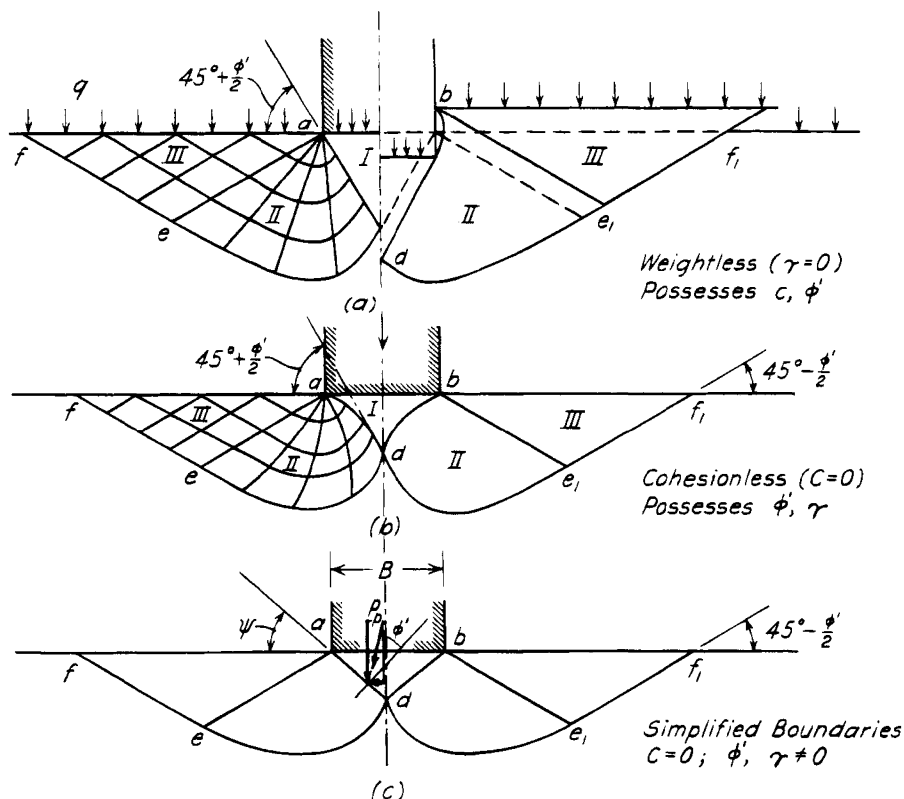


**Figure 33.3** Boundaries of zone of plastic equilibrium after failure of soil beneath continuous footing.

When the bearing capacity of a real footing is exceeded, the soil fails along a surface of rupture similar to those indicated by  $fede f_i$  (Fig. 33.3). The actual surface is not likely, however, to coincide with either of those in Fig. 33.3 corresponding to ideal materials. In the approximate methods it is assumed that the bearing capacity consists in general of the sum of three components, computed separately, representing respectively the contributions of (1) the cohesion and friction of a weightless material carrying no surcharge, (2) the friction of a weightless material on addition of a surcharge  $q$  on the ground surface, and (3) the friction of a material possessing weight and carrying no surcharge. Each component is computed on the assumption that the surface of sliding corresponds to the conditions for that particular component. Because the surfaces differ from each other and from the surface for the real material, the result is an approximation. The error is small and on the side of safety.

The approximate value of the bearing capacity, on the assumption that the shear strength is given by Eq. 26.3 for a soil mass located above water table, can be expressed as:

$$q_d = cN_c + \gamma D_f N_q + \frac{1}{2} \gamma B N_\gamma \quad (33.7)$$

in which  $N_c$  and  $N_q$  are the bearing capacity factors with respect to cohesion and surcharge, respectively. They can be evaluated by means of Eqs. 33.5 and 33.4. The sur-

charge is represented by the weight per unit area  $\gamma D_f$  of the soil surrounding the footing. The bearing capacity factor  $N_\gamma$  accounts for the influence of the weight of the soil. All the bearing capacity factors are dimensionless quantities depending only on  $\phi'$ .

Because a theoretical solution is not available for evaluating  $N_\gamma$  an approximate procedure is used. In this procedure the curved boundaries  $ad$  and  $bd$  of the elastic zone  $abd$  (Fig. 33.3b) are replaced by straight lines (Fig. 33.3c) rising at angles  $\psi$  to the horizontal. The unit weight of the soil is  $\gamma$ . At the instant of failure, the pressure on each of the surfaces  $ad$  and  $bd$  is equal to the resultant passive earth pressure  $P_p$ . Because slip occurs along these faces, the resultant earth pressure acts at an angle  $\phi'$  to the normal on each face. If the weight of the soil within  $adb$  is disregarded, the equilibrium of the footing in the vertical direction requires that

$$Q = 2P_p \cos(\psi - \phi')$$

The average vertical pressure, corresponding to the average bearing capacity, is then

$$q_\gamma = \frac{Q}{B} = \frac{2P_p}{B} \cos(\psi - \phi') \quad (33.8)$$

The problem, therefore, is reduced to determining the passive earth pressure  $P_p$  (Article 32). The point of appli-

cation of  $P_p$  is located at the lower third-point of  $ad$ . By introducing the symbol

$$N_\gamma = \frac{4P_p}{\gamma B^2} \cos(\psi - \phi') \quad (33.9)$$

into Eq. 33.8, we obtain

$$q_\gamma = \frac{1}{2}\gamma B N_\gamma \quad (33.10)$$

the third term in Eq. 33.7. Because the bearing capacity factor  $N_\gamma$  is dimensionless and depends only on  $\phi'$ , values can be computed once for all by the methods explained in Article 32. However, the inclination  $\psi$  is not known. Hence, the computations must be repeated for a given value of  $\phi'$  with various inclinations  $\psi$  until the minimum value of  $N_\gamma$  is found. The results are conservative but agree well with those calculated for particular cases by the more advanced procedures (Meyerhof 1955). Meyerhof's values are plotted in the chart (Fig. 33.4) together with the values of  $N_c$  and  $N_q$  obtained from Eqs. 33.5 and 33.4. The use of the chart greatly facilitates the computation of the bearing capacity.

The soil does not fail as shown in Fig. 33.3c unless it is fairly dense or stiff, so that its settlement curve resembles  $C_1$  in Fig. 33.1. Otherwise the footing sinks into the ground before the state of plastic equilibrium spreads beyond  $e$  and  $e_1$  (Fig. 33.3) and the corresponding settlement curve has no well-defined break (curve  $C_2$  in Fig. 33.1). An approximate value for the bearing capacity  $q_d$

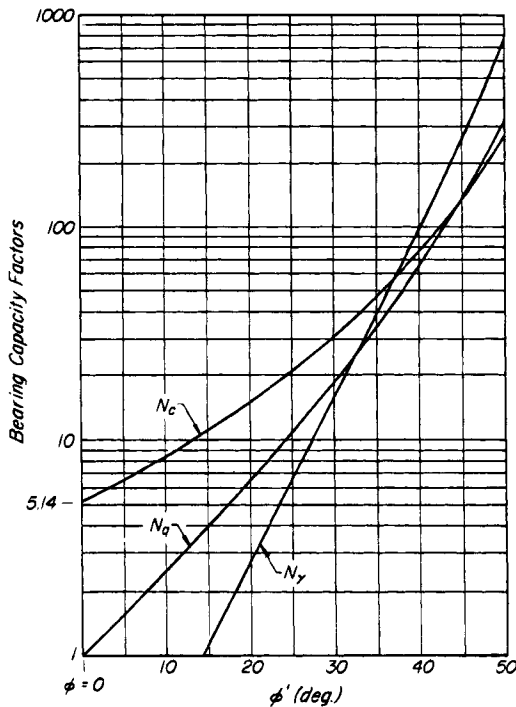


**Figure 33.4** Chart showing relation between bearing capacity factors and  $\phi'$  (values of  $N_\gamma$  after Meyerhof 1955).

of continuous footings on such soils can be obtained by an empirical reduction of the cohesion and friction of the soil.

Experience has shown that even uniformly loaded foundations always fail by tilting. This fact, however, does not invalidate the reasoning in the preceding paragraphs. It merely demonstrates that there are no perfectly uniform subgrades. With increasing load the settlement above the weakest part of the subgrade increases more rapidly than that above the rest. Because of the tilt, the center of gravity of the structure shifts toward the weak part and increases the pressure on that part, whereas the pressure on the stronger parts decreases. These factors almost exclude the possibility of a failure without tilting.

### 33.4 Bearing Capacity of Footings of Finite Length

All the preceding discussions refer to continuous footings. For computing the bearing capacity of square or circular bases, only a few special cases have been solved rigorously; the solutions require the use of numerical procedures. On the basis of the results and of experiments a semiempirical equation has been developed for the bearing capacity  $q_{dr}$  per unit of area of a circular footing with radius  $r$  resting on a fairly dense or stiff soil with shear strength defined by Eq. 26.3.

$$q_{dr} = 1.2cN_c + \gamma D_f N_q + 0.6\gamma r N_\gamma \quad (33.11)$$

The corresponding value for square footings,  $B \times B$ , on dense or stiff soil, is

$$q_{ds} = 1.2cN_c + \gamma D_f N_q + 0.4\gamma B N_\gamma \quad (33.12)$$

The values of  $N$  are given in Fig. 33.4.

According to Eq. 26.5, for undrained failure  $c = s_u$  and  $\phi = 0$ . The bearing capacity at the ground surface is then

$$q_{dr} = q_{ds} = 6.2 s_u \quad (33.13)$$

which is considerably greater than the value  $q_d = 5.14 s_u$  (Eq. 33.6). On the other hand, if  $c = 0$  and  $D_f = 0$ , the bearing capacity  $q_{dr}$  per unit of area is considerably smaller than  $q_d$  for a continuous footing with a width equal to the diameter of the circular footing.

For constant volume undrained failure, the increase in bearing capacity per unit of area produced by the surcharge  $\gamma D_f$  is exactly compensated by the weight of soil removed for construction of the footing. Therefore it is convenient to deal with the *net bearing capacity*

$$q_{d \text{ net}} = q_d - \gamma D_f \quad (33.14)$$

In reality, because the strength of the clay above footing level is not actually zero, the net bearing capacity increases slightly with increasing values of  $D_f$ . For values of  $D_f/B$  not exceeding 2.5, Skempton (1951) proposed

the following simple expression for the net bearing capacity of a rectangular footing with width  $B$  and length  $L$

$$q_{d \text{ net}} = 5 s_u \left( 1 + 0.2 \frac{D_f}{B} \right) \left( 1 + 0.2 \frac{B}{L} \right) \quad (33.15)$$

It is apparent that the value of  $N_c$  has been rounded conservatively from 5.14.

### Problems

1. Compute the bearing capacity per unit of area of a continuous footing 2.44 m wide, supported on a soil for which  $c = 20$  kPa,  $\phi' = 17^\circ$ , and  $\gamma = 19$  kN/m<sup>3</sup>. The load-settlement curve resembles  $C_1$  in Fig. 33.1. The depth of foundation is 2 m. The water table is at depth of 5 m below the ground surface.

Ans. 460 kPa.

2. Compute the bearing capacity per unit of area of a square footing 3 by 3 m on dense sand ( $\phi' = 37^\circ$ ), if the depth of foundation is, respectively, 0, 0.5, 1, 2, 3, and 5 m. The unit weight of the soil is 20 kN/m<sup>3</sup>.

Ans. 1320, 1750, 2180, 3040, 3900, 5620 kPa.

3. A load test was made on a square bearing plate 0.3 by 0.3 m on the surface of a cohesionless deposit of sand having a unit weight of 17.6 kN/m<sup>3</sup>. The load-settlement curve approached a vertical tangent at a load of 17.8 kN. What was the value of  $\phi'$  for the sand?

Ans.  $40^\circ$ .

4. A load test was made on a square plate 0.3 by 0.3 m on a dense cohesionless sand having a unit weight of 18.4 kN/m<sup>3</sup>. The bearing plate was enclosed in a box surrounded by a surcharge 0.6 m deep. Failure occurred at a load of 53 kN. What would be the failure load per unit of area of the base of a square footing 1.5 by 1.5 m located with its base at the same depth in the same material?

Ans. 1080 kPa.

5. A structure was built on a square mat foundation 30 by 30 m. The mat rested at the ground surface on a stratum of uniform soft clay which extended to a depth of 50 m. If failure occurred at a uniformly distributed load of 220 kPa, what was the average value of  $s_u$  (mob) for the clay? Because of the great depth of the zone of plastic equilibrium, the consolidation of the clay prior to failure can be disregarded.

Ans. 37 kPa.

### Selected Reading

- Meyerhof, G. G. (1951). "The ultimate bearing capacity of foundations," *Géot.*, **2**, pp. 301–332. Approximate theoretical solutions for shallow and deep foundations, supplemented by model tests.
- Skempton, A. W. (1951). "The bearing capacity of clays," *Proc. British Bldg. Research Congress*, **1**, pp. 180–189. Discussion for  $\phi = 0$  condition; influence of compressibility on bearing capacity.
- Meyerhof, G. G. (1955). "Influence of roughness of base and ground-water conditions on the ultimate bearing capacity

of foundations," *Géot.*, **5**, pp. 227–242. Review of 1951 paper in light of subsequent developments.

Sokolovski, V. V. (1960). *Statics of Soil Media*. London, Butterworths, 237 pp. General discussion of theory of critical equilibrium, with solutions for several problems of practical importance.

Hansen, J. Brinch (1961). "A general formula for bearing capacity" *Ingeniøren*, **5**, pp. 38–46; also *Bull. 11., Danish Geot Inst.* Brief summary of present state of theoretical developments.

## ARTICLE 34 BEARING CAPACITY OF PIERS AND PILES

### 34.1 Definitions

A pier is a slender prismatic or cylindrical body of masonry that transfers a load through a poor stratum onto a better one. A pile is essentially a very slender pier that transfers a load either through its lower end onto a firm stratum or else through side friction onto the surrounding soil. The relation between the load on a pier or pile and the corresponding settlement is very similar to that for footings. The load-settlement curve approaches either a vertical or an inclined tangent, as shown in Fig. 33.1. The definition of the bearing capacity of piers and piles is identical with that of footings (Article 33).

### 34.2 Bearing Capacity of Cylindrical Piers

Part of the load carried by a pier is transmitted directly to the soil immediately beneath its base, and part is transferred to the surrounding soil by friction and adhesion between the sides of the pier and the soil. At failure the load on a pier with depth  $D_f$  may be expressed as

$$Q_d = Q_p + Q_s = q_p A_p + 2\pi r f_s D_f = q_p A_p + C f_s D_f \quad (34.1)$$

in which  $q_p$  is the bearing capacity per unit of area of the soil beneath the base,  $A_p$  is the base area and  $r$  the radius of the pier,  $C$  is the circumference, and  $f_s$  is the average value at failure of the combined friction and adhesion per unit of contact area between the sides of the pier and the soil. It is commonly called the *skin friction*.

Failure of the soil beneath the base cannot occur without the displacement of at least part of the mass in an outward or an outward and upward direction as indicated by the curved arrows in Fig. 34.1. If the soil within the depth  $D_f$  is appreciably more compressible than that beneath the base, the displacements produce negligible shearing stresses within the depth  $D_f$ . Consequently, the influence of the surrounding soil is practically identical with that of a surcharge having an intensity  $\gamma D_f$ . Under these circumstances the bearing-capacity factors may be taken from Fig. 33.4 and  $q_p$  may be considered equal to  $q_{dr}$  or  $q_{ds}$  (Eqs. 33.11 or 33.12). On the other hand, if the soil is homogeneous, the shearing stresses set up in the

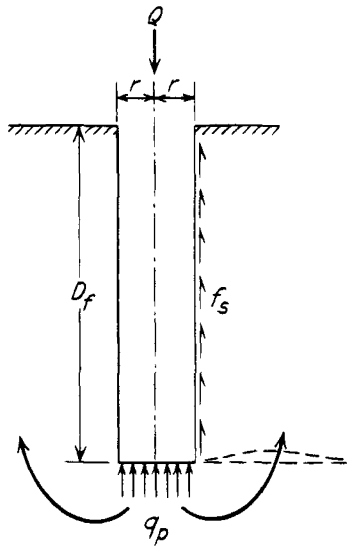


Figure 34.1 Section through cylindrical pier.

soil above base level as a consequence of the displacements alter the shear pattern so that the bearing-capacity factors for shallow foundations (Fig. 33.4) are no longer applicable. The bearing capacity factor  $N_q$  associated with surcharge becomes a function not only of  $\phi'$  but also of the ratio  $D_f/2r$  of the pier. Several investigators have obtained solutions for  $N_q$  based on somewhat different shear patterns; the one that appears to agree most nearly with the results of observations was developed by Berezantzev et al. (1961). Values of Berezantzev's factor  $N_q^*$ , as plotted conveniently by Tomlinson (1986), are shown in Fig. 34.2. They permit calculation of the base resistance  $Q_p$  for a soil in which  $c = 0$ . For a pier in a soil and under a loading condition for which Eq. 26.5 with  $\phi = 0$  and  $c = s_u$  is applicable, the bearing-capacity factor  $N_c$  increases from 5.14 for a loaded area at the surface to a value of 9 for  $D_f/2r$  equal to about 4 or more (Skempton 1951).

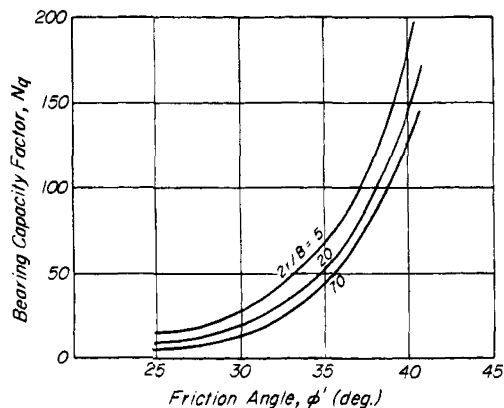


Figure 34.2 Berezantzev's bearing capacity factor  $N_q^*$  (after Tomlinson 1986).

The second term on the right-hand side of Eq. 34.1 contains the skin friction  $f_s$ . The value of  $f_s$  is usually considered to be the sum of two terms

$$f_s = c_a + \sigma'_h \tan \delta \quad (34.2)$$

in which  $c_a$  is the adhesion per unit of area between pier and soil,  $\sigma'_h$  is the average effective horizontal pressure on the vertical surface of the pier at failure, and  $\delta$  is the angle of friction between pier and soil. The values of  $c_a$  and  $\delta$  can be determined by means of laboratory tests. However, both quantities depend, among other factors, on the method of installation. Moreover, the stress conditions at the contact surface are complex. Large-scale experiments and measurements on full-scale piers have indicated that the skin friction per unit of area does not increase with depth below a *critical depth* defined by a critical ratio  $D/2r$  but approaches a constant value. This observation suggests that  $\sigma'_h$ , and probably the vertical pressure near the pier, similarly approach limiting values. Consequently,  $f_s$  is generally and preferably estimated on the basis of empirical data derived from field observations. These conditions are discussed in Articles 52 and 53 in connection with the design of piles and piers.

### 34.3 Bearing Capacity of Piles

Because piles are essentially very slender cylindrical piers, their bearing capacity can also be estimated by Eq. 34.1. The quantity  $Q_p$  is called the *point resistance*. If  $Q_p$  is large compared with  $Q_f$ , the pile is said to be *point-bearing*. On the other hand, if  $Q_p$  is relatively insignificant, the pile is known as a *friction pile*.

The principal difference between piles and piers lies in the method of installation. The construction of piers is preceded by excavation, whereas the driving of piles, which usually consist either of solid bodies or of shells closed at the lower end, involves a displacement of the soil. Occasionally the driving is facilitated by removing part of the soil located in the path of the pile by means of a water jet or a pre-excavator.

If the piles are driven through compressible material to a firm base, a lower limiting value for the point resistance  $Q_p$  can be obtained by means of Eqs. 33.11 and 33.12 for circular and square cross-sections respectively. If the piles are surrounded and underlain by a homogeneous cohesionless material, Eqs. 33.11 and 33.11 may overestimate the point resistance for the reasons discussed under the preceding subheading. The bearing capacity of friction piles depends on the skin friction  $f_s$  (Eq. 34.1). The evaluation of the skin friction on the basis of laboratory tests is even more unreliable for piles than it is for piers, because the computation of the stresses produced by the partial or total displacement of the soil during the process of pile driving is beyond the power of analysis. Therefore, the bearing capacity  $Q_d$  of a friction pile can be determined only by load tests on piles in the field or

else, less accurately, on the basis of empirical values for  $f_s$ . Values of  $f_s$  corresponding to the principal types of soil are given in Article 52. In those cities where friction piles are extensively used, empirical values for  $f_s$ , derived from local experience, are likely to be quite reliable.

### 34.3.1 Pile Formulas

The bearing capacity  $Q_d$  of a point-bearing pile may, under some circumstances, be approximately equal to the resistance  $Q_{dy}$  of the soil against rapid penetration of the pile under the impact of the falling ram of the pile driver. Therefore, there might be a possibility of estimating  $Q_{dy}$ , known as the *dynamic resistance*, from the average penetration  $S$  of the pile under the last few blows of the hammer, provided the weight  $W_H$  of the ram and the height of fall  $H$  are known. Accordingly, many efforts have been made to compute the bearing capacity on the basis of this information. The results of these efforts are known as *pile formulas*. The following paragraphs deal with the fundamental concepts on which the pile formulas are based.

The work performed by the falling hammer is  $W_H H$ , and the work required to increase the penetration of the pile by  $S$  against a resistance  $Q_{dy}$  is  $Q_{dy} S$ . If the entire work of the falling hammer served to increase the penetration of the pile, we could write

$$W_H H = Q_{dy} S$$

from which

$$Q_{dy} = \frac{W_H H}{S}$$

This is Sanders' pile formula, published about 1850. The values obtained by means of this formula are too great, because part of the energy of the falling hammer is converted into heat and into elastic deformations.

If we assume that all the deformations and energy losses occur simultaneously on application of the hammer blow; that is, if the existence of stress waves in the pile and soil is ignored, we can write

$$W_H H = Q_{dy} S + \Delta \quad (34.3)$$

where  $\Delta$  represents the energy lost and therefore unavailable to cause penetration of the pile. If there were no penetration and all the driving energy were consumed in elastic compression of the pile, the energy expended would be

$$W_H H = \frac{1}{2} Q_{dy} S_e$$

where  $S_e$  is the elastic compression of the pile. Moreover,

$$S_e = \frac{Q_{dy} L}{AE}$$

from which

$$S_e = \sqrt{\frac{2W_H H L}{AE}} \quad (34.4)$$

If we assume that the energy loss consists only of the elastic deformation of the pile and is, moreover, not influenced by the penetration of the point of the pile, Eq. 34.3 becomes

$$W_H H = Q_{dy} S + Q_{dy} \frac{S_e}{2} = Q_{dy} \left( S + \frac{S_e}{2} \right)$$

from which

$$Q_{dy} = \frac{W_H H}{S + \frac{1}{2} S_e} \quad (34.5)$$

This expression is known as the Danish formula. Statistical studies suggested that it should be used with a factor of safety of 3 (Sørensen and Hansen 1957).

Numerous attempts have been made to take into account the remaining energy losses. Some of these attempts have resulted in very complicated expressions and procedures. However, inasmuch as all methods based on Eq. 34.3 are fundamentally unsound because they ignore the dynamic aspects of the phenomena (Cummings 1940), the complicated formulas possess no inherent advantage over the simpler ones. The relative merits and reliability of any of the pile formulas can be judged only on the basis of comparisons with the results of load tests.

The *Engineering News formula* (Wellington 1888), even today still widely used in North America, is similar in form to Eq. 34.5 except that the term containing the elastic compression of the pile is replaced by a constant  $c$ . Thus

$$Q_{dy} = \frac{W_H H}{S + c}$$

Wellington regarded the quantity  $c$  as an additional penetration of the point of the pile that would have occurred if there had been no energy losses. He evaluated it on the basis of whatever empirical data he had at his disposal and concluded that  $c$  is approximately equal to 1 in. for piles driven by a drop hammer and 0.1 in. for piles driven by a steam hammer. Because he realized that his estimate involved uncertainties, he proposed that the allowable load  $Q_a$  per pile should not exceed one-sixth of the computed ultimate load  $Q_{dy}$ . By expressing  $H$  in feet and  $S$  in inches, he obtained

$$Q_a = \frac{1}{6} Q_{dy} = \frac{12}{6} \frac{W_H H}{S + c} = \frac{2W_H H}{S + c} \quad (34.6)$$

This equation is known as the *Engineering News formula*.

Because of its simplicity, the *Engineering News formula* has been widely used, but statistical comparisons with the results of load tests on driven piles have shown

such poor correlation and such wide scatter that further use of the formula cannot be justified.

Although comparisons of computed and measured capacities have shown a few of the many pile formulas to be statistically superior to the others, all such formulas are fundamentally unsound because of their neglect of the time-dependent aspects of the dynamic phenomena. Moreover, the validity of any dynamic analysis depends in part on the assumption that the dynamic resistance to penetration is equal to or is at least related to the static capacity of the pile after driving. In fine-grained soft saturated soils, pore pressures are likely to build up during driving and significantly influence the resistance to penetration, whereas under a static load of long duration the pore pressures dissipate and the effective stresses in the soil change correspondingly. Under these conditions, no correlation between dynamic and static resistance can be expected. In free-draining soils such as medium to dense sands, and in stiff to hard clays, dynamic and static resistances, on the other hand, are more closely related. Hence, except where well-supported empirical correlations under a given set of physical and geologic conditions are available, even the use of formulas apparently superior to the *Engineering News* formula is not justifiable.

Most of the defects of pile formulas can be eliminated by a more realistic analysis of the dynamics of pile driving in which the pile is considered to be a long elastic bar subjected to transient stress waves set up by the impact of the hammer. This approach is considered in the following section. Application to design is discussed in Article 52.

### 34.3.2 Transmission of Stresses during Driving

A realistic representation of the dynamics of pile driving must consider the complex chain of events initiated by a single blow of a pile hammer. The energy delivered by the hammer sets up time-dependent stresses and displacements in the pile-head assembly, in the pile, and in the surrounding ground. Because the length of a pile is always large compared with its diameter, a pile does not behave as a concentrated mass but more nearly as an elastic bar in which the stresses travel longitudinally as waves. When the waves are compressive, as at the tip of a pile being driven into a hard material, they cause the pile to penetrate into the ground. Yet, if the compressive stresses are too great, they may damage the pile. On the other hand, when the soil at the tip is soft and driving is easy, the compressive wave may be reflected upward from the end of the pile as a tensile wave. If at some point in the pile the tensile stress is not canceled by other stresses that are compressive, a net tension may develop at least for an instant. The stress may be sufficient to crack a precast concrete pile. Thus, the behavior of the pile, with respect both to its ability to penetrate into the soil and to its structural integrity during driving, is intimately related to the mechanics of stress-wave transmission within the

pile. To the extent that the dynamic force developed at the tip during driving is related to the static bearing capacity of the pile, a knowledge of this force is useful in estimating the static capacity.

The theory of wave transmission in a prismatic elastic bar struck longitudinally by a rigid object was developed more than two centuries ago by St. Venant and Boussinesq and numerical solutions were obtained for several simple boundary conditions. The conditions were so far removed from the complexities of actual pile driving, however, that the solutions had little practical value. The introduction of more realistic conditions became possible only with the development of suitable theoretical models and electronic computation.

According to the theory of longitudinal impact of a prismatic elastic bar, the stress waves travel axially at a velocity

$$c = \sqrt{\frac{E}{\rho}} \quad (34.7)$$

where  $E$  is the modulus of elasticity and  $\rho$  the mass density of the material in the bar. The mass density is defined as

$$\rho = \frac{\gamma_p}{g} \quad (34.8)$$

where  $\gamma_p$  is the unit weight of the material constituting the bar and  $g$  is the acceleration of gravity. The velocity  $c$  of the stress wave is not to be confused with the velocity  $v$  at which a particular point in the bar actually moves. The former, known as the *velocity of longitudinal wave propagation*, or *seismic velocity*, is a constant for a given solid, elastic material. During the passage of a single wave, the longitudinal direct stress in the bar at any point is related to the particle velocity at that point by the simple expression

$$p = \frac{E}{c} v = \rho c v \quad (34.9)$$

The force transmitted across a section of the bar is then

$$P = pA = \rho c A \cdot v \quad (34.10)$$

Because  $v$  is a function of position and time,  $P$  and  $p$  are similarly functions of these quantities. The capability of the bar to transmit longitudinal force is measured by the product  $\rho c A$ , which is designated as the *impedance* of the pile.

The capacity of a pile at a given depth is the force that can be exerted by the surrounding soil against downward displacement. At least this much force must have been transmitted to the soil by the pile during driving for the point to have penetrated to a given position under the last blow of the hammer. In particular, enough force must have been transmitted to the pile to overcome the side

and point resistances. Conversely, no matter how much energy may be applied to the head of the pile, the force that can be transmitted down the pile is limited by the impedance.

Since the impedance  $\rho cA$  determines the maximum force that can be transmitted along the pile as long as the material remains elastic, it is, therefore, a measure of the ability of the pile to develop the required capacity as a consequence of its being driven into the ground. If the impedance of a pile is increased, the potential for obtaining a greater capacity with a particular hammer is also increased, provided the pile is not of such unusually large dimensions with respect to the hammer that its action resembles that of a large mass instead of that of a bar.

The force actually developed at the tip of a pile depends, however, not only on  $\rho cA$  but also on the energy that can be furnished by the hammer and on a wide variety of other factors including the nature of the impulse delivered by the hammer, the stress-transmission characteristics of the cushions and pile-head assembly, the general pattern of distribution of the resistance exerted by the soil along the pile, and the proportion of the total resistance developed along the sides of the pile in comparison to that beneath the point. The properties of the soil also play a decisive role in the behavior of the pile during driving. In addition to the nature of the point resistance, the distribution of the side forces from top to tip of

the pile and the relative magnitudes of side and point resistance may have significant effects.

The foregoing factors influencing the stresses developed in a pile under actual driving conditions can be taken reasonably but approximately into account in a theoretical model (Fig. 34.3), by which the wave analysis has been extended from unrealistically simple cases to those of interest in practice (Glanville et al. 1938, Smith 1960). The pile is assumed to consist of a series of elements, each possessing a weight  $W_n$ , connected by springs with stiffnesses  $K$  associated with the elastic properties of the pile material. The resistances on the side of the pile, which damp the vibrations, are assumed to be of viscoelastic nature and to possess spring constants  $K'$  representative of the soil material. The point resistance is also represented by a viscoelastic element. The weights and stiffnesses of the ram and drive head and the properties of the cushion blocks are represented by appropriate elements.

In the investigation of a specific problem, the velocity of the ram at impact must be introduced, as well as numerical values for all the appropriate weights, stiffnesses, damping factors, and resistances. It is not usually necessary, however, to assign specific numerical values to the point resistance and the side frictional resistance; it is necessary only to estimate the fraction of the total pile resistance likely to be developed by point resistance, and to assume the manner in which the side resistance

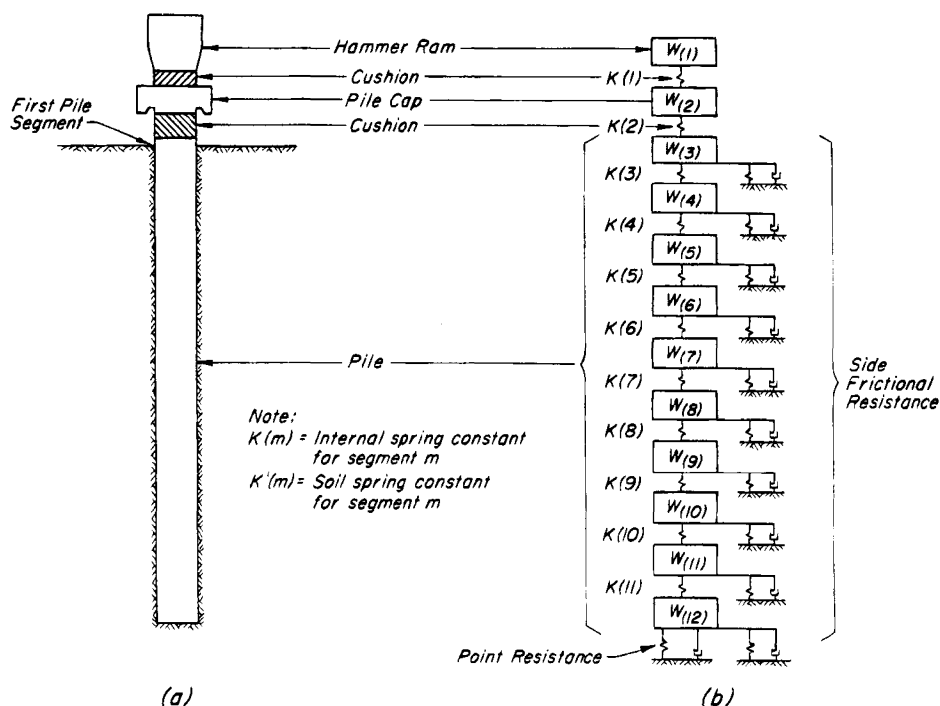


**Figure 34.3** Actual pile (a) and idealized mechanical model (b) considered as basis for dynamic analysis of pile driving (after Davisson 1970b).

is distributed along the pile. The results of a calculation for a given pile under particular soil conditions, driven by a specified hammer, may be expressed in the same form as those derived from the ordinary pile-driving formulas. That is, the ultimate static resistance may be plotted as a function of the resistance to penetration in blows per unit of penetration. A second quantity of significance, the maximum stress in the pile, may also be computed as a function of the resistance to penetration.

The results of wave analyses based on the model illustrated in Fig. 34.3 have proven to be of great practical value (Article 52), but the parameters expressing the stress-strain-time characteristics of the soil, such as elastoplastic spring stiffnesses and viscoelastic damping factors, are not readily related to the soil properties customarily used and understood in soil mechanics. Although the characteristics needed for wave analyses have been evaluated with considerable success by back analyses of pile-driving records and load tests, a procedure based on soil properties in more general use would be preferable. Efforts to this end are showing promise (Lee et al. 1988).

### Problems

1. A reinforced-concrete pile with a cross section 0.4 by 0.4 m was driven through a deposit of fine loose sand and soft clay 20 m thick and into a stratum of dense sand for a distance of 1 m. The water table was located near the ground surface. The loose sand and soft clay had a submerged unit weight of  $7.2 \text{ kN/m}^3$ , and the angle of internal friction of the dense sand was  $35^\circ$ . Compute the point resistance of the pile.

Ans. 79 metric tons.

2. The pile referred to in the preceding problem was driven by means of a steam hammer having a weight  $W_H = 3.56$  metric tons and a stroke  $H = 60$  cm. The penetration of the pile under the last blow was  $S = 1.4$  mm. According to the *Engineering News* formula, what is the ultimate bearing capacity of the pile?

Ans. 542 metric tons.

3. The pile referred to in problem 1 was 21 m long. Its modulus of elasticity was 24 GPa. What is its ultimate capacity according to the Danish formula?

Ans. 236 metric tons.

### Selected Reading

One of the classic papers of soil mechanics is Cummings, A. E. (1940). "Dynamic pile driving formulas," *J. Boston Soc. Civil Engrs.*, **27**, pp. 6–27. It is reprinted in *Contributions to Soil Mechanics 1925–1940*, Boston Soc. Civil Engrs. 1940, pp. 392–413.

## ARTICLE 35 STABILITY OF SLOPES

### 35.1 Introduction

The failure of a mass of soil located beneath a slope is called a *slide*. It involves a downward and outward movement of the entire mass of soil that participates in the failure.

Slides may occur in almost every conceivable manner, slowly or suddenly, and with or without any apparent provocation. Usually, slides are due to excavation or to undercutting the foot of an existing slope. However, in some instances, they are caused by a gradual disintegration of the structure of the soil, starting at hair cracks which subdivide the soil into angular fragments. In others, they are caused by an increase of the porewater pressure in a few exceptionally permeable layers, or by a shock that liquefies the soil beneath the slope (Article 47.4). Because of the extraordinary variety of factors and processes that may lead to slides, the conditions for the stability of slopes often defy theoretical analysis. Stability computations based on test results can be relied on only when the conditions specified in the different sections of this article are strictly satisfied. Various undetected discontinuities in the soil, such as systems of hair cracks, remnants of old surfaces of sliding, or thin seams of water-bearing sand may completely invalidate the results of the computations.

### 35.2 Slopes on Dry Cohesionless Sand

A slope underlain by clean dry sand is stable regardless of its height, provided that the angle  $\beta$  between the slope and the horizontal is equal to or smaller than the angle of internal friction  $\phi'$  for the sand in a loose state, i.e.  $\phi'_{cv}$ . The factor of safety of the slope with respect to sliding may be expressed by the equation,

$$F = \frac{\tan \phi'}{\tan \beta} \quad (35.1)$$

No slope on clean dry sand can exist with a slope angle greater than  $\phi'$ , irrespective of its height.

Because very few natural soils are perfectly cohesionless, the remainder of this article deals with slopes underlain by cohesive materials.

### 35.3 General Character of Slides in Homogeneous Cohesive Soil

A cohesive material having a shearing resistance corresponding to Eq. 26.2, 26.3, or 26.4 can stand with a vertical slope at least for a short time, provided the height of the slope is somewhat less than  $H_c$  (Eq. 28.11). If the height of a slope is greater than  $H_c$ , the slope is not stable unless the slope angle  $\beta$  is less than  $90^\circ$ . The greater the height of the slope, the smaller must be the angle  $\beta$ . If the height is very great compared with  $H_c$ , the slope will fail unless the slope angle  $\beta$  is equal to or less than  $\phi'$ .





If the shape of the surface of sliding is such that it cannot be represented even approximately by an arc of a circle, the procedure must be modified according to the methods described in Article 35.10 in connection with composite surfaces of sliding.

### 35.6 Procedure for Investigating Stability of Slopes

To investigate whether or not a slope on soil with known shear characteristics will be stable, it is necessary to determine the diameter and position of the circle that represents the surface along which sliding will occur. This circle, known as the *critical circle*, must satisfy the requirement that the ratio between the shearing strength of the soil along the surface of sliding and the shearing force tending to produce the sliding must be a minimum.

After the diameter and position of the critical circle have been determined, the factor of safety  $F$  of the slope with respect to failure may be computed by means of the relation (Fig. 35.1)

$$F = \frac{sr \widehat{d_1e_2}}{W_1l_1 - W_2l_2} \quad (35.2)$$

wherein  $r$  represents the radius of the critical circle and  $d_1e_2$  the length of the surface of sliding.

Like the passive earth pressure of a mass of soil, the stability of a slope may be investigated by trial or, in simple cases, by elementary analytical methods. To make the investigation by trial, different circles are selected, each representing a potential surface of sliding. For each circle, the value  $F$  (Eq. 35.2) is computed. The minimum value represents the factor of safety of the slope with respect to sliding, and the corresponding circle is the critical circle.

The elementary analytical solutions can rarely be used to compute the factor of safety of a slope under actual conditions, because they are based on greatly simplified assumptions. They are valuable, however, as a guide for estimating the position of the center of the critical circle and for ascertaining the probable character of the failure. In addition, they may serve as a means for judging whether a given slope will be unquestionably safe, unquestionably unsafe, or of doubtful stability. If the stability seems doubtful, the factor of safety with respect to failure should be computed according to the procedure described in the preceding paragraph.

The solutions are based on the following assumptions: Down to a given level below the toe of the slope, the soil is perfectly homogeneous. At this level, the soil rests on the horizontal surface of a stiffer stratum, known as the *firm base*, which is not penetrated by the surface of sliding. The slope is considered to be a plane, and it is located between two horizontal plane surfaces, as shown in Fig. 35.2. Finally, the weakening effect of tension

cracks is disregarded, because it is more than compensated by the customary margin of safety. The following paragraphs contain a summary of the results of the investigations.

### 35.7 Slope Failures under Undrained Conditions

The average shearing resistance  $s$  per unit of area of a potential surface of sliding in homogeneous clay under undrained conditions (Article 20) is referred to as the mobilized undrained shear strength. That is,

$$s = s_u (\text{mob}) \quad (18.5)$$

If  $s_u (\text{mob})$  is known, the critical height  $H_c$  of a slope having a given slope angle  $\beta$  can be expressed by the equation,

$$H_c = N_s \frac{s_u (\text{mob})}{\gamma} \quad (35.3)$$

In this equation the *stability factor*  $N_s$  is a pure number. Its value depends only on the slope angle  $\beta$  and on the *depth factor*  $n_d$  (Fig. 35.2b), which expresses the depth at which the clay rests on a firm base. If a slope failure occurs, the critical circle is usually a *toe circle* that passes through the toe  $b$  of the slope (Fig. 35.2a). However, if the firm base is located at a short distance below the level of  $b$ , the critical circle may be a *slope circle* that is tangent to the firm base and that intersects the slope above the toe  $b$ . This type of failure is not shown in Fig. 35.2. If a base failure occurs, the critical circle is known as a *midpoint circle*, because its center is located on a vertical line through the midpoint  $m$  of the slope (Fig. 35.2b). The midpoint circle is tangent to the firm base.

The position of the critical circle with reference to a given slope depends on the slope angle  $\beta$  and the depth factor  $n_d$ . Figure 35.3 contains a summary of the results of pertinent theoretical investigations. According to this figure, the failure of all slopes rising at an angle of more than  $53^\circ$  occurs along a toe circle. If  $\beta$  is smaller than  $53^\circ$ , the type of failure depends on the value of the depth factor  $n_d$  and, at low values of  $n_d$ , also on the slope angle  $\beta$ . If  $n_d$  is equal to 1.0, failure occurs along a slope circle. If  $n_d$  is greater than about 4.0, the slope fails along a midpoint circle tangent to the firm base, regardless of the value of  $\beta$ . If  $n_d$  is intermediate in value between 1.0 and 4.0, failure occurs along a slope circle if the point representing the values of  $n_d$  and  $\beta$  lies above the shaded area in Fig. 35.3. If the point lies within the shaded area, failure occurs along a toe circle. If the point is below the shaded area, the slope fails along a midpoint circle tangent to the firm base.

If the slope angle  $\beta$  and the depth factor  $n_d$  are given, the value of the corresponding stability factor  $N_s$  (Eq. 35.3) can be obtained without computation from Fig. 35.3. The value of  $N_s$  determines the critical height  $H_c$  of the slope.

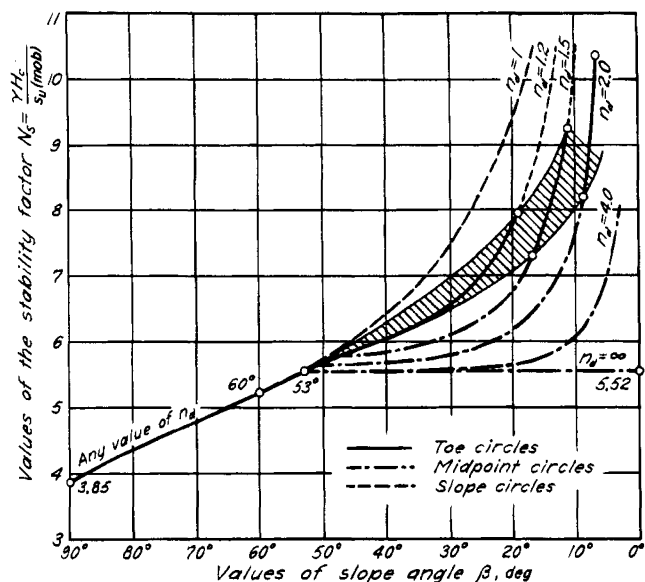


**Figure 35.3** Relation between stability factor  $N_s$  and slope angle  $\beta$  for different values of depth factor  $n_d$  (after Taylor 1937).

If failure occurs along a toe circle, the center of the critical circle can be located by laying off the angles  $\alpha$  and  $2\theta$ , as shown in Fig. 35.2a. Values of  $\alpha$  and  $\theta$  for different slope angles  $\beta$  are given in Fig. 35.4a. If failure occurs along a midpoint circle tangent to the firm base, the position of the critical circle is determined by the horizontal distance  $n_x H$  from the toe of the slope to the circle (Fig. 35.2b). Values of  $n_x$  can be estimated for different values of  $n_d$  and  $\beta$  by means of the chart (Fig. 35.4b).

If the clay beneath a slope consists of several layers with different average undrained shear strengths,  $[s_u]_1$ ,  $[s_u]_2$ , etc., or if the surface of the ground is irregular (Fig. 35.5), the center of the critical circle must be determined by trial and error. Inasmuch as the longest part of the real surface of sliding should be located within the softest stratum the trial circle should also satisfy this condition. If one of the upper layers is relatively soft, the presence of a firm base at considerable depth may not enter into the problem, because the deepest part of the surface of sliding is likely to be located entirely within the softest stratum. For example, if the undrained shear strength  $[s_u]_2$  of the second stratum in Fig. 35.5 is much smaller than the undrained shear strength  $[s_u]_3$  of the underlying third layer, the critical circle will be tangent to the upper surface of the third stratum instead of the firm base.

For each trial circle we compute the average shearing stress  $\tau$  which must act along the surface of sliding to balance the difference between the moment  $W_1 l_1$  of the driving weight and the resisting moment  $W_2 l_2$ . The value of  $\tau$  is

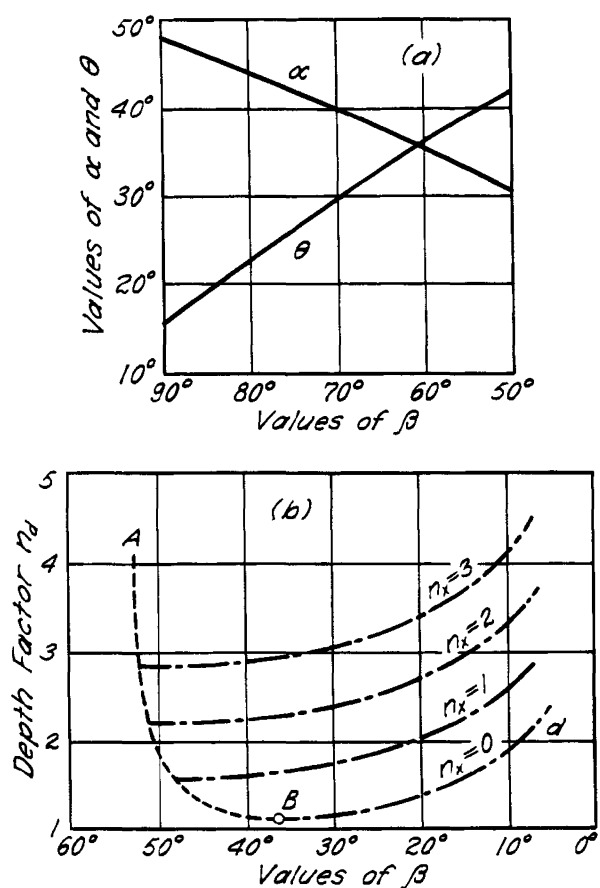


**Figure 35.4** (a) Relation between slope angle  $\beta$  and parameters  $\alpha$  and  $\theta$  for location of critical toe circle when  $\beta$  is greater than  $53^\circ$ ; (b) relation between slope angle  $\beta$  and depth factor  $n_d$  for various values of parameter  $n_x$  (after W. Fellenius 1927).

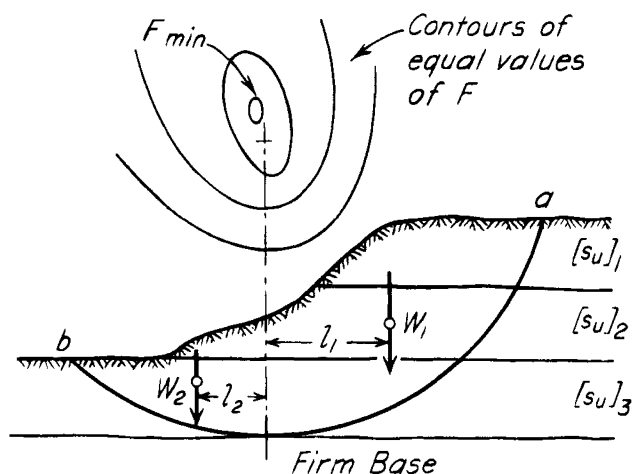


**Figure 35.5** Base failure in stratified cohesive soil.

$$\tau = \frac{W_1 l_1 - W_2 l_2}{r \widehat{ab}}$$

Then, on the basis of the known values of  $[s_u]_1$ ,  $[s_u]_2$ ,  $[s_u]_3$ , etc., we compute the average value of  $s_u$  (mob) of the soil along the sliding surface. The factor of safety of the slope against sliding along the circular trial surface is

$$F = \frac{s_u \text{ (mob)}}{\tau} \quad (35.4)$$

The value of  $F$  is inscribed at the center of the circle. After values of  $F$  have been determined for several trial circles, curves of equal values of  $F$  are plotted (Fig. 35.5). These curves may be considered as contour lines of a depression. The center of the critical circle is located at the bottom of the depression. The corresponding value  $F_{\min}$  is the factor of safety of the slope with respect to sliding.

If it is not obvious which of two layers may constitute the firm base for the critical circle, trial circles must be investigated separately for each possibility and the corresponding values of  $F_{\min}$  determined. The smaller of the two values is associated with the firm base that governs the failure and is the factor of safety of the slope.

### 35.8 Slopes on Soils with Cohesion and Internal Friction

If the shearing resistance of a soil located above water table can be expressed approximately by Eq. 26.3

$$s = c + \sigma \tan \phi'$$

the stability of slopes on the soil can be investigated by the procedure illustrated by Fig. 35.6a. The forces acting on the sliding mass are its weight  $W$ , the resultant cohesion  $C$ , and the resultant  $F$  of the normal and frictional forces acting along the surface of sliding. The resultant cohesion  $C$  acts in a direction parallel to the chord  $de$  and is equal to the unit cohesion  $c$  multiplied by the length  $L$  of the chord. The distance  $x$  from the center of rotation to  $C$  is determined by the condition that

$$Cx = cLx = c \widehat{de} r$$

from which  $x = \widehat{de} r/L$ . Therefore, the force  $C$  is known. The weight  $W$  is also known. Since the forces  $C$ ,  $W$ , and  $F$  are in equilibrium, the force  $F$  must pass through the point of intersection of  $W$  and  $C$ . Hence, the magnitude and line of action of  $F$  can be determined by constructing the polygon of forces.

If the factor of safety against sliding is equal to unity, the slope is on the verge of failure. Under this condition each of the elementary reactions  $dF$  in Fig. 35.6a must be inclined at the angle  $\phi'$  to the normal to the circle of sliding. As a consequence, the line of action of each

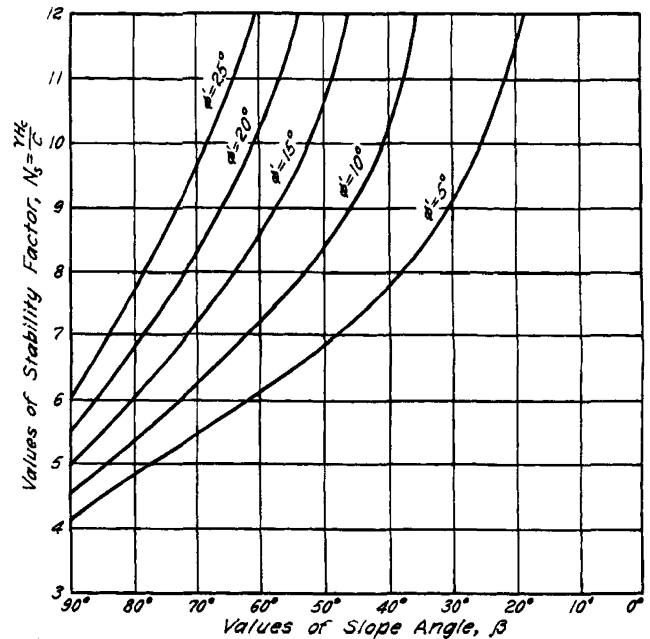
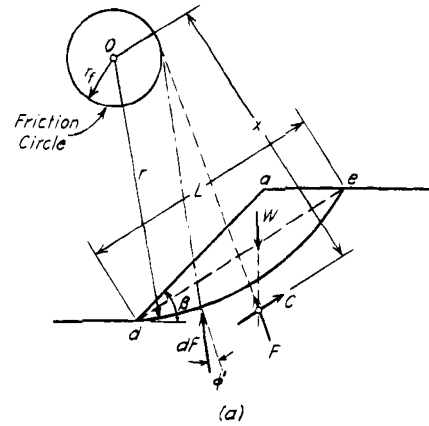


**Figure 35.6** Failure of slope in material having cohesion and friction. (a) Diagram illustrating friction-circle method; (b) relation between slope angle  $\beta$  and stability factor  $N_s$  for various values of  $\phi'$  (after Taylor 1937).

elementary reaction is tangent to a circle, known as the *friction circle*, having a radius

$$r_f = r \sin \phi'$$

and having its center at the center of the circle of sliding. The line of action of the resultant reaction  $F$  is tangent to a circle having a radius slightly greater than  $r_f$ , but as a convenient approximation we assume that at a factor of safety equal to unity the line of action of  $F$  is also tangent to the friction circle. The corresponding error is small and is on the safe side.

For a given value of  $\phi'$  the critical height of a slope that fails along a toe circle is given by the equation,

$$H_c = N_s \frac{c}{\gamma}$$

which is identical with Eq. 35.3, except that  $N_s$  depends not only on  $\beta$  but also on  $\phi'$ . Figure 35.6b shows the relationship between  $\beta$  and  $N_s$  for different values of  $\phi'$ . At a given value of the slope angle  $\beta$ ,  $N_s$  increases at first slowly and then more rapidly with increasing values of  $\phi'$ . When  $\phi' = \beta$ ,  $N_s$  becomes infinite.

All the points on the curves shown in Fig. 35.6b correspond to failures along toe circles, because theory has shown that the possibility of a base failure does not exist unless  $\phi'$  is smaller than approximately  $3^\circ$ . Therefore, if a typical base failure has occurred in a fairly homogeneous soil in the field, it can be concluded that it was a constant volume undrained failure with  $\phi = 0$  and  $c = s_u$ .

### 35.9 Irregular Slopes on Nonuniform Soils, Circular Surface of Sliding

If a slope has an irregular surface that cannot be represented by a straight line, or if the surface of sliding is likely to pass through several materials with different values of  $c$  and  $\phi'$ , the stability can be investigated conveniently by the *method of slices*. According to this procedure a trial circle is selected (Fig. 35.7a) and the sliding mass subdivided into a number of vertical slices 1, 2, 3, etc. Each slice, such as slice 2 shown in Fig. 35.7b, is acted on by its weight  $W$ , by shear forces  $T$  and normal forces  $E$  on its sides, and by a set of forces on its base. These include the shearing force  $S$  and the normal force  $P$ . The forces on each slice, as well as those acting on the sliding mass as a whole, must satisfy the conditions of equilibrium. However, the forces  $T$  and  $E$  depend on the deformation and the stress-strain characteristics of the slide material and cannot be evaluated rigorously. They can be approximated with sufficient accuracy for practical purposes.

The simplest approximation consists of setting these forces equal to zero. Under these circumstances, if the

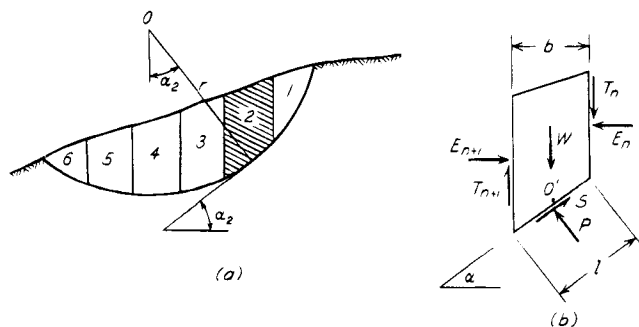


**Figure 35.7** Method of slices for investigating equilibrium of slope located above water table. (a) Geometry pertaining to one circular surface of sliding; (b) forces on typical slice such as slice 2 in (a).

entire trial circle is located above the water table and there are no excess pore pressures, a condition corresponding to a drained failure, equilibrium of the entire sliding mass requires that

$$r \sum W \sin \alpha = r \sum S \quad (35.5)$$

If  $s$  is the shearing strength of the soil along  $l$ , then

$$S = \frac{s}{F} l = \frac{s}{F} \frac{b}{\cos \alpha} \quad (35.6)$$

and

$$r \sum W \sin \alpha = \frac{r}{F} \sum \frac{sb}{\cos \alpha} \quad (35.7)$$

from which

$$F = \frac{\sum (sb / \cos \alpha)}{\sum W \sin \alpha} \quad (35.8)$$

The shearing strength  $s$ , however, is determined by

$$s = c + \sigma \tan \phi'$$

where  $\sigma$  is the normal stress across the surface of sliding  $l$ . To evaluate  $\sigma$  we consider the vertical equilibrium of the slice (Fig. 35.7b), from which

$$W = S \sin \alpha + P \cos \alpha$$

and

$$\sigma = \frac{P}{l} = \frac{P \cos \alpha}{b} = \frac{W}{b} - \frac{S}{b} \sin \alpha \quad (35.9)$$

Therefore

$$\begin{aligned} s &= c + \left( \frac{W}{b} - \frac{S}{b} \sin \alpha \right) \tan \phi' \\ &= c + \left( \frac{W}{b} - \frac{s}{F} \tan \alpha \right) \tan \phi' \end{aligned}$$

and

$$s = \frac{c + (W/b) \tan \phi'}{1 + (\tan \alpha \tan \phi')/F} \quad (35.10)$$

Let

$$m_\alpha = \left( 1 + \frac{\tan \alpha \tan \phi'}{F} \right) \cos \alpha \quad (35.11)$$

Then

$$F = \frac{\sum [c + (W/b) \tan \phi'] b}{\sum W \sin \alpha} \quad (35.12)$$

Equation 35.12, which gives the factor of safety  $F$  for the trial circle under investigation, contains on the right-

hand side the quantity  $m_\alpha$  (Eq. 35.11) which is itself a function of  $F$ . Therefore, Eq. 35.12 must be solved by successive approximations in which a value of  $F = F_1$  is assumed and used for calculation of  $m_\alpha$ , whereupon  $F$  is then computed. If the value of  $F$  differs significantly from  $F_1$ , the calculation is repeated. Convergence is very rapid. The calculations are facilitated by the chart (Fig. 35.8a) from which values of  $m_\alpha$  can be taken (Janbu et al. 1956), and by a tabular arrangement of the computations (Fig. 35.8b).

Inasmuch as the calculations outlined in Fig. 35.8 refer to only one trial circle, they must be repeated for other circles until the minimum value of  $F$  is found.

In general, the slope may be partly submerged and there will be pore pressures acting along the trial circle (Fig. 35.9a). The magnitudes of the pore pressures depend on the conditions of the problem. In some instances they may be estimated by means of a flow net (Article 23), by means of soil tests, or on the basis of field observations. If the level of the external water surface is denoted by  $A - A$ , the weight  $W$  of the slice (Fig. 35.9b) may be written as

$$W = W_a + W_b + zb\gamma_w \quad (35.13)$$

where  $W_a$  is the weight of that part of the slice above  $A - A$ ,  $W_b$  is the submerged weight of the part below  $A - A$ , and  $zb\gamma_w$  is the weight of a volume of water equal to the submerged portion of the slice. If the entire slice is located beneath water level, as slice 5 (Fig. 35.9a), the weight of the water above the slice must be included in  $zb\gamma_w$ . The pore pressure at the midpoint  $O'$  of the base of the slice is  $z\gamma_w + u'$ , where  $u'$  is the excess pore pressure with respect to the external water level. In an undrained failure,  $u'$  includes the shearing-induced pore-water pressure at failure. If the external water level  $A - A$  is located below  $O'$  on the base of the slice (Fig. 35.9b), the pore pressure at  $O'$  is  $h\gamma_w$ , where  $h$  is the height to which the water would rise in a piezometer at  $O'$ . If the pore pressure is due to capillarity,  $h$  is negative.

Because the forces acting on the slice are in equilibrium, they may be represented by the force polygon (Fig. 35.9c). The normal force  $P$  consists of an effective component  $P'$ , the force  $u'l$  caused by the excess pore pressure, and the force  $z'l\gamma_w$  caused by the hydrostatic pressure

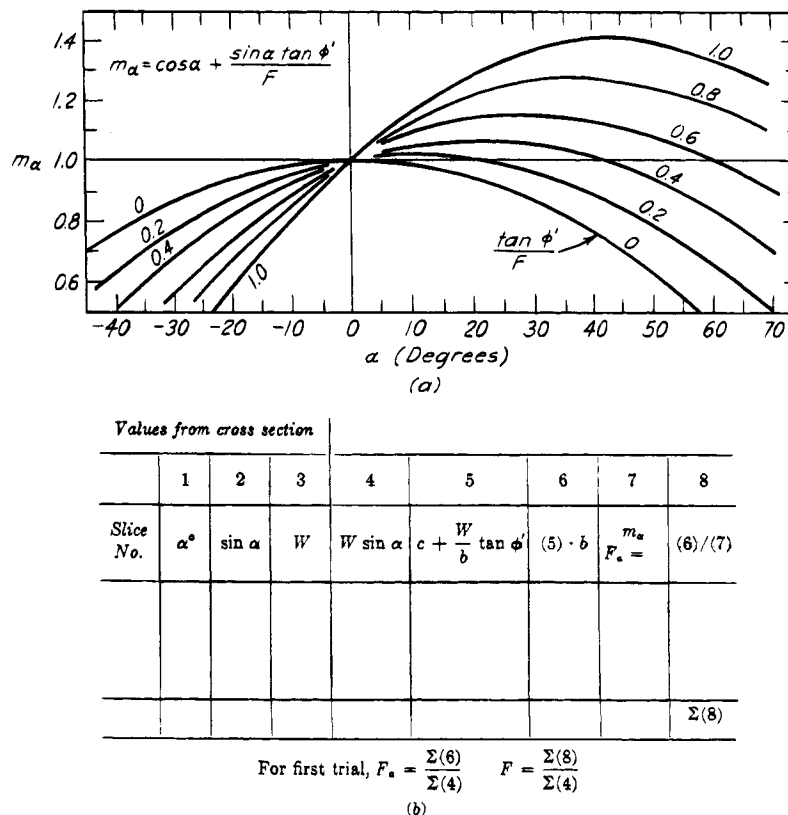


**Figure 35.8** Calculation of factor of safety for slope if surface of sliding is circular and forces between slices are neglected. (a) Chart for evaluating factor  $m_\alpha$ ; (b) tabular form for computation.

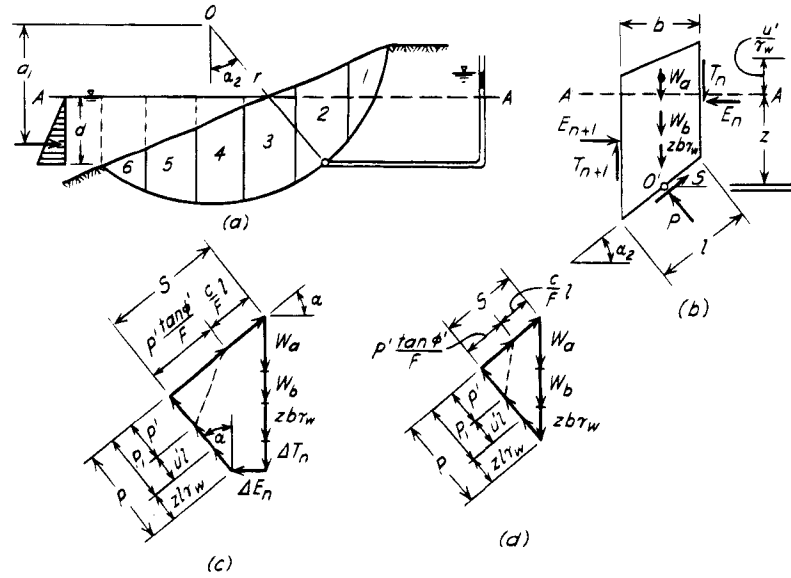


**Figure 35.9** Method of slices for circular surface of sliding if slope is partly submerged. (a) Geometry pertaining to one surface of sliding; (b) forces acting on typical slice, such as slice 2 in (a); (c) force polygon for slice 2 if all forces are considered; (d) force polygon for slice 2 if forces  $T$  and  $E$  on sides of slice are considered to be zero.

of the water with respect to  $A - A$ . The shearing stress  $\tau$  along the surface of sliding is

$$\begin{aligned}\tau &= \frac{s}{F} = \frac{1}{F} (c' + \sigma' \tan \phi') \\ &= \frac{1}{F} \left[ c' + \left( \frac{P}{l} - z\gamma_w - u' \right) \tan \phi' \right] \quad (35.14)\end{aligned}$$

from which

$$\begin{aligned}S &= \tau \cdot l = \frac{1}{F} [c'l + (P - z'l\gamma_w - u'l) \tan \phi'] \\ &= \frac{1}{F} (c'l + P' \tan \phi') \quad (35.15)\end{aligned}$$

Equilibrium of the entire slide with respect to moments about the center of the trial circle requires that

$$\begin{aligned}\sum (W_a + W_b + zb\gamma_w)r \sin \alpha &= \sum S \cdot r + \frac{1}{2}\gamma_w d^2 a_1 \\ &= \frac{1}{F} \sum (c'l + P' \tan \phi')r + \frac{1}{2}\gamma_w d^2 a_1 \quad (35.16)\end{aligned}$$

However, the water below level  $A - A$  is in equilibrium, from which

$$\sum zb\gamma_w r \sin \alpha = \frac{1}{2}\gamma_w d^2 a_1 \quad (35.17)$$

Therefore,

$$\begin{aligned}\sum (W_a + W_b)r \sin \alpha &= \frac{1}{F} \sum (c'l + P' \tan \phi')r \quad (35.18)\end{aligned}$$

and

$$F = \frac{\sum (c'l + P' \tan \phi')}{\sum (W_a + W_b) \sin \alpha} \quad (35.19)$$

The value of  $F$  (Eq. 35.19) depends on  $P'$  which may be determined for each slice from the force polygon (Fig. 35.9c). If the surface of sliding is circular, the influence of the forces  $T$  and  $E$  between the slices is relatively small and  $P'$  can usually be evaluated with sufficient accuracy on the assumption that the forces  $T$  and  $E$  are equal to zero. The force polygon then reduces to Fig. 35.9d, from which

$$\begin{aligned}W_a + W_b + zb\gamma_w &= (z'l\gamma_w + P' + u'l) \cos \alpha \\ &+ \left( P' \frac{\tan \phi'}{F} + \frac{c'l}{F} \right) \sin \alpha \quad (35.20)\end{aligned}$$

and

$$P' = \frac{W_a + W_b - u'b - \frac{c'l}{F} \sin \alpha}{m_\alpha} \quad (35.21)$$

Substitution of Eq. 35.21 into 35.19 gives

$$F = \frac{\sum \frac{[c'b + (W_a + W_b - u'b) \tan \phi']}{m_\alpha}}{\sum (W_a + W_b) \sin \alpha} \quad (35.22)$$

Equation 35.22, like Eq. 35.12, must be solved by successive approximations because the factor of safety  $F$  is contained in  $m_\alpha$  which appears on the right-hand side. It may be noted that the influence of the external water level is fully taken into account by the use of the submerged weight  $W_b$ , and that the excess pore pressure  $u'$  is calculated for the base of each slice as explained in connection with Eq. 35.13.

The procedure described in the preceding paragraphs may be modified to take into account the forces  $T$  and  $E$  between the slices (Bishop 1955, Janbu 1954). If the surface of sliding is circular, however, the improvement in accuracy is not likely to exceed 10 to 15% and the additional effort is not usually justified. On the other hand, if the surface of sliding is not circular the error may be significant. These circumstances will be considered in the next section. The procedures that will be developed may, if desired, be used to take into account the forces between slices for a circular surface of sliding as well (Spencer 1967)

### 35.10 Composite Surface of Sliding

In many instances the geometric or geologic conditions of the problem are such that the surface of sliding may not be even approximately circular. For these conditions, the method of slices can be extended (Janbu 1954, Morgenstern and Price 1965).

A sliding mass with a noncircular surface of sliding is shown in Fig. 35.10. The forces acting on any slice  $n$  are represented in the same manner as those shown in Fig. 35.9*b*, and the polygon of forces is identical to that in Fig. 35.9*c*.

The equilibrium of the entire sliding mass with respect to moments about the arbitrary pole  $O$  requires that

$$\Sigma W_x = \Sigma(Sa + Pf) + \frac{1}{2}\gamma_w d^2 a_1 \quad (35.23)$$

whence, from Eq. 35.15

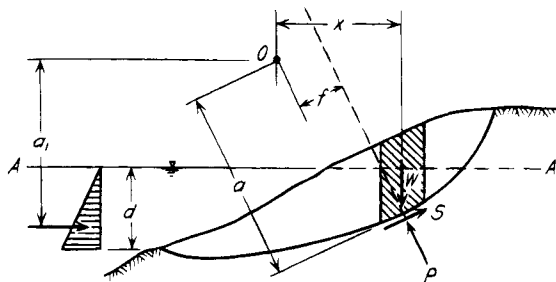


**Figure 35.10** Geometry of method of slices for investigating equilibrium of slope if surface of sliding is not circular.

$$\sum (W_a + W_b + zb\gamma_w)x = \frac{1}{F} \sum (c'l + P' \tan \phi')a + \sum Pf + \frac{1}{2}\gamma_w d^2 a_1$$

and

$$F = \frac{\Sigma(c'l + P' \tan \phi')a}{\Sigma(W_a + W_b + zb\gamma_w)x - \Sigma Pf - \frac{1}{2}\gamma_w d^2 a_1} \quad (35.24)$$

However, the water below level A - A is in equilibrium, whence

$$\Sigma z b \gamma_w x - \frac{1}{2} \gamma_w d^2 a_1 = \Sigma z l \gamma_w f = \Sigma (P - P_1) f \quad (35.25)$$

where

$$P_1 = P - z l \gamma_w$$

Equation 35.24 then becomes

$$F = \frac{\Sigma(c'l + P' \tan \phi')a}{\Sigma(W_a + W_b)x - \Sigma P_l f} \quad (35.26)$$

This expression can be evaluated if  $P'$  and  $P_1$  are known. These quantities may be determined from the force polygon (Fig. 35.9c). Summation of vertical components leads to

$$W_a + W_b + \Delta T_n + z b \gamma_w = z l \gamma_w \cos \alpha + (P' + u' l) \cos \alpha + \frac{1}{E} (c' l + P' \tan \phi') \sin \alpha.$$

from which

$$P' = \frac{W_a + W_b + \Delta T_n - u'b - (c'/F)b \tan \alpha}{m_\alpha} \quad (35.27)$$

Moreover,

$$P_1 = P' + u'l$$

$$= \frac{W_a + W_b + \Delta T_n + (1/F)(u'b \tan \phi' - c'b) \tan \alpha}{m_\alpha} \quad (35.28)$$

By substituting Eqs. 35.27 and 35.28 in 35.26 and combining terms, we find

$$F = \frac{\Sigma[c'b + (W_a + W_b + \Delta T_n - u'b) \tan \phi'](a/m_\alpha)}{\Sigma (W_a + W_b)x - \Sigma \left[ W_a + W_b + \Delta T_n + (u'b \tan \phi' - c'b) \frac{\tan \alpha}{F} \right] (f/m_\alpha)} \quad (35.29)$$

This equation must be solved by successive approximations because the factor of safety  $F$  occurs on the right-hand side explicitly as well as in the quantity  $m_a$ . Furthermore, the value of  $F$  depends on  $\Delta T_n$ . As a first approximation,  $\Delta T_n$  may be set equal to zero. The calculations are facilitated by the chart (Fig. 35.8a) and a tabular



arrangement (Fig. 35.11). Inasmuch as the value of  $F$  determined in this manner refers to only one trial surface, the calculations must be repeated for other surfaces until the minimum value of  $F$  is found. Computer programs are available to expedite the calculations. However, to ensure that the results are reasonable and that no untenable assumption has been incorporated into the routine, a manual check by means of the foregoing procedure is advisable.

For most practical problems involving a noncircular surface of sliding, the assumption that  $\Delta T_n$  is equal to zero leads to sufficiently accurate results. If the cross-section of the surface of sliding departs significantly from a circular shape, the use of Eq. 35.29 with  $\Delta T_n = 0$  is preferable to the assumption of a circular cross-section and the use of Eq. 35.22. However, if greater refinement is justified, values of  $\Delta T_n$  may be inserted in Eq. 35.29 and the factor of safety recalculated. The calculations are laborious and hardly practicable without a computer.

Because the interslice forces  $T$  and  $E$  depend on the deformation and the stress-deformation characteristics of the sliding mass, they cannot be evaluated by limit-equilibrium procedures, but values must be assigned to them arbitrarily. Any set of values  $T_n$  satisfying Eqs. 35.30 and 35.36 will ensure compliance with all conditions for

equilibrium of the slide as a whole and for the horizontal and vertical equilibrium of each slice. However, not all such sets of values are reasonable or possible. For example, the values of  $T_n$  must not exceed the shearing strength of the soil along the vertical boundary of the corresponding slice under the influence of the normal force  $E_n$ . Moreover, tensile stresses should not occur across a significant portion of any vertical boundary between slices. These requirements form one basis for judging the reasonableness of a computer solution.

If the subsoil contains one or more thin exceptionally weak strata, the surface of sliding is likely to consist of three or more sections that do not merge smoothly one into another. In stability computations such a surface cannot be replaced by a continuous curve without the introduction of an error on the unsafe side.

Figure 35.12 represents a slope underlain by a thin layer of very soft clay with undrained shear strength  $s_u$ . If such a slope fails, the slip occurs along some composite surface  $abcd$ . In the right-hand part of the sliding mass, represented by the area  $abf$ , active failure must be expected because the earth stretches horizontally under the influence of its own weight. The central part  $bcef$  moves to the left under the influence of the active pressure on  $bf$ . The left-hand part of the sliding mass  $cde$  experi-

Col.	1	2	3	4	5	6	7	8	9	10	11	12	13	14	15	16	17
Slice	$b$	$a$	$x$	$f$	$\alpha$	$\tan \alpha$	$c$	$\tan \phi'$	$cb$	$ub$	$W_a$	$W_b$	$\Delta T_n$	$W_a + W_b + \Delta T_n$	$(14) - ub$	$(15) \tan \phi'$	$(9) + (16)$
1																	
2																	
:																	
$n$																	

Col.	18	19	20	21	22	23	24	25	26	27	28	29	30
Slice	$(17) \cdot a$	$W_a + W_b$	$(19) \cdot x$	$ub \tan \phi'$	$(21) - cb$	$(22) \tan \alpha$	$F_1$	$\frac{(23)}{F_1}$	$(14) + (25)$	$(26) \cdot f$	$m_a$	$\frac{(18)}{m_a}$	$\frac{(27)}{m_a}$
1													
2													
:													
$n$													

$$\Sigma(20) =$$

$$F_s = \frac{\Sigma(29)}{\Sigma(20) - \Sigma(30)}$$

Repeat steps 24 to 30 incl.

$$\Sigma(29) =$$

$$\Sigma(30) =$$

Figure 35.11 Tabular form for calculating factor of safety of slope by method of slices, if surface of sliding is not circular.

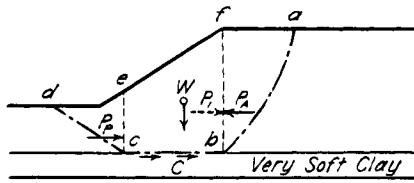


**Figure 35.12** Failure of slope underlain by thin layer of very soft clay.

ences passive failure due to the thrust of the advancing central part *bcef*.

The first step in investigating the conditions for the stability of the slope is to compute the passive earth pressure  $P_p$  of the soil located on the left side of a tentatively selected vertical section *ec* located near the toe of the slope. It is conservative to assume that  $P_p$  acts in the horizontal direction. The next step is to estimate the position of the right-hand boundary *b* of the horizontal part *cb* of the potential surface of sliding and to compute the active earth pressure  $P_a$  on a vertical section *fb* through *b*. The tendency for the mass *bcef* to move to the left is resisted by the passive earth pressure  $P_p$  and the total undrained shear strength  $C$  along *bc*. If the slope is stable, the sum of these resisting forces must be greater than the active earth pressure  $P_a$ , which is assumed to act in a horizontal direction. The factor of safety against sliding is equal to the ratio between the sum of the resisting forces and the force  $P_a$ . The investigation must be repeated for different positions of the points *c* and *b* until the surface of least resistance to sliding is found that corresponds to the least factor of safety.

### Problems

1. A wide cut was made in a stratum of soft clay that had a level surface. The sides of the cut rose at  $30^\circ$  to the horizontal. Bedrock was located at a depth of 12 m below the original ground surface. When the cut reached a depth of 7.5 m, failure occurred. If the unit weight of the clay was  $19.2 \text{ kN/m}^3$ , what was its mobilized undrained shear strength? What was the character of the surface of sliding? At what distance from the foot of the slope did the surface of sliding intersect the bottom of the excavation?

*Ans.* 24 kPa; midpoint circle; 5.25 m.

2. The rock surface referred to in problem 1 was located at a depth of 9 m below the original ground surface. What were the mobilized undrained shear strength of the clay and the character of the surface of sliding?

*Ans.* 22 kPa; toe circle.

3. A cut is to be excavated in soft clay to a depth of 9 m. The material has a unit weight of  $18.3 \text{ kN/m}^3$  and a  $s_u$  (UC) of 34 kPa. A hard layer underlies the soft layer at a depth of 12 m below the original ground surface. What is the slope angle at which failure is likely to occur?

*Ans.*  $\beta = 69^\circ$ .

4. A trench with sides rising at  $80^\circ$  to the horizontal is excavated in a soft clay which weighs  $19.2 \text{ kN/m}^3$  and has an undrained shear strength of 12 kPa. To what depth can the excavation be carried before the sides cave in? At what distance from the upper edge of the slope will the surface of sliding intersect the ground surface?

*Ans.* 2.75 m; 2.46 m.

5. A bed of clay consists of three horizontal strata, each 4.5 m thick. The values for  $s_u$  for the upper, middle, and lower strata are, respectively, 30, 20, and 140 kPa. The unit weight is  $18.4 \text{ kN/m}^3$ . A cut is excavated with side slopes of 1 (vertical) to 3 (horizontal) to a depth of 6 m. What is the factor of safety of the slope against failure?

*Ans.* 1.3.

6. To what depth can the trench in problem 4 be excavated without bracing if the soil is located above water table, and has a cohesion intercept  $c$  of 12 kPa and an angle of internal friction of  $20^\circ$ ?

*Ans.* 4.25 m.

7. To what depth can a permanent trench in problem 4 be excavated without bracing if the clay bed is completely submerged and the effective cohesion intercept  $c'$  is 4 kPa and the angle of internal friction is  $20^\circ$ ?

*Ans.* 2.96 m.

### Selected Reading

An excellent overview of the methods of stability analysis and the assumptions on which they are based is given by D. Nash, "A Comparative Review of Limit Equilibrium, Methods of Stability Analysis," Chap. 2 "Slope Stability," Anderson, M. G. and K. S. Richards, Eds., Wiley, 1987. A similar comparison is found in Fredlund, D. G. and J. Krahn, "Comparison of Slope Stability Methods of Analysis," *Can. Geot. J.*, (1977), **14**, 429–439.

Lafleur, J. and G. Lefebvre (1980). "Groundwater regime associated with slope stability in Champlain clay deposits." *Can. Geotech. J.*, **17**, No. 1, pp. 44–53.

Charles, J.A. and M.M. Soares (1984). "The stability of slopes in soils with nonlinear envelopes." *Can. Geotech. J.*, **21**, No. 3, pp. 397–406.

## ARTICLE 36 STABILITY OF EARTH DAMS

### 36.1 Critical States for Design

The factor of safety of an earth dam with respect to a slope or foundation failure depends to a large extent on the porewater pressures. In a dam of given cross-section on a given foundation, the intensity and distribution of the porewater pressures vary with time between wide limits. For purposes of design it is convenient to distinguish among the porewater pressure conditions corresponding to three stages: during construction, and especially immediately after construction has been completed; after the reservoir has been full long enough to

develop a state of steady seepage in the dam and its foundation; and during or immediately after lowering of the reservoir level. These three stages are briefly designated as the *construction*, *full-reservoir*, and *drawdown states*. The stability of the upstream slope may also be critical upon first filling of the reservoir, especially if the dam has a sloping core. Furthermore, in some instances, the state of the upstream slope may be more critical at an intermediate level, known as *partial pool*, than with the reservoir full.

### 36.2 Evaluation of Porewater Pressures in Critical Design States

During the construction stage, significant pore pressures can develop only in the cohesive portions of the dam and subsoil. They are associated with progressive consolidation. Therefore, the intensity and distribution of the pressures depend not only on the characteristics of the materials and on the boundary conditions for drainage, but also to a large extent on the construction schedule. As an example, Fig. 36.1 shows the porewater pressures observed at the end of construction in the upstream portion of Green Mountain dam in Colorado (Walker and Daehn 1948). Placement of fill was discontinued for the winter when the dam had reached approximately half its final height; the influence of the interruption is evident.

After the dam has been completed and the reservoir has been full for some time, the dam is acted on by the seepage pressures exerted by a steady flow of water percolating out of the reservoir through the dam toward the downstream slope. The corresponding porewater pressures can be estimated on the basis of the flow-net method (Fig. 23.6a) or an equivalent procedure, provided the subsoil conditions are simple enough to permit construction of a reasonably reliable permeability profile of the material on which the dam is founded.

The porewater pressure conditions initiated by a drawdown depend to a large extent on the degree of compressibility of the different constituents of the body of the dam. In the semipervious and relatively incompressible portions, such as those constructed of well-compacted silty sand, most of the water that occupied the voids

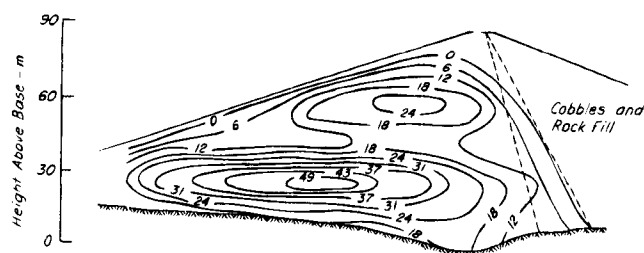


**Figure 36.1** Measured pore pressures in meters of water in impervious section of Green Mountain dam at end of construction (after Walker and Daehn 1948).

before drawdown is retained in the voids; the remainder drains out of the dam at practically unaltered void ratio. It emerges partly through the lower portions of the slopes and, if the subsoil is pervious, partly through the base of the dam. The drawdown condition is illustrated by Fig. 23.6c which shows the flow net for a homogeneous dam of fine, clean, well-compacted sand, at the instant after a sudden, complete drawdown. The dam is assumed to rest on an impervious base. It can be seen that the seepage pressures on the downstream slope remain unchanged from those of the full-reservoir state (Fig. 23.6a), whereas those acting on the lower portion of the upstream slope tend to cause a failure of this portion by sliding. As time goes on, the uppermost flow line (the lower boundary of the capillary fringe) descends and all the seepage pressures decrease.

The impervious compressible portions of the dam, such as those consisting of clay, remain in a completely or almost completely saturated state even after the drawdown. The water is held by capillarity. However, the pore pressures in those portions of the clay located immediately beneath the uppermost flow line change from positive to negative whereas the total stresses remain almost unaltered. Consequently, the effective pressures in the clay increase and the clay starts to consolidate. Most of the excess water flows into the lower part of the clay portion of the dam, reducing its shearing resistance, and ultimately emerges from the lower part of the upstream boundary of the clay portion.

Whatever may be the cross-section of a dam and the geologic profile of its foundation materials, the importance of the undesirable consequences of a drawdown decreases with decreasing rate of drawdown. Hence, to determine the pore pressure conditions for the drawdown state, all the following factors need to be known: the location of the boundaries between materials with significantly different properties; the permeability and consolidation characteristics of each of these materials; and the anticipated maximum rate of drawdown. In addition, the pore pressures induced by the changes in the shearing stresses themselves (Article 15.5.2) need to be taken into consideration. In engineering practice, few of these factors can be determined reliably. The gaps in the available information must be filled by the most unfavorable assumptions compatible with the known facts.

### 36.3 Stability Computations

In every earth dam, except in a homogeneous dam resting on a rigid base, the potential surfaces of sliding pass through the weakest portions of the dam and subsoil (Fig. 36.2). For a given cross-section and a given foundation, the position of these surfaces also depends on the intensity and distribution of the pore pressures. Therefore, the surfaces can rarely be defined as arcs of circles. They can in most instances be represented only by lines with a

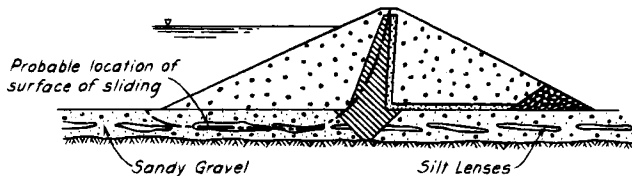


**Figure 36.2** Diagram illustrating likelihood of noncircular surface of sliding in zoned earth dam.

variable radius of curvature or by composite curves. Their position must be ascertained by trial and error, by starting with a curve that is believed to be located close to the surface of minimum resistance. The calculations may be carried out by the procedures outlined in Article 35.

The calculations for each of the three critical states for design require the determination of the corresponding pore pressures. According to the preceding section, this determination must be based on the adaptation of the theories of consolidation and of the flow of water through porous media to the internal and external boundary conditions, as well as on a knowledge of the stress-deformation pore-pressure characteristics of the materials. The latter characteristics are usually expressed in terms of estimated values of the pore-pressure coefficients  $A$  and  $B$  (Article 15.5). If it is possible to estimate the pore pressures at failure for the appropriate mode of shear and to determine the values of  $c'$  and  $\phi'$ , an effective stress stability analysis (ESSA) can be carried out using the equations of Article 35.

The values of  $c'$  and  $\phi'$  for saturated compacted cohesive soils can be determined reliably on the basis of laboratory tests, whereas the choice of appropriate values of porewater pressure at failure requires much experience and judgment. In some situations it may be preferable to use undrained strength stability analysis (USSA) in which the shearing resistance is evaluated directly on the basis of undrained shear tests. For example, the shearing resistance to be used in analyzing the stability of an upstream slope after a drawdown depends on whether the material beneath the upstream slope can experience practically no drainage during the drawdown, or can drain so rapidly as to dissipate practically all the excess porewater pressures as the drawdown progresses. The degree of drainage is judged on the basis of a knowledge of the rate of drawdown and of the permeability and dimensions of the mass of soil affected by the drawdown. For a fully undrained drawdown the values of undrained shear strength corresponding to the consolidation condition preceding the drawdown are used in an USSA. If some drainage is possible during the drawdown, the effect of the associated volume changes on the undrained shear strength of soil can be determined by performing undrained shear tests at different consolidation pressures.

The experience and judgment required to choose the most appropriate values of the undrained shear strength for USSA are fully as great as those needed to evaluate the porewater pressure at failure for use in an ESSA. From this point of view, neither procedure can be said to deserve the preference. Except for circumstances under which the constant volume undrained conditions are applicable, there seems to be a growing tendency to estimate the pore pressures for use in effective stress analyses of stability of earth dams, partly because they can be compared more directly with the results of pore-pressure observations in the field.

### 36.4 Sources of Error in Effective Stress Stability Analyses

The sources of error in stability computations can be divided into three categories: simplifying assumptions introduced into the computations; the assumption of simultaneous failure; and errors in the evaluation of the intensity and distribution of the pore pressures. By far the most important errors are those of the last category. For this reason, the design should be based on the most unfavorable assumptions regarding these pressures consistent with the known physical properties of the materials comprising the dam and its foundation.

### Selected Reading

The effective-stress method of analysis, specifically in connection with rapid drawdown, is exemplified by Bishop, A. W. (1954): "The use of pore-pressure coefficients in practice," *Géot.*, 4, pp. 148–152.

## 36.5 Seismic Stability of Earth Dams

### 36.5.1 Introduction

If an earth dam is located in a region subject to earthquakes, the design must satisfy the condition that even the most severe earthquake likely to occur in the region should not damage the dam to the extent that the reservoir is catastrophically released. Under the rare circumstance that a dam must be located on an active or potentially active fault, the dam must be capable of accommodating the differential movement without permitting internal erosion. Furthermore, whether or not ground rupture occurs, the dam must be able to withstand the shaking associated with the earthquake. The effects of shaking depend primarily on whether the shear strength of the embankment material remains fairly constant during repetitions of the seismic loading or whether the repetitions are associated with significant loss of strength.

If the shear strength does not decrease appreciably as a consequence of cyclic loading or shaking, design requires an estimate of the deformations of the dam as its slopes tend to move downward and outward and its

crest tends to settle correspondingly. If the settlement exceeds the freeboard, overtopping occurs, possibly followed by destruction of the dam and loss of the reservoir. Because the deformations are the result of sliding or shearing movements, analyses pertaining to these conditions are directed toward ensuring a factor of safety great enough to minimize the deformations and to estimate the deformations. The calculations are fairly straightforward.

On the other hand, if the dam or its foundation contains materials subject to loss of shear strength under repeated loading, movements may quickly become very great and cannot be estimated reliably by any simple means. The most severe loss of shear strength occurs as a result of liquefaction of loose saturated cohesionless materials (Article 20.9), and several failures due to this cause are on record. In the design of new dams the possibility of liquefaction is largely precluded by selection and controlled compaction of materials and by suitable treatment of foundations, but the assessment of the liquefaction potential of existing dams remains an important practical problem. Procedures in current use are complex and somewhat controversial.

### 36.5.2 Seismic Shaking with Non-Degrading Shear Strength

In the early 1940's it became customary to account for the effects of earthquakes on dams by including an earthquake-induced force, usually taken as horizontal, in the stability analysis of the dam. The portion of the dam above any arbitrary surface of sliding was assumed to be subjected to a force equal to the mass of the sliding portion multiplied by an acceleration that ranged from about  $0.1g$  for regions of little or no seismic activity to  $0.2g$  or more for locations where destructive earthquakes are possible. Although the procedure, termed a pseudostatic analysis, was preferable to ignoring seismic effects, it was unrealistic because it substituted a constant static force for the random accelerations of a real earthquake and it furnished no indication of the movements or distortions of the dam.

A simple, fundamentally sound, general dynamic analysis was introduced by Newmark (1965) in which the motion of the portion of the dam above any arbitrary surface of sliding, as the result of a series of earthquake acceleration pulses, is calculated on the assumption that the soil along the surface of sliding exhibits rigid-plastic behavior. Although the procedure has been refined and elaborated (Seed and Martin 1966, Ambrayes and Sarma 1967, Makdesi and Seed 1978), the results of applying even the simple analysis are reasonable and useful in practice.

The basic concept of the Newmark procedure is illustrated in Fig. 36.3. A rigid block  $abcd$  (Fig. 36.3a), representing the portion of a dam above an arbitrary surface of sliding, rests on a rigid base  $ef$ . Both the block and

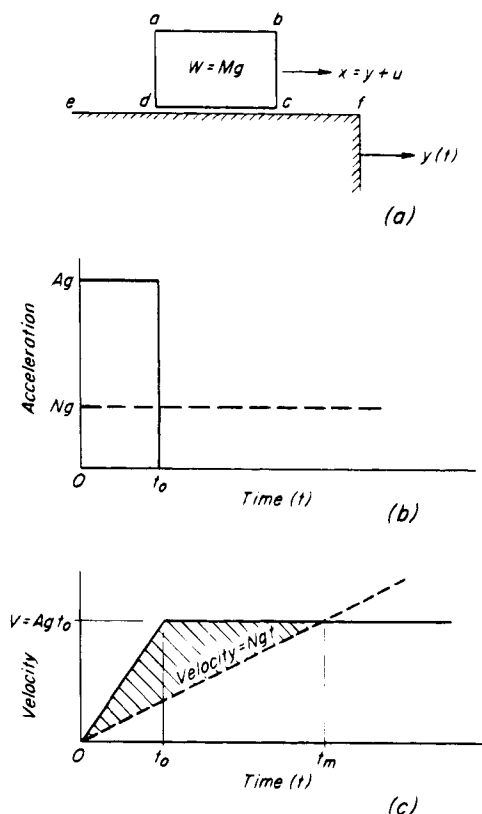


**Figure 36.3** Basic concept of Newmark procedure for dynamic analysis of earth dam. (a) Rigid block on moving support; (b) rectangular block acceleration pulse; (c) velocity response to rectangular block acceleration (after Newmark 1965).

the base move during an earthquake; the movement of the base is  $y(t)$  and that of the block is  $x(t)$ . The differential movement between the two is  $u = x - y$ . The shearing resistance between the block and the base is considered to be proportional to the weight  $W$  of the block; the constant of proportionality is designated as  $N$ . Thus, a base acceleration equal to  $Ng$  is just sufficient to cause slip between the base and the block.

If a constant acceleration  $Ag$  is applied to the block for a time  $t_0$ , the acceleration pulse is represented by the rectangle in Fig. 36.3b. The resisting acceleration  $Ng$  is represented by the dash line; it continues as long as the direction of motion does not change. The corresponding velocities are shown as a function of time in Fig. 36.3c. The block comes to rest relative to the base at a time  $t_m$  when the net velocity becomes zero. Since, at  $t_m$ ,  $V = Ng t_m$

$$t_m = \frac{V}{Ng} \quad (36.1)$$

The maximum displacement  $u_m$  of the block relative to the base is equal to the shaded area (Fig. 36.3c). Thus

$$u_m = \frac{1}{2} V t_m - \frac{1}{2} V t_0 = \frac{1}{2} \frac{V^2}{N g} - \frac{1}{2} \frac{V^2}{A g} = \frac{V^2}{2 g N} \left( 1 - \frac{N}{A} \right) \quad (36.2)$$

The acceleration pulse (Fig. 36.3*b*) corresponds to a constant velocity after  $t_0$  (Fig. 36.3*c*) and thus to an infinite displacement. However, in an earthquake, both positive and negative pulses occur in a random order, as shown by the record for the El Centro earthquake of May 18, 1940 (Fig. 36.4*a*). It can be shown that if a second pulse occurs, of negative magnitude capable of reducing the velocity to zero even without the resisting force, the net displacement with the resistance generally cannot exceed that which would occur without the resistance. Therefore, Eq. 36.2 generally overestimates the displacement.

The foregoing analysis, based on Fig. 36.3*a*, refers to a horizontal surface of sliding on which the resistance is equal in both directions. It might be applicable, for instance, to the portion of a symmetrical earth dam above a horizontal surface of sliding. In reality, most surfaces of sliding are inclined, and the resistance is greater to uphill than to downhill movement. Although Eq. 36.2 remains applicable for calculating the movement for each pulse, the downhill displacements accumulate, whereas the uphill movements are very small and may be neglected. To investigate the influence of unsymmetrical resistance for various values of  $N/A$ , Newmark calculated the accumulated maximum displacements, considering all uphill displacements to be zero, from the records of four different earthquakes with widely different acceleration-time characteristics. The results, normalized to a

maximum peak acceleration of  $0.5g$ , are shown in Fig. 36.5. The expression

$$u_m = \frac{V^2}{2 g N} \left( 1 - \frac{N}{A} \right) \frac{A}{N} \quad (36.3)$$

is seen to be a reasonable upper bound for the accumulated displacements for values of  $N/A$  greater than about 0.1, and a conservative upper bound for smaller values. Because the four earthquakes analyzed by Newmark represent a broad range of experience, Eq. 36.3 may be used for a generally conservative estimate. The factor  $A/N$  may be regarded as the effective number of pulses contributing to the cumulative displacement.

The application of Eq. 36.3 to a particular slope or dam can be carried out by vector analyses of several trial sliding masses with different surfaces of sliding, following procedures similar to those for investigating the static stability of slopes. The method for an assumed circular surface of sliding with radius  $R$  and center  $O$  is illustrated in Fig. 36.6.

The first step is to divide the assumed sliding mass into vertical slices and to determine the shearing resistances  $s_1, s_2, \dots$ . This step requires a careful evaluation of the test and drainage conditions appropriate for the soils under consideration. The values of  $s$  are then combined into their resultant  $S$  (Fig. 36.6*b*), located at a distance from  $O$  such that the moment of  $S$  about  $O$  equals that of the components  $s$ . The weight  $W$  of the sliding mass is determined, and the magnitude and direction of the minimum resistance  $NW$  are assumed (the direction for

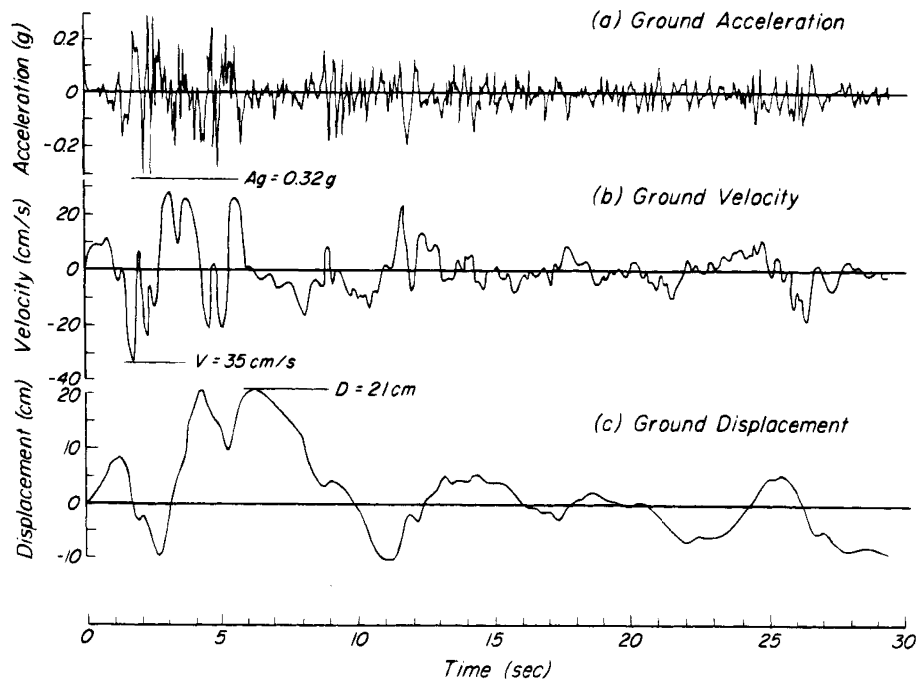
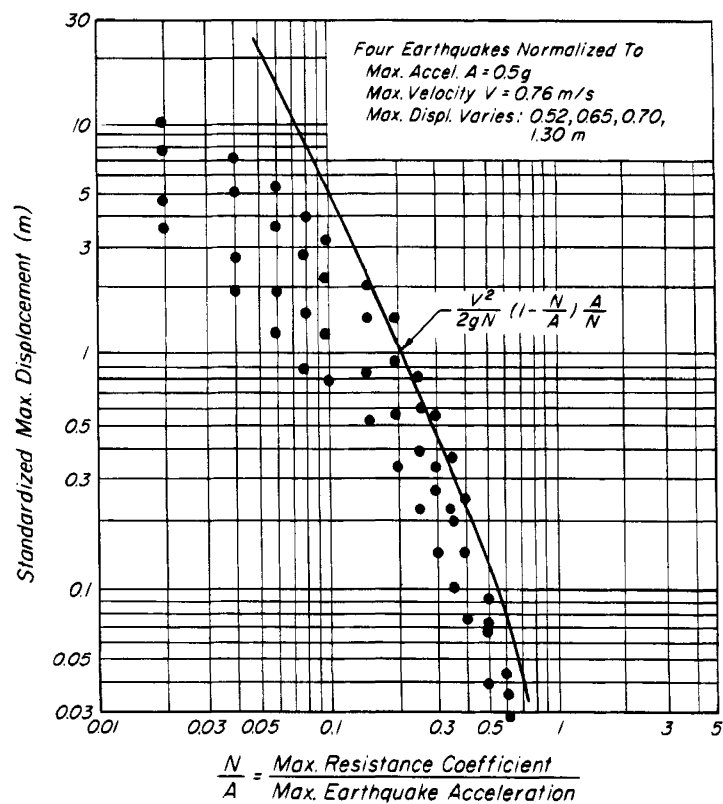
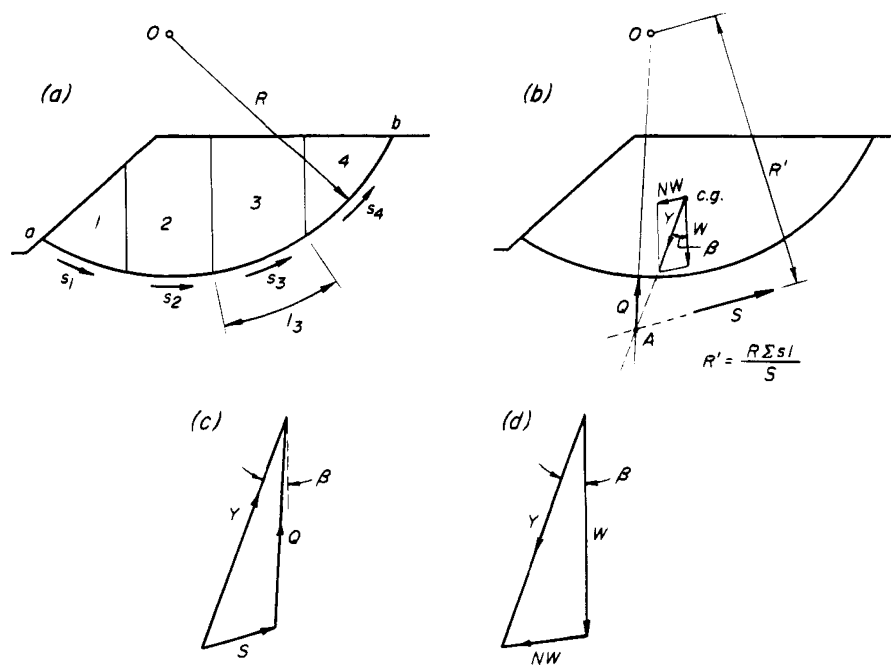


Figure 36.4 North-south component of El Centro earthquake of May 18, 1940.



**Figure 36.5** Standardized displacement for normalized earthquakes neglecting all uphill movements (after Newmark 1965).



**Figure 36.6** Graphical calculation for obtaining minimum resistance  $NW$  of mass above surface  $ab$  to sliding during earthquake. (a) Sliding mass; (b) forces involved; (c, d) vector diagrams.

$NW$  is not likely to be horizontal). The resultant of  $W$  and  $NW$  is  $Y$ , which makes an angle  $\beta$  with  $W$ . The intersection of  $Y$  and  $S$  defines the point  $A$  through which passes the force  $Q$ , the resultant normal force across the surface of sliding. Because  $S$  is known in magnitude and direction, and  $Y$  and  $Q$  in direction, the magnitude of  $Y$  may be determined from the force diagram (Fig. 36.6c). The force  $Y$  can then be decomposed into  $W$  and  $NW$  (Fig. 36.6d). The calculation is repeated for various values of  $\beta$  until the minimum value of  $NW$  for the assumed inclination of  $NW$  is established. The same procedure is repeated for different inclinations of  $NW$  until the inclination and value of the minimum resistance  $NR$  are established.

With the minimum value of  $NW$  determined,  $N$  is calculated and the displacement for a single pulse found from Eq. 36.2. That for the accumulated displacement for several pulses can be obtained from Eq. 36.3.

Equation 36.3 indicates that the accumulated displacement depends primarily on the maximum ground velocity associated with the earthquake motion. Thus, in applying the analysis, one or more earthquake records similar to that in Fig. 36.4 are used. The selection of the ground motions appropriate to a given site requires the cooperation of a seismologist familiar with the location of the dam. Furthermore, because an earth dam is not a rigid block, the maximum acceleration at the elevation of the centroid of the mass of the dam above the surface of sliding under investigation generally differs from the ground motion to which the earthquake record applies.

### 36.5.3 Seismic Shaking with Degrading Shear Strength

If the strength of a soil decreases as a result of earthquake pulses, a Newmark-type analysis is inapplicable. The most striking form of degradation is liquefaction of cohesionless sandy soils; several failures of earth dams containing or resting on such materials have occurred during or shortly after earthquakes, some with disastrous consequences (Seed et al. 1978). Consequently, much attention has been devoted in recent years to developing methods for evaluating the safety of existing dams and for designing proposed dams in seismic areas (Seed 1979b, 1987). Because of the complexity of the subject, only a brief outline is given here.

Earthquakes produce alternating shear stresses,  $\tau$ , throughout a dam and its foundation, corresponding to the variations in acceleration as illustrated in Fig. 36.4a. Laboratory investigations (Seed and Peacock 1971) have established that the susceptibility to liquefaction under undrained conditions, as measured by the number of reversals of shear stress before liquefaction occurs, is a function of the ratio  $\tau/\sigma'_{vo}$ , in which  $\tau$  is the maximum cyclic shear stress, considered to act in a horizontal plane, and  $\sigma'_{vo}$  is the effective vertical pressure before the cyclic

shear is applied. A seismic analysis thus requires calculation of the initial static vertical effective stresses at points throughout the embankment and foundation and of the horizontal shear stresses at corresponding points due to the earthquake selected for analysis. These operations are best accomplished by finite-element procedures that, for the static stresses, take into account nonlinear stress-dependent soil behavior. The dynamic analyses also consider the nonlinear relationships between shear strain and dynamic shear modulus and damping. Values of  $\tau/\sigma'_{vo}$  are thus determined. These values are compared with those associated with liquefaction.

Values of  $\tau/\sigma'_{vo}$  corresponding to liquefaction of level ground during an earthquake of magnitude 7.5 have been related statistically to the standard penetration resistance  $(N_1)_{60}$  (Seed et al. 1984). The correlation, shown in Fig. 20.66, can be modified for earthquakes of other magnitudes. By comparing the values of  $\tau/\sigma'_{vo}$  calculated for the dam with those in Fig. 20.66, after making an adjustment for the slope of the shell of the dam, a conclusion can be drawn whether liquefaction will or will not occur at each of the points for which the comparison is made. If the comparison shows that no liquefaction will occur, the deformation of the dam can be estimated by the procedure for nondegrading soils (Article 36.5.2). If the comparison indicates that some portions of the dam or foundation will liquefy, a stability analysis can be carried out by the methods described in Article 35 in which the shear strengths of the liquefied zones are taken as the critical values (Eqs. 20.40 and 20.41).

Although much progress has been made in recent years in the seismic analysis of dams where liquefaction may be involved, the relative paucity of observational data, in which the earthquake motions and behavior are both adequately known on the basis of field measurements, leaves many serious gaps in knowledge. Consequently, the seismic analysis of embankment dams where liquefaction is a possibility should be undertaken only by experienced specialists fully aware of the latest developments in a rapidly evolving field.

## ARTICLE 37 EARTH PRESSURE AGAINST SUPPORTS IN CUTS

### 37.1 Deformation Conditions Imposed by Supports

Figure 37.1a illustrates one of several methods for supporting an open cut. A row of H-piles is driven along each side of the proposed excavation to a depth of a few meters below grade. The sides of the cut between H-piles are lined by horizontal boards placed directly against the soil as the cut is deepened. The two ends of each board are wedged against the inner flanges of the H-piles. The piles themselves are supported by horizontal struts inserted as excavation proceeds. To design the struts,



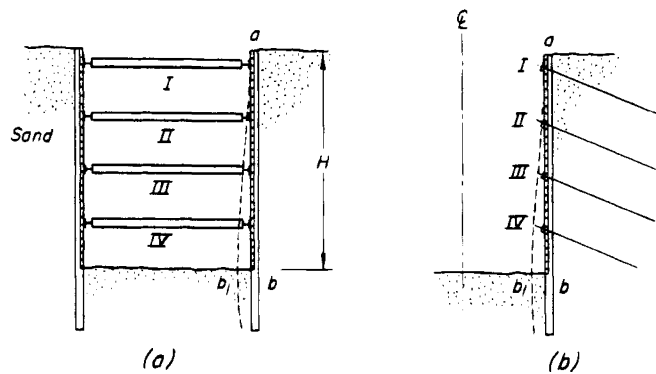


**Figure 37.1** Diagrams illustrating deformation condition for lateral pressure against support system of open cut with (a) struts or (b) tiebacks.

we must know the magnitude and distribution of the earth pressure.

In Article 27 it was shown that the earth pressure depends not only on the properties of the supported soil but also on the restrictions that the construction procedure imposes on the freedom of the supports to yield. Hence, the first step in investigating the earth pressure against an open cut is to examine the nature of these restrictions. When the first row of struts *I* (Fig. 37.1a) is placed, the amount of excavation is still so insignificant that the original state of stress in the soil is practically unaltered. Therefore, the first row of struts is in position before any appreciable yielding of the soil mass occurs. As excavation proceeds to the level of the next row of struts *II*, the rigidity of row *I* prevents further horizontal yielding of the soil located near the ground surface on each side of the cut. However, the H-piles are acted on by the lateral pressure of the soil outside the cut. Under the influence of this pressure, they yield inward by rotating about a line at the level of the uppermost row of struts. Hence, the placement of the second row of struts is preceded by a horizontal yielding of the soil located outside the cut at the level of this row. With increasing depth the yielding increases, because the height of the banks on either side of the cut increases. Therefore, while excavation proceeds, the vertical section *ab* (Fig. 37.1a) advances into position *ab*<sub>1</sub>. Because the strut at the top of the cut prevents the stretching of the upper part of the sliding wedge, the soil can fail only as indicated in Fig. 27.3. Because of this, the active earth pressure against the bracing in the cut may differ from that computed by means of Coulomb's or Rankine's theory. A method must be developed that considers the influence of the deformation conditions on the type of failure.

It has been shown that the deformation conditions represented by line *ab*<sub>1</sub> in Fig. 37.1a involve a failure of the type illustrated in Fig. 27.3. It has also been shown (Article 27) that the failure cannot occur unless the lower edge

*b* of the lateral support (Fig. 37.1a) yields more than a certain distance *bb*<sub>1</sub>. This distance depends on the depth of the cut and on the physical properties of the soil. In the following discussion, we shall assume that this deformation condition is satisfied. The observations on which the assumption is based and the necessary qualifications are presented in Article 46.

Similar deformations occur if the lateral support is provided by earth anchors or tiebacks, as illustrated in Fig. 37.1b. If the tiebacks are horizontal, they exert no vertical force on the wall, but if they are inclined, a substantial vertical component may be introduced. The implications of this component are considered in Article 46. In the present discussion the vertical force is ignored.

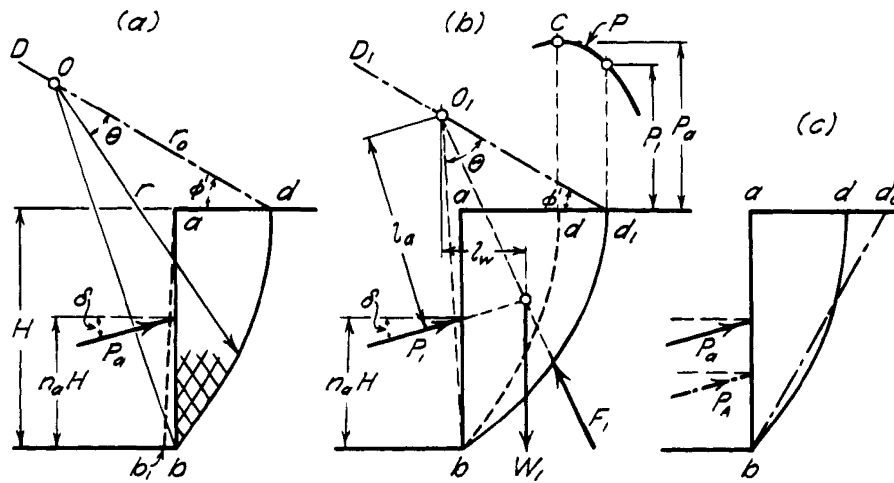
### 37.2 Cuts in Dry or Drained Sand

Figure 37.2 shows a vertical section through one side of a cut with depth *H* in dry or drained sand. The initial position of the H-piles is indicated by the plain line *ab* and the final position by the dash line *ab*<sub>1</sub>. The earth pressure on the bracing, per unit of length of the cut, is designated by *P*<sub>a</sub> to distinguish it from the active earth pressure *P*<sub>A</sub> exerted by a similar mass of sand against a retaining wall of height *H*. Because the upper part of the sliding wedge (Fig. 37.2a) cannot move laterally, the surface of sliding intersects the ground surface at a right angle (see also Fig. 27.3). The real curve of sliding can be closely approximated by a logarithmic spiral having the equation

$$r = r_0 e^{\theta \tan \phi'} \quad (37.1)$$

The center of the spiral is located on a straight line that passes through *d* and makes an angle  $\phi'$  with the horizontal. Because the yield of the lateral support causes the wedge to move downward along the back of the support, the resultant earth pressure acts at an angle  $\delta$  to the horizontal. Theoretical investigations have shown that the point of application of the earth pressure is determined by the shape of the surface of sliding and vice versa. If the curve of sliding is similar to *bd* in Fig. 37.2, theory indicates that the distribution of the sand pressure against the bracing is roughly parabolic, as indicated in Fig. 27.3b, and that the elevation of the point of application *n<sub>a</sub>H* should be between 0.45*H* and 0.55*H*. This theoretical conclusion has been confirmed by pressure measurements in full-sized cuts. Therefore, in the following computation *n<sub>a</sub>* is assumed to be known.

To determine the position of the surface of sliding, an arbitrary point *d*<sub>1</sub> (Fig. 37.2b) is selected on the horizontal surface adjoining the upper edge of the cut. Through this point and through the lower edge *b* of the bank, a logarithmic spiral *bd*<sub>1</sub> is traced with its center on *d*<sub>1</sub>*D*<sub>1</sub>. The reaction *F*<sub>1</sub> on the surface of sliding represented by *bd*<sub>1</sub> passes through the center *O*<sub>1</sub>. Taking moments about *O*<sub>1</sub>, we obtain



**Figure 37.2** Logarithmic spiral method for calculating earth pressure against support of open cuts. (a) Diagram illustrating assumptions on which computation is based; (b) forces acting on sliding wedge; (c) comparison of surface of sliding with that assumed in Coulomb's theory.

$$P_1 l_a = W_1 l_w$$

whence

$$P_1 = \frac{W_1 l_w}{l_a} \quad (37.2)$$

A similar computation is made for spirals through  $d_2, d_3 \dots$  (not shown). By plotting the values  $P_1, P_2 \dots$ , etc., as ordinates above  $d_1, d_2, \dots$ , the curve  $P$  is obtained. The active earth pressure  $P_a$  is equal to the maximum ordinate, corresponding to point  $C$ , and the surface of sliding passes through  $d$ . The width  $ad$  of the top of the wedge which exerts the maximum pressure  $P_a$  is always much smaller than the width of the top of the corresponding Coulomb wedge  $abd_c$  (Fig. 37.2c).

The value of  $P_a$  depends to a certain extent on  $n_a$ . It increases slightly with increasing values of  $n_a$  and is always greater than the corresponding Coulomb value  $P_A$ . For the values  $\phi' = 38^\circ$  and  $\delta = 0^\circ$ , an increase of  $n_a$  from 0.45 to 0.55 increases  $P_a$  from 1.03  $P_A$  to 1.11  $P_A$ . If we assume  $n_a = 0.55$ , any error is on the safe side because this value is the greatest that has been obtained so far by field measurements. The angle  $\delta$  has very little influence on the ratio  $P_a/P_A$ . Hence, for a preliminary estimate, it is sufficiently accurate to assume

$$P_a = 1.1 P_A \quad (37.3)$$

The next step in the investigation is to determine the load in individual struts or tiebacks. The distribution of the lateral pressure is roughly parabolic, as shown in Fig. 27.3b, but from section to section in a given cut it deviates somewhat from the statistical average because of variations in soil conditions and in details of the construction procedure. Consequently, for a given value of  $P_a$  the load differs in individual struts or tiebacks at a given elevation.

The procedure for estimating the maximum pressure that may have to be resisted by the struts or tiebacks in any given row is described in Article 46.3.

### 37.3 Cuts in Saturated Clay Under Undrained Conditions

#### 37.3.1 Heave of the Bottom

Before we consider the earth pressure exerted against the bracing of an open cut in an intact saturated clay under undrained conditions ( $\phi = 0^\circ, c = s_u$ , Article 20), we must investigate whether the bottom may fail by heaving. The weight of the blocks of clay beside the cut tends to displace the underlying clay toward the excavation. If the underlying clay experiences a bearing-capacity failure, the bottom of the excavation heaves and the earth pressure against the bracing increases dramatically.

Figure 37.3a represents a cross-section through a long cut with width  $B$  and depth  $H$ . The block of soil  $abcd$  represents a surcharge  $(HB'\gamma - s_u H)/B'$  on the strip  $cd$ . The bearing capacity of the soil below  $cd$  is equal to  $N_c s_u$  where  $N_c$  is equal to 5.7, corresponding to the bear-

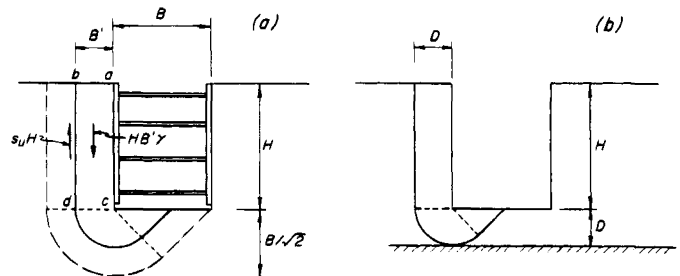


**Figure 37.3** Section through open cut in deposit of soft clay. (a) Failure surfaces for deep deposit; (b) failure surface if hard bottom exists at depth  $D$  below base of cut.

ing capacity of a long footing, considered to be rough because the bracing inside the cut prevents the wall  $ac$  from moving inward. The factor of safety against heaving of the base adjacent to  $ac$  is then

$$F = \frac{5.7 s_u}{H(B'\gamma - s_u)/B'} \quad (37.4)$$

The value of  $F$  decreases with increasing width  $B'$ . However,  $B'$  cannot exceed  $B\sqrt{2}$ ; otherwise the failure surface would extend beyond the opposite boundary of the cut. Hence

$$F = \frac{1}{H} \frac{5.7 s_u}{\left(\gamma - \frac{s_u\sqrt{2}}{B}\right)} \quad (37.5)$$

If a hard base is located at depth  $D$  below the bottom of the cut, Fig. 37.3b,  $B' = D$  and

$$F = \frac{1}{H} \frac{5.7 s_u}{\gamma - s_u/D} \quad (37.6)$$

As the bearing capacity of the underlying soil is approached, large movements of the soil begin to occur irrespective of the strength of the bracing. Therefore, the value of  $F$  is a useful indicator of potential ground movements. The practical implications are discussed in Article 54.3.

For a cut in a clay with a constant value of  $s_u$  to great depth,  $D$  in Eq. 37.6 becomes large and  $F$  approaches the value

$$F = \frac{1}{H} \cdot \frac{5.7 s_u}{\gamma} = \frac{5.7 s_u}{\gamma H} = \frac{5.7}{N_s} \quad (37.7)$$

where

$$N_s = \frac{\gamma H}{s_u} \quad (37.8)$$

is termed the *stability number*. Under some circumstances the stability number is also a useful indicator of potential ground movements. The smaller the value of  $N_s$  with respect to 5.7, the smaller the ground movements.

The preceding discussion assumes a cut having a length that is large compared with its width. In reality, the bearing-capacity factor  $N_c$  depends on the shape of the cut in plan, and on the ratio of depth to width. If it is assumed that the excavated soil is analogous to a single large footing that exerts an upward load  $\gamma H$  at the level  $abcd$ , the values of  $N_c$  may be taken equal to those for footings of the same ratios  $B/L$  of width to length, and  $H/B$  of depth to width (Bjerrum and Eide 1956). The calculations are facilitated by the chart (Fig. 37.4b) (Janbu et al. 1956).

### 37.3.2 Earth Pressure against Supports

If the value of  $F$  (Eq. 37.7) is equal to or greater than unity, the clay below the level of the base of the cut does

not heave and the surface of sliding, represented by Eq. 37.1, terminates at point  $b$  at the bottom of the cut (Fig. 37.2). For  $\phi = 0$  conditions, Eq. 37.1 reduces to that of a circle with radius  $r = r_0$ . Because the circle must intersect the ground surface at a right angle, its center must be located at the level of the surface (Fig. 37.5). The face  $ab$  of the cut is acted on by the horizontal earth pressure  $P_a$  and the adhesion  $s_{ua}H$  between the clay and the sheet-piling.  $P_a$  is computed by taking moments about the center of the circle of the forces that act on the sliding wedge. The driving moment is produced by the weight of the wedge. The resisting moment is equal to the sum of the moment of the resultant earth pressure  $P_a$  and the moments of the forces of adhesion  $s_{ua}H$  and  $s_u \cdot \widehat{bd}$  that act on the boundaries of the wedge.

The value of  $P_a$  depends not only on the ratio  $n_a$ , but also on the ratio  $s_{ua}/s_u$ , in which  $s_{ua}$  is the adhesion developed between the sheeting and the clay. The theory indicates, however, that the influence of  $s_{ua}/s_u$  is small compared with that of  $n_a$ , and negligible compared with that of the shearing strength  $s_u$  itself. This can be seen in Fig. 37.6, in which the earth pressure, expressed in terms of  $K_A = P_a / \frac{1}{2} \gamma H^2$ , has been calculated for various values of  $s_{ua}/s_u$  and  $n_a$  on the assumption that the surface of sliding is circular. The figure also demonstrates that, for values of  $n_a$  not greater than about 0.5, the value of  $K_A$  can be approximated with reasonable accuracy by the Rankine value derived from Eq. 28.10 as follows:

$$K_A = \frac{1}{\frac{1}{2} \gamma H^2} P_A = \frac{1}{\frac{1}{2} \gamma H^2} (\frac{1}{2} \gamma H^2 - 2 s_u H) = 1 - \frac{4 s_u}{\gamma H} \quad (37.9)$$

$K_A$  is represented in the figure by the dash lines. Measurements in full-sized cuts excavated in saturated soft to medium clays have shown that  $n_a$  varies between about 0.30 and 0.50 and is, on the average, about 0.39. The corresponding distribution of lateral pressure, therefore, is not usually triangular but, like that for a sand, approaches a roughly parabolic shape. For a value  $n_a = 0.4$ , representing closely the average for all observed cuts, the approximation expressed by Eq. 37.9 is excellent (Fig. 37.6). Hence, for all practical purposes, the earth pressure can be calculated by Rankine's theory on the assumption that the surface of sliding is a plane rising at  $45^\circ$  from the bottom of the cut (Fig. 37.7a). An active Rankine zone exists within the sliding wedge.

If the value of  $F$  (Eq. 37.7) is less than unity, the clay below the bottom of the cut experiences a base failure and the volume of clay participating in the movement increases. If a firm base exists at depth  $d$  below the bottom, the surface of sliding extends downward to become tangent to the firm base. Above the surface of sliding  $efghk$  (Fig. 37.7b), zone  $bgh$  is a zone of radial shear bounded by planes inclined at  $\pm 45^\circ$  to the horizontal. If the firm base is located at a depth equal to or

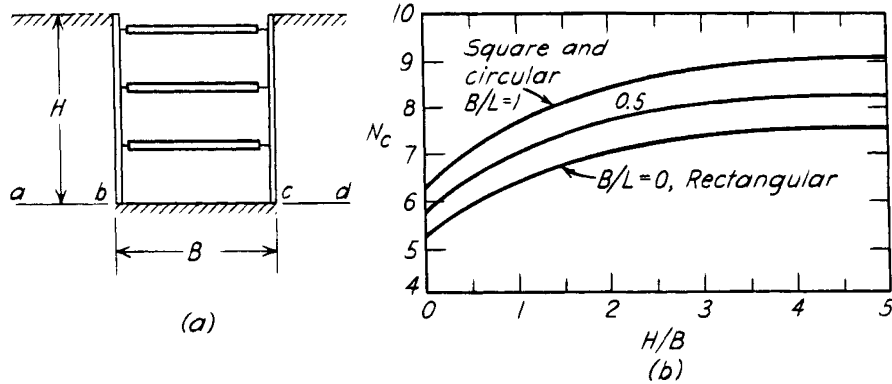


**Figure 37.4** (a) Section through open cut in deep deposit of clay; (b) values of bearing capacity factor  $N_c$  for establishing stability of bottom of cut against heave (after Janbu et al. 1956).

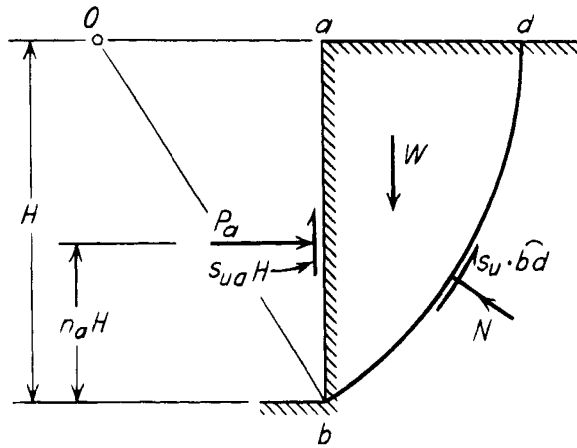


**Figure 37.5** Diagram illustrating assumptions on which calculation of earth pressure is based for cuts in clays under  $\phi = 0$  conditions.

greater than  $B\sqrt{2}$  below the bottom of the cut, the surface of sliding extends only to that depth as shown in Fig. 37.7c.

The influence of the base failure on the earth pressure against the bracing can be investigated by the principle of virtual work (Henkel 1971). In Fig. 37.7b, virtual displacements are indicated by dash arrows. The wedge  $abfe$ , with weight  $W$ , is given a displacement  $\delta$ . The corresponding displacements along the various segments of the surface of sliding are  $\delta\sqrt{2}$ , and the displacement of the resultant earth pressure, assumed horizontal, is  $\delta$ . The resisting force per unit of length along  $ef$  is  $s_u$ , whereas that along  $fghk$  is taken as  $s_{ub}$ . The work done by the weight  $W$  is  $W\delta$ . The work done by the resisting forces along the surface of sliding is:

$$s_u \sqrt{2} H \sqrt{2} \delta + 2 s_{ub} d \sqrt{2} \delta + s_{ub} \frac{\pi d}{4} \sqrt{2} \delta + P_a \delta$$

In addition, internal work is done within the zone of radial

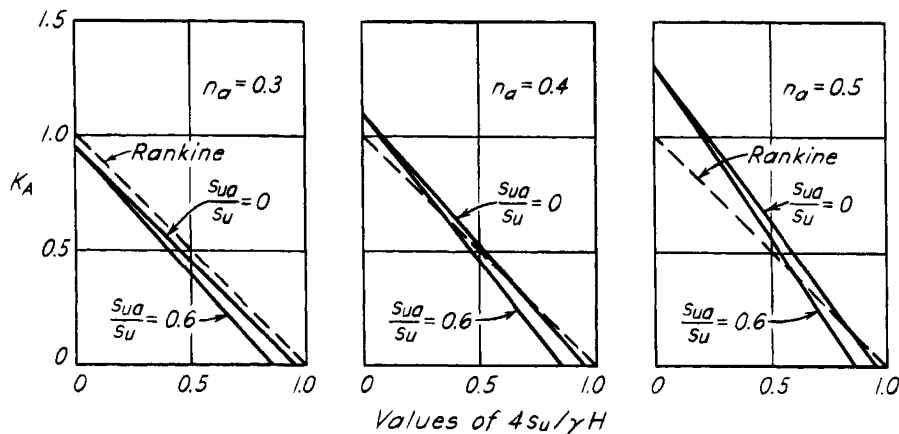


**Figure 37.6** Values of earth-pressure coefficients  $K_A = P_a / \frac{1}{2} \gamma H^2$  for clay soils calculated on assumption that surface of sliding is circular (solid lines) and by means of Rankine's theory (dash lines).

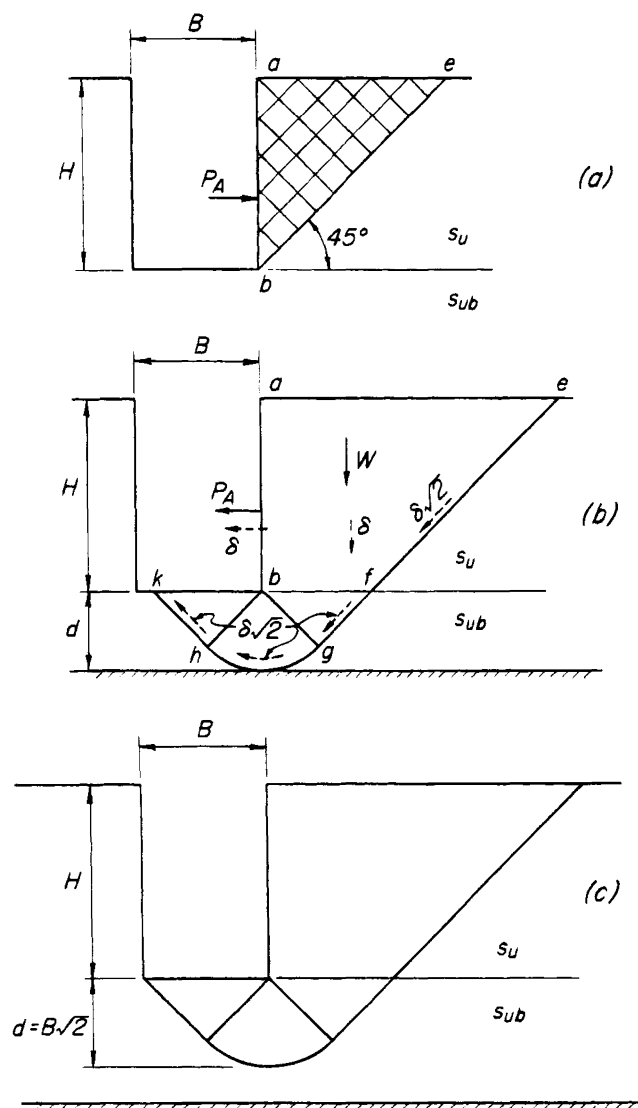


**Figure 37.7** Rankine's failure of clay behind open cut with vertical walls under  $\phi = 0$  conditions when undrained shear strength  $s_{ub}$  below bottom of cut  $\geq \gamma H/(2 + \pi)$ ; (b) when  $s_{ub} < \gamma H/(2 + \pi)$  and depth to firm base is less than  $B\sqrt{2}$ ; (c) when  $s_{ub} < \gamma H/(2 + \pi)$  and depth to firm base  $\geq B\sqrt{2}$ .

shear  $bgh$ , because the virtual displacements along the radial boundaries  $bg$  and  $bh$  are uniform, whereas rigid-body rotation of the zone about  $b$  would require the displacement to increase linearly with increasing distance from  $b$ . Hence, shear strains are induced in the zone with consequent dissipation of energy. It can be shown that the amount of internal energy dissipation is equal to that expended along the boundary  $gh$ . Hence, equating the work done by the weight  $W$  to that of the resisting forces leads to:

$$W\delta = s_u\sqrt{2}H\sqrt{2}\delta + 2s_{ub}d\sqrt{2}\delta + 2s_{ub}\frac{\pi d}{4}\sqrt{2}\delta + P_a\delta \quad (37.9)$$

wherein the third term on the right side is equal to twice the work done along the boundary  $gh$ . Since

$$W = \gamma Hd\sqrt{2} + \frac{\gamma H^2}{2} \quad (37.10)$$

$$P_a = \frac{1}{2}\gamma H^2 - 2s_uH + d\sqrt{2}\left[\gamma H - s_{ub}\left(2 + \frac{\pi}{2}\right)\right] \quad (37.11)$$

Equation (37.11) may be written as

$$P_a = K_A \cdot \frac{1}{2}\gamma H^2 + \frac{1}{2}\gamma H^2 \cdot \frac{2\sqrt{2}d}{H} \left[1 - \frac{(2 + \pi)s_{ub}}{\gamma H}\right] = \frac{1}{2}\gamma H^2 \left[K_A + \frac{2\sqrt{2}}{H} \left(1 - \frac{(2 + \pi)s_{ub}}{\gamma H}\right)\right] \quad (37.12)$$

$$= \frac{1}{2}\gamma H^2[K_A + \Delta K] \quad (37.13)$$

where

$$\Delta K = \frac{2\sqrt{2}d}{H} \left(1 - \frac{(2 + \pi)s_{ub}}{\gamma H}\right) \quad (37.14)$$

is the increment of  $K_A$  due to the bearing-capacity failure of the clay beneath the base of the cut. The value of  $\Delta K$  may be determined from Fig. 37.8, wherein the abscissa

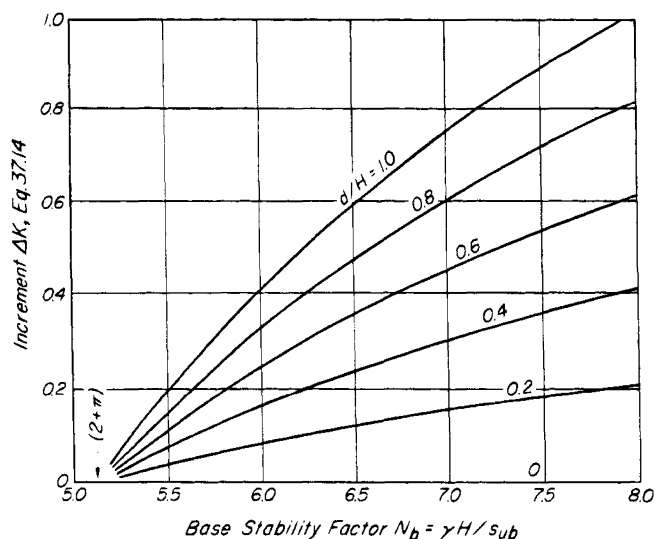


**Figure 37.8** Increment  $\Delta K$  in coefficient of lateral earth pressure against supports of open cut in clay under undrained conditions when base stability factor exceeds 5.14 (after Henkel 1971).

is the base stability number  $N_b = \gamma H/s_{ub}$ . It is evident that for a factor of safety of unity with respect to base failure ( $N_b = 5.14$  for an excavation with a length considerably greater than its width) there is no increment, but for a base stability factor approaching 8 and for a depth to the firm base approaching the depth  $H$  of the cut, the increment can be large. The practical implications of this finding are discussed in Article 46.3.3.

If sheet piles extend below the bottom of the cut, their stiffness reduces the tendency of the clay adjacent to the bottom of the cut to be displaced toward the excavation and, consequently, reduces the tendency toward heave. The effectiveness of the sheeting can be investigated by including the elastic strain energy of the sheet piles in Eq. 37.6 and assuming a reasonable shape for the deflected sheet piles below the lowermost support in the cut (O'Rourke and Jones 1992). In general, if the clay extends to a considerable depth below the cut, the beneficial effects of even relatively stiff sheeting have been found to be small. If the lower ends of the sheet piles are driven into a hard stratum, the effectiveness of the sheet piles is increased appreciably. Support of the lower edge of the piles reduces the maximum bending moment in the embedded portion of the piles; in addition, the vertical load on  $ab$  and  $cd$  (Fig. 37.4a) is reduced by the weight transferred by adhesion between the soil above base level and the sheeting. If the point resistance of the sheet piles is greater than the adhesion, the reduction is equal to the adhesion between the clay and the sheet piles. If it is smaller, the reduction is equal to the point resistance.

If the hard stratum is located a short distance below the bottom of the cut, the lower boundary of the zone of plastic equilibrium is tangent to the upper surface of the hard layer. The tendency for heave is greatly reduced even without sheet piles, and the effectiveness of sheet piles is substantially increased.

### Problems

1. By means of the logarithmic-spiral method, determine the total pressure  $P_a$  against the bracing of a cut 9.14 m deep in cohesionless sand for which  $\gamma = 18.4 \text{ kN/m}^3$  and  $\phi' = 30^\circ$ . The value of  $\delta$  is assumed to be zero. The center of pressure is 4.88 m above the bottom of the cut. Determine also the Coulomb value  $P_A$ .

Ans. 269, 253 kN/m.

2. An open cut is made to a depth of 12.2 m in clay having a unit weight of  $20.4 \text{ kN/m}^3$  and an undrained shear strength of 30 kPa. The point of application of the resultant earth pressure against the bracing is 5.5 m above the bottom. Find the value of the resultant earth pressure.

Ans. 872 kN/m.

3. A braced open cut  $9 \times 46 \text{ m}$  in plan is to be made to a depth of 11 m in a deep deposit of plastic clay having an

undrained shear strength of 29 kPa and a unit weight of  $19.2 \text{ kN/m}^3$ . The sheeting extends less than a meter below the elevation of the bottom of the cut. What is the factor of safety against heave of the bottom?

Ans. 0.93. The bottom will heave when the excavation reaches a depth of 10.3 m.

4. If the excavation in problem 3 consisted of a trench only 1.5 m wide for a length of 46 m, what would be the factor of safety against a heave of the bottom at a depth of 10 m?

Ans. 1.15. The excavation could barely be made.

## ARTICLE 38 ARCHING IN SOILS

The earth pressure on the lateral support shown in Fig. 37.1 is greatest at about midheight of the sides of the cut. Yet, if a few of the horizontal boards supporting the soil at midheight are removed, the exposed part of the sides of the cut remains stable if the soil has at least a trace of cohesion. To explain this fact, we are compelled to assume that the pressure formerly exerted on the boards that were removed was transferred onto those that remained in place. This phenomenon of pressure transfer is known as *arching*.

The essential features of arching can be demonstrated by the test illustrated by Fig. 38.1. A layer of dry cohesionless sand with unit weight  $\gamma$  is placed on a platform that contains a trap door  $ab$ . The trap door is mounted on a scale (not shown) that permits measurement of the pressure on the door. The depth  $H$  of the layer of sand is several times greater than the width of the trap door.

As long as the trap door occupies its original position, the pressure on the trap door as well as that on the adjoining platform is equal to  $\gamma H$  per unit of area. However, as soon as the trap door is allowed to yield in a downward

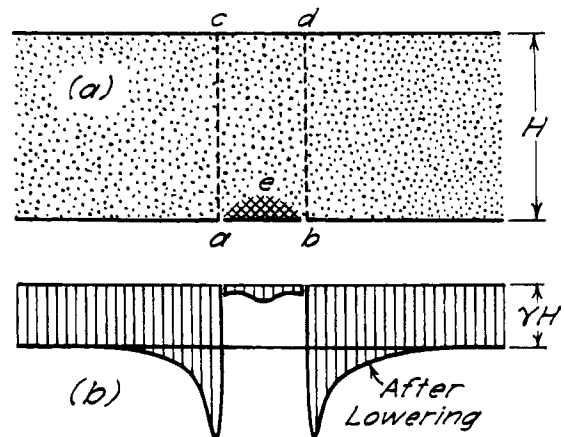


**Figure 38.1** (a) Apparatus for investigating arching in layer of sand above yielding trap door in horizontal platform; (b) pressure on platform and trap door before and after slight lowering of door.

direction, the pressure on the door decreases to a small fraction of its initial value, whereas the pressure on the adjoining parts of the platform increases. This occurs because the descent of the prism of sand located above the yielding trap door is resisted by shearing stresses along its lateral boundaries, *ac* and *bd*.

Theory, as well as the results of tests and experience in tunneling, indicates that the ultimate pressure on the yielding trap door is practically independent of the depth *H* of the layer of sand. It does not exceed the weight of a body of sand having approximately the dimensions indicated by the shaded area *abe* in Fig. 38.1. Hence, if

the sand has a trace of cohesion, the trap door can be removed entirely, and the sand will not drop out of the gap.

### **Selected Reading**

The "conventional" theory of arching over a conduit such as a culvert is detailed in Costes, N. C. (1956): "Factors affecting vertical loads on underground ducts due to arching," *Hwy. Res. Board Bull.* **125**, pp. 12–57. The validity of the results, however, depends on the value of the lateral pressure considered to act on the assumed surfaces of rupture; no reliable means are available for predicting this pressure.

## CHAPTER 6

### *Settlement and Contact Pressure*

#### ARTICLE 39 INTRODUCTION

##### 39.1 Purpose of Settlement Investigations

The term *settlement* indicates the sinking of a building due to the compression and deformation of the underlying soil.

The design of the framework of a building or other structure is, with rare exceptions, based on the assumption that the structure rests on an unyielding base. In reality, the weight of every structure compresses and deforms the underlying soil and, as a consequence, the design assumption is never strictly satisfied. If the base of the structure remains plane, the settlement is irrelevant because the stresses in the framework are not altered. On the other hand, if the weight of the structure causes the loaded area to warp, the base of the structure also becomes warped, and the entire structural framework is distorted. The supplementary stresses caused by this distortion are not considered in the design of the superstructure. Yet in many instances they are important enough to impair the appearance of a building or to cause permanent and irreparable damage.

Because of the complexity of the mechanical properties of soils and the disturbing influences of stratification, the settlement of buildings can be predicted accurately only under exceptional conditions. Nevertheless, a theoretical analysis of settlement phenomena is indispensable because the results permit the engineer at least to recognize the factors that determine the magnitude and the distribution of the settlement. Knowledge of these factors constitutes the prerequisite for converting construction experience into semiempirical rules for the design of foundations (Article 49).

##### 39.2 Theoretical Approach to Settlement Problems

The theoretical methods for dealing with settlement problems must be chosen in accordance with the mechanical properties of the subsoil and the nature of the stratification. If a proposed structure is located above one or more layers of very compressible soil, buried beneath and sepa-

rated by layers of relatively incompressible soil such as sand, the settlement depends only on the physical properties of the soft strata and on the intensity and distribution of the change in vertical pressure on these strata. Experience has shown that the change in vertical pressures can be computed with sufficient accuracy on the assumption that the subsoil of the building is perfectly elastic and homogeneous.

Similarly, if a structure rests on a fairly homogeneous subsoil, the distribution of the change in vertical stresses on horizontal sections can be estimated on the assumption that the subgrade is perfectly elastic. However, the intensity and distribution of all the changes in other stresses are likely to be very different from those in an equally loaded perfectly elastic subgrade and, in addition, the determination of the stress-strain relations for the soil is generally impracticable. Hence, in such instances it may be necessary to investigate the relation of intensity of loading, settlement, and size of loaded area by semiempirical methods.

##### 39.3 Computation of Contact Pressure

After the designer has laid out the foundation in such a manner that the unequal settlement will not be great enough to injure the superstructure, the foundation must be designed. The design requires a computation of the bending moments and shearing stresses in those parts of the foundation, such as footings or rafts, that transfer the weight of the building onto the subgrade. The pressure that acts on the base of footings or rafts is known as *contact pressure*.

The distribution of the contact pressure on the base of some foundations resembles that on the base of a similar foundation supported by an elastic isotropic material, but more often it is entirely different. Furthermore, if the supporting material is clay, the distribution of the contact pressure may change considerably with time. To simplify design, the computation of the bending moments in footings is commonly based on the arbitrary assumption that the footings rest on a uniformly spaced bed of springs.



The procedure is described in Article 42. Experience has shown that it is usually accurate enough for practical purposes. Therefore, the designer needs to be familiar only with the general relationships between the type of soil and the character of the pressure distribution. If the difference between the computed and the real pressure distribution is likely to be large and on the unsafe side, the risk is eliminated by increasing the factor of safety.

## ARTICLE 40 VERTICAL PRESSURE IN SOIL BENEATH LOADED AREAS

### 40.1 Boussinesq's Equations

The application of a concentrated vertical load to the horizontal surface of any solid body produces a set of vertical stresses on every horizontal plane within the body. It is obvious, without computation, that the intensity of the vertical pressure on any horizontal section through the loaded soil decreases from a maximum at the point located directly beneath the load to zero at a very large distance from this point. A pressure distribution of this kind can be represented by a bell- or dome-shaped space, as indicated in Fig. 41.1*b*. Because the pressure exerted by the load spreads out in a downward direction, the maximum pressure on any horizontal section, represented by the maximum height of the corresponding bell-shaped pressure space, decreases with increasing depth below the loaded surface. Yet equilibrium requires that the total increase of pressure on any horizontal section must be equal to the applied load. Therefore, with increasing depth below the surface, the pressure bells become lower but wider.

Both theory and experience have shown that the shape of the pressure bells is more or less independent of the physical properties of the loaded subgrade. Therefore, in connection with practical problems, it is customary and justifiable to compute these stresses assuming that the loaded material is elastic, homogeneous, and isotropic. On these assumptions, a concentrated vertical load  $Q$  (Fig. 40.1*a*) acting on the horizontal surface of a mass of very great extent produces at point  $N$  within the mass a change in vertical pressure having the intensity,

$$\Delta\sigma_v = \frac{3Q}{2\pi z^2} \left[ \frac{1}{1 + (r/z)^2} \right]^{5/2} \quad (40.1)$$

In this equation  $z$  represents the vertical distance between  $N$  and the surface of the mass, and  $r$  the horizontal distance from  $N$  to the line of action of the load.

Equation 40.1 is one of a set of stress equations, known as *Boussinesq's equations*, that determine the entire state of stress at point  $N$  (Fig. 40.1*a*). However, in contrast to the vertical pressure  $\Delta\sigma_v$ , most of the other components of stress at point  $N$  depend to a large extent on the stress-deformation characteristics of the loaded material.

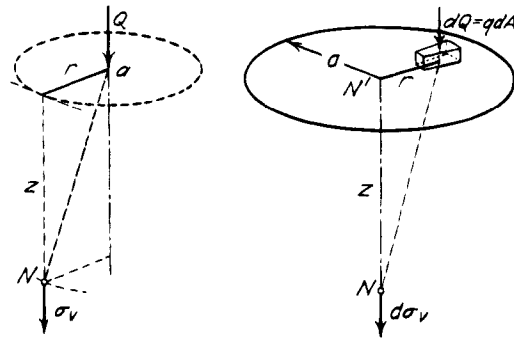


**Figure 40.1** (a) Vertical pressure at point  $N$  in interior of semi-infinite solid acted on by point load  $Q$ ; (b) vertical pressure at point  $N$  beneath center of circular area acted on by load  $q$  per unit of area.

Because soils are not even approximately elastic and homogeneous, the other stress equations of Boussinesq are not so generally suitable for the computation of stresses in soils.

### 40.2 Pressure Distribution on Horizontal Sections beneath Loaded Areas

In computing the change in vertical pressures in the soil beneath a building, it is generally assumed that the building is perfectly flexible. If an area on the surface of a very large mass carries a uniformly distributed and perfectly flexible load of intensity  $q$ , the intensity of the change in vertical pressure at any point  $N$  (Fig. 40.1*b*) within the mass may be computed by dividing the loaded area into small parts  $dA$ , each of which sustains a load,

$$dQ = q dA$$

This load is considered to be concentrated at the centroid of the elementary area  $dA$ . According to Eq. 40.1, each concentrated load produces at point  $N$  a vertical pressure,

$$d\sigma_v = \frac{3q}{2\pi z^2} \left[ \frac{1}{1 + (r/z)^2} \right]^{5/2} dA \quad (40.2)$$

The intensity of the vertical pressure at  $N$  due to the entire load is computed by integrating Eq. 40.2 over the loaded area. For example, if the point  $N$  is located at depth  $z$  beneath the center  $N'$  of a loaded area having the shape of a circle with radius  $a$ , the change in vertical pressure is found to be

$$\Delta\sigma_v = q \left\{ 1 - \left( \frac{1}{1 + \frac{1}{(z/a)^2}} \right)^{3/2} \right\} \quad (40.3)$$

Because of symmetry,  $\Delta\sigma_x = \Delta\sigma_y = \Delta\sigma_r$ . These stresses are found to be

$$\begin{aligned}\Delta\sigma_x &= \Delta\sigma_y = \Delta\sigma_r \\ &= \frac{q}{2} \left( (1 - 2\nu) + \frac{2(1 + \nu)z/a}{[1 + (z/a)^2]^{1/2}} + \frac{(z/a)^3}{[1 + (z/a)^2]^{3/2}} \right) \quad (40.4)\end{aligned}$$

in which  $\nu$  is Poisson's ratio. Thus, in contrast to the vertical stress at point  $N$ , the horizontal stresses are a function of Poisson's ratio; that is, of the elastic properties of the material. For this reason, Eq. 40.3 has more general applicability than Eq. 40.4.

Closed-form solutions for a great variety of loadings, geometries, and elastic properties are readily available (e.g., Poulos and Davis 1974). The change in vertical stress is expressed in terms of dimensionless influence factors. For example, for a uniform load applied over a circular area of radius  $a$  at the surface of the ground

$$\Delta\sigma_v = I(r/a, z/a) q$$

and for a uniform load over a long strip of width  $b$  in the  $y$ -direction

$$\Delta\sigma_v = I(x/b, z/b) q$$

The values of  $I$ , which are applicable to any values of  $a$  or  $b$ , are either tabulated or presented in a graphical form as in Figs. 40.2 and 40.3. The solution for  $\Delta\sigma_v$  at any point in soil subjected to a uniform load over a rectangular area at the ground surface does not have a simple form.

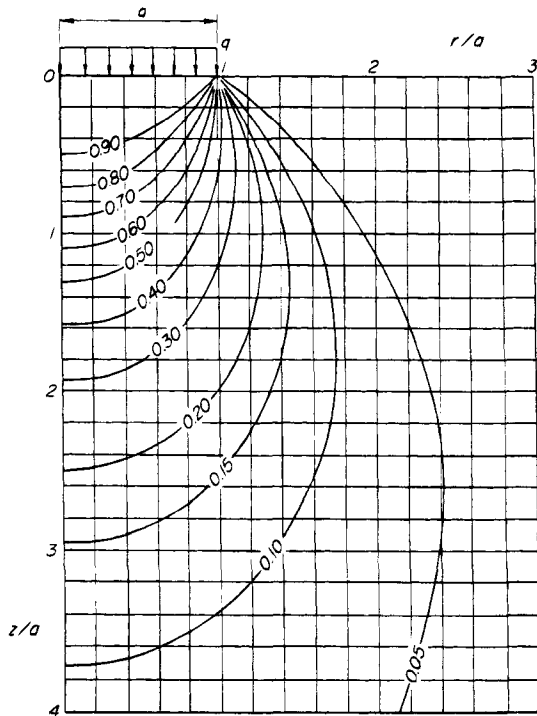


**Figure 40.2** Values of influence factor  $I(r/a, z/a)$  for a uniform load over circular area (after Lambe and Whitman 1969).

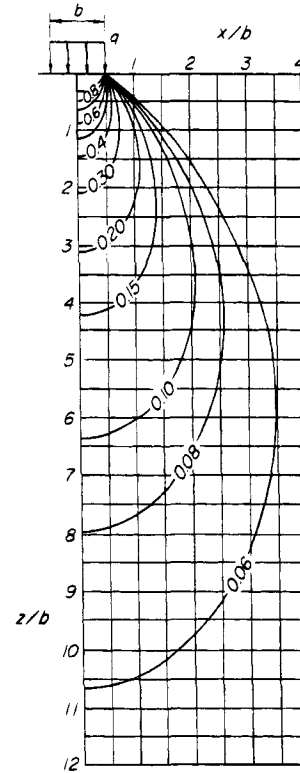


**Figure 40.3** Values of influence factor  $I(x/b, z/b)$  for a uniform load over a strip in  $y$ -direction.

However, an expression has been obtained for  $\Delta\sigma_v$  at any depth  $z$  below the corners of the rectangular area

$$\Delta\sigma_v = I(m, n)q$$

where  $m = a/z$ ,  $n = b/z$ , and  $a$  and  $b$  are the length and breadth of the rectangular area. The values of the influence factor  $I$  for values of  $m$  and  $n$  from 0.01 to 10 are presented in Fig. 40.4. The value of  $\Delta\sigma_v$  at any point  $N$  that is not below a corner of the loaded area is determined by algebraic superposition of  $\Delta\sigma_v$  for rectangles each with a corner at point  $N'$  which is the upward projection of  $N$  to the ground surface. These rectangles are constructed by drawing lines through point  $N'$  parallel to the sides of the rectangular loaded area. The procedure is illustrated in Fig. 40.5 for the two possible situations.

In addition, computer software especially adapted to determining the stress distribution beneath loaded areas, based on Eq. 40.1, is widely used. Thus, calculation of the change in vertical stress  $\Delta\sigma_v$  due to the weight of a building or fill, once a laborious operation for even simple projects, is now routine.

### 40.3 Change of Pressure with Depth

The intensity of the change in vertical pressure along any vertical line beneath a distributed load decreases with increasing values of the depth  $z$  below the surface. There-

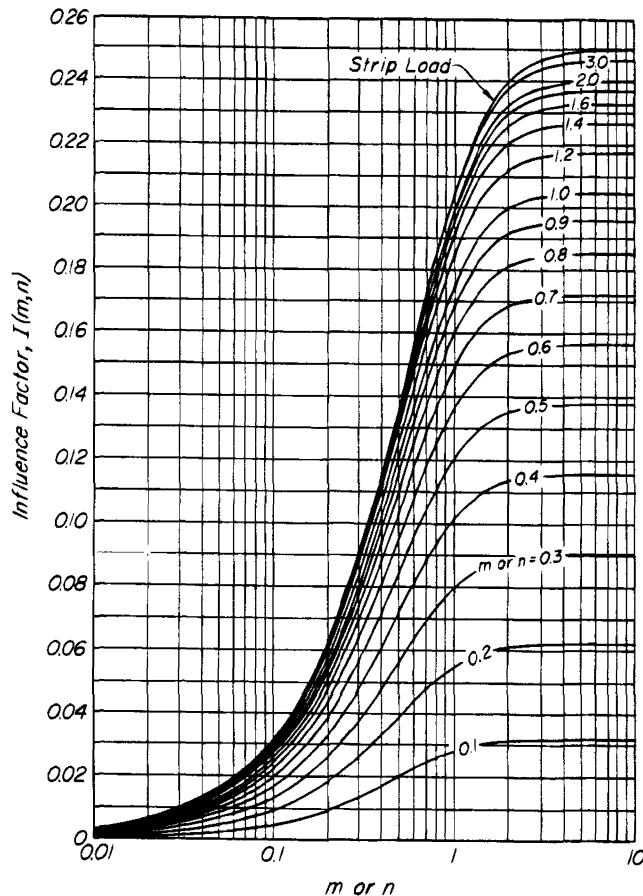
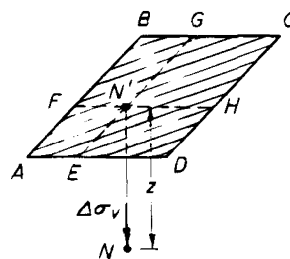


**Figure 40.4** Values of influence factor  $I(m, n)$  for a uniform load over a rectangular area.

fore, if the compressible layer is very thick, the change in vertical pressure in the layer decreases appreciably from the top to the bottom. However, the compression of a thin layer depends merely on the average change in vertical pressure, which is roughly equal to the change in vertical pressure at midheight of the layer. Therefore, if the compressible layer is relatively thin, the variation of pressure with depth can be disregarded and it may be



$$\Delta\sigma_v = (I_{N'EA}F + I_{N'FBG} + I_{N'GCH} + I_{N'NDE})q$$

sufficiently accurate to compute the intensity and distribution of the pressure on a horizontal plane midheight of the layer.

In Fig. 40.6 the abscissas of the curve  $C_a$  represent the intensity of vertical pressure at different depths below the center of a square area  $B \times B$  due to a uniformly distributed load  $q$  per unit of area. If the total load  $B^2q$  is represented by a concentrated load  $Q = B^2q$  acting at the center of the square area, the curve  $C_q$  is obtained instead of  $C_a$ . The figure shows that the curves become almost identical at a depth of about  $3B$ . At any depth greater than  $3B$ , the change in pressure on a horizontal section produced by loading a square area is practically the same as that produced by an equivalent point load acting at the center of the loaded area. Hence, the stresses  $\Delta\sigma_v$  on horizontal sections at a depth of more than  $3B$  can be computed by means of Eq. 40.1.

The removal of soil from the space to be occupied by a basement reduces the vertical pressure at every point below the bottom of the excavation. To compute the resulting change in the stresses, it is assumed that the surface of the soil is located at the level of the bottom

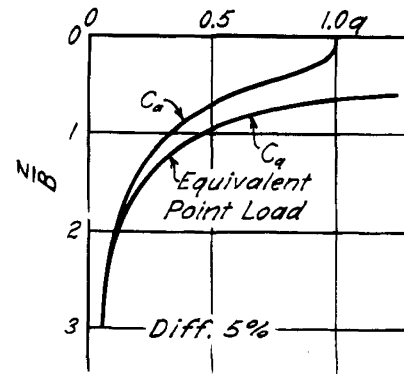
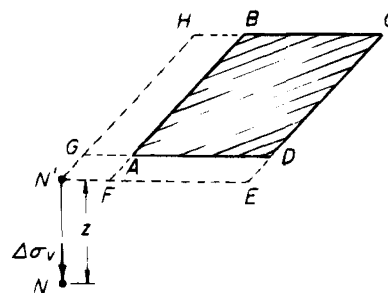


**Figure 40.6** Effect on vertical pressure of replacing uniformly distributed load on square area by equivalent point load at center of square. Curves represent stress along vertical line beneath center of square.



$$\Delta\sigma_v = (I_{N'HCE} - I_{N'HB}F - I_{N'GDE} + I_{N'GA}F)q$$

**Figure 40.5** Superposition of solutions to obtain  $\Delta\sigma_v$  at any point  $N$  in soil subjected to uniform load over a rectangular area at ground surface.

of the excavation, and that the weight of the excavated material acts in an upward direction at this level.

### Problems

1. A point load of 24 kN acts on the surface of an elastic mass of very great extent. What is the intensity of vertical pressure, due to the load, at a depth of 1 m directly below the load? at a depth of 2 m? at a depth of 5 m? What is the intensity of vertical pressure at the same depths at a horizontal distance of 1 m from the line of action of the point load?

Ans. 11.5, 2.86, 0.46; 2.0, 1.64, 0.42 kPa.

2. A circular area on the surface of an elastic mass of great extent carries a uniformly distributed load of 120 kPa. The radius of the circle is 3 m. What is the intensity of vertical pressure at points 3, 6, and 12 m beneath the center of the circle? at points at the same depths beneath the edge of the circle?

Ans. 78, 35, 11; 40, 24, 10 kPa.

3. A building of very great length has a width of 36 m. Its weight constitutes a practically uniform surcharge of 240 kPa on the ground surface. Between the depths of 21 and 27 m there is a layer of soft clay. The rest of the subsoil is dense sand. Compute the intensity of vertical pressure due to the weight of the building, at the following points located in a horizontal plane at midheight of the compressible layer: directly below centerline of building; and 6, 12 and 18 m from the centerline.

Ans. 168, 163, 156, 120 kPa.

4. If the building in problem 3 is 36 m square, compute the stresses at the same points along a section midway between the ends of the building.

Ans. 132, 126, 107, 82 kPa.

5. The excavation for a rectangular building 60 m by 37 m in plan is 6 m deep. The excavated material is a moist sand having a unit weight of 18.4 kN/m<sup>3</sup>. What is the reduction in vertical pressure, due to the removal of weight from the excavated area, at a point 21 m below the original ground surface, at one corner of the building?

Ans. 28 kPa.

### Selected Reading

The following references contain charts, tables, or influence values useful in the calculation of stresses in elastic materials.

- Jurgensen, L. (1934). "The application of elasticity and plasticity to foundation problems," *J. Boston Soc. Civil Engrs.*, **21**, pp. 206–241. Reprinted in *Contributions to Soil Mechanics 1925–1940*, Boston Soc. Civil Engrs., 1940, pp. 148–183.
- Newmark, N. M. (1942). "Influence charts for computation of stresses in elastic foundations," *Univ. of Ill. Eng. Exp. Sta. Bull.* **338**, 28 pp.
- Terzaghi, K. (1943b). *Theoretical Soil Mechanics*, New York, John Wiley and Sons, pp. 481–490.
- Burmister, D. M. (1956). "Stress and displacement characteristics of a two-layer rigid base soil system: influence dia-

grams and practical applications," *Proc. Hwy. Res. Board*, **35**, pp. 773–814.

Osterberg, J. O. (1957). "Influence values for vertical stresses in a semi-infinite mass due to an embankment loading,"

*Proc. 4th Int. Conf. Soil Mech.*, London, **1**, pp. 393–394.

Harr, M. E. (1966). *Foundations of Theoretical Soil Mechanics*, New York, McGraw-Hill, pp. 55–116.

Poulos, H. G. and E. H. Davis (1974). *Elastic Solutions for Soil and Rock Mechanics*, New York, John Wiley and Sons, 411 pp.

## ARTICLE 41 SETTLEMENT OF FOUNDATIONS

### 41.1 Foundations above Confined Strata of Soft Clay

The following paragraphs describe the procedure for estimating the settlement of a building located above a confined layer of soft clay. The weight of the building is transferred by a reinforced-concrete mat foundation (Fig. 41.1a) onto a stratum of sand that contains a layer of soft clay at a depth  $D$  below the mat. The weight of the building is assumed to be uniformly distributed over the area occupied by the mat.

Inasmuch as sand is almost incompressible in comparison with soft clay, the settlement is caused almost entirely by the compression of the clay stratum. Because the clay is restrained by the sand layers from bulging laterally, the compression produced by a given pressure can be computed by the method described in Article 16. However, it is necessary to compute the settlement of several points on the base of the building, because the principal object of the settlement computation is to estimate the amount of warping that the base will experience. If the thickness of the clay stratum is small compared with the depth of the overburden, it can be assumed that the average intensity of the increase in vertical pressures  $\Delta\sigma_v$  in the clay beneath a given point of the foundation is equal to the intensity of the increase in vertical pressure beneath this point at midheight of the stratum. This pressure may be evaluated by the procedures described in Article 40.

The next step is to compute the compression  $S$  of the clay layer below each of the selected points using the procedure outlined in Article 16.6. The increase in effective vertical pressure  $\Delta\sigma'_v$  is equal to the change in vertical pressure  $\Delta\sigma_v$ , computed as outlined in the preceding paragraph. The value  $S$  represents not only the decrease in thickness of the stratum below the given point but also the settlement of the base of the foundation at that point. The depth of influence  $Z_f$ , below which the vertical strains under the foundation are negligible, can be considered to extend from the base of the foundation to a depth at which  $\Delta\sigma_v$  is equal to 10% of  $q$ . For example,  $Z_f$  is equal to 2 times the diameter of a circular area and 6.5 times the width of a strip subjected to uniform load. If the



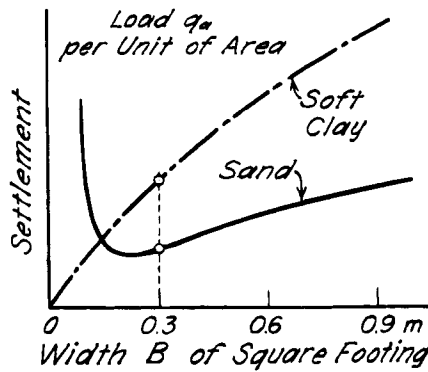


**Figure 41.3** Relation between width of square footing and settlement under same load per unit area (after Kögler 1933).

On the other hand, to determine the influence of the size of the loaded area and the position of the water table on the settlement of footings on cohesionless sand, we must consider the factors that determine the stress-strain properties of the sand (Article 18.2). Theoretical investigations of these relations as well as laboratory tests and field observations have led to the following conclusions (Kögler 1933).

The settlement of a footing with width  $B$  decreases with increasing average value of the initial tangent modulus  $E_i$  of the sand located between the base of the footing and a depth of about  $B$  below the base. Triaxial compression tests demonstrate that the initial tangent modulus of sand increases with increasing effective confining pressure. At any given depth below the surface of the sand, the effective confining pressure is roughly proportional to the effective overburden pressure. If the water table rises to the surface of the sand from a depth greater than  $B$  below the base of the footing, the effective overburden pressure decreases by roughly 50% (Article 15.3). Therefore, the settlement roughly doubles.

At a given load per unit of area of the base of a footing, the depth of the body of sand subject to intense compression and deformation increases as the width of the footing increases. The average initial tangent modulus of the sand also increases. These factors tend to cause the settlement to increase at a decreasing rate with the width  $B$  of the foundation. On the other hand, at very small widths the ultimate bearing capacity of a loaded area is very small (Eq. 33.7); consequently at very small widths, even at low soil pressures, the loaded area may sink into the ground. As a result of these several factors, the settlement varies with the width of the footing approximately as shown by the plain curve in Fig. 41.3.

In practice, the magnitude of the settlement of footings on sand is extremely difficult to predict reliably on the basis of the results of laboratory tests on soil specimens. However, it can be estimated roughly by means of semi-empirical rules based partly on the aforementioned gen-

eral relations and partly on the observed relation between settlement and the results of simple field tests such as penetration tests (Article 50.2).

### Problems

1. The layer of soft clay referred to in problem 3, Article 40, has a natural water content of 45%. The specific gravity of the solid matter of the clay is 2.70, and the unit weight of the dense sand is  $21 \text{ kN/m}^3$ . The free-water level is at the ground surface. From the results of consolidation tests it has been ascertained that  $\sigma'_p/\sigma'_{vo} = 1$  and  $C_c$  is equal to 0.50. Compute the settlement of the edge and of the center of the building resulting from primary consolidation of the clay.

*Ans.* 23, 30 cm.

2. A soil profile consists of 3 m of desiccated crust ( $\gamma = 18 \text{ kN/m}^3$ ) over 3.5 m of organic silt ( $\gamma = 16 \text{ kN/m}^3$ ,  $e_0 = 1.5$ ,  $C_c = 1.3$ ,  $\sigma'_p/\sigma'_{vo} = 1.3$ ,  $C_r/C_c = 0.2$ ,  $C_\alpha/C_c = 0.05$ ,  $c_v = 0.1 \text{ m}^2/\text{day}$ ) over 6 m of blue clay ( $\gamma = 17 \text{ kN/m}^3$ ,  $e_0 = 1.3$ ,  $C_c = 0.6$ ,  $\sigma'_p/\sigma'_{vo} = 1.8$ ,  $C_r/C_c = 0.15$ ) over intact shale. The water table is 3 m below the ground surface. A  $12 \text{ m} \times 12 \text{ m}$  square foundation slab carrying 8 MN will be placed at 1.5 m below the ground surface. Compute settlement at the center of the slab resulting from: (a) primary consolidation of the organic silt, (b) primary consolidation of the blue clay, and (c) secondary compression of the organic silt after 30 years, assuming that as compared with the organic silt the fissured crust is highly permeable and the blue clay is impermeable. For the same assumptions as in (c) sketch porewater pressure isochrones in the organic silt corresponding to 10%, 50%, and 95% primary consolidation.

*Ans.* 10 cm; 1.5 cm; 17 cm.

3. A soil profile at a site consists of 30 m of dense sand ( $\gamma = 20 \text{ kN/m}^3$ ) over 12 m of clay ( $\gamma = 17.6 \text{ kN/m}^3$ ,  $e_0 = 0.7$ ,  $C_c = 0.6$ ,  $\sigma'_p/\sigma'_{vo} = 1.0$ ,  $C_r/C_c = 0.1$ ,  $C_\alpha/C_c = 0.03$ ,  $c_v = 4 \text{ m}^2/\text{yr}$ ) over gravel. The water table is 8 m below the ground surface. The circular base (diameter = 35 m) of an old historic tower structure with a total weight of 116 MN is resting at a depth of 3 m below the ground surface. Compute the settlement of the tower for each of the following situations: (a) the water table drops by 10 m and remains at that position for 2 years before returning to the original elevation, and (b) the porewater pressure in the gravel layer drops by 10 m and remains at that condition for 2 years before returning to the original situation.

*Ans.* 19 cm; 10 cm.

4. A soil profile consists of 13 m of sand ( $\gamma = 20 \text{ kN/m}^3$ ) over 7 m of organic clay ( $\gamma = 16 \text{ kN/m}^3$ ,  $\sigma'_p/\sigma'_{vo} = 1.0$ ,  $e_0 = 1.8$ ,  $C_c = 1.2$ ,  $C_\alpha/C_c = 0.06$ , and  $c_v = 5 \text{ m}^2/\text{year}$ ) over impermeable rock. The water table is 5 m below the ground surface. The  $20 \text{ m} \times 20 \text{ m}$  square foundation of a structure will be placed at 3 m below the ground surface (i.e., in a 3-m-deep excavation). The total weight of the structure is 75 MN. Compute the settlement of the structure: (a) resulting from final primary consolidation of the organic clay, and (b) after 50 years. Sketch and label excess porewater pressure isochrones corresponding to 0%, 30%, and 95% average degree of consolidation of the organic clay.

*Ans.* 42 cm; 54 cm.

## ARTICLE 42 CONTACT PRESSURE AND THEORIES OF SUBGRADE REACTION

### 42.1 Contact Pressure on Base of Rigid Footings

Because the settlement of the base of a perfectly rigid footing is uniform by necessity, the distribution of the pressure on the base of such a footing is identical with the distribution of the load required to produce uniform settlement of the loaded area. If the subgrade consists of a perfectly elastic material, of clay, or of sand containing thick layers of soft clay, a uniformly loaded area assumes the shape of a shallow bowl or trough. To obtain uniform settlement it would be necessary to shift part of the load from the center of the loaded area toward the edges. Hence, the contact pressure on the base of a rigid footing resting on such a subgrade increases from the center of the base toward the rim. On the other hand, if a uniformly loaded area is underlain by sand, the settlement is greater at the edges than at the center. Uniform settlement can be obtained only by distributing the load so that its intensity decreases from a maximum at the center to a minimum at the rim. Hence, the distribution of the contact pressure on the base of a rigid footing on sand has the same characteristics.

Figure 42.1 is a section through a rigid continuous footing with a width  $B$  resting on a perfectly elastic and homogeneous subgrade of very great depth. The load on the footing is  $q_a B$  per unit of length. Computations based on the theory of elasticity have shown that the contact pressure increases as shown in the figure from less than  $0.7q_a$  at the center line to an infinite value at the edges. If the footing rests on a real elastic material, the pressure along the edges cannot exceed a certain finite value  $q_c$ .

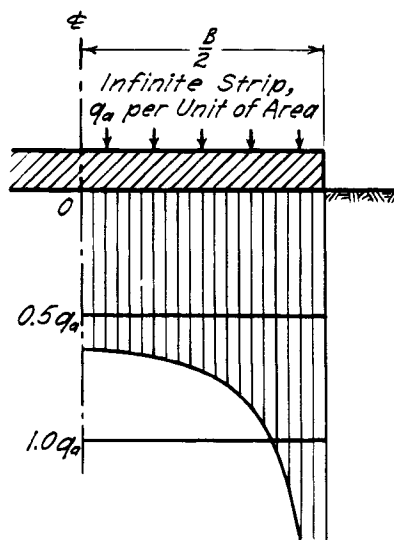


**Figure 42.1** Distribution of contact pressure on base of uniformly loaded rigid footing of very great length, resting on perfectly elastic, homogeneous, and isotropic subgrade.

at which the material passes from the elastic into a semi-plastic or plastic state. The corresponding distribution of the contact pressure is shown in Fig. 42.2a by the curve  $C_1$ .

If the load on the footing in Fig. 42.2a is increased, the state of plastic equilibrium spreads from the edges, and the distribution of contact pressure changes. If the base of the footing is smooth, the distribution becomes perfectly uniform at the instant when the subgrade fails by plastic flow. The curve  $C_u$  represents the distribution at this stage, and the curve  $C_2$  at an intermediate stage.

If either a rigid or a flexible footing rests on the surface of a mass of dry cohesionless sand, theory indicates that the intensity of the contact pressure at any load decreases from a maximum at the center to zero at the edges, as shown in Fig. 42.2b. Experimental investigations have led to the same conclusion (Faber 1933).

Figure 42.2c represents the distribution of contact pressure on the base of a footing supported by a subgrade intermediate in character between purely cohesive and purely cohesionless soils. At small loads the contact pressure increases from the center toward the edges of the footing (curve  $C_1$ ). As the load increases, the pressure at the center increases, whereas that at the edges remains unaltered. At the point of failure the pressure decreases from the center toward the edges, as indicated by curve  $C_u$ .

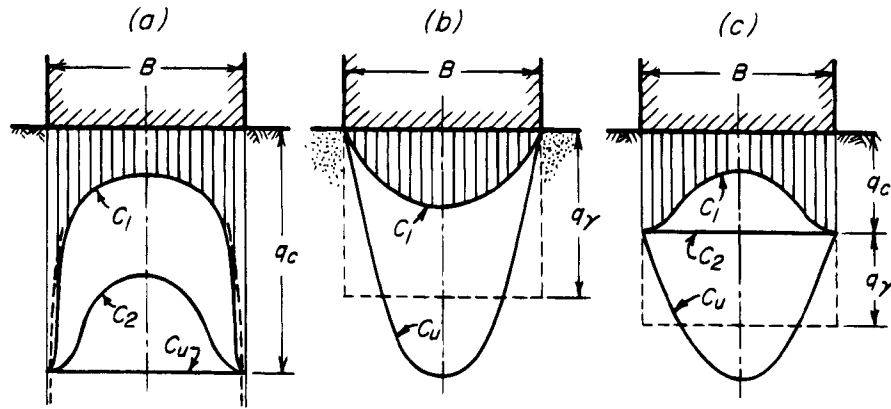
### 42.2 Definition of Subgrade Reaction

Figure 42.2 demonstrates that the relation between the stress-deformation characteristics of the subgrade and the contact pressure on the base of a perfectly rigid footing is by no means simple. If the footing is not rigid, the relation becomes even more complicated. Therefore, even a rough evaluation of the distribution of the real contact pressure is very cumbersome. Yet, without some knowledge of the contact pressure, footings or mats cannot be designed. Therefore, it is customary and necessary to estimate the contact pressure on the basis of simplifying assumptions and to compensate for the error due to these assumptions by an adequate factor of safety.

The simplified procedures are based on the arbitrary and incorrect assumption that the settlement  $S$  of any element of a loaded area is entirely independent of the load on the adjoining elements. It is further assumed, at variance with reality, that the ratio

$$K_s = \frac{p}{S} \quad (42.1)$$

between the intensity  $p$  of the pressure on the element and the corresponding settlement  $S$  is a constant  $K_s$  ( $\text{kN/m}^3$ ). In contrast to the real contact pressure that acts on the base of the footing, the fictitious pressure  $p$  that satisfies Eq. 42.1 is called the *subgrade reaction*. In the following paragraphs of this article the symbol  $p$  is reserved strictly for the subgrade reaction. It is not used with reference



**Figure 42.2** Distribution of contact pressure on base of smooth rigid footing supported by (a) real, elastic material; (b) cohesionless sand; (c) soil having intermediate characteristics. Curves  $C_u$  refer to contact pressure when footing is loaded to ultimate value.

to the real contact pressure. The coefficient  $K_s$  is known as the *coefficient of subgrade reaction*, and the theories based on the aforementioned assumptions are the *theories of subgrade reaction*.

### 42.3 Subgrade Reaction on Rigid Foundations

In connection with a rigid foundation, Eq. 42.1 leads to the conclusion that the distribution of the subgrade reaction  $p$  over the base of the foundation must be planar, because a rigid foundation remains plane when it settles. Hence, to design a rigid foundation in accordance with Eq. 42.1, we merely assume that the subgrade reaction has a planar distribution. In addition, we must satisfy the requirements of statics that (1) the total subgrade reaction is equal to the sum of the vertical loads that act on the subgrade, and (2) the moment of the resultant vertical load about an arbitrary point is equal to the moment of the total subgrade reaction about that point.

As an example, the rigid gravity retaining wall shown in Fig. 42.3 is considered. The width of the base is  $B$ ,

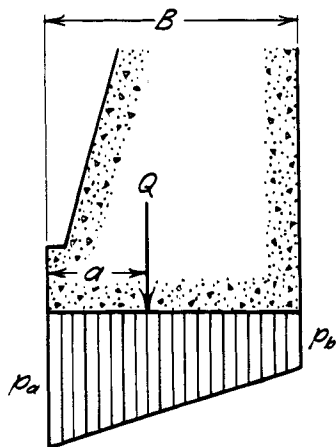


**Figure 42.3** Subgrade reaction on base of rigid gravity retaining wall.

and the resultant  $Q$  of the vertical loads on the base acts at the distance  $a$  from the toe. The subgrade reaction at the toe is  $p_a$ , and at the heel it is  $p_b$ . According to the previous paragraph, the distribution of the reaction is assumed to be linear between these two points. By statics we obtain the two equations,

$$Q = \frac{1}{2}B(p_a + p_b) \quad (42.2)$$

and

$$Qa = \frac{1}{6}B^2p_a + \frac{1}{3}B^2p_b \quad (42.3)$$

These equations can be solved for  $p_a$  and  $p_b$ .

It should be noted that Eqs. 42.2 and 42.3 do not contain the coefficient of subgrade reaction  $K_s$ . In other words, the distribution of subgrade reaction on the base of a rigid footing is independent of the degree of compressibility of the subgrade. This fact makes it easy to visualize the difference between the subgrade reaction and the real contact pressure. If the resultant  $Q$  of the load on a footing passes through the centroid of the loaded area  $A$ , the subgrade reaction is distributed uniformly over the base of the footing and is everywhere equal to  $Q/A$ . On the other hand, the distribution of the real contact pressure on the base of the same footing may be far from uniform, as shown by Fig. 42.2. It depends on the stress-deformation characteristics of the subgrade and on the intensity of the load.

In spite of these obvious discrepancies between theory and reality, the theories of subgrade reaction can be used safely in connection with the routine design of footings, because the errors are within the customary margin of safety and, as a rule, they are also on the safe side.

### 42.4 Subgrade Reaction on Flexible Foundations

If a footing or a mat is not rigid, the distribution of the subgrade reaction depends on both the numerical value of  $K_s$  and the flexural rigidity of the foundation. The



influence of the latter is illustrated by Fig. 42.4, which represents a cross-section through a long rectangular elastic slab. The longer axis of the slab carries a line load  $Q$  per unit of length. The slab rests on an elastic subgrade. Because of the flexibility of the slab, the settlement decreases from the center line toward the edges. Consequently, the subgrade reaction also decreases from a maximum at the center to a minimum at the edges. If the slab is very flexible, the edges may rise, and the subgrade reaction beneath the outer portions of the slab may become zero. In any event, for a given line load  $Q$  and a given width  $B$  of the slab the maximum bending moment in a flexible slab is very much smaller than that in a rigid one.

The subgrade reaction on the base of a relatively flexible member in a foundation can be computed by means of the *theory of elastic beams on a continuous elastic support*. The theory is based on the obvious fact that the vertical displacement of the loaded member due to settlement and bending must at every point be equal to the settlement of the ground surface at the same point. The computation of the settlement of the ground surface is based on Eq. 42.1. In contrast to Eqs. 42.2 and 42.3, which pertain to a rigid foundation, the equations for computing the subgrade reaction on an elastic foundation always contain the value  $K_s$  (Eq. 42.1).

Because the theory of elastic beams on a continuous elastic support is based on Eq. 42.1, it is no more accurate than the theory of subgrade reaction for rigid footings. It can be even less accurate, because it involves the error associated with evaluating  $K_s$ . Because the computations are always cumbersome, the investigation is not justified unless it leads to a considerable saving in the cost of the structure.

In all the theories of subgrade reaction, the coefficient  $K_s$ , which is the ratio between the intensity of load on the fictitious subgrade and the corresponding vertical displacement, is assumed to be a constant that depends only on the physical properties of the subsoil. However, the ratio between the average intensity of pressure on the surface of a given solid and the corresponding settlement is not a constant. For circular footings on an elastic isotropic base the ratio decreases as the radius of the footings increases. For a footing of given size resting on soil it also decreases with increasing values of the intensity of the load. Furthermore, it is different for different points at the base of the same footing. Therefore, the evaluation of  $K_s$  involves many uncertainties.

#### 42.5 Horizontal Subgrade Reaction

If a vertical member such as a pile or pier is subjected to a horizontal load or to moments that cause the member to move laterally through a distance  $\delta$  at any elevation,

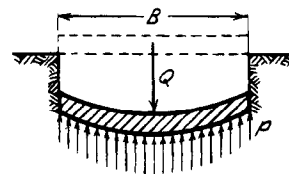


**Figure 42.4** Elastic footing of great length acted on by line load and supported by elastic subgrade. (a) Deformation of footing under load; (b) distribution of subgrade reaction.

the contact pressure between the member and the soil increases on the side of the member that moves toward the soil and decreases on the side that moves away. The latter pressure is small in comparison with the former and is usually ignored in practical problems. In computations the real contact pressure may be replaced by a fictitious subgrade reaction analogous to that beneath a footing. The *modulus of horizontal subgrade reaction*  $K_h = p/\delta$  is usually assumed to be constant for a uniform soil in which the stiffness does not increase significantly with depth, as in a stiff clay, or to increase linearly with depth if the stiffness is a function of overburden pressure, as in a sand or a normally consolidated clay. For such materials, it is usually assumed that

$$K_h = n_h z \quad (42.4)$$

where  $n_h$  is the *coefficient of horizontal subgrade reaction*. The practical application of such calculations, together with appropriate values of  $K_h$  and  $n_h$ , are discussed in Article 52.6.

#### Problems

1. A gravity retaining wall has a base width of 2.5 m. The line of action of the resultant of the vertical and horizontal forces intersects the base at a point 1 m from the toe of the wall. The vertical component of the resultant force is 175 kN/m. What is the subgrade reaction at the toe? at the heel?

Ans. 112, 28 kPa.

2. A footing with a trapezoidal base is 4 m long, 1 m wide at one end, and 2 m wide at the other. It supports two columns along its center line, one at a distance of 0.6 m from the narrow end and the other 1 m from the wide end. The load on the first column is 180 kN, and on the second 360 kN. Assuming that the footing is rigid, what is the subgrade reaction at each end?

Ans. 87 kPa., 93 kPa.

#### Selected Reading

- Hetényi, M. (1946). *Beams on Elastic Foundation*, Ann Arbor, University of Michigan Press, 255 pp.  
 Terzaghi, K. (1955b). "Evaluation of coefficients of subgrade reaction," *Géot.*, 5, No. 4, pp. 297–326.

## PART III

### *Problems of Design and Construction*

Part I contains a description of real soils as disclosed by laboratory and *in situ* tests. Part II is a condensed review of the theoretical procedures available for predicting the performance of ideal materials having properties approximating those of the real soils. Before the theories can be applied to the solution of problems of design and construction, two independent operations must be carried out. First, the significant properties of the subsurface materials must be determined by boring, sampling, and testing. Second, an idealized subsoil, consisting of a few homogeneous units with simple boundaries, must be substituted for the much more complex real one.

In the few instances in which the real soil profile is simple enough to be replaced without intolerable error by an appropriate idealization, theory combined with the results of soil testing makes possible a prediction of the performance of soil-supported structures on a mathematical basis. This procedure has been used successfully, for instance, to predict the magnitude and distribution of the settlement of structures founded above horizontal clay strata of fairly uniform thickness.

In most other instances the results of subsoil exploration inform the designer merely about the general characteristics of the subsurface materials and the location within them of potential sources of trouble. The detailed

characteristics of these sources remain unknown, although, even if they were known, the time and labor involved in securing the data required for an accurate forecast of performance would be prohibitive. Under these circumstances, the designer can do no better than to construct idealized soil profiles showing approximately the outer boundaries of the potentially troublesome weak or compressible zones, and to assign to the materials located within these zones the most unfavorable properties compatible with the available data. The estimates of performance based on these profiles can furnish only upper limiting values for the undesirable consequences of the presence of the zones, but even the knowledge of these values enables the designer to avoid the undesirable consequences by appropriate design. Before the means for investigating the properties of subsurface materials were developed and before the theoretical principles of subsoil behavior were established, the significance or even the existence of troublesome zones remained undetected until they were disclosed by the unanticipated performance of the structures resting on the subsoil.

Part III deals with the practice of subsurface engineering, with the potential sources of trouble that may be encountered in that practice, and with the means at our disposal to anticipate and avoid the detrimental consequences of the potential sources of trouble.

## CHAPTER 7

# *Ground Improvement*

### ARTICLE 43 DRAINAGE PRIOR TO EXCAVATION

#### 43.1 Introduction

Ground improvement refers to any procedures undertaken to increase the strength, decrease the permeability or compressibility, or otherwise render the physical properties of soil more suitable for engineering use. The improvement is accomplished in most instances by drainage, compaction, or preloading. Less frequently, electrical, chemical, or thermal methods are adopted. Among the various procedures the most suitable depends principally on the type of soil to be improved and on whether the soil is being placed as a fill or is to be treated in its present location.

On many jobs, such as the installation of underground utilities, the construction of deep basements for buildings, and the preparation of foundations for dams, the soil must be excavated to a level beneath the water table, and the flow of water into the excavation must be eliminated or reduced to an inconsequential amount. To control the inflow of water, a system of drains must be established either during or, preferably, before removal of the soil. The sides of the excavation are given a slope adequate to maintain stability, or else they are made vertical and are braced with some type of lateral support.

In an excavation with given dimensions, extending to a given depth below the water table, the quantity of water that must be disposed of and the time required for draining the surrounding soil depend on the permeability and the compressibility of the soil. On jobs of average size the planning of the drainage provisions does not require accurate information concerning the permeability of the subsoil. Hence, on such jobs, only routine soil investigations need be made. On large jobs pumping tests are usually made. On every job, regardless of size, the method of drainage and the location of the points at which water will be pumped require careful consideration.

#### 43.2 Methods of Drainage

To obtain satisfactory results at least expense, the method of drainage should be adapted to the average permeability of the soil surrounding the site, to the depth of the cut with reference to the water table, and, on small jobs, to the type of equipment most readily available at the site. The permeability of the soils that constitute most natural deposits varies considerably from point to point. Values within which the coefficient of permeability  $k$  has been found to vary in individual representative deposits of the most common types are given in Table 43.1.

According to their coefficients of permeability, soils may be divided into five groups as indicated in Table 43.2. Soils of high permeability are rarely encountered and, when they are, they are commonly associated with less permeable materials that interrupt their continuity. Practically impervious soils, such as clays, are very common.

Until the late 1800's, the drainage of open excavations was generally accomplished by conducting the water that seeped into the excavation to shallow pits or timbered shafts called *sumps* and by pumping it out of these pits. On small jobs this method of sumping is still practiced. The principle of the method is illustrated by the left-hand side of Fig. 43.1, which represents a vertical section through a wide excavation with sloping sides. Most of the water emerges from the toes of the slopes. It is diverted through drainage ditches into one or several sumps  $S$ . At each sump a pump is installed that lifts the water into a discharge pipe.

The method of pumping from sumps has several disadvantages. First of all, it invites softening and sloughing of the lower part of the slopes, because in this region the seepage velocity and, consequently, the seepage pressures are greatest (Articles 23 and 24). Second, because every natural soil stratum is more or less nonuniform, the water emerges in the form of springs. If the soil contains layers or pockets of fine sand or coarse silt, the springs are likely to discharge

**Table 43.1** Coefficient of Permeability of Common Natural Soil Formations

Formation	Value of $k$ (m/s)
<i>River deposits</i>	
Rhone at Genissiat	Up to $4 \times 10^{-3}$
Small streams, eastern Alps	$2 \times 10^{-4}$ to $2 \times 10^{-3}$
Missouri	$2 \times 10^{-4}$ to $2 \times 10^{-3}$
Mississippi	$2 \times 10^{-4}$ to $10^{-3}$
<i>Glacial deposits</i>	
Outwash plains	$5 \times 10^{-4}$ to $2 \times 10^{-2}$
Esker, Westfield, Mass.	$10^{-4}$ to $10^{-3}$
Delta, Chicopee, Mass.	$10^{-6}$ to $1.5 \times 10^{-4}$
Till	Less than $10^{-6}$
<i>Wind deposits</i>	
Dune sand	$10^{-3}$ to $3 \times 10^{-3}$
Loess	$10^{-5} \pm$
Loess loam	$10^{-6} \pm$
<i>Lacustrine and marine offshore deposits</i>	
Very fine uniform sand, $C_U = 5$ to 2	$10^{-6}$ to $6 \times 10^{-5}$
Bull's liver, Sixth Ave., N.Y., $C_U = 5$ to 2	$10^{-6}$ to $5 \times 10^{-5}$
Bull's liver, Brooklyn, $C_U = 5$	$10^{-7}$ to $10^{-6}$
Clay	Less than $10^{-9}$

**Table 43.2** Classification of Soils According to Their Coefficients of Permeability

Degree of Permeability	Value of $k$ (m/s)
High	Over $10^{-3}$
Medium	$10^{-3}$ to $10^{-5}$
Low	$10^{-5}$ to $10^{-7}$
Very low	$10^{-7}$ to $10^{-9}$
Practically impermeable	Less than $10^{-9}$

a mixture of soil and water instead of clear water. Springs of this type located on the bottom of the excavation are known as *boils*. Starting at the boils, underground erosion may work backward and form tunnels. The collapse of the roofs of these tunnels leads

to subsidence of the ground surface surrounding the excavation, to slumping of the slopes, or to failure of the lateral supports (Article 58).

The probability of the formation of boils can be reduced by surrounding the excavation with a cutoff wall extending to some distance below grade. The wall, consisting of sheet piles or of concrete placed in slurry-filled trenches (Article 59.3.2), intercepts the seepage through all the strata located above its lower edge and reduces the hydraulic gradient at which the water rises toward the bottom of the excavation. Yet, if the soil conditions are unfavorable, even the cutoff wall may not prevent the formation of boils with all their undesirable consequences. On small jobs, such as the excavation of shallow sheeted cuts in fine-grained water-bearing soils, attempts are often made to prevent the formation of boils by dumping gravel into the cut wherever the soil has a tendency to rise with the water, but this procedure is slow and

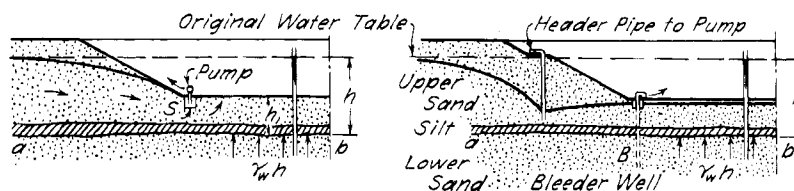


**Figure 43.1** Position of water table while pumping from sumps (left) and from well points (right). Soil conditions lead to failure by heave in spite of pumping unless bleeder wells  $B$  are installed.

hazardous. On a large job, such as the excavation for the foundation of a dam, it may be entirely impracticable.

Accidents and serious delays may also be caused by the hydrostatic pressure acting on the base of a continuous relatively impervious layer, such as  $ab$  in Fig. 43.1, located beneath the bottom of the excavation. The seepage toward the excavation lowers the piezometric level of only the body of water located above  $ab$ , whereas that below  $ab$  remains unchanged. If a piezometric tube is installed at a point located below  $ab$ , the water rises in this tube to the level of the original water table. If

$h$  = vertical distance between  $ab$  and the original water table.

$h_1$  = vertical distance between  $ab$  and the bottom of the excavation.

$\gamma_w$  = unit weight of water

$\gamma$  = unit weight of soil, solid and water combined

the pressure on  $ab$  due to the weight of the overlying soil is  $\gamma h_1$ , and the hydrostatic upward pressure is  $\gamma_w h$ . If  $\gamma_w h$  is greater than  $\gamma h_1$ , and if  $ab$  is fairly horizontal, the bottom of the excavation rises bodily. This phenomenon is known as a *heave*. On the other hand, if  $ab$  is very uneven, the ground heaves only in those places where  $h_1$  is least. Such a local heave is sometimes referred to as a *blow*.

### 43.3 Historical Review of Drainage Techniques

The first attempts to replace the method of pumping from shallow pits by less hazardous procedures were made between 1870 and 1890 in England and Germany. The shallow sumps were replaced by filter wells with a diameter of about 1 m. Toward the end of the century it was realized that the efficiency of the new procedure could be improved by reducing the spacing between wells. This finding led to methods of drainage by pumping from rows of wells. The development of these methods took place along different lines in Europe and in the United States.

In Europe it became customary to install wells at a spacing of 6 to 12 m. Each well was provided with a casing of 0.25-m diameter and a 0.2-m suction tube connected through a horizontal header pipe to a centrifugal pump. The casing was perforated and screened in the pervious zone, and the screen surrounded by a filter. The procedure was referred to as the *Siemens method*, because it was developed by the Siemens Bau Union in Berlin (Kyrieleis and Sichardt 1930).

In the United States the *well-point method* was introduced about 1920. In contrast to the Siemens method, the well-point system consists of drawing the water from wells with a diameter of about 50 mm, spaced at only about 1 to 2 m. The well points are also connected to a header that leads to the pump.

In both methods the header pipe is usually installed on a berm located close to the original water table. Because of

the limited height to which water can be lifted in a suction tube, the water table cannot be lowered more than about 7 m below its original position. Hence, if a project calls for draining the soil to a depth of more than 5 or 6 m, either the water table must be lowered by stages, or else the pumping must be done by pumps that can lift water from any depth below the mouth of the well. Since about 1930 considerable use has been made of vertical turbine and submersible pumps installed inside deep-well casings with diameters ranging from 150 to 500 mm. The spacing of such wells ranges from 6 to 60 m. About 1960 the jet-eductor pump was adapted for use in wells of smaller diameter. The eductor wells usually have a diameter of 100 to 150 mm and are spaced at 2 to 8 m.

Soon after the methods of drainage by pumping from batteries of wells came into general use, it was found that they were ineffective unless the soil had at least medium permeability. As the effective grain size  $D_{10}$  decreased below about 0.1 mm, the time required for draining the site of an excavation increased rapidly and, if  $D_{10}$  was less than 0.05 mm, pumping from wells did not accomplish its purpose. To prevent the rise of the bottom of excavations in cohesionless soils with effective size smaller than 0.05 mm, several different methods were devised.

In Germany, about 1930, development began of procedures to solidify the soil located below the bottoms of proposed excavations by the injection of chemicals that react in the voids of the soil to form an insoluble gel. The procedures are expensive and, if the soil includes zones with a coefficient of permeability less than about  $10^{-6}$  m/s, are likely to be ineffective. Consequently, their practical application in connection with open excavations is quite limited, although they have been found useful in more specialized application such as tunnelling. In the United States it was observed that fine-grained soils such as coarse silt could be consolidated by maintaining a vacuum in the riser pipes of well points. This observation led to the development between 1925 and 1930 of the *vacuum method*. Finally, in about 1934, fine-grained soils were consolidated successfully by the *electro-osmotic method*.

The following paragraphs contain brief discussions of the principal methods of drainage and of the conditions for their success. The effects of drainage on adjoining property are discussed in Article 55.2.

### 43.4 Well-Point Method

The term *well point* refers to the lower perforated end of a 50-mm or 60-mm pipe, commonly 1 m long, that serves the double purpose of well casing and suction tube. The perforations are covered by a wire mesh. The well points are jettied into the ground at a spacing of 1 to 2 m.

If a series of well points is located beneath a continuous stratum with relatively low permeability, the soil above

this stratum is likely to remain undrained. To avoid such an incident and to improve the efficiency of well points in soils of low permeability the following procedure is usually used. After a well point is jetted into the ground, the pressure in the jetting water is increased, whereupon the soil surrounding the riser pipe is scoured out, and a cylindrical hole is formed. During this process all the fine particles of the soil that formerly occupied the scoured space are washed out of the ground, but the coarser particles that remain and accumulate in the lower part of the hole form a cylindrical filter. If the wash water fails to produce a scouring effect, the hole is made by mechanical means, and the filter is constructed by shoveling sand into the hole.

Drainage of a narrow cut can usually be accomplished by pumping from a single row of well points located on one side of the cut, provided the depth of the cut is considerably less than the depth to which the water table can be lowered by the well points. Otherwise, two rows of well points are required, one on each side of the cut. The cost of pumping is usually small compared with that of transporting and installing the well points, unless the soil contains very permeable layers. If the exploratory borings indicate the presence of exceptionally permeable layers, a pumping test should be made for the purpose of estimating the capacity of the pumps that will be required. Otherwise, the pumping equipment is selected on the basis of empirical rules. Commonly, one 150 mm self-priming pump is installed for every 200 m of the length of the row of well points. If the height to which the water has to be lifted above the level of the header pipe is not excessive, a 15-kW motor is sufficient. The drainage requires between about 2 and 6 days.

If the water table must be lowered more than 5 or 6 m, a single-stage system of well points cannot be used. Figure 43.2, for example, shows a section through an open cut with a depth of 15 m below the original water table. By means of the uppermost set of well points *a*, the water table can be lowered only to the level of point *b*, at a depth of less than 7 m below *a*. To carry the excavation to a lower level, a second row of well points interconnected by a header pipe must be installed a few meters above the level of point *b*, and so on. Such an arrangement is known as a *multiple-stage setup*. One row of well points is required for about every 5 m of the depth, and an additional row may be needed along the toe of the slope.

Regardless of the number of stages, the average thickness of the inclined layer of soil that is drained cannot be increased to more than about 5 m (Fig. 43.2a). Beneath this layer the soil is acted on by the seepage pressure of the percolating water. If the depth of the cut is many times greater than 5 m, the drained layer is only skin deep compared with the thickness of the mass of soil

adjoining the slope. The seepage pressures acting within this mass may compromise the stability of the slopes.

### 43.5 Deep-Well Drainage Method

The risk of reducing the stability of a slope because of the seepage pressure of the water flowing toward the thin skin drained by a multiple-stage well-point system can be eliminated by intercepting the flow of seepage by means of deep wells before it enters the space beneath the slope (Fig. 43.2b). Deep wells are also better suited than well points to the predrainage of sites in which a deep excavation is to be made with braced vertical sides. If the permeability of the soil increases with depth, and if the pervious soil extends below the intended position of the lowered water table far enough to ensure submergence of the screen and pump, deep wells of large diameter may prove to be the most economical method of dewatering.

If the soil profile is fairly uniform, the spacing between the deep wells should be determined on the basis of a theoretical study of the flow of water toward the cut. Such an investigation is economically justified, because each unit of a deep-well installation is costly. The spacing usually ranges between 6 and 60 m. The casing has a diameter from about 150 to 500 mm with a screen section 6 to 20 m long usually surrounded by a filter of sand and gravel. The grain-size requirements for the filter material are indicated in Article 14.9. If the screen is slotted, the width of the slot should not exceed the diameter  $D_{70}$  of the material surrounding the screen. If the openings are circular, their diameter should not exceed  $D_{80}$  of the surrounding material. An electrically operated submersible or deep-well turbine pump, capable of lifting water to heights not restricted by suction lift, is installed in each well. The drilling of the holes and installation of the graded filters require special techniques (Powers 1992).

A small quantity of water may flow into an excavation through the gaps between deep wells. To prevent sloughing of the toes of the slopes, it is advisable to remove the water through a row of well points *g* (Fig. 43.2b).

### 43.6 Eductor Well-Point Systems

If the water table must be lowered more than 5 or 6 m but the permeability is relatively low, so that the quantity of water per well is too small for economical use of large-diameter deep-well pumps, a jet-eductor well-point system may be advantageous. The jet-eductor pump, located immediately above the well point, is operated by water furnished to the eductor under high pressure. The well point is established at the bottom of a casing at least 100 mm in diameter, in which are installed the pressure and discharge pipes for the eductor. The casing may be surrounded by a filter.

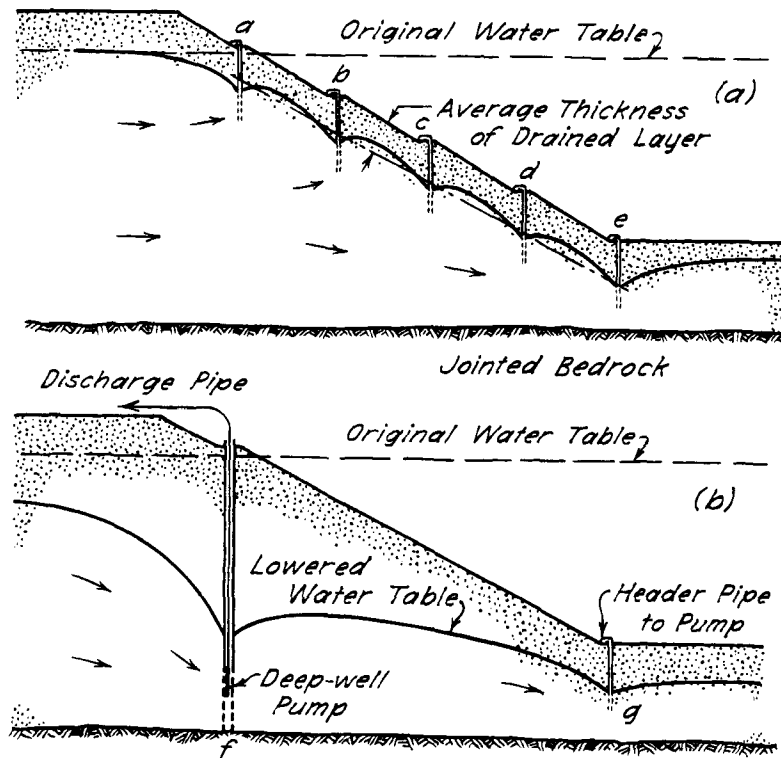


**Figure 43.2** Drainage of deep cut: (a) By multiple-stage setup of well points; (b) by means of deep-well pumps.

Eductor well points are usually spaced at 2 to 8 m and discharge a maximum of about 1 l/s each. They are capable of lowering the groundwater from 15 to 30 m. The efficiency of eductors is considerably lower than that of centrifugal or turbine pumps.

#### 43.7 Bleeder Wells

Because pumping from well points or filter wells lowers the water table to elevations everywhere below the slope or subgrade, the risk of slumps is eliminated. This is an important advantage over the method of pumping from open sumps. However, as previously explained, if the lower ends of the well points or filter wells are located above a relatively impervious stratum, such as *ab* in Fig. 43.1, a heave or a blow may occur in spite of the drainage achieved by pumping from the wells. To prevent such accidents outlets must be provided for the water located below the obstructing layer. These outlets are known as *bleeder wells*. The simplest method for constructing bleeder wells is to jet well points into the ground, to wash an annular space around each riser pipe, and to fill this space with coarse sand.

The saturated unit weight  $\gamma$  of most soils is roughly equal to twice the unit weight  $\gamma_w$  of water. Hence, as a rule, the condition for a heave or blow,

$$\gamma h_1 \leq \gamma_w h$$

is not satisfied unless  $h$  (Fig. 43.1) is greater than  $2h_1$ .

However, in some soil formations the water rises in piezometric tubes to greater elevations from deeper water-bearing strata than from strata nearer the ground surface. This is known as an *artesian condition*. If such a condition prevails, a heave or blow may occur even if  $h$  is considerably less than  $2h_1$ .

To detect the existence of artesian conditions the exploratory holes should be drilled to a depth of at least  $h$  and preferably  $1.5h$  below subgrade level. Whenever a spoon sample is taken, the water should be allowed to rise in the casing until its level becomes stationary, and the elevation of the water level should be determined.

#### 43.8 Vacuum Method

If the average effective grain size  $D_{10}$  of the soil is smaller than about 0.05 mm, the methods of gravity drainage described in the preceding paragraphs fail to produce the desired results, because the water is retained in the voids of the soil by capillary forces. However, the stabilization of very fine-grained soils can be accomplished at least gradually by maintaining a vacuum in the filters that surround the well points (Fig. 43.3). Before the vacuum is produced, both the upper surface of the fine-grained layer and the soil surrounding the filter are acted on by the pressure  $u_a$  of the atmosphere, approximately 100 kPa. After the vacuum has been produced, the pressure on the soil around the filters is almost equal to zero,

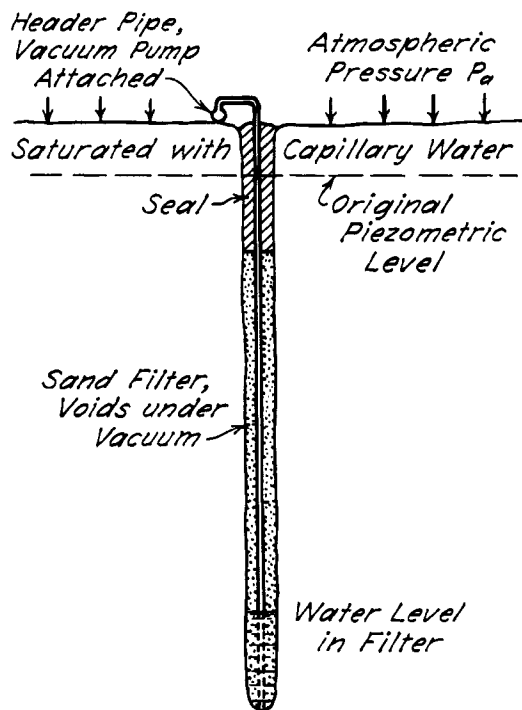


**Figure 43.3** Diagram illustrating principle of the vacuum method of drainage.

whereas that on the surface of the layer remains equal to  $u_a$ . Consequently, water is gradually squeezed out of the soil into the evacuated filters until the effective pressure in the soil adjoining the row of well points has increased by an amount equal to the atmospheric pressure. At the same time the shearing resistance of the soil increases by an amount equal to  $u_a \tan \phi'$ , where  $\phi'$  is the angle of internal friction of the soil. This process is very similar to the stiffening of clay due to desiccation (Article 15.6.4).

The following method is used to construct a filter that can be evacuated. After the well point is jetted into the ground, the pressure of the jetting water is increased until a hole with a diameter of 250 to 300 mm has been scoured out. While the water is still flowing, sand is shoveled into the hole until the top of the sand reaches an elevation a meter or so below the surface of the fine-grained stratum. The water is then turned off, and the rest of the hole is filled with clay or silt which acts as a seal (Fig. 43.3).

The results that can be obtained by this method are illustrated by Fig. 43.4, which shows an open excavation in an organic silt with an average effective grain size less than 0.01 mm. Ninety-five % of the soil passed the No. 200 screen (0.07 mm). The bottom of the excavation was about 5 m below the original water table. Before pumping, the silt was so soft that the crane, visible in the background, had to be moved on a runway of heavy timbers. After two weeks of pumping the soil was so stiff that the sides of the excavation did not require lateral support. The distinct marks left by the excavating tools indicate

the high degree of cohesion that the soil acquired during pumping.

When the vacuum method is used, the well points are commonly spaced at 1 m. The pumping equipment is the same as that for draining soils of medium permeability. One 150-mm pump is used for every 150 m of the length of a row of well points. In addition, one or two vacuum pumps are attached to the header-pipe lines. One 15 kW motor is sufficient to operate the entire pump aggregate. Because of the low permeability of the soil, the water pump discharges for short periods only. The vacuum pumps operate continually. The success of the method depends to a large extent on the quality of the vacuum pumps and on the skill and experience of the foreman.

### 43.9 Drainage by Electro-Osmosis

The principle of this method has been explained in Article 15.6. It has most often been applied in practice to the stabilization of slopes being excavated into cohesionless or slightly cohesive silts below the normal groundwater level. The time required to drain such materials by the vacuum method may be excessive, especially under emergency conditions. Yet, the materials readily become quick under the influence of the seepage pressures directed inward toward the face and upward toward the bottom of the excavation. By an arrangement of electrodes similar to that shown in Fig. 43.5 and the application of a suitable potential, seepage pressures due to electro-osmotic flow can be created in directions away from the faces of the excavation and toward the cathodes. The stabilizing influence of these pressures is in many instances spectacular and occurs as soon as the current is turned on. In addition there are a progressive decrease in the water content of the silt and a corresponding increase in strength (Casagrande 1949, 1962).

The anodes commonly consist of iron pipes, although reinforcing bars or steel rails have also been used. Corrosion is likely to be concentrated at a few points of the anodes; consequently the anodes may become discontinuous whereupon the lower portions are no longer effective. If the anodes consist of pipes, smaller pipes or rods can be inserted in them to restore their continuity. The cathodes may consist merely of iron rods along which the water flows as it escapes to the surface, but should preferably be perforated pipes screened for their full length to permit easier and more rapid escape of the water. The applied potential is usually on the order of 100 volts; the current required for stabilization of even a fairly small excavation is likely to be at least 150 amps. The actual power requirements depend on the resistivity of the soil and vary considerably. Potential gradients in excess of about 50 volts/m may lead to excessive energy loss in the form of heat.

Electro-osmosis causes consolidation of compressible soils such as clays. The consolidation is accompanied by





**Figure 43.4** Open excavation in Camden, N.J., in soft organic silt after consolidation by the vacuum method (courtesy Moretrench Corp.).

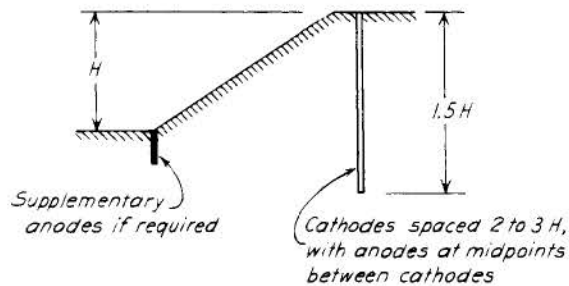


**Figure 43.5** One arrangement of electrodes suitable for stabilizing slope by electroosmosis.

an increase in strength and generally by a decrease in sensitivity. In addition, the clay becomes fissured. The use of electro-osmosis for altering the properties of clays in this manner has not been as frequent as that for the stabilization of slopes in silty materials.

#### 43.10 Summary of Methods of Drainage

The quantity of water that flows toward an excavation with given dimensions and the methods that can be used to best advantage for draining the excavation depend primarily on the average permeability of the adjoining soil. On small jobs the permeability can be estimated with sufficient accuracy on the basis of the results of the routine tests performed on samples from the exploratory borings. On large jobs pumping tests may be appropriate.

To determine whether or not bleeder wells are required, the exploratory borings should be drilled to a depth below subgrade equal at least to the vertical distance between

the original water table and the subgrade level. As often as a sample is taken, the water should be allowed to rise in the casing, and the elevation to which it rises should appear in the boring record.

Excavations in soils with high permeability ( $k$  greater than  $10^{-3}$  m/s) or in very dense mixed-grained soils of medium permeability ( $k$  between  $10^{-3}$  and  $10^{-5}$  m/s) as a rule can be drained without undue risk by pumping from open sumps.

Under favorable conditions uniform soils of medium permeability can also be drained without mishap by pumping from sumps. However, this procedure involves the possibility of the formation of boils on the bottom of the excavation, associated with underground erosion and subsidence of the area surrounding the excavation. To avoid this risk it is preferable to drain soils of medium permeability by pumping from well points or filter wells. The drainage of the soil prior to excavation requires 2 to 6 days.

The greatest depth to which the water table can be lowered by drawing the water from one set of wells or well points is about 6m. If the bottom of the proposed excavation is located at a greater depth, a multiple-stage setup may be used. Two or more header pipes must be installed at a vertical spacing not exceeding about 5m. If limitations of space do not permit a multiple-stage installation, eductor well points may be suitable. If the depth of the excavation exceeds about 15m, it is usually preferable to drain the soil adjoining the site by means of deep-well pumps operating within the casings of large-diameter wells.

Uniform soils of low permeability ( $k$  between  $10^{-5}$  and  $10^{-7}$  m/s) cannot be drained by pumping either from sumps or from wells. Such soils can be stabilized most successfully by the vacuum method. The quantity of water that can be drawn out is very small, but, if the pumping is kept up for several weeks, the soil may become so stiff that the sides of excavations up to 5 m deep can be established at a slope angle of  $60^\circ$  to  $70^\circ$  without risk of failure.

Fine silts and uniform silty soils with a coefficient of permeability between about  $10^{-7}$  and  $10^{-9}$  m/s may be so soft that they will rise in the bottom of an excavation having even a moderate depth. They cannot be drained by gravity or by the vacuum method, but may be stabilized by electro-osmosis. Alternatively, excavations in soft soils of this category may be made by dredging or by the use of compressed air.

Soils with a coefficient of permeability less than about  $10^{-9}$  m/s are with few exceptions very cohesive. Drainage is not practicable by any means except electro-osmosis. However, drainage is seldom necessary, because the shearing strength is normally great enough to maintain the stability of the bottom of an open excavation of moderate depth. The depth to which an excavation can be made in such a soil without the risk of a rise of the bottom can be increased only by reducing the side slopes or, if the sides of the excavation are vertical, by increasing the depth of penetration of the sheet piles or cutoff walls that constitute part of the lateral support (Article 37.3.)

### Selected Reading

An excellent practical treatise on dewatering is Powers, J.P. (1992). *Construction Dewatering*, Wiley, New York, 2nd Ed., 492 pp.

Bjerrum, L., J. Moun, and O. Eide (1967). "Application of electro-osmosis to a foundation problem in a Norwegian quick clay," *Géot.*, **17**, pp. 214–235.

Esrig, M.I. (1968). "Pore pressures, consolidation and electrokinetics," *J. Soil Mech. Found. Eng., ASCE*, **94**, No. 4, pp. 899–921.

Casagrande, L. (1983). "Review of stabilization of soils by means of electro-osmosis—state-of-the-art," Presented to the Geotechnical Section of the BSCES/ASCE, **69**, No. 2, pp. 255–302.

Lo, K.Y., and K.S. Ho (1991). "The effects of electro-osmotic field treatment on the soil properties of soft sensitive clay," *Can. Geotech. J.*, **28**, No. 6, pp. 763–770.

Lo, K.Y., K.S. Ho, and I.I. Incullet (1991). "Field test of electro-osmotic strengthening of soft sensitive clay," *Can. Geotech. J.*, **28**, No. 1, pp. 74–83.

Lo, K.Y., I.I. Incullet, and K.S. Ho (1991). "Electro-osmotic strengthening of soft sensitive clays," *Can. Geotech. J.*, **28**, No. 1, pp. 62–73.

## ARTICLE 44 COMPACTION, PRELOADING, AND OTHER METHODS

### 44.1 Introduction

Even in ancient times it was customary to compact fills to be used as dams or levees, but until the automobile created a demand for hard-surfaced roads in the 1920's most other fills were dumped loosely and allowed to settle under their own weight. It soon became apparent that concrete roads on uncompacted fills were likely to break up and that the surfaces of other types of high-grade pavements had a tendency to become uneven. Avoidance of such undesirable conditions fostered the development of methods of soil compaction that would satisfy the requirements of both economy and efficiency. The more stringent requirements for airfield taxiways and runways and the progressively greater heights of earth dams provided additional incentives. Similarly, the pressure for commercial and industrial development of sites with poor subsoil conditions encouraged the development of methods for improving the properties of the existing materials in place.

### 44.2 Compaction of Fills

#### 44.2.1 Procedure and Equipment

With few exceptions fills for civil engineering projects are spread in layers, each of which is compacted mechanically. Where space permits, the equipment usually consists of rollers of types suited to the nature of the fill material; where space is limited, compaction is usually accomplished by vibrating plates, tampers, or the tires of loaded vehicles. In most instances the soil from the borrow pits requires wetting or drying to bring its moisture content close to a value, known as the *optimum moisture content*, at which the chosen equipment and procedures can achieve the greatest degree of compaction. Ensuring that the water content is maintained close to the optimum value is known as *moisture content control*.

A wide variety of rollers is available. They fall into three principal classes: pneumatic, tamping, or vibratory. In the following paragraphs the characteristics of each class are described. Subsequently the procedures best suited for compaction of various kinds of soil are discussed.

*Pneumatic* rollers usually consist of a load cart, towed by a tractor, supported by a single row of four wheels equipped with tires inflated at pressures ranging from 550 to 700 kPa. The wheels are so mounted that the weight from the cart is transmitted to all wheels even if the surface of the ground is uneven. Fills for buildings are commonly compacted in lifts having compacted thicknesses of 0.15 to 0.30 m with 22.7 Mg (tonne) rollers (25 tons in the English system) and comparatively low tire pressures. For embankments and dams, higher tire pressures, 45.4-tonne rollers, and compacted layers of

0.15 to 0.30 m are usual practice, whereas 90.7-tonne rollers and compacted lift thicknesses of 0.30 to 0.45 m are sometimes used.

The surface of *tamping* or *sheepsfoot* rollers is covered with prismatic attachments or feet, one for approximately each  $0.1 \text{ m}^2$ . The rollers generally used in earth-dam construction have a diameter of about 1.5 m and a length of about 1.8 m. When loaded with ballast they have a mass of about 15.5 tonnes. The feet extend at least 0.23 m from the roller and have areas of 0.003 to  $0.009 \text{ m}^2$ . The contact pressure varies from about 2000 to 4000 kPa. Somewhat smaller and lighter rollers are used extensively for compacting highway fills. Some tamping rollers are self-propelled; others are towed by a tractor.

A *vibratory* roller consists of a smooth steel drum in which vibrations are generated by an unbalanced eccentric mass mounted on the axle of the roller or on the frame supported by the axle. The frequency of the rotating eccentric mass and, hence, the unbalanced force can usually be varied between limits. The drums of comparatively light rollers may have a mass of about 2.7 tonnes, whereas the mass of the drums of heavy rollers for dams may be about 9.1 tonnes. The gross mass of the frame and its appurtenances is roughly equal to that of the drum. The normal operating frequency generally lies between 15 and 30 Hz. The dynamic force generated at the lower frequency is usually about equal to the static weight of the drum, and at the higher frequency may exceed the total weight of the drum and frame. The diameter of the drum is usually about 1.5 m and the length from about 1.8 to 2.7 m.

The dynamic behavior of the system consisting of the soil and compactor is complex (Selig and Yoo 1977, Yoo and Selig 1979, Youd 1972). When the eccentric force in the roller acts downward and the roller impacts the soil, the soil accelerates downward. As the roller force then turns upward the soil rebounds and accelerates upward. Near the maximum upward position of the roller the contact pressure between roller and soil is near zero and the soil begins to fall. In this state the soil particles can be rearranged easily. The next impact of the roller, because the compactor is moving forward, is not at the previously impacted position but is closely adjacent. Thus a shearing deformation is imposed on the soil while its particles are still under small confinement. After the shearing displacement the compressive stresses increase as the roller continues to descend, and the decrease in void ratio accompanying the shear is locked in. The compaction is produced chiefly by the repeated kneading action, which is confined largely to the zone within which the particles are experiencing free fall. The effectiveness of compaction is a function, therefore, of the thickness of the free-fall zone which, in turn, depends on the roller's characteristics and on the relation between its frequency and travel speed. Operating at a frequency close to the

resonant frequency of the system consisting of roller and soil enhances the economy of transmission of energy to the soil by requiring the fewest passes to achieve the specified degree of compaction.

The speed of rollers of all types is usually limited to about 5 km/h. At greater speeds there is likely to be insufficient time for the desired deformations to take place and more passes may be required to achieve the required compaction.

For confined spaces where rollers cannot operate, *vibrating-plate* compactors are used extensively. A single plate usually has a mass of not less than 90 kg and the eccentric weight should rotate at a frequency not less than 25 Hz. The dynamic increment customarily is limited to a value equal to the static weight to minimize jumping of the plate. A variety of hand-held power tampers is also available. Their masses range from about 13 to 100 kg and the diameters of the foot range from about 0.1 to 0.25 m. Irrespective of the type of soil, lift thicknesses must be considerably smaller than for rollers to achieve comparable compaction.

#### 44.2.2 Compaction of Cohesionless Soils

Vibrating rollers are the most effective means for compacting cohesionless soils. Moisture-content control is not necessary. Roller masses customarily range from about 4 tonnes for filters and transitions in earth dams with lift thicknesses of 0.45 m, to about 10 tonnes for rockfill or coarse granular materials for the shells with lift thicknesses of 1 m. A high density is usually produced in 2 to 4 coverages. The frequency typically lies in the range 18 to 25 Hz. Particles as large as the compacted lift thickness do not significantly reduce the effectiveness of compaction.

The applicability of the foregoing generalities may need to be verified on a specific project. For example, D'Appolonia et al. (1969) carried out field tests on a large project to ascertain the optimum layer thickness and number of coverages of a 5.7-tonne roller operating at 27.5 Hz to achieve a relative density of 75% in sand with  $D_{50} = 0.18 \text{ mm}$  and  $C_U \cong 1.5$ . Tests on a single layer 2 m thick led to the results shown in Fig. 44.1 *a*., from which it was judged that 5 coverages would produce the required compaction to a depth of about 0.75 m. Accordingly, a tentative lift thickness of 0.6 m was selected and tests were carried out after several successive layers were compacted. The results, shown in Fig. 44.1 *b*, demonstrated that the procedure was satisfactory and slightly conservative. However, because it was more economical to use lift thicknesses of 0.45 m with only 2 passes per lift, the latter criterion was adopted. The figure also shows that by any procedure the top 0.25 m remained uncompacted. Tests of this type are often justified to establish the most economical procedure to achieve the required compaction at a particular site.

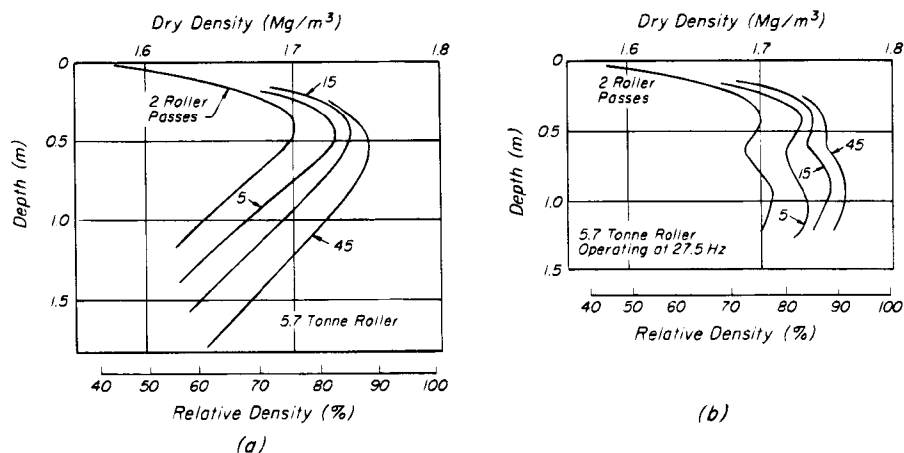


**Figure 44.1** (a) Results of field tests relating dry density of sand layer to number of passes of 5.7-tonne vibrating roller operating on surface of layer 2 m thick. (b) Compaction achieved with same roller operating on 0.6-m lifts (after D'Appolonia et al. 1969).

Moist sands often possess enough apparent cohesion to cause them to bulk when dumped or spread in layers. Their void ratio in this metastable state may considerably exceed that in the loosest stable state. From ancient times it has been customary to destroy the apparent cohesion by flooding or watering the fill. Although the flooding may eliminate the unstable structure, the resulting void ratio is likely to be close to that corresponding to the loosest stable state. Therefore, the practice should be discouraged.

#### 44.2.3. Compaction of Soils with Moderate Cohesion

Soils of a wide variety fall into this category. They include broadly graded glacial tills with silty fines, weathering products of sandstones and siltstones, granular soils with a small percentage of clays of low plasticity; in short, many soils classified as GC, SC, GM, SM, or ML. For all these soils the effectiveness of the compaction procedure depends greatly on the moisture content of the soil. This statement applies especially to almost nonplastic uniform fine-grained soils. If the water content is not almost exactly equal to the optimum, these soils cannot be compacted at all.

If a test embankment is constructed of a soil of uniform properties under carefully controlled conditions in the field, and if the layer thicknesses, type of compacting equipment, and number of passes are all kept constant, it is found that the effectiveness of compaction depends only on the water content of the soil in the layer at the time compaction is started. The effectiveness of compaction is measured by the mass of solids per unit of volume, known as the *dry density*. The relation between dry density and placement water content has the characteristic shape shown by the solid curve *a* in Fig. 44.2. For the conditions of the test, the dry density at the peak of the curve is

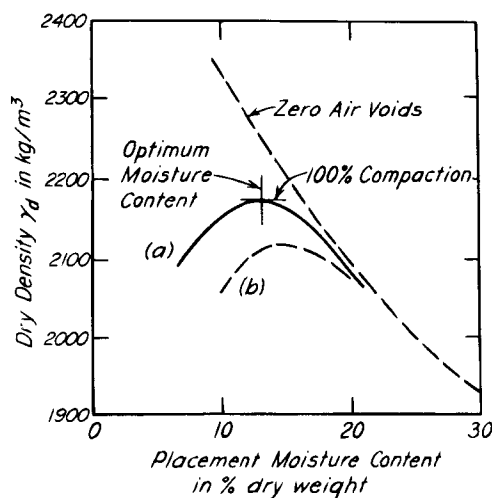


**Figure 44.2** Relation between dry density and placement moisture content for a particular soil (a) under a specific compaction procedure using a given roller. (b) Under the identical compaction procedure but with a lighter roller. Both curves approach zero-air-voids line representing relation for fully saturated soil.

called the *maximum dry density* or the *dry density at 100% compaction*, and the corresponding water content is designated the *optimum moisture content*. Neither of these quantities is a property of the soil itself. If, for example, all conditions are kept unchanged except that a lighter compactor is used, the value of the maximum dry density, as indicated by curve *b*, is lower and the optimum moisture content higher than for the heavier compactor. An increase in the number of passes of the lighter compactor may increase the maximum dry density, but even if it should reach a value comparable to that for curve *a*, the optimum moisture content corresponding to the new value of  $\gamma_{d \max}$  would be likely to exceed that for

the heavier compactor. Similar changes in the moisture-density relations for a given soil accompany variations in thickness of layers and in type or weight of compaction equipment. Hence, the terms *100% compaction* and *optimum moisture content* for a given soil have specific meaning only in connection with a specific compaction procedure. Nevertheless, for any potential borrow material, it is essential to know in advance of construction whether, for the compaction procedure likely to be specified, the moisture content in the field is excessive or deficient with respect to the optimum value for that procedure. Moreover, during placement of a fill the engineer must have the means for determining whether the specified compaction is being achieved even if the character of the borrow materials changes from time to time. These requirements have led to the development of laboratory compaction tests.

The purpose of every laboratory compaction test is to determine in the laboratory a moisture-density curve comparable to that for the same material when compacted in the field by means of the equipment and procedures likely to be used. Most of the current methods are derived from one developed by the California Highway Department in the early 1930's when compaction equipment was of relatively light weight. According to this procedure, now known as the *Standard Proctor test* (Proctor 1933, ASTM D-698), a sample of soil is dried, pulverized, and separated into two fractions by a no. 4 sieve. About 2.7 kg of the finer fraction are moistened with a small quantity of water and thoroughly mixed to produce a damp aggregate that is then packed, in three equal layers, into a cylindrical container of specified dimensions. Each layer is compacted by 25 blows of a standard tamper of mass 2.49 kg that is allowed to fall from a height of 303 mm. When the cylinder has been filled and struck off level at the top, the weight and the water content of the damp soil in the container are determined. From these quantities, the dry density can be computed. In a similar manner the dry density is determined for successively damper mixtures of the aggregate, until the dry density after compaction decreases conspicuously with increasing water content. A curve is plotted showing the relation between dry density and water content. The optimum moisture content according to the Standard Proctor test is the value of water content at which the dry density is a maximum.

Because of the influence of the method of compaction on the moisture-density curve, no standard test of any kind, including the Proctor test, should be expected to produce results of general validity. Conclusive information on the optimum moisture content can be obtained only by making large-scale field tests with the compacting equipment to be used on the job.

From time to time efforts have been made to develop laboratory methods that imitate the common types of field

equipment more closely than does the Standard Proctor test. These efforts have led to various modifications of the original procedure. For the heavy equipment in modern use, especially in connection with the construction of earth dams or of aprons and taxiways for heavy aircraft, the Modified Proctor Test (ASTM D-1557) is likely to be more appropriate. Various types of kneading compactors (Johnson and Sallberg 1962) have been developed that lead to more realistic moisture-density curves, but so far no such tests have been widely accepted.

Typical moisture-density curves for several soils are shown in Fig. 44.3. They were obtained by the Standard Proctor method. It is apparent that not only the shapes but also the positions of the curves change as the texture of the soils varies from coarse to fine.

If the moisture content of the soil in the field is greater than the optimum, the soil should be given an opportunity to dry out. If it is less, water should be added in the borrow pit or by sprinkling before compaction. With reasonable care it is usually possible to maintain the water content within 2 or 3% of the optimum. However, for uniform slightly cohesive nonplastic soils a closer approach to the optimum water content may be required.

The mass density and the water content of the soil are checked in the field by routine sampling and testing. To determine the mass density, a hole having a volume of at least 1.5l is excavated in the compacted soil, and the excavated material is carefully recovered and weighed before any moisture is lost by evaporation. The volume

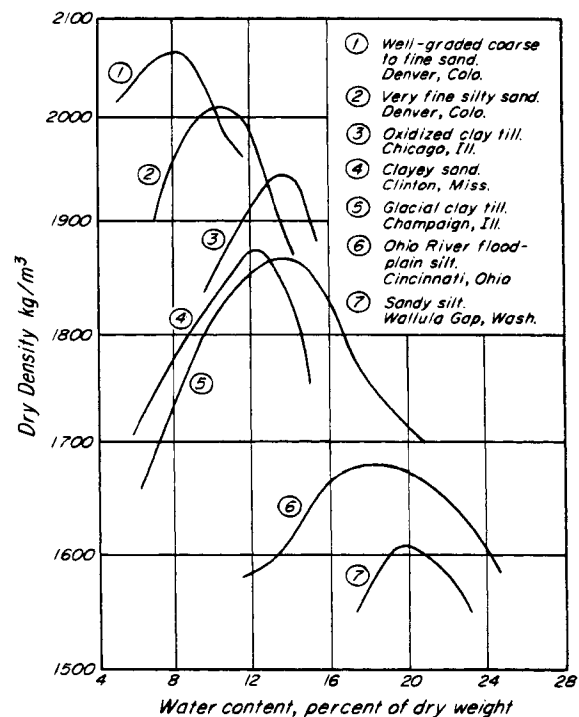


Figure 44.3 Moisture-density relations for various types of soil as determined by ASTM Method D-698.

of the excavated material may be measured by one of several methods. In one of the older, more common procedures, the volume is measured by filling the hole with dry sand in a loose state, after the mass density of the sand in this state has been established. The sand is poured from a container that is weighed before and after the hole is filled. According to a second procedure, a rubber balloon is placed beneath a horizontal cover and forced by the injection of water to accommodate its shape to that of the hole; the volume of the hole is determined by measuring the volume of water injected. An approximate value of the water content can be obtained quickly by determining the loss of weight due to drying the sample in a pan resting on a hot plate. However, after a moderate amount of experience on a given job, an inspector can estimate the water content quite accurately from the appearance and texture of the material. The mass density and water content can be obtained rapidly also by means of nuclear equipment. If the material to be used for a fill is quite variable, or if the job is located in a region subject to frequent rainy spells, compliance with the moisture-content requirements may considerably increase the cost of constructing the fill.

The water content at which a soil is compacted has an effect on all the physical properties of the compacted soil, including the permeability. Experience indicates that an increase in initial water content from a value somewhat below the optimum to a value somewhat above is likely to cause a large decrease in the coefficient of permeability. The decrease seems to increase with increasing clay content of the soil. In studies of a material considered for the core of Mud Mountain Dam, which contained as much as 3% of clay with a high montmorillonite content, it was found that an increase in the water content from 2% below optimum to 2% above decreased the coefficient of permeability about 10,000 times (Cary et al. 1943). An influence of this magnitude is probably a rare exception, but even much less important effects deserve consideration.

In the humid tropics, the degree of saturation of residual soils is often close to 100% and reduction of the moisture content is impracticable. Furthermore, if the soils are dried for the purpose of making compaction tests, the characteristics of the soils may undergo drastic irreversible changes and the laboratory moisture-density curve may have no relation to the field conditions.

This is illustrated by a series of tests on a sample from Java, Indonesia (Fig. 44.4), which had a natural water content of 151%. The compaction curve represented by the open circles was obtained by drying the soil from its natural water content or by adding water; fresh soil was used for each point on the compaction curve. The compaction curves of the dried samples were obtained after drying and then wetting individual samples before compaction.

An extreme example of the error that may be introduced by drying the soil before performing the compaction test is shown in Fig. 44.5, which refers to the Peepeekeo ash, a weathered volcanic soil occurring in the most humid part of the island of Hawaii (Willis 1946). The liquid limit of the ash is about 240% and the plastic limit about 130%. Air-drying renders the soil nonplastic. The natural water content is close to 200%. If a sample is compacted according to the Standard Proctor procedure at this moisture content, the dry density is about  $400 \text{ kg/m}^3$ . If each of a series of samples is allowed to dry to a different water content and then compacted, the relation shown by curve *a* is obtained. However, if the soil is dried to a moisture content of 10% and a moisture-density curve obtained in the usual manner by adding moisture to the dried sample, curve *b* is obtained. It exhibits a peak at a moisture content of 35%, corresponding to a maximum dry density of  $1233 \text{ kg/m}^3$ . Attempts to dry the material in the field to the optimum moisture content determined in this manner are futile. Moreover, use of a roller for compaction turns the soil into a fluid that flows from the embankment. Yet, it has been found that this unpromising material can be used to construct stable highway fills up to 30m high with slopes of 1.5:1 by placing it as gently as possible in 1.2m layers with a very light bulldozer (Hirashima 1948). Although the behavior of the Peepeekeo ash is unusual, similar experiences have been observed to a lesser degree in other tropically weathered soils containing hydrated oxides of iron and alumina, or the clay mineral halloysite (Terzaghi 1958*b*, Jimenez-Quinones 1963). A marked drop in the liquid limit as a consequence of air-drying constitutes grounds for suspicion.

Soils with moderate cohesion can usually be compacted most effectively with pneumatic rollers, although the less plastic varieties may sometimes be densified efficiently by vibrating rollers and the more plastic varieties by sheepfoot rollers.

For buildings, pneumatic rollers with a mass of 25 tonnes or less are customary, with tire pressures of about 500 kPa and compacted lift thicknesses of 0.15 to 0.30 m. For embankments and dams, higher tire pressures, 50-tonne rollers, and compacted layers of 0.15 to 0.30 m are usual practice, although 100 tonne rollers and compacted lift thicknesses of 0.30 to 0.45 m are sometimes used. From 4 to 6 passes commonly achieve the required compaction. On large jobs, or on jobs at which unusual materials are encountered, the number of passes and layer thickness should be determined by field tests at the beginning of the job. Too great a layer thickness results in inadequate compaction of the lower part of each layer and poor bonding of one layer to another.

In confined spaces compaction can sometimes be accomplished by repeated application of wheel loads from vehicles or end loaders. Otherwise impact rammers are

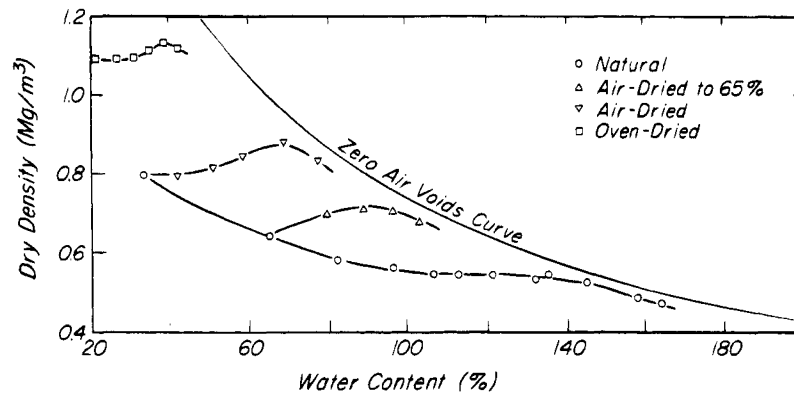


**Figure 44.4** Compaction curves for sample of residual soil from Indonesia (data from Wesley 1973).

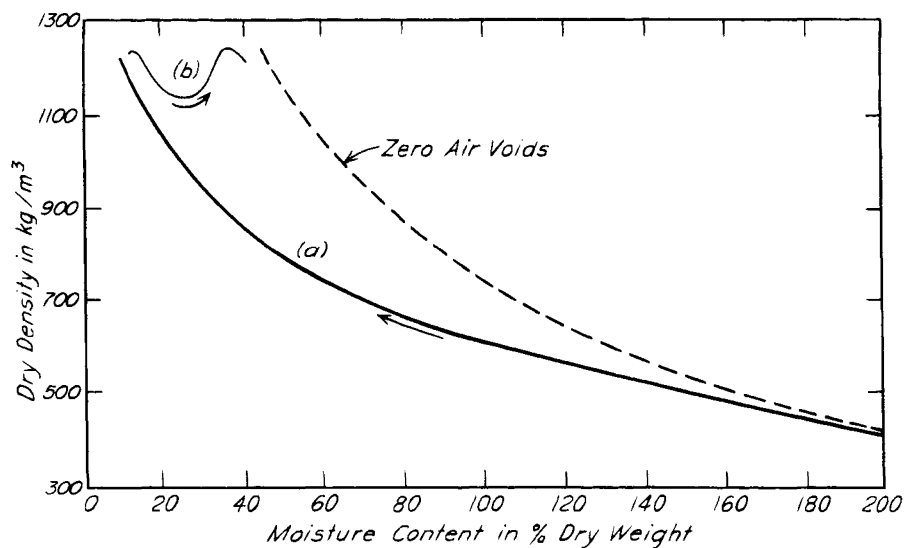


**Figure 44.5** Moisture-density curves obtained by Standard Proctor procedure for Peepeekeo ash from Hawaii. (a) Curve obtained by drying each of successive samples from natural water content to moisture content at which sample is compacted. (b) Curve obtained if soil is dried to  $w = 10\%$ , whereupon water is added and samples compacted in usual manner for performing Proctor test (data after Willis 1946).

generally used. As the effective thickness that can be compacted with such equipment is as small as 0.1 m, great vigilance is required to ensure that the fill is not spread faster than it can be compacted. The optimum moisture content for such equipment is likely to be higher than for the equipment used on the rest of the job.

The feet of tamping rollers penetrate almost to the bottom of a fresh lift and compact the lowermost soil first. With successive passes the feet work their way upward. Layer thicknesses after compaction should generally not exceed 0.15 m; as many as 12 passes per lift may be required. The indented upper surface of a compacted lift aids in knitting the layers together. However, to avoid trapping excessive water, the surface must be smoothed if a rainstorm is imminent; if this is not done

the affected material must be removed or reconditioned before placement resumes. On the other hand, the surface of lifts compacted by pneumatic rollers, if given a slight slope or crown, may effectively shed water but may need to be scarified to improve the bond between layers in fills intended to impede horizontal seepage.

#### 44.2.4 Effect of Compaction on Stresses

Compaction not only increases the density of a soil but it also permanently increases the ratio of the effective horizontal to effective vertical pressures. Thus, it produces an effect similar to that of overconsolidation. This is illustrated in Fig. 44.6 for Ottawa silica sand with  $\phi'_{cv} = 32^\circ$  and  $K_{op} = 0.466$ , which was shaken at 6 Hz under different sinusoidally applied acceleration levels

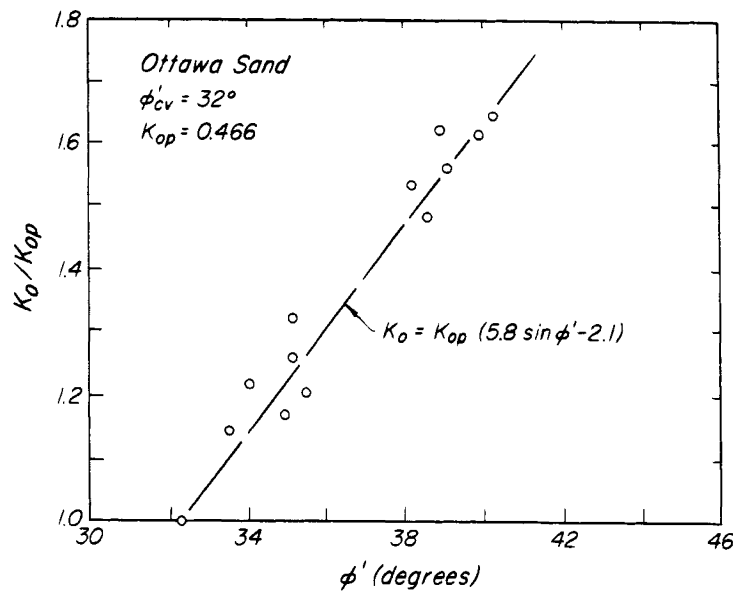


**Figure 44.6** Increase in  $K_0$  of sand with densification (data after Sherif et al. 1984).

for various periods of time (Sherif et al. 1984). In this figure the effect of compaction beyond the initial condition of deposition and consolidation is expressed as an increase in friction angle  $\phi'$ . Similar increases in  $K_0$  caused by cyclic shear or vibration of loose sands have been measured by Pyke (1973) and Bhatia (1982). Vibration of granular soils allows a temporary demobilization of internal friction, whereupon the lateral pressure required to support the soil increases permanently.

Values of  $K_0$  for granular soils compacted in several different ways are summarized in Table 44.1. They indicate that compaction may increase  $K_0$  significantly above the value  $K_{op}$  that applies to normally consolidated sands not subjected to aging (Article 16.5). No reliable measurements currently exist concerning  $K_0$  for compacted cohesive soils. In these soils postcompaction horizontal pressures are likely to be significantly influenced by the time since compaction, by the presence or absence of water, and by the swelling and creep characteristics of the compacted material (Clayton et al. 1991).

When a soil is placed in lifts, each subjected to several applications of vibratory compaction equipment, densification involves cycles of loading, unloading, and reloading, especially of the earlier lifts. Furthermore, field compactors do not apply a uniformly distributed vertical load over the entire area; the load is applied over a localized area and is distributed three-dimensionally into the underlying soil. Various attempts have been made to quantify this process on the basis of the hysteresis associated with loading, unloading, and reloading the soil mass (Sowers et al. 1957, Broms 1971, Seed and Duncan 1986,

Duncan et al. 1991, Mesri et al. 1993). The results are intended to apply to laterally constrained compaction or to the lateral pressure on nondeflecting walls. However, as most actual full-scale lateral pressure measurements have been influenced by the deflection or displacement of the wall (Article 45.7), the number of full-scale observations is insufficient to allow a conclusive evaluation and comparison of existing methods.

The effects of placing and compacting a granular soil are illustrated in Fig. 44.7. It is assumed that a completed backfill will consist of 25 lifts of equal thickness as placed. Immediately after placement and compaction of the entire backfill, the pressure against the wall is represented by  $C_2$ . At no level can the pressure be less than the earth pressure at rest  $K_{op}$ , whereas near the surface it cannot exceed the passive value  $K_p$ . After a period of readjustment the pressure may relax to some long-term value represented by  $C_3$ .

When an intermediate lift, such as lift 10, is placed and compacted, it is then the top lift, and the distribution of pressure  $C_1$  is identical to  $C_2$  below the surface of the lift. Addition and compaction of successive lifts lead to the distribution  $C_2$  at the end of the operation. The pressure diagrams  $C_2$  and  $C_1$  (Fig. 44.7) are analogous to the effective stress path (Fig. 44.8, *a* and *b*) discussed in the following paragraphs.

When the first lift is placed, the average vertical pressure  $\sigma'_v$  in the lift is equal to the product of the unit weight of the soil and the half-thickness of the layer, and the horizontal pressure  $\sigma'_h$  is equal to  $\sigma'_v$  times the coefficient of earth pressure at rest  $K_{op}$ . This state is represented



**Table 44.1** Measurements of  $K_0$  in Compacted Granular Soils

Soil (Reference)	Depth (m)	Lift (cm)	Roller/Compactor	$K_{op}$	$K_0$
Sand (Carder et al., 1977)	0.20	15	BOMAG	0.47	1.7–3.3
	0.50		BW90S		1.0–1.74
	0.70		Static wt = 1300 kg		0.90–1.36
	1.00				0.60–0.90
Yatesville silty sand (Sehn & Duncan, 1990)	0.21	10	WACKER	0.47	1.70
	0.37		BPU 2440A		0.97
	0.55		Vibratory plate, static wt = 121 kg		0.74–1.20
	0.91				0.79
	1.46				0.56–0.80
Uniform sand (Broms & Ingelson, 1971)	0.73	52	Vibratory <sup>1</sup>	0.50	1.4–2.93
	1.22		roller, 3800 kg		0.9–1.91
	1.83		Ten passes		0.52–1.00
Clean sand (Lewis et al., 1985)	0.92			0.49	1.60
Poorly graded dune sand (D'Appolonia et al., 1969)	0.61	24	Deutz Diesel <sup>2</sup>	0.5	1.52 (4 roller passes)
			Vibratory roller Static wt = 5682 kg Operating frequency = 27.5 Hz		2.68 (40 roller passes)
Poorly graded dune sand (D'Appolonia et al., 1969)	0.61	24	Gasoline <sup>2</sup>	0.5	1.13 (4 roller passes)
			Vibratory roller static wt = 2864 kg Operating frequency = 29.5 Hz		1.46 (40 roller passes)

<sup>1</sup> Fill immediately behind the wall was compacted by 300-kg vibratory compactor

<sup>2</sup> Horizontal pressure measured in the free field perpendicular to roller path.

by point 1 in Fig. 44.8a. Under the weight and the dynamic increment of vertical force of the compactor, the state of stress is altered to that represented by point 2. Since the lift is not confined by any overlying soil, passive failure can be expected; consequently  $\sigma'_h$  is limited by the line representing  $K_p$ . Removal of the compactor reduces  $\sigma'_v$  to the value corresponding to the abscissa of point 1, and the state of stress is represented by point 3 on the  $K_p$  line. When the second lift is added, the vertical pressure  $\sigma'_v$  on the first lift is increased by the weight of the second lift, and there is a corresponding increase in  $\sigma'_h$  to the state of stress represented by point 4. Under the weight of the second lift and the weight and dynamic increment of the compactor, the components of stress in the first lift define point 5, and after the removal of the compactor the stresses are reduced to those represented by point 6.

In this illustration, point 6 does not correspond to a passive failure in the first layer, because the failure is prevented by the resistance of the compacted soil above the layer. The successive points 3, 6, . . . , represented by the open triangles in Fig. 44.8a, thus determine the successively increasing lateral pressure  $\sigma'_h$  exerted by the first layer as the number of layers is increased. The points such as 6, 7, 8, and 9 in Fig. 44.8a are generalized in Fig. 44.8b as *a*, *b*, *c*, and *d*.

Inasmuch as any given layer may be regarded as the bottom layer for the layers subsequently placed and compacted above it, the curve defined by the open triangles in Fig. 44.8b represents the values of  $\sigma'_h$  corresponding to the number of lifts above any given level. It is, therefore, analogous to the pressure diagrams  $C_1$  or  $C_2$  (Fig. 44.7).

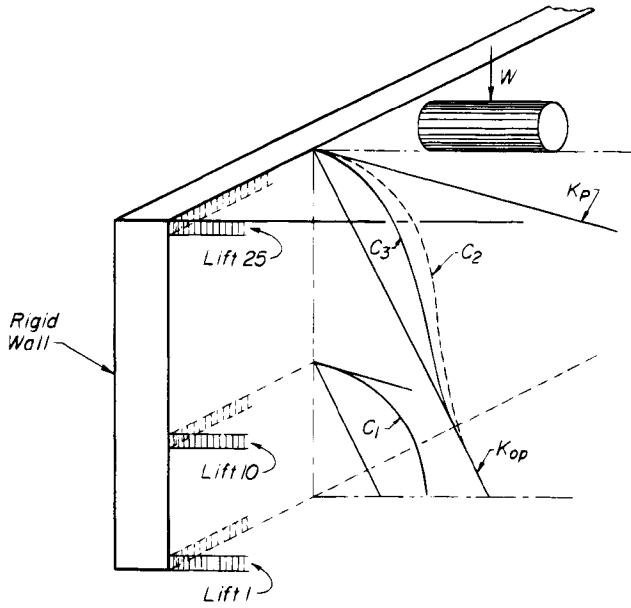


**Figure 44.7** Horizontal pressure of compacted granular backfill against nonyielding wall during placement of lift 10 (curve  $C_1$ ), immediately after placement of lift 25 (curve  $C_2$ ), and after a period of adjustment (curve  $C_3$ ).

With the passage of time, the lateral pressures relax to those indicated by the solid triangles in Figs. 44.8a and 44.8b, and as represented by the line  $de$  in Fig. 44.8b.

The various steps represented by the lines  $ab$ ,  $bc$ , and  $cd$  (Fig. 44.8b) can be quantified by calculation. Placement of the first lift starts the loading along the  $K_{op}$  line (Article 16.5). During compaction, the effective vertical and effective horizontal stresses increase. The increases can be computed by means of linear-elastic stress distribution. When the compactor is removed, unloading progresses according to Eq. 16.6 in the form

$$\sigma'_h = K_m \left( \frac{\sigma'_{vm}}{\sigma'_v} \right)^{\sin \phi'_{cv}} \sigma'_v$$

where  $\sigma'_{vm}$  is the maximum effective vertical stress reached during compaction of the lift,  $K_m$  is the corresponding coefficient of lateral pressure,  $\sigma'_v = \sigma'_{vm} - \Delta\sigma'_v$  and  $\Delta\sigma'_v$  is computed from linear-elastic stress distribution. Placement of the second lift reloads the first lift along a recompression line having a slope  $\bar{K}_r$  (Eq. 16.4). According to an empirical relation for  $\bar{K}_r$  of densified or preloaded granular soils (Mayne 1989)

$$\bar{K}_r = 0.75(1 - \sin \phi')$$

from which

$$\Delta\sigma'_h = 0.75(1 - \sin \phi')\Delta\sigma'_v$$

Compaction of the second lift then loads the first, again approximately according to elastic stress distribution. The

compactor is removed and the process is repeated. The corresponding stress paths are illustrated in Fig. 44.8a. In Fig. 44.8b, each point such as  $d$  defines the stress condition in a lift  $j$  immediately after the completion of the entire backfill consisting of  $n$  lifts ( $n = 25$  in Fig. 44.8b). It also represents a point on the compaction stress paths of other lifts when the  $(n-j)$ th lifts from the current surface of the backfill were subjected to the placement and compaction of a new lift. For example, for the backfill in Fig. 44.8b, consisting of 25 lifts, point  $d$  defines the stress condition at middepth of lift number 22 immediately after the completion of the backfill. It also represents the stress condition in the 4th lifts from the current surfaces of the backfill when the fill was subjected to the placement and compaction of a new lift.

During compaction, the soil is subjected to shear stresses. The upper limiting stress condition is defined by the  $K_p$  line according to

$$K_p = \tan^2 \left( 45 + \frac{\phi'}{2} \right)$$

The  $K_{op}$  line is the lower limit for  $\sigma'_h$ . Since compaction introduces shearing stresses that move the point representing the state of stress away from the  $K_{op}$  stress condition, the compaction-induced horizontal stresses decrease from  $d$  to  $e$  under the subsequent laterally constrained condition according to the empirical relation (Mesri and Hayat 1993b)

$$K_o = K_{op} + \frac{K_{ps} - K_{op}}{2.5} \frac{K_p}{3} \quad (44.1)$$

where  $K_{ps}$  and  $K_0$  are equal to  $\sigma'_h/\sigma'_v$  at points  $d$  and  $e$ ,

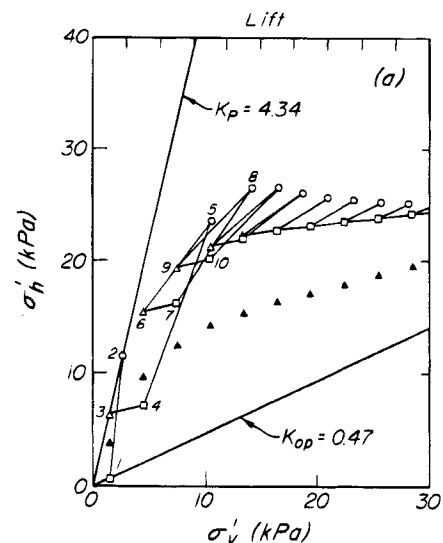


**Figure 44.8a** Effective stress paths during placement and compaction of fill shown in (b). Stress path of each lift starts at  $\sigma'_v = 0$  and ends at  $\sigma'_v$  corresponding to final depth of that lift.

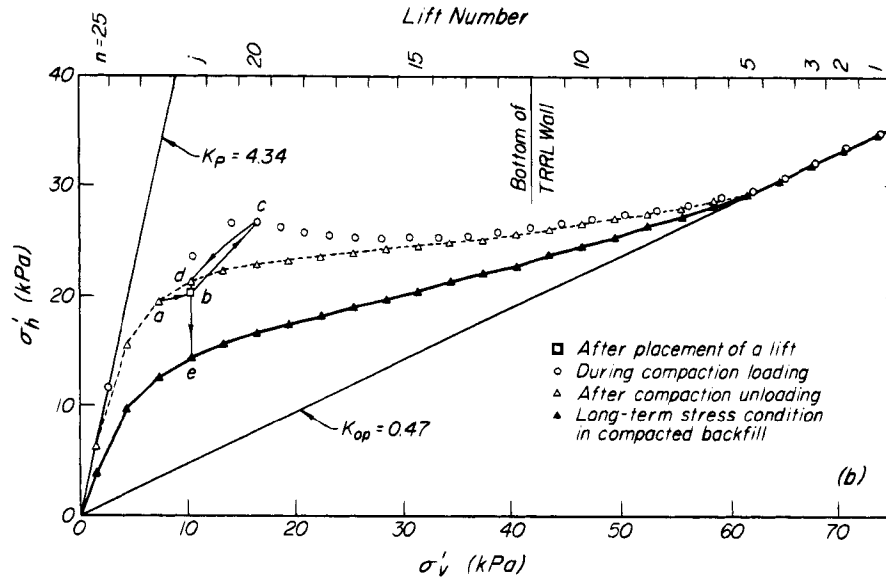


**Figure 44.8b** Horizontal pressure of sand backfill on nondeflecting wall during placement of lift (ab), during compaction (bc), immediately after compaction (cd), and postcompaction (de).

respectively. Laboratory test data and field observations suggest that when the soil is then maintained under a laterally constrained condition, the point representing its state tends to move toward the  $K_{op}$  line. If, for example, the effective vertical stress following passive shear is maintained constant under a laterally constrained condition, the effective horizontal stress decreases toward that represented by the  $K_{op}$  line. A soil subjected to shearing stresses leading to a state differing from that represented by the  $K_{op}$  line comes to equilibrium at a value of earth pressure at rest, defined by Eq. 44.1, somewhere between those defined by  $K_{op}$  and an earth pressure coefficient  $K_{ps}$  corresponding to the maximum preshearing stress condition represented by point *d* and by the open triangles in Fig. 44.8b.

The compaction history of the first lift during the entire filling operation includes the compaction history of all the lifts in the completed backfill. When the filling operation begins, the first lift is the top lift, and when it ends, the first lift has become the bottom lift. During the filling operation the first lift experiences the stress history of every intermediate lift. Therefore, a single computation and tabulation of the stress conditions at middepth of the first lift during the entire filling operation provides the compaction-induced lateral pressure profile for the completed backfill. The profile in Fig. 44.8 actually corresponds to a particular test installation known as the TRRL wall (Carder et al. 1977). Its sand backfill had a unit weight of  $20 \text{ kN/m}^3$ ,  $\phi'_{cv}$  of  $32^\circ$  and  $\phi'$  of  $39^\circ$ . It was placed in 0.15 m lifts, and was compacted by means of an 1800 kg/m vibratory roller 0.9 m long, operating parallel to and 0.15 m distant from the wall. It consisted of 14 lifts, as indicated by the location of the bottom of the

wall in Fig. 44.8b. There was good agreement between the computed and measured lateral pressures against the top half of the wall. However, the computed pressures were larger than those measured against the bottom half, because the actual wall was not nondeflecting (Mesri and Hayat 1993a). Figure 44.8b shows that, after completion of the backfill,  $K_0$  in the first lift was 0.59 and in the next-to-last lift was 2.27.

### 44.3 Compaction of Soils in Place

#### 44.3.1 Procedures and Equipment

If the soil to be compacted is already in place, only about the uppermost meter can be compacted by rollers. The remainder must be treated at depth. The most appropriate method depends primarily on the properties of the soil. Some methods are suitable for a wide variety of soil conditions, others for a limited range. In the following paragraphs the principal procedures are described and the conditions for their successful use are defined. The procedures include vibration combined with water jetting (vibroflotation or vibrocompaction); vibration produced by explosives; the impact of falling weights (dynamic consolidation); pile driving, sand piles and stone columns; and preloading or surcharging with or without sand drains.

#### 44.3.2 Vibration Combined with Water Jetting

Deep deposits of loose clean sand either above or below water table can be compacted effectively by *vibroflotation* (Steuerman 1939). The equipment includes a cylindrical probe containing an eccentric weight, rotating about a vertical axis, which imparts a horizontal vibration to the probe. Water jets direct water downward at the bottom

and outward near the top of the probe. In operation, the probe attached to a follow-up pipe is suspended from a crane, the vibrator actuated, and the bottom water jets turned on. As the vibrating probe is lowered under its own weight the sand around it subsides within a cylindrical zone.

When the required depth of penetration is reached the bottom water jets are turned off and the upper ones turned on. The upward flow maintains a space between the follow-up pipe and the sand. The probe is raised about 0.3 m and vibration is continued for 30 to 60 s while sand is shoveled into the annular space. These operations are repeated until, in this manner, a densified column of sand is formed. Depths as great as 20 m have been treated to achieve final relative densities of 70 to 75%.

The probes in general use (Brown 1977) have a diameter of about 0.4 m and a length of about 1.8 m, have a mass of about 2000 kg, and are connected to follow-up pipes 0.3 m in diameter. The units generally used produce a centrifugal force of 100 kN at 30 rps and a corresponding amplitude of horizontal movement of about 15 mm when unrestrained. The flow of water may reach  $10^{-2}$  m<sup>3</sup>/s at a pressure of 1000 kPa. The influence of these units extends in clean sands to a radial distance of nearly 2 m. More powerful units are available that produce a centrifugal force at 30 rps of 180 kN, experience an amplitude of horizontal movement of about 30 mm when unrestrained, use up to  $2.5 \times 10^{-2}$  m<sup>3</sup>/s of water at a pressure of 1000 kPa, and influence the sand to a distance of nearly 3 m.

Vibroflotation is most effective in compacting very loose sands having grain-size distributions falling entirely within zone B (Fig. 44.9) (Brown 1977). Clay layers, excessive fines, cementation, and organic matter reduce the effectiveness. Soils with distributions falling entirely in zone C are difficult to compact. Gravel (zone A), or a deep water table, reduces the normal penetration rate. Experience and skill are required to supply sand at such a rate that the vibroflot will neither become stuck nor hang loose in the hole and fail to transmit the vibrations to the sand.

A somewhat similar procedure uses a probe consisting of a pipe attached to a vibratory pile driver-extractor. The assemblage is designated by the trade name Terra-Probe. On one project the driver operated at 15 Hz and produced unrestrained 10 to 25 mm vertical vibrations of an open-ended steel pipe 14 m long having a diameter of 760 mm and a wall thickness of 9.5 mm. Circumferential steel bands 150 mm wide and 13 mm thick were spaced at 2-m intervals along the outside of the pipe. The total mass of the probe was 9070 kg. Three water jets, consisting of pipes welded to the side of the probe, were activated while the probe was lowered and then while it was removed slowly with continual vibration.

By this procedure the soil within and immediately outside the pipe is compacted. Depths to 20 m have been treated. In one comparison with the more powerful of the two vibroflotation units described above, it was found that the rate of penetration and extraction of the Terra-Probe was about 4 times as rapid as that of the vibroflot, but about 4 times as many probings were required to obtain similar average relative densities (Brown and Glenn 1976). The materials for which the procedure is suitable are the same as for vibroflotation.

#### 44.3.3 *Compaction Induced by Explosives*

Deposits of loose clean sands below water table have been compacted by detonating charges of explosives at various depths. Although two of the earliest applications of the method were carried out in the United States at Franklin Falls and Denison dams in 1941, most of the development has been conducted by Russian engineers (Ivanov 1972). Shock waves from the detonations temporarily liquefy the sand (Article 20.9) and destroy its original structure, whereupon the grains rearrange themselves in a denser state as the excess water drains away under the influence of the weight of the overlying sand. Increasing the intensity of the charges affects a greater volume of sand but does not increase its compactness; successively exploding smaller charges at the same points, allowing time for drainage between detonations, is much more effective. The charges should not be large enough to cause a breakthrough to the surface. Design of a compaction program requires selection of the depth and spacing of the charges, the size of the charges themselves, and the interval between charges.

At Karnafuli dam a large scour-hole having a volume of 50,000 m<sup>3</sup> was filled by dumping into water a uniform clean sand ( $D_{10} = 0.18$  mm,  $C_u = 2$ ) and compacting the sand by the explosion of a series of charges of 30% special gelatin dynamite, usually of 3.6 kg each, at depths of 3, 6, and 11 m below the surface of the sand. The holes were spaced 6 m horizontally. The lowermost charges were fired first, followed at intervals of 4 hours by the middle and upper charges; a fourth series was then placed and fired at a depth of 4.5 m. The porosity of the sand was reduced from 47 to 43% (Hall 1962).

#### 44.3.4 *Compaction by Dropping Weights*

The systematic dropping of weights on an area is often an effective and economical method of compacting loose underlying materials. The technique is patented and is known as *dynamic consolidation* or *dynamic compaction*. For most applications a mass of about 15 tonnes having a base area of about 4 m<sup>2</sup> is dropped from a height of about 20 m by an ordinary construction crane. The points of impact are usually laid out on a square pattern ranging from  $5 \times 5$  to  $10 \times 10$  m, and 10 or 12 drops are made at each point. The craters are filled and the procedure

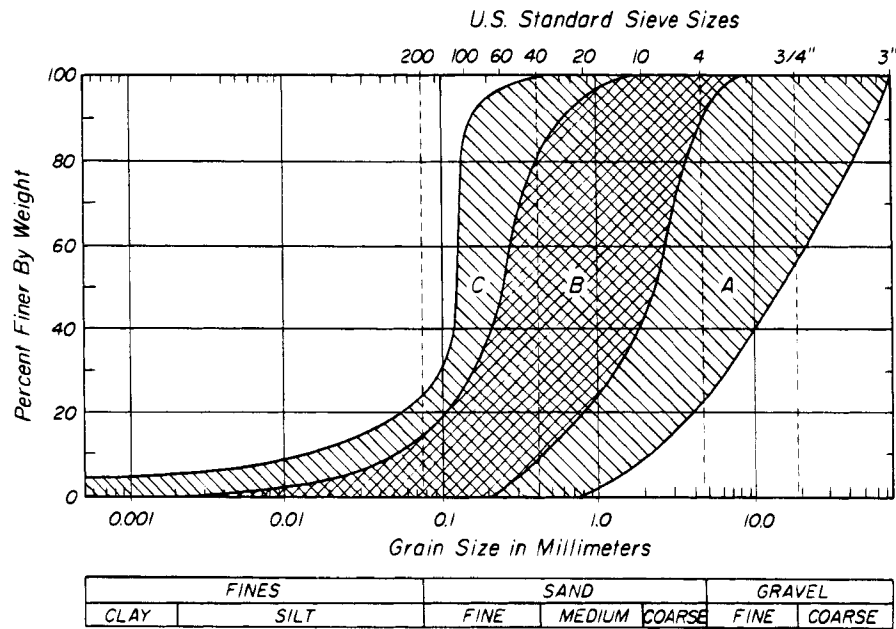


**Figure 44.9** Relation of grain-size distribution of soils to suitability of vibroflotation for compaction. Soils most suitable represented by zone B. Gravels of zone A reduce penetration rate. Soils of zone C are difficult to compact (after Brown 1977).

repeated once or twice after intervals that permit dissipation of some of the excess porewater pressures that may have been created. On the last pass the distance between points of impact is sometimes decreased to produce more uniform compaction of the upper materials, but the upper 1 or 2 m generally require compaction by other means.

The procedure has been used successfully to compact fills containing refuse; it is particularly effective in reducing the voids in trash including boxes, containers, and other debris of low density above the water table (Charles et al. 1981). It has also been used to densify collapsible soils such as loess or colluvium above the water table. If the soils are below water table the procedure creates excess pore pressures that require time for dissipation. The results of tests on a sandy deposit below water table in Yokohama are shown in Fig. 44.10. A 6.4-tonne weight was used with a square grid of 7 m according to the schedule shown in the figure.

In fine-grained soils trenches filled with permeable materials have in some instances been constructed before compaction to facilitate drainage. It has been claimed that use of dynamic compaction in clays leads to the formation of fissures that provide rapid drainage, but the benefits and possible mechanism are controversial; moreover, pore-pressure dissipation and settlement continue for some time after the treatment has been completed.

The depth to which compaction is effective has been estimated at  $D = \sqrt{WH}$ , where  $D$  and  $H$  are, respectively, the depth of compaction and height of fall in meters, and  $W$  the mass in tonnes (Ménard and Broise 1975). How-

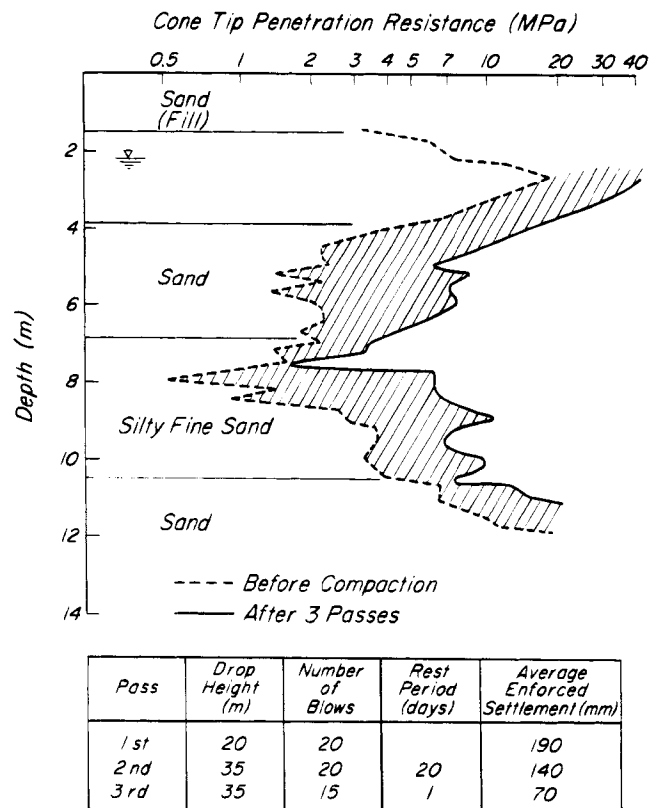


**Figure 44.10** Results of dynamic compaction of sand deposit in Yokohama (courtesy L. Menard).

ever, most investigators have found that the depth of compaction is from 0.5 to 0.8 times the value given by this expression (Mayne et al. 1984). To achieve depths on the order of 40 m, equipment has been built capable of dropping masses as great as 172 tonnes, with base areas of 20 m<sup>2</sup>, from heights of 40 m.

#### 44.3.5 Pile Driving, Sand Piles, and Stone Columns

Cohesionless sands are compacted by the vibrations produced at depth by pile driving. When piles are driven into loose sand, the ground surface between the piles commonly subsides in spite of the displacement of the sand by the piles. In one instance, after cast-in-place concrete piles 14 m long were driven at 1-m centers into fine sand below the water table, the ground surface subsided as much as 1 m, although the volume of the piles was equivalent to a 0.3-m layer. The pile driving reduced the porosity of the sand from about 44 to about 38%.

Sandy soils with some cohesion and cohesive fills can also be compacted by pile driving. However, the compaction of such soils is caused not by the vibrations associated with the driving, but by static pressure which decreases the size of the void spaces. If the soil is located above the water table and the voids are largely filled with air, the compacting effect of pile driving is commonly very satisfactory. However, if the soil is located below the water table, the effect decreases rapidly with decreasing permeability of the soil.

Soft silt below the water table is transformed by pile driving into a semiliquid state. Hence, instead of inducing compaction, pile driving weakens the soil at least temporarily. The compaction of such strata can be accomplished only by some process of drainage, by surcharging, or by a combination of the two.

Because the piles driven for compaction may serve no useful purpose after the compaction is accomplished, or under some conditions may deteriorate, *sand piles* are sometimes used in place of structural piles. A casing with a hinged or detachable end plate is driven to accomplish the densification, filled with sand, and then withdrawn. To force the sand from the casing it may be necessary to cap the casing and introduce compressed air beneath the cap. The pile spacing is usually 3 to 5 diameters. In soils of low permeability the sand piles also serve as drains to accelerate consolidation.

Sand piles are an inherent by-product of densification by vibroflotation or use of the Terra-Probe in cohesionless soils. The vibroflot has also been used to improve weak cohesive soils such as insensitive clays, organic silts, and peats by installing *stone columns*. The vibroflot is lowered through the weak stratum as described for sands. It may be necessary to raise and lower the tool repeatedly while jetting to clean out cohesive cuttings. Backfill is then introduced into the hole in stages; after each stage of

about 1 m the probe is inserted and the fill displaced into the parent soil by vibration. At any stage, filling and vibration are continued until no more fill can be absorbed. In this way a granular column about 0.8 to 1.1 m in diameter is created with its greatest diameter in the softest soils. Various sizes of backfill material have been used; a common selection is a well-graded angular material with maximum size of 150 mm and not more than about 10% smaller than 10 mm. The lateral pressures associated with the compaction induce consolidation of the surrounding material. The spacing is usually from 1.5 to 3 m, but depends on the type of structure and the loading to which the treated soil will be subjected. In some instances the granular columns are considered to be load-carrying units, but methods of estimating the degree of interaction of the columns and the surrounding soil are not yet fully satisfactory (Baumann and Bauer 1974, Thorburn 1975).

#### 44.3.6 Preloading or Surcharging without or with Vertical Drains

Compressible soils such as soft clays, loose silts, and most organic soils may be consolidated by *surcharging* or *preloading*. The area to be treated is covered by a fill having a weight per unit area great enough to consolidate the soil sufficiently to increase its strength or reduce its compressibility to the required extent within the time available for the preloading operation. Because the preloading should compress the soil without causing any significant undrained shear distortion, the magnitude and rate of preloading are designed to provide an adequate factor of safety against undrained failure during the operation. The single most important subsurface information required for proper planning and implementation of a preloading program is the preconsolidation pressure  $\sigma'_p$  profile of the compressible soil (Article 16.4). The undrained shear strength for stability analysis may be determined from  $s_u(\text{mob}) = 0.22 \sigma'_p$ . The preloading is usually done in stages. During each stage,  $s_u(\text{mob}) = 0.22 \sigma'_v$  as soon as the effective vertical stress  $\sigma'_v$  exceeds the preconsolidation pressure  $\sigma'_p$  (Articles 20.5 and 20.6). The value of  $\sigma'_v$  during preloading is determined from  $\sigma'_v = \sigma'_{v0} + \Delta\sigma'_v$ , where  $\sigma'_{v0}$  is the preconstruction *in situ* effective vertical stress and  $\Delta\sigma'_v$  is a function of preload level and degree of primary consolidation.

To eliminate postconstruction primary settlements, the effective vertical stress  $\sigma'_v$  throughout the compressible stratum during preloading must become at least equal to the  $\sigma'_{vf}$  expected under the permanent structure. When the intention is to minimize postconstruction secondary settlements, a surcharge is applied to preconsolidate the soil and is subsequently removed. Therefore, the surcharging in effect produces a preconsolidation pressure  $\sigma'_{vs}$  greater than  $\sigma'_{vf}$ . A surcharge ratio,  $R'_s = (\sigma'_{vs}/\sigma'_{vf}) - 1$  is selected

to achieve the required limit on long-term secondary settlements (Article 16.7).

Preloading of embankment construction for roads and airfields, where the fill is incorporated into the permanent structure, is done mainly to accelerate primary consolidation before paving; some surcharge may be added to minimize long-term secondary settlements. The most efficient method for decreasing the time required for primary consolidation is the use of vertical drains (Article 25.5). In some preloading operations the primary settlement under the permanent load  $\sigma'_{vf}$  is accelerated by applying a surcharge in excess of  $\sigma'_{vf}$  and removing it during primary consolidation. This approach has the disadvantage that it may contribute to undrained instability during preloading. It requires careful analysis of the time rate of primary consolidation, together with field settlement and porewater pressure observations, to ensure that  $\sigma'_v$  becomes at least equal to  $\sigma'_{vf}$  throughout the compressible stratum. It also involves a much more complex method of analysis of postconstruction secondary settlements (Mesri and Feng 1991).

Preloading with earth or rockfill, water load, concrete or steel blocks, or vacuum, without or with vertical drains, is also carried out before construction of permanent structures such as buildings and storage facilities. The preload, which is later completely removed, can be selected so as to achieve any degree of primary compression before construction of the permanent structure or to put any limit on the magnitude of long-term secondary settlements. Economical and efficient preloading programs for important projects require detailed subsurface information on permeability and compressibility of the compressible stratum (Articles 14 and 16) and reliable analysis of the time rate of consolidation (Article 25).

Silty soils containing lenses or layers of sand are likely to consolidate almost as rapidly as the preload can be applied, but much longer times may be required for more impermeable soils. The rate of consolidation can be calculated by means of the theory in Article 25. If the compressible profile includes horizontally discontinuous isolated layers or lenses of sand, the estimates of rate of consolidation may be very unreliable, because the spacing and degree of continuity of the more pervious drainage layers cannot usually be accurately assessed.

If the estimated rate of primary consolidation is too slow, the natural drainage layers are often supplemented by the installation of vertical drains. These may consist of *sand drains*, fabric-encased sand drains also known as *pack drains*, or of *prefabricated wick* or *strip* or *band drains*. The drains are spaced in triangular or square patterns at 1 to as much as 4 m. Sand drains are similar to sand piles and commonly have diameters in the range of 300 to 500 mm. Pack drains with diameters in the range of 100 to 400 mm have been used. Most prefabricated vertical drains have a rectangular cross-section con-

sisting of a plastic core with a nonwoven geotextile filter cover. Typical dimensions of 3.2 to 4.0 mm by 93 to 100 mm lead to values of equivalent diameter for wick drains in the range of 62 to 66 mm. The plastic cores are typically grooved, corrugated, or have a pattern of protruding studs that provide vertical flow channels and support the filter sleeve. The filter sleeve separates the core channels from the soil and permits pore water to enter the drain. The filter sleeve is intended to keep the surrounding soil out of the core channels without being clogged by fine particles that may go into suspension in the smear zone. It must also have sufficient stiffness not to be pressed into the core channels by the effective horizontal pressure in the ground, and must remain biochemically nondegradable during the time required to complete primary consolidation.

Nondisplacement methods of vertical drain installation, for example by jetting, subject the soil to little disturbance, but they are generally uneconomical. Displacement methods are most widely used for both sand, sand pack, and wick drains. A hollow steel mandrel, with the end closed, is either pushed or vibrated at a rate of 0.2 to 0.6 m/s to the required depth in the ground. Both static and dynamic installation rigs of various types, from conventional piling rigs to quite specialized equipment, have been used to install wick drains to depths of more than 30 or 40 m (Hansbo 1994). For sand drains and pack drains, the vertical hole is filled with a clean sand, such as concrete sand with  $D_{10}$  in the range of 0.15 to 0.35 mm as the mandrel is withdrawn. The wick drain is pulled into the ground inside the mandrel that protects the drain during installation. An anchor attached to the tip of the drain holds the wick drain in the ground as the mandrel is withdrawn (Hansbo 1994). The degree and radial extent of soil disturbance depend on the amount of soil that is displaced and, therefore, on the radius of the mandrel,  $r_m$ . Data collected by Lo (1991) suggest that the radius  $r_s$  of the smear zone, expressed in terms of  $r_s/r_m$ , has values in the range of 2 to 4.

Before the preloading fill is placed above the area occupied by the drains, a pervious drainage blanket must be laid down to permit escape of the water emerging from the drains. Whether sand drains are present or not, the preloading fill should not be built up so rapidly or with such steep slopes that a slide or base failure occurs; otherwise, if drains are present, they are likely to become discontinuous and to be rendered ineffective. To avoid such slides, preloading and sand-drain installations are provided with means for observing the settlement of the surface of the soil supporting the preload, the porewater pressures in the subsoil, and the heave or lateral movement of the natural ground beyond the limits of the preload.

## 44.4 Other Methods of Ground Improvement

### 44.4.1 General

Compaction and surcharging are widely practiced and are generally understood by civil engineers and constructors. Most other methods of ground improvement require specialized knowledge in fields other than soil mechanics. They are discussed briefly in the following subsections. More detailed information may be found in the selected readings listed at the end of the article.

### 44.4.2 Injection

Grouting consists of injecting a suspension or solution into the voids of a soil, whereupon the injected materials harden. In most practical applications the objective is to decrease the permeability of the soil; cement, cement-bentonite, clay, and chemical grouts are used for this purpose. The requirements of such grouts are discussed in connection with dam foundations (see Chapter 11). Chemical grouts, especially silicates, are also used to impart cohesion to soils to reduce the danger of runs and subsidences associated with open excavation and tunneling. The approximate ranges of grain size in which various grouts are applicable are shown in Fig. 44.11 (Mitchell 1970).

### 44.4.3 Electro-Osmosis

The principles involved in this method are described in Article 15.7. The most effective application has been in the temporary stabilization of slopes in silts while excavation proceeds below groundwater level. Because silts are too fine to be drained by ordinary dewatering techniques and often possess low undrained strengths, open excavation may be treacherous. By arranging elec-

trodes as shown in Fig. 44.12*b* the seepage may be induced to flow away from the face of the excavation. The seepage pressures then increase the stability of the slope instead of decreasing it (Casagrande 1953, 1962). The stability is, however, vulnerable to an interruption in the power supply, and the shrinkage cracks associated with the consolidation inherent in the phenomenon may be disadvantageous.

### 44.4.4 Freezing

Thawing and degradation of permafrost are readily induced by the apparently minor changes in thermal regime caused by construction activities. The effect on highway subgrades or the subsoil supporting building foundations or pipelines may be devastating. Consequently, in much construction in permafrost areas positive measures are adopted to maintain the subsoil in a frozen state. For example, because piles, which may be necessary for support of structures, readily conduct heat into the permafrost, special devices have been developed to induce freezeback during winter and impede the access of heat during the summer (Long 1964). The skin friction that supports the piles consists largely of the adhesion of ice; if the ice becomes warm the adhesion decreases and the pile settles. Many of the fundamental and practical studies in this field have been carried out by engineers of the USSR (Tsytoich and Sumgin 1937) and Canada (Crawford and Johnston 1971).

The strength and impermeability of frozen ground have led to artificial ground freezing as an aid to excavation below groundwater level in permeable soil and rock, especially for the construction of deep shafts. The procedure is expensive and is rarely justifiable economically unless more conventional methods are impractical on account of specific site conditions. Pipes, usually vertical, are installed at close spacing for circulation of cold brine. Windows between pipes that deviate from their planned position can lead to dangerous conditions. Sufficient time must be allowed before excavation to ensure that the ground is frozen (Sanger 1968).

### 44.4.5 Heating

Thick deposits of unsaturated loess and weak clays have been stabilized in Eastern Europe and the USSR by heating them for 8 to 10 days at temperatures of 600° to 1000°C. Drill holes spaced at about 3 m, with diameters of 0.15 to 0.20 m and depths up to about 15 m, have been sealed and filled with a controlled mixture of air and burning liquid or gas under a pressure of 0.25 to 0.50 atm (Litvinov 1960). The heat produces irreversible changes in loess, including increase in strength and decrease in tendency to collapse and compress. Treatment has competed economically with pile foundations for large structures.

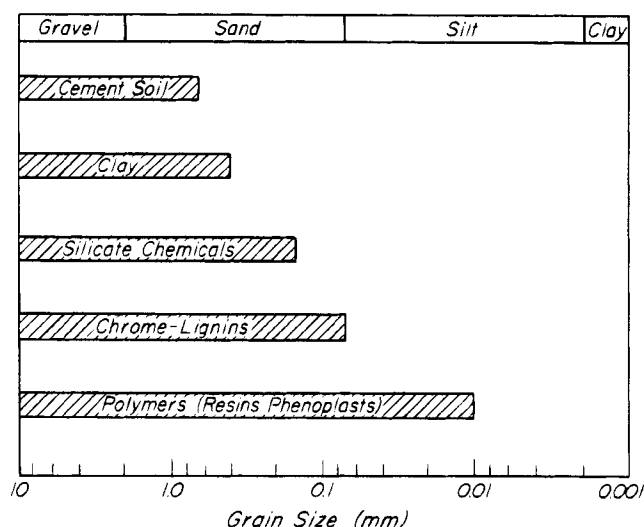
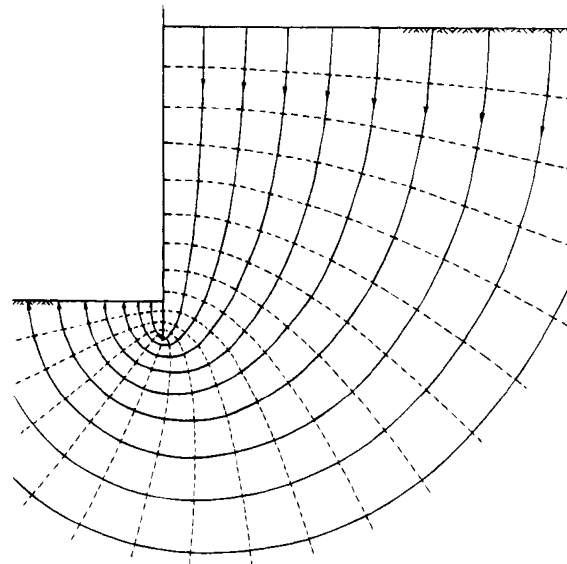
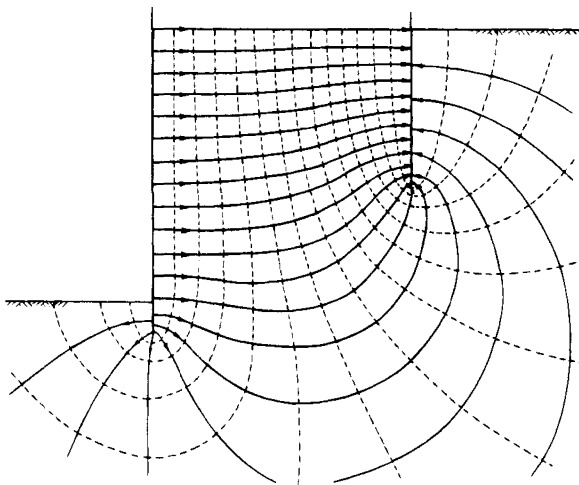


**Figure 44.11** Ranges of grain size in which different types of grout are useful (Mitchell 1970).

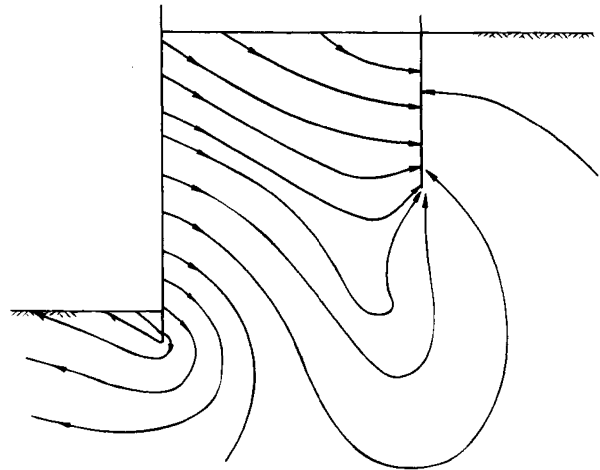




(a) Hydraulic Flow Net



(b) Electro-osmotic Flow Net



(c) Combined Hydraulic and Electro-osmotic Flow Lines

**Figure 44.12** Flow nets illustrating difference in flow patterns toward excavation under (a) gravity flow; (b) electro-osmotic flow; (c) combined gravity and electro-osmotic flow (after Casagrande 1956).

#### 44.4.6 Chemical Additives

Chemical soil stabilization is an extensive field requiring specialized knowledge beyond the scope of soil mechanics. Its principal applications are in highway and airfield engineering. Among the most widely used additives are Portland cement and lime; the latter is generally effective in reducing the plasticity, compressibility, and swelling potential of clays. In most instances the additive is mixed as intimately as is practicable with the soil, whereupon the soil is placed and compacted in layers. Relatively few instances of successful treatment of soil *in situ* have been reported. In Sweden, lime columns have been formed in soft clay by mixing the clay with unslaked lime. The lime

is introduced through the hollow stem of a rapidly rotating auger as the auger is retracted. Columns up to 10 m deep with diameters of 0.5 m, spaced about 1.4 m, were effective in reducing the settlement sufficiently to support light buildings without the pile foundations ordinarily required (Broms and Boman 1979).

#### Selected Reading

A summary of the principal techniques and their applicability is to be found in Moseley, M. P., ed. (1993). *Ground Improvement*, London, Chapman and Hall. Although a

short book (218 pp.), the treatment is thorough and authoritative. The references are a valuable supplement.

"Construction of Fills", 2nd ed., by Edward J. Monahan (New York, John Wiley and Sons, 1994), although intended for practical construction workers, contains much valuable advice and insight concerning the need for compaction, the pitfalls to be avoided, and the human interactions that influence the quality of the completed works.

Several conferences devoted to ground improvement have resulted in publications containing much valuable and detailed information. These include:

- "Placement and Improvement of Soil to Support Structures," Soil Mechanics and Foundations Division ASCE, 1968, 440 pp.
- Ingles, O. G., and J. B. Metcalf (1973). *Soil Stabilization: Principles and Practice*, New York, John Wiley & Sons, Inc., 374 p.
- Proc. of ASCE Symp. on Soil Improvement: History, Capabilities and Outlook*. Report by the Committee on Placement and Improvement of Soils of the Geotech. Eng. of the ASCE (1978), 182 p.
- Proc. International Conference "On Compaction," École Nat. des Ponts Chauss., Paris, 1980.
- Mitchell, J. K. (1981). "Soil improvement—state-of-the-art," *Proc. 10th Int. Conf. Soil Mech. Found. Eng.*, Stockholm, 4, pp. 509–565.
- "Grouting in Geotechnical Engineering," ASCE, 1982, 1018 pp. *Proc. Eighth European Conf. Soil Mech. Found. Eng.* Helsinki, 1983. Conference devoted largely to compaction.
- Proc. of ASCE Symp. on Soil Improvement: A Ten Year Update*, J. P. Welsh, ed., Committee on Placement and Improvement of Soils, Geotech. Special Publ. No. 12 (1987).

## COMPACTION BY ROLLERS

- Hilf, J. W. (1975). "Compacted fill." Chap. 7 in *Foundation Engineering Handbook*, Winterkorn, H. F., and H. Y. Fang, eds., Van Nostrand Reinhold, New York, 244–311.
- Yoo, T-S, and E. T. Selig (1979). "Dynamics of vibratory-roller compaction," *J. ASCE*, **105**, GT10, pp. 1211–1231.

## VIBROFLOTATION AND TERRA-PROBE COMPACTION

- Brown, R. E., and A. J. Glenn (1976). "Vibroflotation and Terra-Probe comparison," *J. ASCE*, **102**, GT10, pp. 1059–1072.

## COMPACTION BY EXPLOSIVES

- Ivanov, P. L. (1972). "Compaction of noncohesive soils by explosives," Trans. for USBR, published by Indian Nat'l. Sci. Doc. Centre, New Delhi, 211 pp.

## COMPACTION BY DROPPING WEIGHTS

- Mayne, P. W., J. S. Jones Jr., and J. C. Dumas (1984). "Ground response to dynamic compaction," *J. ASCE*, **110**, GT6, pp. 757–774.

## SURCHARGING

- Hansbo, S., M. Jamiołkowski, and L. Kok (1981). "Consolidation by vertical drains," *Géot.* **31**, No. 1, pp. 45–66.
- Mesri, G., and T. W. Feng (1991). "Surcharging to reduce secondary settlement," *Proc. Int. Conf. Geotech. Eng. Coastal Development—Theory to Practice*, Yokohama, **1**, pp. 359–364.
- Mesri, G., and D. O. K. Lo (1991). "Field performance of prefabricated vertical drains," *Proc. Int. Conf. Geotech. Eng. Coastal Development—Theory to Practice*, Yokohama, **1**, pp. 231–236.
- Ladd, C. C. (1991). "Stability evaluation during staged construction," *J. Geotech. Eng., ASCE*, **117**, No. 4, pp. 540–615.

## OTHER METHODS

- Mitchell, J. K. (1970). "In-place treatment of foundation soils," *J. ASCE*, **96**, SM1, pp. 73–110. Extensive list of references.
- Aboshi, H., Y. Mizuno, and M. Kuwahara (1989). "Present state of sand compaction piles in Japan," *Proc. Deep Foundation Improvements: Design, Construction, and Testing*, ASTM STP 1089, pp. 32–46.

## CHAPTER 8

# Earth Pressure and Stability of Slopes

### ARTICLE 45 RETAINING WALLS

#### 45.1 Function and Types of Retaining Walls

Retaining walls are structures that support soils at slopes steeper than their angle of repose. Before the advent of reinforced concrete, most retaining walls consisted of stone masonry or mass concrete. Because their resistance to earth pressure was derived from their own weight, they were known as *gravity walls* (Fig. 45.1a). With the introduction of reinforced concrete, *semigravity*, *cantilever* (Fig. 45.1b), and *counterfort* walls came into use and were the dominant types well into the 1980's. The stability of these walls is derived not only from their own weight but also from the weight of backfill resting on their bases. The lateral thrust of the earth pressure is resisted by the structural strength of the wall and is ultimately transmitted by the base of the wall to the foundation material. Concurrently with structural walls, *crib walls* were also used extensively. They consist of interlocking elements of timber, metal, or precast concrete arranged in the form of bins usually filled with granular soil similar to that used as backfill for the wall. Unlike structural walls, crib walls gain their stability not only from their weight but also to some extent from the strength of the fill within the bins.

Although the foregoing types of retaining walls are still in wide use, an increasing fraction of retaining walls since the mid-1960's has consisted of reinforced soil, a composite material in which the soil and reinforcement form a stable unit capable of resisting the backfill pressures and transferring them to the foundation (Fig. 45.1c, d). The soil is compacted in layers between which are placed the reinforcing elements that may consist of steel bars or grids, or of grids or sheets of various polymers. A facing attached to the reinforcement is required to prevent the fill from ravelling but is subject to virtually no pressure. Many types and arrangements of facing and reinforcement, some proprietary, have evolved since the introduction of the original patented system, known as *reinforced earth*, in France (Vidal 1966).

Structural, crib, and reinforced soil walls intended to retain existing slopes usually require excavating a notch into the base of the slope in which to build the wall. Temporary support of the back of the notch may be difficult and expensive, and permanent support is not achieved until the backfill is placed. If the material behind the original slope possesses at least modest frictional resistance, it may be supported by installing reinforcement behind the final slope as excavation proceeds from the top down. The reinforcement usually consists of approximately horizontal steel rods, known as *soil nails*, grouted into drilled holes or driven into the soil at close spacing and connected to a facing also installed as excavation proceeds (Fig. 45.1e). The soil is thus reinforced *in situ* without need to oversteepen the base of the slope temporarily. In contrast to *tiebacks* (Article 46.4), which consist of tendons or rods anchored in stable material well behind the potentially unstable mass of soil, soil nails transform the soil adjacent to the final slope into a unit that serves as the retaining structure.

Irrespective of the type of retention system, two requirements must be satisfied: the stability of the retention system as a whole must have an adequate factor of safety against sliding, overturning, or excessive settlement; and the retention system itself, whether a structural wall or a mass of reinforced soil, must have sufficient strength to withstand the forces to which it will be subjected. These two requirements are categorized as *external stability* and *internal stability*.

#### 45.2 Foundations for Retaining Walls

##### 45.2.1 Introduction

Experience has shown that most retaining wall failures are caused by inadequacy of the foundations. Because an adequate foundation cannot be designed without knowledge of the soil conditions beneath the base of the proposed wall, the subsoil must be investigated by procedures similar to those required for other soil-supported structures. The designer should also know the depth of frost

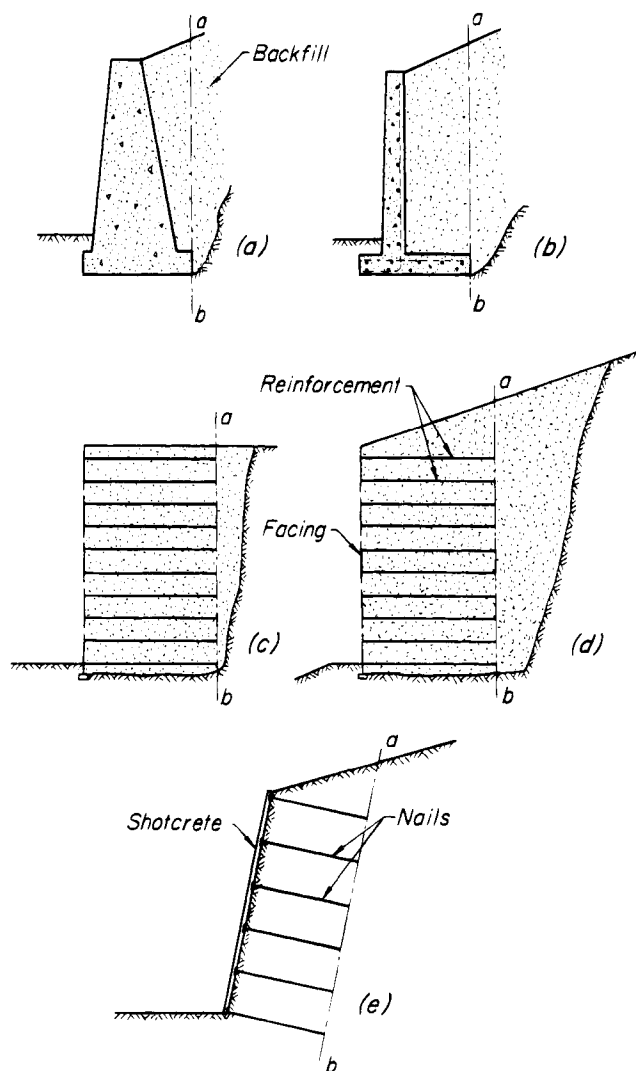


**Figure 45.1** Types of retaining walls: (a) Concrete gravity; (b) reinforced-concrete cantilever; (c) reinforced-soil supporting fill with horizontal surface; (d) reinforced-soil supporting fill with inclined surface; (e) slope supported by soil nailing.

penetration and the depth to which the soil is influenced by seasonal volume changes, so that the base of the foundation can be established below both of these depths (Art. 49).

Foundations for retaining walls must satisfy three conditions: the factors of safety against sliding and overturning must be adequate; the soil pressure beneath the toe of the foundation must be equal to or smaller than the allowable soil pressure (Article 50); and the differential settlement of the foundation must not be excessive.

#### 45.2.2. Safety against Sliding

Sliding of a retaining wall is resisted by the friction between the soil and the base and by the passive earth pressure of the soil in contact with the outer face of the

foundation. It is generally required that the factor of safety against sliding, equal to the horizontal resisting forces divided by the horizontal component of the backfill pressures, be at least 1.5.

The friction between the base and a fairly permeable soil such as a clean or silty sand is equal to the effective normal pressure on the base times the tangent of the friction angle  $\phi'$  between soil and base. In the absence of more specific data, the value of  $\phi'$  may be taken as  $30^\circ$  for a coarse-grained soil containing no silt or clay, and as  $24^\circ$  for a coarse-grained soil containing silt.

If the wall rests on silt or clay, special precautions are required. Immediately before the footing is cast, the soil, to a depth of about 0.1 m, should be removed over the area to be covered by concrete and replaced by a 0.1 m layer of well compacted sharp-grained sand or sand and gravel. The value of  $\phi'$  between the sand and the underlying soil can be assumed as  $20^\circ$ . However, if the undrained shear strength  $s_u$  of the underlying soil is less than the frictional resistance beneath any part of the base, the slip will take place by shear in the soil at some distance below the base. If the normal pressure increases from zero at the heel to  $\sigma'_v$  at the toe (as shown in Fig. 45.2a), failure between  $a_2$  and  $d$ , Fig. 45.2b, would occur by sliding along the contact between the sand layer and the underlying soil, and between  $d$  and  $a_1$  by undrained shear in the soil itself. If the pressure on the base has a uniform value  $\sigma'_v$  per unit of area, the sliding resistance per unit of area

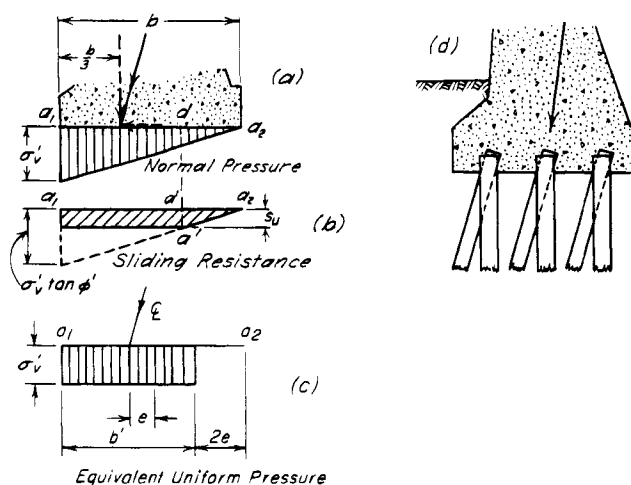


**Figure 45.2** (a) Approximate distribution of contact pressure on base of retaining wall if resultant force intersects base at outer third-point and subgrade remains elastic. (b) Diagram showing resistance to sliding if undrained shear strength of soil beneath base is less than the frictional resistance between base and underlying soil. (c) Diagram showing approximate equivalent uniform soil pressure beneath base of retaining wall subject to vertical component of loading with eccentricity  $e$ . (d) Base of retaining wall supported by vertical and batter piles.

of the base is equal to the smaller of the two values  $\sigma'_v \tan \phi'$  and  $s_u$ .

The second force that resists the sliding of the base is the passive earth pressure of the soil in front of the buried part of the wall. Within the zone of seasonal changes of moisture and temperature, the passive earth pressure is a rather unreliable resistance. The presence of root holes or shrinkage cracks may make the soil so compressible that the passive resistance does not become effective until the wall has advanced through a considerable distance. If the subsoil contains silt and the water table is close to the surface, ice layers may be formed during the winter in the upper part of the soil (Article 15.8). During the subsequent thaw the soil may become so soft that its passive resistance is negligible. Because of these possibilities, the passive earth pressure should be disregarded unless local conditions permit reliable evaluation of its lower limiting value.

If the factor of safety with respect to sliding cannot be raised to 1.5 without the construction of an excessively large or heavy foundation, it is likely to be more economical to establish the wall on a pile foundation containing batter piles driven at an angle to the vertical as shown in Fig. 45.2d. The vertical forces are carried by the vertical piles and by the vertical components of the loads in the batter piles, and the horizontal forces are carried by the batter piles. Vertical piles or drilled piers designed to resist lateral as well as vertical forces (Articles 52.6.2 and 53.5.9) are also sometimes used.

The practice of driving some of the piles beneath the foundations of retaining walls on a batter is by no means universal, because vertical piles can be driven more cheaply. However, because the resistance against horizontal displacement offered by the upper part of vertical piles in soft soil is very small, the absence of batter piles is likely to be associated with a gradual outward movement of the wall. If the weight of the backfill on a plastic subsoil exceeds about one-half the bearing capacity, progressive horizontal movement of the retaining wall or abutment is likely to be excessive, even if the foundation is provided with enough batter piles to resist the backfill pressure (Peck et al. 1948). Under these circumstances it may be necessary to substitute lightweight material for the ordinary types of backfill, or to alter the layout to eliminate the fill. Solid bridge abutments, for example, may be less desirable than open or spill-through abutments through which the backfill extends on a slope. The roadway in front of the slope is then carried on a structure instead of on fill.

### 45.2.3 Safety against Overturning

The factor of safety against overturning is determined by dividing the sum of the moments of forces tending to resist rotation of the wall about its toe by the sum of the

moments of forces tending to produce the overturning. A factor of safety of 2 is customarily required. In reality, this criterion seldom governs the design.

### 45.2.4 Allowable Soil Pressure and Settlement

If the resultant force of all the loads acting on the wall above its base intersects the base of the foundation at the outer third-point, the contact pressure on the base increases roughly from zero at the heel to twice the average pressure at the toe (Fig. 45.2a). Therefore, backfilling tends to produce an outward tilt of the wall. If the wall rests on a firm soil, such as a dense sand or a stiff sand-clay mixture, the tilt of the wall will be inconsequential if the pressure beneath the toe does not exceed the allowable pressure for the given soil (Article 49.4). On the other hand, if the wall rests on a very compressible soil such as soft clay, the tilt can become very large. Progressive consolidation of the clay beneath the toe may increase the tilt for many years. The increased tilt causes the center of gravity of the wall to advance and the soil pressure under the toe to increase further, until finally the wall may fail by overturning. Hence, if a wall rests on a very compressible soil, the foundation should be designed in such a way that the point of application of the resultant pressure is located close to the midpoint of the base.

The triangular distribution of soil pressure shown in Fig. 45.2a is actually an extreme condition unlikely to develop because of yielding of the soil beneath the toe. A convenient approximation, Fig. 45.2c, is to assume that the contact pressure is uniformly distributed over an area extending from the toe over a distance  $b' = b - 2e$ , where  $b$  is the width of the base and  $e$  is the eccentricity of the point of application of the resultant load on the base. This approximation, developed for calculating the bearing capacity of foundations under eccentric load (Meyerhof 1953), will also be found useful in calculating the stability of reinforced-soil walls (Article 45.5.2).

If a retaining wall serves as a bridge abutment, a tilt of the wall changes the clearance between the abutments. Under extreme conditions the clearance may decrease until the superstructure acts as a spacer, or it may increase until it exceeds the span of the superstructure. An increase in clearance is likely to occur if the backfill is underlain by a fairly thick layer of compressible soil such as peat or soft clay. Under the weight of the fill the layer compresses, and the area beneath the backfill settles. Because the abutment is located near the edge of the loaded area, its base becomes inclined, and the wall tilts toward the backfill. The backward tilt due to this cause may be much greater than the forward tilt caused by the pressure of the backfill.

These considerations indicate that the foundation of a retaining wall requires even more careful attention than that of an ordinary building. The general principles that

govern the design of foundations are discussed in Chapter 9.

### 45.3 Backfill of Retaining Walls

#### 45.3.1 Materials

The term backfill refers generally to all the materials supported laterally by the retaining structure. Behind concrete walls it includes the fill between the wall and the vertical section  $ab$  (Fig. 45.1a, b), as well as the fill beyond  $ab$ . If the wall consists of reinforced soil, the backfill is regarded as only that material beyond  $ab$ ; the soil in the reinforced section is usually selected to have physical properties favorable to the soil-reinforcement interaction and is an inherent part of the wall. It may or may not be from the same source as the backfill. On many projects the backfill material is derived from excavations on other parts of the job, and the properties of the fill materials are not known when the wall is designed. The designer may then have to choose whether to specify material of favorable characteristics to be placed within the zone of influence of the backfill on the wall, or to design the wall for the greater pressures that would be exerted by the least favorable material that might be used.

Most backfill materials can be assigned to one of the five categories listed in Table 45.1.

In general, the most favorable materials are permeable coarse-grained soils, preferably with little or no silt or clay content, but such materials may be unavailable or too expensive. Use of less suitable materials is associated with larger earth pressures and increases the cost of the wall. Soft clays, silty clays, or organic soils may be difficult to avoid under some circumstances, but they can be expected to lead to large pressures and progressive movements of the wall. Stiff clays should as a rule not be used, because they are almost certain to experience an increase in water content over the years and to exert swelling pressures that may greatly exceed the lateral resistance of the wall. The swelling pressures are increased if the clay is compacted. Indeed, compaction of any type of backfill, which may be desirable to prevent settlement of the ground surface behind the wall, may

nevertheless produce large lateral stresses. The effects of compaction are discussed in Article 45.6.

All retaining walls are affected adversely by water that may be trapped in or seeping through the backfill. Moreover, in climates where freezing occurs, frost action may seriously endanger the structures. Hence, walls should be designed to eliminate or mitigate these effects. The requirements are discussed in the following sections.

#### 45.3.2 Drainage Provisions for Retaining Walls

For removing water that seeps into the backfill of concrete walls during rainstorms, outlets known as *weep holes* or *back drains* are provided. Weep holes are usually made by embedding 100-mm pipes in the wall, as shown in Fig. 45.3. The vertical spacing between horizontal rows of weep holes should not exceed 1.5 m. The horizontal spacing in a given row depends on the provisions made to direct the seepage water toward the weep holes. The cheapest but least effective method is to place about  $0.03 \text{ m}^3$  of crushed stone or gravel at the intake end of each weep hole. If this method is used, the horizontal spacing of the weep holes should not exceed about 1.5 m. The water that emerges from the weep holes seeps into the ground at the toe of the retaining wall where the soil should be kept as dry as possible. This undesirable condition can be avoided by substituting for each horizontal row of weep holes a longitudinal back drain that extends for the full length of the wall. The outlets of the back drains are located beyond the ends of the wall. The most elaborate system of drainage in common use is the continuous back drain (Fig. 45.4a), which consists of a layer of gravel or of pervious filter fabric covering the entire back of the wall. Outlets are provided at each end of the wall. Even a continuous back drain does not eliminate seepage pressures having horizontal components that add appreciably to the pressures acting against the wall, as shown in the figure (Terzaghi 1936a). Elimination of these components would require an inclined drain that would direct the seepage vertically downward (Fig. 45.4b).

Reinforced soil walls are constructed preferably of free-draining granular materials (type 1, Table 45.1), and the facing often consists of articulated segments that allow

**Table 45.1** Types of Backfill for Retaining Walls

1. Coarse-grained soil without admixture of fine soil particles, very permeable (clean sand or gravel).
2. Coarse-grained soil of low permeability due to admixture of particles of silt size.
3. Residual soil with stones, fine silty sand, and granular materials with conspicuous clay content.
4. Very soft or soft clay, organic silts, or silty clays.
5. Medium or stiff clay.

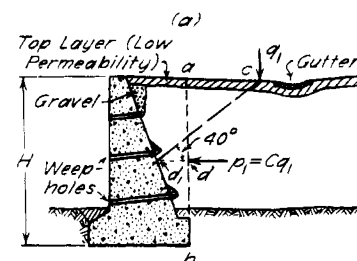


**Figure 45.3** Weep holes for draining backfill of concrete retaining wall.

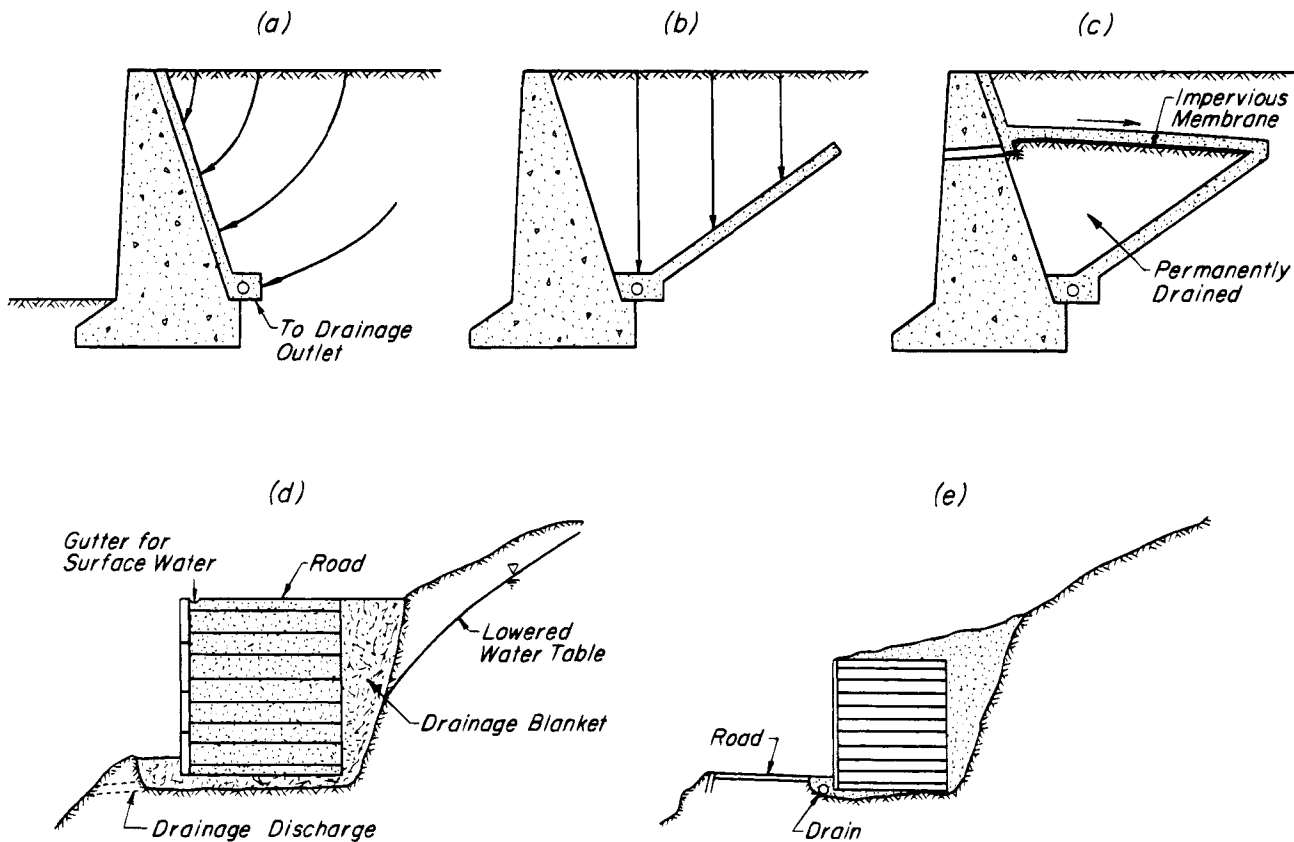


**Figure 45.4** Diagram showing provisions for drainage of backfill behind retaining walls: (a) Back drain; (b) inclined drainage for cohesionless backfill; (c) horizontal drain combined with inclined drainage layer for cohesive backfill; (d and e) drainage blankets behind and beneath reinforced-soil walls.

escape of seepage. Nevertheless, to eliminate seepage pressures similar to those represented in Fig. 45.4a, a drainage blanket behind and beneath the wall is advisable (Fig. 45.4d, e). The blanket itself should be provided with pipe outlets.

To prevent the saturation of backfills of types 2 and 3 (Table 45.1) during the wet season, the surface should be covered by a layer of soil with a permeability considerably smaller than that of the backfill or by an impervious membrane, such as high-density polyethylene, protected by a cover of gravel or other suitable material. The surface should be given a slope toward a conveniently located gutter, as indicated in Fig. 45.3.

If a water or sewer pipe is to be buried in the backfill, the pipe should be surrounded by a gravel drain with an outlet located in such a position that a break in the pipe cannot escape attention.

Backfills of type 5 are necessarily deposited in chunks. They may be protected in such a way, for example as shown in Fig. 45.4c, that a negligible amount of water enters the spaces between the chunks during floods or heavy rains. If this condition cannot be satisfied, the clay should not be used as backfill material. Even with such

protection, the humidity in the voids can, over the years, lead to increasing swelling pressures (Article 15.6.4) and eventually to excessive wall movements; with increasing stiffness of the clay, danger to the wall increases markedly.

#### 45.3.3 Provisions to Reduce Frost Action behind Retaining Walls

If a backfill of types 2 and 3 in Table 45.1 is saturated, the freezing of the pore water adjoining the back of the wall draws water out of the fill toward the zone of freezing and ice layers may be formed parallel to the back of the wall (Article 15.8). If the backfill is permanently separated from the water table by a very permeable or very impermeable material, it constitutes a closed system. In such a backfill the formation of ice layers involves merely a migration of water from the central part of the backfill toward the zone of freezing, but the volume and shape of the backfill remain practically unaltered and the corresponding movement of the retaining wall is likely to be imperceptible. However, if the ground water rises into the backfill, the system is an open one, and the formation of ice layers produces an energetic outward movement of the wall. A continuous drain at the intersection *b* of

the back of a concrete wall and the original ground surface (Fig. 45.5a) would lower the water table into the position *bd*, but it would not prevent the water from being drawn by capillarity toward the zone of freezing, as indicated by the arrows. However, the backfill can be transformed into a closed system by covering the entire area of contact between the backfill and its base, up to a level about 0.5 m above the highest position of the water table, with a blanket of gravel or permeable filter fabric (Fig. 45.5b). The collector drain should be installed behind the inner boundary of the zone of freezing, and its outlets should be protected against obstruction by ice. No serious frost action need be feared if the backfill constitutes a closed system, or if it consists of soils of types 1, 4, or 5.

## 45.4 External Stability of Retaining Walls

### 45.4.1 Forces Acting on Retaining Walls

If a retaining wall is intended to restrain a slope, the possibility should first be considered that a failure may occur by sliding along a surface that passes behind the wall and backfill and beneath the wall. Such a failure can be investigated by the procedures described in Articles 35 and 47. If the factor of safety is found to be inadequate, the slope must be stabilized; otherwise, the slope including the retaining wall may fail.

The next step is to select tentatively the type and dimensions of the retaining structure and to estimate the forces that may act on it. The forces include the earth pressure, the weight of the structure, and the weight of any backfill that may be considered an inherent part of the structure. The earth pressure includes the effects of surcharge, live loads, and earthquakes. If the wall is to be of concrete, the boundary of the part of the backfill considered an inherent part of the structure is usually taken as a vertical plane *ab* through the heel of the base (Fig. 45.1a, b). If the wall is to be of reinforced soil, the boundary *ab* is usually considered to be a plane separating the part of the backfill containing the reinforcing elements from the part containing no reinforcement (Fig. 45.1c, d). The pressure against the boundary so defined is then estimated by means of earth-pressure theory or by semiempirical procedures that have led to satisfactory designs under circumstances discussed in Article 45.4.3. The direct

applicability of earth-pressure theories is subject to several limitations; these are discussed in Article 45.4.2.

Once the forces acting on the wall have been determined, calculations of the factors of safety against sliding, overturning, and bearing-capacity failure can be carried out as indicated in Article 45.2. These calculations determine whether the width of the base of the retaining wall is adequate. The base width of a reinforced-soil wall determined by such an investigation usually establishes the length of the reinforcing elements perpendicular to the axis of the wall, inasmuch as the length required to ensure internal stability is usually less.

### 45.4.2 Use of Earth Pressure Theories for Determining External Pressure on Walls

Methods for computing the earth pressure against retaining walls on the basis of classical earth-pressure theories are presented in Articles 28 to 32. These methods are based on three assumptions:

1. The pressure in the pore water of the backfill is negligible.
2. The soil properties appearing in the earth-pressure equations have definite values that can be determined reliably.
3. The wall can yield by tilting, deforming, or sliding through a distance sufficient to develop the full shearing resistance of the backfill.

If the first and second requirements are not satisfied, the wall will be acted on by various agents and forces beyond the scope of any earth-pressure theory. If the backfill is loosely deposited or inadequately drained, its properties change from season to season, and during the course of each year it passes through states of partial or total saturation alternating with states of drainage or even partial desiccation. All these processes cause seasonal changes in the earth pressure which receive no consideration in the classical earth-pressure theories. For example, pressure cell measurements on the back of a reinforced-concrete retaining wall 10 m high indicated that within 1 year the pressure varied from the average value by  $\pm 30\%$  (McNary 1925).

The implications of the third requirement deserve special consideration because they have led and still lead

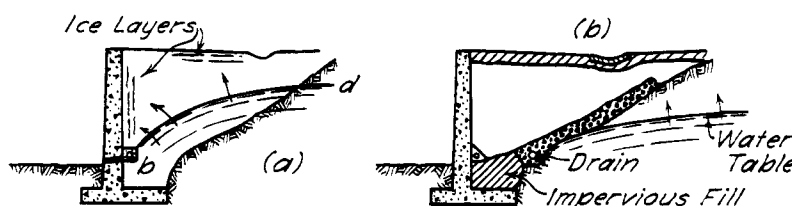


**Figure 45.5** (a) Frost action in backfill of retaining wall provided only with back drain. (b) Method of draining backfill to prevent formation of ice layers.



to considerable confusion. Before the influence of the deformation conditions (Article 27) was understood, measurements and observations of earth pressures produced a wide variety of results because the movements and deformations of the walls on which the observations were made were uncontrolled and often unobserved. The essential relations were first investigated (Terzaghi 1920, 1934c) by means of model tests in which the wall was simulated by a rigid plate held in a fixed position while the backfill was deposited. The plate was then displaced systematically while the pressures were measured. For a dense sand having a horizontal upper surface the variation of the total lateral pressure and that of the elevation of its point of application are shown as a function of outward movement or tilting of the wall in Fig. 45.6. A small angular rotation  $\Delta/H$  of less than 0.1% was sufficient to reduce the pressure from its initial at-rest value to the value of active earth pressure predicted by Coulomb's theory (Article 30). Further rotation was accompanied by a slight increase in pressure. Similar results were obtained if the wall was moved parallel to itself. For loose backfill the required movements to establish the active state were roughly an order of magnitude larger.

These findings indicated that neither small-scale nor large-scale tests or even field measurements could furnish

consistent results unless the walls moved far enough to establish the active state. For granular backfills placed under controlled conditions the required movements were relatively small. Therefore, it was concluded that most conventional walls, if not restrained at their tops, could move far enough without objectionable consequences to reduce the pressure to the active value and that the stability of the walls could, therefore, properly be investigated on the basis of that pressure. This conclusion is subject to several limitations not always realized by designers.

First, if a retaining wall is proportioned to withstand active earth pressure with a suitably conservative margin of safety with respect to sliding, overturning, and bearing capacity, the actual displacements of the wall will be less than those corresponding to the active state, and the pressures will exceed the active values. This condition will not compromise the external stability of the wall unless the wall and its foundation are practically rigid, because before the wall can fail it will have moved or deformed far enough to decrease the pressures to the active values on which the design was based. Nevertheless, if earth-pressure measurements were to be made on such a conservatively designed wall, the pressures would exceed the active values. This apparent contradiction has led to confusion concerning the appropriate basis for

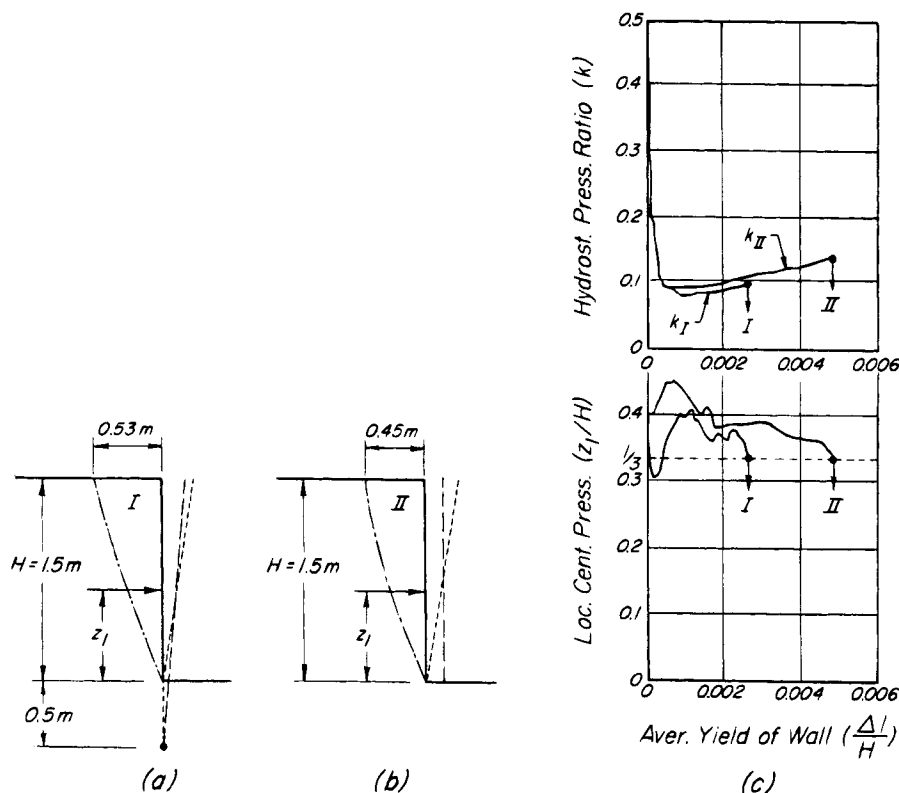


**Figure 45.6** (a and b) Movement of model retaining wall in two different tests, I and II. (c) Relation between average yield of wall, hydrostatic pressure ratio, and location of center of pressure. The arrows I and II indicate slip in tests I and II.

design. Logically, design to resist active earth pressures is appropriate with respect to the external stability of the wall. On the other hand, the structural design of the components of the wall, such as the stem or base slab of a cantilever wall or the reinforcement in a reinforced-soil wall, must take account of the larger pressures that the wall must resist at displacements smaller than those corresponding to the active state.

Second, in the definitive experiments relating wall displacement to lateral pressure (Terzaghi 1920, 1934, Sherif et al. 1982, 1984), the backfill was placed before any appreciable displacement of the wall was permitted, whereupon a predetermined pattern of displacement was imposed. In the field, the displacements take place as backfilling progresses. The deformation conditions, therefore, differ somewhat from those in the experiments. They are more complex, and the deformations depend on the stiffness of the actual wall and its foundation as well as on the details of backfilling. The effect of incremental filling, which inevitably differs from wall to wall, has been investigated by finite-element procedures (Clough and Duncan 1971) and has been shown to be sensitive to details of construction that can be controlled to only a limited extent.

Third, it has become customary to compact the backfill if the ground surface will be required to support pavements, structures, or other installations. The compaction tends to lock in horizontal stresses that may be very large (Sowers et al. 1957, Broms 1971, Duncan and Seed 1986). In a few instances walls have even failed structurally or overturned during compaction. However, if a wall survives the compaction of the backfill, only slight additional movement will be required to develop the full shearing resistance of the backfill, and the deformation conditions on which the theoretical methods of earth-pressure calculation are based are then satisfied.

Thus, the pressure for which a retaining wall should be designed depends on several factors not always clearly separable. These include: (1) whether the economic importance or height of the wall justifies the expenditures necessary to provide a backfill having properties that can be evaluated not only for the time of construction but also throughout the life of the wall; (2) whether the back of the wall can safely move sufficiently to reduce pressures to the active value; and (3) whether the wall can structurally withstand the internal stresses associated with movements smaller than those required to reduce the earth pressures to the active value, including the stresses due to compaction.

The maximum value of the earth pressure of backfills subject to seasonal changes is greater than the Coulomb or Rankine value. Yet, on routine jobs such as the construction of retaining walls along railroads or highways, it would be both uneconomical and impractical to eliminate the seasonal pressure variations by design and con-

struction. Such walls have been customarily designed on the basis of simple semiempirical rules (Article 45.4.3) for estimating the backfill pressure. In their original form these rules were based chiefly on analyses of the stability of actual retaining walls, only a few of which had failed. Because the underlying causes of failure were not taken into consideration in formulating the rules, the design of walls by this procedure led on rare occasions to failure, but in the great majority of cases the walls were safer than necessary. Such rules are still widely used, but the advent of soil mechanics permitted improvements without loss of simplicity.

On the other hand, if a retaining wall constitutes the major part of a large job, or if the height of a wall exceeds about 10 m, it is preferable and likely to be more economical to expend the effort to determine the properties of the backfill, to carry out and monitor such construction procedures as are necessary to satisfy the theoretical requirements for applying an earth-pressure theory, and to design the wall to withstand the theoretical value of the earth pressure.

The physical soil properties that enter into the theoretical earth-pressure computations are the mass density, the angle of internal friction, the cohesion intercept, and the undrained shear strength. No elaborate theoretical calculations are justified unless the values of these properties are determined by means of laboratory tests on representative samples of the backfill material compacted to a density equal to that after deposition and compaction in the field.

The angle of internal friction of fairly permeable soils, such as types 1 to 3 in Table 45.1, can be determined by drained shear tests, because the void ratio of these materials in the field can adapt itself during construction to the change in stresses. The cohesion intercept should be disregarded. The coefficient of wall friction  $\tan \delta$  against a concrete wall can be assumed equal to two thirds of  $\tan \phi'$ . If the fill will not be compacted but will be subjected to traffic vibrations, or if it will sustain heavy surcharges of variable intensity, such as the loads on the floor of storage-warehouse docks, the values of  $\tan \phi'$  and  $\tan \delta$  should be reduced by 20%. If there is a possibility that the wall may settle more than the backfill, the wall friction should be assumed to act against the wall in an upward direction.

The values of  $c$  and  $\phi'$  or  $s_u$  for clay soils, such as types 4 and 5 in Table 45.1, should be determined for conditions immediately after construction by means of undrained triaxial tests performed on samples at the density and water content anticipated in the field at the time the backfill is completed. The adhesion between the clay backfill and the back of a concrete wall should be disregarded, and the value of  $\delta$  taken equal to zero. For long-term conditions,  $c'$  should be disregarded and the value of  $\phi'$  determined by drained tests. The effect of traffic

vibrations does not require consideration. As discussed in Article 45.3.2, stiff clay should not be used as a backfill material unless conditions permit the complete and permanent exclusion of water from the fill; however, this is seldom practicable.

Even if a continuous back drain is provided behind the wall, water percolates during rainstorms through the backfill as shown in Fig. 45.4a. The seepage pressure (Article 23.4) exerted by the percolating water increases the earth pressure exerted by backfills with medium permeability, types 2 and 3 (Table 45.1), as long as percolation continues. This seepage pressure is not taken into account in the earth pressure theories. It should either be estimated by means of a flow net (Article 23) and added to the forces acting against the wall, or it should be eliminated by means of inclined drainage layers, as shown in Fig. 45.4b, or by similarly placed pervious filter fabric. The drainage layers serve the double function of drains and protection against frost action. In addition, the surface of backfills of medium permeability should be covered with a well-compacted layer of less permeable soil, as shown in Fig. 45.3.

A clay backfill is likely to pull away from the back of a concrete wall to a depth of about  $z_o$  (Eq. 28.7). To prevent the accumulation of water in the open fissure during rainstorms, a continuous drain should be inserted between the wall and the backfill to a depth of  $1.5 z_o$  below the crest. The provisions shown in Fig. 45.4c include such a drain.

The quantity of water that percolates through a well-constructed backfill is so small that there is no danger of the drains becoming obstructed by washed-out soil particles. Therefore, it is not necessary that the grain size of the materials in the drainage layers should satisfy the requirements for filter layers (Article 14.9). However, if a geotextile is used as the drain, it should be of a type that remains permeable even when subjected to the weight of the overlying material.

#### 45.4.3 Use of Semiempirical Rules for Estimating External Pressure on Retaining Walls

Perhaps the oldest of the semiempirical methods is the use of charts or tables giving suitable values of the ratio of base width to height for various types of masonry walls and backfills. The principal defect of this approach is that the foundation can not be investigated adequately because the forces that act on it are unknown. Many designers have preferred to use theoretical equations or graphical constructions such as Culmann's (Article 30.3) for calculating the pressure of cohesionless earth and to assign such values to the angle of internal friction as usually led to satisfactory design. However, a great diversity of opinion existed as to the proper values to use for  $\phi'$  under different circumstances.

Nevertheless, the various semiempirical procedures represent a body of valuable experience and summarize much useful information. Today our knowledge of the physical properties of soils permits us to eliminate the most unreasonable values assigned to the parameters. Furthermore, earth-pressure theory can be used to take account of the soil properties and to estimate the influence of a surcharge carried by the backfill or of a backfill that has an irregularly shaped surface. A summary of this information, in the form of an approximate design procedure for practical use, is given in the following paragraphs. Like every such approximate procedure, it is based on more-or-less arbitrary assumptions and it cannot apply to all cases encountered in practice. It should be regarded as a means for producing a design comparable to those for small retaining walls that have generally behaved satisfactorily in the past.

The first step in the design of a wall on a semiempirical basis is to assign the available backfill material to one of the five categories listed in Table 45.1. If the wall must be designed before the nature of the backfill material can be learned, the estimate of the backfill pressure should be based on the most unsuitable material that may be used by the construction forces. If the only available material consists of stiff clay, the semiempirical procedure should not be used.

The second step is to categorize the wall with respect to the shape of the surface of the backfill and the surcharge it carries. The categories are:

1. The surface of the backfill is plane and carries no surcharge.
2. The surface of the backfill rises on a slope from the crest of the wall to a level at some elevation above the crest.
3. The surface of the backfill is horizontal and carries a uniformly distributed surcharge.
4. The surface of the backfill is horizontal and carries a uniformly distributed line load parallel to the crest of the wall.

If the surface of the backfill is plane as in category 1, the backfill pressure may be estimated by means of the chart (Fig. 45.7). The chart is drawn to represent a concrete wall, but it may also be used for a reinforced-soil wall. The first step in using the chart is to determine the height  $H$  of a vertical section, passing through the heel of the wall or enclosing the reinforcement of a reinforced-soil wall, extending from the bottom of the base to the surface of the backfill. The total pressure against this section is  $\frac{1}{2} k_h H^2$ , and the total vertical force on it is  $\frac{1}{2} k_v H^2$ . Values of  $k_h$  and  $k_v$ , normalized to the value of  $\gamma_w$  to facilitate use with any consistent set of units, are given on the right-hand side of Fig. 45.7 in terms of the slope angle  $\beta$  for each of the given types of backfill material. The backfill pressure is assumed to increase in simple

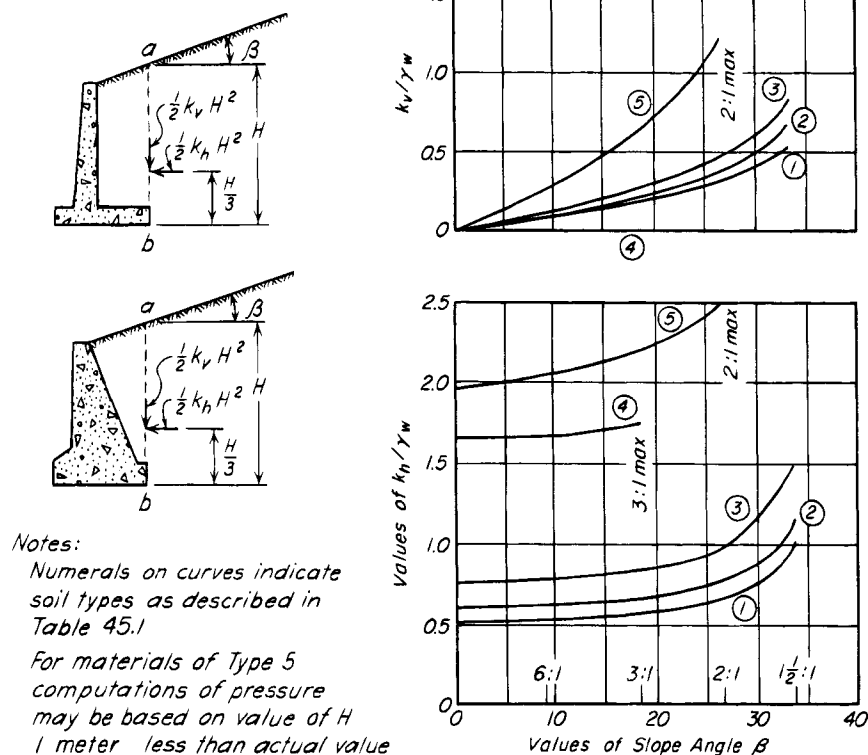


**Figure 45.7** Chart for estimating pressure of backfill against retaining walls supporting backfills with plane surface.

proportion to the depth below point  $a$ . Hence the point of application of the resultant backfill pressure is at the lower third-point of  $H$ .

If the surface of the backfill rises at an angle  $\beta$  to the horizontal for a limited distance and then becomes horizontal (category 2), values of  $k_h$  and  $k_v$  may be estimated from the curves in Fig. 45.8. As before, the chart gives values of the pressure against a vertical section  $ab$  through the heel of the wall. The point of application of the resultant pressure is taken at the lower third-point of  $H$ .

If the surface of the backfill is horizontal and carries a uniformly distributed surcharge  $q$  per unit of area (category 3), the pressure per unit of area against the vertical section  $ab$  at any depth is increased because of the surcharge by an amount

$$p_q = C q \quad (45.1)$$

where  $C$  is a coefficient depending on the type of soil. Values of  $C$  are given in Table 45.2.

If the surface of the backfill carries a line load,  $q_1$  per unit of length, parallel to its crest (category 4), the load is considered to exert a horizontal force against the vertical section  $ab$ ;

$$p_1 = C q_1 \quad (45.2)$$

per unit of length of the wall. The point of application  $d$  of the force  $p_1$  (Fig. 45.9a) can be obtained by drawing a straight line from point  $c$ , which represents the point of application of the force  $q_1$ , at an angle of  $40^\circ$  to the horizontal until it intersects the back of the wall at point  $d_1$ . If point  $d_1$  is located below the base of the wall, the influence of the line load on the surcharge can be disregarded. If point  $c$  is located to the left of the vertical plane  $ab$ , the rule remains unaltered.

The line load  $q_1$  also produces an additional vertical pressure on the upper surface of the heel of a concrete wall. It may be assumed that the pressure  $p_2$  at this level is distributed uniformly over the base  $ef$  of an equilateral triangle with apex at  $c$ . Hence, the intensity of the pressure is:

$$p_2 = \frac{q_1}{ef} \quad (45.3)$$

Only that part of  $p_2$  acting directly on the heel of the wall should be considered in the stability computation.

In most instances the wall friction and adhesion tend to pull the wall down and to reduce the earth pressure.

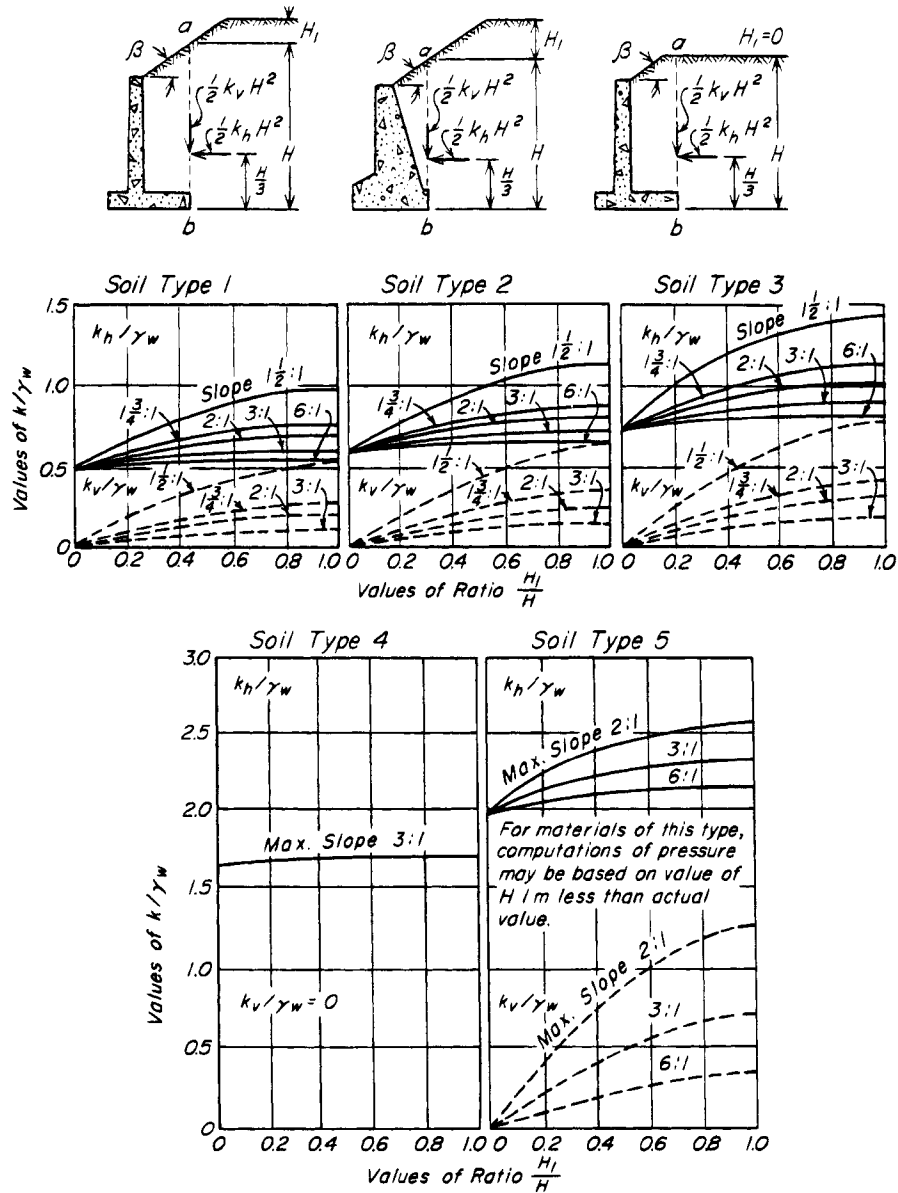


**Figure 45.8** Chart for estimating pressure of backfill against retaining walls supporting backfills with surface that slopes upward from crest of wall for limited distance and then becomes horizontal.

**Table 45.2** Values of  $C$  in Equations 45.1 and 45.2

Type of Soil	$C$
1	0.27
2	0.30
3	0.39
4	1.00
5	1.00

However, if a wall rests on a very compressible foundation, the settlement of the wall with respect to settlement of the backfill may reverse the direction of these forces. This increases the earth pressure considerably (Article 29 and Fig. 29.1). Therefore, if a wall rests on a compressible foundation such as soft clay, the values of backfill pressure should be increased by 50%.

The backfill pressures computed by means of the semi-empirical procedures just outlined include the effect of seepage pressures and various time-conditioned changes in the backfill. Nevertheless, provisions must be made to prevent the accumulation of water behind the wall and

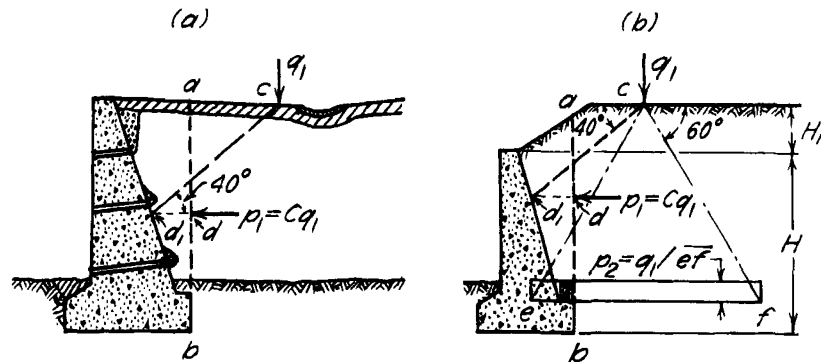


**Figure 45.9** Diagrams illustrating method for estimating magnitude and line of action of force against vertical section through heel of retaining wall, due to surcharge  $q_1$  per unit of length parallel to crest of wall.

to reduce the effect of frost action, as indicated in Article 45.3.

## 45.5 Internal Stability of Retaining Walls

### 45.5.1 Masonry and Concrete Walls

The internal stability of a concrete wall is a matter of structural design in plain or reinforced concrete. The earth pressure against the vertical plane through the heel of the wall is combined with the weight of the backfill and any loads acting on the wall and backfill, and the wall is designed to withstand the corresponding stresses.

Because the wall is designed to have a factor of safety greater than unity against external instability (Article 45.4), its movement will be less than that required to reduce the earth pressure to the active value. Under these conditions the stresses in the wall will exceed the nominal allowable values. Experience has indicated that the overstress is within the customary margins of safety used in structural design and that structural distress rarely develops as a consequence, provided that the backfill consists of free-draining granular materials and is not compacted. Finer materials may experience creep that tends to increase the earth pressure above the active values; this increase is reflected in the semiempirical charts (Figs. 45.7 and 45.8). Compaction may increase the lateral pressure markedly against a rigid or nonyielding wall, as discussed in Article 45.6, and has occasionally led to structural failure (Casagrande 1973). Had the failures not occurred, the walls could have moved sufficiently to reduce the pressure to the lower values indicated by the semiempirical charts.

### 45.5.2 Reinforced Soil

The internal stability of a reinforced-soil wall is achieved by reinforcing the backfill, (Fig. 45.1c, d). The reinforcement usually consists of strips or grids of metal or polymers in which tension is developed primarily by frictional

forces between the reinforcement and the backfill. In types of reinforcement having elements not only perpendicular but also parallel to the face of the wall, such as metal mats or polymer grids, the resistance includes a portion of the passive pressure of the soil in front of the parallel elements. The reinforcement is connected to a wall facing that serves primarily to prevent the escape of backfill. In the following discussion of the principles governing the design of reinforced-soil walls, the assumption is made that the reinforcement consists of metallic strips of rectangular cross-section oriented perpendicular to the face of the wall. This corresponds to the original reinforced-earth system discussed by Vidal in 1963.

The fill is constructed in layers equal in thickness to the vertical distance between the reinforcing elements. Each layer is retained by an increment of facing. To construct a new layer the reinforcing elements are laid on the surface of the preceding one and are connected to the next increment of facing, which must be supported independently while the fill is placed behind it.

Finite-element modeling, small-scale model tests, and measurements on full-scale walls (Schlosser 1990) all indicate that tension in the ties increases from the face of the wall to a maximum and then decreases with increasing distance from the face (Fig. 45.10a). The locus of maximum tension in the ties defines a curved surface forming the boundary of a wedge, known as the *active zone*, that tends to move outward with the wall, away from the mass behind the wedge that may be regarded as the *stable resisting zone*. For internal stability of the wall, the tension in any tie must not exceed the strength of the tie, and the frictional resistance between the tie and the soil of the resisting zone must be great enough to prevent the tie from pulling out of the backfill.

The boundary of the active wedge is a curved surface often approximated for design by the bilinear surface (Fig. 45.10b) or, somewhat more realistically (Fig. 45.10c)

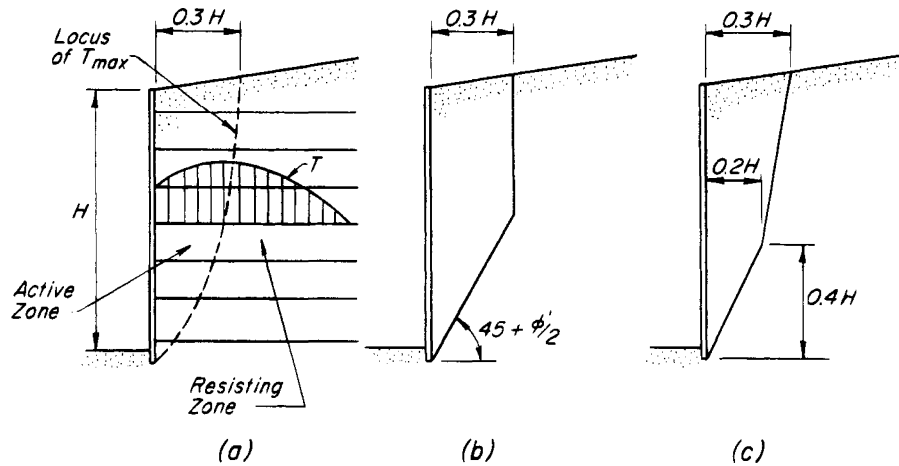


**Figure 45.10** (a) Variation in tension  $T$  in tie in reinforced-soil wall, and locus of maximum tensions defining boundary between active and resisting zones. (b and c) Bilinear surfaces used in design to approximate curved boundary shown in (a).

(Schlosser 1990). At depth  $z$  the intensity of lateral pressure at the boundary of the wedge is

$$\sigma'_h = K\sigma'_v \quad (45.4)$$

and, for a tie at that depth, spaced at a vertical distance  $\Delta H$  and a horizontal distance  $\Delta S$  from its neighbors, the earth pressure to be resisted, and thus the force in the tie, is

$$T = K\sigma'_v \cdot \Delta H \cdot \Delta S \quad (45.5)$$

To resist this force, the tie must neither break nor pull out of the surrounding fill. To prevent breaking, the tie is designed to have an adequate factor of safety against yielding in tension. If the yield strength of the tie is  $f_s$ , the factor of safety against yield is

$$F_{(\text{yield of tie})} = \frac{f_s b_t t_t}{K\sigma'_v \cdot \Delta H \cdot \Delta S} \quad (45.6)$$

where  $b_t$  and  $t_t$  are the width and thickness of the tie, respectively. The resistance against pullout is

$$t_{\text{pullout}} = 2b_t L_R \sigma'_v \tan \delta \quad (45.7)$$

where  $L_R$  is the length of the tie in the resisting zone, and  $\delta$  the angle of friction between tie and backfill. The factor of safety against pullout is then

$$F_{(\text{pullout})} = \frac{2b_t L_R \tan \delta}{K \cdot \Delta H \cdot \Delta S} \quad (45.8)$$

The investigation of a reinforced-soil wall with respect to internal stability consists of selecting tentative values for the horizontal and vertical spacing and length of the ties, determining whether the factor of safety with regard to the strength of the ties is adequate for every lift of the wall, and determining whether the length  $L_R$  provides

sufficient factor of safety against pullout in every lift. The value tentatively chosen for the length is usually that required for stability of the foundation (Articles 45.2.2 to 45.2.4). If the factors of safety are inadequate, adjustments are made to the dimensions, usually by lengthening the ties, until a satisfactory design is achieved.

This relatively straightforward design procedure, however, involves two complexities: evaluation of the vertical effective stress  $\sigma'_v$  for each lift, and evaluation of the earth-pressure coefficient  $K$ . In addition, the value of  $\delta$  is somewhat dependent on the vertical pressure  $\sigma'_v$ .

The vertical effective pressure  $\sigma'_v$  (Eqs. 45.5 and 45.7) may conservatively be taken as  $\gamma z$ , where  $z$  is the depth from the surface of the backfill to the layer of reinforcement. In most instances, however, the overturning moment due to the earth pressure against the back of the wall adds significantly to the vertical pressure in the resisting zone where resistance is developed against pullout, as illustrated in Fig. 45.11. In this figure,  $ab$  represents the back of the wall,  $cd$  the boundary between the active and resisting zones, and  $z$  the depth to the layer of reinforcement being considered. The resultant force of all the loads above  $z$ , including the weight of the backfill, any surcharge loads, and the backfill pressure on  $ab'$  above depth  $z$ , is represented by  $R$ , which acts on section  $c'b'$  at depth  $z$  with an eccentricity  $e$ . According to Meyerhof's approximation (Article 45.2.4), the vertical component of  $R$  may be considered uniformly distributed over a width  $b - 2e$ . Its intensity, which is greater than  $\gamma z$ , is commonly taken as  $\sigma'_v$  in Eqs. 45.5 and 45.7.

The earth-pressure coefficient  $K$  is influenced by the deformation of the wall and by the compaction associated with placement of the layers. Because of the compaction it exceeds the active value near the top of the wall,

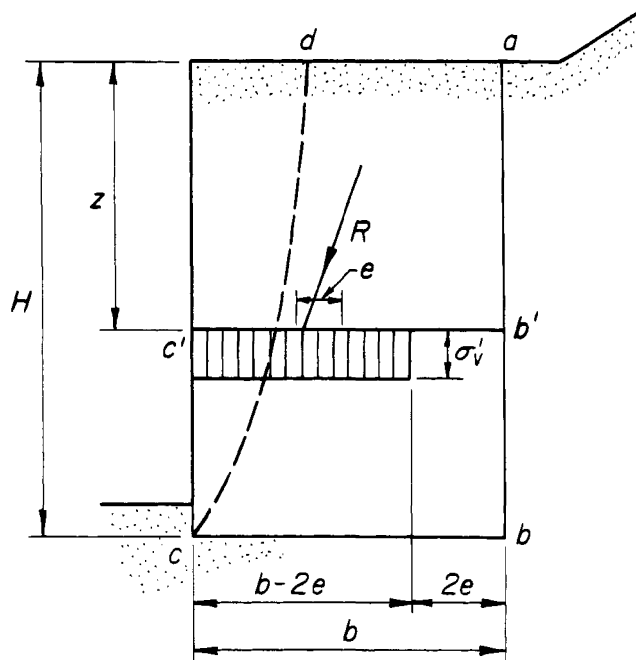


**Figure 45.11** Method for calculating  $\sigma'_v$  on layer of reinforcement at depth  $z$  in reinforced-soil wall.

whereas at depth the deformations cause a reduction to the active value  $K_A$  or even less. For metallic strip reinforcement, field measurements have indicated an appropriate basis for design to be a linear variation with depth from  $K_0$  to  $K_A$  at a depth of 6 m, below which  $K$  remains constant at  $K_A$  (Mitchell and Villet 1987).

Finally, in compacted sands, the shearing strains associated with pulling on the reinforcing strips tend to dilate the sand. The dilatancy, which produces one component of the frictional resistance of the sand (Article 19), decreases with increasing confining pressure and, consequently, with depth (Schlosser 1990). For metallic strips the value of the friction coefficient  $\tan \delta$  is usually assumed to vary linearly from about  $2 \tan \phi'$  at the surface to  $\tan \phi'$  at a depth of 6 m, below which it remains constant (Mitchell and Villet 1987).

The foregoing discussion deals specifically with metallic-strip reinforcement. Because each of the various proprietary systems uses reinforcing elements of different geometry and stress-strain characteristics, the proponents of each system have performed various field and laboratory tests leading to specific data concerning walls constructed according to their system. Some of the proponents have carried out extensive research programs. Information from the various sources has been assembled by agencies concerned with the design of highways and other public works. Details of design procedures contained in the publications of such agencies should be consulted (e.g., Christopher et al. 1990).

The long-term internal stability of reinforced-soil walls depends on the continued integrity of the reinforcing elements. Corrosion may attack metal elements at rates difficult to predict under field conditions, especially when aggressive groundwater or stray electric currents may be present; galvanizing or other protective coatings substantially reduce the rate of attack, but to an extent also subject to uncertainties. Geotextiles and plastics are subject to damage by improperly used compaction equipment, by exposure to the atmosphere and especially to ultraviolet radiation, and by attack by various microorganisms. These factors require consideration when a choice is to be made between a concrete or a reinforced-soil wall. Favorable characteristics of reinforced-soil walls include usually lower first cost, tolerance to differential movements, and ease and speed of construction.

Geotextile reinforcement is appreciably more deformable than metal reinforcement and tends to experience creep. These characteristics require modification of the design procedures described above. They have been the subject of research by the proponents of the various geotextile reinforcement systems, and the findings have been incorporated into suggested design procedures (Christopher et al. 1990).

Although most reinforced-soil walls are constructed of permeable granular materials (type 1, Table 45.1), reinforcement of other soils such as sandy clays and clays has been accomplished successfully. There is need for considerable study and experience, however, before design with these materials can be considered routine. Several failures involving such materials have occurred (O'Rourke and Jones 1990).

### 45.5.3 Soil Nailing

Whereas a reinforced-soil wall consists of alternating layers of soil and reinforcement placed successively as the wall is constructed from the bottom up, soil nailing is a technique for stabilizing an existing mass of soil as a steep face is created by excavating the unwanted soil in front of the face while proceeding from the top down. After each increment of excavation is completed, a layer of steel rods, known as soil nails, is introduced into the slope. The rods are either driven into the slope or are installed in drilled holes and bonded to the soil by grouting. The face of the increment is protected and supported by reinforced shotcrete which may be placed on the soil before the nails are installed if the face tends to ravel, or subsequently if the increment is stable. In any event, the soil must possess enough true or apparent cohesion to stand long enough at the cut slope to permit the increment of excavation to be made and the reinforcement to be installed.

The height to which the final soil-nailed wall can be made depends primarily on the slope, the presence or absence of external loads, the properties of the soil mass, and the force that can be developed in and safely resisted



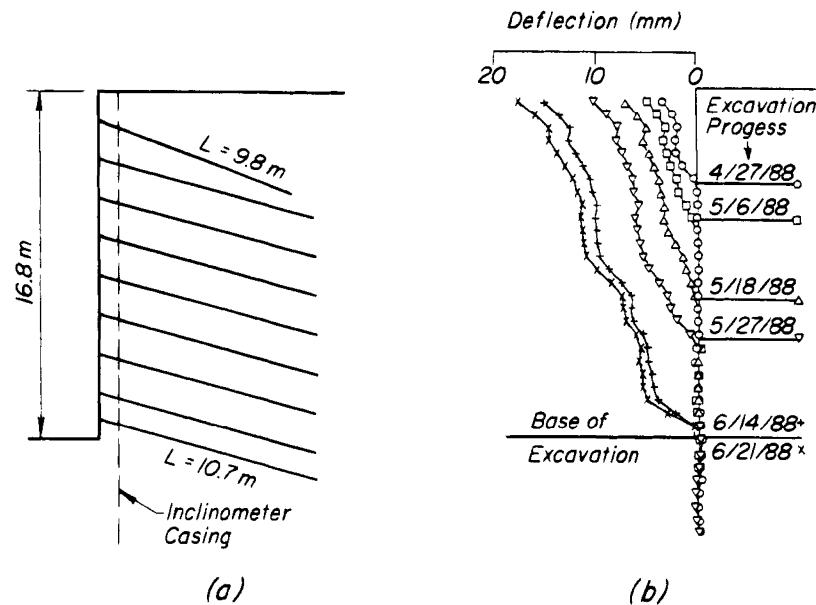


**Figure 45.12** (a) Geometry of soil-nailed wall in heavily overconsolidated glacial deposits in Seattle. (b) Deflected position of face of wall at various excavation stages (after Thompson and Miller 1990).

by the nails. Other variables to be considered by the designer include the inclination and spacing of the nails.

At stresses in the soil and reinforcement corresponding to an adequate factor of safety, measurements on large-scale test walls indicate that the displacements of the face are a maximum at the top of the cut and decrease roughly linearly with depth as shown in Fig. 45.12 (Thompson and Miller 1990). Stresses in the nails reach maximum values that define a curved boundary between an active and a resistant zone; the boundary typically intersects a horizontal ground surface at a distance on the order of  $0.35 H$  to  $0.45 H$  from the face of the wall (Fig. 45.13a).

If the stresses approach failure, however, the entire face moves outward, the bottom moves farther than the top, and the mass of soil defined by the boundary between the active and resistant zones slips downward and outward. The slip is associated with extensive deformations of the nails in a zone extending on both sides of the boundary, as illustrated in Fig. 45.13b. In contrast to the flexible inclusions in reinforced-soil walls, wherein the ties act almost exclusively in tension, the nails in a reinforced slope possess significant bending and shear resistance that aids in supporting the potential sliding mass. The effect of these components of resistance, however,

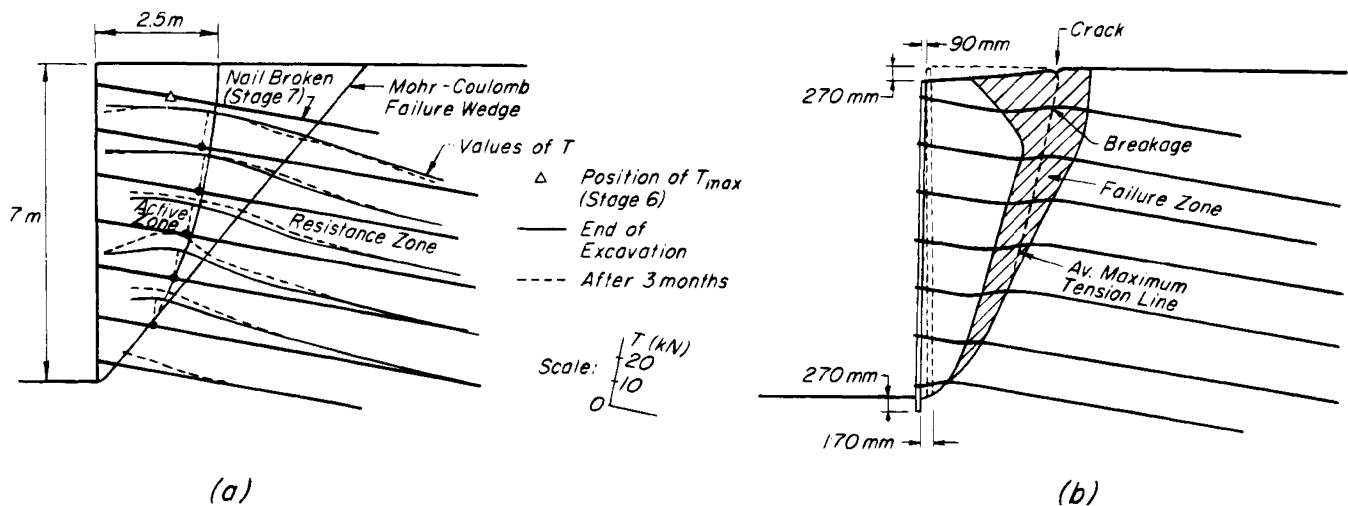


**Figure 45.13** (a) Distribution of tensile forces in nails behind experimental wall. (b) Distortion of nails behind wall and displaced position of wall at failure (after Plumelle et al. 1990).

only comes into play appreciably at large deformations as failure is approached. At conservative factors of safety the principal action of the nails is to provide tensile resistance across the boundary.

Inasmuch as the nails cross the boundary between the active and resistant zone, the internal stability of the nailed slope can be investigated by considering the equilibrium of the potential sliding mass by procedures similar to those discussed in Article 45.5.2 in connection with reinforced-soil walls. Several modifications are required, however. Because the material in which the nails are embedded is usually a natural soil with properties more complex than those in a reinforced soil, evaluation of the shearing resistance along the potential surface of sliding requires a thorough subsurface exploration comparable to that for investigating the stability of a natural slope. The determination of the shearing resistance between the nails and the surrounding soil can rarely be made reliably on the basis of laboratory tests, but usually requires pull-out tests in the field on nails of the same type, installed in the same manner, as those to be used in the wall. Tests of several types of nails are generally needed to establish the ones most suitable under the field conditions.

Several methods are in current use to calculate the global factor of safety against failure along various assumed surfaces of sliding until the surface corresponding to the minimum factor of safety is found. All are based on the principles discussed in Article 35. One such procedure is illustrated in Fig. 45.14. The wall  $ab$  is supported by nails having lengths  $L$  and spaced  $\Delta H$  and  $\Delta S$  vertically and horizontally, respectively. The soil has a small cohesion intercept  $c$  and a friction angle  $\phi'$ . A trial surface of sliding  $bc$  is shown, for illustrative purposes, to intersect the lower nails but to pass beyond the upper ones. The sliding mass is divided into a series of vertical slices; where the nails cross  $bc$  the vertical boundaries of each slice bisect the distance along  $bc$  between the points of intersection of  $bc$  and the nails. The forces acting at failure on a typical slice, such as slice 6 in Fig. 45.14a, are shown in  $b$ . They include the weight  $W$  of the slice and of any surcharge that acts on the ground surface, the lateral interface pressures  $E_5$  and  $E_6$ , the resultant  $F_6$  of the normal force  $N$  and frictional resistance on the base of the slice, the cohesion  $c$  on the base, and the tension  $T_6$ , per unit length of wall, in the nail that intersects the base. This value is limited, of course, by the tensile strength of the nail itself. If it is assumed that the wall is at equilibrium at a factor of safety  $F$ , the resisting forces can be taken as the mobilized cohesion  $c_m = c/F$ , the resultant  $F_m$  of the normal force and the mobilized friction  $N[\tan \phi']/F$ , and the mobilized nail tension  $T_{xm} = T_x/F$ . The nail tension  $T_x$  is the pullout resistance of the nail multiplied by  $x/L$ , where  $x$  is the length of the nail extending into the resisting mass beyond the surface of sliding. A force diagram illustrative of the stability analysis of the entire wall is shown in Fig. 45.14c. Because the

polygon as drawn does not close, it may be concluded that the assumed value of  $F$  is in error; repetition of the procedure for different values of  $F$  is carried out until closure is obtained. For simplicity the interslice forces  $E$  have been taken arbitrarily parallel to the ground surface. The solution is relatively insensitive to this assumption (Long et al. 1990), but the influence of other reasonable assumptions can be investigated by similar procedures. In practical design the iterative graphical solution illustrated in Fig. 45.14 or a similar procedure is usually replaced by a computer calculation (Mitchell and Villet 1987).

Detailed procedures for making the calculations have been developed and incorporated into the publications of various public agencies (FHWA 1991). Some of the procedures (Shen et al. 1981) consider the nails to act only in tension at factors of safety corresponding to working-stress levels. Others (Schlosser 1982) take account of the shear forces in the nails, the corresponding bending resistance, and the passive resistance exerted by the soil against the nails as they resist the deformation across the boundary of the active zone. The latter methods reduce the overconservatism of the former but are more complex and presume a greater degree of sophistication in evaluating the interaction between soil and nail.

Moreover, all methods based on stability analyses leading to an overall or global factor of safety, even if different partial safety factors are assigned to the different elements of resistance, assume that each nail contributes to the resistance in proportion to its pullout capacity within the resisting zone. In contrast, large-scale tests and experience (Plumelle et al. 1990) have shown that the uppermost nails may fail during construction, whereas the lower ones may experience little loading. It has also been noted that a crack frequently develops at the ground surface roughly at the boundary between the active and resisting zones (Fig. 45.13b). These observations suggest that a rational design procedure should permit calculation of the stresses in the nails at the different levels so that an appropriate margin of safety can be achieved for each nail. These aspects have been explored in some detail (Juran et al. 1990), with results that compare favorably with those of large-scale and model tests at failure. The analyses, however, require assigning appropriate values to many parameters, and the agreement may be less satisfactory in forecasting the behavior of new installations than in explaining that of ones already constructed. Relatively few measurements of nail forces in full-scale field installations at failure are likely to be obtained.

An alternative to theoretical calculation of failure stresses in the nails may be field measurements of nail forces at working loads, and assembling the results as nondimensional envelopes representing equivalent pressures from which nail forces can be derived (Thompson and Miller 1990). The concept is analogous to that for determining equivalent pressure diagrams for calculation

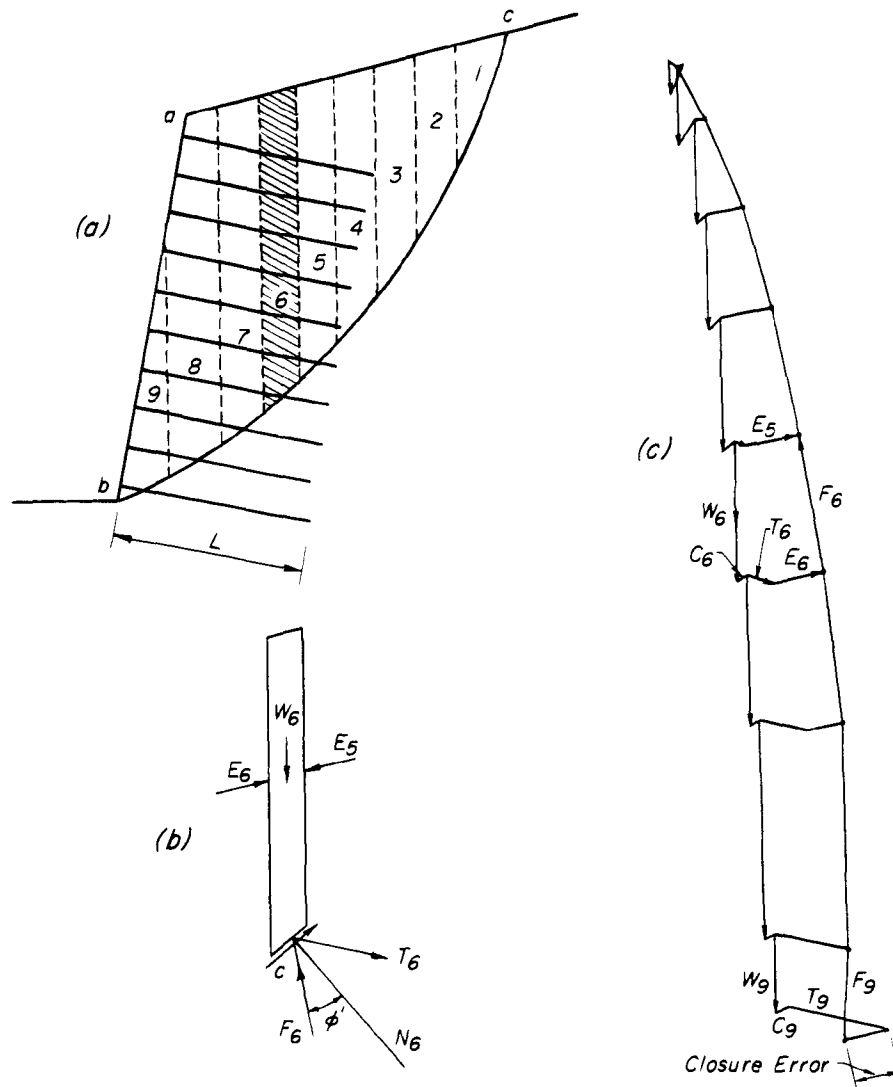


**Figure 45.14** Method for analyzing global stability of soil-nailed slope: (a) Slope subdivided into vertical slices. (b) Forces acting on typical slice 6. (c) Trial force polygon showing closure error indicating incorrect assumption for factor of safety.

of strut loads in open cuts (Article 46.3.1). The procedure seems to have merit, because it has the potential to take into account not only the properties of the soil but also the inevitable variations in construction procedure. The envelope suggested by Thompson and Miller to represent the nail loads in a cut 16.8 m deep in Seattle (Fig. 45.15), represents only a tentative suggestion, inasmuch as the deformation conditions associated with the nailed cut differ from those in the braced cuts for which the envelope was developed. Collection of additional empirical data to develop this approach is a promising endeavor.

The facing of a reinforced-soil wall is acted on by minimal earth pressure, whereas that for a nailed slope must transfer the load in the nail to the soil over the area  $\Delta H \cdot \Delta S$  tributary to the nail. The measurements of tensile forces in the nails of the wall represented in Fig. 45.13a

indicate that a large fraction of the maximum tension at the interface between the active and resisting zones remains in the nail at the face. The facing, usually consisting of shotcrete reinforced with wire mesh, can thus be conservatively designed as a membrane subjected to the pressure  $T_{\max}/\Delta H \cdot \Delta S$ , where  $T_{\max}$  is the estimated maximum force in the nails.

Experience has demonstrated the tendency for a crack to form at the ground surface along the interface between the active and resisting zones. The crack is detrimental because it permits the entrance of surface water and it eliminates whatever shearing resistance might have developed within its depth. In recognition of the detrimental consequences, some engineers consider it advisable to replace the upper set of nails by tiebacks with their anchors located well behind the resisting zone. The tie-

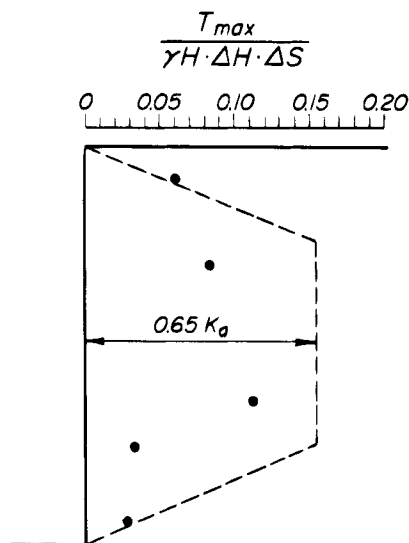


**Figure 45.15** Normalized nail forces measured in cut in Seattle compared with equivalent pressure diagram for braced cut (after Thompson and Miller 1990).

backs are prestressed to counteract the tendency for separation.

If the slope behind the facing would be subject to seepage, drainage must be provided. The design of the drainage system depends on the amount of water that must escape to accomplish the desired results. If the anticipated seepage will be small, vertical filter fabric strips applied before shotcreting and leading to a collector drain at the foot of the wall may suffice. Otherwise it is necessary to install near-horizontal filter drains in drill holes extending well into the slope. Adequate drainage well back from the base of the wall is also necessary if climatic conditions favor the development of frost action.

#### 45.6 Influence of Compaction on Rigid Vertical Walls

Compaction behind walls is usually accomplished by means of vibrating rollers, vibrating plates, or tampers, as the backfill is raised in lifts (Article 44.2). The surface of each lift is subjected locally to a temporary static vertical pressure due to the weight of the compactor, plus a dynamic increment which, at its maximum value, is usually approximately equal to the static pressure. If the wall has a vertical back and can neither move nor deflect, the horizontal pressure after backfilling can be estimated by the procedure described in Article 44.2.4. The calculation can be carried out on a personal computer.

In this section a simple method of hand calculation is described for estimating the postcompaction lateral pressure of compacted granular backfills against vertical non-deflecting structures. Based on the approach of Duncan and Seed (1986), it evaluates the peak and residual lateral

earth pressures produced by placing and compacting level layers of soil of roughly equal thickness. The lateral pressure profile is established by complying with four conditions that govern the effective horizontal pressure  $\sigma'_h$  as illustrated in Fig. 45.16 and described as follows:

1. Lateral pressure resulting from the weight of the compacted backfill

$$\sigma'_h = (1 - \sin \phi') \gamma z \quad (45.9)$$

in which  $\phi'$  is the friction angle and  $\gamma$  the unit weight of the compacted backfill, and  $z$  is the depth below the final surface of the backfill. Equation 45.9 is based on the empirical result that  $\dot{K} = \Delta \sigma'_h / \Delta \sigma'_v$  of compacted granular soils subjected to an increase in  $\sigma'_v$  starting from  $\sigma'_h = \sigma'_v = 0$  is related to  $\phi'$  according to the Jaky equation (Eq. 16.3). In Fig. 45.16, Eq. 45.9 defines the postcompaction lateral pressure of backfill layers that are loaded into the *compression range* by the overburden of subsequent lifts.

2. Lateral pressure limited by the passive Mohr-Coulomb failure condition (Eq. 26.2):

$$\sigma'_h = \tan^2 \left( 45 + \frac{\phi'}{2} \right) \gamma z \quad (45.10)$$

Compacted soil cannot sustain a lateral pressure

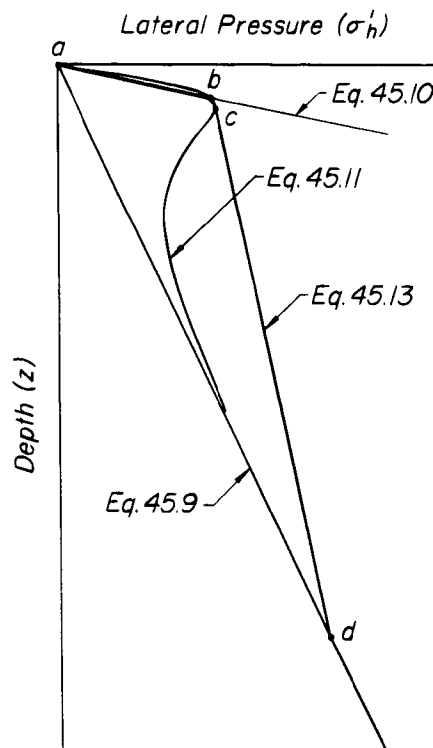


**Figure 45.16** Method for calculating pressure of compacted backfill against vertical back of rigid wall.

exceeding its passive resistance. Thus, near the final surface of the backfill, the lateral pressure is defined by Eq. 45.10.

3. Lateral pressure resulting from the weight of the backfill, plus the residual compaction-induced horizontal stresses:

$$\sigma'_h = (1 - \sin \phi')\gamma z + \frac{1}{4}(5^{\sin \phi'} - 1)\Delta\sigma_h \quad (45.11)$$

The lateral pressure increase  $\Delta\sigma_h$  results from loading the surface of the last lift of backfill by the compactor. The reduction factor  $(5^{\sin \phi'} - 1)/4$  accounts for the unloading as the roller moves away. Field measurements suggest that the lateral pressures on vertical planes perpendicular to the path of the roller are significantly higher than those on planes parallel to it (Seed and Duncan 1983). Therefore, the most efficient compaction is achieved if the direction of rolling is parallel to the wall. The roller can be modeled as a line load of finite length perpendicular to the wall and moving parallel to it. If the wall is assumed to extend in the  $y$ -direction and the line load in the  $x$ -direction, the Boussinesq (1885) point load solution can be integrated to obtain  $\Delta\sigma_x$  for points within the vertical plane that includes the line load. The value of  $\Delta\sigma_h$  is obtained by doubling  $\Delta\sigma_x$  for the free field to take into account stress reflection at the nondeflecting wall. The closed form solution for  $\Delta\sigma_h$  is

$$\Delta\sigma_h = \frac{p}{\pi z} \left( \frac{1}{\left[1 + \left(\frac{z}{x_2}\right)^2\right]^{3/2}} - \frac{1 - 2\nu}{\left[1 + \left(\frac{z}{x_2}\right)^2\right]^{1/2}} + \frac{z}{x_2} - \frac{1}{\left[1 + \left(\frac{z}{x_1}\right)^2\right]^{3/2}} + \frac{1 - 2\nu}{\left[1 + \left(\frac{z}{x_1}\right)^2\right]^{1/2}} + \frac{z}{x_1} \right) \quad (45.12)$$

in which  $x_1$  and  $x_2$  are the shortest distances from the wall to the near and far ends of the line load, respectively. The line load is  $p = W/(x_2 - x_1)$ , in which  $W$  = the total load exerted by the roller, and  $(x_2 - x_1)$  = the length of the roller. Poisson's

ratio  $\nu$  for the backfill can be estimated as 0.42, 0.38, and 0.34 for values of  $\phi'$  for the compacted backfill equal to 30, 40, and 50°, respectively. Equation 45.12, which assumes a uniform fill to infinite depth, is a satisfactory approximation, because the near surface values of  $\Delta\sigma_h$  are unaffected by a rigid base.

4. Lateral pressure profile defined by a line that envelops the residual lateral pressures resulting from the placement and compaction of successive lifts. This line starts from the maximum  $\sigma'_h$  computed by Eq. 45.11 and increases with depth according to

$$\Delta\sigma'_h = \frac{1 - \sin \phi'}{4}(5 - 5^{\sin \phi'})\gamma\Delta z \quad (45.13)$$

Figure 45.16 indicates the manner in which the four conditions described above are used to estimate the pressure against a rigid wall. Near the surface of the backfill, from  $a$  to  $b$ , the lateral pressure on the wall is subject to the passive Mohr-Coulomb failure condition expressed by Eq. 45.10. From  $b$  to  $c$  the overburden and compaction-induced lateral pressure profile is determined by Eq. 45.11. From  $c$  the lateral pressure increases with depth according to Eq. 45.13 until  $d$  is reached. Below  $d$  the overburden pressure exceeds the increases in stress by compaction, and the lateral pressure is directly related to the effective overburden pressure according to Eq. 45.9.

The results of calculations, not only for vibrating rollers but also for vibratory plates and rammer plates, have been assembled on charts supplemented by tables containing adjustment factors to account for different lift thicknesses, distances from the wall, compactor dimensions, and friction angles for the soil (Duncan et al. 1991, 1993. Errors in the results for vibrating rollers were corrected in the 1993 reference). These charts considerably facilitate the calculations.

Somewhat simpler procedures have been suggested by Broms (1971) and Ingold (1979). Both are based in the premise that the vertical pressures beneath the roller can be multiplied by a value of  $K_0$  to obtain the corresponding horizontal pressures. This premise, valid only if the increment of vertical pressure is distributed uniformly over the entire surface of the fill, can be substantially in error beneath a load of limited extent. Hence, it is preferable to compute the distribution of horizontal stresses directly from elastic theory.

## 45.7 Earth Pressure Against Nonyielding Retaining Walls

Backfilled rigid walls in a fixed position, such as massive concrete gravity walls founded on virtually unyielding bedrock, the front part of U-shaped bridge abutments, or the side walls of deep basements, are acted on not by active earth pressure but by pressures approaching earth

pressure at rest. The magnitude of the earth pressure at rest is greater than the active value. It depends not only on the physical properties of the backfill, but also to a large extent on the method of placing and compacting the fill. If the fill is compacted in layers, the procedure illustrated by Fig. 45.16 may be used to estimate the lateral pressure.

Many high concrete gravity walls established on bedrock have been designed to support only the active pressure and have performed satisfactorily, whereas they would have failed had the lateral pressure been equal to the at-rest value. This apparent anomaly has probably arisen because the overturning moment due to the lateral at-rest pressure is partly compensated by the restoring moment due to downward shear forces exerted by the backfill against the back of the wall. These forces are the result of settlement of the backfill as successive lifts of fill are placed. Duncan et al. (1990), who have studied this problem by both precedent and finite-element analyses, conclude that the value of  $k_v$  for a vertical plane through the heel of such a wall is unlikely to be less than 0.1. They also propose that the point of application of the horizontal component of the earth pressure at rest should be taken at 0.4 times the height of the wall. Although use of the active earth pressure and neglect of the vertical shear force in a stability analysis may lead roughly to the same wall dimensions as use of the earth pressure at rest and inclusion of the vertical shear, the latter procedure deserves preference as more nearly representing field conditions.

Relatively few measurements have been made on essentially unyielding walls. Broms and Ingelson (1971, 1972) reported measurements on the abutments of two bridges, both backfilled with sand compacted in layers. At one site the abutment walls, about 3 m high, were supported on rigid piers. The walls, hinged top and bottom, were held apart at their tops by the bridge deck. The depth of backfill was kept equal against the two abutments; consequently, rotations of the walls during filling were minimal. Immediately after backfilling and compaction, the pressures, measured by means of 8 pressure cells on each abutment, exhibited large scatter reflecting small variations in the compaction procedure. Values of the ratio  $K$  of lateral to overburden pressure ranged from 0.3 to 2.1 with an average of about 1.0. Subsequently, as the bridge deck lengthened and shortened as a result of temperature changes, the pressures increased to passive or decreased to active Rankine values. The rotations associated with these extreme values were  $0.0016 H$  and  $0.001 H$ , respectively. At the other site similarly constructed abutments about 10 m high were backfilled with 4 m of medium sand above 6 m of sandy gravel. The sandy gravel was compacted in 0.6-m lifts by a 3-tonne vibratory roller except near the wall, where a 300 Kg vibratory plate compactor was used around vertical ribs that stiffened the wall. At this stage, the horizontal pressures varied roughly linearly with depth at values corresponding to  $K \approx 0.4$ . The upper part of the fill was inaccessible for compaction near the wall. Again, marked variations in lateral pressure were

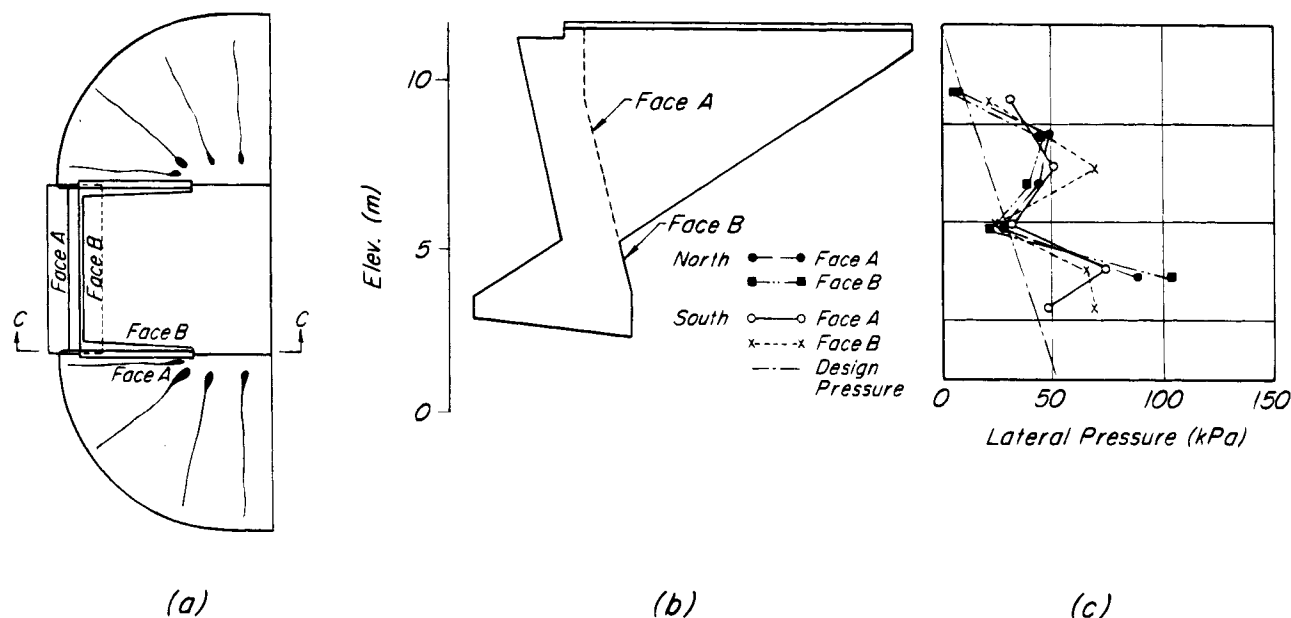


**Figure 45.17** Earth pressure against back of bridge abutment where backfill was confined laterally by wing walls extending only part way to bottom of backfill (after Jones and Sims 1975).

observed as the length of the bridge deck changed between summer and winter.

Pressures acting against the abutments and wing walls of two highway bridges in England were measured by means of pressure cells (Jones and Sims 1975). The wing walls, perpendicular to the abutments and cast monolithically with them (Fig. 45.17*a, b*), allowed the fill to extend alongside the abutments. The fill, a free-draining sand, was placed in 0.15-m layers and compacted by sheepfoot or grid rollers. Immediately adjacent to the walls a vibrating footpath roller was used. Measured pressures at the end of construction were similar at all four abutments. Typical results are shown in Fig. 45.17*c*. Below the wing walls the ratio  $K$  of lateral to overburden pressure was about 0.33, but between the wing walls  $K$  ranged generally between 0.5 and 0.75. Pressures against the wing walls themselves were greatest near the top and least near the bottom where the underlying soil could not be compacted effectively. These data indicate that the pressures against generally used types of rigid structures such as bridge abutments with wing walls depend not only on the type of soil and compaction equipment, but also to a great extent on the ease or difficulty of compaction in confined spaces and on the three-dimensional effects of confinement. Moreover, they indicate that deformations imposed on the backfill by such mechanisms as expansion and contraction of bridge decks may lead to pressures far greater than those existing at the end of construction. If the deformations are smaller than those associated with passive failure, the maximum pressures cannot be evaluated without considering the stress-deformation characteristics of the backfill and structure.

Failure to consider properly the stress-deformation characteristics of subsoil, backfill, and a structure so stiff that it usually would be regarded as rigid can lead to erroneous conclusions. For example, the Port Allen Lock, a massive concrete U-frame on the lower Mississippi River (Fig. 45.18*a*) was designed as a continuous frame. The computed differential settlement of the base slab when the lock was full was made compatible with the computed settlement of the subsoil when acted on by the contact pressure between slab and soil. Under these conditions it was found that the side walls of the lock should deflect inward in spite of the outward hydrostatic pressure. Accordingly, it was expected that the external pressure of the backfill should decrease when the lock was filled. Field observations confirmed that the tops of the walls did indeed deflect inward, but the observed earth pressures increased. This apparent contradiction was resolved by finite-element studies (Duncan and Clough 1971) in which it was shown that the weight of the water in the lock displaced the subsoil as indicated by the arrows (Fig. 45.18*b*), with the result that the backfill tended to move against the retreating wall and thus increase the pressure. Moreover, subsequent studies (Clough and Dun-

can 1972) showed that seasonal temperature strains in the lock structure had an even greater influence on the observed earth pressures than did filling or emptying the lock.

The foregoing examples demonstrate that the interaction of so-called rigid structures with backfill and foundation soils may be complex and largely unrelated to the classical earth-pressure theories. Designs can be based justifiably on these theories only if strains or displacements in the surrounding soil can be related to the limiting conditions to which the theories apply. Otherwise, the interaction must be modeled by finite element or comparable procedures.

Many rigid structures are constructed in braced or tied-back excavations. The earth pressures to which such structures are subjected depend on several factors including the manner in which the bracing loads are transferred to the structures. These matters are discussed in Article 46.

#### 45.8 Large-Scale Model Tests and Field Observations

It has long been recognized that the observational data forming the basis for the existing semiempirical procedures for estimating backfill pressure are meager and that the influence of field conditions and construction methods on the validity of theoretical calculations is virtually unexplored. In an attempt to fill these gaps in our knowledge, two approaches have been pursued in recent years: rather elaborate and carefully controlled measurements on models large enough to permit duplication of at least some construction procedures such as compaction, and necessarily more limited measurements of movements and pressures against actual retaining walls in the field. Although large-scale model tests have the advantage of permitting a systematic investigation of several variables, most such tests have introduced conditions that limit the applicability of the results.

In several series of tests on large models the backfill was placed against a wall held in a fixed position, after which the wall was displaced in a predetermined manner and the backfill pressures measured (Matsuo et al. 1978, Fukuoka et al. 1981 Chiba tests); such tests provide fundamental data on the relation between wall movements and backfill pressure. However, they do not model the effect of incremental backfilling on a yielding wall (Clough and Duncan 1971), nor do they provide information on the amount of movement of the prototype walls. In other tests the movement of the wall has been a function of the design of the model and, although measured, was not necessarily comparable with that of the prototype (Fukuoka et al. 1981 Tohoku tests). Hence, although providing considerable insight, most such tests have not led to consistent conclusions.

Useful field observations should adequately describe the soil used as a backfill, the method of placing and

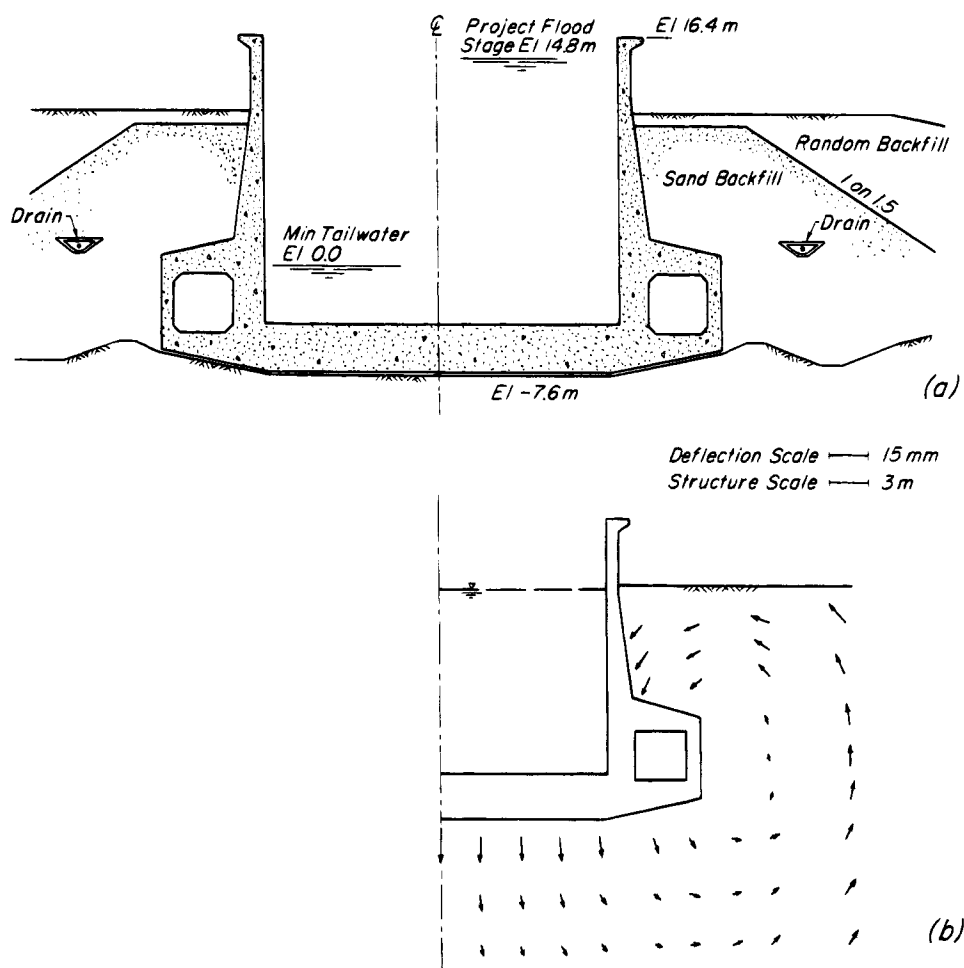


**Figure 45.18** (a) Section through Port Allen Lock (after Kaufman and Sherman 1964). (b) Displacements of soil around lock as calculated by finite-element procedure (after Duncan and Clough 1971).

compacting the backfill, the provisions for drainage, climatic data, foundation conditions, movements of the wall, and measured backfill pressures. Few tests satisfying these conditions have been made. Two tests (Coyle et al. 1974, Coyle and Bartoskewitz 1976) on walls 4 and 3 m high, respectively, and backfilled with clean fine sand, indicated pressures comparable to those suggested by the semiempirical procedures for designing small walls. However, many more such investigations would be required to validate or to warrant refinements in the procedures.

### 45.9 Summary

In connection with the design of retaining walls, the planning of adequate drainage provisions and a careful consideration of the foundation conditions are more important than a correct evaluation of the earth pressure. The pressure exerted by the backfill can be estimated either on the basis of semiempirical rules or by means of earth-pressure theory. The first method has the drawback that

some walls may be excessively safe, others may be barely stable, and occasionally a wall may fail. Nevertheless, for routine jobs the first method is cheaper and preferable. The second method requires that the backfill and the drainage system be constructed in strict compliance with the conditions imposed by the theory. The time and labor involved are not justified unless the retaining wall constitutes a prominent part of an individual job or has a height exceeding about 7 m.

Current design methods are based on the premise that most walls can move, without undesirable consequences, far enough to reduce backfill pressures to the active value. This presumption is generally satisfactory for calculating the overall stability of the walls, although care must be taken to ensure that the movement caused by compaction of the backfill is not excessive. However, the structural design of cantilever or counterfort walls must take account of the greater pressures that will be acting because the conservative factors of safety used in the stability analyses lead to smaller movements than required to



develop the active state. Structures too rigid to experience appreciable movements must be designed for earth pressures corresponding to the compaction stresses induced in the backfill. In some structures, such as rigid-frame bridges, thermal forces may lead to even higher pressures.

Further progress in the design and construction of retaining walls cannot be expected without observations made on full-sized retaining walls in the field, to determine the seasonal variations in the condition of the backfill and their effect on the wall.

### Selected Readings

One of the classic papers containing a graphic description of the causes and types of failure of retaining walls, still worth reading even though the theoretical discussions and proposed design methods are out of date, is "The actual lateral pressure of earthwork," by Sir Benjamin Baker (1881) *Min. Proc. Inst. Civil Eng., London*, **65**, pp. 140–186, discussions pp. 187–241.

The importance of the deformation conditions in determining the magnitude and point of application of the resultant earth pressure was highlighted in the discussion by K. Terzaghi in the paper "Lateral earth pressure; the accurate experimental determination of the lateral earth pressure, together with a resume of previous experiments," by J. Feld, *Trans. ASCE*, 1923, **86**, pp. 1525–1543. The results of the very small-scale tests, disparaged by Feld in his closing discussion, were verified subsequently by Terzaghi's large-scale MIT tests illustrated in Fig. 45.6.

Insight into the design and behavior of conventional retaining walls can be gained from "Behavior and design of gravity earth retaining structures" (1990), by J. M. Duncan, G. W. Clough, and R. E. Ebeling, in "Design and Performance of Earth Retaining Structures," *ASCE Geot. Spec. Publ.*, No. 25, pp. 251–278.

Christopher, B. R., S. A. Gill, J. Giroud, I. Juran, J. K. Mitchell, F. Schlosser, and J. Dunncliff (1990). *Reinforced Soil Structures, Volume I. Design and Construction Guidelines. Volume II. Summary of Research and Systems Information*, U.S. Dept. of Trans. Fed. Hwy. Admin., Publ. No. FHWA-RD-89-043.

FHWA (1991). *Soil Nailing for Stabilization of Highway Slopes and Excavations*. U.S. Dept. of Trans. Fed. Hwy. Admin., Publ. No. FHWA-RD-89-193, 209 p.

## ARTICLE 46 LATERAL SUPPORTS IN OPEN CUTS

### 46.1 Introduction

Open cuts may be intended to remain open permanently, like those for highways or railways, or they may be only temporary, to be backfilled after they have served their

purpose. The sides of permanent earth cuts are inclined at slopes usually not steeper than  $1\frac{1}{2}$  to 1 (Article 47), or else they are supported by retaining walls (Article 45). On the other hand, the sides of temporary cuts are made as steep as the soil conditions permit without undue risk of slope failure (Fig. 43.4), or they are made vertical and are supported by bracing consisting of struts usually extending from side to side of the cut or by tiebacks anchored in the soil outside the cut. The choice depends on economy, on the available space, on the character of the materials outside the cut, and on the advantages that may be derived by keeping the working space unobstructed inside the cut.

Every successful open cut must satisfy two criteria: the supports must have an adequate factor of safety against a structural failure that would permit the support system to collapse; and the movements of the ground adjacent to the cut must not result in intolerable settlements or distortions of adjacent or nearby structures, utilities, or other sensitive installations. Neither criterion can be overlooked. An entire section of the Berlin subway collapsed in the 1930's, because the bracing was designed for earth pressures calculated in accordance with an inappropriate theory. On the other hand, ground movements damaging to a sensitive monumental structure occurred adjacent to a deep open cut in Washington, D. C. (Fig. 54.2), even though the bracing experienced no structural distress. In general, if good workmanship is exercised, movements around cuts in sands and stiff clays are not likely to be excessive, and design can consist of ensuring structural adequacy of the supports followed by an estimate of the ground movements. On the other hand, movements adjacent to cuts in or above clays with low strength relative to the depth of cut may be excessive irrespective of the structural capacity of the supports. Under these circumstances it is preferable (Clough et al. 1989) to begin the design by selecting a support system of suitable geometry and stiffness to ensure that the deformations will be acceptable (Article 54), after which the structural design of the supports can be undertaken.

This article deals with the design of the supports in temporary cuts with vertical sides. If the bottom of a cut in pervious materials is to be located below the water table, the soil adjoining the cut is usually drained before or during excavation. Therefore, the supports can be designed as if the cut were above the water table.

The data needed as a basis for adequate design of the support system depend primarily on the depth of the cut. It is convenient to distinguish between shallow cuts with depths less than about 6 m and deep cuts with greater depths. The bracing of shallow cuts such as trenches for the installation of sewers or water mains is more or less standardized. The customary systems can be used safely under very different soil conditions. Because refinements in the design of such systems would be uneconomical,

only a general soil reconnaissance is needed in advance of construction, and no computations of earth pressure are required. On the other hand, in the design of the support systems for deep cuts such as those for subways, the dimensions of the cut and the character of the adjoining soil should be taken into account, because the savings that can be realized thereby are likely to be much greater than the cost of obtaining the data for design.

Before the advent of modern soil mechanics the design of the support systems for deep cuts was usually based on the assumption that the earth pressure increased like a hydrostatic pressure in simple proportion to the depth below the surface. However, both theory (Article 37) and experience have shown that this assumption is rarely justified. Hence, the discussion of deep cuts in Article 46.3 includes methods for designing supports on the basis of the real pressure distribution.

## 46.2 Bracing of Shallow Cuts

In cohesive soils, cuts with vertical sides can theoretically be made to a depth  $H_c$  (Eq. 28.9) without bracing. The values of  $H_c$  for clays of various consistencies are approximately as follows: very soft, 2.5 m; soft, 2.5–5 m; medium, 5–10 m. Because stiff and very stiff clays are likely to be jointed or fissured, the value of  $H_c$  may be as low as 3 m. The value of  $H_c$  for cohesive sand depends on the cohesion; it commonly lies between 3 and 5 m, but it may be much greater.

In reality, if a cut with entirely unsupported vertical sides is made in cohesive soil, tension cracks are likely to appear on the surface of the ground adjoining the cut a few hours or days after excavation. The presence of such cracks considerably reduces the critical height (Article 35), and sooner or later the sides cave in. To prevent such accidents, which all too often result in fatalities, the upper edges of narrow cuts are braced against each other, as shown in Fig. 46.1a. The horizontal cross-members are usually referred to as *struts* or *braces*. They may consist of timbers or of extensible metal supports known as trench braces. They are tightened by wedges or screw

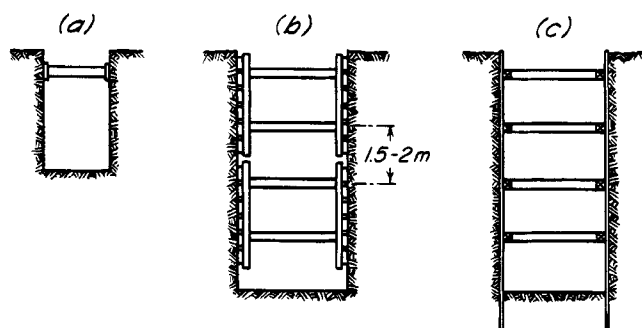


**Figure 46.1** Diagrams illustrating different methods for constructing shallow open cuts: (a) Single row of struts; (b) lagging; (c) sheeting.

jacks and support horizontal timbers that usually consist of 80-mm planks. The braces are usually spaced at about 2.5 m, and the load they carry remains very small unless the cut is located in stiff swelling clay.

If the depth of a narrow cut exceeds about  $\frac{1}{2}H_c$ , struts are usually inserted as excavation proceeds. They are wedged against short vertical timbers known as *soldier beams* that bear against horizontal boards known as *lagging* (Fig. 46.1b). It is usually unnecessary to fit the lagging boards tightly together; if space is left between them, they constitute open lagging. An alternative is to wedge the struts against horizontal timbers known as *wales* that support vertical boards known as *sheeting*. The lowest part of the sides, with a height of about  $\frac{1}{2}H_c$ , can be left unsupported to furnish adequate working space, provided that the soil does not have a tendency to slake or ravel. If it does, the sheets are carried down to the bottom of the excavation, but no struts are required to hold them in place.

In perfectly cohesionless sand or gravel only vertical sheeting can be used. One row of sheeting is usually driven on each side of the cut, and wales and struts are inserted as excavation proceeds. The sheets are generally driven a meter or so at a time, but their lower ends are always kept at least a meter below excavation level (Fig. 46.1c).

The dimensions of the bracing are fairly well standardized, regardless of the type of soil. Struts are spaced at about 2.5 m horizontally and 1.5 to 2 m vertically. Metal trench braces are available for cuts up to 1.5 m in width. For narrow cuts wooden struts are usually 100 by 150 mm. The dimensions increase to about 200 by 200 mm, for cuts 3 m wide. Sheeting or lagging usually consists of planks 150 to 250 mm wide. Bracing of these dimensions can be used safely in cohesionless sand to a depth of about 10 m and in soft clay to depths of about 1.5 m in excess of  $\frac{1}{2}H_c$ .

## 46.3 Support of Deep Cuts

### 46.3.1 General Considerations in Design of Support Systems

The most common methods for supporting the sides of deep cuts are illustrated in Fig. 46.2. When an open cut is excavated, struts or tiebacks are installed as the depth of the excavation increases. In Article 37 it is shown that this procedure is accompanied by an inward movement of the soil on each side of the cut. At the ground surface the movement is restricted to a very small amount, because the uppermost row of supports is inserted before the state of stress in the soil is appreciably altered by excavation. However, the movement that precedes the insertion of supports at lower levels increases as the depth of excavation increases. According to Article 27, this type of yielding is associated with a roughly parabolic

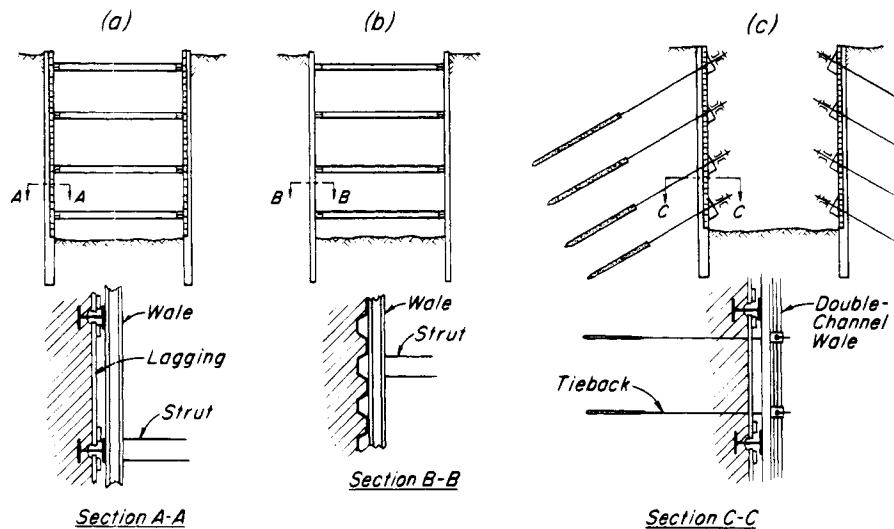


**Figure 46.2** Diagrams illustrating different methods for constructing deep open cuts: (a) Soldier piles, lagging, wales, and struts; (b) sheet piles, wales, and struts; (c) soldier piles, lagging, and tiebacks.

distribution of pressure, and the maximum intensity of pressure occurs near midheight of the cut, whereas the lateral pressure exerted against a structural retaining wall by a backfill with a horizontal surface increases like a hydrostatic pressure in simple proportion to the depth below the surface.

Another fundamental difference between a retaining wall and the support system in a cut is the manner in which failure occurs. A retaining wall constitutes a structural unit, and it fails as a unit. Local irregularities in the magnitude of the backfill pressure are of little consequence. However, any strut or tieback in an open cut can fail as an individual. Because the failure of one support involves an increase of the load on its neighbors, it may initiate a progressive failure of the entire support system.

Finally, the shearing resistance of the soil adjacent to a vertical face does not become fully active until the face has yielded through a certain distance (Article 27). It is impracticable to find out by laboratory tests or any other indirect means whether the process of excavating and supporting a cut is actually associated with enough movement to reduce the total lateral earth pressure to the active value. Furthermore, at a given total pressure on the support system, the loads carried by the individual struts or tiebacks can be very different, because they depend on accidental factors such as the local variations in the adjacent soil, the rate and orderliness with which excavation proceeds, the time that elapses between excavation and insertion of the support at a given point, and the extent and uniformity of prestressing. In view of these facts, no procedure for designing the supports should be trusted until its reliability has been demonstrated by the results of measurements in full-sized cuts. Since about 1940,

many sets of comprehensive measurements have been made in deep cuts in a wide variety of materials. Inasmuch as tiebacks are usually prestressed to loads approximately equal to those anticipated, measured loads in tiebacks to some extent reflect the designer's estimate. Hence, most empirical information concerning values of earth pressure that would be exerted without the prestress has been obtained by measuring strut loads.

Most of the observations consist of measurements of the loads carried by the struts in a given vertical cross-section or in several cross-sections of a cut. The strut-load determinations are usually supplemented by measurements of deflections and settlement. Because reliable direct measurements of the earth pressure against the sheeting have rarely been made, the magnitude and distribution of the earth pressure against the sheeting must be inferred from the strut loads. Leading to a rough but reasonable approximation, the simplest procedure is to assume the load in each strut to be equal to the total earth pressure acting on the sheeting over a rectangular area extending horizontally half the distance to the next vertical row of struts on each side, and vertically half the distance to the horizontal sets of struts immediately above and below. The earth pressure is assumed to be distributed uniformly over the rectangular area. The rectangular area tributary to the uppermost strut in a cross-section extends to the ground surface. For the purpose of the calculation, the bottom of the cut is assumed to be a strut. If the shear in the sheeting at the bottom of the cut has not been measured, the earth pressure per unit of area is assumed to have the same value as that tributary to the lowermost actual strut. The procedure is illustrated in Fig. 46.3.

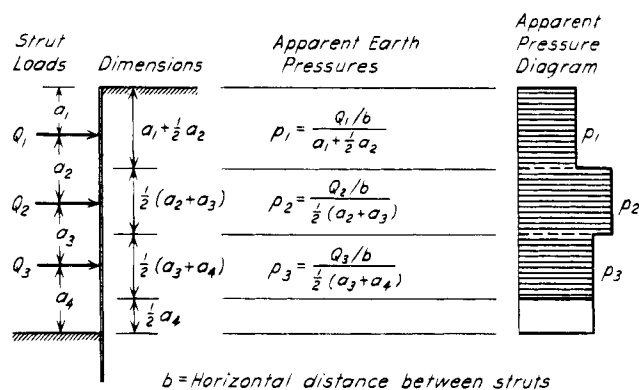


**Figure 46.3** Method of calculating apparent pressure diagram from measured strut loads  $Q$  in open cuts.

The real distribution of the earth pressure against the sheeting may differ appreciably from that calculated in accordance with the foregoing procedure because of the continuity of the sheeting and because of the assumptions concerning the pressures near the bottom of the cut. Moreover, in cohesionless materials the earth pressure at the ground surface must be zero. For these reasons the pressure calculated in this manner is designated the *apparent earth pressure*. However, if the apparent earth pressure is known, the corresponding strut or tieback loads can be computed by following the inverse procedure.

By assigning appropriate stress-deformation characteristics to the soil and to the members of the support system, and by simulating the successive steps in carrying out the excavation and installing the supports, the loads in the support system and the movements of the soil adjacent to a cut can be calculated by finite-element or finite-difference methods (Bjerrum et al. 1972, Clough et al. 1972, Murphy et al. 1975). The results of such calculations are particularly useful in estimating the ground movements associated with open-cut construction and the influence on such movements of the stiffness of the support system. Although some conclusions from finite-element studies are included in this article, more applications will be discussed in Article 54.

### 46.3.2 Deep Cuts in Sand

The earliest reliable measurements of strut loads were made in the late 1930's during construction of the Berlin and New York subways (Spilker 1937, White and Prentis 1940), followed shortly by similar measurements at the Spree Underpass in Berlin and on the Munich subway (Klenner 1941). At all locations the surrounding materials were sands in which the water table before excavation was below the bottom of the cut.

The bracing for the Berlin subway was of the type shown in Fig. 46.2a. The struts were arranged in vertical planes spaced uniformly along the length of the cut, and the loads in the struts were measured in six of these

planes. The apparent earth pressure on four sets of struts is shown in Fig. 46.4a. The apparent pressure diagrams for the other sets lie within the range of those shown.

Although the deposit of sand at the site of this open cut was fairly homogeneous, the various diagrams representing the apparent earth pressure vary considerably from the statistical average. The variations were probably caused to some extent by local differences in the soil properties but to a greater extent by differences in the details of construction procedure at different locations. Yet the distance  $n_a H$  of the center of pressure from the bottom of the cut ranged between the rather narrow limits of  $0.46 H$  and  $0.50 H$ . Similar results were obtained from measurements of seven sets of struts in an excavation for the Munich subway for which  $n_a$  varied from 0.41 to 0.55, and of six sets of struts in an excavation for the New York subway for which  $n_a$  varied from 0.46 to 0.54. Hence, the value of  $n_a$  was found, in all the cuts in sand, to be on the order of 0.5, corresponding to a roughly parabolic distribution of pressure, instead of 0.33, corresponding to a linear increase of pressure with depth. Similar results have been found in subsequent measurements on cuts in sand with depths as great as 19 m (Scott et al. 1972, Briske and Pirlet 1968).

According to Article 37, the total earth pressure for the deformation conditions associated with the excavation and bracing of an open cut in sand should correspond to that calculated on the assumption that the surface of slid-

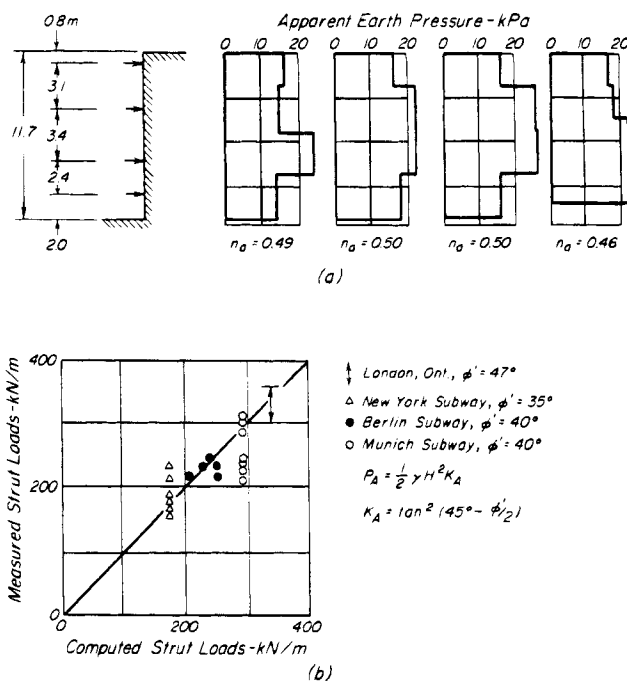


**Figure 46.4** (a) Apparent earth-pressure diagrams for four sets of struts in Berlin subway open cut. (b) Comparison of measured and calculated total loads in vertical sets of struts in various open cuts in sand.

ing is a logarithmic spiral. For a cut of given depth  $H$  in a material of unit weight  $\gamma$ , the horizontal component of the total active pressure depends on the values of  $n_a$ ,  $\phi'$ , and the angle of wall friction  $\delta$  between the horizontal and the direction of the earth pressure on the back of the sheeting. For values of  $n_a$  ranging from 0.4 to 0.6, for a reasonable value of  $\delta$  equal to  $\phi'/2$ , and for values of  $\phi'$  ranging from  $30^\circ$  to  $45^\circ$ , the difference between the coefficient of active earth pressure,

$$K_A = \frac{P_A}{\frac{1}{2} \gamma H^2} \quad (46.1)$$

computed by the logarithmic spiral method, and the Rankine value  $P_A/\frac{1}{2} \gamma H^2$  is smaller than that associated with the evaluation of the angle of internal friction  $\phi'$  itself. Therefore, use of the Rankine coefficient is justified for estimating the total earth pressure in lieu of the coefficient calculated by the less convenient logarithmic spiral method. The reliability of the procedure can be judged in Fig. 46.4b by comparing the sum of the loads in each vertical set of struts in the Berlin, Munich, and New York subways with the total earth pressures calculated on the basis of Eq. 28.1. The measured strut loads include an allowance for the pressure transferred to the soil beneath the bottom of the cut, as shown in Fig. 46.3. The fairly dense sands at the cuts in Berlin and Munich were assigned a value  $\phi' = 40^\circ$ , and the somewhat looser sands in New York a value of  $35^\circ$ . In addition, the results are also shown in Fig. 46.4b for a cut 15 m deep in London, Ontario, where the average value of  $\phi'$  was found in triaxial tests to be about  $47^\circ$  (Scott et al. 1972). The excellent agreement indicates that using Eq. 28.1 to calculate the total earth pressure is fully justified.

On the other hand, the distribution of the apparent earth pressure at a given vertical section may resemble any of the diagrams in Fig. 46.4a. It changes from place to place. Because each support should be designed for the maximum load to which it may be subjected, the design of the supports should be based on the envelope of all the apparent pressure diagrams determined from the measured strut loads. In Fig. 46.5a, the maximum apparent earth pressure for each of the three subway projects has been plotted. The pressure was computed by converting the highest individual strut load at each level into apparent earth pressure. The apparent earth pressure was then expressed in terms of the quantity  $K_A \gamma H$ , where  $K_A$  is the Rankine coefficient  $\tan^2(45^\circ - \phi'/2)$ . The simplest envelope of best fit corresponds to a uniform pressure equal to  $0.65 K_A \gamma H$  for the entire depth of the cut.

Hence, for a similar cut in dense sands, supports should be designed for loads determined from the apparent pressure diagram Fig. 46.5b. This procedure should provide for the highest support loads that can occur. The most probable value of any individual strut or tieback load is about 25% lower than the maximum.

The apparent pressure diagram for design (Fig. 46.5b) has been established on the basis of cuts ranging in depth from about 8 to 19 m. It is emphasized that the apparent pressure diagram for design does not resemble the real distribution of earth pressure against the sheeting of the sides of the cut; it is merely an artifice for calculating values of the strut or tieback loads that will not be exceeded in any real support in a similar open cut. In general, the bending moments in the sheeting or soldier piles, and in wales and lagging, will be substantially smaller than those calculated from the apparent earth pressure diagram suggested for determining support loads.

If the water table is lowered by pumping from open sumps in the cut, ample allowance should be made for seepage pressures against the lower part of the support system. Drainage through spaces between the lagging boards is not sufficient to eliminate seepage pressures. The effect of this type of drainage is similar to that of the drainage layer behind the retaining wall shown in Fig. 45.4a.

### 46.3.3 Cuts in Saturated Clay

Most braced or tied-back cuts in clay are intended to provide working space for the construction of a permanent structure such as a basement or tunnel. During the relatively short time such a cut must function, equilibrium of pore pressures in the adjacent mass of clay is not likely to be achieved, and practically undrained conditions may prevail. The total lateral pressure is then a function of  $K_A$  (Eq. 37.9). Because the value of

$$K_A = 1 - \frac{4s_u}{\gamma H} \quad (37.9)$$

becomes negative for  $s_u > \gamma H/4$ , whereas experience indicates that the supports of even shallow cuts in stiff clays carry some load, it is evident that, for values of  $s_u$  appreciably greater than  $\gamma H/4$ , the state of equilibrium behind the cut is more nearly elastic than plastic and the theories of limiting equilibrium are not applicable. Thus, for cuts in which  $s_u > \gamma H/4$ , or for the first stages of excavation of deep cuts when  $H$  has not yet exceeded  $4s_u/\gamma$ , the total earth pressure can be assessed only on the basis of empirical rules derived from field measurements or by means of finite-element procedures in which the construction sequence is simulated and the soil is assigned appropriate stress-strain relations. In shallow cuts with depths less than about 6 m, the use of standardized bracing eliminates the need for calculating the loads in the supports. In deep cuts the loads in the upper supports at early stages of excavation are rarely as great as they become when the excavation reaches its maximum depth. Hence, for deep cuts, methods of limiting equilibrium can be expected to furnish reasonable values for design of the supports if  $H$  is equal to or exceeds about  $4s_u/\gamma$ ,

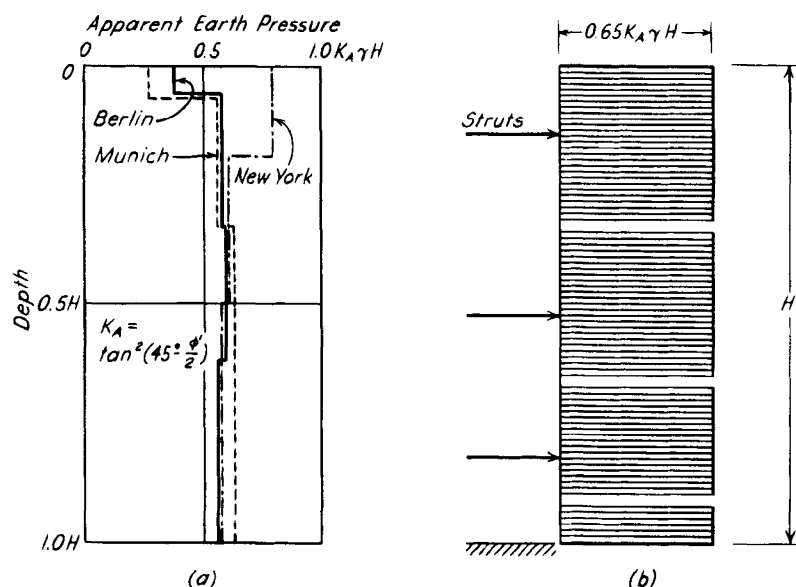


**Figure 46.5** (a) Envelope of apparent earth-pressure diagrams for measured strut loads in sand. (b) Suggested apparent earth-pressure diagrams for design of struts in open cuts in sand.

whereas if  $H < 4s_u/\gamma$ , finite-element or empirical procedures are preferable.

#### 46.3.4 Deep Cuts in Soft to Medium Clay

Numerous observations have been carried out in deep cuts in saturated clays. The values of  $n_a$  usually ranged from 0.30 to 0.50 with an average of 0.39; at one cut the exceptionally high value of 0.59 was found. The measurements leave no doubt that minor and inevitable variations in construction procedure, such as differences in the interval of time between excavation of the clay and placement of the support, are of paramount importance in determining the load that will be carried by the support. This is illustrated by Fig. 46.6, in which each horizontal bar represents the average load in all eight struts at the same level and at the same excavation stage in one open cut in Chicago. The extremities of the bars represent the maximum and minimum values of the strut loads at that level and stage. The cut contained five levels of struts. Excavation was carried out systematically from one level to the next, and after each stage of excavation the eight new struts were carefully installed and prestressed to 100 kN each. Yet, in spite of the unusually uniform construction procedure, individual strut loads in each level varied as much as  $\pm 60\%$  from the average. Similar variations are characteristic for all cuts in which enough strut loads have been measured to provide statistically significant data.

The sums of the loads carried by vertical sets of struts in a given open cut, in which the sets are equally spaced in the horizontal direction, vary much less than the loads in individual struts. Nevertheless, even the variation in total loads is considerable. This is illustrated in Fig. 46.7,

in which each horizontal bar indicates the range in total load as well as the average load in identical vertical sets of struts in each of five different open cuts in Chicago. The cuts contained from 5 to 17 vertical sets of struts. For some of the cuts the variation from the average is as much as  $\pm 30\%$ . The variation is similar in other localities where measurements have been made.

These findings are of outstanding practical importance. They demonstrate that erroneous conclusions concerning the validity of theories for the earth pressures against the bracing of open cuts are likely to be drawn if strut-load measurements have been made on only one or two vertical sets of struts in a given cut. Moreover, the results of any calculations for estimating the loads that must be carried by the individual struts must be interpreted to take into account the inevitable scatter in both the total load on vertical sets of struts and in the load on struts at the same level in different sets.

According to Eq. 37.13, the total earth pressure against a cut in saturated clay is

$$P_a = \frac{1}{2} \gamma H^2 [K_A + \Delta K] \quad (37.13)$$

where  $K_A$  is the Rankine value

$$K_A = 1 - \frac{4s_u}{\gamma H} \quad (37.9)$$

and  $\Delta K$  is the increment in  $K$  if the base stability number  $N_b = \gamma H/s_{ub}$  exceeds about 5.14 (Eq. 37.14). The validity of Eq. 37.9 may be assessed with the aid of Fig. 46.8, in which the total lateral pressure against a variety of cuts in soft to medium clays, as determined from strut-load

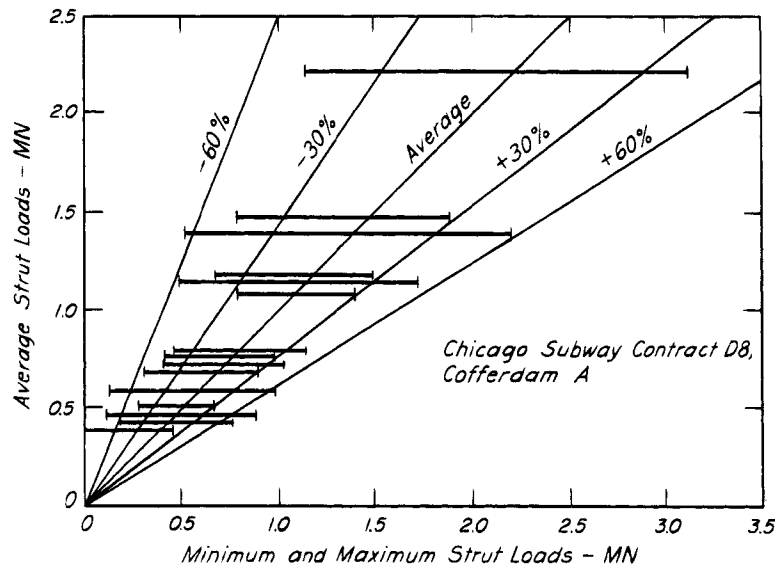


**Figure 46.6** Variation of loads in struts in one open cut in Chicago. Each horizontal bar represents average, minimum, and maximum loads in eight struts at same level and at same stage of excavation.

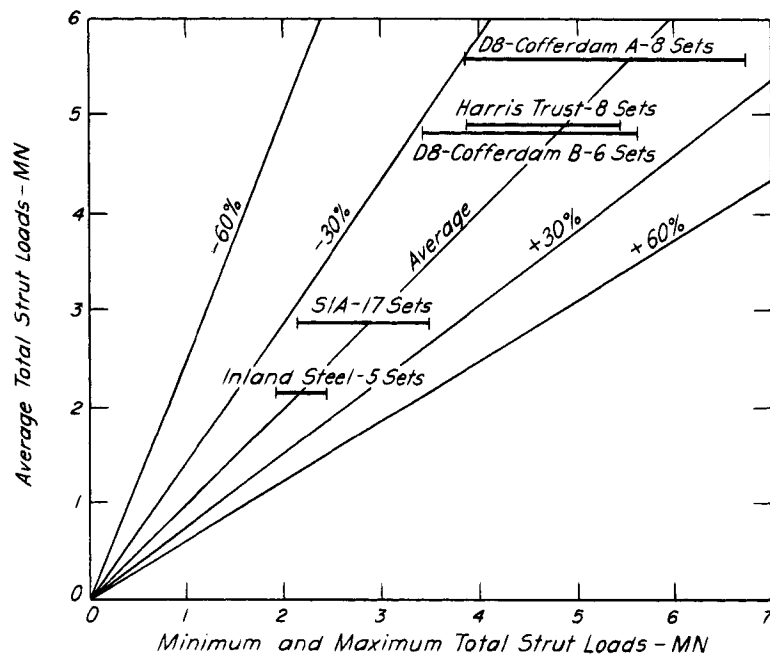


**Figure 46.7** Variation of loads in identical sets of struts in various open cuts in soft to medium clay in Chicago. Each horizontal bar represents average, minimum, and maximum sum of loads in the sets of struts in one open cut when that cut had reached its maximum depth.

measurements is compared to that computed by means of Eq. 37.9. It is evident that all the observed pressures indicated by the solid dots are within about  $\pm 30\%$  of the computed ones. The triangles represent pressures measured in certain cuts in Oslo and Mexico City where the base stability factor was excessive. When these computed values of  $K_A$  are increased by the appropriate values of

$\Delta K$  (Eq. 37.14), the solid circles representing the corrected values are within or close to the  $\pm 30\%$  scatter band. Thus, the use of Eq. 37.14, within the limitations noted in the preceding paragraph, seems justified.

On the other hand, if the average undrained shearing resistance over the depth  $H$  of the cut is less than about  $\gamma H/6$ , corresponding to  $K_A = 1/3$  in Eq. 37.9, the shearing

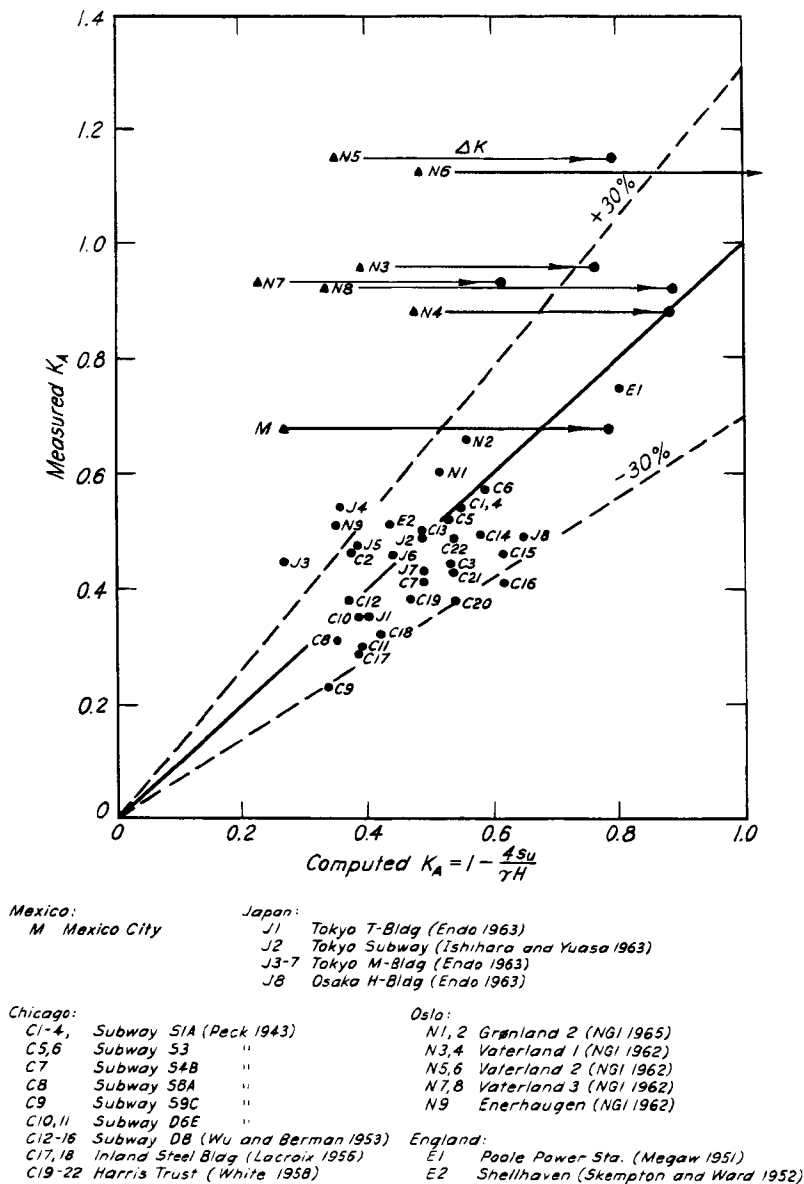


**Figure 46.8** Comparison of measured earth pressures against bracing of open cuts in soft to medium clays with pressures computed by Rankine's theory (After Flaate 1966)

strength will not be fully mobilized, and quasielastic conditions will prevail. It follows that Eq. 37.8 is not applicable to cuts of usual depths, between about 10 and 15 m, in stiff or very stiff clays. Such cuts are discussed in Article 46.3.5.

As was found for cuts in sand, the distribution of the apparent earth pressure varies from cut to cut, and from section to section in the same cut. Because each support should be designed for the maximum load to which it may be subjected, the design of the supports should be based on the envelope of all the apparent pressure diagrams determined from the measured strut loads. In Fig. 46.9 are plotted representative maximum apparent earth-pressure diagrams for cuts in several different localities.

The apparent earth pressure in each instance is expressed in terms of the quantity  $K_A \gamma H$ , where  $K_A$  is defined by Eq. 37.9.

The apparent pressure diagram shown in Fig. 46.10a is considered to be a reasonably conservative basis for estimating the loads for design of supports in cuts in soft to medium saturated clay. In a few instances the maximum apparent pressure diagrams (Fig. 46.9) exhibit somewhat greater pressures over limited vertical distances, but the influence of the excess on the support loads is small and well within the factor of safety for which the supports should be designed. The method of calculation of strut or tieback loads is the same as that described previously for sands.



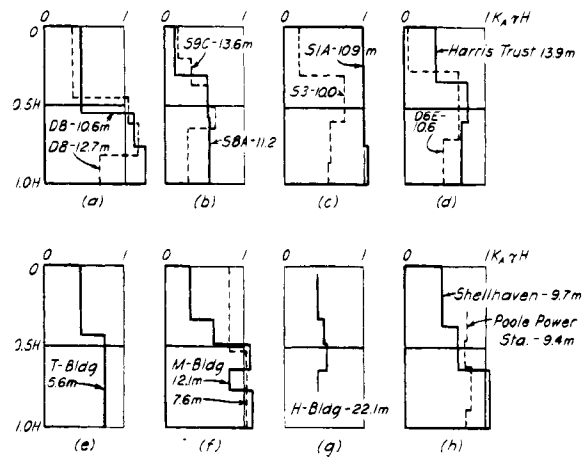


**Figure 46.9** Maximum apparent pressure diagrams for representative open cuts in soft to medium clays: (a to d) Cuts in Chicago; (e and f) cuts in Tokyo; (g) cut in Osaka; (h) cuts in England.

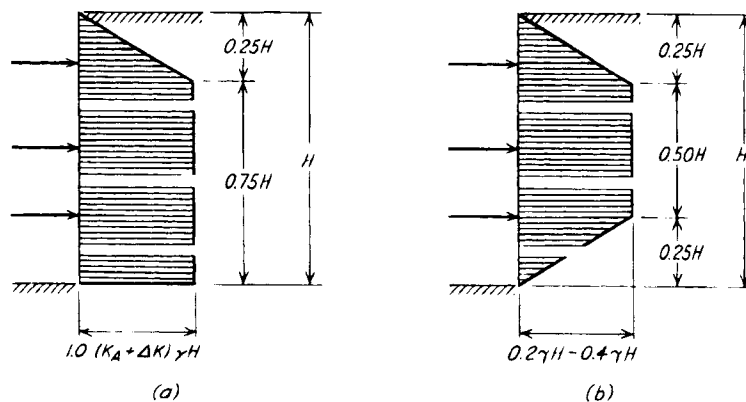


**Figure 46.10** Apparent pressure diagrams for design of struts in cuts excavated in clay soils: (a) Diagram for soft to medium clays; (b) tentative diagram for stiff-fissured clays, lower pressure to be used only when results of observations on similar cuts in the vicinity so indicate. Otherwise, lower limit should be taken as  $0.3\gamma H$ .

Some of the cuts in Chicago were subjected to extended periods of below-freezing weather. The apparent earth pressures corresponding to these conditions have not been included in Fig. 46.9. In some instances they reached magnitudes several times those that had developed at the same stages of excavation before freezing.

#### 46.3.5 Deep Cuts in Stiff Clay

The stability number  $\gamma H/s_u$  for deep cuts in stiff clay is generally less than 4. Consequently, the stresses and deformations correspond to a quasielastic state instead of a state of limiting equilibrium. The magnitude and distribution of earth pressure depend primarily on the value of  $K_0$ , on the *in situ* modulus of elasticity, and on the details of the excavation and support system. The latter include the stiffness of the supports, the depth of excavation before each level of supports is installed, and the prestress to which the supports are subjected.

In very stiff intact nonfissured cohesive soils, even a deep cut should be able to stand without support, although the face of the cut would deform slightly toward the excavation as excavation proceeded. Supports are provided, however, to prevent a failure that might occur on account of an undetected weakness in the soil. If the supports are stiff and, in addition, are highly prestressed, they are likely to experience very large loads, inasmuch as they inhibit the elastic deformations. At the Civic Center subway station in Los Angeles an open cut was excavated to a depth of 23 m in a cohesive soil described locally as a soft siltstone. Heavily prestressed steel bracing in the upper part of the cut buckled locally at connections under loads substantially greater than those for which it was designed, but lateral movements of the walls of the excavation and settlements of the adjacent pavement remained very small. The stiff bracing together with the high prestress attracted load by inhibiting the small

elastic deformations that would otherwise have occurred. Under these circumstances, forecasts of support loads and deformations are best made by finite-element or finite-difference modeling in which the construction sequence is simulated for appropriate values of the soil properties. Because of the inevitable uncertainties in evaluating these properties, it is advisable to measure the stresses and deformations at early stages of the excavation, to adjust the assumed values in accordance with the findings, and to refine the forecast (Roth et al. 1993).

Most stiff clays, however, are weaker than the material described above and contain fissures and other features that reduce their stiffness as compared with the stiffness of intact materials. Under these conditions, empirical data assembled in the form of equivalent pressure diagrams provide an indication of the loads that may be experienced by support systems. Several sets of such data are shown in Fig. 46.11. One set (Fig. 46.11a) was made in a cut only 4 m deep in the stiff fissured crust at the top of the softer deep clays in Oslo (DiBiagio and Bjerrum 1957). Another was made in a deep excavation in typically fissured London clay (Golder 1948). The cuts in Houston (Ulrich 1989a) were made in stiff overconsolidated heavily slickensided and fissured clays locally containing layers or lenses of stiff sandy clays. Although the measured pressures generally fall within the limits of the apparent pressure diagram, there is as yet no sound basis for judging where within the limits the pressures on a new project would fall.

#### 46.3.6 Deep Cuts in Stratified Soils

Relatively uniform deposits of sands or clays, such as those considered in the preceding sections, are seldom encountered. Consequently, most braced cuts are excavated through stratified or lenticular formations containing an assortment of sands, clays, and silts. Even the

simplest of these conditions do not lend themselves to rigorous calculation of the lateral earth pressure by methods of limiting equilibrium. Under several conditions of practical importance, however, sufficient field information is available to justify semiempirical or empirical procedures for estimating apparent pressure diagrams. If a saturated clay deposit contains one or more sand layers or lenses with a total thickness not more than about 25% of the depth of the cut, each layer of sand may be considered to consist of clay having the same thickness as the sand and an undrained shear strength  $s_u$  equivalent to the drained shearing resistance of the sand. It is thus implied that the sands will drain readily during the period of construction and use of the cut, whereas during the same period the clays will remain essentially undrained. A method for calculating the equivalent  $s_u$ , based on the assumption that the surface of sliding is a plane rising at  $45^\circ$  to the horizontal as if the entire mass were indeed clay in an undrained state, is illustrated in Fig. 46.12. The average undrained strength along the entire surface of sliding is then used to calculate the value of  $1 - 4s_u/\gamma H$ . If the value is positive,  $K_A$  is determined from Eq. 37.5 and the apparent pressure diagram (Fig. 46.10a) used to design the bracing. Otherwise, Fig. 46.10b is applicable. As a matter of fact, corrections of this general type were required for the various open cuts in Chicago (Peck 1943) to account for the presence of a layer of sand overlying the deep deposits of clay, and the values of  $K_A$  shown in Fig. 46.9 reflect these corrections.

Little if any information is available if the soils at the site of an open cut are primarily sands containing layers or lenses of soft to medium clays. On the other hand, many sets of strut-load observations have been made in cuts in medium to dense sands containing layers of stiff to hard clays and silts with aggregate thicknesses of as much as 50% of the depth of the cuts. In all instances

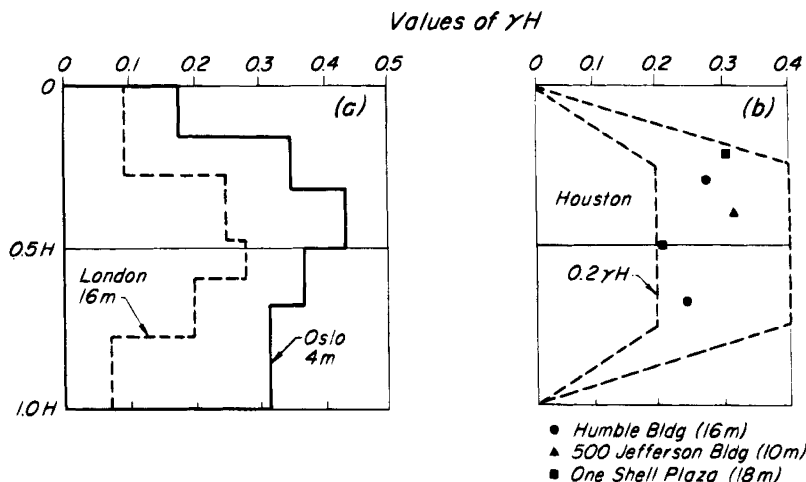


**Figure 46.11** Maximum apparent pressures for cuts in stiff clays: (a) Fissured clays in London and Oslo; (b) stiff slickensided clays in Houston.

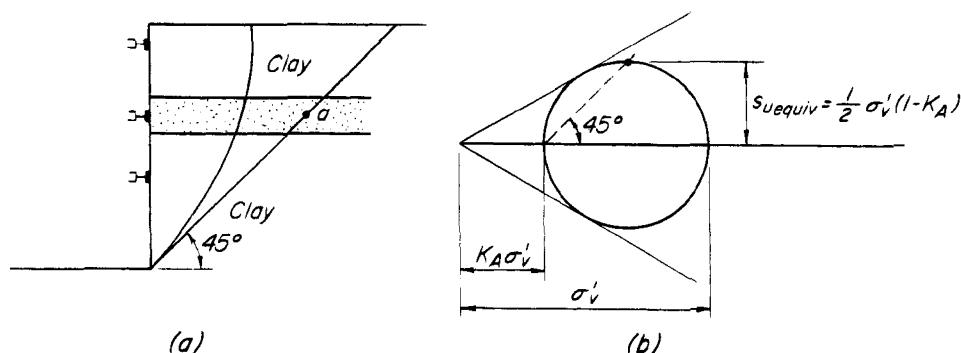


**Figure 46.12** Method for determining equivalent undrained shear strength of sand layer in clay deposit behind braced cut. (a) Location of point *a* on surface of sliding. (b) Stress conditions at point *a* and equivalent undrained shear strength.

the water levels had been drawn down below the bottoms of the cuts. Apparent pressures for five of these cuts, two in Washington, D.C., two in Oakland, California, and one in Cologne, Germany, ranging in depth from 18 to 25 m, are plotted in Fig. 46.13 (O'Rourke 1975). The width of the envelope is about  $0.3\gamma H$ . Values of shearing resistance for the soils at the five cuts were not determined definitively, inasmuch as most of the explorations were carried out by penetration testing. However, on the assumption that the width of the envelope is equal to  $1.0 K_A \gamma H$  (Fig 46.10a), back-calculated values of  $\phi'$  for an equivalent sand range from  $37^\circ$  to  $42^\circ$ , corresponding to dense sandy soils.

#### 46.4 Tiebacks

Because of the similarity of the deformation conditions associated with the construction of strutted and tied-back cuts (Fig. 37.1), the apparent maximum pressure diagrams for determining strut loads can be used with considerable confidence to determine the horizontal components of the loads for design of tiebacks. The practical validity of the procedure has been demonstrated under a wide variety of conditions (Liu and Dugan 1972, Clough et al. 1972, Mansur and Alizadeh 1970, O'Rourke 1975, Ulrich 1989b).

The same considerations of soil mechanics that enter into the design and performance of strutted bracing systems are applicable to tied-back systems. Three further aspects are involved: the imposition of the vertical component of the tieback forces onto the wall if the tiebacks are not horizontal; evaluation of the resistance of each tieback against being pulled out of the ground; and determination of the distance beyond which the anchors must be located to avoid a general failure of the mass of soil in which the anchors are embedded.

The downward load imposed on the wall by inclined tiebacks causes the wall to settle. The downward movement allows the upper end of each tieback to rotate about the anchor, whereupon the wall moves toward the excava-

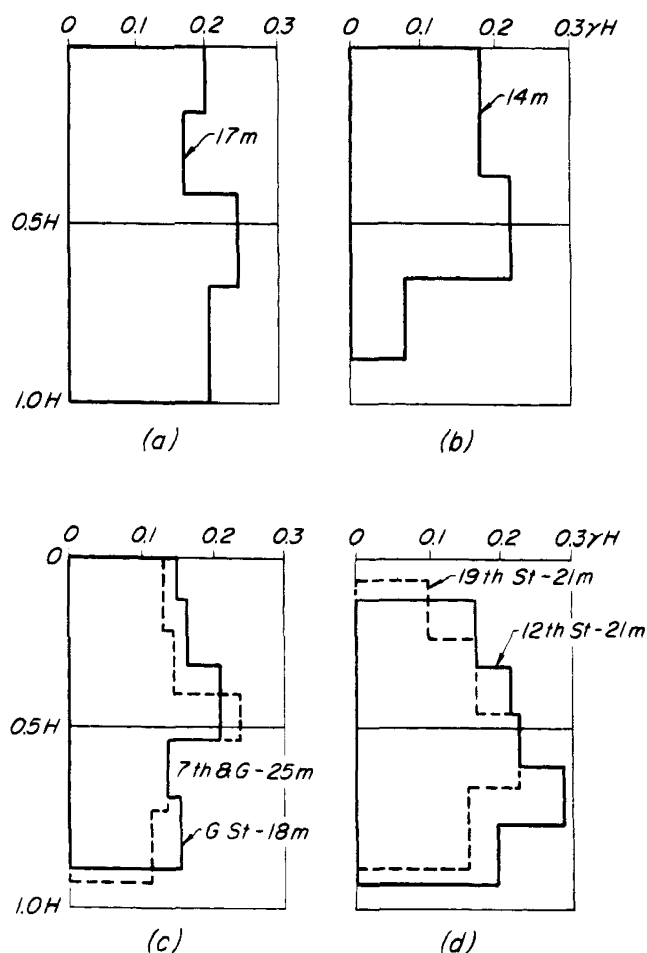


**Figure 46.13** Maximum apparent pressure diagrams for representative deep open cuts in medium to dense sands containing layers of stiff to hard clays and silts. Cuts in (a) Cologne, (b and c) Washington, D.C., (d) Oakland, California.

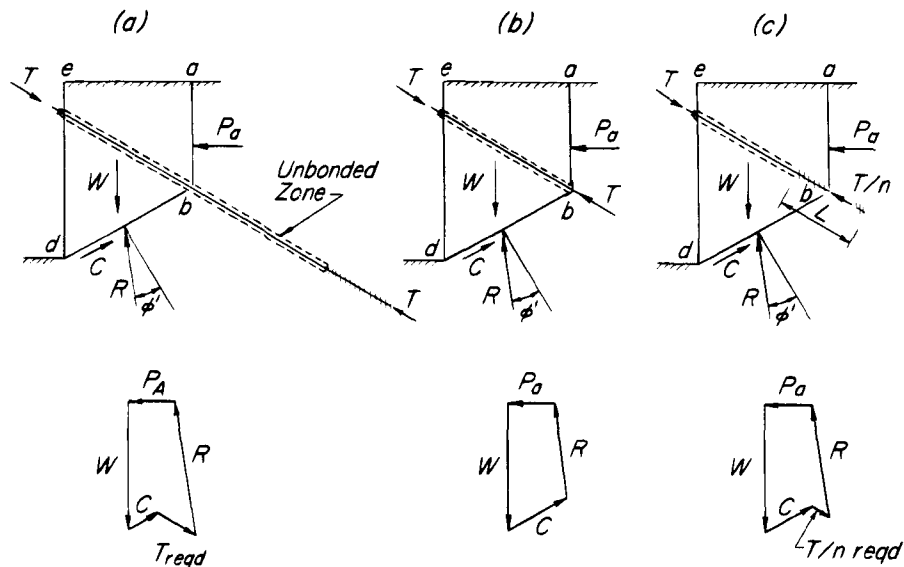


**Figure 46.14** Free-body diagrams representing influence on tiered force  $T$  of different assumptions concerning manner in which tiered force is applied to the soil: (a) Tiered resistance fully developed outside failure wedge; (b) resistance assumed to be concentrated at boundary of wedge; (c) resistance developed only within failure wedge.

tion. The movement causes loss of ground and settlement adjacent to the cut (Article 54). It also tends to unload the lower tiebacks, which are short compared with the upper ones. The lost load must then be partly transferred to the tiebacks above. Thus, good practice requires either that the wall extend down to a stratum on which it can find adequate bearing, or that it penetrate far enough into the underlying strata to develop the capacity to resist the downward loads with minimal settlement. Evaluation of the load-settlement relation for the embedded portion of a wall or soldier pile involves all the complexities and uncertainties associated with determining the same relation for a friction pile (Article 52).

Various procedures, some proprietary, are available for creating the anchorage of a tieback. The anchor is established beyond the limits of any wedge that might participate in a general failure behind the wall. Usually the portion of the tieback passing through the potential failure wedge is separated from it by a bond-breaker that reduces or eliminates transfer of stress from the tie to the soil within the wedge. Although calculations of the pullout resistance of anchors are often made as a guide to preliminary design, the actual capacity is investigated by testing representative anchors to failure. Design loads are established by applying a suitable factor of safety and by restricting the loads to values that will not induce creep. The design loads and the apparent earth pressures to be supported then determine the spacing of the anchors. It is customary to proof-test each tieback to its design load and then to reduce the load to some fraction such as 80% of this value before locking off the tieback. By

this inexpensive routine procedure the adequacy of the individual anchors is ensured.

In principle, stability calculations for the wedge in which the tiebacks are embedded can be made by assuming various positions for the failure surface, constructing the polygon of forces and, if the tiebacks extend beyond the failure surface, determining the required tieback force for equilibrium. In practice, the assessment of stability is complicated by the location of the anchor and the manner in which the stress in the anchor is transferred to the soil. This situation is illustrated for a single anchor in Fig. 46.14. If the anchor is located far behind the failure surface (Fig. 46.14a), the tiered force  $T$  constitutes an external reaction fully effective in adding to the stability of the wedge. On the other hand, if the anchor can be considered to be concentrated at a point  $b$  at the boundary of the wedge (Fig. 46.14b), the tiered reactions  $T$  produce no net external reaction on the wedge and the stability of the wedge depends solely on the resistance of the soil. In reality the anchor resistance is developed over an appreciable length  $L$  (Fig. 46.14c), and some fraction  $T/n$  of the anchor load may be developed beyond the boundary of the wedge. The remainder,  $T - T/n$ , merely stresses the wedge internally. Opinions regarding the appropriate value of  $n$  range from  $n = 2$  (Rankine and Ostermayer 1968) to  $n = 1$  (Schnabel 1982). Experience has indicated, however, that wedge stability will usually be adequate if the anchors are located entirely beyond a plane rising from the base  $d$  of the excavation (Fig. 46.14), at an angle to the vertical of about  $35^\circ$  for granular soils and about  $45^\circ$  for cohesive soils. If a weak zone exists locally behind

the wall, its strength and position may influence the shape and location of the critical surface, and analyses similar in principle to those of Fig. 46.14 should be carried out. In addition, the possibility of failure along a curved surface of sliding encompassing the entire assemblage of wall and tiebacks should be investigated.

The length and inclination of tiebacks is often determined by the location of strata particularly suited or unsuited to the construction of anchors and to the development of resistance without inducing excessive creep. Soft to medium clays and loose silts or sands are usually avoided. The performance and interpretation of tests to establish design capacities and to ensure the performance of each of the installed tiebacks deserve careful attention (Schnabel 1982).

### Selected Reading

Both the methods of construction and the design of supports for open cuts have undergone rapid development in recent years. The innovations were discussed extensively at the ASCE Conference on Design and Performance of Earth Retaining Structures, held at Cornell University in 1990. The papers, covering a broad range of types of earth-supporting structures, were published as ASCE Geotechnical Special Publication No. 25, 904 pp.

## ARTICLE 47 STABILITY OF HILLSIDES AND SLOPES IN OPEN CUTS

### 47.1 Causes and General Characteristics of Slope Failures

Every mass of soil located beneath a sloping ground surface or beneath the sloping sides of an open cut has a tendency to move downward and outward under the influence of gravity. If this tendency is counteracted by the shearing resistance of the soil, the slope is stable. Otherwise a slide occurs. The material involved in a slide may consist of naturally deposited soil, of man-made fill, or of a combination of the two. In this article only slides in natural soil are considered.

Slides in natural soil may be caused by such external disturbances as undercutting the foot of an existing slope or digging an excavation with unsupported sides. On the other hand, they may also occur without external provocation on slopes that have been stable for many years. Failures of this nature are caused either by a temporary increase in porewater pressure or by a progressive deterioration of the strength of the soil.

In spite of the variety of conditions that may cause a slide, almost every slide exhibits the general characteristics illustrated by Fig. 47.1. The failure is preceded by the formation of tension cracks on the upper part of the slope or beyond its crest. During the slide the upper part

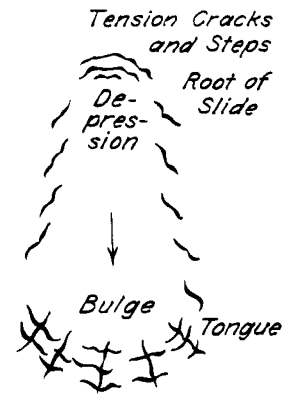


Figure 47.1 Plan of typical slide in cohesive material.

of the slide area, known as the *root*, subsides, whereas the lower part, known as the *tongue*, bulges. Hence, if the original surface of the slope is a plane, the profile of the ground surface along the axis of the slide becomes distorted into an S-shaped curve (Fig. 35.1). The shape of the tongue depends to a certain extent on the type of sliding material. Homogeneous clay with a low degree of sensitivity to disturbance is likely to bulge, as shown in Fig. 47.1. On the other hand, clay with a very sensitive structure or clay with sand pockets is likely to flow like a liquid.

Even on uniform slopes of great length and approximately uniform height, slides seldom occur at more than a few places, separated from each other by considerable distances. For example, the well-known slides in the Panama Canal appear in plan as isolated scars separated by long stretches of intact slope. Slides in long railroad cuts of fairly uniform cross-section exhibit similar characteristics. However, if the geologic conditions are such that the major part of the surface of sliding is located within a horizontal layer of coarse silt or sand that separates two layers of clay, the dimension of the slide measured parallel to the crest of the slope is likely to be very much greater than that perpendicular to the crest. Slides of this type are generally caused by an excess porewater pressure in the sand or silt layer.

### 47.2 Engineering Problems Involving the Stability of Slopes

Construction operations, such as cutting into slopes for highways or commercial developments, placing fills on slopes, or exposing slopes to the water of a reservoir, may initiate sliding in previously stable ground or may reactivate old slide masses. The engineer must judge the likelihood, extent, and consequences of such movements and, where necessary, design measures to prevent them or to mitigate their effects. In some instances similar actions must be taken with respect to potential slides that may arise from natural external causes such as undercutting by streams or shaking by earthquakes.

On the other hand, slides often occur without external provocation as a result of a decrease in shearing resistance of the materials comprising the slope. Usually the decrease that triggers the slide is caused by exceptionally high porewater pressures associated with heavy precipitation or snow melt. Yet, because the probability is very low that unprecedented piezometric conditions would occur during one person's lifetime in a slope that has been stable for hundreds or thousands of years, it is evident that other causes of decreasing shearing resistance are active, such as creep, chemical weathering, or removal of a soluble binder from the soil mass. Here again the engineer must judge the likelihood of a slide that might endanger life or property and, if necessary, design suitable preventive measures.

In many instances, external and internal causes act simultaneously. The shearing stresses in a slope may be increased by cutting, but failure may not occur until porewater pressures reach a critical value associated with climatic conditions.

Successfully coping with landslides requires, perhaps in more than any other aspect of geotechnics, the cooperation of the geologist and the engineer. The geologist's functions include recognition of landslide-prone topography and of old landslides, identification and description of the geologic structure of the ground beneath the slopes, judging the susceptibility of the site to earthquakes, and assessment of the hydrologic conditions not only at the specific site but possibly for several kilometers nearby. The geologist should cooperate with the engineer in the detailed site inspection, in establishing the exploratory program, and in interpreting the results.

The functions of soil mechanics include carrying out the subsurface and laboratory exploration to establish the occurrence and physical properties of the materials in the slope, obtaining piezometric data suitable for quantitative evaluation of pore pressures, establishing reference points and instruments to determine the extent and rate of movement and the geometry of the surface of sliding if a slide is already in progress, and interpreting the data quantitatively in terms of the physical processes involved. Stability analyses may be appropriate for judging the factor of safety against sliding in some instances and for investigating the relative benefits of various remedial measures, but no such analyses are justified unless the geologic features governing the geometry of the slide are taken into account and the physical properties of the soils and porepressure conditions are incorporated realistically.

An aspect of hydrogeology fundamental to the understanding of many problems of the stability of natural slopes is the regime of groundwater flow in the vicinity of slopes and, more specifically, of valleys. Figure 47.2 is a highly idealized flow net representing a cross-section through an upland adjacent to two valleys. The subsurface materials are assumed to be uniformly permeable. From

the recharge area in the upland the water follows the flow lines to the valleys. The discharge into the upper portions of the valley walls has a downward component, but that into the lower parts has an upward component. Consequently, the piezometric level in piezometer A, with its tip well below the valley floor, is higher than that in the shallower piezometer B. The upward seepage pressure represents a destabilizing influence on the slopes in the lower part of the valley. Even in soils having complex patterns of permeability the tendency toward this destabilizing influence is present and is an often overlooked but significant factor tending to reduce the stability of natural slopes. Even when piezometric data are available beneath a slope, they should be interpreted by means of at least roughly drawn flow nets before they are introduced into stability analyses.

The methods for dealing with unstable slopes depend largely on the nature of the soils involved. Hence, for practical purposes it is most suitable to discuss slides in accordance with the types of soil in which they occur. In the following text the causes of several types of slides are described, and present practice in dealing with the engineering aspects of the problems is summarized. Because of the complexity of the subject, the information is no more than an introduction to a study of the stability of slopes in natural soil strata.

### 47.3 Standard Slopes

Experience has shown that slopes at  $1\frac{1}{2}$  (horizontal) to 1 (vertical) are usually stable. The sides of most railway and highway cuts less than 6 m deep rise at that slope, as do those of many deeper stable cuts. Therefore, in many localities a slope of 1.5:1 is considered the standard for railway and highway construction. The standard slopes for flooded cuts such as those for canals range between 2:1 and 3:1.

Steeper than standard slopes on soil, up to 1:1, have been used successfully on some dense residual soils and on mixtures of sand and gravel with boulders. True loess is usually cut at a nearly vertical inclination (0.25:1). On the other hand, it has been found that even the standard slopes are stable only if the cuts are made in *favorable ground*, a term that indicates cohesionless or cohesive sandy or gravelly soil in a moist or dry state. In soft clay or in stiff fissured clay the excavation of even a very shallow cut with standard slopes may cause the soil to move toward the cut, and the movement may spread to a distance from the cut equal to many times the depth. Clay soils containing layers or pockets of water-bearing sand may react to a disturbance of their equilibrium in a similar manner. Deposits with properties of this type constitute *troublesome ground*.

Experienced engineers locate new lines of transportation to avoid cuts in troublesome ground as far as conditions permit. If a project requires long cuts in potentially

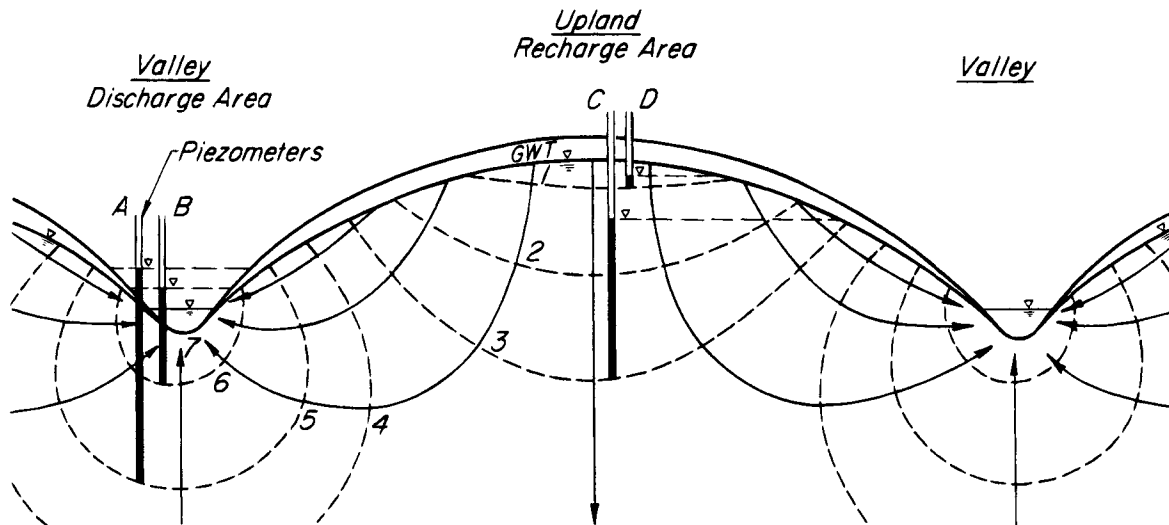


**Figure 47.2** Simplified regional flow system in uniformly permeable materials (after Hubbert 1940).

troublesome soil, estimates are likely to show that costs will be excessive unless the margin of safety is reduced to considerably less than the margin of error in stability computations.

Consequently, in cuts through troublesome soil, local slides are often considered acceptable. At the same time sound engineering requires that the slides should not involve loss of life or serious damage to property. This requirement can be satisfied only by means of extensive and conscientiously executed field observations during and after construction. Such observations make it possible to detect the symptoms of impending slides and to take appropriate measures for avoiding fatal consequences.

#### 47.4 Stability of Slopes and Cuts in Sand

Sand located permanently above the water table is stable ground in which cuts can be made safely at standard slopes. Dense and medium sands located below the water table are also stable. Slides occur only in loose saturated sand that liquefies (Article 20.9). The disturbance required to release a sand slide can be produced either by a shock or by a rapid change in the position of the water table. Once the movement has started, the sand flows as if it were a liquid.

The sand slides along the coast of the island of Zeeland in Holland belong in this category (Müller 1898). The coast is located on a thick stratum of fine quartz sand that consists of rounded grains. The slope of the beach is only about  $15^\circ$ . Yet, once every few decades after exceptionally high tides, the sand liquefies beneath a short section of the coastal belt, flows out, and spreads with great speed in a fan-shaped sheet over the bottom of the adjacent body of water. The tongue of the slide is always very much broader than the root. Figure 47.3 shows a section through one such slide. The final slope of the

ground surface was less than  $5^\circ$ . A slide that occurred at Borssele in 1874 involved nearly  $1,500,000 \text{ m}^3$ .

Because flow slides in sand occur only if the sand is very loose, the tendency toward sliding can be reduced by increasing the density of the sand. This can be accomplished by several different means, such as vibroflotation, dynamic compaction, pile driving, or exploding small charges of blasting powder at many points in the interior of the mass (Article 44.3.3). On slopes of marginal stability, these means may, however, induce a slide.

#### 47.5 Stability of Cuts in Loess

Loess is a cohesive wind-laid soil consisting chiefly of angular and subangular quartz grains with an effective grain size between about 0.02 and 0.006 mm and a low uniformity coefficient. It contains an intricate network of more or less vertical root holes. The cohesion is due to thin films of clay or slightly soluble cementing material that covers the quartz grains and the walls of the root holes. Because the root holes are predominantly vertical, loess has a tendency to break by splitting along vertical surfaces, and its permeability in a vertical direction is large compared with that in a horizontal direction. Its porosity may be as great as 52%.

When loess is located permanently above the water table, it is a very stable soil except that it is readily attacked by erosion. To reduce the erosion as much as possible, cuts in loess are usually given a very steep slope ( $0.25 H:1V$ ). The foot of the slope requires careful protection against temporary saturation during rainstorms. In spite of this precaution, slices break down from time to time, again leaving nearly vertical faces that remain stable for years. To prevent blocking of traffic by the debris it is customary to make the width of cuts in loess greater than that called for by the traffic requirements.

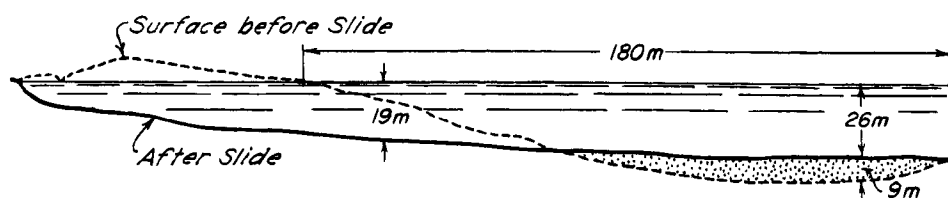


Figure 47.3 Section through flow slide in sand at coast of Zeeland (after Müller 1898).

On the other hand, permanently submerged loess is likely to be very unstable because of its high porosity and because of the leaching or softening effects of submergence. These effects transform the loess into an almost cohesionless material that is not stable unless its porosity is less than about 47% (Scheidig 1934).

The effect of submergence is illustrated by the results of a large-scale experiment performed on a plateau of loess in Turkestan. The loess has an average porosity of 50%. In dry cuts it stands with unsupported vertical faces for a height of more than 15m. The experiment was conducted to find out whether the material would remain stable if an unlined canal were excavated across the plateau and filled with water for irrigation. An open pit, 50 by 20 m in plan, was dug 3 m deep with sides sloping at 1.5 H/1V. The pit was then filled with water and the water level kept constant by replacing the seepage losses. After a few days the slopes started to slough, and the bottom began to subside. This process continued at a decreasing rate for about 6 weeks. At the end of this period the surface surrounding the excavation had cracked and subsided within a distance of about 6m from the original edge of the pit, and the bottom had subsided almost 1m. Within the area of subsidence and sloughing the loess was so soft that it was not possible to walk on it.

#### 47.6 Slides in Fairly Homogeneous Soft Clay

If the sides of a cut in a thick layer of soft clay rise at the standard slope of 1.5:1, a slide is likely to occur before the cut reaches a depth of 3m. The movement has the character of a base failure (see Article 35 and Fig. 35.2b) associated with a rise of the bottom of the cut. If the clay stratum is buried beneath stable sediments, or if it has a stiff crust, the rise occurs when the bottom of the cut approaches the surface of the soft material.

On the other hand, if the soft clay is underlain by bedrock or a layer of stiff clay at a short distance below the bottom of the cut, failure occurs along a toe or slope circle tangent to the surface of the stiff stratum, because the bottom cannot heave (Article 35).

If the base of a mass of soft clay has an irregular shape, the location of the surface of sliding is likely to be determined by that shape. Figure 47.4 illustrates this statement. It represents a section through a slide that occurred during the construction of the Södertälje canal in Sweden. If the soft clay had extended to a considerable

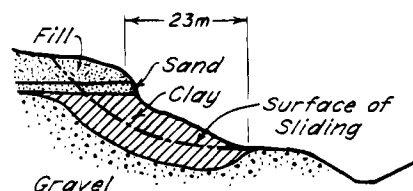


Figure 47.4 Section through toe-circle slide in soft clay on Södertälje Canal in Sweden (after Fellenius et al. 1922).

depth, base failure would have occurred approximately along a midpoint circle. However, the presence of the gravel below the soft clay excluded the possibility of a base failure, and the slide occurred along a toe circle. The movement was so rapid that several workmen were killed (Fellenius et al. 1922).

Experience has shown that sliding failures during construction in masses of homogeneous saturated soft clay take place under undrained conditions. The factor of safety against sliding of the slopes of proposed cuts in such clay can be estimated in advance of construction by the method described in Article 35. However, discontinuities in the clay, consisting of sand or silt partings, may invalidate the results of the computation. The reason is explained in Article 47.8.

#### 47.7 Quick Clay Flows

After a slope on soft clay fails, the movement usually stops as soon as the tongue of the slide (Fig. 47.1) has advanced to a moderate distance from its original position. There is, however, a notable exception to this behavior. In quick clays (Articles 4, 7), such as those that occur in the St. Lawrence River valley, in northern Quebec, and in Norway and Sweden, extensive progressive slides occur from time to time, often without obvious provocation. The movement begins as a small slide, usually at the bank of a stream, but the deformation of the sliding material transforms the clay into a thick slurry that flows out and deprives the new escarpment of its support, whereupon another slip occurs. The disturbance propagates rapidly away from the initial point as the clay is transformed into a fluid matrix of remolded material flowing toward the break in the river bank and carrying with it floating chunks of still intact clay. The principal features of such a flow on one of the northern tributaries of the St. Lawrence River are shown in the block diagram (Fig. 47.5). During



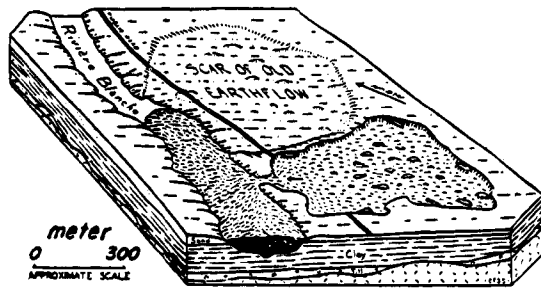


**Figure 47.5** Block diagram showing principal features of flow in quick clay near St. Thuriibe, Quebec (from Sharpe 1938).

the flow a roughly rectangular depression was created with a depth of 5 to 10 m, a length of about 500 m parallel to the river, and a width of 1000 m (Sharpe 1938). Within about half an hour 2,700,000 m<sup>3</sup> of clay moved into the river channel, through a gap 60 m wide. The channel was blocked for more than 3 km, and the upstream water level was raised 8 m. In the great clay flow of Vaerdalen, Norway, in 1893, more than 46,000,000 m<sup>3</sup> flowed out of a narrow gap in less than an hour (Holmsen 1953). In the quick clay flow of Rissa, Norway in April 1978, 5 to 6 million m<sup>3</sup> flowed into lake Botnan in about 5 minutes (Gregersen 1981).

Detailed soil investigations and stability analyses have not permitted definitive conclusions concerning the likelihood that a particular river bank may fail and initiate a flow slide. However, field studies in Norway, undertaken because of the great economic losses caused by flow slides in that country, disclosed that geomorphic factors associated with the triggering of the slides could be recognized (Bjerrum et al. 1969). Only where active erosion in virgin quick clay is occurring are major slides likely. By identifying these rather limited areas and providing erosion protection, it is sometimes possible to safeguard large tracts of land.

#### 47.8 Stability of Slopes on Clay Containing Layers or Pockets of Water-Bearing Sand

In the preceding text we have considered the stability of more or less homogeneous soils. Among the more important nonhomogeneous soil formations are stratified deposits consisting of layers of sand and clay and masses of cohesive soil containing irregular lenses or pockets of sand or silt.

In a sequence of layers of clay and sand or coarse silt, at least some of the latter are likely to be water-bearing during part or all of the year. If a cut is excavated in such a soil, water seeps out of the slopes at various points or along various lines. Therefore, such cuts are commonly referred to as *wet cuts*. They require special attention, particularly if the strata dip toward the slope. The springs that issue along the base of the sand outcrops are likely to cause sloughing, and frost action may also lead to

deterioration. Therefore, it is common practice to intercept the veins of water by drains several meters behind the face of the slope. If the clay strata are soft or fissured, they too may constitute a source of structural weakness. If the cut is deep, a stability investigation should be made to determine the most suitable slope.

Masses of cohesive soil containing irregular lenses or pockets of cohesionless soil are common in regions of former glaciation where the sediments were deposited by melting ice and then deformed by the push of temporarily advancing ice sheets. They have also been encountered in old landslides that took place in stratified masses of sand and clay.

The sand pockets within the clay serve as water reservoirs. During wet weather they become the seat of considerable hydrostatic pressure that tends to cause outward movement of the masses in which they are located. As the soil masses move, they disintegrate into a mixture of saturated silt, sand, and chunks of clay that flows like a thick viscous liquid.

Because the source of instability is the pressure of the water trapped in the sand pockets, stabilization can be accomplished by means of drainage. However, the geological profile is likely to be very irregular, and the spacing of drains may be very difficult to determine in advance even after the soil and hydraulic conditions have been thoroughly investigated by boring, testing, and periodic surveys of the piezometric levels. Under these circumstances an expedient and effective procedure may be the insertion of *horizontal drains*. Such drains usually consist of perforated or slotted metal or plastic pipe of about 50 mm diameter wrapped with filter fabric, inserted into holes drilled nearly horizontally into the soil beneath the slope. The lengths of the drains range from a few meters to more than 100 m. Their horizontal spacing depends on the local conditions; it is often within the range from about 5 to 15m. Several rows at different elevations may prove effective. The drains are usually given a small upward slope into the soil to facilitate the removal of the water by gravity.

The holes for the drains are generally made by a modification of rotary drilling wherein a casing terminating in a hollow bit is advanced by rotation while water is supplied through the interior of the casing and returns around the exterior. The bit is retracted when the hole reaches its final length, the drain is inserted, and the casing withdrawn.

The technique of installation of horizontal auger drains requires adaptation to local conditions, but such drains can often be installed so rapidly and economically that the length and spacing are established on the basis of trial. Several drains may be nonproductive, but those that encounter the pervious pockets may be remarkably effective. Once drainage has been accomplished, the terrain may become as stable as it would have been without the sand inclusions.

### 47.9 Slides in Stiff Clay

Almost every stiff clay is weakened by a network of hair cracks or slickensides. If the surfaces of weakness subdivide the clay into fragments smaller than about 25 mm, a slope may become unstable during construction or shortly thereafter. On the other hand, if the spacing of the joints is greater, failure may not occur until many years after the cut is made.

Slides in clay with closely spaced joints occur as soon as the shearing stresses exceed the average shearing resistance of the fissured clay. Several slides of this type took place in a long railway cut at Rosengarten, near Frankfurt in Germany. The slope of the sides was 3:1. The greatest depth of the cut was 30m, and the average shearing stresses along the surfaces of sliding adjoining the deepest part of the cut were roughly 1 MPa. The clay was very stiff, but large specimens broke readily into small angular pieces with shiny surfaces. Slides started immediately after construction and continued for 15 years (Pollack 1917).

If the spacing of the joints in a clay is greater than about 100 mm, slopes may remain stable for many years or even decades after the cut is made. The lapse of time between the excavation of the cut and the failure of the slope indicates a gradual loss of the strength of the soil. The mechanics of the process of softening are illustrated by Fig. 47.6. Before excavation, the clay is very rigid, and the fissures are completely closed. The reduction of stress during excavation causes deformation of the clay, and some of the fissures open. Water then enters and softens the clay adjoining these fissures. Unequal swelling produces new fissures until the larger chunks disintegrate and the mass is transformed into a soft matrix containing hard cores. A slide occurs as soon as the shearing resistance of the weakened clay becomes too small to counteract the forces of gravity. Most slides of this type occur along toe circles involving a relatively shallow body of soil, because the shearing resistance of the clay increases rapidly with increasing distance below the exposed surface.

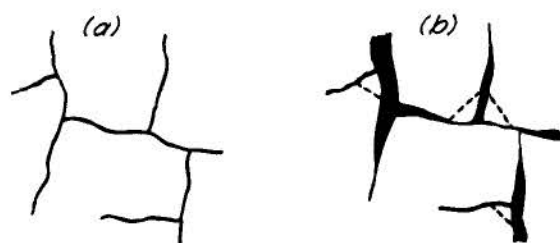


**Figure 47.6** Section through fissured stiff clay mass: (a) Old fissures closed before relief of stress by excavation; (b) relief of stress causes fissures to open, whereupon circulating water softens clay adjacent to the walls (Terzaghi 1936c).

Figure 47.7 shows a slide in very stiff fissured clay beside a railroad cut having side slopes of 2.5:1. The height of the slope was 20m. The characteristic S-shape of the slope after failure is apparent. Failure occurred about 80 years after the cut was excavated. No springs or other indications of percolating water were present.

A study of the records of several delayed slides in stiff clays with widely spaced joints has shown that the average shearing resistance of the clay decreases from a high initial value at the time of excavation to values between 20 and 35 kPa at the time of the slide. Since the process of deterioration may require many decades, it would often be uneconomical to select the slope angle for the sides of cuts in such clays on the basis of the ultimate value of the shearing resistance. However, it is desirable to delay the deterioration as much as possible by draining the strip of land adjoining the upper edge of the cut for a width equal to the depth of the cut and by treating the ground surface of the cut area to reduce its permeability. Should local slides occur at a later date, they can be remedied by local repairs. If delayed slides would endanger life or cause excessive property damage, the slope should be provided with reference points and periodic observations should be made, inasmuch as slides of this type are always preceded by deformations that increase at an accelerated rate as a state of failure is approached. When the movement becomes alarming, the slopes in the danger section should be flattened.

Hard core drains have also been successfully used to prevent movements at danger sections. These drains consist of ribs of dry masonry installed in trenches running up and down the slope at a spacing of about 5 to 7 m. The trenches are excavated to a depth somewhat greater than that to which the clay has been softened. A concrete footwall supports the lower ends of all the ribs. The beneficial effect of this type of construction is commonly ascribed to the action of the ribs as drains, but it is more likely that the principal function of the ribs is to transfer



**Figure 47.7** Slide in very stiff fissured clay.

part of the weight of the unstable mass of clay through side friction to the footwall.

The behavior of poorly bonded clay shales is governed by many of the same considerations as that of stiff clays. Hence, further information concerning slides in heavily overconsolidated clays is contained in the next article.

#### 47.10 Slopes on Shale

From an engineering point of view, shales are of outstanding importance because they constitute about 50% of the rocks that are either exposed at the earth's surface or are buried beneath a thin veneer of sediments. All the rocks of this category consist of deposits of clay or silt that have acquired their present characteristics under the influence of relatively moderate pressures and temperatures.

As the thickness of overlying deposits increases to perhaps thousands of meters, the porosity of a clay or silt deposit decreases; an increasing number of cohesive bonds develops between particles as a result of molecular interaction, but the mineralogical composition of the particles probably remains practically unaltered. Finally, at very great depth, all the particles are connected by virtually permanent, rigid bonds that impart to the material the properties of a rock. Yet, all the materials located between the zones of incipient and complete bonding are called shale. Therefore, the engineering properties of any shale with a given mineralogical composition may range between those of a soil and those of a rock.

The most conspicuous differences among the shales produced by the compaction of identical sedimentary deposits have their origin in the number of permanent interparticle bonds per unit of volume of shale. A relative measure of the degree of bonding is provided by the performance of intact specimens obtained from a depth of a few hundred meters. On submersion, all of these gradually break into fragments. However, the sizes of the fragments depend on the degree of bonding. They may be as great as several millimeters or as small as the individual mineral particles themselves. Between these limits, shales may be said to range from those categorized as well-bonded, of which the extreme types are rock-like shales, and those described as poorly bonded, of which the extreme types are heavily overconsolidated silt- to clay-shales. In addition to the estimated degree of bonding, descriptions of shales should indicate whether the prevalent constituent is clay or silt, as, for example, "poorly bonded clay-shale." Nevertheless, within the limits of any given description the engineering properties of the shale may range as widely as those of clays or silts.

During the removal by geologic processes of the load that was responsible for the transformation of a silt or a clay into shale, the shale expands at practically constant horizontal dimensions. Many of the interparticle bonds, formed during or after compression, are stressed by the subsequent expansion to or beyond the point of failure.

Therefore, shales are commonly weakened by a network of joints. Below a depth of 30 m the joints are completely closed and are spaced a meter or more apart. However, as the depth of overburden is decreased further, the joints open because of unequal expansion of the blocks located between them. The water content of the blocks then increases and their strength decreases like that of any clay or silt during reduction in pressure from the preconsolidation load. During this process, new fissures are formed. The final result depends, like that of the immersion of a shale specimen, on the degree of bonding.

Within the depth of seasonal variations of moisture and temperature the shale undergoes additional alterations and a soil profile consisting of the A- and B-horizons may develop. The B-horizon is likely to be less permeable than the fissured shale beneath. Consequently, in periods of high piezometric levels, it may be subject to surficial sliding.

On shales of any kind, the decrease of the slope angle to its final equilibrium value takes place primarily by intermittent sliding. The scars of the slides give the slopes the hummocky, warped appearance known as *landslide topography*. The details of the performance of shales underlying the slopes depend primarily on the mineral constituents and the degree of bonding. Extreme representatives of the well-bonded shales can be found in the Allegheny region and of the poorly bonded ones among the Cretaceous shales underlying large areas in the interior of the western United States and Canada.

In the Allegheny region of West Virginia, southern Pennsylvania, and eastern Ohio, many slopes are underlain by well-bonded, more or less silty shales. Only a small increase in water content of the blocks between joints is associated with load removal, and slides seldom cut to a depth of more than about 5 m. The resulting landslide topography is illustrated by Figs. 47.8 and 47.9. Steep slopes in side cuts can remain stable for many years. Slope failures, either on hillsides or cuts, occur only during the rainy season. If a failure occurs, the slide material flows for a short time like a viscous liquid and then comes to rest. On account of its relatively high



**Figure 47.8** Slide on gentle slope above well-bonded shale near Barboursville, West Virginia (from Ladd 1935).

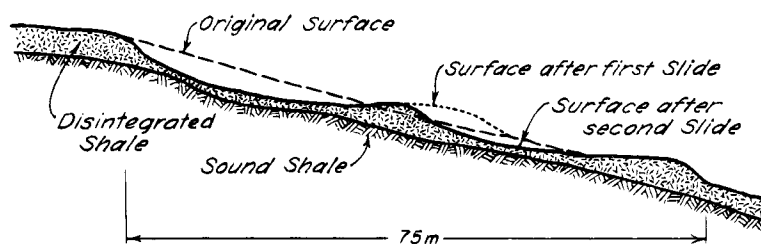


Figure 47.9 Profile of double slide in well-bounded shale (after Ladd 1935).

permeability the slide material can be stabilized by simple means such as the installation of horizontal auger drains.

Whenever an attempt has been made to account for such slides in fairly well-bonded shales by stability computations based on the results of laboratory tests, it has been found that the factor of safety of the slope with respect to sliding should have been more than adequate even on the assumption that the water table at the time of failure was located at the ground surface. The striking and persistent discrepancy between forecast and field performance can be explained most logically by assuming that the slides are preceded by a sudden, but temporary and local, increase of the porewater pressure in the zone of sliding. The shale within this zone consists of macroscopic fragments that are in the process of progressive deterioration. Because of the slope the accumulation of fragments is acted on by shearing forces and the joints between the fragments open. During wet spells the open spaces are filled with water. As soon as the deterioration reaches a critical stage, which occurs in different places at different times, the fragments break down during a wet spell under the combined influence of the overburden and seepage pressures. The weight of the overburden is temporarily transferred to the water, whereupon the effective pressure and the corresponding shearing resistance along a potential surface of sliding are reduced and a slide occurs. It may stop rather abruptly, because the excess porewater pressure dissipates rapidly on account of the relatively high permeability of the accumulation of shale fragments.

The other extreme members of the shale family are the poorly bonded clay shales such as those that prevail in parts of the Dakotas, Montana, and the western prairie provinces of Canada. These shales owe their present engineering properties to intense consolidation under overburdens with a thickness on the order of several hundred meters and to subsequent removal of the load. Beneath a depth measured in tens of meters these shales, too, are very hard. In tunnels extending below this depth it can be seen that they are transected by widely spaced, tight joints, like the well-bonded shales. On the other hand, the changes in water content that have occurred within the uppermost 10 to 20 m as a consequence of unloading are radically different. Whereas in the well-bonded shales

they may be almost imperceptible, in the poorly bonded clay shales they may amount to 10% or more. Consequently, the final result of the removal of load is also very different. Well-bonded shales turn into fairly pervious aggregates of angular, macroscopic rock fragments, but poorly bonded clay shales become stiff plastic clays. The mechanics of the transition from hard shale into a clay-like material is essentially the same as the process responsible for the slides in stiff, fissured clay, illustrated by Fig. 47.6. However, because the permeability of a clay shale is much lower than that of a less heavily preloaded clay, the softening proceeds much more slowly.

During the unloading by erosion of the overburden above poorly bonded clay shales under conditions of no lateral strain, the ratio between the horizontal and vertical normal stresses increases and may approach the coefficient  $K_p$  of passive pressure of the shale (Skempton 1961, Terzaghi 1961). These stresses contribute to the formation of joints and slickensides in the upper part of the shales. Cuts in such shales or stiff clays beneath level terrain may initiate slides, and the slopes may become flatter and flatter by intermittent sliding. As the slope angle decreases, the average shearing stresses also decrease along potential surfaces of sliding. Slides continue to occur at increasing intervals of time until the slopes are reduced to 1 vertical on 10 horizontal or even less. These observations indicate that the loss of strength due to unloading is extremely slow and cannot be predicted reliably on the basis of laboratory tests. Ultimately (Skempton 1964), along surfaces where shearing strains become very large, the resistance may approach the residual strength of the soil (Article 19.2.3). Every slide is preceded by accelerated creep to a depth much greater than that of seasonal variations of moisture and temperature. As soon as the rate of creep attains a value of several centimeters per year a slide occurs. During the slide the shale located above the surface of sliding remains almost intact and retains the character of a fairly stiff and intensely fissured clay.

While a stream is eroding a valley in clay shales or in heavily overconsolidated clays, the horizontal stresses at the sides of the valley are reduced to zero and the shale expands laterally toward the valley. The expansion, which is greater above the level of the valley floor than below,

causes horizontal slippage along initially weak discontinuities such as bedding planes. The slippage, in turn, forms a fault gouge or *shale mylonite* in which the resistance to shear toward the valley has been reduced to the residual value. The valley walls are in a state of marginal equilibrium and, whenever the stream cuts into a slope or erodes a deeper channel, movements are likely to be reactivated along the mylonites. Even small man-made excavations with flat slopes, cut into the valley walls, are likely to rejuvenate old slides or trigger new ones (Brooker and Peck 1993). The slides lead to further disintegration of the shales, general but gradual reduction of shearing strength as swelling occurs, and the development of a band of landslide terrane along both sides of the river valley.

In some of the Cretaceous shales of western United States and Canada, notably in the Bearpaw formation, layers of bentonite formed by the weathering of volcanic ash are interspersed with the more usual shales. The slippages associated with valley formation are concentrated on these layers, which have inherently low residual strengths. Furthermore, because the rebound of the ground due to unloading is a maximum close to the valleys, the bentonite layers tend to swell and to become thicker and weaker near the valley walls. These remarkably unfavorable conditions were present, for example, at the sites of Oahe dam on the Missouri River in South Dakota and Gardiner dam on the South Saskatchewan river in Canada. At the Gardiner dam virtually every construction excavation started a slide, and extremely flat slopes had to be adopted to permit completion of the necessary earthworks. Back calculation of slopes activated by the excavations indicated effective residual friction angles as low as  $2^\circ$  (Jaspar and Peters 1979).

In shales interspersed with layers of more rigid sandstones and siltstones, similar lateral expansion occurs near the valley walls. Joints open in the rigid layers and serve as reservoirs for water pressures during wet periods. Moreover, if the originally horizontal strata have experienced even gentle bending or folding, slip has occurred in the bedding planes to accommodate the shearing stresses caused by the bending, and mylonites at residual strength have probably developed in the shales at their contacts with the more rigid rocks. Under these circumstances, excavations cutting into the strata may cause slides if account has not been taken of the presence or the low shearing resistance of the mylonites.

#### 47.11 Sudden Spreading of Clay Slopes

Experience has shown that failures of clay slopes by sudden spreading tend to occur in cycles with periods of maximum frequency at more or less regular intervals. It is characteristic of this type of failure that a gentle clay slope, which may have been stable for decades or centuries, moves out suddenly along a broad front. At the

same time the terrain in front of the slide heaves for a considerable distance from the toe. On investigation, it has invariably been found that the spreading occurred at a considerable distance beneath the toe, along the boundary between the clay and an underlying water-bearing stratum or seam of sand or silt. The probable causes of these sudden and frequently catastrophic slope failures are illustrated by Fig. 47.10a.

Figure 47.10a represents a section through a valley located above a thick stratum of soft clay that gradually merges toward the left into sand. The clay, which has an average undrained strength  $s_u$ , contains thin horizontal layers of fine sand or coarse silt, such as the layer  $S-S$ . The pore water in  $S-S$  communicates with the water in the large body of sand on the left side of the diagram. The plain lines  $Ad$  and  $Be$ , respectively, represent the water table in the sand during a dry and an exceptionally wet season. The dash lines  $Ab$  and  $Bg$  represent the corresponding piezometric levels for the pore water in  $S-S$ .

A cut  $ab$  has been excavated in the clay to a depth  $H$ . Every horizontal section beneath the cut, including section  $a_1b_1$  through  $S-S$  (Fig. 47.10b) is acted on by shearing stresses tending to move the block  $abb_1a_1$  to the right. If the porewater pressure in  $S-S$  is low, corresponding to the piezometric levels  $Ab$  (Fig. 47.10a), the shearing resistance along  $a_1b_1$  is likely to be considerably greater than the shearing stresses and the slope will be stable, provided that the clay itself is stable on the 1:3 slope.

However, because of unusual precipitation or snowmelt on the surface of the ground above the large body of sand, the piezometric levels in  $S-S$  may rise to the position indicated by  $Bg$  (Fig. 47.10a). Because the rise does not affect the total weight of the block  $abb_1a_1$  (Fig. 47.10b), the vertical pressure  $\sigma_v$  per unit of area on  $a_1b_1$  remains unchanged, but the shearing resistance in  $S-S$  reduces to

$$s = (\sigma_v - u) \tan \phi'$$

If the shearing resistance decreases to the value of the average shearing stress, the slope above  $S-S$  fails by spreading even though it may still possess an adequate factor of safety against sliding along any curved surface located above or cutting through  $S-S$ .

If the value of  $u$  becomes equal to  $\sigma_v$ ,  $s$  reduces to zero. This condition is equivalent to eliminating the resistance of the horizontal section  $a_1b_1$  (Fig. 47.10b), whereupon the slope  $ab$  behaves as if it were vertical. Its critical height would then be  $3.85 s_u/\gamma$  (Fig. 35.3). Thus, failure by spreading will not occur, irrespective of the magnitude of the pore pressure, if  $H$  is less than  $3.85 s_u/\gamma$ .

During exceptionally wet years or during the melting of an exceptionally thick snow cover, the water table rises everywhere. Consequently, the shearing resistance of every water-bearing seam decreases, and slopes may fail that were previously always stable. In 1915 a slide occurred on a very gentle slope about 12 m high, within





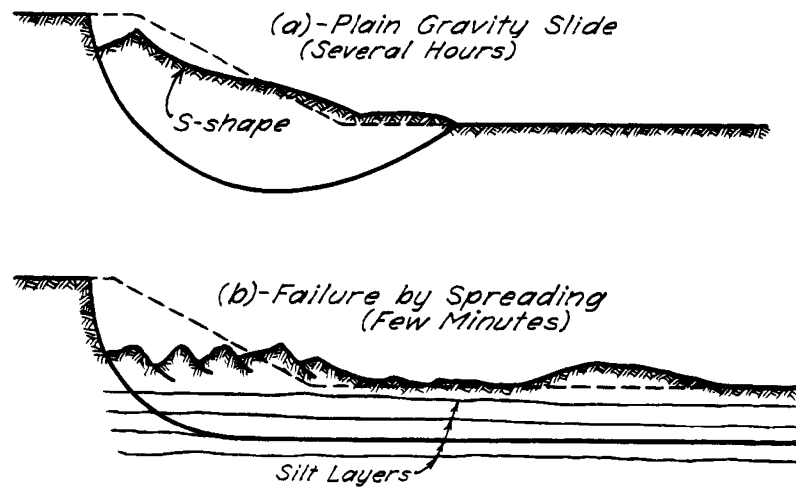


**Figure 47.11** Cross-section through typical slide in varved clay: (a) If porewater pressure in silt layers is inconsequential; (b) if porewater pressure in silt layers is almost equal to overburden pressure.

other localities where the products of ancient weathering have been preserved. Although in detail the variations in subsurface conditions in deeply weathered zones are almost infinite, useful generalizations with respect to landslides can be made on the basis of the weathering profiles typical of various types of rocks.

Most weathering profiles are characterized by the presence of an upper zone of comparatively weak, relatively impermeable residual soil overlying a zone of saprolite and weathered rock of much higher permeability. These zones, of variable thickness, are roughly parallel to the ground surface. In dry seasons the piezometric surface may lie in or below the weathered rock and the overlying materials may even become unsaturated. In wet seasons water may accumulate in the permeable zone where it is trapped by the relatively impermeable residual soil cover. High piezometric pressures on the base of the residual soil lead to sometimes extensive skin slides. In addition, the unsaturated soils may approach saturation, whereupon their suction is lost and they lose their apparent cohesion. Hence, it is not surprising that most landslides in localities such as Hong Kong or Puerto Rico occur in the rainy season.

The zone of high permeability is often sandy and highly erodible. Hence, sliding is often aggravated by subsurface erosion beneath the residual cover as well as by surface erosion where the cover has been removed.

The saprolite and weathered rock contain relict joints and other weaknesses such as shear zones and faults that introduce the possibility of deeper seated failures, again most likely to occur during the rainy season. If these weaknesses are located critically with respect to excavations they may readily lead to slides.

The various products of weathering and landsliding accumulate as colluvium that forms a loose blanket of

weak soils over the residual materials. When piezometric levels rise during the rainy season, the colluvium may slide with or on the residual soils. In many instances it is difficult to distinguish between the colluvial and residual materials. Successive accumulations of colluvium at the foot of a slope lead to stratification that may permit the development of uplift pressures that result in slides.

Under the following subheadings the mechanisms of potential slides are described for several common geologic conditions. Appropriate procedures for design are discussed under the final subheading.

#### 47.12.2 Weathered Metamorphic Rocks

A typical weathering profile for metamorphic rocks is shown in Fig. 47.12a. The development of this profile beneath a typical slope is indicated in Fig. 47.13 (Deere and Patton 1971). Great variations in the depths of the various zones of weathering may occur over short horizontal distances as a result of variations in lithology, but the sequence of the zones is preserved. Faults and shear zones may be much more deeply weathered than adjacent areas. Groundwater level rises markedly in the wet season and springs may emerge at locations governed by details of the structure of the rock. Three typical potential slides are noted on the figure. Slide A, caused by a cut, is a deep-seated movement along relict foliation planes or joints. Slide B is a shallow movement of the IA and IB zones associated with a rising water table. Slide C may occur from uncontrolled erosion of the IC material either beneath or at the surface.

#### 47.12.3 Weathered Granite

A typical weathering profile in granite is shown in Fig. 47.12b, and its development beneath a typical slope is demonstrated in Fig. 47.14. The behavior of the slope is

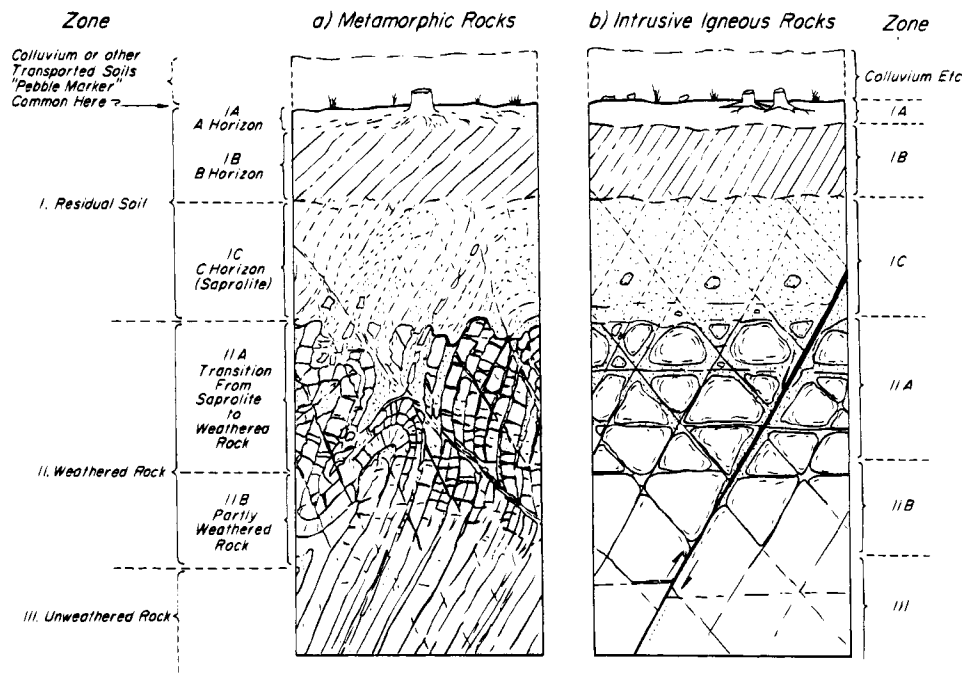


**Figure 47.12** Typical weathering profile for (a) metamorphic and (b) intrusive igneous rocks (from Deere and Patton 1971).

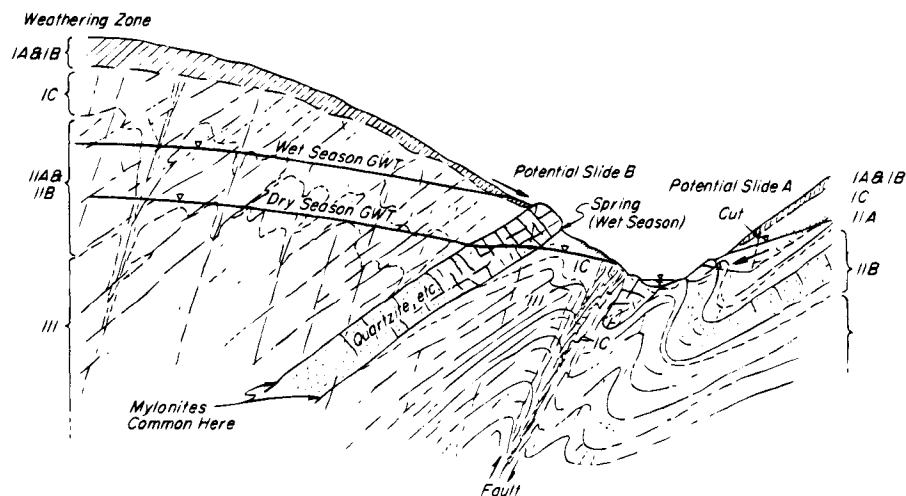


**Figure 47.13** Typical slope in weathered metamorphic rocks (from Deere and Patton 1971).

similar to that in Fig. 47.13, but the directions of weakness, instead of being associated with foliation, are along preexisting joints, faults, shear zones, and stress-relief sheeting joints that tend to form subparallel to the ground surface. Shallow slides, such as A, are common when excess water pressures develop under the residual soil because of exceptionally high rainfall. They may also take place into cuts if the soil is too weak to stand at the cut slope. Slides such as B, less common but more serious,

may develop along one or more joint surfaces exposed in the base of a cut. If a slide does not occur during excavation, it may take place during a subsequent exceptional rainfall or an earthquake.

#### 47.12.4 Weathered Basalts

The weathering of basalts is similar to that of intrusive igneous rocks such as granite. In the transition zone IIA the corestones often display spheroidal weathering. The



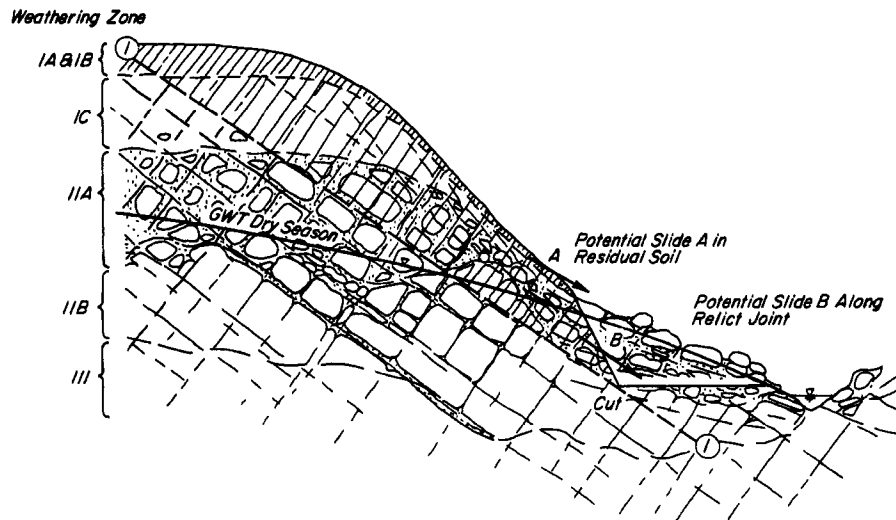


**Figure 47.14** Typical slope in weathered granite (from Deere and Patton 1971).

residual soils usually contain a high iron content and a variety of the more unusual clay minerals including halloysite and nontronite (Grim, 1968), as well as hydrated oxides of iron and aluminum (Article 4.2). These materials may also result from the weathering of volcanic ash and scoria that are often deposited in association with the lava flows.

The upper portion of each lava flow and the ash that falls on the lava may both weather to form soils subsequently interbedded in the basalts. The presence of these weak but relatively impermeable materials often has a controlling influence on the stability of slopes. The basalts themselves tend to be highly permeable horizontally and fairly permeable vertically. Consequently, in the humid tropics they weather rapidly to great depths as evidenced in many road cuts in Hawaii. The groundwater table is usually low, but buried soil layers may intercept downward flow of water and cause springs at slopes. Intrusive dikes in basalts have often altered the adjacent rock to form impervious barriers behind which large quantities of water can be trapped. Large flows of water can be experienced if such a barrier is encountered during excavation.

Because weathering of basalts may be extremely irregular and may produce clays of unusual characteristics, and because buried soil zones of either high or low permeability may be encountered, weathered basalts deserve detailed investigation to assess the stability of slopes.

#### 47.12.5 Weathered Carbonate Rocks

Unlike the weathering products of most igneous and metamorphic rocks, those of limestone, dolomite, and marble consist almost entirely of the insoluble portion of the parent rock. They usually form a nearly structureless residuum, generally clayey but sometimes sandy or pebbly,

with no transition to the undissolved, unweathered rock. However, although sharp, the contact may be extremely irregular. Solution of the carbonates by circulating groundwaters typically leads to voids or caves that may collapse to form sinkholes. Very soft clay is often found in the bottom of incipient or collapsed sinkholes. The overlying material is usually stiffer and is often covered by colluvium.

Few stability problems are associated with limestone or other carbonate terranes unless collapsed or incipient sinkholes are approached or encountered in cuts. The rock boundaries of the solution cavities are likely to be excessively steep or overhanging, and may collapse when the soil filling the cavities is disturbed.

Where cuts are made in thick accumulations of residual soil overlying carbonate rocks, the soil can be considered to be homogeneous and free of structural weaknesses inherited from the parent rock. Design can be based on stability analyses incorporating appropriate soil properties and piezometric conditions.

#### 47.12.6 Design of Slopes

Adequate analytical procedures have been developed in soil mechanics (Article 35.8) and rock mechanics (Patton and Hendron 1974) for calculating the factor of safety of a slope on weathered metamorphic, granitic, or basaltic rock. However, the results of such procedures have no relation to reality unless all the following conditions are satisfied: the geologic profile is reliably known; the relevant physical properties of the materials along potential surfaces of sliding have been established; the locations and attitudes of such relict features as faults, shear zones, and throughgoing joints have been determined; the shearing resistance along such discontinuities is known, including the effects of any infilling or coating materials and

including knowledge of prior movements that might have reduced the strength to residual values; and values have been ascertained for pore pressures that may be expected on the surface of sliding under normal and unfavorable conditions. Because these requirements are at best expensive and difficult to satisfy and involve a considerable element of uncertainty, design based on stability analyses is justifiable only for occasional critical cuts. Moreover, as excavation progresses, detailed observations should be made to determine whether the excavation has disclosed any new aspect of the geologic structures. Appropriate instruments to detect zones of movement and to verify groundwater conditions may also be needed, and modifications to the design may prove necessary. Even so, the possibility of a slide must be anticipated and its consequences considered.

In view of these limitations, slopes on residual soils are designed largely on the basis of precedent, modified as appropriate to take account of the implications of a reasonable amount of preconstruction investigation and of observations by experienced personnel during construction. Figure 47.15 summarizes average slope angles believed by Deere and Patton (1971) to represent generally adopted precedent. However, routine adoption of these slopes is likely to lead to many instances of instability that could be avoided or reduced in severity by modifications based on the findings of detailed surface inspection and judiciously executed subsurface exploration before construction. If such structural features as adverse orientations of relict structural planes of weakness are disclosed, they should be considered in stability calculations together with the results of laboratory or field tests

to establish the shear strength parameters. On the basis of the geologic profile, the measured permeabilities, and observed piezometric levels, a rough groundwater flow net can be sketched to serve as a means for estimating the flow pattern during construction and in subsequent periods of unusual rainfall.

These studies may suggest the need for remedial measures such as internal drainage, particularly if the toe of the cut will be located in an impervious zone close to a more pervious one in which excess pore pressures could reach high values after heavy rainfall.

In any event, surface drainage must be given careful attention to reduce infiltration into pervious zones. Drainage ditches above the cuts and on berms generally should be paved to prevent their destruction by erosion of those weathering products of a friable nature, and the ditches should be carefully maintained. In critical areas the entire slope is sometimes paved with a mortar to prevent surface and subsurface erosion. Such pavements, as used for example in Hong Kong on slopes in weathered granites, are effective, but they are also vulnerable and require vigilant maintenance to ensure that erosion does not occur unnoticed beneath the pavement until destructive collapses occur (Flintoff and Cowland 1982)

In extensively developed localities such as Hong Kong where deeply weathered rocks prevail and periods of torrential rain must be expected, the catastrophic consequences of frequent slides have led to the establishment of organizations to study the conditions and causes of the slides and to devise suitable land-use regulations and preventive measures. The findings of these organizations

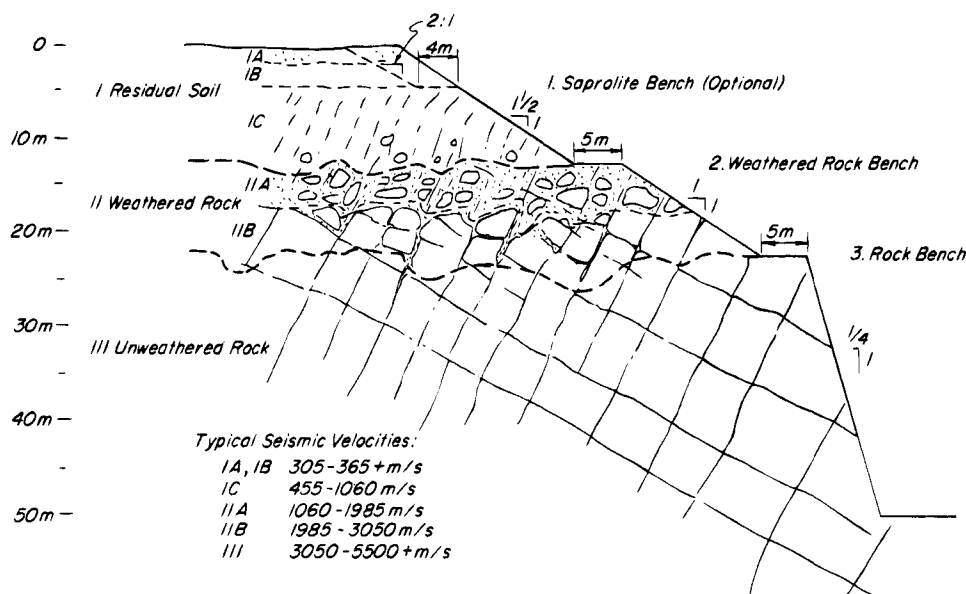


Figure 47.15 Typical layout of cut slope in weathered rock (from Deere and Patton 1971).

should be given careful consideration by any engineer working in the locality or in localities where the geologic and climatic conditions are similar.

### 47.13 Debris Flows

The term *debris flow* is used broadly in this text to include the downward movement of semifluid masses of rock fragments or soil. The velocities of flow range from slow glacier-like advances to violent rushes of more than 20 m/s, and the materials range from mixtures of blocks and fragments of rock to clays and weathered shales. The mechanism of this large group of mass movements lies between the realms of soil and rock mechanics on the one hand and of sediment transport on the other. Soil mechanics provides insight into the conditions and processes responsible for the movements and in some instances may furnish a basis for preventive or remedial measures, but can only rarely furnish quantitative analyses for estimating the degree of safety of a potential flow.

Most catastrophic among debris flows are *debris torrents* (VanDine 1985) in which a saturated mass of rock fragments, boulders, sand, silt, and even pieces of wood ranging from splinters to large logs descends with great speed down confined, preexisting gulleys or channels, destroying bridges and houses in its path and spreading at the mouth of the valley like a fan. Such torrents are common in high mountains in every part of the world. On the western slope of the Wasatch Mountains in Utah, for example, every canyon is said to contain the remnants of at least one debris torrent (Sharpe 1938).

Conditions necessary for the occurrence of debris torrents include, according to VanDine (1985), (1) a drainage area large enough to furnish ample debris and to concentrate sufficient water in the creek bed to saturate the debris already present; (2) a creek bed broadly divided into (a) a steep upper zone where debris can accumulate and where the movement can be initiated, (b) a still relatively steep zone farther downstream in which transportation and erosion occur within valley walls close enough together for the debris to maintain its velocity, and (c) a flatter lower zone where deposition of levees begins and finally a depositional fan is built up; (3) a source of debris adjacent to the upper zone where weathered rock, cohesionless or loose soils, landslide debris or talus are available and where deforestation and poor logging practices have often accelerated erosion; and (4) high intensity of rainfall, possibly coincident with high snowmelt, occurring after intervals long enough to permit accumulation of sufficient debris. Once the torrent begins, the water-saturated front of the flow erodes the valley walls and creek bed and incorporates the eroded material, whereupon the flow becomes self-propagating and more erosive as it moves downstream.

Most debris torrents occur in valleys in which torrents have occurred previously. These areas can be identified

on airphotos and, if possible, avoided for future development. Where a dangerous area cannot be avoided, preventive measures may be considered including check dams to reduce the steep gradients in the area of initiation; reduction of accumulation of debris by terracing, planting, or terracing the slopes; or improvement of the channel to encourage flow of the debris past critical areas. Design of these and other measures is largely judgmental, but methods for prediction and analysis show promise (Hungry et al. 1984).

Possibly at the other end of the scale of debris flows are the *mudflows* that occur in debris derived primarily from clays and clayey shales. The movement takes place on a basal slip surface inclined more steeply near the head of the slide than below. The slope of the lower portion of the slip surface may be flatter than that corresponding to equilibrium conditions for the overlying material at residual shear strength on the assumption that piezometric levels are coincident with the ground surface, yet the debris advances at rates that may be on the order of 0.5 m/year. Steeper slopes produce greater rates of movement.

Piezometric observations in the flowing material near the head of a mudflow in London clay (Hutchinson and Bhandari 1971) indicated piezometric levels above the surface of the flow. It was inferred from the findings that the rate of loading of the head of the mudflow by materials descending from up the slope was more rapid than the rate of dissipation of pore pressures in the debris, and that excess pore pressures developed in the uphill portion of the sliding mass. The resulting large downhill pressures, limited only by the passive resistance of the debris above the slip surface, provided a disturbing force sufficient to cause the mass to move.

Differences in slopes, materials, and climatic conditions produce a vast range of velocities, volumes, and destructive capabilities of debris flows. Among the most violent are *lahars*, flows of freshly deposited volcanic ash which have occurred frequently in storms after volcanic eruptions.

The first step in guarding against the catastrophic consequences of debris flows is recognition of existing and former occurrences. The most effective means for recognition are airphoto interpretation followed by field inspection. Where possible, the sites of former flows should be avoided.

### 47.14 Summary of Approach to Stability of Slopes

The manner and extent of investigating the stability of a slope depend on the nature of the ground, the effects of a failure should it occur, and the cost of measures to reduce the likelihood or consequences of failure.

By far the most important step in the investigation is to judge whether the ground is favorable or troublesome with respect to stability. Because of the infinite variety

of combined soil and hydraulic conditions that may lead to slides, this judgment requires expert geologic reconnaissance, preferably aided by airphoto interpretation, to establish whether or under what conditions the ground is slide prone. Often such features as the orientation of the geologic structure with respect to the course of a river or to the direction of existing cuts for railroads or highways have a significant influence on stability and can be taken into account by the engineer in locating a new facility. Rarely does construction cause a slide in a locality where no evidence exists of previous sliding in similar terrain.

If a new highway or railway must be located through slide-prone or troublesome ground it is likely that some unfavorable situations cannot be avoided. The engineer must then judge whether more extensive investigations and the design of preventive measures are warranted, or whether it may be preferable to use conservative slopes, to provide reasonable drainage and slope protection, to guard against loss of life by installing warning devices such as slide-detector fences, and to allow room at the foot of the cut for equipment to remove slide debris if failures should occur. On the other hand, in highly congested and developed localities where slopes are steep, such as Hong Kong, Caracas, Seattle, and many other cities, cuts and basement excavations into slopes can hardly be avoided, but sliding could cause the collapse of buildings and possibly great loss of life. Obviously, under these circumstances, designing a slope with the intention to accept an occasional slide is intolerable. Thorough investigations, analyses if pertinent, stabilization measures, and field measurements to detect movements in their early stages, are all justified. Unfortunately, even elaborate analyses may have little relevance in a variety of geologic conditions, as indicated in several of the preceding sections. After the most careful studies, and after improvement of stability by such measures as unloading the head of the potential slide, drainage, and providing tiebacks or other restraining devices, a program of observations is mandatory to remove uncertainties in the knowledge of the site, to provide advance warning of unfavorable trends, and to avoid fatal accidents. The prospects for success after such elaborate measures differ greatly in different soil conditions, as exemplified by the discussions of slides in different geologic settings earlier in this article. Prospects for success are probably best in sands and in soft clays, and poorest in deep residual soils in localities having marked rainy seasons.

Few endeavors place as much responsibility on the engineer as judging the extent and justifiable cost of exploration, analysis, and defensive measures in relation to the potentially catastrophic losses in both property and human lives in the event that slides should occur. Formal stability analyses are relevant only if they are based on actual or kinematically and geologically possible surfaces

of sliding and on reliable determination of the physical properties of the materials and of the groundwater conditions. When these conditions are not satisfied, the contribution of soil mechanics, although by no means unimportant, is limited to defining the arrangement and properties of the materials involved, determining the groundwater conditions, and providing knowledge of the laws that govern the interaction between water and the different types of soil. Unfortunately, the engineer who recognizes the inapplicability of stability analyses under these conditions and, therefore, relies on geology, geomorphology, and basic understanding of the behavior of soil and water may be placed on the defensive if no analyses have been made. In presenting recommendations, the engineer should set forth in detail the basis for the conclusions, including the reasons for the irrelevance of calculations in the instance at hand.

### Selected Readings

Several publications deal with the description, mechanism, or correction of landslides from a comprehensive point of view. Among the more useful are:

- Terzaghi, K. (1950). Mechanism of landslides, *Geol. Soc. Am., Engineering geology, Berkeley Vol.*, pp. 83–123. Reprinted in *From Theory to Practice in Soil Mechanics*, New York, John Wiley and Sons, 1960, pp. 202–245.
- Schuster, R. L. and R. J. Krizek, eds. (1978). *Landslides: Analysis and Control*. Transp. Res. Bd. Spec. Rep. 176, Washington, D.C., 234 pp.
- Zaruba, Q. and V. Mencl (1982). *Landslides and Their Control*, 2 ed., Amsterdam and New York, Elsevier, 324 pp.

An outstanding example of the detailed studies and of the knowledge of the geology, geomorphology, and hydrology necessary to understand a large complex slide is: Hendron, A. J. Jr., and F. D. Patton (1986). "A Geotechnical Analysis of the Behavior of the Vaiont Slide" *Civil Eng. Practice, J. Boston Soc. C. E.*, 1, No. 2, pp. 65–130.

Among many excellent papers concerning individual landslides or particular types of landslides, the following have been selected to represent widely different conditions.

- Newland, D. H. (1916). "Landslides in unconsolidated sediments", *N. Y. State Museum Bull.* 187, pp. 79–105. Slides in varved clays on Hudson River.
- Close, U. and E. McCormick (1922). "Where the mountains walked", *Nat. Geog. Mag.*, 41, pp. 445–464. Flow slides in loess in China.
- Seed, H. B. and S. D. Wilson (1967). "The Turnagain Heights landslide, Anchorage, Alaska," *ASCE J. Soil Mech.* 93, No. SM4, pp. 325–353.
- Deere, D. U. and F. D. Patton (1971). "Slope stability in residual soils," *Proc. 4th Pan-American Conf. on Soil Mech. and Fdn. Eng.*, San Juan ASCE, 1, pp. 87–170.

- Tavenas, F., J. Y. Chagnon, and P. LaRoche (1971). "The Saint-Jean-Viannay landslide: observations and eye-witness accounts," *Can. Geot. J.* **8**, No. 3, pp. 463–478.
- Brand, E. W. (1982). "Analysis and design in residual soils," *Proc. ASCE Geotech. Eng. Div., Spec. Conf. on Eng. and Construction in Tropical and Residual Soils*, Honolulu, pp. 89–143. Summary of the experience of the Geotech. Control Office, Hong Kong, with residual granite slides induced by seasonal rainfall and their control.
- VanDine, D. F. (1985). "Debris flows and debris torrents in the Southern Canadian Cordillera," *Can. Geot. J.* **22**, No. 1, pp. 44–68.

## ARTICLE 48 DESIGN AND STABILITY OF EMBANKMENTS

### 48.1 Introduction

Earth embankments are used chiefly for railway and highway fills, levees, and earth dams. Within each group the factors influencing the selection of the side slopes are similar. Earth dams and their foundations are discussed in Chapter 11. In the present article, which deals with the other categories of fills, the choice of slopes is considered first on the premise that the subsoil is stable. Subsequently, the implications of weak subsoil are considered.

### 48.2 Early Practice in Construction of Railway and Highway Fills

Until about the 1930's, railway fills were usually constructed by dumping the borrow material from a timber trestle or over the end of the completed portion of the fill. Such fills were considered satisfactory if they were permanently stable. Because artificial compaction was not used, ballast was not placed beneath the track until the fills had "seasoned" for several years. During this period the fills settled under their own weight. The settlement amounted to about 3% of the height of rock fills, 4% of the height of fills of sandy materials, and about 8% of the height of fills with a considerable clay content. To prevent the development of sags in the track between the ends of a fill, the crest was customarily established at a distance above theoretical grade equal to the expected settlement.

The standard slope of railway fills constructed in this manner was 1.5 (horizontal) to 1 (vertical). However, it was noticed that fills with heights greater than 4 or 5 m were likely to fail either during construction or after a few wet seasons if they contained a high percentage of clay. Therefore, it became the practice to reduce the slope angle of such fills from 1.5:1 at the crest to about 3:1 at the base. The decision whether the character of the clay required flattening of the slopes was commonly left to the engineer in charge of construction. Nevertheless, even the most experienced engineers occasionally misjudged the character of the soil and, consequently, sections of the fills failed. The slopes were then repaired and their

stability increased either by constructing low fills along the toes that moved out or by means of dry masonry footwalls, possibly supplemented by drains.

The earliest highway fills were similarly constructed by loose dumping over the ends of the completed portions. The standard slopes varied in different parts of the United States from 1.5:1 to 1.75:1. Differential settlements of the fills led to unsatisfactory riding characteristics and, frequently, to failure of the road surfaces. Unlike railroad tracks, which could be raised routinely by tamping additional ballast beneath the ties, highway pavements could be leveled only by resurfacing or, beneath concrete pavements, by mud-jacking. Moreover, no time was ordinarily available for seasoning of a highway fill before it was made available to high-speed traffic. Hence, within a decade after the introduction of the modern "hard road," spreading in layers and compaction by hauling equipment and rollers were becoming common practice.

It was recognized that the behavior of fills compacted in this manner depended primarily on the physical properties of the fill material. Consequently, efforts were made by the various state highway departments and the Bureau of Public Roads to correlate the behavior of compacted embankments with the index properties of the fill material. These efforts led to a generally accepted practice of judging the quality of the soil on the basis of its Atterberg-limit values and its maximum compacted dry density as determined by the Standard Proctor test or its local equivalent. Requirements adopted in conformity with experience in some localities were, unfortunately, often copied in other localities without the benefit of similar experience. Restriction of the water content to values within a few percent of the optimum moisture content was rarely specified or required, provided that the specified minimum percentage of the maximum Proctor dry density was achieved.

### 48.3 Modern Practice for Railway and Highway Fills

Inasmuch as most new railroad fills in industrially developed countries are made in connection with improvements in alignment or gradient to permit higher speeds or heavier loads, there is no longer any essential difference in construction procedures for railway or highway fills. Preferably, stable granular materials are used, but economy often dictates the placement of the closest available materials, regardless of their composition, unless they contain highly compressible organic constituents. Under most circumstances the fill is spread by bulldozers in layers about 0.3 m thick and is compacted by rollers until a specified dry density is achieved. Moisture-content control may or may not be specified. Standard slopes remain as steep as 1.5:1 for granular materials, and for cohesive soils vary from about 2:1 for fills 3 m high to as flat as 3:1 for fills 30 m high.

This procedure has led to generally satisfactory results if the water content of the material in the borrow pit does not exceed the appropriate Standard Proctor optimum value (Article 44.2) by more than a few percent. If the borrow material is too wet, serious difficulties and delays may be encountered. Hence, the most important aspect of the soil survey for fine-grained fill materials is to ascertain the relation between the field moisture content and the optimum value. This information should be supplemented by determination of the liquid and plastic limits which serve as a basis for judging the likelihood that the borrow material can be dried to the optimum moisture content under the prevailing climatic conditions.

If the moisture content is excessive and the climate too humid to permit effective drying, no amount of compactive effort can satisfy a requirement in the specifications that 90 or 95% of a standard maximum dry density must be achieved. Under these circumstances, the engineer must investigate the strength that will be developed by the fill material after placement at its natural moisture content and sufficient manipulation by hauling and compaction equipment to eliminate any large voids. Ordinarily only light equipment can work satisfactorily on such a fill. The engineer must then select the slopes of the fill to provide an appropriate factor of safety against exceeding the strength of the material as placed.

The use of fairly stiff clay for the construction of an embankment may involve the danger of subsequent expansion by swelling in contact with water (Article 16.10). If the expansion is unequal, fissures are likely to form, whereupon the structure of the clay may disintegrate and the slopes may start to slough.

The extent of swelling in a fill depends on the inherent swelling capacity of the material and on such factors as the moisture content at which the fill is placed, the degree and method of compaction, and the pressure due to the weight of the overlying part of the embankment. The combined effect of these influences on a fill composed of rolled chunks of a stiff clay can be investigated by preparing samples representative of the clay in its initial state in the fill. Each sample is introduced into an oedometer ring and subjected to a pressure equal to that which will act on the clay at some point in the fill. Water is then admitted to the porous stones that cover the top and bottom of the sample, and the increase in volume is measured. The suitability of the material is judged by its tendency to swell. If the increase in volume under the anticipated vertical pressure in the fill exceeds about 5%, the fill is likely to perform unsatisfactorily.

The expense of carrying out swelling tests and the uncertainties involved in interpreting the results justify attempts to identify those borrow materials that exhibit excessive inherent swelling capacity. In a general way, it has been found that the inherent potential to swell depends

on the plasticity index (Holts and Gibbs 1956a, Seed et al. 1962), as indicated in Table 48.1.

If a clay with high to very high inherent swelling capacity must be used, the effects of swelling may be minimized by placing the clay at the highest practicable moisture content and by using any available nonswelling materials in the outer portions of the fill. The weight of even a meter or so of surcharge over a swelling material substantially reduces the amount of expansion and consequent loss of strength of the clay.

#### 48.4 Levees or Dikes

Levees serve to protect lowlands against periodic inundation by high water, storm floods, or high tides. They differ from earth storage dams in three principal respects: Their inner slopes are submerged during only a few days or weeks per year; their location is determined by flood-protection requirements regardless of whether or not the foundation conditions are favorable; and the fill material must be derived from shallow borrow pits located near the site of the levees. These conditions introduce a considerable element of uncertainty into the design of such structures. Nevertheless, levees were needed in some regions during the earliest days of human civilization, and consequently the art of levee construction was highly developed in these regions.

If the soil conditions in the borrow-pit area change from place to place, the cross-section of a levee is customarily chosen to suit the requirements of the most unfavorable materials that will have to be used. Consideration is also given to the degree of freedom permitted the contractor in choosing the time and method of construction. In some levee districts the method of placing the soil is rigidly controlled, whereas in others the contractor is free to choose among widely different methods of construction. In the past, the influence of the method of construction on the cost of a levee depended chiefly on the ratio between the cost of hand and machine labor. Because this ratio was very different in different countries, efforts to build satisfactory levees at minimum expense led to different rules in different parts of the world. For example, before World War II in countries such as Germany and

**Table 48.1 Approximate Relation Between Plasticity Index and Inherent Swelling Capacity**

Plasticity Index	Inherent Swelling Capacity
0–10	Low
10–20	Medium
20–35	High
35–	Very high

After Seed et al. 1962.

Holland, where hand labor was cheap, levees were carefully compacted and built with steep slopes. At the same time, in the Mississippi Valley no efforts were made to compact levees, because uncompacted levees with gentle slopes were commonly cheaper than carefully compacted ones with much smaller cross-sections (Buchanan 1938). In Europe and Asia many levees of clay were constructed with side slopes of 2:1, whereas clay levees along the Mississippi River were generally given an inner slope of 3:1 and an outer slope of 6:1. Both types of construction grew out of a process of trial and error, and both served their purpose equally well under the conditions that prevailed in the regions where they originated.

Even in the United States, however, steep slopes were justified economically in areas of high land and property values. Whereas levees along the lower Mississippi River were being constructed with flat slopes, the slopes in the industrialized Ohio River valley were much steeper. This trend became more pronounced as time went on and led to increased use of theoretical methods in the design of levees even in regions where levee systems already existed. On the other hand, where economic factors have not changed significantly, soil mechanics can still be used to advantage only for correlating construction and maintenance experience with the index properties of the soils that serve as the construction materials. The information obtained in this manner leads to the elimination of guesswork in classifying the soils encountered in new borrow-pit areas.

The use of theoretical methods in the design of levees on stable subsoil can be justified in a region where few levees have been built previously. Under such circumstances the method of trial and error is too slow and expensive, and there is no experience based on existing levee systems to be used as a guide. The designer is then compelled to use the methods practiced in connection with the design of earth dams (Chapter 11).

#### 48.5 Types of Base Failure

Whenever possible, embankments and earth dams are constructed on firm, relatively incompressible subsoils. However, in many regions railway or highway embankments must be built on broad swampy flats or buried valleys filled with soft silt or clay. Levees must be constructed near the flood channels, irrespective of subsoil conditions. Even earth dams must occasionally be located at sites underlain by undesirable materials. In all these instances the design of the embankment must be adapted not only to the character of the available fill material, but also to the subsoil conditions.

Base failures may occur in several different ways. The fill may sink bodily into the supporting soil. Such an accident is referred to as *failure by sinking* or *breaking into the ground*. On the other hand, the fill together with the layer of soil on which it rests may spread on an

underlying stratum of exceptionally soft clay or on partings of sand or silt containing water under pressure (Article 47 and Fig. 47.11b). This is known as *failure by spreading*. If the embankment retains a body of water, it may also fail by *piping*, as a consequence of backward erosion from springs that emerge from the ground near the toe of the fill. Finally, during major earthquakes, base failures may occur beneath fills located above strata of very loose sand because of liquefaction. The likelihood of liquefaction beneath fills of moderate height can be reduced considerably by compacting the sand by one of the methods described in Article 44. Failure by piping is discussed independently in Article 58. Hence, the present article deals only with base failures by sinking or spreading.

#### 48.6 Methods for Investigating Stability

The design of a fill to be constructed above clay strata should always be preceded by a thorough soil exploration. The results of the exploration inform the designer about the soil profile and the physical properties of the subsoil. The next step is to compute the factor of safety of the fill with respect to a failure of its base (Article 35). Under normal conditions, the foundation conditions are not considered satisfactory unless the factor of safety with respect to a base failure during or immediately after construction is at least 1.5.

The conditions for the stability of the base of fills and the methods for preventing base failures are discussed in the following sequence: fills on very soft or marshy ground, fills on thick strata of fairly homogeneous soft clay, fills on stratified ground containing fairly homogeneous layers of soft clay, and fills on clay containing sand or silt partings. Subsoil conditions of the first two types are likely to be associated with failures by sinking, and those of the last two types with failures by spreading.

#### 48.7 Fills on Very Soft Organic Silt or Clay

Natural deposits of this type are common in regions formerly occupied by shallow lakes or lagoons. The fringes of such shallow deposits are likely to support growths of peat moss or other types of marsh vegetation. The silt or clay brought into the lakes in suspension intermingles with the decayed organic constituents washed in from the fringes. Hence, the fine-grained sediments in such bodies of water are likely to have high organic content. The natural void ratio of the sediments is often greater than 2. The deposits may contain layers of peat or be buried beneath a bed of peat.

If the surface of such a deposit has never before carried an overburden, the subsoil may be unable to sustain the weight of a fill more than a meter or so in height. In many regions soft marshy ground is covered with a mat up to a meter thick that is stiffer than the deeper layers and is effectively reinforced by a dense network of roots.

The mat acts like a raft and may be able to carry, at least temporarily, the weight of a fill several meters high. However, fills on such foundations may continue to settle excessively for many years or decades, and maintenance records show that they may even suddenly break through the mat long after construction. Under these circumstances the engineer may choose between two alternatives: to remove or displace the soft material or to apply the fill at such a rate that the soft soil does not fail but gains sufficient strength by consolidation to support the fill at its final height with acceptable settlement. The latter alternative may require surcharging with or without the use of vertical drains. These procedures are discussed in Article 44.3.6. The following paragraphs deal with excavation or displacement.

The choice of procedures should be preceded by the preparation of a contour map of the firm bottom. If the soft deposits are not more than about 2 m thick, it may be most economical to excavate them. Otherwise the sinking fill may be used to displace them. This procedure is known as the *displacement method*. Although in connection with railway and highway fills it has been widely practiced, surcharging with or without geotextile reinforcement is becoming more prevalent because of the better control that can be exercised.

To accelerate the penetration of the fill material and to shorten the subsequent period of settlement when the displacement method is used, the fill may be built up to a height of 5 or 6 m above final grade, and the excess material removed later. As an alternative the penetration of the fill material may be facilitated by blasting the soft subsoil. If the position of the bottom of the soft stratum is known, the quantity of material required for constructing the fill can be estimated fairly accurately in advance of construction.

The conditions for the equilibrium of a fill with its base established by displacement are illustrated by Fig. 48.1. The contact face  $ab$  is acted on by the active earth pressure exerted by the fill material. The displacement of  $ab$  toward the left is resisted by the sum of the liquid pressure of the soft material and the force required to overcome its shearing strength. If the penetration of the fill is aided by a temporary surcharge or by blasting, the force that produces the corresponding displacement is

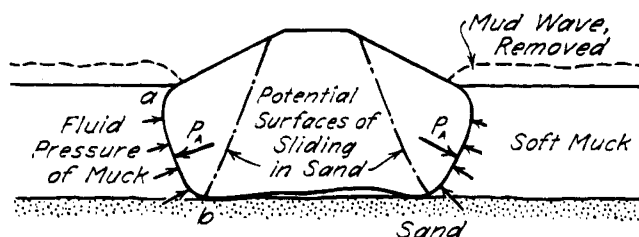


**Figure 48.1** Diagram showing forces that act on soil adjacent to buried part of a fill constructed by the displacement method.

very much greater than the force that acts on  $ab$  after construction. Furthermore, after the fill is completed, the soft material regains a part of the strength lost during the process of displacement. Therefore, if the fill has a cross-section similar to that shown in Fig. 48.1, the progressive settlement of its crest is likely to become inconsequential shortly after construction.

An outstanding example of the successful application of the displacement method is the Kiel canal, built during the years 1887–1895. For a distance of about 20 km the canal had to be established on a layer of peat and very soft organic clay with a thickness up to 10 m. In some sections the soil was too soft to walk on. The method of building the canal in these sections is illustrated by Fig. 48.2. On the inner side of the center line of each of the future dikes, sand fills were constructed as indicated by the dash line. These fills displaced the soft material over a broad belt almost down to firm ground. They served as a base for the dikes and formed the uppermost part of the slopes of the finished canal. To reduce the danger of slides during construction, excavation was not started until 6 months after the fill was placed. Nevertheless, slides did occur at a few points.

#### 48.8 Fills on Soft Homogeneous Clay

In the following discussion, it is assumed that the surface of the clay is very close to the base of the fill, that the thickness of the clay stratum is at least half as great as the base width of the fill, and that the stratum is fairly homogeneous. It is also assumed that negligible consolidation of the clay will occur during filling so that the strength will correspond to undrained conditions (Article 20).

The failure of a fill on such a base has the general character of a base failure along a midpoint circle (Article 35). However, the uppermost part of the surface of sliding is located within the artificial fill, and the shearing resistance per unit of area along this part is different from that along the lower part. The first step in making a stability computation is to ascertain the average undrained shearing resistance  $s_u$  along the lower part on the basis of a strength survey of the clay stratum. The second step is to determine the average shearing resistance  $s_f$  along the part of the surface of sliding located within the fill. In the stability analysis the real fill is replaced by a clay

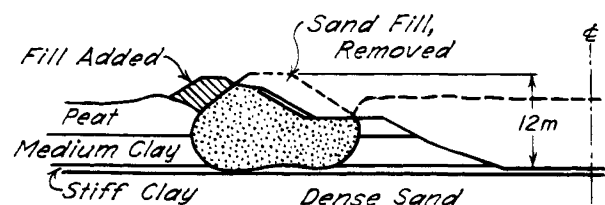


**Figure 48.2** Typical cross-section of Kiel Canal (after Fulscher 1898).



that has an undrained strength equal to  $s_f$ . As a first approximation it is assumed that failure occurs along a midpoint circle; however, the real critical circle must be determined by trial and error. Because of progressive failure, the average shearing strength along the surface of sliding may be less than the weighted average of the peak strengths  $s_u$  and  $s_f$ .

It is usually required that the factor of safety with respect to a base failure should be at least 1.5. Considering the unavoidable errors in estimating the average shearing resistance of the clay, this factor is very low. Nevertheless, to satisfy even this requirement, high fills on soft clay must be provided with very gentle slopes. Hence, if a high fill is also very long, it may be preferable to reduce the factor of safety still further, to 1.2 or 1.1, and to rely on the results of observations during construction to detect impending slides and to prevent the slides by local modifications in the design.

The failure of the base of an embankment on clay is usually preceded by the gradual lateral displacement of the material beneath the toes and by the gradual heave of broad belts located one on each side of the fill. The rate of displacement increases as failure is approached. If the movement is detected in its initial state by means of suitable observations, the failure can be prevented by covering these areas with a layer of fill of suitable thickness.

Slides caused by the failure of a soft clay base generally occur during or immediately after construction, because thereafter the strength of the base gradually increases on account of consolidation. If a slide has already occurred, it is usually possible to ascertain the position of the surface of sliding by means of inclinometers and to compute the average shearing resistance of the clay with considerable accuracy. The value thus obtained serves as a basis for redesign. Figure 48.3 illustrates the procedure. It shows

a section through a highway fill of well-compacted gravel placed on a deposit of organic silty clay (Gottstein 1936). Failure occurred when the top of the fill was 2.5 m below finished grade. A mass of soil having an effective weight  $W$  failed by rotating about the point  $O$ . The driving moment was  $Wl$ . To complete the fill a gravel counterweight  $W_1$  was added with its line of action at a horizontal distance  $l_1$  from  $O$ . The counterweight was given dimensions such that its moment  $W_1l_1$ , plus that due to the shearing resistance along the surface of sliding, exceeded the driving moment of the complete fill by 50%. The right side of Fig. 48.3 shows a section through the finished fill. The upper 2.5 m were made of rolled cinders to keep the weight of the fill as small as possible. After construction of the counterweight there was no movement other than a slight subsidence due to consolidation of the base.

After a fill has been constructed successfully on the surface of a homogeneous mass of clay, its base gradually settles on account of the consolidation of the underlying clay. The magnitude of the settlement can become very great. It should be estimated by means of the procedure outlined in Articles 16 and 41, and the crest of the fill established a corresponding distance above final grade. As consolidation progresses, the bearing capacity of the fill increases.

If time is available to place the fill in stages such that the shearing resistance of the clay increases enough to ensure stability after each stage, steeper slopes may be achieved without infringing on the more conservative factor of safety of 1.5. However, because of the uncertainties in calculated rates of increase in shearing resistance, measurements of pore pressures are required in the clay stratum so that stability analyses can be made and the rate of loading governed by the results. Stage loading is usually associated with the use of vertical drains to

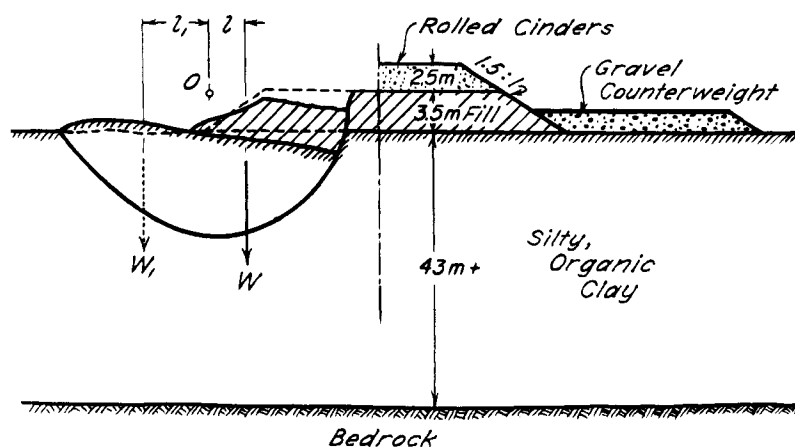


**Figure 48.3** Section through gravel fill on deposit of uniform soft clay. Left side shows principal features of failure during construction; right side shows reconstructed fill stabilized by means of gravel counterweight (after Gottstein 1936).

accelerate the consolidation, as discussed in Article 44.3.6.

Observations on rock fills serving as bases for breakwaters indicate that the settlement of such fills depends not only on the properties of the underlying clay but also to a large extent on the method of construction. In the 1800's the fills were made by dumping large rocks into the water. This procedure completely destroyed the structure of the uppermost layer of clay and caused great local stress concentrations in the underlying material. The settlement of these fills was very large. The older part of the breakwater in the harbor of Spezia, Italy, is an example. Figure 48.4a is a section through the fill. The depth of water was 10 m, and the water content of the soft clay was close to 100%. The results of load tests indicated that the deeper layers had an undrained shear strength of about 25 kPa. Construction was started in 1862. To maintain the crest of the fill at approximately constant elevation in spite of the rapid settlement, it was necessary to add new material to the fill. This in turn accelerated the settlement. During a period of 50 years the material that had to be added was equivalent to a layer 20 m thick. As subsidence increased, the base of the fill assumed the shape shown in Fig. 48.4a.

In 1912 construction of a new section of the breakwater was started. To prevent excessive settlement of the new section, the mud was removed by dredging to a depth between 2 and 5 m below its original surface and replaced by sand with a grain size between 0.2 and 0.4 mm (Fig. 48.4b). Hence, when the fill was constructed, the rocks came to rest on the sand instead of penetrating into the clay, and no local stress concentrations were created in the clay. Probably as a result of this condition, the settlement of the new fill was insignificant compared with that of the old one. At the end of the construction period the settlement was 0.5 m; 9 years later it had reached only 0.8 m. Similar procedures were used successfully in constructing breakwaters in the harbors of Valparaiso, Chile, and Kobe, Japan (Barberis 1935).

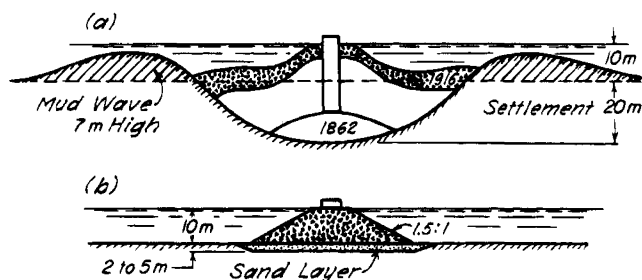


**Figure 48.4** Rockfill breakwater on soft clay in harbor of Spezia, Italy, constructed (a) by dumping rock directly onto clay and (b) by dumping rock onto sand layer that was deposited previously in shallow dredged cut (after Barberis 1935).

## 48.9 Varieties of Failure by Spreading

Failures by spreading have been observed only in connection with fills located above stratified deposits that contain layers of soft clay. Such fills may be safe with respect to breaking into the ground, but they may fail by spreading.

During the last 70 years half a dozen major and several minor dam failures have occurred in this manner. Hence, the stability of fills above clay strata deserves special attention. Outstanding failures due to spreading include Lafayette Dam in California in 1928 (ENR 1929), Marshall Creek Dam in Kansas (ENR 1937), and the Hartford flood-protection dike in Connecticut (ENR 1941).

A study of the records reveals two different types of failure by spreading. One type is distinguished by a relatively slow subsidence of the crest of the fill. The slope, if originally plane, assumes a gentle S-shape, as shown in Fig. 47.11a, and the heave of the ground surface extends only a short distance beyond the foot of the slope. The failures of Chingford Dam near London, England (Cooling and Golder 1942) and of Lafayette Dam are instructive examples of this type. Failures of the other type occur very rapidly, and the heave extends to a great distance from the foot of the slope. During the failure of Lafayette Dam, which was 36 m high, the crest subsided 5 m in about 3 days, over a length of about 150 m. The toe moved out about 6 m, and the heave was confined to a short distance from the foot of the slope. On the other hand, the Hartford dike, only 10 m high, failed in less than 1 min. The crest subsided 5 m over a length of more than 300 m. A row of sheet piles at the foot of the slope moved laterally 20 m, and the heave extended about 50 m from the foot.

Analysis of case records and study of the causes of failure have demonstrated that the catastrophic rapid type of failure occurs only if the clay stratum contains continuous layers or extensive lenses of coarse silt or sand. Therefore, the details of stratification of the clay layer are of decisive importance in determining the mode of failure, and a distinction must be made between clay strata with and without highly permeable partings. In the following discussion we first examine the causes of failure in each of the two types of clay strata and subsequently consider methods for improving the stability of fills located above such strata.

### 48.9.1 Spreading of Fills above Fairly Homogeneous Layers of Soft Clay

The clay stratum below the fill shown in Fig. 48.5a is assumed to be perfectly homogeneous. Shortly after filling starts, the clay begins to consolidate and the stratum becomes stiffer near its upper and lower boundaries. Near midheight, however, the weight of the fill is still carried by excess porewater pressure, indicated by the piezometric levels shown on the left side of the figure, and the shearing

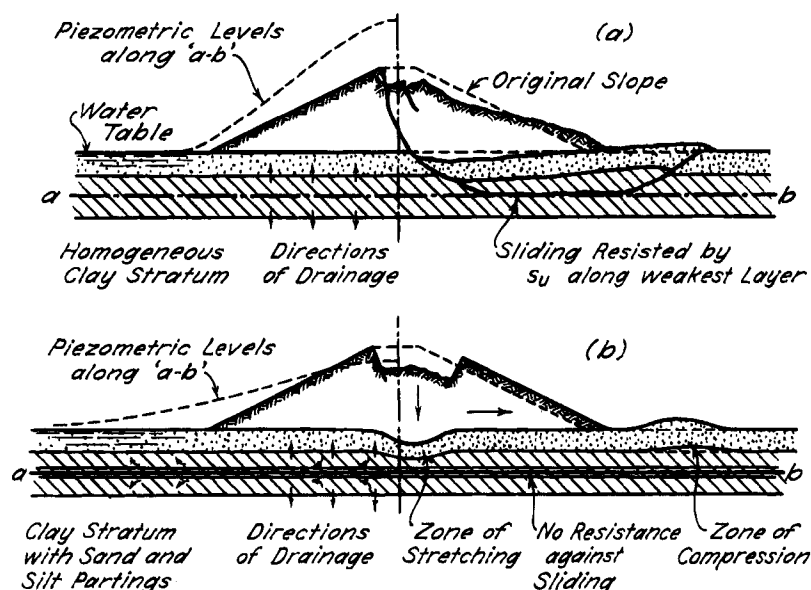


**Figure 48.5** Type of failure of base of fill containing thin clay stratum (a) if clay stratum contains no horizontal pervious partings and (b) if clay stratum contains pervious sand or silt parting.

resistance of the clay remains equal to its initial value. Hence, if failure occurs, the surface of sliding follows some layer of minimum shearing resistance located near midheight of the clay stratum. To estimate the value of the minimum shearing resistance, a survey of the undrained shearing strength must be made. Because the strength of the clay is likely to vary in both the horizontal and vertical directions, the selection of a representative value requires experience, mature judgment, and a thorough investigation of the character of the stratification of the clay bed. It is also essential to make sure that the clay actually does not contain any continuous seams of sand or silt.

After the appropriate value for the undrained shearing resistance has been selected, the factor of safety with respect to sliding can be evaluated by the method described in Article 35 in connection with composite surfaces of sliding. Because there is an appreciable resistance along the horizontal portion of the surface of sliding, the slope assumes the characteristic S-shape shown in Fig. 48.5a.

#### 48.9.2 Spreading of Fills above Clay Strata with Sand or Silt Partings

If the clay contains fairly continuous seams of sand or silt, the excess water from the central part of the stratum drains not only vertically through the top and bottom of the stratum, but also horizontally through the highly permeable seams as shown in Fig. 48.5b. Therefore, the seams may become the seat of high excess porewater pressure. The difference between the excess porewater pressure and the weight of the overlying soil and fill is greatest near the toes of the slopes. In these regions the

shearing resistance of the cohesionless seams may be reduced to zero, and the only resistance to the spreading of the fill is offered by the passive pressure of the earth located above and beyond the surface of sliding. If this pressure is exceeded, the outer parts of the fill move bodily away from the center, and the central part subsides leaving a troughlike depression, as indicated in Fig. 48.5b. Because soil conditions are never exactly symmetrical with respect to the center line of the fill, failure occurs on one side only, but it is hardly possible to predict on which side. The troughlike subsidence characteristic of this type of failure has been observed repeatedly.

The factor of safety against sliding depends on the distribution of the excess hydrostatic pressure within the pervious seams, which in turn depends on unknown local variations in the permeability and on other unknown geologic details. The practical implications of these uncertainties are illustrated by Fig. 48.6. Test borings were made along the center line of the proposed fill shown in the figure. Because no pervious seams were encountered in any of the holes, the designers assumed that during construction the hydrostatic conditions would be as indicated by the dotted piezometric line. These conditions are normal and do not compromise the stability. In reality, the clay contained a seam of fine sand located beneath the right-hand section of the dam. Because porewater pressures are freely transmitted through such seams, the real pressure conditions assumed the character indicated by the dash line, and the fill failed as shown in Fig. 48.5b.

Hence, if the geology of the stratum indicates that the clay may contain highly permeable seams, the risk of failure can be avoided only by providing the fill with

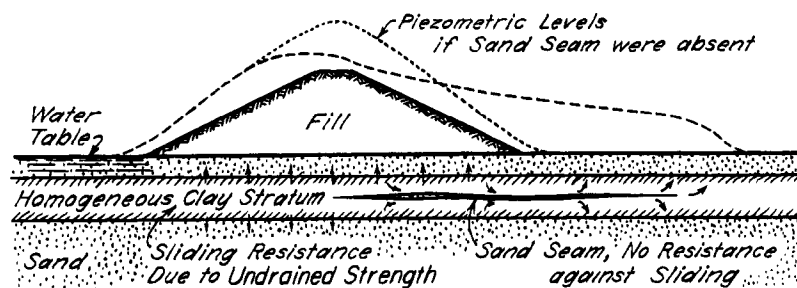


**Figure 48.6** Diagram showing effect on hydrostatic pressure conditions of pervious seam in clay stratum below fill.

very flat slopes at additional cost, or else by using one of the construction expedients described in the following paragraphs.

#### 48.10 Means for Increasing Stability of Fills above Thin Strata of Soft Clay

If the bottom of the soft clay stratum is located at a depth less than about 2 m below the ground surface, it is advisable to remove the clay over the full width of the base of the fill. Otherwise, the designer may choose between two alternatives. The fill may be constructed more slowly than the rate of consolidation of the clay at midheight of the stratum, or provisions may be made to accelerate the process of consolidation by means of vertical drains. Each of these methods deserves consideration, regardless of whether or not the clay strata contain thin permeable seams.

To use the first procedure, the designer must know the rate of consolidation of the inner part of the stratum. Computation alone should not be relied on, because the result may be invalidated by some unnoticed geologic detail such as the presence of highly impermeable seams. It should be used only to make a preliminary estimate of the maximum rate at which the fill can be constructed. To eliminate the risk of failure, the progress of consolidation must be observed in the field during construction by means of porewater pressure gages, and the rate of construction must be adapted to the findings. This is a decided disadvantage, because it does not eliminate the possibility that construction may be intolerably delayed.

If the results of computation show that the normal process of consolidation is too slow to be used as a means for strengthening the base of the fill, acceleration of the process by means of vertical drains should be considered. The procedure is described in Article 44.3.6.

#### 48.11 Summary

On very soft ground high fills can be established by one of two methods. The first consists of displacing the soft ground by the weight of the fill. To avoid excessive settlement after construction, the fill should be built up

to a height of 5 or 6 m above final grade, and the excess material removed after the fill has subsided. The second method consists of accelerating consolidation by means of vertical drains extending to the bottom of the stratum. The drains discharge the water into drainage conduits located at the base of the fill. To determine the most economical procedure, it is necessary to prepare a contour map of the firm base of the soft layer. Wherever the depth of the layer is less than about 2 m, it may be advantageous to remove the soft soil by excavation.

The design of fills to be built above thick beds of soft clay should be preceded by a stability computation. Under normal conditions a factor of safety of 1.5 with respect to sinking should be specified. However, if the fill is very long, it may be more economical to base the design on a factor of safety of 1.2 or 1.1, to locate the weakest spots in the subsoil by means of heave observations during construction, and to cover the areas of heave by a counterweight consisting of a thick layer of fill.

Special vigilance is required if a fill is to be built on stratified soil containing layers of soft clay. Several catastrophic accidents have occurred because the stability of subsoils of this type has been overestimated. If the clay strata contain no sand or silt partings, the resistance against spreading depends on the average shearing resistance of the weakest layers in the subsoil. Because exceptionally weak layers are not necessarily continuous, their presence may escape the attention of even a conscientious investigator. If the clay contains sand or silt partings, the resistance against spreading depends chiefly on the porewater pressure in the partings. This pressure changes during construction, and an accurate forecast of its magnitude is impracticable. Only one reliable safeguard is known against failure due to spreading along such a parting. This is the periodic measurement of the porewater pressure during construction for the purpose of detecting impending danger and the elimination of the pressure by adequate drainage provisions.

#### Selected Readings

An early example of a test fill that experienced foundation failure is "Pendleton Levee Failure (1944)," by K. E.

Fields and W. L. Wells, *Trans. ASCE* 109, pp. 1400–1413. The paper describes the failure and attempts to explain, in terms of the soil-mechanics knowledge of the time, how failure could have occurred at a factor of safety of 1.3. The discussion by K. Terzaghi, pp. 1416–1421, demonstrated that failure occurred by spreading on a sand parting. The paper and discussion illustrate the manner in which progress took place in soil mechanics.

Porter, O. J. (1936). "Studies of fill construction over mud flats including a description of experimental construction using vertical sand drains to hasten stabilization," *Proc. 1st Int. Conf. Soil Mech.*, Cambridge, Mass., 1, pp. 229–235.

Casagrande, A. (1949). "Soil mechanics in the design and construction of the Logan airport," *J. Boston Soc. Civil Engrs*,

36, No. 2, pp. 192–221. Reprinted in *Contributions to Soil Mechanics 1941–1953*, Boston Soc. Civil Engrs. (1953), pp. 176–205. Hydraulically placed clay fill.

AREA (1955). "Soil engineering in railroad construction," *Proc. Am. Rwy. Eng. Assn*, 56, pp. 694–702. Railroad embankment design to avoid common shortcomings.

Moran, Procter, Mueser and Rutledge (1958). *Study of Deep Soil Stabilization by Vertical Sand Drains*, Washington, D.C., U.S. Dept. Commerce, Office Tech. Serv., 192 pp.

Casagrande, A. (1960). "An unsolved problem of embankment stability on soft ground," *Proc. 1st Panamerican Conf. of Soil Mech*, Mexico, 2, pp. 721–746. Railroad fill across Great Salt Lake.

Stamatopoulos, A. C. and P. C. Kotzias (1965). "Construction and performance of an embankment in the sea on soft clay," *Proc. 6th Int. Conf. Soil Mech.*, Montreal, 2, pp. 566–570.

## CHAPTER 9

### *Foundations*

#### ARTICLE 49 FOUNDATIONS FOR STRUCTURES

##### 49.1 Types of Foundations for Structures

The *foundation* is the part of a structure that transmits the weight of the structure onto the natural ground.

If a stratum of soil suitable for sustaining a structure is located at a relatively shallow depth, the structure may be supported directly on it by a *spread foundation*. However, if the upper strata are too weak, the loads are transferred to more suitable material at greater depth by means of *piles* or *piers*. Spread foundations are of two types. If a single slab covers the supporting stratum beneath the entire area of the superstructure, the foundation is known as a *mat* or *raft*. If various parts of the structure are supported individually, the individual supports are known as *spread footings*, and the foundation is called a *footing foundation*. A footing that supports a single column is called an *individual footing*; one that supports a group of columns is a *combined footing*, and one that supports a wall is a *continuous footing*.

The *depth of foundation*  $D_f$  is the vertical distance between the base of the footing or pier and the ground surface, unless the base is located beneath a basement or, if the structure is a bridge, beneath the surface of the river. In these instances the depth of foundation is referred to the level of the basement floor or to that of the river bed. The principal difference between footings and piers lies in the value of the ratio  $D_f/B$ , where  $B$  is the width of the base. For footings  $D_f/B$  commonly ranges between 0.25 and 1, whereas for piers it is usually greater than 5 and may be as great as 20. However, monolithic supports for bridges are also generally called piers, irrespective of the value of  $D_f/B$ . They are designed according to the same principles as those governing the design of footings or piers for buildings.

##### 49.2 Minimum Depth of Building Foundations

The conditions that determine the minimum depth of building foundations are illustrated by Fig. 49.1, which

represents a cross-section through part of a building. The outer portion of the structure does not have a basement but the inner part does.

The first requirement is that the base of every part of the foundation should be located below the depth to which the soil is subject to seasonal volume changes caused by alternate wetting and drying.

This depth usually does not exceed about 1 m, but notable exceptions occur in many parts of the world that experience marked wet and dry seasons where the subsoil consists of clays that shrink and swell significantly. Such seasonal volume changes to great depth are experienced in parts of the southwestern United States, the western prairies of Canada, South Africa, Australia, and many other localities (Simpson 1934, Bozozuk 1962, Jennings 1953). Although the clays may be stiff enough to sustain a load of 200 or 300 kPa without perceptible settlement, the seasonal volume changes require making even light structures so stiff and strong or so flexible that they can sustain the movement without damage, or providing them with pier foundations that extend below the depth of volume change. The design of such piers is considered in Article 53.5.8. Withdrawal of water from the ground by the root systems of large trees located close to buildings has also been responsible for important and detrimental differential settlement.

The base of each part of a foundation should also be located below the depth to which the structure of the soil is significantly weakened by root holes or cavities produced by burrowing animals or worms. The lower boundary of the weakened zone can be discerned readily on the walls of test pits.

In regions with cold winters the foundations of the outside columns or walls should be located below the level to which frost may cause a perceptible heave (Article 15.8). In the northeastern United States this depth may be as great as 1.5 m. Hence, outside walls or columns of heated buildings may require deeper foundations than interior columns.

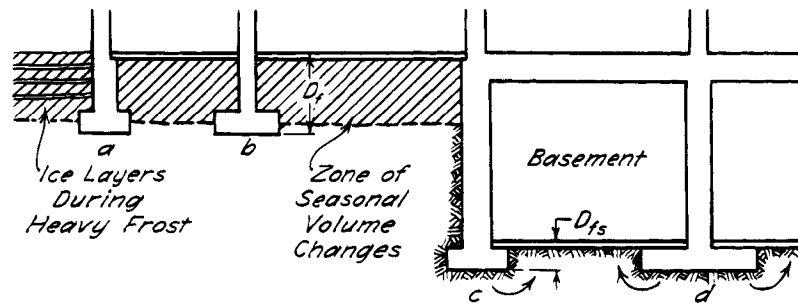


**Figure 49.1** Simplified section through footing foundation of building with basement beneath its central part.

Basement floors are usually located below the minimum depth required for footings of buildings without basements. Consequently, under normal conditions the minimum depth of foundations located within the boundaries of a basement (*c* and *d* in Fig. 49.1) is governed solely by structural requirements. Exceptions to this statement need be considered only if conditions may arise that could subsequently affect the integrity of the soil beneath the footings. In one instance large unequal settlement of a building resting on medium clay was caused by the gradual desiccation of the clay surrounding a deep boiler room. On account of the low humidity and high temperature of the air in the boiler room, the water in the clay evaporated through the concrete walls of the room. In another instance the footings of a building on fine sand settled because of the leakage of water through open joints in a defective sewer located beneath the base level of the footings. The water washed sand into the sewer, and settlement occurred because of the loss of ground. Hence, before the minimum depth of foundation for a building with a basement is established, the possibilities for subsequent artificial changes in the conditions of soil support should be considered.

### 49.3 Minimum Depth of Bridge Foundations

Whenever the water level in a river rises, the soil that constitutes the river bed starts to move throughout the greater part of the length and width of the river, and the bottom of the river goes down. This process is known as *scour*. The minimum depth for the foundation of a bridge pier is determined by the condition that the base of the foundation should be a meter or more below the level to which the river may scour during high water.

In those sections of a river where high banks or dikes prevent flood water from spreading over a wide area, scour can be very deep, even in a channel unobstructed by bridge piers. Figure 49.2 illustrates this possibility. Figure 49.2a is a section through the Colorado River near Yuma, Arizona. The river bed consists of fine silty sand and silt. As the river level rose 4 m, the level of the bottom of the river channel went down as much as 11 m

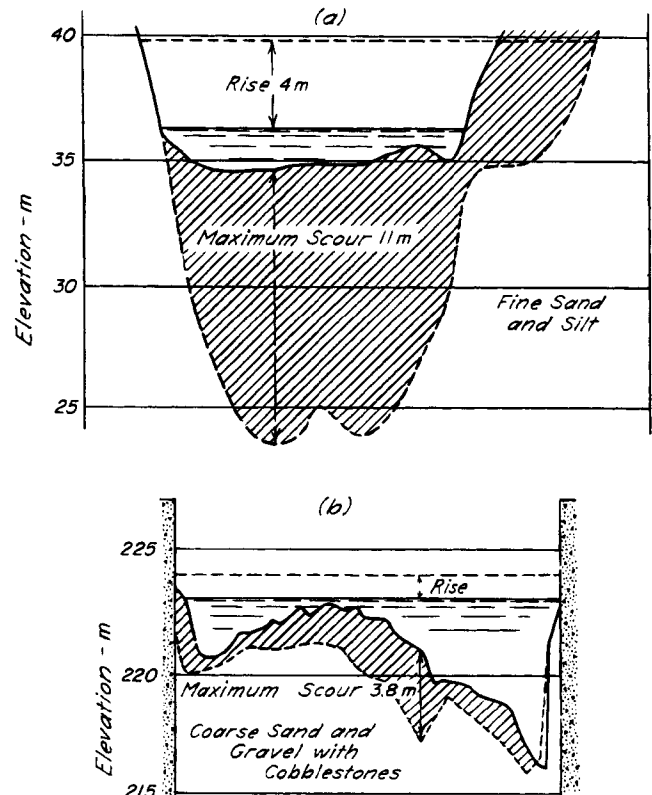


**Figure 49.2** Scour due to high water (a) in unobstructed bed of Colorado River near Yuma, Arizona (after Murphy 1908); (b) between abutments of bridge over Drau River in eastern Alps. Horizontal scale equals 10 times vertical scale.

(Murphy 1908). Figure 49.2b is a section through a mountain stream confined between the abutments of a bridge. The river bed consists of coarse sand and gravel with a high percentage of large cobbles. A rise of the river level of 1 m was associated with a scour ranging between 0.6 and 3.7 m.

Obstruction of the flow by bridge piers increases the amount of scour, particularly in the proximity of the piers. The influence of the shape of the piers on the topography of the depression formed by the scour is illustrated in

Fig. 49.3. The information is based on the results of model tests (Rehbock 1931).

Inasmuch as scour does not always receive the attention it deserves, failure of bridge piers due to this cause is not uncommon. Failure may occur even under conditions that seem to exclude the risk of scour. In a torrential river in Colorado the base of a bridge pier was established at a depth of 3 m below the bottom of the river channel. At that depth the river bed contained boulders up to  $0.2 \text{ m}^3$  in size, so tightly wedged that further excavation would have been impracticable without blasting. Therefore, the base of the pier was established at that depth. Yet, the first high water after construction caused the pier to fail.

Near the east coast of the United States, a bridge pier was founded  $0.6 \text{ m}$  below the surface of a stratum of gravel  $2 \text{ m}$  thick. The gravel was covered with  $2.4 \text{ m}$  of soft mud. During exceptionally high water the pier settled appreciably. After the water level dropped, the gravel was still buried beneath mud. From the records of the failure, it appeared likely that the settlement was due to scour in the gravel, preceded by complete removal of the overlying mud layer. While the high water was receding, a new layer of mud was deposited.

In those parts of a river where the high water has an opportunity to spread over a wide area, the scour may be imperceptible. Locally, the river bed may even be raised. However, bridges are generally located at points where these conditions are not satisfied. Furthermore, at any given cross-section of the river the point of deepest scour may shift from year to year in an unpredictable manner.

Reliable scour forecasts require mature and varied experience in the hydraulics of rivers, often supplemented by hydraulic model tests. Therefore, they can be made only by specialists in this field. On account of the inevitable uncertainties involved in the forecasts, a large margin of safety is required. Rules of thumb relating depth of scour to rise of river level have often proved to be inadequate and should no longer be used.

#### 49.4 Allowable Pressure on the Subsoil

As the load on a given foundation increases, the foundation settles. At low loads the settlement may increase in direct proportion to the load, but with increasing load the rate of increase of settlement usually increases. If the load becomes great enough, the increment of settlement may be excessively or uncontrollably large and the foundation is said to have broken into the ground or to have experienced a bearing-capacity failure. Obviously, the distinction between excessive settlement and failure by breaking into the ground is quite arbitrary in many instances. Nevertheless, it is convenient to consider the two conditions independently, especially because the settlement may increase due to the consolidation of underlying compressible soils even if the loading remains constant.

It is appropriate, therefore, to require that every foundation satisfy two independent conditions. First, the factor of safety of the foundation with respect to breaking into the ground should not be less than a specified value, usually between about 2 and 3. The appropriate value depends on the nature and importance of the structure, the consequences of failure, and the reliability with which the value can be determined. It may differ in the same structure for different types of loadings. Second, the deformation of the base of the structure due to unequal settlement should not be great enough to damage the structure. Because the theoretical methods for evaluating the factor of safety of foundations with respect to breaking into the ground (Article 33) are simple and fairly reliable, they can be used without essential modification in design. On the other hand, the methods for evaluating the magnitude and distribution of the settlement are cumbersome and in many instances unreliable. This fact determines the procedure for estimating the allowable soil pressure whenever the design must be based on considerations of settlement.

Because all substances including soil and rock are compressible, every foundation settles. If the base of a struc-

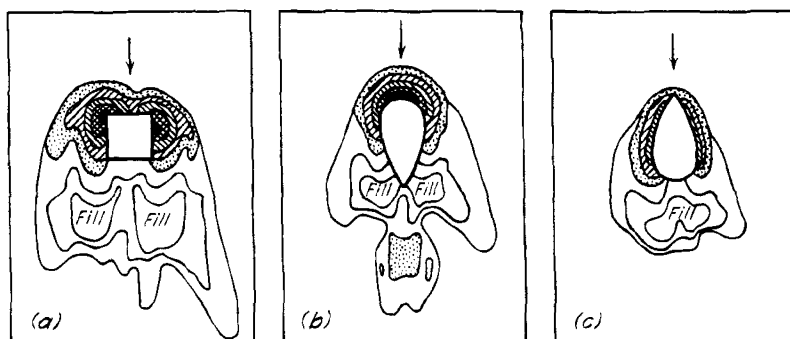


Figure 49.3 Results of hydraulic model tests for investigating effect of shape of bridge piers on scour (after Rehbock 1931).



ture remains plane while settlement proceeds, the magnitude of the settlement may be irrelevant. However, if the base becomes warped during the settlement, the structure may be damaged. For this reason, the distribution of the settlement over the base of the structure is far more important than the maximum value. It is also far more difficult to evaluate.

According to Article 41, the magnitude and the distribution of the settlement of a loaded area depend on the physical properties of the soil located beneath the area, on the size of the area, on the depth of foundation, and on the position of the water table. If a building rests on footings, the estimate of the settlement is further complicated, because the soil conditions prevailing under the different footings are likely to be different (Article 12). An accurate evaluation of the effect of all these factors on the settlement is impracticable. Therefore, under normal conditions the designer is compelled to estimate the settlement on the basis of simple semiempirical rules. The theory of settlement (Article 41) serves merely as a basis for a rational interpretation of the results of soil and load tests and for determining the limits of validity of the semiempirical rules. Refined settlement computations are justified only if the subsoil contains strata of soft clay located below the base of the foundation or the points of the piles (Articles 50–53).

Semiempirical rules for determining settlement are based on observed relations between the results of simple field tests such as penetration tests, the load per unit of area, and the behavior of existing structures. Every relation of this type is a statistical one involving more or less important scatter from the average. Experience shows that a relation developed within a geologically well-defined region always involves less scatter than the corresponding relation for all deposits of a given kind, irrespective of their geologic origin and environment. In this book only relations of the latter type can be considered. On account of the great scatter, they represent a very conservative basis for design. Therefore, whenever extensive construction operations are carried out within a limited area, such as that occupied by a large city, the rules given in the following articles should be checked against local experience. If they are found to be too conservative for the particular region, they should be modified accordingly.

Until local rules are established, the requirements of safety call for design on the basis of the more conservative general rules. Because of the additional expense involved in this procedure, the accumulation of the observational data needed for establishing local rules is a very good investment and should be encouraged. Only in this manner can the engineer exploit the desirable characteristics of the principal local soil types to the fullest extent.

The following articles deal with the methods for adapting the four principal types of foundations to the subsoil conditions.

## Selected Reading

The most comprehensive text on foundation engineering, frequently revised, is *Foundation Design and Construction*, by M. J. Tomlinson (Essex, England, Longman; also New York, John Wiley & Sons, Inc.). Although directed primarily to practice in the United Kingdom, it is applicable worldwide. The 5th Edition, 1986, contains 842 p).

The development of the art of foundation construction, and of geotechnics in general, is described by J. Kerisel (1985). "The History of Geotechnical Engineering up Until 1700," *Golden Jubilee Volume*, 11th ICSMFE, San Francisco, pp. 3–93. An entire session of the 10th ICSMFE, Stockholm (1981), was devoted to Saving Cities and Old Buildings. In Vol. 3 of the Conference Proceedings, pp. 19–178, the 29 papers give interesting descriptions of foundations constructed before the advent of soil mechanics.

The development of the design of footing foundations in Chicago, which epitomizes that in other cities of the world, and the transition to deeper foundations in the late 1800's, are described in R. B. Peck (1948), "History of Building Foundations in Chicago," *Univ. of Illinois Eng. Exp. Sta. Bull.* **373**, 64 p.

## ARTICLE 50 FOOTING FOUNDATIONS

### 50.1 Origin and Shortcomings of Conventional Design Methods

The most important step in the design of a footing foundation is the evaluation of the greatest pressure that can be applied to the soil beneath the footings without causing either failure of the loaded soil or excessive settlement. Before the advent of soil mechanics, the methods for choosing this pressure were based on experience and inadequate knowledge of the properties and behavior of soils. Although the methods contained many shortcomings, they were expedient. Consequently, their general form has been retained and suitable modifications have been introduced to take account of the findings of soil mechanics. Intelligent use of the modified procedures presupposes a familiarity with the methods prevalent during the first half of the 1900's.

Before the 19th century the framework of most large buildings consisted of strong but somewhat flexible main walls of stone or brick masonry interconnected by massive but equally flexible partition walls intersecting each other at right angles. Because such buildings could stand large settlements with little damage, their builders gave scant consideration to foundations other than to increase the wall thickness at the base. If the ground was obviously too soft to support the loads, the walls were established on piles. When exceptional structures were built with large domes, vaults, or heavy individual columns, the designers tended to underdimension the foundations

because they had neither rules nor experience to guide them. As a result, many important buildings either collapsed or were disfigured by subsequent reinforcements.

The development of highly competitive industry during the 19th and 20th centuries led to a demand for large but inexpensive buildings. The types that developed and the equipment they contained were often more sensitive to differential settlement than their predecessors. Furthermore, many of the most desirable sites for industrial buildings were located in regions that had previously been avoided because of notoriously bad soil conditions. Hence, designers found themselves in need of a reliable procedure, applicable under all soil conditions, for proportioning the footings of a given building in such a manner that they would all experience nearly the same settlement.

To satisfy this need the concept of an "allowable soil pressure" was developed during the 1870's in several different countries. The concept was based on the general observation that, under fairly similar soil conditions, footings transmitting pressures of high intensity to the subsoil generally settled more than those transmitting pressures of low intensity. With this in mind designers began to observe the condition of buildings supported by footings that exerted various pressures against the subsoil. The pressures beneath the footings of all those buildings that showed signs of damage due to settlement were considered too great for the given soil conditions. The maximum pressure not associated with structural damage was considered a satisfactory basis for design and was accepted as the *allowable soil pressure* or *allowable bearing value*. The values obtained for each type of soil in a given locality by this purely empirical procedure were assembled into a table of allowable soil pressures that was subsequently incorporated into the building code governing construction in that locality.

Although most building codes contained tables of allowable soil pressures, they did not offer any hint regarding the origin of the values or any explanation of the meaning of the term "allowable soil pressure." These omissions fostered the belief that the settlement of a building would be uniform and of no consequence if the pressure on the soil beneath each footing were equal to the allowable soil pressure. The size of the loaded area and the type of building were believed to be immaterial. Some engineers were even under the delusion that a building with footings that exert the allowable soil pressure would not settle at all.

Many foundations designed on the basis of the allowable-soil-pressure tables were entirely satisfactory, but occasionally the results were disappointing and the structures settled excessively. Because engineers believed that footings would not settle noticeably if the allowable pressure were not exceeded, they attributed the failures to faulty classification of the soil. They

assumed that incorrect allowable pressures had been selected because the terms used to describe the soil in the field and in the building codes did not have the same meaning. To avoid this difficulty, it became customary to select, or at least to verify, the allowable soil pressure by means of load tests.

A load test is made by increasing the load on a bearing plate in small increments and measuring the corresponding settlements. The bearing plate rests on the bottom of a pit, usually at the level of the base of the footings. In accordance with the preference of the engineer who makes the test, the plate may be surrounded by a box and the pit backfilled to final grade (Fig. 50.1a), or the pit may be made so large that the plate rests in the middle of a level area (Fig. 50.1b). The test results are represented by load-settlement curves similar to the one shown in Fig. 50.1c. In the following paragraphs two of the most common methods for performing the tests and interpreting the results are described.

The first method consists of loading a square or circular bearing block of any dimensions chosen by the investigator. The allowable load  $q_a$  per unit of area is taken as some fraction, such as one half, of the average pressure on the block at the time of failure. This procedure is objectionable for several reasons. In the first place, if the load-settlement curve resembles  $C_2$  (Fig. 33.1), there is no definite failure load. Second, the size of the loaded area, which is optional, may have a large influence on the load-settlement relation and on the ultimate bearing capacity per unit of area (Article 33). Hence, by using this first procedure two different investigators can obtain very different values of  $q_a$  for the same soil.

The second method consists of conducting a standard load test, (Article 12.4), which consists of loading a bearing block covering an area of  $0.1\text{ m}^2$ . The allowable load  $q_a$  is arbitrarily defined as one-half the load at which the settlement of the bearing block is 10 mm. (In countries using the English system the area of contact is customarily taken as  $1\text{ ft}^2$ , and the settlement as 0.5 in.) This procedure, although arbitrary, is preferable because two different investigators will at least obtain the same value of  $q_a$  for the same soil.

There are many other methods for performing load tests and many other rules for interpreting the results (i.e., ASTM D1194). Yet, whatever the method may be, the test results reflect the character only of the soil located within a depth of less than about twice the width of the bearing plate, whereas the settlement of the footings depends on the properties of a much thicker soil stratum. Consequently, if the character of the soil changes below a depth of about twice the width of the bearing plate, as it often does, the test results are certain to be misleading. In the past, it was almost universal practice to select the allowable soil pressure without regard for the size of the footings, the type of superstructure, and other vital

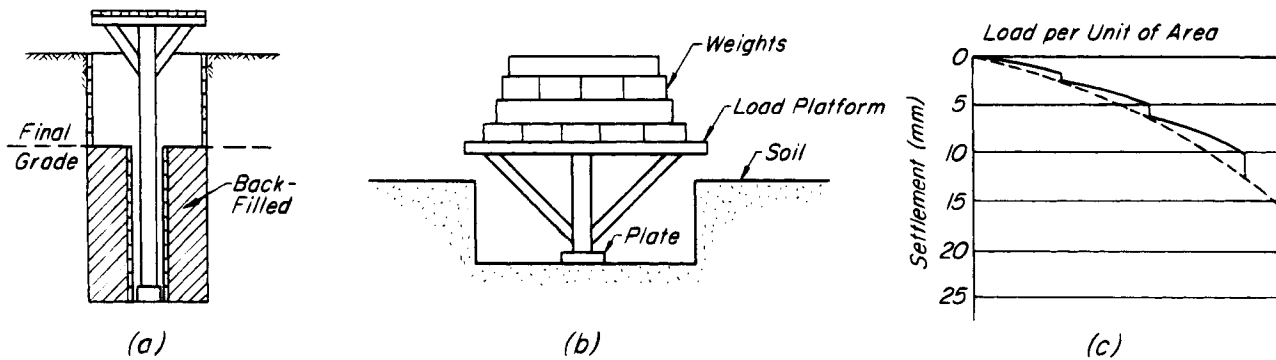


**Figure 50.1** (a and b) Test arrangements for determining relation between load per unit of area and settlement of test plate, as basis for selecting allowable soil pressure. (c) One of several customary methods for plotting results of load test.

characteristics of the proposed project; therefore, it is not surprising that increasing recourse to load tests did not significantly reduce the frequency of faulty footing design. Indeed, numerous complete foundation failures occurred in spite of the conscientious performance of load tests. To reduce the risk of faulty design, the allowable soil pressure must be chosen in accordance with the character of the soil profile and of the foundation itself. Part of the necessary information can be obtained from the theories given in Articles 33, 40, and 41. The rest is derived from construction experience.

Because of the great variety of soils and combinations of soils encountered in practice, no single method for determining the allowable soil pressure is applicable under all circumstances. The procedure must always be adapted to the soil conditions revealed by the subsurface exploration. In particular, the procedure depends on the *significant depth* or *depth of influence*. These terms refer to the depth within which the load on the footing alters the state of stress in the soil enough to produce a perceptible contribution to the settlement.

The significant depth depends not only on the size of the footing and on the load it supports, but also to a high degree on the soil profile and the physical properties of the soils that constitute the individual strata. If the initial tangent modulus of the soil (Article 17.5.1) increases as the depth below a footing increases, the significant depth may be somewhat less than the width  $B$  of the footing. On the other hand, if the soil beneath the footing becomes softer with depth, the significant depth may be equal to several times the width  $B$ .

In the following discussion, four principal types of soil conditions are considered:

1. The footings are supported by nonplastic silt, sand, or sand and gravel that do not contain any layers of soft clay or other highly compressible soil within the significant depth.
2. The footings are supported by clay or plastic silt

that is fairly homogeneous within the significant depth.

3. The footings are supported by soil that contains one or more soft layers within the significant depth.
4. The footings rest on unsaturated soils having a structure that may collapse upon wetting.

#### 50.1.1 Loads, Resistances, and Factors of Safety

The first step in designing a footing is to compute the total effective load that will be transferred to the subsoil at the base of the footing. The total effective or *excess load*  $Q_t$  transferred to the subgrade may be expressed by the equation,

$$Q_t = (Q - W_s) + Q_l = Q_{dn} + Q_l \quad (50.1)$$

$Q$  = permanent or *dead load* on the base of the footing, including the weight of the footing and the soil located above the footing. If the water table is higher than the base of the footing, the hydrostatic uplift (Article 15) on the submerged part of the body of soil and concrete should be deducted.

$W_s$  = effective weight of the soil (total weight of soil reduced by hydrostatic uplift) that was located above the base of the footing before excavation. However, in connection with basement footings such as  $c$  and  $d$  in Fig. 49.1, the weight of the soil previously located above the basement floor should not be deducted, because the soil was removed not only above the base but also above the area adjoining at least one side of the base.

$Q_{dn} = Q - W_s$  = net dead load

$Q_l$  = live load on footing, including that due to wind and snow.

For each of the categories of soil listed at the end of Article 50.1, different types and combinations of loading

produce different effects; moreover, on a given soil the types of loading that govern the ultimate bearing capacity may differ from those that govern settlement.

For example, a footing foundation above a soft or medium clay may be subjected to dead load, live load, and wind load. The dead load remains constant and can be evaluated quite reliably. The live load may be small compared with the dead load, as in some office buildings, or it may be large, as in some warehouses. In any event, the maximum live load that will actually reach a footing cannot usually be determined in design; it has a probabilistic aspect. The maximum wind load that will actually be experienced by the same footing also cannot be evaluated deterministically. Moreover, it is unlikely to occur at the same time the maximum live load is acting. Yet, if at any time the sum of the dead, live, and wind loads should reach the ultimate bearing capacity of the clay, the footing would fail. Whether or not the critical loading is investigated by probabilistic means, the reliability of the design is a function of the uncertainties in loading. Comparable uncertainties also arise in the evaluation of the shear strength of the clay, which governs the ultimate bearing capacity.

In contrast to its ultimate bearing capacity, the settlement of a footing foundation on a soft or medium clay occurs largely as a result of consolidation. The portion of the ultimate settlement due to dead load can be estimated as reliably as the compressibility can be determined. If fluctuations in live loading occur within a time that is short in comparison with the time required to reach a high degree of consolidation, the maximum live load may hardly influence the settlement; the long-term average live load is likely to be the governing value. Wind loads, being transitory, may hardly influence the settlement at all.

Thus, the design of a footing foundation to possess a postulated margin of safety against an outright bearing-capacity failure and to experience no more than a specified settlement involves uncertainties not only with respect to the numerical values for the soil properties, but also with respect to the loads to be taken into account under different conditions.

This situation, which has its counterpart in structural engineering, has led to attempts to rationalize and codify procedures for design. These include the concept of load and resistance factors, sometimes called partial coefficients, for limit-state design.

Limit-state design considers that there are two limit states that must be respected: the *ultimate limit state*, which corresponds to the failure of a slope or to the bearing-capacity failure of a foundation; and the *serviceability limit state*, which corresponds to the development of unacceptable settlements or distortions and which may be determined not only by technical requirements but

also by such subjective criteria as permissible architectural cracking.

Design against ultimate failure has traditionally been based on the equation

$$\frac{\Sigma \text{ resistance}}{\Sigma \text{ load effects}} = F$$

where  $F$  is defined as the overall or *global factor of safety*. Appropriate values of  $F$  have been incorporated in various textbooks and building codes. It is obvious that selection of a suitable value of  $F$  for a particular condition requires considerations comparable to the discussions in the preceding paragraphs. To reduce the subjectivity of this procedure, to achieve a more uniform margin of safety for different types of structures, loadings, and soil conditions, and to develop an approach compatible with ultimate-strength design in structural engineering, design against ultimate failure has been based increasingly on the equation

$$\frac{\Sigma \text{ factored resistances}}{\Sigma \text{ factored load effects}} = 1$$

in which each component of resistance, such as shear strength, is multiplied by a factor less than unity to account for uncertainties in its value and its significance in the type of problem at hand, and each load is multiplied by a factor greater than unity (unless it contributes to resistance) to account for uncertainties in its value. Values for resistance and load factors suggested by the 1985 Canadian Foundation Engineering Manual are listed in Table 50.1. Modification factors are found necessary, however, for particular applications. For the most part,

**Table 50.1 Suggested Load and Resistance Factors**

Category	Item	Factor
		(Load)
Loads	Dead loads	1.25 (0.8)
	Live loads, wind, earthquake	1.50
	Water pressures	1.25 (0.8)
		(Resistance)
Shear strength	Cohesion	0.65
	(stability, earth pressure)	
	Cohesion (foundations)	0.5
	Friction ( $\tan \phi'$ )	0.8

Values in parentheses apply when the load acts to resist failure. (after 1985 Canadian Foundation Engineering Manual).

resistance and load factors have been selected to provide roughly the same global factors of safety as those based on the accumulated experience of the past, but the approach holds promise for improvement as more information becomes available and as probabilistic studies of the variations in loads and soil properties mature.

The serviceability limit state does not lend itself so readily to investigation on the basis of factored loads and resistances, inasmuch as different types and usages of structures correspond to different allowable settlements and distortions. Once the tolerable values are established for a particular design, however, they are usually accepted as the governing values without modification by a factor. However, for soil deposits having wide variations in compressibility, it may be advisable to introduce a serviceability reduction factor less than unity. A value as low as 0.7 has been suggested by Meyerhof. It should be noted that serviceability considerations described here apply only to the proportioning of the foundation, not the actual structural strength design for which Table 50.1 has been suggested. A factor of unity is also usually adopted for the service loads for which the settlements or distortions are computed, provided that time-averaged sustained loads are used for calculating settlements of consolidating clays.

The principal advantages of limit-state design in terms of factored quantities are to provide a unified system for evaluating safety and serviceability in soil mechanics, and to bring geotechnical and structural design into a common framework. However, even though experience and statistical studies may ultimately lead to greater consistency in routine design, good engineering practice will continue to require understanding and application of the fundamental principles of soil mechanics and soil behavior. Hence, in this book, emphasis is directed to the governing fundamentals, and the term factor of safety is generally used in its global sense.

## 50.2 Footings on Sand and Nonplastic Silt

### 50.2.1 Scope

This article deals with footings resting on cohesionless soils having a stable structure. Soils with metastable structures that may collapse upon wetting are discussed in Article 50.5.

Silts can be divided into two categories: those with the characteristics of a rock flour and those that are plastic. The allowable pressure on rock-flour silts can be selected by means of the procedures for sands, and the allowable pressure for plastic silts by the methods used for clay (Article 50.3). The principal difference in evaluating the behavior of nonplastic silts and coarser granular materials is the rate at which pore pressure adjustment may occur. In most sands the rate of drainage is so rapid in relation to the rate of load application that the drained strength

can be counted on in calculating the ultimate bearing capacity. Under some conditions this may not be true for silts, and the pore pressures must be taken into account. The shear strengths may then lie between the consolidated undrained and drained values.

In the remainder of this article, the term sand is interpreted to include nonplastic silts.

### 50.2.2 Relevance and Limitations of Settlement Predictions

Soil mechanics provides the means for calculating the factor of safety of a footing on sand against complete failure by breaking into the ground, and for estimating the settlement to permit judging whether the function of the structure will be impaired by excessive displacement or distortion. Several practical limitations exist, however, on the extent to which it is worthwhile or possible to make a reliable prediction of the settlement of footings on sand.

In the first place, experience has demonstrated that, unless underlain by very loose sands, footings subjected to conventional soil pressures such as those listed in most building codes rarely settle enough to cause distress in the supported structure (Sutherland 1975).

Secondly, the relative density and compressibility of sands, even if deposited under apparently constant geologic conditions, vary significantly and erratically from place to place to such an extent that the settlements of equally loaded footings of the same size on the same sand deposit are likely to vary over a large range of values. This statement is illustrated by the results of a statistical study of settlements at 13 different sites. The findings are shown in Fig. 50.2, in which the vertical axis represents the ratio of the observed settlements of several footings at each site to the mean settlement of the same footings. The sites are characterized by their average standard penetration resistance  $\bar{N}_{60}$ . Corrections have been applied to the settlement ratios to minimize the effects of minor differences in dimensions and depth of embedment of the footings. It is evident that the ratio of maximum to minimum settlements of practically identical footings at the same site may easily be as great as 3 or 4, and that a ratio of maximum to average settlement of 1.6 is a reasonable but not overconservative upper bound.

Finally, even if a homogeneous sand deposit were found, there would be many practical obstacles to making a reliable calculation of footing settlement by the apparently straightforward procedure of determining the vertical pressure at various depths beneath the center of the footing; evaluating, by sampling and testing, the vertical compressibility of the sand at the corresponding depths; calculating the resulting vertical strains between the selected depths; and summing the strains to obtain the settlement. Although the pressures can be approximated with reasonable accuracy, the compressibility eludes

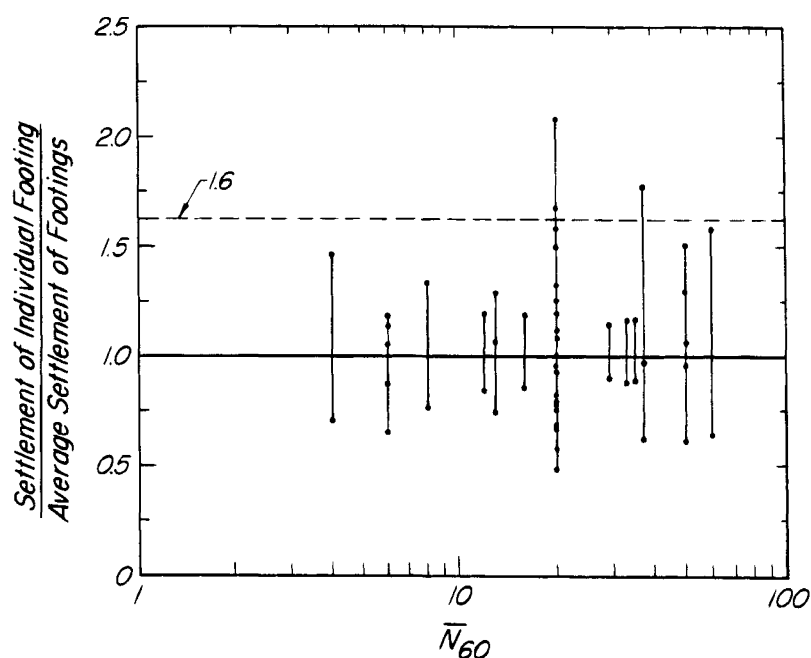


**Figure 50.2** Ratio of settlement of individual equally loaded footings of same size at a given site to average settlement of same footings (after Burland and Burbidge 1985).

direct evaluation. Tests on samples in the laboratory are likely to be misleading because of the practical inability to obtain undisturbed samples. Moreover, the vertical compressibility of sand depends strongly on the lateral stresses, which are a function not only of the degree of overconsolidation or initial lateral stress ratio  $K_0$ , but also of the frictional forces that develop on the base of the footing when it is loaded. These conditions make it virtually impossible to replicate, in either laboratory or field tests, conditions corresponding to the state of stress beneath a footing. Even if possible, such tests would be prohibitively expensive for routine design of simple footing foundations.

In view of the generally satisfactory performance of footings on sand, of the differences in settlement inevitably associated with the inherent variability of even apparently homogeneous sand deposits, and of the infeasibility of determining the state of stress governing the vertical compressibility of the sand beneath the footings, all that soil mechanics can be expected to provide, aside from ensuring an adequate factor of safety against a bearing-capacity failure, is an expedient and reliable approximate procedure for proportioning footings so as not to settle excessively under the design soil pressures.

### 50.2.3 Early Application of Soil Mechanics to Settlement Prediction

In the 1940's, because of the situation discussed above, semiempirical procedures for estimating the settlements of footings on sand were developed in which the compressibility was investigated by penetration tests or small-

scale load tests. The predictions of settlement of the full-size footings followed one of two general approaches. According to one (Buisman 1941, DeBeer 1948), the compressibility was calculated from the results of cone penetration tests by means of an empirical correlation, and the increment of vertical pressure due to the footing was evaluated by Boussinesq's equation (Article 40.1) or some modification thereof.

The other general approach (Terzaghi and Peck 1948) was based on extrapolation of measured or estimated settlements  $S_1$  for small loaded areas with width  $B_1$  to the settlement of the full-size footing with width  $B$ . The extrapolation, based on tests by Press (1933), was expressed as:

$$S = S_1 \left( \frac{2B}{B + 1} \right)^2 \quad (50.1)$$

where  $B$  was in feet. The values of  $S_1$  could be determined by plate load tests, or by use of relations established by field comparisons of the results of standard penetration test  $N$  values, settlement, and width of footing. The principal shortcoming of this procedure was the unreliability of the extrapolation formula (Bjerrum and Eggstad 1963), which is now recognized to be an unacceptable oversimplification of complex phenomena (Article 41.2).

### 50.2.4 Settlement Estimates by Semiempirical Statistical Approaches

Numerous comparisons have been made between the results of settlement observations on actual footings and

estimates based on the foregoing procedures. Various modifications have also been proposed and compared. All comparisons have shown large statistical scatter, due in part to the inevitable variability in the compressibility of natural sand deposits. In addition, the Terzaghi-Peck procedure generally led to significant overestimates of settlement for small footings and underestimates for very large footings or rafts. Most of the comparisons were based on limited data. Now, however, a broad data base of several hundred reliable records of settlements of structures on sand exists and has been used in statistical studies resulting in more reliable methods for estimating the settlements.

### 50.2.5 Method Using Standard Penetration Test

The settlement  $S$  can be expressed in terms of vertical strain  $\epsilon_v$  as

$$S = \int_0^{Z_I} \epsilon_v dz \quad (50.2)$$

where  $Z_I$  represents the depth of influence below which the vertical strains under the foundation are negligible. If the soil is divided into  $n$  sublayers and a linear relationship is assumed between end-of-primary vertical strain  $\epsilon_v$  and effective vertical stress  $\sigma'_v$  in each sublayer, Eq. 50.2 may be rewritten as

$$S_p = \sum_{j=1}^n [Z_I m_v \Delta \sigma'_v]_j \quad (50.3)$$

where

$$\begin{aligned} S_p &= \text{settlement at end-of-primary consolidation} \\ [m_v]_j &= [\Delta \epsilon_v / \Delta \sigma'_v]_j = \text{coefficient of vertical compression of sublayer } j \\ [\Delta \sigma'_v]_j &= \text{increase in effective vertical stress at mid-depth of sublayer } j \\ [Z_I]_j &= \text{thickness of sublayer } j \text{ such that} \\ Z_I &= \sum_{j=1}^n [Z_I] \end{aligned}$$

The coefficient  $m_v$  in Eq. 50.3 differs from the coefficient of volume compressibility  $m_v$  (Article 16.6) determined from a one-dimensional oedometer test, in that it includes the settlement resulting from lateral deformation of the soil.

Because of the difficulties of sampling and testing granular soils, reliable expedient methods are not available for determining the vertical profile of  $m_v$  from laboratory tests. Moreover, errors arise in calculating the change in effective vertical stress in granular soils on the basis of homogeneous isotropic linear elasticity and in estimating the duration of primary consolidation. Consequently, the direct use of Eq. 50.3 for routinely calculating the settlement of footings on sand is impractical and can be

expected to lead to considerable error. On the other hand, it has been observed in the field that, in the recompression range or in the compression range beyond the preconsolidation pressure, a practically linear relation exists between the settlement of a loaded area on sand or gravel and the bearing pressure, for bearing pressures that correspond to a factor of safety against shear rupture of at least 3 (Burland and Burbidge 1985). Inasmuch as the factor of safety against rupture in granular soils beneath actual foundations is at least 3 and often as much as 10 (Stroud 1988), Eq. 50.3 can be replaced by

$$S_c = Z_I \bar{m}_v q \quad (50.4)$$

where  $S_c$  = settlement at end-of-construction and application of permanent live load;  $\bar{m}_v$  = average coefficient of vertical compression of soil within the zone of influence  $Z_I$ ;  $q$  = average gross bearing pressure over the foundation, and

$$q = \frac{P}{A} \quad (50.5)$$

where  $P$  is the total load on the foundation and  $A$  is the area of the foundation.

Burland and Burbidge (1985) assembled more than 200 records of settlement of foundations, tanks, and embankments on sands and gravels. Analyses of these data lead to the empirical expressions:

$$Z_I = B^{0.75} \quad (50.6)$$

$$\bar{m}_v = \frac{1.7}{\bar{N}^{1.4}} \quad (50.7)$$

where  $B$  is the breadth of foundation in meters, and  $\bar{N}$  is the arithmetic mean of the standard penetration test  $N$  values measured within the thickness  $Z_I$  defined by Eq. 50.6. Both  $\bar{m}_v$  and  $N$  are functions of effective confining pressure, but because the influence of the confining pressure is similar on both quantities, it is considered unnecessary to correct  $N$  for the effective overburden pressure. The statistical correlations derived from the settlement records support this conclusion. However, for saturated, very dense fine or silty sands, the measured  $N$  values should be reduced according to:

$$N' = 15 + \frac{1}{2} (N - 15) \quad (50.8)$$

The rod energies for the standard penetration tests in the cases assembled by Burland and Burbidge were not specified, and the empirical correlation represented by Eq. 50.7 was established without correcting the  $N$  values to a standard energy. Because a rod energy ratio of 60% corresponds to the most commonly used procedures, most of the data probably correspond to this ratio. Consequently, in estimating settlements by the standard penetration method,  $N_{60}$  (Article 11.3.2) should be used.

The values of  $\bar{m}_v$ , which were obtained by dividing the measured settlement by  $Z_I$  and  $q$ , are shown in Fig. 50.3, together with a limited number of values of  $m_v = \Delta\epsilon_v/\Delta\sigma'_v$  from oedometer tests on sand. The values of  $m_v$  correspond to a loading intensity of 100 kPa, and the corresponding  $N$  values were obtained over a depth range of 5 to 15 m. It is noteworthy that for the foundation behavior summarized in Fig. 50.3 the relationship between  $\bar{m}_v$  and  $\bar{N}$ , although similar to that between  $m_v$  and  $\bar{N}$ , shows greater scatter.

The empirical equation (Eq. 50.6), which expresses the thickness of sand or gravel beneath the foundation that is significantly influenced by foundation loading, was obtained by two independent interpretations of the settlement records. One interpretation used the few settlement measurements that have been carried out at various depths beneath foundations on granular soils. The widths of the loaded areas ranged from 1 to 30 m. The significant depth  $Z_I$  of sand or gravel was estimated by examining the variation of settlement with depth. Such a set of data, compiled by Burland and Burbidge (1985) and shown in

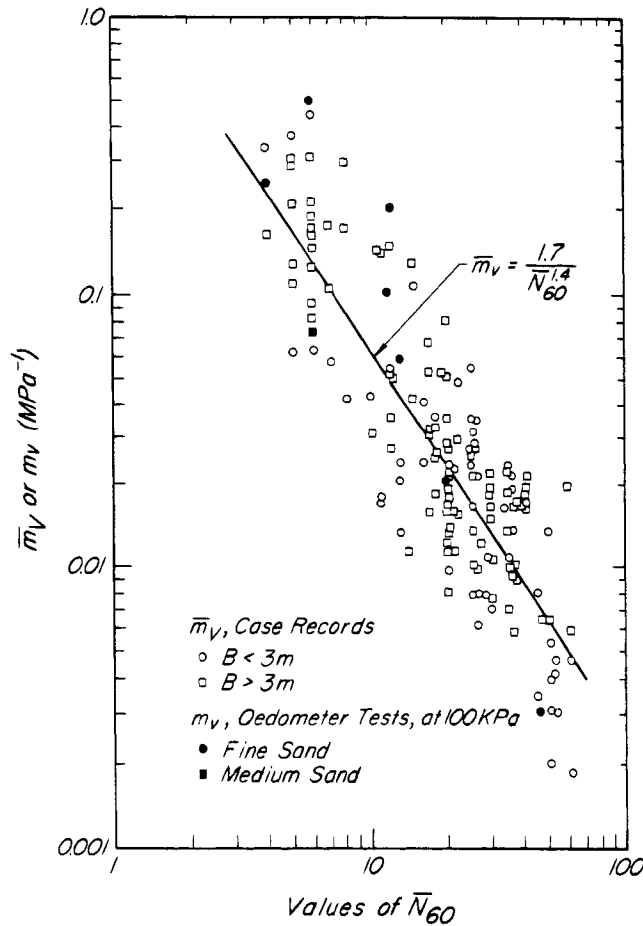


**Figure 50.3** Relation between dynamic standard penetration test  $\bar{N}_{60}$  values and compressibility  $\bar{m}_v$  or  $m_v$  of sand (data from Burland and Burbidge 1985).

Fig. 50.4, is in reasonable agreement with Eq. 50.6. In the second interpretation, Burland and Burbidge prepared plots of  $S_c/q$  against  $B$  for groups of granular soil of different compressibilities defined in terms of  $\bar{N}_{60}$ . One such plot for a group having values of  $\bar{N}_{60}$  in the range of 26 to 40 is shown in Fig. 50.5. Sets of data for five groups of different compressibilities all imply that the settlement  $S_c$  varies according to Eq. 50.4, with  $Z_I$  defined by Eq. 50.6. Thus, two different approaches of settlement records indicate a depth of influence  $Z_I$  in accordance with Eq. 50.6.

Substituting Eqs. 50.6 and 50.7 into Eq. 50.4 we obtain:

$$S_c = B^{0.75} \frac{1.7}{\bar{N}_{60}^{1.4}} q \quad (50.9)$$

The values of  $\bar{m}_v$  in Fig. 50.3 and Eq. 50.7 are in units of MPa. Thus, in Eq. 50.9, values of  $q$  in kPa and  $B$  in m lead to values of  $S_c$  in mm. If the granular soil beneath the foundation has a thickness less than  $Z_I$ , the actual thickness instead of  $B^{0.75}$  is used in Eq. 50.9.

Equation 50.9 does not imply that settlement necessarily increases in proportion to  $B^{0.75}$ , because a change in  $B$  usually results in a change in the arithmetic mean of the  $N_{60}$  values within the depth of influence of the footing.

Equation 50.9 is applicable to normally consolidated sands and gravels. If the materials are preconsolidated, a recompression value of  $\bar{m}_v$  is applicable. Burland and Burbidge found reasonable agreement with the data by using a recompression value equal to one third of that given by Eq. 50.7. Therefore, for average gross bearing pressures greater than  $\sigma'_p$ ,

$$S_c = Z_I \frac{1}{3} \bar{m}_v \sigma'_p + Z_I \bar{m}_v (q - \sigma'_p) \quad (50.10)$$

whence, after substitution,

$$S_c = B^{0.75} \frac{1.7}{\bar{N}_{60}^{1.4}} \left( q - \frac{2}{3} \sigma'_p \right) \quad (50.11a)$$

For average bearing pressures less than  $\sigma'_p$ ,

$$S_c = \frac{1}{3} B^{0.75} \frac{1.7}{\bar{N}_{60}^{1.4}} q \quad (50.11b)$$

If the footing is established at a depth below the ground surface, the removal of the soil above the level of the base renders the sand beneath the base preconsolidated by excavation. Recompression is assumed for bearing pressures up to the preconstruction effective vertical stress  $\sigma'_{vo}$  at the base of the foundation. Thus, for sands normally consolidated with respect to the original ground surface and for values of  $q$  greater than  $\sigma'_{vo}$ ,

$$S_c = Z_I \frac{1}{3} \bar{m}_v \sigma'_{vo} + Z_I \bar{m}_v (q - \sigma'_{vo}) \quad (50.12)$$

Upon substituting Eqs. 50.6 and 50.7,



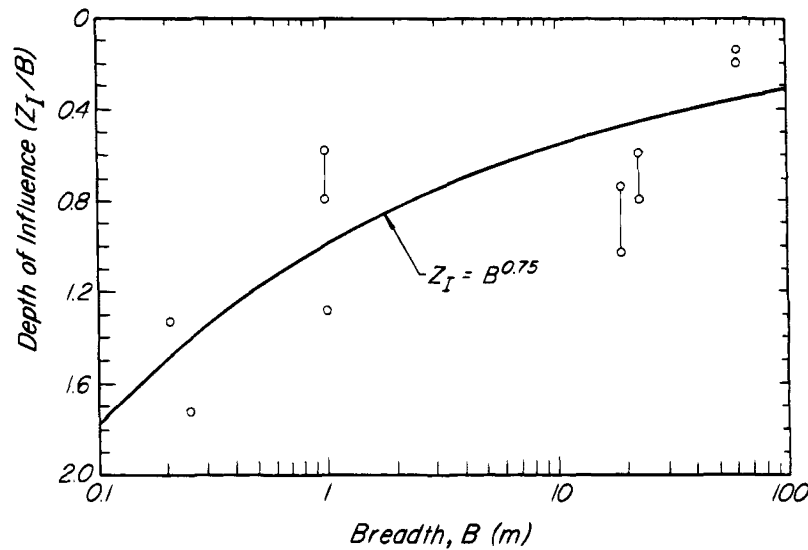


**Figure 50.4** Thickness of granular soil beneath foundation contributing to settlement, interpreted from settlement profiles (after Burland and Burbidge 1985).

$$S_c = B^{0.75} \frac{1.7}{\bar{N}_{60}^{1.4}} \left( q - \frac{2}{3} \sigma'_{vo} \right) \quad (50.13a)$$

and, for values of  $q$  less than  $\sigma'_{vo}$

$$S_c = \frac{1}{3} B^{0.75} \frac{1.7}{\bar{N}_{60}^{1.4}} q \quad (50.13b)$$

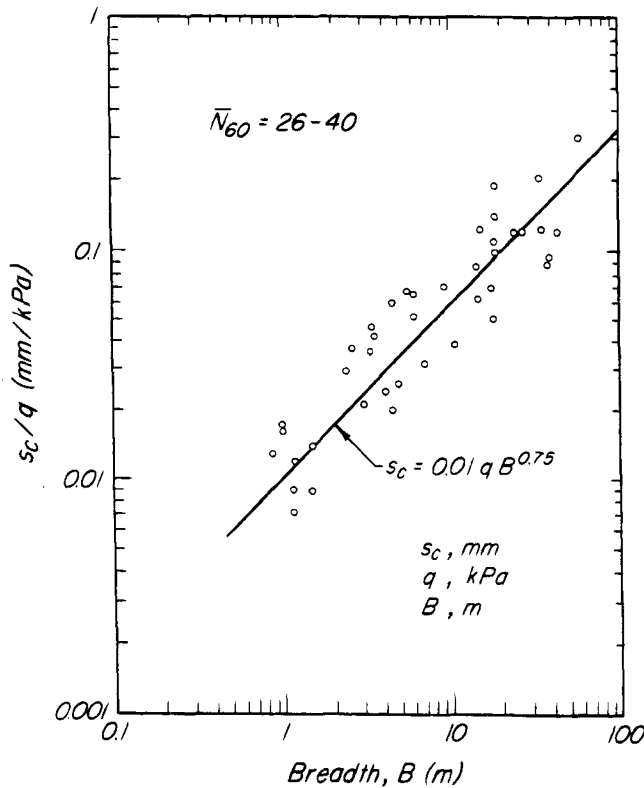


**Figure 50.5** Relation between settlement at end of construction of footing on sand and width of footing, for sands having standard penetration resistances  $\bar{N}_{60}$  between 26 and 60 (after Burland and Burbidge 1985).

If the sand or gravel is preconsolidated with respect to the original ground surface and the load is applied at the base of an excavation, the settlement is calculated by introducing into Eq. 50.11 the preexcavation value of  $\sigma'_p$  at foundation level.

Equations 50.9, 50.11, and 50.12 are applicable to foundations with a length-to-breadth ratio,  $L/B$ , of one. On the basis of a statistical analysis of settlement records, Burland and Burbidge obtained the following relationship between the settlement of foundations with  $L/B > 1$  and that with  $L/B = 1$ :

$$S_c(L/B > 1) = S_c(L/B = 1) \left[ \frac{1.25(L/B)}{(L/B) + 0.25} \right]^2 \quad (50.14)$$

For strip loading where  $L/B$  tends to infinity, the value of  $S_c(L/B > 1)/S_c(L/B = 1)$  becomes 1.56.

An impression of the accuracy to be expected from the standard penetration method can be obtained from Fig. 50.6 which compares computed and measured settlements at end of construction. Although part of the considerable scatter undoubtedly is associated with the relative crudity of the standard penetration test, a major contributor is the inherent variability in compressibility of sand deposits. Hence, there is little improvement to be expected as a result of using more refined or elaborate techniques.

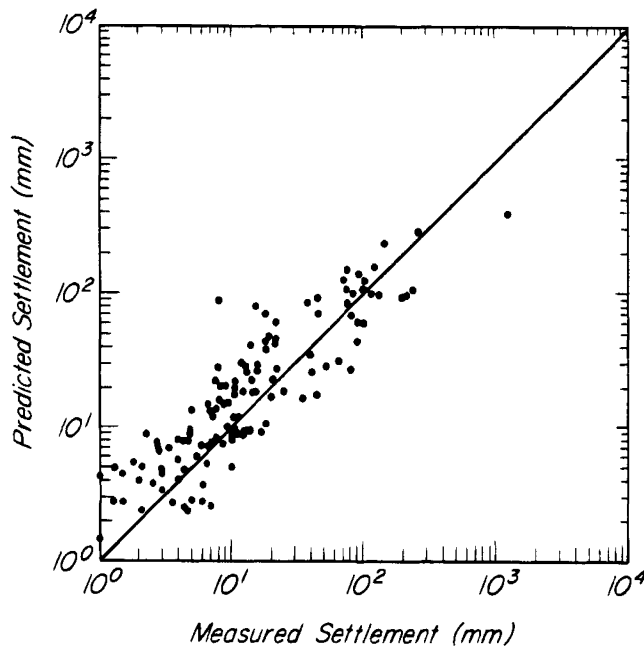


**Figure 50.6** Comparison of measured settlements of footings on sand at end of construction with values predicted by standard penetration test method.

Furthermore, in addition to end-of-primary settlement, footing foundations on sand experience continuing settlement at a decreasing rate as a consequence of secondary consolidation. Prediction of secondary consolidation requires establishing the time at which primary consolidation is complete. For practical purposes this time is usually considered to correspond to the end of construction when all dead loads have been applied. This definition is necessarily arbitrary, as many structures support live loads of a continuing or permanent nature, such as the weight of stored goods in a warehouse or of books in a library. Thus, judgment must be exercised in choosing the date at which primary consolidation is said to end and secondary to begin. As a rule, it is satisfactory to assume that the final 24-hour day of construction represents the duration of the last increment of primary compression. On this basis, the equation of secondary settlement can be expressed as

$$S_c = \epsilon_\alpha Z_f \log \frac{t}{1 \text{ day}} \quad (50.15)$$

where  $\epsilon_\alpha = \Delta\epsilon_v / \Delta \log t$  is the secondary compression strain index, in terms of strain, between one day and the design life  $t$  of the structure, measured in days from the end of construction. The value of  $\epsilon_\alpha$  can be determined by assigning to  $\epsilon_\alpha / \epsilon_c$  the value 0.02 (Article 16.7), and using for  $\epsilon_c = \Delta\epsilon_v / \Delta \log \sigma'_v$  the empirical expression

$$\epsilon_c = \frac{1.4}{\bar{N}_{60}^{1.4}} \quad (50.16)$$

Equation 50.16, which was obtained by analyses of settlement records assembled by Burland and Burbidge, represents the compression index at the final effective vertical stress. It is applicable to normally consolidated sands or to the compression range beyond  $\sigma'_p$ . For values of  $q$  less than  $\sigma'_{vo}$  at the foundation level, or less than the preconsolidation pressure  $\sigma'_p$ , one third of the value of  $\epsilon_c$  from Eq. 50.16 is used to obtain  $\epsilon_\alpha$ . For fluctuating bearing pressures resulting from live loads, building vibrations and wind loading, and minor repeated dynamic events, the secondary settlement may be approximately doubled. An impression of the scatter of results associated with the use of this procedure is obtained from Fig. 50.7, which compares computed and measured postconstruction settlements.

#### 50.2.6 Method Using Cone Penetration Test

The relatively few measurements of settlements at various depths beneath footings in granular soils suggest a vertical distribution of vertical strain,  $\epsilon_v$ , that starts from a finite value at foundation level, increases with depth to a maximum, and then decreases with depth (Schmertmann 1970, Burland and Burbidge 1985). The dash lines in Fig. 50.8 show the distribution of vertical strain at two different intensities of bearing pressure, determined from settlement measurements beneath the slab foundations of buildings on 40 to 50 m of sand of medium density (Kreigel

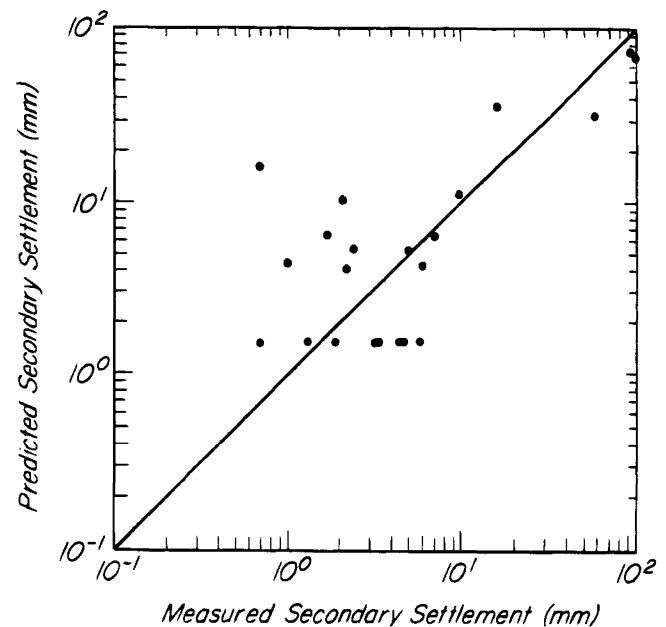


**Figure 50.7** Relation between predicted secondary settlements of footings on sand and settlements predicted by standard penetration test method.

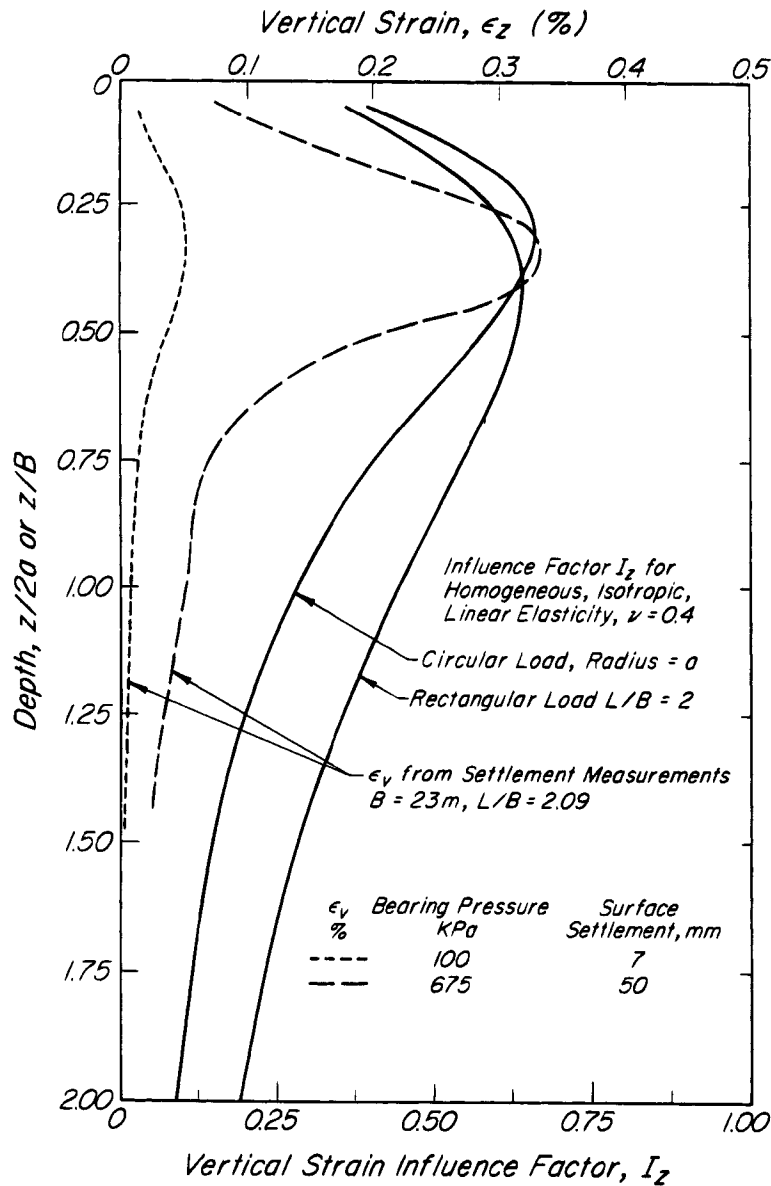


**Figure 50.8** Vertical distribution of vertical strain from settlement measurements beneath foundations on sand (dash lines), and of influence factor  $I_z$  (solid lines) for homogeneous, isotropic, linearly elastic material.

and Wiesner 1973). This distribution differs from that obtained from Eq. 50.2 if, in evaluating Eq. 50.2, the value of  $\epsilon_v = \Delta\sigma'_v/E$  is assumed to be equal to  $\epsilon_v = \Delta\sigma'_z/E$  computed by Boussinesq's theory for a homogeneous, isotropic, linear elastic material. Although the vertical stresses computed by the Boussinesq equation are independent of the lateral deformations in the stressed body, the vertical strains depend on the lateral deformations as determined by Poisson's ratio  $\nu$ . The observed shape of the vertical strain profile can be predicted by an equation

for vertical strain that includes the contribution of lateral deformation:

$$\epsilon_v = \frac{1}{E_s} [\Delta\sigma'_1 + \nu(\Delta\sigma'_2 + \Delta\sigma'_3)] \quad (50.17)$$

where  $\Delta\sigma'_1$ ,  $\Delta\sigma'_2$ , and  $\Delta\sigma'_3$  = increments of effective principal stresses computed from elastic theory;  $E_s$  = drained Young's modulus. For example, under the center of a circular area of radius  $a$  at the surface of a homogeneous

isotropic linear elastic medium, subjected to a uniform surface load per unit of area  $q$  (Article 40.2),

$$\Delta\sigma'_1 = \Delta\sigma_z = q \left( 1 - \left[ \frac{1}{1 + \frac{1}{(z/a)^2}} \right]^{3/2} \right)$$

$$\Delta\sigma'_2 = \Delta\sigma_r$$

$$= \frac{q}{2} \left( (1 - 2\nu) + \frac{2(1 + \nu)za}{[1 + (za)^2]^{1/2}} + \frac{(za)^3}{[1 + (za)^2]^{3/2}} \right)$$

$$\Delta\sigma'_3 = \Delta\sigma_\theta = \Delta\sigma_r \quad (50.18)$$

Substituting Eq. 50.18 into 50.17 leads to an expression for vertical strain at depth  $z$  below the center of the loaded area

$$\epsilon_v = \frac{q}{E_s} I_z \quad (50.19)$$

where the vertical strain influence factor for depth  $z$  is

$$I_z = 1 - \left[ \frac{1}{1 + \frac{1}{(z/a)^2}} \right]^{3/2} - \nu(1 + 2\nu)$$

$$+ \frac{2\nu(1 + \nu)za}{[1 + (za)^2]^{1/2}} - \frac{\nu(za)^3}{[1 + (za)^2]^{3/2}} \quad (50.20)$$

For  $\nu = 0.4$ , the vertical distributions of  $I_z$  according to Eq. 50.20 for a circular loaded area, as well as  $I_z$  for a rectangular area with  $L/B = 2$ , are shown in Fig. 50.8. The shapes of vertical strain profiles from the settlement measurements in sands and from computation using Eq. 50.19 are roughly similar. On the basis of this similarity, Schmertmann (1970) and Schmertmann et al. (1978) recommended that settlement analysis of foundations on granular soils be based on Eq. 50.19.

The actual magnitude and vertical distribution of  $I_z$  depend on the rigidity and shape of the footing as well as on the nature of the stress-strain properties of the granular material and their variation with depth. However, for a simple method of settlement analysis, the vertical profiles of  $I_z$  in Fig. 50.9 can be used. According to this approach the values of  $Z_l/B$  for square and circular footings ( $L/B = 1$ ) and strip footings ( $L/B = 10$ ) are 2 and 4, respectively. For length to breadth ratios between 1 and 10,  $Z_l/B$  is determined from

$$\frac{Z_l}{B} = 2 \left( 1 + \log \frac{L}{B} \right) \quad (50.21)$$

The expression for end-of-construction settlement is then

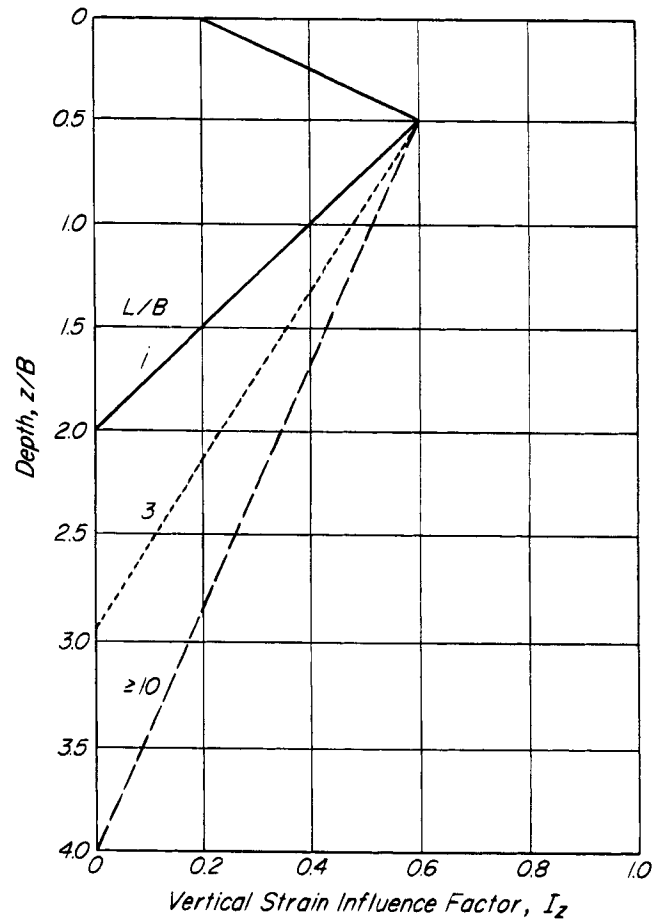


**Figure 50.9** Simplified vertical profiles for influence factor  $I_z$  for vertical strain in sand beneath surface foundations having various ratios of length to breadth.

$$S_c = Z_l \frac{q}{E_s} I_z \quad (50.22)$$

Because  $I_z$  is a function of depth below the footing, and  $E_s$  may also vary with depth, Eq. 50.22 is applied in the form

$$S_c = q \sum_{j=1}^n \left[ Z_l \frac{I_z}{E_s} \right]_j \quad (50.23a)$$

where  $\sum [Z_l]_j = Z_l$ ,  $[I_z]_j$ , and  $[E_s]_j$  are evaluated at mid-depth of  $[Z_l]_j$ . If the thickness of granular soil beneath the footing is less than  $Z_l$ , the  $I_z$  profile is constructed using  $Z_l$  defined by Eq. 50.21. However, the settlement is computed only for  $\sum [Z_l]_j$  corresponding to the thickness of granular soil beneath the footing.

Values of  $I_z$  in Fig. 50.9 are applicable to footings that are placed at the surface. For footings embedded at a depth  $D$  below the ground surface the values of  $I_z$  in Fig. 50.9 are reduced to  $I'_z$  according to Fig. 50.10, based on a photoelastic study by Skopek (1961). According to this

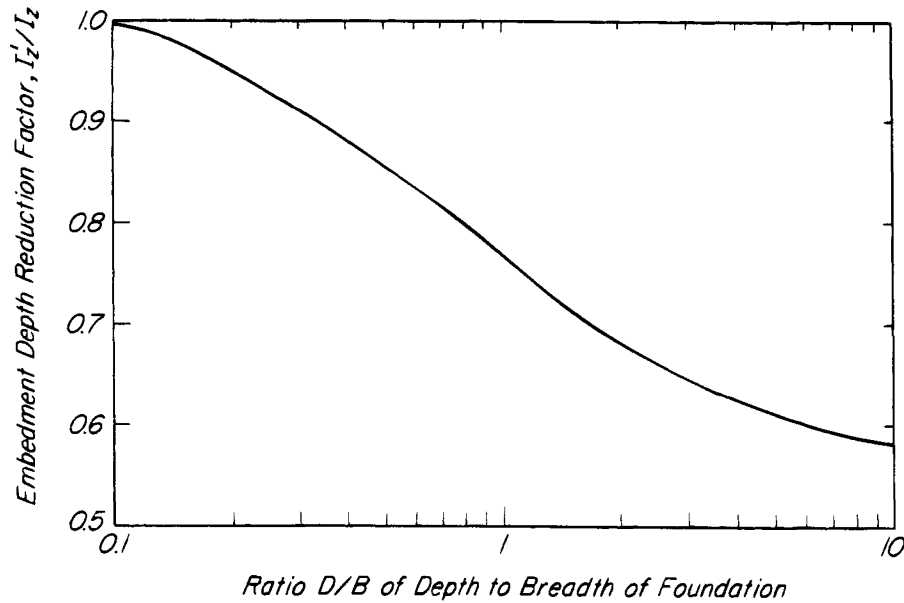


**Figure 50.10** Reduction factor for correcting influence factor  $I_z$  to take account of depth of embedment of foundation on sand.

study the distribution of vertical stress increase beneath an embedded footing corresponds to the Boussinesq distribution at foundation level and merges at  $z/B = 1$  with the Mindlin (1936) distribution which assumes that the load is applied at a depth below the surface of a semiinfinite elastic mass. This finding has been adopted for computing  $I'_z$  for a homogeneous isotropic linear elastic medium with  $\nu = 0.4$ . A small effect of  $L/B$  on  $I'_z/I_z$  has been ignored. For embedded foundations the equation for end of construction settlement is then

$$S_c = (q - \sigma'_{vo}) \sum_{j=1}^n \left[ Z_l \frac{I'_z}{E_s} \right]_j \quad (50.23b)$$

where  $\sigma'_{vo}$  is the preconstruction effective vertical stress at the base of the foundation.

The value of  $E_s$  in Eq. 50.23 is obtained from the cone-penetration-test tip resistance  $q_c$ . The empirical correlation shown in Fig. 50.11 was established by plotting values of  $E_s$  obtained from Eq. 50.23 against the observed settlement for 81 foundations and 92 plate load tests. The value of  $\bar{q}_c$  is the weighted mean of the measured  $q_c$  values of sublayers within the thickness  $Z_l$  defined by Eq. 50.21:

$$\bar{q}_c = \sum_{j=1}^n \frac{[Z_l]_j}{Z_l} [q_c]_j \quad (50.24)$$

According to Fig. 50.11, calculation of the settlement of shallow foundations on sand and gravel can be based on

$$E_s = 3.5 \bar{q}_c \quad (50.25)$$

Equation 50.25 corresponds to axisymmetric circular or

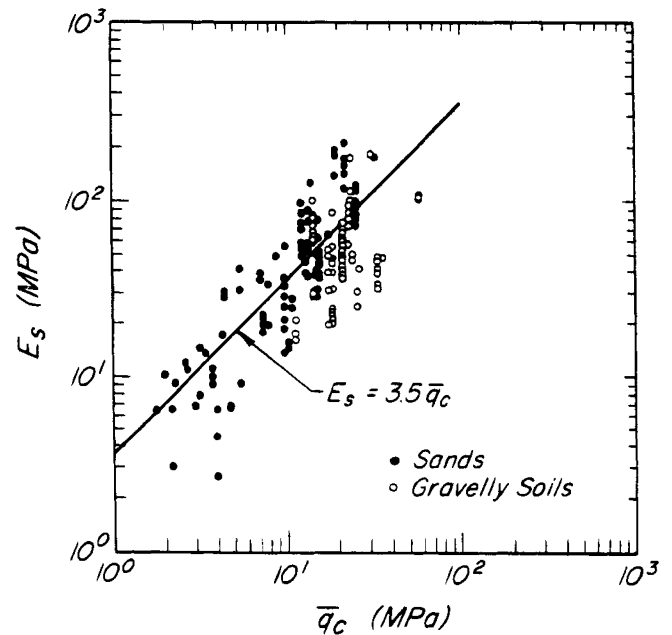


**Figure 50.11** Empirical correlation between drained Young's modulus  $E_s$  and weighted mean cone resistance  $\bar{q}_c$  for square or circular loaded areas, based on settlement analysis of case records and Eq. 50.22.

square loaded areas. Laboratory compression tests on granular soils suggest that  $E_s$  for plane-strain conditions is about 1.4 times that for axisymmetric loading (Cornforth 1964, Lee 1970). Thus,  $E_s$  for loading conditions intermediate between axisymmetric and plane strain (assumed to correspond to  $L/B = 10$ ) can be determined from

$$E_s = \left[ 1 + 0.4 \log \frac{L}{B} \right] E_s(L/B = 1) \quad (50.26)$$

The value of  $E_s$  ( $L/B = 1$ ) is obtained from Eq. 50.25. The results of settlement calculations made according to this procedure are compared with the measurements in Fig. 50.12.

Postconstruction settlement may be computed by using Eq. 50.15; however,  $Z_1$  is determined from Eq. 50.21, and the value of the tangent strain compression index is obtained from:

$$\epsilon_c = \frac{0.1}{\bar{q}_c} \quad (50.27)$$

where  $\bar{q}_c$  is in MPa. Figure 50.13 gives an impression of the accuracy that may be expected in calculating secondary settlement by this procedure.

### 50.2.7 Comparison of Standard Penetration and Cone Penetration Methods

End-of-construction and postconstruction settlements computed by the two methods are compared in Figs. 50.14 and 50.15, respectively. Comparisons are made for three types of information on subsurface conditions: (1) In a few instances independent measurements of  $N$  and  $q_c$  were available for the same site and were used in the respective methods of settlement analyses. (2) Subsurface conditions were defined only by  $N$  values that were used directly in the standard penetration method; the values

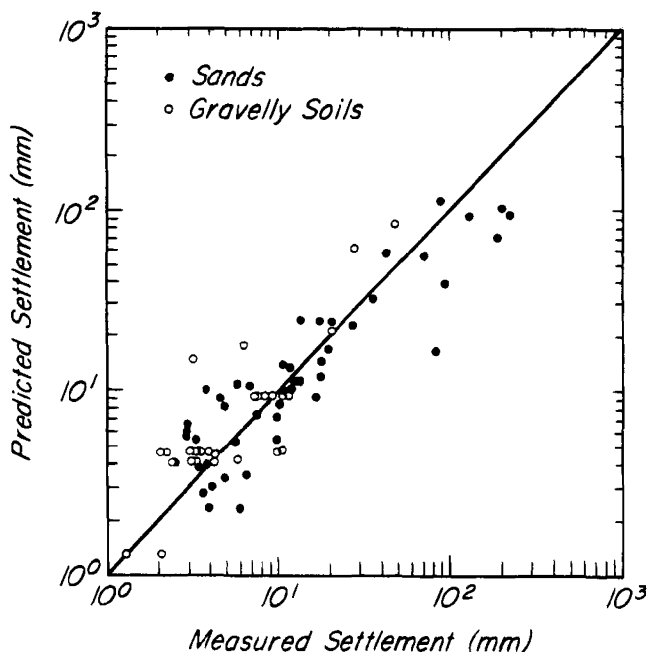


**Figure 50.12** Comparison of end of construction settlements of foundations on sands and gravels as predicted by cone penetration tests and as measured.

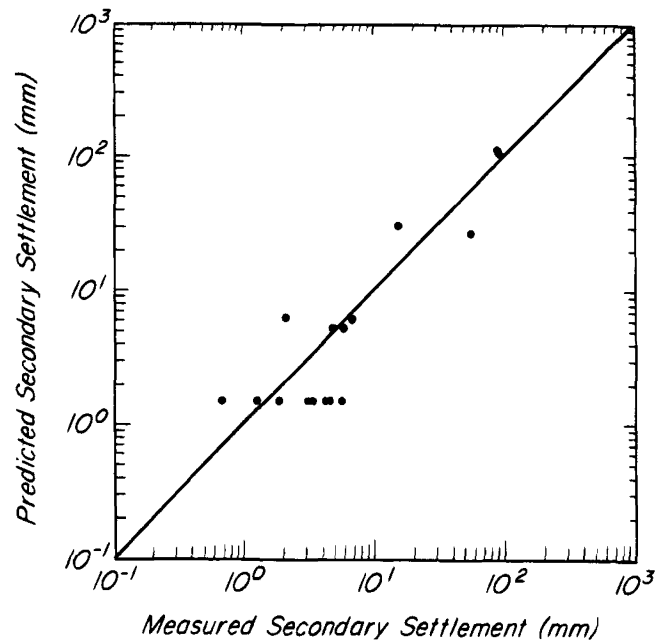


**Figure 50.13** Comparison of secondary settlements of foundations on sand as predicted by cone penetration test method and as measured.

of  $q_c$  for the cone penetration method were then determined from the empirical correlation between  $q_c$  and  $N$  in Fig. 11.15. (3) Only  $q_c$  measurements were available and were used in the cone penetration method; the values of  $N_{60}$  for the standard penetration method were determined by using the  $q_c/N_{60}$  correlation in Fig. 11.15. It is evident that neither method is clearly superior to the other.

### 50.2.8 Design of Footings on Sand and Gravel

Use of Eqs. 50.9, 50.11, 50.13, or 50.23 for calculating settlement requires that the bearing pressure and the width  $B$  of the footing be known. In practice, both of these are unknown initially and are to be determined in design. Moreover, design is usually based on limiting the maximum settlement of any footing supporting a given building to a reasonable value of 25 mm (1 inch).

Inasmuch as the settlement for a given soil pressure increases with increasing width of footing, it is usually sufficient to determine the soil pressure for the footing with the largest total load on the basis of Eq. 50.9, 50.11, 50.13, or 50.23. If the sand deposit were homogeneous with respect to compressibility, proportioning the largest footing to experience settlement  $S_c = 25$  mm for  $N_{60}$  would ensure that all smaller footings would settle less. However, Fig. 50.2 demonstrates that, because of the inherent variability of real soil deposits, the settlements of equally loaded footings of any given size can be expected to vary from the mean by a factor of about 1.6 and perhaps as large as 2. Therefore, to ensure a reasonable probability that the largest footing will not settle

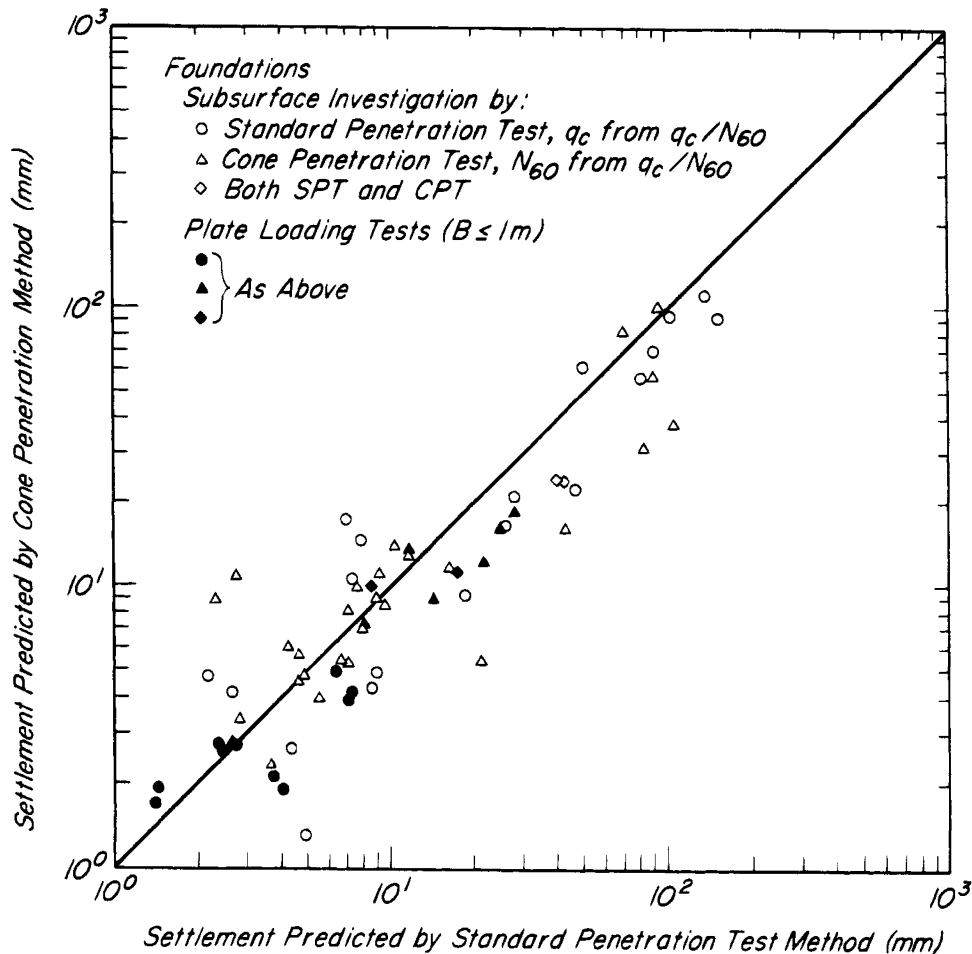


**Figure 50.14** Comparison of end-of-construction settlements for plate-loading tests and for foundations on sands as predicted by standard penetration test method and by cone penetration test method.

more than 25 mm, the value of  $S_c$  in Eqs. 50.9 to 50.23 should be decreased to 25/1.6 or 16 mm. If the  $N_{60}$  values for the various borings beneath a building vary significantly from one part of the site to another, indicating different modes of deposition or history of preloading, the site should be considered to be underlain by separate units, each with its characteristic value of  $N_{60}$ .

If the soil pressure thus determined for the largest footing is then used for all the footings, it is unlikely that any footing will settle more than 25 mm. Experience has indicated that the settlement of the smaller footings within the area of the foundation will be less than 25 mm and that the differential settlement among the footings is unlikely to exceed about 16 mm. However, the factor of safety against a bearing-capacity failure of the smallest footings must be checked to ensure a value of at least 3; otherwise excessive settlements associated with an approaching bearing-capacity failure may develop.

A convenient procedure for design based on the standard penetration method is then to select a tentative value

of bearing pressure for the largest footing, to calculate the required area of the footing and the corresponding value of  $B$  (or values of  $B$  and  $L$  if rectangular), to determine the value of  $\bar{N}_{60}$  for the applicable standard penetration borings to the depth  $B^{0.75}$ , and to solve the appropriate equation (50.9, 50.11, or 50.13) for the settlement. If the settlement differs from 16 mm, the procedure is repeated until agreement is achieved. The bearing pressure thus determined is used to proportion all the footings. However, because of the local variations in relative density of sand deposits in general, and because of the inevitable disturbance of the uppermost materials during construction, a footing on sand should not have a width less than 0.5 m.

According to Article 41.2, if the groundwater table lies above or within the depth of influence  $Z_f$ , the effective confining pressure and the initial tangent modulus of the sand are reduced and the settlement correspondingly increased as compared to the values if the water table were below  $Z_f$ . However, the reduction in confining pres-

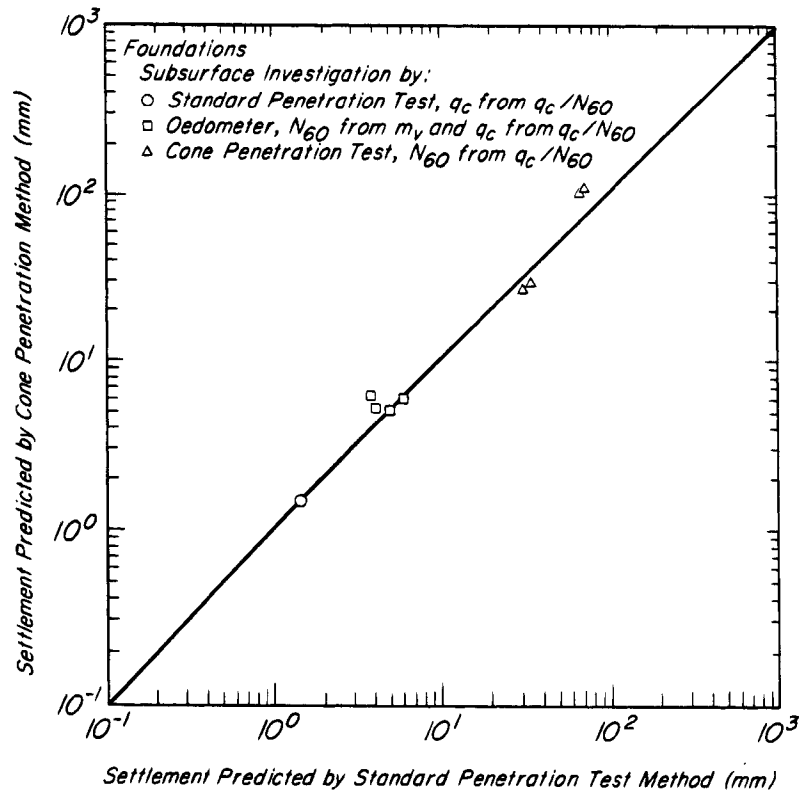


**Figure 50.15** Comparison of postconstruction settlements of foundations on sands as predicted by standard penetration test method and by cone penetration test method.

sure also causes a reduction in the standard penetration test  $N$  values. Burland and Burbidge found from their statistical studies that the two effects largely compensated for each other and that the presence of a high water table could appropriately be neglected in applying the standard penetration method. The same conclusion had been reached earlier by Meyerhof (1965). Hence, in general, no water-table correction is recommended in this book. On the other hand, if for any reason the water table were to rise into or above the zone of influence  $Z_f$  after the penetration tests were conducted, the actual settlement could be as much as twice the value predicted without taking the water table into account.

A convenient method for routine design is the use of the settlement chart (Fig. 50.16), in which Eqs. 50.9, 50.11, and 50.13 are solved directly for the bearing pressure  $q$  corresponding to a settlement of 16 mm for different values of  $\bar{N}_{60}$ . Equation 50.9 can be expressed as

$$q = S_c \frac{\bar{N}_{60}^{1.4}}{1.7 B^{0.75}} = 16 \frac{\bar{N}_{60}^{1.4}}{1.7 B^{0.75}} = 16Q \quad (50.28)$$

for a normally consolidated sand. For a sand having a preconsolidation pressure  $\sigma'_p$ , Eq. 50.11 can be written

$$\text{for } q > \sigma'_p \quad q = 16Q + \frac{2}{3} \sigma'_p \quad (50.29a)$$

$$\text{for } q < \sigma'_p \quad q = 3 \times 16Q \quad (50.29b)$$

If the sand beneath the base of the footing is preconsolidated because excavation has removed a vertical effective stress  $\sigma'_{vo}$ , Eqs. 50.13 can be written

$$\text{for } q > \sigma'_{vo} \quad q = 16Q + \frac{2}{3} \sigma'_{vo} \quad (50.30a)$$

$$\text{for } q < \sigma'_{vo} \quad q = 3 \times 16Q \quad (50.30b)$$

The chart (Fig. 50.16), for an assumed width  $B$  and for the appropriate value of  $\bar{N}_{60}$ , gives values of  $Q$  from which the bearing pressure  $q$  for the applicable conditions of preconsolidation can be calculated by means of Eq. 50.28, 50.29, or 50.30. The chart is constructed for square footings of width  $B$ . For rectangular footings with length  $L > B$ , the value of  $q$  should be reduced in accordance with Eq. 50.14.

The bearing pressures determined by this procedure correspond to a maximum settlement of approximately 25 mm at end of construction. If the secondary settlement (Eq. 50.15) is excessive, the bearing pressure  $q$  should



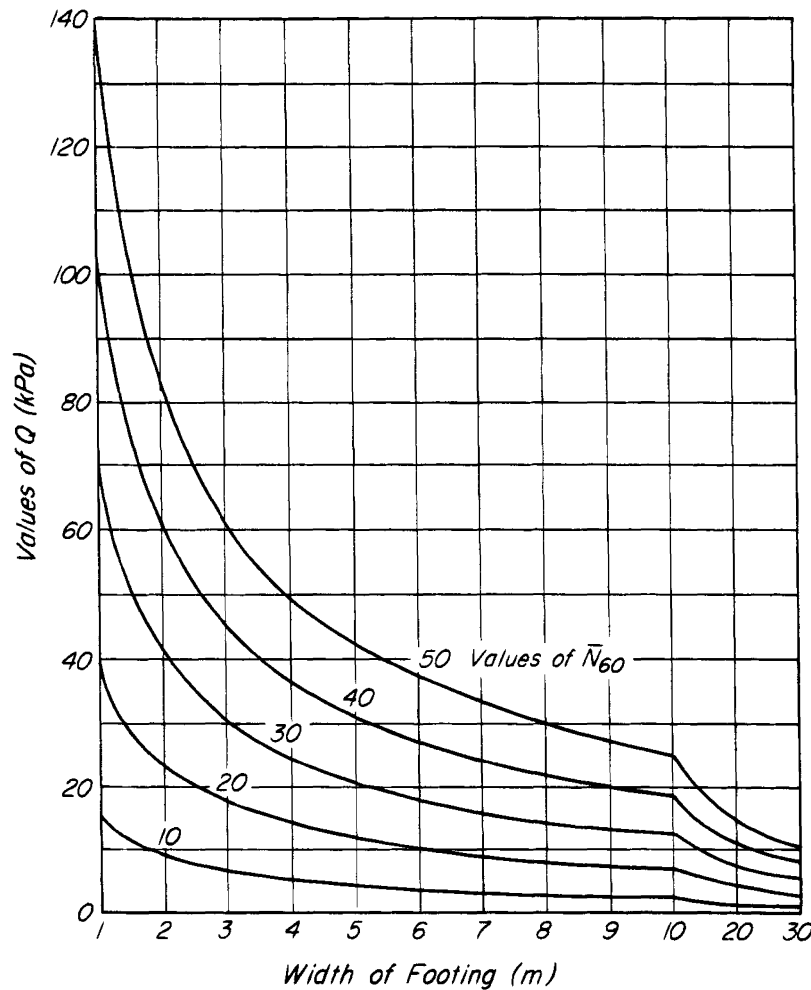


**Figure 50.16** Chart for estimating allowable soil pressure for footing on sand on the basis of results of standard penetration test.

be reduced to decrease the end-of-construction settlement to compensate for the anticipated long-term settlement during the lifetime of the building. Under most circumstances this refinement is unnecessary.

Footings are generally considered unsuitable as foundations on loose cohesionless sands below the water table, not only because of the large dimensions required to provide an adequate factor of safety against a bearing capacity failure and to restrict the settlement, but also because of the susceptibility of the materials to liquefaction. Densification of the sand (Article 44.3) or a deep foundation may be required.

### 50.3 Footings on Clay

In contrast to footings on sand, which are more likely to experience excessive settlement than outright bearing-capacity failure, footings on clay are vulnerable to both types of distress. In particular, a footing underlain by soft to medium clay may fail catastrophically the first time it

is loaded. Therefore, the first step in developing the design of a footing on clay is to determine its ultimate bearing capacity.

If the loads are applied to the footing within a time short compared with the time in which the water content of the clay can be reduced by consolidation, only the undrained shear strength will be mobilized and the net ultimate bearing capacity  $q_{d \text{ net}}$  (Article 33) per unit of area of a footing resting near the surface of the clay may be calculated from

$$q_{d \text{ net}} = 5s_u \left( 1 + 0.2 \frac{D_f}{B} \right) \left( 1 + 0.2 \frac{B}{L} \right) \quad (33.17)$$

wherein  $s_u$  is the undrained strength and  $B$  and  $L$  are the width and length of the footing. The depth of foundation  $D_f$  should not exceed  $2.5B$ . For a circular footing the diameter  $D$  may be taken as  $D = B = L$ .

To compute the bearing capacity of a clay it is necessary to determine the undrained shear strength of the clay

below the proposed footings. This may be done by performing unconfined compression tests on undisturbed samples, by field vane tests, by cone penetration tests, or by use of the pressuremeter (Article 20). The tests should be made at the sites of several footings, the average undrained shear strength determined for each location between the level of the base of the footings and a depth below the base equal to the estimated width of the largest footing, and the smallest of these average values introduced into Eq. 33.17.

The foregoing procedure is valid if the undrained strength is fairly uniform or varies somewhat erratically within the significant depth. As discussed later, it is unconservative if the strength decreases appreciably with depth. To investigate the variability, values of  $s_u$  should be determined at close spacing along the vertical lines explored. The practical minimum spacing depends to some extent on the exploratory tools used. If the investigation is carried out by undisturbed sampling and testing, the sampling should be continuous, the diameter of the samples should be not less than 50 or, preferably, 75 mm, and the vertical spacing of tests should not be greater than about 0.2 m. If a field vane is used, the vertical spacing between tests cannot usually be less than 0.5 m; for this reason it is advisable to stagger the depths at which tests are performed in adjacent vane soundings. Cone penetration tests should be carried out at closer spacing, preferably 0.2 m. Under loads likely to develop, the factor of safety should not be smaller than 3, but if the loads for which the footing is designed are very unlikely to develop, a value as low as  $F = 2$  can be tolerated.

The correlations between standard penetration test  $N$  values and undrained shearing strength of soft to medium clays are too crude to justify their use in proportioning footings. As an expedient, tests can be performed on the spoon samples, but the disturbed condition of the samples may lead to a considerable underestimate of the shearing strength.

The ultimate bearing capacity of intact stiff saturated clays can be determined similarly on the basis of the results of unconsolidated undrained triaxial tests. However, because such materials are usually overconsolidated, the values of the coefficient of consolidation  $c_v$  are large in comparison with those for normally consolidated clays and the pore pressures dissipate more rapidly. Consequently, undrained conditions may not prevail, especially if the rate of increase of dead load during construction is slow in comparison to the rate of porepressure dissipation. Under these circumstances it may prove economical to take the dissipation into account and to base the bearing-capacity calculation on effective-stress parameters.

Most stiff clays contain fissures that separate the clay into fragments. The fissures not only make recovery and testing of samples difficult, but they alter the shearing resistance of the clay mass. Small samples, which may not

include representative numbers of fissures, often exhibit greater shear strengths than more representative large samples, and design based on testing small specimens may be unconservative. In many instances it is preferable to determine the ultimate bearing capacity of such clays by means of load tests. The tests should be made at the level of the base of the footings, on bearing plates 0.6 m square at the bottom of test pits 2 m square. If the consistency of the clay varies considerably between this level and a depth  $B$  (square footings) or  $2B$  (continuous footings), load tests must be made at two or three different levels within this depth. The number of load tests or sets of tests that are required depends primarily on the degree of homogeneity of the clay stratum and the number of footings. The load should be applied in increments until the load-settlement curve (Fig. 33.1) indicates that the bearing capacity of the soil  $q_{d\text{ net}}$  has been reached, or until the pressure is at least three times the value of the maximum pressure that would be transmitted to the ground by the foundation.

The soil pressure that provides an adequate factor of safety against a bearing-capacity failure of the foundation may or may not satisfy the requirement that the settlement will be tolerable. The principal determining factor is whether the clay is normally loaded or overconsolidated.

If the footings rest on normally loaded clay, the magnitude of both the total and the differential settlement can be very large. This can be demonstrated by calculating the end-of-primary settlement of continuous footings of different widths, resting on an insensitive soft normally loaded clay having a natural water content equal to its liquid limit of 40%, when subjected to the very low net soil pressure of 50 kPa. The compression index  $C_c$  of the clay was estimated from Fig. 16.3, and the settlement was calculated by means of Eq. 16.6. The curve that represents the relation between settlement and width of the footing resembles the dash-dotted line in Fig. 41.3. The trend of the curve indicates that the settlement of footings on clay, in contrast to that of footings on sand, increases in almost direct proportion to the width of the footings.

Figure 50.17 shows that the settlement of continuous uniformly loaded footings of constant width on a uniform deposit of normally loaded clay can be very large and that the settlement of footings with different widths can be very different. Furthermore, the settlement of footings with the same width can also be very nonuniform, because the compressibility of natural clay strata may vary considerably in horizontal directions. Indeed, in those parts of such cities as Istanbul or Mexico City that are underlain by soft clays, the unequal settlement of the house fronts can be discerned with the naked eye.

Fortunately, in most localities even soft clays are preconsolidated to some extent by desiccation, aging, or temporary lowering of the water table. In the few regions

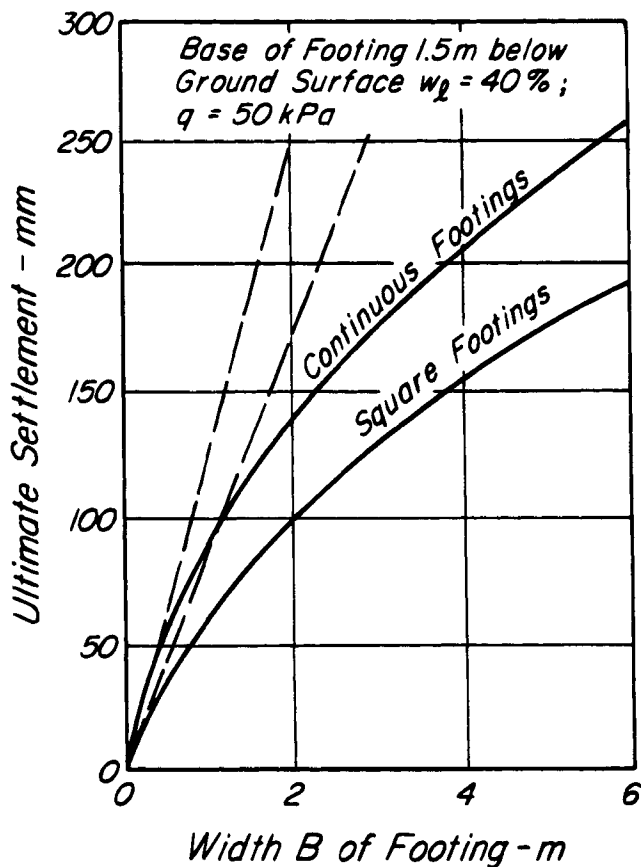


**Figure 50.17** Approximate relation between width  $B$  and ultimate settlement of footing on normally loaded clay.

where structures must be built above normally or almost normally loaded clays, large differential settlements are commonly considered unavoidable. Attempts to reduce the settlement by reducing the soil pressures are ineffective and wasteful. Hence, the design must be a choice between two alternatives. Either the footings are designed on the basis of Eq. 33.17 at the risk of large unequal settlements, or the structure must be provided with another type of foundation (raft, pile, or pier foundation). The characteristics of the alternative types of foundations are discussed in subsequent articles.

Although structures supported by footing foundations on soft clay are likely to settle excessively if the clay is normally loaded, even a slight degree of overconsolidation causes settlements to be radically smaller. Unfortunately, even the best techniques of sampling and testing may be inadequate to detect or to permit reliable evaluation of very small preconsolidation pressures (Simons 1963), and the calculated settlements may be much greater than the real ones. Yet, because the consequences of overestimating the degree of precompression may be very detrimental, the results of such investigations must be used conservatively. A careful study of the behavior of

existing structures on the same deposit often permits the best appraisal of the conditions.

Medium and stiff clays beneath a shallow overburden are always preconsolidated. The allowable soil pressures  $q_a$  corresponding to a factor of safety of 3 against a bearing-capacity failure are almost always less than the preconsolidation pressure. Consequently, the differential settlements of footing foundations on such clays seldom exceed those of adequately designed footing foundations on sand. The maximum settlements, although likely to be greater than those of comparable foundations on sand, are also generally moderate. They can be estimated on the basis of the results of carefully conducted consolidation tests on undisturbed samples. The field  $e$  vs  $\log \sigma'_v$  relation for settlement analysis should be determined in accordance with the procedure outlined for undisturbed precompressed clays (Article 16.9).

### 50.3.1 Footings on Expansive Clays

If the clay is stiff and possesses a high swelling potential (Article 16.10), footing foundations may experience movements that may be extremely damaging to the structure. In semiarid regions the moisture content of the clay within the zone of seasonal change tends to increase and decrease with respect to an equilibrium value that depends primarily on the relative annual rates of precipitation and evaporation. The presence of a building usually decreases evaporation and, in addition, is often accompanied by landscaping and irrigation. Consequently, footings located in the zone of seasonal moisture change may rise. Differential movement is likely not only among the various footings in the building, but between footings and adjacent parts of the structure in contact with the ground.

Various activities at a site lead to an increase in moisture content and, consequently, to a decrease in suction. These include (1) grading, which alters surface drainage and increases water penetration; (2) removing vegetation and stopping transpiration; (3) construction of a structure that covers the ground surface and curtails evaporation while water vapor at a temperature higher than that in the ground migrates toward the cooler covered area and condenses; (4) local filling adjacent to a structure and ready penetration of rainwater into loose backfill; (5) introduction of localized sources of water through leaky water or sewer lines, roof drains, and nonfunctioning subdrains; (6) landscaping and excessive irrigation; and (7) creation of a built-up area, resulting in a perched water table as well as a rise of the deep water table.

Construction and landscaping can lead to highly localized effects of drying and shrinkage. For example, after construction of a slab on ground and during long-term increase of moisture in the ground under the slab, expansive soil under the edge of the covered area may experience seasonal evaporation and shrinkage. The horizontal edge distance subject to drying is approximately equal

to the depth of seasonal moisture fluctuation. Trees lead to desiccation within a radius approximately equal to their height. Heating equipment such as furnaces also produces local drying. In general it is usually possible to avoid postconstruction local drying effects by protecting the edges of slabs on the ground against evaporation, by not planting trees closer to structures than their mature height, and by properly isolating heat-generating equipment from the expansive soil.

Estimates of heave and swelling pressure may be made on the basis of the procedures described in Article 16.10. However, the estimates can serve as no more than a rough guide, because the amount of swelling (or shrinkage) depends to a great extent on the difference between the moisture content in the field at the time the construction is undertaken and the equilibrium moisture content after the construction is completed and the new environment established. Unfortunately, the field moisture content at the start of construction is not likely to be known by the designer.

The tendency of a foundation to heave may be counteracted to some extent by increasing the allowable soil pressure, but the net pressure is limited by the bearing capacity of the clay. Moreover, in lightly loaded structures it may not be possible to develop downward loads large enough to exert the required pressures beneath footings of the smallest practicable size. Furthermore, the swelling can be prevented only in a localized zone beneath the footing where the stresses induced by the footing are concentrated. At a comparatively shallow depth beneath the foundation the intensity of added stress is small, and swelling may occur below this level even if it is entirely prevented above. In the areas between the footings, swelling may be undiminished.

In some instances it may be possible to construct the building on a fill of nonswelling material having a thickness such that the weight of the fill counteracts all or most of the swelling pressure. Other procedures, such as prewetting to a moisture content equal to the equilibrium value, or chemical stabilization, are invoked occasionally. In most instances, however, even light structures are provided with pier foundations extending below the zone of potential movement and precautions are taken to isolate the rest of the structure from the swelling soil (Article 53.5.8).

#### 50.4 Footing Foundations Located on Firm Soil above Soft Layers

The values given for the settlements of footings designed in accordance with the rules discussed under the preceding subheadings are based on the assumption that the soil does not become softer with depth. If this condition is not satisfied, the values cease to be reliable. The reason is illustrated by Fig. 50.18.

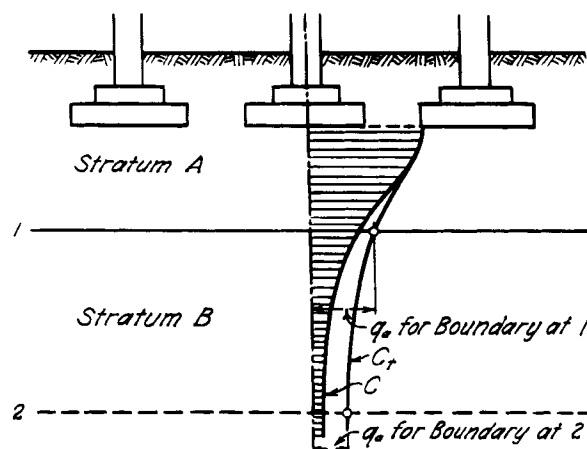


**Figure 50.18** Diagram illustrating method of calculation to ascertain whether allowable soil pressure is exceeded for members of stratified clay subsoil. Curve  $C$  represents variation with depth of vertical pressure beneath single footing neglecting influence of adjacent footings. Curve  $C_i$  represents vertical pressure below same footing, considering influence of adjacent footings.

Figure 50.18 shows the stress conditions beneath a footing that rests on a firm stratum  $A$  located above a soft stratum  $B$ . If the upper boundary of the soft stratum is located close to the base of the footing, the footing may break through the firm layer into the soft deposit. Failures of this type are not uncommon (Skempton 1942). They can be avoided by giving the footing such dimensions that the pressure on the upper boundary of stratum  $B$  does not exceed the allowable bearing value for the soil in that stratum. The pressure at the boundary can be computed by the method described in Article 40. Less accurately, the total footing load can be assumed to be uniformly distributed over the base of a truncated pyramid whose sides slope from the edges of the footing to the upper surface of  $B$  at an angle of  $60^\circ$  with the horizontal.

If the upper boundary of the soft stratum  $B$  is located at a considerable depth below the base of the footings, failure by breaking into the ground cannot occur because stratum  $A$  acts like a thick raft that distributes the entire weight of the building almost uniformly over the surface of  $B$ . The flexural rigidity of this natural raft prevents the surface of  $B$  from heaving beyond the loaded area. Nevertheless, the settlement may be very large. For example, the weight of the building represented in Fig. 50.19 is transmitted by continuous footings onto a stratum of dense sand and gravel that rests, at a depth of 7m below the footings, on a layer of soft clay 15m thick. The footings were designed for a soil pressure of 250 kPa, a conservative value for dense sand and gravel. The greatest pressure on the surface of the clay due to the weight of the building was 110 kPa. During the construction period, which lasted 1 year, the footings settled between 25 and

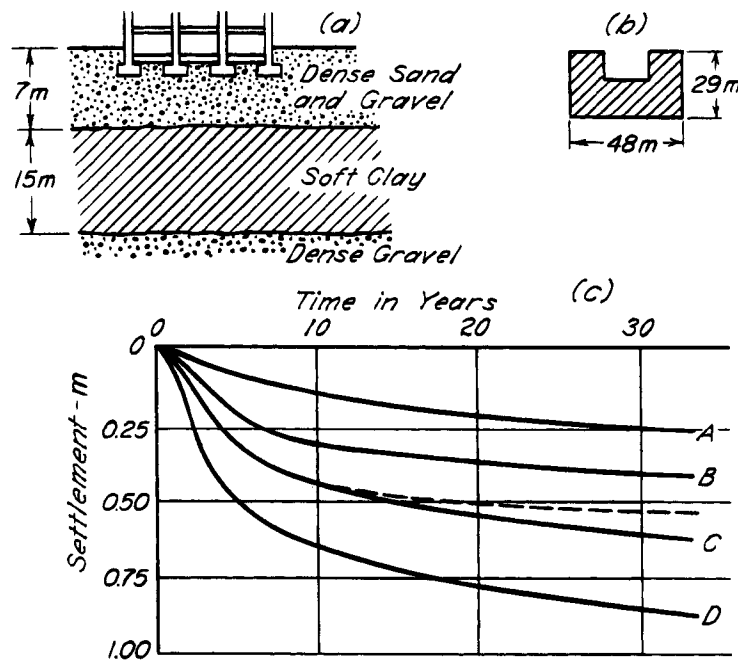


**Figure 50.19** (a) Cross-section through foundation of structure supported by dense sand underlain by soft clay. (b) Plan of structure. (c) Observed time-settlement curves. Dash curve represents time-settlement relation for primary settlement computed from results of consolidation tests (after Terzaghi 1935).

100 mm. During the following 40 years the maximum settlement increased to about 1m. Because the basement floor, which rested on the sand between the footings, neither cracked nor moved with respect to the footings, it is evident that the layer of sand and the footings settled together.

Ten years after construction the deterioration of the building was such that the owners decided to strengthen the foundation. In spite of the symptoms mentioned previously, it was not suspected that the seat of settlement was located below the sand. Hence, the “strengthening” was accomplished by increasing the width of the footings so that the intensity of the pressure exerted by the footings was reduced about 30%. However, since the pressure on the clay remained unchanged, the expensive alterations did not have the slightest effect on the trend of the time-settlement curves shown in Fig. 50.19c.

At a later date undisturbed samples were taken from the clay at some distance from the building. On the basis of the results of consolidation tests the average rate of settlement for the building as a whole was computed. The theoretical trend of the primary settlement, represented by the dash curve in Fig. 50.19c, is very similar to the real one. On account of the secondary compression, however, the real settlement approaches a constant rate ranging for different parts of the structure from 3 to 8 mm per year, whereas the curve of computed primary settlement approaches a horizontal asymptote.

The observations illustrated by Fig. 50.19 show very clearly that the settlement due to consolidation of soft layers located at a considerable depth below the footings is in reality practically independent of the distribution of pressure on the base of the footings, because the firm stratum supporting the footings acts like a natural raft that distributes the load from the footings over the softer strata. Procedures for computing the settlements caused by the consolidation of the lower layers and methods for reducing them are discussed in connection with raft foundations (Article 51). After the foundations are laid out in such a manner that the settlement due to consolidation of the soft layers will be tolerable, the footings can be designed as if the soft strata did not exist. Hence, the presence of the soft strata may compel the designer to change the entire layout of the foundation, but it has no bearing on the allowable soil pressure for the footings.

## 50.5 Footings on Metastable Soils

### 50.5.1 Principal Types of Metastable Soils

The structure of soils that experience large loss of strength or great increase in compressibility on comparatively small changes in stress or deformation is said to be *metastable*. Metastable soils include: (1) extrasensitive clays such as the quick clays of Scandinavia and the St. Lawrence Valley; (2) loose saturated sands susceptible to liquefaction; (3) unsaturated primarily granular soils in

which a loose state is maintained by apparent cohesion, cohesion due to clays at the intergranular contacts, or cohesion associated with the accumulation of soluble salts as a binder; and (4) some saprolites, either above or below the water table, in which a high void ratio has been developed as a result of leaching that has left a network of resistant minerals capable of transmitting stresses around zones in which weaker minerals or voids exist.

Footings on quick clays can be designed by the procedures for clays in general (Article 50.3) or, if a weathered upper zone is present, by the modifications indicated in Article 50.4. Consideration should be given to the possibility of a flow slide (Article 47.7), however, in which all support may be lost. Very loose sands ( $N_{60} \leq \sim 5$ ) should not be used for support of footings; whether somewhat denser sands are suitable depends on the seismicity of the area and the corresponding likelihood of general liquefaction of the sands on which the footings rest. The remainder of this article, therefore, deals with soils in categories 3 and 4 listed in the preceding paragraph.

### 50.5.2 Footings on Unsaturated Soils with Metastable Structure

Soils in this category may be relatively strong and stiff at their natural water content but may experience a radical decrease in volume upon wetting. Hence, they are termed *collapsible soils*. The load-settlement curve for a collapsible soil at its natural water content is influenced principally by the strength of the bonds between particles and the void ratio of the assemblage. The two most prevalent types of collapsible soils are loess (Article 2), which covers large areas in the central part of all the continents except Antarctica, and colluvium and alluvium deposited under semiarid conditions. The latter soils are also widely distributed throughout the world and are prevalent in much of the western and southwestern United States.

As illustrated in Fig. 50.20, the initial portion of the load-settlement curve obtained from a load test on loess usually indicates a relatively small increase in settlement up to a critical pressure  $\sigma_{ver}$  at which a sudden increase occurs and the bearing plate plunges into the ground. The value of  $\sigma_{ver}$  depends, among other factors, on the natural moisture content of the loess. However, the influence of the various factors is so complex that the critical pressure can be determined reliably only on the basis of tests on materials at the site of the proposed structure.

The principal requirement for a footing resting on loess is that the net soil pressure should not exceed  $\sigma_{ver}/F$  where the value of the factor of safety  $F$  should generally not be less than 3 for dead load and 2 for dead load plus live and wind loads. If this requirement is satisfied the settlement of the footing is likely to be inconsequential.

Unless the width of the footing is less than about 1 m, determination of  $\sigma_{ver}$  by means of a load test at the eleva-

tion of the base of the footing may not be indicative of the values at greater depths within the zone of influence of the footing. Hence, it is preferable to investigate  $\sigma_{ver}$  at several depths and to compare the values with the stresses produced at those depths by the footings. This may be done by means of standard load tests (Article 12.4) at several depths. Alternatively, if relatively undisturbed samples can be obtained, confined compression tests can be carried out in consolidation apparatus. In many instances, pressuremeter tests may be more economical. The pressuremeter limit value, although an approximation to  $\sigma_{ver}$ , may somewhat underestimate it because of the anisotropy associated with the near-vertical root holes characteristic of the material.

Cemented desert alluvium and colluvium are notoriously nonhomogeneous and often contain coarse particles that preclude undisturbed sampling and consolidation testing. Standard load tests at depths representative of the materials within the significant depth are appropriate, but pressuremeter tests may be more expedient and economical. The pressuremeter limit values are more likely to approximate  $\sigma_{ver}$  for such soils than for loess because, without the characteristic root holes of loess, they are more nearly isotropic.

Fills compacted on the dry side of the optimum moisture content, including fills containing chunks of clay, may be strong and stiff as compacted. They can be investigated by the procedures described for loess or cemented soils.

However, with respect to all these materials, design should not be based on the critical pressure unless the possibility of future wetting can be precluded. In judging whether wetting can occur, consideration should be given to the potential for ponding associated with regrading for the project, to irrigation close to the structure, and to leakage from water lines and drain pipes. Large and sometimes catastrophic settlements have been experienced for all these reasons. In particular, lightly loaded residences have suffered severe damage in many semiarid regions as a consequence of irrigating shrubbery and lawns. The problem is often compounded by inadequate compaction of fills of the same materials placed at moisture contents below optimum.

If wetting cannot be precluded, three alternatives may be considered: (1) the foundation may be carried to a safe depth by means of piers or piles. (Articles 52 and 53); (2) the collapsible soil may be densified by such means as dynamic compaction (Article 44.3.4); (3) the foundation slab may be posttensioned to prevent its disintegration as differential movements occur, but not to eliminate the movements; or (4) the soil may be induced to collapse by prewetting. The latter procedure has been used successfully for treating the foundations of earth dams or dikes by flooding the area to be loaded, whereupon the material settles under the weight of the super-

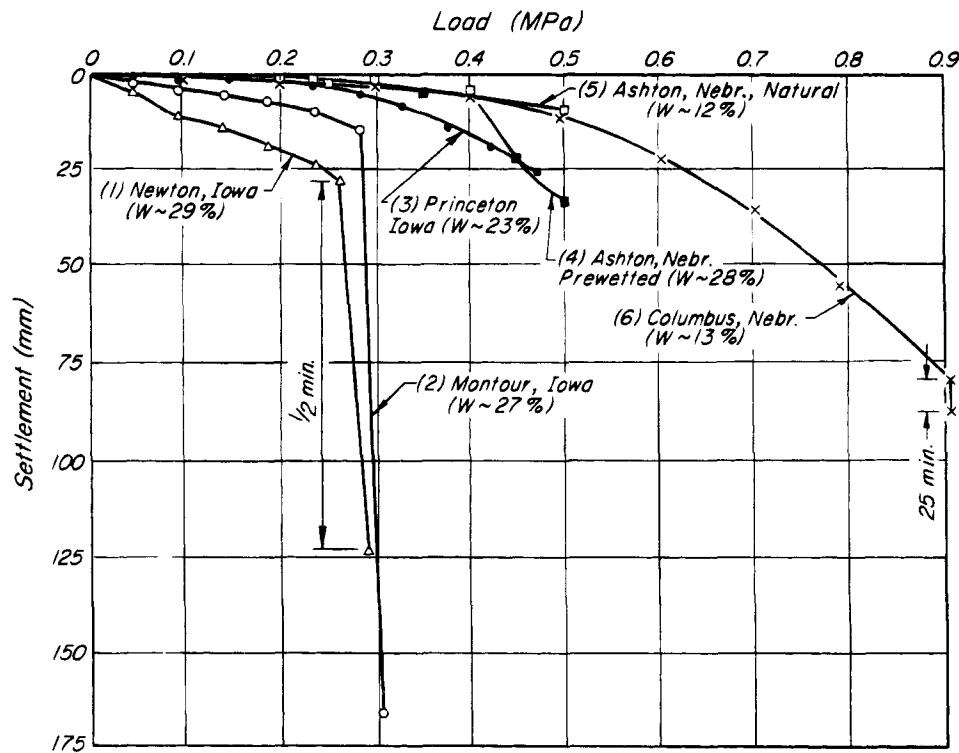


Figure 50.20 Results of standard load tests on loess deposits in Nebraska and Iowa.

posed fill during construction instead of after completion when the reservoir is first filled. Even under favorable conditions, however, penetration of the flooding waters may be slow and nonuniform. Use of the procedure for footing foundations leaves the wetted soil in a loose, wet, highly compressible state; hence flooding is a generally unsatisfactory method of treatment in preparation for footings.

### 50.5.3 Footings on Saprolite

Some saprolites possess a structure, developed as a result of weathering, that may crush at a critical pressure  $\sigma_{ver}$ . The various degrees of weathering likely to have occurred in even a small volume of the material lead to marked inhomogeneity with particle sizes ranging from silts to blocks of rock. The value of  $\sigma_{ver}$  may be determined by the procedures described above for desert alluvium or colluvium. In contrast to the latter materials, however, wetting or submergence may not lead to collapse.

### 50.5.4 Compressibility of Metastable Soils

The compressibility of metastable soils not subjected to wetting may be investigated by means of consolidation tests if satisfactory undisturbed samples can be obtained, by using the initial slopes of load-settlement curves from plate-bearing tests made at suitable depths within the significant depth for the foundation, or by means of the pressuremeter. However, in the relation between modulus

of deformation of the soil  $E_s$  and pressuremeter modulus  $E_{pm}$

$$E_s = \frac{E_{pm}}{\alpha} \quad (11.3)$$

(Article 11.5.3), the rheological coefficients  $\alpha$  proposed by Menard (1965) pertain to sedimented soils without metastable structures. For residual soils and saprolites derived from the granitic, gneissic, or schistose Precambrian basement rocks of the southeastern United States, Martin (1977) found satisfactory agreement between predicted and observed settlements of footing-supported buildings for a value of  $\alpha$  approximately equal to unity.

### Selected Readings

- Peck, R. B. (1948). "History of building foundations in Chicago," *U. of Ill. Eng. Exp. Sta. Bull.* 373, 64 pp.
- Sowers, G. F. (1962). "Shallow foundations," Chapter 6 in *Foundation Engineering*, G. A. Leonards, ed., New York, McGraw Hill, pp. 525-632.
- Meyerhof, G. G. (1965). "Shallow foundations," *ASCE J. Soil Mech.*, 91, No. SM2, pp. 21-31.
- Burland, J. B. and M. C. Burbidge (1985). "Settlement of foundations on sand and gravel," *Proc. Inst. C. E.*, Part 1, 78, pp. 1325-1381.
- Chen, F. H. (1988). *Foundations on Expansive Soils*, New York, Elsevier, 463 p.

Footings on expansive soils are well treated in *Expansive Soils*, by J. D. Nelson and D. J. Miller (1992), New York, John Wiley & Sons, Inc., 259 p. The presentation is sound but not unnecessarily complex.

The Proceedings of the ASCE Geotechnical Engineering Division Specialty Conference on Engineering and Construction in Tropical and Residual Soils, Honolulu (1982), contains two papers dealing with spread foundations: "Settlement predictions in Piedmont residual soil," by J. L. Willmer, G. E. Futrell, and J. Langfelder, pp. 629–646; and "Settlements of a tower on residual soil," by R. D. Barksdale, R. C. Backus, and M. B. Clanou, pp. 647–664. Both refer to conditions in the southeastern United States.

Much useful information, including the results of field observations, is contained in the following publications:

*Settlement of Structures* (1975). Proceedings of a conference organized by the British Geotechnical Society, April 1974, London, Pentech Press. 811 p.

*Vertical and Horizontal Deformations of Foundations and Embankments* (1994). A. T. Yeung and G. Y. Félio, eds., ASCE Geotech. Spec. Publ. 40, 2 Vols., 1906 p.

*Predicted and Measured Behavior of Five Spread Footings on Sand* (1994). J.-L. Briaud and R. M. Gibbens, eds., ASCE Geotech. Spec. Publ. 41, 255 p. Results of Spread Footing Prediction Symposium, College Station, Texas, June 1994.

## ARTICLE 51 RAFT FOUNDATIONS

### 51.1 Comparison between Raft and Footing Foundations

If the sum of the base areas of the footings required to support a structure exceeds about half the total building area, it is often preferable to combine the footings into a single mat or raft. Such a raft is only a large footing and, like a footing, it must satisfy the requirements that the factor of safety with respect to a base failure should be adequate and that the settlement should not exceed an amount acceptable to the designer of the superstructure.

The factor of safety of raft foundations depends on the nature of the subsoil. If the soil consists of very loose sand in a saturated state, it should be compacted before the raft is constructed (Article 44.2.2). If the sand is medium or dense, the factor of safety of a raft is considerably greater than that of footings, and its adequacy can be taken for granted without any computation.

The factor of safety of raft foundations on clay is practically independent of the size of the loaded area. It is commonly very low, and several failures have occurred. One of these is illustrated by Fig. 51.1. The structure, a grain elevator near Winnipeg, Canada, was  $23 \times 59$  m in plan and 31 m high. It rested on a stratum of "firm" clay overlying rock. On the basis of the results of load tests it was estimated that the ultimate bearing capacity of the clay was between 400 and 500 kPa, and the design was

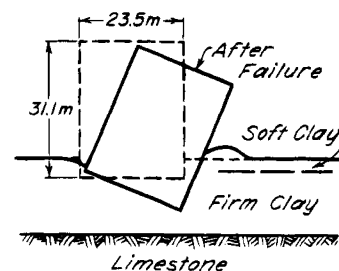


**Figure 51.1** Diagram illustrating failure of grain elevator near Winnipeg, Canada, by breaking into clay stratum.

based on an allowable soil pressure of 250 kPa. When the excess or net load on the raft approached this value, one side of the structure settled 8.8 m, whereas the opposite side rose 1.5 m. The movements took place within less than 24 h (Peck and Bryant 1953, White 1953). To avoid the risk of such a failure, a raft foundation on clay soil should be designed so that the excess load divided by the loaded area does not exceed about one third the value of  $q_{d \text{ net}}$  determined by Eq. 33.15.

The excess load on the base of a raft is computed in the same manner as that on the base of a spread footing (Article 50.1.1). If the raft is located beneath a basement (Fig. 51.3), it constitutes with the basement walls a large hollow footing. Because the loaded soil can rise only outside the area occupied by the raft, as indicated by an arrow, the depth of the overburden is equal to  $D_f$ , measured from the ground surface, and not to  $D_{fs}$ , as for spread footings below basements (Fig. 49.1 c and d). Hence, the excess load  $Q_t$  on the base of the raft is equal to the difference between the total effective load  $Q + Q_t$  at the base of the raft and the total effective weight  $W_s$  of the soil replaced by the basement, or

$$Q_t = (Q + Q_t) - W_s \quad (51.1)$$

If  $q_a$  is the allowable pressure on the subsoil, and  $A$  the area covered by the raft, the foundation must satisfy the condition,

$$\frac{Q_t}{A} \leq q_a \quad (51.2)$$

The relation expressed by Eq. 51.1 indicates that the excess load on the base of a raft can be reduced by increasing the depth of the basement. This reduction increases the factor of safety of the foundation with respect to breaking into the ground and reduces the settlement. The existence of such a relation was recognized by a few engineers in the late 1700's, and they used it to advantage in establishing heavy structures on soft ground without the use of piles.

Although the rules governing the factor of safety of rafts and footings are quite similar, the general character of the settlement of these two types of foundations is



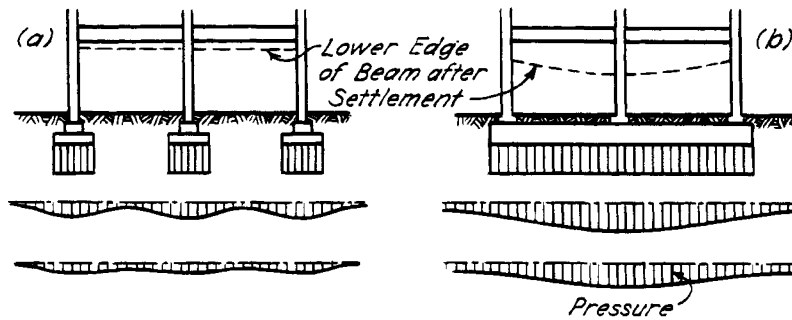


**Figure 51.2** Distribution of pressure in soil beneath buildings supported by (a) widely spaced footings and (b) concrete raft. The load per unit of area is the same beneath the footings and the raft; hence, the total load on the building in (b) exceeds that in (a).

very different. The causes of the difference are illustrated in Fig. 51.2. This figure represents a vertical section through each of two structures, one of which rests on footings and the other on a raft. The footings and the raft both exert on the subsoil the same load per unit of area, as indicated by the rectangular diagrams at the base of the foundations. In addition, the figure shows the intensity and the distribution of the vertical pressure at different depths below the base level of each foundation.

The footings shown in Fig. 51.2a are so far apart that each one settles much as if the others did not exist. If the soil were homogeneous, the footings would settle almost equally; in reality, they settle by different amounts because no natural soil stratum is homogeneous. Because the seat of settlement is located within the uppermost soil stratum, the distribution of the settlement reflects the variations in the compressibility of the soil located within this stratum. It is always erratic and cannot be predicted by any practicable means. This fact determined the proce-

dures that were established for evaluating the allowable soil pressures for footing foundations (Article 50).

The seat of settlement of the raft foundation (Fig. 51.2b) that exerts the same soil pressure as the footings extends to a very much greater depth than that of the footing foundation. Within this depth weak spots are scattered at random, as shown in Fig. 51.3, and their effects on the settlement of a loaded area partly cancel each other. Therefore, the area settles as if the loaded soil were more or less homogeneous. The settlement is not necessarily uniform, but it follows a fairly definite instead of an erratic pattern. The pattern differs, however, if the soil located within the seat of settlement consists of sand or of clay.

## 51.2 Settlement of Raft Foundations

### 51.2.1 Rafts on Sand

Both theory and experience indicate that the settlement of a uniformly loaded area on sand is fairly uniform, provided the area is located at a depth of more than about 3m below the adjacent ground surface. If the depth is smaller, the outer parts of the loaded area are likely to settle somewhat more than the central part unless lateral yield of the sand is prevented within a depth of 2 or 3m from the ground surface.

The differential settlement of the area covered by the raft reflects in a general way the variations in the compressibility of the subsoil. However, because of the random distribution of compressible zones in the subsoil (Fig. 51.3) combined with the stiffening effect of the raft and building frame, the differential settlement of a raft is a smaller fraction of the total settlement than is the differential settlement among the footings of a footing foundation. Experience indicates that the ratio of differential to maximum settlement of a raft on sand is no more than half that of a footing foundation. Therefore, the allowable soil pressure for a raft can be assigned a value equal to twice that given by Eq. 50.23, or twice that obtained from the settlement chart (Fig. 50.16).

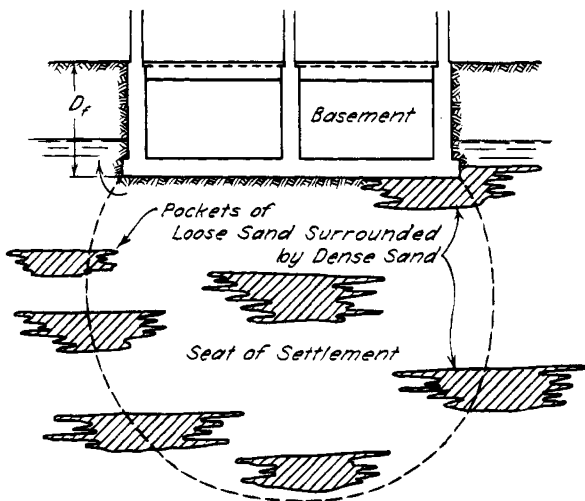


**Figure 51.3** Diagram representing erratic distribution of pockets of loose sand throughout a stratum of dense sand located beneath base of a building.

The foregoing statements imply that, for the same differential settlements that can be tolerated by a building on individual footings, a raft-supported building on sand will experience a maximum settlement of 50 mm instead of 25 mm. A settlement of this magnitude is ordinarily of no concern. However, the loads are presumed to be distributed fairly uniformly over the base of the building. If different parts of a large raft carry very different loads per unit of area, it may be advisable to provide construction joints at the boundaries between these parts.

The depth of the stratum of sand is presumed to be greater than the depth of influence  $Z_f$  (Eq. 50.6) of the raft. If the depth to bedrock is smaller than  $Z_f/2$ , the allowable soil pressure can be increased.

### 51.2.2 Rafts on Clay

The maximum permissible value for the soil pressure beneath rafts on clay, like that beneath footings on clay, is obtained by dividing the ultimate net bearing capacity  $q_{d\text{net}}$  (Eq. 33.17) by a factor of safety  $F$  equal to 3 for dead load and not more than 2 for dead load plus extreme combinations of live load. However, because of the large dimensions of the area covered by a raft and the rapid increase of settlement of clay with increasing size of the loaded area (Fig. 50.17), it is always necessary to find out, at least by a crude estimate, whether the settlement will be tolerable. The computation can be based on the assumption that the loaded clay is laterally confined. The results of the computations show, in accordance with experience, that the base of a uniformly loaded area on clay assumes the shape of a shallow bowl, because the consolidation pressure decreases from the center toward the edges (Fig. 51.2b). The slopes of the bowl are so gentle that the difference between the settlement of two adjacent columns never exceeds a small fraction of the difference between the maximum and the minimum settlement. For rafts on sand, on the other hand, the differences can be almost equal. The effects on the building frame may be radically different.

### 51.3 Design of Raft Foundations

The average gross load per unit of area on the base of a raft is equal to the total effective weight of the building,  $Q + Q_f$ , divided by the total area  $A$  of the base. Because the area occupied by the raft can be only equal to or slightly greater than the area occupied by the building, the designer has little opportunity to change the soil pressure by adjusting the size of the raft. Hence, to satisfy Eq. 51.2,  $W_s$  (Eq. 51.1), must be increased. This can be done by providing the structure with one or more basements of adequate depth. The required depth can be computed by trial.

After the depth of basement has been determined, the next step in the design is to compute the forces that act on the raft. In this operation, the designer must depend

to a large extent on sound judgment. The factors and conditions that need to be considered are illustrated by Fig. 51.4.

Figure 51.4a shows a vertical section through a structure consisting of a heavy tower and two wings. The water table is located below the base of the raft. On this assumption the total soil reaction is equal to the full weight  $Q + Q_f$  of the building including the weight of the raft, whereas the excess load  $Q_e$  (Eq. 51.1) which determines the settlement is equal to the difference between the weight of the structure and the weight  $W_s$  of the soil that has been excavated. If the excess load  $Q_e$  is zero and if, in addition, the structure is rigid, there will be practically no settlement even if the soil reaction is very large. As a rough approximation the soil reaction on the base of a rigid structure may be considered uniform, as indicated by the shaded rectangle in Fig. 51.4a. Yet, the loads are concentrated on the central part of the base of the building. Therefore, the raft and the frame of the structure are acted on by very severe bending moments. The cost of the reinforcement required to carry these moments may be prohibitive.

If the building is flexible, the soil reaction on every part of the raft is roughly equal to the load that acts on it (Fig. 51.4b). The corresponding bending moments are relatively small. However, because of the heavy concentration of loads on the middle part of the raft, this part carries an excess load whereas the excess load on the outer parts is negative. Consequently, the tower will settle more than the wings, as shown in the figure. A difference in settlement is inevitable even if the total excess load on the subsoil is zero. If the building rests on sand, the difference between the settlements of the tower and the wings is likely to be too small to have an injurious effect on the superstructure, and the raft can be designed as if it were acted on by the forces shown in Fig. 51.4b. On the other hand, if the raft rests on clay, the differential settlement due to the nonuniform pressure distribution may be very large. Construction joints between the tower and the wings may slightly improve the stress conditions in the members of the superstructure, but they cannot prevent the settlement of both wings from increasing toward the tower. Hence, it is necessary to make a settlement computation to determine whether the differential settlement is likely to exceed what the structure can stand without injury. If it is, the designer must choose among three alternatives: (1) to increase greatly the strength and rigidity of the raft and superstructure; (2) to specify a pile or pier foundation for the structure; or (3) to provide the tower and the wings with basements of different depths (Fig. 55.4c). In the latter event, the depth of each basement must be determined in such a manner that the settlement of the tower and the wings would theoretically be equal. If this condition is satisfied, the designer can

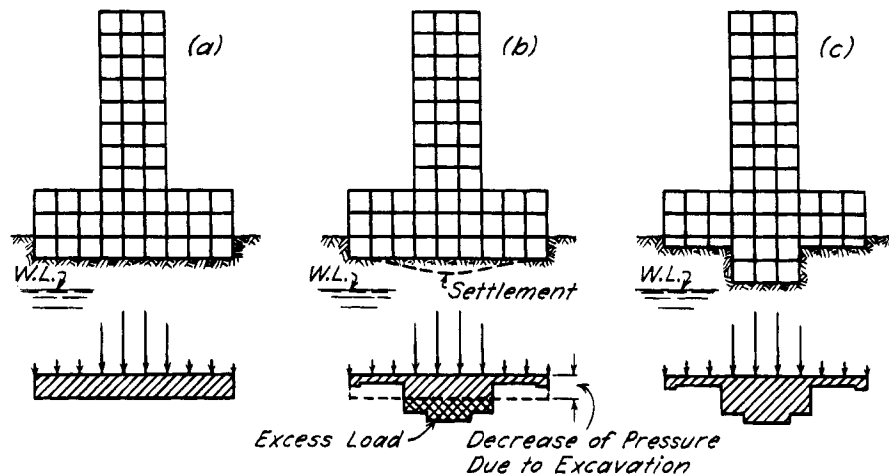


**Figure 51.4** Diagram illustrating three different methods for the design of raft foundations on very compressible subsoil: (a) Rigid superstructure, capable of enforcing uniform settlement; (b) flexible superstructure, capable of sustaining large deflections without damage; (c) flexible superstructure, uniform settlement produced by adapting depths of basements to weight of structure located above them.

be fairly certain that the differential settlement will be tolerable.

The foregoing discussion deals with the aspects of soil mechanics that determine the general suitability of a raft foundation at a given site, with the selection of the allowable soil pressure, and with the estimate of settlement. In contrast to the structural design of the raft itself, these aspects are fairly straightforward. To produce an economical design of adequate strength and stiffness requires an appreciation on the part of the structural designer of the consequences of the assumptions made concerning the soil-structure interaction.

The simplest and most widely used procedure is to assume that the raft behaves like an inverted floor slab acted on by the downward column loads and by a distributed upward soil pressure having its center of pressure coincident with the centroid of the column loads. The structural design of the slab then follows the routine procedure for a flat-slab floor. However, implicit in the procedure is the condition that the points at which the columns meet the slab remain in the same plane. This condition is satisfied to a reasonable degree if the differential settlements among the columns are small and their pattern is erratic, as would be the case, for example, if the subsoil consisted of medium to dense sands and gravels. To compensate for the inability to know in advance where the looser or denser zones occur, it is customary to provide more reinforcement than that required for the same loading on a flat-slab floor, and to furnish reinforcement in both top and bottom of the slab at all locations. Under these conditions, rafts designed according to the flat-slab analogy can be expected to perform successfully. On the other hand, even if the differential settlements

between adjacent columns remain small, but if they exhibit a systematic pattern so as to form, for example, a dish shape, the results may be catastrophic. Such a pattern is likely to develop above a deep deposit of compressible clay. Under these conditions no slab of reasonable dimensions may be able to prevent the deformations, and such measures as providing deep girders or trusses in the basement or even using the strength and stiffness of the superstructure may be required. Many raft foundations, designed in accord with the flat-slab analogy, have failed dismally for lack of appreciation of the potential for systematic, usually deep-seated, settlements.

Structural engineers have also made use of the concept of slabs or beams on elastic foundations as a means to design raft foundations. For simple geometries, solutions are available for the stresses in elastic slabs transmitting loads to an underlying semiinfinite elastic medium of modulus of elasticity  $E$  and Poisson's ratio  $\nu$  (Poulos and Davis 1974). However, the complexities of real structures often make the use of such solutions impracticable. In addition, and more significantly, the difficulty of determining suitable values of  $E$  for real soils and, for compressible clays, the inelastic behavior associated with consolidation, greatly limit the conditions under which the elastic half-space solutions are useful.

Much more widely used and much more adaptable to irregular geometries and loadings is the concept of the modulus of subgrade reaction (Article 42), in which the soil is considered analogous to a bed of independently acting elastic springs. Many solutions are available for calculating moments, shears, and deflections for rafts supported by such a subgrade. Unfortunately, inherent in the concept of the independence of the supporting springs is

the conclusion that the settlement of an area loaded by a uniform pressure is independent of the size of the area or of the presence of loads on adjacent areas. This conclusion may be a reasonable approximation if the subsoil is relatively stiff or dense and if its stiffness increases rapidly with depth, but it is so far from reality for deep compressible soils that its acceptance has led to gross underdesign and to failure of many rafts. The modulus of subgrade reaction  $K_s$  (Eq. 42.1) is not a property of the soil alone; hence, its value determined by small-scale tests such as plate load tests cannot be applied without correction to full-scale foundations. Such corrections have been developed (Terzaghi 1955*b*) for a number of practical problems and are useful under strictly limited conditions, but considerable experience and judgment are required to determine the circumstances under which realistic results and satisfactory designs can be anticipated.

Methods of successive approximation have been used in which the contact pressure between raft and soil has been assumed and the deflection of the raft calculated under the combined action of the building loads and the contact pressure. The settlement of the ground surface at its interface with the raft is also calculated under the action of the assumed contact pressure and compared to the deflection of the raft. The assumed contact pressure is then modified with the objective of reducing the discrepancy between the two deflected shapes, and the procedure is repeated until a reasonable agreement is reached. If the raft selected for the analysis is found to be unsatisfactory, a new design is selected and a new iteration is carried out. Obviously such a procedure is time-consuming and costly, even with computers. Nevertheless, in a few instances, it has been used successfully (Wood 1977, Hooper 1983, Hooper and West 1983).

Finite-element calculations in principle are suitable for the design of structural rafts on compressible foundations, but the complexity of most real structures and their foundation conditions as yet implies prohibitively high costs.

In the preceding discussion, it has been tacitly assumed that a rigid raft does not settle until the load on the raft becomes equal to the weight of the excavated soil. In many instances, the error due to this assumption can safely be ignored. However, if the subsoil is soft and the excavation is deep, the settlement that occurs before the effective load on the raft becomes equal to the effective weight of the excavated soil may be large enough to require consideration. The cause of this settlement is discussed in the next section.

#### 51.4 Heave during Basement Excavation

The excavation for a basement or a subbasement involves the complete removal of the pressure originally exerted against the soil at the base level of the raft. Consequently, the bottom of the excavation rises. During the subsequent period of construction, the weight of the building becomes

equal to and generally exceeds the original overburden pressure; hence, the heave disappears, and the building settles. If the building has a greater weight than the excavated soil, the settlement passes through two stages. The first lasts until the load per unit of area at the base of the raft becomes equal to the original overburden pressure, and the second begins when this pressure is exceeded. The characteristics of the settlement during the second stage have already been described. Those of the first stage may be very different.

At the end of the first stage, when the building load becomes equal to the weight of excavated material, the settlement is equal to or slightly greater than the preceding heave. If the building load is not further increased, the settlement stops shortly after construction is finished. Some buildings with basements deep enough to satisfy this requirement have actually been provided with expensive pile support; it is obvious that the money spent for the piles was wasted. The amount of the heave and subsequent settlement depends on the nature of the subsoil and the dimensions of the excavation. If the excavation is made in sand above the water table, the heave is so small it can usually be disregarded. A soft clay subsoil deforms at practically constant water content like an incompressible elastic material. Hence, the heave can be computed on the basis of the theory of elasticity provided the modulus of elasticity is known. Unfortunately, the value of the initial tangent modulus  $E_i$  (Article 17.5.1) is extremely sensitive to the degree of disturbance of the samples. Consequently, the heave may be grossly overestimated.

If the clay beneath an excavation contains a great number of continuous layers or seams of coarse silt or sand, the water content of the clay may increase to such an extent that the major part of the heave is caused by swelling. Predictions of the rate of swelling, based on the results of laboratory consolidation tests, are likely to be very inaccurate, because the degree of continuity of the pervious strata cannot be learned by sampling in advance of construction.

If the depth of the basement is increased by open excavation beyond a certain value, the bottom of the excavation becomes unstable and fails by heaving, regardless of the strength and nature of the lateral support for the sides (Article 37). The means for estimating the amount of heave and for reducing it are discussed in Article 54.

#### 51.5 Footing Foundations on Natural Rafts

If the footings of a building rest on a thick firm stratum underlain by considerably more compressible ones, the firm stratum acts like a natural raft that distributes the weight of the building over the soft layers. The footings are designed as if the soft strata did not exist, because the settlement due to consolidation of the soft strata is practically independent of the pressure on the base of the footings.

The load responsible for the settlement due to consolidation is equal to the total effective weight of the building reduced by the effective weight of the excavated soil. In the computation of the magnitude and distribution of the consolidation pressure within the soft layers, the weight of the excavated soil is assumed to represent a negative load uniformly distributed over the bottom of the basement. The weight of the building is a positive load that acts on the bases of the footings. At any point in the soft layers the consolidation pressure is equal to the difference between the pressures produced by these two loads. The settlement due to consolidation is estimated on the assumption that the soft soil is laterally confined. The importance of the settlement that may ensue is illustrated by Fig. 50.19.

If the computation shows that the settlement conditions are unacceptable, the concept of the foundation must be changed. This can be done, for instance, by providing the different parts of the building with basements of different depths (Fig. 51.4c) or by supporting the structure on piles or piers.

### 51.6 Footings on Sand in Basements below the Water Table

A basement located below the water table must be provided with a water-tight floor slab interconnecting the footings. If the load on the footings is applied after the slab is concreted, the footings together with the slab constitute a raft the base of which is acted on not only by water pressure but also by a more or less uniformly distributed soil reaction.

To avoid the necessity for making the floor slab strong enough to withstand both pressures, the slab between the footings should not be concreted until the footings carry the full dead load. The load on the base of the footings will then be equal to the full weight of the building reduced by the full hydrostatic uplift on the basement floor, and the interconnecting slab will be acted on by water pressure only. However, the footings must be designed on the assumption that the hydrostatic uplift is inactive, because the water table is not allowed to rise above the basement floor until the footings carry the full dead weight of the structure. The postponement of the construction of the floor slab requires the continuation of pumping until the superstructure is completed. The sequence of operations is shown in Fig. 51.5. To prevent the floor slab from floating, it must be anchored either to the columns or, preferably, to the footings.

#### Selected Reading

Golder, H. Q. (1965). "State-of-the-art of floating foundations," *ASCE J. Soil Mech.*, **91**, No. SM2, pp. 81–88.

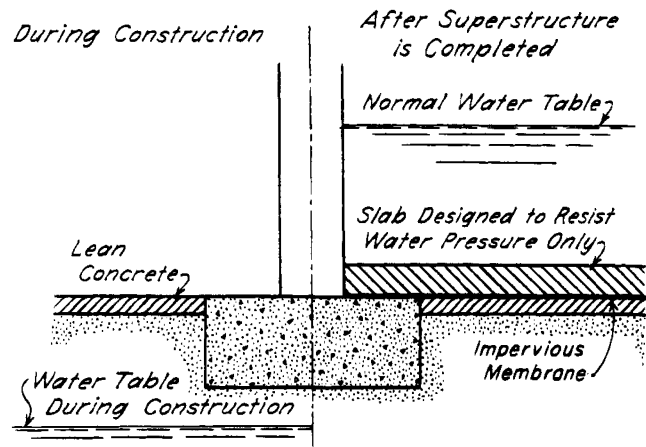


Figure 51.5 Details of footing on sand in basement located below water table.

## ARTICLE 52 PILE FOUNDATIONS

### 52.1 Function of Piles

A structure is founded on piles if the soil immediately below its base does not have adequate bearing capacity or if an estimate of costs indicates that a pile foundation may be the most economical. Piles may also be used to resist lateral or uplift forces or to extend the foundation below the depth of scour.

Piles are made in many forms and of a variety of materials. Descriptions of the principal types and of the methods for installing them can be found in Fuller (1983) and Tomlinson (1986). In this discussion we shall consider only piles of the more common types that are driven into the ground by a mechanical device known as a pile driver. However, the general principles are applicable, with minor modifications, to the design of foundations on other types of piles, installed in a different manner. Piles installed by drilling are essentially small-diameter piers (Article 53).

With respect to the manner in which they transfer their load, piles may be divided into three categories:

1. Friction piles in coarse-grained very permeable soil. These piles transfer most of their load to the adjacent soil through side resistance, often referred to as skin friction. Driving such piles in groups reduces the porosity and compressibility of the soil within and around the groups. Therefore, piles of this category have sometimes been called compaction piles.
2. Friction piles in very fine-grained soils of low permeability. These piles also transfer their load to the soil through side resistance, but they do not compact the soil appreciably. Foundations supported by piles of this type are known as floating pile foundations.

3. Point-bearing or end-bearing piles. These piles transfer their load onto a firm stratum located at a considerable depth below the base of the structure.

In nature, homogeneous soil strata are very rare. Therefore, no sharp boundaries can be established among the categories of piles. The same pile may displace part of the mass of soil through which it is driven without changing the density, whereas the remainder of the soil may undergo compaction. The point of a pile may be embedded in a firm sand stratum capable of supporting the load by point bearing but, nevertheless, a considerable part of the load may be carried by skin friction. Because of the wide variety of soil conditions encountered in practice, any attempt to establish rules for the design of pile foundations necessarily involves radical simplifications and the rules themselves are useful only as guides to judgment. For the same reason, theoretical refinements in dealing with pile problems are of questionable value. Even conclusions based on the results of small-scale model tests may be far from reliable.

## 52.2 Design of Pile Foundations

### 52.2.1 Historical Development

Before the 19th century almost all buildings were established on continuous footings. Piles were used as a means of support, however, if the ground appeared incapable of sustaining the pressure exerted by the footings. Because timber was abundant and labor cheap, as many piles were driven as the ground would take. Settlement caused little concern, because the prevalent type of buildings other than such monumental structures as cathedrals could stand a considerable amount of unequal settlement without injury.

In the 19th century, when industrial development created a demand for heavy but inexpensive structures in locations underlain by soft ground, the cost of pile foundations became an item of consequence, and engineers were expected to specify no more piles than were necessary to provide adequate support for the buildings. This could not be done without at least some knowledge of the ultimate load that an individual pile could carry. Efforts to obtain the necessary information at a minimum expenditure of money and labor led to theoretical speculations that resulted in an impressive assortment of pile-driving formulas. However, the realization slowly grew that the formulas had inherent shortcomings, and it became more and more customary to determine the allowable load per pile on all but the smallest jobs by making load tests on test piles.

The number of piles required to support a given structure, provided that the structure was not eccentrically loaded, was determined simply by dividing the total load by the allowable load per pile. Many foundations designed

in this manner were satisfactory, but now and then excessive and unexpected settlements occurred. These incidents indicated that the settlement of an entire pile foundation was not necessarily related to the settlement of a single test pile, even at the same load per pile. They led to the conclusion that a knowledge of the bearing capacity of a single pile constitutes only part of the information necessary for the design of a satisfactory pile foundation. To find out whether the settlement of a pile foundation will remain within tolerable limits, the designer must consider the stresses produced in the soil by the entire load on the foundation, and must estimate the settlement produced by these stresses. This estimate requires a knowledge of the fundamental principles of soil mechanics. If the results of the investigation show that the settlement may exceed an acceptable value, the design must be changed.

### 52.2.2 Steps in Design of a Pile Foundation

The first requirement for the preliminary design of a pile foundation is a soil profile representing the results of a subsurface exploration. The factors that determine the depth to which the subsoil should be explored are discussed in Article 12.3. Usually, the soil profile provides the information required to decide whether the foundation can best be supported by friction piles, by end-bearing piles, or by piles with a more complex mode of resistance.

The next step in the preliminary design is to select the length and type of pile. If end-bearing piles are appropriate, it may be possible to judge the required length with reasonable accuracy on the basis of the soil profile. Methods for estimating the length of friction piles in sand are generally unsatisfactory, and reliable determinations can be made only by driving and loading test piles. The length of friction piles in soft clay can be determined by making an estimate of the factor of safety of the pile groups against complete failure (Article 52.5.7). The selection of the type of pile is influenced strongly by practical considerations and economics.

After the length and type of pile have been tentatively chosen, the ultimate bearing capacity of a single pile is estimated. This value is divided by an appropriate factor of safety to obtain the *safe design load* per pile. The total number of piles required to support a concentrically loaded structure is determined by dividing the total weight of the structure by the safe design load per pile.

After the number of piles has been determined, the next step is to choose their spacing. The distance  $D$  between the centers of piles with a top diameter  $d$  should rarely be less than  $2.5d$  and preferably not less than  $3d$ . This rule is based on practical considerations. If the spacing is less than  $3d$ , ground movements may displace the piles from their intended locations and out-of-plumb piles may interfere with each other. The heave of the soil is likely to be excessive, and the driving of each new pile may displace or lift the adjacent ones. Moreover, in small groups normal

field tolerances in locating piles may result in large eccentricities and overloading of some piles. On the other hand, a spacing of more than  $4d$  is uneconomical, because it increases the cost of the footings without materially benefiting the foundation. The most suitable value of  $D$  between these limits is selected in accordance with the soil conditions, as explained subsequently.

When the spacing has been decided, the piles are laid out in either a square or a triangular pattern. By multiplying the number of piles by  $D^2$  (square pattern) or by  $\frac{1}{2}D^2\sqrt{3}$  (triangular pattern), the total area required for the pile-supported parts of the foundation is obtained. If this area is considerably smaller than half the total area covered by the structure, the structure is usually established on pile-supported footings; if it is considerably greater, the structure is founded on a pile-supported raft, and the spacing of the piles is increased so that the pile layout forms a continuous pattern. If the intensity of loading on different parts of the raft is very different, the spacing between piles is adapted to the intensity on each of the parts. Finally, if it is doubtful whether the structure should be established on footings or on a raft, the decision is made after a comparison of the costs of the two alternatives.

If the foundation is supported by friction piles in soft clay or plastic silt, an estimate must be made of the ultimate bearing capacity of the pile groups, and the load on the groups must not be allowed to exceed this value divided by a factor of safety not less than 2 and preferably equal to 3. The consequences of ignoring this condition can be catastrophic. In several instances, structures together with the supporting piles and the soil located between the piles have sunk suddenly into the ground, although the load per pile did not exceed the safe design load. The procedure for estimating the bearing capacity of pile groups is described in Article 52.4.

If the load per pile is such that the bearing capacity of the pile groups is not exceeded, the foundation will not fail suddenly by sinking into the ground. However, adequate bearing capacity does not exclude the possibility of excessive settlement, because the settlement of an entire pile foundation has no simple relation to the settlement of a single pile under the load per pile assigned to the foundation. The settlement of the foundation may range between a few millimeters and a meter or so, in accordance with the soil conditions, the number of piles, and the area covered by the structure. Settlements of less than about 50 mm are generally not harmful, but settlements of 150 mm or more may have very undesirable effects on the superstructure. Hence, if a foundation rests on friction piles driven into soft clay, or if the points of point-bearing piles are located above soft strata, a settlement computation is mandatory. Failure to make such a computation has been responsible for many unsatisfactory pile foundations.

The final step in the design of the foundation is the structural design of the pile-supported footings or raft. The computations of bending moments and shears are commonly based on the assumption that each pile carries the same load. Theoretical considerations and the results of field tests (Swiger 1941, O'Neill et al. 1982, O'Neill 1983) both lead to the conclusion that this assumption is usually incorrect, but the error involved in the assumption of equally loaded piles is usually well within the customary margin of safety for reinforced-concrete design. Shear reinforcement in pile caps, however, should make allowance for the likelihood that the pile heads may be located several centimeters from their proper position.

It is evident from the foregoing discussion that the estimate of the ultimate bearing capacity of a single pile is an essential element in the design of the foundation. Yet, the actual ultimate bearing capacity, and thus the validity of the design, remain unknown until the piles are driven and tested. As will be discussed subsequently, only load tests carried to failure can establish the ultimate bearing capacity with reasonable certainty. Without such tests, the designer must rely on indirect procedures such as the use of pile-driving or static formulas or wave analyses together with a generous factor of safety.

If load tests are carried out to validate the design, the designer may choose to have them conducted either before or after the bids are taken. The first alternative permits development or revision of the design and specifications to fit the actual conditions, but requires mobilization of testing equipment and personnel before the foundation contractor has been selected. The second saves the expense of mobilizing the test equipment twice but may lead to delay and modification of the contract if the results of the tests are unsatisfactory. In some instances the designer may require only that the test piles carry, without excessive settlement, a load equal to the design load multiplied by an arbitrarily selected factor of safety. Such tests are known as *proof tests*.

## 52.3 Ultimate Loads and Safe Design Loads for Single Piles

### 52.3.1 Side Resistance and Point Resistance

In a general way, the term *ultimate load* or *bearing capacity* of a single pile indicates the load at which the settlement of the pile increases continuously with no further increase in load, or at which the settlement begins to increase at a rate far out of proportion to the rate of increase of the load. Whatever the load may be, it is carried partly by the resistance of the soil directly beneath the point and partly by side resistance, as indicated in Fig. 52.1a. Therefore, the ultimate bearing capacity  $Q_d$  can be considered rather arbitrarily to consist of two parts:  $Q_p$ , which is due to point resistance, and  $Q_s$ , which is due to side resistance. Hence,

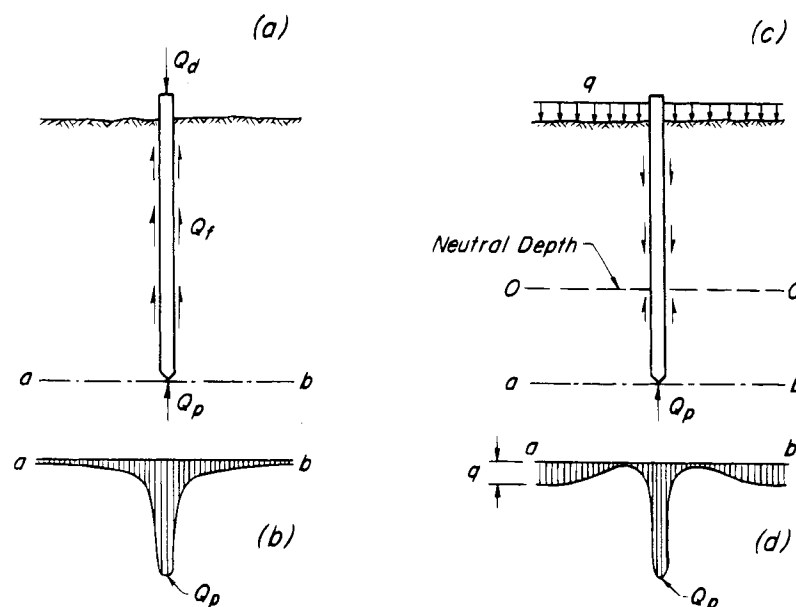


**Figure 52.1** (a) Loaded friction pile in soft clay. (b) Distribution of pressure on horizontal section through point of pile. (c) Unloaded pile in compressible soil settling under influence of surcharge  $q$ . (d) Distribution of pressure on horizontal section through point of pile.

$$Q_d + W'_p = Q_p + Q_s \quad (52.1)$$

where  $W'_p$  is the weight of the pile less the weight of the displaced soil. For driven piles  $W'_p$  is usually small in comparison to  $Q_d$  and will be neglected in the remainder of this article.

In Fig. 52.1b,  $ab$  represents a horizontal section through the point of the pile, and the shaded areas indicate the pressure on this section due to the load on the pile. The total pressure at ultimate bearing capacity is obviously equal to  $Q_d$ . Although various methods have been used to compute the distribution of this pressure, the results of the computations cannot be relied on, because all the methods are based on idealized assumptions concerning the homogeneity and stress-deformation properties of the soil. Authoritative information on the pressure distribution could be obtained by direct measurements, but so far no such measurements have been made. However, there is no doubt that the distribution depends not only on the dimensions of the pile, but also on the nature of the soil and the conditions of stratification. It is also likely to change appreciably with time.

Moreover, the distribution of pressure on section  $ab$  at loads less than the ultimate bearing capacity depends on the magnitude of the load with respect to the ultimate value and on the relative displacements between the pile and the surrounding soil. Under some conditions the side resistance is replaced by downward forces, known as *negative skin friction*, that may greatly increase the load on the point. Negative skin friction is illustrated in Fig. 52.1c. The pile, which carries no structural load, was

driven through a recently placed fill underlain by a compressible soil that is consolidating under the weight of the fill. Because the pile is less compressible than the surrounding soil, forces of friction and adhesion develop between the pile and the surrounding material whereby part of the weight of the surrounding material is transferred to the pile. The corresponding distribution of pressure on section  $ab$  through the point of the pile is shown in Fig. 52.1d. On account of the large pressure on the point, the pile may settle appreciably even though it is subjected to no external structural load. Because the soil alongside the pile is much more compressible than the pile itself, the dragdown forces on the upper part of the pile force the lower part to slip downward with respect to the adjacent soil. Consequently, there is a neutral depth above which negative skin friction occurs and below which the skin friction acts upward.

Figure 52.1c merely illustrates the phenomenon of negative skin friction. In practice the pile is likely to carry a structural load in addition to the dragdown force. Moreover, the consolidation of the adjacent soil may have a variety of causes including the increased compressibility of the soil due to the remolding associated with pile driving and the increase in effective stress caused by lowering the water table. Failure to recognize the potential for negative skin friction has been responsible for many examples of excessive settlement; indeed, recognizing the conditions under which it may develop is more important than the ability to estimate with precision the additional downward load or the amount of settlement.



### 52.3.2 Relations between Driving Resistance and Depth

If the depth to which a pile has penetrated is plotted against the number of hammer blows per unit of penetration, a resistance diagram is obtained. Typical diagrams are shown in Fig. 52.2. The shape of the penetration curve indicates almost unmistakably into which of the three main categories the pile belongs. Figure 52.2a shows curves typical for piles driven into loose and into dense sand. In both types of sand the penetration resistance increases with depth. On the other hand, the pile represented by Fig. 52.2b was driven through soft clay, and the penetration resistance became practically constant. The sharp break in the curve in Fig. 52.2c indicates that the pile point passed from soft silt into a fairly dense sand. Such a break is typical for point-bearing piles. Figure 52.2d represents the depth-resistance curve for a pile driven through fill and peat into a sand stratum containing layers and pockets of clay. The curve consists of inclined sections such as *ab* followed by nearly vertical ones. The abrupt transitions may indicate the passage of the point of the pile from sand into soft silt or clay; if the soil below the level of point *b* had been similar to that above it, the curve would have continued as indicated by the dash line *bc*. Because the depth-resistance curve has several steps, the point of the pile evidently passed through several lenses or layers of sand alternating with soft clays. Quite similar abrupt transitions may be caused by the passage of the point of the pile from dense layers of sand into loose ones. By correlating the resistance diagrams with the soil profile on a given job, a reliable conception can usually be obtained of the material in which each pile is embedded. In particular, one can determine whether the point of the pile has reached a suitable bearing stratum.

### 52.3.3 Use of Pile-driving Formulas for Estimating Ultimate Bearing Capacity

When a point-bearing pile encounters a firm stratum, the penetration resistance increases sharply (Fig. 52.2c). In a general way, the greater this increase, the greater is likely to be the point resistance of the pile. This observation has led to various attempts to express the relationship between the bearing capacity of a pile and the resistance to penetration just before driving is discontinued. The results are known as pile-driving formulas (Article 34.3.1).

In every such formula the calculated ultimate bearing capacity depends on the penetration *S* under the last blow of the hammer. According to Fig. 52.2b, for instance, the value of *S* that appears in the formulas would, for friction piles in clay, be practically independent of depth. As a result, application of any of the formulas would lead to the conclusion that the ultimate bearing capacity of such piles is also independent of depth. However, experience has shown that the ultimate bearing capacity of friction piles in clay increases approximately in direct proportion to the length of the piles. This fact alone demonstrates that no pile-driving formula is applicable to friction piles in soft silt or clay. As a matter of fact, in cities where the prevalence of thick deposits of soft soils calls for extensive use of friction piles, no experienced engineer even considers using a pile formula. Instead, the bearing capacity is estimated on the basis of empirical values for the average skin friction per unit of area, and the point resistance is disregarded. If a more reliable estimate is needed, load tests are made.

Even for point-bearing piles and other piles for which the penetration resistance increases with depth, the agreement between the real ultimate bearing capacity and that computed on the basis of any one of the pile-driving

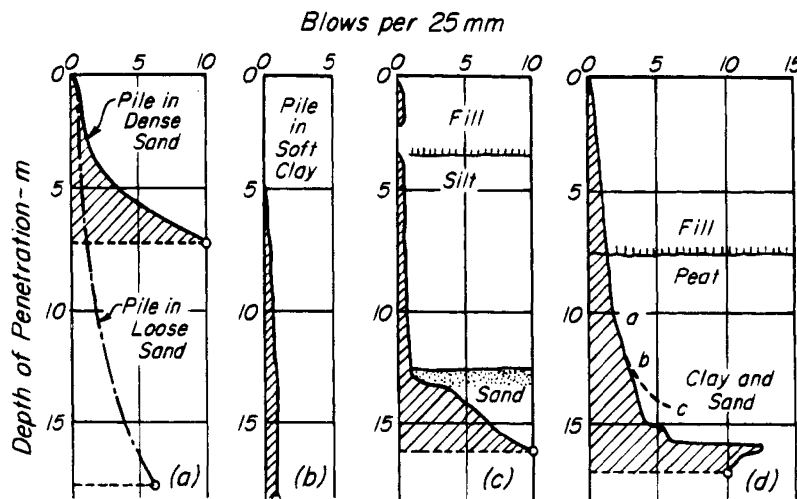


**Figure 52.2** Relation between blows per 25 mm of penetration and total depth of penetration for wood piles driven into subsoils of various characteristics.

formulas is, in general, so poor and erratic that it does not justify continued use of these formulas except under limited circumstances. These circumstances should be restricted to well-defined geologic settings where many load tests have been made on piles of the types and general dimensions being considered and where one or another of the pile-driving formulas has been found to predict capacities in reasonable agreement with experience and the results of the load tests.

#### 52.3.4 *Use of Wave Equation in Design*

Dynamic analyses by means of the wave equation (Article 34.3.2) are useful in two ways: (1) they provide the designer with much general insight into the factors governing the choice of pile type and driving equipment and the capacity that can be developed at various lengths of embedment once the pile profile has been established; and (2) they permit estimates of pile capacity on the job on the basis of field measurements during pile driving. The first use is a design function and is discussed in the following paragraphs; the second is a part of construction control and is considered in Article 52.3.6.

In contrast to the pile-driving formulas, which have an unsound theoretical basis, wave equation analyses take rational account of the principal factors that influence the bearing capacity of a pile. For example, the influence of the type of pile in many of the more elaborate pile-driving formulas is incorrectly characterized by the ratio of the weight of the pile to that of the hammer; the greater the ratio the less the predicted capacity. In contrast, wave analysis demonstrates that the property of the pile that limits the force that can be transmitted to the point is its impedance  $pcA$  (Article 34.3.2). Other factors being equal, the greater the impedance, which is proportional to the weight per unit length of the pile, the greater the potential for obtaining a high capacity with a particular hammer. For example, if the impedances of various types of cylindrical piles, all having the same external diameter of 254 mm, are compared to the impedance of a timber pile of the same cross-section, it is found that a steel pipe with a 7.1-mm wall can be driven to 1.9 times the capacity of the timber pile. Corresponding ratios for a steel pipe with a 9.2-mm wall, a precast concrete pile, and a 7.1-mm pipe filled with concrete are 2.3, 3.1, and 4.6, respectively. The influence of filling the pipe with concrete is notable.

The force actually developed at the tip of a pile, however, depends not only on  $pcA$  but also on the energy that can be furnished by the hammer and on a wide variety of other factors including: (1) the nature of the impulse delivered by the hammer; (2) the stress-transmission characteristics of the cushions and pile-head assembly; (3) the general pattern of distribution of the resistance exerted by the soil along the pile; and (4) the proportion of the

total resistance developed along the sides of the pile in comparison with the resistance beneath the point.

Hammers differ greatly in the manner in which they deliver energy to the anvil or hammer cushion. Diesel hammers exert very brief peak forces followed by forces of relatively great duration in comparison with those exerted by steam hammers. The total energy actually transmitted by a hammer can best be ascertained by continuous measurement of the velocity of the ram as it approaches the pile, reverses direction, and rises again. Such measurements have shown that the efficiency of poorly maintained or improperly operated hammers may be extremely low.

To prevent damage to both the hammer and the pile, cushion blocks are almost always inserted between hammer and pile. For the most satisfactory results, the type and dimensions of the cushion block and the characteristics of the hammer should be chosen to satisfy two criteria: (1) to develop a peak driving force in the pile equal to 1 to 1.5 times the desired ultimate capacity without overstressing the pile; and (2) to transmit an adequate amount of energy to the pile. The second requirement leads to economy in driving; it sometimes must be sacrificed to achieve the first. Various combinations of hammer, cushioning, and pile can be investigated by wave analyses to determine the best means for achieving the desired capacity or, in many instances, to determine whether a particular pile is capable of developing the capacity under the action of a particular hammer. The advantage of making such determinations in the office, before carrying out expensive field work, is obvious. Indeed, the ability to make the studies places an obligation on the designer to check whether the proposed requirements are compatible with the specified type of pile and other conditions. This use of wave analysis is by far the most valuable contribution of the technique to foundation engineering.

The properties of the soil obviously play a major role in the behavior of the pile during driving. However, in making a wave analysis it is not usually necessary to assign specific numerical values to the point resistance and the side resistance; it is sufficient to estimate the fraction of the total pile resistance likely to be developed by point resistance and to assume the manner in which the side resistance is distributed along the pile. In addition, estimates must be made of the damping factors associated with the viscous or velocity-dependent resistance of the soil alongside and beneath the point of the pile (represented by the dashpots in Fig. 34.3) and of the recoverable or elastic downward movement (quake) following each blow of the hammer. These quantities can be evaluated from the results of measurements, but it is not practical to do so on a routine basis. Instead, they are assigned empirical values that have been found generally satisfactory, although in some instances they require adjustment

to achieve agreement between calculated and observed resistance-penetration records.

The results of a calculation for a given pile under particular soil conditions, driven by a specified hammer, may be expressed by plotting the ultimate static resistance as a function of the resistance to penetration in blows per unit of penetration. A second quantity of significance, the maximum stress in the pile, may also be computed as a function of the resistance to penetration. The results of such a calculation are shown in Fig. 52.3 for a steel pipe pile having the characteristics shown in the figure. It was assumed that 50% of the pile resistance was carried by the tip and that the remaining 50%, carried by skin friction, was distributed uniformly along the length of the pile. It was further assumed that the pile was driven by a No. 1 Vulcan hammer operating at 70% efficiency. A cushion block consisting of alternate disks of aluminum and micarta was postulated.

The solid curve in Fig. 52.3 represents the ultimate resistance as a function of the blows per 25 mm during driving. The curve applies strictly only to the specific length and embedment for which the calculation was made, but the results are rather insensitive to changes in length and only small errors are introduced even at substantially different lengths. On the assumption that the dynamic driving resistance is equal to the static resistance, the curve represents the ultimate capacity of the

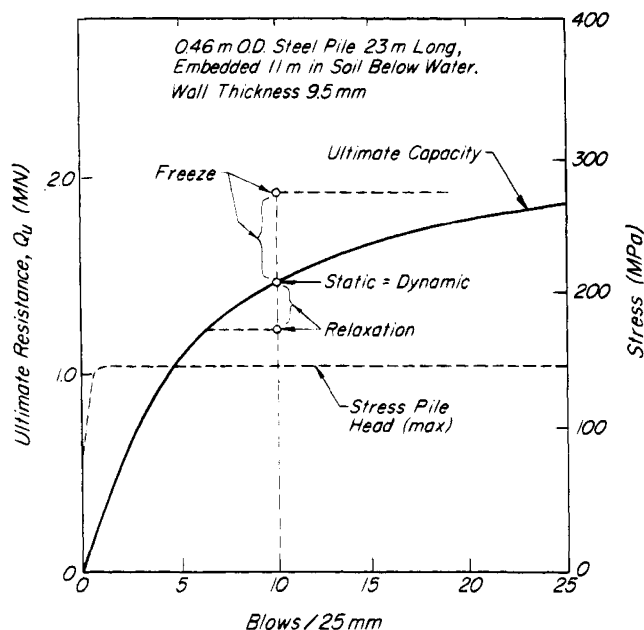


**Figure 52.3** Resistance curve from dynamic analysis of steel pipe pile by application of wave equation. Soil reaction assumed to be 50% at tip, 50% side friction distributed uniformly along 11 m embedded length. Driven by No. 1 Vulcan hammer operating at 70% efficiency, with aluminum-micarta cushion block (after Davisson 1970b).

pile if driven to a given penetration resistance. At 10 blows/25 mm, for example, the ultimate resistance is indicated as 1.50 MN.

If a load test were to be made on the pile and if the static resistance were equal to the dynamic resistance, the test load at ultimate capacity should correspond to the computed load of 1.50 MN. In some types of ground the capacity tends to increase after driving. This phenomenon is known as *freeze*; its effect is to increase the capacity, as shown in the figure. On the other hand, in some materials stress *relaxation* occurs and the capacity after driving decreases. The occurrence of freeze or relaxation is significant in design and can be investigated by means of a calculation, such as that indicated in Fig. 52.3, together with the results of a load test. After the magnitude of freeze or relaxation has been ascertained in this manner, the information can be used to modify the computations that might be carried out for piles of other dimensions, materials, or driving conditions at the site.

During driving, the resistance of the soil along the sides of the pile is likely, because of the continued disturbance, to be a minimum. However, it is not, in general, equal to zero. The side resistance during driving plus the subsequent freeze would be numerically equal to the total side resistance on the single pile, if the static point resistance did not change before the load test was made. Not infrequently, however, the point resistance during driving exceeds that which can be developed later. If relaxation decreases the point resistance, the increase of load ascribed to freeze in Fig. 52.3 is the sum of the increase in side resistance and the decrease of the point resistance after driving. Thus, freeze is not due exclusively to side resistance; it may be a combination of changes in side and point resistance. Figure 52.3 also shows that for any driving resistance the stress in the pile is on the order of 150 MPa, a value well below the yield point of the material. Therefore, in this instance, driving should not damage the pile.

Studies with the wave equation demonstrate clearly that, except for the influence of freeze and relaxation, the attainment of a specified capacity by a particular pile in a given soil depends partly on the impedance of the pile and partly on the success with which pile, cushioning, and hammer are matched. The system must effectively transmit the driving energy to the point, and it must also keep the driving stresses within safe limits with respect to failure or crippling of the pile.

For a particular combination of pile, hammer, and cushioning, the relation between ultimate driving resistance or capacity and blows per unit of penetration, as exemplified by the resistance diagram (Fig. 52.3), is practically independent of the soil conditions, inasmuch as the influence of the soil profile is reflected only in the effects of quake and damping and of the ratio of point to side resistance. The soil conditions, on the other hand, largely

determine the penetration of the pile per blow and are thus implicitly contained in the driving record for the pile. If the efficiency of the hammer on the job is equal to that assumed in the calculation, but the penetration per blow is not as small as that corresponding to the required capacity, the soil conditions are not adequate for the support of the pile as driven.

### 52.3.5 Determination of Bearing Capacity by Load Test

In principle, the ultimate bearing capacity of a pile can be determined by increasing the vertical load on the pile until failure occurs; the load at failure is the ultimate bearing capacity. In practice, so decisive a result is obtained only for piles under a limited set of soil conditions. In soft clays extending to a depth greater than the embedment of the pile, for example, the settlement of the head of the pile is likely to increase modestly with increasing load until either the pile plunges, if the applied load consists of dead weights, or the pile moves downward under a constant or even a decreased load, if the load is applied by jacking. Under these circumstances, no interpretation is necessary to establish the value of the ultimate bearing capacity. Under most other conditions, however, the settlement of the top of the pile increases at an increasing rate with respect to the increase in load until it becomes obvious that the settlement would be intolerable for the supported structure even if the resistance of the pile to penetration would continue to increase. Under these circumstances, some reasonable but arbitrary criterion must be chosen to establish the value of the ultimate bearing capacity. Because many such criteria have been proposed, and because the load-settlement curve for a given pile is itself somewhat dependent on the test procedure, even a full-scale pile load test leaves room for interpretation in establishing the bearing capacity of the pile. For the same reason, the definition of factor of safety against the bearing-capacity failure of a single pile is somewhat arbitrary.

In spite of these limitations, a load test remains the only definitive way to establish the ultimate bearing capacity of a single pile. The need for such tests arises under two circumstances: in design, to determine whether the designer's estimate of capacity and length for the piles to be specified is appropriate; and during construction, to determine whether the production piles meet the specifications. Because the designer wishes to ensure a certain factor of safety, the ultimate bearing capacity must be determined unless it is so great that other factors would limit the design load per pile. Under these circumstances the test might be carried to a load equal to only twice the anticipated load per pile. During construction, only proof tests may be required in which, again, the load may be carried to a value that, in the designer's judgment,

ensures adequate capacity in view of the probable variation among all the piles on the job.

The equipment and procedures for conducting pile load tests have been developed and refined over the years and are set out in standard specifications such as ASTM D1143. In many jurisdictions the required procedures are incorporated in the building codes. The details, especially those concerning the recording of all pertinent details of the installation of the test pile, should be carefully observed. In addition, acceleration and strain measurements near the head of the pile may be made to permit comparison with a wave analysis and to aid in evaluating other piles on the job that may not be subjected to load tests.

Several different loading scenarios are in common use. The most information, which includes an indication of the extent to which the settlement under the working load is elastic, is obtained from the conventional or *Slow Maintained Load* (SML) test. The SML test is presently the most widely used procedure; it is also the most time consuming. In the SML test the load is applied in increments, usually by jacking against a reaction. Under each increment the settlement of the head of the pile is observed as a function of time until the rate of settlement becomes very small. A new increment is then added. As the capacity of the pile is approached, the size of the increments is decreased to permit better definition of the load at which the capacity of the pile is reached. The rise of the head of the pile is measured when the load is removed. The settlement of the tip should also be measured if the type of pile permits.

The results of typical SML load tests are shown in Fig. 52.4 in which the total load is plotted as a function of the settlement of the pile head. Curve *a* represents a pile that plunged suddenly when the load reached a definite value termed the *ultimate pile load* or *pile capacity*. Curves *b* and *c*, on the other hand, show no well-defined breaks; consequently, the determination of the ultimate pile load is to some degree a matter of interpretation. A convenient procedure (Davisson 1973) that eliminates personal bias and takes account of the significant variables is illustrated in the figure. The elastic deflection of the pile is computed by means of the expression  $PL/AE$  and plotted on the load-settlement diagram as line  $OO'$ ; for the best interpretation the scales of the diagram should be chosen so that the slope of  $OO'$  is about  $20^\circ$ . The line  $CC'$  is drawn parallel to line  $OO'$  with an intercept on the settlement axis equal to  $(4 + 8d) 10^{-3}$  m where  $d$  is the diameter of the pile in meters. In the English system of units the intercept is  $(0.15 + 0.1d)$  inches, where  $d$  is in feet. The intercept is a measure of the tip settlement required to develop the capacity. The ultimate load is defined as the load at which the line  $CC'$  intersects the load-settlement curve. This criterion is applicable to load-settlement records obtained from tests in which each load

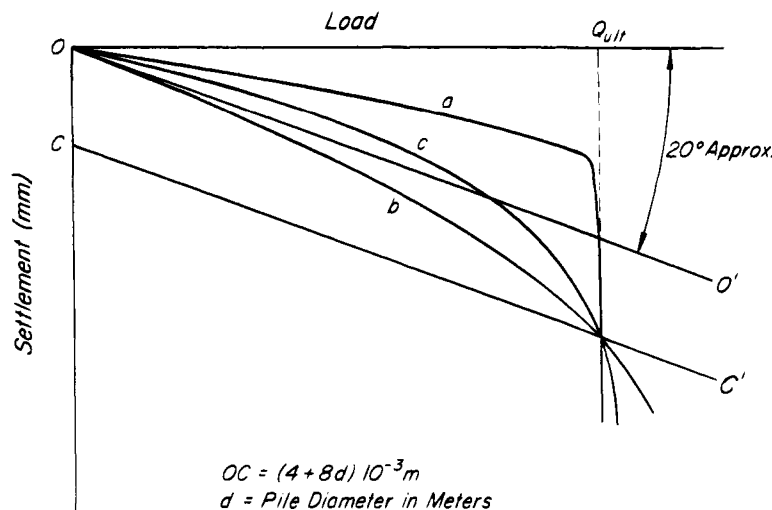


**Figure 52.4** Typical results of load tests on (a) friction pile; (b) end-bearing pile; (c) pile deriving support from both end-bearing and friction.

increment is held for periods not exceeding 1 h. It may be overly conservative, however, for load-settlement records based on holding periods of 24 h or longer, if creep or consolidation settlements at the tip become significant portions of the total.

The cost of a load test depends greatly on its duration, especially if the job is delayed while the results are awaited. Specifications that require maintaining the final load (usually twice the design load) for several days are rarely justifiable. In most instances the performance under twice the design load in 24 h or more can be judged by applying 2.25 times the design load for 1 h, or by raising the load in a proof test to failure or to the limits of the equipment.

The duration of a load test can be shortened substantially by using either the *constant rate of penetration* (CRP) or the *quick maintained load procedure* (QML). In the CRP test the applied load is increased to maintain a constant rate of penetration, measured at the head of the pile, of about 0.75 mm/min for cohesive soils or about 1.5 mm/min for granular soils. The load is increased until maintaining the specified rate of penetration requires no further increase in load; the corresponding total load is considered the ultimate bearing capacity. In the QML test, the pile is loaded at intervals of 2.5 min in increments of about 15% of the estimated design load until continuous jacking is required to maintain the load; as before, the maximum load is considered to be the ultimate bearing capacity.

In a conventional load test the load is applied to the head of the pile by jacking against a reaction. The reaction is furnished by dead weights supported on a platform above the test pile or by a beam or structural frame attached to anchor piles driven on each side of the test pile. Either arrangement is cumbersome and, especially

for very large loads, presents safety hazards unless the design and execution are expertly done. These disadvantages may be avoided in testing displacement piles of circular or square cross-section by use of the *Osterberg load cell* (Osterberg 1989), a fitting that in effect constitutes the lowermost portion of the pile. It contains a hydraulic jack or bellows driven as part of the pile to the desired depth or resistance. The bellows is then activated, whereupon its lower part forces the base of the pile downward, and its upper part applies a force of the same magnitude that tends to lift the shaft of the pile. The force and the movements of the tip and top of the pile are measured independently; the data permit plotting the load-settlement relation for the point of the pile and the load-rise relation for the shaft. The point load can be increased until the point-bearing capacity is reached or until the reaction provided by the side resistance of the shaft is exceeded. Under the first circumstance, the test establishes the value of the point resistance and a lower limit for the shaft resistance. Under the second, the test establishes the ultimate shaft resistance and a lower limit for the ultimate point resistance. This information is often adequate for validating the design. On completion of the test the bellows in its extended position is filled with grout to maintain the point resistance developed during the test. Steel pipe piles are readily fitted for the Osterberg cell; concrete piles must be cast with a hole along the axis to accommodate the necessary hydraulic lines and measuring devices.

### 52.3.6 Use of Wave Equation for Estimating Ultimate Bearing Capacity

The widespread use of pile-driving formulas in spite of their known shortcomings arose from the designer's need to be able to assign a capacity to each pile before the

design drawings were completed and construction commitments made. By requiring that each pile be driven to the resistance corresponding to the postulated ultimate load in accordance with a particular formula, the designer could transfer the responsibility for the foundation to the constructor. Moreover, if the specification were satisfied, the constructor could also claim freedom from liability if the foundation proved to be unsatisfactory. These non-technical advantages of the use of pile-driving formulas were powerful reasons for their use.

Moreover, by and large, the practice of relying on pile-driving formulas for all but friction piles in clay was successful; relatively few pile foundations failed because the bearing capacity of individual piles was exceeded. This relative success had several causes including the high factor of safety inherent in most of the formulas, which implies overconservatism and excessive costs, the high  $pcA$  values for many piles, and the ability of engineers to make reasonable assessments of the capacity of various piles on the basis of the soil profile. The latter ability remains an important asset, and the contribution of soil mechanics to its enhancement is discussed in subsequent sections of this article. Nevertheless, an unfortunately large minority of unsatisfactory pile foundations was associated with reliance on pile-driving formulas even with the exercise of judgment based on broad knowledge of soil behavior.

In the past, the only assurance that individual piles in a foundation would perform as anticipated lay in carrying out one or more pile load tests with their inherent expense and potential for delay. In the attempt to avoid these drawbacks, there has been an increasing tendency to carry out field measurements from which wave analyses can be made for production piles. Whereas before a pile is driven, the hammer-cushion model (Fig. 34.3) is needed to evaluate the input to the pile, measurements during driving can establish the actual input as a function of time. The force is measured by means of accelerometers mounted near the top of the pile, and the axial strain is measured in the same cross-section. These data can be used as input into a mathematical model of the pile-soil system and subjected to a wave-equation analysis with the aid of a computer program such as CAPWAP (Rausche et al. 1972). The output includes the driving resistance as indicated by the number of hammer blows per unit of penetration of the pile. If the calculated driving resistance differs from the measured resistance, the soil parameters used in the analysis can be adjusted until agreement is reached. Thus, the analysis would appear to have the potential for predicting pile capacity more reliably than a wave analysis using the hammer-cushion model. Experience indicates that this potential is not necessarily realized, inasmuch as the combination of soil parameters used successfully to predict capacity of one production pile on a given job may not prove successful for another.

With currently available measuring and data-processing equipment, neither a conventional wave analysis nor CAPWAP can calculate a predicted pile capacity rapidly enough to display the capacity blow by blow at the time of driving. To provide this ability, the Pile Driving Analyzer (PDA) has been developed (Rausche et al. 1985). Known as the Case Method, the procedure indicates the pile capacity associated with each blow of the hammer. To reduce the time for data processing and calculation and thus to make possible real-time readout, an algorithm is programmed into the equipment that uses the field measurements together with empirical input factors. Use of the factors, empirically related to the type of soil, has led in many instances to satisfactory agreement with the results of load tests, but exceptions have not occurred infrequently. Consequently, without corroborative load tests, use of the PDA cannot be considered a fully dependable means for determining pile capacity.

Although determination of pile capacity by use of the wave equation or procedures derived from such analyses has often led to satisfactory foundations on the basis of a nominal factor of safety of 2, notable exceptions have occurred. A comparison of capacities for five piles at one site is shown in Fig. 52.5 (data from Davisson 1991). All piles, of medium to long length, were of prestressed concrete and were driven with an open-top diesel hammer. Piles 1, 2, and 5 were believed to terminate in dilatant material in which temporary pore pressures could develop during driving, whereas piles 3 and 4 extended into underlying soils not likely to dilate. According to the figure, pile 1 would have failed if designed for a factor of safety of 2 by any of the predictive methods, and pile 5 would have fared only marginally better. On the other hand, on the basis of the PDA, pile 3 would have been appreciably overdesigned. It is also evident that there was no systematic order in the degree of conservatism associated with the three predictive procedures. Therefore, it can be concluded that dynamic measurements are not a reliable substitute for pile load tests (Selby et al. 1989). On a given job, however, use of the Pile Driving Analyzer can be an effective means for relating the capacities of production piles to those of piles on which both static load tests and dynamic measurements have been made.

### 52.3.7 *Single Pile Entirely in Sand*

When a single pile is driven into very dense sand, refusal against further penetration is met at a shallow depth, whereas in very loose sand, piles can be driven to great depth without encountering appreciable resistance. Irrespective of the relative density, part of the resistance is derived from point bearing and part from skin friction. The total resistance, like that for a prismatic or cylindrical pier, may be expressed by Eq. 34.1.

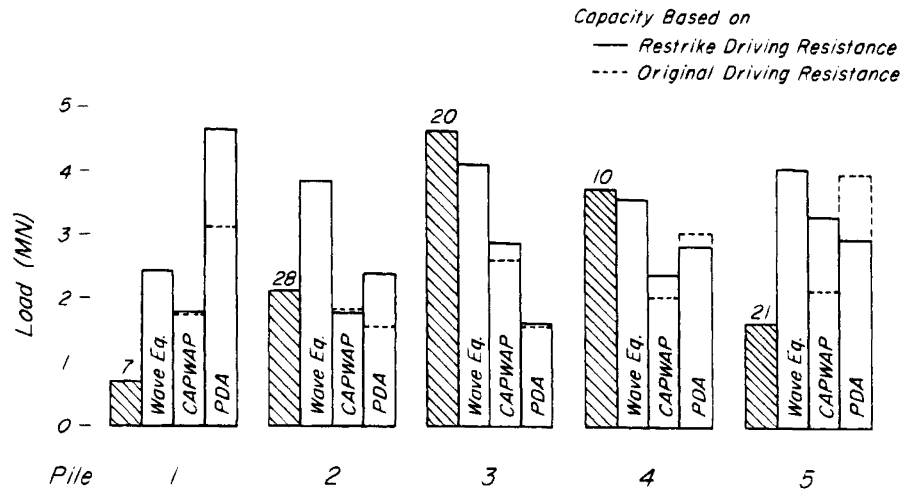


**Figure 52.5** Comparison of pile capacities of 5 precast concrete test piles on same job, as determined by load test (hatched areas) and as determined by wave equation, CAPWAP, and pile driving analyzer (PDA). Numerals above load-test values indicate final driving resistance in blows per 25 mm (after Davisson 1991).

$$Q_d = Q_p + Q_s = q_p A_p + C f_s D_f \quad (34.1)$$

As for a shallow foundation, the bearing capacity of the point per unit of area is given by  $\sigma'_{vb} N_q$  where  $\sigma'_{vb}$  is the vertical effective pressure at tip or base level and  $N_q$  is a bearing capacity factor. However, because the soil beneath the tip is displaced outward and upward, shearing stresses are induced in the soil above tip level; these stresses alter the shear pattern below tip level with respect to that for a shallow footing and increase the value of  $N_q$  to  $N_q^*$  as described by Berezantzev (Article 34). Moreover, the skin friction varies along the length of the pile. If at any depth the skin friction per unit of area is assumed to be equal to

$$f_s = K \sigma'_v \tan \delta \quad (52.2)$$

where  $K$  is the ratio of effective lateral to effective vertical pressure,  $\sigma'_v$  is the effective vertical pressure at depth  $z$ , and  $\delta$  is the angle of friction between pile and sand, then Eq. 34.1 becomes:

$$Q_d = \sigma'_{vb} N_q^* A_p + C \int_0^{D_f} K \sigma'_v \tan \delta \, dz \quad (52.3)$$

If Eq. 52.3 is used to evaluate the ultimate bearing capacity of a pile in sand by introducing the assumptions that  $\sigma'_v$  is equal to the effective overburden pressure at depth  $z$  and that  $K$  and  $\delta$  are constants, both  $Q_p$  and  $Q_s$ , and thus  $Q_d$ , should increase directly with the depth of penetration of the pile. In contrast, model tests (Kerisel 1961, Vesic 1967) and load tests on full-scale piles (Vesic 1970, Tavenas 1971) have shown that  $Q_d$  increases linearly with depth only until a *critical depth* is reached, below which it increases much more slowly or becomes practically constant. For a cylindrical pile the critical depth appears to depend on the diameter  $d$  of the pile and on the initial

relative density of the sand. If the sand is initially loose, the ratio  $D/d$  at which the critical depth is reached may be as small as about 7; if the sand is dense, the ratio may be as great as about 20.

Whereas the relatively small or negligible increase of total capacity below the critical depth has been well established by driving single piles to incrementally greater depths and testing the piles to failure after each increment, information regarding the distribution of skin friction as a function of depth or regarding the relative fractions of the total load carried by skin friction and point resistance is far less satisfactory. The data have been obtained by measuring the vertical strains at various depths in instrumented piles during load testing. From the strains and the moduli of deformation of the piles, the amount of the applied load remaining in the piles at these depths and, consequently, the load transferred to the soil by skin friction can be calculated. Unfortunately, in most of the studies reported in the literature up to the early 1970's, the initial strain readings were considered to be those at the start of loading of the test piles. Residual stresses in the piles associated with their installation were not accounted for (Hunter and Davisson 1969). Because the soil beneath and alongside the lower part of a pile experiences elastic rebound after each blow of the hammer, the lower part of the pile tends to be lifted by a combination of upward pressure on the point and upward skin friction. The upper part of the pile then tends to slide upward with respect to the surrounding soil and is thus subjected to downward skin-friction. The pile reaches equilibrium when the sum of the upward skin friction and point pressure equals the downward skin friction. These forces may be quite large, as shown by Fig. 52.6, which represents the results of measurements on a cylindrical precast con-

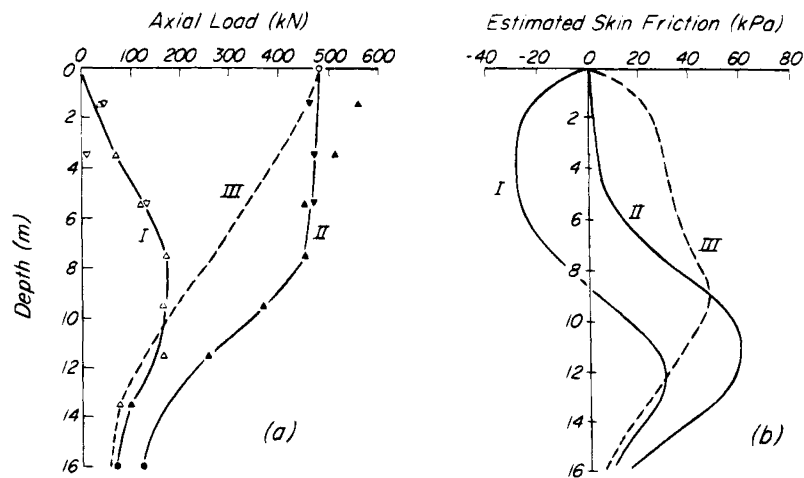


**Figure 52.6** Results of load tests on prestressed concrete pile 0.28 m diameter and 16 m long driven in loose, medium to coarse sand in Norway: (a) axial load in pile after driving (I) and after application of test load (II); (b) skin friction under same conditions. Curves III represent values of axial load and skin friction that would have been deduced from observations if residual stresses (I) had been ignored. The difference between curves II and III in each diagram represents the error due to ignoring the residual stresses in the pile (after Gregerson et al. 1973).

crete pile 16 m long driven into a loose sand in Norway. The figure also shows the incorrect values of axial load, point resistance, and skin friction that would have been deduced from the measurements if the residual stresses had not been taken into account. Insight into the mechanism can be gained from dynamic wave analyses (Darrag and Lovell 1989), together with estimates of the stresses under idealized conditions. In general, ignoring the residual stresses leads to an overestimate of side resistance and a corresponding underestimate of tip resistance.

Ordinary structures above dense sand, other than bridge piers subject to scour and structures subject to uplift, seldom require pile support. In looser sands, piles may be installed to keep settlements within acceptable limits; such piles must also possess a suitable margin of safety against a bearing-capacity failure. The designer's main interest is to specify a pile that will develop the required capacity economically at a predictable depth of penetration. As a first step the designer needs to know the depths to which piles of different types can be driven into the sand by customary equipment and what the corresponding capacities will be. At this stage the best guide is a good knowledge of the relative density and stratigraphy of the sand deposit at the site coupled with knowledge of local driving experience or of experience elsewhere in similar deposits. If the subsurface investigation has disclosed the presence of some layers of sand that have a greater relative density than others, it is probable that some of the types of piles under consideration would attain the required supporting capacity in these layers; hence, a critical study of the soil profile as disclosed by penetration testing is a valuable aid. Yet, because the depth that can be attained

and the bearing capacity of the pile depend on many variables, such experience is not gained easily. It is not surprising, therefore, that even the most experienced engineers and pile-driving contractors occasionally misjudge the outcome.

Equation 52.3 may be generalized to allow for variations in dimensions and soil properties with depth by considering the piles to be subdivided into  $n$  sections of vertical length  $\Delta L$  and perimeter  $C$ , each in contact with sand of specific properties. Hence,

$$Q_d = \sigma'_{vb} N_q A_p + \sum_{j=1}^n [K \sigma'_v \tan \delta \cdot C \cdot \Delta L]_j \quad (52.4)$$

Although calculations based on this equation are straightforward and are carried out often, the results are likely to have little resemblance to reality, because the quantities  $K$ ,  $\sigma'_{vb}$ ,  $\sigma'_v$ , and  $\delta$  cannot be evaluated reliably. Some of the reasons are:

1. the coefficient of earth pressure  $K$  is not a constant but is influenced by the local displacement and compaction caused by insertion of the pile,
2. the effective vertical stress  $\sigma'_v$  is not the free-field overburden pressure  $\sigma'_{vo}$ , because the insertion and presence of the pile cause stress redistribution; this redistribution is analogous to the arching around an excavated shaft, and
3. the friction angle  $\delta$  between pile and soil is unlikely to be equal to that determined by direct shear tests of the pile material sliding on the sand because of rearrangement and crushing of the grains of sand next to the pile during pile driving.



Consequently, determination of the ultimate capacity of a pile in sand by means of a static formula such as Eq. 52.4 and physical properties determined by laboratory tests is not justified by logic. Nevertheless, the formula provides a basis for developing semiempirical procedures for estimating capacities by correlating experience gained from static load tests. With this aim, Dennis and Olson (1983*a, b*) assembled the records of all the load tests they could discover, on piles of various types in different soils, for which information of sufficient quality was available to justify statistical studies. Of these, about 100 provided data on the ultimate failure of piles in adequately described sand. The statistical analyses consisted of subdividing the data on the basis of the description of the sands and the type of pile, and of assuming sets of reasonable values for  $K$ ,  $\delta$ , and  $N_q$ . Upper limiting values were placed on skin friction and point resistance. Various combinations of the reasonable values were inserted into Eq. 52.4 until the combination was determined that led to a mean ratio of computed to measured capacities closest to 1.0 for all the tests and that displayed the least scatter.

For example, some 30 load tests pertained to cylindrical closed-ended steel piles. By taking  $K$  equal to 0.8 and by assigning reasonable values to  $\delta$  and  $N_q$  in accordance with the standard penetration resistances, Olson (1990) developed a table of soil properties (Table 52.1) for use in Eq. 52.4 that resulted in a mean ratio of computed to measured capacities of 1.00 and the small scatter indicated on Fig. 52.7. Similar analysis of a smaller number of parallel-sided precast concrete piles indicated that Table 52.1 and Eq. 52.4 can also be used for piles of this type.

Such a semiempirical approach, wherein load-test data are correlated by means of theory as represented by Eq. 52.4, appears to be a promising avenue for improving practice. It is evident, however, that the number of adequately documented load tests of good quality will need to be greatly increased to establish a more adequate data base for the statistical studies.

Numerous correlations and procedures have been proposed for estimating the capacity of piles in sand on the basis of various *in situ* or laboratory tests. Several of these have met with success where used under a limited range of conditions in limited geologic environments, because these limitations reduce the number of variables that control pile capacity. The cone penetrometer (Article 11.4.2) has been found to be particularly useful. Well-established local experience and methodology are valuable assets to the practicing engineer and should be used. A deeper understanding leading to general methods that take account of all the significant variables may have to await the broad data base and statistical studies discussed above.

Once a forecast of pile capacity is made for a given job, its validity should be checked by means of one or more load tests. The tests may be supplemented by

**Table 52.1 Soil Properties Used in Final Analyses**

Soil Type	Range in $N$ Values	$\delta$ (deg)	$f_{lim}$ (kPa)	$N_q$	$q_{lim}$ (MPa)
Gravel	0–4	(20)	(70)	(12)	(3)
	5–10	(25)	(85)	(20)	(5)
	11–30	(30)	(100)	(40)	(10)
	over 30	(35)	(120)	(60)	(12.5)
Sand/ gravel	0–4	(20)	(70)	(12)	(3)
	5–10	(25)	(85)	(20)	(5)
	11–30	(30)	(100)	(40)	(10)
	over 30	(35)	(120)	(60)	(12.5)
Sand	0–4	(20)	(50)	(50)	(2)
	5–10	30	55	120	6
	11–30	35	95	120	95
	31–50	40	130	120	9.5
	51–100	40	165	130	10
	over 100	40	190	220	26.5
Sand/ silt	0–4	10	(50)	(10)	(0.5)
	5–10	10	(50)	(20)	(2)
	11–30	15	(70)	50	5.5
	31–50	20	100	100	8
	51–100	(30)	(100)	(100)	(10)
	over 100	(34)	(1000)	(100)	(10)
Silt	0–4	(10)	(50)	(10)	(2)
	5–10	15	(50)	(10)	(2)
	11–30	20	(70)	(10)	(2)
	31–50	20	(70)	(12)	(3)
	over 50	(25)	(70)	(12)	(3)

Numbers in parentheses were not used in the analyses.

dynamic measurements for wave analyses to permit extrapolation of the load-test results to the remaining piles and to determine whether there is a loss of capacity due to relaxation after driving ceases. Unless the sand is below the water table and is fine enough to permit the accumulation of porewater pressures during driving, the effect of relaxation is likely to be small. In any event, control of the pile-driving operation is based on the relation between driving resistance and the number of blows per unit of penetration of the production piles as compared with the relation for the load-test pile or piles. Although this relation has traditionally been furnished by a pile-driving formula, the theoretically unsound basis (Article 34.3.1) and statistical unreliability of such formulas amply demonstrate that they should no longer be used. Information in the same convenient form is given by the results of a wave analysis as exemplified in Fig. 52.3. When calibrated to the driving records of the load-test piles, the results of the wave analysis can be used with confidence,

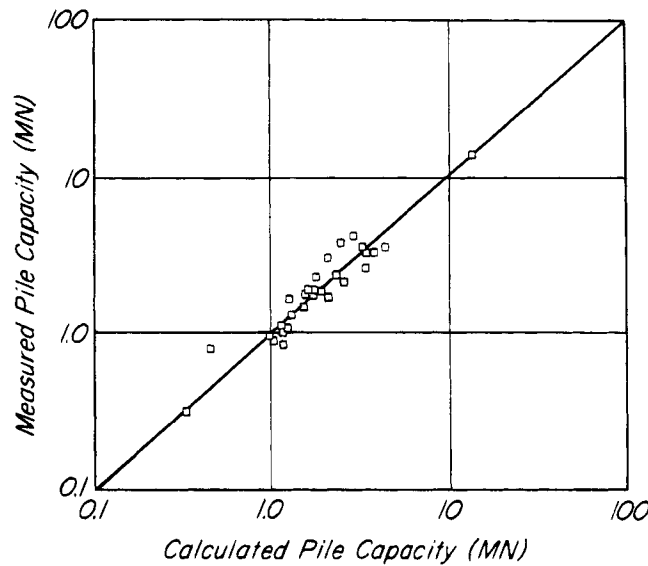


**Figure 52.7** Comparison of measured and calculated axial load capacities of driven steel piles (after Olson 1990).

provided that the efficiency of the pile hammer is the same for the production piles as for the load-test piles. The pile driving analyzer (Article 52.3.6) can be used similarly.

In many applications piles in sand must resist tensile or pullout forces. Although static calculations permit estimating the pullout resistance, the results must be interpreted with conservatism. The uplift forces transmitted by the pile to the sand reduce  $\sigma'_v$  (Eq. 56.3) and also have an influence on  $K$ . These effects are not understood fully. It is reasonable to expect that the total skin friction available to resist pullout would be less than that acting during downward penetration, although some statistical studies of the available data base have not confirmed this expectation (Dennis and Olson 1983a). Where uplift resistance is critical, pullout tests (ASTM D3689) should be conducted. They are relatively inexpensive.

The influence of taper on the bearing capacity of piles in sand can be approximated by replacing  $\tan \delta$  in Eq. 52.3 by  $\sin(\omega + \delta) \sec \omega$ , where  $\omega$  is the taper of the pile expressed as an angle. Because the circumference of a tapered pile changes with depth,  $C$  must be placed under the integral. On the basis of this expression and the values of  $\phi'$  estimated from standard penetration resistances, Nordlund (1963) interpreted the results of more than 60 load tests on piles with various tapers in sand. Although there was considerable scatter in the results, the increase in bearing capacity for a taper of  $1^\circ$  ranged from a factor of about 2.5 to 4 for sands ranging from loose to dense and for piles of equal average diameter; for a taper of  $0.5^\circ$  the factor correspondingly ranged from about 1.5 to 4.

Olson and Long (1989) were able to collect data from load tests on 18 pairs of piles in sand. The piles in each

pair were in close proximity and of the same length and average diameter; one pile was tapered, the other not. The geometry of the tapered piles was characterized by the ratio  $(D_{\text{top}} - D_{\text{bottom}})/D_{\text{bottom}}$ , where  $D$  is the diameter of the pile. Use of this ratio led to less scatter in the results than expressing the taper in degrees. The ratio of the capacity of the tapered pile to that of the untapered pile in a pair is shown in Fig. 52.8 as a function of  $(D_{\text{top}} - D_{\text{bottom}})/D_{\text{bottom}}$ . The results are comparable to those of Nordlund but are of more general validity because they do not depend on a determination or an estimate of  $\phi'$ . Nevertheless, the scatter of the results together with the small number of pairs of piles in the data base indicate the need for many additional similarly paired load tests before the influence of taper can be quantified reliably.

Some offshore drilling platforms are supported by piles driven into sands beneath depths of water of more than 150 m to design capacities as great as 18 MN. The design and construction of such piles have challenged and extended the state of the art. Initial predictions of the depth of penetration and capacity have usually been based on static calculations and Eq. 52.3. Usually the critical depth has been assumed to vary linearly as a function of relative density from about  $D_{cr}/d = 10$  for a loose sand to about  $D_{cr}/d = 20$  for a dense sand, and the value of  $\sigma'_{vb}$  for calculating the point resistance below the critical depth has been taken as  $\gamma' D_{cr}$ . The value of  $K$ , while certainly not less than  $K_0$ , has been based on judgment and has usually been considered equal to  $2K_0$  to allow for the compaction associated with a driven pile. For a steel pile  $\tan \delta$  has been taken as  $\frac{2}{3} \tan \phi'$ , and for a concrete pile as  $\tan \phi'$ , although statistical studies (Dennis 1982) have indicated little difference in  $\tan \delta$  for steel or

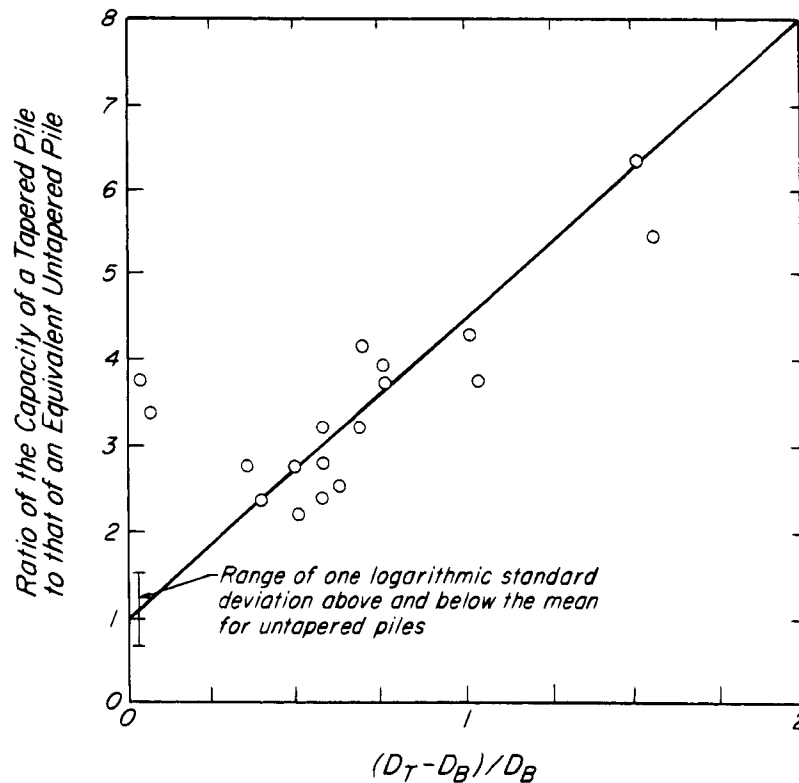


**Figure 52.8** Influence of the change in diameter on the capacity of tapered piles in sand (after Olson and Long 1989).

concrete piles. In addition, an upper limit of about 25 kPa for very loose sands and about 100 kPa for very dense sands has usually been imposed on the skin friction. The wave equation has been used extensively to assess whether a selected pile could be driven to the required resistance. In several instances it was found that no existing pile hammer could deliver the required energy; this finding led to the development and use of hammers of far greater capabilities than those available in the 1960's.

Most of the experience with friction piles in sand has been gained with siliceous materials or other particles of high crushing strength. However, extensive deposits of carbonate sands exist in which the grains consist largely of shell fragments and oolites, often weakly cemented at a high void ratio. Consequently, they are readily crushed near an advancing pile (Murff 1987). Such sands do not dilate significantly during shear and thereby cause an increase in frictional resistance around and beneath the pile. Limited experience suggests that the maximum skin friction on a pile driven in such materials may be less than 20% and the maximum point resistance as little as 50% of that exerted by a noncarbonate sand (McClelland 1974).

### 52.3.8 Single Pile in Sand below Weak Deposits

Piles are often driven through soft materials to obtain support in underlying sands. In general, the discussions in

the preceding section remain applicable, but considerably more data exist because a number of heavily industrialized cities are located above such deposits, and semiempirical procedures for design have been developed and validated by experience. Economy dictates that the piles should be no longer than necessary. In dense sands a high capacity can be achieved with a modest penetration, but to avoid great length in loose sands the piles, usually of precast reinforced concrete, are often provided with enlarged bases. Large parts of Belgium and Holland rest on thick deposits of peat or organic silts and clays underlain by sands; thus, it is no accident that the best-known procedures for exploration and design were developed in these countries beginning in about the 1930's. They make use of the cone penetrometer (Article 11.4.2), originally known as the Dutch cone.

All the procedures require vertical profiles of the cone resistance to establish the depth of the surface of the sand and the variations in point resistance  $q_c$  below the surface. In some methods values of  $\phi'$  are inferred from those of  $q_c$  (Article 19.1) and the pile capacity is calculated by the static analyses described in the preceding section. Simpler procedures are based on the premise that the cone resistance  $q_c$  per unit of area is equal to the point resistance per unit of area of a pile founded at the same depth. Such an equivalence requires that the tip of the

pile be embedded in the sand far enough to develop confining conditions above the tip comparable to those above the cone penetrometer, and that the properties of the sand in the stressed zone below the pile correspond to those of the stressed zone beneath the penetrometer. The significance of these requirements was investigated in detail by deBeer (1963).

Different investigators have proposed somewhat different procedures for using the results of cone penetration tests to predict the capacity of piles driven through weak strata to end bearing in sand. Perhaps the simplest, proposed by Van der Veen and Boersma (1957), averages the values of cone resistance from a distance of three pile diameters above the tip of the pile to one diameter below. To account for the scatter exhibited in the 15 load tests in Amsterdam on which the comparison was based, Van der Veen recommended use of a factor of safety of 2.5 with the pile resistance so determined. It is evident that the procedure recognizes that the properties of the sand surrounding the pile above the point are significant in determining the resistance of the pile to penetration. Variants of the Van der Veen procedure and limitations applicable under various conditions have been proposed (de Ruiter and Beringen 1978, Schmertmann 1978); several are summarized in Hunt (1986) and Tomlinson (1986).

If the soft materials above the sand are likely to consolidate after the piles are driven, the piles will be subjected to the added load of negative skin friction; they should be designed to resist the load or means should be adopted to reduce or eliminate it. The precast concrete piles with enlarged bases, mentioned previously, are advantageous in this respect.

The magnitude of the negative skin friction may be approximated as the product of the undrained shearing resistance of the surrounding material and the surface area of the pile above the bearing stratum. Experience has indicated that a very small relative movement between pile and soil is sufficient to develop the full dragdown force. More precise calculations are sometimes warranted. They take account of the location of the neutral depth (Article 52.3.1), the relation between permanent and transient working loads, and time effects (Fellenius 1972, Alonso et al. 1984).

### 52.3.9 Side Resistance on Single Pile in Saturated Clay

In contrast to a friction pile in sand, the point resistance of a pile embedded in soft clay is usually insignificant; it seldom exceeds 10% of the total capacity. The mobilized shear strength or side resistance per unit of contact area depends largely on the properties of the clay and except for very long piles does not depend strongly on the depth of penetration. It is also fairly independent of the method of installing the pile. The resistance against pulling is usually, but not always, nearly equal to the resistance

against further penetration under load. All these relations are much simpler than the corresponding ones for a friction pile in sand. On the other hand, the relations between side resistance and time are much more complex and as yet are unpredictable. The side resistance usually increases during the first few weeks after the pile is driven, but the amount of increase varies considerably with the nature of the soil.

The curve in Fig. 52.9 represents a somewhat exceptional increase in bearing capacity of a friction pile with time. The pile was driven into soft brown clay with streaks of silt. The liquid limit of the clay was between 37 and 45%, the plastic limit between 20 and 22%, and the natural water content slightly below the liquid limit. During the pile-driving operations the soil turned almost liquid, and the side resistance had a very small value. Although the piles penetrated 300 mm under a single blow, they rose 250 mm when the hammer was lifted, and a special device had to be used to prevent the piles from rising. Yet, within a month the side resistance increased to more than three times its initial value.

When a pile is driven into soft clay, the clay in the path of the penetrating pile is displaced and becomes severely distorted. After the pile is driven, the disturbed clay surrounds it like a shell (Cummings et al. 1950, Flaate 1972). Beyond the outer boundaries of this shell the disturbance of the soil structure is quite small. If a large number of piles is driven in a small area, the effects of disturbance may be cumulative and may extend well beyond the limits of the pile-driving operations. Consequently, settlements of adjacent structures have in some

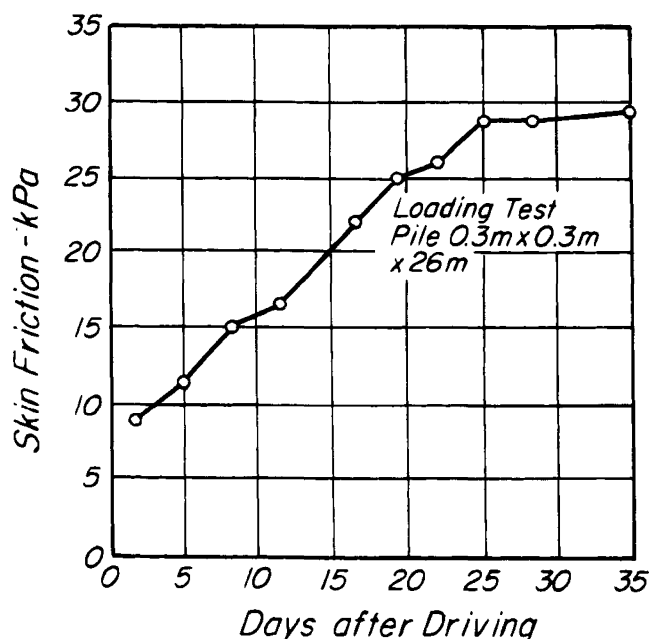


Figure 52.9 Diagram illustrating increase of ultimate bearing capacity of friction pile with time.

instances been induced (Casagrande 1947, Lambe and Horn 1965). On the other hand, the shell of badly disturbed clay around each pile usually consolidates rapidly and becomes stiffer than the undisturbed clay; it is likely to adhere to the pile if the pile is pulled. If a pile is driven into an extremely sensitive or quick clay, the shell of disturbed material is likely to be only a few centimeters thick and to behave like a liquid during pile driving. The displaced material flows upward along the pile to the surface (Leggett 1950) where it accumulates, but the soil outside the liquid shell remains virtually undisturbed. Within the shell the liquefied material regains strength by consolidation and thixotropy, but the final strength is not necessarily equal to that of the undisturbed soil.

Driving piles into saturated clay or silt produces a temporary increase in porewater pressure (Lambe and Horn 1965). In a silt, the excess pressures may temporarily liquefy the silt for a considerable distance. Yet, within a few days or weeks the silt may become as solid and stable as it was originally.

In spite of the influence of disturbance and the diverse time effects that take place immediately after a pile is driven into soft clay or soft plastic silt, the ultimate shear strength mobilized between clay and pile is approximately equal to the undrained shear strength from unconfined compression tests, averaged over the length of the pile, on samples of C quality. In stiffer clays the mobilized shear strength is smaller than  $\bar{s}_{uo}$  (UC), and the ratio

$$\alpha = \frac{\bar{s}_{uo} \text{ (UC)}}{s_u \text{ (mob)}} \quad (52.5)$$

decreases with increasing strength of the clay. The empirical correction factor  $\alpha$ , proposed by Tomlinson (1957), was used by Dennis and Olson (1983b) to analyze full-scale loading tests on steel pipe piles and untapered precast concrete piles driven into clays and silts and axially loaded in compression or tension. The set-up time between pile driving and loading was usually 2 to 4 weeks. The measured side capacity was obtained by subtracting from the measured pile capacity the calculated tip capacity, taken as  $9 \bar{s}_{uo}$  (UC) for the compression tests and zero for the tension tests. The values of  $\alpha$  are shown in Fig. 52.10, together with values computed by Stas and Kulhawy (1984) for cast-in-place drilled shafts in clays and silts, loaded in compression or tension. Because these values are applicable to data from specimens of C quality, they are underestimates for specimens of E quality (such as those recovered in deep water by driving samplers at the bottom of a wireline) and are overestimates for specimens of A quality.

Figure 52.10 can be used to estimate the mobilized side resistance of piles and shafts with penetration lengths less than about 30 m. As the length of embedment increases beyond about 30 m the value of  $\alpha$  decreases.

Piles of such great length experience significant elastic shortening that results in relatively small shear strain or slip at great depth as compared to that at shallow depths. Thus, the maximum shear strength at the interface is developed only over a limited length of the pile. Statistical studies suggest that for embedments greater than about 50 m values of  $\alpha$  from Fig. 52.10 should be multiplied by 0.56. For embedments between 30 and 50 m the reduction factor can be considered to vary linearly from 1.0 to 0.56 (Dennis and Olson 1983 *a,b*). The reduction is of consequence in the design of some types of offshore oil platforms that are supported by several single piles with embedded lengths of 50 to 200 m and diameters of 1 to 4 m driven into clays with values of  $\bar{s}_{uo}$  (UC) ranging from 24 to 700 kPa (Kraft et al. 1981).

Factors, other than the quality of  $\bar{s}_{uo}$  (UC) data and the length of embedment, that influence  $\alpha$  and the scatter in Fig. 52.10 include the degree of disturbance of soil caused by pile installation, the set-up time before the pile load test, the differences in mode and rate of shear, and progressive failure effects in the pile load test as compared with the unconfined compression test.

Several investigators (Chandler 1968, Burland 1973, Meyerhof 1976, Esrig and Kirby 1979) have proposed that the skin friction per unit of area on a pile in clay should be expressed in terms of effective stresses. For example, Burland proposed the expression

$$f_s = \beta \sigma'_v \quad (52.6)$$

On the assumption that the clay next to the pile is completely remolded, and thus that its cohesion intercept  $c'$  is zero and its effective angle of internal friction is  $\phi'$ , then

$$\beta = K_s \tan \phi' \quad (52.7)$$

where  $K_s$  is the final coefficient of earth pressure on the pile. If  $K_s$  is approximated by the coefficient of earth pressure at rest  $K_0 = 1 - \sin \phi'$ , then

$$\beta = (1 - \sin \phi') \tan \phi' \quad (52.8)$$

When average values of  $\beta$  are calculated on the basis of load tests on piles in soft to medium clay they are found to vary from about 0.1 to 0.5, with an average of 0.32, whereas laboratory tests would indicate values of 0.2 to 0.3. Moreover, values of  $\beta$  for short piles range from about 0.25 to 0.5, whereas those for very long piles range from about 0.10 to 0.25 (Meyerhof 1976). Thus, the  $\beta$  method also reflects empirically the influence of length of embedment.

On the assumption that the lateral pressure against the pile shortly after pile driving could not exceed the passive pressure at any depth, Vijayvergiya and Focht (1972)

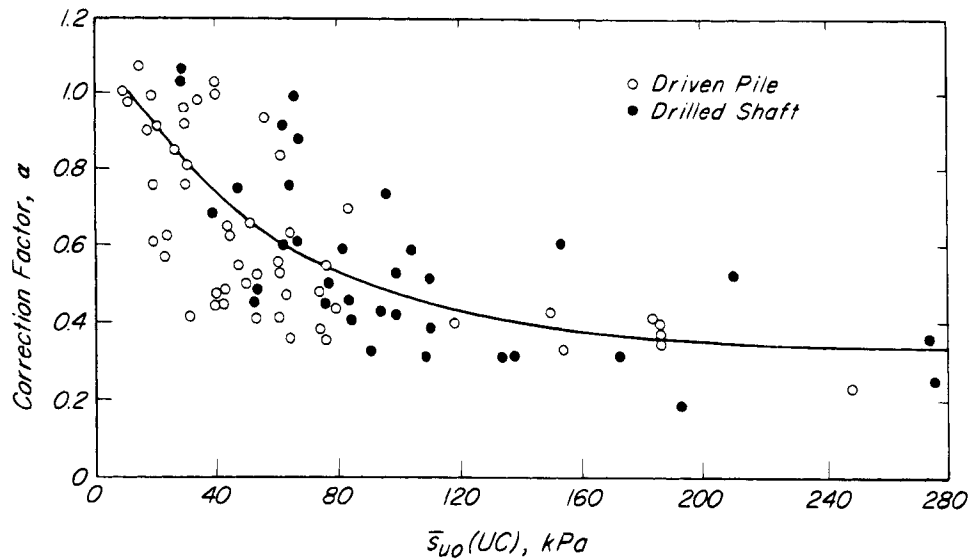


**Figure 52.10** Correction factor for  $s_{uo}$  (UC) from specimens of *C* quality for piles with penetration lengths less than 50 m in clay. (Data from Dennis and Olson 1983, Stas and Kulhawy 1984.)

suggested that the frictional resistance per unit of embedded area would be proportional to  $\sigma'_h$ . From Eq. 26.9

$$\sigma_h = \sigma_v + 2s_{uo} \text{ (UC)}$$

or

$$\sigma'_h = \sigma'_v + 2s_{uo} \text{ (UC)}$$

Assuming that the *in situ* effective vertical stress is not altered by pile installation

$$\sigma'_h = \sigma'_{vo} + 2s_{uo} \text{ (UC)}$$

Vijayvergiya and Focht proposed as the correction factor

$$\lambda = \frac{Q_s}{A_s} \frac{1}{\bar{\sigma}'_{vo} + 2\bar{s}_{uo} \text{ (UC)}} \quad (52.9)$$

where  $\bar{\sigma}'_{vo}$  and  $\bar{s}_{uo}$  (UC) are, respectively, the average values of effective overburden pressure and undrained shear strength along the pile length. This is an undrained strength stability analysis (USSA) method (Article 26). Because  $\bar{\sigma}'_{vo}$  and, in general,  $\bar{s}_{uo}$  (UC) increase with depth,  $Q_s$  inherently includes a length effect.

More recent efforts (Azzouz et al. 1990) have been directed to analytical and experimental studies of the coefficient  $\beta$  by expressing  $\beta$  as the product  $\rho K_c$ , wherein  $\rho$  is a dimensionless parameter representing the peak undrained shearing resistance corresponding to a unit normal effective stress acting on the shaft prior to shearing (analogous to the ratio  $s_u/\sigma'_p$ ), and  $K_c$  is a lateral earth-pressure coefficient corresponding to conditions after consolidation of the clay around the pile but before shearing. The coefficient  $\rho$  is fairly insensitive to the overconsolidation ratio of the deposit. The coefficient  $K_c$  is

influenced principally by the effects of installation of the pile on the stresses in the soil, including the manner of porepressure dissipation, and by the plasticity of the clay. Analytical models are being developed and refined to predict each component of  $\beta$  and techniques are being devised to measure the relevant pressures in the field as a function of time. The results are providing insight into the behavior and show promise of improved predictions, but development and evaluation of the procedures have not yet reached the stage of practical application. At present the empirical base for judging the relative merits of the several procedures is inadequate to demonstrate that any of them is clearly superior to the  $\alpha$  method.

#### 52.3.10 Action of Point-bearing Piles

In contrast to friction piles, point-bearing piles are assumed to transfer the load through their points onto a firm stratum. Nevertheless, a considerable part of the load is carried at least temporarily by side resistance. This has been demonstrated by load tests in both the laboratory and the field (Vey 1957, D'Appolonia and Romualdi 1963, D'Appolonia and Hribar 1963). However, if the pile passes through a very compressible soil such as soft silt or clay, the pressure transferred to the compressible soil by skin friction gradually consolidates it, and the pile consequently tends to settle. The settlement is resisted only by the soil in which the point is embedded and, as time goes on, the pressure on the point increases until the major part of the load on the pile is carried by the point. If the load assigned to the pile in the foundation exceeds the point resistance, the resulting settlement can be very large. Yet, the danger is not revealed by the results of a load test on a single pile, even if the load test is

applied for several weeks. Hence, it is more important to know the point resistance than the total bearing capacity of a point-bearing pile.

### 52.3.11 Evaluation of Safe Design Load

The term *safe design load*  $Q_a$  indicates the load at which the factor of safety with respect to a downward plunging or sinking of a single pile has a value consistent with the customary safety requirements.

Even if the ultimate bearing capacity has been determined by means of a load test, the factor of safety should not be taken as less than 2 because of uncertainties associated with the variation of subsurface conditions over the site, with differences in rates of loading during the load test as compared to the service loadings, and with the assignment of a value for the ultimate bearing capacity based on an interpretation of the load-settlement curve.

The general character of load-settlement curves ranges between the two extremes shown in Fig. 52.11. The curve in Fig. 52.11a is typical for friction piles embedded in coarse-grained soils and for point-bearing piles that transfer their load onto sand strata. Because the settlement curve gradually approaches an inclined tangent as the load on the pile increases, the ultimate bearing capacity must be assigned a value determined by a suitable convention such as that illustrated in Fig. 52.4. The safe design load on such piles should not exceed the ultimate bearing capacity divided by a factor of safety of at least 2.

The load-settlement curves for friction piles differ considerably from each other. An extreme possibility is represented in Fig. 52.11b. The test pile was driven 11 m through soft silt and clay with layers of peat. The point did not reach a firm stratum. Under loads of less than 200 kN the settlement of the pile was modest, but when

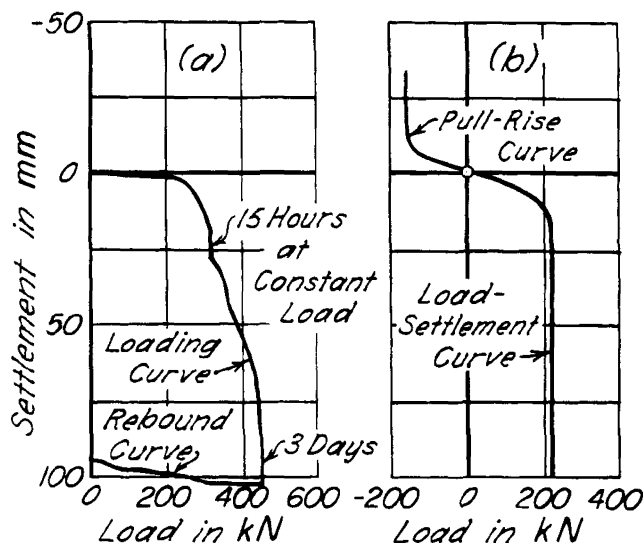


Figure 52.11 Typical load-settlement curve for: (a) point-bearing pile; (b) friction pile.

the load became equal to this value the pile suddenly sank several feet and did not stop until the loading platform hit the ground. The pull-rise curve, also shown in the figure, is similar to the load-settlement curve. The safe design load for such piles can be considered equal to the ultimate bearing capacity,  $Q_d$ , divided by a factor of safety of not less than 2.0.

### 52.4 Ultimate Bearing Capacity of Pile Groups

Both theory and experience have shown that pile groups may fail as units by breaking into the ground before the load per pile becomes equal to the safe design load. Such a failure is illustrated in Fig. 52.12. Hence, the computation of the safe design load must be supplemented by a computation of the ultimate bearing capacity of the entire group. Let  $A_g$  = area of pile group in plan;  $S$  = surface area of embedded portion of pile group (equal to  $D_f [2B + 2L]$  in Fig. 52.12);  $s_u$  = average undrained shearing resistance of soil between surface and depth  $D_f$ ;  $q_d$  = ultimate bearing capacity, per unit of area, of a loaded area with area  $A_g$  and depth  $D_f$ . This quantity may be estimated by means of the appropriate equations (Article 33).

If the piles and the confined mass of soil sink as a unit like a pier, the ultimate bearing capacity  $Q_g$  of the group is given with sufficient accuracy by

$$Q_g = q_d BL + S s_u \quad (52.10)$$

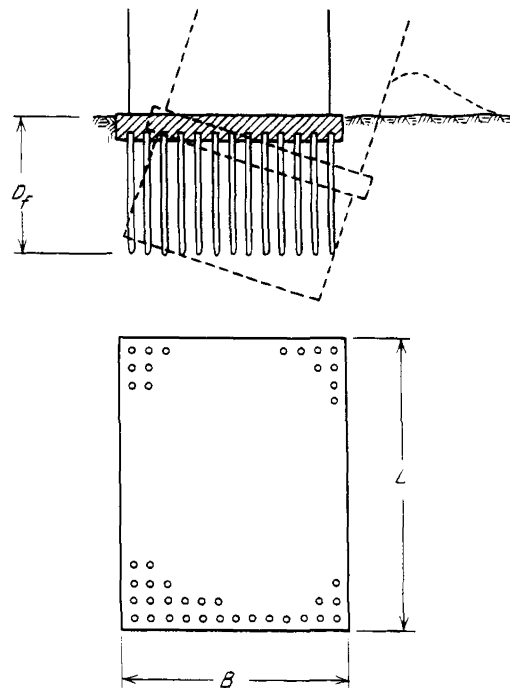


Figure 52.12 Diagram illustrating failure due to breaking into ground of entire pile cluster, including the soil located between the piles.

Computations based on this equation have shown that a base failure can hardly occur unless the pile group consists of a large number of friction piles embedded in silt or soft clay, as shown in Fig. 52.12, or else of point-bearing piles that transfer their load onto a firm but thin stratum underlain by a thick deposit of silt or soft clay. A pile group can be considered safe against such a failure if the total design load does not exceed  $Q_g/3$ . If this condition is not satisfied, the design of the foundation must be changed.

## 52.5 Behavior of Pile Foundations

### 52.5.1 Friction Pile Foundation in Sand

Dense sand is an excellent subsoil that does not need any reinforcement by piles. If piles have to be installed in dense sand for some purpose such as to transfer the weight of a bridge pier to a level below that of the deepest scour or to develop tensile resistance, it is usually necessary to aid the penetration of the pile by jetting. Hence, in the following paragraphs we consider only piles driven into loose sand. Furthermore, we assume that the sand within which the piles are driven is not underlain by any material more compressible than the sand itself.

The most suitable spacing  $D$  between the centers of piles with a top diameter  $d$  is usually about  $3d$ . If the safe pile load has been determined by means of a pile loading test, each pile in a cluster should be driven until the number of blows per unit of penetration becomes equal to that at which the driving of the test pile was discontinued. Driving should proceed outward from the center of the cluster; otherwise, the inner piles cannot be driven to as great a depth as the others.

After the piles have been installed, each cluster constitutes the core of a column of compacted sand embedded in loose sand. If the load per pile of such a foundation does not exceed the safe design load, the settlement is not likely to be greater than that of a similar structure supported by footings on dense sand. However, if the sand stratum containing the piles is interspersed with pockets or layers of silt or clay, the settlement may be much greater, because the pressure transmitted through the skin of the piles onto these layers causes them to consolidate.

If all other conditions are the same, the skin friction against the piles increases with increasing relative density of the sand. While a pile is being driven, the density of the surrounding sand increases (Plantema and Nolet 1957). Large-scale experiments have shown that the compaction caused by driving one pile influences the bearing capacity of any other pile located within a distance equal at least to five times the diameter of the pile (Press 1933, Petrasovits 1973).

Unfortunately, no simple relation exists between the settlement of a single pile under its working load and the

settlement of a group of piles or an entire pile foundation under the same load per pile (Terzaghi 1938b). The reason is apparent from the following discussion.

The settlement of a single pile or of an entire group of piles has two components: one arising from the settlement of the pile or piles with respect to the sand in which they are embedded, and one having its seat in the sand beneath the points. The first is the result of transfer of load to the adjacent soil by skin friction. It includes the penetration of the tips into the underlying sand. The second is due to the compression of the sand beneath the tips as a consequence of the increase in vertical effective stress.

When the piles in a group are driven, the sand between them is densified, and a load test on one of the piles provides the relation between load and settlement for that single pile. Almost all the settlement consists of the first component, because the load from the single pile stresses the underlying sand to a very limited depth. If all the piles are subjected to the same load per pile, however, the stresses in the sand below the level of the pile tips are increased, because the sand beneath the pile tips is stressed to a much greater depth than when only the single pile is loaded. The second component of settlement then becomes significant, even though the seat of settlement, like that beneath a large footing or raft (Article 50.2.5), is limited because the modulus of deformation of the sand increases with depth.

The first component is influenced greatly by the increase in relative density caused by the displacements and vibrations produced by pile driving; the second is influenced primarily by the increase in stress due to the loading and by the compressibility of the sand in the zone of influence of the stress. Both components are obviously influenced, in quite different ways, by the number of piles in the group. With increasing size of the group, at constant load per pile and spacing, the first component might be expected to decrease and the second to increase. The few available empirical data indicate that, in general, the settlement of a single pile is less, and possibly much less, than that of the same pile under the same load in a group, but they do not permit establishing a general relation between size of a pile group and settlement.

On the basis of the data available in 1953, Skempton proposed the relation shown in Fig. 52.13. Other studies (Berezantzev et al. 1961) have generally confirmed an increase in settlement with size of loaded area for equally spaced, equally loaded piles. However, most of the information contained in Fig. 52.13 is based on observations by Feagin (1948) concerning the settlements of large lock-and-dam structures, supported by timber piles, on the Mississippi River. The settlements were measured after several hundred cycles of filling and emptying the locks and thus undoubtedly included substantial effects of cyclic loading (Article 21). Until many more observations



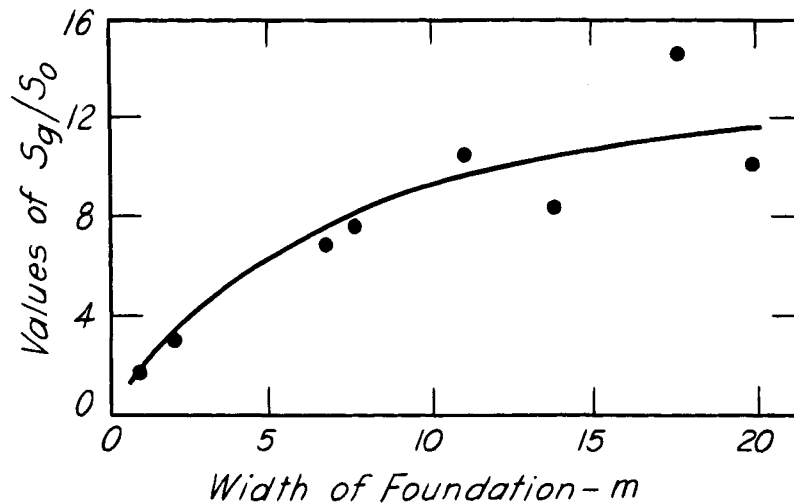


**Figure 52.13** Approximate empirical relation between width  $B$  of group of piles in sand and the ratio  $S_g/S_0$ , wherein  $S_g$  represents the settlement of a group of piles with width  $B$  and  $S_0$  represents the settlement of a single isolated test pile subject to the same load as each of the piles in the group (after Skempton 1953).

have been made, of structures subjected to more usual loadings, Fig. 52.13 or any similar relations (Vesic 1977) should be considered highly conservative approximations. In many instances a reasonable estimate of the settlement of a large group can be made by adding to the settlement of a test pile at working load the vertical compression of the sand beneath the elevation of the pile tips, calculated as if the added stresses at that level corresponded to the total pile load distributed uniformly at a depth equal to two thirds of the depth of pile penetration. This approximation to the distribution of added load is discussed in more detail in Article 52.5.7.

The foregoing comments concerning a test pile refer to a single pile subjected to a load test after all the piles in the group have been driven. When, as is often the case, a load test at a site is made on a pile before the other piles are driven, the first component of settlement, which is governed largely by the densification of the sand above tip level, will be greater than that of the same pile after the remaining piles have been driven. If this increase should bring the settlement of the test pile and that of the group into closer agreement, the result would be purely coincidental.

### 52.5.2 Piles Driven through Compressible Strata into Sand or Gravel

In Article 52.3.9 it was pointed out that the settlement of a single point-bearing pile passing through compressible strata depends more on the point resistance than on the total bearing capacity of the pile. The same general statement can be made regarding the settlement of the entire foundation. If the load per pile is equal to or less than the point resistance, the settlement is likely to be of no consequence. On the other hand, if it is greater, the settle-

ment may be large and detrimental. However, in any event the average settlement of the foundation will be many times greater than the settlement of a single pile acted on by the safe design load. The latter statement is illustrated by the following example (Terzaghi 1938b).

An apartment house in Vienna, Austria, was constructed on continuous footings 1 m wide, supported by cast-in-place concrete piles driven through about 6 m of loose fill into fairly dense gravel. Each pile carried a load of 200 kN. In Fig. 52.14b, curve  $C_0$  shows the result of a load test on a single pile, and  $C$  the load-settlement curve for the same pile during construction of the building. When the load due to the weight of the building reached its final value of 216 kN, the settlement of the pile was very much greater than that of the same pile during the load test. Curves of equal settlement for the entire foundation 11 weeks after the building was completed are shown in Fig. 52.14a. Their complete lack of symmetry suggests that the seat of settlement was in the upper part of the gravel stratum and that the settlement reflected primarily the local variations in compressibility of this stratum. If the walls had been perfectly flexible, the curves of equal settlement would extend without any break across the expansion joint at midlength of the building. The discontinuities indicate that the walls acted as semirigid beams that bridged the weakest spots in the supporting stratum. However, from a practical point of view the settlement was irrelevant, because the maximum differential settlement did not exceed 15 mm. The foundation was successful because the load per pile was smaller than the point resistance.

If the load per pile does not exceed about one half of the point resistance, the settlement of the foundation will

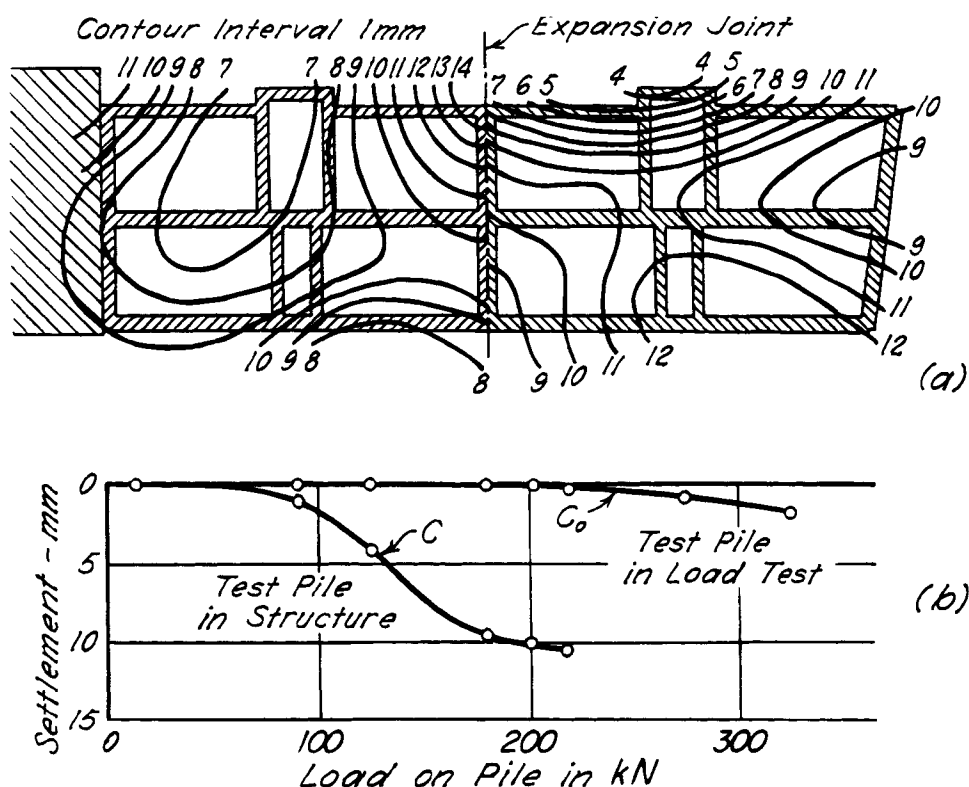


**Figure 52.14** (a) Settlement contours one year after construction of brick buildings supported by continuous footings on conical piles bearing on dense gravel stratum. (b) Load-settlement relations for single pile under test load and under same load beneath structure.

be inconsequential regardless of the spacing of the piles. A spacing of  $3d$  satisfies all practical requirements. The center piles in a cluster should be driven first to ensure that their points will have adequate penetration into the bearing stratum.

In some localities the bedrock is covered by a composite stratum consisting of irregular pockets of sand and gravel alternating with pockets of more compressible material such as clay, or rock fragments embedded in clay. This composite base is buried beneath soft sediments. The conventional exploratory borings do not necessarily reveal its composite character. However, while a test pile is being driven, the variations in the character of the subsoil come into prominence. The depth-resistance curve (Fig. 52.2d) represents such a condition. In any event, the individual piles of a cluster driven into a subsoil with an erratic soil profile are likely to meet refusal at very different depths. If the soil located between the points of piles with very different lengths consists only of loose sand, the performance of the cluster under load may be perfectly satisfactory. On the other hand, if it contains pockets of soft clay or silt, the settlement of the pile-supported footing may be excessive. Hence, if adjacent foundation piles meet refusal at very different depths, a boring should be made nearby to determine the cause of the difference. If the boring shows that the soil contains

pockets of highly compressible material below the level of the shortest piles, it is necessary to enforce the penetration of all the piles to a level below the bottom of the zone that contains the pockets. If this cannot be done by preboring, a larger hammer may be required. Jetting should be avoided. All those piles that meet refusal above the level of the lowest soft pockets should be disregarded and replaced by piles with adequate length.

On flood plains and along the seacoast the construction of pile foundations is often preceded by placing a fill over the site of the proposed structure. If the subsoil consists of loose sand or other highly permeable and relatively incompressible soils, the effect of the fill on the piles can be disregarded, although the potential for liquefaction should be evaluated. On the other hand, if the subsoil contains layers of soft silt or clay, the presence of the fill considerably increases the load on the piles as a result of negative skin friction (Article 52.3.1) and thus causes an increase in settlement. This condition was first recognized in Holland, where many buildings located in the coastal plains rest on point-bearing piles driven through about 20 m of very soft strata to refusal in a bed of sand. Wherever the site was covered by a thick layer of fill shortly before the piles were driven, the buildings supported by the piles settled excessively.

If the piles beneath such a building are widely separated, the added load per pile due to negative skin friction can be calculated as indicated in Article 52.3.8. If the piles are arranged in clusters or groups, however, the dragdown force per pile may be less than that on widely separated piles. It consists of two components, one due to the weight of the fill within the area enclosed by the group, and another due to the downward shearing stresses on the prism of soil enclosing the group. The first component is equal to

$$Q_I = \frac{A}{n} \gamma H \quad (52.12)$$

wherein  $A$  is the area of a horizontal section included within the boundaries of the cluster,  $n$  the number of piles,  $H$  the thickness of the fill, and  $\gamma$  its unit weight. The second component cannot become greater than

$$Q_{II} = \frac{PHs_u}{n} \quad (52.13)$$

where  $P$  is the perimeter of the cluster,  $H$  the thickness of the compressible stratum, and  $s_u$  the average undrained shearing resistance of the compressible stratum. With increasing spacing of the piles in the group, both  $Q_I$  and  $Q_{II}$  increase. Hence, to reduce the effects of negative skin friction the spacing between the piles can be reduced, but the advantage may be more than offset by increased heave, lateral movements, and interference among the piles. Providing a bituminous coating for the piles is preferable, as described subsequently in this article.

If  $Q$  is the load per pile exerted by a building on piles driven through new fill and soft clay into a sand stratum, the lower ends of the piles will ultimately receive a load

$$Q_t = Q + Q_I + Q_{II} \quad (52.14)$$

If this load is greater than the point resistance of the pile, the settlement of the foundation will be excessive, regardless of what ultimate bearing capacity a load test may indicate. Hence, if a foundation on point-bearing piles is to be established at the site of a recent fill, both the point resistance and the value of  $Q_t$  (Eq. 52.14) should be determined. If the load  $Q$  includes a short-term or transient component, the transient fraction may be transferred by positive skin friction to the stratum responsible for the dragdown on the pile. If the duration of the transient load is too brief to induce significant consolidation of the underlying compressible material, the transient load will not increase the penetration of the point of the pile. This favorable condition is considered in some detail by D'Appolonia and Romualdi (1963) and Fellenius (1972).

Various expedients are used to reduce the effects of negative skin friction. For example, in Holland it became customary to use precast concrete piles with shafts of small cross-section as compared to that of the points (Plantema and Nolet 1957). The procedure most widely

used is to coat the piles with bitumen with a thickness of 1 or 2 mm (Baligh et al. 1978, Clemente 1981). The reduction, often on the order of 80% or more, depends to a considerable extent on the properties of the bitumen, which should be selected in accordance with the temperature of the soil. Coarse-grained soils tend to penetrate the coating; protection in the form of a casing or a plastic sleeve (Fuyuka et al. 1982) may be advisable. In any event, the perimeter of a pile should be small compared to its gross cross-sectional area; for example, a circular pipe pile is more efficient in reducing dragdown than an H-pile.

Where negative skin friction is likely to develop, inclined or batter piles may be subjected to severe bending. Their use under these conditions should be avoided.

### 52.5.3 Piles Driven to Sound Bedrock

Under ideal conditions piles supported by sound bedrock act like piers, and unless heave has occurred (Article 52.5.8) the settlement does not exceed the elastic shortening of the piles under the load imposed by the structure and any negative skin friction. However, the points of timber piles are likely to be injured by brooming, whereupon the beneficial effect of the rigid point support is lost. H-piles and pipe piles may be deformed locally and are customarily provided with fittings to reinforce the points. If the points encounter a smooth but inclined rock surface, they may travel down the slope without giving any visible indication of their progressive deflection. When the weight of the building is added, the deflection may increase still further, the piles may bend or break, and the foundation may fail. Steep slopes of very hard rock beneath soft clay underlie many cities in Scandinavia; to cope with these conditions, steel piles are provided with special points (Oslo points) consisting of a round hardened steel bar having a hollow-ground lower end that chisels a contact area into the rock below the point (Bjerrum 1957). Successful installation of these piles requires a special driving technique.

### 52.5.4 Piles Driven into Decomposed Bedrock

Decomposed rocks, particularly of metamorphic origin, may be as compressible as medium clay. Yet, they usually contain fragments of fairly intact rock that interfere with driving the piles through the compressible zone. Under these circumstances reliable information on the probable settlement can be obtained only by securing undisturbed cores of the decomposed material and making a settlement forecast on the basis of the results of consolidation tests. If the settlement may conceivably exceed the tolerable value, some method such as drilling must be used to penetrate the resistant fragments.

### 52.5.5 *Piles Driven through Compressible Strata into Stiff Clay*

Under these conditions most of the load on the piles is carried ultimately by the points. This produces a large concentration of stress in the clay near the point of each pile. The results of a load test on a single pile may be perfectly reassuring, because the major part of the load during the test is carried by skin friction, and the consolidation of the clay near the pile points develops very slowly. However, as time goes on, the settlement due to this consolidation may become very large.

The spacing of the piles should not be less than  $3d$ , to reduce as much as possible the disturbance of the clay constituting the bearing stratum. A spacing of  $3.5d$  is preferable. The difference between the ultimate settlement of the single test pile and of the entire foundation is likely to be unimportant. Loss of support due to heave of the bearing stratum is unlikely (Article 52.5.8).

If the area to be occupied by the foundation has been covered by a recent fill, the foundation should be designed for a load  $Q_i$  per pile (Eq. 52.14) to take account of negative skin friction.

### 52.5.6 *Piles Embedded in Firm Stratum Underlain by Soft Clay*

If the bearing stratum, such as a thick layer of dense sand, is located above a layer of soft clay, the settlement of the pile foundation is the sum of two independent items. The first part is equal to the settlement that would take place if the sand stratum were not underlain by compressible material. The factors that determine this part of the settlement are discussed under the preceding subheadings. The second part is due to the gradual consolidation of the compressible layer located beneath the stratum in which the points of the piles are embedded. Whereas the first part is negligible if the foundation is properly designed, the second may be very large and detrimental. This possibility has often been overlooked.

In one instance about 5000 wood piles 25 m long were driven to firm bearing in dense sand through fill and through 15 to 20 m of loose fine sand containing thin layers of silt and soft clay. The piles were arranged in clusters and capped by footings. The load per pile was about 140 kN, less than one quarter of the ultimate bearing capacity as determined by load tests. No measurable settlement was anticipated; yet, the foundation actually settled more than 0.6 m. The seat of settlement was a layer of clay 9 m thick, located 7.5 m below the points of the longest piles. The water content of the clay was close to the liquid limit.

The settlement of a pile foundation due to the consolidation of a soft layer below the bearing stratum can be computed by the procedures given in Articles 16 and 41, on the assumptions that the structure is perfectly flexible

and that the loads act directly on the surface of the bearing stratum. The total load that produces the consolidation is equal to the difference between the effective weight of the building and the effective weight of the excavated soil (Article 51). The reliability of this procedure is illustrated by Fig. 52.15. Figures 52.15a and b represent a simplified plan and vertical section through a steel frame building with cut-stone facing, respectively. The structure rests on about 10,000 wood piles 8 m long, driven so that their points came to bearing in the upper part of a layer of dense sand. The load per pile is 135 kN. Because the average settlement of the test pile was only 6 mm under 270 kN, the designers did not expect that the maximum settlement of the entire foundation would exceed this value. The real maximum settlement, however, had already exceeded 0.3 m within 2 years after construction. The contours of observed settlement, in millimeters, at the end of the construction period are shown on the left side of Fig. 52.15c. The right side shows curves of equal computed primary settlement, plotted as a fraction of the maximum primary settlement. In spite of the simplifying assumptions made in the calculations, the computed differential settlement is in good agreement with the actual settlement. According to the results of the settlement analysis, the final maximum primary settlement would be about 0.5 m, but the real settlement has been considerably greater because of the secondary compression (Article 16.7).

To get information about the magnitude of the settlement due to consolidation of compressible strata located beneath the pile points, the exploratory borings must be supplemented by at least several undisturbed-sample borings from which continuous samples of all the highly compressible strata are secured. The program for testing the samples and the method of computation are identical with those outlined for the settlement of raft foundations located above soft clay strata (Article 51.2.2). If the computation indicates that the settlement may exceed a tolerable value, other methods for constructing the foundation must be considered.

If the computation indicates that the settlement will be tolerable, the spacing between piles may be determined by means of the rules for foundations on point-bearing piles embedded in sand.

### 52.5.7 *Floating Pile Foundations in Deep Soft Deposit*

In some types of soft ground, piles of any kind can be driven to great depth without appreciable resistance against further penetration. The depth-penetration diagrams for such piles resemble that shown in Fig. 52.2b. These conditions call for a floating pile foundation, wherein the minimum length of the piles is determined not by a specified resistance against further penetration under the blows of a hammer, but by the requirement

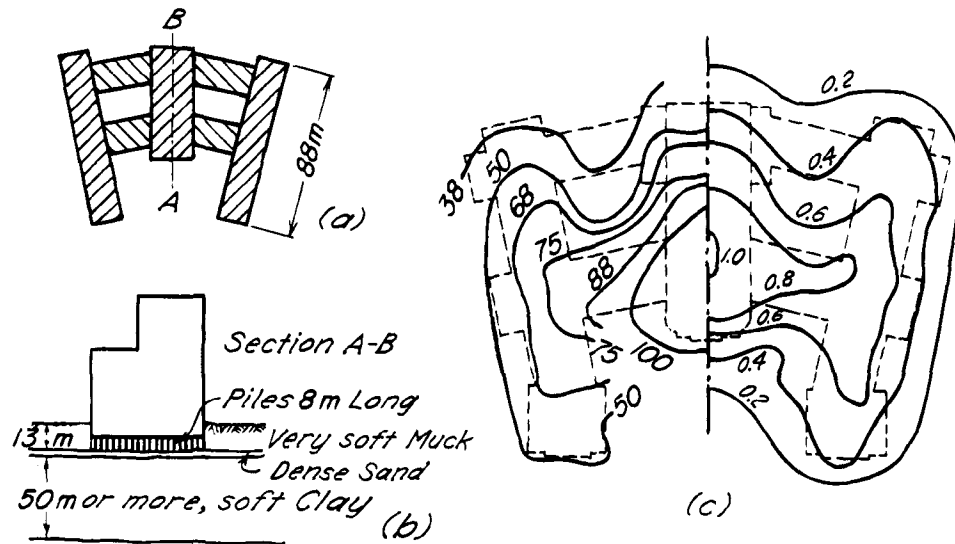


**Figure 52.15** (a and b) Plan and cross-section of structure supported by piles driven into dense sand layer above deep clay deposit. (c) Settlement contours for structure. Contours on left side represent observed settlement in millimeters at completion of structure; contours on right side represent lines of equal relative settlement based on computation and results of consolidation tests.

that the factor of safety of the pile groups with respect to a base failure should be equal to at least 2 or 3. The ultimate bearing capacity  $Q_g$  of each group can be estimated by means of Eq. 52.10. The value of  $s_u$  in this equation can best be determined by loading to failure several test piles of different length. However, before the computation can be made, the spacing between piles must be decided.

According to Eq. 52.10, the ultimate bearing capacity of a friction pile group increases with increasing spacing. Furthermore, at a given load per pile the settlement of a cluster consisting of a given number of piles decreases as the spacing increases. It would seem that a fairly large spacing is advantageous; however, as yet, empirical data concerning the effect of spacing on the settlement are very scarce. In 1915 two groups of friction piles embedded in soft silty clay were loaded with 2 MN per group (Staniford 1915). Each group contained 16 piles 23 m long. In one group the piles were spaced at 0.75 m, and in the other group at 1.06 m. After 40 days both groups had settled 0.11 m but after 270 days the settlement of the group with the closer spacing was 0.28 m, and that of the other group only 0.20 m. Inasmuch as such an advantage must be paid for by constructing very much larger footings, it is doubtful that a spacing in excess of  $3.5d$  is economical.

If the number of piles in a group is increased at a given spacing and at a given load per pile, both the intensity of the greatest stress in the soil and the depth of the highly stressed zone increase. This can be seen by comparing the right-hand sides of the diagrams in Fig. 52.16, *a* and *b*. Hence, the settlement of a pile-supported foundation

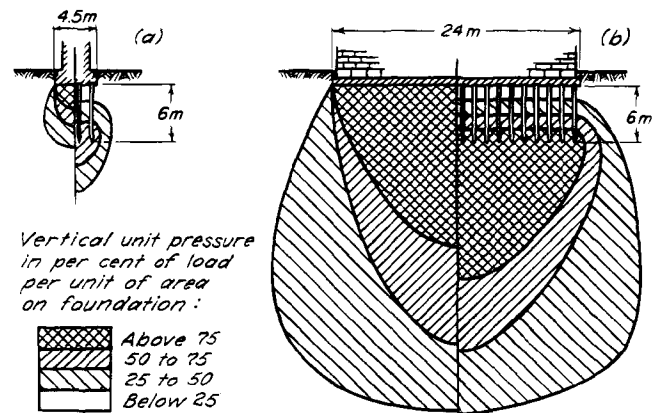


**Figure 52.16** Diagram representing increase of vertical pressure in soil beneath friction pile foundations having piles of equal lengths carrying equal loads. In (a) width of foundation is small compared with pile length; in (b) width of foundation is large compared with pile length.

covering a large area is greater than that of a smaller foundation supported by equally loaded piles of the same length and driven at the same spacing. Moreover, the settlement of a foundation covering a given area and supporting a given total load decreases with increasing length of the piles, in spite of the fact that fewer piles are needed to carry the load. These conclusions are confirmed by experience in every city where the soil conditions call for floating pile foundations.

On the left sides of Fig. 52.16, *a* and *b*, are shown the intensity and the distribution of the stresses in the soil

computed on the assumption that no piles are present. The ultimate settlement of the pile foundations shown on the right side of the diagrams can be estimated roughly on the basis of the following simplifying assumption. Above the level of the lower third-point of the length of the piles the water content of the clay remains unchanged, and below this level consolidation proceeds as if the building were supported on a flexible raft located at that level. The presence of the piles is disregarded. According to this assumption, the benefit derived from the piles is equivalent to replacing the subsoil by a practically incompressible material that extends from the base of the foundation to a depth equal to two thirds of the length of the piles. If this depth is several times greater than the width of the footings and the footings are widely spaced, the settlement of the pile foundation will be small, no matter how compressible the subsoil may be. On the other hand, if this depth is considerably smaller than the width of the loaded area and the loaded area is large, the ultimate settlement may be excessive even under a moderate load. These conclusions have been confirmed consistently by experience. Both experience and theory have also shown that raft foundations supported by uniformly loaded and equally spaced friction piles, like simple raft foundations, always tend to assume the shape of a shallow bowl.

If the structure contains a basement, the load that produces consolidation is equal to the difference between the effective weight of the building and the effective weight of the soil that was excavated to form the basement (Article 51.3).

#### 52.5.8 Heave and Lateral Movement due to Pile Driving

If a pile is driven through silt or clay, the neighboring piles may rise. If the piles were driven to end-bearing on rock or a stratum of hard soil, their points may lose contact with the point-supporting material. Composite or spliced piles may even separate at the joint. Subsequent application of load causes a settlement equal to the preceding rise. Hence, if the rise is excessive, the piles should be redriven. On the other hand, if the piles were driven through weak strata for some distance into a stiffer stratum from which the piles will receive their support by side resistance, displacements may cause the piles to heave, but the heave may not diminish their capacity. Redriving is then unnecessary (Klohn 1963, Koutsoftas 1982).

Heave may be reduced by predrilling to remove part of the soil that would otherwise be displaced, or by using a pile, such as an H-pile, that has a small cross-section. However, even H-piles may cause enough displacement to produce large heave under some conditions (Olko 1963), particularly if a plug of soil forms between the flanges.

Wherever conditions conducive to heave exist, the elevations of the tops of the piles should be monitored. If

the type of pile permits, tell-tales should be used to detect heave of the points. If it is not obvious that contact with a hard bearing stratum has been lost and that redriving will therefore be needed, load tests should be performed to determine whether the capacity of the heaved piles has been impaired. Criteria for redriving can then be established to control the job.

The displacements may cause not only heave but also lateral movements, especially if there are adjacent excavations extending below the level from which the piles are driven (Hagerty and Peck 1971). Where the movements are likely to be objectionable, they can be reduced by removing part of the soil in the space to be occupied by each pile. This is usually done by *predrilling* with an auger or by *coring* with a rotary cutting tool combined with water jets that transform the clay into a slurry where the pile is to be located.

#### 52.5.9 Efficiency Equations

The preceding discussions have demonstrated that the settlement of a pile foundation exceeds that of a single pile under a load equal to the load per pile in the foundation. The realization of this fact led to various attempts to express the influence of the number and spacing of the piles on the settlement of the foundation by so-called efficiency equations (Seiler and Keeney 1944, Masters 1943, Feld 1943). However, the extraordinary variety of soils encountered in piling practice excludes the possibility of establishing a limited number of sufficiently accurate efficiency equations of general validity. The effect of the number and spacing of the piles on the ratio between the settlement of a single pile under a given load and that of a group under the same load per pile depends to a large extent on the sequence and properties of the soil strata. Furthermore, at a given length and spacing of the piles the ratio changes to a considerable extent with the load per pile. Nevertheless, in none of the existing theories are these vital facts given adequate consideration. Because of the great number and diversity of the factors involved, it seems very doubtful, to say the least, whether the efficiency equations represent a step in the right direction. Estimates of the ratio based on the theory of elasticity may be logically more defensible but, as discussed in Article 52.5.1, they have inherent shortcomings.

At the present state of knowledge it is preferable to consider every case individually and to evaluate the probable settlement of a proposed pile foundation on the basis of the physical properties of the soils onto which the load is transmitted by the piles. Examples of the use of this procedure have been given under the preceding subheadings. If the probable settlement exceeds the tolerable maximum, the design must be modified. The maximum tolerable settlement of pile foundations is determined by

the same factors as those that govern the permissible settlement of footing and raft foundations (Articles 50 and 51).

If the distribution of the loads over the area to be occupied by a structure is very uneven, the secondary stresses in the structure due to unequal settlement can be appreciably relieved by dividing the structure into blocks separated from each other by continuous vertical joints.

#### 52.5.10 Selection of Type of Pile

The designer of a pile foundation can choose among several different types of piles, any one of which may provide adequate support for the proposed foundation. The final choice is governed by economic considerations and by conditions imposed by the character of the job.

Until the early 1900's untreated timber piles were used almost exclusively. This type of pile is relatively cheap, but it has two major disadvantages. First, an untreated wood pile must be cut off below the lowest water table; if the water table is subsequently lowered on account of a permanent change in groundwater conditions, the uppermost parts of the pile disintegrate within a relatively short time. Second, a wood pile may break if it is driven too hard, although the foreman may not detect anything unusual. The risk of deterioration may be reduced by impregnation with wood preservatives, but the risk of breakage can be reduced only by stopping the driving of the pile while its bearing capacity is still relatively low. Because concrete or steel piles can be driven harder than wood piles without risk of damage, the safe design load for such piles is considerably greater than that for wood piles. Recognition of this fact in practice is exemplified by the values that represent the loads commonly assigned to piles of various types. Such values are given in Table 52.2. However, under many circumstances the design loads differ widely from those in the table.

Although the safe design loads for piles of different types vary, the spacing between piles of all types is practically the same. Therefore, the footings required to transfer a given load onto wood piles are considerably larger and more expensive than footings supported by concrete or steel piles. Furthermore, the bases of footings resting on concrete or steel piles can be established at any convenient elevation, whereas those of footings on untreated wood piles must be located below the lowest position of the water table. These advantages in many instances compensate for the additional cost of concrete or steel piles.

Before the beginning of the 20th century all concrete piles were the precast, reinforced type. During the next decade cast-in-place piles became widely used, and the manufacture of concrete piles developed into a highly specialized industry. Later, prestressed concrete piles also entered the field. Structural steel sections and steel pipe have similarly become commonplace. The piles from which the designer may choose differ in their method of

**Table 52.2 Customary Range of Working Loads on Driven Piles<sup>a</sup>**

Type	Load (MN)
Timber (200 mm tip diam.)	0.1–0.3
Concrete, precast, or prestressed	
250 mm diameter	0.2–0.6
450 mm square	0.7–2.0
Steel pipe or shell, concrete-filled, not mandrel-driven	
273 × 4.8 mm pipe	0.3–0.5
273 × 6.4 mm pipe	0.4–0.7
324 × 6.4 mm pipe	0.5–0.8
350 × 7.8 mm pipe	0.6–0.9
400 × 9.5 mm pipe	1.0–1.2
Monotube, 7-gage	0.3–0.5
Steel pipe or shell, concrete-filled, mandrel-driven <sup>b</sup>	
Raymond Step-taper with 260 mm point	0.3–0.5
Raymond Step-taper with 308 mm point	0.4–0.7
305 mm corrugated, 16 gage	0.3–0.6
254 × 3.2 mm pipe	0.3–0.5
Steel H-section <sup>c</sup>	
HP 10 × 42*	0.5–0.8
HP 12 × 53*	0.5–1.0
HP 14 × 89*	1.0–1.6
HP 14 × 117*	1.5–2.0

<sup>a</sup>Indicated maximum loads can be exceeded if freeze or setup (Article 52.3.4) occurs after pile has been driven to resistance corresponding to tabulated value.

<sup>b</sup>Use of the mandrel permits driving these piles to a resistance great enough to warrant working loads based on the full structural capacity of the pile.

<sup>c</sup>When driven with adequate hammer to resistance indicated by wave equation H-piles may be stressed to as much as 90MPa under working loads; in soils likely to deform the tips, the same stress may be allowed if the piles are equipped with drive points.

\*Nominal width in inches; weights in pounds per lineal foot.

installation, their shape, the texture of their surface, and several other aspects. Almost every type of pile has features that make it exceptionally suitable under certain soil conditions and less suitable or inapplicable under others. If vibrations due to pile driving cannot be tolerated for some reason, a pile must be adopted that can be jacked or augered down or else installed in a drill hole. These factors must be considered by the designer in connection with every pile job. Proper choice of a pile type requires

judgment, experience in pile driving, and thorough grounding in the principles discussed in this article.

## 52.6 Piles Subjected to Lateral Loads

### 52.6.1 Lateral Resistance of Single Piles

Single piles are often used to support lateral loads or combined lateral and vertical loads. The piles themselves at working loads exhibit essentially elastic behavior, but the surrounding soil may be in states ranging from elastic to plastic and furthermore may be subject to cyclic degradation. Hence, design of such structural members represents a complex problem of soil-structure interaction. In general, laterally loaded piles may be categorized with respect to their embedded length as *short* or *long*. In a short pile the embedded portion remains practically rigid under the action of the load; it displaces primarily by rotation, and its capacity is determined by the passive resistance of the surrounding soil. The objective of design is to ensure an adequate factor of safety against passive failure; in some instances it is also necessary to limit the lateral displacement or rotation of the pile at the ground line. In a long pile the lateral capacity is governed not by the resistance of the soil but by the moments or stresses in the pile. The objectives of design are to limit these moments or stresses to structurally acceptable values and to ensure that the corresponding deflection and rotation of the pile at the ground line are within acceptable limits.

The distinction between short and long piles is a function not only of the geometry of the piles but also of the stress-deformation characteristics of both the piles and the surrounding soils. The piles are characterized by their elastic stiffness  $EI$  and the soils by their stress-strain characteristics, usually expressed in terms of the modulus of horizontal subgrade reaction (Article 42.5) or as  $p$  vs  $y$  curves, described subsequently. For soils having a modulus of subgrade reaction  $k_h$  that is constant with depth, roughly representative of stiff overconsolidated clays, a relative stiffness factor may be defined as

$$R = \sqrt[4]{EI/k_h} \quad (52.15)$$

For soils in which the modulus of subgrade reaction increases linearly with depth such that  $k_h = n_h z$ , roughly representative of sands, the relative stiffness factor is defined as

$$T = \sqrt[5]{EI/n_h} \quad (52.16)$$

If the embedded length is  $D_f$ , a short pile is characterized by  $D_f/T$  or  $D_f/R$  equal to or less than 2. For a long pile,  $D_f/T$  is equal to or greater than 4, or  $D_f/R$  equal to or greater than 3.5.

The ultimate lateral capacity of short piles can be estimated by methods proposed by Broms (1965) who provides charts to facilitate the calculations. However, most

practical problems fall into the category of long piles, for which values of moment and deflection are required as functions of depth. An approximate and often adequate analysis for such piles can be obtained by the use of dimensionless plots that furnish values of moment and deflection for values of  $k_h$  that are constant with depth or that represent a two-layer system with a stiffer upper layer (approximating the stiffness of many clay deposits with stiff crusts), or for values of  $n_h$  that are constant with depth (Davisson 1970a). Corrections can be made for the effect of the degree of fixity of the head of the pile, a significant variable. Although the moments and deflections are influenced appreciably by the variation of  $k_h$  with depth, they are relatively insensitive to the absolute values of  $k_h$  or  $n_h$ . Hence, these values can be estimated (Table 52.3). They can also be determined conveniently by means of the pressuremeter.

Use of the dimensionless plots is an efficient first step in the design of a laterally loaded pile, as it permits judging what, if any, unfavorable conditions may exist. Often, no further investigation is needed. However, if more refined studies are indicated, they can be carried out by means of the  $p$  vs  $y$  method (Reese and O'Neill 1988). This method also makes use of the concept of subgrade reaction, but at any depth on the buried part of the pile the relation between lateral deflection  $y$  and pressure  $p$  (force per unit of length of pile) is postulated in accordance with the physical characteristics of the soil. Figure 52.17 is a schematic representation of a pile subjected at various depths to lateral soil reactions  $p$  which vary with deflection  $y$  in accordance with the  $p$  vs  $y$  curves applicable to the soil at the corresponding depths.

For an elastic pile the equation governing the pile-soil interaction is

$$EI \frac{d^4 y}{dx^4} + P_x \frac{d^2 y}{dx^2} - p - W = 0 \quad (52.17)$$

**Table 52.3 Estimated Values for  $k_h$  for Laterally Loaded Piles**

Soil Type	Value
Granular soils	$n_h$ ranges from 0.5 to 50 kPa/mm, is generally in the range from 3 to 30 kPa/mm and is approximately proportional to the relative density.
Normally loaded organic silt	$n_h$ ranges from 0.1 to 0.8 kPa/mm.
Peat	$n_h$ is approximately 0.05 kPa/mm.
Cohesive soils	$k_h$ is approximately 67 $s_u$ .

*Note:* the effects of group action and repeated loading are not included in these estimates.

(after Davisson 1970a)



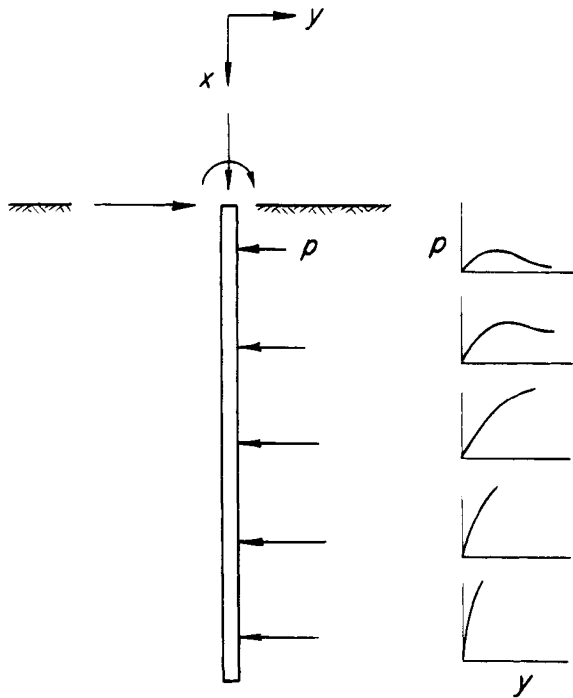


**Figure 52.17** Schematic illustration of family of  $p$  vs  $y$  curves for analysis of lateral capacity of vertical pile.

where  $EI$  is the flexural rigidity of the pile,  $P_x$  is the axial load,  $p$  is the lateral soil reaction per unit of length, and  $W$  is the distributed load along the length of the pile. The differential equation is solved by subdividing the pile into discrete elements and expressing the equation in difference form. If the  $p$  vs  $y$  relations reasonably represent the soil behavior, the solution permits evaluation of the bending moments in the pile and of the deflections and moments or shears at points of interest. The principal condition not in accordance with reality is that the  $p$  vs  $y$  curves are assumed to be independent of each other. This assumption introduces a small error into the calculations.

Detailed procedures have been developed for establishing the  $p$  vs  $y$  curves for soils of various types under the anticipated states of stress pertinent to a given installation. The application of the procedures requires considerable judgment and a thorough knowledge of the stress-deformation-time properties of soils. In several instances, the results have been compared with measured deflections and moments in instrumented piles and, by double integration and differentiation of measured moments, field  $p$  vs  $y$  curves have been deduced for comparison with those assumed. If allowance is made for the inherent errors in this procedure, the comparisons have been reasonable.

The iterative nature of the solution of Eq. 52.17 requires use of a computer. Detailed programs are available. Reference should be made to the extensive literature on the subject (Reese and O'Neill 1988).

### 52.6.2 Lateral Resistance of Pile Groups

The lateral resistance of a group of vertical piles is less than the resistance of a single pile multiplied by the number of piles in the group, and the lateral deflection of the group exceeds that of a single pile subjected to the same load per pile. On the basis of load tests on small-scale model piles in sand (Prakash 1962), the effect may be estimated by decreasing the value of  $k_h$  or  $n_h$  by a group reduction factor that depends on the center-to-center spacing of the piles in the direction of application of the horizontal load. Values of the reduction factor suggested by Davisson (1970) are shown in Table 52.4. For spacings greater than 8 times the width or diameter of the piles, no reduction is necessary. The pile spacing in the direction perpendicular to the direction of the load should be at least 2.5 times the pile diameter.

**Table 52.4** Group Reduction Factors for Coefficient of Subgrade Reaction

Center-to-Center Spacing in Direction of Load	Group Reduction Factor for $k_h$ or $n_h$
$3d$	0.25
$4d$	0.40
$6d$	0.70
$8d$	1.00

(after Davisson 1970a)

### 52.6.3 Effect of Repeated Lateral Loads on Vertical Piles

Repeated or cyclic lateral loads cause a reduction in the resistance of the soil and a corresponding increase in deflection. On the basis of limited model and full-scale tests, Davisson (1970a) suggests that if the load is cycled 50 times or more, the subgrade modulus  $k_h$  is reduced to about 30% of that applicable to the initial loading. Long and Reese (1987) noted a substantially greater reduction of lateral resistance of a full-size pile in stiff fissured clay having access to free water than for a comparable pile in soft clay. They attributed the inferior behavior of the stiff clay to the softening effect of water in the fissures and to the removal of particles by erosion as the water flowed in and out of the gap that developed between pile and soil.

According to Davisson, the combination of the effects of cyclic loading and group action could in some instances reduce the effective value of  $k_h$  to as little as 10% of that applicable to a single pile under its initial loading. Where piles may experience repeated lateral loading, particularly if the ground surface is submerged, a cyclic load test on one of the piles may be advisable.

### Selected Reading

- A summary of current practice is contained in Vanikar, S. N. (1985). *Manual on Design and Construction of Driven Pile Foundations*, U. S. Dept. of Transp., Fed. Hwy. Admin. Publ. No. FHWA-DP-66-1. The chapters on "Piled Foundations" in *Foundation Design and Construction*, by M. J. Tomlinson, 5th ed. (1986), New York, John Wiley and Sons, contain much useful information for the designer, with special emphasis on British practice. Although out of date with respect to available types of piles, *Foundation Design and Practice*, by J. H. Thornley (1951, New York, Columbia Univ. Press) includes an excellent treatment of economic and practical aspects, including the choice of type of pile.
- The success of a pile foundation depends not only on its design but also on the details of its installation, including conscientious inspection and supervision. These aspects are treated in detail in *Engineering of Pile Installations*, by Frank M. Fuller, McGraw-Hill, 1983, 287 p.
- The article by J. D. Parsons (1966). "Piling difficulties in the New York area," *ASCE J. Soil Mech.*, **92**, No. SM1, pp. 43-64, is an exemplary addition to the meager documentation of the behavior of piles and pile foundations under adequately described conditions.
- The assessment of the status of design and construction of pile and pier foundations discussed in Peck, R. B. (1965). "Pile and pier foundations," *ASCE J. Soil Mech. Found. Eng.*, **91**, No. SM2 is unfortunately largely still applicable today.

## ARTICLE 53 PIER FOUNDATIONS

### 53.1 Function of Piers

Piers are prismatic or cylindrical columns that have essentially the same function as piles or pile clusters. If piers are constructed to support a bridge, their sole purpose may be to transfer the loads to a level below that of the deepest scour. In semiarid regions with highly plastic clays, piers are used to transfer the loads to a level below the zone of periodic shrinking and swelling (Article 16.10). In most other instances, piers serve like piles to transfer the loads onto or into a firm stratum located beneath softer ones.

### 53.2 Distinction between Piers and Piles

Because piers and piles serve the same purpose, no sharp differentiation can be made between the two. In this book the distinction is based on the method of installation. A pile is installed by driving, a pier by excavating. Thus, a foundation unit installed in a drill hole, although often called a cast-in-place pile, would in this text be regarded as a small-diameter pier. This choice of definitions is based on geotechnical considerations: the two different methods of installation produce radically different effects in the surrounding supporting soil. The following examples illustrate the possibilities.

If a pile is driven through soft ground into a stratum of dense sand, the point of the pile displaces and compacts the sand. The point resistance of such a pile is likely to be many times greater than that of a cylindrical pier with equal diameter, because the process of installing the pier does not compact the sand but, instead, gives it an opportunity to expand. It may be intended to transfer the weight of a structure onto unweathered bedrock overlain by a thick layer of weathered rock which, in turn, is buried beneath soft sediments. The weathered rock may be as compressible as medium or even soft clay, but it may contain large fragments of less decomposed material. These fragments would prevent the points of piles from being driven to unweathered rock, whereas they could be removed from the excavation for a pier.

If a structure is underlain by a medium clay that rests in turn at comparatively shallow depth on a deep deposit of stiff clay, it may be possible to support the entire load from each column on a single machine-drilled pier with an enlarged base resting just below the upper surface of the stiff clay. Such a foundation may be far more economical than friction piles in the stiff clay. On the other hand, if the clay deposits contain seams of waterbearing silt and sand, it may not be possible to enlarge the base without collapse or without inflow of loose wet material that would deprive the pier of firm support and might make the placement of sound concrete impracticable.

The most suitable method for constructing piers of large base dimensions is determined chiefly by the subsurface conditions. If an attempt is made to build such a pier by a method that is not practicable under the given soil conditions, the contractor will be compelled to change the method during construction. An emergency change of procedure always involves a considerable loss of time and money. Therefore, the engineer who specifies a pier foundation should be familiar with the prerequisites for success. The most common methods of construction are sinking caissons and excavating shafts. Caissons are rarely used for piers with diameters less than about 3 m, whereas the dimensions of shafts range from as little as about 300 mm to many meters.

### 53.3 Caissons

#### 53.3.1 Methods of Construction

Strictly speaking, a caisson is a shell within which the excavation is made. The shell descends into the ground to the level of the base of the foundation and eventually becomes an integral part of the pier. The oldest type of caisson is the drop shaft or open caisson (Fig. 53.1 *a* to *c*). The shell sinks under its own weight as the soil at the bottom of the caisson is excavated. If the bottom is located above the water table, or if the water is removed by pumping from an open sump, the excavation can be made by hand (Fig. 53.1*a*); otherwise, the soil is removed by

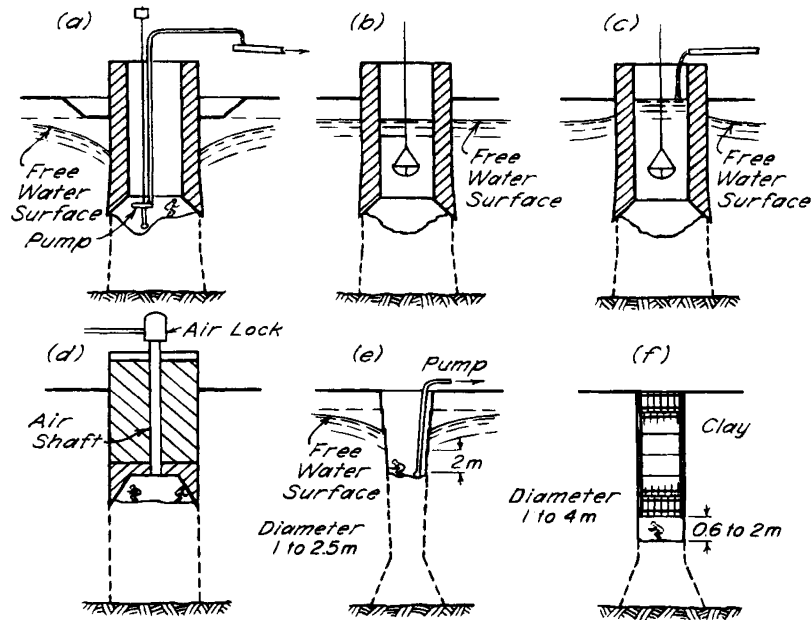


**Figure 53.1** Diagrams illustrating methods for constructing piers: (a to c) Open caisson method; (d) compressed air caisson; (e) open shaft with telescoping steel-shell lining (Gow method); (f) open shaft lined with wood lagging and steel rings (Chicago method).

dredging (Fig. 53.1 *b* and *c*) and the bottom of the caisson sealed with underwater concrete when grade is reached. Obstacles in the path of the cutting edge, such as buried logs or boulders, may delay the sinking of the caisson by several days or weeks. If they cannot be removed within a reasonable length of time, the work may have to be continued by the compressed-air method (Fig. 53.1 *d*). As the caisson descends, air pressure is maintained in the working chamber at the value of the hydrostatic pressure in the pore water at the level of the cutting edge. For physiological reasons the use of air pressure is limited to a depth of about 35 m below the water table. Beyond a depth of 12 m the cost increases rapidly. The compressed-air method may also be used in water-bearing ground instead of dewatering, if the specifications call for cleaning the bottom of the pier excavation in the dry before placing the concrete.

Dredging in sand usually removes a volume of sand greater than the volume of the caisson. If the sand is loose, the quantity excavated may easily be twice that displaced by the caisson. The excess volume is associated with loss of ground and settlement of the nearby ground surface. However, the loss can be prevented almost entirely by maintaining the water level inside the caisson several feet above the external water table, as shown in Fig. 53.1 *c*. The excess head produces a flow of water downward from the caisson into the sand located below the bottom of the excavation, and the corresponding seepage pressure counteracts the tendency of the sand to rise.

To avoid disrupting the flow, the excavating tools must be hoisted out of the caisson slowly.

In choosing between the dredging and compressed-air methods for sinking a caisson, several factors should be considered. If obstacles in the soil are encountered when the dredging method is being used, they may cause unpredictable delays. The compressed-air method avoids this risk, because the workers have access to the obstacles. It has the added advantage that the base for the pier can be prepared carefully, and all loose material removed. On the other hand, the use of compressed air is inherently much more expensive, and it may impair the health of the workers. In constructing a bridge pier it is not uncommon to lower a caisson by dredging until the bearing stratum is approached or reached, whereupon the caisson is converted to the compressed-air type. In this manner the economy of open dredging is combined with the greater certainty of the pneumatic method during preparation of the bottom for placement of concrete.

### 53.3.2 Estimate of Skin Friction during Sinking of Caissons

While excavation is being carried on within a caisson of the drop-shaft type, the soil next to the caisson is supported laterally by the walls of the shaft. Sections are added to the shaft above the ground surface, and as excavation proceeds, the caisson slides down. The downward movement is resisted by skin friction. To overcome the skin friction, lightweight drop shafts, such as those of steel, must be loaded with dead weights. On the other

hand, heavy caissons, such as those of reinforced concrete, may descend under their own weight.

Adding weights to the top of a caisson is a cumbersome procedure that considerably increases the cost of construction. Therefore, concrete caissons are generally designed so that their weight exceeds the skin friction at every stage of construction. Hence, the design requires evaluating the skin friction. Experience has demonstrated that methods for evaluating the skin friction on the basis of soil tests are unreliable. The principal source of information is the record of loads required to start caissons that had become stuck. These records suggest that for a given soil the skin friction per unit of contact area reaches a fairly constant value below a depth of about 8 m. Table 53.1 presents values that have been obtained for caissons ranging in depth from 8 to 40 m. For each material the range of values is fairly close to that for skin friction on piles in the same material. However, no perfect agreement should be expected, because in a given material  $f_s$  depends on the shape of the lowest part of the caisson, on the method of excavation, and on the diameter of the caisson. Values from other jobs in the vicinity should not be relied on unless all the circumstances attending the caisson sinking are known. In clay the skin friction is likely to increase with time.

The friction between the walls of concrete caissons and fine-grained soils such as silt or clay can be considerably reduced by providing the outside of the caissons with a smooth coating tough enough not to be rubbed off while the caisson descends. Such a coating was used on the caissons for the piers of the San Francisco-Oakland Bay bridge. The results of friction tests made before construction indicated that it reduced the friction between the concrete and a fairly stiff clay by about 40%.

During the 1960's several deep basements were constructed through silty soils in Japan as caissons, some as large as a city block. In several instances the work was finished under compressed air, and means were developed for injecting bentonite slurry through the walls of the caissons as a lubricant. Although technically successful, the use of such caissons has, for economic reasons, been supplanted by open excavations carried out within enclo-

sures formed by diaphragm walls constructed in slurry-filled trenches (Article 54.6).

### 53.4 Piers Constructed in Open Excavations

Many piers, particularly for bridges, are constructed in open excavations with sides supported by sheeting held by bracing or tiebacks. If the construction is located in a body of water, the enclosure is known as a cofferdam. The system of support is described in Article 46.

When the excavation has reached a suitable depth, the bottom is cleaned. If water is present, it is collected in a sump and pumped out so that the concrete can be cast against a firm base. The concrete usually extends to the lateral limits of the excavation, at least until it has the required thickness to serve as a footing. Above this level the concrete is usually placed in formwork to become a structural shaft. The behavior of the pier differs from that of a shallow footing to the extent that the embedment into the ground influences the bearing capacity and settlement.

If the excavation has been made by dredging under water inside the cofferdam, the bottom is sealed by concrete placed under the water by tremie. The thickness of the tremie seal must be great enough to resist the hydrostatic uplift when the cofferdam is unwatered so that the remainder of the pier can be constructed in the dry.

#### 53.4.1 Piers on Sand

The buried part of a bridge pier may be completely surrounded by sand that has a low compressibility and is capable of carrying a considerable part of the load on the pier by skin friction. The base of such a pier is usually located at a moderate depth below the maximum depth of scour (Article 49.3). During exceptionally high water, most of the sand surrounding the pier is temporarily removed. Hence, even in connection with bridge piers entirely surrounded by sand, it should be assumed that the entire load on the pier is carried by the base.

The ultimate bearing capacity of a pier on sand beneath compressible deposits can be calculated with sufficient accuracy by means of Eqs. 33.7, 33.13, or 33.14, in which the term  $\gamma D_f N_q$  is considered to be the effective weight of the soil between the level of the base of the pier and the ground surface or the lowest level to which the surrounding soil can be removed by scour. Because of the influence of this term, the ultimate bearing capacity increases rapidly with increasing depth of foundation. Hence, unless the pier is comparatively shallow and has a small width or unless scour can occur, it can usually be taken for granted that it will not experience a base failure. The allowable bearing value is then determined exclusively by considerations of settlement.

Various observations indicate that the settlement of the base of a pier on sand at a depth of about four or more

**Table 53.1 Values of Skin Friction during Sinking of Caissons**

Type of Soil	Skin Friction $f_s$ (kPa)
Silt and soft clay	8–30
Very stiff clay	50–100
Loose sand	13–35
Dense sand	35–70
Dense gravel	50–100

times the width of the base is likely to be about half the settlement of an equally loaded footing near the ground surface covering the same area on sand of the same characteristics. Therefore, the allowable bearing value for a pier on sand can be assumed to be twice the value that would be admissible for a footing resting on the same sand in the same state (Article 50.2). If the pressure on the base of the piers does not exceed this value, the maximum settlement is not likely to exceed 25 mm. Furthermore, if the bases of all the piers have approximately the same width, the differential settlement among the piers will not exceed about 15 mm. If the designer believes that larger settlements can be tolerated, the bearing values may be increased accordingly.

A modification of this procedure may be required if the base of a bridge pier is located fairly close to the level to which scour may remove the sand. The scour temporarily reduces the depth of foundation of the pier to much less than 4 times the width of the base. Hence, the pressure on the base of such piers should not exceed that appropriate for footings of the same area resting on the same sand in a saturated condition.

#### 53.4.2 *Piers on Clay*

The ultimate bearing capacity of a pier founded on a stratum of stiff clay located beneath soft compressible deposits is determined by Eq. 33.17, in which  $D_f$  is taken as the vertical distance between the top of the stiff clay and the level of the base of the pier. The value of  $N_c$  is not increased above the value corresponding to that for a shallow footing, because the low strength and compressible character of the overlying materials prevent the development of the zones of plastic equilibrium characteristic of a homogeneous cohesive material (Article 34). Consequently, the procedure is conservative because the strength of the overlying material increases the ultimate bearing capacity of the pier to some extent.

The total load that can safely be applied to the clay beneath the pier is equal to the sum of the allowable load on the base of the pier and the effective weight of the soil excavated during construction. Hence, the design load on large piers, at a given allowable load on the base, can be considerably increased by making the piers hollow. This fact has been used many times in the design of bridge piers.

On clay the settlement of piers, like that of footings, depends to a large extent on the history of loading of the clay. Pier foundations on normally loaded clay are uneconomical, and their settlement is prohibitive. Therefore, piers are established only on overconsolidated clay. Yet, if the area covered by a pier is large, the overconsolidated state of the underlying clay does not necessarily preclude important progressive settlement. This statement is illustrated by the following observation. Near the end

of the 19th century, bridge piers were established by the compressed-air method on a thick stratum of very stiff precompressed clay beneath the Danube River. The base of each pier was 23 m long and 6 m wide. The effective load on the bases of the piers ranged between 0.33 and 0.48 MPa. For a very stiff clay this load is well below the critical value for a base failure. Yet within half a century the differential settlement among the piers reached 75 mm. The value of the maximum settlement could not be ascertained, but there is no doubt that it was much greater than the differential settlement. Hence, if the base of a pier on stiff clays covers a large area, a settlement computation should be made. The uncertainties involved in the determination of the settlement of loaded areas on overconsolidated clay are discussed in Article 16.

#### 53.4.3 *Hand-excavated Shafts*

In the past, piers for buildings were constructed in hand-dug shafts, and hand excavation is still required in locations not accessible to drilling equipment. However, in the industrialized countries most piers are now constructed as plain or reinforced concrete shafts cast in cylindrical holes drilled by mechanical equipment. Significant progress has been made in means to cope with adverse soil and water conditions. Inasmuch as the success and economy of drilled-shaft construction depend greatly on selecting equipment and procedures appropriate to the subsurface conditions at the specific site, most of the following discussion deals with the geotechnical aspects of drilled-shaft construction and design. However, the occasional necessity for hand excavation justifies a brief description.

Two traditional open-shaft methods for establishing piers by hand excavation are the Gow method (Fig. 53.1e) and the Chicago method (Fig. 53.1f). Neither procedure can be used unless the water can be removed by pumping or bailing. In the Gow method the sides of the excavation are supported by a series of steel cylinders, each of which is 50 mm smaller in diameter than the one above. The cylinders are driven with a light hammer while the soil is being excavated by hand. The lowest part of the shaft is usually belled out. After the excavation has been completed, the cylinders are recovered one by one as the shaft is filled with concrete.

The Chicago method is used exclusively in clay. A cylindrical hole is dug by hand for a depth which varies from as little as 0.6 m in soft clay to 2 m in stiff clay. The sides of the excavation are accurately trimmed and lined with vertical boards held against the clay by two or more steel rings. The hole is then deepened a similar distance and lined in the same manner. When the bottom reaches final elevation, the hole is filled with concrete. If the clay is homogeneous, water causes no difficulty, but if water-bearing strata of sand or silt are encountered, special construction expedients may be required.

### 53.5 Drilled Shafts

#### 53.5.1 Methods of Construction

Most drilled shafts are constructed by means of truck- or crawler-mounted equipment including a mast for handling drills, casing, and reinforcing cages; a rotary table that turns a vertical rod or kelly bar; and augers or drilling buckets attached to the kelly for advancing and cleaning the hole. Usually the equipment has the capability of "crowding," or pressing the auger or bucket into the ground. Special buckets are used if enlargements or bells are to be formed at the bottom of the hole. The diameters of the shafts vary from as little as about 0.3 m for short piers to as much as about 6 m; bells can be formed beneath the latter to diameters up to about 10 m. Depths for the larger holes have reached more than 75 m. Many types of auxiliary equipment are available for special purposes such as breaking boulders or chopping or drilling into rock. Casing can be used to support the walls temporarily or permanently; support may also be provided by keeping the hole filled with slurry. Specialty contractors throughout the world have developed equipment and techniques to deal with conditions prevalent in their areas of operation.

Soil mechanics enters into the construction and design of drilled shafts in two ways. Its most important contribution is the exploration and definition of subsurface conditions, particularly the occurrence of boulders and of free water, that determine the potential construction difficulties and corresponding equipment and techniques at the site. If the conditions are misjudged, the equipment brought to the site may prove inadequate, collapses and delays may ensue, and under extreme conditions the contractor may be obliged to discontinue operations until more suitable equipment is obtained. Such situations are likely to be extremely costly. Second, soil mechanics provides the means to design the piers to carry the imposed loads at tolerable settlements and lateral movements; the design includes the determination of the most appropriate depth of the piers.

#### 53.5.2 Construction Implications of Subsurface Conditions

Forming a drilled pier in a stiff clay containing no large boulders or other obstructions and admitting no free water to the hole before the concrete is placed is a rapid and economical procedure that can usually be carried out without complications. Most departures from these ideal conditions require additional equipment and preparation on the part of the contractor, call for greater expertise, and if unanticipated can lead to delays, defective foundations, and unnecessarily increased costs. An appreciation of the consequences of the various departures provides insight into the requirements for subsurface exploration.

Quite apart from its geotechnical implications, the presence of even such a small amount as 25 or 50 mm of water in the bottom of the drilled hole may seriously degrade the quality of the concrete shaft. The water tends to rise as the concrete is introduced and to wash the cement from the aggregate as it rises. An estimate is needed, therefore, of the inflow that might occur during the interval between cleaning the bottom and placing the first concrete. If the inflow should be excessive, it would be necessary to use one of several specialized procedures to ensure satisfactory quality of the concrete (Greer and Gardner 1986, Reese and O'Neill 1988).

Boulders may reduce progress while tools are introduced to break them or while grab buckets are used to extract them. Often, boulders that would cause difficulties in small shafts can be removed with comparative ease in shafts of larger diameter. Many controversies and much litigation have arisen because the field notes taken during the exploratory drilling program and the logs derived from the notes failed to record the details that could have indicated the presence of boulders. The potential for seepage should also receive special consideration in the exploratory program, because if the walls of the shaft are subject to deterioration as a consequence of seepage, the reduced progress may lead to instability of the hole.

If an otherwise cohesive soil contains layers or pockets of sand or silt, it is crucial to determine whether the potentially cohesionless materials are below groundwater level. If they are, and if they are encountered unexpectedly, they are likely to flow into the hole and cause it to collapse. If their presence is known in advance, such unstable zones can be cut off a casing within which the auger or drilling bucket can operate, by drilling through water kept at a level high enough to produce seepage pressures directed from the hole into the surrounding soil, or by introducing a mud slurry into the hole. All these procedures slow production and increase costs as compared with drilling through inherently stable soils, but the added costs are minimized if the conditions are correctly anticipated.

In primarily cohesionless soils the use of casing or slurry is mandatory; the optimum choice of the defensive measures requires a detailed knowledge of the permeability, grain size, and relative density of the soils and of the groundwater conditions.

If an attempt is made to drill a shaft into soft clay, base failure at which no further progress is possible can be expected when the overburden pressure  $\sigma_{vo}$  approaches  $9 s_u$ , and the clay may squeeze toward the hole at values of  $\sigma_{vo}$  exceeding about  $5 s_u$ . The squeeze is likely to lead to excessive settlement and lateral movement of adjacent shafts or nearby structures and utilities. The movement can be reduced by keeping the hole filled with slurry, but if the bottom is to be cleaned or a bell formed in stiffer underlying material, the hole will require casing before

the slurry is pumped out. Removal of the casing during concreting requires precautions to avoid inclusions of clay or slurry in the pier.

Formation of a bell, whether by machine or hand excavation, is affected even more adversely by unfavorable seepage conditions, slickensides, or local cohesionless pockets than is advancing the cylindrical hole. Therefore, special attention to the details of subsurface conditions is needed in any zones where formation of bells is considered.

The foregoing descriptions of ground conditions and their implications with respect to the construction of drilled shafts are by no means comprehensive. They serve to indicate the nature of the role of soil mechanics in successful drilled-shaft construction practice. In addition to having the results of a detailed subsurface investigation, the designer of a drilled-shaft foundation needs to be aware of construction practices and of their relation to subsurface conditions in the area where the project is to be located; otherwise the design may not achieve the safety and economy inherent in drilled-shaft construction. Similarly, the constructor needs to assess the subsurface conditions carefully and realistically to select the equipment and procedures most likely to accomplish the work economically with the fewest unpleasant surprises.

Because the cost of setting up for drilling is comparatively low, it is often prudent to include one or more full-scale predesign test holes at the site of an unusual or a large job. In this way, inferences from drillholes and other exploratory procedures can be evaluated and misunderstandings avoided, with savings often many times the cost of the test holes.

### 53.5.3 Behavior of Drilled Shafts under Compressive Load

Like other types of foundations, drilled shafts must have an adequate factor of safety against a bearing-capacity failure and must not settle excessively. These two requirements are, however, not so clearly separable as in footing foundations. The complexity arises because the downward movement required to mobilize the shaft resistance differs from that to mobilize the base resistance.

A relative downward displacement of a shaft with respect to the surrounding soil of 10 to 15 mm is sufficient in almost all materials to develop the maximum shaft resistance. On the other hand, the ultimate base resistance is not usually reached until the downward movement of the base is much larger: on the order of 5% of the diameter in clays and appreciably more in sands. Thus, it is evident that the working load on the base of most shafts is limited by considerations of settlement rather than ultimate capacity.

If the purpose of a drilled shaft is to transfer the load to a firm stratum below weak materials, the capacity of the foundation will obviously be controlled by the base

resistance; shaft resistance is likely to be inconsequential and can be ignored. On the other hand, if the foundation does not reach a bearing stratum, skin friction is likely to be the dominant resistance. It will be shown in the following subsections that base resistance plays a minor role in uniform clays. In sands, settlements are likely to be excessive if the skin friction is exceeded, unless the base pressure is selected specifically to limit settlement. The base pressure so selected is a very small fraction of the ultimate bearing capacity. Hence, although much attention has been devoted to the complex problem of evaluating the theoretical ultimate bearing capacity of the base of a pier in sand, the results are seldom of practical significance, because even a crude approximation will suffice.

If the supporting medium is rock, the hole may be carried into the rock to form a socket that effects the load transfer. Under these conditions the skin friction on the shaft above the rock, unless it increases the load by drag-down, is essentially immaterial. In downtown Chicago, highly compressible clays are underlain by much stiffer ones in which bells can be formed to transfer the load to the hardpan beneath. If the hardpan is inadequate, the shafts are carried through all the soils to or into the dolomitic limestone below. Again, apart from investigating the adequacy of the hardpan to support the loads in direct bearing, the function of soil mechanics reverts to considerations of construction rather than design. Similarly, drilled shafts are rarely used in loose sand except to transfer loads to more resistant or less compressible materials beneath. If the objective is to eliminate progressive settlements due to vibrations, the existence of any positive skin friction is discounted.

In many localities the bearing stratum is so variable that even an extensive program of boring and sampling or of *in situ* testing cannot establish in advance the depth at which suitable support can be found. Among the geologic conditions under which these conditions are likely to exist are residual soils and saprolites in which weathering has taken place to different depths, stiff clays and shales with extensively slickensided zones, and solutioned limestones containing voids or cavities filled with soft residual materials. Such conditions are not uncommon in regions where drilled shafts are suitable foundations. Inspection of the bottom of the hole, sometimes including probing or drilling, may be needed, carried out by a person with the experience to decide whether the bottom is adequate, whether the sides of the socket can provide the necessary support, or whether the shaft must be deepened. Familiarity with the conditions in the vicinity is a prime asset for the inspector. Downhole inspections should never be made without adequate equipment and precautions, particularly with respect to poisonous gases.

### 53.5.4 Bearing Capacity of Drilled Shafts

Like that of a single driven pile, the ultimate bearing capacity of a drilled shaft can, in principle, be calculated by the static formula

$$Q_d + W_p = Q_p + Q_s = q_p A_p + C f_s D_f \quad (34.1)$$

Whereas for driven piles the properties of the soil are radically altered by the vibrations and displacements associated with installation, the main influence of drilled-shaft installation is a relaxation of the *in situ* stresses, although to some extent this relaxation is reduced by the pressure of the fluid concrete placed in the hole. Drilling with the aid of a slurry also influences the values of  $f_s$ . Therefore, it is not surprising that the correlation between Eq. 34.1 and the results of load tests should differ for drilled shafts and for piles.

For a shaft embedded entirely in sand, Eq. 34.1 can be modified as for a single driven pile:

$$Q_d + W_p = \sigma'_{vb} N_q A_p + C \int_0^{D_f} K \sigma'_v \tan \delta \, dz \quad (53.1)$$

where  $\sigma'_v$  is the effective vertical stress at depth  $z$ ,  $\sigma'_{vb}$  the corresponding stress at the base of the pier,  $N_q$  the appropriate bearing capacity factor,  $K$  the ratio of lateral to vertical effective stress, and  $\delta$  the friction angle at the interface between shaft and sand.

In developing correlations for practical use, some investigators have attempted to take into account as many pertinent variables as possible by modifying the factors  $\sigma'_{vb}$ ,  $N_q$ ,  $K$ , and  $\tan \delta$  in Eq. 53.1 by coefficients to be evaluated by theory, laboratory investigations, or other suitable means (e.g., Kulhawy 1991). Others have preferred to lump all the components of  $N_q$  and of  $K \tan \delta$  into single variables to be evaluated by correlations with load tests (e.g., Reese and O'Neill 1988, Long and Shimel 1989). Although the former approach may be fundamentally preferable, the present state of knowledge favors the latter approach for practical applications.

Very few load tests of cylindrical drilled piers in sand have been made in which the base resistance has been measured separately from the total resistance. In most instances the sand has been characterized by the standard penetration resistance  $N_{60}$ . The data are summarized in Fig. 53.2. As a rough approximation Reese and O'Neill (1988) have suggested

$$q_p = 0.06 N_{60} \text{ (MPa)} \quad (53.2)$$

with an upper limit of 4.3 MPa. Furthermore, the values of  $q_p$  plotted in Fig. 53.2 do not represent the ultimate load, which is unknown, but the base pressure at an arbitrary settlement such as 5% of the diameter; the bases could have sustained greater pressures at greater settlements. Because the base diameters in the reported tests did not exceed about 1.5 m, Reese and O'Neill suggested

that for greater diameters the values of  $q_p$  from Eq. 53.2 should be reduced by the ratio 1.5/(base diameter) to restrict the settlement to that corresponding to the diameter of 1.5 m.

As a practical consideration the ultimate bearing capacity of the base of a pier in sand, except possibly for a pier of very small diameter, is of little significance, because the base has the capacity to support loads far greater than those at which the settlement of the supported structure would become intolerable. At a customary tolerable settlement of 25 mm under working loads, for example, the base resistances of the piers represented in Fig. 53.2 ranged from 10 to 22% of their respective ultimate total capacities. Thus, even a considerable underestimate of the base resistance would not lead to a serious encroachment on the overall factor of safety.

The unit side resistance at any depth  $z$  (Eq. 53.1) is expressed as  $K \sigma'_v \tan \delta$ . All these quantities are influenced strongly by the stress and deformation conditions associated with construction of the shaft. The lateral pressure  $K \sigma'_v$  reflects not only the initial at-rest value  $K_0$  and changes caused by excavation, but also the pressure exerted at the interface by the fresh concrete. The concrete pressure itself is a function of the slump or consistency at the time of placement and of the rate of placement in relation to the time of initial set (Bernal and Reese 1983). The interface friction angle  $\delta$  depends on the relative density of the sand at the interface resulting from the disturbances associated with drilling and concreting, as well as on the effect of any slurry used in drilling. The impracticality of separately evaluating these and other possibly unrecognized factors led O'Neill and Reese (1978) to combine all influences except  $\sigma'_v$  into a single variable

$$\beta = K \tan \delta \quad (53.3)$$

to be evaluated by correlating the expression

$$C \int_0^{D_f} \beta \sigma'_v \, dz$$

with the results of load tests on instrumented piers in which the load transferred from the piers to the surrounding sand could be determined. The correlations indicated that  $\beta$  was governed primarily by the depth and could be approximated by

$$\beta = 1.5 - 0.246 z^{0.5} \quad 1.2 \geq \beta \geq 0.25 \quad (53.4)$$

where  $z$  is in meters.

In practice, relatively few drilled shafts have been constructed entirely in sand, and most of the correlations pertain to slightly cemented materials. Hence, O'Neill and Reese point out the need to use the results with caution. They suggest an upper limiting value of unit side resistance of 0.2 MPa, and in addition propose that the



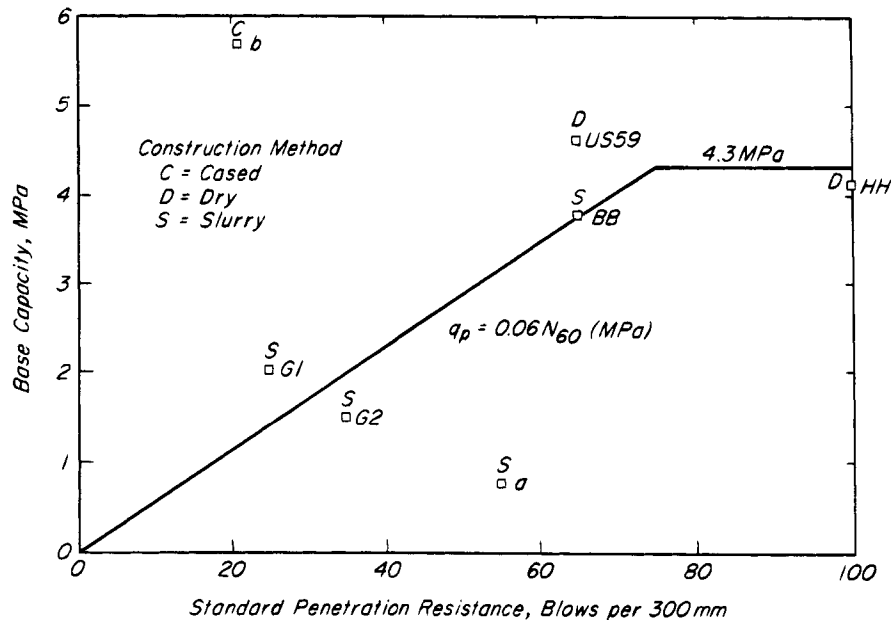


**Figure 53.2** Relation between measured ultimate base capacity (capacity at settlement equal to 5% of base diameter) and standard penetration resistance for cylindrical drilled piers terminating in sand. (Data from Touma and Reese 1982.)

unit side resistance should be considered constant for depths below 26 m, the depth at which Eq. 53.4 indicates that  $\beta$  becomes constant. If a less conservative design is considered, it should be validated by the results of full-scale load testing.

Although few shafts derive their support entirely from sand, many shafts are constructed in deposits of clay interspersed with strata of sand. The foregoing approach has led to capacities in good agreement with the results of load tests under these circumstances (Reese and O'Neill 1988). However, it is apparent that a much larger data base of reliable information is needed before the procedure can be fully evaluated or improved (Long and Shimel 1989).

In the foregoing discussion of the bearing capacity of a shaft in sand, it has been assumed that excess pore pressures associated with construction or loading dissipate so rapidly that they are of no practical consequence; that is, that drained conditions prevail. For shafts in clay, however, the period of porepressure adjustment is so slow that undrained conditions are likely to prevail at least during the first loading of the foundation. Because porepressure dissipation tends to increase the capacity, design is based on the reasonable but conservative assumption of undrained conditions. The results of conventional load tests obviously conform to these conditions.

Under these circumstances, Eq. 34.1 can be written:

$$Q_d + W_p = Q_p + Q_s = s_u N_c A_p + C s_{ua} D_f \quad (53.5)$$

where  $s_u$  is the undrained shearing resistance  $\bar{s}_{uo}$  (UC) mobilized at the base of the pier,  $N_c$  is the bearing-capacity factor associated with a foundation having a depth of

embedment that is large compared to the diameter, and  $s_{ua}$  is the adhesion between clay and pier. For shafts having a ratio of depth to diameter of at least 2.5,  $N_c = 9$ . As for piles in clay (Article 52.3.9), the adhesion  $s_{ua}$  for shafts in soft clay or soft plastic silt has been found, on the basis of full-scale loading tests, to be approximately equal to the undrained shear strength  $s_{uo}$  (UC) from unconfined compression tests, averaged over the depth of the pier, on samples of C quality. In stiffer clays the mobilized adhesion is smaller than  $s_{uo}$  (UC), and the ratio

$$\alpha = \frac{\bar{s}_{uo} \text{ (UC)}}{s_{ua} \text{ (mob)}} \quad (53.6)$$

decreases with increasing strength of the clay. Values of  $\alpha$  computed for cast-in-place drilled shafts in clays and silts, loaded in compression or tension, are shown in Fig. 52.10 (Stas and Kulhawy 1984), together with similar data from the analysis of full-scale loading tests on driven steel pipe piles and untapered precast concrete piles (Tomlinson 1957, Dennis and Olson 1983b). The measured side capacity was obtained by subtracting the calculated base capacity, taken as  $9 \bar{s}_{uo}$  (UC) for compression tests and zero for tension tests, from the measured total capacity.

It is likely that for piers, like piles,  $\alpha$  decreases as a function of depth, but the data are meager. The decrease is usually neglected except for very deep shafts. Further discussion of the depth effect is included in Article 52.3.8 in connection with pile foundations. Reese and O'Neill (1988) suggest that for stiff clays  $\alpha$  be taken as zero in

the upper 1.5 m of a drilled shaft to allow for desiccation or seasonal decreases in adhesion, and for a distance equal to the diameter of the shaft above the bottom or above the top of the bell if the shaft is belled. Between these limits they propose a constant value of 0.55. They also suggest an upper limit for  $\alpha_{s_{uo}}$  (UC) of 275 kPa. In a statistical study of 41 well-documented load tests on shafts in stiff clays or stiff clays interstratified with sands or silts, Long and Shimel (1989) found good agreement between the load-test results and predictions based on the suggestions of Reese and O'Neill, but they noted that the agreement would be improved if the adhesion for a distance of one diameter above the top of the bell were not excluded. They found that the use of slurry did not significantly affect the side resistance, although it was associated with greater variation in base resistance than was concreting in the dry. When casing was left in place in the shafts, however, the capacity was markedly reduced.

### 53.5.5 Settlement of Drilled Shafts

The settlement of a drilled shaft includes two components: that required to develop the side friction and base capacity and that caused by the increase in stress in the compressible materials around and beneath the shaft. A small additional component may be the axial shortening of the shaft itself.

Under most circumstances the first component of settlement does not exceed about 25 mm if the factor of safety with respect to side friction is adequate and if the base resistance constitutes a small fraction of the total capacity. These conditions prevail, for example, if the shaft is located in a deep deposit of stiff clay. On the other hand, if a comparatively short shaft with a large base diameter were located in sand, much of the total capacity would be furnished by base resistance that could be developed only as a result of large settlement. Under such circumstances, the settlement can be restricted to acceptable limits only if, at working loads, the factor of safety with respect to base failure is large compared to that for side friction. A global factor of safety of 2.5 might, under such circumstances, be associated with intolerable settlement.

To provide a means for the designer to judge the potential behavior of a pier under consideration, Reese and O'Neill (1988) have assembled the results of measurements on full-scale drilled shafts in which the load carried by side shear could be evaluated separately from the base load, and the corresponding settlements of shaft and base could be similarly separated. The findings are generalized in the sets of curves (Fig. 53.3) for shafts in sands and for shafts in clays. In designing a shaft the designer tentatively selects a depth, diameter of shaft, and diameter of base if an enlarged base is being considered. These dimensions are chosen to provide an appropriate global

factor of safety against the sum of the side and base ultimate capacity. The curves are then used to estimate the corresponding settlement at working loads. If the settlement would be excessive, the dimensions of the shaft are adjusted and the procedure repeated. In the final design, the factor of safety with respect to shaft resistance will be likely to differ from that for base resistance. The load in the shaft can then be calculated under working conditions and the elastic shortening of the shaft determined; except for deep shafts it is likely to be inconsequential.

The settlements so determined will occur simultaneously with application of the working load. In addition, immediate or delayed settlement will occur due to the compressibility of the stressed soil near and beneath the shaft. This component of settlement is likely to be small under the usual circumstances in which drilled shafts are used, but its magnitude can be estimated by the procedures discussed in connection with pile foundations. If several shafts deliver their load to a natural raft consisting of a stiff stratum underlain by more compressible materials, a settlement analysis is required.

### 53.5.6 Load Tests on Drilled Shafts

The general comments in Article 52.3.5 concerning load tests on piles are applicable to drilled shafts. For units of high capacity, however, the arrangements for providing the necessary reaction become very expensive, and field verification of capacity by direct loading is seldom done. On the other hand, the Osterberg load cell (Article 52.3.5) is readily adaptable to use beneath shafts of large diameters and to measurement of large loads. As of 1990 total loads of more than 50 MN had been measured, and installations made on shafts with diameters as great as 1.4 m. The device has the further advantage that the stress induced at the base of the pier by expansion of the bellows is maintained by filling the bellows with grout. Thus, in sands, the base settlement under working loads is negligible in contrast to the large settlement normally required to develop the base resistance.

### 53.5.7 Uplift Capacity of Drilled Shafts

Drilled shafts are often used to resist uplift forces. The weight of the shaft itself constitutes an appreciable resistance. Full-scale tests have indicated that the side friction resisting uplift is approximately equal to that available to resist downward loads. However, it is prudent to design for a higher factor of safety, particularly in sands, because the additional capacity associated with the base resistance, albeit at large settlement, is not available. Moreover, the maximum shaft resistance is mobilized at small upward movements; consequently, failure may occur with little warning. It is advisable to disregard the shaft resistance within the zone of seasonal volume change. Moreover,

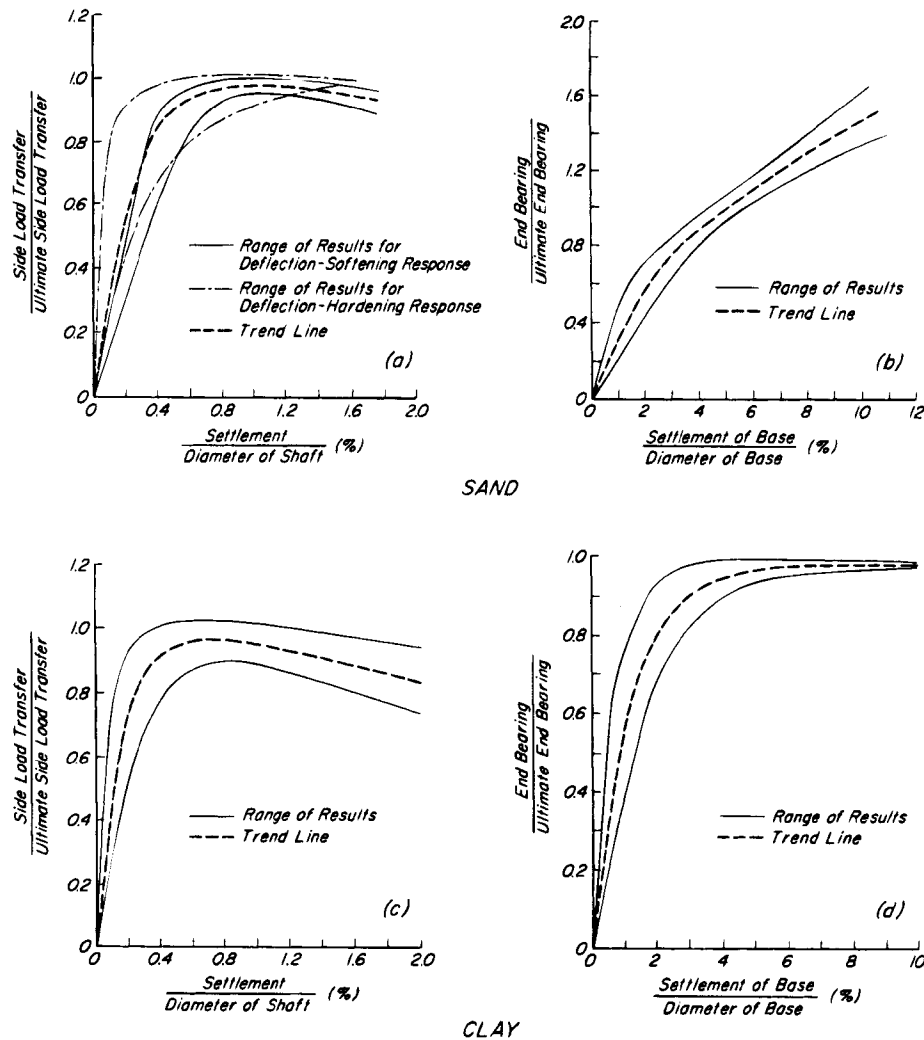


**Figure 53.3** Normalized curves showing load transfer in (a) side resistance and (b) end bearing versus settlement for drilled shafts in cohesionless soil; (c and d) similar relations for clay (after Reese and O'Neill 1988).

if ice lenses due to frost action might develop near the ground surface, the shaft should be surrounded by material not susceptible to frost action to a depth below the zone of frost penetration, or the shaft should be reinforced to withstand the tension.

The uplift resistance in clay may be increased by enlarging the base of the shaft by means of a bell. If the shaft diameter is  $d_s$  and the base diameter  $d_b$ , the area against which the uplift resistance is developed is  $\pi(d_b^2 - d_s^2)/4$ , and the ultimate uplift resistance due to the bell is

$$Q_u + W_p = N_c s_u \frac{\pi}{4} (d_b^2 - d_s^2) \quad (53.7)$$

If the top of the bell is at a depth at least as great as  $2.5 d_b$ ,  $N_c$  may be taken as 9 and may be assumed to vary linearly from 0 to 9 for depths ranging from 0 to  $2.5 d_b$

(Vesic 1971, Reese and O'Neill 1988). Although side resistance may not be negligible on the upper part of a deep shaft terminating in a bell, it is advisable to depend only on the resistance of the bell. Of course, the shaft and bell must be reinforced to withstand the uplift.

The value of  $s_u$  to be used in Eq. 53.7 can be taken as the average value of  $s_u$  (UU) from the bottom of the bell to a height of about  $2 d_b$  above the base. However, if the soil above the base is weakened by slickensides, even though a bell can be formed, the value of  $s_u$  should be reduced by as much as 30%. Moreover, if the soil is highly compressible, a similar reduction should be made to allow for local instead of general shear failure, and an estimate of the consolidation of the clay should be made to permit judging whether the upward movement of the shaft would be excessive.

### 53.5.8 Drilled Shafts in Expansive Soils

In many arid and semiarid parts of the world the subsoil consists of stiff overconsolidated highly plastic clays to considerable depth. Shrinking and swelling occur in the dry and wet seasons, respectively, with consequent rising and settling of the ground surface. Interruption of evaporation, for instance by construction of a building or pavement, may also result in heaving of the ground surface. Because the movements are characteristically nonuniform, serious cumulative damage develops to structures having foundations supported in the active zone. Drilled piers have been used extensively to establish the support for structures below the zone of volume change; indeed, the equipment and techniques for drilled-pier construction were developed primarily in localities where expansive soils underlie large areas.

The most important step in designing a drilled shaft to circumvent the problems associated with expansive soils is to determine the depth of the active zone so that the shaft can develop its resistance below that depth. Under some circumstances there may also be a zone of negative porewater pressure below the active zone. Moisture drawn from the wet concrete may reduce the resistance to uplift. Hence, particular attention should be paid to groundwater conditions, especially to the possibility that the groundwater table in the active zone may be separated by a zone of moisture deficiency from the true groundwater level in the inert underlying formation. In this respect, in particular, detailed knowledge of performance of deep foundations in the locality is a prime asset to the geotechnical engineer.

Estimating the uplift force on a shaft involves considerable uncertainty. It is customary to assume the unit uplift stress to be equal to the undrained shear strength  $s_u$  (UC) of the surrounding clay for the full depth of the active and moisture-deficient layers. This assumption is probably conservative because of the slight increase of moisture content that occurs next to the shaft as a result of the construction operations. A fundamentally more attractive alternative is to determine the horizontal pressure required to prevent swelling of a vertically confined undisturbed sample when allowed to imbibe water, starting at the field moisture content. The unit uplift force on the shaft is taken as the product of this pressure and the tangent of the residual angle of internal friction of the material, presuming that the drilling operations have reduced the shear strength to the residual value. Observations on a drilled and belled pier in San Antonio after a year of service, however, indicated a shear stress about 30% greater than the value calculated in this manner (O'Neill and Poormoayed 1980).

Because the uplift force depends on the degree of saturation or moisture content at the time the shaft is installed, it is advantageous to construct the shaft near the end of

the wet season; however, ponding to increase the moisture content before construction is relatively ineffective.

Attempts have been made to surround the portion of the shaft in the active zone by a surface casing permitting the soil to expand without contact with the shaft. This procedure is effective, but it should be used only if the soil below the casing has no potential to swell. Precautions should also be taken to ensure that surface water does not enter the annular space and eventually seep into the expansive soil.

By far the most prevalent procedure is to extend the pier far enough into the material below the zone of potential swelling to develop sufficient resistance to overcome the net uplift forces on the shaft, and to reinforce the shaft to withstand the tensile stresses. The anchorage may be provided by a sufficiently long shaft or by a bell, as discussed in Article 53.5.5.

If the shaft is part of a foundation supporting a structure, the structure must be isolated from the underlying soil. Otherwise, uplift forces will be exerted on the structure far in excess of those for which the shafts are designed. Structural floors supported by grade beams, all with clearance greater than the anticipated long-term heave of the ground surface, are customarily used to transfer the building loads to the piers.

### 53.5.9 Lateral Resistance of Drilled Shafts

The behavior of a drilled shaft under lateral loading is essentially no different from that of a laterally loaded pile. This subject is treated in Article 52.6. In general, piers are less likely than piles to behave as infinitely long units, and more attention is directed toward determining their ultimate moment capacity and stiffness. The use of  $p$  versus  $y$  curves and electronic calculation is routine (Reese 1984).

### Selected Reading

*Construction of Drilled Pier Foundations*, by David M. Greer and Wm. S. Gardner (1986, New York, John Wiley & Sons, Inc., 246 p.) is a readable and authoritative discussion of the equipment and procedures that are of overriding importance in achieving a satisfactory drilled pier foundation.

Reese, L. C. and M. W. O'Neill (1988). *Drilled Shafts: Construction Procedures and Design Methods*. U.S. Dept. of Trans. Fed. Hwy. Admin., Publ. No. FHWA-HI-88-042 or ADSC-TL-4.

The many publications of the International Association of Foundation Drilling (ADSC), 10925 Estate Lane, Suite 145, Dallas, TX 75235, deal with all aspects of design and construction of drilled piers. Intended primarily to ensure the quality of the practice of its members and to promote the use of drilled piers, the publications are useful to designers as well.

## CHAPTER 10

### *Settlement Due to Extraneous Causes*

#### ARTICLE 54 SETTLEMENT DUE TO EXCAVATION IN OPEN CUTS

##### 54.1 Characteristic Movements

The deformations associated with an internally braced or tied back cut depend on the stress-deformation properties of the affected soils, the dimensions of the excavation, and the type and workmanship of the support system. Removal of the excavated material reduces the vertical stresses not only directly beneath the bottom of the excavation but, to a lesser extent, at locations outside the excavated area. Consequently, to the extent that the soil behaves elastically, the soil beneath the excavation and the ground surface adjacent to it displace upward. As the depth of excavation increases, however, the soil alongside acts increasingly like a surcharge with respect to the material beneath the bottom and tends to produce a bearing-capacity failure (Fig. 37.4). The stresses then correspond more nearly to plastic than to elastic conditions; the soil beneath the bottom continues to rise, but that alongside tends to settle. Moreover, the inward movements of the walls of the cut tend to induce states of plastic equilibrium behind the walls with accompanying settlement of the adjacent ground surface (Fig. 27.3a). Hence, as the depth of a cut increases there is a gradual transition from near-elastic toward plastic states. Whether the ground surface adjacent to the cut rises or settles depends on the relative extent to which the transition has occurred in various parts of the affected soils. Except in very stiff cohesive soils, excavations of customary depths usually result in adjacent settlement (Fig. 54.1).

By using nonlinear stress-strain relations and by simulating excavation in stages, the behavior of braced or tied back excavations can be investigated quantitatively by finite-element procedures (Mana and Clough 1981, Clough and Tsui 1974). The results of such studies are particularly useful in assessing the influence of such variables as the stiffness of various wall systems, the vertical spacing between struts or tiebacks, the use of sloping berms in lieu of structural members, or the stiffnesses of

various soil strata alongside and beneath the excavation. Generalized results from these studies are presented later in this article. Nevertheless, because of the difficulties inherent in quantifying the necessary soil properties for analyses, and because of the great and usually unpredictable variations in construction details, progress, and workmanship, digests of field observations and semiempirical rules remain the most reliable basis for prediction of settlements caused by excavating and supporting open cuts.

Measured movements associated with a strutted excavation 18 m deep in dense sands and stiff clays in Washington, D. C., are shown on Fig. 54.2. The side walls consisted of timber lagging supported by steel H-beams set as soldier piles in predrilled holes backfilled with weak concrete (Article 46.3). Inward movement of the soldier piles was measured by inclinometers and reached successive positions on the days after start of construction shown by the numerals. The positions of the bottom of excavation at various times and the locations of the successive struts are similarly shown at the appropriate number of days. The rise of buried reference points between day 1 and the time of their exposure by excavation or, for those points below final excavation level, between days 1 and 116, is indicated by vertical arrows drawn to the same scale as that for the lateral movement of the soldier piles. Outside the soldier piles similar reference points indicated settlements of comparable magnitudes. Inclinometers at distances of 5 and 10 m from the edge of the cut reflected the deflected shapes of the soldier piles but to extents decreasing with increasing distance. The building on the right had been underpinned by jacked piles before excavation began. It settled about 13 mm during excavation, somewhat less than it settled as a consequence of the underpinning itself.

The set of observations exemplifies the behavior of many braced cuts. It also demonstrates the significant influence of details of construction procedure. The large bulge experienced by the soldier piles at a depth of about

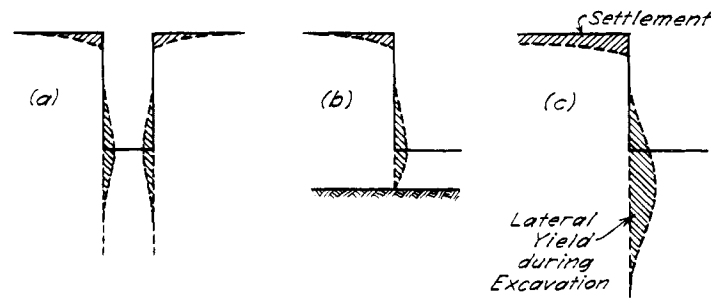


**Figure 54.1** Diagrams indicating settlement of ground surface adjacent to areas in which excavation operations are carried out: (a) Settlement due to lateral yield of clay beside narrow deep cut; (b) settlement due to lateral yield of clay beside wide deep cut above stiffer soil; (c) settlement due to lateral yield of clay beside and below wide deep cut in soft clay of great depth.

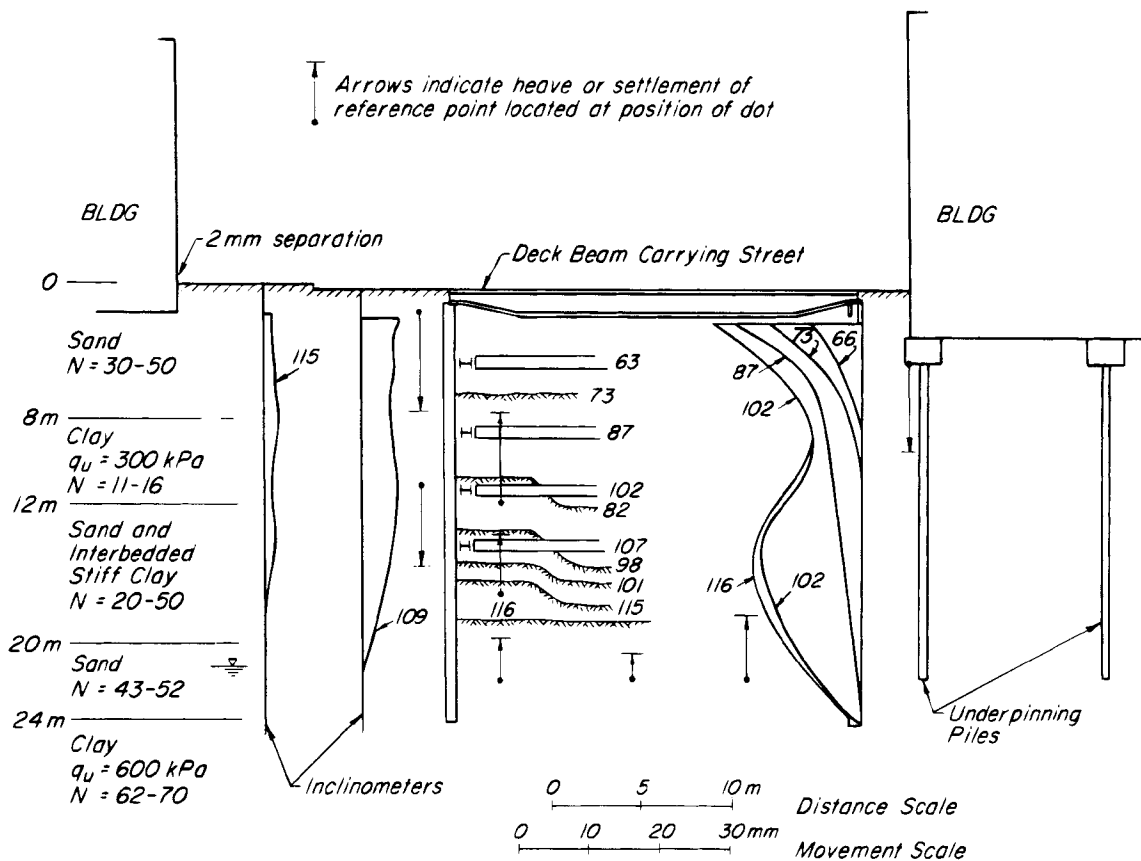


**Figure 54.2** Movements accompanying excavation and bracing of open cut 18 m deep in Washington, D.C. Numerals indicate number of days after start of construction (after O'Rourke 1975).

15 m between days 87 and 102 is a consequence of excavating below the strut placed on day 87 to a depth of about 17.5 m without installing any additional struts until days 102 and 107. An unbraced vertical distance of about 8 m existed just before day 102. The impracticability of foreseeing or excluding the possibility of such occurrences limits the accuracy of any forecast whether based on precedent or finite-element calculation.

The inward movement of the walls of the excavation is associated with settlement of the adjacent ground surface and stretching of the near-surface soil toward the cut. Both components of movement may be harmful to structures resting on or within the affected soil. The volume between the original ground surface and the surface in its settled position is closely related to the volume between the original and final positions of the walls. For

well constructed and supported cuts in drained sands and in stiff clays the ratio of the former to the latter is about 0.5; for soft to medium saturated clays it is about 1.0. Therefore, settlement and damage to adjacent buildings can be minimized by taking all practical measures to minimize the lateral movements. Nevertheless, for a cut of given dimensions, constructed by a particular method in a given soil, there are inevitably certain losses of ground and settlements that cannot be reduced by even the best of workmanship. Estimates of the inevitable settlements are required to permit judging the extent of damage that may occur to nearby buildings and to reach sound conclusions regarding the need to underpin or protect them; the estimates are also needed to allow an evaluation of the effect of the excavation on nearby utilities. If the settlements would be excessive for a particular method of construction, the cost of the ensuing damage must be compared with the cost of adopting a different method associated with smaller inevitable settlements.

The magnitude of the settlement of the ground surface adjacent to a cut and its variation with distance from the edge of the cut depend on many factors. Among the most important are the nature of the soil, the type of support and extent of prestressing of the struts or tiebacks, whether the wall rests on a firm support or can settle, and the success with which, in cohesionless soils, groundwater has been controlled (Goldberg et al. 1976). General experience is summarized by the set of curves (Fig. 54.3)

on which have been plotted a few points selected for discussion from the large store of available data. The figure refers to walls consisting of soldier piles and lagging or of sheet piles, and to soil deposits in which any cohesionless members are in a drained state. The discussion is divided into three parts: cuts in sand, cuts in soft to medium clays, and cuts in stiff clays or cohesive sands.

## 54.2 Cuts in Sand

### 54.2.1 Sand Above Water Table

If the adjacent ground surface carries no load, the settlement of a medium to dense sand beside a well braced or tied back cut is unlikely to exceed 0.5% of the depth of the cut or to extend beyond a distance equal to half the depth of the cut. If the ground is heavily loaded these values may double. The magnitude and extent of the movements are likely to be somewhat greater if the sand is loose. Thus, the settlements should be represented by points in zone I (Fig. 54.3). Points falling outside this zone are usually a consequence of local loss of ground associated with insertion of soldier piles or lagging, of the driving of sheet piles, or of inadequate dewatering.

### 54.2.2 Effect of Lowering the Water Table in Sand Strata

Pumping from sand that does not contain any clay strata increases the effective pressure, but the corresponding

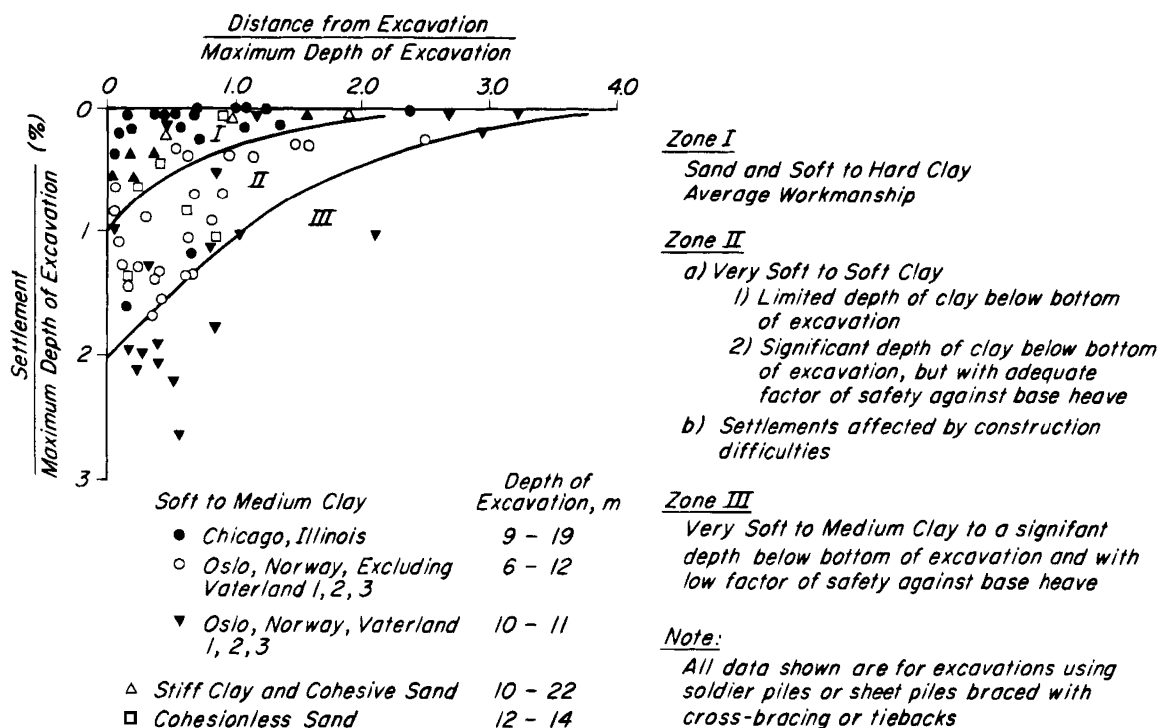


**Figure 54.3** Summary of settlements adjacent to open cuts in various soils as function of distance from edge of excavation.

settlement is usually small unless the sand is very loose. However, if the water table is raised and lowered periodically, the settlement may become important, because every temporary increase of effective pressure increases the settlement. This can be demonstrated by means of laboratory tests on laterally confined sand. The magnitude of the increment of settlement decreases with increasing number of cycles and approaches zero, but the final total settlement is several times greater than the settlement produced by the first cycle. The looser the sand, the greater is the settlement.

During construction in an open excavation fluctuations of the lowered water table are usually insignificant. Therefore, if pumping causes large settlements in any but very loose sand, the settlements are probably due to causes other than the increase of the effective weight of the drained portion of the sand. The most common cause is careless pumping from an open sump (Article 43.2). Several instances of settlement due to this cause are described in Article 58.2. In all these instances one or more subsurface conduits were formed by backward erosion from springs that discharged into a pit. The settlement produced by the erosion led to the formation of shallow and narrow troughs located above the conduits. The width and depth of the troughs increased with increasing distance from the springs, and the troughs terminated in sink holes. Settlement of this type can be avoided by pumping from well points or by providing the sump with a filter lining.

Loss of ground can also occur on one or both sides of an open cut lined by watertight sheet piles. The loss is caused by the erosive action of water as it rises toward the bottom of the cut along the inner face of the sheet piles. It can be avoided by providing the sides of the cut with a permeable instead of an impermeable lining (Prentis and White 1950). The following observation demonstrates the efficacy of this procedure. A subway cut was made in New York through fine sand and coarse silt close to buildings founded on pile-supported footings. The points of the piles did not rest on a hard stratum. In one section of the cut the bracing was of the type shown in Fig. 46.2a. The sheeting consisted of boards placed horizontally with spaces between them, as shown in Fig. 54.4a. The spaces were packed with marsh hay to permit free flow of water into the cut without allowing sand to enter. In a second section the sheeting consisted of steel sheet piling driven along the sides of the cut. The sheeting compelled the water to enter the cut by percolating under the sheet piles, as indicated in Fig. 54.4b. Therefore, conditions were favorable for the development of erosion by springs, and the footings of the adjacent buildings settled about 150 mm. Excavation of the section with permeable sheeting, on the other hand, produced no noticeable settlement.

### 54.3 Cuts in Soft to Medium Clays

If the factor of safety against heave of the bottom of the cut (Eq. 37.4) is greater than about 1.5, the lateral movement of the wall and, hence, the settlement of the adjacent ground surface are functions primarily of the width-to-depth ratio of the cut, of the value of the factor of safety against base heave (Eqs. 37.6 and 37.7), and of the construction procedure.

If the cut is very narrow (Fig. 54.1a) or if the bottom of the cut is located close to the surface of a firm stratum (Fig. 54.1b), the lateral yield spreads only a short distance from the sides of the cut. Therefore, the settlement of the ground surface is restricted to relatively narrow belts located on each side of the cut. The width of these belts does not exceed the depth of the cut. Beyond this distance the settlement is inconsequential. By careful bracing the inward yield of the clay can be kept within 0.5% of the depth of the cut, and the greatest surface settlement is of the same order of magnitude. Appreciably greater settlements are usually due to poor workmanship.

If the cut is wide and the clay is soft to a great depth below the bottom, the lateral yield involves a wide and deep body of clay (Fig. 54.1c). The corresponding settlement may extend to a distance considerably greater than the depth of the cut. For values of the factor of safety  $F$  against base failure (Eqs. 37.5 or 37.7) greater than about 3 the points representing the settlement of the adjacent ground surface are likely to lie within zone I (Fig. 54.3). For smaller values of  $F$  the movements are larger. The maximum lateral movement depends on  $F$ , the depth of the cut  $H$ , the structural stiffness  $EI$  of the wall, the vertical distance between supports, and the vertical distance that excavation is advanced below the lowermost set of supports installed at any given stage of construction. On the assumptions that the supports are spaced vertically at approximately equal distances and the excavation is extended the minimum practical distance below the elevation of a set of supports before that set is installed, the maximum lateral movement  $\delta_{h \max}$  is a function of the *system stiffness*, defined as  $EI/\gamma_w h_{av}^4$ , where  $EI$  is the flexural stiffness of the wall itself per unit of length along the wall, and  $h_{av}$  is the average vertical spacing between struts. The results of finite-element studies to establish the relationships among these quantities are indicated by the family of curves (Fig. 54.5a), and a comparison of the results of field observations with those predicted by the finite-element studies is shown in Fig. 54.5b (Clough et al. 1989).

The theoretical studies represented by Fig. 54.5a do not pertain solely to conditions prevailing when the cut has reached its final depth. In most localities the shear strength  $s_u$  varies with depth; it is not unusual, for example, that the soil profile consists of a stiff crust underlain by a much softer material having a strength that increases



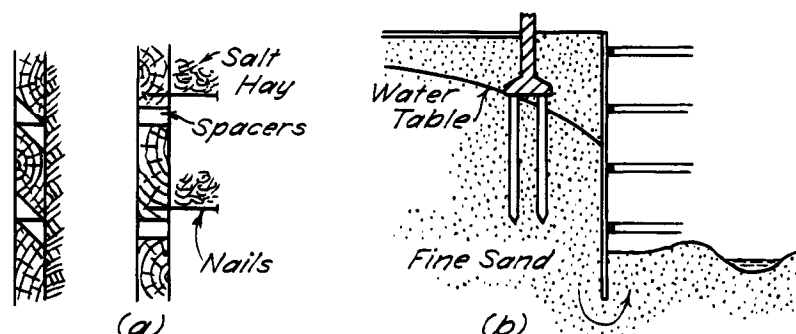


**Figure 54.4** (a) Louvre-type sheeting successfully used in part of open cut in water-bearing sand to prevent loss of ground. (b) Continuous steel sheeting used in other sections of the same cut. Adjacent foundations settled on account of loss of ground by erosive action of rising water veins (after Prentis and White 1950).

with depth, often in abrupt steps. Under such circumstances the factor of safety against basal heave may be a minimum when the excavation depth is well above the final grade, and the value of maximum lateral movement may be governed by conditions at an intermediate depth. Therefore, in practical applications of Fig. 54.5, the value of  $F$  should be calculated for a series of excavation depths in accordance with the actual shear-strength profile of the clay. If at some intermediate depth  $F$  should be close to unity, distortion of the support system and excessive ground movements would be expected unless preventive measures were adopted as discussed subsequently.

It is evident from Fig. 54.5 that a significant reduction of the maximum lateral wall movement of a cut in a particular deposit of clay can be achieved only by a disproportionally large increase in system stiffness. For example, for a value of  $F$  of 1.4 and a system stiffness of about 36, the maximum lateral deflection is about 1% of the depth of the cut. To reduce the maximum movement to half this value, a system stiffness of 300 would be required. Thus, in some instances, reduction of movements to acceptable values may require more radical measures than mere modification of the bracing system. Such measures are discussed subsequently.

The maximum lateral deflection  $\delta_{h \max}$  of the wall of the excavation support system is only an index to the general movements around the cut. Assessment of the potential damage to adjacent structures and utilities requires an estimate of the magnitude and distribution of the settlement of the adjacent ground surface and of the horizontal displacements of the soil alongside the cut. The distribution of settlement usually has the characteristic shape shown by the inset in Fig. 54.6. The maximum value ordinarily occurs a short distance beyond the edge of the cut because the wall usually develops some resistance to penetration in the underlying materials and supports the immediately adjacent clay by adhesion. The maximum settlement,  $S_{\max}$ , is approximately equal to the maximum lateral movement  $\delta_{h \max}$ . Finite-element studies

and field observations indicate that the curves representing the distribution of surface settlement  $S$  on sections perpendicular to the walls of a cut fall within the rectangular envelopes shown in Fig. 54.6, and that the envelopes are functions of the factor of safety  $F$  against basal heave (Mana and Clough 1981). On the basis of Fig. 54.6, a curve can be sketched to represent a reasonable approximation to the anticipated surface settlement.

The displacements of the ground surface toward the cut, which result in translation or horizontal straining of near-surface structures or utilities, can also be expressed in terms of the maximum lateral deflection of the wall. These horizontal displacements are a rather complex function of the distance from the wall. If the wall is supported by struts placed as the cut is deepened, the uppermost struts restrain the movement of the soil near the cut, but at lower elevations the inevitable inward deflection of the wall as excavation deepens results in horizontal movements of the surface farther from the edge. Consequently, the near-surface soil may be compressed horizontally within distances approximating the depth of excavation, and stretched horizontally at greater distances. Finite-element studies (Clough et al. 1989) indicate that the lateral displacements toward the cut are a function not only of the depth of excavation, but also of the factor of safety  $F$  against failure of the base of the excavation by heave. Figure 54.7 indicates the results of such a study, in which the horizontal surface displacements are expressed in terms of the maximum lateral displacement  $\delta_{h \max}$  of the wall. The figure may be expected to provide reasonable approximations to the horizontal surface movements in a strut-braced excavation. However, if the supports consist of tiebacks, less restraint is likely to be provided at the top of the cut, and the pattern of deformation may differ correspondingly.

Design with the aid of Fig. 54.5 first requires determining the ground movements that may be considered tolerable as a result of the construction. This determination

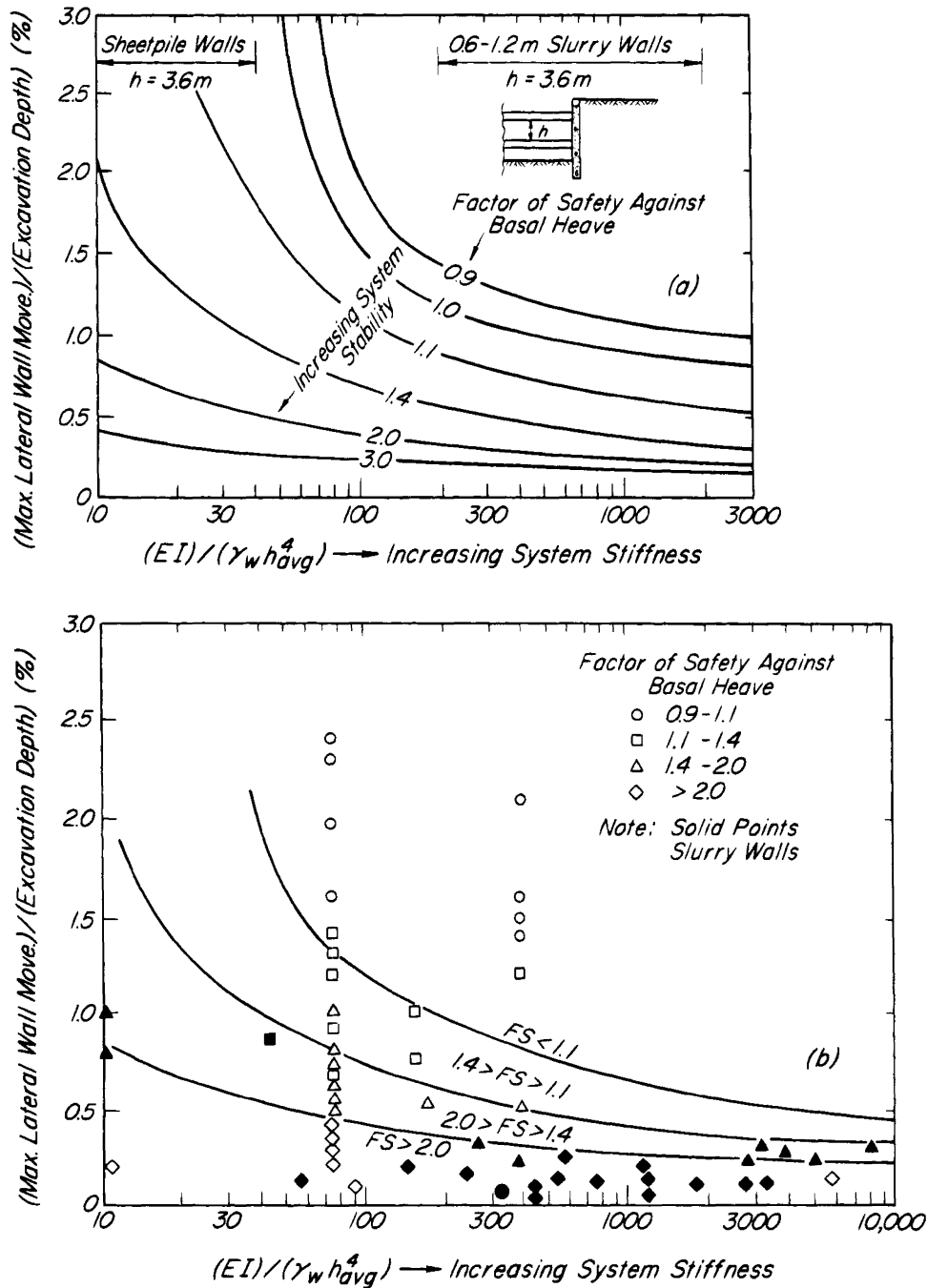


**Figure 54.5** Relation among maximum lateral wall movement, system stiffness, and factor of safety against basal heave for cuts in plastic clay: (a) calculated by finite-element solutions; (b) comparison with field measurements (after Clough et al. 1989).

permits establishing the value of  $\delta_{h \max}$ . From the soil profile, values of  $F$  are calculated for successive stages of excavation. A layout of the wall and system of struts and tiebacks is then assumed, from which the system stiffness  $EI/\gamma_w h_{av}^4$  is computed. From Fig. 54.5 the value of  $\delta_{h \max}$  is determined and compared with the tolerable

value. If the results are unsatisfactory, a new layout for the support system is selected and the procedure is repeated. When a satisfactory layout is achieved, the struts or tiebacks and other aspects of the support system are designed on the basis of the loads determined in accordance with Article 46.

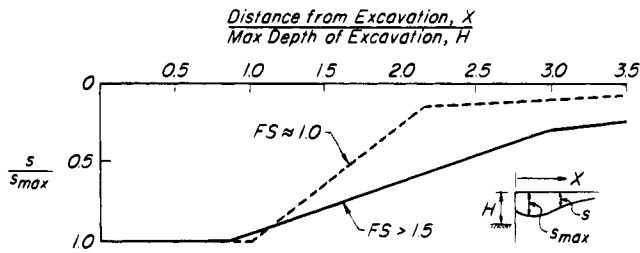


**Figure 54.6** Envelope of curves representing settlement of ground surface adjacent to braced open cut in soft to medium clay as function of factor of safety  $F$  against basal heave (after Mana and Clough 1981).

The movements associated with excavating a wide cut in a very deep deposit of medium clay of moderate sensitivity ( $S_t = 3-7$ ) are illustrated by Fig. 54.8, which represents the excavation for a subway in Oslo (NGI 1962e). The average undrained shearing resistance was about 40 kPa. Heavy steel sheet piles were driven on both sides of the cut to a depth of about 2m below final grade; bedrock was at a depth of more than 10m below the bottom of the excavation. While the excavation progressed the sheet piles moved inward, in spite of the

successive insertion of struts, as shown in the figure. Correspondingly, the soil beneath excavation level rose, as indicated by the dash lines representing the upward movements of reference points  $H1$  and  $H2$ , and the surface of the ground settled adjacent to the cut. Up to 80 days after the start of excavation, the factor of safety against basal heave was greater than about 3.2 (Fig. 54.8b), and all the movements were small. Between days 80 and 109,  $F$  decreased to about 1.5 and heave of the bottom and inward movements of the sheet piles increased markedly. During the same interval, the settlement spread from the edge of the cut to a distance of more than twice the depth of excavation, and cracks developed in the three-story brick building. The increase of the settlement with decreasing  $F$  is shown in Fig. 54.8b, in which the settlement is represented by the volume of subsidence adjacent to one side of the cut, per lineal meter measured along the cut.

Although the settlements adjacent to the cut represented in Fig. 54.8 might have been reduced by increasing the depth of the sheet piles, the reduction would have been very small. This conclusion is based on the large changes in curvature experienced by the compara-

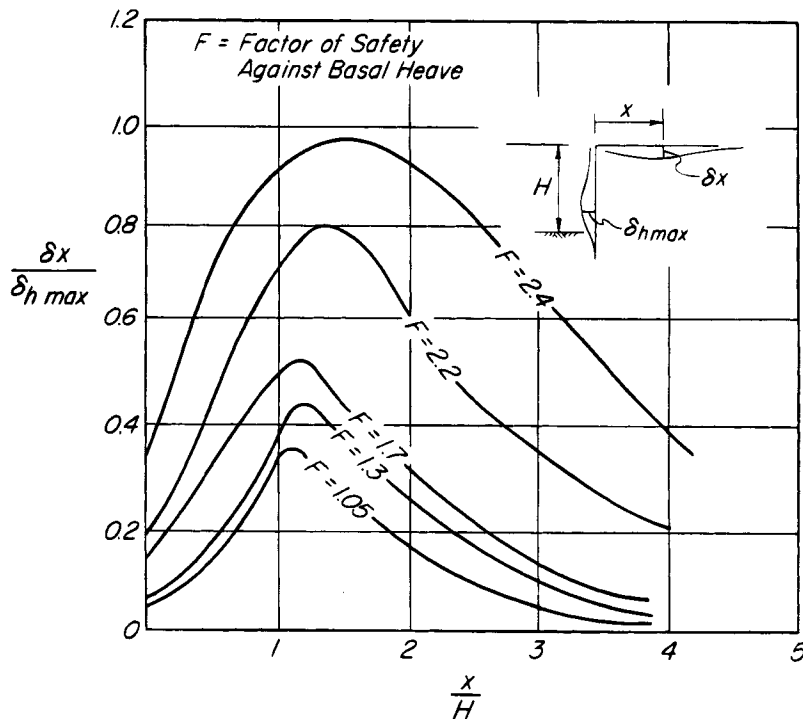


**Figure 54.7** Horizontal movement  $\delta_x$  toward wall of braced open cut in clay, at distance  $x$  from face of cut, for various values of factor of safety  $F$  against heave of bottom of cut, as determined by finite-element calculations (after Clough et al. 1989). Values of maximum lateral movement  $\delta_{h\max}$  to be determined from Fig. 54.7.

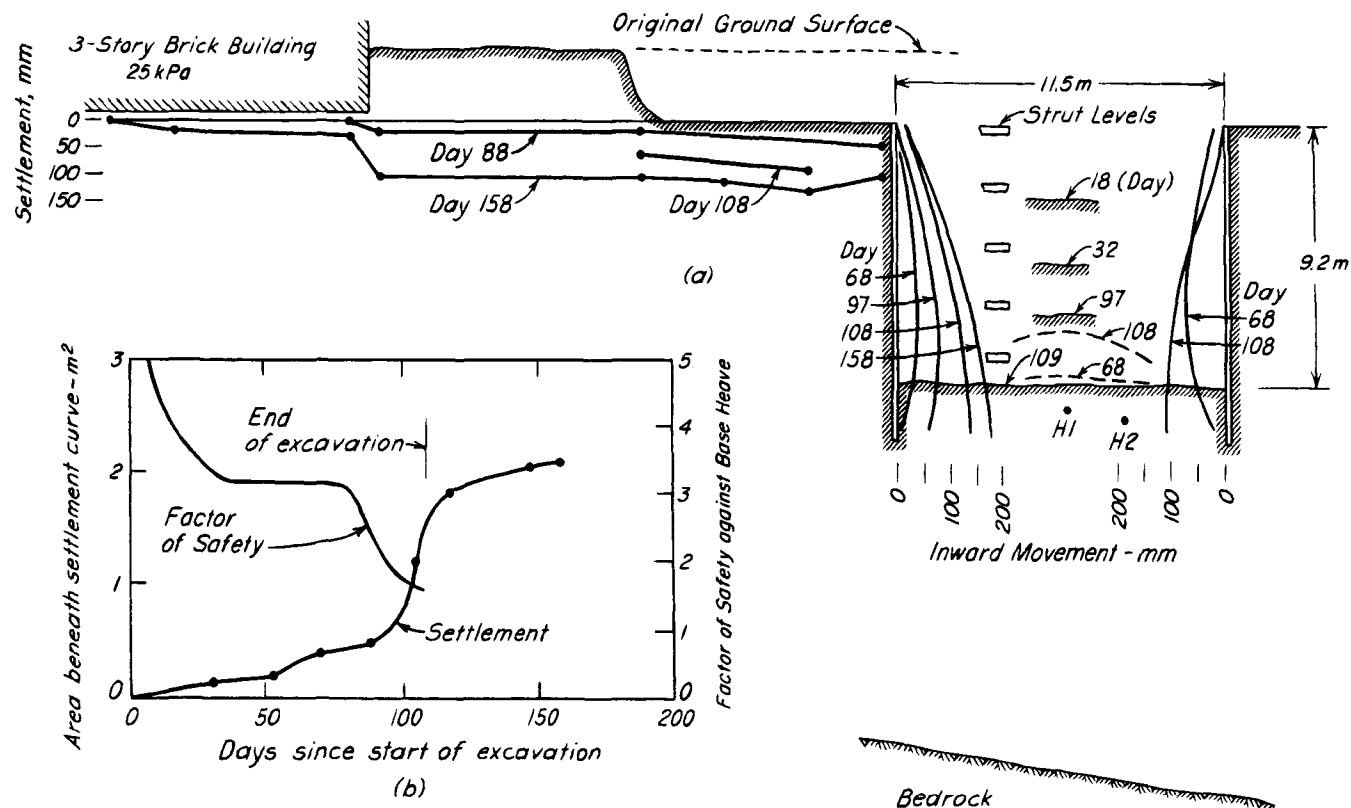


**Figure 54.8** Diagrams showing results of measurements of adjacent settlement, heave of bottom, and lateral yield of sheet piling at sides of open cut in deep deposit of medium clay in Oslo: (a) Successive positions of ground surface and sheeting on designated days; (b) progress of settlement and decrease of factor of safety  $F$  against bottom heave as function of time since start of excavation (after NGI 1962e).

tively stiff sheet piles even at intermediate stages of excavation. As a matter of fact, before construction of the cut the elevation of the surrounding ground surface was lowered by excavating to a depth of about 2 m. This increased the value of  $F$  at the bottom of the cut from 1.2 to 1.5 and doubtless substantially reduced the potential movements.

#### 54.4 Cuts in Stiff Clays or Cohesive Sands

The settlements adjacent to well supported cuts in such materials are usually small and are represented by points in zone I (Fig. 54.3). At two cuts reaching depths of 17 and 19 m through stiff fissured clays in Houston (Ulrich 1984) the adjacent ground surface experienced a net rise, represented by points above zone I. Appreciable rises have been noted adjacent to shallow subway cuts in Mexico City where the strength of the clay is relatively large in comparison with its initial tangent modulus.

Cuts in stratified soils consisting of stiff clays, dense sands, and cohesive sands, exemplified by Fig. 54.2, are also likely to be represented by points in zone I.

#### 54.5 Wide Cuts with Berms

If a cut is too wide for practical use of cross-lot bracing the walls are often supported by tiebacks. Where this is not practical, either because of right-of-way limitations or inability of the adjacent soil to provide adequate anchorage, inclined struts or *rakers* are often used (Fig. 54.9a). After the walls have been installed, the soil in the central part of the excavation is removed to grade while berms are left around the periphery to support the walls and to reduce the tendency toward base failure. Often the central portion of the permanent foundation or base slab is cast, after which the tops of the walls are supported by rakers reacting against the base slab. The berms are then successively cut down and additional rakers installed as lower portions of the walls are exposed.

The lateral movements of the walls and the corresponding settlements depend not only on the dimensions of the berms and location of the rakers, but in clays also on the stability number (Eq. 37.8). The beneficial influence of the berms has often been overestimated for values of stability number greater than about 3. The relation among

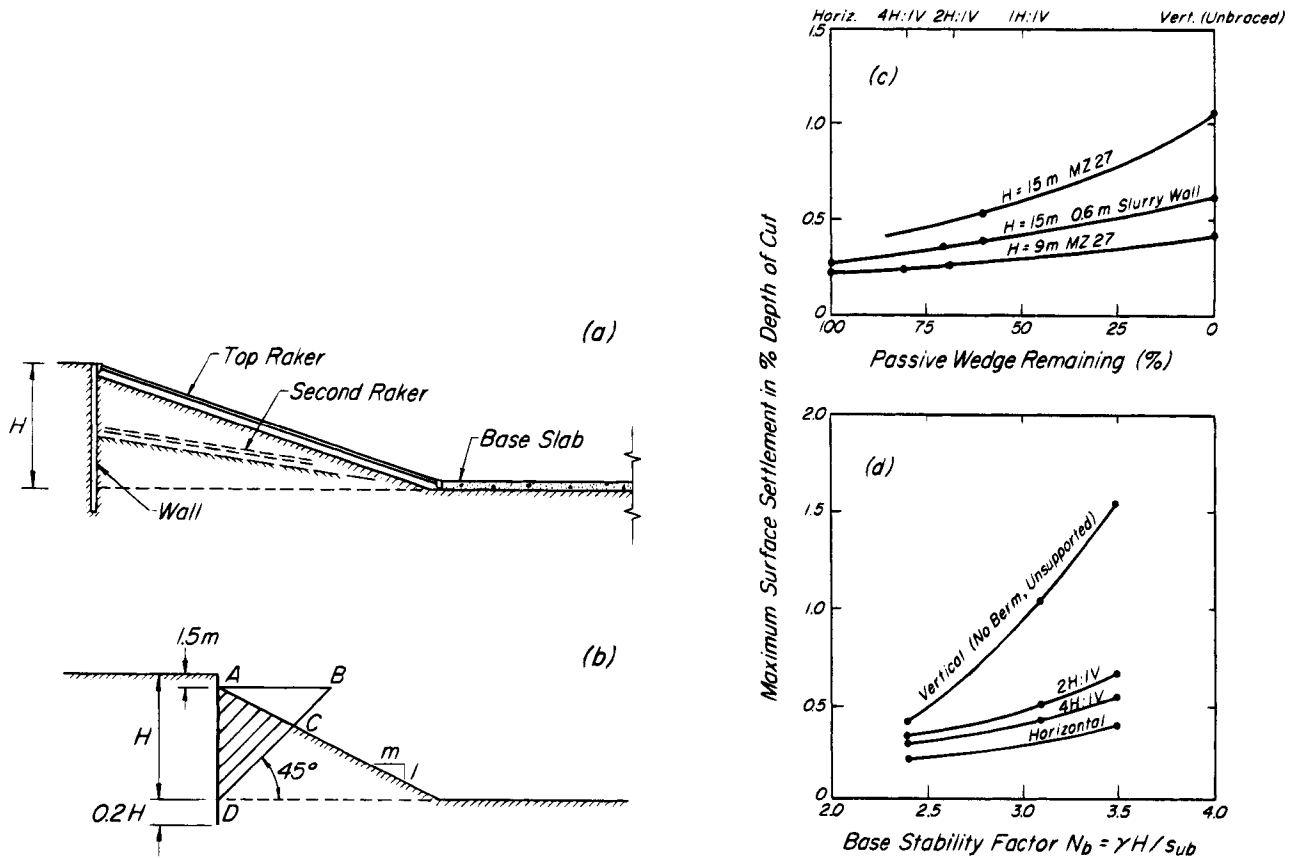


**Figure 54.9** Effect of berms in reducing settlement adjacent to wide cut in clay: (a) Components of berm and raker system; (b) geometry of excavation for calculations of settlement; (c) relation of settlement to slope of berm and stiffness of wall; (d) relation of settlement to slope of berm and base stability factor (after Clough and Denby 1977, Clough and Schmidt 1981).

the stability number, dimensions of berm, and maximum settlement adjacent to several cuts of typical dimensions has been investigated by finite-element procedures (Clough and Denby 1977) and the results found to be in reasonable agreement with measurements on two full-sized cuts. The principal findings are illustrated in Fig. 54.9, *c* and *d*.

The geometry of the cuts to which the calculations pertain is shown in Fig. 54.9*b*. The final depth of excavation is  $H$ ; the wall penetrates into the clay beneath final grade a distance  $0.2H$ . The berm, with a slope of  $1V:mH$ , begins at a depth of 1.5 m below the original ground surface, where the reaction of the first raker is applied. The wedge  $ABD$ , with its lower surface rising at  $45^\circ$ , is termed the *passive wedge*; the shaded area  $ACD$  is designated the *passive wedge remaining* at the excavation stage shown. As indicated in Fig. 54.9*c* the adjacent settlements are a function of the percentage of the passive wedge remaining, equal to  $100 \cdot \text{Area } ACD / \text{area } ABD$ , or  $m/(m+1)$ . The undrained shearing strength is assumed to have a value of 50 kPa at the ground surface and to

increase with depth by an amount  $0.3 \sigma'_v$  where  $\sigma'_v$  is the vertical effective pressure before excavation.

The influence of the slope of the berm is indicated in Fig. 54.9*c*. It is evident that the maximum settlement adjacent to the cut increases significantly as the slope of the berm becomes steeper. The influence of the stiffness of the wall itself can be judged by comparing the settlements adjacent to the two 15-m walls, one of which consists of MZ-27 sheet piles ( $EI = 50,000$  kPa/m) and the other of a 600-mm concrete slurry wall ( $EI = 403,000$  kPa/m). The influence of the depth of the cut is illustrated by comparing the settlements for the 9-m and 15-m cuts for which the walls consist of MZ-27 sheet piles. The former is braced by rakers at two levels; four levels are provided for the latter.

The significance of the slope of the berm and of the base stability factor  $N_b$  is illustrated in Fig. 54.9*d*. The walls to which this chart refers are all of MZ-27 sheet piles; the depth  $H$  is 9 m; and the value of  $s_u = 25 + 0.3 \sigma'_v$  (kPa). Two trends are evident: the settlements increase rapidly with increasing  $N_b$  and with increasing

steepness of berm. For a given value of  $N_b$ , the settlements associated with a 2:1 berm are roughly double those that would be associated with excavation to a constant level with supports inserted as the excavation proceeds. Berms steeper than 2:1, especially for values of  $N_b$  greater than about 2.5, are relatively ineffective.

Where settlements adjacent to a wide cut must be severely restricted, the rakers are sometimes installed in trenches excavated in the berms before the next general reduction of the size of the berms is carried out.

In some instances the rakers react not against a completed portion of the foundation slab but against pile-supported or soil-supported inclined footings or kicker blocks. Such supports often experience excessive movement even though their nominal factor of safety may seem adequate. They must be designed to limit deflection.

#### 54.6 Measures for Reduction of Settlement

The settlement adjacent to an open cut can be minimized by reducing the vertical spacing between struts or tiebacks, by increasing the bending stiffness of the walls, by excavating no deeper than necessary for insertion of the struts or tiebacks, and by appropriate prestressing of the supports. For cuts in soft to medium clay the maximum lateral movement  $\delta_{h \max}/H$  of a supported wall, and hence the settlement, have been found empirically and by finite-element studies to be functions of the factor of safety  $F$  against basal heave and the ratio  $EI/\gamma_w h_{av}^4$  as shown in Fig. 54.5. Movements of walls in granular materials wherein upward seepage pressures are not present beneath the bottom of the excavation are comparable to those indicated by Fig. 54.5 for values of  $F$  roughly equal to 2.

The stiffness of a typical wall consisting of soldier piles and lagging is approximately an order of magnitude smaller than that of a reinforced concrete slurry wall 600 mm thick. By decreasing the vertical spacing between supports by about 44% in the soldier pile wall the value of  $EI/h^4$  can be increased a corresponding amount. Whether it is preferable to decrease the spacing or to install a stiff wall becomes a matter of economics and practicality at a particular site.

As the factor of safety  $F$  against basal heave of an excavation underlain by clays of great depth decreases from 2 or 3 to 1.2 or less, the lateral movements are associated with increasing tendency toward base failure and cannot be controlled entirely by increasing the stiffness ratio  $EI/h^4$ . Three general methods are available for reducing the tendency to heave: the effective width of the excavation can be decreased, as illustrated in Fig. 54.1a; a vertical pressure  $\sigma_v$  can be applied to the bottom of the excavation; or the depth of the cut can be decreased by lowering the level of the adjacent ground surface for a considerable distance from the cut. All three methods have been used successfully.

The effective width can be reduced by making the excavation in compartments. For example, the area to be excavated may first be surrounded by tremie concrete walls cast in trenches constructed by the slurry method to a depth well below the bottom of the future general excavation. Slurry walls are then constructed across the width of the cut to form a series of compartments. The compartments are then successively excavated and braced. Finally the transverse slurry walls are removed above the general excavation level. Obviously, this method is slow and expensive.

The factor of safety against basal heave has been increased to an acceptable value in a few instances by constructing the side walls, supporting a structural roof on the walls, and carrying out the excavation beneath the roof under compressed air. This procedure was used, for example, on the original Oslo subway (Eide et al. 1974). In other instances excavation has been carried out by dredging under water and placing a tremie concrete base slab, capable of resisting the heave and lateral forces, before unwatering (NGI 1966). In either procedure excess hydrostatic pressures beneath the base slab must be controlled before the stabilizing air or water surcharge is removed.

If a firm base exists at a considerable depth below the bottom of the excavation, it may be practicable to construct walls or soldier piles of sufficient strength and stiffness to withstand without excessive movement the lateral pressure between the lowest support and the top of the firm base in which the walls are embedded. To control the lateral movements and settlements adjacent to the Embarcadero Station of the San Francisco Bay Area Rapid transit system (Fig. 54.10), unusually stiff walls and close vertical spacing of struts were required (Armento 1973). At a depth of excavation of 12 to 15 m the factor of safety against basal heave was as little as 0.7 on account of the presence of 9 to 12 m of clay having an undrained shear strength of 20 to 40 kPa beneath the excavation level. Thus, at that stage, large ground movements would inevitably have occurred unless extraordinary precautions were taken. The walls were therefore designed as soldier piles consisting of built-up steel beams having overall distances back to back of flanges up to 1.23 m. The piles were installed to depths as much as 11 m below final excavation depth in slurry-filled auger holes of diameters slightly less than the outside distance between flanges. The space between adjacent soldier piles was excavated by clamshell bucket while being kept filled with slurry. The slurry was then displaced by tremie concrete. Such a wall is known as a soldier-pile tremie-concrete, or *SPTC*, wall. The success of the procedure may be judged by the magnitude of the lateral movements shown in Fig. 54.10c. The maximum displacement of about 25 mm occurred below midheight of the cut. In spite of the large embedment below final

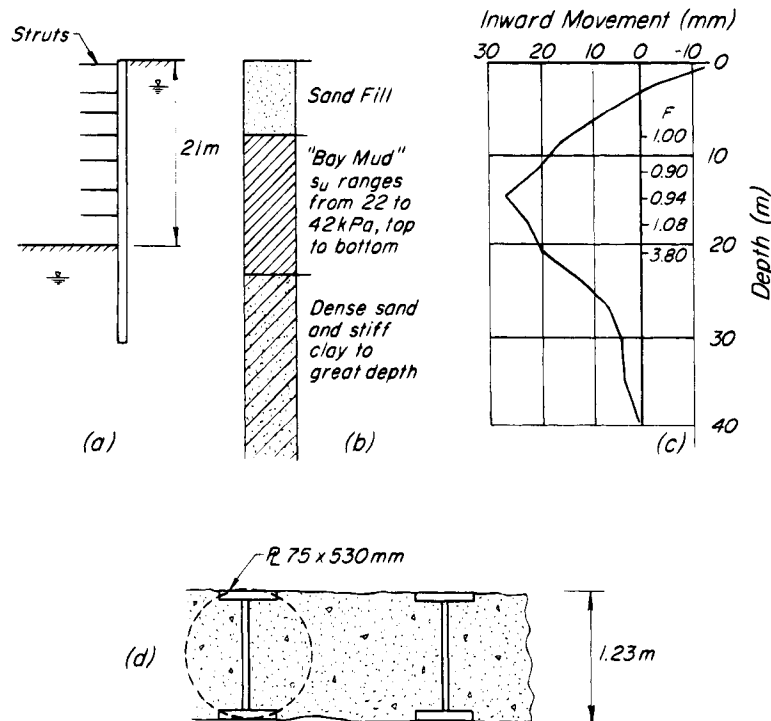


**Figure 54.10** Deep braced excavation for Embarcadero Station on San Francisco Bay Area Rapid Transit: (a) Cross-section showing strut levels; (b) soil profile; (c) lateral displacements of SPTC wall after completion of excavation, together with values of factor of safety  $F$  against base heave for excavation to depths shown; (d) detail of SPTC wall.

grade some rotation of the wall occurred at the bottom, and an appreciable part of the lateral movement took place below final grade of the cut. To avoid consolidation settlement of the surrounding area the water level was maintained at its original elevation outside the SPTC wall, but to avoid a blow-up of the base due to water pressure in the sandy members of the underlying soils the water level was lowered between the walls.

### Selected Reading

The results of investigations made to determine the settlement during construction and of the factors influencing it are contained in the following:

- Terzaghi, K. (1938b). "Settlement of structures in Europe and methods of observations," *Trans. ASCE*, **103**, pp. 1432–1448. Effect of filling of oil tanks on settlement of neighboring tanks.
- Terzaghi, K. (1942). "Shield tunnels of the Chicago subway," *J. Boston Soc. Civil Engrs.* **29**, pp. 163–210. Record of heave and settlement due to shoving a shield through soft clay.
- Peck, R. B. (1943). "Earth-pressure measurements in open cuts, Chicago subway," *Trans. ASCE*, **108**, pp. 1008–1036. Record of settlements due to excavation of open cuts in soft clay.

- Terzaghi, K. (1943a). "Linerplate tunnels of the Chicago subway," *Trans. ASCE*, **108**, pp. 970–1007. Settlements caused by the construction of linerplate tunnels in soft clay.
- Ireland H. O. (1955). *Settlements due to Foundation Construction in Chicago, 1900–1950*, Ph.D. thesis, Univ. of Illinois, 128 pp.
- Norwegian Geotechnical Institute, *Technical Reports* Nos. 1–8, Oslo, 1962–1966. Series of reports on measurements made in connection with excavations for braced open cuts in Oslo, including observations of settlement, movement of sheeting, and heave of bottom.
- Boscardin, M. D. and E. J. Cording (1989). "Building response to excavation-induced settlement," *J. Geotech. Eng., ASCE*, **115**, No. 1, pp. 1–21.

## ARTICLE 55 SETTLEMENT DUE TO INCREASING STRESS IN SUBSOIL

### 55.1 Effect of Adjacent Loads

The application of a load to one portion of the ground surface above any type of soil causes the surface of the adjacent soil to tilt. The distance within which the tilt is of any practical importance depends on the soil profile as well as the dimensions of the loaded area. If the subsoil contains soft clay, the magnitude and distribution of the settlement can be roughly estimated on the basis of the results of soil tests. If the subsoil is sand, the settlement

cannot be computed and estimates can be based only on the records of precedents.

If rafts on sand are designed in accordance with the rules contained in building codes, they are likely to settle as much as 50 mm. Exceptionally, they may settle even more. Because the greatest part of this settlement occurs during construction, the structure itself will not be damaged unless it is very sensitive. However, the tilt of the adjoining ground surface toward the loaded area may be great enough to damage neighboring structures. In New York, for example, a 20-story building was constructed on a lot between two 7-story buildings supported by spread footings on a deposit of fine sand. The new building rested on a raft at a depth of 6 m below the ground surface. The soil pressure was 200 kPa in excess of the weight of the soil removed. Because the building itself settled only 46 mm and the settlement was fairly uniform, the building remained intact. Yet, the neighboring buildings were damaged by shear cracks and by distortion of door and window frames.

If the subsoil consists of soft clay, the effect of the weight of a new building on its neighbors can be much greater, although not necessarily more detrimental. In Istanbul a tall building was erected on a site separated from that of its equally tall neighbor by a narrow alley. The new structure caused such a large tilt of the old one that the cornices of the two structures came into contact with each other.

## 55.2 Effect of Pumping on Clay Strata

If the subsoil contains layers of soft clay, silt, or peat, lowering of the groundwater table may cause large settlements. In Mexico City, for example, where the subsoil consists of highly compressible clays with horizontal layers of water-bearing sand, the withdrawal of water by drainage and by pumping from sand layers has been accompanied by a general irregular subsidence of the whole area. Between 1900 and 1960 the surface in some places settled more than 8 m. Similarly, in the Santa Clara Valley in California, the operation of 2000 wells to provide water for irrigation initiated a process of pro-

gressive settlements. The floor of this valley is underlain by a thick bed of marine clay that contains layers of water-bearing sand and gravel at a depth of 30 to 60 m. In 1918 the withdrawal of water began to exceed the natural supply, and the piezometric levels began to descend. By 1956 the corresponding settlement had reached locally as much as 2.5 m (Poland 1958). The increasingly severe flooding of the Piazza San Marco in Venice turned worldwide attention to subsidence due to pumping from sand layers interspersed among compressible clays. Settlements of 0.12 m occurred in the period 1952 through 1970. During about the same period, moreover, the nearby city of Ravenna, also in the deep alluvial valley of the Po River, subsided some 0.84 m, largely as a result of groundwater pumping but also in part because of recovery of natural gas (Carbognin et al. 1978). Even localities underlain by stiff clays have experienced significant subsidences. Lowering of the water levels beneath Houston by some 75 m between 1905 and 1951 was accompanied by a subsidence of as much as 0.6 m associated with local faulting and sharp differential settlements of ordinary structures (Lockwood 1954). Similarly, subsidences in London on the order of 0.2 m occurred between 1865 and 1931; during the same period the piezometric levels declined roughly 60 m. (Wilson and Grace 1942). Similar phenomena have occurred above oil fields, notably in Long Beach, California (Berbower 1959) and at Lake Maracaibo, Venezuela (Collins 1935).

The physical causes of this phenomenon are illustrated in Fig. 55.1, which represents a section through a bed of saturated clay overlying a pervious sand layer. In Fig. 55.1a the piezometric level is assumed to be at the ground surface; in *b* it has been lowered through the distance  $\Delta H$  by pumping from the layer of sand. Before pumping, the effective vertical pressure on a section *ab* is

$$\sigma'_v = \gamma' H_1$$

where  $\gamma'$  is the submerged unit weight of the clay (Article 15.3). During and after pumping the effective vertical pressure gradually increases and approaches a final value

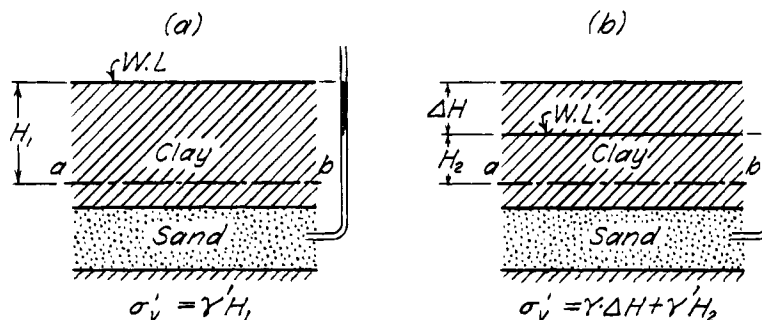


**Figure 55.1** Diagrams illustrating cause of settlement of clay surface due to pumping from underlying water-bearing sand.



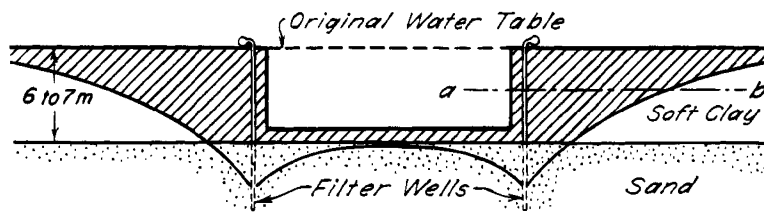


**Figure 55.2** Simplified cross-section through excavation for Vreeswijk Locks, Holland, showing position of water table lowered by filter wells during excavation (after Brinkhorst 1936). Vertical scale greatly exaggerated.

$$\sigma'_v = \gamma \Delta H + \gamma' H_2$$

where  $\gamma$  is the total unit weight of the saturated clay. The change in effective vertical pressure due to the lowering of the piezometric level is

$$\gamma \Delta H + \gamma' H_2 - \gamma' H_1 = \Delta H(\gamma - \gamma') = \gamma_w \Delta H$$

Therefore, lowering the water table by a distance  $\Delta H$  ultimately increases the effective vertical pressure on a horizontal section through the clay by an amount equal to the weight of a column of water  $\Delta H$  in height. This increase involves a progressive settlement of the surface of the clay due to consolidation. The rate and magnitude of the settlement can be computed on the basis of the theory of consolidation and the results of soil tests (Articles 16,25). However, in areas of large regional subsidence due to the consolidation of great thicknesses of stiff soils, the results are not likely to be reliable because the compressibility of the soils is altered substantially by the sampling procedures, and the location and degree of continuity of drainage layers often cannot be assessed.

If the clay strata are soft and thick, and if the water table is lowered through a considerable distance, the settlement due to pumping is likely to be very great and to spread over a large area. A record of settlement of this type was obtained during the construction of the Vreeswijk locks in Holland. At the site of the locks the subsoil consisted of 6 to 7 m of clay and peat underlain by a thick layer of water-bearing sand. The bottom of the pit was 6 m below the ground surface and covered an area 52 m wide by 270 m long.

Before construction the water level was 0.2 m above the ground. During excavation it was lowered, by pumping from filter wells that extended into the sand, to the position indicated in Fig. 55.2. As a result of the pumping, the effective vertical pressure on any horizontal section such as  $ab$  was increased gradually by an amount equal to the height of the shaded area above  $ab$  times the unit weight of water. Because the height of the shaded area was a maximum adjacent to the excavation, the settlement was greatest at the edge of the cut. Even at a distance of 40 m, the settlement amounted to 0.6 m, and it was noticeable as far as 1000 m (Brinkhorst 1936).

On several construction projects the subsidence adjacent to the dewatered zone has been prevented or greatly reduced by surrounding the site by sheet piles and injecting water outside the sheeting by means of well points or filter trenches (Zeevaert 1957, Parsons 1959). The injected water is commonly obtained from the dewatering system. Provision should be made for cleaning the injection wells because of their tendency to become clogged, particularly by bacterial action. The subsidence in the vicinity of Long Beach was virtually stopped after a program of repressurization of the oil-bearing formations by the injection of water was put into effect in 1959.

### Selected Reading

- Wilson, G. and H. Grace (1942). "The settlement of London due to under-drainage of the London clay," *J. Inst. Civil Engrs., London*, **19**, pp. 100-127.
- Zeevaert, L. (1953). "Pore pressure measurements to investigate the main source of surface subsidence in Mexico City," *Proc. 3d Int. Conf. Soil Mech., Zurich*, **2**, pp. 299-304.
- Lockwood, M. G. (1954). "Ground subsides in Houston area," *Civ. Eng.*, **24**, No. 6, pp. 48-50.
- Poland, J. F. (1958). "Land subsidence due to ground-water development," *ASCE J. Irr. and Drainage Div.*, **84**, Paper 1774, 11 pp.
- Saxena, S. K., ed. (1978). *Evaluation and Prediction of Subsidence*, Intern. Conf. on Evaluation and Prediction of Subsidence, Pensacola Beach, Florida, ASCE, New York.
- Johnson, A. I., ed. (1991). *Land Subsidence*, Proc. 4th Int. Symp. on Land subsidence, Houston, Texas, IAHS Publ. No. 200, 690 pp.

## ARTICLE 56 SETTLEMENT CAUSED BY VIBRATIONS

### 56.1 Factors Determining Magnitude of Settlement

Any structure founded on cohesionless soil is likely to settle excessively if the soil is subject to vibrations from such sources as moving machinery, traffic, pile driving, blasting, or earthquakes. On the other hand, the settlement caused by vibration of a foundation on clay is usually so small that it is unlikely to cause serious damage under

any circumstances. This conspicuous difference between the effect of vibrations on sand and on clay has already been emphasized in the discussion of the methods for the compaction of fills. (Article 44.2.). On account of its sensitivity to vibrations, sand can be compacted most effectively by vibratory equipment, whereas clay can be compacted only by static forces. Therefore, only the effects of vibrations on sand will be considered.

In Article 21 it is shown that the settlement of the surface of sand due to a pulsating load is many times greater than that produced by static action of the peak value of the load. At a given peak value the settlement depends on the frequency of the pulsations. The greatest settlements occur within a range of about 10 to 40 Hz. Inasmuch as the frequency of the unbalanced forces in many types of machinery, such as steam turbines, diesel power units, and air or gas compressors, lies within this range, the effect on settlement of the operation of these machines is particularly conspicuous.

### 56.2 Examples of Settlement Due to Induced Vibrations

The following examples demonstrate the magnitude of the settlements that may be caused by the vibration of machinery. In Germany a coal-handling plant,  $50 \times 20$  m in plan, contained coal crushers mounted on concrete blocks 3 m square. The building rested on footings supported by a bed of fairly dense sand 18 to 40 m deep. Although the allowable soil pressure of 140 kPa was very conservative, the unequal settlement assumed such proportions that the building was damaged severely and had to be underpinned. In another locality turbogenerators were installed in a powerhouse founded on fairly dense sand and gravel. The number of revolutions was 25/s. The maximum settlement of the foundations exceeded 0.3 m within a year after the power plant started to operate.

Traffic may generate vibrations of a periodic character (Taniguchi and Sawada 1979). Experience has shown that continued exposure to such vibrations is likely to produce considerable settlement. In Holland it has been observed that new buildings adjoining old main highways commonly tilt away from the highways. The cause of the tilt is the precompaction by traffic vibrations of the subsoil beneath and next to the highway, whereas the sand supporting the rear part of the buildings was still in its original condition. In Berlin some of the foundations of the elevated railway settled as much as 350 mm during 40 years of operation. They rested on fairly dense sand and were designed on the basis of an allowable soil pressure of 350 kPa. In Munich where most buildings rest on 6 m of dense sand and gravel overlying rock, truck traffic of increasing intensity caused settlements of such magnitude that several streets had to be closed entirely to trucking. Within a 10-year period, the damage to adjacent structures rose to about \$1,500,000.

Pile driving may also be responsible for the settlement of adjacent areas. The frequency of the hammer blows of conventional drivers is far below that corresponding to resonance but each blow gives rise to a series of vibrations of the soil at the resonant frequency. In one instance about 100 piles were driven into a deposit of sand and gravel so loose that piles as long as 15 m could be driven without jetting. Within the area occupied by the piles the ground surface settled 150 mm. The settlement decreased with increasing distance from the edge of the area to a value of 2 mm at a distance of 15 m.

The effect of blasting is somewhat similar to that produced by a mild earthquake (Article 56.3). Most damage attributed to blasting arises, however, not from settlement but from the transient ground motions and the air blast associated with the shock.

Occasionally, pile driving and blasting give rise to complaints or suits for damage, whereupon the engineer may be called on to determine whether or not the complaints are justified. One method of investigation that eliminates the personal equation is illustrated by the following examples.

In the first instance the owner of a house complained that vibrations due to pile driving were causing damage to his structure. To check the validity of his complaint, a fully loaded truck of the heaviest type was driven past the house at maximum legal speed, while seismographic observations were made in the house at points where the owner claimed the vibrations were strongest. During pile-driving operations the seismic observations were repeated. The results indicated that the vibrations caused by pile driving were milder than those caused by the truck. Because the owner was not justified in objecting to vibrations smaller than those caused by trucks passing his house at the maximum legal speed, his claim to damages was disallowed.

In the second instance an owner also protested against blasting in the vicinity of his house, whereupon a similar truck experiment was made. After the experiment charges differing in size were fired, and the corresponding vibrations were observed in the house. The contractor was given permission to blast with charges not greater than those that caused vibrations equivalent to the ones produced by the truck.

The settlements of machine foundations can be reduced most effectively by avoiding frequencies at which resonance occurs. Present knowledge (Barkan 1962, Novak 1970) permits fairly reliable estimates of the resonant frequencies under the simplest conditions, but the complexities of actual installations are usually so great that unrealistic simplifying assumptions have to be made and, as a consequence, undesirable conditions of resonance may occur. Various procedures have been tried to alter the resonant frequency of such systems, including permanently lowering the groundwater level, adding weight to

the foundation base, or injecting chemical grout into the granular subsoil. In some instances these procedures have been highly successful, but in many they have not served their purpose. Careful design of the machines to reduce unbalanced forces to a minimum is mandatory.

No generally applicable procedures are available for reducing the influence of vibrations reaching the subsoil of a structure from an external source. One method is to surround the structure with a deep ditch. The sides of the ditch should preferably be unsupported. If space is so limited that the ditch must be provided with vertical sides braced against each other, the bracing must be designed so that it does not transmit the vibrations from one side of the ditch to the other. Observations suggest that protective ditches are most effective if the frequency of vibration is high. The detrimental effects of blasting can be considerably reduced by the introduction of millisecond delays in the sequence of firing.

### 56.3 Settlement due to Earthquakes

Prolonged intense earthquakes have caused spectacular settlements of the surface of cohesionless deposits. The floors of the deeply filled alluvial valleys of the Kenai peninsula subsided as much as 1.5 m during the Good Friday earthquake of 1964 in Alaska; the differential settlements severely damaged highways, railways, and buildings. Nevertheless, even during a very mild earthquake in Vienna, it was observed that a grain bin with a width of 15 m and a height of 24 m settled 43 mm more on one side than on the other. The absolute maximum settlement is unknown. The bin was supported by short conical piles embedded in very fine, fairly dense water-bearing sand. The load was 400 kPa over the total area. When the bin was filled for the first time, the settlement was practically uniform and amounted to only about 5 mm.

When a granular soil is subjected to cyclic shear stresses such as those induced by earthquake shaking, the tendency for rearrangement of soil particles to more stable positions results in a tendency for volume decrease. If the permeability of the soil, the drainage boundary conditions, and the rate of shearing allow a drained response, compression of the soil and the consequent settlements take place during the shaking. On the other hand, if the response is undrained (Article 18.2), as is often the case for saturated sand deposits subjected to earthquakes, the compression and settlements occur after the shaking. Undrained shaking of loose sands, followed by dissipation of the shear-induced porewater pressures after the earthquake, typically results in settlements greater than those produced by drained shaking, especially if the sand liquefies.

Large ground deformations, including vertical settlements and horizontal displacements, may be caused by lateral spreading of unconfined liquefied sand deposits

or by the escape of liquefied sands from beneath the foundations of structures through earthquake-induced boils, fissures, and cracks (Dobry 1994). The amount of settlement of this type cannot be computed, but the settlement can be prevented by predensification of the sand at the construction sites. This article concerns only earthquake-induced settlement of sand that remains confined after the earthquake and experiences one-dimensional compression. Differential settlement of the ground may still occur under these conditions as a result of variations of thickness and density of the sand deposits or because of the deformation and drainage boundary conditions.

The settlement of a granular soil deposit subjected to earthquake shaking can be computed by integrating the vertical strain  $\epsilon_v$  over the thickness  $L$  of the deposit or, more conveniently, by the summation

$$S = \sum_{j=1} [\epsilon_v L]_j$$

where  $[\epsilon_v]_j$  is the vertical strain of sublayer  $L_j$  and  $\sum L_j = L$ . The earthquake-induced shear stress at middepth of each sublayer is computed by means of Eq. 20.33. This shear stress is then used to estimate the vertical strain from a relation between vertical strain and shear stress obtained by combining shear stress versus shear strain and vertical strain versus shear strain data from laboratory tests. The compressibility and undrained yield strength of the granular soil, determined by the relative density, are expressed in terms of standard penetration test  $(N_1)_{60}$  values.

#### 56.3.1 Settlement due to Drained Shaking

A reasonable method for estimating the settlement of granular soils subjected to drained shaking has been developed by combining the results of several series of laboratory tests on sands. Iwasaki et al. (1978) defined useful shear stress-shear strain relations by means of a series of stress-controlled drained cyclic torsional shear tests on 13 reconstituted loose to dense sands (mean grain diameter, uniformity coefficient, fines content, minimum void ratio and maximum void ratio, in the range of 0.16–0.99 mm, 1.2–4.6, 0–8%, 0.49–0.92, and 0.72–1.42, respectively). The specimens were subjected to consolidation pressures of 25 to 200 kPa before shear. Silver and Seed (1969) established typical volumetric strain-shear strain relationships as a function of relative density and number of shear strain cycles (magnitude of earthquake) on the basis of a series of strain-controlled drained cyclic simple shear tests on a silica sand (a uniform angular quartz sand with mean grain diameter of 0.65 mm and minimum and maximum void ratios of 0.64 and 0.97, respectively). Reconstituted sand specimens were prepared in the relative density range of 45 to 80% and were subjected to vertical consolidation

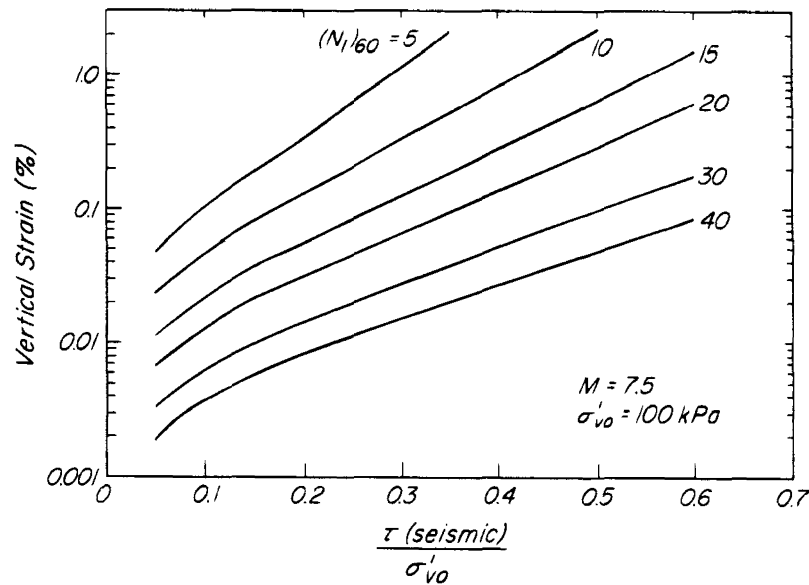


**Figure 56.1** Relation between vertical strain and normalized seismic shear stress for drained shaking.

pressure of 25 to 200 kPa before shear. Tokimatsu and Seed (1984) presented vertical strain-shear strain data from Silver and Seed (1969) for a magnitude 7.5 earthquake, expressing relative density in terms of  $(N_1)_{60}$ . By combining the laboratory data of Iwasaki et al. and Tokimatsu and Seed, the relations between vertical strain and normalized shear stress (Fig. 56.1) are obtained. Vertical strains for earthquake magnitudes other than 7.5 and at effective overburden pressures  $\sigma'_{vo}$  different from 100 kPa can be obtained by using the correction factors in Tables 56.1 and 56.2.

Settlement analysis assuming drained shaking is most applicable to dry granular soils and to coarse sands and gravels. At a number of sites subjected to earthquakes, observed settlements less than 50 mm, significantly smaller than values computed assuming undrained shaking, suggest a drained response in some saturated sand deposits. However, at other sites on saturated sand depos-

**Table 56.2** Correction Factor for Effective Overburden Pressure

$\sigma'_{vo}$ (kPa)	$C_0 = \frac{\epsilon_v}{\epsilon_v(\sigma'_{vo} = 100 \text{ kPa})}$
10	0.31
25	0.51
50	0.73
75	0.87
100	1.00
150	1.21
200	1.42

**Table 56.1** Correction Factor for Earthquake Magnitude

M	$C_M = \frac{\epsilon_v}{\epsilon_v(M = 7.5)}$
8.5	1.25
7.5	1.00
6.75	0.85
6.0	0.60
5.25	0.40

(Tokimatsu and Seed 1984)

its an analysis assuming drained shaking underestimated the settlements of buildings, storage tanks and embankments by factors of 10 to 30; these sites apparently experienced undrained shaking (Shahien 1996).

### 56.3.2 Settlement due to Undrained Shaking

A reasonable method for estimating  $\epsilon_v$  for undrained shaking has been developed on the basis of a series of laboratory tests on Fuji River sand, a uniform subangular sand with mean grain diameter of 0.40 mm, and minimum and maximum void ratios of 0.53 and 1.06, respectively (Nagase 1985, Nagase and Ishihara 1988). Stress-controlled undrained cyclic simple shear tests were performed on saturated reconstituted specimens consolidated to 196 kPa. After each test, the shear-induced porewater pressures were allowed to dissipate by drainage, and the vertical strain was measured. At each relative density, the tests

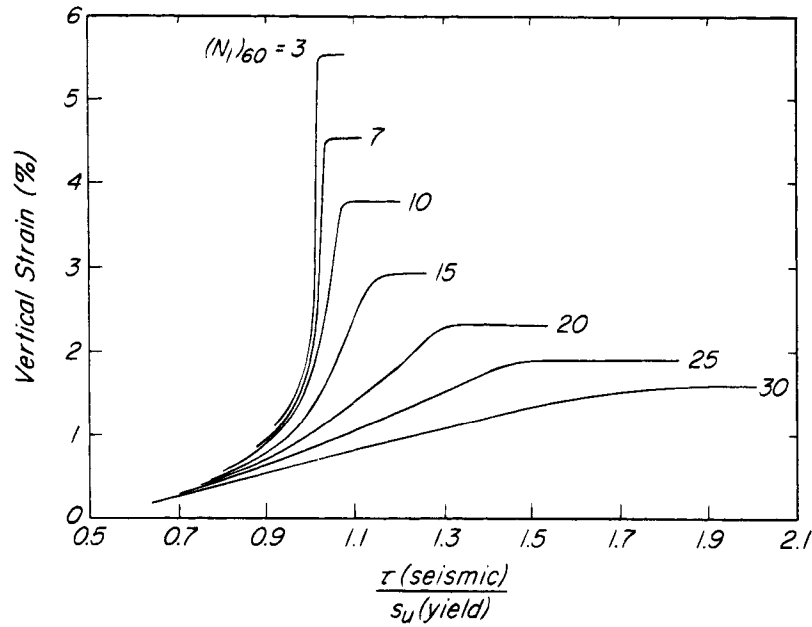


**Figure 56.2** Relation between vertical strain and seismic shear stress level for undrained shaking.

**Table 56.3** Correction Factor for Yield Strength

M	$C_y = \frac{s_u(\text{yield})}{s_u(\text{yield}, 7.5)}$
8.5	0.89
7.5	1.00
6.75	1.13
6.0	1.32
5.25	1.50

(Seed et al. 1985)

resulted in relations between cyclic shear stress and shear strain and relations between vertical strain and shear strain. Ishihara and Yoshimine (1992) combined these results to obtain relations, for various values of  $(N_1)_{60}$ , between the vertical strain and the ratio of seismic shear stress to undrained yield strength  $s_u(\text{yield})$ . In Fig. 56.2  $s_u(\text{yield})$  for magnitude 7.5 earthquakes is obtained from the  $s_u(\text{yield})/\sigma'_{vo}$  versus  $(N_1)_{60}$  relation (Fig. 20.66). Shear stress levels for earthquakes other than 7.5 are obtained from the correction factors in Table 56.3.

Predictions of settlement by the method based on undrained shaking are comparable with the observed set-

tlements of saturated sand deposits beneath level ground; they are equal to or smaller than the observed settlement of buildings, storage tanks, and embankments on saturated sand deposits (Shahien 1996). One-dimensional settlement analysis assuming undrained shaking predicts settlements up to 0.5 m with reasonable accuracy. Observed settlements in excess of 0.5 m and as much as 3 m, which have been observed on structures above saturated sands subjected to earthquakes, have resulted from the lateral flow of liquefied sand. These settlements are not included in the one-dimensional compression analysis.

### Selected Reading

- Crandell, F. J. (1949). "Ground vibration due to blasting and its effect upon structures," *J. Boston Soc. Civil Engrs.* **36** pp. 245–268. Reprinted in *Contributions to Soil Mechanics 1941–1953*, Boston Soc. Civil Engrs., 1953, pp. 206–229.
- Barkan, D. D. (1962). *Dynamics of Bases and Foundations*. Translated from the Russian by L. Drashevskaya, New York, McGraw-Hill, 434 pp.
- Richart, F. E. Jr., J. R. Hall, Jr. and R. D. Woods (1970). *Vibration of Soils and Foundations*. Englewood Cliffs, N. J., Prentice-Hall.
- Prakash, S. (1981). *Soil Dynamics*. New York, McGraw-Hill, 426 pp.

## CHAPTER 11

### *Dams and Dam Foundations*

#### ARTICLE 57 TYPES OF DAMS AND POTENTIAL MODES OF FAILURE

##### 57.1 Types of Dams and Foundations

Earth and rockfill dams may rest on rock, weathered rock, or soil. High concrete dams are almost invariably founded on rock, but some types of low concrete dams may be established on soil.

The design of an earth or rockfill dam should be adapted to the available construction materials. At most sites both pervious and impervious materials can be obtained. The dam may then be made up of a relatively impervious inner zone or core that retains the water and of outer zones that provide the required stability. Such dams are called *zoned*. The relative quantities in the different zones are determined chiefly by economic considerations. A dam consisting almost entirely of clay may be provided with a thin filter drain that maintains the downstream portion of the dam in a permanently drained state. On the other hand, a dam made entirely of pervious material must include an impervious membrane. If the dam consists exclusively of rock fill, the membrane sometimes consists of a reinforced concrete slab or a bituminous concrete pavement on the upstream face.

The conditions under which a concrete dam is established on soils are usually encountered in large rivers flowing on alluvial deposits of great depth. The major part or all of such a dam often serves as a spillway containing gates to control the level of the river for power or navigation. The dam consists of rigid units separated from each other by sealed joints that can accommodate moderate differential displacement among the units.

##### 57.2 Causes of Failure

An earth or rockfill dam may fail on account of overtopping, slope failure, spreading or sliding, internal erosion, or subsurface erosion. A concrete dam may fail by sliding or by subsurface erosion, and may be damaged by unequal settlement. Excessive leakage through, beneath, or around

a dam of either type does not in itself constitute a failure, but it may have embarrassing financial consequences.

Overtopping of an earth dam, once a major cause of failure, can be avoided by conservative spillway design, attention to the possibility of large rapid landslides into the reservoir, and generous freeboard. Slope failures and failures by spreading or sliding can be avoided by design in accordance with Articles 36 and 48 supplemented during construction by field observations, principally by measurement of porewater pressures. Furthermore, failures of these types are most likely to occur during construction; they cause unanticipated expenditures and delays but they are not catastrophic.

Failures of concrete dams by sliding can be catastrophic because they are apt to occur when the reservoir is full. They are most likely if the dams have been founded on soil or rock containing nearly horizontal weak layers not noticed or not properly evaluated during design. Bedding-plane shear zones have often developed in stratified, alternately strong and weak rocks adjacent to a river during valley cutting, and the strength in such zones may be at the residual value (Article 19.2.3). The strength may be reduced further by pore pressures. Hence, the possibility of such conditions deserves serious consideration.

Catastrophic failures of either concrete or embankment dams can also occur as a result of subsurface erosion. They are likely to occur without any apparent warning, at full reservoir, sometimes many years after the reservoir has been put into operation. The erosion may start at springs fed by seepage and proceed insidiously upstream toward the reservoir, following lines of least resistance along foundation slabs, conduits, or irregularities in the bedrock, or it may develop entirely in the subsoil in a pattern that depends on unknown details of the stratification. When the erosion channel reaches the reservoir it enlarges rapidly; the release of water may destroy the dam and its foundation and devastate the valley downstream. Failure of a dam by subsurface erosion thus ranks among the most serious accidents in civil engineering.

Internal erosion within the body of zoned embankment dams may also have serious consequences. The water-retaining element or core of such dams, usually consisting of clay or other relatively impervious soils, may develop cracks as a result of differential settlements or other causes, may not be sealed tightly against the foundation or abutments, or under the influence of seepage pressures may tend to migrate, particle by particle, into the coarser shell materials intended to support the core. The loss of core material by migration or erosion may result in sinkholes, in weakening and dislocation of the fill material, and sometimes in a breakthrough to the reservoir. If this occurs, the results can be as catastrophic as those of subsurface erosion. To prevent such accidents, filters (Article 14.9) are inserted between the core and the shells and at any other locations where seepage through the dam or its foundation or abutments has the potential to initiate erosion. The design and construction of such filters deserve the greatest care and attention. Unfortunately, the trend toward the use of wide broadly graded filters instead of zoned filters in which each zone is narrowly graded has led to numerous instances of near-failure and expensive remedial work, and to several outright failures. Although various gradation criteria have been developed for broadly graded filters, the practical difficulties of avoiding segregation during placement (Article 59.9) have often nullified the criteria.

Because of the disastrous consequences of failure of a dam by subsurface or internal erosion, the conditions that lead to the erosion and the means for avoiding the danger are described in detail in Articles 58 and 59.

## ARTICLE 58 MECHANISMS OF SUBSURFACE EROSION

### 58.1 Influence of Geologic Factors on Mechanics of Piping

A typical failure caused by piping is illustrated in Fig. 58.1. The dam, of the slab-and-buttress type, rested on a reinforced-concrete base slab provided with an upstream cutoff wall 3 m deep and a downstream cutoff 2 m deep. Failure occurred suddenly by a rush of water beneath the dam. A 16-m gap was left in the subsoil and was bridged over by the structure.

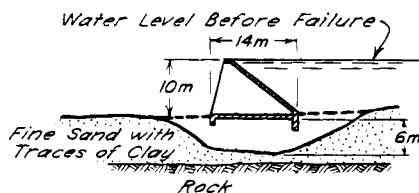


**Figure 58.1** Failure of Ashley Dam near Pittsfield, Massachusetts, due to piping (*Eng. News* 1909).

If a dam rests on a perfectly homogeneous, cohesionless subsoil, the factor of safety with respect to piping can be computed as shown in Article 24. The theory presented in that article, in agreement with laboratory tests, leads to the following conclusions: (1) the head  $h_c$  at which piping occurs is independent of the grain size of the subsoil, and (2) failure occurs almost instantaneously as soon as the hydraulic head becomes equal to the critical head at which the seepage pressures lift the ground adjacent to the downstream edge of the structure. Piping failures of this kind are referred to as *piping due to heave*.

In reality, most piping failures occur at hydraulic heads  $h'_c$  much smaller than the head  $h_c$  computed on the basis of theory. They occur from a few to many years after the reservoir is filled for the first time. Moreover, the ratio  $h'_c/h_c$  decreases rapidly with decreasing grain size. The conspicuous and almost universal time-lag between application of head and failure indicates that most piping failures are caused by a process that reduces the factor of safety with respect to piping gradually and inconspicuously until the point of failure is reached. The only process that can produce such results is *subsurface erosion*, progressing along a narrow belt toward the reservoir. As will be pointed out in Article 58.2, such a process cannot take place in a homogeneous body of cohesionless sand. In nonhomogeneous material the locations of lines of least resistance against subsurface erosion and the hydraulic gradient required to produce a continuous channel along these lines depend on geologic details that cannot be ascertained by any practicable means.

### 58.2 Mechanics of Subsurface Erosion

The destruction of dams by either type of piping is usually so complete that the sequence of events can seldom be reconstructed. However, subsurface erosion occurs under other circumstances, such as by careless pumping from an open sump or by natural tapping of a body of ground water through erosion of a river bank. These processes commonly leave evidence that remains open to inspection. Therefore, they constitute the principal sources of our knowledge of the characteristics of subsurface erosion. The following paragraphs contain abstracts of the records of pertinent observations.

Figure 58.2 represents a cross-section through a gently inclined blanket of gravel that rests on a deep bed of very fine uniform loose sand. At A a pit was dug for the foundation of a new machine. Although the pit was surrounded by sheet piles that extended to a considerable depth below final grade, the pump discharged a mixture of sand and water. The quantity of sand removed was far in excess of the volume of the pit. Before final grade was reached, the building collapsed. At the same time a sink hole, 1 m deep and 6 m in diameter, appeared at B, at a distance 100 m from the pit. Between A and B the ground surface was intact. Hence, the loss of ground can be

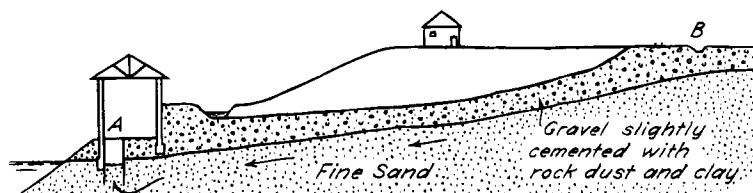


**Figure 58.2** Diagram illustrating underground erosion produced by pumping mixture of sand and water from sump A. Sinkhole at B 100 m from A.

accounted for only by the movement of soil particles in a relatively narrow subterranean conduit. It is most likely that the conduit was located immediately below the gravel blanket, because the slightly cemented gravel was capable of forming an unsupported roof.

In the Rhineland pumping was continued for 13 years in a sand pit. The bottom of the pit was located between 5 and 6 m below the original water table. During this period three of the springs that discharged into the sump cut backward and eroded tunnels in the slightly cohesive sand. Each tunnel terminated in a sink hole on the ground surface. The largest tunnel was 1 to 2 m wide and in its length of 50 m had an average grade of only 6%. The sinkhole above the end of this tunnel was 2.5 m deep and 11 m in diameter.

In another instance an open cut was excavated for the construction of a sewer. The excavation passed through fairly stiff clay into fine sand that was drained by pumping from an open sump. While pumping proceeded, a narrow strip of the ground surface subsided about 0.3 m. The formation of the trough started at the sump and gradually proceeded to a distance of about 200 m. The width of the trough increased from a fraction of a meter at the sump to more than 3 m at the farther end.

Although the piping phenomena described in the preceding paragraphs took place in very different soil formations, they had two important features in common. First, the material overlying the eroded soil always possessed at least a trace of cohesion, sufficient to form a roof over the erosion tunnel. Because an unsupported roof cannot be maintained in homogeneous cohesionless sands, such materials are not subject to subsurface erosion unless, of course, they lie beneath an artificial roof such as the base of a concrete dam.

The second feature common to all the examples is that the subsidence of the roof always occurred at a great distance from the discharge end of the tunnel. This fact indicates that the erosive capacity of a spring increases as the length of the tunnel increases. The reason is illustrated by the flow nets in Fig. 58.3. The thin dash curves indicate equipotential lines, or contour lines of the water table, whereas the solid curves represent the flow lines. The dash-dot lines indicate the boundary of the intake area. With increasing length of the tunnel, the number of

diverted flow lines increases. Thus, the discharge from the spring becomes greater, and the rate of erosion increases.

Progressive subsurface erosion starting at springs near the toe of a dam also proceeds along lines leading toward the reservoir, as shown in Fig. 58.3. The frequent occurrence of springs at the downstream edge is known to everyone who has had experience with dams. If a spring is powerful enough to start erosion in the first place, the erosion will almost certainly become more serious as time goes on, because the flow from a given spring increases with the length of the eroded tunnel (Fig. 58.3). Finally, the dam will fail by piping.

### 58.3 Empirical Rules for Estimating Factor of Safety

On account of the frequency and the serious consequences of failures of dams by piping, empirical rules for evaluating the factor of safety against piping were established long before the mechanics of the process were clearly understood. The first rules of this kind (Bligh 1910) were set up after the catastrophic failure in 1898 of the Narora Dam on the Ganges River in India. They were derived from a compilation of case records, and were based on the assumption that the sole cause of piping was erosion along the surface of contact between the soil and the base of the dam. The path that a water particle followed along this surface was called the *line of creep*. If the length  $L$  of the line of creep was such that the average hydraulic gradient  $i = h/L$  was less than a certain critical value for the foundation material, the dam was believed to be safe. The quantity

$$C_c = \frac{L}{h_{cr}} \quad (58.1)$$

was called the *creep ratio*. The value  $h_{cr}$  represented the greatest height to which the water level in the reservoir could rise with reference to tailwater level without producing failure by piping. The available failure records indicated that the ratio  $C_c$  increased with increasing fineness of soil from about 4 for gravel to about 18 for fine sand and silt.

The first step in designing a dam on the basis of Eq. 58.1 was to estimate the creep ratio  $C_c$  of the subsoil. This was done by means of a table containing the values



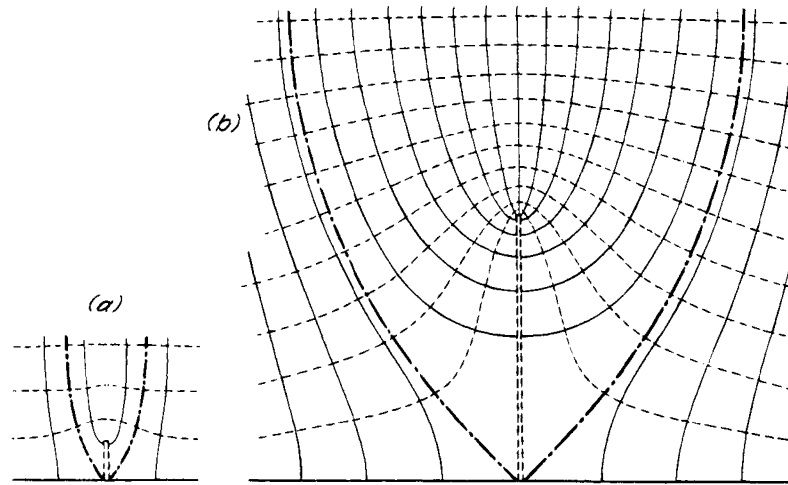


**Figure 58.3** Flow nets illustrating increase of intake area of spring as length of erosion tunnel increases: (a) incipient state; (b) after erosion has proceeded to considerable distance from spring.

of  $C_c$  for the principal types of soil. The required length  $L$  of the creep line was then obtained by multiplying the creep ratio  $C_c$  by the hydraulic head  $h_{cr}$  created by the dam. The foundation was laid out in such a manner that the length of the creep line was at least equal to  $L$ . For example, the length of the line of creep for the dam shown in Fig. 58.4 is

$$L = t_1 + t_2 + B + t_3 + t_4 = B + \sum t$$

and this distance must be at least as great as  $C_c h_{cr}$

During the next 30 years it was gradually recognized that vertical sections of the line of creep contribute more toward reducing the danger of piping than horizontal sections of equal length. The reason for the difference is that the subsoil of dams generally has a sedimentary origin, and sedimentary deposits are always less permeable in the vertical direction than in the horizontal directions (Article 14.8). If  $k_h$  and  $k_v$  are the coefficients of permeability in the horizontal and vertical directions, respectively, the loss in head per unit of length of vertical

sections of the line of creep is roughly equal to the ratio  $k_h/k_v$  times that of horizontal sections. The value of the ratio ranges between 2 or 3 and much larger values, in accordance with the details of stratification and the variations of the permeability in the vertical direction.

To take account of the greater efficiency of vertical sections of the line of creep, the original procedure was modified by the assumption that every horizontal section of the line of creep was only one third as effective as a vertical section of the same length. On this assumption, the equation

$$C_w = \frac{\frac{1}{3}B + \sum t}{h_{cr}} \quad (58.2)$$

was obtained. The value  $C_w$  is known as the *weighted creep ratio*. Because Eq. 58.2 corresponds approximately to the ratio  $k_h/k_v = 3$ , it is obvious that it does not take into account the wide range of values that this ratio can have in the field.

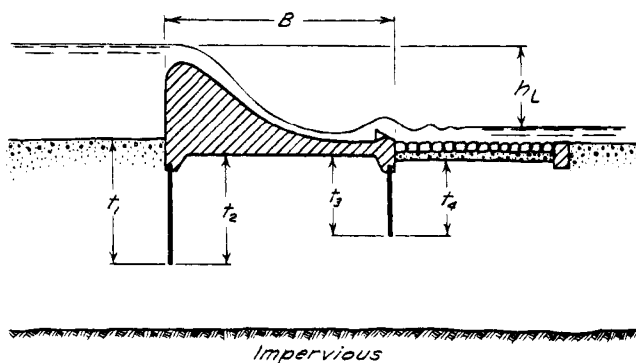


**Figure 58.4** Diagram indicating dimensions used for computation of length of line of creep.

**Table 58.1** Weighted Creep Values  $C_w$  (Eq. 58.2)

Very fine sand or silt	8.5
Fine sand	7.0
Medium sand	6.0
Coarse sand	5.0
Fine gravel	4.0
Medium gravel	3.5
Coarse gravel including cobbles	3.0
Boulders with some cobbles and gravel	2.5

From E. W. Lane (1935).

Table 58.1 is an abstract of a list of safe values for  $C_w$ , based on a digest of about 280 dam foundations of which 24 had failed (Lane 1935).

The line-of-creep approach to the problem is purely empirical. Like every other procedure based solely on statistical data, it leads to design with an unknown factor of safety. Experience and experiments have shown that the values of  $C_w$  (Eq. 58.2) are widely scattered from the statistical average for a given soil. The values of  $C_w$  contained in Table 58.1 represent maximum rather than average values, and the values of  $h_{cr}$  obtained by means of Eq. 58.2 and Table 58.1 represent the smallest heads at which piping under field conditions has ever occurred. For a single row of sheet piles driven into homogeneous sand the weighted creep ratio  $C_w$  at failure by piping through heave would be approximately 0.67 irrespective of the grain size. Yet, under field conditions, dams have failed at creep ratios ranging from 2.5, for boulders with cobbles and gravel, to 8.5 for fine sand and silt. This discrepancy indicates that the real factor of safety against piping by heave of dams designed on the basis of Eq. 58.2 and Table 58.1 is very high. On the other hand, the wide scattering of the values of  $C_w$  from the statistical average indicates that, against failure by subsurface erosion, the factor of safety of some existing dams designed by the empirical rules must be excessive; that of others may be barely tolerable; and an unprecedented combination of several unfavorable circumstances may even lead to failure.

#### 58.4 Subsurface Erosion Initiated by Scour

In contrast to subsurface erosion initiated by the progressive removal of material through springs, erosion can also occur when water impinges on or flows against an erodible soil, as through a transverse crack in the core of a dam or through an open joint in a rock abutment against which erodible fill has been placed. If the water carrying the eroded particles can escape downstream, an erosion tunnel can form quickly. The outlet of the erosion tunnel formed shortly before the catastrophic failure of Teton Dam in 1976 is shown in Fig. 58.5. The core material, a wind-blown silt, was placed against open untreated joints in the abutment. During the first filling of the reservoir, water flowing through cracks in the core or through the joints themselves could rapidly remove the eroded material. Only a few hours elapsed between the first appearance of muddy water from springs downstream and the complete destruction of the dam.

#### 58.5 Means for Avoiding Subsurface Erosion

Theory and experience lead to the following conclusions. Most of the piping failures on record have been caused by subsurface erosion involving the progressive removal of materials through springs; this condition invalidates

the theory of piping by heave (Article 24.2). The factor of safety with respect to piping by subsurface erosion cannot be evaluated by any practicable means. However, if the removal of subsurface material is reliably prevented, the conditions for the validity of the theory of piping by heave are satisfied and the critical head can be computed. It is, moreover, very much greater than the critical head for subsurface erosion. The means for preventing subsurface erosion depend on the importance of the project and the pattern of stratification of the subsoil.

The foremost requirement is to avoid, by appropriate design of the foundation, local concentrations of flow lines. Such concentrations were, for example, responsible for the failure of Hauser Lake Dam in Montana (Fig. 58.6a). The subsoil consisted of 20 m of gravel. The water was retained by a skin of steel plates supported by a steel framework that rested on large footings. The presence of the footings produced a local concentration of flow lines, as shown in the figure. The dam failed in 1908, one year after the first filling (Sizer 1908). Because it did not fail immediately, the cause was undoubtedly subsurface erosion. A second example is shown in Fig. 58.6b, which represents a section through a dam across the Elwha River in Washington. The structure rested on gravel and coarse sand underlain by bedrock. While the reservoir was being filled, large springs developed at the downstream toe. To reduce the flow, a row of sheet piles was driven to a depth between 9 and 12 m, at a distance of 2.5 m from the toe. This obstruction caused a concentration of flow lines, as shown in the figure, and subsurface erosion occurred. The dam failed before the sheet-pile wall was completed.

If local concentrations of flow lines are avoided, design on the basis of Eq. 58.2 is acceptable from the point of view of safety but the factor of safety may range from a high value to one close to unity; the real value depends on factors that are unknown. Hence, on important projects, provisions should be made to eliminate the possibility of subsurface erosion by one or more of the following procedures: (1) lowering the piezometric levels beneath the downstream edge of the foundation by means of relief wells; (2) establishing the downstream portion of the foundation on an inverted filter; and (3) observing the terrain downstream from the foundation during the first filling of the reservoir and placing inverted filters over the areas where springs begin to come out of the ground. This procedure was followed, for example, on Vermilion Dam (Terzaghi and Leps 1960). On minor projects such elaborate provisions may not be economically justified, and design based on Eq. 58.2 may be appropriate.

The greatest difficulties associated with preventing piping by subsurface erosion are encountered in sedimentary deposits in which layers of inorganic silt are in direct



**Figure 58.5** Erosion tunnel on downstream face of Teton Dam just before its collapse and failure of dam by piping (United States Bureau of Reclamation photo).

contact with layers of clean coarse sand or gravel. Erosion occurs in the silt and the silt is carried into suspension into the relief wells or toward the springs. If the exit of the sand layer is covered with a filter fine enough to prevent the escape of silt, the filter obstructs the flow of the water out of the sand layer. Such conditions of stratification often exclude the possibility of reliably preventing subsurface erosion by means of filters, and the foundation of even an important structure must be designed on the basis of a conservative interpretation of Eq. 58.2. If relief wells are installed, special precautions must be taken (Article 59.2).

Means to prevent subsurface erosion along cracks through the cores of dams or along core-rock interfaces are described in Article 59.

### 58.6 Susceptibility of Soils to Erosion

The foregoing discussion has indicated that piping by subsurface erosion, involving grain-by-grain removal of

particles, occurs most readily in fine-grained cohesionless materials above which a roof of at least slightly cohesive soils can form. Thus, inorganic silts and very fine sands are potentially troublesome, and protective filters are designed to prevent the migration of these materials. However, some clays may lose their cohesion when exposed to water of a particular chemical composition (Arulanandan et al. 1975), whereupon the particles disintegrate and become susceptible to piping. Such clays are known as *dispersive* (Sherard et al. 1976). The tendency to disperse is not disclosed by the usual index properties. Hence, the presence of dispersive clays is usually investigated by the *pinhole test* wherein water of the expected chemical characteristics is passed through a specimen in which a small hole has been drilled, and the enlargement of the hole is noted under standard conditions. If dispersive clays are likely to participate in subsurface erosion, the protective filters must be designed to retain them. Graded filters will almost surely be required because of

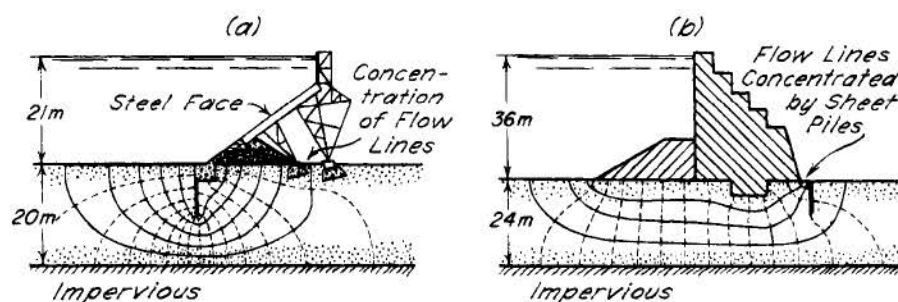


**Figure 58.6** Flow nets showing concentration of flow lines responsible for failure by piping of two dams: (a) Hauser Lake Dam, Montana; (b) Elwha River Dam, Washington.

the fine filter sizes required to satisfy the filter criteria for the clay.

### Selected Readings

Descriptions of the failure of three modern dams by sub-surface erosion (Baldwin Hills, Teton, and Walter Bouldin) are contained in Chapter 2, Lessons from Notable Events, in *Advanced Dam Engineering for Design, Construction, and Rehabilitation*, (1988). Robert B. Jansen, ed., New York, Van Nostrand Reinhold, pp. 8–59.

## ARTICLE 59 EARTH AND ROCKFILL DAMS

### 59.1 Basis for Design

In designing an earth or rockfill dam, the foundation, abutments, and embankment should be considered as a unit. The entire assemblage must retain the reservoir safely without excessive leakage. In addition, the design must permit diversion of the river during construction and must provide suitable spillway facilities for handling floods. The layout of the project is also influenced by facilities needed for producing power, providing for irrigation, permitting the passage of fish, and satisfying other environmental requirements. Finally, the design should be economical.

Soil mechanics enters into the evaluation of foundation and abutment conditions and of materials for construction; into the estimate and control of seepage through, around, and beneath the embankment; into selection of safe slopes; into methods of placement and control of the embankment materials; into the estimate of deformations and the evaluation of their consequences; and into the means for observing the behavior of the completed works. It may also be concerned with the stability of construction slopes and of the slopes around the reservoir after impoundment. This article deals principally with control of seepage and with the utilization and arrangement of materials to ensure stability and to exclude the possibility of failure by piping or subsurface erosion.

The distinctions among the disciplines of soil mechanics, rock mechanics, and engineering geology become obscure and meaningless at the interface between an embankment dam and foundations or abutments of rock. Findings from the latter disciplines will be invoked where they influence the soil-mechanics aspects of the design.

### 59.2 Seepage Control

Provisions for seepage control have two independent functions: reduction of the loss of water to an amount compatible with the purpose of the project, and elimination of the possibility of a failure of the structure by piping. Many dams have been in successful service for decades in spite of losses of water amounting to several

m<sup>3</sup>/s. Therefore, the rational design of measures for reducing seepage should be initiated by an estimate of the largest quantity of water that may escape from the reservoir if no attempt were made to intercept percolation through any but the most conspicuously pervious strata encountered in the borings. In many instances it will be found that the cost of reducing the loss of water further would be far in excess of the value of the additional water that can be retained.

Compliance with the requirement that the loss of water should not exceed a specified amount calls first of all for a knowledge of the coefficients of permeability  $k_h$  and  $k_v$  of the subsoil. The information is needed even when the feasibility of the project is being studied. Below the water table  $k_h$  should be determined by pumping tests, whereas  $k_v$  is estimated on the basis of the boring records. The sediments located above the water table should be assigned the highest values compatible with the results of the pumping tests supplemented by the boring records.

The safety of a dam with respect to a failure by piping has no relationship to the amount of water that escapes from the reservoir. Large losses of water may be associated with a high degree of safety against piping. Hence, the means for eliminating the danger of piping require independent consideration. The danger of failure of a dam by piping increases rapidly with increasing values of the hydraulic gradient at which the water percolates through the “impervious” portion of the dam and along the contact between this portion and the natural ground. Piping through the core can be eliminated reliably by adequately designed and constructed transition zones and filters. However, the prevention of piping along the contact between the core and the natural ground requires more than the application of routine procedures. The designer’s attention, therefore, must be concentrated on this contact.

### 59.3 Cutoffs

#### 59.3.1 Efficiency of Cutoffs

If part or all of the base of a dam is located on pervious sediments, water will escape from the reservoir by under-seepage. If the loss is estimated to be excessive, it must be reduced by means such as constructed or grouted cutoffs or impervious blankets. If a dam forms part of a high-head power development, it may be economically justifiable to collect the seepage and to pump it back into the reservoir during periods of low demand.

The depth and permeability of the sediments and the loss of water considered tolerable determine whether constructed cutoffs are extended over their full length to impervious materials (complete cutoffs), or are terminated at some depth between the base of the dam and the top of the impervious formation (partial cutoffs). Cutoffs may consist of clay-filled trenches with sloping or vertical sides (Fig. 59.1a), of sheet piles, of concrete panel walls

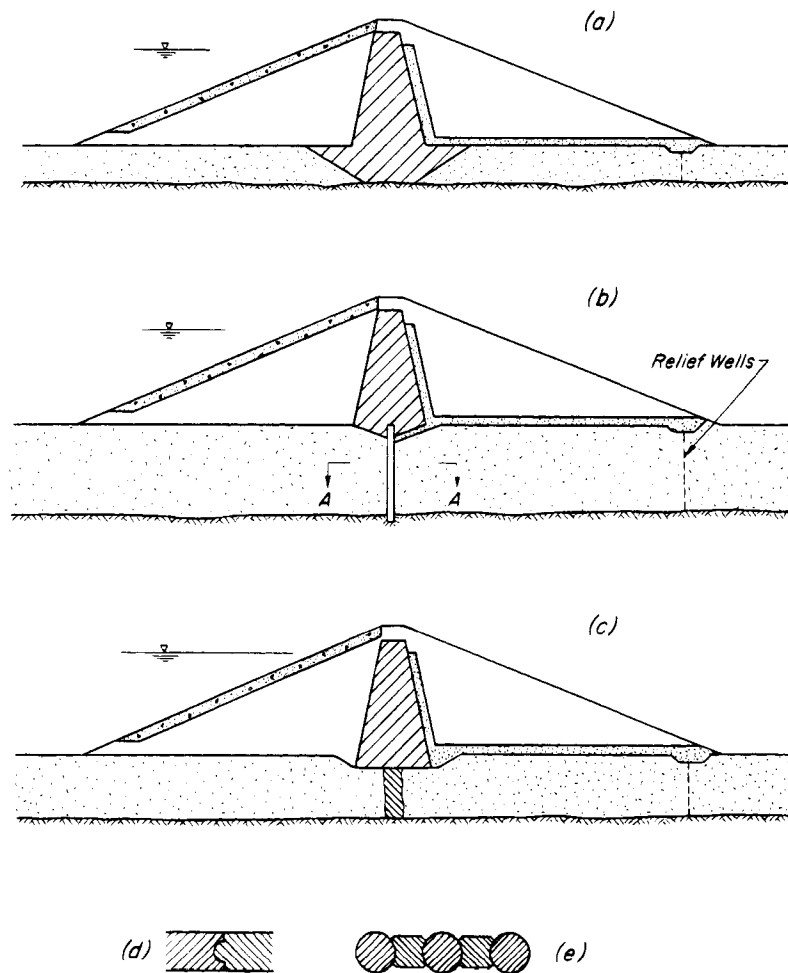


**Figure 59.1** Types of cutoffs: (a) clay-filled trench; (b) concrete wall constructed in slurry-filled excavation; (c) slurry trench; (d) section A-A through panel wall shown in (b); (e) Section A-A through interlocking-cylinder wall shown in (b).

cast in slurry-filled trenches (Fig. 59.1*b, d*), of interlocking cast-in-place concrete piles (Fig. 59.1 *b, e*), or of any of several modifications or variations of these types. As a result of constructing a cutoff, the piezometric elevation immediately upstream from the cutoff exceeds the corresponding elevation immediately downstream by an amount  $h'$ . The efficiency of a cutoff can be expressed conveniently by the ratio

$$E = \frac{h'}{h} \quad (59.1)$$

where  $h$  is the total head, equal to the difference between the elevation of the water level at full reservoir and the tailwater level. In the design stage  $E$  is estimated with the aid of the flow net (Article 23.5) on the assumption that the cutoff is perfectly watertight. For tight, complete cutoffs,  $E = 100\%$ .

The real efficiency cannot be determined until the reservoir is filled for the first time, and then only on the basis of the results of readings on piezometers located

immediately upstream and downstream of the cutoff. In many instances the observations have shown that the real efficiency is very much less than the designer anticipated. The magnitude of the difference between the estimated and the real values of  $E$  depends on the type and depth of the cutoff, the foundation conditions, and the workmanship as it reflects the qualifications of the contractor's personnel. Hence, in the selection of the type of cutoff all these factors should be considered.

The only type of cutoff of which the efficiency can be controlled positively by conscientious supervision is a compacted clay cutoff established in an open cut with sloping sides. However, before construction the subsoil conditions at the bottom of the trench are known at only a few points. Therefore, the specifications for preparing the base for the cutoff and placing the lower part of the cutoff material may require radical modification after the trench has been opened. Such modifications were needed, for example, at Mammoth Pool Dam (Terzaghi 1962). The depth to which a clay cutoff deserves the preference

over other types depends to a considerable extent on economic considerations.

All other types of cutoffs may turn out to be defective in spite of conscientious supervision. For any given type, the difference between the computed and real efficiency increases with increasing depth. Under unfavorable conditions the real efficiency may be so low as to make the cutoff practically ineffective.

For example, even if sheet-pile cutoffs are intact they are not water-tight because of leakage across the interlocks. In addition, the locks may break because of defects in the steel or when a pile hits an obstacle. Once the lock is split, the width of the gap increases rapidly with increasing depth and may assume dimensions of many meters. Such gaps have often been encountered in open excavations carried out within sheet-pile enclosures. The measured efficiency of complete sheet-pile cutoffs beneath several of the large dams on the Missouri River was found to be as low as about 10%, even though sheet piles were driven into shale (Lane and Wohlt 1961).

### 59.3.2 Construction by Use of Slurry

Several types of cutoffs are constructed with the aid of soil-bentonite slurries. The principal function of the slurry is to stabilize the walls of the excavation, which may consist of a trench, a slot, or a cylindrical hole, until the slurry is replaced by the permanent impermeable material that will constitute the cutoff. In the *slurry trench* cutoff (Fig. 59.1c), the trench is usually excavated by a backhoe, clamshell, or dragline and the slurry displaced by a well-graded relatively impermeable mixture of silt, sand, and gravel that often includes the material originally excavated from the trench. The cutoff beneath Wanapum Dam on the Columbia River was constructed in this manner in 1962 to a depth of 24 m with a minimum thickness of 3 m. Because the trench terminated on hard rock, a 1 m layer of concrete was placed on the carefully cleaned bottom to form a seal before backfilling and grouting were done under the seal (Engstrom 1963). At Dike D-20 on the James Bay Project in Quebec, a slurry-trench cutoff to a maximum depth of 24 m extended to a glacial till. The design called for careful cleaning of the bottom of the trench and keying it into the till, but the boulders embedded in the till made these operations difficult. Because it was found that a few windows were left at the bottom of the trench, relief wells were added downstream to control the seepage as the reservoir rose.

Continuous concrete diaphragms known as *panel walls* (Fig. 59.1b) are constructed in sections usually about 0.6 m wide and 5 m long. A slot with these horizontal dimensions is excavated with slurry support by means of a special clamshell bucket mounted on a stiff kelly bar. Heavy chopping tools are available to key the bottom of the slot into bedrock or to advance the slot through resistant materials. The slurry is displaced by tremie concrete

to form the panel. One end of the panel usually abuts a completed panel and fits into a semicylindrical groove left for that purpose (Fig. 59.1d). At the other end a pipe is placed vertically in the slot before the concrete is introduced. The pipe serves as the form for the semicylindrical groove into which the next panel will fit; it is removed as soon as the tremie concrete has taken its initial set. If desired, the panels may be reinforced with prefabricated cages lowered into the slots before the tremie concrete is introduced.

Panel cutoffs have been constructed successfully to depths as great as 100 m, but even shallower ones occasionally contain windows. Great care and skill are required to make sure that the slurry level is not lowered accidentally, as caving may occur during even a brief lapse. Care is also required to ensure that sediments do not accumulate at the bottom of a panel before the concrete is introduced, that the alignment and continuity of the joints are maintained, and that slurry does not accumulate on the surface of the joint with the preceding panel and form a gap between the concreted panels. Experience, including exposure of panel walls by excavation, has demonstrated that defects have occurred in even the most carefully controlled walls and that no such wall can be assumed to be perfect. After impoundment begins, piezometric observations are required to establish the actual efficiency of the wall, and the design should envisage additional means for control of such seepage and seepage pressures as may develop.

Several variations of panel walls are available, including the use of a deformable "plastic" concrete that can accommodate settlements of the material through which the wall passes.

Interlocking concrete piles cast in slurry-filled holes (Fig. 59.1e) have been used widely, especially to great depths where verticality is essential or where the bedrock is hard and the rock profile steep and irregular. At Manicouagan 3, Quebec, the cutoff consists of such piles in two rows 3 m apart with a maximum depth of 128 m (Lefebvre et al. 1977). Wolf Creek Dam, in Kentucky, was rehabilitated by constructing a cutoff through the core and underlying alluvium and as far as 30 m into hard but karstic limestone to a total depth of 90 m (Couch and Ressi 1979). Construction of such walls is costly and time-consuming; panel walls are usually selected for shallower depths.

### 59.3.3 Injected Cutoffs in Soils

The formation of cutoffs by injections of cement, chemical, or clay grouts has been practiced for several decades, especially in Europe. At present, diaphragm walls are used more widely, although grouting is usually used in attempts to seal defects beneath or through cutoff walls of other types. Until about 1925 the injected substance consisted almost invariably of neat Portland cement.

However, neat cement does not penetrate the voids of a granular material unless the effective size  $D_{10}$  exceeds about 0.5 mm if the material is loose, or 1.4 mm if it is dense. These conditions are seldom satisfied. Microfine cement with grain size of 1–10  $\mu\text{m}$  is being used to get grout into openings finer than can be penetrated by ordinary Portland cement. In 1925 Joosten patented a procedure for solidification and impermeabilization by the successive injection of solutions of sodium silicate and calcium chloride. The procedure and several similar ones derived from it are used widely, although the cost is usually prohibitive in connection with large cutoffs. A period of experimentation followed, chiefly in France, culminating in the practice of injecting mixtures of cement and clay in varying proportions, with occasional admixtures of chemicals usually acting as deflocculants. More recently, solutions have been developed which polymerize in the voids and plug them; all of these are very expensive, and some of the substances are toxic. An essential feature of all grouting procedures is successive injection, usually from the same grout holes, of progressively finer zones in the deposit. Inasmuch as grout cannot be made to penetrate the finer materials as long as more pervious zones are available, the coarser materials are treated first, usually with the less expensive and thicker grouts, whereupon the finer portions are penetrated with less viscous fluids.

Large-scale tests performed in river sediments at Aswan, Serre Ponçon, and Mangla Dams have led to the conclusion that the coefficient of permeability of the grouted sediments ranges from  $10^{-6}$  to  $10^{-7}$  m/s, irrespective of the coefficient of permeability of the untreated sediments (Wafa 1961, Guelton et al. 1961, Skempton and Cattin 1963). Based on these values, the thickness of the grout curtain can be adapted to the upper limiting value of seepage loss that can be tolerated.

Grout curtains in soils have one or more shortcomings. The sizes and locations of those portions of the sediments not penetrated by the grout are unknown. Yet, if a layer of very fine untreated sand, for instance, crosses a grout curtain, water percolates through it under a high gradient and may scour out a gap. Most chemical grouts are compressible; therefore, seepage pressures of long duration may puncture the curtain. The result of grouting operations depends to an uncomfortably large degree on the skill and experience of the grouting personnel. On important projects large-scale grouting tests should be performed, even though they do not furnish any information on the long-time performance of the curtain.

#### 59.3.4 Injected Curtains in Rock

If the impervious portion of a dam rests not on soil but on bedrock, the consequences of flow through the rock mass must be considered. The permeability of most rock foundations arises from joints, faults and shear zones,

and solution cavities. Seldom is the permeability of the intact rock between these discontinuities of significance. To cut off seepage around and beneath the dam, a jointed rock is often treated by injection of cement grout. *Curtain grouting* consists of drilling holes around the periphery of the valley along the axis of the dam to depths great enough to encounter most open joints or to depths equal to some arbitrary fraction such as two-thirds of the reservoir head, of circulating water to wash any erodible filling from the joints, and of injecting grout under pressure. The initial grout holes are usually spaced at intervals of 6 to 12 m. After they are grouted, additional holes are drilled to split the spacing and are grouted. The procedure continues until the final holes accept virtually no grout. The grouting in each hole is usually done in stages wherein sections of the hole are isolated, generally by expandable packers, and grouted successively. The grout pressures and mixes are subjects of controversy, but it is universally agreed that excessive pressures, especially near the faces of the abutments, can damage the rock. If the jointing or other discontinuities are pervasive, a grout curtain of several parallel lines can be constructed (Deere 1982).

Curtain grouting is ineffective at shallow depths and is usually supplemented by *blanket grouting* beneath the area of contact of the bedrock and the core, and possibly beneath part of the downstream filter zone adjacent to the core. Blanket-grout holes are generally shallow, often about 8 m deep, and are filled with grout under little or no pressure with the objective of blocking the near-surface joints through which water might circulate and erode the fine-grained embankment material.

The beneficial aspects of curtain grouting have been seriously questioned (Casagrande 1961). There is strong evidence that many grout curtains contain defects and that the presence of even carefully constructed curtains may have little effect on the pressure of the water in the discontinuities in the rock. These pressures, known as *cleft water pressures*, are controlled more effectively by drainage; indeed, drain holes should be considered a standard requirement downstream of grout curtains in rock foundations. Nevertheless, a well-constructed grout curtain may substantially reduce the quantity of flow beneath and around the embankment. In some instances, economy favors avoiding the loss of water. Of greater significance is the reduction of erosive action of large flows at the interface between embankment and foundation or abutment, with consequent reduction of the likelihood of sub-surface erosion by scour.

In karstic terrains many attempts have been made to cut off the flow through solution cavities by grouting. Few have been permanently successful. Most such cavities are at least partly filled with residual or transported materials that cannot be entirely flushed out before grouting but that gradually erode under the gradients imposed by the



reservoir. The cutoff wall at Wolf Creek Dam, for example, was required after sinkholes, subsidences, and muddy flows developed at an accelerating rate after 20 years of apparently successful performance, and after an extensive emergency grouting program proved futile.

#### 59.4 Upstream Blankets

As an alternative to a cutoff as a means for reducing leakage through sediments of great depth, an upstream blanket may be considered. Its function is to increase the length of the path through which water must travel from the reservoir to the nearest exit, and thereby to decrease the average hydraulic gradient. The effectiveness depends to a large extent on the ratio between the coefficients of permeability of the sediments in the horizontal and vertical directions. This ratio is almost always unknown and can be quite large (Articles 12.5, 14.8). However, if the loss of water is estimated on the assumptions that the ratio is unity and the value of  $k$  is equal to that in the horizontal direction, the estimated quantity will represent an upper limiting value.

The floor of many reservoirs is covered by an upper layer that is less pervious than the underlying sediments but that has been locally removed by stream erosion or must be excavated near the dam to permit construction. Frequently the effectiveness of the upstream blanket can be greatly enhanced by repairing the known defects in the upper layer and by connecting it to the natural blanket. Such a procedure proved to be highly beneficial at Vermilion Dam in California (Terzaghi and Leps 1960). In many reservoirs, loss of water decreases with time because of deposition of silt on the floor.

If the fine-grained artificial or natural blanket material is underlain by coarse sediments, such as cobbles or openwork gravel, or by open-jointed bedrock, sinkholes may develop in the blanket and permit the seepage to increase dramatically. At Tarbela Dam in Pakistan, the blanket, which extended 1.7 km upstream (Fig. 59.2), was reinforced by dumping additional material through the reservoir until the underlying openwork gravels developed natural filters due to the migration of finer constituents (Lowe 1978). The partial failure of the ring dam at Sir Adam Beck II station in Niagara Falls, Ontario, was caused to some extent by migration of blanket material into a joint in the underlying dolomite (Peck 1980).

#### 59.5 Drainage Provisions

The water that escapes from the reservoir through the subsoil and through gaps in the cutoff comes out of the ground in the form of springs downstream from the impervious portion of the dam. The location of the springs is unknown before the reservoir is filled for the first time. Subsurface erosion starting at the springs may lead to failure by piping. If this risk exists, the pervious downstream portion of the dam should be established on an

inverted filter, and any springs that emerge downstream from the dam should be covered by such a filter. Nevertheless, if the subsoil should contain an impervious layer terminating beneath the reservoir, the pressure of the water beneath this layer might lift the overlying sediments near the toe, whereupon the dam would fail by piping by heave. This possibility can be investigated by systematic porepressure observations in the subsoil near the toe during an early stage of filling of the reservoir. If it exists, relief wells should be installed in the vicinity of the toe. They serve the double purpose of relieving the hydrostatic excess pressures beneath the valley floor and of drying up or at least reducing the discharge of the springs.

Relief wells are designed to discharge water without suspended solids. They are generally spaced initially at 15 to 30 m and are equipped with provisions for measuring discharge. A piezometer is established between each adjacent pair of relief wells. As time goes by, the discharge from the relief wells may decrease for one of several reasons: the reservoir may be silting up; the wells may be plugging with silt; or the well screens may be becoming obstructed by chemical deposits or products of corrosion. If the decrease in the discharge is caused by silting of the reservoir, the water levels in the piezometers at full reservoir go down; in all other circumstances they go up. Excessive discharge of silt should be prevented by sealing off any silt layers or lenses during installation of the wells. Minor accumulations of silt should be flushed out periodically. For this reason, and to permit replacement of deteriorated screens, the heads of the wells should be readily accessible. If the observations during the first years after filling the reservoir indicate that the dam would be safe without the relief wells, supervision and maintenance of the wells can be discontinued.

Relief wells for the control of excess pressures beneath permanent dams were developed to a high degree by the Corps of Engineers, U.S. Army, in projects on the Mississippi-Missouri River system. They formed an integral part of the design of major structures such as Randall Dam (Thorfinnson 1960).

#### 59.6 Zoned Dams

##### 59.6.1 Purpose of Zones

A dam must be sufficiently impermeable to retain the reservoir, stable enough to withstand the forces to which it will be subjected, and capable of resisting internal erosion or piping. The different materials near a particular site are likely to possess characteristics that satisfy these requirements to different degrees. Hence, they are selected and arranged in the dam to accomplish the requirements most efficiently and economically. The arrangement for this purpose is termed *zoning*. Most embankment dams consist of a core of relatively impermeable soil, flanked by shells intended to support the



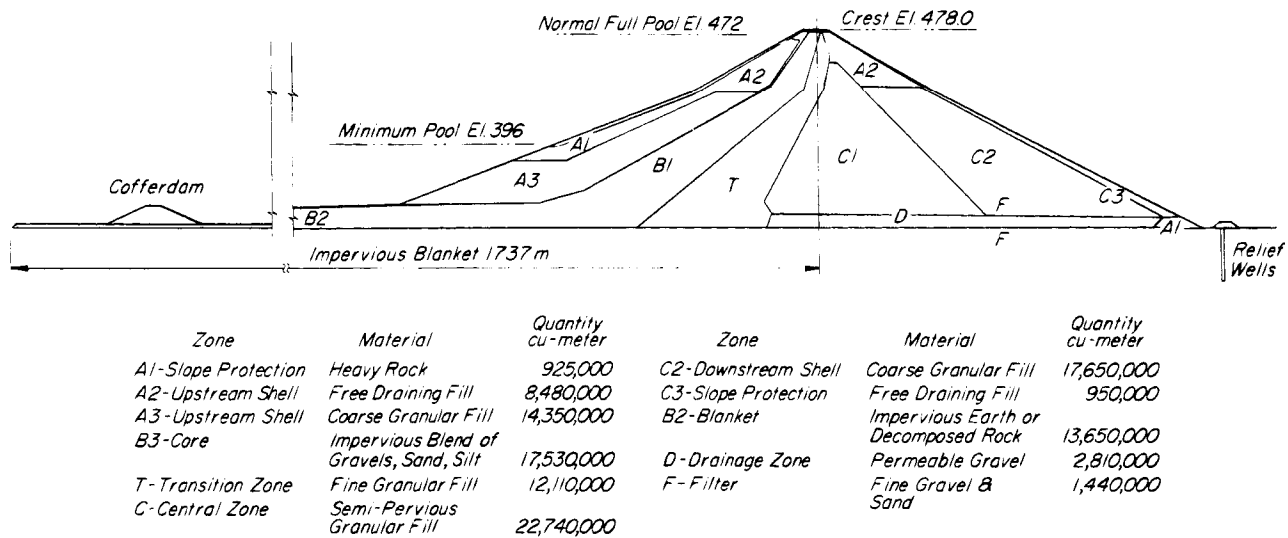


**Figure 59.2** Cross-section through Tarbela Dam, Pakistan. Underseepage through highly pervious valley, filled to a depth of 213 m with glaciofluvial deposits, was controlled by long upstream blanket and downstream relief wells (after Lovell 1970).

core, and separated from the shells by filters or transition zones to prevent internal erosion and to control pore-water pressures.

### 59.6.2 Arrangement of Zones

The *core*, usually near and somewhat upstream of the axis of the dam, is the principal barrier to flow of water through the dam. It generally consists of the most impervious suitable material that is available. Because no core is perfectly impervious and because it is always possible that a core may contain a pervious zone or a crack, the zone immediately downstream of the core is designed to serve as a *filter* to prevent migration of particles from the core into the downstream shell. Downstream of the filter is the *downstream shell*. It has the primary function of supporting the core and downstream filter under all conditions including full reservoir and during an earthquake. It may consist of inherently strong, stable material such as gravel or rockfill, or of weaker materials with a flatter downstream slope. It is beneficial to keep the downstream shell in a permanently drained condition. Hence, if the dam rests on a pervious foundation, a *filter drain* is placed between the shell and the foundation. By this procedure the shell is effectively isolated from both reservoir water and groundwater and much of it can be designated a *random zone* in which any stable compactable material can be placed. If the grain sizes of the core and shell differ too greatly to be accommodated by a single filter, additional filters or *transition zones* are introduced, each constituting a filter for the one upstream. Each successive zone from upstream to downstream must have the capacity to carry the inflowing seepage to the next zone without building up excess water pressure. The

material near the downstream face of the dam is selected to provide resistance to erosion.

Immediately upstream from the core is the *upstream transition zone*. Although it is often designed to satisfy the requirements of a filter against the core, its function differs from that of the downstream filter. Its primary function is to furnish material to fill and plug any crack or open zone that might extend through the core. Therefore, it should consist of lightly compacted cohesionless material, of fairly uniform grain size, that can be readily moved into a void by flowing or seeping water. Moreover, it should be of a size that would be retained by the filter downstream of the core. Upstream of the core and upstream transition zone is the *upstream shell*. Like that of the downstream shell, its function is to support the core. Unlike the downstream shell, however, the upstream shell is submerged by the reservoir and subject to its fluctuations. The stability under full reservoir is usually greater than that after a drawdown (Article 36), and to mitigate the effects of drawdown at least the upper and outer portions of the upstream shell are constructed of free-draining material. In general, the finer portions of the remainder of the upstream shell material are placed closer to the core, and the coarser portions nearer to the upstream face. Because the upstream face of the dam is likely to be subjected to wave action, an outer zone of *riprap* is furnished within the elevations where the attack may occur. If materials having the potential to lose strength by swelling must be used in the upstream shell, they must have sufficient cover of stable material to prevent the swelling or else the upstream slopes must be flat enough to be stable after the swelling and softening occur.

The foregoing comments present a considerably idealized conception of the cross-section of an earth or rockfill dam. In reality, the selection of materials and the dimensions of the zones are strongly influenced by the properties of the potential borrow materials, their relative costs in place in the dam, and the practicability of using materials from necessary excavations. Many earth dams, for example, require spillway or intake cuts from which large volumes of soil or rock must be removed. Whether incorporation of these materials into the dam is economical depends, among other factors, on the stage of embankment construction when the cuts must be made and, thus, whether stockpiling and double handling would be necessary. For these reasons, it can rarely be said that there is one best design for a given site, and many different arrangements have been used successfully (Fig. 59.3). Although simplicity in the zoning is desirable, the as-built cross-sections of dams often show complexities because the borrow pits contained smaller volumes of suitable material than expected, materials from structural excavation became available, or weather conditions prevented placement of some materials during parts of the year. One of the advantages of embankment dams is their adaptability, within rather broad limits, to conditions as they are disclosed by construction. The zoning of a well-designed dam allows for as much flexibility of this type as possible within the framework of the contract.

The zoning and cross-section are also strongly influenced by the local foundation and abutment conditions. Rarely can a foundation be considered impermeable, and often the permeability is not only high but variable to a degree that cannot be determined reliably before the reservoir is filled. In considering the provisions for control of seepage, the embankment, foundations, and abutments should be considered as a whole. Moreover, the slopes of the embankment are often governed not by the embankment materials but by the strength of the foundation.

Compaction (Article 44.2) is an essential component of the construction of all modern earth and rockfill dams. Compacted materials are stronger, are less susceptible to erosion, and are less compressible and of more uniform compressibility than uncompacted ones.

All these attributes are significant with respect to dams, but the consequences of the deformations associated with compressibility are the least obvious and deserve detailed consideration.

### 59.7 Deformation of Earth and Rockfill Dams

An earth or rockfill dam is inherently flexible and able to withstand differential movements appreciably larger than can be tolerated by concrete structures of comparable height. Nevertheless, for several reasons it is usually advantageous to minimize such movements by compacting the embankment materials to decrease their compressibility. The unfavorable effects of differential movements

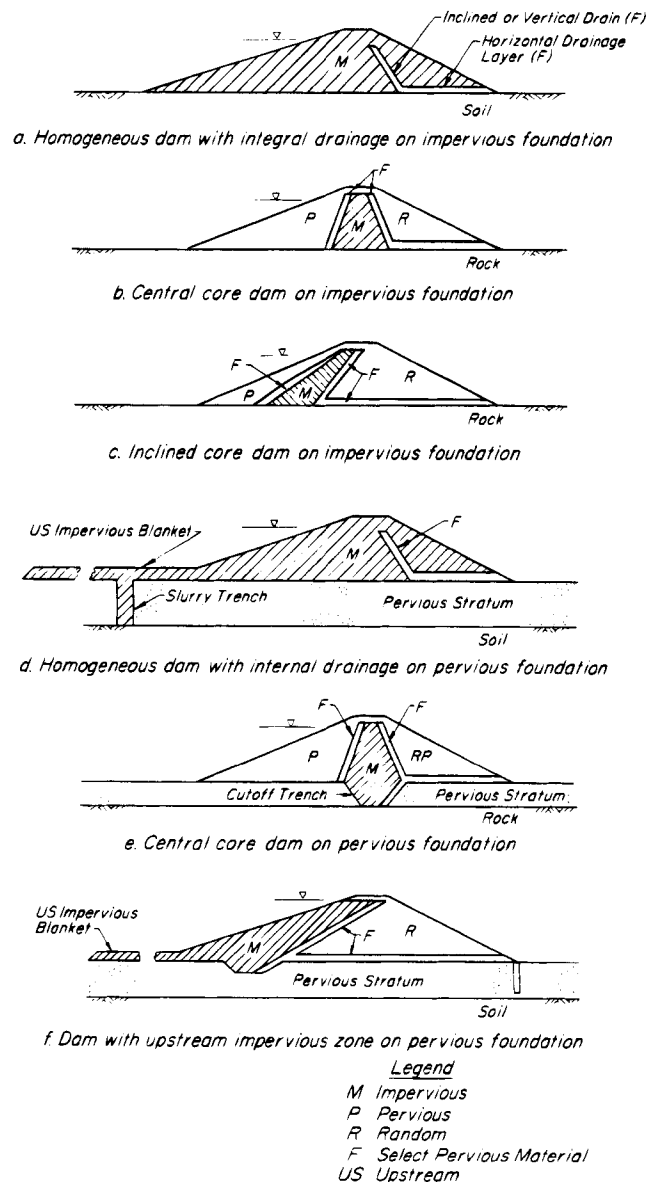


**Figure 59.3** Types of earthfill and rockfill dam sections: (a) homogeneous dam with internal drainage on impervious foundation; (b) central core dam on impervious foundation; (c) inclined core dam on impervious foundation; (d) homogeneous dam with internal drainage on pervious foundation; (e) central core dam on pervious foundation; (f) dam with upstream impervious zone on pervious foundation (Wilson and Marsal 1979).

include stress transfer or arching, which may reduce effective stresses where higher pressures would be advantageous, and the development of extension strains, which might lead to cracks in the upstream-downstream direction.

The behavior of Lower Notch Dam, Ontario, illustrates the foregoing statements. A cross-section of the valley along the axis of the dam is shown in Fig. 59.4a. The width of the bedrock valley at the original stream level

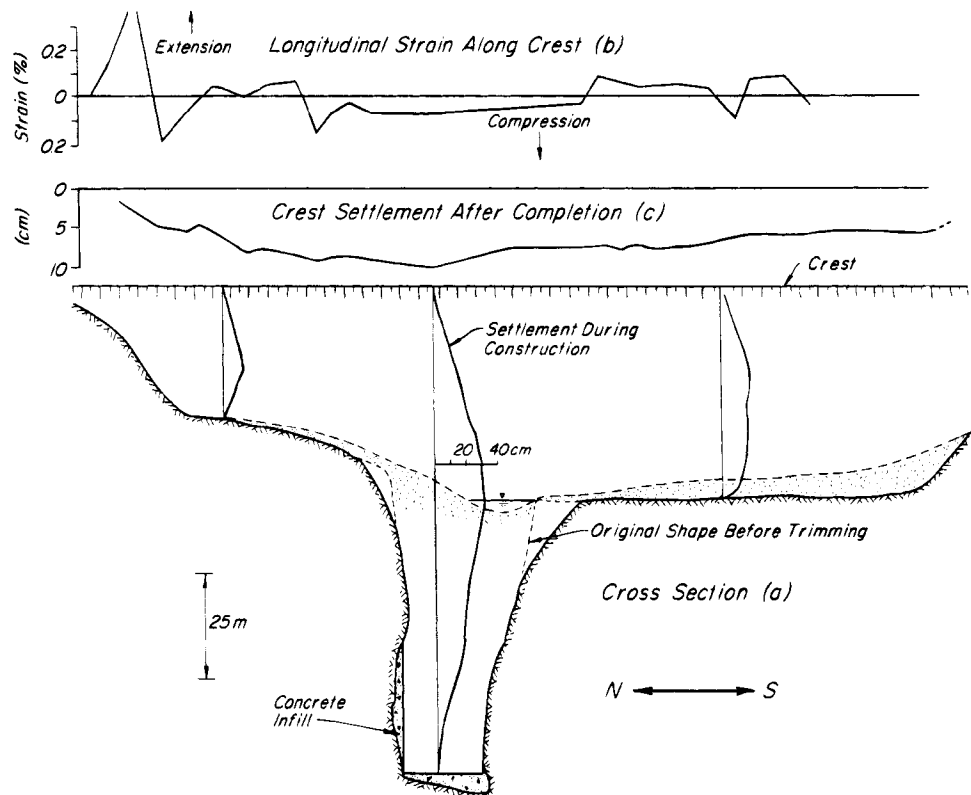


**Figure 59.4** (a) Cross-section of Lower Notch Dam, Ontario, showing settlements during construction. (b) Longitudinal strains along crest. (c) Crest settlement 4 years after completion.

was about 120 m, but an inner sediment-filled gorge less than 30 m wide extended to a depth of 75 m. The sediment was excavated and a compacted embankment built to a height of 125 m above the bottom of the inner gorge. As construction progressed, settlements were measured along vertical lines with the results, at the end of construction, shown in the figure. The maximum settlement of approximately 0.3 m at midheight of the gorge section is rather small for a dam with a height of 120 m, but at the rock walls corresponding to the same elevation the settlement was zero. As a consequence of the downward movement of the earth fill with respect to the adjacent walls, substantial shear forces were transferred to the walls. The vertical pressure at the base of the fill in the gorge was correspondingly reduced, and pressure cells at the bottom of the gorge indicated only about half the full weight of the fill directly overhead.

After completion of the fill the settlement of the crest slowly increased and in 4 years reached a maximum of about 0.1 m over the deepest part of the gorge. The shape of the settlement curve (Fig. 59.4c) reflects that of the valley. Longitudinal strains along the crest of the dam were measured and are also shown in the figure. They clearly indicate compression of the crest above and beside the gorge, and extensions at greater distances, corresponding to continued lateral movements toward the subsiding

area at the gorge. The concentrated zones of extension and compression at the south abutment represent local movements not associated with the inner gorge.

Stress transfer may also occur in planes at right angles to the axis of a dam. If, for example, a near-vertical core is more compressible than the adjacent transition and shell materials, its tendency to settle produces shearing forces between the core and the shells that add to the vertical pressures in the shells and reduce those in the core. Conversely, if the core is more rigid than the shells, it attracts vertical load.

Deformations of the foregoing types and the corresponding stress transfer may be greatly increased and complicated if the dam rests on a compressible foundation itself subject to differential settlements.

The pattern of deformations and corresponding stress transfer discussed in the preceding paragraphs develops to some degree in all embankment dams (Wilson and Marsal 1979). It becomes a concern only if extension strains may lead to cracking, or if stress reduction becomes so great that water pressures may induce cracks, or that the soil, even if well compacted, may be readily eroded.

Extension strains do not lead to cracking in a field of compressive stresses. Hence, cracks are more likely to occur near the crest of a dam than in the interior. However,

if the abutments exhibit unfavorable geometry, such as overhangs or niches, compressive stresses may not be able to develop to a sufficient degree, cracking may occur, and seepage may initiate erosion. Hence, such geometry should be corrected.

If the stress transfer reduces the stresses at a point in the core to the extent that the difference between the water pressure and the total minor principal stress exceeds the tensile strength of the core material, there is at least a theoretical possibility that a crack may be induced by *hydraulic fracturing*. The phenomenon of hydraulic fracturing has been induced many times unwittingly in the cores of dams as a consequence of introducing water into boreholes being made for installing piezometers, for sampling, or for grouting. The theoretical criterion given above, however, seems to be an oversimplification. Laboratory investigations with simulated boreholes indicate that the actual value of the hydraulic fracturing pressure is usually larger than that indicated by the criterion. Fracturing could be induced readily in the laboratory at a slot comparable to an open joint in a rock foundation, but not at predictable water pressures and only because the soil adjacent to the slot was in a loose condition that permitted the entry of the water. The water then could fracture the soil by a wedging action and could also induce sloughing (Jaworski et al. 1981).

The pattern of stress redistribution can be investigated by finite-element techniques in which the stiffnesses of the various materials are introduced into the mathematical model and the weight of the embankment is applied in increments to simulate the construction procedure. Such studies are useful as an indication of potentially undesirable geometric details and of means for improving them. For example, at Lower Notch Dam the steep upper part of the inner gorge (Fig. 59.4a) was trimmed back substantially to reduce extension strains. The quantitative results, however, should not be taken at face value in design because of the impracticability of determining in advance the properties and constitutive relations for the foundation and embankment materials, including the effects of time and of exposure of the dam and its surroundings to the reservoir water.

Transverse cracking in the cores of earth and rock-fill dams is undesirable and should be avoided by all practicable means. Narrow compressible cores between less compressible shells, particularly if they include geometric discontinuities as at Hyttejuvet and Balderhead Dams (Fig 59.5) have proven troublesome (Kjaernsli and Torblaa 1968, Vaughan et al. 1970). Geometrics favoring stress concentrations conducive to extension strains or to large stress reduction due to load transfer should be improved as much as practicable. Upstream curvature of the axis of the dam is desirable where possible. In a few instances (Wilson and Marsal 1979) where large concen-

trations of deformation could not be avoided, deformable sections have been built into dams. Nevertheless, after all reasonable precautions have been taken to avoid cracking, the design should proceed on the assumption that cracks will occur, and appropriate defensive measures should be incorporated.

Deformations of the upstream shell occur as a result of raising the reservoir for the first time. Because the shell usually consists of large particles, the stresses due to the weight of the fill as construction proceeds are transmitted from particle to particle through relatively few point contacts. If the particles are angular, the stresses near the points are high and some of the particles break. To a large extent, the compression of a rockfill under its own weight is the result of such corner breakage. The process requires time, because breakage of one corner causes stresses to increase at nearby points of contact whereupon another corner may break and cause further stress redistribution. Inasmuch as wetting a rock reduces its strength, raising the reservoir for the first time weakens the rock and may cause corners to break that had reached equilibrium, although highly stressed, under dry conditions. On the other hand, the stresses in rounded particles adjacent to points of contact are very much less than those near sharp points. Consequently, the effect of submergence is much smaller in soils with rounded particles, and wetting is likely to produce only small settlements in transition zones or filters of rounded grains. Moreover, core materials compacted near optimum moisture content are little affected by a rise in water level. Consequently, an upstream rockfill shell during its first submergence is likely to settle with respect to the transitions or core. If the dam is high enough, the accumulated settlements result in an escarpment in the crest accompanied by a longitudinal crack. Such cracks have appeared in almost all rockfill dams with a height of more than about 100 m. They could be prevented or reduced by copious watering of the rockfill during placement and compaction, but because they do not impair the function of the dam and are easily repaired by regrading the crest, watering is seldom undertaken. In the past, however, when many dams were constructed of uncompacted rockfill dumped in high lifts, watering was standard practice. High dams with shells of rounded particles, such as the 244-m Mica Dam or the 213-m W. A. C. Bennett Dam in British Columbia, have shown no tendency for longitudinal cracking upon reservoir filling.

Filling the reservoir for the first time causes deformations not only of the upstream shell but of the upstream transition zones and core as well. The more slowly the submergence occurs, the more readily these zones, particularly the core, can adjust to the deformations without cracking. Although the rate of rise cannot always be controlled, it should be kept as low as practicable, prefera-

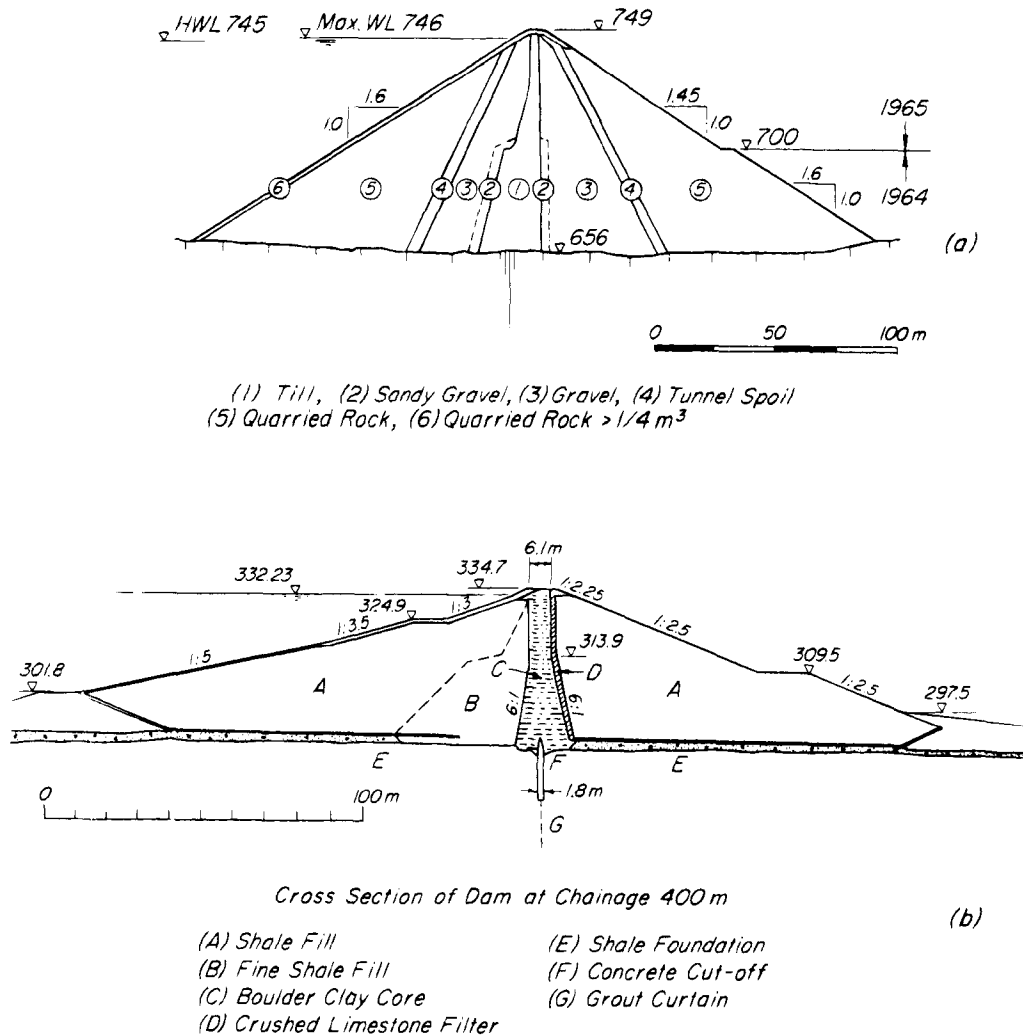


**Figure 59.5** Cross-section of (a) Hyttejuvet Dam in Norway and (b) Balderhead Dam in England. Both dams experienced cracking and piping at the abrupt change of section in their extremely narrow cores. (a) After Kjaernsli and Torblaa (1968); (b) after Vaughan et al. (1970).

bly a fraction of a meter per day in contrast to several meters per day.

### 59.8 Slopes

If the foundation materials are weak, they govern the slopes of the dam almost irrespective of the properties of the embankment materials. On the other hand, if the foundation is strong and rigid, the quality of the embankment materials governs.

An outstanding example of the influence of poor foundation conditions on embankment slopes is Gardiner Dam in Saskatchewan (Jaspar and Peters 1979). The Bearpaw formation underlying the site is a highly overconsolidated bentonitic clay shale containing many preconstruction shear zones along which the strength had been reduced to a residual value of  $c' = 0$  and  $\phi_r = 9^\circ$  or less. Although the dam is only 64 m high, its slopes vary from 1 on

1.75 at the top to 1 on 85 at the downstream toe. The design was revised several times (Fig. 59.6a) as observations during construction provided more definitive information concerning the foundations. By contrast, the 125 m LG-4 Main Dam on the James Bay project in northern Quebec, with a foundation of unweathered granite and gneiss, makes effective use of excellent construction materials in a simple cross-section with upstream and downstream slopes of 1 on 1.7 and on 1 on 1.8, respectively (Fig. 59.6b) (Paré et al. 1984).

The slopes of most dams are tentatively established on the basis of experience and precedent in consideration of the foundation conditions, availability and properties of materials, height of the dam, and possibly other factors specific to the project. After a preliminary cross-section has been developed, stability analyses are conducted to determine whether the factors of safety satisfy the mini-

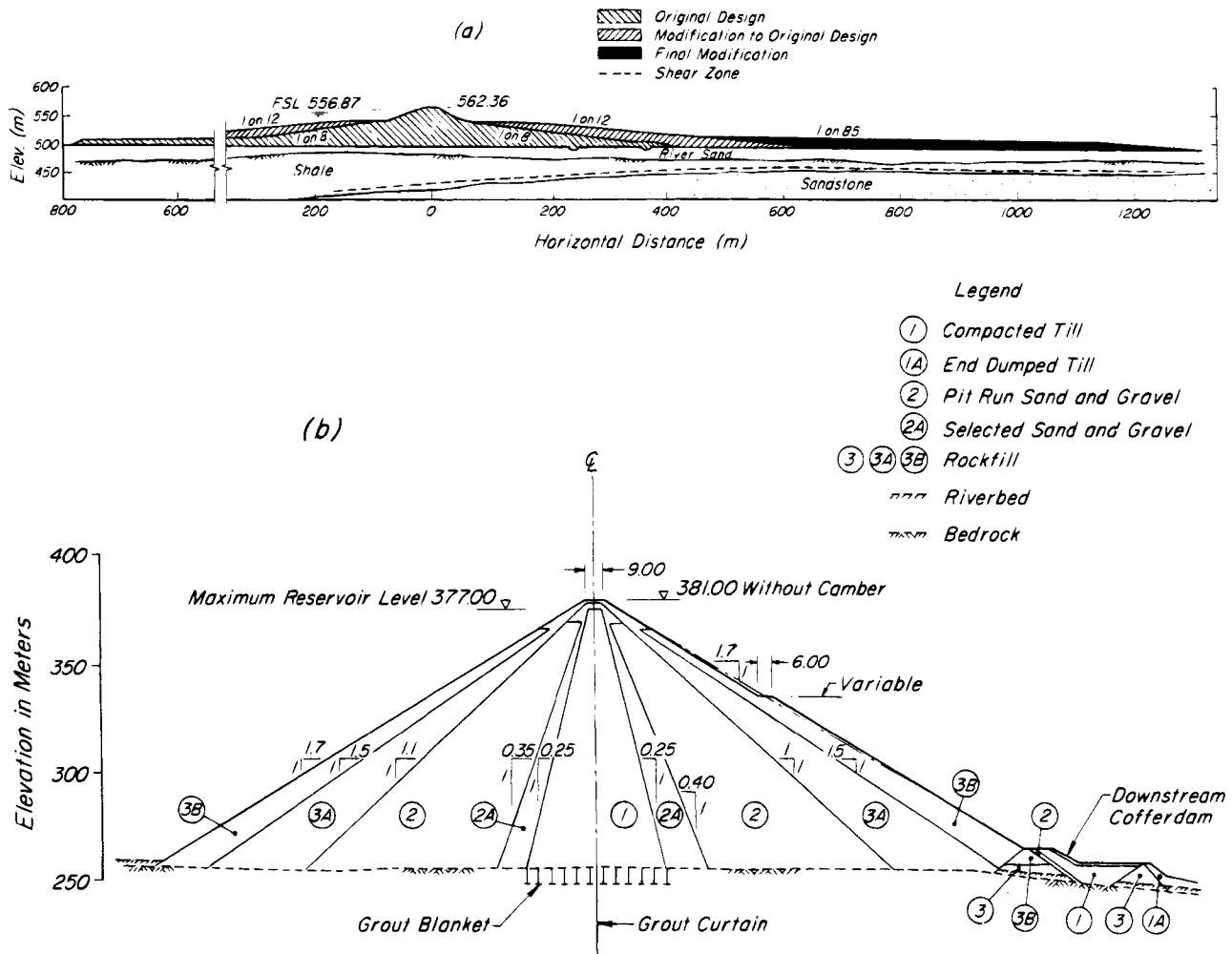


**Figure 59.6** (a) Cross-section of Gardiner Dam, Saskatchewan, on Bearpaw shale, showing revisions of slopes during design and construction. (b) Cross-section of LG4 Main Dam, James Bay Project, Quebec, on unweathered granite and gneiss of Canadian Shield.

imum requirements, usually postulated by some authority, corresponding to end of construction, steady seepage, drawdown, and earthquake (Article 36). If necessary, the design is modified in accordance with the findings.

In carrying out stability analyses, the investigator should be wary of methods of calculation and computer programs in which the critical surface of sliding is derived from the analysis without sufficiently taking into account the presence of weak zones in the foundation. Rarely is a circular surface of sliding a good approximation when the geologic features of the foundation govern stability (Article 36.3). Gardiner Dam (Fig. 59.6a) is an outstanding but by no means unique example of the radical and detrimental influence on the stability of a dam of a single, easily overlooked weak feature in the foundation. It also exemplifies the extent to which the assumption of a circular surface of sliding may be inappropriate. It is preferable to make simple calculations based on an investigation and assessment of the geologic and geohydrologic conditions,

along with a realistic appraisal of the properties of the materials involved, than to undertake sophisticated calculations that may impose unappreciated limitations on the validity of the analyses.

### 59.9 Materials

A major objective of site investigation is to determine the location, extent, and characteristics of all materials in the vicinity that might be incorporated into the dam. Preferably the investigation proceeds as the layout of the project develops and information becomes available regarding the quantities required, the amounts and kinds of materials that may become available from excavations for spillways and other facilities, and whether portions of the potential borrow areas may become flooded during construction. Because the layout itself is determined to some extent by the cost and availability of materials, the program of site investigation and the development of the

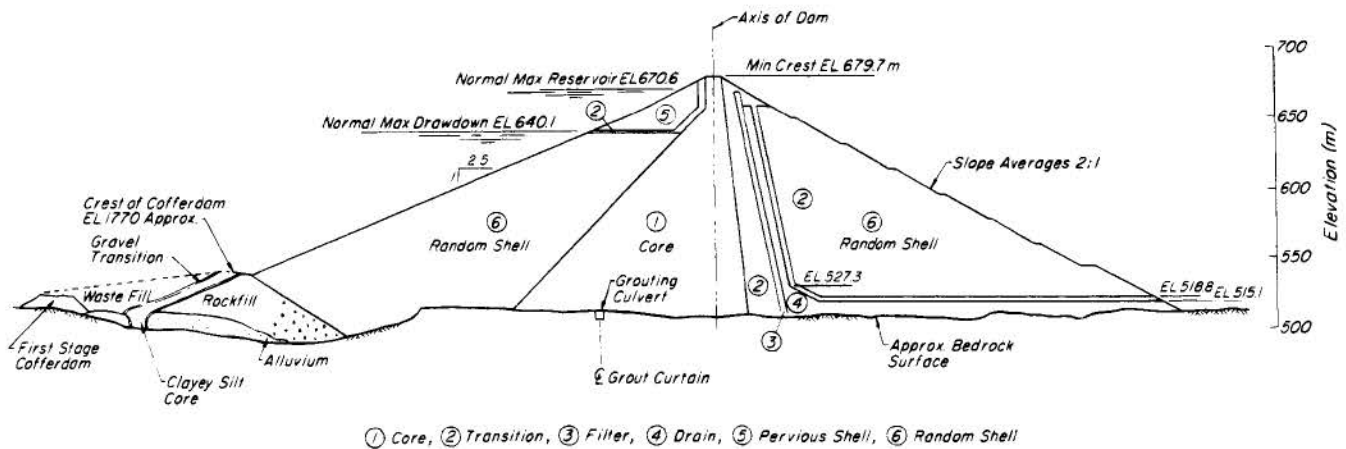


**Figure 59.7** Cross-section of W.A.C. Bennett (Portage Mountain) Dam, British Columbia, consisting entirely of glaciofluvial materials from one borrow area (after Morgan and Harris 1967).

design are not independent operations but deserve close coordination and interaction.

Successful embankment dams have been built of almost all types of earth materials. Indeed, the art of embankment-dam engineering consists not of performing sophisticated tests and carrying out calculations of stability and deformation but of selecting and using the local materials in the best way to satisfy the requirements of safety and economy. If the site investigation and the design do not proceed hand in hand from the earliest stages, guided by persons of experience and judgment, no amount of refinement at later stages can compensate for premature faulty decisions.

Although, in the absence of a variety of materials, dams have been built almost entirely of clay (Fig. 59.3a) or almost entirely of sand (Fig. 59.3b), experience favors composite sections. For such sections, borrow pits would ideally provide (1) impervious soils of low compressibility and high resistance to erosion, at field moisture contents close to optimum; (2) free-draining cohesionless materials suitable for the upstream drawdown zone; (3) granular materials suitable for filters and transitions; and (4) granular materials, stable, with low compressibility when compacted, preferably fairly pervious, for the shells. Seldom are all these desirable components found close to a dam site; processing, usually by screening, is often required. Almost the entire embankment of the W.A.C. Bennett Dam (Fig. 59.7), for example, was obtained from a single borrow pit. About half the material went directly to a random zone. The rest was screened to sizes suitable for the remaining zones. No material was wasted; a small amount of silt was added to the fraction reserved for the core (Morgan and Harris 1967).

Processing by screening, when specified in the contract, is inexpensive. In fact, the increase in volume associated with separation into fractions, each of more uniform grain size than the original deposit, often com-

pensates for the cost of processing. Processing by screening is also useful in reducing segregation at the boundaries between cores, filters, and transitions. When a broadly graded material is stockpiled, dumped by trucks, or bulldozed into windrows, the coarsest constituents invariably collect near the edges (Fig. 59.8). Consequently, even though the grain-size distribution of a filter zone on the average satisfies the filter criteria, the critical portion of the zone adjacent to the material to be protected may not, and internal migration will then be fostered under conditions of steady seepage. Because even the greatest vigilance can hardly avoid segregation under field conditions, the materials should be processed to produce more uniform grain sizes and, if necessary, to increase the number of zones.

As it is usually impractical to determine the grain-size characteristics of a borrow area in advance of construction with sufficient accuracy to judge the quantities that will be produced in the various ranges of size, the need for



**Figure 59.8** Photograph showing segregation of crushed-rock transition materials at edge of windrow.

flexibility in zoning and for random zones in the embankment is apparent.

The foregoing discussion, limited to only a few aspects of exploration and placement, justifies the following generalizations: The design of an embankment dam, including the exterior slopes, must be based on judgments regarding the quantities and properties of borrow materials that cannot be known reliably until construction is well advanced or perhaps even completed. Therefore, calculations of factors of safety, deformations, and seepage will lead to results only as reliable as the estimated properties. The most valuable contribution of soil mechanics at the design stage is the ability to judge what will be the properties of the materials that can actually be produced or derived from the borrow areas after they have been placed in the dam. In making these judgments, the engineer is guided by the results of explorations, laboratory tests, and possibly field tests, but above all by experience including any findings from field observations on similar projects involving similar materials. On critical projects, observations and measurements during construction will provide data and may justify more refined analyses.

In general, compaction (Article 44.2) increases strength, uniformity, and resistance to erosion. It reduces compressibility and deformations. Therefore, all modern embankment dams are compacted. The lifts should be thin enough to ensure that the lower part of each lift is compacted to the required degree; the maximum size of particles should not be so great as to interfere with compaction. By compaction of cohesive soils, particularly if the water content is at or somewhat below the optimum value, not only are the shear strength and rigidity increased but also the brittleness under low ambient pressures. Therefore, it may be advisable to minimize the deformations in the lower part of a clay core by thorough compaction at moisture contents slightly dry of optimum, but to increase the water contents slightly in the upper part to reduce the tendency to crack. The moisture content should not, however, be so low in any part of the core as to induce collapse of the soil structure upon saturation.

Uniformity of compaction of the core is an important deterrent to internal erosion. Local loose zones, such as may occur at the base of a poorly compacted layer, are especially susceptible. The juxtaposition of a poorly compacted zone in the core and the segregated edge of a filter is particularly unfavorable.

### **59.10 Contact between Embankment and Foundation**

When core material at or slightly above optimum moisture content is compacted against an intact rock surface, seepage along the interface is negligible and there is no possibility of erosion of the core material. However, rock is invariably jointed and may possess other defects as well. Core material cannot be compacted against an open joint;

if water flows in the joint the readily erodible poorly compacted soil sloughs into the opening and may be carried away. At the abutments the rock-core contact should not flare outward in the downstream direction; if it does, the water pressure tends to separate the core from the rock surface. Moreover, if the rock surface overhangs and the adjacent core settles, an opening may be created beneath the overhang through which water may flow. Near the upper part of the core, where ambient pressures are low, abrupt changes in the slope of the rock may induce tension cracks transverse to the core with the possibility for subsurface erosion. If the downstream portion of the core contact is attacked by erosion, the protective filter adjacent to it may also be eroded. Therefore, steps must be taken to protect the vulnerable areas.

Curtain and blanket grouting to reduce the flow in the rock and downstream drains to direct the flow away from the contact area are generally used. These measures are not usually sufficient. If a grout curtain is successful in providing a barrier to flow, it leads to piezometric levels in the rock just upstream of the curtain equal to the reservoir level and thereby creates a high hydraulic gradient across the curtain, a gradient much greater than that associated with flow through the same foundation if ungrouted. Because even the best of grout curtains contains imperfections, local zones of high flow under the large gradient are likely to occur. If they coincide with the zones of susceptibility to erosion described in the preceding paragraph, failure could ensue; for instance, this mechanism is believed to be a principal factor in the failure of Teton Dam (Chadwick et al. 1976).

In addition to removing all rock that can be loosened without blasting, vertical faces of steps higher than about 3 m are generally trimmed back to about 70° with the horizontal, joints are cleaned out to a depth of about three times their width and filled with dental concrete, narrower joints are filled with slush grout broomed into the cracks, overhangs are corrected by trimming or by infill concrete, and features in the bottom of the valley such as potholes or depressions from which blocks have been plucked by glaciers are filled with lean concrete. In some instances the irregularities are covered by shotcrete, but indiscriminate shotcreting is undesirable because of the tendency of the shotcrete to crack and, in effect, become jointed itself. Foundation and abutment preparation may be expensive and time consuming, but it is nevertheless essential.

After preparation of the rock surface, the first core fill is placed. Usually the core material is from the same source as that for the main body of the core but the particles larger than about 10 cm are removed and the water content is raised above optimum enough to allow the material to be squeezed into continuous contact with the prepared foundation or abutment. The fill at the con-



tact is compacted by hand-held equipment, small mechanical compactors, or the wheels of a heavy truck.

Some rocks, especially shales and mudstones, slake rapidly on exposure. They must be treated and covered rapidly. Often the area of foundation or abutment that can be exposed at one time must be severely limited. The slaked material is likely not only to be more erodible than the fresh rock, but also weaker.

Where the core rests on a soil foundation instead of rock, a shallow core trench (Fig. 59.9) is usually excavated to ensure contact with unweathered, undisturbed foundation material. Because the foundation soil may contain pervious zones, downstream drainage is usually provided by means of filter drains, as shown in the figure.

In many localities the foundation soil is underlain at a modest depth by bedrock. In glaciated areas, for example, till may overlie rock from which older sediments were scoured. All the defects in the rock discussed in connection with foundations on rock are likely to exist under the foundation soil, but they are not visible and, therefore, cannot be treated with the care described above. In exchange for this disadvantage, the soil cover constitutes a medium through which underflow occurs at hydraulic gradients that may be much smaller than those beneath a core-bedrock contact. If, however, a cutoff wall is constructed to the rock, high gradients will exist and, in the event of a defect in the cutoff, may lead to a concentration of flow. Under these various conditions, downstream drainage provisions, possibly including relief wells, are required, and surveillance of springs near the downstream toe as well as piezometric observations are essential. Additional drainage, weighted filter berms, or both may be indicated.

Where the core is extended to bedrock through loose pervious soils in areas of potentially active seismicity it may be necessary to remove or densify the soils beneath all or part of the shells to eliminate or reduce the consequences of liquefaction (Article 20.9). Because it is often impractical to remove the pervious materials beneath cofferdams which will eventually be incorporated into the

dam, it is sometimes considered tolerable, where the probability of a major earthquake is low, to remove or densify only the loose foundation soils within the limits of two planes descending at arbitrarily chosen slopes (usually 1:1), one from the upstream and one from the downstream shoulder of the crest of the dam. Outside these limits the shoulders would be expected to slump and to require extensive repairs if a strong earthquake should occur, but the core would have adequate lateral support to retain the reservoir until the water could be drawn down and repairs completed.

The foregoing examples of conditions and treatments are not comprehensive. Different conditions prevail in regions of deeply weathered rocks, in karstic terrains, and in deep alluvial valleys, for example. For these reasons no all-encompassing procedures can be given. Each project must be considered in view of its own circumstances. Engineering geology furnishes the information for visualizing the physical conditions that may be encountered. Soil mechanics provides an understanding of the consequences of the conditions, the means to prevent or reduce the undesirable consequences, and methods of observing and evaluating the performance of the foundation and dam during and after impoundment. It also permits rational design of remedial measures if needed.

## 59.11 Embankment Dams with Membranes

### 59.11.1 Upstream Facings

During the mid-1800's, numerous dams in the gold fields of the western United States were constructed of dumped rockfill with timber upstream skins sealed to the bedrock. From this beginning evolved the concrete-faced rockfill dam, often an economical type in mountainous regions where rock is plentiful and where suitable core and filter materials for conventional earth dams are either scarce or difficult to place under the prevailing climatic conditions. Until the 1960's the fill for such dams almost invariably consisted of quarried rock, with blocks having masses up to 20 tonnes placed by dumping in lifts of 15 to 50 m

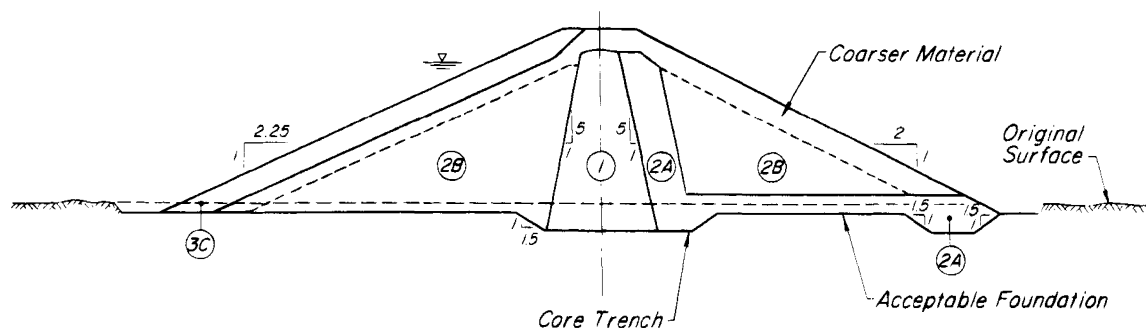


**Figure 59.9** Section through 15-m dike on Opinaca Reservoir, James Bay project, showing core trench in foundation of glacial till. Zone 1, till core; zone 2A, granular filter; zone 2B, sand and gravel shells with coarser materials placed near the slopes; zone 3C, rockfill.

while being copiously watered. The slopes corresponded to the angle of repose, usually between 1.1H:1V and 1.4H:1V. The practice culminated in several dams more than 100 m high. The facings, of reinforced concrete, were cast on a bedding zone in panels about 15 m square separated by joints, and were keyed into shallow vertical cutoff walls formed in trenches blasted into the rock at the upstream toes. The facings of all these dams experienced large settlements perpendicular to the slope as well as movements in the plane of the facings. The horizontal joints in the upper parts of the facings and the vertical joints near the upper parts of the abutments tended to open, often with large leakage. The connection between the cutoff wall and the facing was particularly vulnerable. In spite of their shortcomings and frequent need for repairs of their facings, such dams had an excellent record for safety.

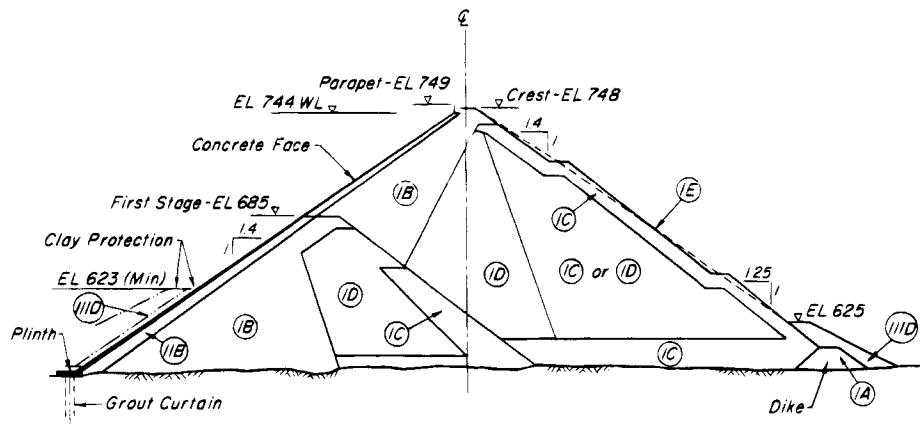
With the advent of heavy vibratory compacting rollers in the latter half of the 1960's it became possible to achieve economical, far better compaction of rock fill by compaction in layers than by dumping in high lifts, whereupon interest in concrete-faced rockfill dams increased. Their performance was improved not only because of the reduced settlements due to compaction, but also on account of better details of design. By 1982 at least eight had been constructed with heights greater than 100 m. According to recent practice the rock fill is usually compacted in lifts of about 1 m and 2 m in the upstream and downstream halves, respectively. Material with a permeability of about  $10^{-6}$  m/s, sometimes consisting of crusher-run rock with a maximum size of 120 to 150 mm, is placed immediately under the concrete facing and compacted, not only to provide bedding for the facing but also to form a relatively impermeable barrier to leakage. The horizontal width of the bedding zone, about 4 m at the top of the dam, increases gradually to the base. To avoid damaging the rock by blasting to construct a curtain wall, it is now customary to cast a slab or plinth on the cleaned and surface-treated rock, to dowel the plinth to the bedrock, and to carry out blanket grouting beneath it. A grout curtain is also often constructed along the line of the plinth. The concrete facing, reinforced with about 0.5 percent of steel in both directions, is cast in continuous strips upslope without horizontal joints, and with unkeyed vertical joints across which reinforcement is carried. The perimeter joint usually contains a thin filler and two independent waterstops. The thickness of the slab is customarily 0.3 m at the crest and increases toward the base by  $0.002d$  to  $0.003d$ , where  $d$  is the vertical distance below the crest in meters.

The size of the rock is selected to increase in a general way downstream and toward the base of the dam, so that any excessive leakage through the facing and bedding zone escape harmlessly. Leakage in recent dams, how-

ever, has been small. At Areia Dam in Brazil, 160 m high, for example (Fig. 59.10), it is less than 100 l/s (Pinto et al. 1985).

Asphaltic concrete has been used as a facing for rockfill dams since the late 1930's. The principal development has been carried out by German engineers, and most such dams are located in Germany. A few are located in the United States, including Homestake Dam (1966) in Colorado, 69 m high. Several early dams were constructed in Algeria, among them the Iril Enda Dam, 75 m high, built in 1954. For convenience and safety in construction of the facing, the upstream slope is usually about 1.7H:1V. The construction of the rock fill is similar to that for concrete-faced dams, with an upstream zone of smaller rock as a base for the membrane. The design of the membrane itself has undergone a considerable evolution. Early membranes consisted of a bonding or equalizing layer of bitumen up to a few centimeters thick followed by one or two layers of asphaltic concrete with a total thickness of about 60 mm, a drainage layer about 110 mm thick of pervious bituminous concrete, and an upper layer of dense bituminous concrete about 120 mm thick, made up of two 60-mm sublayers. The drainage layer usually led the water to an inspection gallery. In more recent dams there has been a trend to elimination of the pervious bituminous drainage layer in favor of a facing built up of two or more layers of dense bituminous concrete each about 60 mm thick. The carefully designed bituminous mixes are placed in strips from the bottom toward the top and compacted with vibrating rollers drawn upward. Although an asphaltic concrete membrane is inherently flexible, cracking may occur where tensile strains develop between the membrane and the cut-off wall. It is minimized by making the transition as gradual as possible and compacting the rock fill thoroughly near the boundary.

Soil mechanics enters only peripherally into the design and construction of an embankment dam with an upstream membrane if the dam is supported by competent rock. Since the membrane protects the entire embankment from reservoir water, the water pressure increases the frictional resistance of the fill material. In addition, rapid drawdown does not lead to stability conditions less favorable than those corresponding to construction or to an empty reservoir. Therefore, the upstream slope can be at least as steep as the downstream slope. At some sites this steepening significantly shortens the diversion works. The volume of fill is correspondingly less than for a dam with internal core or membrane. The steeper slopes make greater demands on the foundation, however, so the effect of weak seams or zones deserves careful investigation and analysis. A principal requirement is that the fill be permeable enough to discharge all leakage without reducing



Material	Classification	Zone	Method of Placement	Compaction
Rockfill I	Massive Basalt (Up to 25% Basaltic Breccia)	IA	Dumped	—
		IB	Compacted in 0.80m Layers	Four Passes 9-tonne Vib. Roller Water = 25% of Fill Volume
		IC	Compacted in 1.60m Layers	" "
	Intercalation of Massive Basalt and Basaltic Breccia	ID	Compacted in 0.80m Layers	" "
	Massive Basalt (Selected Rock - Min. 0.80m)	IE	Placed Rock (Downstream Face)	—
Transition II	Crushed Sound Basalt	IIB	Well Graded Max Size 150mm Compacted in 0.40m Layers	Layers: 4 Passes of Vib. Roller Face: 6 Passes of Vib. Roller (Upslope)
Earthfill III	Impervious Soil	IIID	Maximum Size 20mm Compacted in 0.30m Layers	Pneumatic Roller or Construction Equipment

**Figure 59.10** Cross-section through 160-m concrete-faced Foz do Areia rockfill dam, Brazil (Pinto et al. 1985).

stability either through development of seepage pressures or internal erosion of the fill materials.

### 59.11.2 Internal Membranes

Although the use of Portland cement concrete for facing embankment dams, particularly rockfill dams, is common practice, internal core walls of concrete are rare. In the early days of embankment-dam development, unreinforced core walls were found to be susceptible to cracking. Thin cast-in-place reinforced walls have been used occasionally but are expensive and difficult to build because of the incompatibility of procedures for construction of the concrete and earth-fill components of the dam. Because a concrete wall is stiffer than the earth or rock fill in which it is embedded, it inevitably is subjected to negative skin friction (Article 52.3.1) with corresponding compressive stresses in the concrete, as the embankment settles. Concrete panel walls or continuous diaphragm walls have on a few occasions been constructed through compacted embankments, for instance at Wolf Creek and Mud Mountain Dams, as remedial measures. The measures were successful partly because they were constructed after most of the deformations of the dam and foundation had already occurred.

On the other hand, asphaltic concrete has been used extensively, especially in Germany and other parts of Europe, in place of soil as a core material. It has the advantage as compared to concrete of considerable flexibility and compressibility that permit it to adjust to the deformations of the dam. Finstertal Dam in Austria, a rockfill dam with a height of 149 m, has a slightly inclined asphaltic concrete core 96 m high with a thickness increasing from 0.5 m at the crown to 0.7 m near the base. It is flanked by an upstream transition zone of screened glacial till at least 3 m wide containing fines intended to move into any cracks that might form in the membrane, and a downstream transition 2 m or more wide to serve as a drain. A cross-section is shown in Fig. 59.11. Homogeneity, adequate compaction, and freedom of contamination of the elements of such a thin diaphragm, including the transition zones, require extraordinary precautions. A single machine has been developed to control the placement of all three elements and compact them simultaneously (Pircher and Schwab 1980).

In general, soil mechanics enters into the design and construction of an embankment dam with an internal membrane in much the same fashion as in dams with earth cores. Because membranes are remarkably thin,

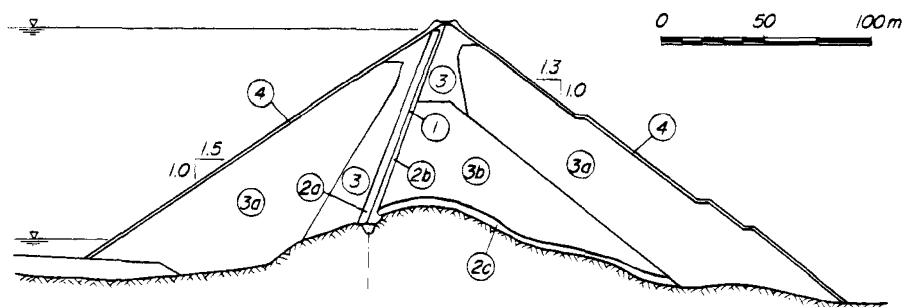


**Figure 59.11** Cross-section through Finstertal Dam, Austria: Zone 1 asphaltic concrete core membrane; zone 2a, impervious screened till; zone 2b, pervious crushed rock; zones 2c, 3a, rockfill; zone 3b, glacial till from excavations; zone 4, boulders of  $\frac{1}{2}$  to 1 m. (after Pircher and Schwab 1980).

however, construction control is considerably more demanding, and the need to make reliable estimates of deformations is greater. Finally, the design should ensure that the dam will be safe with respect to stability and internal erosion even if the membrane should prove to be defective.

### 59.11.3 Synthetic Membranes and Filter Fabrics

Thin membranes of synthetic materials such as butyl rubber and polyvinyl chloride, which are essentially impermeable, have been used extensively for linings of small reservoirs and canals and have occasionally been incorporated into dams. At Mission (Terzaghi) Dam in British Columbia (Terzaghi and Lacroix 1964) the upstream face consisted of a clay blanket protected by an overlying layer of granular material and underdrained by a pervious till. Because the dam was located above a deep compressible deposit, the designers anticipated areas in which differential movements of the clay blanket would cause the formation of cracks that would tend to remain open because of the pressure of the water flowing through them. A vinyl membrane was placed over the area of possible tension cracks to transmit an effective stress equal to the water pressure to the surfaces of the clay beside an incipient crack and keep it closed (Fig. 59.12).

Both butyl and vinyl plastic membranes are capable of elongations of over 200%. Therefore, they can withstand considerable differential settlement. They have considerable resistance to puncture, but are not highly resistant to tearing. Under some circumstances they may be attacked by bacteria. They should be placed on prepared surfaces, usually of sand, and require a protective covering not only against the action of waves and mechanical damage but against sunlight. Where compressible soils abut rigid elements, such as concrete outlet pipes, the membranes should be given slack to allow for differential movements, but pleats or folds are likely to crease and ultimately crack. The vulnerability of such membranes requires that leakage should be rendered harmless by

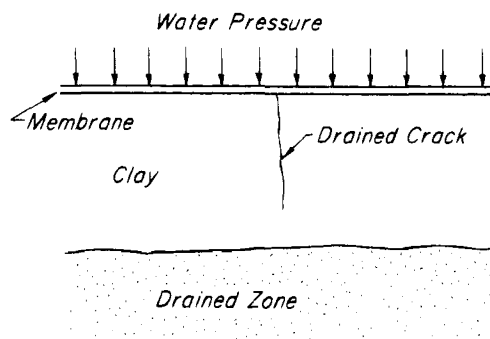


**Figure 59.12** Use of plastic membrane combined with under-drain to close crack in clay core of Mission (Terzaghi) Dam in British Columbia (Terzaghi and Lacroix 1964).

being conducted to underdrains protected by filters. Because of their low frictional resistance, membranes are not usually placed on slopes steeper than  $2H:1V$ ; in some instances the resistance has been increased by providing indentations on the surface of the sheets during manufacture, or by applying fine-grained particles with an adhesive.

The Rio Macho No. 1 project in Costa Rica required the construction of dikes with heights up to about 20 m to retain a reservoir located above an old landslide on a gentle slope. The underlying materials were a heterogeneous mixture of peats, organic silts, and colluvium. To avoid reactivating the slide it was necessary to prevent infiltration from the reservoir. This was done by covering the bottom of the reservoir with vinyl plastic with a thickness of 0.51 mm and the slopes with butyl plastic with a thickness of 0.76 mm. The membranes were bedded on a 75-mm layer of rolled granular material for which the maximum grain size was to be 2 mm if angular, or 4.75 mm if rounded. The same material, also 75 mm thick, was placed above the membrane but not rolled, and covered with 250 mm of pitrun gravel or similar material. The underdrainage system was subdivided into zones from which the outflow could be identified. During

the first two years of service several leaks were observed; they were repaired while the reservoir was drawn down. Most of these occurred at junctions of the membranes with rigid structures or at local places where the rolled base had been damaged during construction, as by small excavations that had not been compacted properly when backfilled. Subsequent to these early repairs, the reservoir has performed satisfactorily for some 20 years.

Since about 1970 permeable synthetic fabrics with considerable tensile strength, tear resistance, and ability to stretch have been used increasingly. Not only do they serve the purpose of filter zones between materials of grain-size distributions so different that migration of particles would otherwise occur, but their tensile strength affords significant resistance to such undesirable behavior as the horizontal spreading of embankments over weak soils. Consequently, they have been widely adopted in the construction of haul roads on soft soils, as filters between drainage blankets and the underlying soil in sand-drain installations, and as barriers to the fouling of ballast by clay subgrades and the resultant formation of ballast pockets beneath railroad tracks (Koerner and Welsh 1980). Their use in zoned dams to replace one or more filter zones, to protect gravel drains from clogging, or to reduce the undesirable consequences of segregation at the boundaries between zones would appear to be advantageous. As yet, however, the long-time stability of the synthetic materials when buried in earth materials, the possibilities for clogging when subjected for many years to high pressures, and the possibility for damage and leakage at points where high stresses are transmitted through the fabrics from large particles on opposite sides have not been evaluated sufficiently to justify routine use in major dams. On the other hand, on the James Bay Project in Quebec, for example, filter fabrics were used effectively in the construction of several large cofferdams, particularly to permit placement of an impervious blanket of till directly on rockfill. A variety of materials was used and some were later excavated for evaluation. As such experience accumulates, dependence on filter fabrics with appropriate safeguards may prove justifiable in major dams.

### Selected Readings

The most comprehensive and authoritative publication dealing with the soil-mechanics aspects of earth and rock-fill dams is *Current Trends in Design and Construction of Embankment Dams* prepared by S.D. Wilson and R.J. Marsal at the request of the committee on International Relations of the International Commission on Large Dams and published as a monograph by the American Society of Civil Engineers in 1979.

*Advanced Dam Engineering for Design, Construction, and Rehabilitation*, Robert B. Jansen, ed., New York,

Van Nostrand Reinhold, (1988) deals with the design, construction, and performance of all types of modern dams, with sections prepared by specialists in the field.

Several symposia on specific aspects of embankment dams have resulted in useful publications. These include:

"Foundations for Dams." ASCE (1974), 472 p.

"Grouting in geotechnical engineering," ASCE (1982), 1018 p.

"Concrete Face Rockfill Dams—Design, Construction and Performance," ASCE (1985), 658 p.

An interesting historical summary is: *Development of Dam Engineering in the United States*, prepared in Commemoration of the Sixteenth Congress of the International Commission on Large Dams by the United States Committee on Large Dams. E.B. Kollgaard and W.L. Chadwick, eds. (1988). New York, Pergamon Press 1072 p.

A classic early paper is Terzaghi, K. (1929a). "Effect of minor geologic details on the safety of dams," *Am. Inst. Min. and Met. Eng.*, Tech. Publ. 215, pp. 31–44.

## ARTICLE 60 CONCRETE DAMS ON SEDIMENTS

### 60.1 Modes of Failure

A concrete dam may fail by subsurface erosion or by sliding on its base, and it may be damaged by unequal settlement. Subsurface erosion is discussed in Article 58. Sliding and settlement are considered here.

### 60.2 Safety with Respect to Sliding

The potential surface of sliding in the subsoil of a concrete dam may be located in very permeable material such as clean sand, in a soil of intermediate permeability such as silt, or else in clay which is practically impermeable. In the following discussion, only the two extreme possibilities are considered.

If the surface of sliding is located in sand, the total sliding resistance  $S$  per unit of length of the dam is

$$S = (P - U) \tan \phi'_c$$

in which

$P$  = total vertical pressure on base of dam due to weight of dam and vertical component of water pressure on the inclined faces of the dam

$U$  = total neutral pressure on base of dam

$\phi'_c$  = angle of friction between concrete and sand

Because the value of  $\tan \phi'_c$  is always at least 0.6, and because the neutral pressure  $U$  can usually be reduced to a very small value by suitable drainage provisions, it is seldom difficult to eliminate the danger of sliding.

On the other hand, if the substrata contain horizontal layers of soft clay, or if the dam rests on a thick clay stratum, it may be very difficult to establish adequate resistance against sliding. After the clay beneath a dam becomes consolidated, sliding is resisted both by cohesion

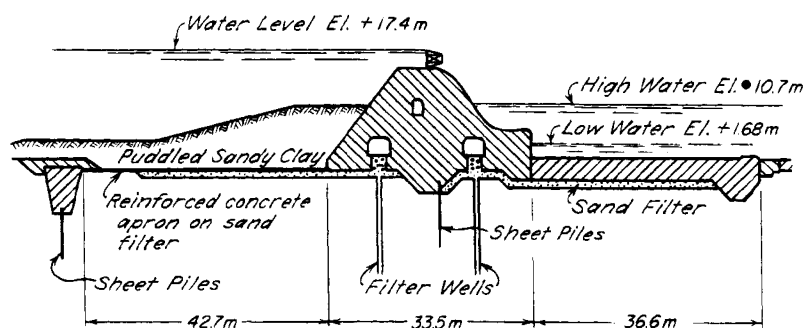


**Figure 60.1** Section through dam resting on thick deposit of clay. Stability against sliding increased by weighted underdrained concrete apron on upstream side. Svir III, USSR (after Graftio 1936).

and by friction under drained conditions. However, because of the low permeability of the clay, consolidation proceeds very slowly; furthermore, the rate of consolidation can seldom be reliably forecast. Therefore, it is usually advisable to assume that undrained conditions still prevail at the end of the period of construction (Article 20).

To make the dam shown in Fig. 60.1 safe against sliding before the underlying clay consolidated, its base width was increased from 34 to 77 m by a reinforced concrete apron on the upstream side. Because the apron was an integral part of the dam, sliding was resisted by undrained shearing strength over the full length of 77 m. The factor of safety increased steadily because of consolidation of the clay under the weight of the dam itself as well as the weight of the water above the apron. To make the weight of the water effective the under side of the apron was drained.

Failure to recognize the presence of bedding-plane shears at residual strengths in bedded deposits containing shales or stiff clays has been responsible for failures of both embankment and concrete dams. Effective-stress analyses require evaluation of the excess pore pressure in the shear zone. These pressures arise not only from the weight of the dam itself, but also in many instances from artesian conditions associated with the local hydrogeology. Dissipation of the excess pressures may proceed extremely slowly.

### 60.3 Settlement Considerations

If a dam is of a rigid type or contains rigid elements, a settlement forecast is needed before construction to determine whether joints are required between various parts of the structure and, if so, how much movement should be anticipated. The methods for making the forecasts are no different from those that have been described for estimating the settlement of buildings (Article 41). To supplement the available information concerning the future settlement, the observational method can often be used to advantage. The following history of a dam across

the Svir River in Russia describes an early example (Graftio 1936).

The dam includes a reinforced-concrete powerhouse section (Fig. 60.2) and a plain concrete overflow section (Fig. 60.1). It rests on a deposit of stratified heavily precompressed clay at least 100m thick. It was believed that settlement forecasts based on laboratory tests on samples of such materials were likely to be unreliable and to overestimate the settlements.

Furthermore, the schedule of operations precluded the possibility of making elaborate soil investigations before construction. Therefore, it was decided to base the preliminary settlement computations on the results of tests of a few representative samples obtained from a test shaft. The forecast showed that a joint was necessary between the powerhouse and the adjacent overflow section and that no rigid connection could be tolerated between the body of the dam and the adjoining aprons.

The preliminary settlement computations also indicated that filling the reservoir would cause the powerhouse to tilt upstream about  $1^\circ$ . Because the turbines had to be installed before the reservoir was filled, and the computed tilt far exceeded the value considered admissible by the turbine designers, it was decided to install the turbine shafts out of plumb in such a manner that they would

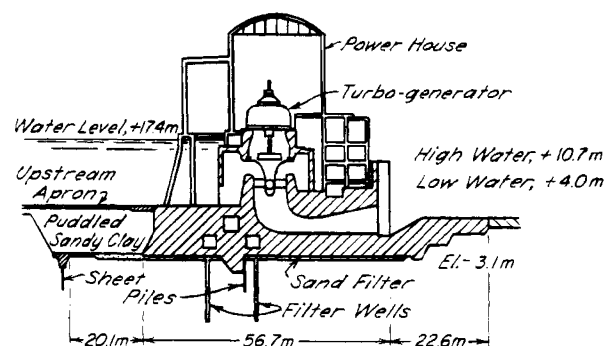


**Figure 60.2** Section through powerhouse portion of dam resting on thick deposit of clay. Svir III, USSR (after Graftio 1936).

become vertical when the reservoir was filled. To secure a more accurate value for the tilt, the results of the preliminary soil tests were used as a basis for computing the displacement of many points on and beneath the ground surface at different stages of construction. As construction proceeded, the displacements were measured. It was found that the real displacements were consistently equal to 0.35 times the computed displacements. Therefore, the turbine shafts were mounted with a downstream tilt of

0.35° and, when the reservoir was filled, the shafts were practically vertical.

#### **Selected Reading**

- Terzaghi, K. (1929*a*). "Effect of minor geologic details on the safety of dams," *Am. Inst. Min. and Met. Eng.*, Tech. Publ. 215, pp. 31–44.
- Lane, E.W. (1935). "Security from under-seepage—masonry dams on earth foundations," *Trans. ASCE*, **100**, pp. 1235–1351.

## References

- Aboshi, H., Y. Mizuno, and M. Kuwahara (1989). "Present state of sand compaction pile in Japan," *Proc. Deep Foundation Improvements: Design, Construction, and Testing*, ASTM STP 1089, pp. 32–46.
- Abramento, M. and C.S. Carvalho (1989). "Geotechnical parameters for the study of natural slopes instabilization at "Serra do Mar", Brazil," *Proc. 12th Int. Conf. on Soil Mech. and Found. Eng.*, Rio de Janeiro, 3, pp. 1599–1602.
- Adachi, K. (1989). "Sampling of cohesionless and gravelly soils," *The Art and Science of Geotechnical Engineering*, Englewood Cliffs, N.J., Prentice Hall, pp. 206–220.
- Alonso, E.E., A. Josa, and A. Ledesma (1984). "Negative skin friction on piles: a simplified analysis and prediction procedure," *Géot.*, 34, No. 3, pp. 341–357.
- Alperstein, R. and S.A. Leifer (1976). "Site investigation with static cone penetrometer," *ASCE J. Geot.*, 102, No. GT5, pp. 539–555.
- Ambrayes, N.N. and S.K. Sarma (1967). "The response of earth dams to strong earthquakes," *Géot.*, 17, No. 3, pp. 181–213.
- Andresen, A. and L. Bjerrum (1958). "Vane testing in Norway," *Norwegian Geotech. Institute*, Publ. No. 28.
- Andresen, A. and P. Kolstad (1979). "The NGI 54-mm samplers for undisturbed sampling of clays and representative sampling of coarser materials," *Proc. Int. Symp. on Soil Sampling*, Singapore, pp. 1–9.
- AREA (1955). "Soil engineering in railroad construction," *Proc. Am. Rwy. Eng. Assn.*, 56, pp. 694–702.
- Armento, W.J. (1973). "Cofferdam for BARTD Embarcadero subway station," *ASCE J. Soil Mech.*, 99, No. SM10, pp. 727–744.
- Arulalandan, K., P. Loganathan, and R.B. Krone (1975). "Pore and eroding fluid influences on surface erosion of soil," *ASCE J. Geot.*, 101, No. GT1, pp. 51–66.
- ASCE (1961). "Sonic pile-driver shows great promise," *Civ. Eng.*, 31, No. 12, Dec., p. 52.
- Asaoka, A. (1978). "Observational procedure of settlement prediction," *Soils and Foundations*, 18, No. 4, pp. 87–101.
- Atterberg, A. (1908). "Studien auf dem Gebiet der Bodenkunde" (Studies in the field of soil science), *Landw. Versuchsanstalt*, 69.
- Atterberg, A. (1911). "Über die physikalische Bodenuntersuchung und über die Plastizität der Tone" (On the investigation of the physical properties of soils and on the plasticity of clays), *Int. Mitt. für Bodenkunde*, 1, pp. 10–43.
- Atterberg, A. (1916). "Die Klassifikation der humusfreien und der humusarmen Mineralböden Schwedens nach den Konsistenzverhältnissen derselben" (The classification of Swedish mineral soils with little or no humus content, according to their consistency limits), *Int. Mitt. für Bodenkunde*, 6, pp. 27–37.
- Azzouz, A.S., M.M. Baligh, and C.C. Ladd (1981). "Three-dimensional stability analyses of four embankment failures," *Proc. 10th Int. Conf. on Soil Mech. and Found. Eng.*, Stockholm, 3, pp. 343–346.
- Azzouz, A.S., M.M. Baligh, and C.C. Ladd (1983). "Corrected field vane strength for embankment design," *J. Geotech. Eng.*, ASCE, 109, No. 5, pp. 730–734.
- Azzouz, A.S., M.M. Baligh, and A.J. Whittle (1990). "Shaft resistance of piles in clay," *ASCE J. Geot.*, 116, No. GT2, pp. 205–221.
- Babbitt, H.E. and D.H. Caldwell (1948). "The free surface around, and interference between, gravity wells," *Univ. of Illinois Eng. Exp. Sta. Bull.*, 374, 60 pp.
- Baguelin, F., J.F. Jezequel, and A. La Mehaute (1974). "A self-boring placement method of soil characteristics measurement," *ASCE Conf. on Subsurface Exploration for Heavy Construction*, pp. 312–332.
- Bailey, S.W. (1975). "Chlorites," *Soil Components Edited by Giesekeing*, New York, Springer-Verlag, 2, pp. 191–263.
- Baker, B. (1881). "The actual lateral pressure of earthwork," *Min. Proc. Inst. Civil Engrs.*, London, 65, pp. 140–186; Discussions pp. 187–241.
- Baker, R., G. Kassiff, and A. Levy (1973). "Experience with psychrometric technique," *Proc. 3rd Int. Conf. on Expansive Soils*, Haifa, 1, pp. 83–95.
- Baldi, G., R. Bellotti, V. Ghionna, M. Jamiolkowski, and E. Pasqualini (1981). "Cone resistance of a dry medium sand," *Proc. 10th Int. Conf. on Soil Mech. and Found. Eng.*, Stockholm, 2, pp. 427–432.
- Baligh, M.M., V. Vivatrat, and H. Figi (1978). "Dragdown on bitumen-coated piles," *ASCE J. Geot.*, 104, No. GT11, pp. 1355–1370.
- Barberis, M.C. (1935). "Recent examples of foundations of quay walls resting on poor subsoil, studies, results obtained," *16th Int. Congr. Navigation*, Brussels, 2nd section, 3rd communication.
- Barentsen, P. (1936). "Short description of a field-testing method with coneshaped sounding apparatus," *Proc. 1st Int. Conf. Soil Mech.*, Cambridge, Mass., 1, pp. 7–10.
- Barkan, D.D. (1962). *Dynamics of Bases and Foundations*. New York, McGraw-Hill, 434 pp.
- Barksdale, R.D., R.C. Backus, and M.B. Clanou (1982). "Settlements of a tower on residual soil," *Proc. ASCE Geotech. Eng. Div. Specialty Conf. on Eng. and Construction in Tropical and Residual Soils*, Honolulu, pp. 647–664.



- Barron, R.A. (1944). *The Influence of Drain Wells on the Consolidation of Fine-grained Soils*, Providence, R. I. District, U.S. Engineers Office.
- Barron, R.A. (1948). "Consolidation of fine-grained soils by drain wells," *Trans. ASCE*, **113**, pp. 718–754.
- Baumann, V. and G.E.A. Bauer (1974). "The performance of foundations on various soils stabilized by the vibro-compaction method," *Can. Geot. J.*, **11**, No. 4, pp. 509–530.
- Begemann, H.K.S. (1953). "Improved method of determining resistance to adhesion by sounding through a loose sleeve placed behind the cone," *Proc. 3rd Int. Conf. Soil Mech.*, Zurich, **1**, pp. 213–217.
- Begemann, H.K.S. (1965). "The friction jacket cone as an aid in determining the soil profile," *Proc. 6th Int. Conf. Soil Mech.*, Montreal, Canada, **1**, pp. 17–20.
- Belcher, D.J. (1945). "The engineering significance of soil patterns," *Photogrammetric Engineering*, **11**, No. 2, pp. 115–148.
- Berbower, R.F. (1959). "Subsidence problem in the Long Beach Harbor District," *ASCE J. Waterways and Harbors Div.*, **85**, No. WW2, pp. 81–97.
- Berezantzev, V.G., V.S. Khristoforov, and V.N. Golubkov (1961). "Load bearing capacity and deformation of piled foundations," *Proc. 5th Int. Conf. Soil Mech.*, Paris, **2**, pp. 11–15.
- Bernal, J. and L.C. Reese (1983). "Study of the lateral pressure of fresh concrete as related to the design of drilled shaft," *Research Report 308-IF*, Center for Hwy. Research, Univ. of Texas at Austin, November.
- Berry, P.L. and T.J. Poskitt (1972). "The consolidation of peat," *Géot.*, **22**, No. 1, pp. 27–52.
- Bertram, G.E. (1940). "An experimental investigation of protective filters," *Harvard Soil Mechanics Series*, No. 7, Cambridge, 21 pp.
- Beskow, G. (1935). "Tjälbildningen och Tjällyftningen med Särskild Hänsyn till Vägar och Järnvägar" (Soil freezing and frost heaving with special application to roads and railroads), *Sveriges Geologiska Undersökning*, Stockholm, Series Cv, No. 375, 242 pp.
- Bhatia, S.K. (1982). *The Verification of Relationships for Effective Stress Method to Evaluate Liquefaction Potential of Saturated Sands*, Ph.D. thesis, Univ. of British Columbia, Vancouver.
- Bishop, A.W. (1948). "A new sampling tool for use in cohesionless sands below ground water level," *Géot.*, **1**, No. 2, pp. 125–131.
- Bishop, A.W. (1954). "The use of pore-pressure coefficients in practice," *Géot.*, **4**, pp. 148–152.
- Bishop, A.W. (1955). "The use of the slip circle in the stability analysis of slopes," *Géot.*, **5**, pp. 7–17.
- Bishop, A.W. (1966). "The strength of soils as engineering materials," *Géot.*, **16**, pp. 91–128.
- Bishop, A.W. (1971). "Shear strength parameters for undisturbed and remolded soil specimens," *Proc. of the Roscoe Memorial Symp.*, R.H.G. Parry, ed., Cambridge Univ., pp. 3–58.
- Bishop, A.W. (1973). "The influence of an undrained change in stress on the pore pressure in porous media of low compressibility," *Géot.*, **23**, No. 3, pp. 435–442.
- Bishop, A.W. (1976). "The influence of system compressibility on the observed pore-pressure response to an undrained change in stress in saturated rock," *Géot.*, **26**, No. 2, pp. 371–375.
- Bishop, A.W. and G. Eldin (1950). "Undrained triaxial tests on saturated sands and their significance in the general theory of shear strength," *Géot.*, **2**, No. 1, pp. 13–32.
- Bishop, A.W. and R.E. Gibson (1963). "The influence of the provisions for boundary drainage on strength and consolidation characteristics of soils measured in the triaxial apparatus," *Laboratory Shear Testing of Soils*, ASTM STP No. 361, pp. 435–451.
- Bishop, A.W., G.E. Green, V.K. Garga, A. Andresen, and J.D. Brown (1971). "A new ring shear apparatus and its application to the measurement of residual strength," *Géot.*, **21**, No. 4, pp. 273–328.
- Bishop, A.W. and D.J. Henkel (1962). *The Measurement of Soil Properties in the Triaxial Test*, 2nd ed., London, Edward Arnold, 228 pp.
- Bishop, A.W., D.L. Webb, and P.I. Lewin (1965). "Undisturbed samples of London clay from the Ashford Common shaft: strength-effective stress relationships," *Géot.*, **15**, No. 1, pp. 1–31.
- Bjerrum, L. (1954). "Geotechnical properties of Norwegian marine clays," *Géot.*, **4**, pp. 49–69.
- Bjerrum, L. (1957). "Norwegian experiences with steel piles to rock," *Géot.*, **7**, No. 2, pp. 73–96.
- Bjerrum, L. (1967). "Engineering geology of Norwegian normally-consolidated marine clays as related to settlement of buildings," *Géot.*, **17**, No. 2, pp. 83–118.
- Bjerrum, L. (1972). "Embankments on soft ground," *ASCE Conf. on Performance of Earth and Earth-Supported Structures*, Purdue Univ., **2**, pp. 1–54.
- Bjerrum, L. (1973). "Problems of soil mechanics and construction on soft clays," *Proc. 8th Int. Conf. on Soil Mech. and Found. Eng.*, Moscow, **3**, pp. 111–159.
- Bjerrum, L. and O. Eide (1956). "Stability of strutted excavations in clay," *Géot.*, **6**, pp. 32–47.
- Bjerrum, L. and Å. Eggstad (1963). "Interpretation of loading test on sand," *Proc. European Conf. Soil Mech.*, Wiesbaden, **1**, pp. 199–203.
- Bjerrum, L., C.J. Frimann Clausen, and J.M. Duncan (1972). "Earth pressures on flexible structures: a state-of-the-art report," *Proc. 5th European Conf. Soil Mech.*, Madrid, **2**, pp. 169–196.
- Bjerrum, L., S. Kringstad, and O. Kummeneje (1961). "The shear strength of a fine sand," *Proc. 5th Int. Conf. Soil Mech.*, Paris, **1**, pp. 29–37.
- Bjerrum, L. and B. Kjaernsli (1957). "Analysis of the stability of some Norwegian natural clay slopes," *Géot.*, **7**, No. 1, pp. 1–16.
- Bjerrum, L. and A. Landava (1966). "Direct simple-shear tests on a Norwegian quick clay," *Géot.*, **16**, No. 1, pp. 1–20.
- Bjerrum, L., T. Loken, S. Heiberg, and R. Foster (1969). "A field study of factors responsible for quick clay slides," *Proc. 7th Int. Conf. Soil Mech.*, Mexico, **2**, pp. 531–540.
- Bjerrum, L., J. Moum, and O. Eide (1967). "Application of electro-osmosis to a foundation problem in a Norwegian quick clay," *Géot.*, **17**, pp. 214–235.

- Bjerrum, L. and C. Soydemir (1972). "Anisotropy of marine clays (DSS-CCV anisotropy tests on plastic Drammen clay)," *Norwegian Geotechnical Institute, Report 50320-1*, 5 pp.
- Bligh, W.G. (1910). "Dams, barrages, and wiers on porous foundations," *Eng. News*, **64**, pp. 708–710.
- Blight, G.E. (1963). "The effect of nonuniform pore pressures on laboratory measurements of the shear strength of soils," *Laboratory Shear Testing of Soils*, ASTM STP No. 361, pp. 173–191.
- Boreli, M. (1955). "Free-surface flow toward partially penetrating wells," *Trans. American Geophysical Union*, **36**, No. 4, pp. 664–672.
- Boscardin, M.D. and E.J. Cording (1989). "Building response to excavation-induced settlement," *J. Geotech. Eng., ASCE*, **115**, No. 1, pp. 1–21.
- Boussinesq, J. (1885). *Application des Potentiels à l'Étude de l'Équilibre et du Mouvement des Solides Élastiques*, Paris, Gauthier-Villard.
- Bozozuk, M. (1962). "Soil shrinkage damages shallow foundations at Ottawa, Canada," *Eng. J. Canada*, **45**, pp. 33–37.
- Brand, E.W. (1982). "Analysis and design in residual soils," *Proc. ASCE Geotech. Eng. Div., Spec. Conf. on Eng. and Constr. in Tropical and Residual Soils*, Honolulu, Hawaii, pp. 89–143.
- Briaud, J.-L. (1992). *The Pressuremeter*, Rotterdam, Balkema, 322 pp.
- Brinkhorst, W.H. (1936). "Settlement of the soil surface around the foundation pit," *Proc. 1st Int. Conf. Soil Mech.*, Cambridge, Mass., **1**, pp. 115–119.
- Briske, R. and E. Pirlet (1968). "Messungen über die Beanspruchung des Baugrubenverbaues der Kölner U-Bahn" (Strain measurements on the excavation wall in the Cologne subway), *Bautechnik*, **45**, No. 9, pp. 290–299.
- Bromhead, E.N. (1979). "A simple ring shear apparatus," *Ground Eng.*, **12**, No. 5, 40 pp.
- Broms, B.B. (1965). "Design of laterally loaded piles," *ASCE J. Soil Mech.*, **91**, No. SM3, pp. 79–99.
- Broms, B. (1971). "Lateral earth pressures due to compaction of cohesionless soils," *Proc. 4th Conf. Soil Mech.*, Budapest, pp. 373–384.
- Broms, B.B. and P. Boman (1979). "Lime columns: a new foundation method," *ASCE J. Geot.*, No. GT4, pp. 539–556.
- Broms, B.B. and I. Ingelson (1971). "Earth pressure against the abutments of a rigid frame bridge," *Géot.*, **21**, No. 1, pp. 15–28.
- Broms, B.B. and I. Ingelson (1972). "Lateral earth pressure on a bridge abutment," *Proc. 5th European Conf. Soil Mech.*, Madrid, **1**, pp. 117–123.
- Broms, B.B. and N. Flodin (1988). "History of soil penetration testing," *Proc. Int. Symp. on Penetration Testing, ISOPT-1*, **1**, pp. 157–220.
- Brooker, E.W. and R.B. Peck (1993). "Rational design treatment of slides in overconsolidated clays and clay shales," *Can. Geot. J.*, **30**, No. 3, pp. 526–544.
- Brown, F.S. (1941). "Foundation investigations for the Franklin Falls dam," *J. Boston Soc. Civil Engrs.*, **28**, pp. 126–143.
- Brown, R.E. (1977). "Vibroflotation compaction of cohesionless soils," *ASCE J. Geot.*, **103**, No. GT12, pp. 1437–1451.
- Brown, R.E. and A.J. Glenn (1976). "Vibroflotation and Terra-Probe comparison," *ASCE J. Geot.*, **102**, No. GT10, pp. 1059–1072.
- Bruggen, J.P. v. (1936). "Sampling and testing undisturbed sands from boreholes," *Proc. 1st Int. Conf. Soil Mech.*, Cambridge, Mass., **1**, pp. 3–6.
- Buchanan, S.J. (1938). "Levees in the lower Mississippi valley," *Trans. ASCE*, **103**, pp. 1378–1395; Discussions pp. 1449–1502.
- Buisman, A.S.K. (1941). *Grondmechanica*. (Nederlandsch—Indische Nooduitgave). Bandoengsche Technische Hoogeschoolfonds, Kleijne, Bandoeng, 349 pp.
- Burland, J. (1973). "Shaft friction in piles in clay; a simple fundamental approach," *Ground Engrg.*, **6**, No. 3, pp. 30–42.
- Burland, J.B. and M.C. Burbidge (1985). "Settlement of foundations on sand and gravel," *Proc. Institution of Civil Engineers*, Part 1, **78**, pp. 1325–1381.
- Burmister, D.M. (1956). "Stress and displacement characteristics of a two-layered rigid base soil system: influence diagrams and practical applications," *Proc. Hwy. Res. Board*, **35**, pp. 773–814.
- Cadling, L. and S. Odenstad (1950). "The vane borer," *Proc. Swedish Geot. Inst.*, No. 2, 88 pp.
- Cambeftor, H. (1955). *Forages et sondages* (Borings and soundings). Paris, Eyrolles, 396 pp.
- Campanella, R.G., P.K. Robertson, and D. Gillespie (1983). "Cone penetration testing in deltaic soils," *Can. Geot. J.*, **20**, No. 1, pp. 23–35.
- Campbell, J.D. (1973). *Pore Pressures and Volume Changes in Unsaturated Soils*, Ph.D. thesis, Univ. of Illinois at Urbana-Champaign, 104 pp.
- Canadian Foundation Engineering Manual*, 2nd Ed. (1985). Canadian Geotechnical Society. BiTech Publishers, Vancouver, Canada, 456 pp.
- Caquot, A. and J. Kerisel (1948). *Tables for the Calculation of Passive Pressure, Active Pressure and Bearing Capacity of Foundations*, Transl. from the French by Maurice A. Bec., Paris, Gauthier-Villars, 120 pp.
- Carbognin, L., P. Gatto, G. Mozzi, and G. Gambolati (1978). "Land subsidence of Ravenna and its similarities with the Venice case," *ASCE Conf. on Evaluation and Prediction of Subsidence*, Pensacola, Florida, pp. 254–266.
- Carder, D.R., R.G. Pocock, and R.T. Murray (1977). "Experimental retaining wall facility—lateral stress measurements with sand backfill," *Transport and Road Research Laboratory Report No. LR 766*, Crowthorne, England.
- Carlson, L. (1948). "Determination in situ of the shear strength of undisturbed clay by means of a rotating auger," *Proc. 2nd Int. Conf. Soil Mech.*, Rotterdam, **1**, pp. 265–270.
- Carrillo, N. (1942). "Simple two and three dimensional cases in the theory of consolidation of soils," *J. of Math. and Physics*, **21**, No. 1, pp. 1–5.
- Cary, A.S., B.H. Walter, and H.T. Harstad (1943). "Permeability of Mud Mountain Dam core material," *Trans. ASCE*, **108**, pp. 719–728; Discussions pp. 729–737.
- Casagrande, A. (1931). "Discussion: a new theory of frost heaving," *Proc. Hwy. Res. Board*, **11**, pp. 168–172.
- Casagrande, A. (1932a). "Research on the Atterberg limits of soils," *Public Roads*, **13**, pp. 121–136.

- Casagrande, A. (1932b). "The structure of clay and its importance in foundation engineering," *J. Boston Soc. Civil Engrs.*, **19**, No. 4, pp. 168–209.
- Casagrande, A. (1935a). "Discussion: security from under-seepage masonry dams on earth foundations," *Trans. ASCE*, **100**, pp. 1289–1294.
- Casagrande, A. (1935b). "Seepage through dams," *J. New England Water Works Assn.*, **51**, No. 2, pp. 131–172.
- Casagrande, A. (1936a). "Characteristics of cohesionless soils affecting the stability of slopes and earth fills," *J. Boston Soc. Civil Engrs.*, **23**, No. 1, pp. 13–32.
- Casagrande, A. (1936b). "The determination of the pre-consolidation load and its practical significance," *Proc. 1st Int. Conf. Soil Mech.*, Cambridge, Mass., **3**, pp. 60–64.
- Casagrande, A. (1947). "The pile foundation for the new John Hancock building in Boston," *J. Boston Soc. Civil Engrs.*, **34**, pp. 297–315.
- Casagrande, A. (1948). "Classification and identification of soils," *Trans. ASCE*, **113**, pp. 901–991.
- Casagrande, A. (1949). "Soil mechanics in the design and construction of the Logan airport," *J. Boston Soc. Civil Engrs.*, **36**, No. 2, pp. 192–221.
- Casagrande, A. (1958). "Notes on the design of the liquid limit device," *Géot.*, **8**, No. 2, pp. 84–91.
- Casagrande, A. (1960). "An unsolved problem of embankment stability on soft ground," *Proc. 1st Panamerican Conf. Soil Mech. and Found. Eng.*, Mexico, **2**, pp. 721–746.
- Casagrande, A. (1961). "Control of seepage through foundations and abutments of dams," *Géot.*, **11**, No. 3, pp. 161–181.
- Casagrande, A. (1965). "Role of the 'calculated risk' in earthwork and foundation engineering," *ASCE J. Soil Mech.*, **91**, No. SM4, pp. 1–40.
- Casagrande, A. (1975). "Liquefaction and cyclic deformation of sands—a critical review," *Proc. 5th Pan American Conf. on Soil Mech. and Found. Eng.*, Buenos Aires; also published as *Harvard Soil Mechanics Series*, No. 88, Cambridge, 51 pp.
- Casagrande, A. and R.E. Fadum (1940). "Notes on soil testing for engineering purposes," *Harvard Univ. Grad. School of Engineering Publ.* 268, 74 pp.
- Casagrande, L. (1949). "Electro-osmosis in soils," *Géot.*, **1**, No. 3, pp. 159–177.
- Casagrande, L. (1953). "Review of past and current work on electro-osmotic stabilization of soils," *Report to the Bureau of Yards and Docks*, Contract No. NOY-76303, Cambridge, 83 pp.
- Casagrande, L. (1962). "Electro-osmosis and related phenomena," *Revista Ingenieria*, Mexico, **32**, No. 2, pp. 1–62 (Spanish and English text).
- Casagrande, L. (1973). "Comments on conventional design of retaining structures," *ASCE J. Soil Mech.*, **99**, No. SM2, pp. 181–198.
- Casagrande, L. (1983). Review of stabilization of soils by means of electro-osmosis—state-of-the-art. Presented to the Geotechnical Section of the BSCES/ASCE, **69**, No. 2, pp. 255–302.
- Castro, G. (1969). "Liquefaction of sands," *Harvard Soil Mechanics Series*, No. 81, Cambridge, 112 pp.
- Cedergren, H.R. (1989). *Seepage, Drainage, and Flow Nets*, 3rd ed., New York, John Wiley and Sons, 465 pp.
- Cepeda-Diaz, A.F. (1987). *An Experimental Investigation of the Engineering Behavior of Natural Shales*, Ph.D. thesis, Univ. of Illinois at Urbana-Champaign.
- Chadwick, W.L. et al. (1976). *Failure of Teton Dam*, Rept. of Independent Panel to review cause of Teton Dam failure, U. S. Govt. Printing Office, Washington, D. C.
- Chan, A.C.Y. and N.R. Morgenstern (1986). "Measurement of lateral stresses in a lacustrine clay deposit," *Proc. 39th Canadian Geotechnical Conf.*, Ottawa, pp. 285–290.
- Chan, H.T. and T.C. Kenney (1973). "Laboratory investigation of permeability ratio of New Liskeard varved soil," *Canadian Geotech. J.*, **10**, No. 3, pp. 453–472.
- Chandler, R.J. (1968). "The shaft friction of piles in cohesive soils in terms of effective stress," *Civ. Eng. and Pub. Wks. Review*, **63**, pp. 48–51.
- Chandler, R.J. (1984). "Recent European experience of landslides in overconsolidated clays and soft rocks," *Proc. IV Int. Symp. on Landslides*, **1**, pp. 61–81.
- Chandler, R.J. (1988). "The in situ measurement of the undrained shear strength of clays using the field vane," *Proc. Int. Symp. on Vane Shear Strength Testing in Soils: Field and Laboratory Studies*, ASTM STP No. 1014, pp. 13–44.
- Chapman, G.A. and I.B. Donald (1981). "Interpretation of static penetration tests in sand," *Proc. 10th Int. Conf. on Soil Mech. and Found. Eng.*, Stockholm, **2**, pp. 455–458.
- Charles, J.A., D. Burford, and K.S. Watts (1981). "Field studies of the effectiveness of dynamic consolidation," *Proc. 10th Int. Conf. Soil Mech.*, Stockholm, **3**, pp. 617–622.
- Charles, J.A. and M.M. Soares (1984). "The stability of slopes in soils with nonlinear envelopes," *Canadian Geotech. J.*, **21**, No. 3, pp. 397–406.
- Charles, J.A. and K.S. Watts (1980). "The influence of confining pressure on the shear strength of compacted rockfill," *Géot.*, **30**, No. 4, pp. 353–367.
- Chellis, R.D. (1961). *Pile Foundations*, 2nd ed., New York, McGraw-Hill, 704 pp.
- Chen, F.H. (1988). *Foundations on Expansive Soils*, 2nd ed., Elsevier, New York, 463 p.
- Chen, W.F. (1975). Limit analysis and soil plasticity, In *Developments in Geotechnical Engineering*, **7**, Elsevier, Amsterdam, 638 pp.
- Christian, J.T., J.W. Boehmer, and P.P. Martin (1972). "Consolidation of a layer under a strip load," *ASCE J. Soil Mech.*, **98**, No. SM7, pp. 693–707.
- Christopher, B.R., S.A. Gill, J.P. Giroud, I. Juran, J.K. Mitchell, F. Schlosser, and J. Dunncliff (1990). Design and construction guidelines for reinforced soil structures, Vol. I; Summary of research, Vol. II; Rep. No. FHWA-RD-89-043, Fed. Hwy. Adm., Washington, D.C.
- Clayton, C.R.I., I.F. Symons, and J.C. Hiedra-Cobo (1991). "The pressure of a clay backfill against retaining structures," *Canadian Geotech. J.*, **28**, No. 2, pp. 282–297.
- Clemente, F.M. Jr. (1981). "Downdrag on bitumen coated piles in a warm climate," *Proc. 10th Int. Conf. Soil Mech.*, Stockholm, **2**, pp. 673–676.
- Close, U. and E. McCormick (1922). "Where the mountains walked," *Nat. Geog. Mag.*, **41**, pp. 445–464.

- Clough, G.W. and G.M. Denby (1977). "Stabilizing berm design for temporary walls in clay," *ASCE J. Geot.*, **103**, No. GT 2, pp. 75–90.
- Clough, G.W. and J.M. Duncan (1971). "Finite element analysis of retaining wall behavior," *ASCE J. Soil Mech.*, **97**, No. SM12, pp. 1657–1673.
- Clough, G.W. and J.M. Duncan (1972). "Temperature effects on behavior of Port Allen lock," *Proc. ASCE Conf. on Performance of Earth and Earth-supported Structures*, Lafayette, Ind., **1**, pp. 1467–1479.
- Clough, G.W. and T.D. O'Rourke (1990). "Construction induced movements of insitu walls," *ASCE Spec. Geotech. Publ. No. 25*, pp. 439–470.
- Clough, G.W. and Schmidt, B. (1981). "Design and performance of excavations and tunnels in soft clay," Chap. 8 in *Soft Clay Engineering*, E.W. Brand and R.P. Brenner, eds., Amsterdam, Elsevier, pp. 569–631.
- Clough, G.W., E.M. Smith, and B.P. Sweeney (1989). "Movement control of excavation support systems by iterative design," *Proc. ASCE Conf. on Foundation Engrg.*, Evanston, Ill., pp. 869–884.
- Clough, G.W. and Y. Tsui (1974). "Performance of tied-back walls in clay," *ASCE J. Geot.*, **100**, No. GT12, 1259–1273.
- Clough, G.W., P.R. Weber and J. Lamont, Jr. (1972). "Design and observation of a tied-back wall," *Proc. ASCE Conf. on Performance of Earth and Earth-Supported Structures*, Lafayette, Ind., pp. 1367–1389.
- Collins, J.J. (1935). "New type sea wall built for subsiding lake shore in Venezuela," *Eng. News-Record*, **114**, No. 12, pp. 405–408.
- Cooling, L.F. and H.Q. Golder (1942). "The analysis of the failure of an earth dam during construction," *J. Inst. Civil Engrs.*, London, **20**, No. 1, pp. 38–55; Discussions, Supplement to No. 8, pp. 289–304.
- Cornforth, D.H. (1961). *Plane Strain Failure Characteristics of a Saturated Sand*, Ph.D. thesis, Univ. of London.
- Cornforth, D.H. (1964). "Some experiments on the influence of strain conditions on the strength of sand," *Géot.*, **14**, No. 2, pp. 143–167.
- Cornforth, D.H. (1973). Prediction of drained strength of sands from relative density measurements, ASTM STP No. 523, pp. 281–303.
- Costes, N.C. (1956). "Factors affecting vertical loads on underground ducts due to arching," *Hwy. Res. Board Bull.*, **125**, pp. 12–57.
- Couch, F.B. Jr. and A.D. Ressi di Cervia (1979). "Seepage cutoff wall installed through dam is construction first," *Civ. Eng.*, **49**, No. 1, pp. 62–66.
- Coulomb, C.A. (1776). "Essai sur une Application des Règles des Maximis et Minimis à quelques Problèmes de Statique Relatifs à l'Architecture" (An attempt to apply the rules of maxima and minima to several problems of stability related to architecture), *Mém. Acad. Roy. des Sciences*, Paris, **7**, pp. 343–382.
- Coulson, J.H. (1970). *The Effects of Surface Roughness on the Shear Strength of Joints in Rock*, Ph.D. thesis, Univ. of Illinois at Urbana-Champaign.
- Coyle, H.M. and R.E. Bartoskewitz (1976). "Earth pressure on precast panel retaining wall," *ASCE J. Geot.*, **102**, No. GT5, pp. 441–456.
- Coyle, H.M., R.E. Bartoskewitz, L.J. Milberger, and H.O. Butler (1974). "Field measurements of lateral earth pressures on a cantilever retaining wall," *Transp. Res. Rec.*, **517**, pp. 16–29.
- Crandell, F.J. (1949). "Ground vibration due to blasting and its effect upon structures," *J. Boston Soc. Civil Engrs.*, **36**, pp. 245–268. Reprinted in *Contributions to Soil Mechanics 1941–1953*, Boston Soc. Civil Engrs., 1953, pp. 206–229.
- Crawford, C.B. and G.H. Johnston (1971). "Construction on permafrost," *Can. Geot. J.*, **8**, No. 2, pp. 236–251.
- Crooks, J.H.A. (1981). "A qualitative stress-strain (time) model for soft clays," *Laboratory Shear Strength of Soils*, ASTM STP No. 740, pp. 685–699.
- Crooks, J.H.A. and J. Graham (1976). "Geotechnical properties of the Belfast estuarine deposits," *Géot.*, **26**, No. 2, pp. 293–315.
- Culmann, C. (1875). *Die graphische Statik* (Graphic statics). Zurich, Meyer and Zeller, 644 pp.
- Cummings, A.E. (1940). "Dynamic pile driving formulas," *J. Boston Soc. Civil Engrs.*, **27**, pp. 6–27.
- Cummings, A.E., G.O. Kerkhoff, and R.B. Peck (1950). "Effect of driving piles into soft clay," *Trans. ASCE*, **115**, pp. 275–285.
- D'Appolonia, E. and J.A. Hribar (1963). "Load transfer in a step-taper pile," *ASCE J. Soil Mech.*, **89**, No. SM6, pp. 57–77.
- D'Appolonia, E. and J.P. Romualdi (1963). "Load transfer in end-bearing steel H-piles," *ASCE J. Soil Mech.*, **89**, No. SM2, pp. 1–25.
- D'Appolonia, D.J., R.V. Whitman, and E. D'Appolonia (1969). "Sand compaction with vibratory rollers," *ASCE J. Soil Mech.*, **95**, No. SM1, pp. 263–284.
- Darcy, H. (1856). *Les fontaines publiques de la ville de Dijon* (The water supply of the city of Dijon). Dalmont, Paris, 674 pp.
- Darrag, A.A. and C.W. Lovell (1989). "A simplified procedure for predicting residual stresses for piles," *Proc. 12th Int. Conf. Soil Mech.*, Rio de Janeiro, **2**, pp. 1127–1130.
- Davis, E.H. and H.G. Poulos (1972). "Rate of settlement under two- and three-dimensional conditions," *Géot.*, **22**, No. 1, pp. 95–114.
- Davisson, M.T. (1970a). "Lateral load capacity of piles," *Hwy. Res. Rec.*, **333**, pp. 104–112.
- Davisson, M.T. (1970b). "Design pile capacity," *Proc. Conf. on Design and Installation of Pile Foundations and Cellular Structures*, Lehigh Univ., Envo. Publ. Co., pp. 75–85.
- Davisson, M.T. (1973). "High capacity piles," in *Innovations in Found. Constr. Soil Mech. Div.*, Ill. Sect. ASCE, Chicago, Ill., pp. 81–112.
- Davisson, M.T. (1991). "Reliability of pile prediction methods," *Proc. Deep Fdns. Inst. Conf.*, Chicago.
- De Alba, P., C.K. Chan, and H.B. Seed (1975). "Determination of soil liquefaction characteristics by large-scale laboratory tests," *Earthquake Engineering Research Center*, Report No. EERC-75/14, Univ. of California at Berkeley.
- de Beer, E.E. (1948). "Données concernant la résistance au cisaillement déduites des essais de pénétration en profondeur," *Géot.*, **1**, pp. 22–39.

- de Beer, E.E. (1948). "Settlement records of bridges founded on sand," *Proc. 2nd Int. Conf. on Soil Mech. and Found. Eng.*, Rotterdam, **2**, pp. 111–121.
- deBeer, E.E. (1963). "The scale effect on the transposition of the results of deep-sounding tests on the ultimate bearing capacity of piles and caisson foundations," *Géot.*, **13**, No. 1, pp. 39–75.
- de Beer, E.E., E. Lousberg, M. Wallays, R. Capentier, J. DeJaeger, and J. Paquay (1977). "Bearing capacity of displacement piles in stiff fissured clays," Belgian Governmental Institute for Scientific Research in Industry and Agriculture, *IRSIA-IWON Research, Report 39*.
- Deere, D.U. (1982). "Cement—bentonite grouting for dams," *Proc. ASCE Conf. on Grouting in Geot. Engrg.*, New Orleans, pp. 279–300.
- Deere, D.U. and F.D. Patton (1971). "Slope stability in residual soils," *Proc. 4th Panamerican Conf. Soil Mech.*, Puerto Rico, **1**, pp. 87–170.
- De Mello, V.F.B. (1971). "The standard penetration test," *Proc. 4th Pan Am. Soil Mech. Conf.*, San Juan, **1**, pp. 1–86.
- Denby, G.M. and G.W. Clough (1980). "Self-boring pressuremeter tests in clay," *J. Geotech. Eng., ASCE*, **106**, No. 12, pp. 1369–1387.
- Dennis, N.D. (1982). *Development of Correlations to Improve the Prediction of Axial Pile Capacity*, Ph.D. thesis, Univ. of Texas.
- Dennis, N.D. and R.E. Olson (1983a). "Axial capacity of steel pipe piles in sand," *Proc. ASCE Conf. on Geot. Practice in Offshore Engrg.*, Austin, Texas, pp. 389–402.
- Dennis, N.D. and R.E. Olson (1983b). "Axial capacity of steel pipe piles in clay," *Proc. ASCE Conf. on Geot. Practice in Offshore Engrg.*, Austin, Texas, pp. 370–388.
- deRuiter, J. and F.L. Beringen (1978). "Pile foundations for large North Sea structures," *Marine Geot.*, **3**, pp. 2.
- DiBiagio, E. and L. Bjerrum (1957). "Earth pressure measurements in a trench excavated in stiff marine clay," *Proc. 4th Int. Conf. Soil Mech.*, London, **2**, pp. 196–202.
- Dobry, R. (1994). "Foundation deformation due to earthquakes," *Proc. of Settlement '94, ASCE, Geotech. Spec. Publ. No. 40*, College Station, Texas, **2**, pp. 1846–1863.
- Donovan, N.C. (1972). *Earthquake Hazards of Buildings. Building Practices for Disaster Mitigation*, Building Science Series 46, National Bureau of Standards, U.S. Department of Commerce, Washington, D.C., pp. 82–111.
- Duncan, J.M. and C. Chang (1970). "Nonlinear analysis of stress and strain in soils," *J. Soil Mech. Found. Eng., ASCE*, **96**, No. 5, pp. 1629–1653.
- Duncan, J.M. and G.W. Clough (1971). "Finite element analysis of Port Allen lock," *ASCE J. Soil Mech.*, **97**, No. SM8, pp. 1053–1068.
- Duncan, J.M., G.W. Clough, and R.M. Ebeling (1990). "Behavior and design of gravity earth retaining structures," *Proc. ASCE Conf. on Design and Performance of Earth Retaining Structures*, Ithaca, N.Y., pp. 251–277.
- Duncan, J.M. and R.B. Seed (1986). "Compaction-induced earth pressures under  $K_0$  conditions," *ASCE J. Geot.*, **112**, No. GT1, pp. 1–22.
- Duncan, J.M., G.W. Williams, A.L. Sehn, and R.B. Seed (1991). "Estimation earth pressures due to compaction," *ASCE J. Geot.*, **117**, No. 12, pp. 1833–1847.
- Duncan, J.M., G.W. Williams, A.L. Sehn, and R.B. Seed (1993). "Estimation earth pressures due to compaction. Closure," *J. Geotech. Eng., ASCE*, **119**, No. 7, pp. 1172–1177.
- Dunncliff, J. (1988). *Geotechnical Instrumentation for Monitoring Field Performance*, John Wiley & Sons, Inc., New York, 577 pp.
- Dupuit, J. (1863). *Études théoriques et pratiques sur le mouvement des eaux dans les canaux découverts et à travers les terrains perméables* (Theoretical and experimental studies of the flow of water in open channels and through permeable ground), 2nd ed., Paris, Dunod, 304 pp.
- Durgunoglu, H.T. and J.K. Mitchell (1975). "Static penetration resistance of soils," *Proc. ASCE Specialty Conf. on In Situ Measurement of Soil Parameters*, Raleigh, **1**, pp. 151–171.
- Dyvik, R., T. Berre, S. Lacasse, and B. Raadim (1987). "Comparison of truly undrained and constant volume direct simple shear tests," *Géot.*, **37**, No. 1, pp. 3–10.
- Eden, W.J. and R.J. Mitchell (1970). "The mechanics of landslides in Leda clay," *Canadian Geotech. J.*, **7**, No. 3, pp. 285–296.
- Eden, W.J. and R.J. Mitchell (1971). "The mechanics of landslides in Leda clay reply," *Canadian Geotech. J.*, **8**, No. 1, pp. 148–149.
- Eide, O., G. Aas, and T. Josang (1974). "Special application of cast-in-place walls for tunnels in soft clay in Oslo," *Proc. 5th European Conf. Soil Mech.*, Madrid, **1**, pp. 485–498.
- Endo, M. (1963). "Earth pressure in the excavation work of alluvial clay stratum," *Proc. Int. Conf. Soil Mech. and Found. Eng.*, Budapest, pp. 21–46.
- Eng. News (1909). "The undermining of a reinforced-concrete dam at Pittsfield, Mass.," **61**, No. 13, pp. 345–347.
- Engstrom, U.V. (1963). "Innovations at Wanapum Dam," *Civ. Eng.*, **33**, No. 10, pp. 43–47.
- ENR (1929). "Reconstruction of Lafayette dam advised," *Eng. News-Record*, **102**, pp. 190–192.
- ENR (1937). "Foundation of earth dam fails," *Eng. News-Record*, **119**, p. 532.
- ENR (1941). "Foundation failure causes slump in big dike at Hartford, Conn.," *Eng. News-Record*, **127**, p. 142.
- Escario, V., J.F.T. Jucá, and M.S. Coppe (1989). "Strength and deformation of partly saturated soils," *Proc. 12th Int. Conf. on Soil Mech. and Found. Eng.*, Rio de Janeiro, **1**, pp. 43–46.
- Esrig, M.I. (1968). "Pore pressures, consolidation, and electrokinetics," *J. Soil Mech. Found. Eng., ASCE*, **94**, No. 4, pp. 899–921.
- Esrig, M.I. and R.C. Kirby (1979). "Soil capacity for supporting deep foundation members in clay," *ASTM Spec. Tech. Publ.*, **670**, pp. 27–63.
- Faber, O. (1933). "Pressure distribution under bases and stability of foundations," *The Structural Engineer*, **11**, New Series, pp. 116–125, 241–248.
- Fadum, R.E. (1941). *Observations and Analysis of Building Settlements in Boston*, Sc.D. thesis, Harvard Univ.
- Fadum, R.E. (1948). "Concerning the physical properties of clays," *Proc. 2nd Int. Conf. Soil Mech.*, Rotterdam, **1**, pp. 250–254.
- Fahlquist, F.E. (1941). "New methods and technique in subsurface explorations," *J. Boston Soc. Civil Engrs.*, **28**, No. 2, pp. 144–160.

- Feagin, L.B. (1948). "Performance of pile foundations of navigation locks and dams on the upper Mississippi River," *Proc. 2nd Int. Conf. Soil Mech.*, Rotterdam, **4**, pp. 98–106.
- Feld, J. (1923). "Lateral earth pressure; the accurate experimental determination of the lateral earth pressure, together with a resume of previous experiments," *Trans. ASCE*, **86**, pp. 1448–1505.
- Feld, J. (1943). "Discussion: timber friction pile foundations," *Trans. ASCE*, **108**, pp. 143–144.
- Fellenius, B.H. (1972). "Down-drag on piles in clay due to negative skin friction," *Can. Geot. J.*, **9**, No. 4, pp. 323–337.
- Fellenius, W. (1927). *Erdstatische Berechnungen* (Calculation of stability of slopes). Berlin, (Revised ed. 1939, 48 pp.)
- Fellenius, W., F. Blidberg, L.v. Post, and J. Olsson (1922). *Statens Järnvägars Geotekniska Kommission 1914–22 Slutbetänkande* (State Railways Geotechnical Committee 1914–22. Final Report). Stockholm, 180 pp.
- FHWA (1991). *Soil Nailing for Stabilization of Highway Slopes and Excavations*, U.S. Dept. of Trans. Fed. Hwy. Admin., Publ. No. FHWA-RD-89-193, 209 pp.
- Fieldes, M. and G.G.C. Claridge (1975). "Allophane," *Soil Components Edited by Giesecking*, Springer-Verlag, **2**, pp. 351–393.
- Fields, K.E. and W.L. Wells (1944). "Pendleton Levee failure," *Trans. ASCE*, **109**, pp. 1400–1413.
- Finn, W.D.L. (1981). "Liquefaction potential: development since 1976," *Proc. Int. Conf. on Recent Advances in Geotech. Earthquake Eng. and Soil Dynamics*, Rolla, Missouri, pp. 655–681.
- Finn, W.D.L. and D. Shead (1973). "Creep and creep rupture of an undisturbed sensitive clay," *Proc. 8th Int. Conf. on Soil Mech. and Found. Eng.*, Moscow, **1.1**, pp. 135–142.
- FitzHugh, M.M., J.S. Miller, and K. Terzaghi (1947). "Shipways with cellular walls on a marl foundation," *Trans. ASCE*, **112**, pp. 298–324.
- Flaate, K. (1966). *Stresses and Movements in Connection with Braced Cuts in Sand and Clay*, Ph.D. thesis, Univ. of Illinois, Urbana, 264 pp.
- Flaate, K. (1972). "Effects of pile driving in clays," *Can. Geot. J.*, **9**, No. 1, pp. 81–88.
- Fletcher, G.F.A. (1965). "Standard penetration test: its uses and abuses," *ASCE J. Soil Mech.*, **91**, No. SM4, pp. 67–75.
- Flintoff, W.T. and J.W. Cowland (1982). "Excavation design in residual soil slopes," *Proc. ASCE Specialty Conf. on Engrg. and Constr. in Tropical and Residual Soils*, Hawaii, pp. 539–556.
- Fredlund, D.G. and J. Krahn (1977). "Comparison of slope stability methods of analysis," *Canadian Geot. J.*, **14**, No. 3, pp. 429–439.
- Fredlund, D.G. and H. Rahardjo (1993). *Soil Mechanics for Unsaturated Soils*, New York, John Wiley and Sons, 517 pp.
- Frivik, P.E., N. Janbu, R. Saetersdal, and L.I. Finborud (1980). *Ground Freezing 1980. Developments in Geotech. Eng., Volume 28*, Elsevier, Amsterdam, 411 p.
- Fukuoka, M., T. Akatsu, S. Katagiri, T. Iseda, A. Shimazu, and M. Nakagaki (1981). "Earth pressure measurements on retaining walls," *Proc. 9th Int. Conf. Soil Mech.*, Tokyo, Case History Vol., pp. 237–296.
- Fuller, F.M. (1983). *Engineering of Pile Installations*, New York, McGraw-Hill, 286 pp.
- Fülscher, J. (1897–1899). "Der Bau des Kaiser Wilhelm-Kanals" (Construction of the Kaiser Wilhelm canals). *Zeitschrift für Bauwesen*, **47**, 1897, column 117–142, 275–304, 405–454, 525–586; **48**, 1898, column 41–82, 205–282, 441–490, 693–752; **49**, 1899, column 99–126, 269–304, 425–464, 621–675.
- Fuyuka, T., T. Todoroki, and M. Kasuga (1982). "Reduction of negative skin friction with steel tube NF pile," *Proc. 7th S.E. Asian Geot. Conf.*, Hong Kong, **1**, pp. 333–347.
- Gibson, R.E. (1961). "The progress of three-dimensional consolidation in an anisotropic clay stratum," *Symp. on Found. Eng.*, Indian National Society of Soil Mechanics and Foundation Engineering, New Delhi, pp. 1–19.
- Gibson, R.E., G.L. England, and M.J.L. Hussey (1967). "The theory of one-dimensional consolidation of saturated clays," *Géot.*, **17**, No. 3, pp. 261–273.
- Gibson, R.E. and P. Lumb (1953). "Numerical solution of some problems in the consolidation of clay," *Proc. Instn. Civ. Engrs.*, **1**, Part 1, pp. 182–198.
- Gibson, R.E. and J. McNamee (1957). "The consolidation settlement of a load uniformly distributed over a rectangular area," *Proc. 4th Int. Conf. on Soil Mech. and Found. Eng.*, London, **1**, pp. 297–299.
- Giesecking, J.E. (1975a). "Organic components," *Soil Components Edited by Giesecking*, Springer-Verlag, **1**, 534 pp.
- Giesecking, J.E. (1975b). "Inorganic components," *Soil Components Edited by Giesecking*, Springer-Verlag, **2**, 684 pp.
- Gilboy, G. (1928). "The compressibility of sand-mica mixtures," *Proc. ASCE*, **54**, pp. 555–568.
- Glanville, W.H., G. Grime, E. Fox, and W.W. Davies (1938). "An investigation of the stresses in reinforced concrete piles during driving," *Dept. Sci. Ind. Research, Bldg. Research Sta., England*, Tech. Paper 20, 111 pp.
- Godskesen, O. (1936). "Investigation of the bearing-power of the subsoil (especially moraine) with 25 × 25-mm pointed drill without samples," *Proc. 1st Int. Conf. Soil Mech.*, Cambridge, MA, **1**, pp. 311–314.
- Golder, H.Q. (1948). "Measurement of pressure in timbering of a trench in clay," *Proc. 2nd Int. Conf. Soil Mech.*, Rotterdam, **2**, pp. 76–81.
- Golder, H.Q. (1965). "State-of-the-art of floating foundations," *ASCE J. Soil Mech.*, **91**, No. SM2, pp. 81–88.
- Golder, H.Q. and A.W. Skempton (1948). "The angle of shearing resistance in cohesive soils for tests at constant water content," *Proc. 2nd Int. Conf. on Soil Mech. and Found. Eng.*, Rotterdam, **1**, pp. 185–192.
- Goldberg, D.T., W.E. Jaworski, and M.D. Gordon (1976). *Lateral Support Systems and Underpinning*, Fed. Hwy. Admin. Rep. FHWA-RD-75-128, 3 volumes.
- Gottstein, E. v. (1936). "Two examples concerning underground sliding caused by construction of embankments and static investigations on the effectiveness of measures provided to assure their stability," *Proc. 1st Int. Conf. Soil Mech.*, Cambridge, Mass., **3**, pp. 122–128.
- Graftio, H. (1936). "Some features in connection with the foundation of Svir 3 hydro-electric power development," *Proc. 1st Int. Conf. Soil Mech.*, Cambridge, Mass., **1**, pp. 284–290.

- Graham, J., M.L. Noonan, and K.V. Lew (1983). "Yield states and stress-strain relationships in a natural plastic clay," *Canadian Geotech. J.*, **20**, No. 3, pp. 502-516.
- Graham, J., R.B. Pinkney, K.V. Lew, and P.G.S. Trainor (1982). "Curve-fitting and laboratory data," *Canadian Geotech. J.*, **19**, No. 2, pp. 201-205.
- Greer, D.M. and W.S. Gardner (1986). *Construction of Drilled Pier Foundations*, New York, John Wiley and Sons, 246 pp.
- Gregersen, O. (1981). "The quick clay landslide in Rissa, Norway," *Proc. 10th Int. Conf. on Soil Mech. and Found. Eng.*, Stockholm, Sweden, **3**, pp. 421-426.
- Gregersen, O.S., G. Aas, and E. DiBiagio (1973). "Load test on friction piles in loose sand," *Proc. 8th Int. Conf. Soil Mech.*, Moscow, **2.1**, pp. 109-117.
- Grim, R.E. (1968). *Clay Mineralogy*, 2nd ed., New York, McGraw-Hill, 596 pp.
- Guelton, M., P. Baldy, and C. Magne (1961). "La Barrage de Serre-Ponçon, Conception d'Ensemble" (Serre-Ponçon dam, concept of the project), *Travaux*, **45**, pp. 298-315.
- Hagerty, D.J. and R.B. Peck (1971). "Heave and lateral movements due to pile driving," *ASCE J. Soil Mech.*, **97**, No. SM11, pp. 1513-1532.
- Hall, C.E. (1962). "Compacting a dam foundation by blasting," *ASCE J. Soil Mech.*, **88**, No. SM3, pp. 33-51.
- Hansbo, S. (1957). "A new approach to the determination of the shear strength of clay by the fall-cone test," *Proc. Swedish Geotech. Inst.*, No. 14, 46 pp.
- Hansbo, S. (1960). "Consolidation of clay, with special reference to influence of vertical sand drains," *Proc. Swedish Geotechnical Institute*, **18**, Linköping.
- Hansbo, S. (1979). "Consolidation of clay by band-shaped prefabricated drains," *Ground Engr.*, **12**, No. 5, pp. 16-25.
- Hansbo, S. (1981). "Consolidation of fine-grained soils by prefabricated drains," *Proc. 10th Int. conf. on soil Mech. and Found. Eng.*, Stockholm, **3**, pp. 677-682.
- Hansbo, S. (1994). *Foundation Engineering. Developments in Geotechnical Engineering*, No. 75, New York, Elsevier, 519 pp.
- Hansbo, S., M. Jamiolkowski, and L. Kok (1981). "Consolidation by vertical drains," *Géot.*, **31**, No. 1, pp. 45-66.
- Hansen, B. (1961). "Shear box tests on sand," *Proc. 5th Int. Conf. on Soil Mech. and Found. Eng.*, Paris, **1**, pp. 127-131.
- Hansen, B. (1965). *A Theory of Plasticity for Ideal Frictionless Materials*, Copenhagen, Teknisk Forlag, 471 pp.
- Hansen, J. Brinch (1961). "A general formula for bearing capacity," *Ingeniøren*, **5**, pp. 38-46; also Bull. 11, Danish Geotechnical Inst.
- Hanzawa, H. (1979). "Undrained strength characteristics of an alluvial marine clay in the Tokyo Bay," *Soils and Foundations*, **19**, No. 4, pp. 69-84.
- Hanzawa, H. (1980). "Undrained strength and stability analysis for a quick sand," *Soils and Foundations*, **20**, No. 2, pp. 17-29.
- Hanzawa, H. and T. Kishida (1982). "Determination of in situ undrained strength of soft clay deposits," *Soils and Foundations*, **22**, No. 2, pp. 1-14.
- Hanzawa, H., E. Matsuda, and M. Hirose (1980). "Evaluation of sample quality of sandy soil obtained by the modified Bishop sampler," *Soils and Foundations*, **20**, No. 3, pp. 17-31.
- Hanzawa, H., T. Matsuno, and K. Tsuji (1979). "Undrained strength and stability analysis of soft Iraqi clays," *Soils and Foundations*, **19**, No. 2, pp. 1-14.
- Harder, L.F. (1988). "The Use of Penetration Tests to Determine the Liquefaction Resistance of Sands during Earthquakes," Ph.D. thesis, Univ. of California at Berkeley.
- Harder, L.F. and H.B. Seed (1986). "Determination of penetration resistance for coarse-grained soils using the Becker Hammer Drill," *Earthquake Engineering Research Center, Report No. EERC-86/06*, Univ. of California at Berkeley.
- Hardin, B.O. and V.P. Drnevich (1972). "Shear modulus and damping in soils: design equations and curves," *J. Soil Mech. Found. Eng., ASCE*, **98**, No. 7, pp. 667-692.
- Harr, M.E. (1962). *Groundwater and Seepage*, New York, McGraw-Hill, 315 pp.
- Harr, M.E. (1966). *Foundations of Theoretical Soil Mechanics*, New York, McGraw-Hill, 381 pp.
- Hartman, J.P. and J.H. Schmertmann (1975). "FEM study of elastic phase of pressuremeter test," *ASCE Conf. on In Situ Measurement of Soil Properties*, Raleigh, N.C., **1**, pp. 190-207.
- Hazen, A. (1892). "Physical properties of sands and gravels with reference to their use in filtration," *Rept. Mass. State Board of Health*, p. 539.
- Hendron, A.J. Jr. and F.D. Patton (1986). "A geotechnical analysis of the behavior of the Vaiont slide," *Civil Engrg. Practice*, J. Boston Society Civil Eng., **1**, No. 2, pp. 65-130.
- Hénin, S. and S. Caillère (1975). "Fibrous minerals," *Soil Components Edited by Giesecking*, Springer-Verlag, **2**, pp. 335-349.
- Henkel, D. (1971). "The calculation of earth pressure in open cuts in soft clays," *The Arup Journal*, London, **6**, No. 4, pp. 13-15.
- Hertwig, A., G. Früh and H. Lorenz (1933). "Die Ermittlung der für das Bauwesen wichtigsten Eigenschaften des Bodens durch erzwungene Schwingungen" (The determination by means of forced vibrations of soil properties of special importance for construction work), *Degebo. Veröffentlichung*, **1**, 45 pp.
- Hetényi, M. (1946). *Beams on Elastic Foundation*, Ann Arbor, Univ. of Michigan Press, 255 pp.
- Hilf, J.W. (1975). "Compacted fill," Chap. 7 in *Foundation Engineering Handbook*, Winterkorn and Fang, eds., Van Nostrand Reinhold, pp. 244-311.
- Hirashima, K.B. (1948). "Highway experience with thixotropic volcanic clay," *Proc. Hwy. Res. Board*, **28**, pp. 481-494.
- Holden, J.C. (1971). *Laboratory Research on Static Cone Penetrometers*, Univ. of Florida at Gainesville, Dept. of Civil Eng., CE-SM-71-1.
- Holmsen, P. (1953). "Landslips in Norwegian quick-clays," *Géot.*, **3**, pp. 187-194.
- Holtz, W.G. and H.J. Gibbs (1956). "Engineering properties of expansive clays," *Trans. ASCE*, **121**, pp. 641-677.
- Hooper, J.A. (1983). "Interactive analysis of foundations on horizontally variable strata," *Proc. Institution of Civil Engineers*, **75**, No. 2, pp. 491-524.

- Hooper, J.A. and D.J. West (1983). "Structural analysis of circular raft on yielding soil," *Proc. Institution of Civil Engineers*, **75**, No. 2, pp. 205–242.
- Hubbert, M.K. (1940). "The theory of groundwater motion," *J. Geol.*, **48**, Nov.–Dec., pp. 785–944.
- Hungr, O., G.C. Morgan, and R. Kellerhals (1984). "Quantitative analysis of debris torrent hazards for design of remedial measures," *Canadian Geot. J.*, **21**, No. 4, pp. 663–677.
- Hunt, R.E. (1984). *Geotechnical Engineering Investigation Manual*, New York, McGraw-Hill, 983 pp.
- Hunt, R.E. (1986). *Geotechnical Engineering Analysis and Evaluation*, New York, McGraw-Hill, 729 pp.
- Hunter, A.H. and M.T. Davisson (1969). *Measurement of Pile Load Transfer*. ASTM Spec. Tech. Publ. 444, pp. 106–117.
- Huntington, W.C. (1957). *Earth Pressures and Retaining Walls*, New York, John Wiley and Sons, 534 pp.
- Hutchinson, J.N., and R.K. Bhandari (1971). "Undrained loading, a fundamental mechanism of mudflows and other mass movements," *Géot.*, **21**, No. 4, pp. 353–358.
- Hvorslev, M.J. (1936). "A ring shearing apparatus for the determination of the shearing resistance and plastic flow of soils," *Proc. 1st Int. Conf. on Soil Mech. and Found. Eng.*, Cambridge, **2**, pp. 125–129.
- Hvorslev, M.J. (1939). "Torsion ring shear tests and their place in the determination of the shearing resistance of soils," *Proc. ASTM Symp. on Shear Testing of Soils*, **39**, pp. 999–1022.
- Hvorslev, M.J. (1948). *Subsurface Exploration and Sampling of Soils for Civil Engineering Purposes*, Waterways Exp. Sta., Vicksburg, Miss., 465 pp.
- Hvorslev, M.J. (1960). "Physical components of the shear strength of saturated clays," *Proc. ASCE Research Conf. on Shear Strength of Cohesive Soils*, pp. 169–273.
- Ingles, O.G. and J.B. Metcalf (1973). *Soil Stabilization: Principles and Practice*, New York, John Wiley & Sons, Inc., 374 p.
- Ingold, T.S. (1979). "The effects of compaction on retaining walls," *Géot.*, **29**, No. 3, pp. 265–283.
- Ireland, H.O. (1955). *Settlements due to Foundation Construction in Chicago, 1900–1950*, Ph.D. thesis, Univ. of Illinois, 128 pp.
- Ishihara, K. (1985). "Stability of natural deposits during earthquakes," *Proc. 11th Int. Conf. on Soil Mech. and Found. Eng.*, San Francisco, **1**, pp. 321–376.
- Ishihara, K. (1993). "Liquefaction and flow failure during earthquakes," *Géot.*, **43**, No. 3, pp. 351–415.
- Ishihara, K. and Y. Koga (1981). "Case studies of liquefaction in the 1964 Niigata earthquake," *Soils and Foundations*, **21**, No. 3, pp. 35–52.
- Ishihara, K. and K. Ogawa (1978). "Liquefaction susceptibility map of downtown Tokyo," *Proc. 2nd Int. Conf. on Microzonation for Safer Construction: Research and Application*, **2**, pp. 897–910.
- Ishihara, K. and F. Yamazaki (1980). "Cyclic simple shear tests on saturated sand in multi-directional loading," *Soils and Foundations*, **20**, No. 1, pp. 45–59.
- Ishihara, K. and Y. Yuasa (1963). "Earth pressure measurements in subway construction," *Proc. 2nd Asian Regional Conf. on Soil Mech. and Found. Eng.*, Tokyo, pp. 337–343.
- Ishihara, K. and M. Yoshimine (1992). "Evaluation of settlements in sand deposits following liquefaction during earthquakes," *Soils and Foundations*, **32**, No. 1, pp. 173–188.
- Ivanov, P.L. (1972). *Compaction of Noncohesive Soils by Explosions*, Trans. for U. S. Bur. Recl. and published by Indian Nat'l. Sci. Doc. Centre, New Delhi, 211 pp.
- Iwasaki, T., F. Tatsuoka, and Y. Takagi (1978). "Shear moduli of sands under cyclic torsional shear loading," *Soils and Foundations*, **18**, No. 1, pp. 39–56.
- Iwasaki, T., F. Tatsuoka, K. Tokida, and S. Yasuda (1978). "A practical method for assessing soil liquefaction potential based on case studies at various sites in Japan," *Proc. 2nd Int. Conf. on Microzonation for Safer Construction: Research and Application*, **2**, pp. 885–896.
- Jacob, C.E. (1950). "Flow of ground water," in *Engineering Hydraulics*, H. Rouse, ed., New York, John Wiley and Sons, pp. 321–386.
- Jakobson, B. (1946). *Kortfattat Kompendium i geoteknik*, Statins Geotekniska Institut Medd 1, Stockholm.
- Jaky, J. (1944). "A nyugalmi nyomás tenyezése" (The coefficient of earth pressure at rest), *Magyar Mémek és Építész-Egylet Közönl.*, pp. 355–358.
- Jaky, J. (1948). "Pressure in silos," *Proc. 2nd Int. Conf. on Soil Mech. and Found. Eng.*, Rotterdam, **1**, pp. 103–107.
- Jamiołkowski, M., C.C. Ladd, J.T. Germaine, and R. Lancellotta (1985). "New developments in field and laboratory testing of soils," *Proc. 11th Int. Conf. on Soil Mech. and Found. Eng.*, San Francisco, **1**, pp. 57–153.
- Janbu, N. (1954). "Application of composite slip surfaces for stability analysis," *Proc. European Conf. on Stability of Earth Slopes*, Sweden, **3**, pp. 43–49.
- Janbu, N., L. Bjerrum, and B. Kjaernsli (1956). "Veiledning ved løsning av fundamenteringsoppgaver" (Soil mechanics applied to some engineering problems), in Norwegian with English summary, *Norwegian Geot. Inst. Publ.* **16**, 93 pp.
- Janbu, N. and K. Senneset (1974). "Effective stress interpretation of in situ static penetration tests," *Proc. European Symp. on Penetration Testing, ESOPT-1*, Stockholm, **2.2**, pp. 181–193.
- Jansen, R.B. ed. (1988). *Advanced Dam Engineering for Design, Construction, and Rehabilitation*, New York, Van Nostrand Reinhold, 811 pp.
- Jaspar, J.L. and N. Peters (1979). "Foundation performance of Gardiner Dam," *Can. Geot. J.*, **16**, No. 4, pp. 758–788.
- Jaworski, G.W., J.M. Duncan, and H.B. Seed (1981). "Laboratory study of hydraulic fracturing," *ASCE J. Geot.*, **107**, No. GT6, pp. 713–732.
- Jayawickrama, P.W. and R.L. Lytton (1992). "Conductivity through macropores in compacted clay," *Proc. 7th Int. Conf. on Expansive Soils*, Dallas, **1**, pp. 99–104.
- Jefferies, M.G., J.H.A. Crooks, D.E. Becker, and P.R. Hill (1987). "Independence of geostatic stress from overconsolidation in some Beaufort Sea clays," *Canadian Geotech. J.*, **24**, No. 3, pp. 342–356.
- Jennings, J.E. (1953). "The heaving of buildings on desiccated clay," *Proc. 3rd Int. Conf. Soil Mech.*, Zurich, **1**, pp. 390–396.
- Jimenez-Quinones, P. (1963). *Compaction Characteristics of Tropically Weathered Soils*, Ph.D. thesis, Univ. of Illinois, 135 pp.



- Johnson, A.I., ed. (1991). "Land subsidence," *Procs of the 4th International symposium on Land subsidence, Houston, Texas*, IANS Publication No. 200, 690 pp.
- Johnson, A.W. and J.R. Sallberg (1962). "Factors influencing compaction test results," *Hwy. Res. Board Bull.*, **319**, 148 pp.
- Johnson, H.L. (1940). "Improved sampler and sampling technique for cohesionless materials," *Civ. Eng.*, **10**, pp. 346–348.
- Jones, C.J.F.P. and F.A. Sims (1975). "Earth pressures against the abutments and wing walls of standard motorway bridges," *Géot.*, **25**, No. 4, pp. 731–742.
- Juran, I., G. Baudrand, K. Farrag, and V. Elias (1990). "Design of soil nailed retaining structures," *ASCE Conf. on Design and Performance of Earth Retaining Structures*, Ithaca, N. Y., pp. 644–659.
- Jurgenson, L. (1934). "The application of elasticity and plasticity to foundation problems," *J. Boston Soc. Civil Engrs.*, **21**, pp. 206–241.
- Karpoft, K.P. (1955). "The use of laboratory tests to develop design criteria for protective filters," *Proc. American Society for Testing and Materials*, **55**, pp. 1183–1198.
- Kaufman, R.I. and W.C. Sherman (1964). Engineering measurements for Port Allen Lock. *J. Soil Mech. Found. Eng.*, ASCE, **90**, No. 5, pp. 221–247.
- Kenney, T.C. (1963). "Permeability ratio of repeatedly layered soils," *Géot.*, **13**, No. 4, pp. 325–333.
- Kenney, T.C. (1964). "Sea-level movements and geologic histories of the post-glacial marine soils at Boston, Nicolet, Ottawa and Oslo," *Géot.*, **14**, No. 3, pp. 203–230.
- Kenney, T.C. (1967a). "The influence of mineral composition on the residual strength of natural soils," *Proc. Geotech. Conf. on Shear Strength Properties of Natural Soils and Rocks*, Oslo, **1**, pp. 123–129.
- Kenney, T.C. (1967b). "Slide behaviour and shear resistance of a quick clay determined from a study of the landslide at Selnes, Norway," *Proc. of the Geotech. Conf. on Shear Strength Properties of Natural Soils and Rocks*, Oslo, **1**, pp. 57–64.
- Kenney, T.C. (1976). "Formation and geotechnical characteristics of glacial-lake varved soils," *Bjerrum Memorial Volume, Norwegian Geotechnical Institute*, Oslo, pp. 15–39.
- Kenney, T.C. (1977). "Residual strengths of mineral mixtures," *Proc. 9th Int. Conf. on Soil Mech. and Found. Eng.*, Tokyo, **1**, pp. 155–160.
- Kenney, T.C., R. Chahal, E. Chiu, G.I. Ofoegbu, G.N. Omenge, and C.A. Ume (1985). "Controlling constriction sizes of granular filters," *Canadian Geotech. J.*, **22**, No. 1, pp. 32–43.
- Kenney, T.C. and H.T. Chan (1973). "Field investigation of permeability ratio of New Liskeard varved soil," *Canadian Geotech. J.*, **10**, No. 3, pp. 473–488.
- Kenney, T.C., D. Lau, and G.I. Ofoegbu (1984). "Permeability of compacted granular materials," *Canadian Geotech. J.*, **21**, No. 4, pp. 726–729.
- Kenney, T.C., W.A. van Veen, M.A. Swallow, and M.A. Sungaila (1992). "Hydraulic conductivity of compacted bentonite-sand mixtures," *Canadian Geotech. J.*, **29**, No. 3, pp. 364–374.
- Kerisel, J.C. (1961). "Deep foundations in a sandy medium." (French), *Proc. 5th Int. Conf. Soil Mech.*, Paris, **2**, pp. 73–83.
- Kerisel, J. (1985). "The history of geotechnical engineering up until 1700," *Proc. 11th Int. Conf. on Soil Mech. and Found. Eng.*, San Francisco, Golden Jubilee Volume, pp. 3–93.
- Kimura, T. and K. Saitoh (1983). "Effect of disturbance due to insertion on vane shear strength of normally consolidated cohesive soils," *Soils and Foundations*, **23**, No. 2, pp. 113–124.
- King, F.H. (1899). "Principles and conditions of the movements of ground water," *U.S. Geol. Soc. 19th Ann. Rept.*, Part 2, pp. 59–294.
- Kirkebo, S. (1994). *A Numerical Study of Excavations in Low Permeable Soils*, Dr. Ing. thesis, Dept. of Geotechnical Eng., The Norwegian Institute of Technology.
- Kjaernsli, B. and I. Torblaa (1968). Leakage through horizontal cracks in the core of Hyttejuvet Dam, NGI Publ. 80, pp. 39–47.
- Klenner, C. (1941). "Versuche über die Verteilung des Erd-druckes über die Wände ausgesteifter Baugruben" (Tests on the distribution of the earth pressure over the walls of braced excavations), *Bautechnik*, **19**, pp. 316–319.
- Klohn, E.J. (1963). "Pile heave and redriving," *Trans. ASCE*, **128**, Part 1, pp. 557–577.
- Koerner, R.M. and J.P. Welsh (1980). *Construction and Geotechnical Engineering Using Synthetic Fibers*, New York, John Wiley and Sons, 267 pp.
- Kögler, F. (1933). "Discussion: Soil mechanics research," *Trans. ASCE*, **98**, pp. 299–301.
- Kolb, C.R. and W.G. Shockley (1959). "Engineering geology of the Mississippi valley," *Trans. ASCE*, **124**, pp. 633–645.
- Kollgaard, E.B. and W.L. Chadwick, eds. (1988). *Development of Dam Engineering in the United States*. Prepared in Commemoration of the Sixteenth Congress of the International Commission on Large Dams by the United States Committee on Large Dams, New York, Pergamon Press, 1072 pp.
- Kondner, R.L. (1963). "Hyperbolic stress-strain response: cohesive soils," *J. Soil Mech. Found. Eng.*, ASCE, **89**, No. 1, pp. 115–143.
- Konrad, J.M. (1990). "Minimum undrained strength versus steady-state strength of sands," *J. Geotech. Eng.*, ASCE, **116**, No. 6, pp. 948–963.
- Koutsoftas, D.C. (1982). "H-pile heave: a field test," *ASCE J. Geot.*, **108**, No. GT8, pp. 999–1016.
- Koutsoftas, D.C. and C.C. Ladd (1985). "Design strengths for an offshore clay," *J. Geotech. Eng.*, ASCE, **111**, No. 3, pp. 337–355.
- Kovacs, W.D. (1979). "Velocity measurement of free-fall SPT hammer," *ASCE J. Geot.*, **105**, No. GT1, pp. 1–10.
- Kraft, L.M., Jr., R.P. Ray, and T. Kagawa (1981). "Theoretical t-z curves," *J. Geotech. Eng.*, ASCE, **107**, No. 11, pp. 1543–1561.
- Kriegel, H.J. and H.H. Wiesner (1973). "Problems of stress-strain conditions in subsoil," *Proc. 8th Int. Conf. on Soil Mech. and Found. Eng.*, Moscow, **1.3**, pp. 133–141.
- Kulhawy, F.H. (1991). "Drilled shaft foundations," *Foundation Engineering Handbook*, H.Y. Fang, ed., Van Nostrand Reinhold, 2nd ed., pp. 537–552.

- Kyrieleis, W. and W. Sichert (1930). *Grundwasserabsenkung bei Fundierungsarbeiten* (Groundwater lowering for foundation construction), 2nd ed., Berlin, J. Springer, 286 pp.
- La Gatta, D.P. (1970). "Residual strength of clays and clay-shales by rotation shear tests," *Harvard Soil Mechanics Series*, No. 86, Cambridge.
- La Rochelle, P., M. Roy, and F. Tavenas (1973). "Field measurements of cohesion in Champlain clays," *Proc. 8th Int. Conf. on Soil Mech. and Found. Eng.*, Moscow, **1.1**, pp. 229–236.
- La Rochelle, P., J. Sarrailh, F. Tavenas, M. Roy, and S. Leroueil (1981). "Causes of sampling disturbance and design of a new sampler for sensitive soils," *Canadian Geotech. J.*, **18**, No. 1, pp. 52–66.
- Lacasse, S.M., C.C. Ladd, and M.M. Baligh (1978). "Evaluation of field vane, Dutch cone penetrometer and piezometer testing devices," *Research Report*, Mass. Inst. of Tech., Cambridge.
- Lacroix, Y. (1956). *Measurements of earth pressure against bracing of Inland Steel Building Excavation, Chicago, Ill.* Paper presented before the ASCE, Pittsburgh, Oct. 19, 1956.
- Ladd, C.C. (1991). "Stability evaluation during staged construction," *J. Geotech. Eng., ASCE*, **117**, No. 4, pp. 540–615.
- Ladd, C.C., O. Dascal, K.T. Law, G. Lefebvre, G. Lessard, G. Mesri, and F. Tavenas (1983). *Report of the Subcommittee on Embankment Stability of the Committee of Specialists on Sensitive Clays of the NBR Complex*, SEBJ, Montreal, Annexe II.
- Ladd, C.C., R. Foott, K. Ishihara, F. Schlosser, and H.G. Poulos (1977). "Stress-deformation and strength characteristics," *Proc. 11th Int. Conf. on Soil Mech. and Found. Eng.*, Tokyo, **2**, pp. 421–494.
- Ladd, C.C. and A.E.Z. Wissa (1970). "Geology and engineering properties of Connecticut valley varved clays with special reference to embankment construction," *Research Report R70-56-264*, Dept. of Civil Eng., MIT, Cambridge.
- Ladd, G.E. (1935). "Landslides, subsidences and rock-falls," *Proc. Am. Rwy. Eng. Assn.*, **36**, pp. 1091–1162.
- Lafleur, J. (1984). "Filter testing of broadly graded cohesionless tills," *Canadian Geotech. J.*, **21**, No. 4, pp. 634–643.
- Lafleur, J. and G. Lefebvre (1980). "Groundwater regime associated with slope stability in Champlain clay deposits," *Canadian Geotech. J.*, **17**, No. 1, pp. 44–53.
- Lambe, T.W. and H.M. Horn (1965). "The influence on an adjacent building of pile driving for the M.I.T. Materials Center," *Proc. 6th Int. Conf. Soil Mech.*, Montreal, **2**, pp. 280–284.
- Lambe, T.W. and R.V. Whitman (1969). *Soil Mechanics*, New York, John Wiley & Sons, Inc., 553 pp.
- Lane, E.W. (1935). "Security from under-seepage—masonry dams on earth foundations," *Trans. ASCE*, **100**, pp. 1235–1351.
- Lane, K.S. and P.E. Wohlt (1961). "Performance of sheet piling and blankets for sealing Missouri River reservoirs," *Proc. 7th Congr. on Large Dams*, Rome, **4**, pp. 255–279.
- Larsen, E.S. and H. Berman (1934). "The microscopic determination of the nonopaque minerals," 2nd ed. *U.S. Dept. of Interior Bull.* **848**, 266 pp.
- Larsson, R. (1977). "Basic behavior of Scandinavian soft clays," *Swedish Geotechnical Institute, Report No. 4*, 108 pp.
- Larsson, R. (1980). "Undrained shear strength in stability calculation of embankments and foundations on soft clays," *Canadian Geotech. J.*, **17**, No. 4, pp. 591–602.
- Larsson, R. and G. Sällfors (1981). "Hypothetical yield envelope at stress rotation," *Proc. 10th Int. Conf. on Soil Mech. and Found. Eng.*, Stockholm, **1**, pp. 693–696.
- Law, K.T. and R.D. Holtz (1978). "A note on Skempton's A parameter with rotation of principal stresses," *Géot.*, **28**, No. 1, pp. 57–64.
- Lee, C.H. (1953). "Building foundations in San Francisco," *Proc. ASCE*, **79**, Separate 325, 32 pp.
- Lee, K.L. (1970). "Comparison of plane strain and triaxial tests on sand," *J. Soil Mech., ASCE*, **96**, No. 3, pp. 901–923.
- Lee, S.L., Y.K. Chow, G.P. Karunaratne, and K.Y. Wong (1988). "Rational wave equation model for pile-driving analysis," *ASCE J. Geot.*, **114**, No. GT3, pp. 306–325.
- Lebedeff, A.F. (1928). "Methods of determining the maximum molecular moisture holding capacity of soils," *Proc. 1st Int. Conf. Soil Science*, Washington, **1**, pp. 551–560.
- Lefebvre, G. (1981). "Fourth Canadian Geotechnical Colloquium: Strength and slope stability in Canadian soft clay deposits," *Canadian Geotech. J.*, **18**, No. 3, pp. 420–442.
- Lefebvre, G., C.C. Ladd, G. Mesri, and F. Tavenas (1983). *Report of the Subcommittee on Sampling and Laboratory Testing of the Committee of Specialists on Sensitive Clays of the NBR Complex*, SEBJ, Montreal, Annexe III.
- Lefebvre, G., C.C. Ladd, and J.J. Paré (1988). "Comparison of field vane and laboratory undrained shear strengths in soft sensitive clays," *Int. Symp. on Vane Shear Strength Testing in Soils: Field and Laboratory Studies*, ASTM STP No. 1014, pp. 233–246.
- Lefebvre, G., J.J. Paré, and O. Dascal (1987). "Undrained shear strength in the surficial weathered crust," *Canadian Geotech. J.*, **24**, No. 1, pp. 23–34.
- Lefebvre, G. and C. Poulin (1979). "A new method of sampling in sensitive clay," *Can. Geot. J.*, **16**, No. 1, pp. 226–233.
- Lefebvre, G., O. Dascal, and G. St-Arnaud (1977). "Arching in the foundations of a large dam," *Proc. 9th Int. Conf. Soil Mech.*, Tokyo, **1**, pp. 623–628.
- Legget, R. (1950). "Discussion: effect of driving piles into soft clay," *Trans. ASCE*, **115**, pp. 319–322.
- Leonards, G.A. (1979). "Stability of slopes in soft clay," *6th Pan American Conf. on Soil Mech. and Found. Eng.*, Lima.
- Leroueil, S., G. Collins, and F. Tavenas (1983). "Total and effective stress analyses of slopes in Champlain Sea clays," *SGI Report No. 17*, pp. 293–321.
- Leroueil, S., F. Tavenas, and J.-P. LeBihan (1983). "Propriétés caractéristiques des argiles de l'est du Canada," *Canadian Geotech. J.*, **20**, No. 4, pp. 681–705.
- Lessard, G. (1982). *Biogeochemical Phenomena in Quick Clays and Their Effects on Engineering Properties*, Ph.D. thesis, Univ. of California at Berkeley.
- Lea, N.D. and C.O. Brawner (1963). "Highway design and construction over peat deposits in lower British Columbia," *Highway Research Record*, No. 7, pp. 1–32.
- Lewis, M.R., M.G. Donnelly, and L.W. Young (1985). "Discussion:  $K_A$  and  $K_O$  behind rotating and non-yielding walls," *J. Geotech. Eng., ASCE*, **111**, No. 8, pp. 1039–1041.

- Liao, S.S.C. and R.V. Whitman (1986). "Overburden correction factors for SPT in sand," *J. Geotech. Eng., ASCE*, **112**, No. 3, pp. 373-377.
- Litvinov, I.M. (1960). "Stabilization of settling and weak clayey soils by thermal treatment," *Hwy. Res. Bd. Spec. Rep.* 60, pp. 94-112.
- Liu, T.K. and J.P. Dugan, Jr. (1972). "An instrumented tied-back deep excavation," *Proc. ASCE Conf. on Performance of Earth and Earth-Supported Structures*, Lafayette, Ind., **1**, pp. 1323-1339.
- Lo, D.O.K. (1991). *Soil Improvement by Vertical Drains*, Ph.D. thesis, Univ. of Illinois at Urbana-Champaign.
- Lo, K.Y. and K.S. Ho (1991). "The effects of electroosmotic field treatment on the soil properties of a soft sensitive clay," *Canadian Geotech. J.*, **28**, No. 6, pp. 763-770.
- Lo, K.Y., K.S. Ho, and I.I. Inculet (1991). "Field test of electro-osmotic strengthening of soft sensitive clay," *Canadian Geotech. J.*, **28**, No. 1, pp. 74-83.
- Lo, K.Y., I.I. Inculet, and K.S. Ho (1991). "Electro-osmotic strengthening of soft sensitive clays," *Canadian Geotech. J.*, **28**, No. 1, pp. 62-73.
- Locat, J. and D. Demers (1988). "Viscosity, yield stress, remolded strength, and liquidity index relationships for sensitive clays," *Canadian Geotech. J.*, **25**, No. 4, pp. 799-806.
- Lockwood, M.G. (1954). "Ground subsides in Houston area," *Civ. Eng.*, **24**, No. 6, pp. 48-50.
- Long, E.L. (1964). "The long thermopile," *Civ. Eng.*, **34**, No. 4, Apr., p. 36.
- Long, J.H. and L.C. Reese (1987). "Behavior of two piles in clay subjected to cyclic lateral loads," *Proc. Conf. Prediction and Performance in Geot. Engrg.*, Calgary, pp. 97-104.
- Long, J.H. and S. Shimel (1989). "Drilled shafts: a database approach," *Proc. ASCE Found. Engrg. Congress*, Evanston, Ill.
- Long, J.H., W.F. Sieczkowski, Jr., E. Chow, and E.J. Cording (1990). "Stability analyses for soil nailed walls," *Proc. ASCE Conf. on Design and Performance of Earth Retaining Structures*, Geotech. Spec. Publ. No. 25, pp. 676-691.
- Lorenz, H. (1934). "Neue Ergebnisse der dynamischen Baugrunduntersuchung" (New results of dynamic investigations of foundation soils), *Zeitschrift des Vereins deutscher Ingenieure*, **78**, pp. 379-385.
- Louden, A.G. (1952). "The computation of permeability from simple soil tests," *Géot.*, **3**, No. 4, pp. 165-183.
- Lovell, L.A. (1970). "Design features of Tarbela Dam in West Pakistan," *World Dams Today* 70, Japan Dam Assn., pp. 111-114.
- Lowe, J. (1960). "Current practice in soil sampling in the United States," *Hwy. Res. Board Special Rept.* 60, pp. 142-154.
- Lowe, J. (1978). "Foundation design: Tarbela dam, Pakistan," *4th Nabor Carrillo Lecture*, Mexican Soc. Soil Mech., 148 pp.
- Lowe, J. (1988). "Seepage analysis," *Advanced Dam Engineering for Design, Construction, and Rehabilitation*, R.B. Jansen, ed., New York, Van Nostrand Reinhold, pp. 270-275.
- Lumb, P. (1965). "The residual soils of Hong Kong," *Géot.*, **15**, No. 2, pp. 180-194.
- Lund, A. (1949). *An Experimental Study of Graded Filters*, M.Sc. thesis, Univ. of London.
- Lundgren, H. and K. Mortensen (1953). "Determination by the theory of plasticity of the bearing capacity of continuous footings on sand," *Proc. 3rd Int. Conf. Soil Mech.*, Zurich, **1**, pp. 409-412.
- Lunne, T., S. Lacasse, N.S. Rad, and L. Décourt (1990). "SPT, CPT, pressuremeter testing and recent developments on in situ testing," *Norwegian Geotech. Inst. Pub.* 179, 89 pp.
- Lysmer, J. and F.E. Richart, Jr. (1966). "Dynamic response of footings to vertical loading," *ASCE J. Soil Mech.*, **92**, No. SM1, pp. 65-91.
- Lytton, R.L. (1992). "Use of mechanics in expansive soils engineering," *Proc. 7th Int. Conf. on Expansive Soils*, **2**, Dallas, pp. 13-23.
- MacEwan, D.M.C. and A. Ruiz-Amil (1975). "Interstratified clay minerals," *Soil Components Edited by Giesekeing*, Springer-Verlag, **2**, pp. 265-334.
- Makdesi, F.I. and H.B. Seed (1978). "Simplified procedure for estimating dam and embankment earthquake-induced deformation," *ASCE J. Geot.*, **104**, No. GT7, pp. 848-867.
- Mana, A.I. and G.W. Clough (1981). "Prediction of movements for braced cuts in clay," *ASCE J. Geot.*, **107**, No. GT6, 759-777.
- Mansur, C.I. and M. Alizadeh (1970). "Tie-backs in clay to support sheeted excavation," *ASCE J. Soil Mech.*, **96**, No. SM2, pp. 495-509.
- Marachi, N.D., C.K. Chan, and H.B. Seed (1972). "Evaluation of properties of rockfill materials," *J. Soil Mech. Found. Eng., ASCE*, **98**, No. 1, pp. 95-114.
- Marcuson, W.M., M.E. Hynes, and A.G. Franklin (1990). "Evaluation and use of residual strength in the seismic stability of embankments," *Earthquake Spectra*, **6**, No. 3, pp. 529-572.
- Marsal, R.J. (1973). "Mechanical properties of rockfill," *Embankment Dam Engineering*, Casagrande Vol., New York, Wiley, pp. 109-200.
- Marsal, R.J. and M. Mazari (1962). *El Subsuelo de la Ciudad de México* (The subsoil of Mexico City), 2nd ed., Universidad Nacional Autónoma de México, Facultad de Ingeniería, 614 pp.
- Marsland, A. (1971). "Large in situ tests to measure the properties of stiff fissured clay," *Proc. 1st Australian Conf. on Geomech.*, Melbourne, **1**, pp. 180-189.
- Marsland, A. (1974). "Comparisons of the results from static penetration tests and large in situ plate tests in London clay," *Proc. European Symp. on Penetration Testing*, Stockholm.
- Marsland, A. and J.J.M. Powell (1979). "Evaluating the large-scale properties of glacial clays for foundation design," *Proc. 2nd Conf. on Behavior of Offshore Structures*, **1**, pp. 435-464.
- Marsland, A. and R.S.T. Quarterman (1982). "Factors affecting the measurement and interpretation of quasi static penetration tests on clays," *Proc. European Symp. on Penetration Testing II*, Amsterdam, **2**, pp. 697-702.
- Marsland, A. and R.S.T. Quarterman (1988). "The interpretation of cone penetration tests in clays, with particular reference

